# WATERSHED AND STREAM MECHANICS

U.S. Department of Agriculture

SOIL CONSERVATION SERVICE

# WATERSHED AND STREAM MECHANICS

Prepared for

United States Department of Agriculture

Soil Conservation Service

Washington, D.C. 20013

by

D. B. Simons

R. M. Li

N. Duong

N. Kouwen

V. M. Ponce

E. V. Richardson

K. Schneider

S. A. Schumm

R. K. Simons

Research Institute of Colorado

Fort Collins, Colorado 80526

March 1980

TABLE OF CONTENTS


| Chapter | | Page |
|---|---|---|
| 1 | INTRODUCTION | 1-1 |
| | 1.1 INTRODUCTION | 1-1 |
| 2 | PHYSICAL PROCESSES GOVERNING WATERSHED AND CHANNEL RESPONSE | 2-1 |
| | 2.1 INTRODUCTION | 2-1 |
| | 2.2 CLASSIFICATION OF WATERSHEDS AND RIVERS | 2-2 |
| | 2.3 PHYSICAL PROCESSES GOVERNING WATERSHED RESPONSE | 2-10 |
| | 2.4 PHYSICAL PROCESS VARIABLES AND RIVER MECHANICS GOVERNING CHANNEL RESPONSE | 2-18 |
| | 2.5 QUALITATIVE ORDER OF MAGNITUDE ANALYSIS OF FORCES ACTING ON A RIVER--AN EXAMPLE | 2-29 |
| | 2.6 QUALITATIVE ANALYSIS OF CHANNEL RESPONSE FOR SELECTED EXAMPLES | 2-41 |
| | 2.7 SUMMARY | 2-53 |
| 3 | OVERVIEW OF STREAM MECHANICS AND RIVER SYSTEMS ANALYSIS | 3-1 |
| | 3.1 INTRODUCTION | 3-1 |
| | 3.2 CURRENT STATE-OF-THE-ART | 3-2 |
| | 3.3 PHYSICAL PROCESSES IMPORTANT TO THE ANALYSIS | 3-7 |
| | 3.4 CRITERIA OF USEFUL MATHEMATICAL MODELS | 3-8 |
| | 3.5 PROCEDURAL STEPS FOR MODEL DEVELOPMENT | 3-10 |
| | 3.6 OVERVIEW OF SOME CASE STUDIES | 3-12 |
| | 3.7 DATA NEEDS FOR ANALYSIS | 3-32 |
| | 3.8 LEVEL OF ANALYSIS | 3-32 |
| | 3.9 SUMMARY | 3-38 |
| 4 | FLUVIAL GEOMORPHOLOGY | 4-1 |
| | 4.1 THE FLUVIAL SYSTEM | 4-1 |
| | 4.2 VARIABLES | 4-4 |
| | 4.3 DRAINAGE BASIN MORPHOLOGY | 4-11 |
| | 4.4 DRAINAGE BASIN DYNAMICS | 4-17 |
| | 4.5 CHANNEL MORPHOLOGY | 4-32 |
| | 4.6 CLASSIFICATION | 4-58 |
| | 4.7 DISCUSSION | 4-63 |
| 5 | OPEN CHANNEL FLOW | 5-1 |
| | 5.1 INTRODUCTION | 5-1 |
| | 5.2 BASIC PRINCIPLES | 5-3 |
| | 5.3 STEADY UNIFORM FLOW | 5-15 |
| | 5.4 STEADY RAPIDLY VARYING FLOW | 5-26 |
| | 5.5 STEADY FLOW AROUND BENDS | 5-32 |
| | 5.6 RAPID FLOW IN BENDS AND TRANSITIONS | 5-34 |
| | 5.7 GRADUALLY VARIED STEADY FLOW | 5-37 |
| | 5.8 UNSTEADY FLOW | 5-43 |
| | 5.9 GRADUALLY VARIED UNSTEADY FLOW | 5-49 |
| | APPENDIX 5A | 5-74 |
| | 5A.1 Bridge Constrictions with No Backwater (Neglecting Energy Losses) | 5-75 |
| | 5A.2 Backwater from Downstream Diversion Dam | 5-75 |
| | 5A.3 Standard Step Method for Backwater Computations | 5-78 |
| | 5A.4 Energy and Momentum Coefficients for Rivers | 5-81 |
| | 5A.5 Average Pressure and Elevation of a River Cross Section | 5-88 |

| Chapter | | Page |
|---|---|---|
| 6 | RESISTANCE TO FLOW | 6-1 |
| | 6.1 INTRODUCTION | 6-1 |
| | 6.2 BASIC CONCEPTS FOR DESCRIBING RESISTANCE TO FLOW | 6-1 |
| | 6.3 RESISTANCE TO FLOW IN OPEN CHANNELS WITH FLAT BED AND RIGID BOUNDARY | 6-10 |
| | 6.4 RESISTANCE TO FLOW IN SAND BED CHANNELS | 6-31 |
| | 6.5 RESISTANCE TO FLOW IN COBBLE AND GRAVEL BED STREAMS | 6-63 |
| | 6.6 RESISTANCE TO FLOW IN VEGETATED CHANNELS | 6-90 |
| | APPENDIX 6A | 6-108 |
| 7 | SEDIMENT TRANSPORT | 7-1 |
| | 7.1 INTRODUCTION | 7-1 |
| | 7.2 TRANSPORT CONCEPTS | |
| | 7.3 APPLICATION OF SEDIMENT TRANSPORT FORMULAS | 7-46 |
| | 7.4 SAMPLE CALCULATIONS | 7-48 |
| | APPENDIX 7A | 7-72 |
| | 7A.1 Size Frequency Distribution | 7-72 |
| | 7A.2 Quartile and Moment Measures | 7-79 |
| | 7A.3 Shape Distribution | 7-82 |
| | 7A.4 Specific Weight of Deposited Sediment | 7-82 |
| | APPENDIX 7B | 7-85 |
| | 7B.1 Sediment Transport Equation from Nonlinear Regression Analysis | 7-85 |
| 8 | CHANNEL DESIGN | 8-1 |
| | 8.1 INTRODUCTION | 8-1 |
| | 8.2 DESIGN OF STABLE CHANNELS: PERMISSIBLE VELOCITY AND TRACTIVE FORCE | 8-2 |
| | 8.3 UTILITY OF VEGETATION AND ITS IMPACT ON CHANNEL STABILITY | 8-26 |
| | 8.4 METHODS OF DETERMINING STABILITY OF GRASSED CHANNELS | 8-27 |
| | 8.5 PRACTICAL CONSIDERATIONS | 8-35 |
| 9 | CHANNEL PROTECTION | 9-1 |
| | 9.1 INTRODUCTION | 9-1 |
| | 9.2 CHANNEL IMPROVEMENT | 9-5 |
| | 9.3 RIVER TRAINING AND STABILIZATION | 9-13 |
| | 9.5 SCOUR AND DEGRADATION | 9-22 |
| | APPENDIX 9A | 9-33 |
| | 9A.1 Introduction | 9-34 |
| | 9A.2 Representative Grain Size for Riprap | 9-42 |
| | 9A.3 Relation between Velocity and Shear | 9-47 |
| | 9A.4 Riprap Design on an Embankment | 9-50 |
| | 9A.5 Design Aid for Side Slope Riprap | 9-52 |
| | 9A.6 Filter Design | 9-55 |
| | 9A.7 Straub's Equation for Clear-water Scour | 9-58 |
| | 9A.8 Determination of Flow Parameters on an Embankment | 9-62 |

Chapter Page

10 UTILIZATION OF HYDROLOGIC INFORMATION SYSTEM . . . . . 10-1
10.1 INTRODUCTION . . . . . 10-1
10.2 DATA STORAGE . . . . . 10-3
10.3 BASIC CONCEPTS OF A COMPUTERIZED DATA BASE SYSTEM . . . 10-7
10.4 CODASYL CONCEPTS OF DATA BASE MANAGEMENT . . . . . 10-9
10.5 DATA STORAGE AND RETRIEVAL SYSTEM FOR RIVER BASIN ANALYSIS . . . . . 10-12
10.6 A CASE STUDY: THE YAZOO DATA STORAGE AND RETRIEVAL SYSTEM . . . . . 10-12

11 WATER AND SEDIMENT ROUTING . . . . . 11-1
11.1 INTRODUCTION . . . . . 11-1
11.2 CLASSIFICATION OF FLOOD ROUTING METHODS . . . . . 11-2
11.3 NUMERICAL MODELING . . . . . 11-4
11.4 TYPES OF FINITE DIFFERENCE SCHEMES . . . . . 11-9
11.5 STABILITY AND CONVERGENCE . . . . . 11-11
11.6 WATER AND SEDIMENT ROUTING . . . . . 11-15
11.7 DEGRADATION BELOW A DAM (T OR C WILLIAMSBURG WATERSHED, NEW MEXICO) . . . . . 11-19
11.8 DEGRADATION AND AGGRADATION ASSOCIATED WITH GRAVEL MINING (SAN JUAN CREEK, CALIFORNIA) . . . . . 11-31

12 SURFACE WATER HYDROLOGY . . . . . 12-1
12.1 INTRODUCTION . . . . . 12-1
12.2 SPATIAL REPRESENTATION OF WATERSHEDS . . . . . 12-2
12.3 MODEL COMPONENTS . . . . . 12-13
12.4 EXCESS RAINFALL ESTIMATION . . . . . 12-17
12.5 WATER ROUTING . . . . . 12-21
12.6 EXAMPLE OF APPLICATION . . . . . 12-40
12.7 PEAK FLOOD PREDICTION FOR AN ARID WATERSHED . . . . . 12-48
12.8 DATA NEEDS . . . . . 12-54

13 WATERSHED SEDIMENT YIELD . . . . . 13-1
13.1 INTRODUCTION . . . . . 13-1
13.2 TYPES OF APPROACH . . . . . 13-8
13.3 BASIC SEDIMENT ROUTING AND YIELD EQUATIONS . . . . . 13-17
13.4 MODEL APPLICATION . . . . . 13-24
13.5 DATA NEED . . . . . 13-24
13.7 SUMMARY . . . . . 13-30

14 STAGE DISCHARGE RELATIONSHIP . . . . . 14-1
14.1 THE EFFECT OF ALLUVIAL BEDFORMS ON STAGE-DISCHARGE RELATIONS . . . . . 14-2
14.2 DISCONTINUITIES IN STAGE-DISCHARGE RELATIONS DUE TO BEDFORMS CHANGE . . . . . 14-6
14.3 HYSTERESIS PHENOMENON IN STAGE-DISCHARGE RELATIONS DUE TO CHANGING BEDFORMS . . . . . 14-6
14.4 EFFECT OF GRAVEL, SAND, OR SILT TRANSPORT IN DEPTH-DISCHARGE RELATIONS OF COBBLE AND BOULDER BED RIVERS . . . . . 14-14
14.5 EFFECT OF SCOUR AND FILL ON STAGE-DISCHARGE RELATIONS . 14-14
14.6 DYNAMIC EFFECTS ON STAGE-DISCHARGE RELATIONS DUE TO UNSTEADY, NONUNIFORM FLOW IN BOTH RIGID AND ALLUVIAL CHANNELS . . . . . 14-25

Chapter Page

14.7 SOLUTION OF THE FULL DYNAMIC MOMENTUM EQUATION TO DESCRIBE THE STAGE-DISCHARGE RELATION . . . . . 14-26
14.8 CONVERSION FROM DISCHARGE TO STAGE . . . . . 14-26
14.9 CONVERSION FROM STAGE TO DISCHARGE . . . . . 14-30
14.10 TEST RESULTS OF DYNAMIC STAGE-DISCHARGE RELATION . . . 14-32
14.11 CONCLUSIONS . . . . . 14-32

15 RESERVOIR SEDIMENTATION . . . . . 15-1
15.1 TYPES OF RESERVOIRS . . . . . 15-1
15.2 VOLUME OF DEPOSITION . . . . . 15-2
15.3 PATTERNS OF DEPOSITION . . . . . 15-7
15.4 CONCLUSIONS . . . . . 15-36

# CHAPTER 1

# INTRODUCTION

## 1.1 INTRODUCTION

The river and watershed system is an integral part of the dynamic ecosystem. Streamflows, sediment transport rates, and channel morphology reflect the major responses resulting from watershed management and/or river utilization activities. Knowledge of river mechanics, geomorphology, and watershed management is essential for formulating and selecting design alternatives by planners and/or engineers of the U.S. Soil Conservation Service (SCS). The basic principles affecting the dynamics and hydraulic response of streams to any natural conditions and/or man-made alteration are not generally covered in college curriculum, particularly at the undergraduate level. An understanding of stream mechanics is necessary for proper planning and design of any channel change. This is particularly true of work in natural streams, streams with bed load, and streams that carry heavy sediment loads. Analysis using principles of stream mechanics, which is a dynamic condition as compared to a static rigid-boundary condition, will provide more realistic designs that do not require excessive maintenance. In response to this need, the National Training Committee of the SCS has approved a training course on stream mechanics. Two courses have been conducted. The first course was held from August 13 to 24, 1979 and the second course from February 11 to 22, 1980. Positive comments and suggestions were made by the participants of the first two courses and the SCS has determined that such a course should be a part of the regular training courses offered in the future. This set of "class notes" will be utilized as the course reference for SCS personnel in the future.

This reference can be used to teach the principles of stream dynamics and present quantitative procedures for analysis of channel modifications, etc. It reviews the dynamics of stream systems considering geologic, hydrologic, and hydraulic perspectives. Principles of both rigid boundary and alluvial (movable bed) channels are presented. Effects and analysis of stream morphology, watershed, and river response are discussed. In addition, quantitative and qualitative analyses of stream response and stabilization are included for practical application to analyze all types of channel modifications encountered in SCS program work.

The training course provides an awareness and understanding of the basic principles of watershed and river hyraulics and the dynamic boundary response. Upon completion of the training, the participant is able to:

1. Identify and classify streams according to the hydraulic and bed material parameters,

2. Outline the proper steps and physical parameters needed to analyze and design stream alterations for any purpose, and

3. Prepare design concepts for stream modification features to serve irrigation, improve fisheries, maintain or minimize environmental effects created by man-made alterations, and control damage and destruction occurring through natural stream morphology.

Lectures given in the second course February 11-22, 1980 were utilized to develop this manuscript. A brief description of the lectures and responsible lecturers follows.

1. Overview of Stream Mechanics and River System Analysis by Dr. D. B. Simons

   Current methods of analysis - geomorphic, engineering, and modeling; physical processes important to the analysis; criteria for analysis - geomorphic, engineering, modeling (physical and mathematical models).

2. The Fluvial System by Dr. S. A. Schumm

   A geomorphic perspective of the landscape with emphasis on the significance of time and the system concept. Consideration of the major independent variables that control landform evolution and morphology.

3. Drainage Basin Morphology by Dr. S. A. Schumm

   Quantitative description of drainage basin morphology and the components of a drainage basin (hillslopes, drainage networks).

4. Open Channel Flow I and II by Dr. E. V. Richardson

   Fundamental equations of open-channel flow with application to steady uniform and non-uniform flow conditions. Particular emphasis on resistance to flow, flow through transitions, water surface profile and importance of the Froude number.

5. Channel Morphology I by Dr. S. A. Schumm

   Description and classification of alluvial channels. Effects of water and sediment discharge on channel morphology.

6. Channel Morphology II by Dr. S. A. Schumm

   Unstable channels, river metamorphosis, and river pattern thresholds. Summary and applications of the geomorphic approach.

7. Unsteady-Open-Channel Flow by Dr. V. M. Ponce

   Fundamentals of unsteady open-channel flow; overview of flood routing methods--governing equations, kinematic, dynamic, and inertial waves, Muskingum-Cunge Method.

8. Numerical Modeling by Dr. V. M. Ponce

   Fundamentals of numerical modeling and its application to open-channel flow problems; finite difference schemes; explicit and implicit schemes; properties of numerical solution.

9. Drainage Basin Dynamics by Dr. S. A. Schumm

The erosional development of drainage networks and the influence of basin morphology on runoff and sediment yield. The complex response of drainage basins and the recognition of geomorphic thresholds.

10. Sediment Transport I by Dr. D. B. Simons

Definition of terms; characteristics of sediment; beginning of motion; suspended sediment, bed load, bed material transport, washload; methods of estimating sediment transport - Einstein, modified Einstein, Meyer-Peter, Müller, Colby, stream power, and other methods.

11. Sediment Transport II by Dr. D. B. Simons

Evaluation of usefulness of methods; application of methods - Einstein, modified Einstein, Colby, Meyer-Peter, Müller and others; modification of methods for specific applications - watersheds, rivers, and reservoirs.

12. Surface Water Hydrology I and II by Dr. R. M. Li

Governing physical processes of surface water; spatial representation of watersheds; distribution of rainfall; excess rainfall estimation; water routing; data needs; examples of application; programmable calculator programs.

13. Watershed Water and Sediment Yield by Dr. R. M. Li

Review of methods for estimating water and sediment yield; on-site soil erosion models; single and multiple watershed models; data needs; parameter estimation; and model applications.

14. Utilization of Hydrologic Information System by Dr. N. Duong

Data storage and retrieval system for managing stage-discharge, discharge, stage, sediment, channel cross section, control structure, reservoir and precipitation data; query language for easy access and retrieval of desired data.

15. Resistance to Flow in Sand Bed Streams by Dr. E. V. Richardson

Alluvium, sediment transport terms, bed configurations, and sediment properties; the effect of bed configuration and changes in bed configuration on sediment transport, resistance to flow, Manning's n, stage discharge relations, and flow velocity; methods of measuring sediment properties, the effect of sediment size, water temperatures, depth, and slope on bed form and these on resistance to flow and sediment transport.

16. Resistance to Flow in Cobble and Gravel Bed Streams by Dr. R. M. Li

Scales of roughness; bed material characteristics; process of fluid mechanics - wave drag, free surface drag, and instabilities; roughness geometry; flow resistance equation; applications.

17. Resistance to Flow in Vegetated Channel by Dr. N. Kouwen
Retardance curves for selected vegetated condition; physically based resistance function; applications.

18. Channel Morphology by Dr. E. V. Richardson
The basic characteristic stream form, slope, velocity, cross section roughness and how they respond to natural and man-made changes. Methods of predicting qualitative and quantitative changes.

19. Physical Processes Governing Watersheds and Channel Response by Dr. D. B. Simons
Classification of watershed and rivers; physical processes governing watershed and channel response; major variables and principles of river mechanics governing channel response.

20. Stage-Discharge Relationship by Mr. R. K. Simons
Single and looped stage-discharge rating curves; factors affecting stage-discharge relationships; flow dynamic effects; backwater effects; sedimentation and erosion effects; reliability of stage-discharge relationships; application.

21. Design of Static Equilibrium Channels by Dr. E. V. Richardson
Details of the design of stable channels that will not transport sediment; problems associated with the design and the control of sediment.

22. Design of Dynamic Equilibrium Channels I by Dr. D. B. Simons
Major variables for channel design; qualitative order of magnitude analysis of forces affecting the response and stability of channels and river systems; discussion of the concept of stable alluvial channels - natural channels and canals.

23. Design of Dynamic Equilibrium Channels II by Dr. D. B. Simons
The dynamics of watershed and channel systems; the design of channels - beginning of motion, permissible velocity, regime concepts; design of systems; levels of analysis; data needs for analysis; data storage and retrieval systems; case studies.

24. Design of Stable Channels with Vegetation by Dr. N. Kouwen
Methods of design for stability - maximum permissible velocity, permissible tractive force, equivalent stone size, and maximum permissible depth; physically based method for determining stability; and practical considerations.

25. Reservoir Sedimentation by Dr. D. B. Simons
Physical processes; major variables - hydrologic, hydraulic, geometry of the system, sedimentation, and sediment transport; commonly accepted methods of analysis; state-of-the-art methodologies; methods of controlling reservoir sedimentation; effects of reservoir deposition on spillway

design, flood control, hydro-power, and channel system - bank erosion, aggradation, and degradation; consolidation of reservoir sediments.

26. Response of River System to Watershed Development by Dr. R. M. Li

Qualitative response of river system; qualitative analysis of river response, quantitative analysis of river response.

27. Water and Sediment Routing by Dr. R. M. Li

Methods of water and sediment routing in rivers; degradation and aggradation analysis; general and local scour below dams.

28. Channel Protection by Dr. E. V. Richardson

The fundamentals of local and general scour and methods of predicting their magnitude; channel modifications to improve the flow line, decrease erosion and provide flood protection methods; river training and sizing of riprap, spurs and jetties.

Each lecturer was responsible for preparing the class notes in consultation with Dr. Fred Theurer of SCS and Drs. Daryl B. Simons and Ruh-Ming Li of Colorado State University. The integrated class notes were edited and prepared by Drs. Daryl B. Simons and Ruh-Ming Li with capable assistance from Ms. Kris Schneider and Ms. Tammy McFall along with Ms. Janna Fullerton. Special thanks are due to Ms. Lee Ann Mitchell for typing the material. In order to provide the continuity of presented material in a systematic and orderly way, the sequence of chapters presented in this training reference has been modified from those of the second course. In addition, overlapping information has been eliminated.

# CHAPTER 2

# PHYSICAL PROCESSES GOVERNING WATERSHED AND CHANNEL RESPONSE

## 2.1 INTRODUCTION

Written or mathematical descriptions of a natural system rely on understanding the physical processes that govern the system. This holds true for climatologic, hydrologic, hydraulic, and biologic systems. Only by recognizing and comprehending the myriad of complex processes can a system be correctly analyzed and future reponse of the system adequately estimated.

The fluvial system composed of a watershed, channels, and those entities that act on and react to them is a prime example of a highly nonlinear complex system. The fluvial system includes hydrologic, hydraulic, geologic, soil, climatologic, biologic, and man's influences as subsystems or components. Each of these components is governed by physical processes that often affect other components. Because of the overlap and complex nature of the processes, fluvial system components are often difficult to fully understand. However, current knowledge of the governing physical processes will permit a better depiction of the fluvial system.

In general, two types of forces are common to all components of the fluvial system, those resulting from gravity and those resulting from inertia, friction, and cohesion. Gravity is involved in rainfall, infiltration, runoff, sediment movement, mass wasting, weathering, plant growth, and man's activities. Conversely, inertia, friction and/or cohesive forces sometimes counteract the actions of gravity by developing flow resistance, landslide stability, and erosion resistance. Because gravity and friction-cohesion forces affect many processes, the effects can be either positive or negative. For example, although gravity promotes downslope water movement resulting in soil erosion, it also prevents some soil particles from being eroded due to their weight.

Several approaches can be taken in delineating and analyzing physical processes that govern the fluvial system. As a first step, watersheds and rivers can be classified into different groups based on physical characteristics. These characteristics are usually a direct result of the physical processes that govern the system and therefore provide an initial view of the controlling phenomena. Once subdivided, watersheds and rivers can be described in terms of the processes that control their response. After these processes are understood as well as possible, their relative importance can be evaluated. For example, raindrop splash is often an important process in upland watershed erosion but has little if any effect on a large rivers such as the Mississippi. These important physical processes should be considered to determine qualitative and quantitative response of the system.

## 2.2 CLASSIFICATION OF WATERSHEDS AND RIVERS

### General

Classification of watersheds and rivers is usually based on observable physical characteristics. These characteristics are the result of governing physical processes (including man's influence) that determine system configuration.

Classification systems utilize qualitative and quasi-quantitative descriptions. Qualitative descriptions are those that identify easily visualized physical characteristics of the described system. Examples of these are descriptive terms for rivers such as meandering, straight, and braided. Quasi-quantitative descriptions use numerical values to relate qualitative descriptions to one another. For example, a river with a certain degree of sinuosity, slope, and characteristic discharge can be classified as meandering based on the values of these variables. Use of quantitative means of description allows comparisons between areas on a more theoretical and less subjective basis.

Classifications reflect morphology of the system in question. Although physical processes controlling watershed and river systems overlap considerably, each has a set of processes that is extremely important. Therefore, classification systems for watersheds and river channels can provide considerable insight into the controlling physical processes.

### Watershed Classification

There are many factors that combine to characterize a watershed (Figure 2-1). However, at present there does not seem to be a widely accepted or employed classification system used to categorize upland watersheds due to the wide diversity of watersheds and watershed conditions and the more intense interest in river classification systems. However, as the United States population expands and interest in environmental issues increases, more emphasis will be placed on water, mineral resources, timber, energy, recreation, and residential uses on upland watersheds. This will necessitate a better understanding of processes and responses. Such an understanding can be partially attained through better classification schemes.

Research has identified various methods for quantifying watersheds according to morphological measures. Horton (1945) was one of the first to recognize and utilize the relationship between stream order and number and length of streams in that order. In general, drainage area and stream length increase as the stream order increases. But as stream order increases, the number of streams in that order decreases. Qualitatively, this means that a large stream has a large drainage basin and is longer than a small stream. However, the Horton analysis of a drainage basin does not provide a quantitative basis for these qualitative observations. Langbein et al. (1947) and Strahler (1952, 1957) developed methods for determining additional watershed indices. Many of the most widely used morphological characteristics and their related measurement techniques have been summarized by Chow (1964). Some of

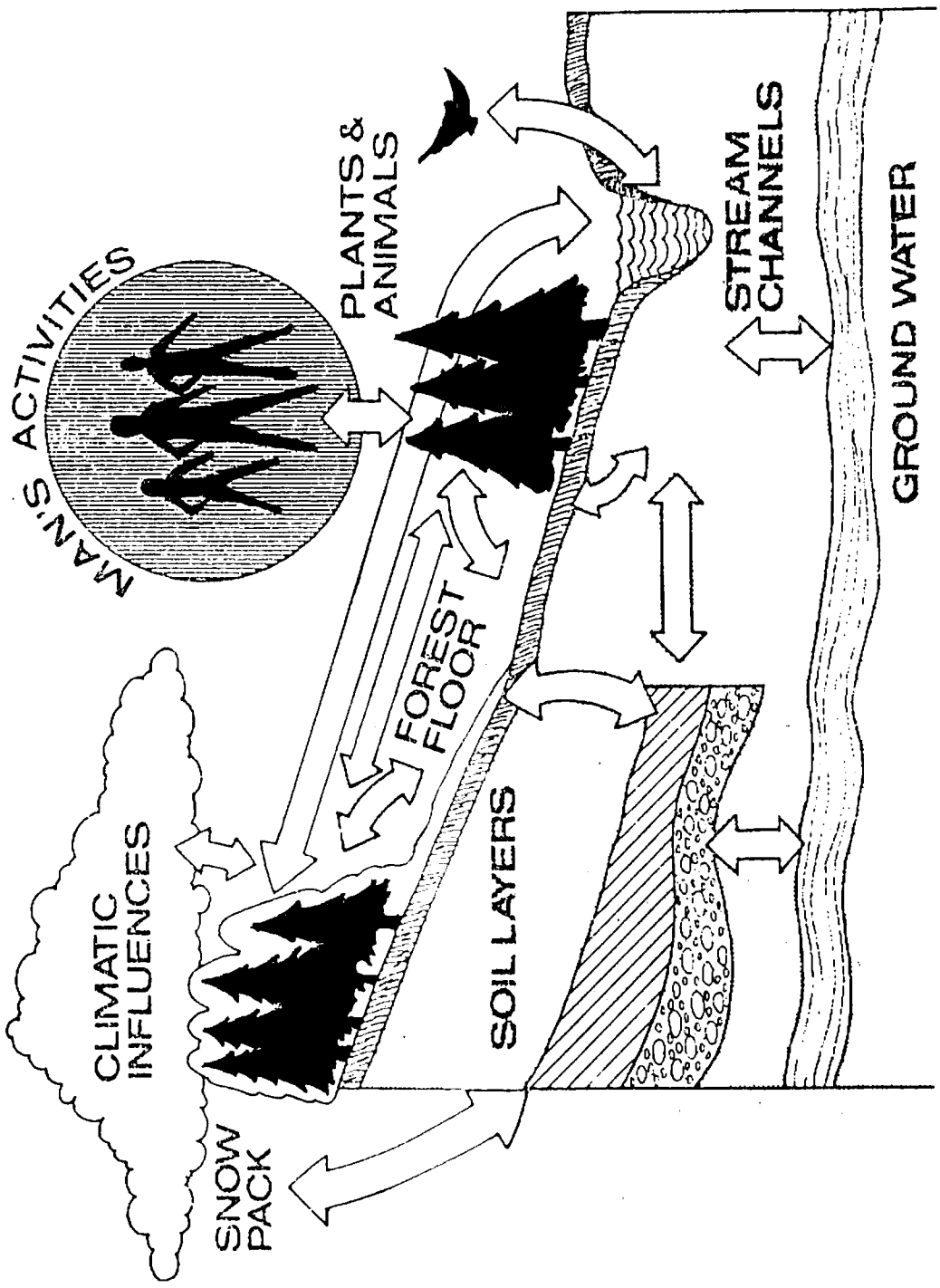


Figure 2-1. Some common factors used for characterizing watersheds.

widely used characteristics include watershed area, stream length, average main stream slope, drainage density (miles of stream per square mile of watershed area), watershed shape such as circularity ratio (ratio of basin area to area of circle with same perimter as basin), and watershed slope (such as average overland slope or relief ratio which is the total watershed relief divided by the distance from the outlet to the furthest point on the basin divide).

Little more in the way of watershed classification has been utilized beyond morphological measures. However, a watershed cannot be completely described by these measures alone. Indices of soils, geology, vegetation, hydrology, and hydraulics are also needed to more accurately describe the watershed. Pfankuch (1975) and Rosgen (1975) presented methods for delineating important watershed channel characteristics that can lead to numerical and descriptive classifications of the channels. This is a positive step that should be extended to other parts of the watershed system. For example, a rating system or classification of sediment sources and yields from watersheds would aid in describing this aspect. Simons, Ward, and Li (1979) have delineated important sources of sediment in watersheds. However, more effort to establish a quantification scheme is needed.

It is possible using experience gained from years of field inspections and modeling to develop a framework of watershed classification. This proposed framework (Table 2-1) is based on the primary needs of modeling and quantifying descriptions as determined from past experience.

Table 2-1. Proposed frameworks for classification of watersheds.

| Key Component | Possible Descriptors |
|---|---|
| GEOMETRY | Location, area, slope, drainage density, length of streams, channel characteristics |
| SOIL | Type, distribution, dominant size, erosivity, depth, texture |
| GEOLOGY | Bedrock and surficial types and distribution, structure, effects on hydrology and soils |
| VEGETATION | Overstory and understory types and distribution, interception, transpiration, stage of succession |
| CLIMATE | Precipitation type, seasonal occurrence, duration, frequency, temperature, evaporation |
| HYROLOGY | Surface water, groundwater, infiltration interflow, peak discharges, yearly hydrographs, ephemeral or perennial discharge |
| SEDIMENT YIELD | Sources, erosion and transport mechanisms, sediment hydrograph characteristics |
| MAN'S INFLUENCE | Degree of development, type of development or construction activity, impacts on other components |

As Table 2-1 indicates, there is the possibility for many combinations of components for watershed classification. Such a system provides a common basis for comparison of different watersheds. For example, a watershed may be classified according to Table 2-2.

Although Table 2-2 presents general descriptions, it illustrates the myriad pieces of information needed to fully describe and classify a watershed.

River Classification

In contrast to the lack of a widely used watershed classification system are the numerous schemes applied to rivers. Davis (1899) first suggested that rivers could be divided into three stages: youth, maturity, and old age. These stages were later subdivided based on the presence or absence of rapids, falls, meanders, oxbow lakes, flood plains, canyons, and other factors. In general a stream can range from youth to old age as it flows from watershed to ocean.

Although this system does not account for spatial variability, it provides an initial common classification language. Thornbury (1969) presented common valley classifications based on land surface development. Although not precisely analagous, these surface patterns are often used for stream classification. These patterns are recognized as antecedent, superposed, consequent, and subsequent. Antecedent streams or valleys antidate structures that they cut across, such as a valley through an updomed area or a fault zone. A superposed stream extends across structures that are older than the stream but were covered by the original stream bed material. Erosion eventually removed this material and superposed the river on the structure. Consequent streams are a result of initial land slope, while subsequent streams have been shifted from original consequent courses to ones following weaker belts of rocks.

Schumm (1963, 1971) quantified the stream types by using discharge and type of sediment load (Table 2-3). These two independent variables determine alluvial channel (compared with bedrock channels that are controlled by the rock and its structure) morphology or how the stream shapes its channel.

Simons et al. (1975) discusses how rivers or segments of rivers, can also be classified as straight, meandering, braided, or some combination of these (Figure 2-2). Reaches of a river that are relatively straight over a long distance are generally unstable, as are divided flow reaches and those with rapidly migrating bends. Long straight reaches can be created by natural or man-made cut-offs of meander loops when long reaches of sinuous meandering channels with relatively flat slopes are converted to shorter reaches with steeper slopes. Straight reaches can also be man-induced by contraction works such as dikes and revetment used to reduce or control sinuosity.

Table 2-2. Example of a watershed classification using component system proposed in Table 2-1.

| Key Component | Selected Descriptors |
|---|---|
| GEOMETRY | Area = 10 sq. miles<br>Average channel slope = 0.05<br>Average overland slope = 0.25<br>Narrow, deep channel; width/depth = 3 |
| SOIL | Gravelly sand loam predominates, sand sizes predominate<br>Moderately erodible (gravel offers protection)<br>Typically 20"-30" deep |
| GEOLOGY | Granitic rocks--primarily granodiorite some basalt flows<br>Major fault in watershed and basalt-granodiorite contact provides zones of groundwater discharge |
| VEGETATION | Ponderosa pine (second growth) overstory<br>Minimal understory from recent fire<br>Sixty percent canopy cover<br>Forty percent ground cover |
| CLIMATE | Winter snowfall $\tilde{\sim}$ 70% of yearly total<br>Spring rain showers $\tilde{\sim}$ 15% of yearly total<br>Summer thunderstorms $\tilde{\sim}$ 15% of yearly total<br>Yearly precipitation average $\tilde{\sim}$ 25 inches<br>Average January minimum temperature = 10° F.<br>Average July maximum temperature = 83° F. |
| HYDROLOGY | Mixed ground and surface water flow<br>Geologic controls force most of groundwater to surface at basin mouth<br>Ephemeral stream<br>Storm flow controlled by interflow |
| SEDIMENT YIELD | Primarily surface and rill erosion<br>A few small landslides, little channel erosion<br>Bedload transport of sand size particles |
| MAN'S INFLUENCE | Increased erosion near an unprotected roadway<br>Some soil disturbance on logged areas |

Table 2-3. Classification of alluvial channels.

| Mode of Sediment Transport and Type of Channel | Channel Sediment (M) Percent | Bedload (Percentage of Total Load) | Channel Stability | | |
|---|---|---|---|---|---|
| | | | Stable (Graded Stream) | Depositing (Excess Load) | Eroding (Deficiency of Load) |
| Suspended Load | 20 | 3 | Stable suspended-load channel. Width-depth ratio less than 10; sinuosity usually greater than 2.0; gradient relatively gentle. | Depositing suspended load channel. Major deposition on banks cause narrowing of channel; initial streambed deposition minor. | Eroding suspended-load channel. Streambed erosion predominant; initial channel widening minor. |
| Mixed Load | 5-20 | 3-11 | Stable mixed-load channel. Width-depth ratio greater than 10; less than 40; sinuosity usually less than 2.0; greater than 1.3; gradient moderate. | Depositing mixed-load channel. Initial major deposition on banks followed by streambed deposition. | Eroding mixed-load channel. Initial streambed eroson followed by channel widening. |
| Bed Load | 5 | 11 | Stable bed load channel. Width-depth ratio greater than 40; sinuosity, usually less than 1.3; gradient relatively steep. | Depositing bed load channel. Streambed deposition and island formation. | Eroding bed load channel. Little streambed erosion; channel widening predominant. |

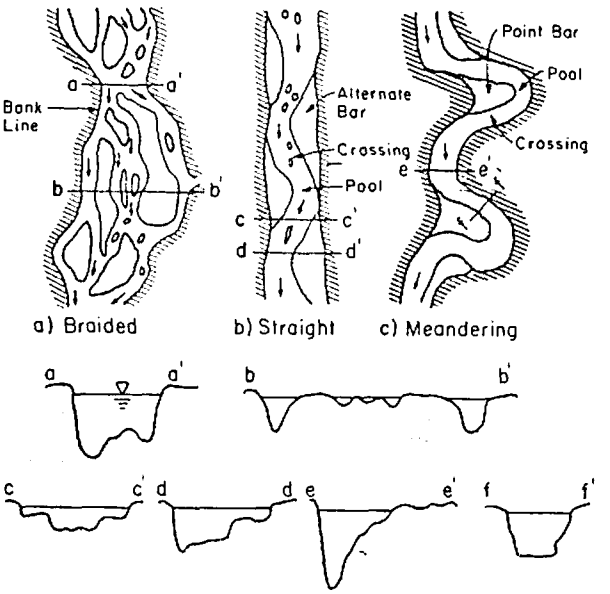


Figure 2-2. Typical river channel patterns (after Simons et al., 1975).

A braided channel is relatively wide with poorly defined unstable banks and characterized by a steep, shallow water course with multiple channel divisions around alluvial islands. Braiding is one pattern that can maintain quasi-equilibrium among the variables of discharge, sediment load, and transport capacity. Lane (1957) concluded two primary causes for the braided condition generally are: 1) the stream is supplied with more sediment than it can carry, resulting in deposition of part of the load and 2) steep slopes that produce a wide shallow channel where bars and islands readily form.

One or both factors could be responsible for a braided pattern. If the channel is overloaded with sediment, deposition ensues, the bed aggrades, and channel slope increases in an effort to maintain a graded condition. As the channel steepens, the velocity increases and multiple channels develop and cause the overall channel system to braid. Multiple channels that form when bars of sediment accumulate within the main channel are generally unstable and change position over time and with stage fluctuations.

Another cause of braiding is easily eroded banks. If the banks are easily eroded such as sand and gravel banks, the stream widens at high flow and during periods of low flow bars form that may become stabilized by armoring and vegetation, forming islands. In general, a braided channel has a steep slope, large bed-material load in comparison with suspended load, and relatively small amounts of silts and clay in the bed and banks. The exact response of a braided stream is difficult to predict because it is unstable, rapidly changes alignment, carries large quantities of sediment, and is wide and shallow even at flood flow.

A meandering channel is one that consists of alternating bends giving an S-shaped appearance to the plan view of the river. Lane (1957) concluded that a meandering stream has a channel alignment consisting principally of pronounced bends, the shapes of determined predominantly by the varying nature of terrain. The meandering river consists of a series of deep pools in the bends and shallow crossings in the short straight reach connecting the bends. The thalweg flows from a

pool through a crossing to the next pool, forming the typical S-curve of a single meander loop.

As shown schematically in Figure 2-2, the pools tend to be relatively triangular in section with point bars located on the inside of the bend. In the crossing the channel tends to be more rectangular, widths are greater and depths are relatively shallow. During periods of low flow local slope is steeper and velocities are larger in the crossings than in the pools. At low stages the thalweg is located very close to the outside of the bend. At higher stages, the thalweg tends to straighten. More specifically, the thalweg moves away from the outside of the bend encroaching on the point bar to some degree. In extreme cases, shifting of the current causes chute channels to develop across the point bar at high stages. In the crossings, the channel is relatively more shallow than in the pools and banks may be more subject to erosion.

Because of the physical characteristics of straight, braided, and meandering streams, all natural channel patterns integrade. Although braiding and meandering patterns are strikingly different, they actually represent extremes in a continuum of channel patterns. Assuming that the pattern of a stream is determined by the interaction of numerous variables whose range in nature is continuous, it is not surprising that a river may exhibit braiding, straight, and meandering forms. Alteration of the controlling parameters in a reach can change the character of a given stream from meandering to braided or the reverse. Studies have quantified this concept of a continuum of channel patterns. Khan (1971) related sinuosity, slope, and channel pattern (Figure 2-3). Any natural or artificial change that alters channel slope such as the cutoff of a meander loop, can result in modifications to the existing river pattern. A cutoff in a meandering channel shortens channel length i.e., increases slope, and tends to move plotting position of the river to the right on Figure 2-3. This indicates a tendency to evolve from a controllable meandering pattern to a less controllable braided pattern that rapidly varies with time, has high velocities, is subdivided by sandbars, and carries relatively large quantities of sediment. Conversely, a decrease in slope could change an unstable braided river into a more stable meandering pattern.

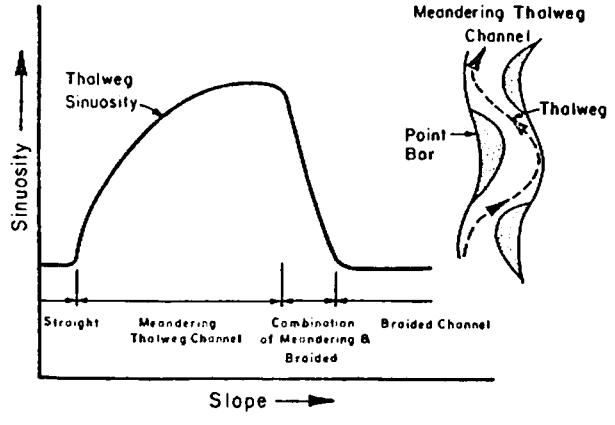


Figure 2-3. Sinuosity compared with slope with constant discharge relative to channel patterns (channel patterns are illustrated in Figure 2-2).

Lane (1957) suggested relationships among slope, discharge, and channel patterns in meandering and braided streams and observed that an equation of the form

$$SQ^{\frac{1}{4}} = K \qquad (2\text{-}1)$$

fits a large amount of data from meandering sand streams. Here S is the channel slope, Q is the water discharge, and K is a constant. Figure 2-4 summarizes Lane's results. If a river is meandering with a discharge and slope that borders on transitional, a relatively small increase in channel slope could initiate a tendency toward a transitional or braided character.

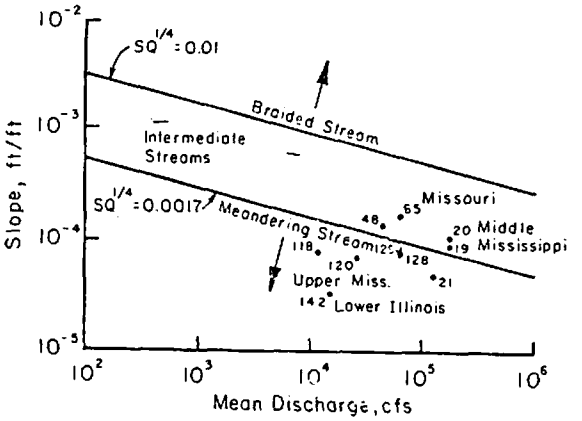


Figure 2-4. Slope-discharge relation for braiding or meandering in sand bed streams (Lane, 1957).

Another classification scheme that uses vegetation pattern, sinuosity, and bank characteristics has been proposed by Culbertson, Young, and Brice (1967). Their contribution is summarized in Figure 2-5. Using this approach, a more descriptive classification can be developed.

There are other more complex classification schemes available (e.g. Garg, 1972). Many of these have been compiled by Rundquist (1975). However, no matter what classification scheme is used, it should be remembered that classification only applies to that segment being analyzed. Because river channels are very dynamic, the river form can change dramatically from location to location, in turn changing classification.

Watershed and river channel classification systems are a reflection of the physical processes that govern their observable characteristics. Understanding physical processes aids in classifying as well as determining future response of the system to natural or man-induced changes. Response of the system has been briefly presented in Figures 2-3 and 2-4. However, a more concise understanding of controlling factors is needed before the entire response of the system can be predicted.

## 2.3 PHYSICAL PROCESSES GOVERNING WATERSHED RESPONSE

Governing physical processes or quantities in watersheds can be divided into seven broad groups of topography, soils, geology, vegetation, climatic conditions, hydrology and hydraulics, and man's influence. These divisions are similar to those presented in Table 2-1

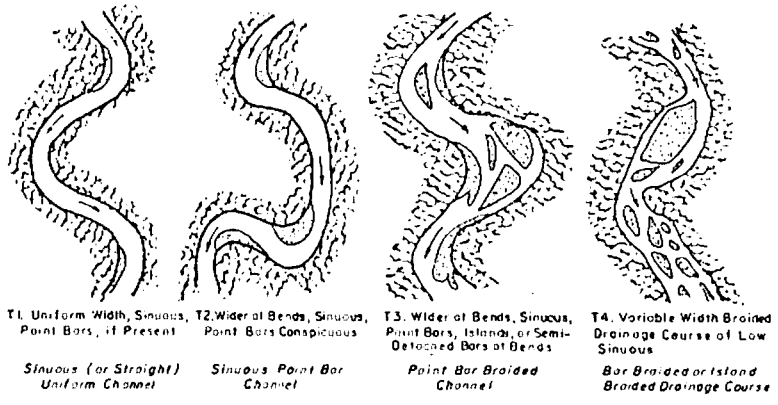


(a) Variability of Unvegetated Channel Width: Channel Pattern at Normal Discharge

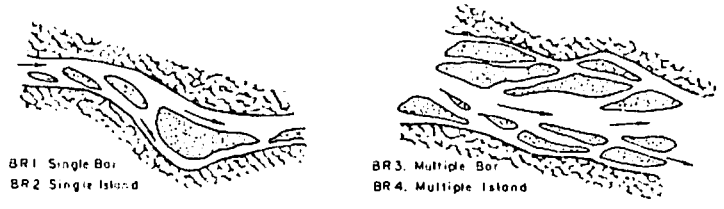


(b) Braiding Patterns

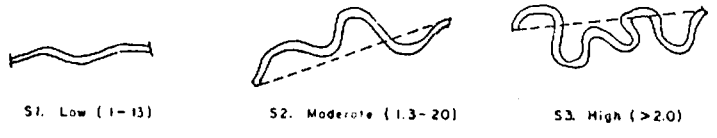


(c) Types of Sinuosities

Figure 2-5. Classification of river channels (after Culbertson et al., 1967).

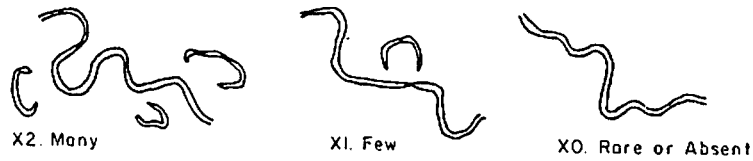


(d) Oxbow Lakes on Floodplain

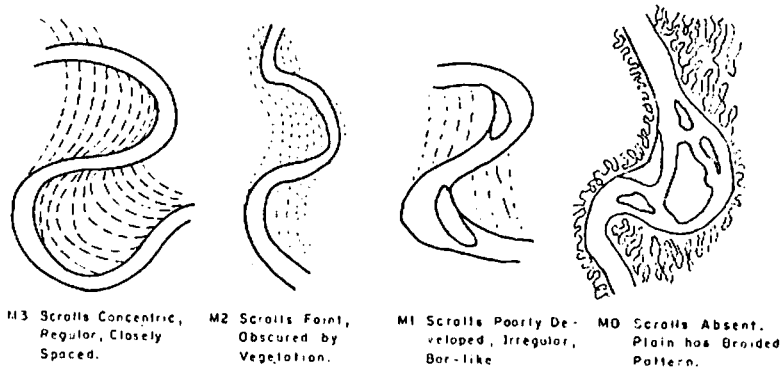


(e) Types of Meander Scroll Formations

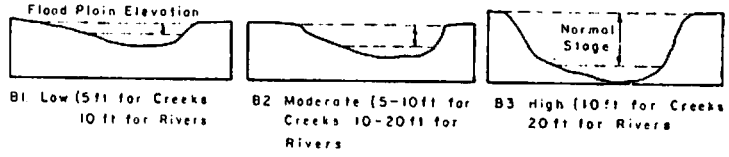


(f) Types of Bank Heights

Figure 2-5 (continued).

L0. No Levees

L1. Levees Mainly on Concave Bank

L2. Levees Well Developed on Both Banks

(g) Types of Natural Levee Formations

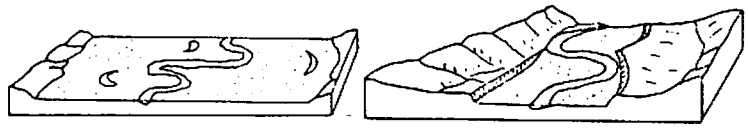

F2. Broad in Relation to Channel Width

F1. Narrow, Confined by Terraces or Valley Sides

(h) Types of Modern Floodplains

V0. Very Limited or No Vegetation Along Banks

V2. Narrow Belt of Dense Vegetation Along Both Bends

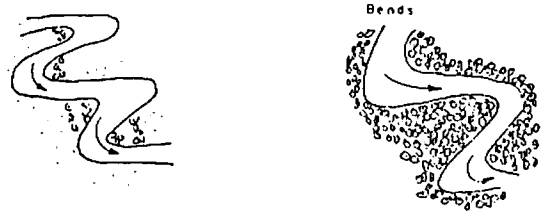

V1. Vegetal Growth on Inside of Bends of the Channel

V3. Dense Vegetation Growth in the River Basin

(i) Types of Vegetal Patterns

Figure 2-5. (continued).

and are reconsidered as actual physical processes that govern the response of a watershed. Because all parts of a natural system are interrelated to some degree, there is overlap between groupings that is not detailed.

Topography including land and channel slopes, aspect, and surface and channel geometry is an expression of morphological, geologic, and other erosive forces that have acted on the watershed. In turn these forces are modified by the topography they have created. For example, channel slope governs water discharge rate and sediment transport rate. Conversely, discharge rate and sediment transport can alter channel form to produce a new slope. Aspects of land surfaces influence vegetative growth and soil moisture conditions, that in turn affect water yield. Channel and surface geometry affect depth and velocity of water flow, thus altering sediment transport.

Soils

Watershed soil characteristics depend to a large extent on the parent geologic materials and predominant weathering processes. For example, light-colored silaceous type igneous rock will usually produce more granular materials than igneous rock containing relatively higher proportions of dark-colored minerals. This is caused by chemical reactions and formation of clay materials from constituent minerals comprising the rocks. Abundance or lack of clay minerals, affect the soil properties that govern or influence watershed response or other processes. Infiltration is a key example of a process controlled by soil characteristics. In general sandier, more porous soils have higher infiltration rates than do clay types. This differentiation tends to create faster runoff from the clay soils, whereas sandy soils (unless saturated) may not permit surface runoff. However, sandy soils lend themselves more to groundwater or interflow processes because of the rapid drainage characteristics. Soil mineralogy also influences soil moisture relationships, water quality, and vegetation growth. Size of surface soil particles or aggregates determines (given other conditions) the rate of water and wind erosion of soil. Soil type is a factor in the major types of sediment sources in watersheds: surface and rill gullies, landslides, and channels (Simons, Ward, and Li, 1979). Soil characteristics are important physical quantities that describe watershed response.

Geology

Geology is important because it affects soils, vegetation, topography, and hydrology. The effects on soils and vegetation were previously discussed. General topography (ridges, cliffs, plateaus, valleys) and the resultant channel and land surface configuration are dictated by erosion resistant rocks, large scale erosive forces such as glaciation, and bedrock structure. Long-term surface adjustments through folding, faulting, isostatic rebound (e.g., rise in land surface after removal of ice), vulcanism, and changes in sea level are all important geologic processes. The effect of geology on hydrology is varied and extensive, resulting from the above mentioned processes and other influences on climate such as the abrupt rise of the Sierra Nevada

Mountains that create a wet climate to the west and a dry, rain-shadowed climate to the east. Determining the relative importance of ground and surface water contributions in a basin is another influence that geology has on watershed hydrology. Typically, crystalline igneous terrain unless highly fractured is not noted for sustained baseflow during dry periods. Sedimentary and metamorphic (in some cases) terrains are more often capable of sustaining baseflow. This difference is related to rock type and structure.

Vegetation

Vegetation plays an important role in water balance and soil stability in a watershed. It is known that vegetation, usually trees or large brush, is a major consumer of water in watersheds. Through transpiration, interception, and evaporative processes vegetation can substantially reduce water yield from a watershed. Reduction in the amount of vegetation or introduction of less consumptive types can decrease water consumption by plants. However, reduction in vegetation may have detrimental effects in that vegetation is important in the protection of soil from erosion. Vegetation can reduce the amount of water reaching the ground through interception, reduce rainfall intensities by providing an energy-absorbing cover, bind or reinforce surface materials into more erosion resistant aggregates, reduce landslide hazards through binding and lowering soil water content, reduce overland and channel erosion by providing added roughness to retard water velocity, and provide organic debris for stream channels, creating stairstep configurations, thus lowering flow energy and transport capacity. Trees and large brush also assist in maintaining water quality by shading stream channels.

Climate

Climate and associated meteorological components are important processes affecting response in a watershed. These components are influenced by topography, vegetation, and geologic features, but to a much lesser extent than they affect these and other watershed processes and quantities. Important climatic or meteorological processes are related to precipitation, temperature, solar radiation, and wind.

Precipitation occurs as a solid, liquid, or aerosol (mist, fog) all of which eventually manifest themselves in the watershed in liquid form. Snowfall and snowpack present unusual problems in that the melt rate, distribution, sublimation, interception, inter-snow packs and sub-snow packs, waterflow, and wind effects are all long-term processes with lag effects that are complex and not easily delineated. In addition, freeze-thaw effects caused by temperature variations within and external to the snowpack add more complexity to the heat and mass transfer aspects of the pack. Also, little is known about the erosion processes that occur at the snowpack-soil surface interface. Although snow and snowpack processes are important in many watersheds, in governing water yield, runoff hydrographs, and sediment yield, a better understanding of these complex processes are required. Since rainfall is already in liquid form, is more easily understood in terms of its related processes. Of primary importance are volume, time distribution intensity,

spatial distribution, and duration. Intensity affects runoff occurrence and soil erosion from raindrop splash, whereas volume, intensity, duration, and spatial duration determine (along with other processes) the water hydrograph and yield from a storm. Mist or fog although not recognized as primary sources of runoff, can create antecedent moisture conditions such as reduced interception or increased soil moisture, that can alter the water balance during subsequent storms.

Temperature not only affects type of precipitation, but infiltration rate because higher temperature water is less viscous and flows faster through the soil. Temperature also influences snowpack dynamics, vegetation growth, and freeze-thaw phenomena.

Solar radiation is extremely important but often hard to utilize to the long-term response of a watershed. Fortunately, incoming solar radiation is constant for the time span of most interest. Alterations or influences on radiation reaching a soil surface occur from airborne particulates, gases, water vapor, and vegetation. Although important in studying long-term balances, such as water yield in a watershed, we often neglect solar radiation when examining short-term phenomena such as storm runoff. Solar radiation does influence to a major extent most climatic processes, vegetation, snowpack dynamics, and soil-water balance. Solar radiation and its effects on other processes must be considered in watershed analyses.

Often wind is not given enough credit as an important process in watersheds. However, it does affect evaporation, sublimation, snow redistribution, transpiration, rainfall intensity and distribution, wind erosion, vegetation stability, and landslide potential (from vibrating soil caused by wind sway in trees). Wind is usually considered in water-balance energy-balance studies, but neglected in short-term rainfall runoff storm analyses because of variability.

Hydrology and Hydraulics

Hydrology and hydraulic processes in watersheds are heavily influenced and interrelated with the other important processes. Two important processes should be recognized as belonging to this broad group. These are water flow and sediment transport. Controlling both are gravity, resistance, and other related watershed processes. Water flow is the result of many complex interactions. It can be described by two basic concepts, continuity and momentum. Continuity is mass balance which means in general, input minus output is the change in storage of the system. For example, if two inches of rain produce one inch of runoff, then the other inch is retained in the system or lost to other outputs such as evaporation, transpiration, or regional groundwater flow. The momentum equation is a force balance of inertial, gravity, and frictional components. These two concepts govern water movement. Similarly, the movement of sediment is described by the sediment continuity concept. Again this concept like water continuity, describes the input, output, and storage change of sediment in the watershed.

Complementary to these concepts are those dealing with specifics of water and sediment movement. In steep watersheds the energy slope in the momentum concept or equation can be assumed equal to land surface or

channel slope. Such an assumption permits major simplifications in descriptive modeling of a watershed. This assumption is permissible because other components in the momentum equation are relatively minor compared to surface slope. Descriptive relations for infiltration, evapotranspiration, and groundwater flows are also important in organizing and identifying each segment of the water continuity equation. Sediment transport is usually considered in three parts:

1. bed load - sediment movement primarily along the surface,
2. suspended load - sediment transport primarily in the flow with some contact with the bed, and
3. wash load - fine particles not found in appreciable quantities in the bed material suspended in the flow.

Bed load and suspended load can be described by transport equations as they are related to water discharge. However, wash load is more dependent on supply conditions. In upland watersheds the concept of supply and capacity is crucial as it determines sediment yield. Typically, transport capacity for small sizes (e.g., wash load) is in excess of supply. Therefore, yield is related to supply. Conversely, for large sizes capacity is much less than supply (e.g., large cobbles in a mountain stream), therefore capacity controls. In general, hydrology and hydraulics of a watershed are expressions of other physical processes and accounting on balance concepts. Understanding these processes must be coupled with understanding other processes.

Man's Influence

Man's influences are not natural physical processes in a strict sense. They do, however, tend to affect other processes to some degree and in doing so create watershed responses that can be beneficial or deleterious. Although there are many influences, such as dam building, intermountain diversions, removal of vegetation, alteration of hillslopes, road building, energy and mineral resource acquisition, and recreational and agricultural uses, only a simple example will be presented here that encompasses several processes.

Timbering is a well known and long practiced resource acquisition activity in the United States. However, sometimes techniques have been used that alter the natural processes and create adverse impacts. For example if a watershed is clear-cut, water yield may increase and provide more water for domestic and industrial use because the trees are no longer transpiring the water. However, increased water yield may result in higher streamflow levels that produce more channel erosion and instability. At the same time, removal of vegetation can expose the soil surface to rainfall and snowmelt erosion, thus promoting sediment yield. Increased groundwater levels and lack of vegetative anchoring may lead to higher landslide risk in steep watersheds. Landslides, if they do occur, produce large quantities of sediment that affect the sediment yields and other activities. Loss of cover and increased organic debris can have an adverse water quality impact on the stream through increased sediment, water temperatures, and BOD loading.

The above simple example illustrates several key concepts. First, physical processes controlling watershed response are varied, complex, and interrelated. Second, man's influence can have ripple effects as

they are passed between processes and third, understanding watershed response must encompass several distinct but related subjects.

## 2.4 PHYSICAL PROCESS VARIABLES AND RIVER MECHANICS GOVERNING CHANNEL RESPONSE

### General

In general, the physical process groupings described previously for watersheds are also applicable to stream or river channels. However, the importance of each can differ considerably between the watershed and channel system. In addition, specific effects of each element in the broad groups can be quite different for the two systems. For example, vegetation in the watershed affects several different processes whereas in the channel it usually affects flow resistance and stability of river banks and islands.

Major physical processes in an alluvial channel are those related to water discharge, channel slope and shape, geology and soils, sediment transport, vegetative effects, and again, man's influence. As in the watershed, each of these is intertwined in a set of complex relationships. Again bedrock channels have a restricted set of conditions while alluvial channel conditions are more general.

Water discharge is a key process, resulting from other processes, that affects channel shape and sediment transport. Discharge variables of velocity, depth, and flow area are important in analysis of channel response. Coinciding with these are channel shape, channel slope and flow resistance from grains and bed forms. Geology and soils of the channel bottom and banks help determine relative erodibility of the system and therefore, its response to other changes or alterations. Local variation in geology, soils, vegetation, and flow rate plays important role in determining bank stability in channels. Sediment transport in channels differs among watersheds because there is often more material available for transport than can be carried. Vegetation is an important variable in channel systems. Often, it is bank vegetation that resists erosion during periods of high flow. Similarly, vegetation tends to stabilize interchannel bars and islands thus producing an added resistance in the channel. These banks and bars can substantially alter flow lines and channel movement.

A more complete understanding of the physical processes governing channel response can be attained through a study of important river mechanics concepts, processes, and relations. Some of these were previously presented in Section 2.2 and Figures 2-3 and 2-4 as related to channel form. Other important processes and variables will be considered in this chapter and the chapters that follow.

### Variables Affecting Alluvial Channels

Because of the number of interrelated variables that can react simultaneously to natural or imposed changes in a river system, river response to both natural and man-imposed forces is complex and varied in nature, but it is predictable. Simons and Richardson (1966) detailed the variables affecting alluvial channel geometry and bed roughness and

concluded that the nature of these variables is such that, unlike rigid boundary hydraulics problems, it is not possible to isolate and study the role of an individual variable. For example, evaluation of the effects of increasing channel depth on average velocity is hampered because related variables such as flow resistance also respond to the changing depth. Not only will velocity respond to a change in depth, but also form of bed roughness, channel cross section shape and sediment discharge. Position and shape of alternate, middle, and point bars can also be expected to change.

Variables that influence alluvial channel flow include velocity, depth, slope of energy grade line, density of water-sediment mixture, apparent viscosity of water-sediment mixture, gravitational constant, representative fall diameter of bed material, gradation of bed material, density of sediment, shape factor of particles, shape factor of the reach of the stream, shape factor of the cross section of stream, seepage force in the bed of the stream, concentration of bed-material discharge, fine material concentration, and particle terminal fall velocity. Dimensional analysis of these variables verifies the importance of the Froude number ($V\sqrt{gy}$), Reynolds number ($V\gamma\rho/\mu$), and a relative roughness parameter ($D/y$).

Bed Forms and Resistance to Flow

The bed of an alluvial river is not a smooth regular boundary, but is characterized instead by forms that vary in size, shape, and location created by changes in flow, temperature, sediment load, size of bed material, and other variables. These bed forms produce a major portion of the flow resistance exhibited by alluvial channels, and in turn feedback by exerting a significant influence on flow parameters such as depth, velocity and sediment transport.

Bed Form without Sediment Movement

If the bed material of a stream moves at one discharge but not at a smaller discharge, bed configuration at the smaller discharge will be a remnant of the bed configuration formed when sediment was moving. In general, Shields' relation (Figure 2-6) is adequate to define beginning of motion of bed material. In this figure the dimensionless shear stress $F_*$ represented by

$$F_* = \frac{\tau}{(\gamma_s - \gamma)D_s} \tag{2-2}$$

where $\tau$ is the shear on the bed, $\gamma_s$ is the unit weight of sediment, $\gamma$ is unit weight of water, and $D$ is particle size is related to the boundary Reynolds number $R_*$ as

$$R_* = \frac{U_* D_s}{\nu} \tag{2-3}$$

where $U_*$ is the shear velocity and $\nu$ is the kinematic viscosity of water. After the beginning of motion, the bed will become rippled for

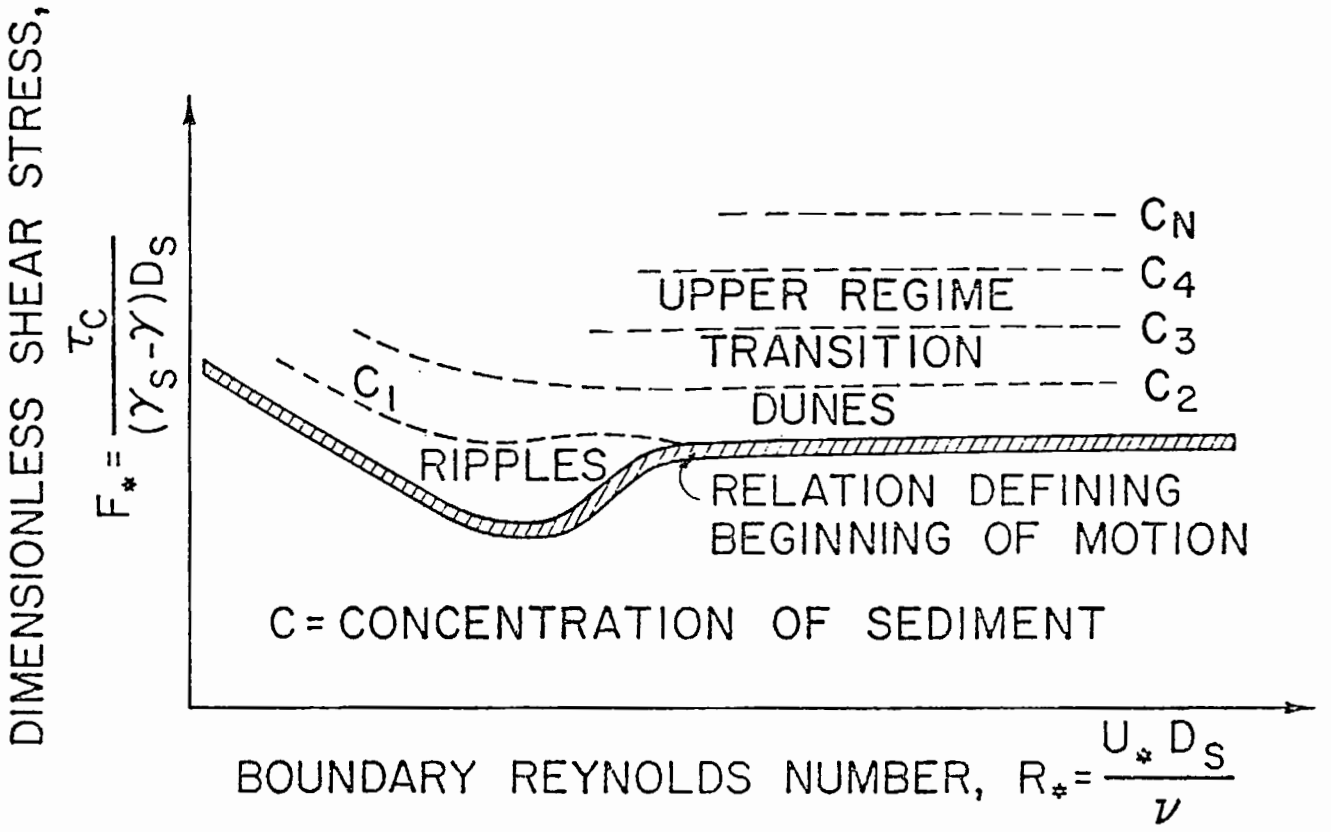


Figure 2-6. Generalized Shields' relation for beginning of motion showing relative bed form positions.

sand material smaller than 0.6 mm. Dunes will develop for material no coarser than 0.6 mm. Resistance to flow is small for a plane bed without sediment movement and is caused by sand grain roughness. Values of Manning's n range from 0.012 to 0.016 depending on size of bed material.

Bed Form with Sediment Movement

Profiles of typical bed forms and their relation to the water surface are shown in Figure 2-7. Using these bed forms as a criteria, flow in alluvial channels can be divided into two regimes separated by a transition zone. These two flow regimes are characterized by similarities in the shape of bed form, mode of sediment transport, process of energy dissipation, and phase relation between bed and water surface. These regimes and associated bed forms include:

1. Lower Flow Regime (low stream power)
   a. Ripples
   b. Ripples superimposed on dunes
   c. Dunes
2. Transition Zone
3. Upper Flow Regime (high stream power)
   a. Plane bed (with sediment movement)
   b. Antidunes
   c. Chutes and pools

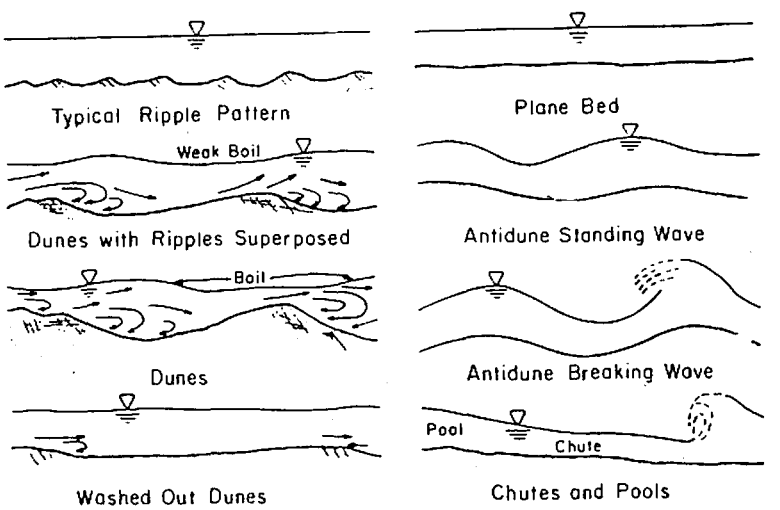


Figure 2-7. Typical bed forms in sand-bed channels (Simons and Richardson, 1966).

Simons and Richardson (1966) used flume and stream data to develop a graphical relation among stream power ($\tau V$), median fall diameter, and bed form. This relation shown in Figure 2-8 indicates the form of bed roughness that may occur if depth, slope, velocity, and fall diameter of the bed material are known. Another useful relation (Figure 2-9) schematically shows the effect of bed form on roughness coefficients such as Manning's n. As the bed configuration passes through lower regime to upper regime, Manning's n changes from a typical value of 0.012 to 0.016 for plane bed without sediment motion to values as high as 0.04 for a dune bed. If stream power increases, upper regime plane bed conditions will develop that may produce a decrease in roughness to values as small as 0.010 to 0.015.

In natural streams a large increase in discharge with little or no change in stage is possible as a result of a change in bed configuration from dunes to plane bed. Figure 2-10 shows a break in the depth-discharge relation resulting from this phenomena. Conversely, an increase in depth with constant slope and bed material can change a dune bed to plane bed or antidunes., A decrease in depth can reverse the regime.

Bars

In natural channels other types of bed configurations or forms occur. These bed configurations are generally called bars and are related to plan form geometry and channel width.

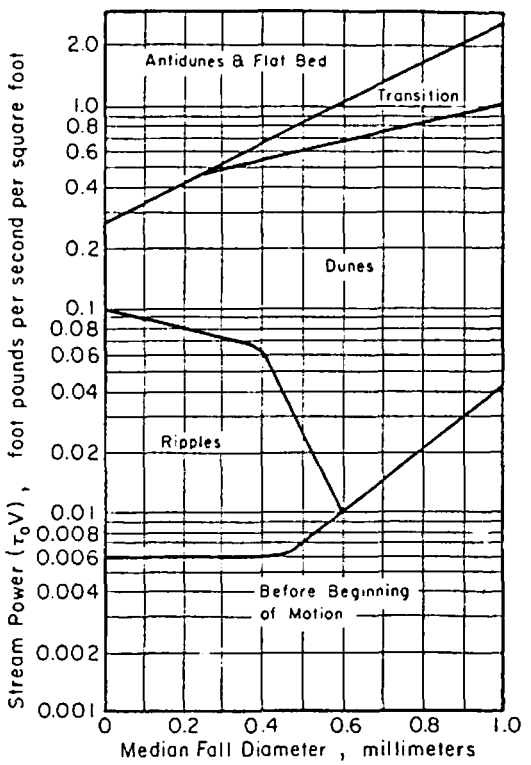


Figure 2-8. Relation of stream power and median fall diameter to form of bed roughness.

Bars are bed forms having lengths about the same size as the channel width or greater, and heights comparable to the mean depth of the generating flow. Several different types of bars occur and are classified as:

1. Point Bars - occur adjacent to the convex bank of channel bends. Point bar shape may vary with changing flow conditions, but point bars do not move relative to the bends.

2. Alternate Bars - occur in straighter reaches of channels and tend to be distributed periodically along the reach, with consecutive bars on opposite sides of the channel. Their lateral extent is significantly less than the channel width. Alternate bars slowly move downstream.

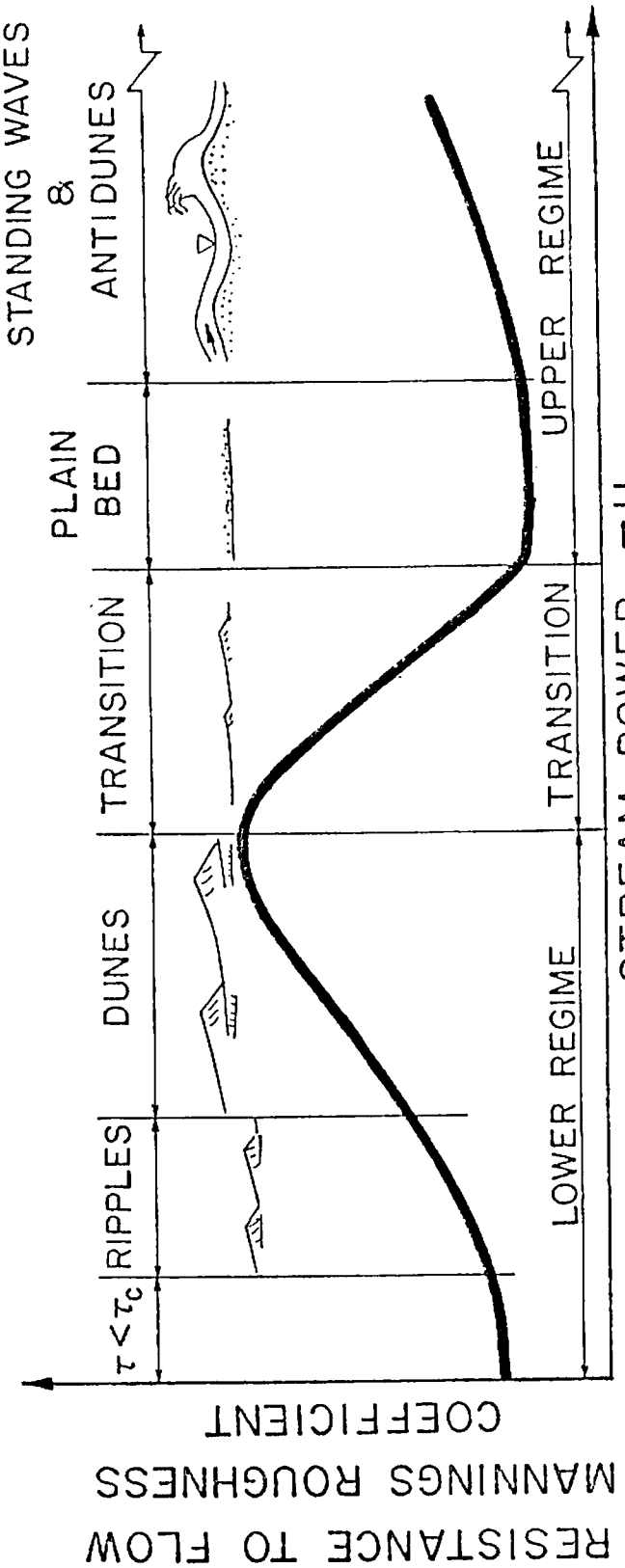


Figure 2-9. Generalized variation of resistance with changing bed forms.

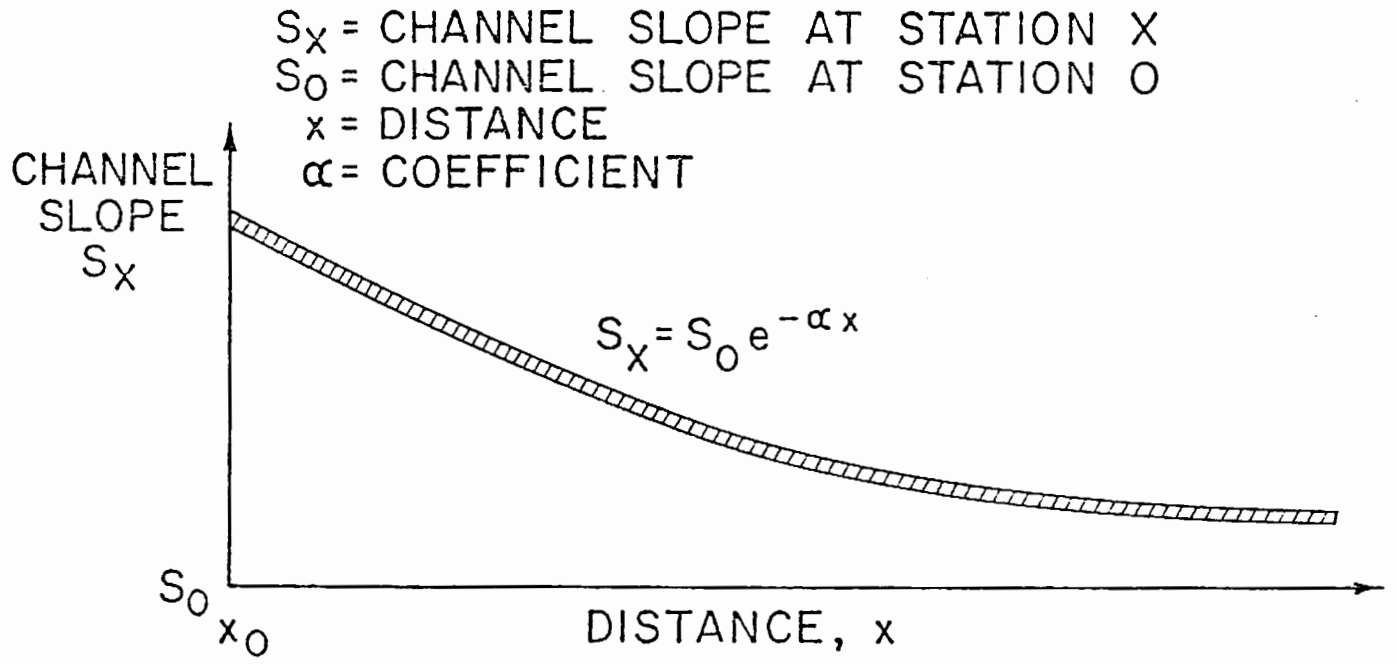


Figure 2-10. Generalized variation of channel slope with distance.

3. Transverse Bars (middle bars) - also occur in straight channels. They occupy nearly the full channel width of the producing divided and multiple flow channels. They occur as isolated and as periodic forms along a channel. They also move slowly downstream.

4. Tributary Bars - occur immediately downstream from points of tributary or other lateral inflow into a channel.

Longitudinal sections indicate that bars are approximately triangular with long gentle upstream slopes and short downstream slopes at approximately the angle of repose. They are similar to dunes in form but much larger. Bars appear as small barren islands during low flows. Portions of the upstream slopes of bars are often covered with ripples and dunes. Bars significantly affect development of new flow alignments as well as resistance to flow, particularly if these bars are armored.

Hydraulic Geometry

Hydraulic geometry is a general term used to denote relationships between bankful discharge, channel morphology, hydraulics, and sediment transport. In natural alluvial channels morphologic, hydraulic, and sedimentation characteristics of the channel result from a large variety of factors. Generalized hydraulic geometry relations apply to channels within a physiographic region and can be computed from data available for gaged rivers. Hydraulic geometry relations express the integral effect of all hydrologic, meterologic, vegetative, and geologic variables in a drainage basin.

Hydraulic geometry relations of alluvial streams are necessary for river engineering computations and river modeling. Forerunners of these relations were the regime theory equations of stable alluvial canals. A generalized version of hydraulic geometry relations was developed by Leopold and Maddock (1953) for different regions in the United States and for different types of rivers. Hydraulic geometry relations include:

$$W = a\,Q^{b} \qquad y_o = c\,Q^{f}$$

$$V = k\,Q^{m} \qquad Q_T = p\,Q^{j}$$

$$S = t\,Q^{z} \qquad n = r\,Q^{y}$$

where $W$ is channel width, $y_o$ is channel depth, $V$ is average velocity of flow, $Q_T$ is total bed-material load, $S$ is energy gradient, $n$ is Manning's roughness coefficient, and $Q$ is discharge defined below. Leopold and Maddock (1953) have shown that in a drainage basin two types of hydraulic geometry relations can be defined: 1) those relating $W$, $y_o$, $V$, and $Q_T$ to the variation of discharge at a station and 2) those relating these same variables to the discharges of a given frequency of occurrence at various stations on a channel. Because $Q_T$ was not available, they used $Q_s$ the suspended load transport rate. The former relations are called at-station relationships and the latter are downstream relationships.

Hydraulic geometry relations were theoretically developed at Colorado State University (Simons and Li, 1975). These relations are almost identical to those proposed by Leopold and Maddock. The at-station relations derived at Colorado State University are:

$$W \sim Q^{0.26} \tag{2-4}$$

$$y_o \sim Q^{0.46} \tag{2-5}$$

$$S \sim Q^{0.00} \tag{2-6}$$

$$V \sim Q^{0.30} \tag{2-7}$$

Equation 2-7 implies that slope is constant at a cross section. This is not precisely true since at low flow effective channel slope is determined by the thalweg that flows from pool through crossing to pool. At higher stages the thalweg straightens somewhat thus shortening the path of travel and increasing the local slope. In extreme cases river slope approaches valley slope at flood stage. During high floods flow often cuts across point bars developing chute channels. This direction of travel verifies the shorter path the water takes and that a steeper channel prevails under this condition.

Similarly, derived downstream relations for bank-full discharge are:

$$y_b \propto Q_b^{0.46} \tag{2-8}$$

$$W_b \propto Q_b^{0.46} \tag{2-9}$$

$$S \propto Q_b^{-0.46} \tag{2-10}$$

$$V_b \propto Q_b^{0.08} \tag{2-11}$$

where the subscript b indicates the bank-full condition.

## Sediment Transport in Alluvial Channels

Sediment in a river usually originates in the drainage basin. Eroded material is carried into the river and along the river's course by flowing water. Ultimately, this material is deposited in the lower reaches of the river, on the river delta, or for the finer material in the sea. This constant displacement of material implies a slow but continuous change in the longitudinal profile of the river eventually ending in the destruction of the upland region drained by the river. As a result, it must be anticipated that large quantities of sediment will pass through a river system each year.

### Longitudinal Stream Profile

The longitudinal profile of a stream shows slope or gradient. It is a representation of the ratio of fall to length of a stream over a given reach. Because a river channel is often steepest in the upper regions, most river profiles are concave upward. As with other channel characteristics, shape of the profile is a result of a number of interdependent factors representing a balance between transport capacity of the stream, and size and quantity of supplied sediment load.

Shulits (1941) among others, provided an equation describing the concave horizontal profile of a channel in terms of distance along the stream as

$$S_x = S_o e^{-\alpha x} \tag{2-12}$$

where $S_x$ is the slope at any station a distance $x$ downstream of a reference station, $S_o$ is the slope at the reference station, and $\alpha$ is a coefficient of slope reduction (Figure 2-10).

Similarly, grain size of the bed material decreases in a downstream direction. Transport processes reduce the general size of sediment particles by abrasion and hydraulic sorting. Abrasion is size reduction by mechanical actions such as grinding, impact, and rubbing, while hydraulic sorting results in differential transport of particles of varying sizes. For sedimentary particles of similar shape, roughness, and specific gravity the end result of these processes is observed reduction of bed material size along the direction of transport. Change in particle size with distance downstream can be expressed as

$$D_{50x} = D_{50o} e^{-\beta x} \tag{2-13}$$

where $D_x$ is size of bed material at distance $x$ downstream of a reference station, $D_o$ is median size of bed material at the reference station, and $\beta$ is a wear or sorting coefficient (Figure 2-11). This trend is found in large and small channels.

The longitudinal profile of an alluvial river is dynamic, continually adjusting to changed input conditions of water and sediment discharge. Altered input conditions change channel geometry, roughness, and other parameters including channel gradient.

## Sediment Yield

The quantity of sediment delivered to the channel depends on watershed processes discussed in previous sections. Capacity of a stream to transport sediment depends on hydraulic properties of the stream channel. Such variables as slope, roughness, channel geometry, discharge, velocity, turbulence, fluid properties, and size and gradation of the sediment are closely related to hydraulic variables controlling capacity of the stream to carry water. Total sediment load of a stream is the sum of bed material load and wash load, the sum of bed load and susended load, or the sum of measured and unmeasured load.

## Bed-Load Transport

Because bed material is transported as suspended load and bed load, different physical laws controlling these modes must be incorporated into any method for predicting total transport of bed material. Transport of bed load is usually related to the tractive force or shear on the bed as in the historic Du Boys formula of

$$q_b = K \tau_o (\tau_o - \tau_c) \tag{5-14}$$

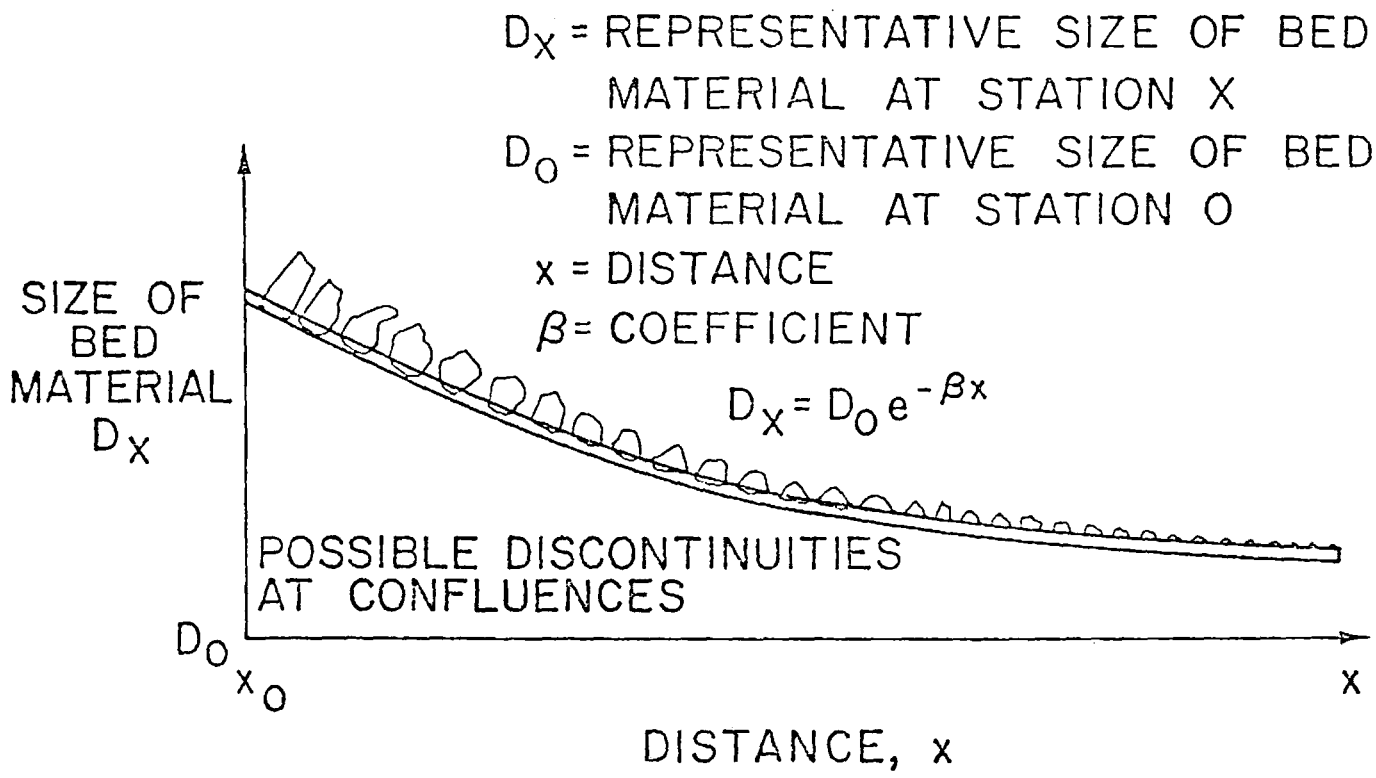


Figure 2-11. Generalized variation of size of bed material size with distance.

where $q_b$ is bedload discharge per unit width of section per unit time, K is a sediment parameter, $\tau_o$ is intensity of bed shear, and $\tau_c$ is critical shear at which motion is initiated (Figure 2-6).

Bed-Material Transport

As implied by the above definitions, distinction between bed-material load and wash load is important and is reiterated here. Bed material is transported at the capacity of the stream and is functionally related to measurable hydraulic variables. Wash load, however, is not transported at the capacity of the stream, depending instead on supply, and is not functionally related to hydraulic variables. While there is no sharp demarcation between wash load and bed material load, one criteria assumes bed-material load consists of particle sizes equal to or greater than 0.062 mm (the division between sand and silt). Another reasonable demarcation is to use a sediment size finer than the smallest 10 percent of the bed material as a point of division.

Sediment particles which constitute bed material load are transported either by rolling or sliding along the bed (bed load) or in suspension. Again there is no sharp distinction between bed load and suspended load. A particle of the bed material load may move part of the time in contact with the bed and at other times is suspended by the flow. Generally, the amount of bed material moving in contact with the bed of a large sand bed river is only a small percentage of bed material moving in suspension.

Fine material moving as wash load usually will not pose direct problems for development activities in the channel system. However, large concentrations of fine material can affect the capacity of a stream to transport bed material through its influence on fluid properties such as viscosity and density.

The processes, variables, and mechanics controlling the response of channel systems are varied and complex. It is impossible to consider all factors at one time. Therefore an analysis to delineate the most important variables is needed. One method is use of physical process models and parameter sensitivity tests. Another way is by order of magnitude analyses. The following section presents such an evaluation of important forces in river channels.

## 2.5 QUALITATIVE ORDER OF MAGNITUDE ANALYSIS OF FORCES ACTING ON A RIVER--AN EXAMPLE

General

Previous sections have primarily dealt with qualitative analyses of the processes and forces acting in watersheds and river channels. In this section, a quasi-quantitative approach is described and applied to a major New England River (Simons, Andrew, Li, and Alawady, 1979). This analysis is general in nature and can be applied to other rivers. Through such an analysis a better understanding of the key or important variables can be gained.

Evaluation of Forces

The tractive force method described by Chow (1959) has been utilized to evaluate bank erosion on different rivers. It is an acceptable method and has been used in the design and stability evaluation of alluvial canals. The method proposed and utilized by the U.S. Army Corps of Engineers is limited to straight reaches of channel that are principally affected by shear stresses exerted on the bed and banks by flowing water. In this example the banks of the channel are subjected to additional forces produced by operation of numerous power dams and their pools. The analysis made in this example considered all significant factors including the tractive force and effective durations based upon the physical system. This is different from the tractive force method, which considers the tractive force alone. Typical average depth, average velocity, and average sediment transport for natural rivers and upper and lower pools are given in Figures 12-12, 12-13 and 12-14, respectively. The definition of a natural river is one that is usually unaffected by backwater caused by a downstream dam. Computed depth is roughly within 10 percent of the normal depth of the river. Figure 2-14 indicates that the sediment-transporting capacity is significantly lower in pools than in the natural river. These figures were determined using a dam height of 30 feet, a channel bed slope of 0.00029, and a typical channel cross section.

Magnitudes of the forces acting on the river banks can be expressed as a percentage of the tractive force exerted on the channel bed by flowing water. This flowing water tractive force can be approximated by the relation

$$\tau = \gamma d S \tag{2-15}$$

where $\tau$ is shear stress, $\gamma$ is specific weight of the water-sediment mixture, $d$ is depth of flow at the location where shear stress is to be estimated, and $S$ is slope of energy gradient.

As an alternative, shear stress acting on the channel boundary can be estimated by the relation

$$\sqrt{\tau/\rho} = \frac{u_1 - u_2}{5.75 \log \frac{y_1}{y_2}} \tag{2-16}$$

where $\rho$ is density of water and $u_1$ and $u_2$ are the point velocities measured at distances $y_1$ and $y_2$ from the boundary of the channel.

For best results $y_1$ and $y_2$ should be as close as possible to the boundary. This relation provides a better approximation of boundary shear stress in reaches affected by power dams since shear stress is independent of the channel and is sensitive to velocity distribution.

To estimate stability of a river channel critical shear stress which is sufficient to initiate movement of bed material is first determined. This critical shear stress can be approximated from Shields'

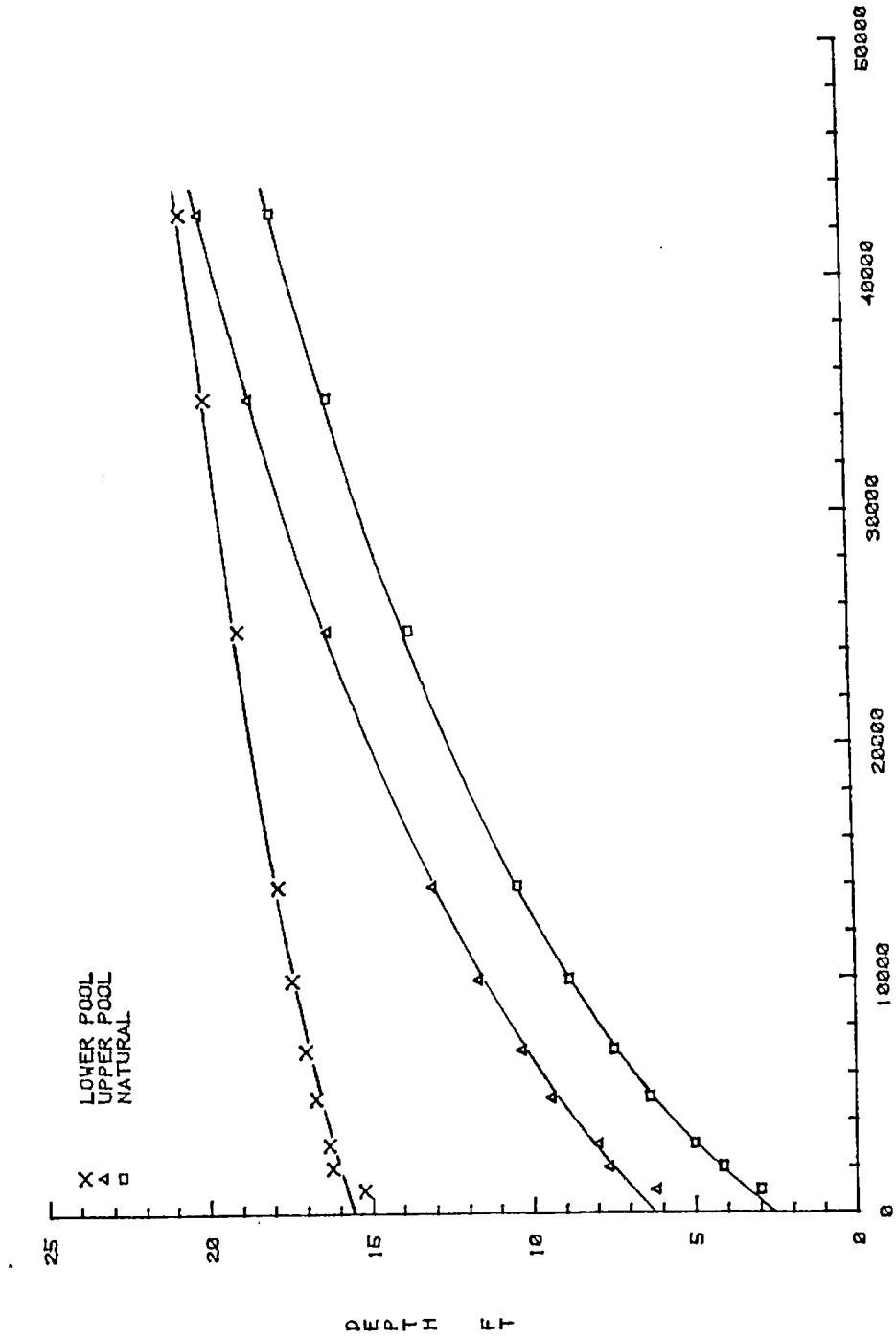


Figure 2-12. Water discharge as compared to depth for typical reaches.

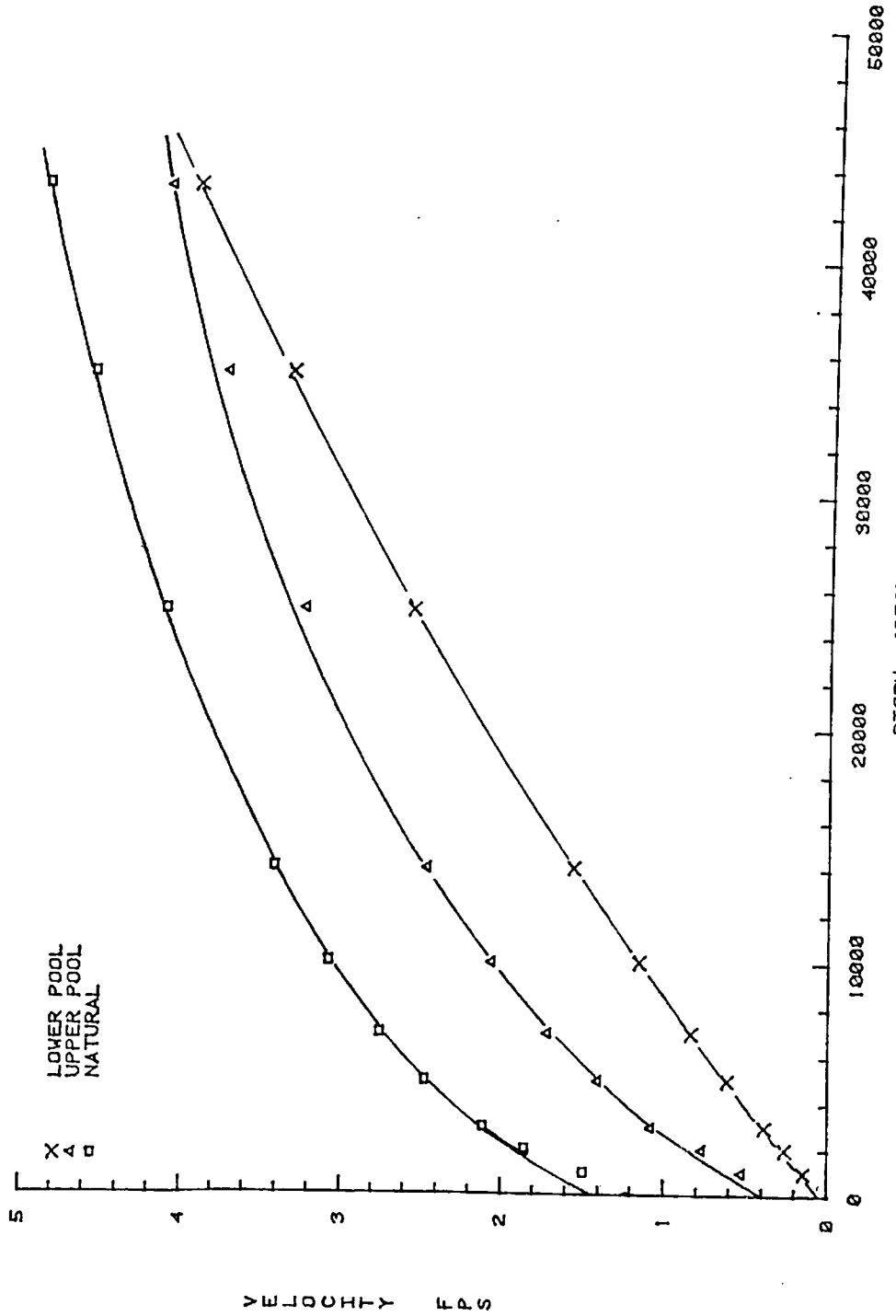


Figure 2-13. Water discharge as compared to velocity for typical reaches.

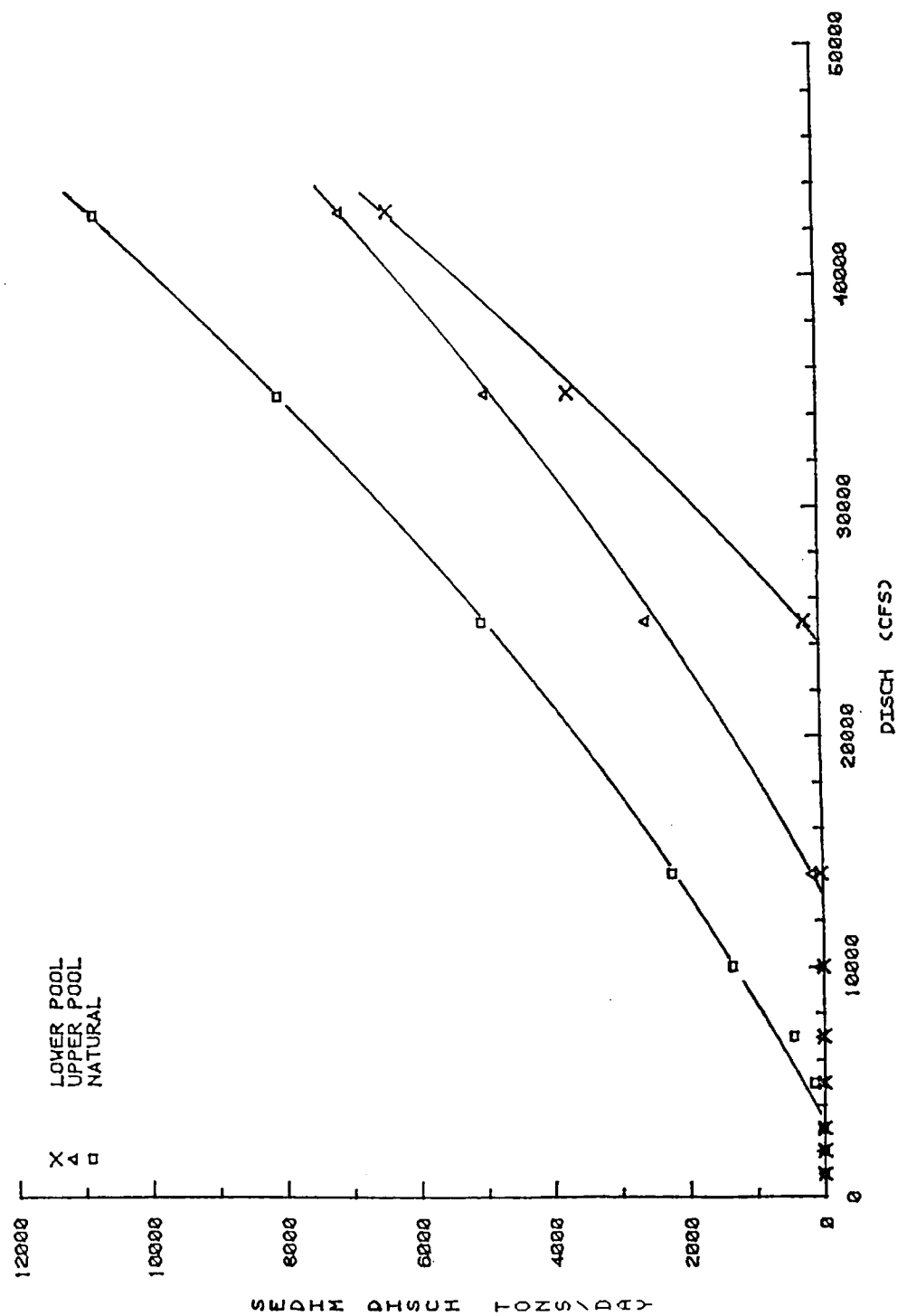


Figure 2-14. Water discharge as compared to sediment discharge for typical reaches.

diagram previously presented in Figure 2-6 if $\tau$ at motion is taken as critical shear $\tau_c$. In Figure 2-6, $D_s$ is the particle size, $U_*$ is the shear velocity, $\nu$ is the kinematic viscosity, $\Delta\gamma$ is the difference between specific weight of sediment and water, and Re is the particle Reynolds number. When Re > 500, the term $\tau/\Delta\gamma D$ has a constant value equal to 0.06. Hence, knowing $\Delta\gamma$ and D, the critical shear stress $\tau_c$ can be estimated. If the shear stress acting on the bed or boundary of the river determined by Equations 2-15 and 2-16 is greater than critical shear stress $\tau_c$, the bed material will be in motion. If the rate of transport on a segment of river exceeds inflow of sediment from upstream or lateral inputs, degradation of the river bed will occur. Aggradation will occur if the converse is true. After estimating shear stress acting on the river bed and critical shear stress, the next step is to estimate actual shear stress acting on the banks. If this exceeds the critical shear stress, bank erosion will result. Consequently, the river bank will be unstable unless protected by vegetation, riprap, or other stabilization measure. Critical shear stress for the river bank material can be estimated utilizing Shields' diagram to give critical bed shear stress, and then reducing this value by a factor K to allow for the gravitational component of forces on the bank particles:

$$K = \frac{(\tau_s)_c}{(\tau_b)_c} = \cos\theta \sqrt{1 - \frac{\tan^2\theta}{\tan^2\phi}} \qquad (2\text{-}17)$$

where $(\tau_s)_c$ and $(\tau_b)_c$ are the critical shear stresses on the side and bed respectively, $\theta$ is the angle of the side slope, and $\phi$ is the angle of repose of the bank material.

For wide channels the maximum value of shear stress on the bank is 0.77 times the maximum shear stress on the bed

$$\tau_s = 0.77\ \tau_b \qquad (2\text{-}18)$$

As when analyzing the stability of the bed of a channel, the banks wil be unstable if the tractive force acting on the banks except the critical tractive force for the bank material.

Only the shear stress exerted on the river banks as caused by flowing water was evaluated. Consequently, it is necessary to add effects of other forces acting on the banks to the tractive force. These additional increments of shear stress can be determined from Table 2-4.

In this table, the relative magnitude ($M_B$) and relative duration ($D_B$) of the forces causing bank erosion for noncohesive and stratified bank materials have been assessed qualitatively and rated from 1 to 9 in ascending order of estimated effect. This qualitative assessment was accomplished through examination of available data, review of current theory, personal experience, and sound professional judgment. The shear stress acting on a noncohesive bank within a reach of natural river is considered the most significant force exerted upon that bank and as such is rated as 9. The least significant effect under a similar river condition is the freeze-thaw action, and it is ranked as 1. In relation

Table 2-4. Relative magnitudes and duration of erosive forces.

| Factors & Variables Causing Bank Erosion | River Condition | Relative Magnitude of Forces | | Relative Duration of Forces | Relative Magnitude of Bank Erosion | | | |
|---|---|---|---|---|---|---|---|---|
| | | Noncohesive | Stratified | | Noncohesive* | | Stratified** | |
| (1) | (2) | (3) | (4) | (5) | (6) | (7) | (8) | (9) |
| Shear Stress or Velocity | Natural river | 9 | 8 | 9 | 81 | 1.0 | 72 | 1.0 |
| | Natural river with high banks | 9 | 8 | 9 | 81 | 1.0 | 72 | 1.0 |
| | Pools; low banks | 9 | 8 | 7 | 63 | .78 | 56 | .78 |
| | Pools; low banks with vegetation | 7 | 6 | 6 | 42 | .52 | 36 | .50 |
| | Pools; high banks | 8 | 7 | 7 | 56 | .69 | 49 | .68 |
| | Pools; high banks with vegetation | 6 | 5 | 6 | 36 | .44 | 30 | .42 |
| Floor Variation | Natural river | 2 | 2 | 1 | 2 | .02 | 2 | .03 |
| | Natural river with high banks | 2 | 2 | 1 | 2 | .02 | 2 | .03 |
| | Pools; low banks | 2 | 2 | 1 | 2 | .02 | 2 | .03 |
| | Pools; low banks with vegetation | 1 | 1 | 1 | 1 | .01 | 1 | .01 |
| | Pools; high banks | 2 | 2 | 1 | 2 | .02 | 2 | .03 |
| | Pools; high banks with vegetation | 1 | 1 | 1 | 1 | .01 | 1 | .01 |
| Stage Variation | Natural river | 3 | 3 | 2 | 6 | .07 | 6 | .08 |
| | Natural river with high banks | 4 | 3 | 2 | 8 | .10 | 6 | .08 |
| | Pools; low banks | 3 | 3 | 1 | 3 | .04 | 3 | .04 |
| | Pools; low banks with vegetation | 2 | 2 | 1 | 2 | .02 | 2 | .03 |
| | Pools; high banks | 5 | 4 | 1 | 5 | .06 | 4 | .06 |
| | Pools; high banks with vegetation | 3 | 3 | 1 | 3 | .04 | 3 | .04 |
| Pool Fluctuations | Natural river | 3 | 3 | 2 | 6 | .07 | 6 | .08 |
| | Natural river with high banks | 4 | 3 | 2 | 9 | .11 | 6 | .08 |
| | Pools; low banks | 4 | 3 | 3 | 12 | .15 | 9 | .13 |
| | Pools; low banks with vegetation | 3 | 3 | 3 | 9 | .11 | 9 | .13 |
| | Pools; high banks | 5 | 4 | 3 | 15 | .19 | 12 | .17 |
| | Pools; high banks with vegetation | 4 | 4 | 3 | 12 | .15 | 12 | .17 |
| Wind Waves surface erosion & piping | Natural river | 2 | 2 | 1 | 2 | .02 | 2 | .03 |
| | Natural river with high banks | 1 | 1 | 1 | 1 | .01 | 1 | .01 |
| | Pools; low banks | 3 | 3 | 2 | 6 | .07 | 6 | .08 |
| | Pools; low banks with vegetation | 2 | 2 | 1 | 2 | .02 | 2 | .03 |
| | Pools; high banks | 2 | 2 | 1 | 2 | .02 | 2 | .03 |
| | Pools; high banks with vegetation | 1 | 1 | 1 | 1 | .01 | 1 | .01 |

*Standardized values based on the shear stress on noncohesive bank and natural river. For example, for condition of pool, low bank, 63/81 = 0.78.

**Standardized values based on the shear stress on stratified bank and natural river. For example, for condition of pools, low banks, 56/72 = 0.78.

Table 2-4. (Continued).

| Factors & Variables Causing Bank Erosion | River Condition | Relative Magnitude of Forces | | Relative Duration of Forces | Relative Magnitude of Bank Erosion | | | |
|---|---|---|---|---|---|---|---|---|
| | | Noncohesive | Stratified | | Noncohesive* | | Stratified** | |
| (1) | (2) | (3) | (4) | (5) | (6) | (7) | (8) | (9) |
| Boat waves surface erosion & piping | Natural river | 2 | 3 | 2 | 4 | .05 | 6 | .08 |
| | Natural river with high banks | 2 | 2 | 2 | 4 | .05 | 4 | .06 |
| | Pools; low banks | 3 | 4 | 2 | 6 | .07 | 8 | .11 |
| | Pools; low banks with vegetation | 3 | 3 | 2 | 6 | .07 | 6 | .08 |
| | Pools; high banks | 4 | 5 | 2 | 8 | .10 | 10 | .14 |
| | Pools; high banks with vegetation | 3 | 4 | 2 | 6 | .07 | 8 | .11 |
| Freeze-Thaw | Natural river | 1 | 1 | 1 | 1 | .01 | 1 | .01 |
| | Natural river with high banks | 1 | 1 | 1 | 1 | .01 | 1 | .01 |
| | Pools; low banks | 1 | 1 | 1 | 1 | .01 | 1 | .01 |
| | Pools; low banks with vegetation | 1 | 1 | 1 | 1 | .01 | 1 | .01 |
| | Pools; high banks | 1 | 1 | 1 | 1 | .01 | 1 | .01 |
| | Pools; high banks with vegetation | 1 | 1 | 1 | 1 | .01 | 1 | .01 |
| Ice | Natural river | 2 | 2 | 1 | 2 | .02 | 2 | .03 |
| | Natural river with high banks | 3 | 2 | 1 | 3 | .04 | 2 | .03 |
| | Pools; low banks | 2 | 2 | 1 | 2 | .02 | 2 | .03 |
| | Pools; low banks with vegetation | 1 | 1 | 1 | 1 | .01 | 1 | .01 |
| | Pools; high banks | 2 | 2 | 1 | 2 | .02 | 2 | .03 |
| | Pools; high banks with vegetation | 1 | 1 | 1 | 1 | .01 | 1 | .01 |
| Seepage Forces | Natural river | 2 | 3 | 2 | 4 | .05 | 6 | .08 |
| | Natural river with high banks | 3 | 3 | 2 | 6 | .07 | 6 | .08 |
| | Pools; low banks | 2 | 3 | 2 | 4 | .05 | 6 | .08 |
| | Pools; low banks with vegetation | 2 | 3 | 2 | 4 | .05 | 6 | .08 |
| | Pools; high banks | 3 | 4 | 2 | 6 | .07 | 8 | .11 |
| | Pools; high banks with vegetation | 2 | 3 | 2 | 4 | .05 | 6 | .08 |
| Gravitational Forces | Natural river | 2 | 2 | 2 | 4 | .05 | 4 | .06 |
| | Natural river with high banks | 3 | 4 | 3 | 9 | .11 | 12 | .17 |
| | Pools; low banks | 2 | 2 | 2 | 4 | .05 | 4 | .06 |
| | Pools; low banks with vegetation | 1 | 2 | 1 | 1 | .01 | 2 | .03 |
| | Pools; high banks | 3 | 4 | 3 | 9 | .11 | 12 | .17 |
| | Pools; high banks with vegetation | 2 | 3 | 2 | 4 | .05 | 6 | .08 |

*Standardized values based on the shear stress on noncohesive bank and natural river. For example, for condition of pool, low bank, 63/81 = 0.78.
**Standardized values based on the shear stress on stratified bank and natural river. For example for condition of pools, low banks, 56/72 = 0.78.

to this scale, other factors causing bank erosion in the Connecticut River have been rated accordingly. A similar rating scale has then been established with regard to the relative duration of these forces. The shear stress is acting as long as the water is flowing and is rated as 9 in the relative duration. Freezing and thawing effect is usually active for a short period of time and is rated as 1.

From these two rating scales, the relative magnitude of bank erosion ($R_B$) has been defined as $R_B = (M_B)(D_B)$ for both the noncohesive and stratified bank conditions. The resulting values have then been standardized to the shear stress acting on a noncohesive bank within a natural river reach. As an example of this table, to determine the relative effect of pool fluctuations upon low, stratified banks within the operation limits of a pool, the $M_B$ value is 3 (Column 4), the $D_B$ value is 3 (Column 5), and the resulting relative magnitude of bank erosion ($R_B$) is ($M_B$) x ($D_B$) = 9 (Column 8). The relative magnitude of the bank erosion for a stratified bank within a natural river reach is 72 and the standardized value is thus $9/72 \cong 0.13$ (Column 9).

Incremental values of shear stress acting on the banks of a natural river with high banks formed of noncohesive material are tabulated in Table 2-5. For these conditions, total effective tractive force acting on the bank can be estimated by adding the 0.52 $\gamma dS$ from the preceding tabulations taken from Table 2-4 to shear stress exerted by the flowing water on the banks of the channel. In summary, if shear stress is 0.77 $\gamma dS$, then total effective shear stress will be 1.29 $\gamma dS$. If this value exceeds the critical shear stress acting on the banks, erosion of the banks will occur unless protected.

If the bank line is subjected to erosion, size of riprap required to stabilize the bank line can be estimated from Shields' diagram. In this case estimated effective shear stress acting on the river bank can be substituted for $\tau$ in $\tau/(\gamma_s-\gamma)D_s$. If $R_* > 500$, then

$$\frac{1.29\ \gamma dS}{(\gamma_s-\gamma)D_s} = 0.06 \qquad (2\text{-}19)$$

The median diameter of the required size of riprap can be approximated by solving for $D_s$. Considering the numerator term 1.29 $\gamma dS$ is not a constant, but a function of river geometry and the forces acting on the river banks, its value can be approximated for each condition or evaluated as above.

The preceding analysis applies to essentially straight reaches of river channel. This method of analysis can be extended to apply to the outside banks of a river system by considering the lateral velocity distribution resulting from the properties of the river bend (Figure 2-15). The procedure requires an estimate of the increase in boundary shear stress acting on the outside bank of a river bend.

For straight channels the flow of water is more or less evenly distributed so the velocity remains basically constant across a cross section of the stream. In a curved channel the velocity of flow is generally higher on the outside of the bend and smaller on the inside.

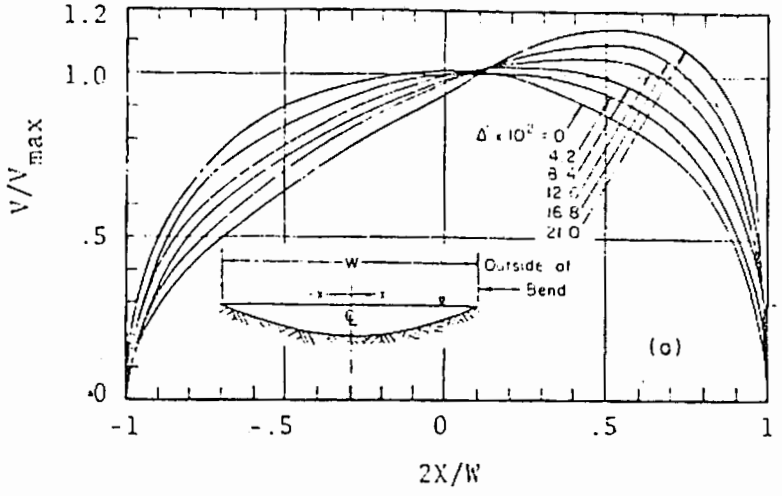


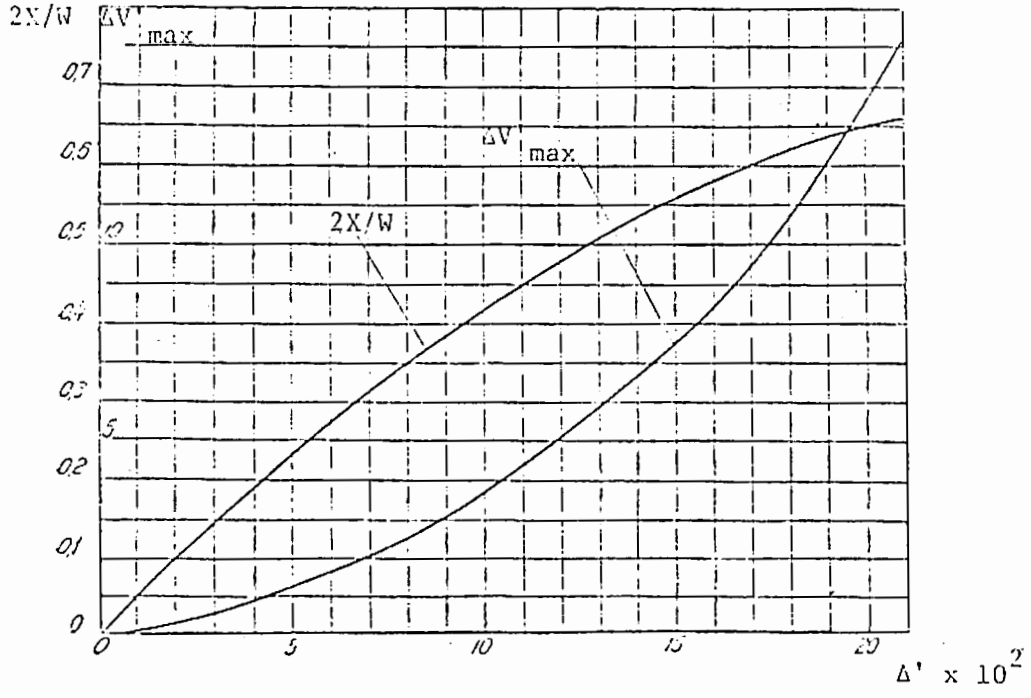


Figure 2-15. Lateral distribution of velocity in a bend (after Karaki, Mahmood, Richardson, Simons and Stevens, 1973).

Table 2-5. Example of estimated incremental values of shear stress from different processes.

| Variable Causing the Force on the River Bank | Magnitude of Equivalent Shear Stress |
|---|---|
| flood variation | 0.02 γdS |
| normal stage variation | 0.10 γdS |
| pool fluctuations | 0.11 γdS |
| wind waves | 0.01 γdS |
| boat waves | 0.05 γdS |
| freezing and thawing | 0.01 γdS |
| ice | 0.04 γdS |
| seepage forces | 0.07 γdS |
| gravitational forces | 0.11 γdS |
| | Σ = 0.52 γdS |

These changes in velocity cause even larger changes in the shear stress acting on the bed and banks of the river. The factor by which the mean shear stress is increased for the outside of bends in curved channels changes depending on the curvature of the channel. For sharp bends with a small radius of curvature, the boundary shear stress on the outside of a bend is approximately twice that of a straight channel.

To illustrate, a river bend has a radius of curvature, $R_c$ = 1500 feet and width W = 300 feet.

$$\frac{\tau_{bend}}{\tau_{straight}} = 1.5 \qquad (2\text{-}20)$$

For this case, the shear stress in the bend is about 1.5 times that in the straight reach. With this value established, the effect of the other forces acting on the bank can be added to the computed value to determine the total effective shear stress acting on the bank. Then the stability of the bank can be evaluated and if riprap is required, it can be sized as described in the preceding paragraphs.

Considering river bends in general, the shear stress in the bend way can be evaluated for each case. For more severe conditions, the shear stress acting on the outside bank in the bend may be as much as 1.5 times as large as for the straight reach.

Table 2-4 was developed based on theoretical consideration of causative factors and available data. Further examinations of Table 2-4 follow.

A summation of the relative magnitude of bank erosion for different factors causing erosion is determined from Table 2-4 and is given in Table 2-6. This table indicates the relative importance of these factors. In decreasing importance they are: shear stress (velocity),

Table 2-6. Sum of relative magnitude of bank erosion for different factors.

| Variables Causing Erosion | Sum of Relative Magnitude of Bank Erosion | |
|---|---|---|
| | Noncohesive | Stratified |
| Shear stress or velocity | 359*(1.0)** | 315 (0.88) |
| Flood variation | 10 (0.03) | 10 (0.03) |
| Stage variation | 27 (0.08) | 24 (0.07) |
| Pool fluctuation | 63 (0.18) | 54 (0.15) |
| Wind waves, surface erosion and piping | 14 (0.04) | 14 (0.04) |
| Boat waves, surface erosion and piping | 34 (0.09) | 42 (0.12) |
| Freeze-thaw | 6 (0.02) | 6 (0.02) |
| Ice | 11 (0.03) | 10 (0.03) |
| Seepage forces | 28 (0.08) | 36 (0.10) |
| Gravational forces | 31 (0.09) | 40 (0.11) |

*Values are obtained from summing the relative magnitude of basic erosion for each variable.
**Standardized values based on the shear stress (or velocity) in noncohesive banks. For example, for flood variation, 10/359 = 0.03.

Table 2-7. Sum of relative magnitude of bank erosion for different conditions.

| Conditions | Sum of Relative Magnitude of Bank Erosion | | |
|---|---|---|---|
| | Noncohesive | Stratified | Average |
| Natural river | 112*(1.00)** | 107 (0.96) | 109.5 (0.98) |
| Natural river with high bank | 124 (1.11) | 112 (1.00) | 118.0 (1.05) |
| Pools: low banks | 103 (0.92) | 97 (0.87) | 100.0 (0.89) |
| Pools: low banks with vegetation | 69 (0.62) | 66 (0.59) | 67.5 (0.60) |
| Pools: high banks | 106 (0.95) | 102 (0.91) | 104.0 (0.95) |
| Pools: high banks with vegetation | 69 (0.62) | 69 (0.62) | 69.0 (0.62) |

*Values are obtained from summing the relative magnitude of basic erosion for each river condition.
**Standardized values based on the natural river with noncohesive banks. For example, for pools with low and noncohesive banks, 100/112 = 0.89.

Table 2-8. Number of erosion sites per mile for different reaches.

| | Natural River | Pools |
|---|---|---|
| Number of erosion sites | 19.0 | 84 |
| Total river mile | 20.8 | 120.2 |
| Number of erosion sites per mile | 0.91 | 0.70 |

pool fluctuation, boat waves, gravitational forces, seepage forces, stage variation, wind waves, ice, flood variation, and freeze-thaw. In general, the stratified soil is slightly less susceptible to bank erosion than the noncohesive banks except when considering boat waves, seepage forces, and gravitational forces. Overall, the predominant force causing bank erosion is the shear stress (or velocity).

Further analysis of Table 2-4 provides a measure of the relative magnitude of bank erosion for different conditions (Table 2-7). This table demonstrates that a reach with a high bank is more susceptible to erosion, and vegetation is important in stabilizing the bank. Furthermore, the natural river has a higher potential for bank erosion that do the pools. The average sum of relative magnitude of bank erosion for a natural river is 113.75 and that for pools is 84.75. In other words, the natural river is roughly 1.34 (113.75/84.75 = 1.34) times more susceptible to major bank erosion than pools.

The number of erosion sites per mile for the natural river is 0.92 and that for pools is 0.68 (Table 2-8). Therefore, the measured data indicate the natural river is 1.35 (0.91/0.70 = 1.30) times more susceptible to bank erosion than pools. This is very close to the theoretical evaluation with a value of 1.34. The most common type of erosion is the "sloughing." In addition, most observed erosion sites are located in pools, straight reach, stratified soil, and vegetated area. The above statistics cannot be directly utilized to interpolate the causes of erosion; an unbiased statistical approach that considers erosion sites per mile for a particular classification. For example, the length of vegetated bank line is much longer than the unvegetated zone in these two areas. A direct interpolation without a proper adjustment on a linear mile basis will indicate that the total number of observed erosion sites with vegetated banks erroneously exceeds those with barren areas.

Based on the above discussion, the theoretical approach as presented in Table 2-4, is justified considering physical significance and field observations. However, further investigation of causative factors is needed to improve the information gap and the developed method.

The use of quasi-quantitative order of magnitude analysis to determine important processes acting in a channel provides useful information about those variables that are most needed in river response analyses. In the above example, shear stress was found to be relatively more important to erosion than were other river processes. Therefore, this process should be studied in more detail.

In general, river or watershed response analyses must require two preliminary steps. First, controlling processes must be identified and second, the most important processes delineated.

## 2.6 QUALITATIVE ANALYSIS OF CHANNEL RESPONSE FOR SELECTED EXAMPLES

### General

Previous sections have formed a basis for qualitatively analyzing channel response to different activities. This section takes those

ideas and introduces new ones to permit evaluation of selected channel modifications. Many channels have achieved approximate equilibrium over long reaches. For engineering purposes, such reaches can be considered stable. However, this does not mean significant changes over a short period of time or over a period of several years cannot occur. This is evidenced by streams that contain long reaches that are actively aggrading or degrading as well as stable reaches.

Regardless of the degree of channel stability, man's local activities may produce major changes in river characteristics both locally and throughout an entire reach. Frequently, the result of a river improvement is a greater departure from equilibrium than which originally prevailed. Good design must seek to enhance the natural tendency of the stream toward equilibrium conditions. This requires an understanding of the direction and magnitude of change in channel characteristics caused by the actions of man and nature. This understanding can be obtained by: 1) studying the river in a natural condition, 2) having knowledge of the sediment and water discharge, 3) being able to predict the effects and magnitude of man's future activities, and 4) applying to these a knowledge of geology, soils, hydrology, and hydraulics of alluvial rivers.

Predicting the response to channel development is a very complex task. There are a large number of variables involved in analyses that are interrelated and can respond to changes in a river system and the continual evolution of river form. Channel geometry, bars, and forms of bed roughness all change with changing water and sediment discharges. Because prediction of channel response is necessary, useful methods have been developed to qualitative and quantitative estimate changes in channel systems.

Qualitative Prediction of General River Response

Quantitative prediction of response can be made if all of the required data are known with sufficient accuracy. Usually, the data are not sufficient for quantitative estimates and only qualitative estimates are possible.

Lane (1955) studied the changes in river morphology in response to varying water and sediment discharge. Leopold and Maddock (1953), Schumm (1971), and Santos and Simons (1972) have all investigated channel response to natural and imposed changes. These studies support the following general relationships:

1. Depth of flow $y$ is directly proportional to water discharge $Q$.

2. Channel width $W$ is directly proportional to both water discharge $Q$ and sediment discharge $Q_s$.

3. Channel shape, expressed as width to depth $W/y$ ratio is directly related to sediment discharge $Q_s$.

4. Channel slope $S$ is inversely proportional to water discharge $Q$ and directly proportional to both sediment discharge $Q_s$ and median grain size $D_{50}$.

5. Sinuosity s is directly proportional to valley slope and inversely proportional to sediment discharge $Q_s$.

6. Transport of bed material $Q_s$ is directly related to stream power $\tau_o V$ and concentration of fine material $C_F$, and inversely related to the fall diameter of the bed material $D_{50}$.

A very useful relation for predicting system response was developed by Simons et al. (1975) establishing a proportionality between bed-material transport and several related parameters.

$$Q_s \sim \frac{(\tau_o V)WC_F}{D_{50}} \tag{2-21}$$

where $\tau_o$ is bed shear, V is cross sectional average velocity, and $C_F$ is concentration of fine material load. Equation 2-21 can be modified by substituting $\gamma DS$ for $\tau_o$, and

$$Q = AV = WDV \tag{2-22}$$

from continuity, yielding

$$Q_s \sim \frac{(\gamma DS)WV}{D_{50}/C_F} = \frac{\gamma QS}{D_{50}/C_F} \tag{2-23}$$

If specific weight $\gamma$ is assumed constant and concentration of fine material $C_F$ is incorporated in the fall diameter, this relation can be expressed simply as

$$QS \sim Q_s D_{50} \tag{2-24}$$

Equation 2-24 is essentially the relation proposed by Lane (1955), except fall diameter which includes the effect of temperature on transport has been substituted for the physical median diameter used by Lane.

## Applications of Qualitative Analysis

Equations 2-23 and 2-24 are most useful for qualitative prediction of channel response to natural or imposed changes in a river system. A well-known example is the downstream response of a river to the construction of a dam (Figure 2-16). Aggradation in the reservoir upstream of the dam will result in relatively clear water being released downstream of the dam. That is, $Q_s$ will be reduced to $Q_s$ downstream.

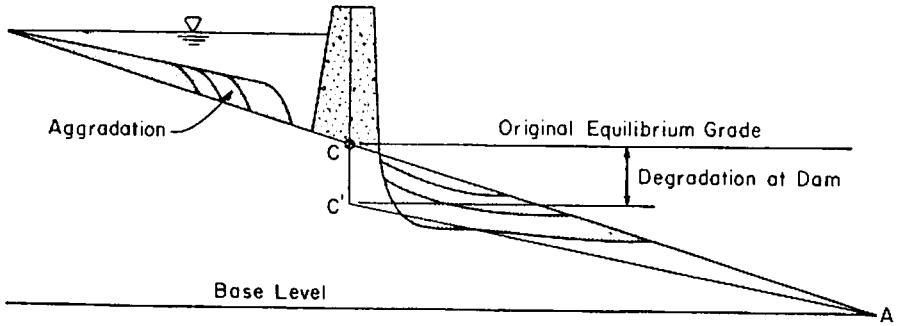


Figure 2-16. Channel adjustment above and below a dam.

Assuming fall diameter and water discharge remain constant, slope must decrease downstream of the dam to balance the proportionality of Equation 2-25

$$Q_s^- D_{50}^o \sim Q^o S^- \qquad (2\text{-}25)$$

In Figure 2-16 the original channel gradient between the dam and a downstream geologic control (line CA) will be reduced to a new gradient (line C'A) through gradual degradation below the dam. With time the pool behind the dam will fill and sediment would again be available to the downstream reach. Then, except for local scour gradient C'A would increase to original gradient CA to transport the increase in sediment load. Upstream the gradient would eventually parallel the original gradient, offset by height of the dam. Thus, dams with small storage capacity may induce scour and then deposition over a relatively short time period.

Quantitative results in addition to qualitative indications of trends are also of interest. The geomorphic relation $QS \sim Q_s D_{50}$ is only an initial step in analyzing long-term channel response problems. However, this initial step is useful because it warns of possible future difficulties in designing channel improvement and flood protection works and provides a good estimate of response to all types of river development.

Qualitative Analysis Examples of River Response

Consider next several relatively simple situations commonly encountered by engineers, scientists, and geologists in the river environment. Each case is introduced by a sketch that shows the physical situation prior to a selected natural or man-induced change. Below the sketch some major local effects, upstream effects, and downstream effects resulting from natural processes or development activity are given. It is necessary to emphasize that only gross local, upstream, and downstream effects are identified. For more detail on regimes of flow, bed forms, and resistance to flow and their effects on river response refer to Simons and Sentürk (1977).

Initial river conditions are sometimes given in terms of storage dams, water diversions, or other works of man. These examples are used in illustrations relating to common experience. For more details refer to Simons et al. (1975). In general, the effect of a storage reservoir is to cause a sudden increase of base level for the upstream section of the river. The result is aggradation of the channel upstream, degradation downstream, and a modification of the downstream flow hydrograph. Similar changes in the channel result if the base level is raised by some other mechanism, such as uplift from tectonic activity. The effect of diversions from rivers is to decrease river discharge downstream of the diversion with or without an overall reduction of the sediment transport. Similarly, changes in water and sediment input to a river reach often occur due to river development projects upstream from the reach under consideration or as a result of natural causes.

Figure 2-17 illustrates the confluence of a tributary stream with the main channel. Average water surface elevation in the main channel acts as the base level for the tributary. It is assumed here that base level in the main channel has been lowered by a natural change in river environment or by man-induced change such as lowering reservoir level on the main stem. Applying Equation 2-24 to the tributary stream shows that increase in slope $S^+$ must be balanced by increase in sediment transport $Q_s^+$. Thus, under new imposed condition, the local gradient of the tributary stream is significantly increased. This increased energy gradient induces headcutting and causes a significant increase in water velocities in the tributary stream. The result is bank instability, possible major changes in geomorphic characteristics of the tributary stream and increased local and general scour.

Response to the converse situation, raising the base level, can be illustrated by considering river response to construction of a dam (Figure 2-18). Whenever base level of a channel is raised, a pool is created extending a distance upstream depending on channel gradient and dam height. This results in a "backwater" effect. As water and sediment transported by the river encounters this pool, most of the sediments drop out forming a delta-like formation at the head of the pool which slowly advances downstream. Deposition of sediment at the entrance to the pool induces aggradation in the channel upstream. This aggradation may extend several miles upstream after a long period of time, producing significant changes in river geometry, and increased flood stages by raising the channel bed. Again, Equation 2-24 provides an indication of the response. The decrease in slope $S^-$ must be accompanied by a decrease in transport capacity $Q_s^-$ or $Q_s^{\circ -} \sim Q_s^- D_{50}^{\circ}$. It is possible that the river may become sufficiently perched so at some high flow the river could abandon the old channel and adopt a new one.

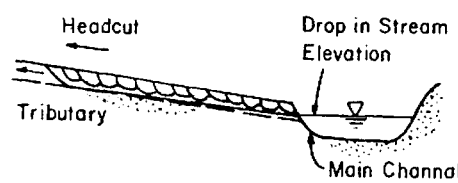


| Local Effects | Upstream Effects | Downstream Effects |
|---|---|---|
| 1. Headcutting | 1. Increased velocity | 1. Increased transport to main channel |
| 2. General scour | 2. Increased bed material transport | 2. Aggradation |
| 3. Local scour | 3. Unstable channel | 3. Increased flood stage |
| 4. Bank instability | 4. Possible change of form of river | 4. Possible change of form of river |
| 5. High velocities | | |

Figure 2-17. Lowering of base level for tributary stream (Simons et al., 1975).

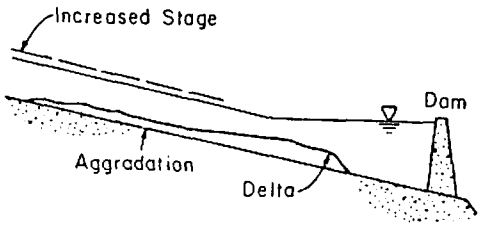


| Local Effects | Upstream Effects | Downstream Effects |
|---|---|---|
| 1. Aggradation of bed | 1. See local effects | 1. See downstream effects, Fig. 3.19 |
| 2. Loss of waterway capacity | 2. Change in base level for tributaries | |
| 3. Change in river geometry | 3. Deposition in tributaries near confluences | |
| 4. Increased flood stage | 4. Aggradation causing a perched river channel to develop or changing the alignment of the main channel | |

Figure 2-18. Raising base level in main channel.

As noted in Figure 2-18, the effects of raising the base level of the main channel include an increase in base level for any tributaries entering the pool formed by the main stem dam. The impact of this change on the tributaries is shown in Figure 2-19.

Change in gradient of the tributary stream in most cases causes significant deposition. This can be seen from Equation 2-24 where a decrease in slope is accompanied by a decrease in sediment transport or

$$Q^{o}S^{-} \sim Q_{s}^{-} D_{50}^{o}$$

assuming constant conditions of water discharge and size of bed material. In this case an alluvial fan develops that in time can divert the river or reduce the waterway. In general, streams on alluvial fans shift laterally so that the future location of the channel is uncertain.

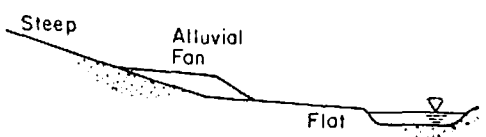


| Local Effects | Upstream Effects | Downstream Effects |
|---|---|---|
| 1. Alluvial fan reduces waterway | 1. Erosion of banks | 1. Aggradation |
| 2. Channel location is uncertain | 2. Unstable channel | 2. Flooding |
| | 3. Large transport rate | 3. Development of tributary bar in the main channel |

Figure 2-19. Raising base level for tributary stream.

A similar situation occurs naturally where a steep tributary stream draining an upland region reaches the flatter floodplain of the parent stream.

The impact of construction of a dam on the reach upstream of the dam is also outlined in Figure 2-18. Construction of an upstream storage dam provides a desilting basin for the water flowing in the system. In most instances all of bed material load coming into a reservoir deposits within the reservoir. Water released from the reservoir is quite clear. The existing river channel is the result of its interaction with normal water-sediment flows over a long period of time. With the sediment-free flows the channel below the dam is too steep and sediments are entrained from the bed and the banks bringing about significant degradation. Channel banks may become unstable due to degradation and there is a possibility that the river, as its profile flattens, may change its plan form (Figure 2-20). Assuming that prior to dam construction the reach below the dam plotted as an intermediate stream (point 1), the decrease in slope at constant water discharge could move the stream's plotting position to point 2 in the meandering region of the chart. In the extreme case, it is possible that degradation may cause dam failure and the release of a flood wave.

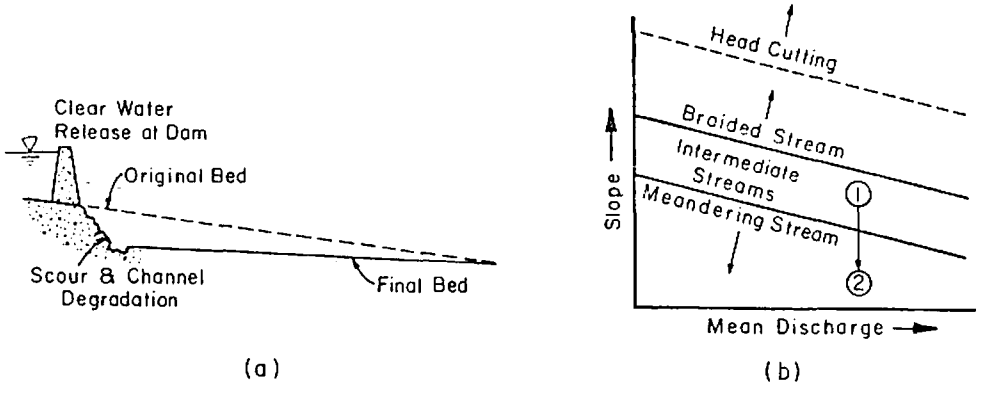


| Local Effects | Upstream Effects | Downstream Effects |
|---|---|---|
| 1. Channel degradation | 1. See upstream effects, Fig. 3.17 | 1. Degradation |
| 2. Possible change in river form | | 2. Reduced flood stage |
| 3. Local scour | | 3. Reduced base level for tributaries, increased velocity and reduced channel stability causing increased sediment transport to main channel |
| 4. Possible bank instability | | |
| 5. Possible dam failure | | |

Figure 2-20. Clear water release below a dam.

Figure 2-21 illustrates a situation where artificial cutoffs have straightened the channel below a given reach. Straightening the channel downstream of Reach A significantly increases channel slope. This causes higher velocities, increased bed material transport, degradation, and possible headcutting through Reach A. This can result in unstable river banks and a braided stream form. Original plotting position (point 1) is moved to point 2 in the braided region by increase in channel slope. In addition, straightening the main channel brings about a drop in base level and tributary streams flowing into the affected reach of the main channel are subjected to conditions outlined in Figure 2-17.

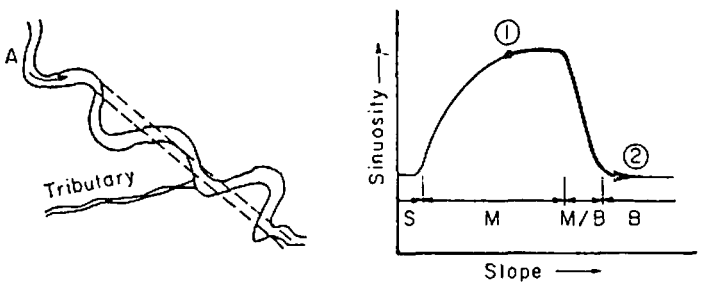


| Local Effects | Upstream Effects | Downstream Effects |
|---|---|---|
| 1. Steeper slope | 1. See local effects | 1. Deposition downstream of straightened channel |
| 2. Higher velocity | | 2. Increased flood stage |
| 3. Increased transport | | 3. Loss of channel capacity |
| 4. Degradation and possible headcutting | | |
| 5. Banks unstable | | |
| 6. River may braid | | |
| 7. Degradation in tributary | | |

Figure 2-21. Straightening of a reach by construction of cutoffs.

On the other hand, if the straightened section is designed to transport the sediment loads that the river is capable of carrying both upstream and downstream of the straightened reach, bank stability may not decrease. Such a channel should not undergo significant change over either short or long periods of time. It is possible to build modified reaches of main channels that do not introduce major adverse responses due to local steepening of the main channel. In order to design a straightened channel so that it behaves essentially as the natural channel in terms of velocities and magnitude of bed material transport, it is usually necessary to build a wider shallower section.

## Qualitative Analysis of Response of Large Scale Systems

Simple examples presented above lead into more complex ones for large scale problems or systems. However, it should be noted that the large scale systems are analyzed by the same procedures as smaller examples.

### Impact of Construction of a Large Dam on a River System Upstream of a Diversion to an Irrigated Area

A particular river system carried significant percentages of fine sediments comprised of silts and clays during the majority of the year. An irrigation diversion system was developed long before there was any construction of dams upstream of the diversion structure (Figure 2-22). The main feeder canal diverts water from the river system to the irrigated area at the diversion structure. Thereafter, it flows around a side hill, comprised of rather permeable materials including sands and gravels, passes through a city area where there is relatively dense development along both sides of the canal, and then continues downstream to serve the distant irrigated area.

A large storage dam was constructed on the river immediately upstream of the diversion structure. The reservoir acts as a desilting basin and water released below this dam is essentially clear. This clear water flows down the short reach of river channel and is then diverted to the irrigation canal. This release of clear water may cause some degradation immediately downstream of the dam before it enters the canal. There has been some degradation in the main canal and erosion has exposed more permeable bed and bank materials thus increasing seepage losses. There are several major detrimental consequences from the increased seepage losses including 1) significant decrease in the amount of water that can be delivered to the farm units for irrigation and 2) seepage from the canal system has a potential to cause a rise in the water table. Increase in the water table level may cause extensive damage to adjacent buildings by basement flooding.

There are other potentially detrimental factors that can adversely affect the irrigation system. For example, with clear water in the canal system it will be a suitable environment for growth of aquatic plants. With these plants choking the channels there will be added water losses and it will be difficult to convey required water to the downstream irrigation systems. Therefore, some type of periodic treatment would be required to keep the channels free of vegetation. On the

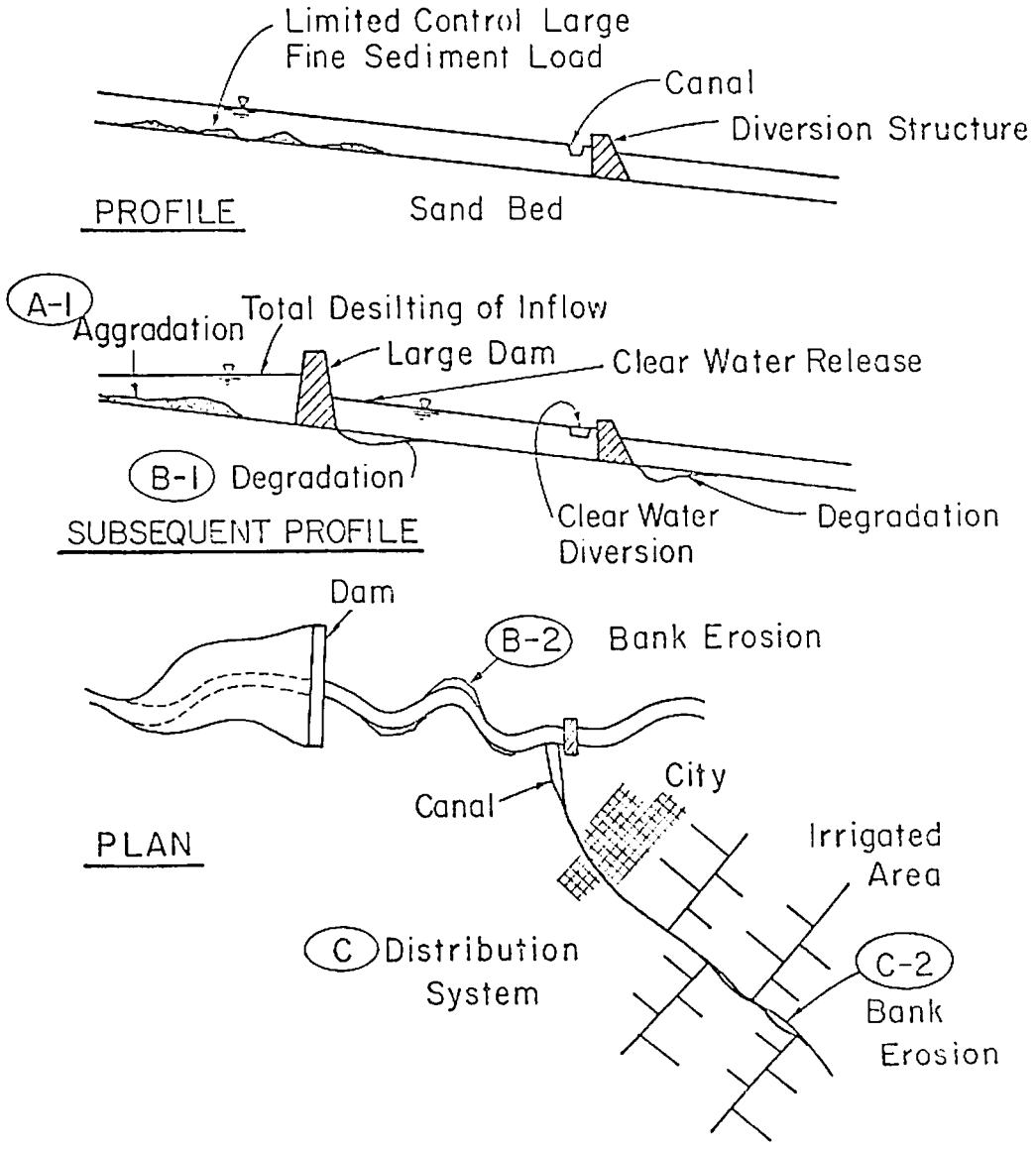


Figure 2-22. Impact of construction of a large dam on a river system upstream of a diversion to an irrigated area.

farm units where land has been irrigated by diversions from head ditches into furrows, the head ditches were designed and spaced so that a fairly efficient application of water could be made with water containing silts and clays. With silt and clay in the water, relatively long runs were possible. If the same lengths of runs are used with clear water there are excess seepage losses and before the water reaches the ends of the furrows, all of it is infiltrated thus building up the groundwater level. This means that the distribution system on the farm units must be dramatically changed. Length of runs may have to be cut in half. This will require more head ditches and more nonproductive space. Numerous ditches may also add to problems of harvesting.

As referred to previously, clear water tends to scour banks and degrade the bed of the canal system. If the attack is sufficiently severe, channel stabilization may be required or some type of lining may be required to minimize the losses of water and provide stability.

The Response of a River System and Intervening Reaches of Channel to the Construction of Major Reservoirs (Simons and Li, 1977)

In analysis of river systems it is common to find water resources development projects that involve the construction and use of major reservoirs. Such a case is outlined in Figure 2-23. The reservoir identified as A has been constructed on a major river. Reservoir B further downstream is planned for subsequent development. At location C there is a city that will be affected by the backwater from reservoir B. With this general background, responses of the system to these developments can be considered. Reservoir A stores on the order of 10,000,000 acre feet of water. However, even though it is large, it only stores a small percent of the water that is annually discharged from this watershed, as illustrated by inserted hydrograph. This particular hydrograph points out that approximately five times the volume of the reservoir flows down the river system each year. All sediment carried into the reservoir is trapped and the quantity of water that is desilted is approximately equal to five times the volume of the reservoir, about 50,000,000 acre feet per year. The sediment load carried by the river ranges from average to large for similar sized rivers. This means that desilting of such a large volume of water causes a large volume of sediment to be deposited within reservoir A each year. This deposition can significantly decrease storage capacity for hydropower, irrigation, and flood control in a relatively short time. Furthermore, essentially clear water is released downstream of the dam. The channel is comprised of materials ranging from fine sand, silts, and clays to coarse gravel. Coarser materials in the bed of the stream will tend to limit degradation induced downstream of the dam by release of clear water. It is essential to not only evaluate the rate at which the loss of live storage occurs in the reservoir but to document the rate and magnitude of ultimate degradation so that the structure's safety can be adequately considered.

Reservoir B is considered next. This particular reservoir has approximately the same storage capacity as reservoir A. Waters released into this particular reservoir will be essentially clear insofar as the water coming through reservoir A is concerned. On the other hand, two other river systems flow into reservoir B. These are

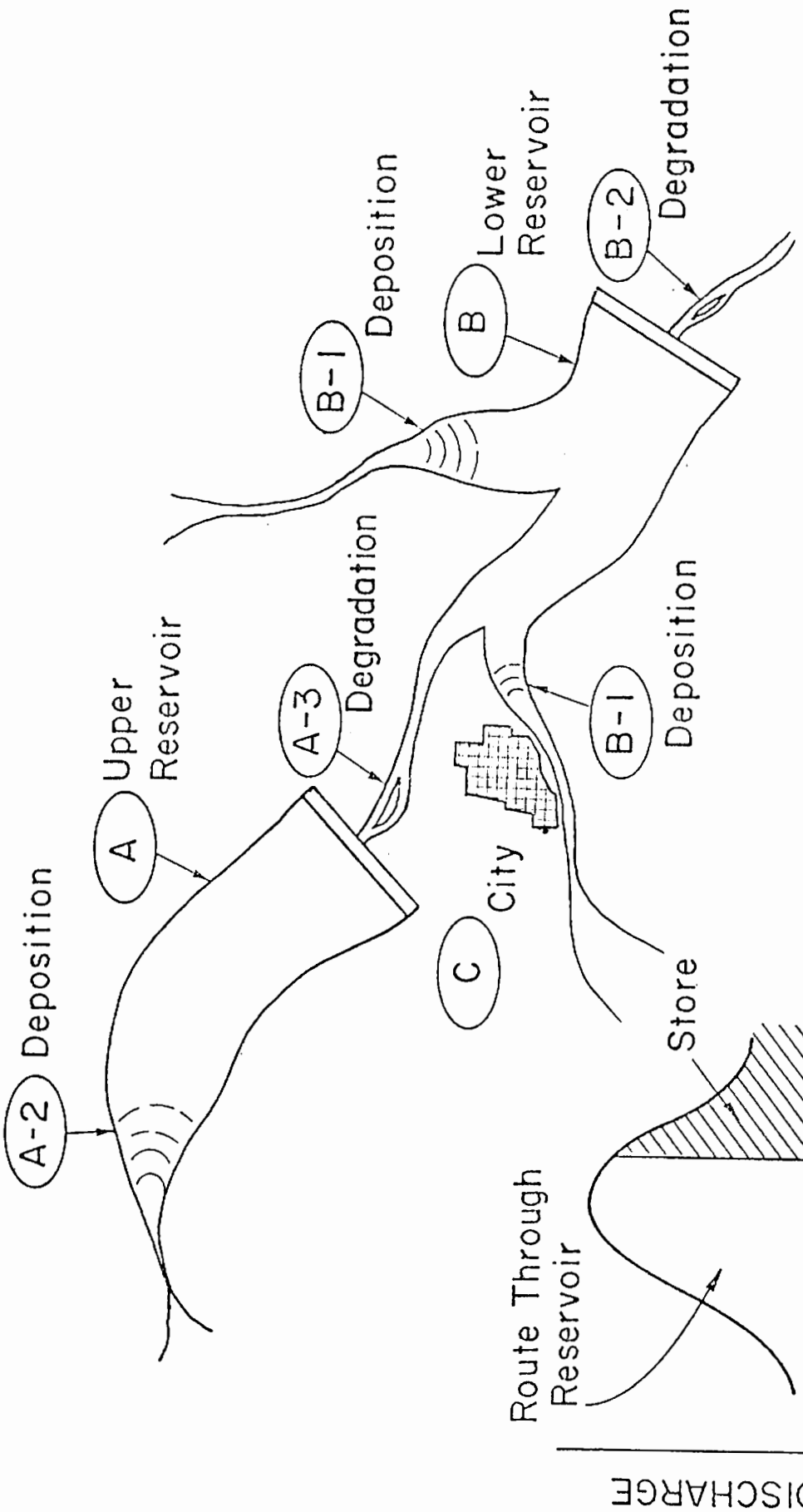


Figure 2-23. The response of a river system and intervening reaches of channel to the construction of major reservoirs.

not desilted and consequently carry significant quantities of sediment into the reservoir. Once again it is necessary to consider the rate of loss of live storage as a consequence of inflowing sediments. It should also be recognized that ultimately reservoir A will lose the capacity to store sediment and sediments may be discharged from reservoir A to reservoir B. On the other hand, there is the possibility that reservoirs upstream of reservoir A will be constructed. This type of activity can significantly increase the lifetime of reservoirs such as A and B. This is typical of what has happened to downstream reservoirs due to the construction of upstream reservoirs along the Colorado River.

Because of the importance of sediment in terms of economics of operation of the reservoirs over long periods of time, an interesting problem with respect to reservoir B is to attempt to construct it in such a way that relatively large quantities of sediment can be discharged annually from it instead of being stored within it. This would involve building a large gated structure in such a way that reservoir B could essentially run as an open river during those periods of high flow when water could be passed through the system. Then, toward the end of the runoff period, it would be necessary to close the gates in time to allow filling of the reservoir. With this type of operation it would be necessary to empty the reservoir annually. Otherwise, it would not be possible to pass excess sediments through the reservoir system. Hence, it can be seen that there are many trade-offs that have to be considered when determining economics of these systems as well as the response of the rivers and impacts that may result.

Location C is considered next. Here a city is located on a river discharging into an arm of reservoir B. Backwater from the reservoir may require construction of flood protection works for the city. In addition, determining water levels in the vicinity of the city is not adequate. It is necessary to route water and sediment down the river system into the reservoir to determine rates of deposition, location of deposition, and how these deposits of sediment may increase river stage, aggravate the flooding situation, increase groundwater level, and perhaps cause other adverse responses.

As the above simple examples and case histories illustrate, knowledge of the qualitative responses of a system to changes is important in understanding quantitative changes. Without this knowledge, mathematical and physical models can be constructed that do not and cannot truly represent the system being studied.

## 2.7 SUMMARY

A key to mathematical modeling of watershed or channel responses to natural or man-induced changes is through understanding of important physical processes. These processes can be broadly grouped as topography, soils, geology, vegetation, climate, hydrology and hydraulics, and man's influence. Processes differ somewhat between watershed and channel systems, but they share a common trait of being interrelated and complex. Identification of physical processes must coincide with determination of the most important ones. This can be

done through sensitivity analysis of mathematical models that describe the process or by relative order of magnitude comparisons. Once the processes are understood, they can be used to qualitatively predict system response or can be used to construct more representative mathematical models. Qualitative analysis often provides a check for results obtained from mathematical models. Either way knowledge of physical processes is necessary in understanding natural systems.

REFERENCES

Chow, V. T., 1964, Handbook of Applied Hydrology. McGraw Hill Book Company, New York, 1000+p.

Culbertson, D. M., Young, L. E., and Brice, J. C., 1967, Scour and Fill in Alluvial Channels. U. S. Geological Survey, Open File Report.

Davis, W. M., 1899, The Geographical Cycle. Geographical Journal, Vol. 14, pp. 481-504.

Garg, M. M., 1972, River Classification by Photos and Map. M. S. Thesis, Colorado State University, Fort Collins, 1972.

Horton, R. E., 1945, Erosional Developments of Streams and Their Drainage Basins; Hydrophysical Approach to Quantitative Morphology. Geol. Soc. Am. Bull., Vol. 56.

Karaki, S., Mahmood, K., Richardson, E. V., Simons, D. B. and Stevens, M. A., 1975, Highways in the River Environment - Hydraulic and Design Considerations. Colorado State University, Fort Collins, Colorado, CER73-74EVR-SK-KM-DBS-MAS49, September (Federal Highway Administration, U. S. Department of Transportation, May 1975).

Khan, Hamidur, R., 1971, Laboratory Studies of Alluvial River Channel Patterns. Ph.D. Dissertation, Civil Engineering Department, Colorado State University, Fort Collins.

Lane, E. W., 1955, The Importance of Fluvial Morphology in Hydraulic Engineering. ASCE Proc., Vol. 81, No. 745, 17 p.

Lane, E. W., 1957, A Study of the Shape of Channels Formed by Natural Streams Flowing in Erodible Material. Missouri River Division Sediment Series No. 9, U. S. Army Engineer Division, Missouri River, Corps of Engineers, Omaha, Nebraska.

Langbein, et al., 1947, Topographic Characteristics of Drainage Basin. U. S. Geological Survey Water Supply Paper 968-C. In Contributions to the Hydrology of the United States.

Leopold, L. B. and Maddock, T., Jr., 1953, The Hydraulic Geometry of Stream Channels and Some Physiographic Implications. U. S. Geological Survey Professional Paper 252, 57 p.

Pfankuch, D. J., 1975, Stream Reach Inventory and Channel Stability Evaluation. U. S. Department of Agriculture Forest Service, Northern Region.

Rosgen, D. L., 1975, Watershed Response Rating System. In Forest Hydrology, Part II. U. S. Department of Agriculture Forest Service, Northern Region, Missoula, Montana.

Rundquist, L. A., 1975, A Classification and Analysis of Natural Rivers. Ph.D. Dissertation, Department of Civil Engineering, Colorado State University, Fort Collins, Colorado.

Santos-Cayade, J. and Simons, D. B., 1972, River Response, paper presented at the 1972 River Mechanics Institute, Colorado State University, published in Environmental Impact on Rivers edited by H. W. Shen, Colorado State University, Fort Collins, Colorado, 1973.

Schumm, S. A., 1963, A Tentative Classification of Alluvial River Channels. U. S. Geological Survey Circular 477.

Schumm, S. A., 1971, Fluvial Geomorphology: The Historical Perspective. In Chapter 4 of River Mechanics, Vol. I, H. W. Shen, Ed., Fort Collins, Colorado.

Schulits, S., 1941, Rational Equation of River-Bed Profile. Trans., AGU, Vol. 22, pp. 622-630.

Simons, D. B., Andrew, J., Li, R. M., Alawady, T., 1979, Connecticut River Streambank Erosion Study of Massachusetts, New Hampshire and Vermont. Prepared for U. S. Army Corps of Engineers, Waltham, Massachusetts.

Simons, D. B. and Li, R. M., 1977, In-Field Estimation of Infiltration Parameters. Colorado State University Report, prepared for USDA Forest Service, Rocky Mountain Forest and Range Experiment Station, Flagstaff, Arizona.

Simons, D. B. and Li, R. M., 1975, Watershed Segmentation by a Digital Computer for Mathematical Modeling of Watershed Response. Prepared for USDA Forest Service, Rocky Mountain Forest and Range Experiment Station, Flagstaff, Arizona, December.

Simons, D. B. and Richardson, E. V., 1966, Resistance to Flow in Alluvial Channels. USGS Professional Paper 422-J.

Simons, D. B. and Senturk, F., 1977, Sediment Transport Technology. Water Resources Publication, Fort Collins, Colorado.

Simons, D. B., Ward, T. J. and Li, R. M., 1979, Sediment Sources and Impacts in the Fluvial System. In Modeling of Rivers, H. W. Shen, Ed., John Wiley and Sons, New York.

Strahler., 1952, Hypsometric (arca-altitude) Analysis of Erosional Topography. Geological Society of America Bulletin, No. 63.

Strahler., 1957, Quantitative Analysis of Watershed Geomorphology. Transactions, American Geophysical Union, Vol. 38, No. 6.

Thornbury., 1969, Principles of Geomorphology. 2nd Edition. John Wiley & Sons.

# Chapter 3

# OVERVIEW OF STREAM MECHANICS AND RIVER SYSTEMS ANALYSIS

## 3.1 INTRODUCTION

Increasing interest in water resource and land use planning has stimulated development of particular and general watershed and river system models for predicting response of ecological systems. The models, whether physical process simulation or conceptual, are intended to be utilized for estimating physical quantities that describe major eco-system responses to precipitation such as water yield, sediment yield, changes of land and river morphology, and transport of pollutants. Methods for estimating water, sediment, and other pollutant transport yields are required for analysis of the economic feasibility and trade-offs of proposed water resources or land use development in watershed and river systems and for predicting possible adverse environmental impacts associated with the proposed development.

A mathematical model is simply a quantitative expression of a process or phenomenon. In a conventional method of analysis, a series of manual calculations may be required. With advancement of numerical techniques and computer technology, a series of tedious computations can be conducted efficiently, repeatedly, and adequately through the formulation and construction of a mathematical model. Utilizing a well developed model, an array of "what-if" questions can be answered with minimum of time and effort. Since no process can be entirely understood and observed, any mathematical expression of a process involves some level of uncertainty. This uncertainty can be minimized by considering the governing physical processes in the analysis and properly designing, calibrating and verifying the model. Model development, verification, and application requires consideration of the nature of the problems, physical environment, objective of the study, time, manpower, and money. Since time, manpower, and money are limited, model users and developers must decide on the degree of complexity of the model, and the extensiveness of the verifications that are to be performed. According to Overton and Meadows (1976), if a highly complex mathematical representation of the system under study is made, risk of not representing the system will be minimized but difficulty of obtaining a meaningful solution will be maximized. Data requirements, programming effort, and computer time will be large, and the overall complexity of the mathematical handling may render problem formulation intractable. Further, resource constraints of time, money, and manpower may be exceeded. Conversely, if a simplified mathematical model is selected or developed without proper examination of physical significance, risk of not representing the physical system will be maximized but difficulty in obtaining a solution will be minimized. Figure 3-1 illustrates the concept of "trade-offs" in model complexity. Knowledge of governing physical processes and sensitivity of system response is most important in determining the appropriate level of analysis. It is possible to select or develop a model that is simple to use and involves a minimum level of risk if the governing physical processes are emphasized.

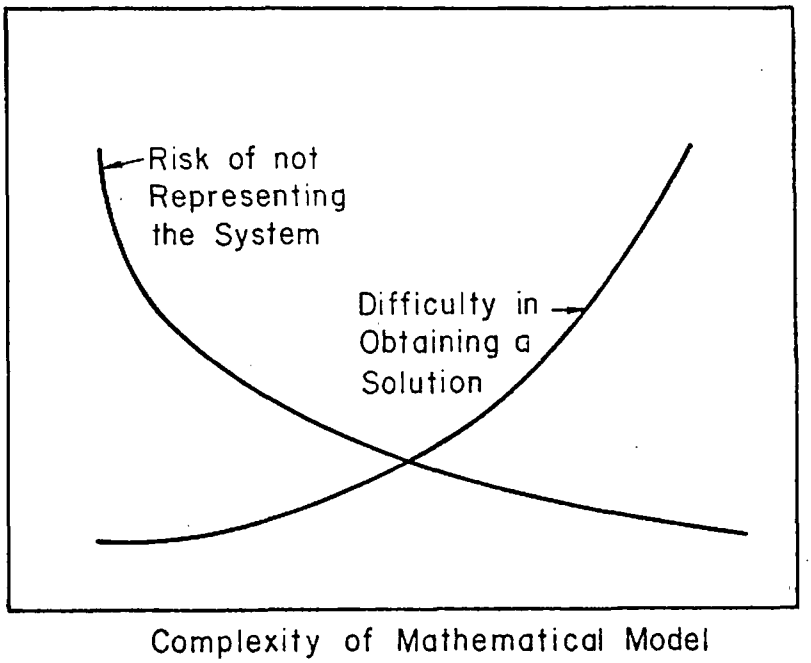


Figure 3-1. The model complexity trade-off diagram (after Overton and Meadows, 1976).

Physical processes governing watershed and river responses are very complicated. Therefore, many past studies have utilized a statistical interpretation of observed response data. The unit hydrograph method for water routing, Universal Soil Loss Equation for soil erosion, and hydraulic equations for stream morphology are examples of these types of studies. It is difficult to predict the response of a watershed to various watershed developments or treatments using such methods, because they are based on the assumption of homogeneity in time and space. Mathematically simulating governing physical process is a more viable way to estimate the time-dependent response of watersheds and river systems to precipitation with varying land use and water resources development. By analzying basic ecosystem processes and the impact of management activities on specific processes it is possible to predict the cause-effect relationships between management activities and ecosystem response. With the aid of systems analysis techniques, a desirable combination of management activities can be selected considering both environmental and resource goals.

This chapter presents a brief assessment of the current state-of-the-art utilized to analyze watershed and river systems, physical processes important to analysis, criteria related to the development of mathematical models for various applications, procedural steps involved in model development, and examples of applications of models to watershed and river systems.

## 3.2 CURRENT STATE-OF-THE-ART

Mathematical models used to simulate the effects of management activities on ecosystem responses can be classified as one of three types: regression, "black box" simulation, and physical process

simulation. If models are hybrids of components that fall into two or all three of these categories, they are classified according to the dominant traits of the model as a whole (Simons and Li, 1979).

A general weakness of regression models available for use in water and land resources management (e.g., the Musgrave approach to soil erosion, U.S. Forest Service, 1976 is that the variables representing water and land uses and conditions are not specific enough to reflect the effects of many individual management activities. In addition, regression models usually require sufficient observed data to correlate meaningful relations. This is often the most serious drawback to this approach. Furthermore, it is difficult to predict time and space dependent processes using regression equations.

Lumped parameter ("black box" or "simulation programming") type of model interprets input-output relations using oversimplified forms which may or may not have physical significance. All processes related to movement of water and sediment through the watershed are "lumped" together into several coefficients. The classic example of a lumped parameter model is the rational formula for estimating peak discharge i.e., $Q = CIA$ where $Q$ is peak discharge, $I$ is rainfall input, $A$ is drainage area, and $C$ is the runoff coefficient representing the major hydrologic processes. Such a model is easy to use, but has limited physical meaning and may be inaccurate. In most cases, it is impossible to predict the effects of alternative combinations and sequences of management activities occurring on complex upland watersheds utilizing lumped parameter models. Further, simulation programming models can only be made to represent a particular watershed by calibrating numerous internal model coefficients using water and sediment flow data documented for existing or past vegetation and soil conditions. In the absence of adequate data for model calibration with significantly different future vegetation and soil conditions, predicted future water and sediment flow using simulation programing models must be suspect.

Physical process simulation models, however, avoid "lumping" physically significant variables by decomposing components such as infiltration and sediment detachment from raindrop splash. By delineating the selected phenomena into its separate components, each individual process can be analyzed, refined, or altered to meet the needs of the user. Consequently, as each process component is upgraded, the model becomes more representative of the physical system. Use of component process models also allows input of variables that have physical significance to the user and the field situation. All of the above characteristics of component process models allow greater flexibility than other types of models. Advantages of physical process component models over other types are numerous. In general, physical process simulation models are superior to regression type models or "black box" type mathematical models. Input variables to process models are physically significant because they indicate system response caused by changing one or more physically significant values. Physical process simulation models are dynamic simulation systems. They are not assumed stationary in either time or space and therefore with little calibration they can be used to predict future response of the system in real time and space. Furthermore, since these models are formulated according to physical processes, they are applicable to areas in which governing physical processes are the same.

Numerous mathematical models are available for predicting the response of watershed and river systems. A comprehensive review of nonpoint water quality modeling in wildland management was conducted by the U.S. Forest Service (1976). Herein, a brief review of available component models for predicting system response from watershed and river systems is given.

Physical process simulation models include those models relating to the physical processes such as surface runoff, subsurface flow, raindrop splash erosion, overland flow erosion, channel flow routing, channel bank erosion, degradation, and aggradation. Streamflow models have received a great deal of attention in ecosystem modeling. A great deal of research has been conducted on the components within the hydrologic cycle with water as the prime carrier of sediment and pollutants. Research on streamflow and the hydrologic cycle provides necessary ingredients for advancement of the physical process simulation model for estimating transport of sediment and other pollutants. Determination of resistance to flow is usually the most important item for calibraton of streamflow models. Resistance to flow is a function of bed material size, bed form, river stage, temperature, etc. It is often difficult to predict resistance to flow in cobble and boulder bed rivers. Recent studies at Colorado State University by Simons et al. (1979) further demontrated the dynamics of flow resistance in mountain rivers. They indicated that released sediment from upstream watershed or bank erosion during a flood fills the space between and may completely cover the roughness elements. Thereafter the cobble channel behaves as a sand bed upper regime channel with a reduced resistance to flow. A better understanding of resistance to flow for a variety of river and land surface conditions is needed.

Methodologies presented in the literature identify three basic types of mathematical approaches to watershed and river analysis: 1) the analytical solution, 2) the finite difference method, and 3) the finite-element method. Hann and Young (1972) and Simons et al. (1977a) provide a review of finite difference models using both implicit and explicit solution techniques. Analytical solutions are usually limited by simplified assumptions and are applicable to restricted conditions. The finite-element technique has been actively applied recently, especially to the modeling of microscopic flow phenomena. In the finite-element method the original continuous problem is reduced to a system of ordinary differential equations in time. These can be solved by traditional techniques. Due to the fundamentals of finite-element formulation, completely arbitrary geometries may be modeled. Thus, spatial programming is not required to fit highly irregular boundaries. In addition, the feature of variable element size can be used to create a fine mesh of elements in areas of high varible gradients in order to obtain the desired accuracy and detail in sensitive regions. Common boundary conditions are also handled easily by the finite-element method. The major drawback to the finite-element method is the required computer time. This constraint will be less significant in the future as numerical techniques and computer software advancements occur.

Degradation, aggradation, and movement of sediment and other pollutants in watersheds and river systems are closely related to water movement. Streamflow and water routing models have received the most

intensive study. The ability of the majority of available streamflow and water routing models to relate wildland activities to their unique environments and to account for spatial diversity is not well demonstrated. A model that will predict effects of management activities and represent spatial and temporal variability of both activities and processes is needed.

Existing sediment models in watershed systems deal mainly with surface erosion. Process models for unstable channel erosion or models for predicting mass wasting and its interaction with channels are not yet available. Almost all existing surface erosion models are based on either the Musgrave approach or the Universal Soil Loss Equation (U.S. Forest Service, 1976). These models are difficult to use because they are insensitive to spatial and temporal variability of management activities. In 1975, Simons et al. (1975a) developed a numerical model to simulate physical processes governing sediment movement on small watersheds. The model can predict effects of management activities on sediment yield in both time and space. This model is being modified to accommodate unstable channel erosion and deposition, a more complex watershed system, and long-term simulation of response considering interstorm periods. In addition, for coupling the nitrogen, phosphorous, etc. movement with water and sediment, it has been modified to route the sediment according to sediment sizes (Li et al., 1977). This is necessary because different sizes of sediment have different uptake rates for different contaminants.

It is important to recognized that a river is a dynamic system. An alluvial river is generally continuously changing its position and shape as a consequence of hydraulic forces acting on its bed and banks and as a result of the interaction of these forces with the biological processes of the river environment. These changes may be slow or rapid and may result from natural events or from man's activities. When a river channel is modified locally, the change frequently causes modification of channel characteristics both up and downstream and can be propagated for long distances. Many available river routing models either neglect the dynamic response due to sediment movement or are insensitive to man's activities. In a parallel study completed at Colorado State University by Simons et al. (1975b) a one-dimensional water and sediment routing model was used to simulate dynamic response of river-bed elevation resulting from operation of locks and dams. Their model can be used to study the short- and long-term impacts of the effects of different operational schemes for locks and dams, the effects of pools on behavior and form of the tributary rivers, the impact of changes in water and sediment inflows on morphology of the river and adjacent lands, and the impacts of dredging and dredged material disposal on the hydraulic response and sedimentation in the channel.

In a recent study conducted by Simons et al. (1978b) for the U.S. Army Corps of Engineers, Vicksburg District, sedimentation problems of the Yazoo River Basin were investigated. This is a large and comprehensive mathematical modeling effort including about one-fourth of the State of Mississippi, 27 major rivers, four major reservoirs, and several smaller streams and reservoirs. In analyzing large river systems like the Yazoo, development of a data storage and retrieval system is imperative.

Sediment transport is one of the most important variables needed for evaluating erosion, sedimentation, and channel morphology. Capacity of a stream to transport sediment depends on hydraulic properties of the stream channel. Such variables as slope, roughness, channel geometry, discharge, velocity, turbulence, fluid properties, and size and gradation of the sediment are closely related to the hydraulic variables controlling the capacity of the stream to carry water, and are subject to mathematical analysis. Total sediment load of a stream is the sum of bed material load and wash load, or bed load and suspended load, or measured and unmeasured load.

Because bed material is transported as both suspended load and bed load the different physical laws governing these modes of transport must be incorporated into any method for predicting total transport of bed material. As implied by the definitions, the distinction between bed mateial load and wash load is of importance. Bed material is transported at the capacity of the stream and is functionally related to measurable hydraulic variables. Wash load is not usually transported at the capacity of the stream but depends instead on its availability and is not functionally related to hydraulic variables. While there is no clear demarcation between wash load and bed material load, one general guideline assumes that bed material load consists of sizes equal to or greater than 0.062 mm (division between sand and silt). Another reasonable criteria is to choose a sediment size finer than the smallest 10 percent of the bed material as the point of division between wash load and bed material load.

Sediment particles that constitute bed material load are transported either by rolling or sliding along the bed (bed load) or in suspension. Again, there is no sharp distinction between bed load and suspended load. A particle of the bed material load can move part of the time in contact with the bed and at other times be suspended by the flow. Generally, the amount of bed material moving in contact with the bed of a large sand bed river is only a small percentage of the bed material moving in suspension. These two modes of transport follow different physical laws which must be incorporated into any equation for estimating the bed material discharge of a river.

Limited quantities of fine material moving as wash load usually will not pose direct inhibiting development activities in the riverine environment. However, large concentrations of fine materials can influence the capacity of a stream to transport bed material through it influence on fluid properties such as viscosity and density, bank stability, growth of aquatic plants, the biomass of the channel, etc.

For a detailed treatment of currently used suspended and bed material load transport theories refer to Vanoni (1976) and Simons and Sentürk (1977). Data on sediment transport in steep channel systems is generally unavailable due to the difficulty associated with collecting data in the laboratory and field environments. Yet many streams in the upland watershed are steep and mountainous channels. Recently, Bathurst et al. (1979) reported a laboratory effort on sediment transport in steep channels with slopes ranging from one to twenty-five percent.

Hydraulic geometry is a general term applied to alluvial channels to denote relationships between discharge, the channel morpohology, hydraulics, and sediment transport. In self-formed alluvial channels, the morphologic, hydraulic, and sedimentation characteristics of the channel are determined by a large variety of factors. In general, these relations apply to channels within a physiographic region and can be derived from data available on gaged rivers. It is understood that hydraulic geometry relations express the integrated effect of all the hydraulic, hydrologic, meteorologic, and geologic variables in a drainage basin.

Geometric relations describing alluvial streams are necessary in river engineering and river modeling. Forerunners of such relations are the regime equations developed to design stable alluvial canals. A generalized version of hydraulic geometry relations was developed by Leopold and Maddock (1953) for different regions in the United States and for different types of rivers. Geometric relations are usually applied to provide an approximation of river response. In addition, Lane's geomorphic response relation stating that the product of the water discharge and slope is proportional to the product of the sediment discharge and the bed material size (Simons and Sentürk, 1977) is useful in qualitative analysis of river response. For a detailed description of current knowledge on river morphology refer to Schumm (1977) and Simons and Sentürk (1977).

## 3.3 PHYSICAL PROCESSES IMPORTANT TO THE ANALYSIS

Physical processes governing watershed and river response are complicated. Two primary inputs to the ecosystem are climatic inputs and man's activities. Climatic inputs include precipitation (rain or snow), solar radiation, air currents, and moisture. Man's activities important to watershed and river analysis include weather modification, urban development, watershed management, fire, energy resource acquisition, water resources development, land-use zoning, mining activites, water supply and irrigation, recreational development, development and operation of transportation systems, application of fertilizers, herbicides and pesticides, locks and dam construction and operation, river channelization, river training, transbasin water diversions, timber planting and harvesting, and grazing and browsing. Processes that govern responses from watersheds and rivers are numerous. Key physical processes are atmospheric, vegetative, ground surface, overland flow, mass wasting, stream, soil, and groundwater processes. Atmospheric processes deal with aerosolization, transport phenomena, diffusion, dispersion, convection, and particle dynamics. Vegetative processes include interception, evaporation, transpiration, nitrogen fixation, litter production, ground cover functions, plant succession, and thermal balance modulation. Ground surface processes account for infiltration, depression storage, evaporation, thermal balance, litter accumulation and decay, and raindrop splash soil erosion. The overland flow processes involve water flow routing (both surface and subsurface), sediment detachment and transport, pollutant absorption and transport, rill development and thermal diffusion. The mass wasting processes are important on watersheds having relatively unstable soil. They include mudflows, slides, debris, avalanches, stream bank failure, soil creep,

dry ravel, and soil piping. The stream and river processes are of great concern to both engineers and environmentalists, and are often referenced as principal indicators of the impacts of watershed and river basin development. They include water routing, sediment transport, gully development, degradation, aggradation, geomorphology, bank erosion, deltas and fan formulation, pollutant uptake and storage, pollutant transport, dissolved oxygen balance dissolved solids, and routing of forest litter and debris. The soil processes involve weathering, pollutant storage, nitrate reactions, pollutant adsorption, thermal balance, and water percolation. The groundwater processes include flow movement, pollutant transport, diffusion, dispersion, recharge, heat exchange, nitrogen and phosphorous transport, and dissolved oxygen.

It is important to consider that different variables and physical processes have varying degrees of importance, depending on the purpose of analysis and the size and characteristics of the particular watershed and river ecosystem being analyzed, including the types of climatic conditions, soils, geology, vegetative cover, land-use activities, and water and sediment inflows. In order to determine which of these variables and/or processes must be included in the analysis, it may be necessary to evaluate the importance of many variables and/or processes by sensitivity analyses.

Degradation, aggradation, and movement of pollutants are closely related to water and sediment movement. Therefore, understandng the physical processes related to water and sediment routing is of fundamental importance for effective analysis of watershed and river response. In spite of the complexity of problems involved in water and sediment routing in watershed and river ecosystems, the governing equations are the same. They are the continuity equation of water, the flow momentum equation, the continuity equation of sediment, the flow energy equation, and some supplementary equations such as flow resistance relations, channel geometry equations, and sediment supply equations. For a detailed discussion of governing physical processes refer to Chapter 2 or the paper by Simons, Ward and Li (1979).

## 3.4 CRITERIA OF USEFUL MATHEMATICAL MODELS

For all practical purposes, a useful mathematical model for predicting watershed and river system response to potential management actions should meet the following criteria:

1. Temporal resolution should be both short- and long-term. Management practices usually have both short- and long-term effects on our environment and short-term projects often have prolonged effects. Thus, temporal resolution should accommodate addressing both short- and long-term response questions.

2. Spatial resolution should be flexible. Specific management plans and activities are very often limited to small watersheds. Most watersheds subject to legal requirements for environmental quality and water resources management are quite

large and often encompass complete river basins or sub-basins. As a consequence, spatial resolution should accommodate both small watersheds and river systems as a whole.

3. The model should be widely applicable. That is, although the model parameters may be area or regionally specific, the model itself should not be area or regionally specific. The only feasible way to develop such a moel is to consider the physical based model can represent appropriate cause-effect relationships between management practices and ecosystem response in a general way.

4. The model should be sensitive to the desired management activities. That is, it must be possible to explicitly represent management activities and simulate system response resulting from these activities. For example, if grazing is a desired management activity for evaluating watershed response, then the model should be formulated to represent grazing activity through changing model parameters that could be altered according to grazing intensity.

5. Uncertainties due to varying climatic and spatial input should be considered. That is, simulation must consider variations in both mean values and extreme events. This requires a probabilistic approach to describe the stochastic structure of model inputs.

6. The model should be developed within the constraints of available data. Models intended for practical application should not have requirements for data that are excessively difficult, costly, or time consuming to collect or acquire. If a large quantity of data is required, an effective data storage and retrieval system is necessary.

7. The model should be oriented for use by management personnel. Perspective of the user must be foremost in all model development work. Models intended for use by managers mut readily fit into specific decision-making processes and situations for which they are to be employed, if information resources are to be generated efficiently and used effectively. Therefore, in order for usable models to be designed and implemented, developers must be in effective communication with target users throughout the develpment process. Involving users in model design helps insure that the researcher has full knowledge of the decision-making environment, the actual problems managers face, and the user's perception of the situation being modeled. The model will thereby be more relevant and the user will better trust its validity and capabilities.

8. The model should be easily transformed for use at several levels of accuracy and resolution. Models operable at several levels of accuracy and resolution will be required in order to provide the full range of tools needed for land and river

management. Providing usable and realistic models and guidelines for professionals operating in the field in many cases will first require developing and testing relatively complex process models. Once the processes involved are thoroughly understood and sensitive parameters identified, these models can then be regionalized and generalized to provide simplified models and guidelines for field users.

9. The model computer software system should be developed in a modular fashion. Experience has shown that nonmodular all-purpose models are expensive to develop, difficult to use and control, and have large data requirements--all of which tend to detract from their field usability. Adopting the modular approach offers an opportunity to build a coordinated nucleus of standardized system components for use in analyzing a wide spectrum of watershed and river systems. This nucleus would be made up of components that provide common storage and retrieval, analysis, and display. Modular systems also have the advantage that individual components can be updated or replaced as needed without disrupting other components of the system.

10. Full model documentation is an important obligation in providing a useful and viable tool. The documentation should include not only the formulation theory, system flow charts, computer code, and test results but also sufficient examples, guidelines, and precautions for users to implement and correctly use the model.

## 3.5 PROCEDURAL STEPS FOR MODEL DEVELOPMENT

Development of a model for analysis usually involves spatial design, temporal design, model formulation, mathematical solution, model calibration, parameter sensitivity analysis, qualitative examination of physical significance, model simplification, regionalization and generalization, validation, testing and refinement under operational field applications, and documentation.

Spatial and temporal designs of a simulation model are important to a realistic representative of the time-space structure of a watershed or river system. For example, designing a realistic space structure for the hydrologic analysis of small watersheds would involve devising a systematic means for either manual or computer-aided determination of hydrologic response units as a function of such attributes as watershed geometry, topography, vegetation distribution, soil distribution, and the like. A computer program for automatically segmenting a watershed and grouping segments into desired response units was developed by Simons and Li (1975). At the time of applying the model in a specific situation, general spatial and temporal designs must explicitly fit the watershed or basin being studied in accordance with the purpose of the analysis. For example, spatial design of a large river basin would have to consider the nature and location of the river and its tributaries, and the location of all pertinent gaging stations, structures, and confluences. The explicit temporal design would be made using the historic hydrologic record of the basin. This record might include

historic maximum, minimum and mean precipitation, temperature, moisture contents and water flows, river stages, precipitation patterns, flow volumes, and the effect of man's activities such as reservoir construction on the hydrologic record. Temporal design is then used to generate the system input for evaluating explicit response of the future system.

After spatial and temporal designs are completed, major physical processes governing the system response can be identified. Then a series of mathematical equations can be assembled to represent the governing processes, constituting the conceptual formulation of the model. Model formulation should be guided by the criteria of a useful mathematical model presented earlier. Successful model formulation requires a blend of theoretical and practical considerations, as the following discussion illustrates.

For simulating dynamic response of water and river systems, perhaps the most important governing equations include the continuity equation for water, the continuity equation for sediment, and the momentum equation (or the energy equation). These three equations can be solved simultaneously or can be approximated by solving the water continuity equation and the momentum equation first and then refined by using the sediment continuity equation. The second approach is usually applicable because the movement of sediment is much slower than that of water. Numerical solution of these three equations can proceed in two directions. Either an attempt can be made to convert the original system of partial differential equations into an equivalent system of ordinary differential equations by using the method of characteristics or one can replace the partial derivatives in the original system with quotients of finite-differences by using the explicit method or the implicit method.

For the flood routing problem, precise values of the parameters describing flow resistance are usually unknown, but the ranges are determined from measured data. However, to pinpoint parameter values that produce the best model response, model calibration is necessary. The simplest calibration technique is the trial and error method. But except for methods that contain parameters with very narrow searching ranges the trial and error procedure is inefficient. Therefore, in the mathematical modeling of system responses, calibration of model parameters often relies on an optimization scheme. There are many optimization techniques available for the purpose of model calibration. However, usefulness of a particular optimization technique is dependent on formulation of the model being calibrated. For hydrologic model calibration Rosenbrock's (1960) optimization technique for finding the optimum set of parameters has proven to be the most promising and efficient method.

After development, the sensitivity of model outputs to changes in each model parameter should be examined. Sensitivity analysis facilitates model parameter calibration, identifies data needs, and provides useful information for model simplification. Another important examination is to evaluate the model qualitatively using physical significance as a guide. At this stage, trends and extremes simulated by the need to model are examined to assure that they are meaningful considering physical significance and field experience.

Simplification is directed toward developing widespread applications of methods derived from the more complicated process simulation models. In general, the more complicated models explicitly deal with time and space, solving finite difference formulations of the various processes at each time-space point. The simplified model retreats from this approach and averages the processes over both time and space. While the more complex model usually provides the better solution, its main disadvantage is that often it is relatively expensive to use and requires knowledge of computer applications and mathematical formulations and assumptions that are often beyond the capability of the average field user. Limitations of regression type or "black box" models and user restrictions imposed by the more complex physical process models have necessitated development of simpliied physical process component models. Such simplified models can provide the field user with an easy to use, yet reliable methodology for estimating system response (Simons et al., 1977a).

In order to further facilitate application of the model, model parameters may also be regionalized. This can be achieved by extensive application of the model in a particular geographical area, leading to a generalized regional version of the model. An example of regionalization and generalization is given by the Agricultural Research Service (1975).

Model testing, evaluation, refinement, and documentation are continuous processes. As more field data becomes available, the model can be improved so that more accurate predictions are possible.

## 3.6 OVERVIEW OF SOME CASE STUDIES

### General

The following describes several case histories that illustrate the complexity of water and river systems, the associated development and utilization of mathematical modeling techniques to achieve improved planning, analysis, and design.

### Variation of a Canal Cross Section with Time

A canal was constructed to carry a discharge of approximately 2,000 cu ft per second. The canal cross section was approximately 80 ft wide and had an average depth of approximately 10 ft. The side slopes were originally constructed at 1½:1 (Figure 3-2). The segment of this particular canal was constructed through a sand hill area so the bank material is very erodible. When a canal is constructed with banks consisting of such material, large width-to-depth ratios result as the channel adjusts. This can be illustrated by comparing wetted perimeter with discharge relationships for channels with different types of bank materials ranging from highly erodible sands that will yield wide channels to cohesive materials that tend to resist erosion and may be quite narrow. When flow was introduced into this sand bank channel, rapid erosion of the banks occurred. This caused the channel to widen from 80 ft to a width on the order of 150-200 ft. There was a corresponding reduction in depth. Widening of the channel encroached on the

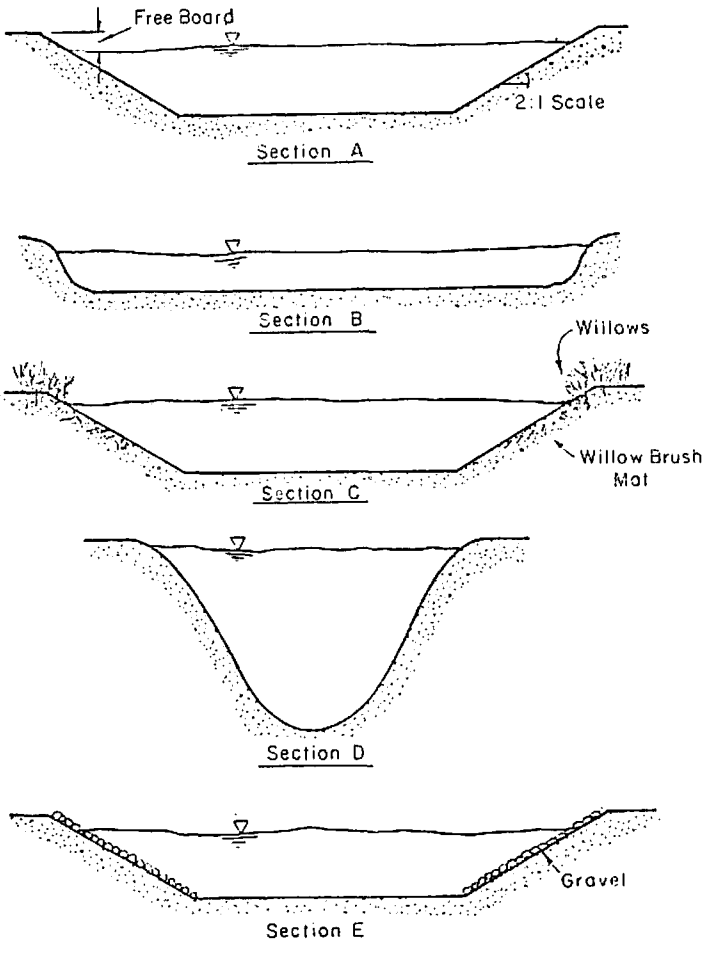


A. Original channel constructed in sand hills area

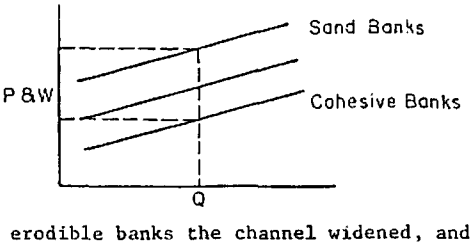


B. With sandy erodible banks the channel widened, and encroached on the right-of-way.

C. Channel was reconstructed to its original dimensions. A willow brush mat was placed on the bank and willows were planted.

D. Willow growth developed rapidly, the banks were reinforced with roots extending into the flow. The roots slowed the local velocity and trapped fine sediment particles that were being carried in suspension. The deposition of fine sediment caused the canal to develop a narrow and deep cross section which restricted the flow causing a backwater upstream that reduced freeboard and caused local flooding.

E. The channel was once more reconstructed to its original dimensions and the banks were riprapped with local river gravel. The gravel armor has done an excellent job of stabilizing the channel cross section. The Lane, Simons, Shields, etc. methods can be used to determine the size, gradation and thickness of gravel blankets to stabilize the channel and river banks, and reduce the supply of sediment downstream.

Figure 3-2. Variation of a channel cross section with time.

right-of-way and introduced numerous other problems. Hence, it was decided to reconstruct the canal cross section to its original dimensions and stabilize the banks into that position, using willow mattresses. At the same time the growth of willows in the banks was encouraged. Willow growth developed rapidly. Roots from the willows extended into the flow. The roots from the willows slowed the local velocity and trapped fine sediments consisting of silts and clays that were transported in the flow. The result was deposition of fine sediments on the banks. As deposition occurred, the root system continued to extend itself from there into the channel. The net result was the development of a very narrow, deep channel that restricted the flow to such an extent that backwater effects caused serious encroachment on the freeboard and the canal upstream. In some instances, the backwater caused overflow and bank failure. Therefore, it was decided to reconstruct the canal once more to its original dimensions. This was done and the banks were riprapped with local river gravel to provide protection from erosion of the flowing water. The gravel armor has done an excellent job of stabilizing the canal cross section. Furthermore, the water losses introduced by extensive growths of vegetation along the bank line have been eliminated. This type of problem can be easily handled in terms of designing the size of riprap required. Reference can be made to Simons and Sentürk (1977) that outlines the Lane method and other methods including those recently developed at Colorado State University to determine the size, gradation, and thickness of gravel bank cuts required to stabilize such systems.

The importance of the effects of silts and clays, or wash load on river and canal geometry cannot be over-emphasized. In the early 1900's when irrigation systems were being developed in the Imperial Valley of California water diverted from the Colorado River to these systems carried large quantities of wash load. Channels were sized according to current engineering knowledge but the concentrations of silts and clays in the flowing water diverted to the canals was such that berming occurred in the canals. The berms consists of materials that held water well, were fairly fertile, and encouraged rapid growth of vegetation and grasses. As in the foregoing case, the channel narrowed dramatically with time as a consequence of the growth of vegetation at the water line, extension of roots into the water, and trapping of fine sediments. In some instances these channels became almost pipe-like. The berms would grow out over the flowing water partly covering the channel. This change in channel geometry constricted the water cross section and increased the resistance to flow. Hence, it was necessary to regularly restore these channels to their original dimensions in order for them to convey the required quantities of water to the irrigation system.

In subsequent years there has been a rapid development of large storage facilities on the Colorado River. More and more of the sediments that normally flowed downstream are now trapped in upstream reservoirs. As a consequence, the irrigation system alluded to that originally received large quantities of silts and clays with the water diverted to it no longer does so. In fact, upstream reservoirs trap the majority of the sediments and most of these canal systems now operate with almost a clear water environment. That is, the water diverted from the river system and its reservoirs is largely free of sediment. This

change in the quality of the water brought about by upstream storage and control caused the reverse of the situation to occur in these canals. With the removal of silts and clays the water entering the canals had an opportunity to attack the banks and bed, eroding them. Where the materials were sufficiently erodible, the channels widened, depths reduced, and another set of adverse conditions developed. In this case it was possible to reconstruct these canals to desirable dimensions and armor them with properly sized gravel or riprap. This type of protection has very effectively held the channels in the desired location with the desired cross-sectional dimensions. Again, design of stabilization works for such systems can be handled as was cited above.

To further illustrate the possible effects of silts and clays on channel geometry, let us refer to a river system in the western United States that up until the early 1900's carried relatively large quantities of silts and clays during periods of high flow while the channel was actively changing form. At that particular time the channel was relatively stable, there was vigorous growth of vegetation on bars and on the bank line, and for a significant part of the year the channel was reasonably stable. Major channel changes only occurred during major flow events. In the early 1900's a major earthquake in the area caused a large landslide to form a dam of considerable size across the river valley. This results in a lake. The lake is of sufficient size that it has essentially removed the silts and clays that normally flow in the river at high stages. In the absence of silts and clays downstream, durin hig flow events the banks and bars were attacked and new bars were formed, but these new bars and bank lines had little silts and clays in them as a consequence of the desilting upstream and they were unable to hold moisture for a sufficiently long period to allow the growth of vegetation. Consequently, in recent decades the bank lines have changed, new bank lines have formed, but without silts and clays in the newly deposited material, and no new vegetation has been able to grow. The end result has been the elimination of a significant amount of riparian vegetation along the stream line, greatly reducing the beauty of the stream system and in many ways deteriorating it from the viewpoint of recreational use, fisheries habitat, etc. Once again, the potential for change exists when the wash load concentrations flowing in either canals or rivers are altered.

As a final example of the importance of wash loads on river and canal morphology, a study was conducted by Colorado State University in Venezuela that extended over a period of years. This study dealt primarily with the geomorphology and hydraulics of rivers and the relationship of these river systems to the watersheds. Vegetation developed and grew along certain segments of the bank line and floodplain. In other sections or locations vegetation sometimes started growing but died before a root system could be developed due to an inadequate supply of water and nutrients. Conducting extensive soil sampling along the banks and in the floodplains of these rivers showed that in every case where a substantial growth of vegetation was occurring, there was a significant percentage of silts and clays. Hence, where a river system experiences natural cutoffs that subsequently fill with finer sediments, an environment is developed that can support rapid and vigorous growth of vegetation. In those segments of the floodplain that consist largely of gravels and sands, the area drains so rapidly that significant vegetation usually does not develop.

Degradation Analysis of a Small Dam

There are many small dams that are built for a single purpose including flood control, low head hydropower generation, erosion control, irrigation, etc. The major impacts include aggradation in the upstream and degradation (local scour and general scour) in the downstream reach (Figure 3-3). Baffled chute spillways are often utilized as the emergency spillways for these small dams to dissipate the energy associated with the design of freeboard discharge. The required analysis involves the determination of the magnitude of degradation to be expected downstream from the emergency spillway chute during passage of the design hydrograph. Such an analysis is required to determine how far the baffled outlet end of the chute must extend below the present channel grade. In order to provide enough information for adequate design, different conditions that depict future water and sediment inflows to the dam prior to the occurrence of the design hydrograph are required. Examples of cases that could be considered follow.

Case I considers that the reservoir is 90 percent filled with sediment resulting from a series of small floods, prior to the occurrence of the design hydrograph. These small floods pass all of the flow through the principal spillway. Degradation due to the design hydrograph would be neglibile and the total expected scour depth below the structure is equal to the general scour depth resulting from the flows through the principal spillway. Case II assumes that immediately following closure of the dam water storage has reached the top of the dam and the sediment storage capacity has enough room for the sediment yield associated with the design hydrograph. Under this condition, the emergency spillway chute would pass the freeboard hydrograph with essentially clear water. This is because nearly all of the sediment will be trapped upstream of the dam. The third condition, Case III may represent the worst possible condition which assumes that after a long period of operation, two 50-year floods and one 100-year flood occur prior to the passing of the design hydrograph. The total expected scour is the sum of the general scour due to flows through the principal spillway for a long period of operation and the general and local scour resulting from a sequence of two 50-year floods, one 100-year flood, and the freeboard hydrograph. This condition is very unlikely to occur yet constitutes the worst possible condition in determining the degradation below the emergency spillway structure. Determination of the change in sediment storage is vital for the evaluation of both Cases I and III. This requires the estimation of the annual sediment yield and sediment yields resulting from various sizes of storms from the watershed. The magnitude of scour can be determined utilizing a sediment routing procedure and considering the size fractions of bed material. This computational procedure will involve use of a sediment transport equation, the sediment continuity equation, the armoring effect of coarse materials, and the channel geometry equation. Figure 3-4 shows the time-lapse change of local and general scour for Case II. The local scour depth defined in this study is measured from the present bed level. This local scour depth represents a combination of general scour and local scour according to established definitions. In order to check applicability of the mathematical model, a large scale physical model (1:30)

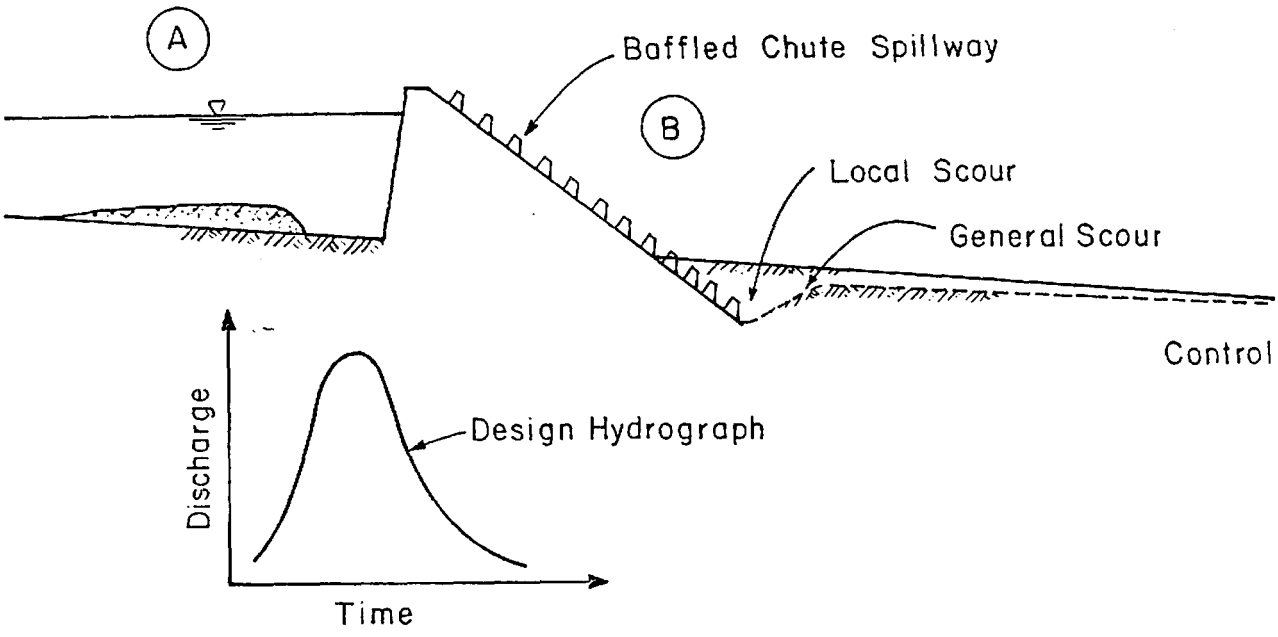


A. Major upstream effects of small reservoir

   1. Aggradation

   2. Decreased capacity

B. Major downstream effects of small reservoir

   1. Degradation (local scour and general scour)

   2. Bank erosion

Figure 3-3. Impact of construction of a small dam.

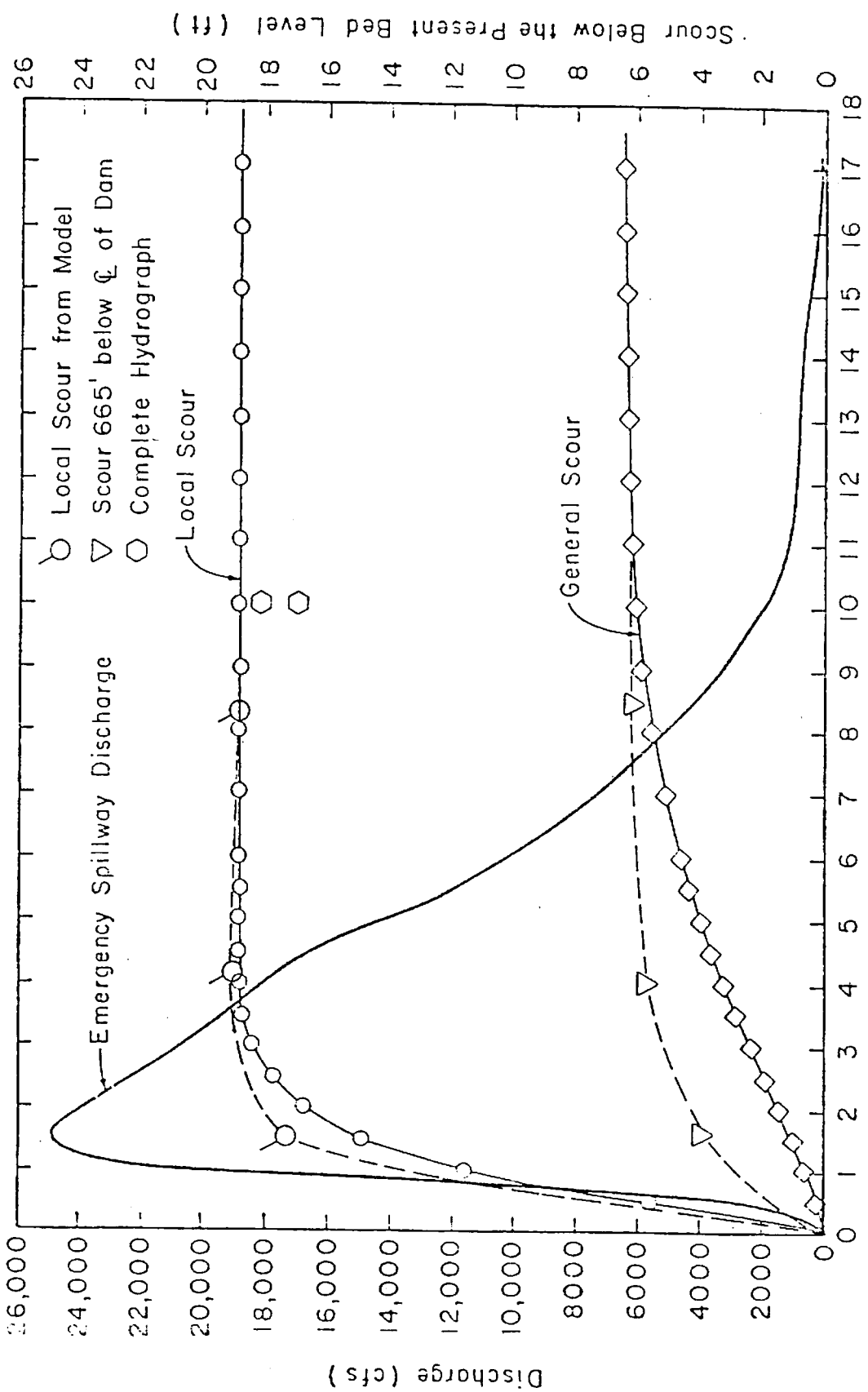


Figure 3-4. Local and general scour with the existing downstream control (6970 ft from the structure).

was utilized by a federal agency to estimate local and general scour for the design freeboard hydrograph. Results from both totally independent model approaches were extremely close, demonstrating a successful application of the technology of routing sediment by size fractions.

## Gravel Mining Impact in Streams

Gravels are important natural resources that are required for construction. As population grows, acquisition of gravels is steadily increasing. Removal of gravels from streams may induce either positive or negative impacts on the stability of stream morphology. Unwise gravel mining activities often result in significant adverse impacts on the river environment. Figure 3-5 illustrates such a case history. Since 1969 a gravel mining company has excavated approximately 6,500,000 tons of gravel and sand in the San Juan Creek, Orange County, California. This gravel and sand mining activity resulted in a vertical cut of approximately 55 ft of the stream bed near the Casper regional park before the end of 1977. Three storms in early 1978 induced a series of significant stream morphology changes. Measured profiles before and after each of the storms are plotted in Figure 3-5. The deepest erosion depth was about 30 ft and extended approximately 3,500 ft upstream of the park boundary. The time lapse changes of elevation at the original gravel pit boundary (Station 16+00) is given in Figure 3-6. Simulation results are excellent when compared with field measurements. One point worth mentioning is that the simulated results of the 1978 storms were predicted utilizing the calibrated sediment transport parameters based on the data from two 1969 storms. A major effort to rehabilitate the Casper park was required. In order to evaluate various alternatives, a mathematical model for routing sediment by size fraction was developed and utilized. Four engineering alternatives were evaluated. Alternative I is a "do nothing" plan terminating the mining of sand and gravel. This alternative would allow natural healing processes in the form of aggradation to take place. No mitigation measure would be imposed on the existing stream. Alternative II is essentially the same as Alternative I except it permits regular mining of sand and gravel. Alternative III proposes construction of a drop structure located near the upstream end of the gravel pit. Alternative IV proposes construction of a series of small gabion check dams near and upstream of the gravel pit boundary coupled with regular gravel mining.

## Removal of Dams from River Systems

Many dams are in existence in the United States and the world. The removal of dams from river systems happens from time to time either by man or by other causes such as natural disasters. Potential impacts on the downstream reach caused by the removal of a dam are illustrated in Figure 3-7. Impacts resulting from a released wave of sediment include: 1) sediment migrates downstream, 2) conversion of gravel bed stream to sand bed stream, and 3) the sand wave will form sand bars, dunes, etc. that may increase or decrease resistance to flow, velocity, sediment transport, stage, flood, etc. A careful environmental impact analysis is often required to assess the short- and long-term effects of the downstream system. Movement of a sand wave through a river system as results from removal of a dam is a complicated problem. This problem

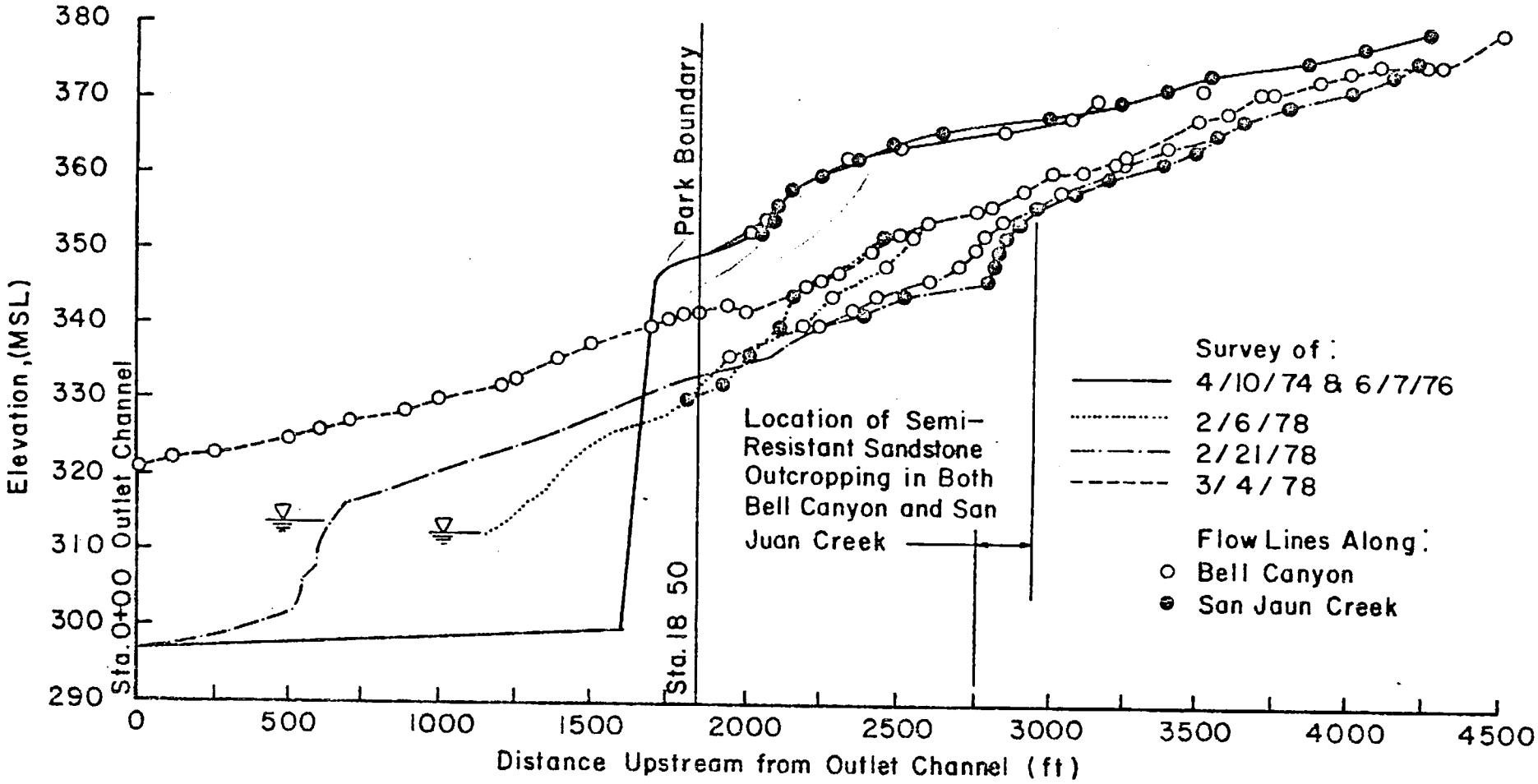


Figure 3-5. Measured bed profiles.

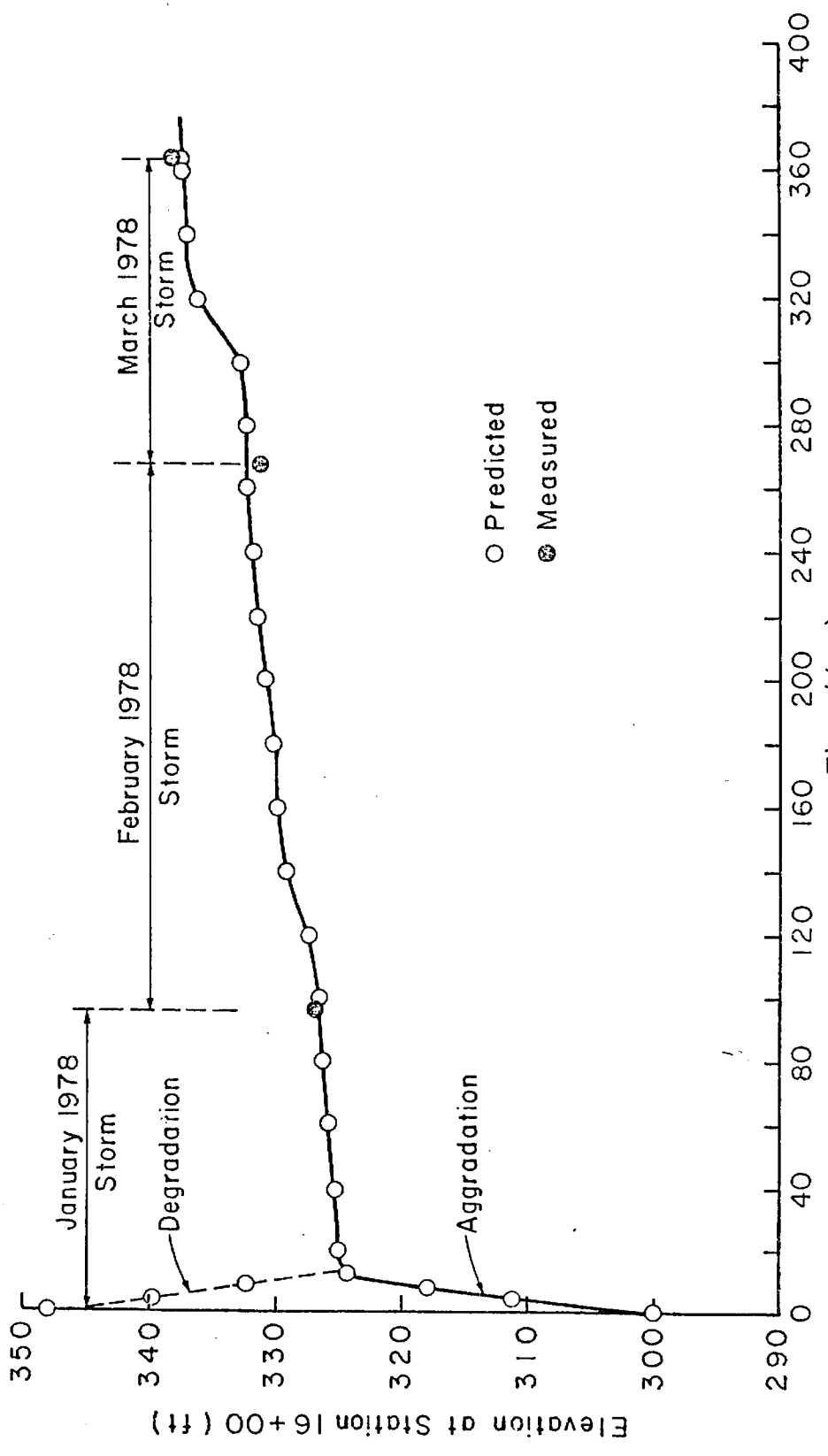


Figure 3-6. Time lapse changes of elevation at the original gravel pit boundary (Station 16+00).

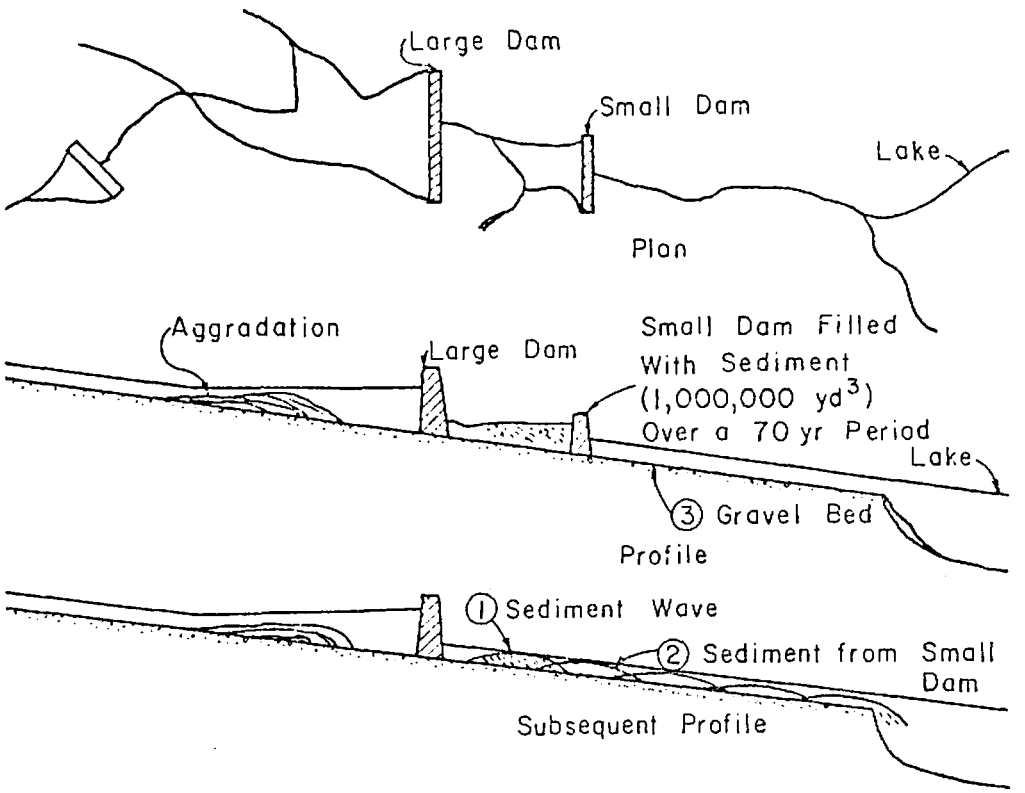


1. Released wave of sediment (1,000,000 $yd^3$)

2. Sediment wave moved downstream

3. Converted gravel bed stream to sand bed stream

4. The sand wave will form sand bars, dunes, etc. that may increase or decrease resistance to flow, velocity, sediment transport, stage, flooding, etc.

5. It is necessary to eliminate the rate at which the wave of sediment will move downstream and what will be the short- and long-term effects?

Figure 3-7. Response of river to removal of small dam.

includes the rate of sand wave movement, degradation upstream of the old dam site, deposition of the material along the upstream channel, possible changes in water surface elevations and velocities, and possible effects on the channel stability and flood potential. Simple but realistic assumptions are needed to obtain a solution to this problem in a practical and economical way. Dominant physical processes considered in the analysis should include: flow of water, sediment transport, sediment routing, degradation, aggradation, and bed control due to the presence of an armor layer at small to intermediate discharges. The governing equations include the continuity equations for water and sediment, momentum equation, and energy equation. Processes governing water and sediment movement are unsteady in nature, therefore a routing procedure is needed. In order to simplify the problem, a known discharge assumption can be used if the study reach is not too long and the primary objective of analysis is to analyze the movement of sand waves.

Flood Hydrograph from a Watershed with a Series of Cascade Sub-basins

Most of the conventional methods for determining the flood hydrographs from watersheds are based on the average basin characteristics. Resulting hydrographs usually are nearly symmetrical in shape and fairly short in duration (Figure 3-8b). An inspection of the basin characteristics including shape and topography (Figure 3-8a) will suggest that the hydrograph shape is questionable. Topography of the watershed should be approximated by a series of cascade sub-basins when a large variation of slopes exists. The multiple watershed model would yield a more reasonable hydrograph shape similar to Figure 3-8c. When determining a probable maximum flood, a large discrepancy can result between these two approaches.

Flow Around a Sharp Bend

Because of restriction due to space and other reasons, it is sometimes necessary to divert a large flow around a sharp bend with a short radius. Figure 3-9 introduces a system of sharp bends with breaking bed slopes. If the design flow is large, such as a probable maximum flood, hydraulic design is difficult. To assess adequacy of the system shown in Figure 3-9, it is necessary to evaluate the hydraulic characteristics, hydraulic performance, and stability of the system. Major hydraulic considerations require determination of: 1) depth of flow, 2) velocity of the flow, 3) regime of flow, 4) superelevation of the water surface in the bend, 5) the depth of aggradation near the bend, 6) the increase in depth of flow caused by separation in the bend, and 7) riprap requirements along the bend.

Depth of flow and velocity can be determined utilizing the slope of the system and a proper Manning's resistance coefficient. With this system the stream power (the product of average velocity and boundary shear stress) will be sufficiently large that the flow will be in upper regime with antidunes. These antidunes occur in the form of unstable surface waves that have a maximum amplitude approximately equal to the depth of flow. As the water and sediment traverse the bend, the water is superelevated on the outside of the channel. The channel will carry

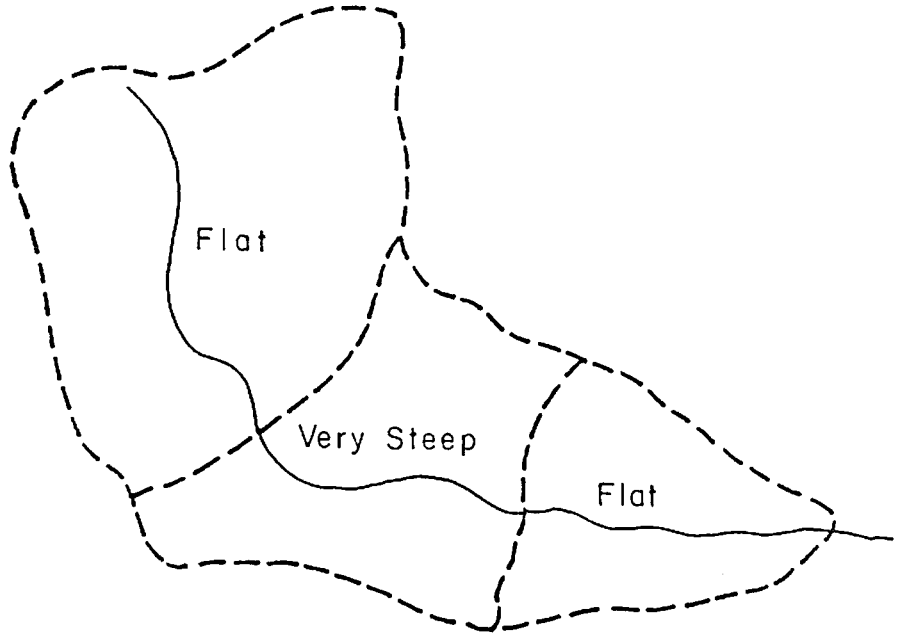


(a) Basin Map

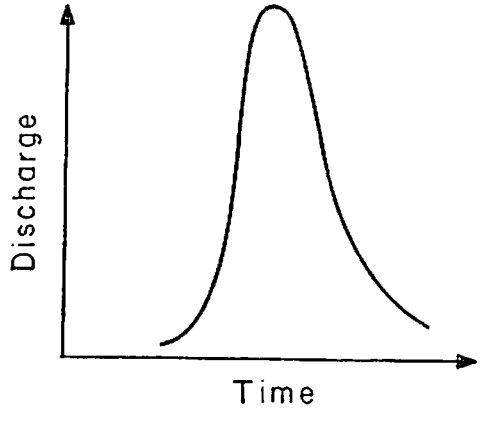


(b) Hydrograph Utilizing Average Basin Characteristics

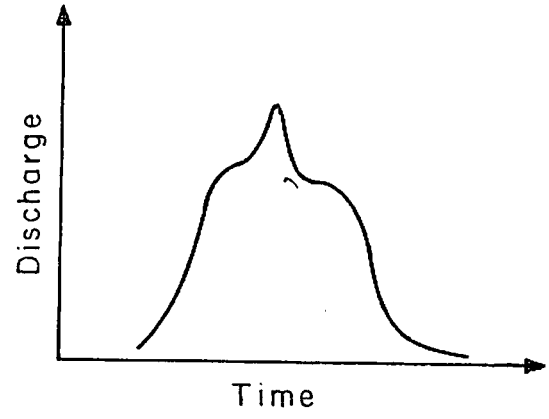


(c) Hydrograph Considering Cascade Sub-basins

Figure 3-8. Flood hydrographs.

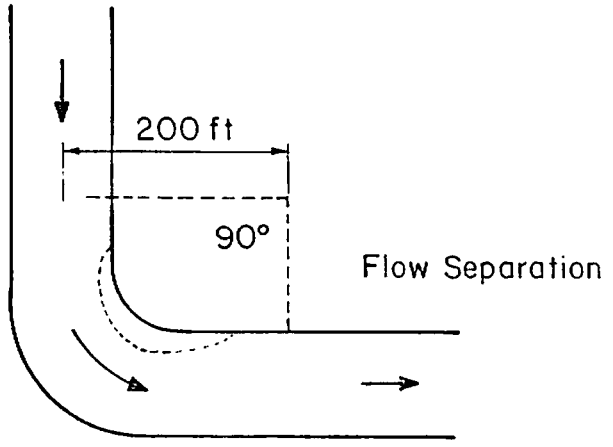


(a) Plan View

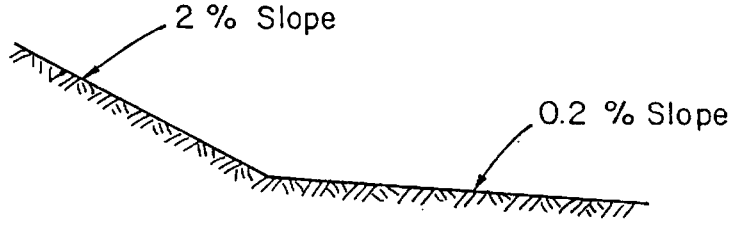


(b) Bed Profile

Figure 3-9. Flow around a bend with breaking slopes.

both water and sediment and because of nonuniformity of sediment transport caused by variations in channel slope and cross-sectional geometry, it will experience local aggradation and degradation which will affect the channel's capacity to transport water and sediment. Also, the high velocity flow will cause separation of the flow from the boundary resulting in a reduction in the effective cross-sectional area, deposition of a point bar, and an increase in depth of flow. Relatively large bed materal load and variation in the sediment transporting capacity of each element of the system will induce local aggradation and degradation until the system adjusts to a new equilibrium.

Flow Diversion Problems

Flow diversion problems frequently occur in the urbanized areas. Flow diversion would cause unbalanced sediment distribution in the channel system that may result in aggradation in some reaches and degradation in other reaches. Figure 3-10 illustrates an example of potential problems. If the degree of urbanization is increased, more serious problems associated with degradation, aggradation, and channel bank erosion will be introduced. The flood protection project for the school would be evaluated according to short- and long-term response of the system.

Evaluation of Data Collection Program

Data is the key element for monitoring and studying the system response of a watershed or river. Increasing use of mathematical models for evaluatng proposed land use practices has verified the necessity of obtaining good sets of data for development, modification, calibration, verification, sensitivity analysis, and successful application of models. Unfortunately, many existing data sets are neither accurate nor adequate for detailed system analysis utilizing mathematical models. When a data collection network has been improperly designed and operated it often provides inaccurate and inadequate information that is neither spatially or temporally consistent. In other situations data is collected that is unnecessary considering the purposes of study. In addition poor data sets are not usually identified, resulting in a waste of considerable time and effort in their collection and analysis. It is very important that a clearly-defined methodology be developed for evaluating and/or designing data monitoring and collection programs of existing and proposed data collection networks. With an adequate data collection, evaluation, and design scheme it is possible to efficiently and economically collect useful data. There are many cases in which hydrologists or hydraulic engineers are requested to evaluate a specific data collection program.

The data collection methodology adopted should be dependent on type of data required, frequency and accuracy of sampling, manpower requirement, and economic constraints. Measurements can be automatic or man-operated depending on instruments. For evaluating and/or designing a data collection program, spatial and temporal designs of the data collection program, spatial and temporal designs of the data collection network are the most important items. For example typical questions are: How many gaging stations are required?, Where should they be

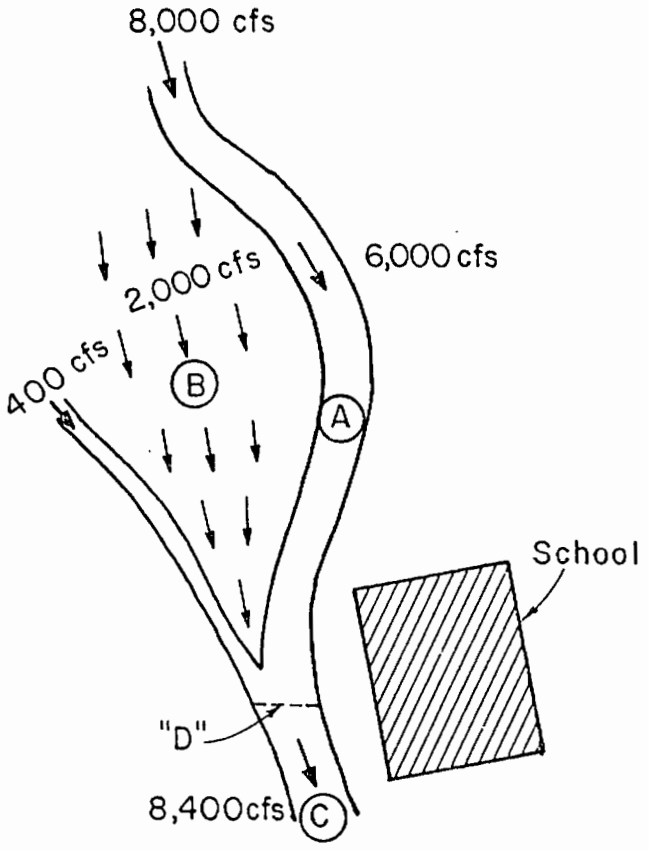


A. Reach above "D"

   1. Aggradation

   2. Increase stage

B. Flow diversion area

   1. Aggradation or degradation depending on physical environment

   2. Aggradation if highly urbanized

C. Reach below "D"

   1. Degradation

   2. Bank erosion

Figure 3-10. Flow diversion problems.

located?, When should they be operated? Adequacy of spatial and temporal designs is dependent on the purpose of the study, spatial and temporal variability of a physical environment, and desired accuracy of analysis. A systematic approach to the solution of this problem should be developed. This approach will include identification of the problems, survey and evaluation of the current data base, application of available mathematical models to determine sensitivity and hence the importance of each element of data and to evaluate the adequacy of spatial and temporal designs of the data collection program. Often available data do not adequately describe spatial and temporal variations in the system. Application of physical process simulation models calibrated by utilizing available data to generate the spatial and temporal variations is the most feasible way to examine the temporal and spatial data requirements.

Bunay-Barry Canal Design

A general layout of the Wadi Canal system, Yemen Arab Republic is given in Figure 3-11. Because the canal system intakes water from the river draining a steep watershed in the arid area, problems encountered in the Wadi Canal system are unique in many respects compared to usual canal design problems. Unsteady input of water and sediment to the canals, high sediment load of the Wadi, and heterogeneous distribution of bed and transported material all contribute to the complexity of the problems involved.

Source of water for the canals is the flood flows of the Wadi Zabid which fluctuates to a great extent considering both the discharge and the sediment. In the past water has been diverted by a temporary earth dike constructed across the Wadi. When a large flow occurred in the Wadi, the dike was destroyed and it was usually impossible to rebuild the dike until the next dry season. Concrete diversion weirs are being constructed to command the remodeled canal system. The canal should be designed either to transport the sediment through it or to have both stable banks and bed for the design discharge. If the primary objective is to transport sediment inflow, the canal design bed slope must be fairly steep since the banks would erode unless stabilized. Conversely, if the primary objective of the design is to have both stable banks and bed, design of the bed slope must be flatter. This would greatly reduce the capability of the canal to transport any measurable bed material load. This design alternative would be attractive if the sediment concentration in the water supplied to the canal was relatively small.

Impact of Construction of a Large Dam on a River System Upstream of a Diversion to an Irrigated Area

A particular river system and its watershed was of such a nature that during most of the year the water flowing in the river channel carried significant percentages of fine sediments comprised of silts and clays. An irrigation system was developed that diverted water from this river long before there was any construction of dams upstream of the diversion structure (Figure 3-12). The main canal diverts water from the river system to the irrigated area at a diversion structure. Thereafter, it flows around the side hill comprised of rather permeable

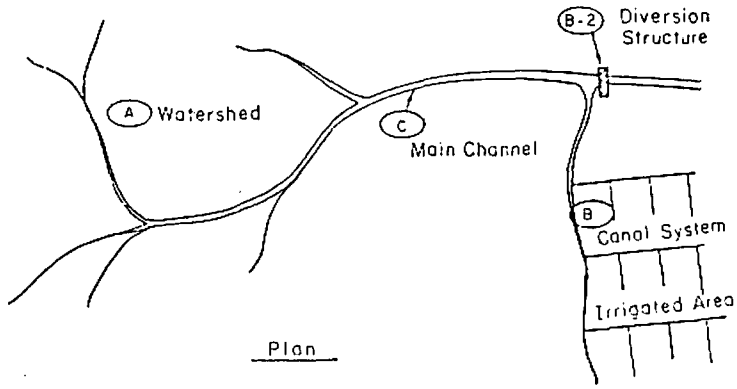


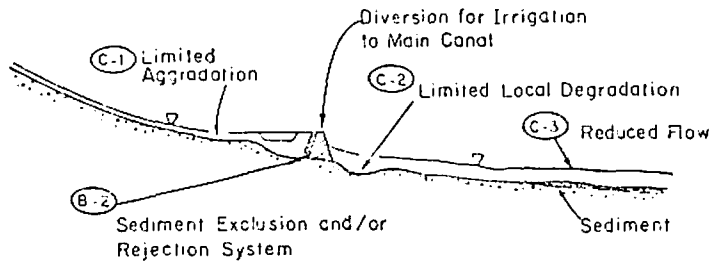


Profile

A. Watershed Characteristics

1. Steep slopes
2. Small flows
3. Large velocities
4. Relatively coarse bed and bank materials
5. Large sediment transport rates

B. Canal System Characteristics

1. Designed to operate on a flat gradient to assure stability of banks and beds of the canal system
2. Sediment delivered to the canal system has been reduced by use of sediment excluders at the diversion dam. Even so, it is difficult to reduce the sediment load to the point where the canal system can carry the sediment without depositing part of it in the canals, laterals, ditches, etc.

C. Effect on Main Channel

1. Limited aggradation upstream of diversion dam
2. Limited local degradation downstream of diversion dam
3. Downstream flow reduced due to diversion for irrigation. This reach will receive more sediment than it normally would from upstream, after the small reservoir upstream of the diversion dam is filled with sediment. Hence, significant aggradation may occur over time downstream of the diversion structure.

Conclusion

In this type of system it is virtually impossible to design a system that will not experience aggradation and require maintenance. However, with a detailed analysis of the systems the problems can be minimized.

Figure 3-11. Watershed, river and irrigation systems.

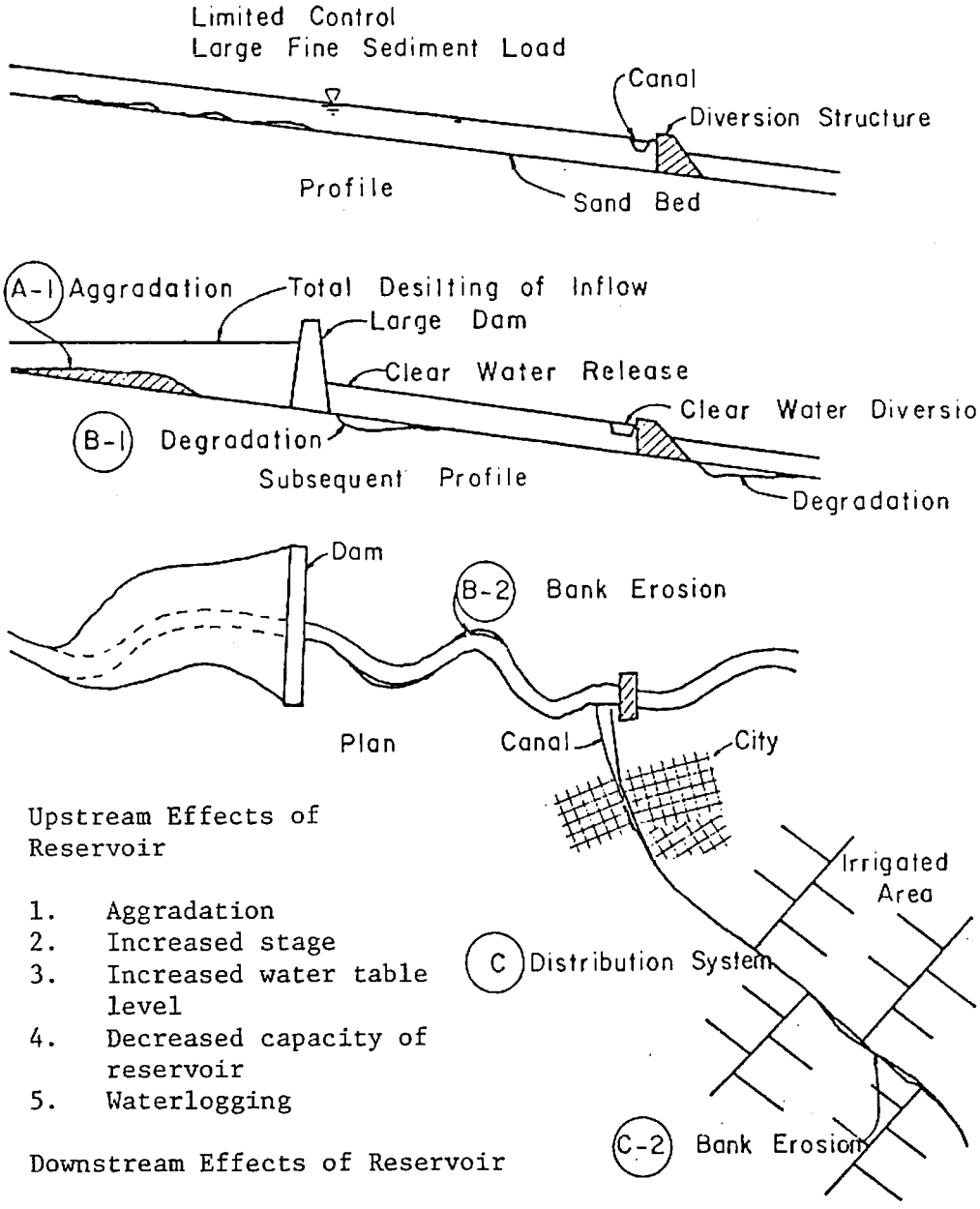


A. Upstream Effects of Reservoir

1. Aggradation
2. Increased stage
3. Increased water table level
4. Decreased capacity of reservoir
5. Waterlogging

B. Downstream Effects of Reservoir

1. Degradation
2. Bank erosion

C. Effects on Distribution System

1. Degradation
2. Bank erosion
3. Increase seepage losses
4. Growth of aquatic plants
5. Reduce efficiency of irrigation system requiring redesign

Figure 3-12. Impact of construction of a large dam on a river system upstream of a diversion to an irrigated area.

materials including sands and gravels, passes through a city area where there is relatively dense development along both sides of the channel, and then continues downstream to serve the distant irrigated area.

Recently, a large storage dam was constructed on a river immediately upstream of the diversion structure that serves the irrigation system. The reservoir is in effect a desilting basin, and water released from there is essentially clear. This clear water released from the dam flows down the short reach of river channel and is then diverted by means of the diversion dam to the irrigation canal. This release of clear water may cause some degradation immediately downstream of the dam as one would anticipate. Then the essentially clear water enters the canal. There has been some degradation in the main channel and bank erosion that has exposed more permeable bed and bank materials. This has increased seepage losses. There are several major detrimental factors as a consequence of the increased seepage from the canal.

1. A significant decrease in the amount of water that can be delivered to the farm units for irrigation.

2. The seepage from the canal system has the potential to cause a rise in the water table. The increase in the level of the water table may cause extensive damage to adjacent buildings by filling the basement levels with water.

There are, of course, other potentially detrimental factors that can adversely affect the irrigation system. For example, with clear water in the canal system it will be an ideal environment for the growth of aquatic plants. With these plants choking the channels, there will be added water losses and it will be difficult to convey the water required to the irrigation systems. Therefore, some type of periodic treatment will be required to keep the channels free of vegetation. There is another important issue on the farm units. Where land has been irrigated by diversions from head ditches into furrows, the head ditches were spaced so that a fairly efficient application of water could be made with water containing silts and clays. With silt and clay in the water, relatively long runs were possible. When one attempts to use these same lengths of runs with clear water there are excess seepage losses and, in fact, before the water reaches the ends of the furrows, all of it is infiltrated thus building up the groundwater level. This means that the distribution systems on the farm units must be dramatically changes. Length of runs may have to be cut in productive space. The numerous ditches may also add to problems of harvesting.

As referred to previously, the clear water tends to scour the banks and degrade the bed of the canal system. If the attack is sufficiently severe, channel stabilization of some nature may be required or, as another possibility, some type of lining may be required to minimize the losses of water and to provide stability to the system.

In summary, it is important to stress that canals and river systems develop in accordance with the forces to which they are subjected. When conditions are altered, a variety of responses is initiated in rivers, canals, and watersheds that supply water to the river systems. It is

necessary then in carrying out these developments to utilize methods of analysis such as mathematical models to investigate the potential for change and to help identify both the favorable and adverse factors that may result from the development and subsequent changes to the system. In addition, it should be stressed that systems are continually being subjected to changes and once one has an operational model for the system one can periodically evaluate long-term response resulting from changes in upstream and downstream developments in the basin. The necessity for overall basin planning cannot be over emphasized. To carry out a meaningful investigation for basins and sub-basins the mathematical approaches utilizing process models and management models are essential.

## 3.7 DATA NEEDS FOR ANALYSIS

### General

Evaluating the adequacy of available data for supporting various phases of a river system study is an essential element of the analysis. Consideration must be given to gaps in the available data and related supplemental data collection requirements as well as techniques for data synthesis and data sensitivity analysis.

Data needs are, of course, dependent on the complexity of the system being analyzed and the methods of analysis employed. Data requirements for a basin-wide study to include both watershed and channel modeling are presented in Tables 3-1 and 3-2 which outline, respectively, the data necessary to support channel and tributary modeling and that required for watershed modeling. These tables are arranged in matrix form and include a description of the data and an assessment of its degree of importance to the particular phase of the study.

## 3.8 LEVEL OF ANALYSIS

Various levels of analysis can be formulated, verified, and utilized depending on level of accuracy required, available data, constraints, magnitude of projected watershed and river changes, rate of changes, whether or not the watershed or channel is on the threshold of a major change considering its geometry, hydraulics, hydrology, and sediment transport.

Level 1. This includes the office work and limited field investigations needed to determine if significant watershed and river response may occur. This would require hand-held calculator applications.

Level 2. This level involves conducting field work to establish baseline data (present conditions) and project changes that will result from alterations in flow, etc. Either hand-held calculator applications or simple computer models could be used in this level of analysis.

Level 3. Additional data (some data could be synthesized) must be obtained to utilize the present state-of-the-art methods to simulate changes continuously and/or for major events. This level would require computer application of either simple or complicated state-of-the-art models.

Table 3-1. Basic data needs for channel modeling.

| | Description of Data | Degree of Importance |
|---|---|---|
| A. | Maps and Charts | |
| | Topographic map of river environment | Primary |
| | Geologic map of river environment | Secondary |
| | Hydrographic charts | Primary |
| B. | Aerial and Other Photos | |
| | Large scale photos of river and surrounding terrain | Secondary |
| | Small scale aerial photos of river and surrounding terrain | Primary |
| | Color infrared photos for flow patterns, scour zones, and vegetation | Secondary |
| C. | Hydraulic Structures (existing and planned structures) | |
| | Plans and design details | Primary |
| | Alterations and repairs | Secondary |
| | Scour | Primary |
| | Operation procedure | Primary |
| D. | Hydrology and Hydraulics | |
| | Discharge records | Primary |
| | Flow velocity records | Primary |
| | Stage records | Primary |
| | Flood frequency curves | Secondary |
| | Sediment discharge records (bed material and wash load) | Primary |
| | Resistance to flow | Primary |
| E. | Channl Geometry | |
| | Cross sections | Primary |
| | Islands | Primary |
| | Flood plain | Primary |
| | Bed slope | Primary |
| | Water surface slope | Primary |
| | Bars | Primary |
| | Sinuosity | Secondary |
| | Controls (falls, rapids, restriction, rock outcropping, dams, diversions) | Primary |
| F. | Hydrography | |
| | Water hydrograph | Primary |
| | Sediment hydrograph (bed material and wash load) | Primary |
| G. | Sediment size | |
| | Bed material size distribution | Primary |
| | Bank material size distribution | Primary |
| H. | Environmental data | |
| | Riparian community | Secondary |
| | Salinity of water | Primary |
| | Turbidity | Secondary |

Table 3-1. (Continued).

| | Description of Data | Degree of Importance |
|---|---|---|
| | Water temperature | Secondary |
| | Fish habitat | Secondary |
| | Chemical quality | Secondary |
| I. | Climatologic data | |
| | Precipitation | Secondary |
| | Wind | Secondary |
| | Air temperature | Secondary |

Table 3-2. Basic data needs for watershed modeling.

| | Description of Data | Degree of Importance |
|---|---|---|
| A. | Maps and charts | |
| | Topographic maps of watersheds | Primary |
| | Soil maps of watersheds | Primary |
| | Geologic maps of watersheds | Primary |
| | Vegetation maps of watersheds | Primary |
| | Land use maps of watersheds | Primary |
| B. | Aerial and Other Photos | |
| | Aerial photos | Primary |
| | Color infrared photos of watersheds | Primary |
| C. | Soil and Geologic Data | |
| | Hydraulic conductivity | Primary |
| | Capillary section | Primary |
| | Soil porosity | Primary |
| | Particle size distribution | Primary |
| | Soil moisture | Primary |
| | Rock outcropping | Primary |
| | Armoring size and distribution | Primary |
| D. | Forest Inventory Data | |
| | Total vegetation volume | Secondary |
| | Total litter volume | Secondary |
| | Canopy cover density | Secondary |
| | Ground cover density | Secondary |
| | Interception storage capacity of a typical canopy | Secondary |
| | Evapotranspiration of a typical canopy | Secondary |
| E. | Hydrology and Hydraulics in Water System | |
| | Flow discharge records | Primary |
| | Flow velocity records | Primary |
| | Flow stage records | Primary |
| | Resistance to flow | Primary |
| | Sediment discharge records (bed material and wash load) | Primary |
| F. | Climatological Data | |
| | Precipitation | Primary |
| | Wind | Primary |
| | Radiation | Primary |
| | Air temperature | Primary |
| | Humidity | Secondary |
| | Precipitation frequency curves | Secondary |
| G. | Hydrographic Data | |
| | Water hydrographs | Primary |
| | Sediment hydrographs | Primary |
| H. | Environmental Data | |
| | Wildlife | Secondary |
| | Fish habitat | Secondary |
| | Turbidity | Secondary |
| | Chemical quality | Secondary |
| | Water temperature | Secondary |

Table 3-2. (Continued).

| Description of Data | Degree of Importance |
|---|---|
| I. Land Use Data (historical and present records) | |
| Forested areas | Primary |
| Urban areas | Primary |
| Industrial areas | Primary |
| Recreational areas | Secondary |
| Agricultural areas | Primary |

It must be noted that certain categories of data including hydrogolic, hydraulic, channel geometry, and hydrographic, are extremely dynamic in nature and strongly a function of past and present conditions. Therefore, available data should be validated against today's river system conditions to determine their acceptability for the analysis.

Level 4. This level includes the research to develop and/or modify state-of-the-art technology to improve Level 3 analysis. This might incorporate sediment routing by size fraction. This approach would utilize an interactive data storage and retrieval system and could include data essential for the analysis of water quality, biology, recreation, etc.

Level 5. This level incorporates the management model with Level 3 and/or Level 4 analysis as one component of the comprehensive system of models.

All levels of analysis should be capable of evaluating watershed and river responses to all levels of watershed management and streamflow alteration. The methods of analysis must include the stream system and the watershed. The data required and recommended level of analysis for various levels of analysis follow.

Level 1

| Needs | Data Required | Method of Analysis |
|---|---|---|
| Knowledge of present system | Recorded data:<br>climatic<br>hydrologic<br>hydraulic<br>Maps<br>Aerial photos<br>Field data:<br>type of river<br>bank erosion<br>stability<br>bed and bank material<br>vegetation<br>channel geometry<br>watershed characteristics<br>riffle and pool sequence<br>velocity<br>geology<br>control<br>structures<br>Proposed structures, water rights, etc. | Geomorphic, transport, hydrologic and hydraulic relations required for a qualitative analysis. An exaple is to use Lane relation (Simons and Sentürk, 1977) hydraulic geometric equations, etc. |

Level 2

| Needs | Data Required | Method of Analysis |
|---|---|---|
| Requires more accurate and detailed data. Also needs more information on changes in above as function of space and time | All data for Level 1 plus: detail data on study subreaches, cross setion in the sub-reaches, stage-discharge relations, suspended sediment, bed material, channel slope, etc. | Conduct Level 1 type study supported with additional data on sediment transport, geomorphic relations, stage duration, flow distribution, peak flows, minimum flows, etc. Determine more precise values of the system response |

| | |
|---|---|
| Information on:<br>verticals at a cross section, engineering and natural controls, land-use changes, and watershed impacts.<br>Decide whether to treat river as rigid or alluvial system. | If results indicate:<br>1. Large changes in time and space<br>2. Thresholds<br>3. High costs<br>4. Need for greater accuracy<br>5. Cannot satisfy legal, etc., constraints then go on to Level 3 analysis |

Level 3

Use the current state-of-the-art models and techniques to route water and sediment for major runoff events or simulate continuously if necessary. Generally, a known discharge model will provide sufficient accuracy.

Develop methodologies to accommodate all interests including water resources development, water quality, recreation, biology, river mechanics, etc.

Develop and utilize a common data storage and retrieval system. Such an approach is necessary to conduct an accurate, economical, efficient and sufficients analysis.

Level 4

Use the current models to identify short- and long-term data needs and research needs. Then conduct research to improve Level 3 type models and analysis. Also, could proceed with a higher level of sophistication involving water quality, sediment routing by size fraction, two-dimensional modeling, improve watershed modeling components, etc.

Level 5

Incorporate the management models such as linear programming, dynamic programming, screening, direct search, and/or nonlinear programming optimization techniques with Level 3 and/or Level 4 model as one component of the comprehensive system of models.

## 3.9 SUMMARY

In this chapter, an overview of some case studies is made to illustrate types of problems that are often encountered in analysis of watershed and river systems. General data needs for analysis are discussed and an effective system for data management is presented. Then, a general approach to determine the required level of analysis is recommended.

## REFERENCES

Agricultural Research Service, United States Department of Agriculture, 1975, Control of water pollution from croplad, Vol. I-A, Manual for Guideline Development, November.

Bathurst, J. C., Li, R. M., and Simons, D. B., 1979, Hydraulics of mountain rivers, Civil Engineering Department, Colorado State University, Fort Collins.

Hann, R., Jr. and Young, P., 1972, Mathematical models of water quality parameters for rivers and estuaries, Technical Report No. 45, Water Resources Institute, Texas A and M University, College Station, Texas.

Leopold, L. B. and Maddock, T., Jr., 1953, The hydraulic geometry of stream channels and some physiographic implication, U.S. Geological Survey Professional Paper 252, 1953, 57 p.

Li, R. M., Simons, D. B., and Simons, R. K., 1977, A mathematical model for evaluating on-site soil erosion, prepared for USDA Forest Service, Rocky Mountain Forest and Range Experiment Station, Flagstaff, Arizona, February.

Overton, D. E. and Meadows, M. E., 1976, Stormwater Modeling, Academic Press, New York.

Rosenbrock, H. H., 1960, An automatic method for finding the greatest or least value of a function, The Computer Journal, Vol. 3, 1960, pp. 175-184.

Schumm, S. A., 1977, The Fluvial System, Wiley Interscience, 338 p.

Simons, D. B. and Li, R. M., 1975, Watershed segmentation by a digital computer for mathematical modeling of watershed response, prepared for USDA Forest Service, Rocky Mountain Forest and Range Experiment Station, Flagstaff, Arizona, December.

Simons, D. B. and Li, R. M., 1979, Analysis of watershed and river systems, In: Modeling of Rivers, H. W. Shen, ed., John Wiley and Sons, New York.

Simons, D. B., Li, R. M., Brown, G. O., Chen, Y. H., Ward, T. J., Duong, N., and Ponce, V. M., 1978, Sedimentation study of the Yazoo River basin--Phase I General Report, prepared for U.S. Army Corps of Engineers, Vicksburg, Mississippi, June.

Simons, D. B., Li, R. M., and Spronk, B. E., 1978, Storm water and sediment runoff simulation for a system of multiple watersheds, prepared for USDA Forest Service, Rocky Mountain Forest and Range Experiment Station, Flagstaff, Arizona, April.

Simons, D. B., Li, R. M., and Ward, T. J., 1977a, Simple procedural method for estimating on-site soil erosion, prepared for USDA Forest Service, Rocky Mountain and Forest Range Experiment Station, Flagstaff, Arizona, February.

Simons, D. B., Ponce, V. M., Li, R. M., Chen, Y. H., Gessler, J., Ward, T. J., and Duong, N., 1977a, Flood flows, stages and damages, CER77-78DBS-VMP-RML-HYC-JG-TJW-ND9, prepared for Land-Use Studies, Colorado State University Experiment Station, November.

Simons, D. B., Schumm, S. A., Stevens, M. A., Chen, Y. H., and Lagasse, P. F., 1975b, A geomorphic study of pools 24, 25 and 26 in Upper Mississippi and Lower Illinois Rivers, prepared for the Waterways Experiment Station, Vicksburg, Mississippi.

Simons, D. B. and Sentürk, F., 1977, Sediment Transport Technology, Water Resource Publications, Fort Collins, Colorado.

Simons, D. B., Ward, T. J., and Li, R. M., 1979, Sedment sources and impacts in the fluvial system, In: Modeling of Rivers, H. W. Shen, ed., John Wiley and Sons, New York.

U.S. Forest Service, 1976, Non-point water quality modeling in wildland management: A State-of-the-art Assessment, USDA Forest Service Interagency Agreement No. EPA-IAG-05-0660, Washington, D.C.

Vanoni, V. A., editor, 1976, Sedimentation engineering, ASCE Manual and Report of Engineering Practice, No. 54, prepared by ASCE Task Committee for the preparation of the Manual on Sedimentation of the Sedimentation Committee of the Hydraulics Division.

# CHAPTER 4

# FLUVIAL GEOMORPHOLOGY

## 4.1 THE FLUVIAL SYSTEM

Fluvial geomorphology has as its object of study not only individual channels but the entire drainage system (Kruska and Lamarra, 1973). For example, it is rarely possible to understand even a short reach of an alluvial channel in isolation from its upstream and downstream controls. In the simplest case the reach is an integration of upstream geology, morphology, and hydrology (the hydrology itself may be strongly influenced by drainage-basin morphology).

Figure 4-1 which is divided for convenience of discussion into three parts is a sketch of an idealized fluvial system. The parts are referred to as Zones 1, 2, and 3 in a downstream direction. The uppermost is the drainage basin, watershed, or sediment-source area (Zone 1). This is the area from which water and sediment are derived. It is primarily the zone of sediment production, although sediment storage does not occur there in important ways. Zone 2 is the transfer zone where for a stable channel, input of sediment can equal output. Zone 3 is the sediment sink or area of deposition.

These three subdivisions of the fluvial system may appear artificial because obviously sediments are stored, eroded, and transported in all the zones. Nevertheless, within each zone one process is

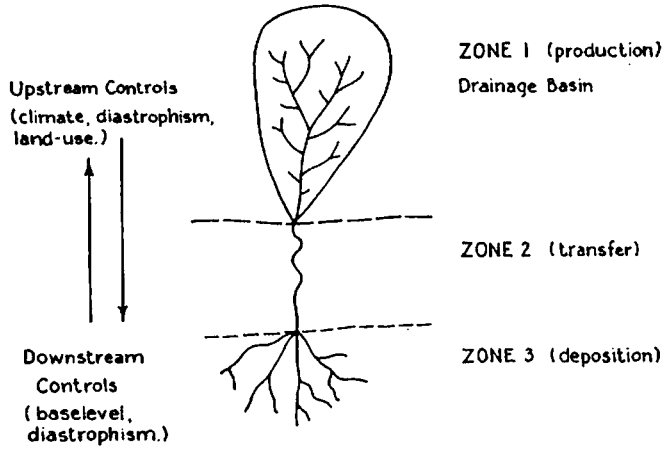


Figure 4-1. Idealized fluvial system. (From Schumm, 1977.)

usually dominant and it is convenient to think of Zone 1 as the sediment producer, and in the ideal case Zone 2 is a zone of transfer or predominant transport. Eventually the sediment is deposited in Zone 3 on an alluvial fan, alluvial plain, delta, or in deeper waters.

Zone 1 is the area of greatest interest to watershed scientists and hydrologists, as well as geomorphologists involved with evolution and

growth of drainage systems. Zone 2 is of major concern to the hydraulic and river-control engineer and to geomorphologists concerned primarily with river-channel morphology.

Landforms may reflect their past history and most show the influence of current processes. Therefore, scrutiny of the landscape should reveal much about past and present events and even future response of the system to changes imposed upon it. In this way geomorphic principles can be applied to the fields of geology, astrogeology, archaeology, hydrology, civil and agricultural engineering, regional planning, and law (Schumm, 1969b).

There appear to be three ways in which a geomorphologist's knowledge of the landscape can be applied to practical problems. The first is simply in evaluation of existing conditions. For example, photogeologists use differences in drainage density and drainage patterns to delineate specific rock types and locate geologic structures. The second is an attempt to predict what will happen in the future both with constant and changing environmental conditions. For example, what will happen to a river as flood peaks are increased by urbanization or weather modification? This type of projection of current information (prediction) is the result of the development of an understanding of cause and effect relations in geomorphic systems. The third is an attempt to interpret the past (retrodiction). Of course, this is the traditional approach of geologists to historical problems but it may also have real significance. For example, past behavior of rivers may significantly influence their present morphology.

In order to accomplish the objectives of evaluation, prediction, and retrodiction it is necessary to apply not only specific information concerning erosional and depositional processes but also geomorphic principles. W. M. Davis' (1899) model of erosional development of landforms was based on variables grouped under the headings of structure, process, and stage. In this presentation on the fluvial system process might be eliminated from consideration. Nevertheless because erosional and depositional processes tend to operate at different intensities under different climatic regimes and different geologic constraints, the intensity and duration of activity of the process is still of concern. Structure, of course, applies to all geologic controls, both structural and lithologic. Finally, there is stage or time. The geologist and geomorphologist will not question the progressive change of the fluvial landscape through time but when dealing with an interval shorter than that involved in the erosional cycle many others feel that the landscape is relatively static. That is, the erosion of the river bend is an unnatural event and it must be controlled. This is nonsense from a geomorphic point of view because one can normally expect such changes to take place. Three principles upon which the interpretation of the fluvial system can be based are as follows:

1. The landscape is dynamic. One can expect erosional and depositional changes to occur over relatively short periods of time. In many cases these changes result from unstable situations generated by changing hydrologic conditions or changing land-use patterns, but the

normal progressive change of the landscape must not be mistaken for instability.

2. Landscape changes are usually complex (Schumm and Parker, 1973). When a landscape or landscape component is subjected to the influence of an external variable such as climatic change, man's influence, or changing base level, it will respond but because a landscape is a complex system, the response itself will be complex. That is, when A is changed we can expect B to occur but in addition, C and D may also result. Secondary responses can be anticipated but we are frequently unable to precisely predict their nature. Therefore, it is important to recognize that either natural or man-induced landform changes will almost certainly be more complicated than most textbooks suggest.

3. Geomorphic thresholds exist and result in abrupt and unexpected landform change (Schumm, 1973, 1977). Examples cited later will make this concept clear but it means that with progressive change of an independent variable, a landform may not respond until a critical condition is attained. The bedform changes that occur during a progressive increase of stream power are a good example (Simons et al., 1965). In addition, as landforms change through time they may develop to a morphologically critical condition, when a dramatic and abrupt change occurs. A trivial example of this type of inherent geomorphic threshold is the changing form of a river meander. Through time a meander bend may deform until its neck is very narrow, and then during the event of a major flood it will cutoff. The immediate cause of the cutoff is the high discharge but, nevertheless, the situation was developed through a long period of normal erosion. Events of this general type may be fairly common and the identification of incipiently unstable landforms should be a major goal of geomorphologists.

## Thresholds

One of the critical problems and questions in geomorphology is determining the stress conditions that will cause a dramatic change in the geomorphic system with significant modification of the landscape. This of course depends on the external stress applied and the strength of the material to which the stress is applied. It is in this context that thresholds are generally considered. A gradual increase in external stress eventually produces a dramatic response in the system. These are referred to as extrinsic thresholds (Schumm, 1973) because they depend on an external influence. A good example is the response of sediment to an increase in the velocity and depth of flow of water. The sediment remains immobile until movement eventually begins at a shear or velocity threshold. In addition at higher thresholds abrupt changes in the bedforms develop on the channel floor (Simons et al., 1965). These hydraulic thresholds show that there need not always be a progressive reaction of a system to a slowly increasing stress.

Also another type of threshold inherent to the system is the intrinsic threshold. An example is the long-term progressive weathering of slope materials that eventually results in mass movement (Kirkby, 1973). In semiarid regions sediment storage in a valley through time progressively increases valley slope until failure (erosion) occurs.

This is an intrinsic geomorphic threshold. It is the result of landform change through time to a condition of incipient instability, without a change of external influences (Schumm, 1977).

A common example of a geomorphic threshold is progressive increase in channel sinuosity and meander amplitude until a cutoff or channel avulsion results on alluvial plains and deltas. This is due to channel lengthening and gradient reduction accompanying increases in sinuosity and delta size.

It is important to stress that the concept of intrinsic geomorphic thresholds and especially geomorphic thresholds, means that changes in fluvial erosion and deposition need not always be attributed to external (extrinsic) influences such as climate, tectonics, and baselevel change. This conclusion is contrary to the usual geologic assumption of progressive change interrupted only by external influences and has significant implications for interpretation of erosional and depositional events and the distribution of erosional and depositional features in the landscape.

## 4.2 VARIABLES

A hierarchy of variables that are significant to the morphology and mechanics of Zone 1 is shown in Table 4-1. The variables are arranged in a sequence that reflects increasing degrees of dependence, insofar as this can be done for such a complex system. It should be noted that only upstream controls are given.

Time, initial relief, geology, and climate (variables 1-4, Table 4-1) are the dominant independent variables that influence progress of erosional denudation of a landscape and its hydrology. Vegetational type and density (variable 5) depend on lithology (soils) and climate (variable 6) or mass remaining above baselevel is determined by the factors above it in the table. Relief in turn strongly influences the runoff and sediment yield per unit area within the drainage basin (variable 7). Runoff acting on soil and geologic materials produces a characteristic drainage network morphology (variable 8 - drainage density, channel shape, gradient, and pattern) and hillslope morphology (variable 9 - angle of inclination, length, and profile form) within the constraints of relief, climate, lithology, and time. These morphologic variables in turn strongly influence the volumes of runoff and sediment that are eventually discharged from Zone 1 (variable 10). It is this volume of sediment and water that to a major extent determines channel morphology and the nature of fluvial deposits that form in Zones 2 and 3 (variables 11 and 12).

Some of the variables given in Table 4-1 for example, geology (lithology, structure, and soils) and climate (temperature and precipitation), represent a group of variables and are considered in the discussions that follow. Other variables that can be grouped for discussion purposes are variables 2, 6, 8, and 9 (morphology) and variables 7 and 10 (hydrology).

Table 4-1. Fluvial system variables (From Schumm and Lichty, 1965).

| Drainage system variables |
|---|
| 1. Time |
| 2. Initial relief |
| 3. Geology (lithology, structure) |
| 4. Climate |
| 5. Vegetation (type and density) |
| 6. Relief or volume of system above baselevel |
| 7. Hydrology (runoff and sediment yield per unit area within Zone 1) |
| 8. Drainage network morphology |
| 9. Hillslope morphology |
| 10. Hydrology (discharge of water and sediment to Zones 2 and 3) |
| 11. Channel and valley morphology and sediment characteristics (Zone 2) |
| 12. Depositional sysem morphology and sediment characteristics (Zone 3) |

Time (Variable 1)

Time refers to the passage of time since the inception of the erosional process and in itself has no effect on the landscape. Instead it records the accomplishments of the system. Depending on the time span considered, time may be either an extremely important variable or of relatively little significance in consideration of the fluvial system. For example, during a short period of time there may be no change in the morphology of stream channel but during a longer period (graded time) the channel may adjust to hydrologic events. Whereas during long periods of geologic (cyclic) time there can be a progressive change in channel character. (For a fuller discussion see Schumm and Lichty, 1965 and Schumm, 1977).

Morphology (Variables 2, 6, 8, and 9)

The initial movement of water and sediment in Zone 1 reflects precipitation, soil characteristics, and slope. For a fluvial landscape to form, water must move and erode. The resulting drainage network and its morphologic character then influence the amount and manner in which water and sediment are discharged to Zones 2 and 3 (variable 10). The inception and effect of runoff on slopes and beneath them through the soil, although of great importance are not discussed. Rather only the effect of two morphologic variables relief or slope (variables 2 and 6) and drainage density (variable 8) on the hydrology of Zone 1 (variable 10) are considered.

Relief (Variables 2 and 6)

Initial relief (variable 2) that is dependent on the magnitude of uplift and the relief at any time during the erosional development of Zone 1 (variable 6) determines the magnitude of the component of gravitational force acting along slopes and channels and the potential energy of Zone 1. Therefore, the rate at which denudational processes operate and their effects on basin morphology are significantly influenced by relief and slope.

Relief and slope strongly influence the movement of water and sediment (variables 7 and 10). For example, when sediment-yield data from small drainage basins that are underlain by sandstone and shale, are plotted against the average slope (relief/length ratio, relief of basin divided by basin length), an exponential relationship between the two variables is apparent (Figure 4-2).

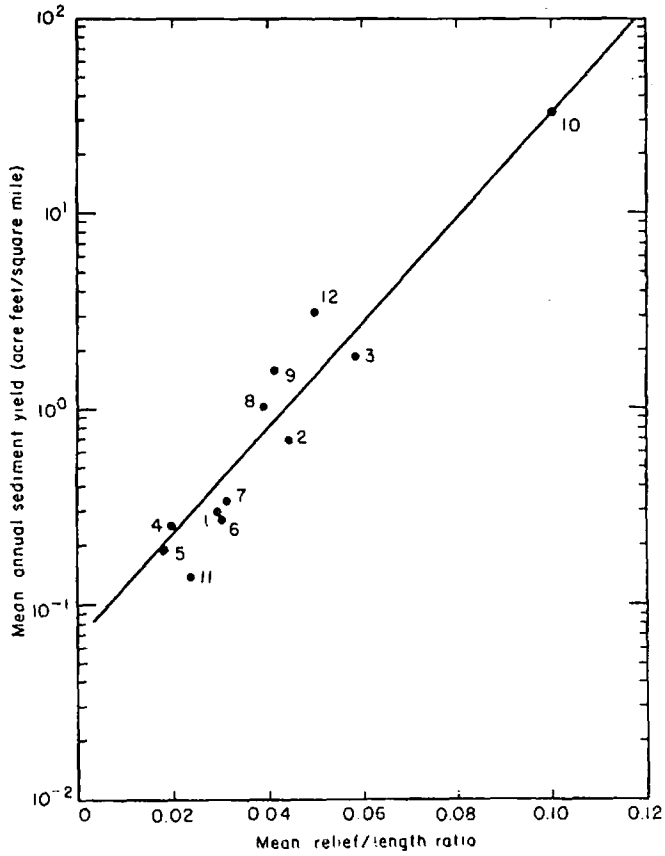


Figure 4-2. Relation of mean annual sediment yield to relief/length ratio for small drainage basins in western United States. Each point is an average value for several basins. Data from a total of 59 basins are represented. The number beside each point indicates rock type and location as follows: 1) resistant sandstone, Utah, 2) friable sandstone, Utah, 3) shale, Utah, 4) sandstone, New Mexico, Arizona, 5) conglomerate and sandstone, New Mexico, Arizona, 6) sandstone, New Mexico, Arizona; 7) sandy shale, Wyoming, 8) sandstone and shale, Wyoming, 9) shale, Wyoming, 10) 10) shale, siltstone, Wyoming, 11) sandstone, Wyoming, 12) shale, Colorado (From Hadley and Schumm, 1961).

## Drainage Texture (Variable 8)

The spacing of the drainage channels within Zone 1 expressed as drainage density is an index of efficiency of Zone 1 in disposing of water and sediment. The effect of relief has already been clarified.

Both mean annual runoff and sediment yield are found to be significantly greater from drainage basins with high drainage densities but similar relief/length ratios. See the later discussion of Cornfield, Washington drainage basin.

Geology (Variable 3)

Geology includes lithologic character of rocks, as well as structure, the influence of fractures (joint and faults), and other deformational features and their distribution.

Rivers draining areas that differ greatly in the physical character of rocks and soils show significant morphologic differences, as the erodibility of the soils, hydrologic character of the system, and the size and quantity of sediment load moved from the basin differ. On a regional basis, drainage pattern itself reflects these controls. For example, drainage density is high in a region of weak rocks and impermeable soils and low for resistant rocks and highly permeable soils (Table 4-2).

Table 4-2. Lithologic units, Cheyenne River basin (from Table 2 and p. 175, Hadley and Schumm, 1961)

| Stratigraphic units | Mean infiltration (in/hr) | Sediment yield (acre/ft/sq. mile) | Drainage density (miles/sq. mile) |
|---|---|---|---|
| Wasatch Formation | 9.2 | 0.13 | 5.4 |
| Lance Formation | 5.0 | 0.5 | 7.1 |
| Fort Union Formation | 1.3 | 1.3 | 11.4 |
| Pierre Shale | 1.0 | 1.4 | 16.1 |
| White River group | 0.18 | 1.8 | 258 |

As important as lithology is to erosion and sediment transport, relatively little can be said other than that weak rocks erode rapidly and resistant rocks erode slowly. A difficulty is that, for most studies of sediment yield, the data have not been stratified geologically. For example, Figure 4-2 shows a statistically significant relation between drainage basin slope and sediment yield. However, morphology is not the only significant control. Basins underlain by shales and siltstones plot high and those underlain by sandstone and conglomerates plot low (Figure 4-2). Another variable is infiltration capacity. Weak rocks that produce sandy soils with a high infiltration capacity produce less runoff and therefore little sediment (Table 4-2). Therefore, there is major lithologic control of the relation of Figure 4-2.

Climate (Variable 4)

Geomorphologists assume that climate and climate change effects are reflected in erosional and depositional processes and ultimately in the landscape. For example, morphoclimatic regions have been identified

wherein the climate determines to a signficant extent both the efficiency and type of erosion process and the resulting landforms (Stoddart, 1969 and Wilson, 1968) but there is no quantitative description of these supposed differences. However, the effects of the greatly different river flow regimes experienced throughout the world (Parde, 1964 and Beckinsale, 1969) and the different types of sediments provided by tropical as compared to semiarid, arctic, and arid rock weathering are detectable. For example, comparison of the hydraulic geometry of perennial streams of humid and subhumid regions with that of ephemeral streams of semiarid regions shows that, in contrast to the case of perennial streams, depth of ephemeral streams increases less rapidly and gradient decreases less rapidly in a downstream direction. This probably is due to the high water loss in ephemeral stream channels and to the increase in suspended sediment concentration in a downstream direction (Leopold et al., 1964, Table 7-5). In addition, obvious differences in the morphology of slopes of different aspect, north compared with south, for example, are directly attributable to the microclimatic character of the valley sides.

Vegetation (Variable 5)

There can be no question of the highly significant effect of vegetation on landforms and erosion rates. In the United States vegetational bulk or weight increases approximately as the cube of mean annual precipitation (Langbein and Schumm, 1958) and a significant reduction in erosion and sediment yield can be anticipated as precipitation increases or as vegetation increases in a given climatic situation. Figure 4-3 shows such a relation from an experimental area in Utah. The relationship is exponential and an extrapolation of the curve indicates a maximum of 50,000 pounds per acre of erosion with zero ground cover. However, there is no reason to believe that this value will be achieved. Although in Figure 4-3 an asymptotic approach to the y axis is indicated by the rapid increase of erosion and small percentages of ground cover, there is a maximum rate of erosion for a given soil or rock type that must be reached before ground cover is zero. The curve would plateau at that value as the dashed line suggests. If this is true, then Figure 4-3 suggests that with less than approximately 8.0 percent cover vegetation is probably relatively ineffective in controlling erosion. On the other hand, above about 70 percent cover, additional vegetation will not significantly reduce erosion. These limits to vegetational effectiveness for erosion control should be given consideration before expensive attempts are made to slightly improve vegetational cover on the drylands. The above discussion is based on the assumption that a threshold, above which vegetational cover becomes important for erosion control, exists.

Hydrology (Variables 7 and 10)

All previously discussed variables significantly control runoff and sediment yield from Zone 1, which in turn greatly influence Zones 2 and 3. In this section the products of Zone 1 are considered primarily in relation to climatic controls.

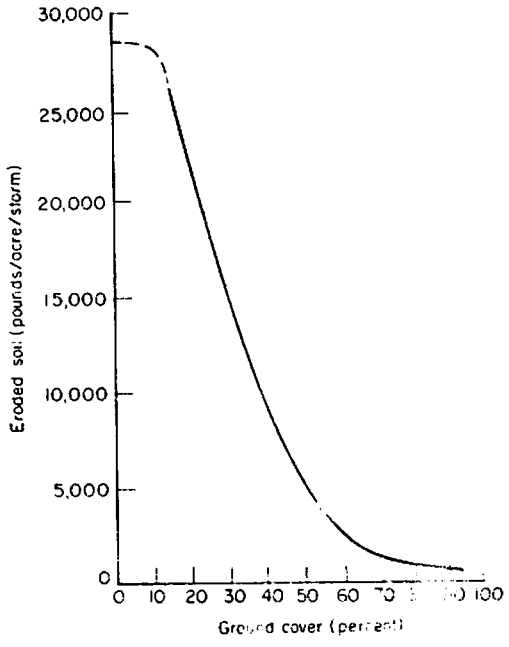


Figure 4-3. Relation of eroded soil to ground cover from an experimental watershed in Utah. Dashed extension of curve is hypothetical. (After Noble, 1965.)

In any study of hydrologic variables only modern records can be utilized and many of these are of short duration. In addition, records of stream discharge are far more abundant than records of sediment loads. Therefore, much more is known concerning runoff than sediment movement.

Runoff

Runoff is the precipitation that appears in surface streams. It is therefore water that plays the principal role in fashioning and modifying the fluvial landscape.

Langbein et al. (1949) used data from gaging stations at which discharge was not materially affected by diversions or regulations to illustrate the general relation between climate and runoff (Figure 4-4). The position of each of the curves depends on mean annual temperature which was adjusted to remove seasonal rainfall on runoff effects. For example, a given amount of precipitation yields less runoff during warmer months than during cool months.

The family of curves shows that when annual precipitation increases, annual runoff increases and as temperature increases with constant precipitation, runoff decreases. These relations are straightforward and need no elaboration.

Sediment Yield

Sediment yield is the total amount of sediment moved from a drainage basin. It is usually calculated from measurements of sediment

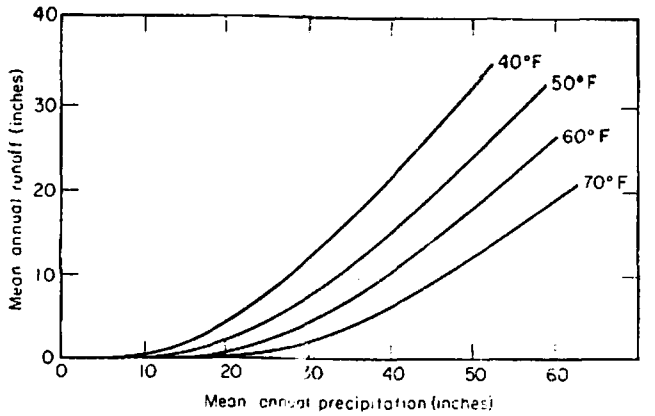


Figure 4-4. The effect of average temperature on the relation between mean annual runoff and mean annual precipitation. (After Langbein et al., 1949.)

concentration in a stream that does not include bed load, or from the amount of sediment deposited in a reservoir that is a measure of total sediment load.

Langbein and Schumm (1958, Figure 4-2) define the relation between annual sediment yield and annual precipitation for drainage basins averaging about 1500 square miles in the conterminous United States at an annual mean temperature of 50°F (Figure 4-5). Although precipitation is the dominant climatic factor influencing sediment yields, temperature effects needs to be considered because more precipitation is required to produce a given amount of runoff in a warm climate than in a cool climate. The curve of Figure 4-5, therefore, is the relationship between sediment yield and precipitation adjusted to an annual mean temperature of 50°F (Langbein and Schumm, 1958, p. 1076). The definition of the 50°F curve is based on known values of runoff for each drainage basin from which the sediment-yield data were obtained. These observed values of runoff were converted to an "effective precipitation," or the annual precipitation required to produce the known runoff at 50°F by use of the 50°F rainfall/runoff curve of Figure 4-4. For example, if the mean annual runoff from a drainage basin is 10 inches at a mean annual temperature of 50°F, the effective precipitation required to produce this runoff is about 33 inches. To produce the same runoff at 60°F about 39 inches of precipitation is required.

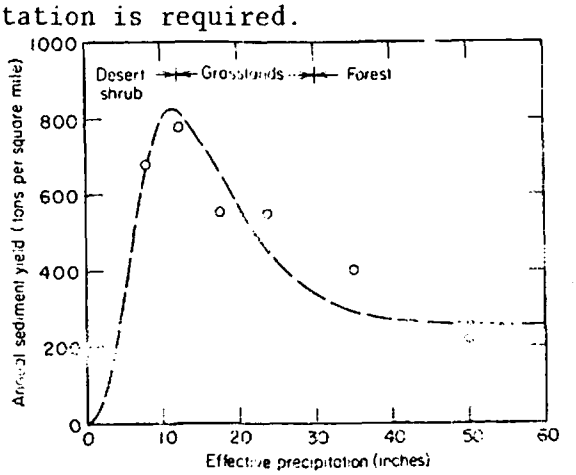


Figure 4-5. Variation of sediment yield with climate as based on data from small watersheds in the United States. (From Langbein, W. B. and Schumm, S. A., 1958).

The sediment yield curve reveals that at 50°F sediment yield is a maximum of approximately 12 inches of precipitation, and then decreases with lesser and greater amounts of precipitation. This variation in sediment yield with precipitation can be explained by the interaction of precipitation and vegetation on runoff and erosion. As precipitation increases above zero, sediment yields increase rapidly because more runoff is available to move sediment. Opposing this trend is vegetation that becomes more abundant as precipitation increases. Above 12 inches of precipitation sediment-yield rates decrease under the influence of the more effective grass and forest cover. However, where monsoonal climates prevail, sediment-yield rates may increase again above 50 inches of precipitation under the influence of highly seasonal climates (Fournier, 1949).

## 4.3 DRAINAGE BASIN MORPHOLOGY

Geomorphologists are fortunate in that the object of study is entirely exposed to scrutiny. Unlike geologists who must draw conclusions about form and characteristics of sedimentary units based on only limited exposures, geomorphologists see landforms on the surface displayed for complete description. Therefore, he can use standard statistical sampling techniques to obtain a quantitative description of the landforms. These techniques have been utilized most significantly in the study of drainage basins and their components.

A drainage basin or watershed is simply the area that gathers water from precipitation and delivers it to a larger stream, lake, or ocean. It is an area limited by a drainage divide and occupied by a drainage network. Drainage basins, therefore, are the components of continents and are of all sizes. For example, the Mississippi River drainage basin is a hierarchy of drainage basins, the largest of which is the Mississippi-Ohio-Missouri River system, one of the largest river systems on earth, and the smallest is a single, small unbranched badland tributary located in the Missouri River basin.

Drainage basin is a convenient unit of the landscape because it can be defined at any cross section along a river. Above that cross section the upstream drainage basin supplies water and sediment to the cross section.

If drainage basin and channel morphology are closely related to the climatic and hydrologic character of the basin, then it is necessary to describe the drainage basin quantitatively in order to relate the geomorphic character to the climatic and hydrologic character of the watershed and for this reason, among others, numerous descriptors of basin morphology have been developed.

### Morphometric Analysis

The quantitative description of a drainage basin is referred to as morphometric analysis, and before we can proceed to a discussion of the reason for certain watershed characteristics and its response to change, the basin and certain critical components of the watershed must be described. Obviously, drainage basins are extremely complex units of the earths surface, being composed of divides, hillslopes, terraces, floodplains and channels, each of which can be investigated separately.

From the air the most characteristic feature of a drainage basin is its drainage network which is displayed in a variety of patterns and textures. On the ground the observer is more impressed with the characteristics of the valley-sides' slopes. Nevertheless, the character of the drainage network is important because it can be used to interpret geologic conditions responsible for certain patterns, and in addition, the texture of the pattern is controlled by and has an influence on the hydrology of the drainage basin. In fact, detailed study of drainage basin morphology was given impetus by a paper by hydrologist Robert E. Horton (1945). His paper demonstrated that the drainage basin and drainage network could be dissected and the components studied, according to a stream-order numbering system. Figure 4-6 shows a third-order drainage network with each channel segment or link identified by a number. Note that in the Horton method (Figure 4-6a) the highest order channel extends from the basin mouth to the uppermost tributary, whereas in the Strahler system (Figure 4-6b) the third-order number is applied to the entire basin but only to the lowermost link. The Shreve magnitude numbering scheme (Figure 4-6c) is also shown. The Strahler and Shreve classifications are the most frequently used in the analysis of drainage networks today. It should be noted that not only tributaries are numbered but also segments and links of the main channels. Hence, one can speak of a second order drainage basin and of second order links.

Horton and others have studied the network components and relations were established between stream order number and frequency or number of streams of each order and length gradients and drainage area of streams of each order (Figure 4-7). Figure 4-6 should convince the observer that there are more first-order streams than any other order and that the first-order streams on the average are shorter and occupy smaller drainage basins. It has also been demonstrated that stream discharge increases systematically with order number (Figure 4-8). These relations indicate that the drainage network has developed in response to the erosive forces acting on the erodible materials comprising the drainage basin. The result is a drainage pattern with characteristics that can be related to erodibility of material comprising the drainage basin as well as climatic and hydrologic controls.

The geomorphologist is limited only by his ingenuity in developing measures of drainage basin morphology (see Gregory and Walling, 1973). Nevertheless, a problem frequently arises as to the accuracy of the required data that are obtained from maps, aerial photographs, and measurements in the field.

Field work is often tedious and can be expensive and time consuming, but there can be no substitute for it. Drainage density is an important measure of the texture of the topography, and yet great care must be taken when measurements of drainage density are obtained from maps and photographs. For example, during the preparation of topographic maps cartographers rarely understand or appreciate the needs of the geomorphologist. Therefore, the drainage network that is shown by blue lines on topographic maps are not a total representation of that network. The blue lines on topographic maps in many cases designate streams that contained water when the aerial photographs were taken. It is understandable that depending on the time of year, the length of blue lines on a topographic map will vary.

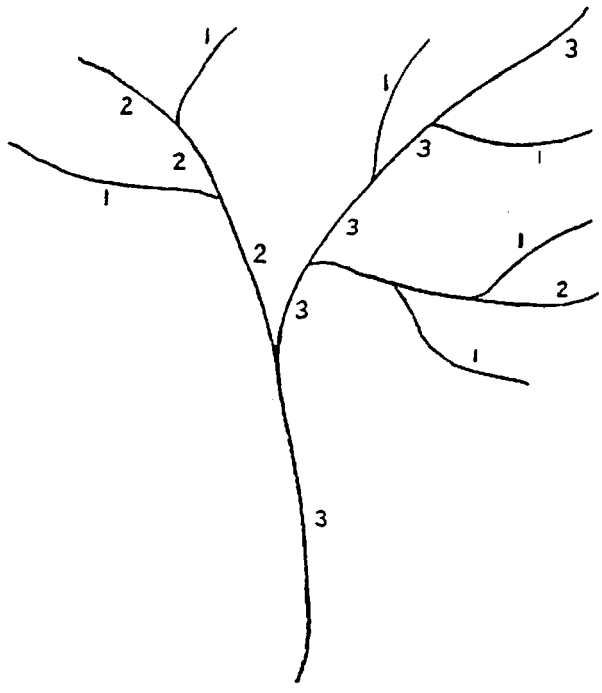


(a) HORTON'S STREAM ORDERS

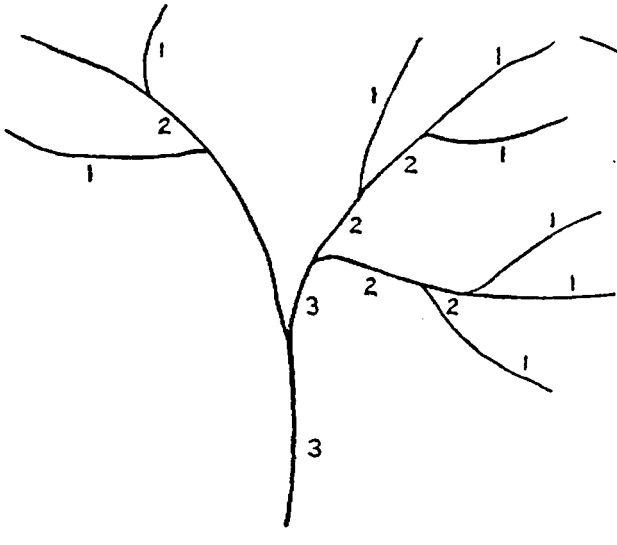


(b) STRAHLER'S STREAM ORDERS

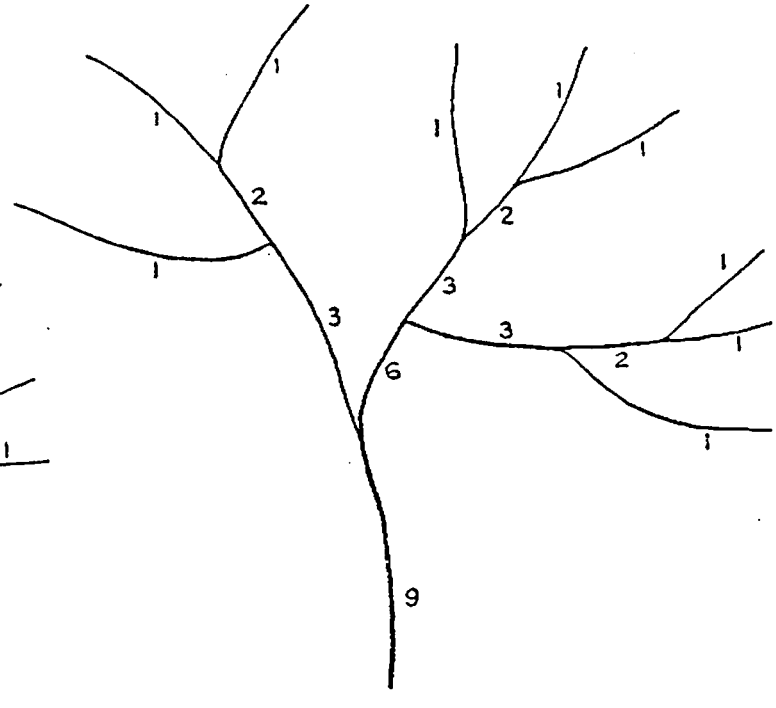


(c) SHREVE'S STREAM MAGNITUDE (M)

Figure 4-6. Comparison of stream ordering systems.

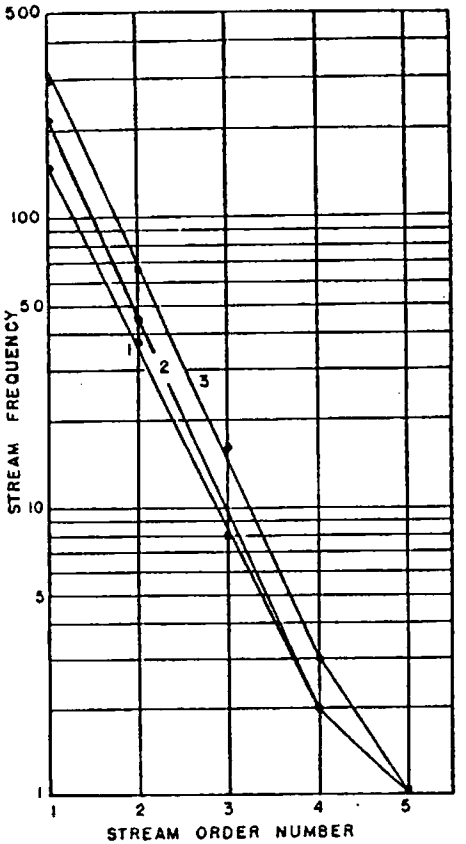


Figure 4-7a. Relation of number of streams of each order to order number 1) Perth Amboy, 2) Chileno Canyon, 3) Hughesville area.

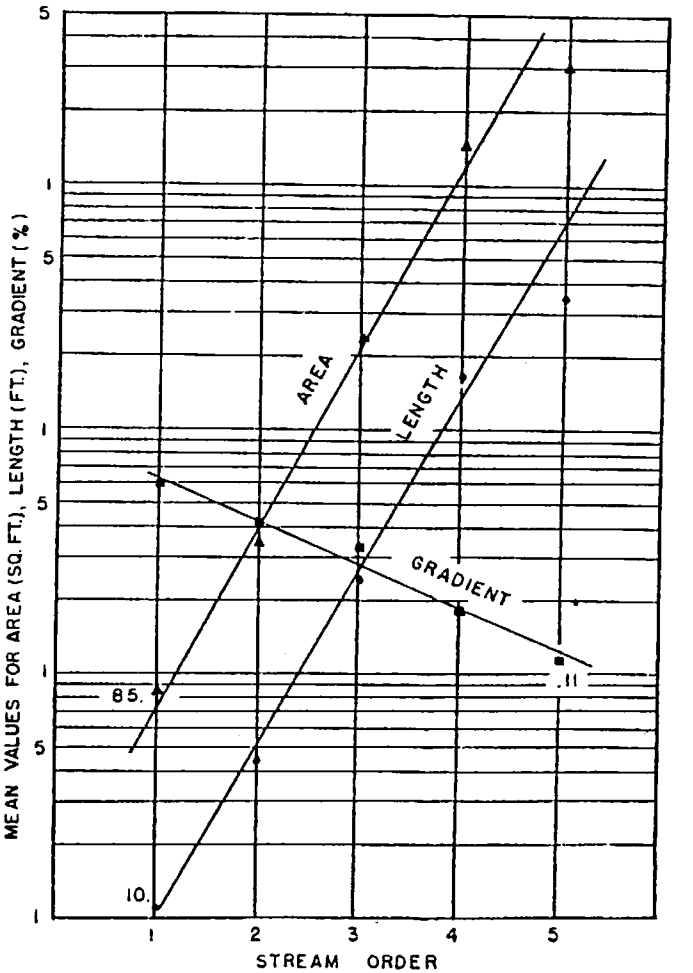


Figure 4-7b. Relation of mean basin area, mean stream length, and mean stream gradient to stream order.

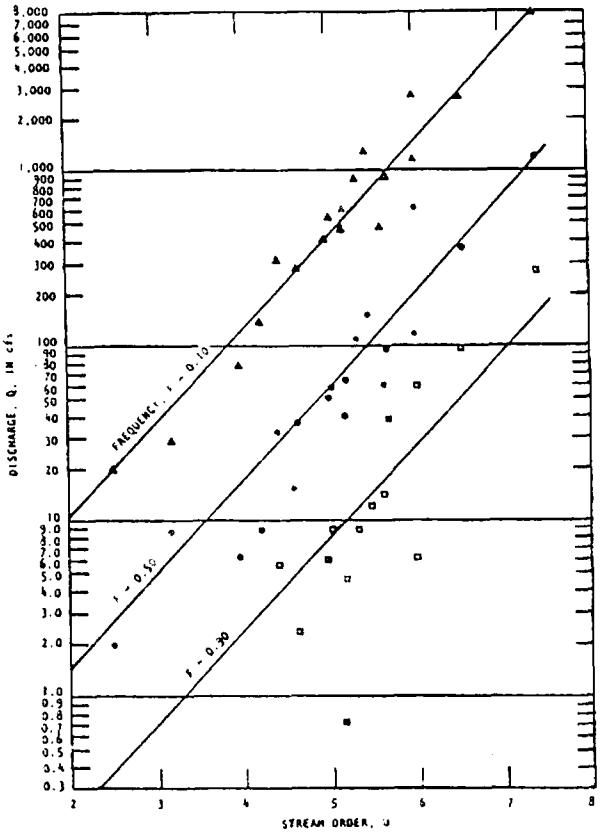


Figure 4-8. Discharge as related to proportional stream order and frequency of occurrence. (From Stall and Fok, 1968.)

A study by the U.S. Geological Survey revealed that when four cartographic engineers were instructed to measure drainage density they produced measured values of drainage density from 2.3 to 5.8. When for the same area special maps of the area were prepared, it was discovered that drainage density of perennial streams was 3.42 and total drainage density was 10.31 (Figure 4-9). It is apparent that some cartographers were measuring only perennial streams or wet channels and others were attempting to measure not only the perennial but also the dry ephemeral-stream channels within the drainage basin. This study emphasizes the danger of attempting to use topographic maps alone to study of drainage basin morphology.

The ability to study drainage basins on maps and photographs depends to a large extent on the texture of topography. Texture is simply the coarseness or fineness of dissection of the drainage network. Drainage density varies from values of less than one to values in excess of a thousand in extremely fine-textured badland areas where erosion is very rapid. The difficulty of comparing drainage density variation for areas of different lithology is brought out clearly in Figure 4-10 that shows change in drainage density values that are obtained as photograph and map scale changes. Measurements of basins underlain by granite and sandstone show relatively minor and perhaps insignificant changes in

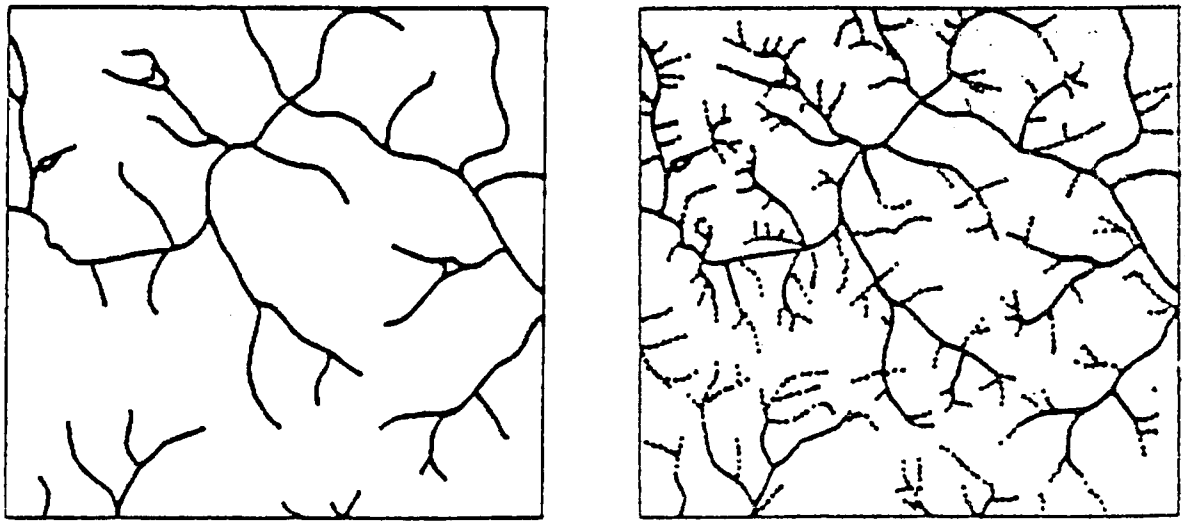

(a) Beaver Ruin Creek area (b) Beaver Ruin Creek area

Figure 4-9. Yellow Creek area; a) perennial streams, b) perennial and ephemeral streams.

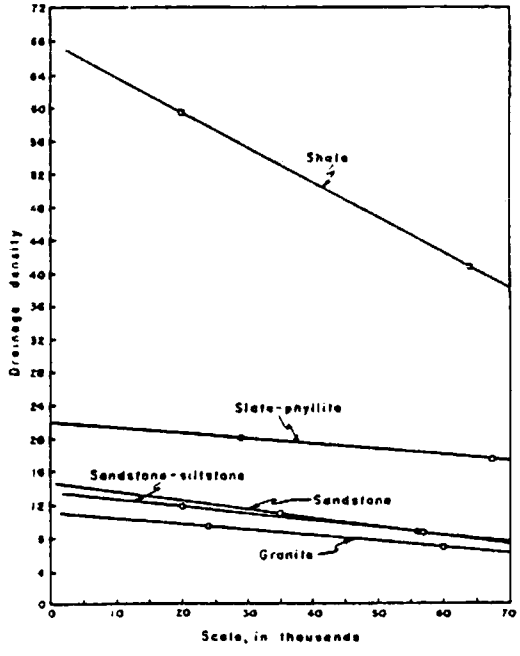


Figure 4-10. Graph showing relation of scale of photographs to drainage density of several different rock types. (From Ray and Fisher, 1960.)

drainage density as the photographs scale changes from 1/10,000 to 1/70,000 compared with drainage basins formed on shale that show

significant decrease in drainage density. Hence, comparisons of fine-textured topography should be made on photographs or maps of similar scale.

The preceding discussion was meant as a warning to those who use morphometric data. Remember that for some important descriptors, such as drainage density, subjectivity and differences of map and photograph scales may prevent a comparison of results obtained by more than one investigator.

## 4.4 DRAINAGE BASIN DYNAMICS

If as noted above, a drainage basin and drainage network evolve with regard to climatic and lithologic controls, then there should exist clear relations between drainage-basin morphology and hydrologic character. For example, in small drainage basins where land use, geology, and climate are similar highly significant relations can be established between runoff and sediment yield from these basins. In Figures 4-11 and 4-12 such relationships are presented for the Cheyenne River basin in Wyoming. As the drainage density increases the drainage basin is drained more efficiently and therefore, the water leaves the basin more rapidly and in greater quantities. The greater the relief and drainage density, the greater the erosion and sediment yields will be. Relations shown in Figures 4-11 and 4-12 are good because they were developed for small drainage basins in an area of relatively uniform climate, vegetation, and land use. A change in any of these variables throughout the region would have complicated these simple geomorphic hydrologic relations considerably.

Another important hydrologic characteristic of drainage basins that may be confusing is the inverse relation between sediment yield per unit area and drainage area (Figure 4-13). Obviously the larger a drainage basin the more water and sediment is delivered from the basin, but on a unit area basis an increase of drainage area reduces sediment production. This apparent anomaly can be explained when the drainage basin is viewed in its entirety. Usually the upstream part of the basin near the drainage divide is the steepest and downstream the valley widens, slopes become gentler, and the stream gradient and drainage density decline. Hence, more sediment per unit area is produced in the headwaters and the opportunity for sediment storage increases downstream. This will be better understood when the evolution of a basin through time is considered.

### Morphogenesis

As a historically oriented science, a major concern of geomorphologists is evolution of landscape and of course, this includes drainage basin evolution.

The question of how the geomorphologist is to obtain information on the erosional evolution of drainage basins and evolutionary development of drainage patterns arises. There appear to be three methods to accomplish this. Both experimentally and in the field, detailed studies of rapidly-eroding small drainage basins (e.g., badlands) can provide some

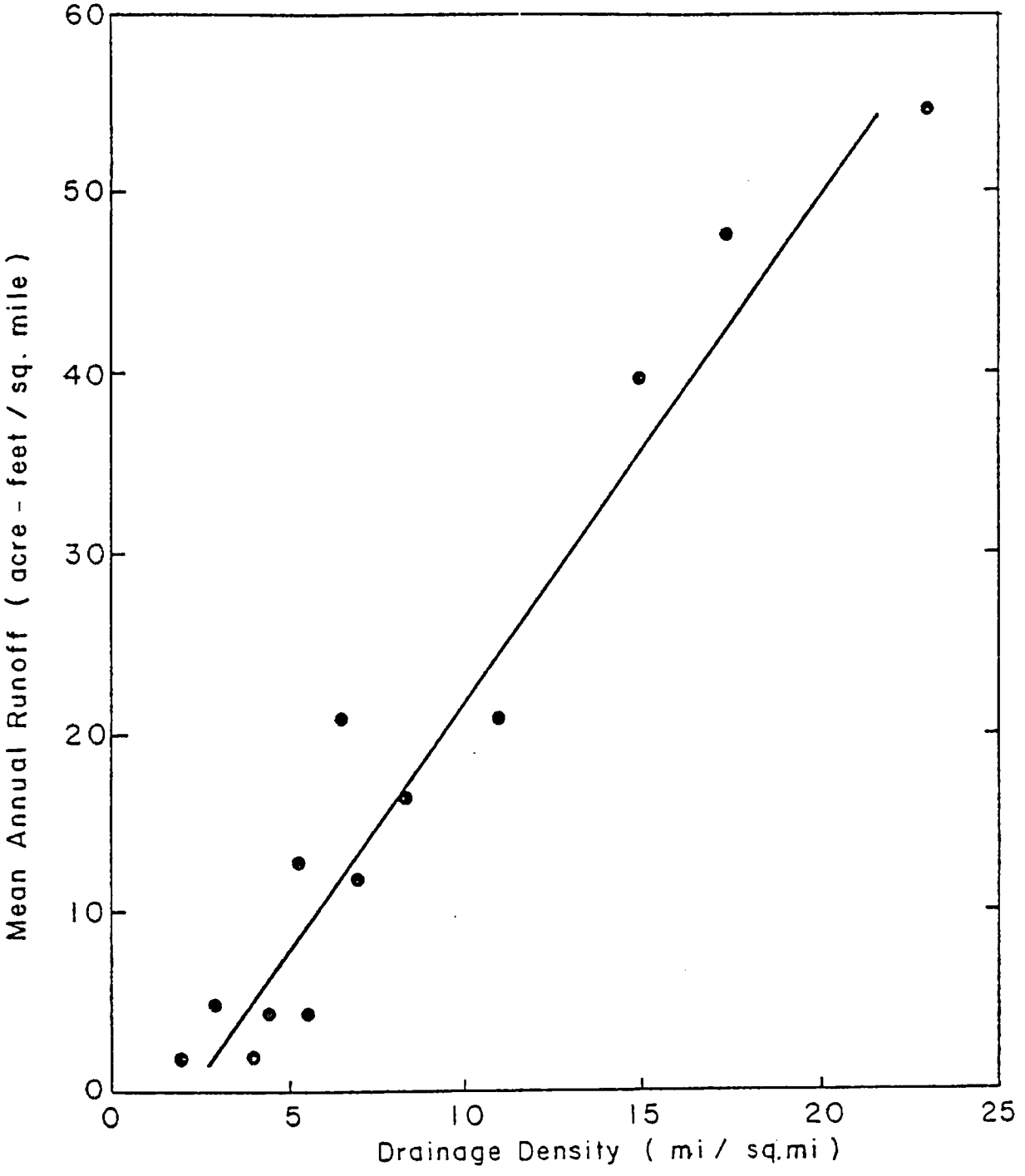


Figure 4-11. Relation between runoff and drainage density for small drainage basins on Fort Union Formation, Wyoming. (From Hadley and Schumm, 1961.)

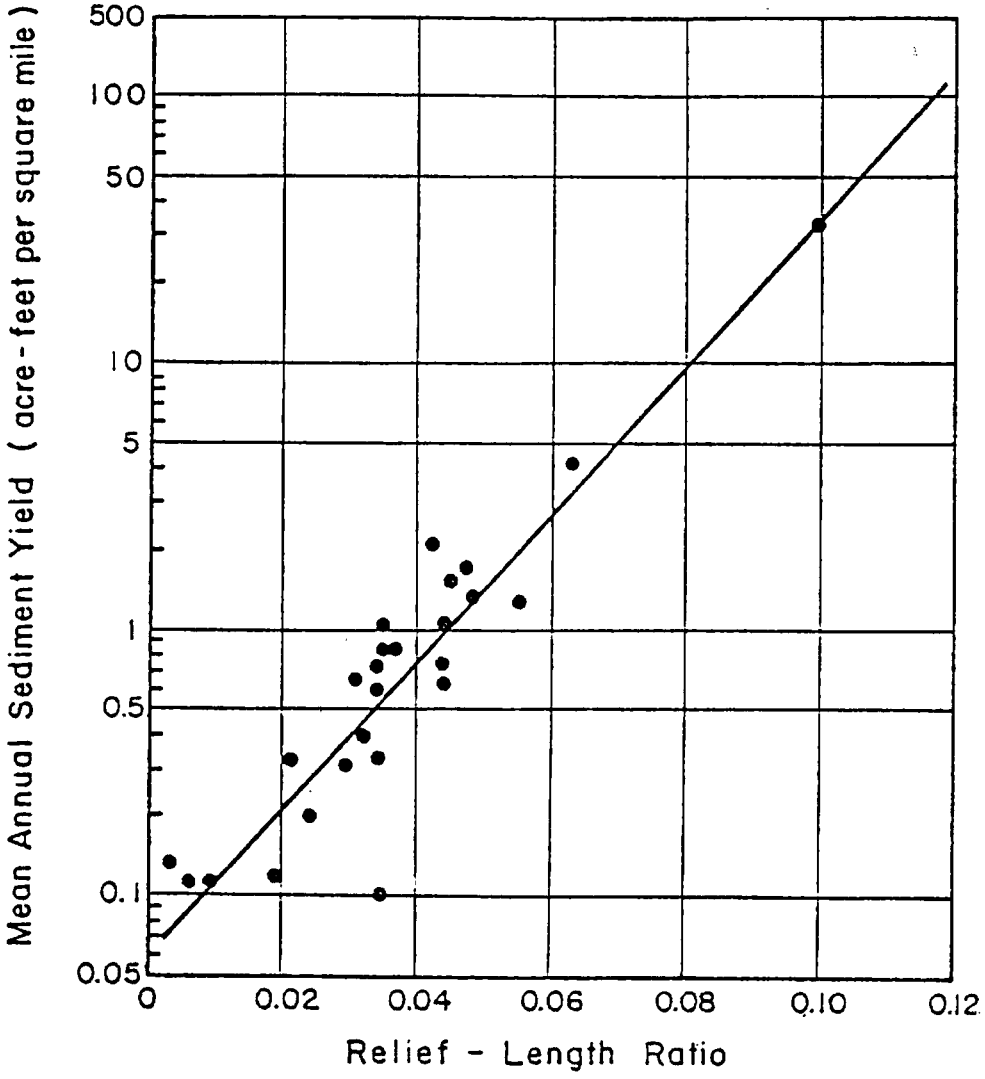


Figure 4-12. Relation between sediment yield and relief-length ratio for small drainage basins on Fort Union Formation, Wyoming. (From Hadley and Schumm, 1961.)

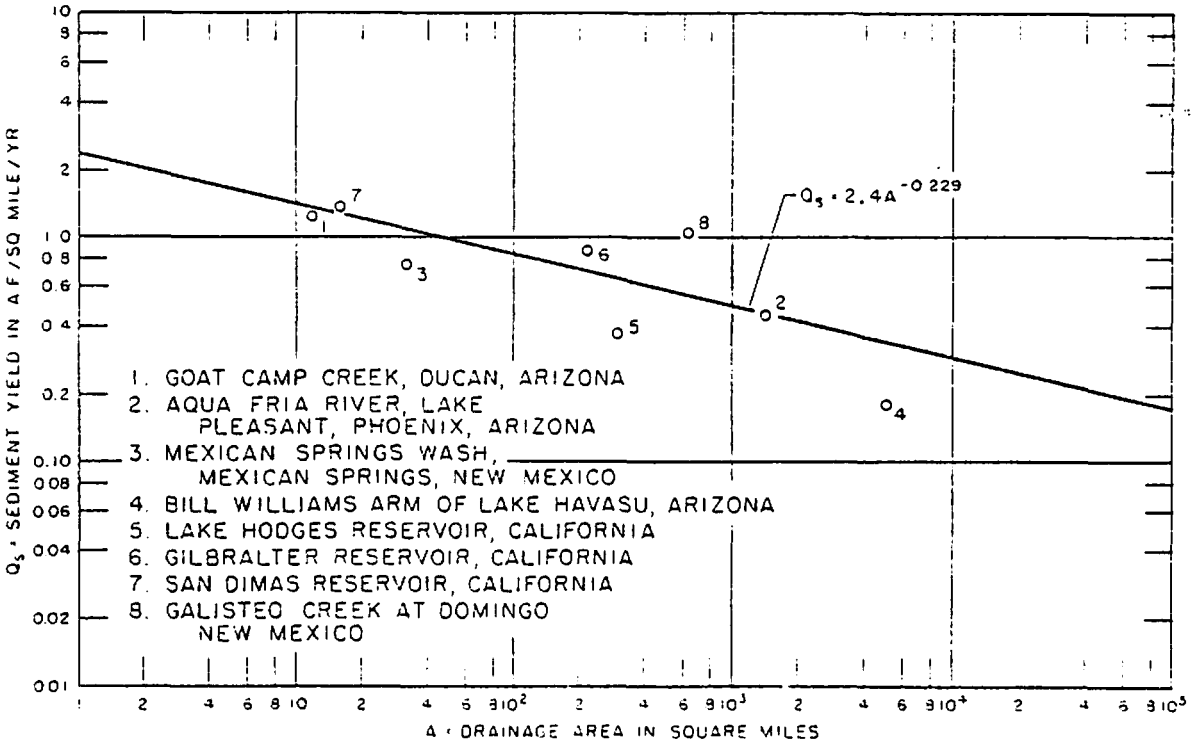


Figure 4-13. Sediment yield decrease with increase of drainage area for basins in Southwestern U.S.A. (From Strand, 1975.)

information. However, in the past the geomorphologist has usually relied on the space for time substitution, in other words, in a given area he selects a sequence of landforms that appear to show evolutionary development and arranges them in an order that portrays such development. A study by Glock of drainage pattern evolution is a good example (Figure 4-14). Glock divided the evolutionary process into five stages: 1) initiation, the first development on a stream pattern on a pristine surface, 2) elongation, the growth of channels into the available area and the blocking out of the network, 3) elaboration, the filling in of the network by the addition of lower order tributaries, 4) maximum extension, is when drainage density is greatest and the drainage network completely fills the available space, and 5) integration involves the loss of identity of the small order streams with progressive reduction of drainage density through time. Glock's scheme is reasonable and in fact at least a part of it is demonstrated by Ruhe's studies of drainage pattern or developed on till sheets of different ages in Iowa (Figure 4-15). Comparison of drainage patterns on four till sheets show a rapid increase in drainage density and in stream frequency through time to a maximum when drainage network growth ceases.

Another method to observe and document drainage network evolution is by experimental studies of network evolution. Several studies of this type have been carried out in the rainfall-erosion facility (REF) at Colorado State University. When precipitation was applied to a gently sloping surface composed of two intersecting planes that concentrated the runoff, a dentritic drainage pattern began to develop in the

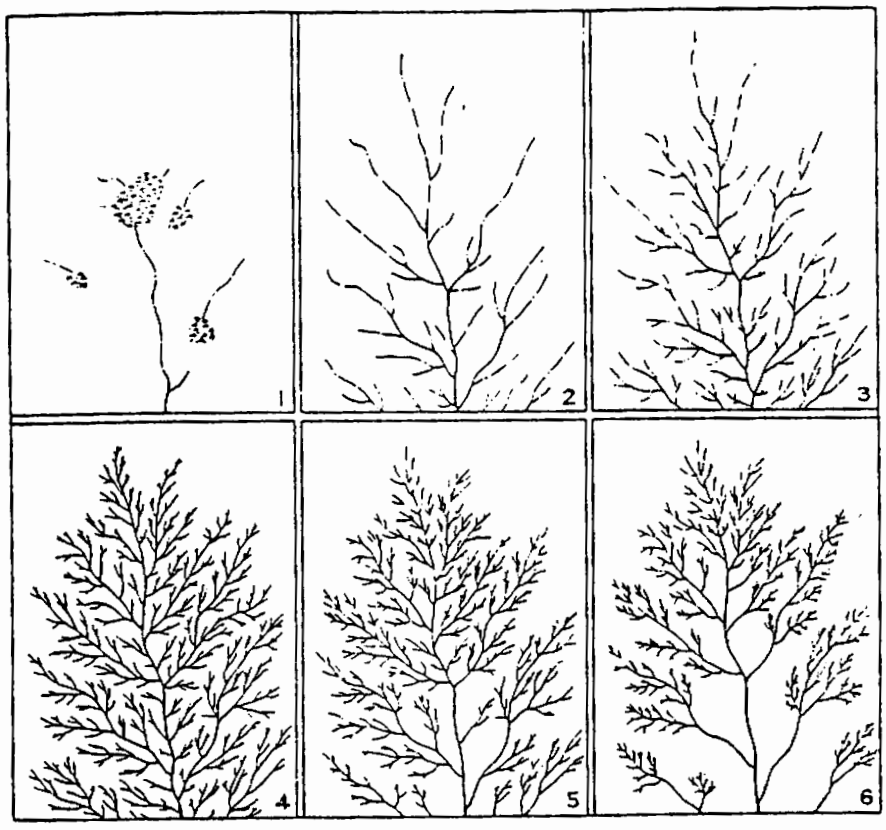


Figure 4-14. An ideal diagrammatic summary of the development of a drainage system given for purposes of comparison only. The first four parts show extension, thus: 1) initiation, 2) elongation, 3) elaboration, and 4) maximum extension. Parts 5 and 6 represent steps during integration.

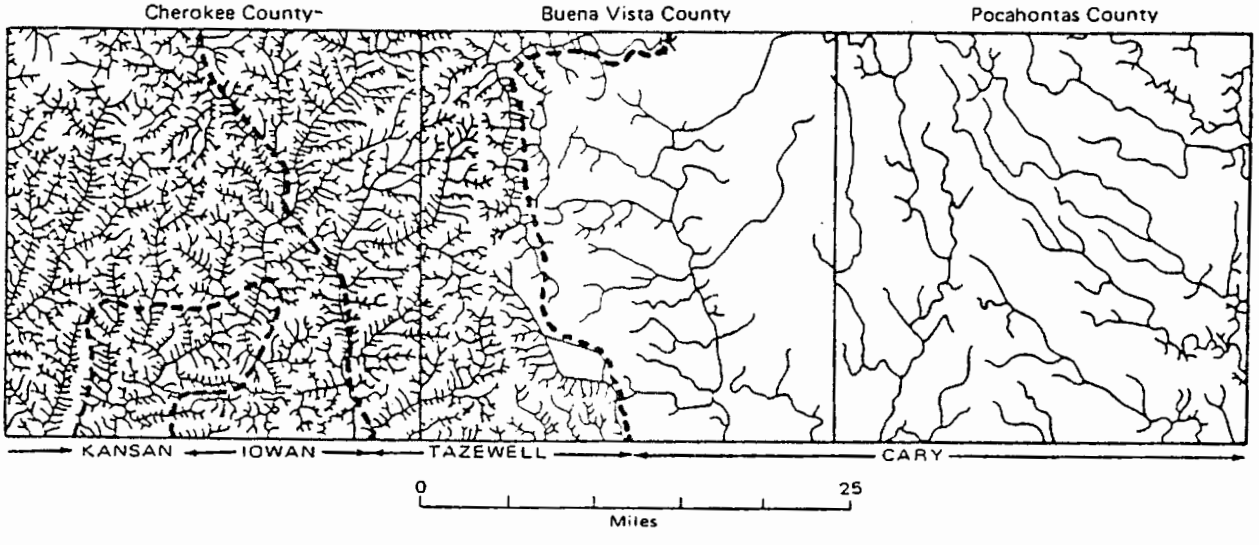


Figure 4-15. A drainage net on land surfaces of glacial drift country in northwestern Iowa. From Ruhe (1952), by permission of American Journal of Science.

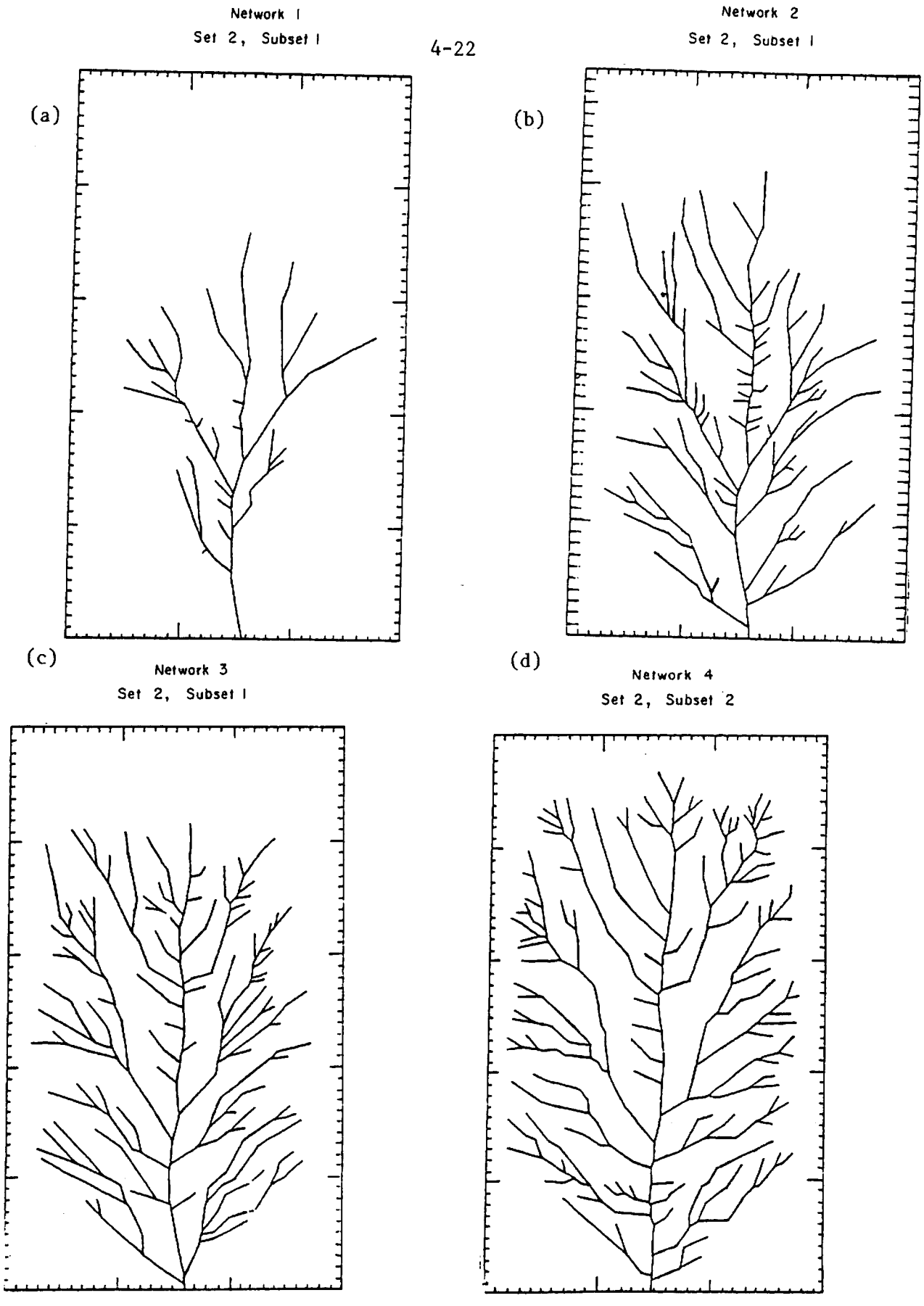


Figure 4-16. Experimental study of drainage network development (Parker, 1977).

(e)

Network 1
Set 2, Subset 3

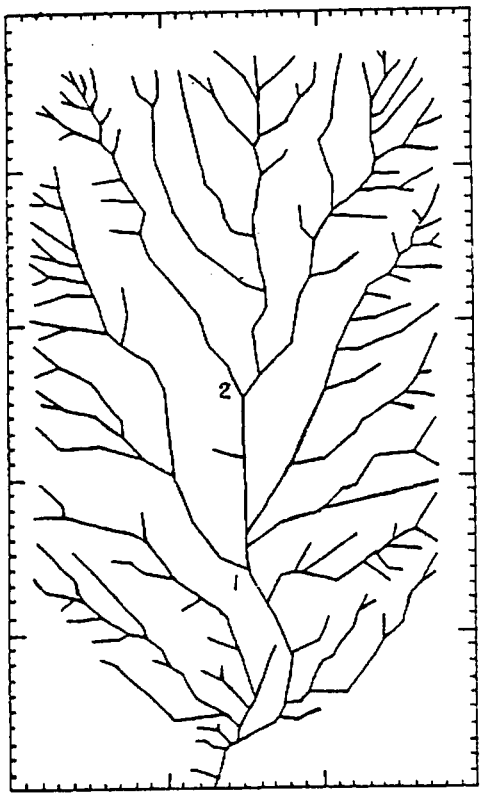


(f)

Network 2
Set 2, Subset 3

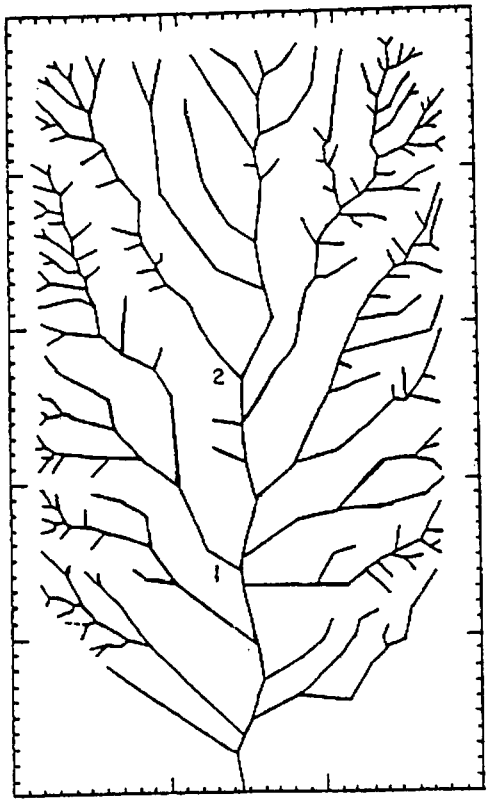


(g)

Network 3
Set 2, Subset 3

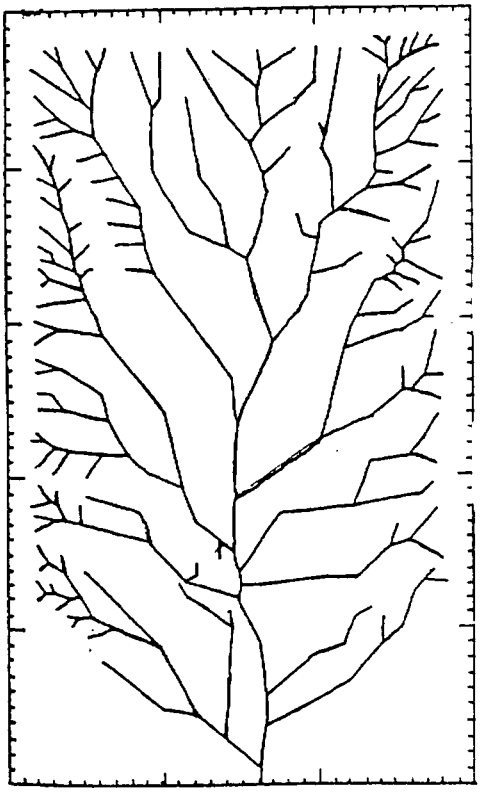


(h)

Network 4
Set 2, Subset 3

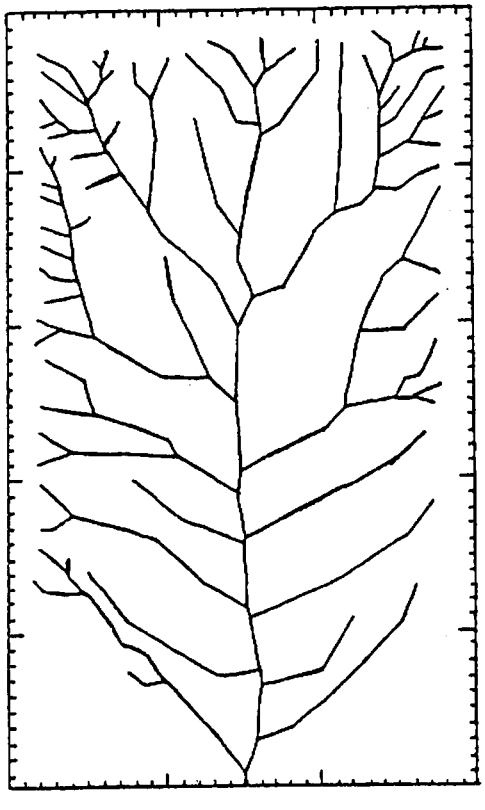


Figure 4-16. Continued.

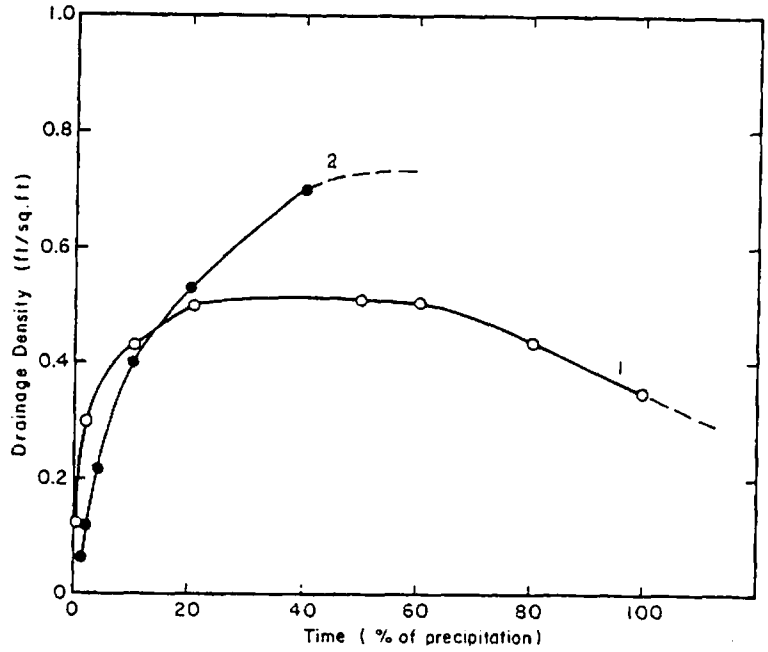


Figure 4-17. Drainage density change during two experiments in REF. Curve 1 is for pattern developed on 3.2 percent slope with stable baselevel. Curve 2 is for pattern developed on 0.75 percent slope with baselevel lowering prior to beginning of experiment (after Parker, 1976). Time is expressed as a percentage of the total water applied to the REF during experiment 1 (curve 1).

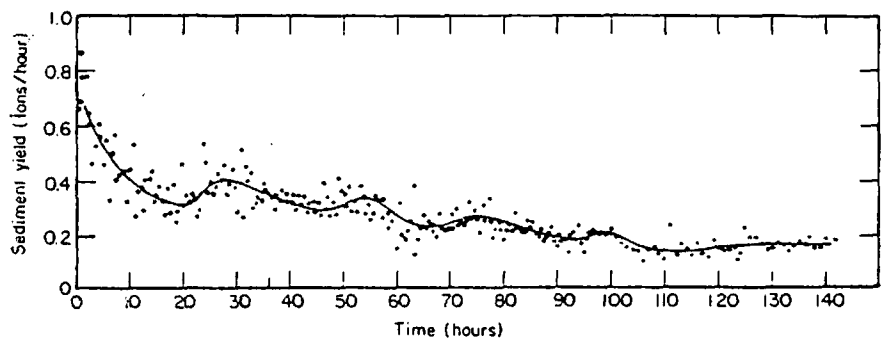


Figure 4-18. Sediment-yield variations during experimental drainage basin evolution (from Parker, 1976). Mean lines is based on a moving mean of 3 points with an average of 10 points. Note secondary peaks at about 25, 55, 75, and 100 hours.

REF (Figure 4-16). As more artificial precipitation was applied there was a rapid increase in drainage density and stream frequency (Figure 4-16 a, b, c, d, and 4-17) and then maximum extension of the drainage network was achieved (Figures 4-17 and 4-16). For this experiment drainage density remained relatively constant for a considerable time at maximum extension. However, as one views the drainage patterns it is apparent that this constancy of drainage density is a result of dynamic change within the drainage pattern itself (Figure 4-16 f, g, h). For example, during the period of constant drainage density there is a loss of lower-order tributaries in the center of the drainage basin and the addition of first order tributaries at the periphery of the drainage network. So network growth is continuing at the margins of the network in those areas of steeper slope the older interior portions of the network enter Glock's phase of integration and channel loss (Figure 4-16 g, h). Erosion begins near the basin outlet and initially there is very high sediment production (Figure 4-18). However, the rate of sediment yield decreases rapidly from this peak through time. This is partly due to the decreasing network growth rate but also as the main channels enlarge and valleys widen there is an increasing opportunity for storage of alluvium in the drainage basin. Growth of the experimental drainage network conforms to Glock's study and provides an interesting insight into the mechanism of a drainage basin, and it is very much like the expected result as based on Davis' cycle of erosion.

Response

Discussion of drainage basin controls and drainage network evolution reveals there is an orderly growth pattern reflecting the nature of materials and the applied eroding forces. During experimental studies a drainage network filled the available space and developed a drainage density that at maximum extension is characteristic of the terrain. In fact when the inverse of drainage density is calculated it provides a measure of a unit drainage area required to maintain a unit length of stream channel. When this value is converted to meters a figure emerges that indicates the average drainage area required to maintain 1 meter length of channel. In badlands one square meter is sufficient but in coarser textured topography much higher values are required. This number ideally should be a constant for any drainage basin but except for an early stage of maximum drainage development this is not the case (e.g. Figure 4-17). Nevertheless, that such a number can be determined shows the influence of earth materials involved in network development. This is also an explanation for orderly drainage patterns and for variations of drainage patterns that one sees because as lithology changes so does the drainage density.

It is clear that a natural change such as a climate or lowering of baselevel will cause basin rejuvenation and an extension of the network with an increase of drainage density, runoff, and sediment yield. Recall also the changes in the drainage patterns exemplified by expansion and contraction of flow in intermittent and ephemeral streams during and following a storm (Figure 4-9). Man's activities such as lumbering and farming, and the effects of overgrazing may have the same results. Forest fires also induce serious erosion and drainage pattern expansion by destruction of protective vegetative cover.

Table 4-3. Hydrologic and geomorphic data from Cornfield Wash.

| Drainage basin number | Drainage area sq miles | Relief ratio, h/l | Incised channel drainage density ΣL/A | Texture-slope product, ΣL/Axh/l | Mean annual sediment yield, acre ft per sq mile | Mean annual runoff, acre ft per sq mile |
|---|---|---|---|---|---|---|
| 1 | 0.29 | 0.046 | 5.6 | 0.26 | 6.8 | 63.4 |
| 2 | 0.87 | 0.026 | 2.1 | 0.055 | 1.7 | 22.1 |
| 3 | 0.25 | 0.036 | 3.0 | 0.11 | 2.2 | 36.8 |
| 4 | 1.18 | 0.023 | 0.6 | 0.014 | 0.6 | 16.3 |
| 5 | 1.04 | 0.035 | 1.3 | 0.046 | 0.9 | 20.5 |
| 9 | 0.09 | 0.048 | 3.2 | 0.15 | 2.8 | 59.9 |
| 13 | 0.33 | 0.043 | 3.1 | 0.13 | 3.7 | 44.5 |

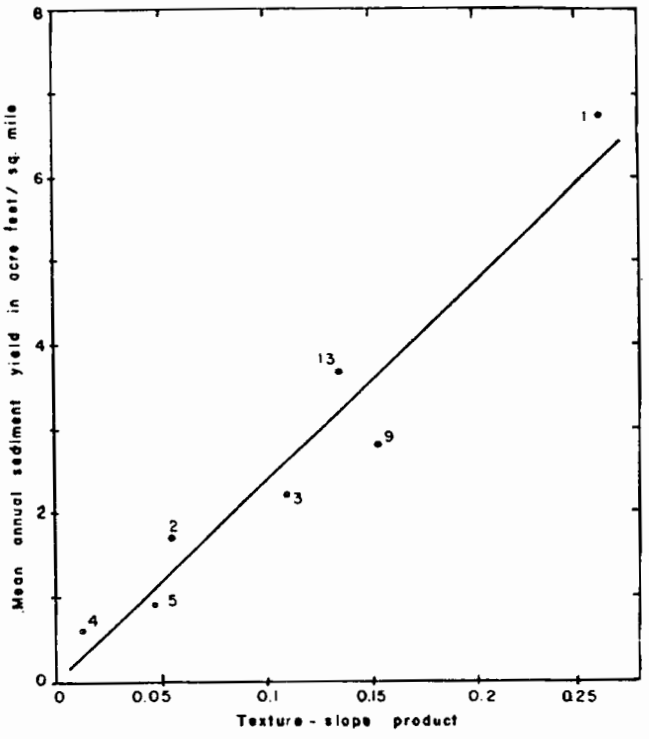


Figure 4-19. Relation between mean annual sediment yield and texture-slope product (incised channel drainage density times relief ratio) for Cornfield Wash drainage basins. Equation of regression line is $y = 25x$.

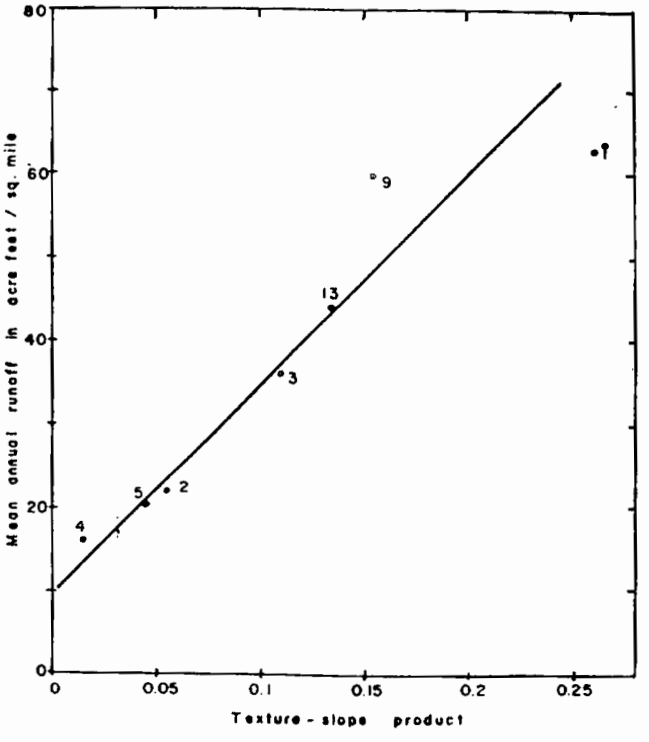


Figure 4-20. Relation between mean annual runoff and texture-slope product (incised-channel drainage density times relief ratio) for Cornfield Wash drainage basins. Equation of regression line is $y = 250x - 10$.

The preceding suggests that the evolutionally development of a drainage basin and landscape will be complex. Any change in an external variable such as climate, land use, or tectonics will have its effect on the drainage pattern.

An example of low difference in the erosional development of small drainage basins' influence on the hydrologic character of these basins is provided by the Cornfield Wash drainage area in New Mexico (Schumm, 1969).

Cornfield Wash is located about 55 miles west of Albuquerque in the Rio Puerco drainage basin. It has a drainage area of 21.3 sq miles which receives about 11 inches of precipitation annually. It is a grassland underlain by horizontal shales and sandstones of the Menefee formation of late Cretaceous Age. Twelve earthfilled dams were constructed in the area during 1950, and runoff and sediment yield have been measured in the reservoirs. Subsequently other dams were constructed within five of these twelve basins. Therefore, the records of only seven basins are comparable and will be considered here. In Table 4-4 hydrologic data collected during 10 years of record (1951-60) are presented with some geomorphic variables that have been found useful in describing morphology of small drainage systems.

Sediment yield is closely related to runoff for the Cornfield Wash basins and both are related to geomorphic variables. Relief ratio, (relief of a drainage basin divided by length) is a simple descriptive parameter that can be calculated by using a map or aerial photographs and an altimeter.

Drainage density (total length of stream channels divided by drainage area) has been related to mean annual runoff for small drainage basins in Wyoming. In the Wyoming study the lengths of all drainage lines were measured, but at Cornfield Wash only the lengths of incised channels were measured (Figure 4-11).

Both incised-channel drainage density and relief ratio are significantly related to runoff and sediment yield from the seven small drainage basins (Table 4-3) but a better correlation is obtained by plotting the product of drainage density and relief ratio against the hydrologic variables. Incised-channel drainage density reflects the texture of dissection or efficiency of the drainage network. When this variable is combined with basin slope (relief ratio) both the gravitational effects on the drainage system and efficiency of the drainage system are combined to provide a geomorphic texture-slope index with dimensions of length $\{L/L \times L/L^2 = 1/L\}$. When this index is plotted against sediment yields and runoff, which are both expressed as a volume per unit area $\{L^3/L^2 = L\}$, direct correlations are obtained (Figures 4-19 and 4-20).

In addition to providing a means of estimating average runoff and sediment yield rates from small watersheds on the Menefee Formation of northern New Mexico, the relations between geomorphic and hydrologic variables provide a ready means for delineation of high sediment producing areas within a larger drainage system. For example, if it is necessary with limited means to prevent as much sediment as possible

from leaving the area, dams could be constructed on channels draining from basins that have both a high relief ratio and a high incised-channel density (high texture-slope product) e.g. Basins 1, 3, 9, and 13 (Table 4-3).

On the other hand if a stock water supply is required, a drainage basin that provide moderate runoff but low sediment yield could be selected (low texture-slope product). For example, the relief ratios of Basins 2 and 4 are almost identical, but Basin 4 (Table 4-3) has a low incised-channel density and a low sediment yield, conversely, basin 2 has a three-fold greater incised-channel drainage density, and the texture-slope product is four times greater. Basin 4 produces about two-thirds the runoff of Basin 2 but only one-third as much sediment. Geomorphic variables provide a basis for selecting small drainage systems for specific purposes. A detailed morphometric analysis of a drainage basin requires good quality aerial photographs and maps. However, the information used above could have been obtained from aerial photographs and a minor amount of field work.

The variables discussed above describe the small drainage systems as a unit but within each of these units there are specific areas from which the greatest amounts of sediment and runoff are produced. For example, studies of erosional development of bandland drainage basins indicate that initially erosion is greatest in the lower part of each basin. As the basin evolves, this zone of maximum erosion moves up the drainage system until the later stages of basin erosion when it concentrates along the divides. Figure 4-21 shows that assuming a flat surface into which the drainage channels have incised, when 50 percent of total possible erosion within a drainage system has occurred, almost 80 percent of the lower one-fifth of the basin but only 25 percent of the upper one-fifth of the basin has been eroded. Therefore, within a drainage system a zone of maximum erosion should exist. In most cases this should be located near the drainage divide but depending on the recent geologic and erosional history of the region, it might well be located nearer the mouth of the system. If this zone of maximum erosion could not be located by inspection of aerial photographs or by field reconnaissance, then average slope curves should provide information on its location within the drainage system.

In summary it is essential to recognize the complexity of Zone 1 both in space and through time. For example, the concept of intrinsic geomorphic thresholds is a basis for the explanation of distribution of erosional features in the landscape and it may provide the techniques needed for predicting sites of erosional and depositional change that can lead to a preventive conservation approach to erosion problems.

For example field studies in semiarid valleys of Wyoming, Colorado, New Mexico, and Arizona reveal that discontinuous gullies (short but troublesome gullied reaches of valley floors) can be related to the slope of the valley-floor surface (Schumm and Hadley, 1957) and the beginning of network rejuvenation by gully erosion in these valleys tends to be localized on steeper reaches of the valley floor. Carrying this one step farther with the concept of geomorphic thresholds in mind, it seems that for a given region of uniform geology, land-use, and climate a critical threshold valley slope should exist above which an alluvial valley floor is unstable.

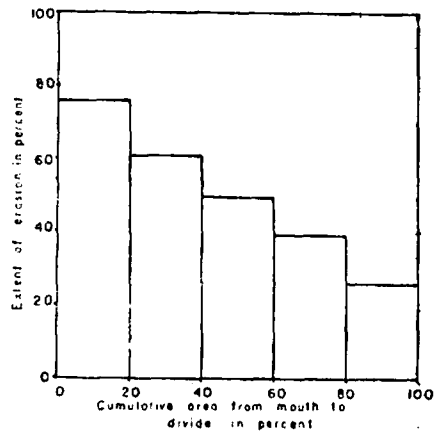


Figure 4-21. Bar chart illustrating distribution of erosion within a small drainage system (11). Bars indicate amount of total possible erosion that has occurred within each 20 percent segment of basin area, after 50 percent of total possible basin erosion has occurred. Maximum erosion has occurred near mouth of basin (76 percent in lower 20 percent of basin). Minimum erosion has occurred in upper 20 percent of area, where during the same period of time only 26 percent of the total possible erosion has occurred.

To test this hypothesis measurements of valley-floor gradient were made in the Piceance Creek basin of western Colorado, an area with numerous discontinuous gullies but with no orderly pattern of distribution (Figure 4-22). Within this area, valleys were selected in which discontinuous gullies were present. The drainage area above each gully was measured on maps and valley slopes were surveyed. Since records of runoff or flood events exist the drainage basin area was considered a variable, reflecting runoff and perhaps flood discharge. When valley slope is plotted against drainage area the relationship is inverse (Figure 4-22) with gentle valley slopes characteristic of large drainage areas. As a basis for comparison, similar measurements were taken for valleys in which there were no gullies and these data are also plotted in Figure 4-22. The lower range of slopes of unstable valleys coincide with higher range slopes of stable valleys. In other words, for a given drainage area it is possible to define a valley slope above which the valley floor is unstable (Patton and Schumm, 1975). Brice (1966) found a similar but less well defined relation for valleys in Nebraska.

It should be noted that the relationship does not pertain to drainage basins smaller than approximately 5 square miles. In these small basins, variations in vegetative cover which are perhaps related to the aspect of the drainage basin or to variations in the properties of alluvium prevent recognition of a critical threshold slope. Only two areas larger than 5 square miles with stable valley floors plotted above the threshold line. It may be concluded that these valley floors are incipiently unstable and that a major flood may eventually cause erosion and trenching of the alluvium stored in these valleys.

Using Figure 4-22 the threshold slope above which trenching or valley instability will take place in the Piceance Creek area may be defined. This has obvious implications for land management, for if the slope at which valleys are incipiently unstable can be determined, corrective measures can be taken to artificially stabilize such critical reaches as they are identified.

The concept of thresholds as applied to alluvial deposits in the western United States is shown by Figure 4-23 in which the decreasing stability of an alluvial fill is represented by a line indicating increase of valley slope toward a condition of instability (line 2) with time. A similar relationship would pertain if, with constant slope sediment loads slowly decrease with time. Superimposed on the ascending line of increasing slope are vertical lines showing variations of valley floor stability caused by flood events of different magnitudes. The effect of even large events is minor until the stability of the deposit has been so reduced by steepening the valley gradient that during one major storm, erosion begins at time A. It is important to note that the large event is only the most apparent cause of failure, as it would have occurred at time B in any case.

These studies of alluvial deposits in drylands suggest that large infrequent storms can be erosionally significant, but major permanent changes result only when a geomorphic threshold has been exceeded. It is for this reason that high-magnitude, low-frequency events may at times have only minor and local effects on a landscape.

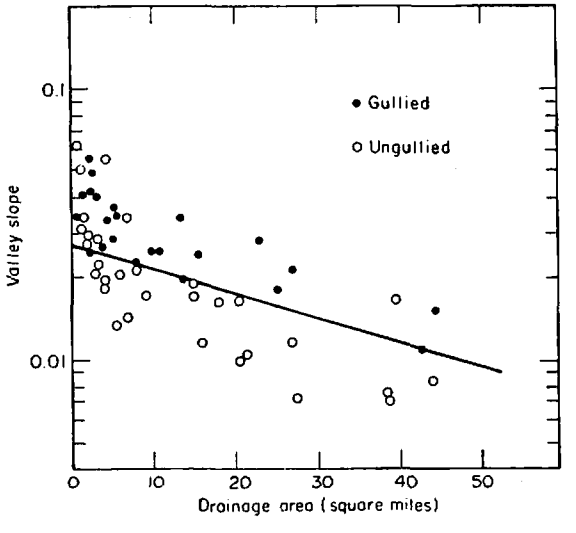


Figure 4-22. Relation between valley-floor slope and drainage area for small drainage basins, Piceance Creek area, Colorado. (From Patton and Schumm, 1975.)

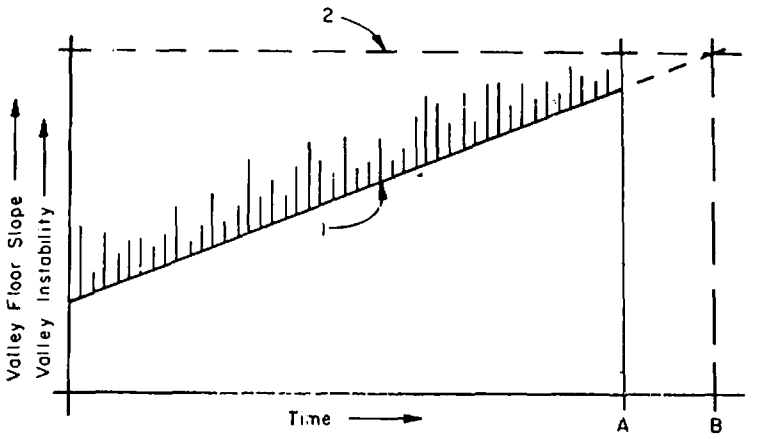


Figure 4-23. Changing valley floor stability through time. Line 1 shows increasing instability of valley floor as it approaches failure threshold (line 2). (From Schumm, 1968.)

The concepts of complex response and geomorphic thresholds are supported by both the response of the experimental drainage basin after rejuvenation and the situation in the Piceance Creek area. It is not suggested that these concepts are applicable everywhere. Rather they are useful in areas of high sediment production or areas of rugged, youthful topography. Nevertheless, the natural storage, flushing, and reworking of alluvium in the valley systems of a drainage basin can be a important aspect of development of alluvial deposits in Zones 2 and 3.

## 4.5 CHANNEL MORPHOLOGY

Sediment and water moving through stable alluvial channels are the independent variables that determine the size, shape and pattern of the channel. Numerous empirical relations have been developed that relate channel morphology to water and sediment discharge. A review of some of these follow.

Lane (1955) summarized these relations by presenting a qualitative relation among bed material load $Q_s$, mean water discharge Q; median sediment size $d_{50}$, and gradient S, as

$$Q_s \cdot d_{50} \simeq Q \cdot S \qquad (4\text{-}1)$$

He concluded that a channel will be maintained in steady-state equilibrium when changes in sediment load and sediment size are compensated for by changes in water discharge and river gradient.

Bed material load is defined as that part of the stream's sediment load that consists of sediment sizes comprising a significant part of the stream bed. Emphasis on significant representation excludes the small percentage of silt and clay usually found in most bed material (Einstein, 1950, pp. 6, 7). The other component of total sediment load, as defined by Einstein, is wash load which is part of the total load not significantly represented in the bed. It is held in suspension by the turbulence of flowing water and moves at the velocity of the water. This distinction is necessary because during sampling of sediment loads bed material load is caught in the suspended sediment sampler, although this coarser material may be only in temporary suspension. Einstein's definition suggests that bed load is composed of sand-size and larger sediment compared with suspended load which is composed of sediment smaller than sand (smaller than about 0.06 to 0.07 mm). In the following text bed load is used to mean sediment larger than silt which although often in suspension will eventually be deposited on the bed. A sediment particle of sand size and larger normally only remains in suspension during a flood, and then is redeposited as the flood wanes. Suspended sediment load refers to wash load composed of silt and clay. This distinction is important because the two types of sediment have significantly different physical properties. Silt and clay have cohesion and are difficult to erode and sands are moved readily depending on size and shape (Hjulstrom, 1935 and Schumm, 1960). Therefore, a river in which a large proportion of the sediment load is silt and clay should be morphologically different from a river with a sediment load that is predominantly sand size and larger, or bed load.

All available evidence indicates that the greater the quantity of water that moves through a channel, the larger is the cross section of that channel. Preceded by numerous studies of canal morphology and stability (Leliavsky, 1955) and Leopold and Maddock (1953) demonstrated that for most rivers, the water surface width b and depth d increase with mean annual discharge $Q_m$ in a downstream direction:

$$b = kQm^{0.5} \tag{4-2}$$

$$d = kQm^{0.4} \tag{4-3}$$

The coefficients of Equations 4-2 and 4-3 are different for each river and when data from a number of rivers are plotted against discharge the scatter covers an entire log cycle. That is, for a given discharge there is an order of magnitude range of width and depth. Therefore, other variables apparently influence channel dimensions.

One such hydrologic variable that has not been given due consideration is peak or maximum discharge. It is rare to find streams that drain geologically similar areas and yet have very different flood peaks. Two such rivers may be the Rios Guanipa and Tonoro in northeastern Venezuela (Stevens et al., 1975). Although hydrologic data were collected for only the rainy season (June-September, 1969) meteorological data indicate that the hydrologic results should be similar for longer periods. A comparison of morphology and hydrologic character of both rivers is presented in Table 4-4. The major differences in width and sinuosity (ratio of channel to valley length) appear to be the result of the great difference in flood characteristics. Although the

Table 4-4. Characteristics of Rios Tonoro and Guanipa (From Stevens et al., 1975).

| River | Drainage area (sq. miles) | Valley slope (ft/mile) | Channel width (ft) | Sinuosity | Median sediment size (mm) | Mean annual discharge (Q) (cfs) | Maximum annual discharge ($Q_p$) (cfs) | $Q_p/Q$ |
|---|---|---|---|---|---|---|---|---|
| Tonoro | 500 | 0.8 | 600 | 1.1 | 0.35 | 400 | 18,900 | 47 |
| Guanipa | 1100 | 0.7 | 50 | 2.3 | 0.35 | 600 | 3,700 | 6 |

records are short they indicate that rivers with high ratios of peak to mean discharge are morphologically different from rivers with low ratios.

The remaining variable that significantly controls river morphology is sediment load. Lacey (1930) concluded from an analysis of regime canal data that the wetted perimeter of a channel is directly dependent on discharge but channel shape reflects sediment load size. Coarse sediment produces channels of a high width/depth ratio and fine sediment produces narrow and deep cross sections. Considerable research into the hydraulics and morphology of coarse load Canadian rivers show that they do differ in dimensions from the rivers studied by Leopold and Maddock (1953). For example, analysis of data from 70 reaches of gravel-fed streams in Alberta yields the following relations (Bray, 1973)

$$b = 2.38\ Q_2^{0.527} \tag{4-4}$$

$$d = 0.266\ Q_2^{0.333} \tag{4-5}$$

in which $Q_2$ is the discharge for a flood with a 2-year recurrence interval and b and d are average water surface width and depth, respectively, at the 2-year discharge. Comparison with Equations 2 and 3 indicates that gravel-bed streams at a given discharge will be wider and shallower but according to Bray the addition of median grain size to Equations 4-4 and 4-5 did not improve them significantly.

In addition to the size of the transported sediment relative amounts of bed load and suspended load also significantly influence the morphology of sand-bed streams. For example, along the Smoky Hill-Kansas River system in Kansas discharge increases in a downstream direction while channel width decreases from about 300 feet to less than 100 feet in central Kansas. Farther east there is a marked increase in channel width. These and other changes are attributed to changes in the type of sediment load introduced by major tributary streams (Schumm, 1968). Tributaries introduce large suspended-sediment loads where the width decreases and large bedloads or sand loads are added where width increases.

The collection of data on channel dimensions, bed and bank sediments, and water discharge at 36 cross sections permits development of additional empirical equations for channel dimensions. Of all the channels located in the semiarid to subhumid regions of the Great Plains of the United States and on the Riverine Plains of New South Wales, Australia none contains more than approximately 10 percent gravel. Thus the bed material is sand (Schumm, 1968, pp. 40, 45). However, the channels show a considerable range of dimensions and hydrology: width 27 to 800 feet, depth 2.4 to 18 feet, width/depth ratio 4 to 75, sinuosity 1.05 to 2.5, and mean annual discharge 21 to 5000 cfs.

The channels are defined as stable because there has been no progressive channel adjustment during the last 10 years of record and are described as alluvial channels because their bed and banks are

composed of sediment that is transported by the river. Data are not available for total sediment loads, but bed and bank samples were collected that are assumed to reflect the type of sediment transported. Although there were no systematic changes in the average size of the bed and bank materials, it was determined that the shape of the channels is closely related to the percentage of silt and clay in the sediments forming the perimeter of channel M. Silt-clay was measured as the sediment smaller than 0.074 mm (200 mesh sieve). The width/depth ratio F of these channels was found to be related to the percentage of silt-clay in the perimeter of the channel M according to Figure 4-24.

$$F = 255M^{-1.08} \tag{4-6}$$

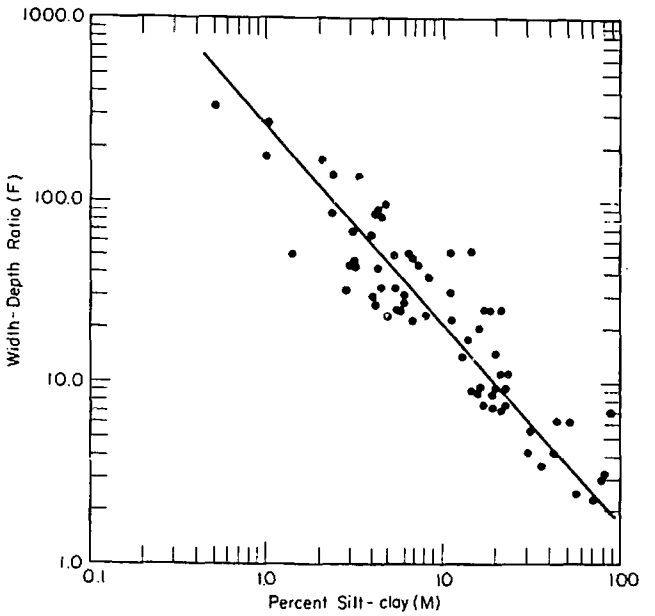


Figure 4-24. Relation between width/depth ratio and percentage of silt and clay in channel perimeter for stable alluvial streams. (After Schumm, 1960.)

M apparently is an index of the type of sediment being transported through the channel and is also an indication of bank stability. For five locations, where both total sediment load data are available and M has been calculated, it was inversely related to the percentage of the total load that is sand or bed load Qb, at a given discharge, as follows (Schumm, 1968)

$$M = \frac{55}{Qb} \tag{4-7}$$

Because of the great range of channel size and discharge of the channels studied, the type of sediment load is considered to be a more important control on stable channel shape than the total quantity of sediment transported through a channel. For example, in one channel a small quantity of bed load may exert the dominant control if it is the

total load, whereas in another channel the same amount of bed load may exert much less influence on channel shape because it is only a small part of the total sediment load. Therefore when suspended sediment load and discharge are constant, an increase in the quantity of bed load will cause an increase in channel width and width/depth ratio. This is probably related to increased gradient and velocity of flow associated with the increase of bed load (Leopold and Maddock, 1953). For example, the experimental results presented in Figure 4-25 for small channels with a constant discharge of 0.15 cfs demonstrate an increase of width/depth ratio with increased bed load (Khan, 1971).

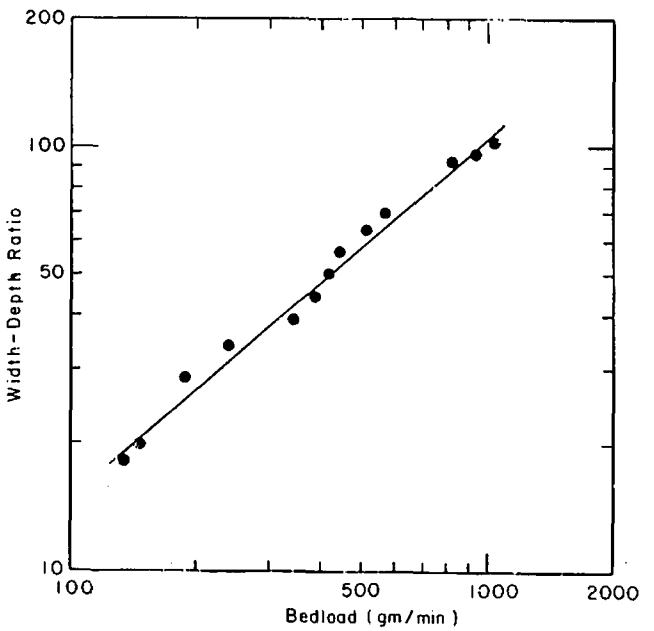


Figure 4-25. Relation between width/depth ratio and sand load in experimental channels at constant discharge of 0.15 cfs (From Khan, 1971).

In summary, for the range of channels studied, type of sediment load exerts the main control on shape. Therefore, for a single channel with constant discharge and amount of suspended load a change of bed load is reflected in a change of both shape and gradient.

Further analysis of the river data produced the following relations for channel width and depth (in feet)

$$b = 37 \frac{Qm^{0.38}}{M^{0.39}} \tag{4-8}$$

$$d = 0.6\, M^{0.342}\, Qm^{0.29} \tag{4-9}$$

Eighty-eight percent ($r = .93$) of the variability of width can be accounted for by mean annual discharge $Qm$ in cfs and channel silt-clay

or type of sediment load M, both being about equally important. The relationship for channel depth is not as good, with about 81 percent (r = .89) of the variability of channel depth accounted for. Nevertheless, only about 40 percent of the variability of channel dimensions is accounted for by discharge alone. It should be noted that width and depth as used here are the bank-full width and depth of channel in contrast to water width and depth used in Equations 4-2 and 4-5.

To summarize for the alluvial rivers, no relation between size of bed sediment and channel dimensions was detected, but when an index of the type of sediment load M was combined with discharge, good correlations with width and depth were obtained. Hence, one may conclude that variations in channel dimensions among many rivers are probably attributable to differences of sediment type. Local changes of channel dimensions may, of course, be strongly affected by variations of resistance of bank sediments (Fisk, 1944, Simons and Albertson, 1960, and Ackers, 1964).

Channel Gradient

If not influenced by uplift or variations in bedrock, the gradient of a stream will usually show a downstream decrease that is associated with an increase of discharge and a decrease in size of sediments (Shulits, 1941 and Lane, 1955). In fact, Lane's relation (Equation 4-1) indicates that gradient is directly related to both bed-material load and grain size and inversely related to water discharge. Sediment size can be readily obtained at any cross section, and when samples are obtained near gaging stations, both sediment size and discharge can be related to gradient. Hack (1957) determined for streams in Virginia and Maryland that drainage area was closely related to mean annual discharge. He then used drainage area as an index of discharge and found that a ratio of median grain size ($d_{50}$ in mm) to drainage basin area (A in square miles) was related to gradient ($S_c$ in feet per mile) as follows:

$$S_c = 18 \left(\frac{d_{50}}{A}\right)^{0.6} \qquad (4\text{-}10)$$

Hack (1957) and Brush (1961) concluded that downstream decreases of stream gradient depend on the resistance of the rocks being eroded and supplied to the channels. For example, Brush found that, for a given distance downstream or length of channel (L in miles) gradient decreased most rapidly for shale, then limestone, and least for sandstone, as shown by the following equations:

$$S_c \text{ (shale)} = 0.034L^{-0.81} \qquad (4\text{-}11)$$

$$S_c \text{ (limestone)} = 0.019L^{-0.71} \qquad (4\text{-}12)$$

$$S_c \text{ (sandstone)} = 0.46L^{-0.67} \qquad (4\text{-}13)$$

Bray (1973) found the following expected relation among gradient, discharge $Q_2$ and sediment size $d_{50}$ for rivers of Alberta

$$S_c = 0.965\, Q_2^{-0.334}\, d_{50}^{0.58} \qquad (4\text{-}14)$$

When data on type of sediment load M were used with mean annual discharge Qm, the following multiple regression equation resulted for the Great Plains and Australian rivers

$$S = 60M^{-0.38}Qm^{-0.32} \qquad (4\text{-}15)$$

Seventy-one percent of the variability of gradient can be accounted for by Qm and M (r = .84, standard error is 0.07 log units). The range of grain size of the bed material was too small to permit an evaluation of effect of grain size on the gradient of these rivers.

A plot of the slope of the alluvial valley surface on which each of the channels flowed compared with gradient of the stream shows that valley slope is correlated with channel slope (Figure 4-26). Although this seems trivial, if the valley slope reflects past discharges and sediment loads (Table 4-1), then it is an independent variable influencing modern channel gradient. It is interesting that in Figure 4-26 for channels with a low silt-clay content, the gradient and valley slope are almost identical and for others with a high silt-clay content the valley slope is three times that of the channel gradient. This suggests that, although valley slope can exert an important influence on gradient of a modern channel, the difference between valley and channel slope can be the result of a change of the type of sediment moved through the channel (Schumm, 1968, p. 51). This matter is considered again when variability of channel patterns is discussed.

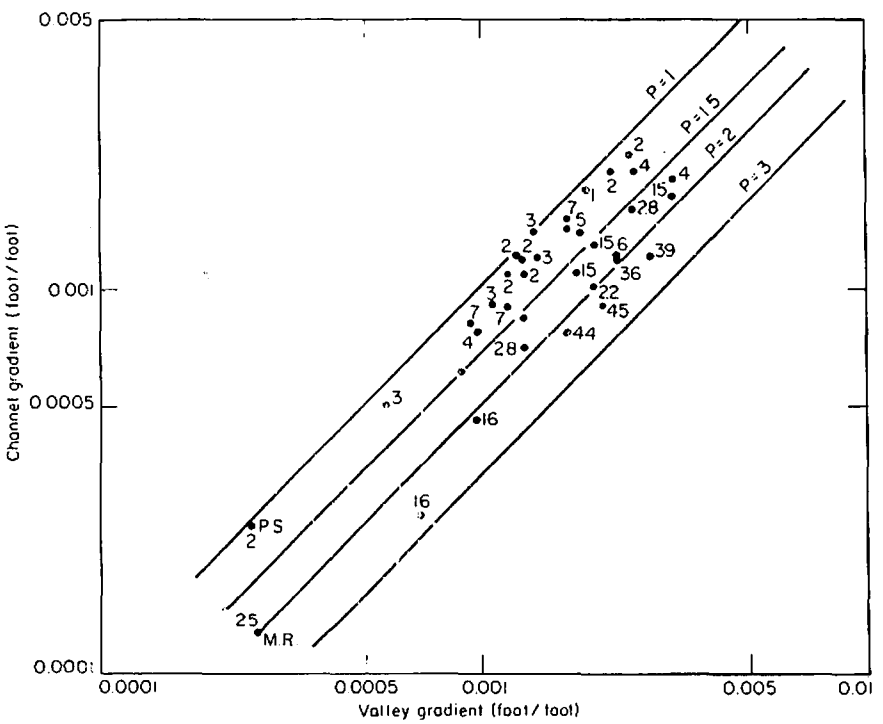


Figure 4-26. Relations between alluvial valley slope and channel gradient. Numbers beside points indicate percentage of silt-clay in channels M. Four lines of equal sinuosity P are shown. M. R. identifies Murrumbidgee River and P. S. identifies paleochannel 2 (Figure 5-34). (From Schumm, 1968.)

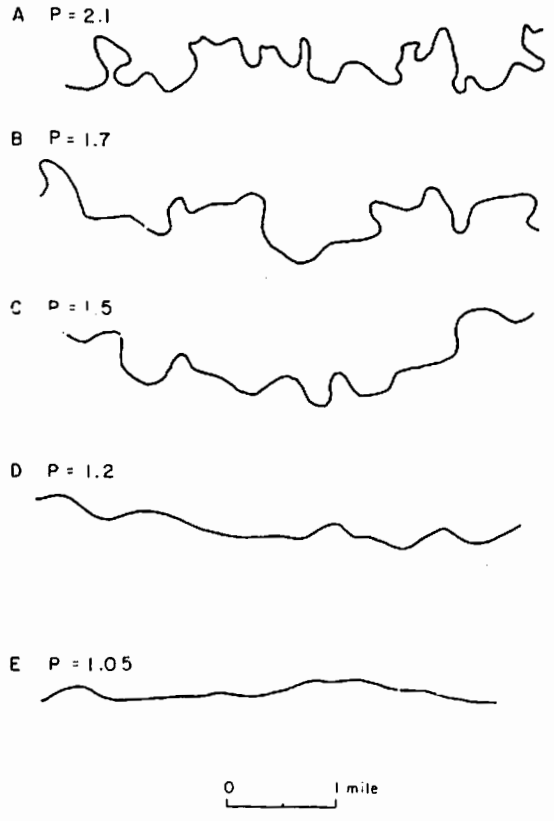


Figure 4-27. Examples of channel patterns. P is sinuosity (ratio of channel to valley length). (From S. A. Schumm, 1963).

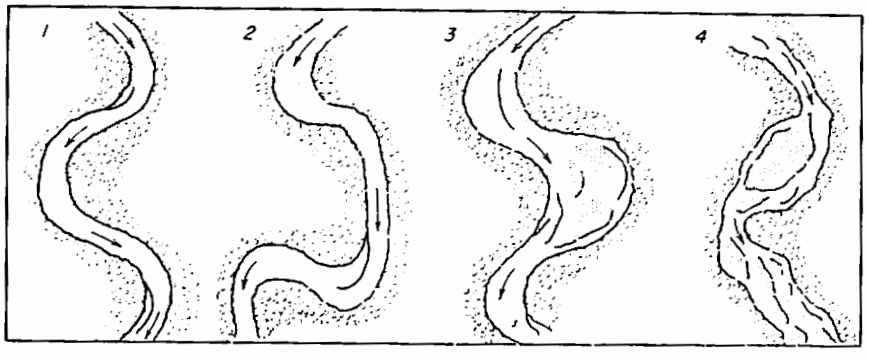


Figure 4-28. Variability of sinuous channel patterns. (1) Sinous channel, uniform width, narrow point bars. (2) Sinuous point-bar channel, wider at bends. (3) Point-bar braided channel, wider at bends. (4) Island-braided channel, variable width. (From Culbertson et al., 1967.)

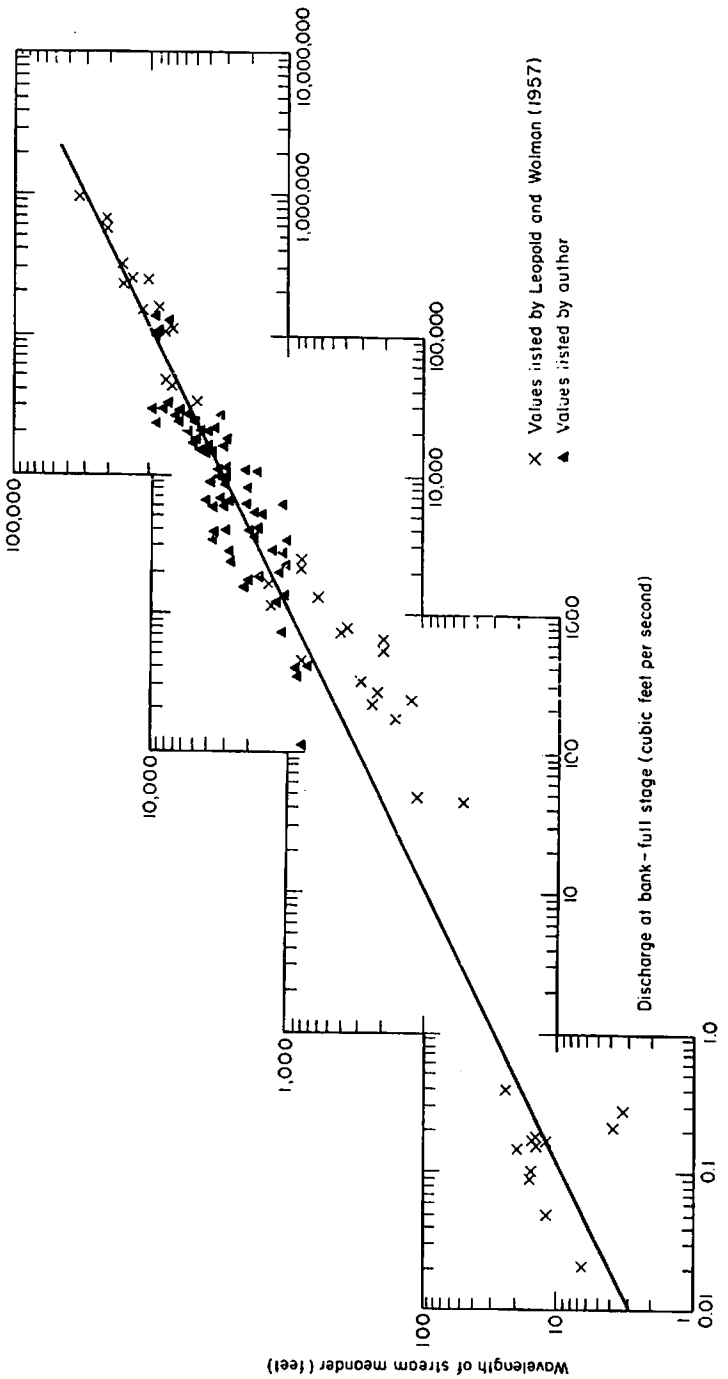


Figure 4-29. Relations between meander wavelength and bankfull discharge. (From Dury, 1964.)

In summary, the gradient of a stream is strongly influenced by the hydrology and geology of the drainage basin. The latter provides sediment of various quantities and sizes and the former provides the transporting medium. Together they determine longitudinal profile and gradient of an alluvial river.

## Channel Patterns

Rivers display a continuum of patterns from straight to highly sinuous (Figure 4-27). It should be emphasized that any division between straight and meandering channels is arbitrary and a meandering stream may be of low sinuosity, perhaps as low as 1.2, if the channel displays a repeating pattern of bends. In addition, sinuous channels have been subdivided on the basis of variations in channel width and bar pattern (Figure 4-28).

Channel patterns described above and in Figures 4-27 and 4-28 are single-channel patterns but multiple-channel patterns exist. Although at low water braided streams have islands of sediment or relatively permanent vegetated islands exposed in the channels, this should not obscure the fact that the islands are in a single, large channel. However, any type of single channel can be part of a multiple-channel distributary system.

All previous work on meandering has demonstrated that meander dimensions are related to discharge of water through the channel (Leopold and Wolman, 1957, Dury, 1964, and Speight, 1965, 1967). In fact the channel need not meander to have a pool and crossing or pool and riffle spacing related to discharge (Keller, 1975). Dury (1964) found that meander wavelength (g in feet) is related to mean annual flood (Qma in cfs) as follows (Figure 4-29)

$$\lambda = 30\ Qma^{0.5} \tag{4-16}$$

It should be noted that there is a 10-fold variation of meander wavelength at a given discharge (Figure 4-29). When information on type of sediment load $M$ is included, the following vastly improved relation is obtained for both mean annual discharge (Qm in cfs) and mean annual flow (Qma in cfs)

$$\lambda = 1890\ \frac{Qm^{0.34}}{M^{0.74}} \quad (r = .96, \text{ standard error is } 0.16 \text{ log units}) \tag{4-17}$$

$$\lambda = \frac{Qma^{0.48}}{M^{0.74}} \quad (r = .93, \text{ standard error is } 0.19 \text{ log units}) \tag{4-18}$$

Additional relations among channel width, discharge, and width of the meander belt have been reviewed by Leliavsky (1955, pp. 133-135).

For stable alluvial rivers of the Great Plains, the degree of meandering or sinuosity $P$ (ratio of channel length to valley length) is related to $M$ as follows

$$P = 0.94\ M^{0.25} \quad (r = .91) \tag{4-19}$$

Hence, Equations 4-6 and 4-19 show that streams transporting little bed load are relatively narrow, deep, and sinuous. However, it is true that rivers that transport small quantities of sand are not always sinuous and some rivers that appear to be transporting only very fine sediment are straight.

Sinuosity

A partial explanation of these sinuosity differences among rivers may reside in the relations of Figure 4-26. If tectonic factors have not modified valley slope, the gradient of the alluvial surface should be at precisely the inclination required for movement of the water-sediment mixture through the valley. The fact that the surface of the alluvium is too steep requires an explanation that depends on an understanding of stream regimen changes during perhaps the past 15,000 years. All rivers flow on the upper surface of alluvium that fills valleys cut into bedrock. Deep valleys and the alluvium probably are the result of changes in baselevel, climate, and hydrologic conditions during and following the Pleistocene epoch.

The alluvium filling the valleys decreases in size from gravel and coarse sand at the base of the deposit to silt, clay, or fine sand at the present valley surface, presumably reflecting changed sediment transport conditions and availability of coarse sediment. Great variability of sediment type occurs in these alluvial deposits but all available information shows a decrease in size of alluvium toward surface of the fill.

Depending on the type of rocks exposed within a drainage basin, the sediment load of one of these rivers might have changed from gravel and sand to sand alone or from silt, clay, sand, and gravel to predominantly silt and clay during deposition. For example, in a stream draining areas underlain by sandstone the size and quantity of the sediment decreased but the proportion of bed load to total load probably changed little. A stream draining areas of sandstone and shale underwent not only a decrease in size of sediment load but also a reduction in ratio of bed load to total load. As a result a stream draining areas of mixed sediments, after deposition of the coarser sediment ceased, was flowing on alluvium with a gradient in excess of that required for transport of finer load. Reduction of gradient by degradation could only be partly effective, for with incision the stream would encounter coarser sediments transported during a previous regime and development of an armor of coarse sediment would prevent further degradation. Formation of a sinuous course appears to have been the only alternative. Rivers draining areas of relatively coarse or sandy sediments were less affected by the change in size and type of sediment load and continued to flow on a gradient that is today essentially that of the valley itself, because they have historically been transporting relatively large amounts of bed load.

An increase in sinuosity and accompanying decrease in stream gradient reflects the need to dissipate energy (in excess of that expended in friction and sediment transport) that becomes available as the

bed load decreases. Thus the rivers with sandy channels (low M) plot high (low sinuosity) in Figure 4-26 and rivers with high silt-clay channels plot low.

Apparent exceptions to this conclusion may occur. For example, streams draining mountain meadows may meander yet their beds are composed of cobbles. An explanation is that the coarse sediment acts as an armor over which the stream meanders. Under the present regime these coarse sediments are not moved. Therefore, the predominant sediment load is transported in suspension. In addition it appears probable that although a stream is transporting fine sediments, the valley gradient may be so gentle as to inhibit meandering. Examples of this may be the Mississippi River below New Orleans (Fisk, 1944) and the Illinois River (Rubey, 1952). Both rivers flow on surfaces that slope very gently downstream, and both rivers are essentially straight, although they transport fine sediments.

It appears that valley gradient can be an independent variable influencing the present pattern of an alluvial river. This is an appealing explanation for development of a sinuous river course. It is not an original one but it can be supported by field evidence. For example, the points labeled M. R. and P. S. in Figure 4-26 represent two channels on the Riverine Plain and New South Wales, Australia. One is a paleochannel (P. S.) that was functioning at least 10,000 year ago. It contains and therefore must have transported, large quantities of sand (low M) across an alluvial plain at the slope of the plain (sinuosity about 1.0). Since the time that this channel was functioning, the climate has changed, vegetational cover in the headwaters has improved, and the quantity of sand to be moved has decreased markedly (Schumm, 1968). The modern Murrumbidgee River (M. R.), which drains the same sediment source area, now meanders across the alluvial plain with a sinuosity of about 2. To reduce its gradient the paleochannel could have either incised into the plain or developed a sinuous course. Incision required movement of tremendous quantities of sediment and to reduce the gradient by half, incision in the headwaters would have had to have been great. A much simpler means of reducing gradient required development of a sinuous course, and it was by this method that gradient reduction was accomplished and the pattern of the Murrumbidgee River established.

## Channel Adjustment

The engineer is well aware of the type of channel response that results from efforts to control river behavior and engineering literature is replete with discriptions of local, but rapid, channel response to man's influence. The geologist on the other hand, recognizes in alluvial deposits the river terraces, evidence of long-term adjustment of entire river systems to the effects of change of climate, mountain-building processes, and sea-level fluctuations.

Equations developed for stable alluvial channels demonstrate that for most changes of hydrologic regime that involve both a change in discharge and type of sediment load, many aspects of channel morphology will adjust. In addition, reaction of a channel to altered discharge

and type of load may result in changes of channel dimensions contrary to those indicated by standard regime equations. That is, it is conceivable that under certain circumstances with a decrease of discharge, depth will decrease and width will increase.

Equations 4-6, 4-8, 4-9, 4-14, 4-17, and 4-19 provide a basis for discussion of natural and man-induced changes of river morphology. River adjustment within the framework of these equations is discussed. However, first it should be reemphasized that these equations result from an analysis of stable alluvial rivers that transport only small quantities of gravel and are for the most part located in subhumid and semiarid regions. Although the equations can be expected to have a wide application, parameters must change as more data from a wider range of geologic and hydrologic conditions are accumulated. Therefore, the following treatment stresses directions of change rather than magnitude.

Equations 4-2, 4-3, 4-8, 4-9, and 4-16 to 4-18 indicate that channel width b, depth d, and meander wavelength $\lambda$ are directly related to discharge Q. Equations 4-14 and 4-15 demonstrate that gradient S is inversely related to discharge. From these equations the following generalized relation is obtained

$$Q \simeq \frac{b,\ d,\ \lambda}{S} \tag{4-20}$$

Either mean annual discharge Qm or mean annual flood Qma could be used in this and subsequent equations. Considerable independent information is available to demonstrate that the relations expressed by Equation 4-20 are valid. However, effects of flood peaks as discussed earlier are not included in these relations but may well have the same influence as Qm and Qma.

Equations 4-8, 4-15, 4-17, and 4-18 demonstrate that channel width, meander wavelength, and gradient are inversely related to the type of sediment load M. Equations 4-9 and 4-19 indicate a direct relationship among channel depth, sinuosity P, and type of sediment load M. The percentage of silt-clay in the perimeter of a stable channel reflects the nature of sediment load moving through that channel that can be expressed as the percentage of total load that is bed load $Q_b$. However, for one channel or for channels of similar average discharge, M probably will vary inversely with the quantity of bed load that moves through the channel (Equation 4-7). Therefore, $1/Q_s$ can be substituted for M in these equations if discharge is constant. From this substitution the following generalized relation is developed

$$Q_s \simeq \frac{b,\ \lambda,\ S}{d,\ P} \tag{4-21}$$

Width/depth ratio F is not included in Equation 4-21 although it is highly dependent on M or $Q_s$ because both width and depth appear separately. Nevertheless, the relation between width/ depth ratio and M (Equation 4-6) is useful for interpreting changes of channel width and depth in subsequent relations.

To discuss in more detail the effects of changing discharge and sediment load on channel morphology, a plus or minus exponent is used to indicate how with an increase of discharge or bed load the various aspects of channel morphology change. For the relatively straightforward cases of an increase or decrease in discharge or bed load alone, Equations 4-22 through 4-25 are obtained.

$$Q^+ \simeq b^+, d^+, \lambda^+, S^- \quad (4\text{-}22)$$

$$Q^- \simeq b^-, d^-, \lambda^-, S^+ \quad (4\text{-}23)$$

$$Q_s^+ \simeq b^+, d^-, \lambda^+, S^+, P^- \quad (4\text{-}24)$$

$$Q_s^- \simeq b^-, d^+, \eta^-, S^-, P^+ \quad (4\text{-}25)$$

An increase or decrease in discharge alone could be caused by diversion of water into or out of a river system or climate change. An increase of $Q_s$ can result from increased erosion in the catchment area induced by deforestation or by an increase in the area under cultivation, climate change, or uplift. A decrease of $Q_s$ can result from improved land use, a program of soil conservation, or climate change.

An increase or decrease in discharge changes the dimensions of the channel and its gradient. An increase or decrease in bed load at constant mean annual discharge changes not only channel dimensions, but also gradient width/depth ratio and sinuosity.

In nature however, rarely does a change in discharge or sediment load occur alone. Generally, any change in discharge is accompanied by a change in type of sediment load and vice versa. Under these circumstances it should no longer be assumed that M which can have the same value for both very large and very small streams is related to the reciprocal of $Q_s$ because discharge is changing. However, changes of average discharge Q in a river are always considerably less than the order of magnitude differences of discharge between large and small rivers. Hence, it is probable that M can be an index of both type of sediment load $Q_b$ and quantity of bed load $Q_s$ in a river subject to moderate changes of average discharge.

Using the plus or minus exponents to indicate an increase or decrease in a variable, four combinations of changing discharge and sediment load can be considered. Consider for example, the case where both discharge and bed load increase, perhaps as a result of diversion of water from a bed load channel into a suspended load channel. Equation 4-26 suggests the nature of the resulting channel changes.

$$Q^+ Q_s^+ \simeq b^+, d^{\pm}, \lambda^+, S^{\pm}, P^-, F^+ \quad (4\text{-}26)$$

Equation 4-19 indicates that with an increase of both discharge and bed load, sinuosity should decrease and width, meander wavelength, and width/depth ratio should increase. The influences of increasing discharge and of bed load on channel depth and gradient are in opposite directions and it is not clear in what manner gradient and depth should change. However, by including width/depth ratio F in Equation 4-26 an

estimate of the direction of change of depth can be obtained. Width/depth ratio is predominantly influenced by type of load (Equation 4-6) and therefore increases in Equation 4-26. This suggests that depth will remain constant or decrease because both width and width/depth ratio increase. Channel gradient will probably increase because sinuosity decreases thereby straightening the channel and increasing its slope.

When both $Q_s$ and $Q$ decrease, for example as a result of dam construction, the reverse of Equation 4-26 pertains:

$$Q^- Q_s^- \simeq b^-, d^{\pm}, \lambda^-, S^{\pm}, P^+, F^- \quad (4\text{-}27)$$

When, as is common in nature, changes in Q and $Q_s$ are in opposite directions, the following relations are obtained

$$Q^+ Q_s^- \simeq b^{\pm}, d^+, \lambda^{\pm}, S^-, P^+, F^- \quad (4\text{-}28)$$

$$Q^- Q_s^+ \simeq b^{\pm}, d^-, \lambda^{\pm}, S^+, P^-, F^+ \quad (4\text{-}29)$$

The situation expressed in Equation 4-28 could result from a combination of controls, for example dam construction with impoundment of sediment and diversion of water into the channel from another source. The situation expressed by Equation 4-29 could result from increased water and land use, thereby decreasing discharge and increasing bed load. Both could result from climate change.

Equation 4-29 shows that with an increase in discharge but a decrease in bed load, the channel depth and sinuosity will increase while gradient and width/depth ratio will decrease. With an increase in depth and a decrease in width/depth ratio, channel width will probably decrease. Meander wavelength will remain unchanged or will either increase or decrease depending on the magnitude of the changes of discharge and load. However, as sinuosity increases, it seems likely that meander wavelength would decrease.

The above relations demonstrate qualitatively how channel metamorphosis occurs with changes of discharge and sediment load. The magnitude of the changes of channel characteristics can be estimated through the use of Equations 4-6, 4-8, 4-9, 4-15, and 4-17 to 4-19 if the magnitudes of the changes of discharge and bed load or channel silt-clay content are known (Schumm, 1969, 1977).

Significantly different channel dimensions, shapes, and patterns associated with different quantities of discharge and bed load indicate that as these independent variables change, major adjustments of channel morphology can be anticipated. When changes of channel width and depth, as well as of sinuosity and meander wavelength, are required to compensate for a hydrologic change then a long period of channel instability can be anticipated with considerable bank erosion and lateral shifting of the channel occurring before stability is restored.

Horizontal Instability

Horizontal instability of a river may take two forms, avulsion and pattern change. Avulsion is the shift of the channel from one part of

the valley to another by development of a new course. Pattern change can be due to cutoffs that reduce channel sinuosity or to growth of meanders.

Pattern Variability

The same river may have patterns ranging from essentially straight to very meandering and even braided. Variations of pattern between river systems can be explained by differences in geologic history of the systems and by differences in water discharge and sediment load. However, variations of sinuosity along one river that is presumably transporting constant sediment load at a constant discharge are less readily explained. If an increase of sinuosity is one means by which the gradient of a river is reduced, a serious problem arises. How can a river remain stable with essentially constant water and sediment discharge, if its gradient changes from reach to reach? Such a situation appears to invalidate the well-established regime equations that relate gradient to discharge and sediment load.

The answer appears to be that in many cases gradient varies only slightly but slope of the valley floor on which the river flows varies significantly. That is, within a valley there are reaches of valley floor that are steeper and gentler than the average gradient. To maintain a relatively constant gradient the river lengthens its course by meandering on the steeper reaches. Thus, if other causes are eliminated, high sinuosity reaches of a channel should reflect a steeper valley slope and vice versa.

Figure 4-30 shows that the sinuosity of the Mississippi River varies with valley slope. Data used to prepare Figure 4-18 were obtained from the 1911 to 1915 survey of the Mississippi River between Cairo, Illinois, and Head of Passes, Louisiana, a river distance of 1020 miles. This old survey was used because it provided information on the river before artificial cutoffs shortened the river by about 150 miles.

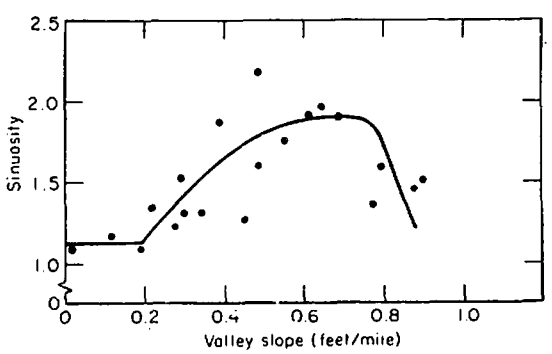


Figure 4-30. Relation between valley slope and sinuosity for the Mississippi River between Cairo, Illinois and Head of Passes, Louisiana. Data was obtained from 1911 to 1915 surveys before modification of the channel patterns by artificial cutoffs. (From Schumm et al. 1972.)

Although the scatter is large, the lowest sinuosity evidently occurs on the gentlest valley slopes (left side of plot), which is characteristic of the lower 200 miles of river. Low values of sinuosity at the steepest valley slopes occur where natural chute cutoffs have developed and the flow now divides around large islands.

It should be emphasized that length and sinuosity of meandering rivers change naturally as meander loops are enlarged and then cut off. Thus, along a given reach of a meandering river sinuosity varies about a mean with time explaining much of the scatter in Figure 4-30. For example, the very low point (slope of 0.009, sinuosity of 1.2) represents a reach north of Memphis, Tennessee where several cutoffs occurred naturally during the late 19th century.

The highest points represent a reach in which a large bend is prevented from cutting off by a bedrock control. Without human interference sinuosity of very sinuous reaches will decrease because of cutoffs. Sinuosity of the reach north of Memphis should however increase as new bends develop and enlarge.

Research by Lane (1957) and Leopold and Wolman (1957) indicates that there is a gradient or discharge threshold above which rivers tend to be braided (Figures 4-31 and 4-32). Experimental work reported by Schumm and Khan (1972) shows that for a given discharge, as valley floor slope is progressively increased, a straight river becomes sinuous and then eventually braided at high values of stream power and sediment transport (Figure 4-33). Rivers that are situated close to the meandering-braided threshold should have a history characterized by transitions in morphology from braided to meandering and vice versa.

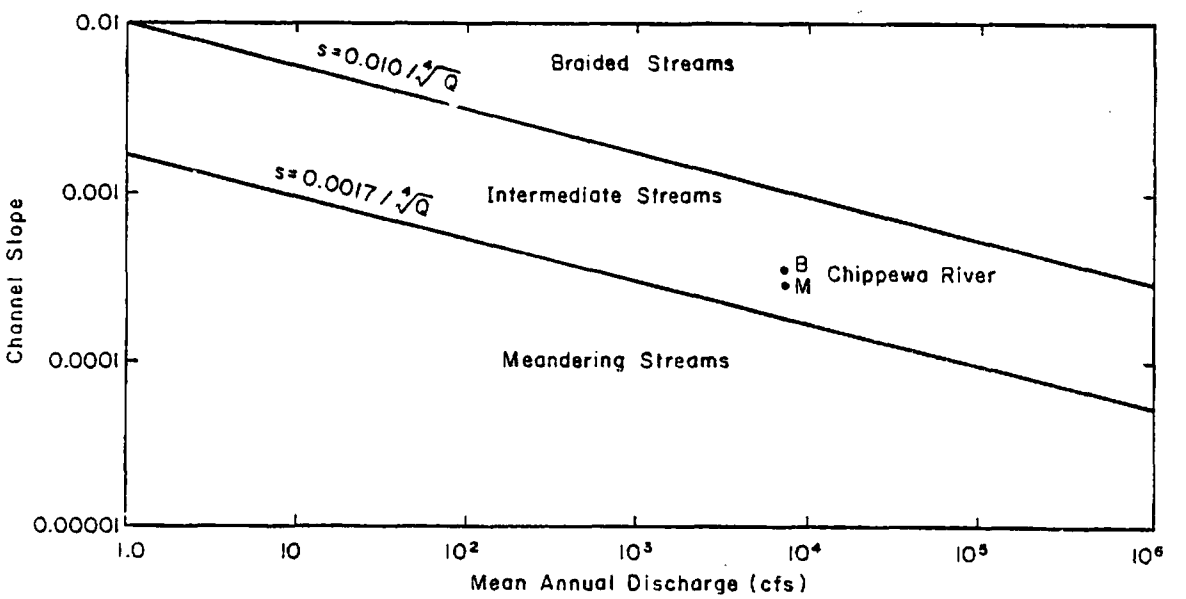


Figure 4-31. Lane's (1957) relation between channel patterns, channel gradient, and mean discharge. The regression lines were fitted to data from streams that Lane classified as highly meandering to braided. Letters B and M identify position of the braided and meandering reaches of the Chippewa River (From Schumm and Beathard, 1976).

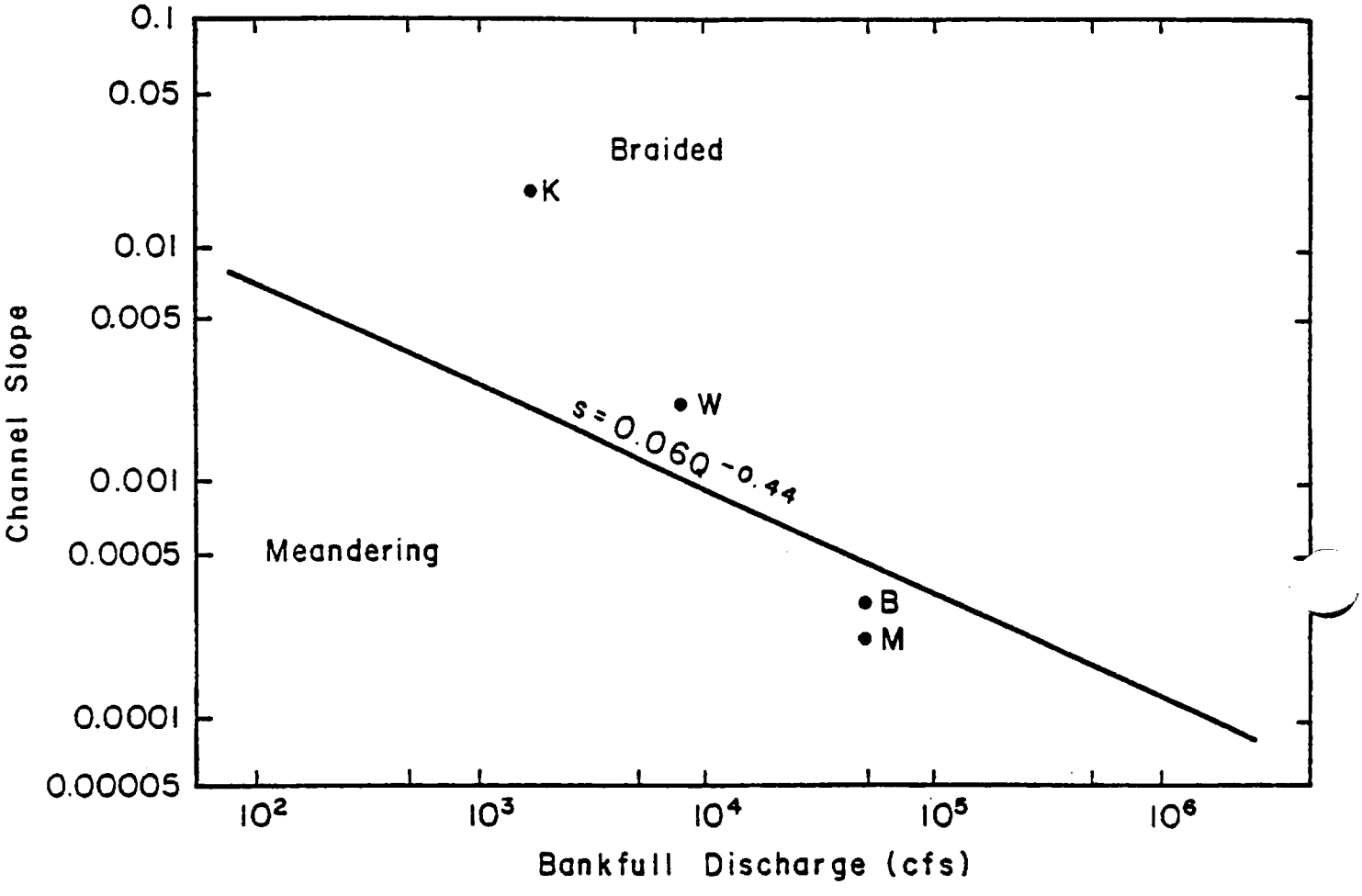


Figure 4-32. Leopold and Wolman's (1957) relation between channel patterns, channel gradient, and bankfull discharge. Letters B and M identify braided and meandering reaches of Chippewa River. Letters K and W refer to Kowhai and Wairau Rivers (From Schumm and Beathard, 1976).

In most cases it is difficult to determine if a river is susceptible to the type of treatment discussed in the preceding sections. Perhaps the best qualitative guide to river stability is a comparison of the morphology of numerous reaches and determination of change in the position of morphology of the channel during the last few centuries. Another approach might be to determine position of the river on the Leopold-Wolman (1957) or Lane (1957) gradient-discharge graphs (Figures 4-31 and 4-32). If a braided river plots among the meandering channels or vice versa it is a likely candidate for change because it is unstable.

An example of the method by which this may be accomplished is provided by the Chippewa River of Wisconsin a major tributary to the Mississippi River (Schumm and Beathard, 1976). The Chippewa River rises in northern Wisconsin and flows 320 km to the Mississippi River entering 120 km below St. Paul. It is the second largest river in Wisconsin with a drainage basin area of 24,600 square km.

From its confluence with the Mississippi to the town of Durand 26.5 km up the valley, the Chippewa is braided. The main channel is characteristically broad and shallow and contains shifting sand bars. Bankfull width as measured from U.S. Geological Survey topographic maps is 333 m. Sinuosity of this reach is low (only 1.06). However, in the 68 km reach from Durand to Eau Claire the Chippewa River abruptly changes to a meandering configuration with a bankful width of 194 m and sinuosity of 1.49. The braided reach has a channel gradient of .00033 and the meandering reach has a gradient of .00028.

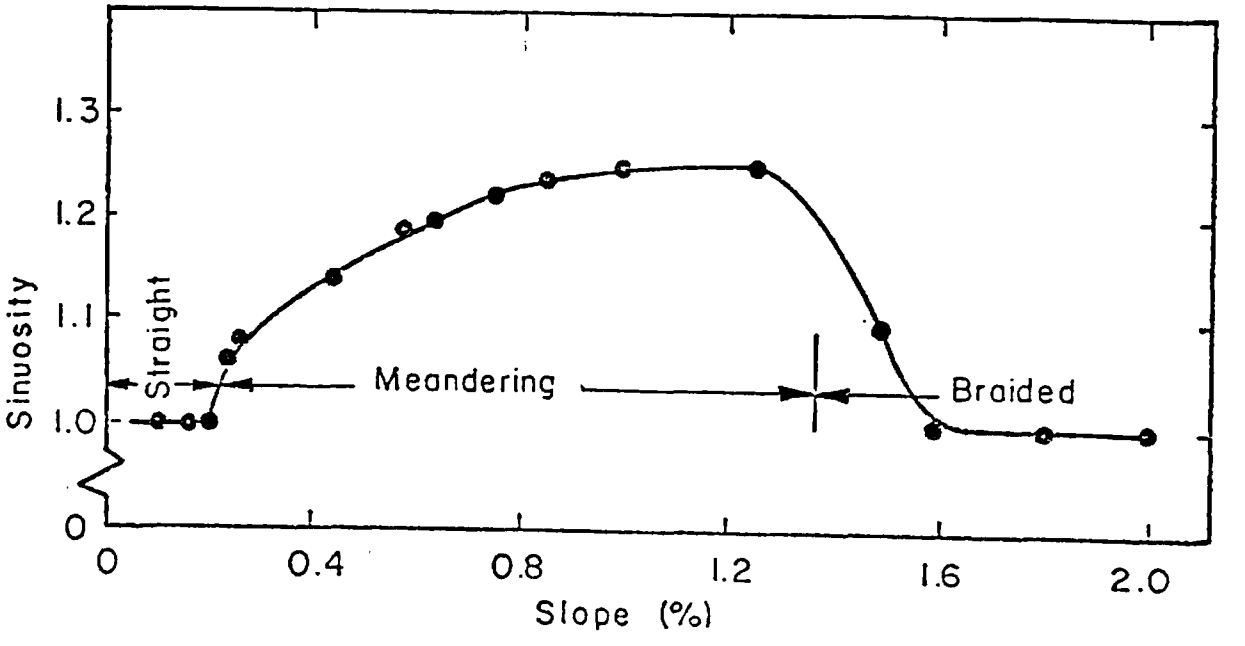


Figure 4-33. Relation between flume slope and sinuosity (ratio of channel length to length of flume or length of valley) during experiments. The change from a straight to a sinuous pattern and from a sinuous to a braided pattern occurs at two threshold slopes. Absolute value of slope at which such changes occur will be influenced by discharge. Discharge was maintained at 0.15 cfs during the experiments (After Schumm and Khan, 1972).

The relations described by Leopold and Wolman (1957) and Lane (1957) provide a means of evaluating the relative stability of modern channel patterns of the Chippewa River. Bankfull discharge was plotted against channel slope in Figure 4-32 for both the braided and the meandering reaches of the Chippewa. The value used for bankfull discharge is 1503 cms, (53,082 cfs) which is the flood discharge having a return period of 2.33 years. The braided reach plots higher than the meandering reach but both are well within the meandering zone defined by Leopold and Wolman. This suggests that the braided reach is anomalous. That is, according to this relation the lower Chippewa is expected to display a meandering pattern rather than a braided one. Even when the 25-year flood of 98,416 cfs is used, the braided reach still plots within the meandering region of Figure 4-32.

When Chippewa data are plotted on Lane's graph (Figure 4-31), the same relation exists. The Chippewa falls in the intermediate region but within the range of scatter about the regression line for meandering streams. Again the braided reach is seen to be anomalous because it plots closer to or above the braided stream regression line. Position of the braided reach as plotted on both figures, indicates that this reach should be meandering and historical studies reveal that it had a sinuosity of about 1.3 in the late 18th century but an avulsion changed the position and pattern of the channel.

It appears that the lower Chippewa has not been able to adjust as yet to its new position and steeper gradient, and the resulting bed and bank erosion has supplied large amounts of sediment to the Mississippi. Normal configuration of the lower Chippewa is sinuous and if it could be induced to assume such a pattern, high sediment delivery from the Chippewa could be controlled. An appropriate means of channel stabilization and sediment load reduction in this case is the development of a sinuous channel.

Since the above suggestions were made (Schumm and Beathard, 1976), more detailed studies of the Chippewa River basin indicate that upstream sediment production must be controlled especially where the upper Chippewa River is cutting into the Pleistocene outwash terraces. If contribution of sediment from these sources were reduced, the lower Chippewa could resume a sinuous course.

An indication that the pattern conversion of the Chippewa could be successful if the upstream sediment sources were controlled is provided by the Rangitata River of New Zealand (Schumm, 1979). The Rangitata River is the southernmost of the major rivers that traverse the Canterbury Plains of the South Island. It leaves the mountains through a bedrock gorge. Above the gorge the valley of the Rangitata is braided and it appears that the Rangitata should be a braided stream below the gorge as are all the other rivers that cross the Canterbury Plain. However, below the gorge the Rangitata is meandering. A few miles farther downstream, the river cuts into high Pleistocene outwash terraces and abruptly converts from a meandering to a braided stream. The braided pattern persists to the sea. If the Rangitata could be isolated from the gravel terraces, it probably could be converted to a single-thalweg sinuous channel because the Rangitata is obviously a river near the pattern threshold.

Other New Zealand rivers are near the pattern threshold, and therefore are susceptible to pattern change. In fact, New Zealand engineers are attempting to accomplish this pattern change in order to produce a "single-thread" channel which will reduce flood damage and be less likely to acquire large sediment loads from their banks and terraces. For example the Wairau River, a major braided stream, has been converted from uncontrolled braided mode to a slightly sinuous single-thalweg, relatively more stable channel (Pascoe, 1976). Increase in sinuosity is only from 1.0 to 1.05, and was accomplished by construction of curved training banks. On Figure 4-32 the Wairau River plots close to the threshold line and with reduction of sediment load produced by bank stabilization it appears that the pattern threshold can be successfully crossed.

Farther to the south near Kaikoura, the Kawhai River is being modified in the same manner as the Wairau (Thomson and MacArthur, 1968). Whereas much of the sediment load in the Wairau River is derived from bank and terrace erosion that can be controlled, high sediment loads are delivered to the Kawhai River directly from steep and unstable mountain slopes. On Figure 4-32 the Kowhai River plots well above the threshold line and without a major reduction in upstream sediment, it may be difficult to maintain a single-thalweg channel at this location.

Variability of the Rangitata River pattern indicates that braided single-thalweg conversions should be possible for the Chippewa and Wairau Rivers. However, not all braided rivers can be so readily modified, as this depends on their position with regard to the pattern thresholds on Figures 4-31, 4-32 and 4-33.

This geomorphic approach to channel evaluation and management deserves further consideration. Consider the sinuosity of an idealized river that flows at constant discharge over a highly variable alluvial valley slope (Figure 4-34). At position 1 the channel has just sufficient velocity to move its sediment load and further decrease in slope by a sinuosity increase would cause aggradation. Therefore the channel by necessity remains straight. At A the threshold between straight and meandering channels is crossed at a relative slope of 2. The line A-A' indicates the sinuosity at which channel gradient is 2, as sinuosity increases with valley slope. Assuming that at a valley slope of 2 the channel must be straight to transport its sediment load at a gradient of 2, at position 2 the maximum sinuosity that can be achieved is 1.25 because at a higher sinuosity the channel gradient is less than 2. At this position sinuosity can range between 1.0 and 1.25, and the channel could be straightened with little channel response because the increase of gradient would be slight as sinuosity is decreased. At position 3 a sinuosity of 1.7 is possible. Theoretically, it should be possible for sinuosity to achieve this value and still transport the sediment load but practically it will not be possible as the pattern roughness of the channel increases with increased sinuosity. Therefore, the flow velocity will be decreased (Chow, 1959, p. 109), and maximum sinuosity will be less than that suggested by line A-A'. The curve X,Y,Z shows what may be optimum sinuosity. The shape is obviously based on experimental results (Figure 4-34).

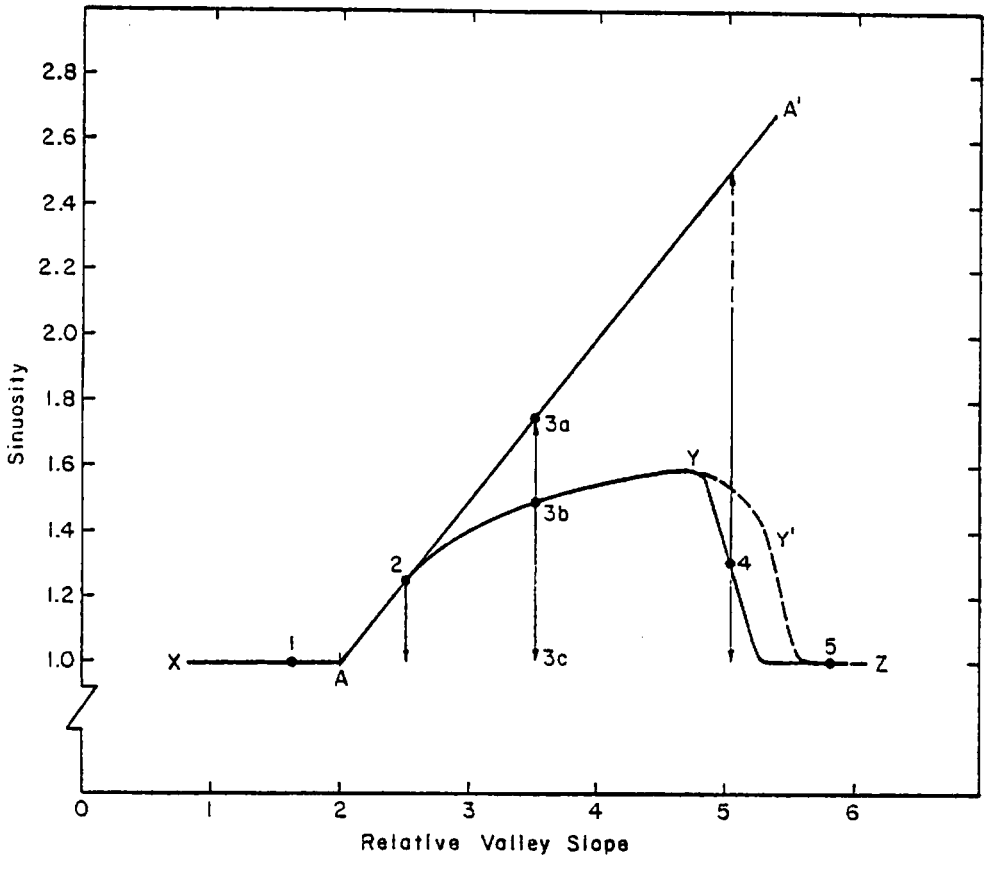


Figure 4-34. Diagram based on Figure 4-33 showing possible range of sinuosity with changes of relative valley slope. Vertical lines indicate the range of sinuosity at a given position on curve X,Y,Z.

A considerable range of sinuosity is possible at position 3. The channel can be meandering or straight and depending on sinuosity the gradient of the channel will be as steep as the valley slope 3.5 when the channel is straight 3c or gentler 2.0, when channel sinuosity is 1.75 position 3a. If the average curve X,Y,Z indicates optimum sinuosity at a given valley slope, then it is clear that the channel with a sinuosity well above this value probably is unstable and will by cutoffs revert toward a sinuosity of about 1.5 (position 3a to 3b). A straight channel at the same valley slope will develop a sinuous course in order to reduce its gradient (position 3c to 3b). The channel at position 3c will undoubtedly have a higher sediment load than the channels at positions 3a and 3b because it will be eroding its channel and banks.

The river engineer should carefully examine variations of sinuosity along a river. Where sinuosity is abnormally high and other factors such as tributary influences and valley slope changes can be eliminated, a program of alignment by selective meander cutoffs may improve channel stability as it is shifted from position 3a to 3b (Figure 4-34). On the other hand, when sinuosity is abnormally low, a shift from position 3c

to 3b will be beneficial and probably can be achieved by placing of dikes or other structures that induce a sinuosity into the channel. Perhaps this can be achieved by increasing roughness with artificial riffles (Keller, 1975).

At position 4 in the transition zone between meandering and braided it may be possible to shift the threshold zone to the right (Y-Y'-Z) by utilizing structural controls that reduce velocity and stream power, thereby forcing a divided flow or a braided channel into the meandering mode. Hence, at position 4 a channel may shift between meandering and braided depending on discharge and sediment load variations. At position 5 the valley slope may be too steep and sediment loads too great for the channel to be anything but straight and man-induced controls can not be effective in maintaining a sinuous channel at this position on Figure 4-34.

The suggestion made here is that if one can identify the range of patterns along a river, then within that range the most appropriate channel pattern and sinuosity probably can be identified. Thus, the engineer can work with the river to produce its most efficient or most stable channel. Obviously, a river can be forced into a straight configuration or made more sinuous but there is a limit to the changes that can be induced beyond which the channel cannot function without a radical morphologic adjustment as suggested by Figure 4-34. These limits probably can be determined by the use of sediment transport equations but in essence the approach to channel control presented here is geomorphic and based on the threshold concept.

Vertical Instability

In addition to the pattern changes or horizontal instability discussed in the last section, scour and fill of channels or vertical instability also produces major channel control problems and leaves a complex record for stratigraphic and sedimentologic interpretation.

High sediment loads can also cause local deposition or plugging of a channel with subsequent backfilling upstream and in fact this seems to be the dominant process in semiarid and arid regions. Local baselevel control caused by deposition in the channel diverts the flow, gradient is reduced locally, and deposition moves progressively upstream. There can be several sites of deposition of this type in a large valley and local backfilling above each eventually produce a continuous surface of deposition.

During a study of deposition of ephemeral-stream channels in the western United States it was concluded that the nature of sediment moved through and deposited in the channel strongly influenced the processes of deposition and the nature of channel erosion (Schumm, 1961). For example in sediment containing a large percentage of silt and clay, erosion primarily by vertical incision produced a deep narrow trench. However in sandy sediment, bank erosion and channel widening took place. The major difference was change from incision to lateral erosion.

Field observations of actively aggrading channels of ephemeral streams formed the basis for the preparation of Figure 4-35. In the figure generalized cross sections of filled channels are presented. Channels shown in the figure were not observed in cross section. Nevertheless, the downstream changes in channel shape and sediment character in the backfilling channels gave a good indication of probable appearance of channels in section. Differences in stratification appear to be related to differences in type of sediment produced in the study areas. The following discussion of active channel aggradation, as studied in four areas in which channel deposition was typical of that sketched in Figure 4-35, explains the differences in channel-fill stratification.

In the Sage Creek, South Dakota channel (Figure 4-35a) the percentage of silt-clay at the stable cross sections M was about 67 since Sage Creek drained an area of siltstone and claystone. Deposition occurred initially around slump blocks that had fallen into the channel. The highly cohesive sediment was not immediately swept away because

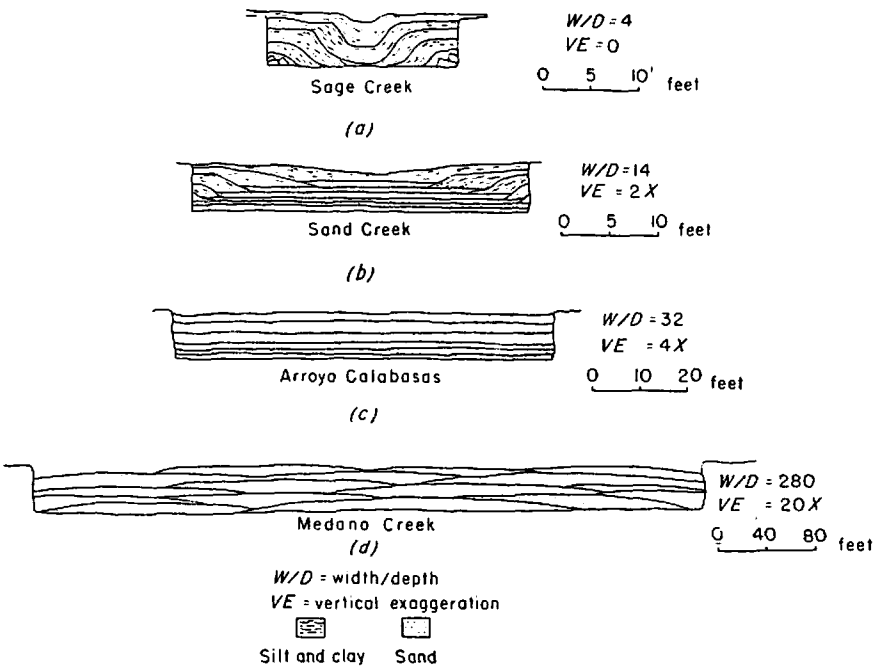


Figure 4-35. Channel-fill deposits in ephemeral-stream channels. (From Schumm, 1960.)

of its resistance to disintegration. As deposition continued it was greatest on the channel sides causing narrowing of the channel.

In the Sand Creek, Nebraska area (Figure 4-35b) the percentage of silt-clay at the stable channel sections was 20, reflecting the sandy nature of the shales exposed in the drainage area. As deposition began the sand was deposited in essentially horizontal layers on the floor of the channel and as this coarser material was deposited the percentage of silt-clay increased downstream. The amount of finer sediment in the channel increased in a downstream direction and lateral deposition became important as the channel filled. The two types of deposition continued contemporaneously, fines on the banks and coarser sediments on

the floor of the channel but in the later stages of filling all the deposited material was silt-clay. Horizontally stratified sands were restricted to the lower part of the fill and progressively toward the center near the top of the fill (Figure 4-35b). This deposition produces a fining-upward sequence that is the result of sediment sorting in the channel. As backfilling occurs the coarser sediments are deposited further upstream during each flood event. The result is a deposit of the type shown in Figure 4-36.

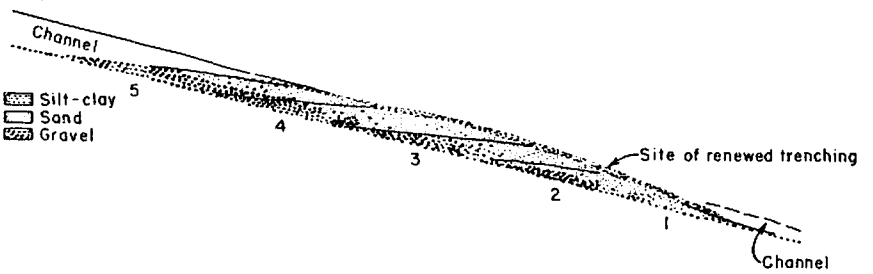


Figure 4-36. Longitudinal section through alluvial deposit formed by backfilling, showing development of graded bedding due to upstream shift of depositional units.

In the Arroyo Calabasas, New Mexico channel that drains an area of coarse Tertiary alluvium, channel silt-clay was less than 10 percent. The channel filled from bottom to top (Figure 4-35c) and stratification was relatively horizontal. The Medano Creek, Colorado channel is 600 feet wide and it receives an abundant supply of aeolian sand from the Great Sand Dunes. Convex surface of deposition were noted in this wide sandy channel (Figure 4-35d). During the study water was flowing over a width of 100 to 150 feet on a part of the channel cross section lying at an altitude several feet above the lowest part of the channel. In wide sandy channels or on floodplains where water loss into the fill is great that part of the channel on which water is flowing may be raised by deposition. Resulting fill may appear in section as a series of overlapping convexities unless planed flat by subsequent high flood flows.

In summary, type of stratification exposed in a channel-fill deposit may be dependent to a large extent on sediment character. Fine-grained cohesive sediments tend to adhere to the channel banks forming concave stratification. Noncohesive sediments are deposited directly on the channel floor causing horizontal stratification in the fill. Even convex stratification can be formed by a stream occupying only part of a wide sandy channel as it builds up bed.

Actually, the channel-fill deposits are only a part of the fluvial sedimentary complex. During and after a channel is filled, sediment-laden water spreads over the floodplain to form a variety of deposits (these are considered in the next chapter).

## 4.6 CLASSIFICATION

To focus attention on the most important factors that determine river morphology and to summarize previous material, a classification of channels may be useful. All rivers may be separated into two major groups depending on freedom to adjust shape and gradient. Bedrock controlled channels are those so confined between outcrops of rock that the material forming the bed and banks determines the morphology of the channel. Alluvial channels on the other hand are free to adjust dimensions, shape, pattern, and gradient in response to change and flow through channels with bed and banks composed of material transported by the river under present flow conditions.

Rivers have been classified according to their stage of development in the erosion cycle as youthful, mature, and old (Davis, 1899) and also according to the history of development on a land surface as antecedent, superposed, consequent, and subsequent (Thornbury, 1969, p. 113). However, none of these classifications considers two independent variables, discharge and type of sediment load, on which morphology of alluvial channels depends.

As demonstrated, discharge is an independent variable that largely determines size of stream channels and amplitude and wavelength of meanders. Discharge, however, is not a valid basis for a classification of stream channels unless size is considered most important, although a qualitative distinction among stream channels can be made on the basis of discharge characteristics (i.e., ephemeral and perennial streams).

Another independent variable that must be considered is sediment load. Channels are frequently referred to as muddy or sandy, or as cobble or boulder channels. This implies that size of material in and transported through the channel may be a prime consideration. Although it is true that in a downstream direction many river characteristics appear to change as grain size changes (Nevins, 1965), there can be great changes in the morphology of a stream when the median grain size of bed material is essentially constant. For this reason classification is based on the nature of the sediment load or predominant mode of sediment transport. Type of load and mode of transport are simplified here to mean the transportation of sediment as either suspended load or bed load.

The term bed load as used is synonymous with bed-material load and the term suspended load as used is synonymous with wash load. In channels of the Great Plains rivers, bed material load is usually composed of sand and wash load is composed of silt and clay. Although a single grain size that would form the boundary between suspended load and bed load cannot be selected from available sediment transport data, it is suggested that in general silt and clay are transported in suspension and sand and coarser sediment are transported on or near the streambed.

On the basis of relations previously discussed, alluvial river channels can be classified primarily according to type of sediment load as bedload, mixed load, and suspended load channels. Actually, a

Table 4-5. Classification of alluvial channels.

| Mode of sediment transport and type of channel | Channel sediment (M) (percent) | Bedload (percentage of total load) | Channel stability | | |
|---|---|---|---|---|---|
| | | | Stable (graded stream) | Depositing (excess load) | Eroding (deficiency of load) |
| Suspended load | >20 | <3 | Stable suspended-load channel. Width/depth ratio <10; sinuosity usually >2.0; gradient, relatively gentle | Depositing suspended load channel. Major deposition on banks cause narrowing of channel; initial streambed deposition minor | Eroding suspended-load channel. Streambed erosion predominant; initial channel widening minor |
| Mixed load | 5-20 | 3-11 | Stable mixed-load channel. Width/depth ratio >10, <40; sinuosity usually <2.0, >1.3; gradient moderate | Depositing mixed-load channel. Initial major deposition on banks followed by streambed deposition | Eroding mixed-load channel. Initial streambed erosion followed by channel widening |
| Bed load | <5 | >11 | Stable bed-load channel. Width/depth ratio >40; sinuosity usually <1.3; gradient, relatively steep | Depositing bed-load channel. Streambed deposition and island formation | Eroding bed-load channel. Little streambed erosion; channel widening predominant |

continuous series of channels exists and with this classification braided, meandering, and straight channels can be recognized.

Based on the nature of unstable channel behavior during erosion and deposition as discussed earlier, a second major division of alluvial channels can be made (Table 4-5). Differences can be considered of with respect to total sediment load delivered to the channel. An excess of total load causes deposition, a deficiency causes erosion, and between the extremes lies the stable channel. Although a given river channel often cannot be clearly identified in the field as stable, eroding, or depositing, it is possible to think of all rivers as falling into one of these three classes.

The stable channel is one that shows no progressive change in gradient, dimensions, or shape. Temporary changes occur during floods, but the stable channel, if the classification were not restricted to short segments of the river, would be identical to the graded stream as defined by Mackin (1948).

The eroding channel is one that is progressively degraded and/or widened by bank erosion. Conversely, the depositing channel is one that is being aggraded and/or having sediment deposited on its banks. Classification of river channels on the basis of stability as eroding, stable, or depositing emphasizes the diversity among rivers and stream channel. Each of the three classes can be considered as distinct from the others.

Classification of alluvial channels is summarized in Table 4-5. Nine subclasses of channels are shown, based on channel stability and predominant mode of sediment transport. Although variations in the proportions of bed load and suspended load are transitional, it is possible to think in terms of a suspended load channel transporting perhaps 0 to 3 percent bed load, a bed load channel transporting greater than 11 percent bed load, and a mixed-load channel transporting from 3 to 11 percent bed load. Boundaries between these groups are based on the relation between M and the percentage of bed load (Equation 4-7) and on the known characteristics of streams having varying amounts of silt and clay in their channels. Ranges of channel shape and sinuosity are established for each subclass, but gradient is expressed qualitatively because gradient depends to a large extent on discharge that can vary greatly for a given value of M. Although sinuosity as has been shown may depend on valley slope, a characteristic sinuosity range can be established for each type of stream.

In summary, alluvial-stream channels have been classified on the basis of one of the two independent variables influencing stream morphology. Discharge is not used as a basis for the classification because it controls mainly the size of the channels. Type of material transported or mode of transport as bed load or suspended load appears to be a major factor determining the character of a stream channel and classification of channels is based on this relation. Absolute size of sediment load may be less important than manner by which it moves through the channel. Channel stability depends on balance or lack of balance between sediment load and transportability, and three classes of channels result: stable, eroding, and depositing.

Classification is applicable only to segments of a river system because characteristics of a stream channel change significantly within a short distance if it becomes unstable or receives sediment of a different type from a tributary. Therefore, the classification is of channels rather than of river systems and must be considered to tentative until more data become available on total sediment load and the influence of sediment size on channel shape and pattern.

Classification is based on research confined to sandbed streams and thus may not be applicable to gravel and cobble rivers. For a description of these channels see Galay et al. (1973), Lewis and McDonald (1973), and Kellerhals et al. (1972). However, Mollard (1972) has used the classification based on type of load to classify a wide range of Canadian rivers.

Figure 4-37 attempts to summarize available information on channel pattern, type, and associated variable.

Five basic channel patterns are shown as follows:

1. Straight channel, straight thalweg (deepest part of channel). Channel is relatively stable.

2. Straight channel, sinuous thalweg. Channel is generally stable but thalweg shift and bar migration occur (Figure 4-38).

3. Meandering.
   a. Uniform channel width, small point bars. Channel is stable but neck cutoffs occur (Figure 4-38).
   b. Channel wider at bends, large point bars. Chute and neck cutoffs and meander shift produce a relatively unstable channel.

4. Meander - braided transition, large point bars with frequency chute cutoffs. Unstable channel with sinuous thalweg (Figure 4-38).

5. Braided channel. Unstable channel with multiple thalweg and numerous bars and islands (Figure 4-38).

Classification of Figure 4-37 indicates the relative stability of a river and therefore should be especially useful to those utilizing riparian lands. For instance although the occurrence of a pattern 1 straight channel (Figure 4-37) may be rare, it means that the banks are relatively stable and erode slowly. However, if the channel is straight because it has been channelized, it can be unstable. In the case of a Pattern 2 straight channel, the banks are relatively stable but the thalweg and alternate bars shift.

Channel patterns 3a and 3b are meandering channels, the banks of which are not straight and parallel. Shifting the thalweg or deepest part of the channel and the banks of this channel follows a more or less regular pattern that can be anticipated.

Pattern 4 is transitional between meandering and braided and in fact such a pattern may represent a change from pattern 3 to the braided stream pattern 5. Some investigators have subdivided braided channels into those with unvegetated bars and those with permanent vegetated islands. The vegetated islands reflect more stable conditions.

As shown in Figure 4-37, type of sediment load, sediment size (limited experience only), sediment load, flow velocity, stream power, width-depth ratio, and channel gradient are related to channel pattern and relative stability of alluvial channels.

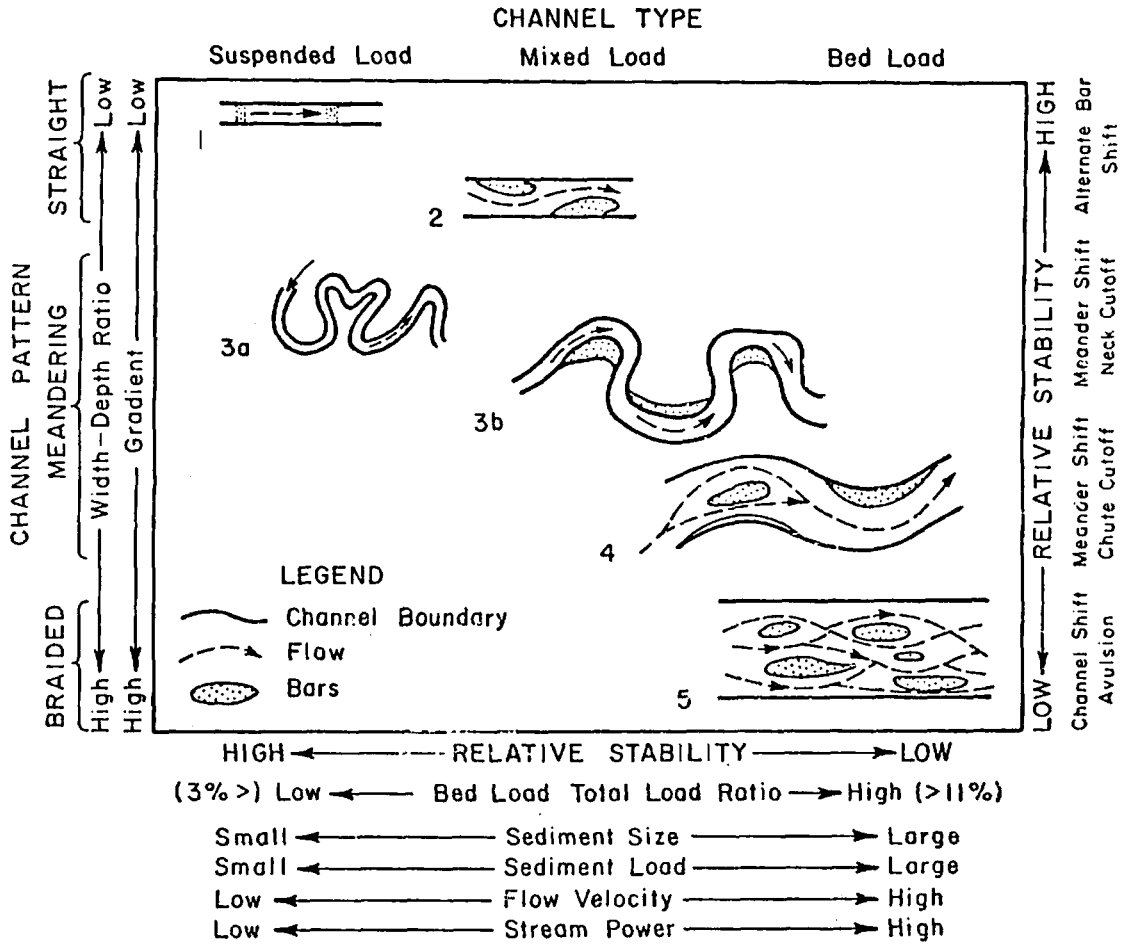


Figure 4-37. Channel classification based on pattern and type of sediment load, showing types of channels, their relative stability and some associated variables. (After Schumm and Meyer, 1979).

As indicated by Figure 4-37, channel pattern not only changes from pattern 1 to 5 but other morphologic aspects of the channel also change. That is, for a given discharge gradient increases and width-depth ratio increases. In addition, peak discharge, sediment size, and sediment load will probably increase from pattern 1 to 5. Naturally with such geomorphic and hydrologic changes, hydraulic differences can be expected

and flow velocity, tractive force, and streampower increase from pattern 1 to 5. Obviously then, channel stability decreases from pattern 1 to 5 with patterns 4 and 5 being the least stable.

Since the alluvial channel, is flowing in erodible sediments and the stress exerted by the flowing water often exceeds the strength of sediment forming the bed and banks the channel it will change naturally with time. Figure 4-38 illustrates six types of natural channel changes. Examples a and b are within channel shifts of bars and islands. In case b, as the alternate bars shift slowly downstream, and the thalweg shifts position. Hence, at one time a bank location is protected by the alternate bar, whereas at some later time the bar has shifted downstream, and the bank can be subjected to erosion. Examples c, d, e, and f show a change of channel position either gradually by meander shift or relatively quickly by neck or chute cutoffs or by avulsion.

In addition to meander shift (Figure 4-38e), meanders may also increase in amplitude. This is accomplished by erosion of the cutbank or outside of the bend while sediment is deposited on the inside bank or point bar.

Continual reworking of sediment demonstrates that the floodplain of a meandering stream is not a permanent feature but is composed of material in temporary storage on its journey downstream.

Meander migration is inherent to sinuous rivers, and over a period of years a river will sweep back and forth across its floodplain, reworking floodplain deposits, destroying all surface features, and replacing them with point bar deposits.

In addition to and in part as a result of meander migration, cutoffs also modify meandering channels. Meander cutoffs commonly occur in two ways either by neck cutoffs or by chute cutoffs (Figure 4-38c, d). By increasing local slope and causing increased scour upstream and deposition downstream both processes shorten the channel.

## 4.7 DISCUSSION

The equations presented in this chapter indicate the significant influence that water and sediment discharge exert on channel morphology. Changes in the hydrologic character of Zone 1, for whatever cause, can result in river metamorphosis and drastic change in sediment moved to Zone 3.

A genetic classification of river channels has been presented based on channel stability and type of sediment load. Classification of rivers will not be wholly adequate but differences in pattern and channel shape as identified can be of use in interpretation of river behavior from aerial photography when no other data are available (Kellerhals et al., 1976). Also the cross section and nature of its sediments can aid in prediction of the nature of fluvial sedimentary deposits by the sedimentologist and exploration geologist.

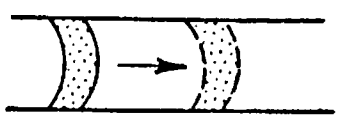

a. Transverse Bar Shift

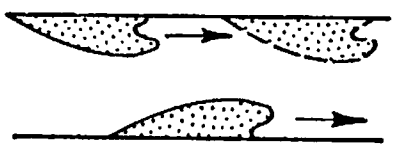

b. Alternate Bar Shift

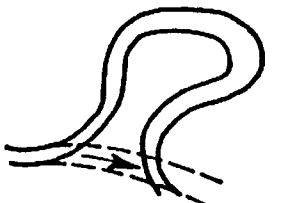

c. Neck Cutoff

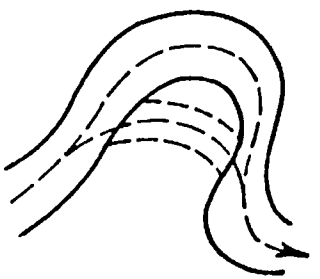

d. Chute Cutoff

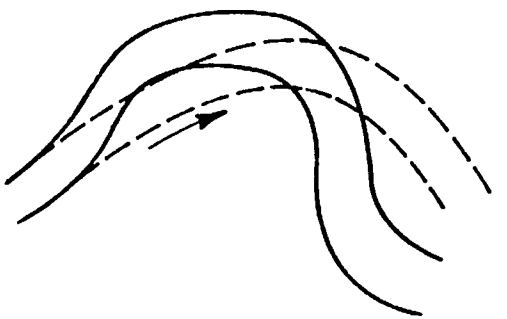

e. Meander Shift

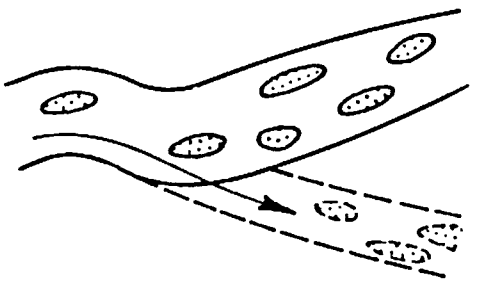

f. Avulsion

(Solid lines indicate current status and dashed lines indicate future potential changes.)

Figure 4-38. Types of channel change.

Evaluation of the relative stability of a channel depends on the training and goals of the investigator and therefore the time span considered. While meander shift may be a catastrophe to a landowner and a challenge to the river control engineer, it may be the anticipated result of natural channel development to the geomorphologist who would conclude that these natural changes should be permitted to occur. If a river is considered as an organism with a history, then its relative stability and propensity of change can be more fully comprehended. Therefore, much channel "instability" may, in fact, be a natural and predictable adjustment to geomorphic controls. This perspective hopefully has potential for the better understanding of and management of rivers.

Two types of threshold conditions have been identified with regard to channel patterns. Extrinsic thresholds of sediment load (slope) and stream power (velocity) determine if the river will be straight, meandering, or braided. Intrinsic geomorphic pattern threshold when exceeded, results in a change from relatively high to relatively low sinuosity (Figure 4-33). The exceeding of a pattern threshold that introduces a period of channel instability and high sediment transport can provide an explanation for an increased rate of sedimentation in a fluvial deposit when none is warranted by climatic or other evidence.

The fact that such pattern thresholds exist provides the river management with an approach to river control involving an appreciation of river history. Intrinsic thresholds can be exceeded at any time but usually only for reaches of relatively high sinuosity during large floods.

Empirical equations presented in this chapter have also been used to provide an estimate of the hydrology of ungaged channels and of paleochannels. For example Brown (1971) determined that channel cross-sections are provided good estimates of bank-full discharge for channels in Kentucky, Tennessee, and Minnesota with perennial flow. Hedman (1970) used low-water channel widths and depths to estimate annual runoff and Schumm (1972) used width/depth ratio and width in a series of equations to estimate paleochannel discharge, gradient, and meander wavelength.

SYMBOLS

| | |
|---|---|
| A | Drainage area ($km^2$ or square miles) |
| b | Water surface width either at mean annual discharge (Leopold and Maddock), at $Q_2$ (Bray), or at channel bank-full width (Schumm) (feet or m) |
| d | Water depth either at mean annual discharge (Leopold and Maddock), at $Q_2$ (Bray), or at maximum bank-full depth of channel (Schumm) (feet or m) |
| $d_{50}$ | Median grain size (mm) |
| F | Width/depth ratio |
| L | Channel length (miles) |
| M | Silt-clay in channel perimeter (percent) |
| P | Sinuosity (ratio of channel length to valley length or ratio of valley slope to channel slope) |
| Q | Mean annual water discharge (Lane) (cfs) |
| Qma | Mean annual flood (cfs) |
| Qm | Mean annual discharge (cfs) |
| $Q_2$ | Discharge for flood with 2-year recurrence interval (cfs) |
| $Q_s$ | Bed material load (weight or volume) |
| $Q_b$ | Bed load (percentage of total load) |
| R | Hydraulic radius, area of channel cross section divided by wetted perimeter (feet or m) |
| S | Slope of energy line (percent, tangent) |
| Sc | Channel gradient (percent, feet/mile, tangent) |
| Sv | Valley floor slope (percent, feet/mile, tangent) |
| V | Velocity (feet/second, m/second) |
| $\lambda$ | Meander wavelength (km, feet, miles) |
| $\tau$ | Tractive force (qRS; weight per unit area) |
| $\gamma$ | Specific weight of water (weight per unit volume) |
| $\omega$ | Stream power (tV; foot pounds per second per foot) |

## REFERENCES

Ackers, P., 1964, Experiments on small streams in alluvium: J. Hydraul. Div., Am. Soc. Civil Eng. Proc. HY4, pp. 1-37.

Beckinsale, R. P., 1969, River regimes, in R. J. Chorley (editor), Water, earth and man, Methuen, London, pp. 455-472.

Bray, D. I., 1973, Regime relations for Alberta gravel-bed rivers, in Fluvial processes and sedimentation: National Research Council of Canada; Ottawa, pp. 440-452.

Brice, J. C., 1966, Erosion and deposition in the loess-mantled Great Plains Medicine Creek drainage Basin, Nebraska: U.S. Geol. Surv. Prof. Paper 352-H, pp. 255-339.

Brown, D. A., 1971, Stream channels and flow relations: Water Resour. Res., v. 7, pp. 304-310.

Brush, L. M., Jr., 1961, Drainage basins, channels and flow characteristics of selected streams in central Pennsylvania: U.S. Geol. Surv. Prof. Paper 282-F.

Chow, Ven Te, 1959, Open-channel hydraulics: McGraw-Hill, New York, 680 pp.

Culbertson, D. M., Young, L. E., and Brice, J. C., 1967, Scour and fill in alluvial channels: U.S. Geol. Surv. Open-File Report, 58 p.

Davis, W. M., 1899, The geographical cycle, Geog. J., V. 14, pp. 481-504.

Dury, G. H., 1964, Principles of underfit streams: U.S. Geol. Surv. Prof. Paper 452-A, 67 pp.

Einstein, H. A., 1950, The bed-load function for sediment transportation in open channel flows: U.S. Dept. Agric. Tech. Bull. 1926, 71 pp.

Fisk, H. N., 1944, Geological investigation of the alluvial valley of the lower Mississippi River: Mississippi River Commission, Vicksburg, Miss., 78 pp.

Fournier, M. F., 1949, Les facteurs climatiques de l'erosion du sol, Bul. Assoc. Geogr. Fr. 203 (11 Juin 1949), pp. 97-103.

Galay, V. J., Kellerhals, R. and Bray, D. I., 1973, Diversity of river types in Canada, in Fluvial Process and Sedimentation: Proc. Hydrol. Symp., National Research Council of Canada, pp. 217-250.

Gregory, K. J. and Walling, D. E., 1973, Drainage basin form and process, Wiley, New York, 456 pp.

Hack, J. T., 1957, Studies of longitudinal stream profiles in Virginia and Maryland: U.S. Geol. Surv. Prof. Paper 294-B, pp. 45-97.

Hadley, R. F. and Schumm, S. A., 1961, Sediment sources and drainage basin characteristics in upper Cheyenne River basin, U. S. Geol. Surv. Water-Supply Paper 1531-B, pp. 137-196.

Hedman, E. R., 1970, Mean annual runoff as related to channel geometry of selected streams in California: U.S. Geol. Surv., Water-Supply Paper 1999-E, 17 pp.

Hjulstrom, F., 1935, Studies of the morphologic activity of rivers as illustrated by the River Fjris: Geol. Inst. Uppsala Univ. (Sweden) Bull., v. 25, pp. 293-452.

Horton, R. E., 1945, Erosional development of streams and their drainage basins: Hydrophysical approach to quantitative morphology, Geol. Soc. Am. Bull., v. 50, pp. 275-370.

Keller, E. A., 1975, Channelization: a search for a better way: Geology, v. 3, pp. 245-248.

Kellerhals, R., Church, M. and Bray, D. I., 1976, Classification and analysis of river processes: J. Hydraul. Div., Am. Soc. Civil Eng., v. 102, pp. 813-829.

Kellerhals, R., Neill, C. R. and Bray, D. I., 1972, Hydraulic and geomorphic characteristics of rivers in Alberta: Research Council of Alberta, River Engineering and Surface Hydrology Report 72-1, 52 pp.

Khan, H. R., 1971, Laboratory study of river morphology: unpublished Ph.D. Dissertation, Colorado State University, 189 pp.

Kirkby, M. J., 1973, Landslides and weathering rates: Geol. Appl. Idrageol., Vol. 8, pp. 171-183.

Kruska, J. and Lamarra, V. A., Jr., 1973, Use of drainage patterns and densities to evaluate large scale land areas for resource management, J. Environ. Syst., 3:85-100.

Lacey, G., 1930, Stable channels in alluvium: Inst. Civil Eng., Proc., v. 229, pp. 259-384.

Lane, E. W., 1955, The importance of fluvial morphology in hydraulic engineering: Am. Soc. Civil Eng. Proc., v. 81, No. 745, 17 pp.

Lane, E. W., 1957, A study of the shape of channels formed by natural streams flowing in erodible material: M. R. D. Sediment Series No. 9, U.S. Army Engineer Division, Missouri River, Corps of Engineers, Omaha, Nebraska.

Langbein, W. B., et al., 1949, Annual runoff in the United States, U.S. Geol. Surv. Circ. 52, 14 pp.

Langbein, W. B. and Schumm, S. A., 1958, Yield of sediment in relation to mean annual precipitation, Am. Geophys. Union Trans., v. 39, pp. 1976-1084.

Leliavsky, S., 1955, An introduction to fluvial hydraulics: Constable, London, 256 pp.

Leopold, L. B. and Maddock, T., Jr., 1953, The hydraulic geometry of stream channels and some physiographic implications: U.S. Geol. Surv. Prof. Paper 242, 57 pp.

Leopold, L. B. and Wolman, M. G., 1957, River channel patterns: braided, meandering and straight: U.S. Geol. Surv. Prof. Paper 282-B.

Leopold, L. B., Wolman, M. G. and Miller, J. P., 1964, Fluvial Processes in Geomorphology, Freeman, San Francisco, Calif., 522 pp.

Lewis, C. P. and McDonald, B. C., 1973, Rivers of the Yukon North Slope, in Fluvial processes and sedimentation: Proc. Hydrol. Symp. National Research Council of Canada, pp. 251-271.

Mackin, J. H., 1948, Concept of the graded river: Geol. Soc. Am. Bull., v. 59, pp. 463-512.

Mollard, J. D., 1972, Airphoto interpretation of fluvial features, in Fluvial processes and sedimentation: Research Council of Canada, pp. 341-380.

Nevins, T. H. F., 1965, River classification with particular reference to New Zealand: N. Z. Geogr. Cong., 4th Proc., v. 4, pp. 83-90.

Noble, E. L., 1965, Sediment reduction through watershed rehabilitation, U.S. Dept. Agric. Misc. Publ. 970, pp. 114-123.

Parde, M., 1964, Fleuves et rivieres, Paris, Librairie Armand Colin, 223 pp.

Parker, R. S., 1976, Experimental Study of drainage system evolution: unpublished report, Colorado State University, Fort Collins, CO.

Parker, R. S., 1977, Experimental study of drainage basin evolution and its hydrologic implications, Colorado State Univ., Hydrology Paper 90, 58 pp.

Patton, P. C. and Schumm, S. A., 1975, Gully erosion, northwestern Colorado: A threshold phenomenon, Geology, v. 3, pp. 88-90.

Ray, R. G. and Fisher, W. A., 1960, Quantitative photography: A geologic research, Photogrammetric Eng., v. 25, p. 143-150.

Rubey, W. W., 1952, Geology and mineral resources of the Hardin and Brussels Quadrangles, Illinois: U.S. Geol. Surv. Prof. Paper 218, 179 p.

Ruhe, R. V., 1952, Topographic discontinuities of the Des Moines lobe, Amer. Jour. Sci., v. 250, p. 46-56.

Schumm, S. A., 1960, The effect of sediment type on the shape and stratification of some modern fluvial deposits: Am. J. Sci., Vol. 258, pp. 177-184.

Schumm, S. A., 1961, The effect of sediment characteristics on erosion and deposition in ephemeral-stream channels, U.S. Geol. Surv. Prof. Pap., 352-C:31-70.

Schumm, S. A., 1963, The disparity between present rates of denudation and orogeny: U.S. Geol. Surv. Prof. Paper 454-H, 13 p.

Schumm, S. A., 1968, River adjustment to altered hydrologic regime, Murrumbidgee River and paleochannels, Australia: U.S. Geol. Surv. Prof. Paper 598.

Schumm, S. A., 1969, A geomorphic approach to erosion control in semiarid regions, Am. Soc. Agric. Eng. Trans., 12:60-68.

Schumm, S. A., 1972, Fluvial paleochannels: Soc. Econ. Paleontol. and Mineral. Spec. Publ. 13, pp. 98-107.

Schumm, S. A., 1973, Geomorphic thresholds and the complex response of drainage systems, in Marie Morisawa (editor), Fluvial geomorphology, Publications in Geomorphology, State University of New York, Binghamton, pp. 299-310.

Schumm, S. A., 1977, The fluvial system, Wiley-Interscience, New York, 338 p.

Schumm, S. A., and Beathard, R. M., 1976, Geomorphic thresholds: an approach to river management, in Rivers 76, v. 1, 3rd Symposium of the Waterways: Harbors and Coastal Engineers Division of the American Society of Civil Engineers, pp. 707-724.

Schumm, S. A., and Hadley, R. F., 1957, Arroyos and the semiarid cycle of erosion, Am. J. Sci., v. 255, pp. 161-174.

Schumm, S. A., and Khan, H. R., 1972, Experimental study of channel patterns: Geol. Soc. Am. Bull., v. 83, pp. 1755-1770.

Schumm, S. A., Khan, H. R., Winkley, B. R. and Robbins, L. G., 1972, Variability of river patterns: Nature, Phys. Sci., v. 237, pp. 75-76.

Schumm, S. A. and Lichty, R. W., 1965, Time, space and causality in geomorphology, Am. J. Sci., v. 263, pp. 110-119.

Shulits, S., 1941, Rational equation of river-bed profile: Am. Geophys. Union Trans., v. 22, pp. 522-631.

Simons, D. B., and Albertson, M. L., 1960, Uniform water conveyance channels in alluvial materials: J. Hydrol. Div., Am. Soc. Civil Eng. Proc. HY5, pp. 33-71.

Simons, D. B., Richardson, E. V. and Nordin, C. F., Jr., 1965, Sedimentary structures generated by flow in alluvial channels, Soc. Econ. Paleontol. Mineral. Spec. Publ. 12, pp. 34-52.

Speight, J. G., 1965, Meander spectra of the Anabunga River: J. Hydrol., v. 3, pp. 1-15.

Speight, J. G., 1967, Spectral analysis of meanders of some Australian Rivers, in Landform studies from Australia and New Guinea: Aust. National University Press, p. 48-63.

Stall, J. B. and Fok, Yu-Si, 1968, Hydraulic geometry of Illinois streams, Univ. of Illinois, Water Resources Center Research Report 15, 47 p.

Stevens, M. A., Simons, D. B., and Richardson, E. V., 1975, Non-equilibrium river form: J. Hydraul. Div., A. S. C. E., v. 101, pp. 557-566.

Stoddart, D. R., 1969, Climatic geomorphology: Review and re-assessment, Prog. Geogr., 1:161-222.

Strand, R. I., 1975, Bureau of Reclamation procedures for predicting sediment yield, Agricultural Research Service, ARS-S-40, pp. 10-15.

Wilson, L., 1968, Morphogenetic classification, in R. W. Fairbridge (editor), The encyclopedia of geomorphology, Reinhold, New York, pp. 717-729.

Chapter 5

# OPEN CHANNEL FLOW

## 5.1 INTRODUCTION

In open channel flow, the water surface is not confined; surface configuration, flow pattern and pressure distribution within the flow depend on gravity. In rigid boundary open channel flow, no deformations or movements of the bed and banks are considered, whereas in mobile boundary hydraulics the bed configuration depends on the flow. This chapter is restricted to a one-dimensional analysis that is, the direction of velocity and acceleration are only large in one direction and are so small as to be negligible in all other directions.

Open channel flow can be classified as: 1) uniform or nonuniform flow, 2) steady or unsteady flow, 3) laminar or turbulent flow, and 4) tranquil or rapid flow. In uniform flow, the depth and discharge remain constant with respect to space; also, the velocity at a given depth is the same everywhere. In steady flow, no change occurs with respect to time. In laminar flow, the flow field can be characterized by layers of fluid, one layer not mixing with adjacent ones. Turbulent flow is characterized by random fluid motion. Tranquil flow is distinguished from rapid flow by a dimensionless number called the Froude number, Fr. If $Fr < 1$, the flow is tranquil; if $Fr > 1$, the flow is rapid, and if $Fr = 1$, the flow is called critical.

Open channel flow can be nonuniform, unsteady, turbulent and rapid at the same time. Because the classifying characteristics are independent, sixteen different types of flow can occur. These terms, uniform or nonuniform, steady or unsteady, laminar or turbulent, rapid or tranquil, and the two dimensionless numbers (the Froude number and Reynolds number) are explained more fully in the following sections.

### Definitions

Velocity. The velocity of a fluid particle is the time rate of displacement of the particle from one point to another. Velocity is a vector quantity. That is, it has magnitude and direction. In cartesian coordinates, the mathematical representation of the fluid velocity is

$$V = \frac{ds}{dt} = \frac{\partial x}{\partial t} + \frac{\partial y}{\partial t} + \frac{\partial z}{\partial t} \tag{5-1}$$

Streamline. A streamline is an imaginary line within the flow which is tangent everywhere to the velocity vector.

Acceleration. Acceleration is the time rate of change of the velocity vector, either of magnitude or direction or both. Mathematically, acceleration is expressed by the total derivative of the velocity vector or

$$\frac{DV}{Dt} = \frac{dv_s}{dt} + \frac{dv_n}{dt} = \frac{\partial v_s}{\partial t} + \frac{1}{2}\frac{\partial (v_s^2)}{\partial s} + \frac{\partial v_n}{\partial t} + \frac{1}{2}\frac{\partial (v_n^2)}{\partial n} \tag{5-2}$$

where the subcript s is along the streamline and n refers to the direction normal to the streamline. The tangential acceleration component is

$$a_s = \frac{\partial v_s}{\partial t} + \frac{1}{2}\frac{\partial (v_s^2)}{\partial s} \tag{5-3}$$

and the normal acceleration component is

$$a_n = \frac{\partial v_n}{\partial t} + \frac{1}{2}\frac{\partial}{\partial n}(v_n^2) \tag{5-4}$$

The first terms in Equations 5-3 and 5-4 are the change in velocity, both magnitude and direction, with time at a point. This is called the local acceleration. The second term in each equation is the change in velocity, both magnitude and direction, with distance. This is called convective acceleration.

Uniform flow. In uniform flow there is no change in velocity along a streamline with distance; that is

$$\frac{\partial v_s}{\partial s} = 0$$

and

$$\frac{\partial v_n}{\partial n} = 0$$

Nonuniform flow. In nonuniform flow velocity varies with position so

$$\frac{\partial v_s}{\partial s} \neq 0$$

and

$$\frac{\partial v_n}{\partial n} \neq 0$$

Flow around a bend ($\partial v_n/\partial n \neq 0$) and flow in expansions or contractions ($\partial v_s/\partial s \neq 0$) are examples of nonuniform flow.

Steady flow. In steady flow the velocity at a point does not change with time; that is

$$\frac{\partial v_s}{\partial t} = 0$$

and

$$\frac{\partial v_n}{\partial t} = 0$$

Examples of unsteady flow are channel flows with waves, flood hydrographs, and surges. Unsteady flow is difficult to analyze unless time changes are small.

Laminar flow. In laminar flow mixing of the fluid and momentum transfer is accomplished by molecular activity.

Turbulent flow. In turbulent flow mixing of the fluid and momentum transfer is accomplished by random fluctuations of finite "lumps" of fluid.

Flow is laminar or turbulent depending on the value of the Reynolds number ($Re = \rho VL/\mu$), which is a dimensionless ratio of inertial forces to viscous forces. Here $\rho$ and $\mu$ are the density and dynamic viscosity of fluid, $V$ is the fluid velocity and $L$ is a characteristic dimension, usually the depth in open channel flow. In laminar flow, viscous forces are dominant and $Re$ is relatively small. In turbulent flow, $Re$ is large; that is, inertial forces are very much greater than viscous forces.

In turbulent flow over a hydraulically smooth boundary viscous forces near the boundary are the dominant resistance to flow. With a hydraulically rough boundary, form drag is more significant than viscous drag and is the dominant reason for resistance to flow. Between these two types of roughnesses there is an intermediate condition where viscosity and form drag affect the flow.

Turbulent flows are predominant in nature. Laminar flow occurs very infrequently in open channel flow.

Tranquil flow. In open channel flow the flow pattern, surface configuration, depth, and changes in these quantities in reponse to changes in channel geometry depend on the Froude number ($Fr = V/\sqrt{gL}$), which is the ratio of inertia forces to gravitational forces. The Froude number is also the ratio of the flow velocity to the velocity of a small gravity wave in the flow. When $Fr < 1$, the flow is tranquil, and surface waves (with velocity $\sqrt{gL}$) propagate upstream as well as downstream. Control of tranquil flow depth is always downstream.

Rapid flow. When $Fr > 1$, the flow is rapid and surface disturbances can propagate only in the downstream direction. Control of rapid flow depth is always at the upstream end of the rapid flow region. When $Fr = 1.0$, the flow is critical and surface disturbances remain stationary in the flow.

## 5.2 BASIC PRINCIPLES

### Introduction

The basic equations of flow in open channels are derived from the three conservation laws. These are: 1) the conservation of mass, 2) the conservation of linear momentum, and 3) the conservation of energy. The conservation of mass is another way of stating that (except for mass-energy interchange) matter can neither be created nor destroyed. The principle of conservation of linear momentum is based on Newton's second law of motion which states that a mass (of fluid) accelerates in the direction of and in proportion to the applied forces on the mass.

Analysis of flow problems can be greatly simplified if no acceleration of flow exists or if the acceleration is primarily in one direction, accelerations in other directions being negligible. However, a very inaccurate analysis may occur if one assumes accelerations are small or zero when in fact they are not. The developments in this chapter assume one-dimensional flow and the derivations of the equations utilize a control volume. A control volume is an isolated volume in the body of the fluid, through which mass, momentum, and energy can be convected. The control volume may be assumed to be fixed in space or moving with the fluid.

## Conservation of Mass

Consider the short reach of river shown in Figure 5-1 as a control volume. The boundaries of the control volume are the upstream cross section, designated section 1, the downstream cross section, designated section 2, free surface of the water between sections 1 and 2, and the interface between water, banks, and bed.

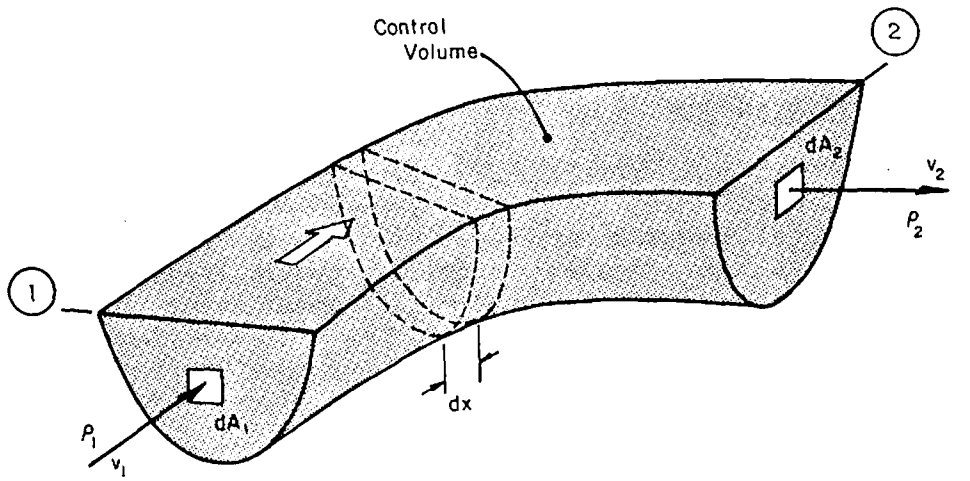


Figure 5-1. A river reach as a control volume.

The statement of the conservation of mass for this control volume

| | | | | | |
|---|---|---|---|---|---|
| Mass flux out of the control volume | - | Mass flux into the control volume | + | Time rate of change in mass in the control volume | = 0 |

Mass can enter or leave the control volume through any or all of the control volume surfaces. Rainfall would contribute mass through the surface of the control volume and seepage passes through the interface between the water, banks, and bed. In the absence of rainfall, evaporation, seepage, and other lateral mass fluxes, mass enters the control volume at section 1 and leaves at section 2.

At section 2, the mass flux out of the control volume through the differential area $dA_2$ is $\rho_2 v_2\, dA_2$. The values of $\rho_2$ and $v_2$ can vary from position to position across the width and throughout the depth

of flow at section 2. The total mass flux out of the control volume at section 2 is the sum of all $\rho_2 v_2 \, DA_2$ through the differential areas that make up the cross section area $A_2$, and may be written as

$$\sum_{A_2} \rho_2 v_2 dA$$

Therefore

$$\begin{array}{l}\text{Mass flux} \\ \text{out of the} \\ \text{control volume}\end{array} = \sum_{A_2} \rho_2 v_2 \, dA_2$$

Similarly

$$\begin{array}{l}\text{Mass flux} \\ \text{into the} \\ \text{control volume}\end{array} = \sum_{A_1} \rho_2 v_2 \, dA_2$$

The amount of mass inside a differential volume $d\forall$ inside the control volume is

$$\rho \, d\forall$$

and the total mass inside the control volume $\forall$ is then the sum of the mass inside or

$$\begin{array}{l}\text{Mass inside} \\ \text{the} \\ \text{control volume}\end{array} = \sum_{\forall} \rho \, d\forall$$

The statement of conservation of mass for the control volume calls for the time rate of change in mass. In mathematical notation, the rate of change is

$$\frac{\partial}{\partial t} \{\sum_{\forall} \rho \, d\forall\}$$

so that

$$\begin{array}{l}\text{Time rate of} \\ \text{change in mass} \\ \text{in the control} \\ \text{volume}\end{array} = \frac{\partial}{\partial t} \{\sum \rho \, d\forall\}$$

For the reach of river, the statement of the conservation of mass becomes

$$\sum_{A_2} \rho_2 v_2 \, dA_2 - \sum_{A_1} \rho_1 v_1 \, dA_1 + \frac{\partial}{\partial t} \{\sum_{\forall} \rho \, d\forall\} = 0 \qquad (5\text{-}5)$$

It is often convenient to work with average conditions at a cross section so we define an average velocity $V$ such that

$$V = \frac{1}{A} \sum_{A} v \, dA \qquad (5\text{-}6)$$

or in integral form,

$$V = \frac{1}{A} \int_A v \, dA \tag{5-7}$$

The velocity $V$ is the average velocity at the cross section.

If the density of the fluid does not change from position to position in a cross section or in the reach, $\rho_1 = \rho_2 = \rho$. When the flow is steady

$$\frac{\partial}{\partial t} \{\int_{\forall} \rho \, d\forall\} = 0$$

and Equation 5-5 reduces to the statement that inflow equals outflow or

$$\rho V_2 A_2 - \rho V_1 A_1 = 0$$

That is

$$V_1 A_1 = V_2 A_2 = Q \tag{5-8}$$

where $Q$ is the volume flow rate or the discharge.

Equation 5-8 is the familiar form of the conservation of mass equation for river flows. It is applicable when the fluid density is constant, the flow is steady and there is no lateral inflow or seepage.

Conservation of Linear Momentum

The curved reach of river shown in Figure 5-1 is rather complex to analyze in terms of Newton's Second Law because of the curvature in the flow. Therefore, as a starting point, the differential length of reach dx is isolated as a control volume.

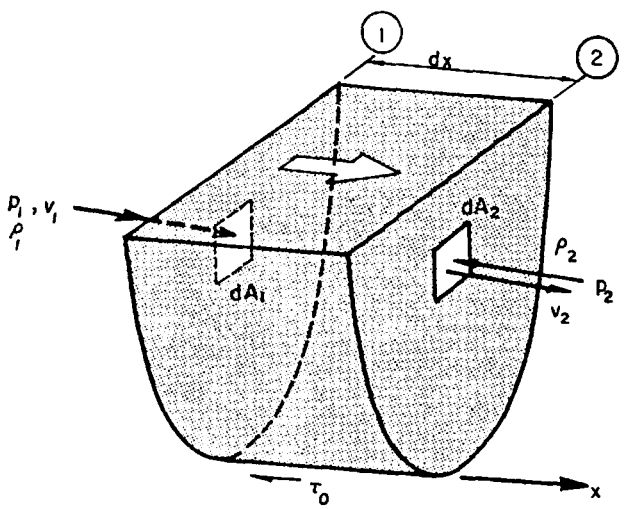


Figure 5-2. The control volume for conservation of linear momentum.

For this control volume shown in Figure 5-2, the statement of conservation of linear momentum is

| | | | | |
|---|---|---|---|---|
| Flux of momentum out of the control volume | - | Flux of momentum into the control volume | | |
| | + Time rate of change of momentum in the control volume | = | Sum of the forces acting on the fluid in the control volume. | |

The terms in the statement are vectors so we must be concerned with direction as well as magnitude.

Considering the conservation of momentum in the direction of flow (x-direction in Figure 5-2), the outflow section (section 2), the flux of momentum out of the control volume through the differential area $dA_2$ is

$$\rho_2 v_2 \, dA_2 \, v_2$$

Here $\rho_2 \, v_2 \, dA_2$ is the mass flux (mass per unit of time) and $\rho_2 v_2 \, dA_2 \, v_2$ is the momentum flux through the area $dA_2$. The total momentum flux out through section 2 is

$$\sum_{A_2} \rho_2 v_2 \, dA_2 \, v_2$$

so

$$\text{Flux of momentum out of control volume} = \sum_{A_2} \rho_2 v_2 \, dA_2 \, v_2$$

Similarly, at the inflow section (section 1)

$$\text{Flux of momentum into the control volume} = \sum_{A_1} \rho_1 v_1 \, dA_1 \, v_1$$

The amount of momentum in the control volume is

$$\sum_{\forall} \rho v \, d\forall$$

so

$$\text{Time rate of change of momentum in the control volume} = \frac{\partial}{\partial t} \left\{ \sum_{\forall} \rho v \, d\forall \right\}$$

At the upstream section, the force acting on the differential area $dA_1$ of the control volume is

$$p_1 dA_1$$

where $p_1$ is the pressure from the upstream fluid on the differential area.

The total force in the x-direction at section 1 is

$$\sum_{A_1} p_1 \, dA_1$$

Similarly, at section 2, the total force is

$$-\sum_{A_2} p_2 \, dA_2$$

There is a fluid shear stress acting along the interface between the water, bed, and banks. The shear on the control volume is in the opposite direction to the direction of flow and results in a force

$$-\tau_o P \, dx$$

where $\tau_o$ is the average shear stress on the interface area, $P$ is the average wetted perimeter and $dx$ is the length of the control volume. The term $P \, dx$ is the interface area.

If the x-direction is normal to the direction of gravity, the statement of conservation of momentum in the x-direction for the control volume is

$$\sum_{A_2} \rho_2 v_2 v_2 \, dA_2 - \sum_{A_1} \rho_1 v_1 v_1 \, dA_1 + \frac{\partial}{\partial t} \left\{ \sum_{\forall} \rho v \, d\forall \right\} = \sum_{A_1} p_1 dA_1 - \sum_{A_2} p_2 dA_2 - \tau_o P \, dx \qquad (5\text{-}9)$$

In the limit, the summations can be replaced with integrals so that Equation 5-9 becomes

$$\int_{A_2} \rho_2 \, v_2^2 \, dA_2 - \int_{A_2} \rho_1 v_1^2 \, dA_1 + \frac{\partial}{\partial t} \left\{ \int_{\forall} \rho v \, d\forall \right\} = \int_{A_1} p_1 \, dA_1 - \int_{A_2} p_2 \, dA_2 - \tau_o P \, dx \qquad (5\text{-}10)$$

which is the integral form of the momentum equation.

Again, as with the conservation of mass equation, it is convenient to use average velocities instead of point velocities. A momentum coefficient $\beta$ is defined so that when average velocities are used instead of point velocities, the correct momentum flux is considered.

The momentum coefficient is

$$\beta = \frac{1}{\rho V^2 A} \int_A \rho v^2 \, dA \qquad (5\text{-}11)$$

which reduces to

$$\beta = \frac{1}{V^2 A} \int v^2 \, dA \qquad (5\text{-}12)$$

if there is no variation in fluid density at a cross section. By assuming $\rho_1 = \rho_2 = \rho$, Equation 5-10 is reduced to

$$\rho\beta_2 V_2^2 A_2 - \rho\beta_1 V_1^2 A_1 + \rho \frac{\partial}{\partial t} \{\int_{\forall} v \, d\forall\}$$

$$= \int_{A_1} p_1 \, dA_1 - \int_{A_2} p_2 \, dA_2 - \tau_o P \, dx \qquad (5\text{-}13)$$

If the flow is steady

$$\frac{\partial}{\partial t} \{ \int_{\forall} v \, d\forall\} = 0 \qquad (5\text{-}14)$$

The pressure force and shear force terms on the right-hand side of Equation 5-14 are usually abbreviated as $\Sigma F_x$ or

$$\Sigma F_x = \int_{A_1} p_1 \, dA_1 - \int_{A_2} p_2 \, dA_2 - \tau_o P \, dx \qquad (5\text{-}15)$$

Then, for steady flow of constant density fluid, the conservation of momentum equation becomes

$$\rho\beta_2 V_2^2 A_2 - \rho\beta_1 V_1^2 A_1 = \Sigma F_x \qquad (5\text{-}16)$$

For steady flow with constant density, the conservation of mass equation (Equation 5-8) was

$$V_1 A_1 = V_2 A_2 = Q$$

With this expression, the steady flow conservation of linear momentum equation takes on the familiar form

$$\rho Q (\beta_2 V_2 - \beta_1 V_1) = \Sigma F_x \qquad (5\text{-}17)$$

Conservation of Energy

The First Law of Thermodynamics can be written

$$\dot{Q} - \dot{W} = \frac{dE}{dt} \qquad (5\text{-}18)$$

where $\dot{Q}$ = the rate at which heat is added to a fluid system
$\dot{W}$ = the rate at which a fluid system does work on its surroundings
$E$ = the energy of the system

Then $dE/dt$ is the rate of change of energy in the system.

The statement of conservation of energy for a control volume is then

| | | | |
|---|---|---|---|
| Flux of energy out of the control volume | - | Flux of energy into the control volume | |
| | + | Time rate of change of energy in the control volume | $= \dot{Q} - \dot{W}$ |

The choice of a control volume is arbitrary. Because of the complexities resulting from having to integrate over the cross-sectional area, the control volume, which includes the entire cross section of the river is inconvenient. Therefore, the control volume is reduced to the size of a streamtube connecting $dA_1$ and $dA_2$ as shown in Figure 5-3. The streamtube is bounded by streamlines through which no mass or momentum enters.

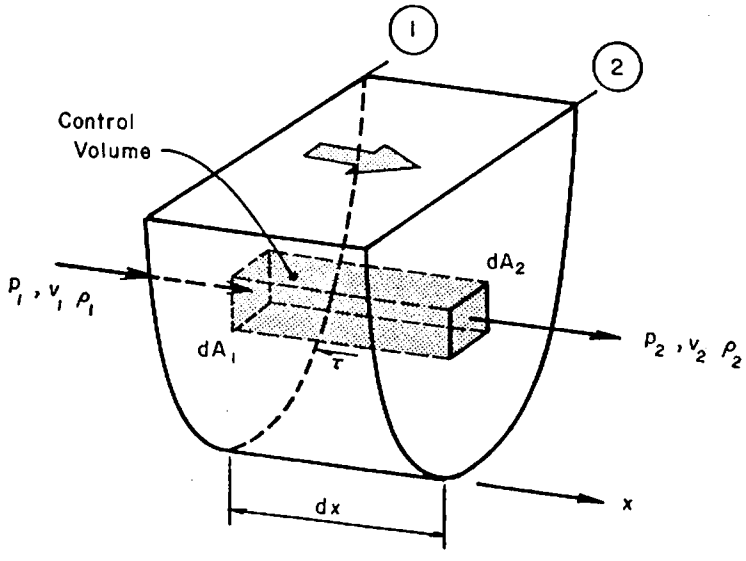


Figure 5-3. The streamtube as a control volume.

For steady constant density flow in the streamtube

| | |
|---|---|
| Flux of energy out of the control volume | $= \rho_2 e_2 \, dA_2 \, v_2$ |

and

| | |
|---|---|
| Flux of energy into the control volume | $= \rho_1 e_1 \, dA_1 \, v_1$ |

Here $e$ is the energy per unit of mass. Accordingly, the total energy in a control volume of size $\forall$ is

$$E = \int_{\forall} \rho e \, d\forall \qquad (5\text{-}19)$$

Because the flow is steady

$$\begin{array}{l}\text{Time rate of}\\ \text{change of energy} \\ \text{in the control volume}\end{array} = 0$$

Unless one is concerned with thermal pollution, evaporation losses, or problems concerning the formation of ice in rivers, the rate at which heat is added to the control volume can be neglected; that is

$$\dot{Q} \cong 0 \tag{5-20}$$

The work done by fluid in the control volume on its surroundings can be in the form of pressure work $W_p$, shear work $W_\tau$, or shaft work (mechanical work) $W_s$. For the streamtube shown in Figure 5-3, no shaft work is involved.

The rate at which the fluid pressure does work on the control volume boundary $dA_1$ in Figure 5-3 is

$$-p_1\ dA_1\ v_1$$

and on boundary $dA_2$, the rate of doing pressure work is

$$p_2\ dA_2\ v_2$$

At the other boundaries of the streamtube, there is no pressure work because there is no fluid motion normal to the boundary. Hence, for the streamtube

$$\dot{W}_p = p_2\ dA_2\ v_2 - p_1\ dA_1\ v_1 \tag{5-21}$$

Along the interior boundaries of the streamtube there is a shear stress resulting from the condition that the fluid velocity inside the streamtube may not be the same as the velocity of the fluid surrounding the streamtube. The rate at which the fluid in the streamtube does shear work on the control volume is

$$\dot{W}_\tau = \tau P\ dx\ v \tag{5-22}$$

where $\tau$ is the average shear stress on the streamtube boundary, $P$ is the average perimeter of the streamtube, $dx$ is the length of the streamtube and $v$ is the fluid velocity at the streamtube boundary. The product $P\ dx$ is the surface of the streamtube subjected to shear stresses.

For steady flow in the streamtube, the statement of the conservation of energy in the streamtube shown in Figure 5-3 is

$$\rho_2 e_2 v_2\ dA_2 - \rho_1 e_1 v_1\ dA_1 = p_1 v_1 dA_1 - p_2 v_2\ dA_2 - \tau P v\ dx \tag{5-23}$$

If the density is constant in the streamtube, the conservation of mass for the streamtube is

$$v_2\ dA_2 = v_1\ dA_1 = dQ$$

and

$$\rho_2 = \rho_1 = \rho \tag{5-24}$$

Now Equation 5-23 reduces to

$$(\rho e_1 + p_1)dQ - (\rho e_2 + p_2)dQ = \tau P v \, dx \tag{5-25}$$

The energy per unit mass $e$ is the sum of the internal, kinetic and potential energies or

$$e = u + \frac{v^2}{2} + gz \tag{5-26}$$

where $u$ = the internal energy associated with the fluid temperature
$v$ = the velocity of the mass of fluid
$g$ = the acceleration due to gravity
$z$ = the elevation above some arbitrary reference level

This expression for $e$ is substituted in Equation 5-25 to yield

$$u_1 + \frac{v_1^2}{2} + gz_1 + \frac{p_1}{\rho} = u_2 + \frac{v_2^2}{2} + gz_2 + \frac{p_2}{\rho} + \frac{\tau P v dx}{\rho dQ} \tag{5-27}$$

By dividing through by $g$ and calling the term

$$\frac{u_2 - u_1}{g} + \frac{\tau P v dx}{\rho g dQ}$$

the head loss $h_\ell$, the energy equation for the streamtube becomes

$$\frac{v_1^2}{2g} + \frac{p_1}{\gamma} + z_1 = \frac{v_2^2}{2g} + \frac{p_2}{\gamma} + z_2 + h_\ell \tag{5-28}$$

If there is no shear stress on the streamtube boundary and if there is no change in interval energy ($u_1 = u_2$), the energy equation reduces to

$$\frac{v_1^2}{2g} + \frac{p_1}{\gamma} + z_1 = \frac{v_2^2}{2g} + \frac{p_2}{\gamma} + z_2 \tag{5-29}$$

which is the Bernoulli Equation.

Generally, there is not sufficient information available to do a differential streamtube analysis of a reach of river so appropriate changes must be made in the energy equation. A reach of river such as that shown in Figure 5-1 can be pictured as a bundle of streamtubes. We know the statement of the conservation of energy for a streamtube. It is Equation 5-28 which can be rewritten

$$\left(\frac{v_1^2}{2g} + \frac{p_1}{\gamma} + z_1\right) v_1 \, dA_1$$

$$= \left(\frac{v_2^2}{2g} + \frac{p_2}{\gamma} + z_2\right) v_2 \, dA_2 + h_\ell \, vdA \qquad (5\text{-}30)$$

because

$$v_1 \, dA_1 = v_2 \, dA_2 = vdA$$

for the streamtube. By summing the energies in all the streamtubes making up the reach of river, we can write

$$\frac{\alpha_1 V_1^2}{2g} + \frac{\bar{p}_1}{\gamma} + \bar{z}_1 = \frac{\alpha_2 V_2^2}{2g} + \frac{\bar{p}_2}{\gamma} + \bar{z}_2 + H_L \qquad (5\text{-}31)$$

Equation 5-31 is the common form of the energy equation used in open channel flow. It is derived from Equation 5-30 by integrating Equation 5-30 over the cross section area; that is

$$\int_A \left(\frac{v^2}{2g} + \frac{p}{\gamma} + z\right) vdA = \left\{ \frac{\alpha V^2}{2g} + \frac{\bar{p}}{\gamma} + \bar{z} \right\} Q \qquad (5\text{-}32)$$

where $\alpha$ is the kinetic energy correction factor defined by the expression

$$\alpha = \frac{1}{V^3 A} \int v^3 \, dA \qquad (5\text{-}33)$$

to allow the use of average velocity $V$ rather than point velocity $v$. The average pressure over the cross section is $\bar{p}$, defined as

$$\bar{p} = \frac{1}{VA} \int_A p \, vdA \qquad (5\text{-}34)$$

The term $\bar{z}$ is the average elevation of the cross section defined by the expression

$$\bar{z} = \frac{1}{VA} \int_A z \, vdA \qquad (5\text{-}35)$$

and $Q$ is the volume flow rate or the discharge. By definition

$$Q = \int_A vdA \qquad (5\text{-}36)$$

Also

$$H_L = \frac{1}{VA} \int_A h_\ell \, vdA \qquad (5\text{-}37)$$

In summary, the expression for conservation of energy for steady flow in a reach of river is written

$$\frac{\alpha_1 V_1^2}{2g} + \frac{\bar{p}_1}{\gamma} + \bar{z}_1 = \frac{\alpha_2 V_2^2}{2g} + \frac{\bar{p}_2}{\gamma} + \bar{z}_2 + H_L \qquad (5\text{-}38)$$

The tendency in river work is to neglect the energy correction factor even though its value may be as large as 1.5. Usually it is assumed that the pressure is hydrostatic and the average elevation head $\bar{z}$ is at the centroid of the cross-sectional area. However, it should be kept in mind that Equations 5-33, 5-34 and 5-35 are the correct definitions of the terms in the energy equation.

Hydrostatics

When the only forces acting on the fluid are pressure and fluid weight, the differential equation of motion in an arbitrary direction x is

$$-\frac{\partial}{\partial x}\left(\frac{p}{\gamma} + z\right) = \frac{a_x}{g} \qquad (5\text{-}39)$$

In steady uniform flow (and for zero flow), the acceleration is zero and we obtain the equation of hydrostatics

$$\frac{p}{\gamma} + z = \text{Constant} \qquad (5\text{-}40)$$

However, when there is acceleration, the piezometric head varies in the flow. That is, the piezometric head is not constant in the flow. This is illustrated in Figure 5-4. In Figure 5-4a the pressure at the bed is equal to $\gamma y_o$ whereas in the curvilinear flow (Figure 5-4b) the pressure is larger than $\gamma y_o$ because of the acceleration resulting from a change in direction.

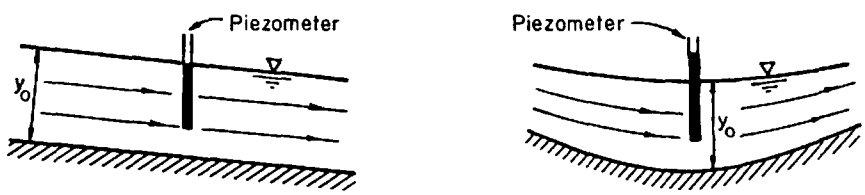


(a) Steady uniform flow

(b) Steady nonuniform flow

Figure 5-4. Pressure distribution in steady uniform and in steady nonuniform flow.

In general, when fluid acceleration is small (as in gradually varied flow) the pressure distribution is considered hydrostatic. However, for rapidly varying flow where the streamlines are converging, expanding, or have substantial curvature (curvlinear flow), fluid accelerations are not small and the pressure distribution is not hydrostatic.

In Equation 5-40, the constant is equal to zero for gage pressure at the free surface of a liquid, and for flow with hydrostatic pressure throughout (steady, uniform flow or gradually varied flow) it follows that the pressure head $p/\gamma$ is equal to the vertical distance below the free surface. In sloping channels with steady uniform flow, the pressure head $p/\gamma$ at a depth $y$ below the surface is equal to

$$\frac{p}{\gamma} = y \cos\theta \qquad (5\text{-}41)$$

Note that $y$ is the depth (perpendicular to the water surface) to the point, as shown in Figure 5-5. For most channels, $\theta$ is small and $\cos\theta \cong 1$.

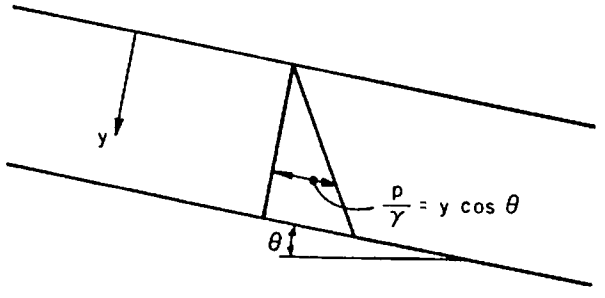


Figure 5-5. Pressure distribution in steady uniform flow on large slopes.

## 5.3 STEADY UNIFORM FLOW

### Introduction

In steady uniform open channel flow there are no accelerations, streamlines are straight and parallel, and the pressure distribution is hydrostatic. The slope of the water surface $S_w$ and the bed surface $S_o$ and the energy gradient $S_f$ are equal. Consider the unit width of the channel shown in Figure 5-6 as a control volume. According to Equation 5-38, the conservation of energy for this control volume is

$$\frac{\alpha_1 V_1^2}{2g} + \frac{\bar{p}_1}{\gamma} + \bar{z}_1 = \frac{\alpha_2 V_2^2}{2g} + \frac{\bar{p}_2}{\gamma} + \bar{z}_2 + H_L$$

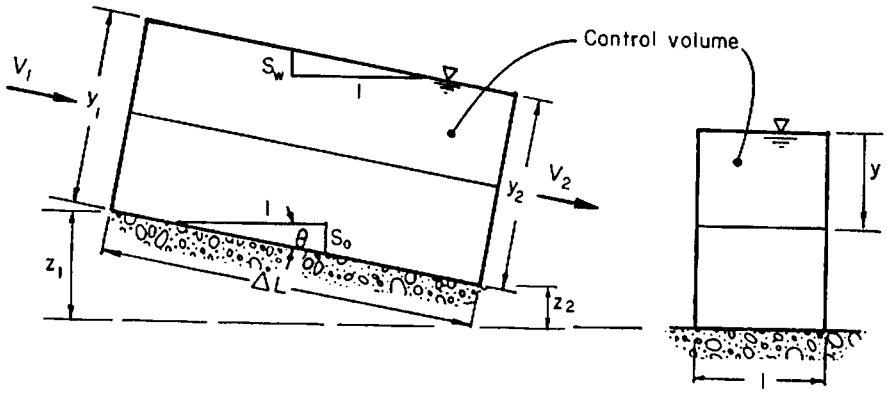


Figure 5-6. Steady uniform flow in a unit width channel.

The pressure at any point y below the surface is y cosθ. Then according to Equation 5-34

$$\bar{p}_1 = \frac{1}{V_1 y_1} \int_0^{y_1} \gamma y \cos\theta \, v_1 \, dy$$

Assuming only small variations in the point velocity v with y,

$$\bar{p}_1 \cong \frac{\gamma y_1 \cos\theta}{2}$$

Similarly

$$\bar{p}_2 \cong \frac{\alpha y_2 \cos\theta}{2}$$

Also according to Equation 5-35

$$\bar{z}_1 \cong z_1 + \frac{y_1 \cos\theta}{2}$$

and

$$\bar{z}_2 \cong z_2 + \frac{y_2 \cos\theta}{2}$$

With the above expressions for $\bar{p}_1$, $\bar{p}_2$, $\bar{z}_1$, and $\bar{z}_2$ the energy equation for this control volume reduces to

$$\frac{\alpha_1 V_1^2}{2g} + \frac{y_1 \cos\theta}{2} + z_1 + \frac{y_1 \cos\theta}{2} = \frac{\alpha_2 V_2^2}{2g} + \frac{y_2 \cos\theta}{2} + z_2 + \frac{y_2 \cos\theta}{2} + H_L$$

or

$$\frac{\alpha_1 V_1^2}{2g} + y_1\cos\theta + z_1 = \frac{\alpha_2 V_2^2}{2g} + y_2\cos\theta + z_2 + H_L$$

For most natural channels $\theta$ is small and $y\cos\theta \cong y$. The velocity distribution in the vertical is normally a log function for which $\alpha_1 \cong \alpha_2 \cong 1$. Then the energy equation becomes

$$\frac{V_1^2}{2g} + y_1 + z_1 = \frac{V_2^2}{2g} + y_2 + z_2 + H_L \tag{5-42}$$

and the slopes of the bed, water surface and energy gradeline are respectively

$$S_o = \sin\theta = \frac{z_1 - z_2}{\Delta L} \tag{5-43}$$

$$S_w = \frac{(z_1+y_1) - (z_2+y_2)}{\Delta L} \tag{5-44}$$

and

$$S_f = \frac{L}{\Delta L} = \frac{(\frac{V_1^2}{2g} + y_1 + z_1) - (\frac{V_2^2}{2g} + y_2 + z_2)}{\Delta L} \tag{5-45}$$

Steady uniform flow is an idealized concept for open channel flow and is difficult to obtain even in laboratory flumes. For many applications, the flow is steady and the changes in width, depth or direction (resulting in nonuniform flow) are so small that the flow can be considered uniform. In other cases, the changes occur over such a long distance the flow is a gradually varied flow.

Variables of interest for steady uniform flow are: (1) the mean velocity V, (2) the discharge Q, (3) the velocity distribution v(y) in the vertical, (4) the head loss $H_L$ through the reach, and (5) the shear stress, both local $\tau$ and at the bed $\tau_o$. The variables are interrelated and which variable we determine and how we determine it depends on the data available. For example, if the discharge and cross-sectional area are known, the mean velocity is easily determined for some suitable equation such as Manning's or Chezy's equaton.

## Shear-Stress and Velocity Distribution

Shear stress $\tau$ is the internal fluid stress which resists deformation. The shear stress exists only when fluids are in motion. It is a tangential stress in contrast to pressure, which is a normal stress.

The local shear stress at the interface between the boundary and the fluid can be determined quite easily if the boundary is hydraulically smooth; that is, if the roughness at the boundary is submerged in a viscous sublayer as shown in Figure 5-7. Here, the thickness of the

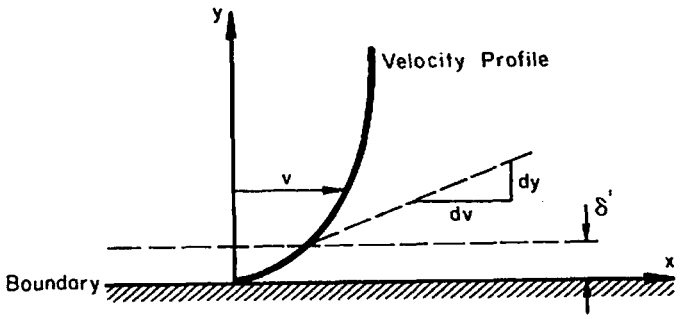


Figure 5-7. Hydraulically smooth boundary.

laminar sublayer is $\delta'$. In laminar flow, the shear stress at the boundary is

$$\tau_o = \mu\left(\frac{dv}{dy}\right)_{y=0} \tag{5-46}$$

The velocity gradient is evaluated at the boundary. The dynamic viscosity $\mu$ is the proportionality constant relating boundary shear and velocity gradient in the viscous sublayer.

When the boundary is hydraulically rough, there is no viscous or laminar sublayer. The paths of fluid particles in the vicinity of the boundary are shown in Figure 5-8.

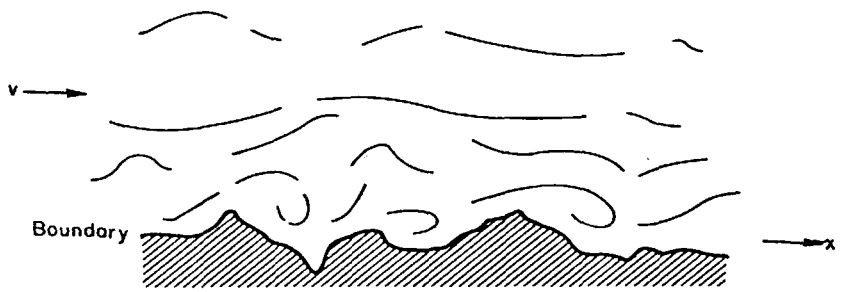


Figure 5-8. Hydraulically rough boundary.

The velocity at a point near the boundary fluctuates randomly about a mean value. The random fluctuation in velocity is called turbulence. For the hydraulically rough boundary

$$\tau_o \neq \mu \frac{dv}{dy}$$

so another method of expressing $\tau_o$ is required. So far, the only satisfactory way of determining the boundary shear stress at a rough boundary has been by experimental means.

If we follow a unit of mass of fluid in the flow near a rough boundary, the path is erratic. As shown in Figure 5-9a, the particle has a vertical component of velocity $v_y$ as well as a horizontal component $v_x$.

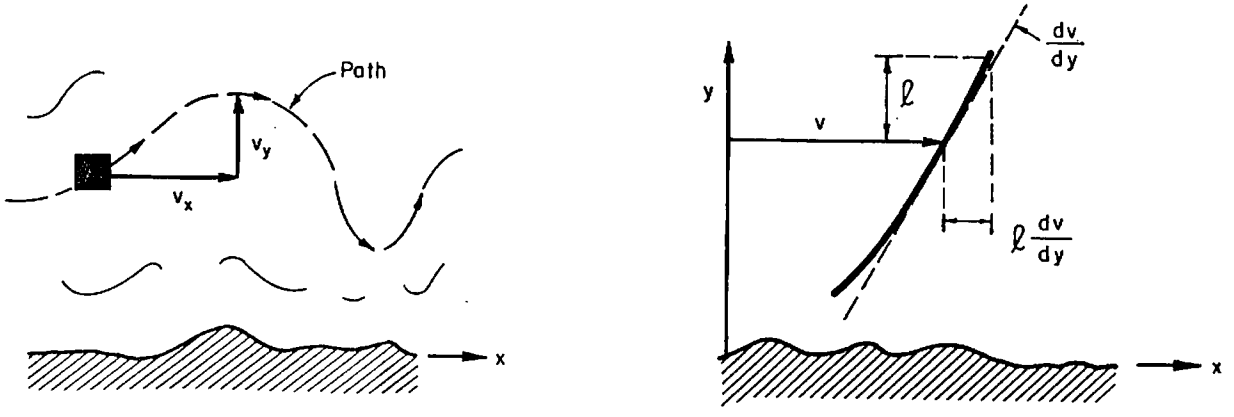


(a) Path of the particle

(b) Velocity profile

Figure 5-9. Velocities in turbulent flow.

The two components of velocity in Figure 5-9a can be written as

$$v_x = \bar{v}_x + v'_x \tag{5-47}$$

and

$$v_y = \bar{v}_y + v'_y \tag{5-48}$$

where $\bar{v}_x$ and $\bar{v}_y$ are the time-averaged mean velocities in the x and y direction and $v'_x$ and $v'_y$ are the fluctuating components.

Through experimental correlations it has been found that the boundary shear stress for turbulent flow at the boundary is

$$\tau_o = -\rho\overline{v'_x v'_y} \tag{5-49}$$

The term $v'_x v'_y$ is the time-average of the product of $v'_x$ and $v'_y$ at a point in the flow. It is called the Reynolds shear stress.

Prandtl (1925) suggested that $v'_x$ and $v'_y$ are related and furthermore that $v'_x$ is related to the velocity gradient dv/dy shown in Figure 5-9. He proposed to characterize the turbulence with a dimension called the "mixing length" $\ell$. Accordingly

$$v'_x \sim \ell \left(\frac{dv}{dy}\right) \tag{5-50}$$

$$v_y' \sim \ell \left(\frac{dv}{dy}\right) \tag{5-51}$$

and

$$\tau \sim \rho \ell^2 \left(\frac{dv}{dy}\right)^2 \tag{5-52}$$

If it is assumed that the mixing length can be represented by the product of a constant $\kappa$ and $y$ (i.e., $\ell = \kappa y$), then for steady uniform turbulent flow

$$\tau = \rho \kappa^2 y^2 \left(\frac{dv}{dy}\right)^2 \tag{5-53}$$

Using different reasoning von Kármán (1930) derived the same equation. Equation 5-53 can be rearranged to the form

$$\frac{dv}{dy} = \frac{\sqrt{\tau_o/\rho}}{\kappa y} \tag{5-54}$$

where $\kappa$ is the von Kármán universal velocity coefficient. For rigid boundaries, $\kappa$ has the average value of 0.4. The term $\tau_o$ is the shear stress at the bed. The term $(\tau_o/\rho)^{1/2}$ has the dimensions of velocity and is called the shear velocity. Integration of Equation 5-54 yields

$$\frac{v}{\sqrt{\tau_o/\rho}} = \frac{1}{\kappa} \ln \frac{y}{y'} = \frac{2.31}{\kappa} \log \frac{y}{y'} \tag{5-55}$$

Here ln is the logarithm to base e and log is the logarithm to base 10. The term $y'$ results from evaluation of the constant of integration assuming $v = 0$ at some distance $y'$ above the bed.

The term $y'$ depends on the flow and has been experimentally determined. The many experiments have resulted in characterizing turbulent flow into three general types:

1. Hydraulically smooth boundary turbulent flow where the velocity distribution, mean velocity and resistance to flow are independent of the boundary roughness of the bed but depend on fluid viscosity. Where $\delta'$ is equal to $11.6\nu/\sqrt{\tau_o/\rho}$, $y' = \delta'/107$.

2. Hydraulically rough boundary turbulent flow where velocity distribution, mean velocity and resistance to flow are independent of viscosity and depend entirely on the boundary roughness. For this case, $y' = k_s/30.2$ where $k_s$ is the height of the roughness element.

3. Transition where the velocity distribution, mean velocity and resistance to flow depends on both fluid viscosity and boundary roughness. Then

$$\frac{\delta'}{107} < y' < \frac{k_s}{30.2}$$

There are many forms of Equation 5-55 depending on the experimental and the method of expressing y'. In this manual, the Einstein method of expressing y' is employed. The Einstein form of the von Kármán-Prandtl velocity distribution, mean velocity and resistance to flow equations are:

$$\frac{v}{V_*} = 5.75 \log \left(30.2 \frac{xy}{k_s}\right) = 2.5 \ln \left(30.2 \frac{xy}{k_s}\right) \tag{5-56}$$

$$\frac{V}{V_*} = \frac{C}{\sqrt{g}} = 5.75 \log \left(12.27 \frac{o}{k_s}\right) = 2.5 \ln \left(12.27 \frac{o}{k_s}\right) \tag{5-57}$$

where

$x$ = a coefficient given in Figure 5-10

$k_s$ = the height of the roughness elements. For sand channels, $k_s$ is the $D_{65}$ of the bed material

$v$ = the local mean velocity at depth $y$

$y_o$ = the depth of flow

$V$ = the depth-averaged velocity

$V_*$ = the shear velocity $\sqrt{\tau_o/\rho}$ and for steady uniform flow is $\sqrt{gRS_f}$

$\tau_o$ = the shear stress at the boundary and for steady uniform flow

$= \gamma RS_f$

$R$ = the hydraulic radius equal to the area divided by the wetted perimeter

$S_f$ = the slope of the energy gradeline

$\delta'$ = the thickness of the viscous sublayer

$$= \frac{11.6\nu}{V_*} \tag{5-58}$$

$C/\sqrt{g}$ = the Chezy discharge coefficient in the equation

$$V = C\sqrt{RS_f} \quad \text{or} \quad C = \left(\frac{8g}{f}\right)^{1/2} \tag{5-59}$$

$f$ = the Darcy-Weisbach resistance coefficient and is given by the expression

$$f = \frac{8\tau_o}{\rho V^2} \tag{5-60}$$

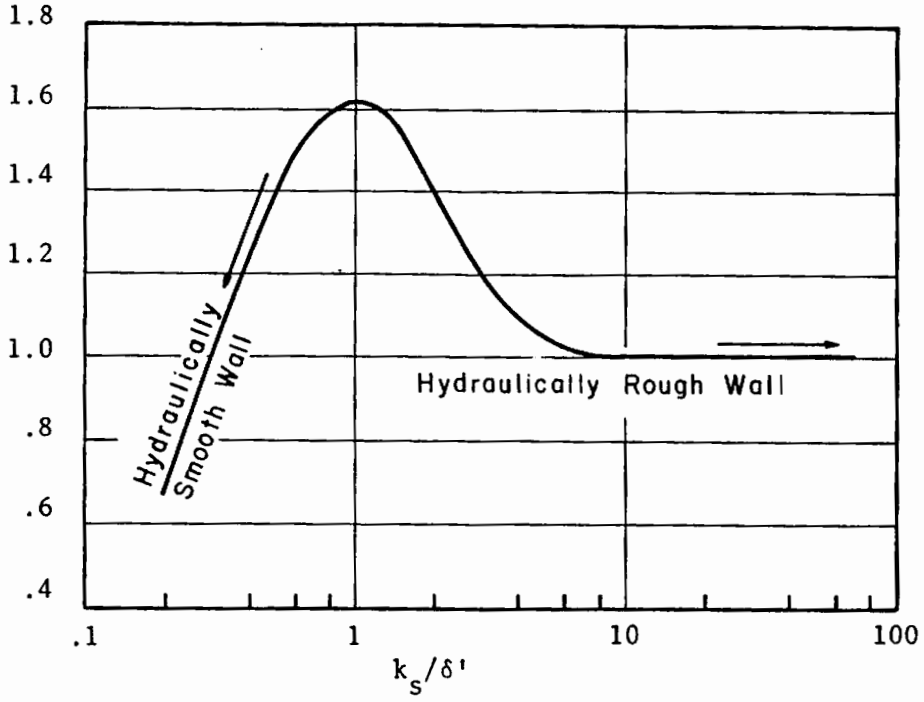


Figure 5-10. Einstein's multiplication factor x in the logarithmic velocity equations (Einstein, 1950).

## Empirical Velocity Equations

Because of the difficulties involved in determining the shear stress and hence the velocity distribution in turbulent flows, the empirical approach to determine mean velocities in rivers has been prevalent. Two such empirical equations are in common use. They are Manning's equation

$$V = \frac{1.486}{n} R^{2/3} S_f^{1/2} \tag{5-61}$$

and Chezy's equation

$$V = CR^{1/2} S_f^{1/2} \tag{5-62}$$

where

V = the average velocity in the cross section
n = Manning's roughness coefficient
R = the hydraulic radius equal to the cross-sectional area A divided by the wetted perimeter P
$S_f$ = the energy slope of the channel
$C^f$ = Chezy's discharge coefficient known as Chezy's C

In these equations, the boundary shear stress is expressed implicitly in the roughness coefficient n or in the discharge coefficient C. By equating the velocity determined from Manning's equation with the velocity determined from Chezy's equation, the relation between the coefficients is

$$C = \frac{1.486}{n} R^{1/6} \tag{5-63}$$

If the flow is gradually varied, Manning's and Chezy's equations are used with the energy slope $S_f$ replaced with an average friction slope $S_{f_{ave}}$. The term $S_{f_{ave}}$ is determined by averaging over a short time increment at a station or over a short length increment at an instant of time, or both.

Over many decades, a catalog of values of Manning's n and Chezy's C has been assembled so that an engineer can estimate the appropriate value by knowing the general nature of the channel boundaries. An abbreviated list of Manning's roughness coefficients is given in Table 5-1. Additional values are given by Barnes (1967) and V. T. Chow (1959). Manning's n for sandbed channels is discussed in detail in another chapter.

Table 5-1. Manning's roughness coefficients for various boundaries.

| Rigid Boundary Channels | Manning's n |
|---|---|
| Very smooth concrete and planed timber | 0.011 |
| Smooth concrete | 0.012 |
| Ordinary concrete lining | 0.013 |
| Wood | 0.014 |
| Vitrified clay | 0.015 |
| Shot concrete, untrowelled, and earth channels in best condition | 0.017 |
| Straight unlined earth canals in good condition | 0.020 |
| Rivers and earth canals in fair condition-some growth | 0.025 |
| Winding natural streams and canals in poor condition-considerable moss growth | 0.035 |
| Mountain streams with rocky beds | 0.040-0.050 |
| **Alluvial Sandbed Channels (no vegetation)[1]** | |
| Tranquil flow, Fr < 1 | |
| plane bed | 0.014-0.020 |
| ripples | 0.018-0.030 |
| dunes | 0.020-0.040 |
| washed out dunes or transition | 0.014-0.025 |
| plane bed | 0.010-0.013 |
| Rapid flow, Fr $\tilde{\sim}$ 1 | |
| standing waves | 0.010-0.015 |
| antidunes | 0.012-0.020 |

[1]Data is limited to sand channels with $D_{50}$ < 1.0 mm.

Average Boundary Shear Stress

The shear stress at the boundary $\tau_o$ for steady uniform flow is determined by applying the conservation of mass and momentum principles to the control volume shown in Figure 5-11. Recall that the statement of the conservation of mass is

| Mass flux out of the control volume | - | Mass flux into the control volume | + | Time rate of change in mass in the control volume | = 0 |
|---|---|---|---|---|---|

and the statement of the conservation of linear momentum is

| Momentum flux out of the control volume | - | Momentum flux into the control volume | + | Time rate of change of momentum in the control volume | = | Sum of the forces acting on the fluid in the control volume |
|---|---|---|---|---|---|---|

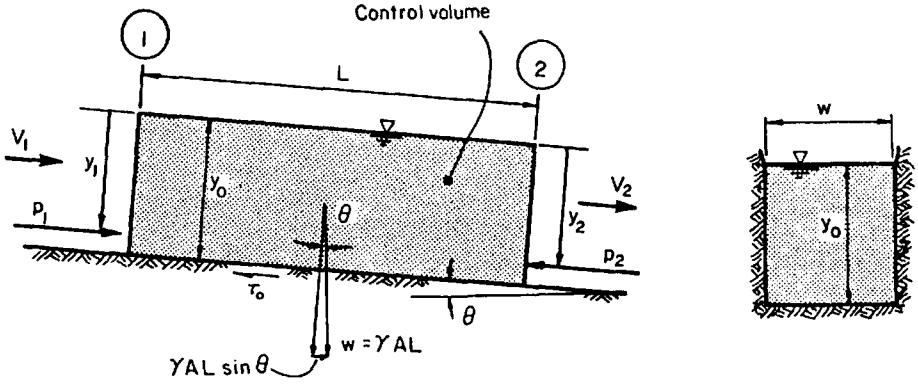


Figure 5-11. Control volume for steady uniform flow.

As the flow is steady

| Time rate of change in mass and momentum in the control volume | = 0 |
|---|---|

| Mass flux into the control volume | $= \rho y_o W V_1$ |
|---|---|

and

| Mass flux out of the control volume | $= \rho y_o W V_2$ |
|---|---|

The conservation of mass is then

$$\rho y_o W V_2 - \rho y_o W V_1 = 0$$

or

$$V_1 = V_2 \tag{5-64}$$

The conservation of momentum in the downstream direction is composed of the terms

Momentum flux out of the control volume $= \rho V_2 \, y_o W \, V_2$

where $\rho V_2$ is the momentum of a unit volume at the outflow section, and $y_o W$ is the outflow cross section area.

Similarly,

Momentum flux into the control volume $= \rho V_1 \, y_o W \, V_1$

The pressure force acting on the control boundary at the upstream section is

$$F_1 = \int_o^{y_o} p_1 W \, dy$$

As the flowlines are parallel

$$p_1 = \gamma y$$

so

$$F_1 = \int_o^{y_o} \gamma W y \, dy = \frac{\gamma y_o^2 W}{2} \tag{5-65}$$

Similarly at the downstream section the force acting on the boundary is

$$F_2 = \frac{-\gamma y_o^2 W}{2} \tag{5-66}$$

The body force is the weight of the fluid in the control volume and the downstream component of this body force is

$$\gamma AL \sin\theta$$

where $\theta$ is the slope angle of the channel bed. The average boundary shear stress is $\tau_o$ acting on the wetted perimeter P. The shear force $F_s$ in the x-direction is

$$F_s = \tau_o PL \tag{5-67}$$

With the above expressions for the components, the statement of conservation of linear momentum becomes

$$\rho V_2 y_o W V_2 - \rho V_1 y_o W V_1 = \gamma AL \sin\theta + \frac{\gamma y_o^2 W}{2} - \frac{\gamma y_o^2 W}{2} - \tau_o PL \tag{5-68}$$

which reduces to

$$\tau_o = \gamma \frac{A}{P} \sin\theta \tag{5-69}$$

The term A/P is called the hydraulic radius R. If the channel slope angle is small

$$\sin\theta \cong S_o \tag{5-70}$$

and the average shear stress on the boundary is

$$\tau_o = \gamma R S_o \tag{5-71}$$

If the flow is gradually varied nonuniform flow, the average boundary shear stress is

$$\tau_o = \gamma R S_f \tag{5-72}$$

where $S_f$ is the slope of the energy gradeline.

## 5.4 STEADY RAPIDLY VARYING FLOW

### Introduction

Steady flow through relatively short transitions where the flow is uniform before and after the transition can be analyzed using the Bernoulli equation. Energy loss due to friction may be neglected, at least as a first approximation. Refinement of the analysis can be made as a second step by including friction loss. For example, the water surface elevation through a transition is determined using the Bernoulli equation and then modified by determining the friction loss effects on velocity and depth in short reaches through the transition. Energy losses resulting from separation cannot be neglected, and transitions where separation may occur need special treatment which may include model studies. Contracting flows (coverging streamlines) are less susceptible to separation than expanding flow. Also, any time a transition changes velocity and depth such that the Froude number approaches unity, problems such as waves, blockage or choking of the flow may occur. If the approaching flow is rapid (supercritical), a hydraulic jump may result. Transitions for rapid flow are discussed in a later section.

Transitions are used to contract or expand a channel width (Figure 5-12a), to increase or decrease in bottom elevation (Figure 5-12b), or to change both the width and bottom elevation. The first step in the

analaysis is to use the Bernoulli equation (neglecting any head loss resulting from friction or separation) to determine the depth and velocity changes of the flow through the transition. Further refinement depends on importance of freeboard, whether flow is rapid, and whether flow approaches critical.

The Bernoulli equation for flow in Figure 5-12b is

$$\frac{V_1^2}{2g} + y_1 = \frac{V_2^2}{2g} + y_2 + \Delta z \tag{5-73}$$

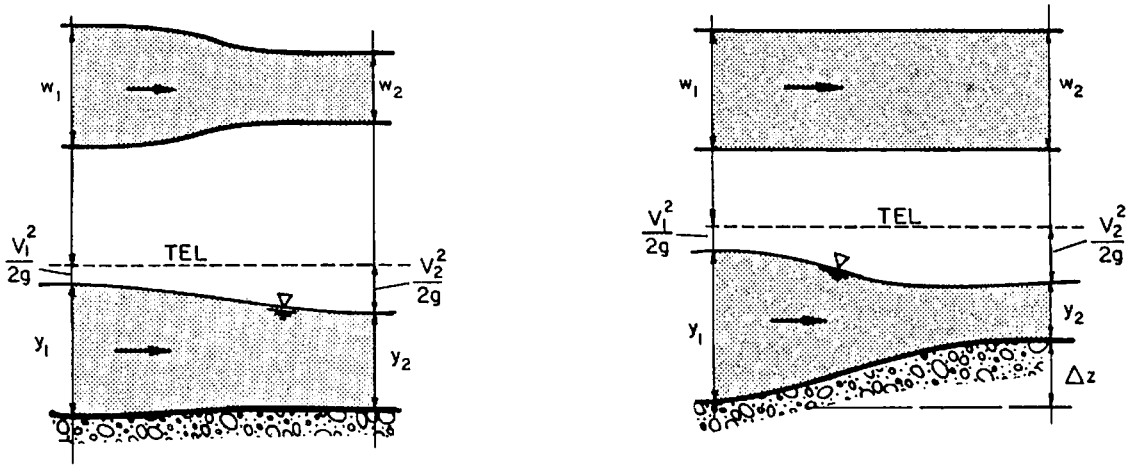


(a) Width contraction

(b) Bed rise

Figure 5-12. Transitions in open channel flow.

or

$$H_1 = H_2 + \Delta z \tag{5-74}$$

where

$$H = \frac{V^2}{2g} + y \tag{5-75}$$

The term $H$ is called the specific head, and is the height of the total head above the channel bed.

In the analysis of flow through transitions, the Bernoulli equation gives a numerical solution to the problem but very little descriptive information of the depth variation. Only after the analysis is completed will it be known if the depth will increase or decrease as the fluid passes through the transition or even if the flow is physically possible. On the other hand, by investigating the various interrelations between the variables (H, V and y) in the specific head equation, the variation of depth through a transition can be predicted.

There are two conditions for analyzing the flow through transitions. In the first condition, the width is constant and the elevation of the stream bed changes; that is, $q = Q/W$ is constant and H and y vary (Figure 5-12b). In the second, the width changes and the elevation of the stream bed (neglecting the slope) is constant; that is, H is constant.

Specific Head Diagram

For simplicity, the following specific head analysis is done on a unit width of channel so that Equation 5-75 becomes

$$H = \frac{q^2}{2gy^2} + y \tag{5-76}$$

For a given q, Equation 5-76 can be solved for various values of H and y. When y is plotted as a function of H, Figure 5-13 is obtained. There are two possible depths called alternate depths for any H larger than a specific minimum. Thus, for specific head larger than the minimum, the given flow may have a large depth and small velocity or small depth and large velocity. Flow cannot occur with specific energy less than the minimum. The single depth of flow at the minimum specific head is called the critical depth $y_c$ and the corresponding velocity, the critical velocity $v_c = q/y_c$. To determine $y_c$ the derivative of H with respect to y is set equal to 0.

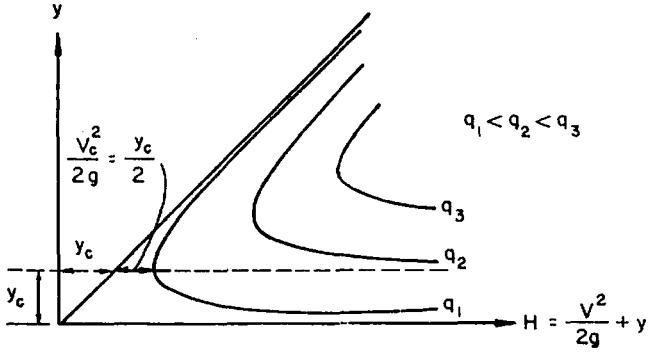


Figure 5-13. Specific head diagram.

$$\frac{dH}{dy} = - \frac{q}{gy^3} + 1 = 0 \tag{5-77}$$

and

$$q = (gy_c^3)^{1/2} \tag{5-78}$$

or

$$y_c = (\frac{q^2}{g})^{1/3} = 2 \frac{V_c^2}{2g} \tag{5-79}$$

Note that

$$V_c^2 = y_c g \tag{5-80}$$

or

$$\frac{V_c}{\sqrt{gy_c}} = 1 \tag{5-81}$$

But

$$\frac{V}{\sqrt{gy}} = Fr \tag{5-82}$$

Also

$$H_{min} = \frac{V_c^2}{2g} + y_c = \frac{3}{2} y_c \tag{5-83}$$

Thus flow at minimum specific energy has a Froude number equal to one. Flows with velocities larger than critical (Fr > 1) are called rapid or supercritical and flows with velocities smaller than critical (Fr < 1) are called tranquil or subcritical. These flow conditions are illustrated in Figure 5-14, where a rise in the bed causes a decrease

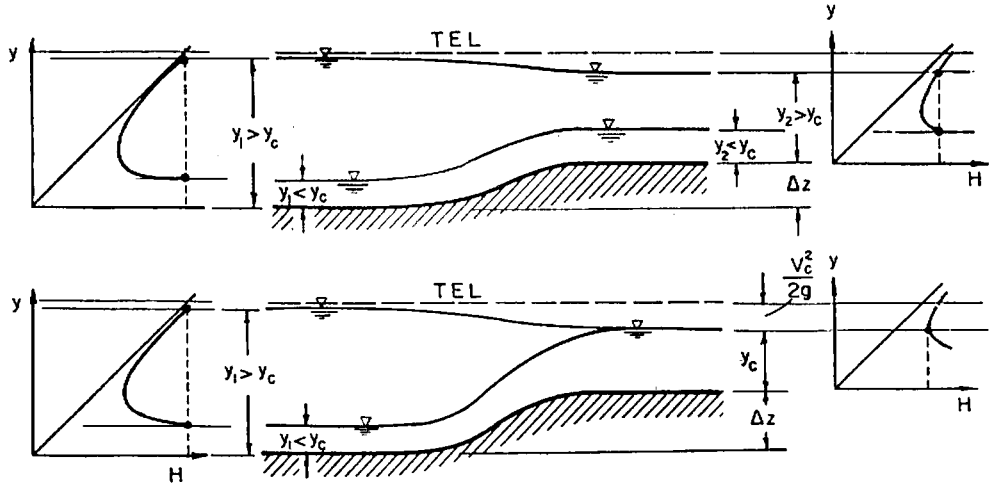


Figure 5-14. Changes in water surface resulting from an increase in bed elevation.

in depth when the flow is tranquil and an increase in depth when the flow is rapid. Furthermore there is a maximum rise in the bed for a given $H_1$ where the given rate of flow is physically possible. If the rise in the bed is increased beyond $\Delta z_{max}$ for $H_{min}$ then the approaching flow depth $y_1$ would have to increase (increasing H) or the flow would have to be decreased. Thus, for a given flow in a channel, a rise in the bed level can occur up to a $\Delta z_{max}$ without causing backwater.

Discharge Diagram

For a constant H, Equation 5-76 can be solved for y as a function of q. By plotting y as a function of q, Figure 5-15 is obtained and

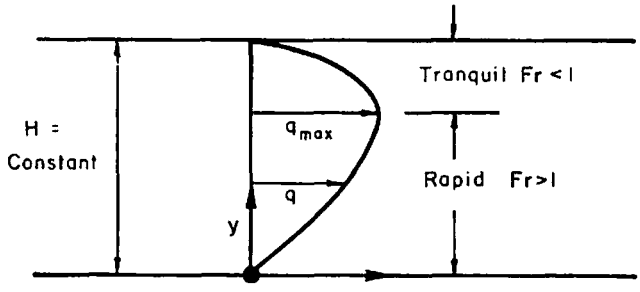


Figure 5-15. Specific discharge diagram.

for any discharge smaller than a specific maximum, two depths of flow is possible. To determine the value of y for $q_{max}$ Equation 5-76 is rearranged to obtain

$$q = y\sqrt{2g(H-y)} \tag{5-84}$$

The differential with respect to y is set equal to zero

$$\frac{dq}{} = 0 = \sqrt{\frac{g}{2}} \frac{(2H-3y)}{(H-y)^{1/2}} \tag{5-85}$$

from which

$$y_c = \frac{2}{3} H = 2 \frac{V_c^2}{2g} \tag{5-86}$$

or

$$V_c = \sqrt{gy_c} \tag{5-87}$$

Thus for maximum discharge at constant H, the Froude number is 1.0 and the flow is critical. From this

$$y_c = \frac{2}{3} H = 2 \frac{V_c^2}{2g} = \left(\frac{q_{max}^2}{g}\right)^{1/3} \tag{5-88}$$

For critical conditions, the Froude number is 1.0, the discharge is a maximum for a given specific head and the specific head is a minimum for a given discharge.

Flow conditions for constant specific head for a width contraction are illustrated in Figure 5-16. The contraction causes a decrease in flow depth when the flow is tranquil and an increase when the flow is rapid. The maximum contraction possible for these flow conditions is to the critical depth. Then the Froude number is one, the discharge per foot of width $q$ is a maximum, and $y_c$ is 2/3 H. A further decrease in width causes backwater. That is, increase $y_1$ upstream to get a larger specific energy and increase $y_c$ in order to get the flow through the decreased width.

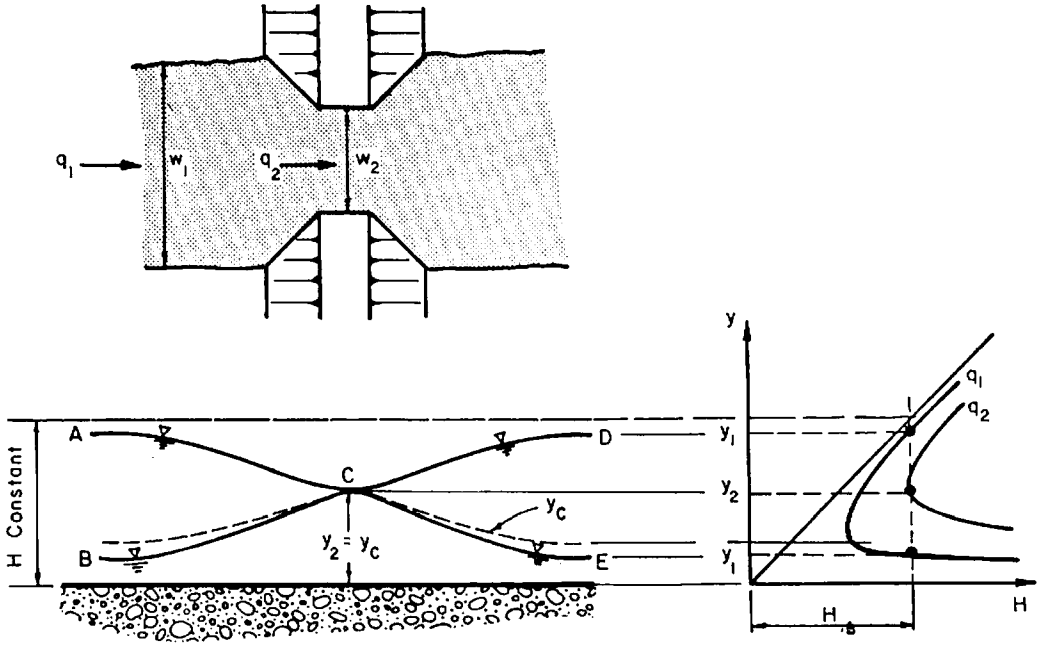


Figure 5-16. Change in water surface elevation resulting from a change in width.

The flow in Figure 5-16 can go from point A to C and then back to D or down to E depending on the boundary conditions. An increase in slope of the bed downstream from C and no separation would allow the flow to follow the line A to C to E. Similarly the flow can go from B to C and back to E or up to D depending on boundary conditions. Figure 5-16 is drawn with the side boundary forming a smooth streamline. If the contraction were a bridge abutment, the upstream flow would follow a natural streamline to a verna contracta but downstream the flow would probably separate. Tranquil approach flow could follow line A-C but the downstream flow probably would not follow either line C-D or C-E but would have an undulating hydraulic jump. There would be interaction of the flow in the separation zone and considerable energy would be lost. If the slope downstream of the abutments was the same as upstream, then the flow could not be sustained

with this amount of energy loss. Backwater would occur, increasing the depth in the constriction and upstream, until the flow could go through the constriction and establish uniform flow downstream.

## 5.5 STEADY FLOW AROUND BENDS

Because of the change in flow direction with results in centrifugal forces, there is a superelevation of the water surface in river bends. The water surface is higher at the concave bank than at the convex bank. The resulting transverse slope can be evaluated quantitatively. Using cylindrical coordinates (Figure 5-17), the differential pressure in the radial direction arises from the radial acceleration or

$$\frac{1}{\rho}\frac{\partial p}{\partial r} = \frac{\theta}{r} \tag{5-89}$$

The total superelevation between the outer and inner bend is

$$\Delta z = \frac{1}{\rho g}\int_{p_i}^{p_o} dp = \frac{1}{g}\int_{r_i}^{r_o}\frac{V_\theta^2}{r}\,dr \tag{5-90}$$

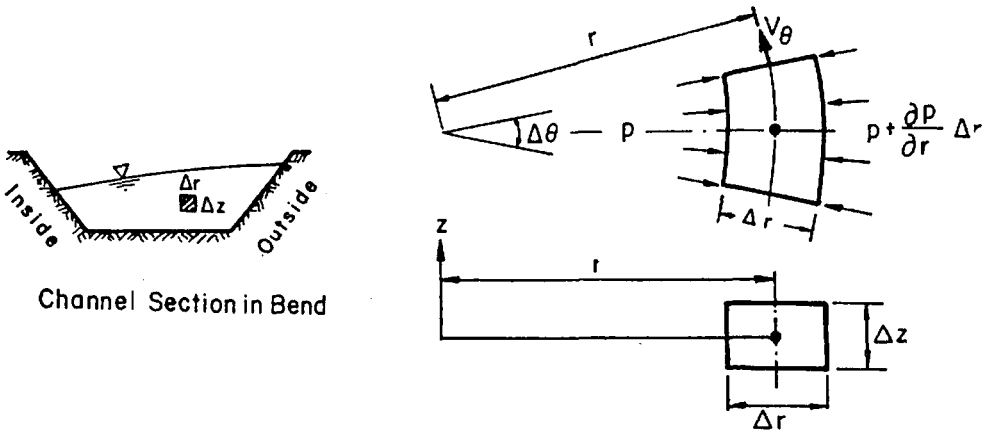


Figure 5-17. Definition sketch of dynamics of flow around a bend.

Two assumptions are made:

1. The radial and vertical velocities are small compared to the tangential velocities such that $V_\theta \tilde{\sim} V$.

2. The pressure distribution in the bend is hydrostatic i.e., $p = \gamma y$.

Then

$$\Delta z = \frac{1}{g}\int_{r_i}^{r_o}\frac{V^2}{r}\,dr \tag{5-91}$$

To solve Equation 5-91, the transverse velocity distribution along the radius of the bend must be known or assumed. The results obtained assuming various velocity distribution follow.

Woodward (1920) assumed V equal to the average velocity Q/A and r equal to the radius to the center of the stream $r_c$ and obtained

$$\Delta z = \frac{1}{g} \int_{r_i}^{r_o} \frac{V^2}{r_c} dr \tag{5-92}$$

or

$$\Delta z = z_o - z_i = \frac{V^2}{g r_c} (r_o - r_i) \tag{5-93}$$

in which $z_i$ and $r_i$ are the water surface elevation and the radius at the inside of the bend, and $z_o$ and $r_o$ are the water surface elevation and the radius at the outside of the bend.

By assuming the velocity distribution to approximate that of a free vortex, Shukry (1950) obtained

$$\Delta z = \frac{1}{g} \int_{r_i}^{r_o} \frac{C^2}{r^3} dr = \frac{C^2}{2g} \left\{\frac{1}{r_i^2} - \frac{1}{r_o^2}\right\} \tag{5-94}$$

in which C = rV, the free vortex constant. By assuming the depth of flow upstream of the bend equal to the average depth in the bend, Ippen and Drinker (1962) reduced Equation 5-94 to

$$\Delta z = \frac{V^2}{2g} \frac{2W}{r_c} \left\{\frac{1}{1-\left(\frac{W}{2r_c}\right)^2}\right\} \tag{5-95}$$

For situations where high velocities occur near the outer bank of the channel, a forced vortex may approximate the flow pattern. With this assumption and assuming a constant average specific head, Ippen and Drinker (1962) obtained

$$\Delta z = \frac{V^2}{2g} \frac{2W}{r_c} \left\{\frac{1}{1 + \frac{W^2}{12\, r_c^2}}\right\} \tag{5-96}$$

By assuming that the maximum velocities are close to the centerline of the channel in the bend and that the flow pattern inward and outward from the centerline can be represented as forced and free vortices, respectively, then

$$\Delta z = \frac{1}{g} \int_{r_i}^{r_c} \frac{C_i^2 r^2}{r} dr + \frac{1}{g} \int_{r_c}^{r_o} \frac{C_o^2}{r^3} dr \tag{5-97}$$

and when $r = r_c$, $V = V_{max}$.

Therefore, $C_i = \frac{V_{max}}{r_c}$ and $C_o = V_{max}\, r_c$

and Equation 5-97 becomes

$$\Delta z = \frac{V_{max}^2}{2g} \{2 - (\frac{r_i}{r_c})^2 - (\frac{r_c}{r_o})^2\} \qquad (5\text{-}98)$$

The differences in superelevation that are obtained by using the different equations are small, and in alluvial channels the resulting erosion of the concave bank and deposition on the convex bank leads to further error in computing superelevation. Therefore, it is recommended that Equation 5-93 be used to compute superelevation. For lined canals with sharp radii of curvature, superelevation should be computed using Equations 5-95 and 5-98.

## 5.6 RAPID FLOW IN BENDS AND TRANSITIONS

### Bends

Rapid flow or supercritical flow in a curved prismatic channel produces cross wave disturbance patterns which persist for long distances in a downstream direction. These disturbance patterns are the result of nonequilibrium conditions which persist because the disturbances cannot propagate upstream or even propagate directly across the stream. Therefore, the turning effect of the walls is not felt on all filaments of the flow at the same time and the equilibrium of the flow is destroyed. The waves produced form a series of troughs and crests in the water surface along the channel walls.

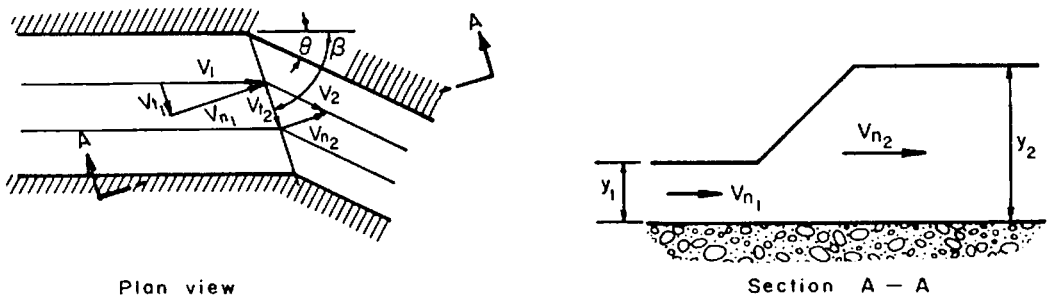


Figure 5-18. Definition sketch for rapid flow in a bend.

Figure 5-18 is a definition sketch to aid in the analysis of cross wave patterns in a bend with rapid flow. The water surface elevation in a bend can be computed if the following major assumptions are made: 1) the flow is two-dimensional, 2) the velocity is constant throughout the cross section, 3) the channel is horizontal, 4) there are no boundary shear stresses, and 5) the channel walls are vertical. The outer wall

which turns the flow inward produces an oblique hydraulic jump and a corresponding positive disturbance line or positive wave front propagates across the channel. The inner or convex wall causes an oblique expansion or negative wave to propagate across the channel with a corresponding negative disturbance line or wave front. From analysis of Figure 5-18 and the hydraulic jump equation the following formulas can be derived.

The initial velocity perpendicular to the wave front is given by

$$V_{n1} = \{\frac{gy_2}{2} (1 + \frac{y_2}{y_1})\}^{1/2} \quad (5\text{-}99)$$

The wave front angle is given by

$$\sin\beta \frac{V_{n1}}{V_1} = \frac{\sqrt{gy_1}}{V_1} \{\frac{y_2}{2y_1} (1 + \frac{y_2}{y_1})\}^{1/2}$$

or

$$\sin\beta \cong \frac{1}{Fr_1} \quad (5\text{-}100)$$

The relationship of the deflection angle $\theta$ and the Froude number is given by

$$\theta = \sqrt{3} \tan^{-1} \{(\frac{3}{Fr^2-1})^{1/2}\} - \tan^{-1} \{(\frac{1}{Fr_1^2-1})^{1/2}\} + \text{const.} \quad (5\text{-}101)$$

where the constant may be determined from the condition that for $\theta = 0$, the depth $y$ is the initial depth $y_1$.

For practical applications, Equation 5-101 is very involved and inconvenient to use even with graphical charts. Knapp (1951) developed a much simpler equation which gives adequate results. The depth at the first maximum may be computed from

$$y = \frac{V^2}{g} \sin^2 (\beta + \frac{\theta}{2}) \quad (5\text{-}102)$$

Equation 5-102 results from experimental observations of a constant velocity occurring at a cross section. The locations of the first maximum may be found from

$$\theta = \tan^{-1} \{\frac{2W}{(2r_c + w) \tan\beta}\} \quad (5\text{-}103)$$

where $r_c$ is the radius of curvature and $W$ is the channel width as shown in a plan view of the cross wave pattern given in Figure 5-19. The disturbance wave pattern oscillates about a plane located at the normal depth. The distance along the wall to the first maximum subtends a central angle $\theta$ and this distance represents half a wave length.

The amplitude of the disturbance pattern in the downstream tangent is dependent on whether the new disturbance pattern created in the

change of flow from curved to straight reinforces or damps out the disturbance pattern already in existence. When the curve has central angles of $\theta$, $3\theta$, $5\theta$, etc., where $\theta$ is given by Equation 5-103, the two disturbance patterns reinforce each other and the resulting disturbance pattern in the tangent section oscillates about the normal depth with an amplitude approximately $V^2W/r_c g$. By adopting central angles of $2\theta$, $4\theta$, $6\theta$, etc., the disturbance pattern generated by the change from a straight to curved channel will cancel out the disturbance created by the initial curve in the channel.

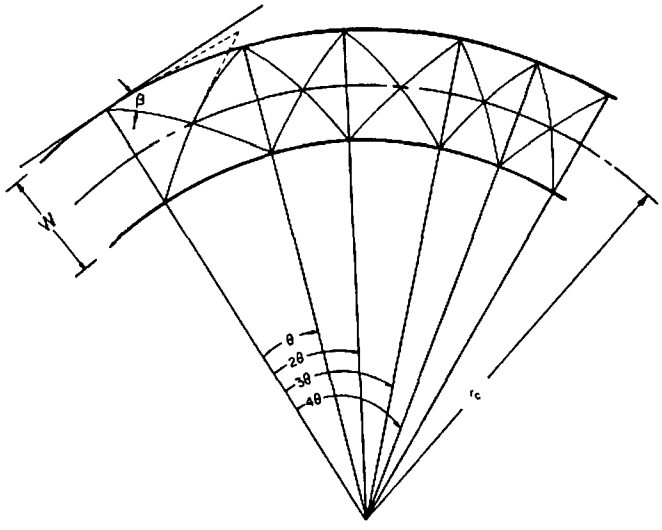


Figure 5-19. Plan view of cross wave pattern for rapid flow in a bend.

Two methods have been used in the design of curves for rapid flow in channels. One method is to bank the floor of the channel and the other is to provide curved vanes in the flow. Banking of the floor produces lateral forces which act simultaneously on all filaments and causes the flow to turn without destroying the flow equilibrium. Curved vanes break up the flow into a series of small channels and since the superelevation is directly proportional to the channel width, each small channel has a smaller superelevation.

Transitions

Contractions and expansion in rapid flow produce cross wave patterns similar to those observed in curved channels. The cross waves are symmetrical with respect to the centerline of the channel. Ippen and Dawson (1951) have shown that in order to minimize the disturbance downstream of a contraction, the length of the contraction should be

$$L = \frac{W_1 - W_2}{2 \tan\theta} \tag{5-104}$$

where $W$ is the channel width and the subscripts 1 and 2 refer to sections upstream and downstream from the contraction. The contraction angle is $\theta$ and should not exceed 12°. The relationship between the channel widths and depths $y$ can be determined from the continuity of the flow $W_1 y_1$ channel widths and depths $y$ can be determined from the continuity of the flow $W_1 y_1 V_1 = W_2 y_2 V_2 = Q$ or

$$\frac{W_1}{W_2} = \left(\frac{y_2}{y_1}\right)^{3/2} \left(\frac{Fr_2}{Fr_1}\right) \tag{5-105}$$

For an expansion, Rouse et al. (1951) have found experimentally that the most satisfactory boundary form is given by

$$\frac{z}{W_1} = \frac{1}{2} \left(\frac{x}{W_1 Fr_1}\right)^{3/2} + \frac{1}{2} \tag{5-106}$$

where $x$ is the longitudinal distance measured from the start of the expansion or outlet section and $z$ is the lateral coordinate measured from the channel centerline. A boundary developed from this equation diverges indefinitely. Therefore, for practical purposes, the divergent walls are followed by a transition to parallel lines.

## 5.7 GRADUALLY VARIED STEADY FLOW

### Introduction

Thus far, two types of steady flow have been considered. They are uniform flow and rapidly varying nonuniform flow. In uniform flow, acceleration forces are zero and energy is converted to heat as a result of viscous forces within the flow; there are no changes in cross section or flow direction and the depth (called normal depth) is constant. In rapidly varying flow, changes in cross section, direction, or depth take place in relatively short distances; acceleration forces are not zero; viscous forces can be neglected (at least in the first approximation).

Different conditions prevail for each of these two types of steady flow. In steady uniform flow, the slope of the bed, the slope of the water surface, and the slope of the energy gradeline are all parallel and are equal to the head loss divided by the length of channel in which the loss occurred. In rapidly varying flow through short streamlined transitions, resistance is neglected and changes in depth due to acceleration are dominant. In this section; a third type of steady flow is considered. In this type of flow, changes in depth and velocity take place slowly over large distances, resistance to flow dominates and acceleration forces are neglected. This type of flow is called gradually varied flow, and the study involves 1) the determination of the general characteristics of the water surface and 2) the elevation of the water surface or depth of flow.

In gradually varied flow, the actual flow depth $y$ is either larger than or smaller than the normal depth $y_o$ and either larger than or smaller than the critical depth $y_c$. The water surface profiles which are often called backwater curves, depend on the magnitude of the actual depth of flow $y$ in relation to the normal depth $y_o$ and the critical depth $y_c$. Normal depth $y_o$ is the depth of flow that would exist for steady-uniform flow as determined using the Manning or Chezy velocity equations, and the critical depth is the depth of flow when the Froude number equals 1.0. Reasons for the depth being different than the normal depth are changes in slope of the bed, changes in cross section, obstruction to flow, imbalances between gravitational forces accelerating the flow and shear forces retarding the flow.

In working with gradually varied flow, the first step is to determine what type of backwater curve would exist. The second step is to perform the numerical computations.

Classification of Flow Profiles

The classification of flow profiles is obtained by analyzing the change of the various terms in the total head equation in the x-direction. The total head is

$$H_T = \frac{V^2}{2g} + y + z \tag{5-107}$$

or

$$H_T = \frac{Q^2}{2gA^2} + y + z \tag{5-108}$$

Then assuming a wide channel for simplicity

$$\frac{dH_T}{dx} = - \frac{q^2}{gy^3} \frac{dy}{dx} + \frac{dy}{dx} + \frac{dz}{dx} \tag{5-109}$$

The term $dH_T/dx$ is the slope of the energy gradeline $S_f$, it is assumed. For short distance and small changes in $y$, the energy gradient can be evaluated using the Manning or Chezy velocity equations.

When Chezy's equation (Equation 5-62) is used the expression for $dH_T/dx$ is

$$- \frac{dH_T}{dx} = S_f = \frac{q^2}{C^2 y^3} \tag{5-110}$$

The term $dy/dx$ is the slope of the water surface $S_w$ and $dz/dx$ is the bed slope $S_o$. For steady flow, the bed slope is (from Equation 5-62)

$$S_o = \frac{q^2}{C_o^2 y_o^3} \tag{5-111}$$

where the subscript "o" indicates the steady uniform flow values.

When Equations 5-110 and 5-111 are substituted into Equation 5-109, the familiar form of the gradually varied flow equation

$$\frac{dy}{dx} = S_o \left\{ \frac{1 - \left(\frac{C_o}{C}\right)^2 \left(\frac{y_o}{y}\right)^3}{1 - \left(\frac{y_c}{y}\right)^3} \right\} \qquad (5\text{-}112)$$

is obtained.

If Manning's equation is used to evaluate $S_f$ and $S_o$, Equation 5-112 becomes

$$\frac{dy}{dx} = S_o \left\{ \frac{1 - \left(\frac{n}{n_o}\right)^2 \left(\frac{y_o}{y}\right)^{10/3}}{1 - \left(\frac{y_c}{y}\right)^3} \right\} \qquad (5\text{-}113)$$

The slope of the water surface $dy/dx$ depends on the slope of the bed $S_o$, the ratio of the normal depth $y_o$ to the actual depth $y$ and the ratio of the critical depth $y_c$ to the actual depth $y$. The difference between flow resistance for steady uniform flow $n_o$ to flow resistance for steady nonuniform flow $n$ is small and the ratio is taken as 1.0. With $n = n_o$, there are twelve types of water surface profiles. These are illustrated in Figure 5-20 and summarized in Table 5-2.

Table 5-2. Characteristics of water surface profiles.

| Class | Bed Slope | Depth | Type | Classification |
|---|---|---|---|---|
| Mild | $S_o>0$ | $y>y_o>y_c$ | 1 | $M_1$ |
| Mild | $S_o>0$ | $y_o>y>y_c$ | 2 | $M_2$ |
| Mild | $S_o>0$ | $y_o>y_c>y$ | 3 | $M_3$ |
| Critical | $S_o>0$ | $y>y_o=y_c$ | 1 | $C_1$ |
| Critical | $S_o>0$ | $y<y_o=y_c$ | 3 | $C_3$ |
| Steep | $S_o>0$ | $y>y_c>y_o$ | 1 | $S_1$ |
| Steep | $S_o>0$ | $y_c>y>y_o$ | 2 | $S_2$ |
| Steep | $S_o>0$ | $y_c>y_o>y$ | 3 | $S_3$ |
| Horizontal | $S_o=0$ | $y>y_o$ | 2 | $H_2$ |
| Horizontal | $S_o=0$ | $y_c>y$ | 3 | $H_3$ |
| Adverse | $S_o<0$ | $y>y_c$ | 2 | $A_2$ |
| Adverse | $S_o<0$ | $y_c>y$ | 3 | $A_3$ |

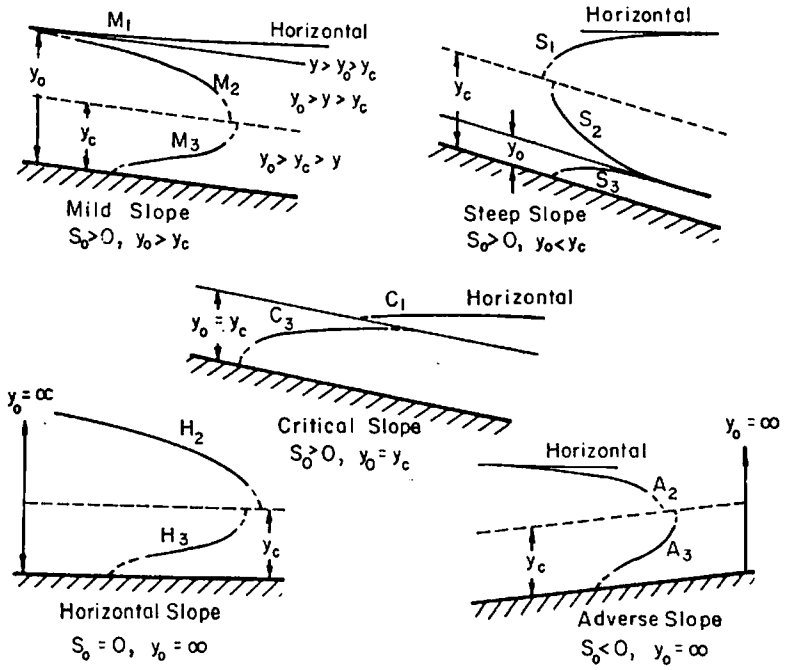


Figure 5-20. Classification of water surface profiles.

Note:

1. With a type 1 curve ($M_1$, $S_1$, $C_1$), the actual depth of flow $y$ is greater than both normal depth $y_o$ and the critical depth $y_c$. Because flow is tranquil, control of the flow is downstream.

2. With a type 2 curve ($M_2$, $S_2$, $A_2$, $H_2$), the actual depth $y$ is between the normal depth $y_o$ and the critical depth $y_c$. The flow is tranquil for $M_2$, $A_2$ and $H_2$ and thus the control is downstream. Flow is rapid for $S_2$ and the control is upstream.

4. For a mild slope, $S_o$ is smaller than $S_c$ and $y_o > y_c$.
5. For a steep slope, $S_o$ is larger than $S_c$ and $y_o < y_c$.
6. For a critical slope, $S_o$ equals $S_c$ and $y_o = y_c$.
7. For an adverse slope, $S_o$ is negative.
8. For a horizontal slope, $S_o$ equals zero.
9. The case where $y \to y_c$ is of special interest because the denominator in Equation 5-112 approaches zero.

When $y \to y_c$, the assumption that acceleration forces can be neglected no longer holds. Equations 5-112 or 5-113 indicate that dy/dx is

perpendicular when $y \rightarrow y_c$. For cross sections close to the cross section where the flow is critical (a distance from 50 to 10 ft), curvilinear flow analysis and experimentation must be used to determine the actual values of y. When analyzing long distances (100 to 1000 ft or longer) one can assume qualitatively that y reaches $y_c$. In general, when the flow is rapid (Fr $\geq$ 1), the flow cannot become tranquil without a hydraulic jump occurring. In constrast, tranquil flow can become rapid (cross the critical depth line). This is illustrated in Figure 5-21.

When there is a change in cross section or slope at an obstruction to the flow, the qualitative analysis of the flow profile depends on locating the control points, determining the type of curve upstream and downstream of the control points, and then sketching the backwater curves. It must be remembered that when flow is rapid (Fr $\geq$ 1), the control of the depth is upstream and the backwater proceeds in the downstream direction. When flow is tranquil (Fr < 1), the depth control is downstream and in the computations must proceed upstream. The backwater curves that result from a change in slope of the bed are illustrated in Figure 5-21.

Computation of Water Surface Profiles

There are many computer programs available for the computation of the elevation or depth of flow for water surface profiles. Herein, the standard step method is described. However, as with most computer programs, a qualitative analysis of the general characteristics of the backwater curves as described in the preceding section must be made. This is necessary in order to know whether the analysis proceeds upstream or downstream. Most available computer programs cannot solve the water surface profile equations when flow changes from rapid to tranquil or vice versa.

The standard step method is derived from the energy equation

$$\frac{V_1^2}{2g} + y_1 + \Delta z = \frac{V_2^2}{2g} + y_2 + H_L \qquad (5\text{-}114)$$

From Figure 5-22

$$\frac{V_1^2}{2g} + y_1 + S_o\,\Delta L = \frac{V_2^2}{2g} + y_2 + S_f\,\Delta L \qquad (5\text{-}115)$$

$$H_1 + S_o\,\Delta L = H_2 + S_f\,\Delta L \qquad (5\text{-}116)$$

and

$$\Delta L = \frac{H_2 - H_1}{S_o - S_f} \qquad (5\text{-}117)$$

The procedure is to start from some known y, assume another y either upstream or downstream depending on whether the flow is tranquil or rapid, and compute the distance $\Delta L$ to the assumed depth using Equation 5-117.

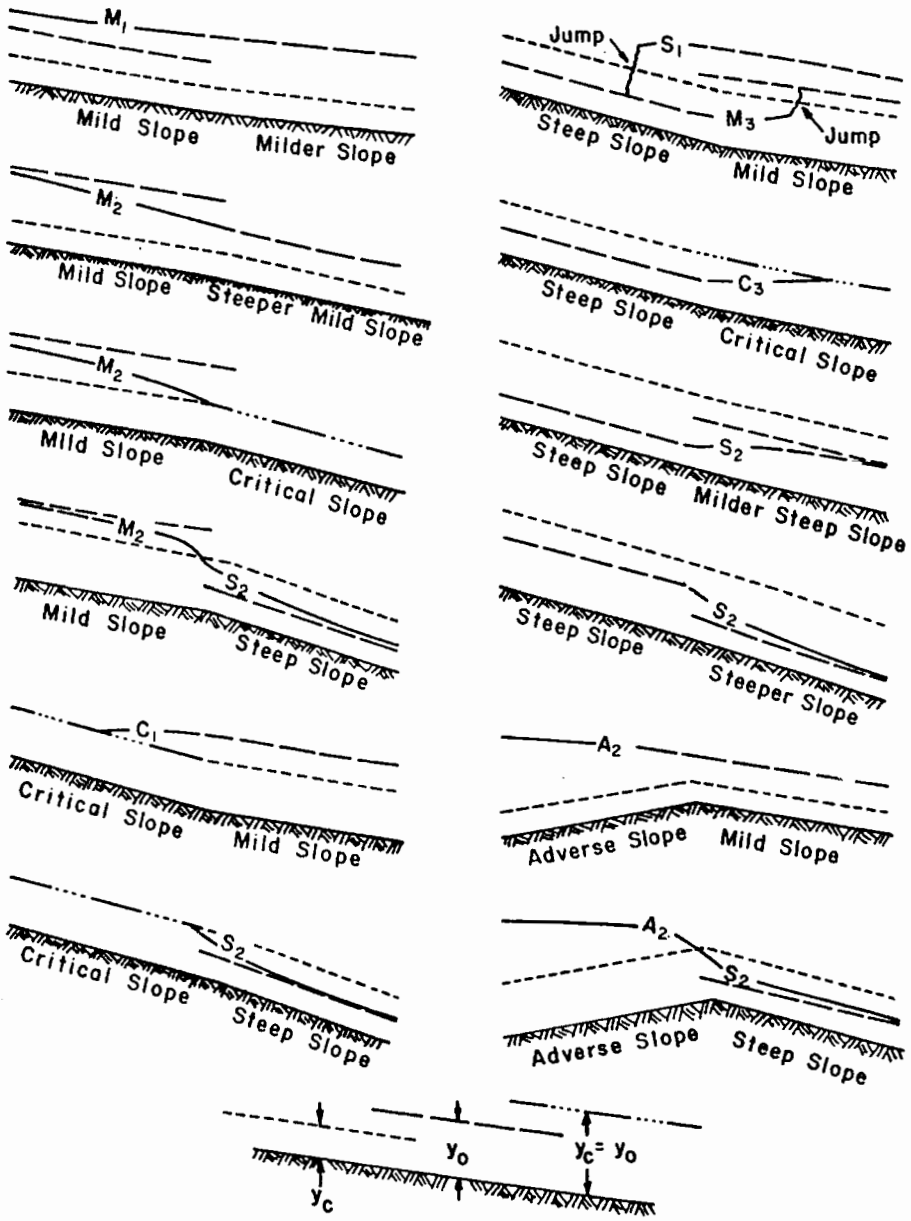


Figure 5-21. Examples of water surface profiles.

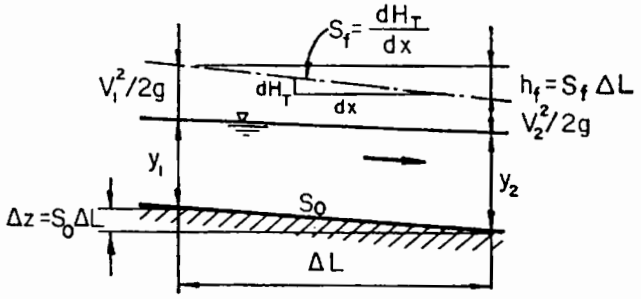


Figure 5-22. Definition sketch for step method computation backwater curves.

## 5.8 UNSTEADY FLOW

Unsteady flows of interest to the designer of waterway crossings and encroachments are: (1) waves resulting from disturbances of the water surface by wind and boats, (2) waves resulting from the surface instability that exists for flows with Froude numbers close to 1.0, (3) waves resulting from flow disturbance resulting from change in direction of flow with Froude numbers greater than 2.0, (4) surges or bores resulting from sudden increase or decrease in the flow by opening or closing of gates or the movement of tides on coastal streams, (5) standing waves and antidunes that occur in alluvial channel flow, and (6) flood waves resultng from the progressive movement downstream of stream runoff or gradual release from reservoirs.

Waves are an important consideration in bridge hydraulics when designing slope protection of embankments and dykes, and channel improvements. In the following paragraphs, only the basic one-dimensional analysis of waves and surges is presented. Other aspects of waves are presented in other sections.

### Gravity Waves

The general equation for the celerity C of a small amplitude gravity wave (velocity of the wave relative to the velocity of flow) is

$$C = \left\{\frac{g\lambda}{2\pi} \tanh \frac{2\pi y_o}{\lambda}\right\}^{1/2} \qquad (5\text{-}118)$$

where the terms are defined in Figure 5-23.

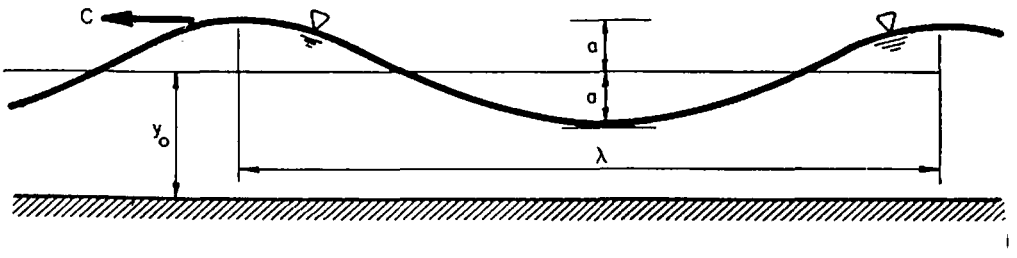


Figure 5-23. Definition sketch for small amplitude waves.

For deep water waves (short waves)

$$\frac{y_o}{\lambda} > \frac{1}{2}$$

and

$$C = \left\{\frac{g\lambda}{2\pi}\right\}^{1/2} \qquad (5\text{-}119)$$

For shallow water waves (long waves)

$$\frac{y_o}{\lambda} < \frac{1}{20}$$

and

$$C = \{gy_o\}^{1/2} \tag{5-120}$$

If T is the time (period) of travel of one water crest to another at a given point, then

$$C = \frac{\lambda}{T} \tag{5-121}$$

In Equation 5-119, the celerity is independent of depth and depends on gravity and wave length. This is the celerity of ocean waves. In Equation 5-120, the celerity is a function of gravity and depth and is used for small amplitude waves in open channels. These equations apply only to small amplitude waves; that is, $a/\lambda << 1$.

The celerity of finite amplitude shallow water waves has been determined both analytically using Bernoulli's equation and experimentally and is given by the expression

$$C = \{\frac{(y_o + 2a)^2}{(y_o + a)y_o}\, gy_o\}^{1/2} \tag{5-122}$$

When $2a$ is small in comparison to $y_o$

$$C = \{(1 + \frac{2a}{y_o})\, gy_o\}^{1/2} \tag{5-123}$$

Generally as $2a/y_o$ approaches unity the crest develops a sharp peak and breaks.

In the above equations, C is measured relative to the fluid. If the wave is moving opposite to the flow then, when $C > V$, the waves move upstream; when $C = V$, the wave is stationary; and when $C < V$, the wave moves downstream. When V equals C for small amplitude flow,

$$V = \sqrt{gy_o}$$

The definition of the Froude number is

$$Fr = \frac{V}{\sqrt{gy_o}} \tag{5-124}$$

Thus, the Froude number is the ratio of the velocity of flow to the celerity of a small-amplitude wave. When $Fr < 1$ (tranquil flow), a small amplitude wave moves upstream. When $Fr > 1$ (rapid flow), a small amplitude wave moves downstream and when $Fr = 1$ (critical flow), a small amplitude wave is stationary. The fact that waves or surges cannot move upstream when the Froude number is equal to or greater than 1.0 is important to remember when determining the control points for gradually varied flows and for determining when the stage-discharge relation at a cross section can be affected by downstream conditions.

## Surges

A surge is a rapid increase in the depth of flow. A surge may result from sudden release of water from a dam, or from an incoming tide. If the ratio of wave height $2a$ to the depth $y_o$ is less than unity, the surge has an undulating wave form. If $2a/y_o$ is greater than one, the first wave breaks and produces a discontinuous surface. The breaking wave dissipates energy and the previous equations for wave celerity do not hold. However, by applying the momentum and continuity equations for a control volume encompassing the surge (Figure 5-24), the equation

$$C = \{gy_1 [\frac{1}{2} \frac{2}{y_1} (\frac{2}{y_1} + 1)]\}^{1/2} \tag{5-125}$$

for the velocity of the surge can be derived.

Equation 5-125 gives the velocity of a surge as it moves upstream as the result of a sudden total or partial closure of a gate, or of an incoming tide, or of a surge that moves downstream as the result of a sudden opening of a gate. The lifting of a gate in a channel not only causes a position surge to move downstream, it also causes a negative

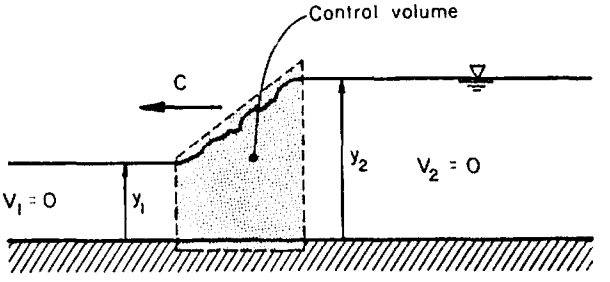


Figure 5-24. Sketch of a surge and its control volume.

surge to move upstream. Equation 5-125 is approximately correct for the celerity of the negative surge if the height of the surge is small compared to the depth. As it moves upstream a negative surge quickly flattens out.

## Hydraulic Jump

When the oncoming velocity of flow is rapid or supercritical the surge is a moving hydraulic jump. When $V_1$ equals the celerity of the surge the jump is stationary and Equation 5-125 is the equation for a hydraulic jump. Equation 5-125 can be rearranged to the form

$$\frac{V_1}{\sqrt{gy_1}} = Fr_1 = \{\frac{1}{2} \frac{y_2}{y_1} (\frac{y_2}{y_1} + 1)\}^{1/2} \tag{5-126}$$

or

$$\frac{y_2}{y_1} = \frac{1}{2} \{(1 + 8Fr_1^2)^{1/2} - 1\} \tag{5-127}$$

Equation 5-127 has been experimentally verified along with the dependence of the jump length and energy dissipation on the Froude number of the approaching flow. The results of these experiments are given in Figure 5-25.

When the Froude number for rapid flow is less than two, an undulating jump with large surface waves is produced. The waves are propagated for a considerable distance downstream. In addition, when the Froude number of the approaching flow is less than three, the energy dissipation of the jump is not large and jets of high velocity flow can exist for some distance downstream of the jump. These waves and jets can cause erosion a considerable distance downstream of the jump.

Roll Waves

Shallow flow on steep slopes may surge or pulsate. The waves formed are called roll waves. They are observed in shallow flow over spillways, in steep alluvial channels and in steep lined channels.

There is no simple criterion for determining when roll waves form, their velocity or their size. Their formation, size and velocity depend on the roughness and slope of the channel, the initial depth of flow, the length of channel and the nature of any disturbance that triggers

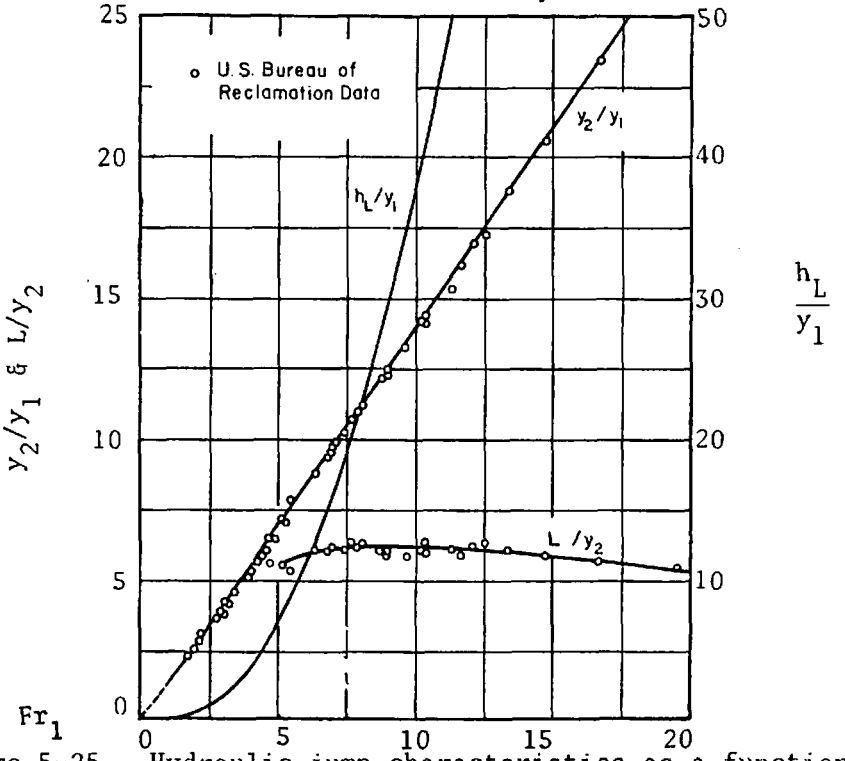


Figure 5-25. Hydraulic jump characteristics as a function of the Froude number.

them. Roll waves form when the Froude number is greater than two or the slope is approximately four times greater than the critical slope. They can cause the resistance to flow to increase.

## 5.9 GRADUALLY VARIED UNSTEADY FLOW

### General

The remainder of this chapter presents an overview of unsteady flow concepts for flood waves in open channels. First, the governing equations are introduced, leading to a classification of open channel flow waves into: 1) kinematic, 2) diffusive, 3) inertial, and 4) dynamic. This theoretical background enables an improved understanding of flood routing concepts and methodologies. Flood routing is classified into reservoir routing and stream channel routing. The level pool method for reservoir routing and the Muskingum method for stream channel routing are treated in detail. Finally, a note is given on the range of applicability of kinematic and diffusive wave models.

### Governing Equations

The governing equations of gradually varied unsteady open channel flow are the equation of water continuity and the equation of motion. These are often referred to in the literature as the Saint Venant equations.

#### The Water Continuity Equation

The equation of water continuity for unsteady open channel flow is

$$\frac{\partial Q}{\partial x} + \frac{\partial A}{\partial t} = q_L \tag{5-128}$$

in which $Q$ is water discharge, $A$ is flow area, and $q_L$ is lateral inflow. In the absence of lateral inflow, Equation 5-128 reduces to

$$\frac{\partial Q}{\partial x} + \frac{\partial A}{\partial t} = 0 \tag{5-129}$$

Expressed per unit of channel width, Equation 5-129 reduces to

$$\frac{\partial q}{\partial x} + \frac{\partial d}{\partial t} = 0 \tag{5-130}$$

in which $q$ is water discharge per unit of channel width, and $d$ is depth of flow.

Equation 5-130 can also be expressed as

$$d \frac{\partial u}{\partial x} + u \frac{\partial d}{\partial x} + \frac{\partial d}{\partial t} = 0 \tag{5-131}$$

in which the first term is prism storage, the second term is wedge storage, and the third term is rate-of-rise.

The lumped form of the equation of water continuity is obtained by integrating Equation 5-129 over a channel reach or reservoir to yield the storage equation

$$I - O = \frac{dV}{dt} \tag{5-132}$$

in which I is inflow, O is outflow and V is reach storage.

The Equation of Motion

The equation of motion is derived by applying Newton's second law of motion to the force balance in gradually varied unsteady open channel flow. This yields

$$\frac{\partial Q}{\partial t} + \frac{>}{\partial x}\left(\frac{Q^2}{A}\right) + gA\frac{\partial y}{\partial x} + gA\,S_f = 0 \tag{5-133}$$

in which y is water surface elevation, g is acceleration of gravity and $S_f$ is friction slope.

If Equation 5-133 is expressed for a unit-width channel, the equation of motion becomes

$$\frac{\partial}{\partial t}(ud) + \frac{\partial}{\partial x}(u^2 d) + gd\frac{\partial}{\partial x}(z+d) + gd\,S_f = 0 \tag{5-134}$$

in which u = mean velocity, d = flow depth, and z = bed elevation.

Equation 5-134 is often used in reduced form. The derivatives are operated to yield

$$d\frac{\partial u}{\partial t} + u\left[\frac{\partial d}{\partial t} + \frac{\partial}{\partial x}(ud)\right] + ud\frac{\partial u}{\partial x} + gd\frac{\partial d}{\partial x} + gd\frac{\partial z}{\partial x} + gd\,S_f = 0 \tag{5-135}$$

The terms enclosed in brackets are a statement of the water continuity without lateral inflow, and equal zero by definition. Furthermore, if $Mz/Mx = -S_o$, Equation 5-135 reduces to

$$\frac{1}{g}\frac{\partial u}{\partial t} + \frac{u}{g}\frac{\partial u}{\partial x} + \frac{\partial d}{\partial x} - S_o + S_f = 0 \tag{5-136}$$

which is the equation of motion in its reduced form.

Classification of Shallow Water Waves

One of the most interesting and important phenomena in unsteady open channel flow is that of the propagation of shallow waves. Shallow waves are those for which the water depth is small in comparison with the wavelength. Deep waves, on the other hand, are those for which the water depth is much larger than the wavelength. Shallow waves are commonly present in river and canal flow, in which the wave can "feel" the presence of the channel bottom. Deep waves belong more to the realm of the ocean environment.

Shallow water waves in open channel flow are commonly classified according to the relative magnitude of the various forces responsible for the motion. These forces are of three types: body, surface and inertia forces. The body force is the component of gravity resolved along the direction of motion. The surface forces can be either normal (pressure) or tangential (stresses). The normal force is the pressure gradient along the direction of motion. The tangential forces are the bottom and water surface stresses. The bottom stresses are caused by friction, while the water surface stresses are normally attributed to wind. The latter are usually neglected in open channel flow calculations. The two types of inertial forces are convective inertia and local inertia.

In Equation 5-136 $(1/g)(\partial u/\partial t)$ represents the local inertia force, $(u/g)(\partial u/\partial x)$ represents the convective inertia force, $(\partial d/\partial x)$ represents the pressure gradient force, $S_f$ represents the friction force along the channel bottom, and $S_o$ represents the gravity force.

A kinematic wave is defined as that wave in which the inertia terms (both local and convective) are neglected on the grounds of being very small in comparison with the remaining terms. The two types of kinematic waves are a nondiffusive-kinematic wave (kinematic wave) which neglects not only the inertia terms but also the pressure gradient term and a diffusive-kinematic wave (diffusive wave) which neglects only the inertia terms.

The reasons for the use of kinematic and diffusive waves are ease of solution and applicability. Without the neglected terms, the equations of open channel flow are considerably simplified and more amenable to mathematical treatment. Furthermore, there are a large number of practical cases in which the neglect of terms is indeed justified. Therefore, the proper use of these simplified wave models hinges on their applicability to a particular problem situation.

An inertial wave is defined as that wave in which the friction and gravity components of the motion are either zero or negligible. Therefore, such a wave is governed strictly by the inertia and pressure gradient forces. Inertial waves arise in connection with unsteady open channel flow phenomena involving sudden changes in mean velocity and flow depth.

A dynamic wave is defined as that wave in which all forces (local inertia, convective inertia, pressure gradient, friction and gravity) interact freely with no one particular force predominating over the others. As such, it is the most general type of shallow water wave, an asset to be certainly recognized. However, its solution is quite elaborate since it takes into consideration the complete equation of motion together with the equation of water continuity.

A summary of the classification of shallow water waves treated here is given in Table 5-3.

Table 5-3. Classification of shallow water waves.

| | Forces and Terms | | | | |
|---|---|---|---|---|---|
| | Inertia | | Surface | | Body |
| | Local | Convective | Pressure Gradient | Friction Slope | Bottom Slope |
| Wave | $\frac{1}{g}\frac{Mu}{Mt}$ | $\frac{u}{g}\frac{Mu}{Mx}$ | $\frac{Md}{Mx}$ | $S_f$ | $-S_o$ |
| Kinematic | | | | √ | √ |
| Diffusive | | | √ | √ | √ |
| Inertial | √ | √ | √ | | |
| Dynamic | √ | √ | √ | √ | √ |

Kinematic Waves

This section discusses the nondiffusive-kinematic wave, referred to simply as kinematic wave. The following section will cover the diffusive-kinematic wave, referred to as diffusive wave.

The kinematic wave model assumes that the inertia and pressure gradient terms in the equation of motion are negligible compared to the friction and gravity terms. Without the inertia and pressure gradient terms, Equation 5-136 reduces to

$$S_f = S_o \tag{5-137}$$

This equation could be construed as a statement of uniform flow. Therefore, the kinematic wave is sometimes erroneously associated with the uniform flow condition. The wavelike features of the kinematic wave, however, are preserved through the equation of water continuity, which does contain information on the nonuniformity and unsteadiness of the flow.

The behavior of the kinematic wave model is described by the kinematic wave equation. This equation is derived from Equation 5-137 and the equation of water continuity, Equation 5-129. Equation 5-137 can be expressed as a uniform flow resistance formula, for which there is a choice of either Manning's or Chezy's

$$Q = \frac{1.486}{n} AR^{2/3} S_f^{1/2} \tag{5-138}$$

or

$$Q = CA(R\ S_f)^{1/2} \tag{5-139}$$

in which R = hydraulic radius, n = Manning's coefficient, and C = Chezy's coefficient. Be definition, R = A/P, in which P is the wetted perimeter. In general, the wetted perimeter is a function of the flow area, and the P-A relationship describes the shape of the cross section. Once this relationship is known at a given cross section, Equations 5-138 and 5-139 describe a unique Q-A relationship, since n and C are taken as constants, and $S_f = S_o$ = constant. Thus, the discharge-area relation reduces to

$$Q = \alpha\ A^{\beta} \tag{5-140}$$

in which $\alpha$ = a coefficient containing information on the resistance factor, the bottom slope, and the shape of the cross section, and $\beta$ = an exponent containing information on the type of resistance formula (Manning or Chezy) and the shape of the cross section.

The kinematic wave equation is derived by multiplying Equation 5-129 by $\partial Q/\partial A$, leading to

$$\frac{\partial Q}{\partial t} + \left(\frac{\partial Q}{\partial A}\right) \frac{\partial Q}{\partial x} = 0 \tag{5-141}$$

The term in parenthesis in Equation 5-141 is the kinematic wave celerity (also referred to as the Kleitz-Seddon celerity), obtained from Equation 5-140

$$\frac{\partial Q}{\partial A} = \frac{dQ}{dA}\bigg|_{x_o} = \alpha\beta A^{\beta-1} \tag{5-142}$$

from which

$$\frac{\partial Q}{\partial A} = \beta \frac{Q}{A} = \beta u \tag{5-143}$$

u being the mean flow velocity.

Equation 5-141 is a quasilinear first order partial differential equation. It is quasilinear because the kinematic wave celerity is a function of the mean flow velocity, which increases with discharge. Since it is a first order equation, it can only describe convection (wave travel) and not diffusion (wave attenuation). Its quasilinear property enables the deformation (wave skewness) of the hydrograph, manifested as a steepening rising limb and flattening receding limb as the wave moves downstream. If left uncontrolled, the wave steepening will eventually develop into the so-called "kinematic shock," which resembles a dynamic shock but in the absence of inertia.

In summary, the neglect of the inertia and pressure gradient terms of the equation of motion leads to the kinematic wave equation. This equation provides for convection (wave travel) and deformation (wave skewness), but does not take into account diffusion (wave attenuation). The diffusive property is lost as part of the neglected terms.

Diffusive Waves

This section covers the diffusive-kinematic wave, commonly referred to as diffusive wave.

The diffusive wave model assumes that the inertia (local and convective) terms of the equation of motion are negligible as compared to the pressure gradient, friction, and gravity terms. Without the inertia terms, Equation 5-136 reduces to

$$S_f = S_o - \frac{\partial d}{\partial x} \tag{5-144}$$

The behavior of the diffusive wave model is described by the diffusive wave equation. For the sake of simplicity, this equation is derived herein assuming a wide channel governed by Chezy friction. The equation of water continuity is recast as

$$B \frac{\partial d}{\partial t} + \frac{\partial Q}{\partial x} = 0 \tag{5-145}$$

in which B = channel width. Equation 5-144 is substituted into Equation 5-139, leading to

$$Q = CA[R(S_o - \frac{\partial d}{\partial x})]^{1/2} \tag{5-146}$$

Taking into consideration the wide channel assumption, Equation 5-146 reduces to

$$Q = CBd^{3/2} (S_o - \frac{\partial d}{\partial x})^{1/2} \tag{5-147}$$

Differentiating Equation 5-147 with respect to x, and substituting $\partial Q/\partial x$ into Equation 5-145, leads to

$$\frac{\partial d}{\partial t} + c_k \frac{\partial d}{\partial x} = \mu \frac{\partial^2 d}{\partial x^2} \tag{5-148}$$

in which $c_k = 1.5\ u$ is the kinematic wave celerity corresponding to a wide channel with Chezy friction, and $\mu = ud/2S_f$ is the diffusion coefficient (or also, hydraulic diffusivity). Note that unlike Equation 5-141, Equation 5-148 contains both a convection and a diffusion term. Diffusive wave equations with discharge or flow area as the dependent variable can also be derived, albeit under some additional assumptions.

The diffusive wave equation is a quasilinear second order partial differential equation. As such, it can account for the convection, diffusion and deformation of the hydrograph. Unlike the kinematic wave, the deformation (steepening of the rising limb) cannot proceed uncontrolled, since the diffusive character of the wave would tend to counteract the steepening tendency. Therefore, the kinematic shock phenomenon which often plagues kinematic wave computations is totally absent in computations using the diffusive wave.

In summary, the neglect of the inertia terms in the equation of motion leads to the diffusive wave equation. This equation provides for convection, diffusion, and deformation of the hydrograph. The diffusive features of the wave can be linked to the presence of the pressure gradient term.

Inertial Waves

The inertial wave model assumes that the friction and gravity terms are negligible as compared with the inertia and pressure gradient terms. Without the friction and gravity terms, Equation 5-136 reduces to

$$\frac{1}{g}\frac{\partial u}{\partial t} + \frac{u}{g}\frac{\partial u}{\partial x} + \frac{\partial d}{\partial x} = 0 \qquad (5\text{-}149)$$

The water continuity equation, expressed in terms of velocity and flow depth and neglecting lateral inflow, is

$$\frac{\partial d}{\partial t} + d\frac{\partial u}{\partial x} + u\frac{\partial d}{\partial x} = 0 \qquad (5\text{-}150)$$

Equations 5-149 and 5-150 constitute a set of two quasilinear first order partial differential equations describing the inertial wave model. Their analytical solution is carried out by linearizing the dependent variables u and d around reference values $u_o$ and $d_o$. The linearized equations are then used to solve for one dependent variable at a time, leading to a second order partial differential equation describing a wave with velocity $c_i$ defined by

$$c_i = u_o \pm \sqrt{gd_o} \qquad (5\text{-}151)$$

Equation 5-151 is the inertial wave celerity (also referred to as the Lagrangian celerity). It describes the speed of travel of free surface flow waves in the absence of gravity and friction. Notice that the inertial wave has two solutions, unlike the kinematic and diffusive waves which have only one solution (precisely because of their lack of inertia). Depending on the value of the Froude number

$$F_o = \frac{u_o}{\sqrt{gd_o}} \qquad (5\text{-}152)$$

the solutions can either travel one upstream and one downstream ($F_o$ F 1), or travel both downstream ($F_o$ J 1). For $F_o = 1$, one of the solutions is a stationary (still) wave.

The analytical solution of the one dimensional wave equation describing the inertial wave model does not lead to wave diffusion. Therefore, the inertial wave model cannot account for wave attenuation.

In summary, the neglect of the gravity and friction terms in the equation of motion leads to the inertial wave equation. This equation provides for convection (wave travel) at the well-known inertial wave celerity. It does not take into account diffusion, which is lost as part of the neglected terms.

Dynamic Waves

A dynamic wave is defined as that wave in which all forces (inertia, surface, and body) interact freely, with no one particular force predominating over the others. Its solution is based on the complete equation of motion, Equation 5-136, and the equation of water continuity. These equations constitute a set of two quasilinear first order partial differential equations for which no complete analytical solution is available to date. However, a particular solution derived by using the tools of linear analyis can provide a wealth of information on the characteristics of the dynamic wave.

Following Ponce and Simons (1977), Equations 5-131 and 5-136 are linearized around reference values. A sinusoidal solution is forced on the linearized system of equations, leading to a homogeneous system of linear algebraic equations. The nontrivial condition for the determinant of the coefficient matrix enables the determination of the celerity and attenuation characteristics of the dynamic wave. These are shown to be functions of the reference flow Froude number $F_o$ and a dimensionless wave number $\hat{\sigma}$ defined as

$$\hat{\sigma} = \frac{2\pi}{L} L_o \tag{5-153}$$

in which $L$ = wavelength, and $L_o = d_o/S_o$ = the length of channel necessary for the reference flow to drop a head equal to its depth. Notice that $\hat{\sigma}$ contains information on the size of the wave phenomena, the bottom slope, and the channel friction.

There are three well-defined bands in the spectrum of dimensionless wave numbers $(0 < \hat{\sigma} < \infty)$: 1) a kinematic band, corresponding to the smaller wave numbers, in which the wave celerity is essentially the kinematic wave celerity; 2) an inertial band, corresponding to the larger wave numbers, in which the wave celerity is essentially the inertial wave celerity; and 3) a dynamic band, corresponding to wave numbers in the intermediate range, in which the wave celerity lies in between the kinematic and inertial wave celerity values. Such a trend is depicted in Figure 5-26, which shows the dimensionless wave number $\hat{\sigma}$ in the abscissae, and the dimensionless relative celerity $\hat{c}_r$ defined as

$$\hat{c}_r = \frac{c}{u_o} - 1 \tag{5-154}$$

in the ordinates. Figure 5-26 shows that for small values of $\hat{\sigma}$, the relative celerity $\hat{c}_r$ approaches asymptotically the relative kinematic wave celerity value (0.5 for the case of wide channels with Chezy friction). For large values of $\hat{\sigma}$, the relative celerity $\hat{c}_r$ approaches asymptotically the relative inertial wave celerity value $(1/F_o)$. For intermediate values of $\hat{\sigma}$, the relative dynamic wave celerity is between 0.5 and $1/F_o$.

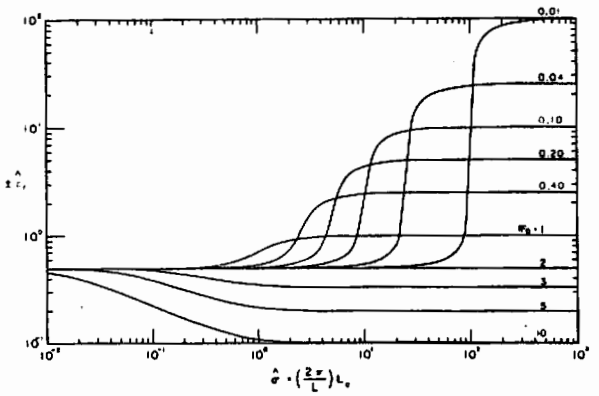


Figure 5-26. Dimensionless relative celerity $\hat{c}_r$, versus dimensionless wave number $\hat{\sigma}$; curve parameter = Froude number $F_o$, $(0.01 \leq F_o \leq 10)$.

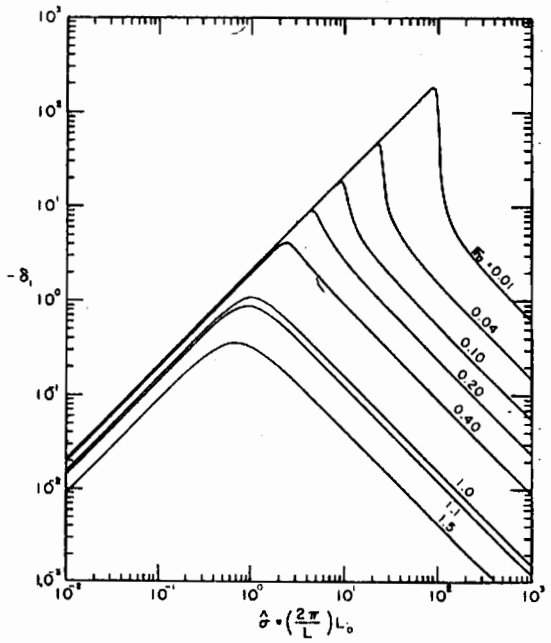


Figure 5-27. Primary wave logarithmic decrement $-\delta_1$ versus dimensionless wave number $\hat{\sigma}$; curve parameter = Froude number $F_o$, $(F_o < 2)$.

The attenuation characteristics for the spectrum of dimensionless wave numbers is portrayed in Figure 5-27. The ordinate is a decay parameter $\Delta$ referred to as logarithmic decrement, defined in

$$a_1 = a_0 e^{\delta} \tag{5-155}$$

in which $a_0$ = initial wave amplitude and $a_1$ = wave amplitude after one period of propagation. This figure depicts the variation of the logarithmic decrement of the primary wave (that traveling always in the same direction as the main flow) as a function of $\hat{\sigma}$, and for $F_o < 2$. The decay rate is a minimum at both extremes of the $\hat{\sigma}$ spectrum; $\hat{\sigma} \to 0$ corresponds to the kinematic wave case; $\hat{\sigma} \to \infty$ corresponds to the inertial wave case. In the intermediate $\hat{\sigma}$ range, the decay rate is very high, indicating that the primary dynamic wave has markedly strong dissipative tendencies. For a more detailed discussion on the characteristics of the dynamic wave, reference is made to Ponce and Simons (1977).

In summary, the dynamic wave takes into account all forces present in open channel flow. It can describe convection, diffusion and deformation. The celerity and attenuation are functions of the reference flow Froude number and a dimensionless wave number characteristic of the unsteady component of the motion and the channel properties. The dynamic wave celerity lies between the kinematic and inertial wave celerity values. The attenuation of the dynamic wave is markedly strong, with a maximum around the midrange values of the dimensionless wave number.

## Flood Routing

The following is an overview of flood propagation phenomena in open channels. First, some fundamental concepts on the nature of floods are introduced. This leads naturally into flood routing and a classification of flood routing methods. The remainder of the chapter describes briefly some of the most important methods, emphasizing their major features and giving a rationale for their use.

### Nature of Flood Waves

It is perhaps an oddity that the nature of flood waves is most readily grasped by looking at the system rather than at the flood wave itself. The system could be either a channel, a reservoir (or lake), or a channel-reservoir combination. This distinction is of fundamental importance, as will be shown here. The channel case is usually associated with the existence of a finite (nonzero) water surface slope. The reservoir case is normally taken to imply a zero water surface slope.

Flood waves travel downstream in a channel or reservoir and, in general, are subject to attenuation. The rate of travel (flood wave velocity) and the rate of attenuation depend on the system in which the flood wave is moving.

Flood waves in stream channels travel at an average velocity closely corresponding to that given by the Kleitz-Seddon law

$$c = \left.\frac{dQ}{dA}\right|_{x_o} = \frac{1}{B}\frac{dQ}{dy} \qquad (5\text{-}156)$$

They attenuate at a rate which is a function of the magnitude of the various forces involved in the motion. Kinematic waves do not attenuate, diffusive waves attenuate at a small to moderate rate, and dynamic waves are subject to very strong attenuation. Strictly speaking, Equation 5-156 is valid only for flood waves which do not attenuate i.e., kinematic waves. However, it can also be used as an approximation for flood waves subject to moderate attenuation i.e., diffusive waves. Figure 5-28 depicts the typical behavior of flood waves in stream channels.

Flood waves in lakes and reservoirs travel at an infinite velocity i.e., there is an instantaneous response (outflow hydrograph) to the excitation (inflow hydrograph). However, the system exerts a diffusing effect on the flood wave, with the result that the peak of the outflow hydrograph is attenuated and delayed. A significant characteristic of flood waves through reservoirs is that at the time when the inflow and outflow are equal, the outflow is a maximum. Figure 5-29 depicts the typical behavior of flood waves in lakes and reservoirs.

## Flood Routing

Although flood waves appear to have well-defined properties, in practice it is often necessary to carry out elaborate calculations in order to determine these properties. The reason for this is the variability of the natural environment, manifested in the need to handle large amounts of data. Flood routing is defined as the process of tracing by calculation the movement of a flood wave. The calculations can proceed along one of the following two lines: either by considering only temporal variations (lumped case), or by considering both temporal and spatial variations (distributed case). The lumped case is the classical reservoir routing situation, formulated in terms of one first order ordinary differential equation (the storage equation). The distributed case corresponds to stream channel routing, formulated in terms of two first order partial differential equations. The latter are commonly referred to as the equations of gradually varied unsteady open channel flow, or also, as the Saint Venant equations.

Under certain conditions, the Saint Venant equations with appropriate simplifications can be combined into one second order partial differential equation describing convection and diffusion. This equation can be used to describe flood movement in a large number of practical applications.

## Classification of Flood Routing Methods

A knowledge of the nature of flood waves provides a good basis on which to develop a classification of flood routing methods. The most general classification is that of reservoir (or lake) routing and

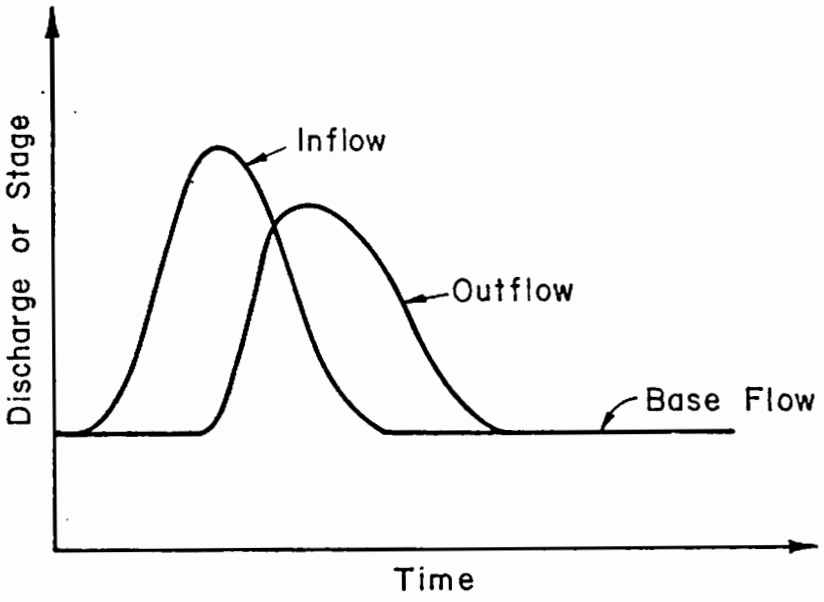


Figure 5-28. Typical inflow and outflow hydrographs for flood waves in stream channels.

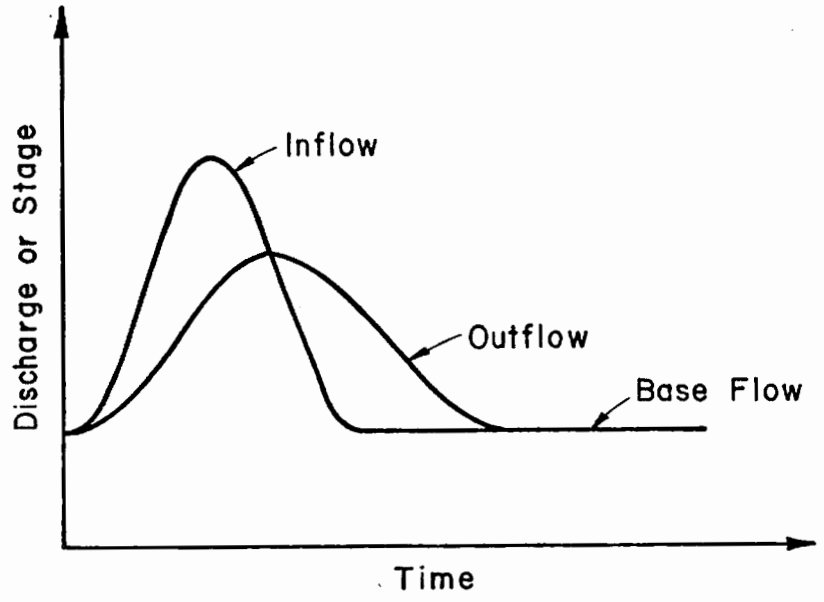


Figure 5-29. Typical inflow and outflow hydrographs for flood waves in lakes and reservoirs.

stream channel routing. The essential difference between these two is that in the reservoir routing case the water surface slope is zero, while in stream channel routing it has a nonzero value. Several other criteria could be used to classify flood routing methods. Among these, the following are readily identified: 1) the equations used to formulate the problem, 2) the overall approach to data collection, and 3) the approach to obtaining a solution.

According to the equations used to formulate the problem, flood routing methods can be classified as mass-balance methods, and mass-and-momentum-balance methods. The mass-balance methods use the ordinary differential equation of storage plus an auxiliary storage-outflow relationship. The mass-and-momentum-balance methods use the Saint Venant equations or appropriate simplifications. The use of the complete Saint Venant equations leads to the dynamic wave model, while the simplified forms lead to kinematic and diffusive waves.

According to the approach to data collection, flood routing methods can be classified as hydrologic, in which the parameter estimation is based on hydrologic observations for individual channel reaches, and hydraulic, in which the parameter estimation is based on actual measurements of channel characteristics at individual cross-sections.

According to the approach to obtaining a solution, flood routing methods can be classified as analytical and numerical. The analytical methods are based on the solution of differential equations specified on a continuous domain of space and time. The numerical methods are based on the solution of algebraic equations on a discrete domain. Analytical solutions use the tools of classical mathematics such as linear analysis and Laplace transforms, while numerical solutions use characteristic or finite difference methods.

Table 5-4 provides a summary of the classification of flood routing methods presented herein.

Table 5-4. Classification of flood routing methods.

| | |
|---|---|
| Based on Equations Used | Mass-balance: Storage equation and an auxiliary storage-outflow relationship.<br>Mass-and-momentum-balance: Saint Venant equations (dynamic wave) or appropriate simplifications (kinematic and diffusive waves). |
| Based on Approach to Data Collection | Hydrologic Routing: Observations for channel reaches.<br>Hydraulic Routing: Measurements of channel characteristics at individual cross-sections. |
| Based on Solution Technique | Analytical Routing: Differential equations; continuous domain.<br>Numerical Routing: Algebraic equations; discrete domain. |

Reservoir Routing

The reservoir routing methods follow directly from the differential equation of water storage

$$I - O = \frac{dV}{dt} \qquad (5\text{-}157)$$

in which I = inflow, O = outflow, V = volume of storage, and t = time. A significant role is played by the equation relating the outflow rate to the pool level, and therefore, to the volume of storage (V-O relationship).

A widely recognized method of reservoir routing is the level pool (or Puls) technique. Equation 5-157 is discretized over a time interval Wt to yield

$$\frac{1}{2}(I_1+I_2) - \frac{1}{2}(O_1+O_2) = \frac{1}{\Delta t}(V_2-V_1) \qquad (5\text{-}158)$$

in which the subscripts 1 and 2 refer to conditions at the start and end of the time interval $\Delta t$, respectively. Equation 5-158 is rearranged to

$$N_2 = N_1 - O_1 + \frac{1}{2}(I_1+I_2) \qquad (5\text{-}159)$$

in which

$$N_i = \frac{V_i}{\Delta t} + \frac{O_i}{2} \qquad (i=1,2,\ldots) \qquad (5\text{-}160)$$

is referred to as the storage indication quantity.

The input data consists of the inflow hydrograph and a relationship between storage and outflow (V-O). A suitable Wt is chosen, and the inflow hydrograph is discretized in time, yielding a series of I values. The V-O relationship and Equation 5-160 are used to derive an N-O relationship. A known initial value of O is used to obtain an initial value of N through the N-O relationship. The calculation proceeds by a sequential application of the following two steps: 1) updating the value of N by using Equation 5-159 and 2) updating the value of O by using the N-O relationship. The series of O values computed in this way depict the hydrograph attenuation and delay typical of reservoir routing methods (see Figure 5-29).

Stream Channel Routing

A feature common to all stream channel routing methods is that they consider the balance of mass and momentum, whether this is explicitly stated or not. Historically, stream channel routing methods have developed along three major paths. These are: 1) the classical approach, in which an algebraic inflow-outflow-storage relationship is substituted for the equation of motion, 2) the numerical approach, which relies on the numerical solution of the complete Saint Venant equations, and 3) the simplified approach, which uses a convection-diffusion equation.

The Classical Approach

The classical approach originated in the realization that, unlike reservoir routing, in stream channel routing the reach storage V is a function not only of the outflow O but also of the inflow I. This led naturally into the formulation of several hypotheses for this relationship. One of the most widely recognized of these hypotheses is that of the Muskingum method, which dates back to 1934, and is stated as

$$V = K[XI+(1-X)O] \tag{5-161}$$

in which K and X = parameters to be determined by calibration using historical flood data for the reach under study.

Equations 5-157 and 5-161 lead to the Muskingum routing equation, stated as

$$O_2 = C_1 I_1 + C_2 I_2 + C_3 O_1 \tag{5-162}$$

from which the outflow at the new time level $O_2$ can be calculated from a knowledge of the inflow at the present level $I_1$, the inflow at the new time level $I_2$, and the outflow at the present time level $O_1$. The coefficients $C_1$, $C_2$, and $C_3$ are the Muskingum coefficients, and they are functions of the Muskingum parameters K and X, and the time interval Wt.

The Numerical Approach

The development of the numerical approach to flood routing was triggered by the advent of the electronic computer and the quantum increase in computational power that ensued. Paralleling the availability of the computer, significant progress was made in the field of applied mathematics, particularly with reference to the numerical solution of partial differential equations. Towards the mid-fifties, these advances made possible the early successful attempts to solve the Saint Venant equations by numerical methods with the aid of the computer. Later developments were concentrated on increasing the efficiency and reliability of the numerical approach to flood routing.

The numerical solution of the Saint Venant equations can be carried out by either: the method of characteristics, or finite difference methods. In the method of characteristics, the two partial differential equations (water continuity and motion) are replaced by four ordinary differential equations which are solved numerically on a characteristic grid. The intersections of characteristic lines on the x-t plane define the characteristic grid (see Figure 5-30).

In the finite difference methods, the functions (e.g., discharge Q, flow area A, stage y) and their derivatives (e.g., $\partial Q/\partial x$, $\partial A/\partial t$) are expressed in terms of their values on a rectangular grid defined on the x-t plane (see Figure 5-31). A finite difference scheme is a formula expressing a relationship between neighboring values on the

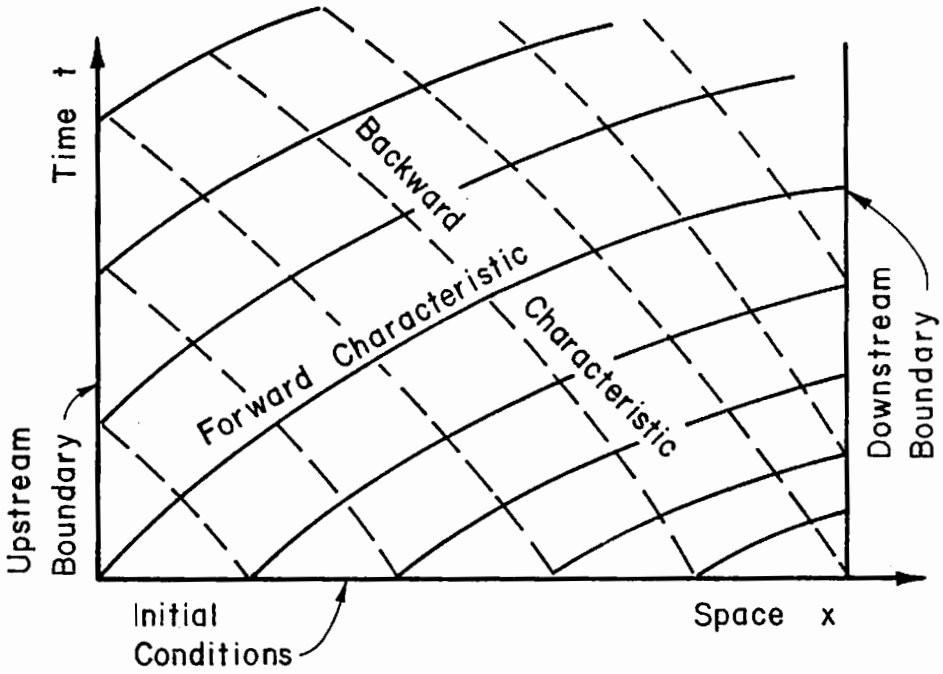


Figure 5-30. Characteristic grid on the x-t plane.

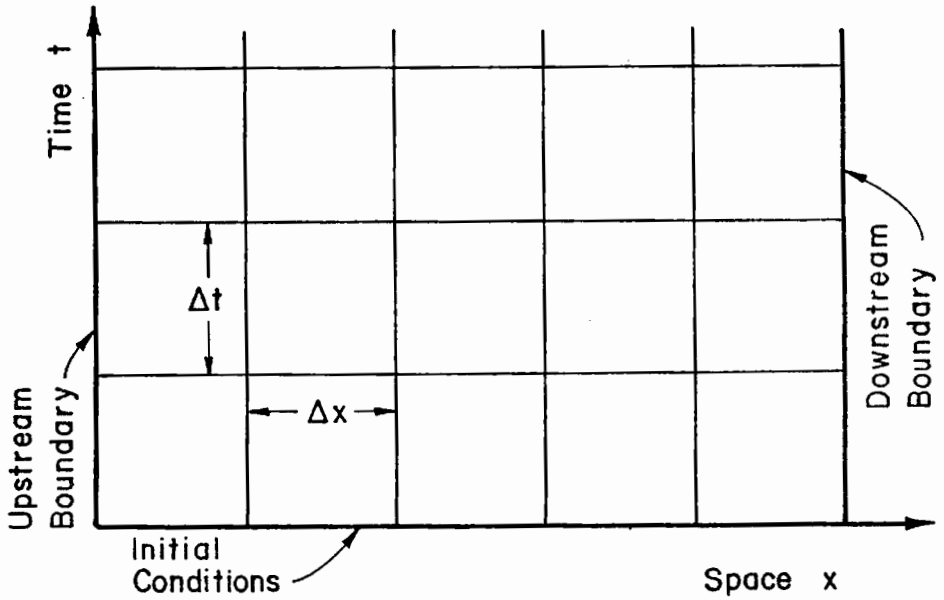


Figure 5-31. Rectangular (finite difference) grid on the x-t plane.

rectangular grid. There are two types of finite difference schemes the explicit, and the implicit. Explicit schemes are those that advance the solution in time and space by solving for the unknown variables, one grid point at a time. Implicit schemes advance the solution in time by simultaneously solving for the unknown variables at a number of grid points.

Explicit schemes are relatively simple to formulate, but are usually limited to a small time step $\Delta t$ by considerations of numerical stability. Implicit schemes require the inversion of a matrix, but are not subject to the strict stability criterion of explicit schemes. In general, implicit schemes are more efficient than explicit schemes in their use of computational resources.

There is a marked difference between the classical and numerical approaches. The latter is based on the complete equations, and therefore, can describe nonlinear effects, looped stage-discharge relationships and other physical details which the classical approach simply cannot consider. On the other hand, the numerical approach represents an altogether higher level of sophistication, demanding not only a thorough understanding of the physical processes, but also a knowledge of numerical methods and computer programming. Nevertheless, the increasing use of computers in all aspects of engineering analysis and design guarantees that the numerical approach will continue to play a leading role in the future. The challenge, of course, remains to keep the numerical approach in the proper perspective, making sure that it does not substitute for sound physical reasoning and competent engineering judgment.

The Simplified Approach

The simplified approach to flood routing has its origins in the observations of Hayami (1951). Hayami pointed out that, given all the irregularities present in natural channels, it is striking that the flow appears steady and nearly uniform in the mean. He reasoned that the disturbances caused by these irregularities quickly damp away as part of a large scale process of longitudinal mixing. This led Hayami to the formulation of a differential equation of flood waves describing convection and diffusion. Later, Lighthill and Whitham (1955) used similar physical reasoning to formulate their kinematic wave theory.

In essence, the simplified approach to flood routing is based on the realization that in a large number of practical cases, the inertia terms of the equation of motion play an exceedingly small role. Without these terms, the Saint Venant equations can be combined into one second order partial differential equation describing convection and diffusion. Furthermore, if the pressure gradient term of the equation of motion is also neglected, the resulting equations can be combined into a first order partial differential equation describing only convection. The convection-diffusion equation forms the basis of the diffusive wave model. Likewise, the convection-only equation is referred to as the kinematic wave model. Both models can describe flood wave movement, provided sufficient care is exercised in their use.

Several comments are necessary regarding the simplified approach to flood routing. First, its solution is based on one partial differential equation; therefore, only one dependent variable (usually discharge Q) can be calculated at a time. The remaining dependent variable (either stage y or flow area A) is calculated from a single-valued rating curve. Strictly speaking, this procedure is correct only as an approximation to the unsteady features of the flood wave which do include a loop in the rating curve (see Figure 5-32).

Second, it is noted that the simplified approach leads to a quasilinear (variable coefficient) partial differential equation. This equation can be solved either in its original form, or linearized (assuming constant coefficients) in the interest of mathematical expediency. Of course, the quasilinear features of the wave movement are lost in the linearized solution, a situation which can lead to a decrease in the overall accuracy of the simplified approach.

Third, the quasilinear features of the wave movement may lead to physically unrealistic results in a highly simplified model such as the kinematic wave. The quasilinear property is manifested as a steepening rising limb and a flattening receding limb as the wave moves downstream (see Figure 5-33). If left uncontrolled, the wave steepening will eventually develop into the so-called kinematic shock, which resembles a dynamic shock but in the absence of inertia. Such problems are altogether avoided in diffusive wave computations. The diffusive wave has its own built-in diffusive properties which tend to counteract the steepening tendency, thus impeding the development of the shock. Therefore, the kinematic shock is totally absent in computations using the diffusive wave.

## Relation Between Various Approaches to Stream Channel Routing

Given the apparently widely differing nature of the various approaches to stream channel routing treated here, the question remains, is there an all-encompassing link? Or stated in other terms, is there a unifying theory hidden behind the maze of approaches, methods, and techniques? The answer to these questions can be found in the work of Cunge (1969) who demonstrated the correspondence between the classical approach (e.g., Muskingum method) and the simplified approach (e.g., the convection-diffusion method of Hayami). Since the latter could be construed as a particular case of the numerical approach, the stage was set for a unified theory of flood movement. It is recognized that all stream channel routing methods can be classified as either kinematic, diffusive, or dynamic wave models. The dynamic wave model is the most general, encompassing the other two as particular solutions. While losing somewhat in generality, the diffusive wave model remains widely applicable, encompassing the kinematic wave as a particular solution. The kinematic wave model has a limited range of applicability, being restricted to the cases of very steep bottom slopes (e.g., overland flow) or very long duration (slow-rising) hydrographs.

### Muskingum Method

The classical approach to stream channel routing is based on the assumption that the storage V in a given channel reach is a function of both inflow I and outflow O. The group of procedures that

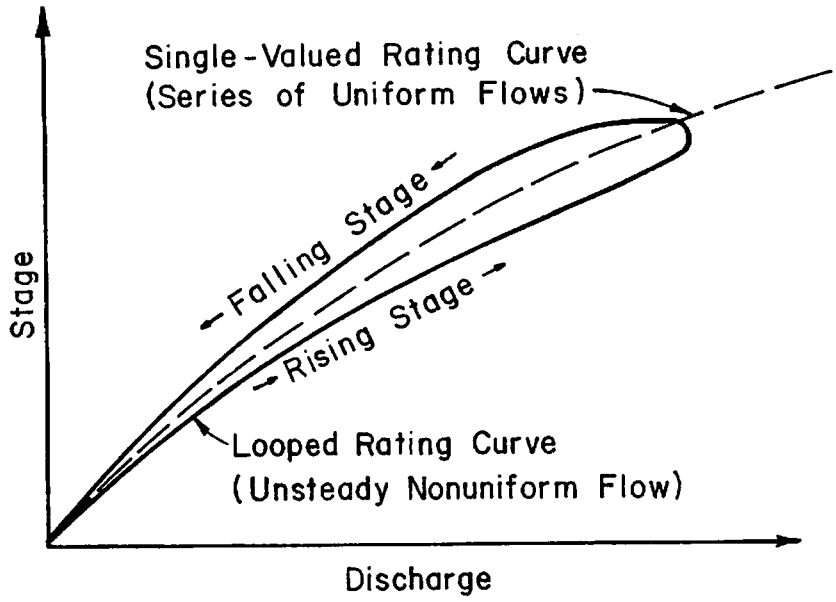


Figure 5-32. Schematic of single-valued and looped rating curves in open channel flow.

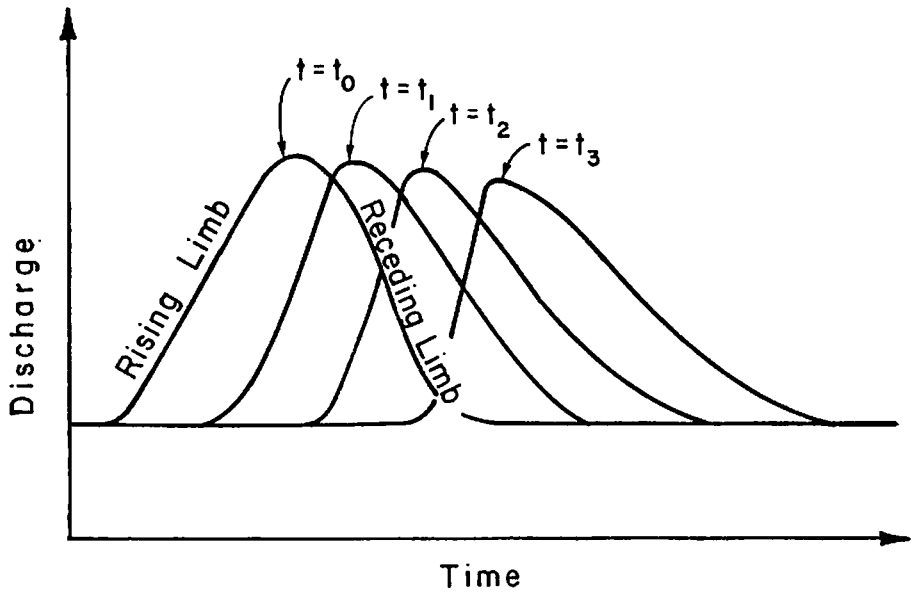


Figure 5-33. Schematic portrayal of the effect of the quasilinear property of a flood wave, manifested as a steepening rising limb and flattening receding limb as the wave moves downstream.

approximate in some way the relationship between storage, inflow, and outflow are referred to here collectively as the classical approach, or also, as coefficient methods of routing. As their name indicates these methods involve the use of coefficients in a certain type of routing equation. The coefficients as well as the parameters from which they are derived are purely empirical, and are determined by calibration using historical flood records for the reach under study.

Perhaps the best known and most widely used of the coefficient methods is the Muskingum method, developed by the U.S. Army Corps of Engineers in connection with flood control schemes in the Muskingum River Basin, Ohio. The original Muskingum method was formulated along the following lines. The water continuity equation is expressed in its spatially-integrated form, Equation 5-132. The equation of motion is replaced by a linear storage-inflow-outflow relationship of the following form

$$V = K[XI + (1-X)O] \tag{5-163}$$

in which $K$ and $X$ are parameters to be determined by calibration using historical flood records on a given reach.

Equation 5-132 can be discretized in time (Figure 5-34) to yield

$$\frac{I_{n+1} + I_n}{2} \quad \frac{O_{n+1} + O_n}{2} = \frac{V_{n+1} - V_n}{\Delta t} \tag{5-164}$$

Likewise, Equation 5-163 can be expressed at time levels $n$ and $(n+1)$ as

$$V_n = K[XI_n + (1-X)O_n] \tag{5-165}$$

and

$$V_{n+1} = K[XI_{n+1} + (1-X)O_{n+1}] \tag{5-166}$$

respectively. Substituting Equations 5-165 and 5-166 into Equation 5-164, the following routing equation is obtained

$$O_{n+1} = C_1 I_n + C_2 I_{n+1} + C_3 O_n \tag{5-167}$$

in which the coefficients $C_1$, $C_2$ and $C_3$ are defined as

$$C_0 = \Delta t/K + 2(1-X) \tag{5-168}$$

$$C_1 = (\Delta t/K + 2X)/C_0 \tag{5-169}$$

$$C_2 = (\Delta t/K - 2X)/C_0 \tag{5-170}$$

$$C_3 = [2(1-X) - \Delta t/K]/C_0 \tag{5-171}$$

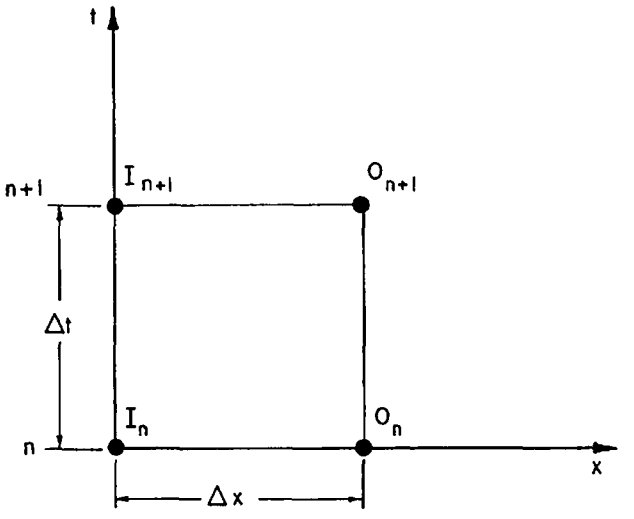


Figure 5-34. Schematic of the discretization of the Muskingum Method.

Much has been written on the Muskingum method, particularly in reference to the determination of the parameters K and X. The parameter K has the units of time, and has come to be closely associated with the average travel time i.e., the time it takes the average flood discharge to travel the length of the reach. The parameter X is a weighting factor used for the purpose of matching the attenuation of the calculated hydrograph to that of the observed data. The recommended range for X is $0 \leq X \leq 0.5$. A value of $X = 0$ implies reservoir-type behavior i.e., storage being only a function of outflow. A value of $X = 0.5$ indicates that the flood hydrograph is not being subject to attenuation. Values of $X > 0.5$ are associated with computational instability.

The predictive accuracy of the Muskingum method hinges upon the correct determination of the parameters K and X. These are a function of the flood characteristics, i.e., the hydrograph travel time and attenuation rate, and are usually determined by a process of trial and error calibration. However, since the flood characteristics are likely to vary from one flood to another, it would be rash to assume that the parameters determined from one set of flood records could be used to predict the behavior of an altogether different flood. This, in effect, limits the predictive capability of the method to floods similar to that used in the calibration, and any attempt at extrapolation is unwarranted.

The use of constant parameters in the classical Muskingum method is tantamount to an assumption of linearity, and this is in contradiction with the quasilinear property of flood waves. In addition, the neglect

of the looped discharge-stage relations can be justified only as an approximation to the natural phenomena. Nevertheless, the classical Muskingum method remains an expedient way of obtaining approximate answers for a number of practical problems. A comparatively recent improvement, referred to as the Muskingum-Cunge method, considerably enhances the predictive capability of the method, while remaining within the same computational framework. The basic concepts underlying the Muskingum-Cunge method are given in the following section.

Muskingum-Cunge Method

The Muskingum-Cunge method of stream channel routing is a variation due to Cunge (1969) of the classical Muskingum method. It is based on the realization that a four-point numerical analog of the kinematic wave equation and the Muskingum storage relationship lead to the same routing equation. In effect, the kinematic wave equation can be written as follows

$$\frac{\partial Q}{\partial t} + c\,\frac{\partial Q}{\partial x} = 0 \qquad (5\text{-}172)$$

in which $Q$ is the flood wave discharge to be convected with the celerity $c$. In general, $c$ is a function of $Q$, however, for compatibility with the use of constant parameters $K$ and $X$, the assumption of constant $c$ is made here.

Equation 5-172 is discretized on the x-t plane as shown in Figure 5-35 to yield

$$\frac{X(Q_j^{n+1} - Q_j^n) + (1-X)\,(Q_{j+1}^{n+1} - Q_{j+1}^n)}{\Delta t} + c\,\frac{Y(Q_{j+1}^n - Q_j^n) + (1-Y)\,(Q_{j+1}^{n+1} - Q_j^{n+1})}{\Delta x} = 0 \qquad (5\text{-}173)$$

in which $X$ and $Y$ = weighting factors, $\Delta x$ = space interval $\Delta t$ = time interval, and $c$ has been taken as constant. Setting $Y = 0.5$, Equation 5-173 can be expressed as

$$\frac{Q_j^n + Q_j^{n+1}}{2} - \frac{Q_{j+1}^n + Q_{j+1}^{n+1}}{2} = \frac{\frac{\Delta x}{c}\left[XQ_j^{n+1} + (1-X)\,Q_{j+1}^{n+1}\right] - \frac{\Delta x}{c}\left[XQ_j^n + (1-X)\,Q_{j+1}^n\right]}{\Delta t} \qquad (5\text{-}174)$$

In one time increment, the left-hand side of Equation 5-174 is I-O, the right-hand side is dV/dt if

$$V = \frac{\Delta x}{c}\,[XI + (1-X)O] \qquad (5\text{-}175)$$

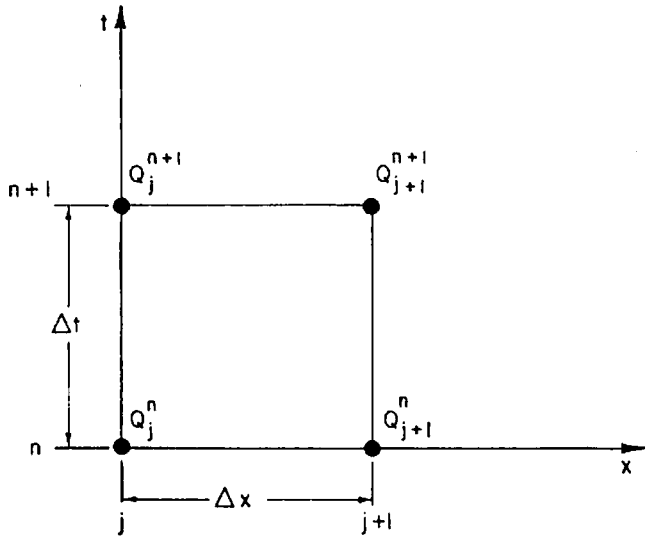


Figure 5-35. Schematic of the discretization of the Muskingum-Cunge Method.

which is recognized as Equation 5-163, provided $K = \Delta x/c$. Clearly then, the parameter $K$ is the travel time of a representative flood discharge i.e., the time it takes that discharge to travel the reach length $\Delta x$ with the celerity $c$.

The parameter $X$ is recognized as a weighting factor. The use of weighting factors in discrete solutions is ostensibly for the purpose of introducing a certain amount of numerical diffusion i.e., a diffusion due solely to the finite size of the grid. Cunge (1969) was able to use this property of discrete solutions to obtain an estimate of $X$ based on hydraulic quantities. He derived the numerical diffusion coefficient $\mu_n$ of the discretized kinematic wave equation as

$$\mu_n = c\Delta x(\frac{1}{2} - X) \tag{5-176}$$

By matching this diffusion coefficient with the physical diffusion coefficient of the convection-diffusion equation, the following expression for $X$ is obtained

$$X = \frac{1}{2}\left(1 - \frac{q_o}{S_o c\Delta x}\right) \tag{5-177}$$

With $K = \Delta x/c$ and Equation 5-177, the coefficients $C_0$ to $C_3$ (Equations 5-168 to 5-171) can be calculated as a function of the flood wave, channel, and grid characteristics. Furthermore, by defining the Courant number $C$ as the following ratio of celerities

$$C = \frac{c}{\left(\frac{\Delta x}{\Delta t}\right)} = c\,\frac{\Delta t}{\Delta x} \tag{5-178}$$

and the cell Reynolds number D as the following ratio of diffusivities

$$D = \frac{\left(\frac{q_o}{2S_o}\right)}{\left(\frac{c\Delta x}{2}\right)} = \frac{q_o}{S_o c\Delta x} \qquad (5\text{-}177)$$

the coefficients $C_0$ to $C_3$ can be expressed in the following reduced form

$$C_0 = 1 + C + D \qquad (5\text{-}180)$$

$$C_1 = (1 + C - D)/C_0 \qquad (5\text{-}181)$$

$$C_2 = (-1 + C + D)/C_0 \qquad (5\text{-}182)$$

$$C_3 = (1 - C + D)/C_0 \qquad (5\text{-}183)$$

Calculation of the Parameters

Equations 5-180 to 5-183 enable the calculation of the Muskingum coefficients in terms of measurable physical quantities and the characteristics of the grid. These are: 1) the equilibrium (or reference) unit-width discharge $q_o$, 2) the celerity c corresponding to this discharge, 3) the bottom slope $S_o$ for channels of regular cross-section (or alternatively, the equilibrium energy slope for channels of irregular cross-section), 4) the time interval $\Delta t$, and 5) the space step (or reach length) $\Delta x$.

Depending on the modeling needs and resources, the calculation of the parameters in the Muskingum-Cunge method can proceed in one of two ways, either by using constant parameters, or variable parameters. The essential difference between the two is that the use of constant parameters has implicit in it the assumption of linearity, while this is not the case in computations using variable parameters. In the constant parameter method, the linear behavior is associated with a reference value of discharge, the calculation of the parameters being based on this reference value. The accuracy of the computations is shown to be dependent on the choice of reference discharge. For practical purposes, a reference discharge close to the average flood discharge is recommended.

In the variable parameter method, an attempt is made to account for the quasilinear property of flood waves (see Figure 5-33). This invariably results in an improved definition of certain features of the flood wave, specially in reference to the hydrograph shape and time to peak. Several approaches to the calculation of the variable parameters have been developed e.g., see Miller and Cunge (1975), Price (1978), and Ponce and Yevjevich (1978). While there are minor differences in detail between these approaches, that of Ponce and Yevjevich is preferred here due to its simplicity.

Following Ponce and Yevjevich (1978), the value of $\Delta t$ is fixed by considerations of accuracy, the value of $\Delta x$ is also fixed (reach

length), and the value of $S_o$ (equilibrium energy slope) is specified for a given reach. The calculation of variable parameters is based on the variation of the unit-width discharge q and the celerity c. These are defined at grid point (j,n) as

$$q = \left.\frac{Q}{B}\right|_{j,n} \tag{5-184}$$

and

$$c = \left.\frac{dQ}{dA}\right|_{j,n} = \left.\frac{1}{B}\frac{dQ}{dy}\right|_{j,n} \tag{5-185}$$

In determining C and D, the values of q and c are calculated either directly, by using a three-point average of the values of q and c at grid points (j,n), (j+1,n) and (j,n+1) or by iteration, using a four-point average of the values of q and c at grid points (j,n), (j+1,n), (j,n+1) and (j+1, n+1). To improve convergence in the iterative four-point procedure, the results of the three-point procedure can be used as the first guess of the iteration.

Applicability of Simplified Models

The choice between the classical and simplified approaches on one hand, and the complete numerical models on the other hand, involves consideration of accuracy, ease of application, familiarity with a particular method, and other economic factors. The following advantages of the classical and simplified approaches to stream channel routing are readily recognized. The ease of formulation, manifested in shorter training periods, lower program development costs, lower run costs, and smaller computer size needs and also the applicability for a wide range of practical problems, since the inertia terms can be shown to be negligible in a large number of applications.

The major disadvantage is the loss of accuracy resulting from the various assumptions that are made in order to simplify the problem. For instance, upstream wave motions such as those produced in the vicinity of tributary flows or by dams and other control devices, cannot be accounted for in the classical and simplified methods, due primarily to their kinematic formulation. Computational details aside, the simplified methods provide a reasonably good answer to a wide range of problems with a minimum investment of resources. In addition, as shown by Ponce et al. (1978), their range of applicability can be clearly delineated in terms of readily identifiable hydraulic quantities.

Criteria for Applicability of Simplified Approach

According to Ponce et al. (1978), the error due to the use of the kinematic wave model (error in hydrograph peak accumulated after an elapsed time equal to the hydrograph duration) is within 5%, provided the following inequality is satified

$$\frac{TS_o u_o}{d_o} \geq 171 \tag{5-186}$$

in which T = hydrograph duration, $S_o$ = equilibrium energy slope (or bottom slope, for channels of regular cross-section), $u_o$ = reference mean velocity, and $d_o$ = reference flow depth. When applying Equation 5-186 to check the validity of the kinematic wave model, the reference values should correspond as closely as possible to the average flow conditions.

The error due to the use of the diffusive wave model (error in hydrograph peak accumulated after an elapsed time equal to the hydrograph duration) is within 5%, provided the following inequality is satisfied

$$TS_o\left(\frac{g}{d_o}\right)^{1/2} \geq 30 \qquad (5\text{-}187)$$

For instance, assume $S_o = 0.001$, $u_o = 3$ fps and $d_o = 10$ ft. The kinematic wave model will apply for hydrographs of duration larger than 6.59 days. Likewise, the diffusive wave model will apply for hydrographs of duration larger than 0.19 days.

## REFERENCES

Barnes, Harry H. Jr., 1967, Roughness Characteristics of Natural Channels: U. S. Geol. Survey Water-Supply Paper 1848, 213 p.

Chow, V. T., 1959, Open Channel Hydraulics: John Wiley and Sons Inc., New York, New York.

Cunge, J. A., 1969, On the Subject of a Flood Propagation Computation Method (Muskingum Method), Journal of Hydraulic Research, Vol. 7, No. 2, pp. 205-230.

Einstein, H. A., 1950, The Bed Load Function for Sediment Transportation in Open Channel Flows: U. S. Dept. of Agriculture Tech. Bull. 1026, 70 p.

Hayami, S., 1951, On the Propagation of Flood Waves, Bulletin No. 1, Disaster Prevention Research Institute, Kyoto University, Kyoto, Japan, December, pp. 1-16.

Ippen, A. T. and Dawson, J. H., 1951, Design of Channel Contractions: Trans. ASCE Vol. 116, pp. 326-346.

Ippen, A. T. and Drinker, P. A., 1962, Boundary Shear Stresses in Curved Trapezoidal Channels: ASCE Hyd. Div. J., Vol. 88, No. HY5, Sept.

Karman, T. von, 1930, Mechanische Ähnlichkeit und Turbulenz: Nach. Ges. Wiss. Göttingen, Math. Phys. Klasse, Vol. 58, and Proc. 3rd Intern. Congr. Appl. Mech., Stockholm, Pt. I, Vol. 85 (1930).

Knapp, R. T., 1951, Design of Channel Curves for Supercritical Flow: Trans., ASCE, Vol. 116, pp. 296-325.

Lighthill, M. J. and Whitham, G. B., 1955, On Kinematic Waves, I. Flood Movement in Long Rivers, Proceedings of the Royal Society of London, Vol. A229, May, pp. 281-316.

Miller, W. A. and Cunge, J. A., 1975, Simplified Equations of Unsteady Flow, Chapter 5 in Unsteady Flow in Open Channels, K. Mahmood and V. Yevjevich, eds., Water Resources Publications, Fort Collins, Colorado, pp. 183-257.

Ponce, V. M. and Simons, D. B., 1977, Shallow Wave Propagation in Open Channel Flow, Journal of the Hydraulics Division, ASCE, Vol. 103, HY12, Proc. Paper 13392, December, pp. 1461-1476.

Ponce, V. M., Li, R. M., and Simons, D. B., 1978, Applicability of Kinematic and Diffusion Models, Journal of the Hydraulics Division, ASCE, Vol. 104, HY3, March, pp. 353-360.

Ponce, V. M. and Yevjevich, V., 1978, Muskingum-Cunge Method with Variable Parameters, Journal of the Hydraulics Division, ASCE, Vol. 104, HY12, December, pp. 1663-1667.

Prandtl, L., 1925, Über die ausgebildete Turbulenz: ZAMM 5, and Proc. 2nd Intern. Congr. Appl. Mech., Zürich (1926).

Price, R. K., 1978, A River Catchment Flood Model, Proceedings of the Institution of Civil Engineers, Vol. 65, Part 2, September, pp. 655-668.

Rouse, H., Bhoota, B. V., and Hsu, E. Y., 1951, Design of Channel Expansions: Trans. ASCE, Vol. 116, pp. 347-363.

Shukry, A., 1950, Flow Around Bends in Open Flume: Trans. ASCE, Vol. 115.

Woodward, S. M., 1920, Hydraulics of the Miami Flood Control Project: Technical Reports, Miami Conservancy District, Dayton, Ohio, Pt. VII.

# APPENDIX 5A

## PROBLEMS

### 5A.1 BRIDGE CONSTRICTIONS WITH NO BACKWATER (Neglecting Energy Losses)

A stream is rectangular in shape and 100 ft wide. The design discharge is 5000 cfs and the uniform depth for this discharge is 10 ft. Neglecting energy losses what is the maximum amount of constriction that can be imposed without causing backwater at the design discharge?

The upstream flow rate per unit width is

$$q = \frac{Q}{W} = \frac{5000}{100} = 50 \text{ cfs/ft}$$

the average velocity is

$$V = \frac{Q}{A} = \frac{5000}{1000} = 5.00 \text{ fps}$$

and the specific head is (from Equation 5-75)

$$H = \frac{V^2}{2g} + y = \frac{5^2}{64.4} + 10 = 10.39 \text{ ft}$$

According to the section on the discharge diagram, the maximum unit discharge that can occur with this specific head is (from Equation 5-88)

$$q_{max} = \{g\ (\tfrac{2}{3} H)^3\}^{1/2}$$

$$= \{32.2(\tfrac{2}{3} \times 10.39)^3\}^{1/2}$$

$$= 103.4 \text{ cfs/ft}$$

Therefore, the width of channel which will accommodate this unit discharge is

$$W = \frac{Q}{q_{max}} = \frac{5000}{103.4} = 48.3 \text{ ft.}$$

and the amount of the constriction is 100 - 48.3 = 51.7 ft.

Note, as discussed previously, this contraction could cause an undulating hydraulic jump downstream. When energy losses are considered there will be some backwater at this constriction. This backwater is evaluated by conventional methods such as those given in "Hydraulics of Bridge Waterways" (Federal Highway Administration, 1970).

### 5A.2 BACKWATER FROM A DOWNSTREAM DIVERSION DAM

A small diversion dam is to be placed across a stream downstream of a highway bridge. The purpose of the dam is to head up water for diversion into a canal. At the bridge, the design flood discharge was

5000 cfs. The river is 100 ft wide and has a uniform flow depth of 10 ft for the design discharge. What is the maximum height of the dam that will not cause backwater at the bridge?

The unit discharge in the river at design flood discharge is

$$q = \frac{Q}{W} = \frac{5000}{100} = 50 \text{ cfs/ft}$$

the velocity is

$$V = \frac{q}{y_o} = \frac{50}{10} = 5.00 \text{ fps}$$

and the specific head is (from Equation 5-75)

$$H = \frac{V^2}{2g} + y_o = \frac{5^2}{2g} + 10 = 10.39 \text{ ft}$$

As a first approximation assume no energy loss in the reach. Then at the dam, the elevation of the total energy line is 10.39 ft above the bed (see Figure 5A-1). At the dam

$$H_{min} + \Delta Z_{max} = 10.39 \text{ ft}$$

that is, the dam can be built to a height of $\Delta Z_{max}$ which decreases the specific head at the dam to $H_{min}$. From Equation 5-83

$$H_{min} = \frac{3}{2} y_c$$

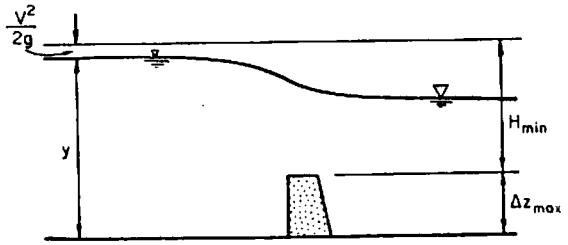


Figure 5A-1. Backwater curve upstream of the dam.

and from Equation 5-79

$$y_c = \left(\frac{q^2}{g}\right)^{1/3}$$

$$= \left(\frac{50^2}{32.2}\right)^{1/3} = 4.27 \text{ ft}$$

so

$$H_{min} = \frac{3}{2}(4.27) = 6.40 \text{ ft}$$

Thus

$$\Delta Z_m = 10.39 - 6.40 = 4.0 \text{ ft}$$

If the dam is built to a crest elevation 4.0 ft above the bed, critical flow will occur at the dam for a flow of 5000 cfs and the dam will cause no backwater.

How much backwater will the dam cause for a flow of 1000 cfs if the normal depth for this discharge is 5 ft and the dam height is 4.0 ft?

Upstream of the dam

$$q = \frac{Q}{W} = \frac{1000}{100} = 10 \text{ cfs/ft}$$

and

$$V_o = \frac{q}{y_o} = \frac{10}{5} = 2 \text{ fps}$$

At the dam the flow is critical so from Equation 5-79

$$y_c = \left(\frac{q^2}{g}\right)^{1/3}$$

$$= \left(\frac{10^2}{32.2}\right)^{1/3} = 1.46 \text{ ft}$$

and from Equation 5-83

$$H_{min} = \frac{3}{2} y_c$$

$$= \frac{3}{2}(1.46) = 2.19 \text{ ft}$$

The specific head upstream of the dam is then (assuming no energy loss)

$$H = H_{min} + \Delta Z$$

or

$$H = 2.19 + 4.00 = 6.19 \text{ ft}$$

Also, the specific head upstream of the dam is (from Equation 5-76)

$$H = \frac{q^2}{2gy^2} + y$$

Therefore

$$\frac{q^2}{2gy^2} + y = 6.19$$

or

$$y^3 - 6.19\ y^2 + \frac{10^2}{64.4} = 0$$

The solution is

$$y = 6.14 \text{ ft}$$

As the normal depth is only 5 ft, the backwater is

$$\Delta y = 6.14 - 5.00 = 1.14 \text{ ft}$$

That is, the depth upstream of the dam is increased 1.14 ft by the 4.0-ft high dam when the flow is 1000 cfs.

## 5A.3 STANDARD STEP METHOD FOR BACKWATER COMPUTATIONS

Consider an abrupt change of slope in a lined rectangular channel 100 ft in width. The discharge is 5000 cfs. Upstream of the slope change, the flow is at the normal depth of 10 ft. The normal depth in the downstream reach is 3 ft. Manning's n for both reaches is 0.012.

In both the upstream and downstream reaches, the flow per unit width is

$$q = \frac{5000}{100} = 50 \text{ cfs/ft}$$

and the critical depth is (from Equation 5-79)

$$y_c = \left(\frac{q^2}{g}\right)^{1/3} = \left(\frac{50^2}{32.2}\right)^{1/3} = 4.27 \text{ ft.}$$

Upstream where the flow is at normal depth, $y = y_o > y_c$ so the flow is tranquil here.

The bed slope is obtained from Manning's equation for normal flow (from Equation 5-61)

$$S_o = \frac{n^2 V_o^2}{2.21 R_o^{4/3}}$$

Here

$$V_o = \frac{q}{y_o} = \frac{50}{10} = 5.00 \text{ fps}$$

$$A_o = y_o W = 10\ (100) = 1000 \text{ sq ft}$$

$$P_o = 2y_o + W = 2\ (10) + 100 = 120 \text{ ft}$$

$$R_o = \frac{A_o}{P_o} = \frac{1000}{120} = 8.33 \text{ ft}$$

$$S_o = \frac{(0.012 \times 5)^2}{2.21(8.33)^{4/3}} = 0.000095$$

Downstream where the flow has attained its normal depth, $y = y_o < y_c$ so in the downstream reach flow is supercritical.

The bed slope in the downstream reach is obtained as follows

$$V_o = \frac{q}{y_o} = \frac{50}{3} = 16.67 \text{ fps}$$

$$A_o = y_o W = 3 \times 100 = 300 \text{ sq ft}$$

$$P_o = 2y_o + W = 2\ (3) + 100 = 106 \text{ ft}$$

$$R_o = \frac{A_o}{P_o} = \frac{300}{106} = 2.83 \text{ ft}$$

$$S_o = \frac{n^2 V_o^2}{2.21 R_o^{4/3}} = \frac{(0.012 \times 16.67)^2}{2.21\ (2.83)^{4/3}}$$

$$= 0.004523$$

At the change in slope the flow must pass through the critical depth. Then, in the reach immediately upstream $y_o > y > y_c$ so the backwater curve in this reach is an $M_2$ type (Table 5-2).

Downstream, $y_o < y < y_c$ so the backwater curve in this reach is a $S_2$ type (Table 5-2).

The two backwater curves are sketched in Figure 5A-2.

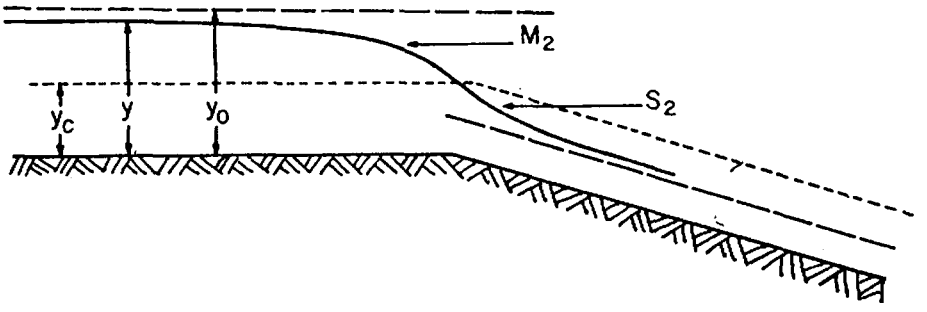


Figure 5A-2. Sketch of backwater curves.

For the upstream reach, flow is subcritical so the standard step method computations start at the change in slope and proceed upstream.

At the change in slope

$$y = y_c = 4.27 \text{ ft}$$

$$A = yW = 4.27\ (100) = 427 \text{ sq ft}$$

$$V = \frac{q}{y} = \frac{50}{4.27} = 11.71 \text{ fps}$$

$$\frac{V^2}{2g} = \frac{11.71^2}{64.4} = 2.13 \text{ ft}$$

$$H = \frac{V^2}{2g} + y = 4.27 + 2.13 = 6.40 \text{ ft}$$

$$P = 2y + W = 2\ (4.26) + 100 = 108.52 \text{ ft}$$

$$R = \frac{A}{P} = \frac{427}{108.54} = 3.93 \text{ ft}$$

$$S_f = \frac{n^2 V^2}{2.21\ R^{4/3}} = \frac{(0.012 \times 11.71)^2}{2.21(3.93)^{4/3}} = 0.001438$$

Let's compute the distance upstream to where the flow is 4.50 ft deep. The flow conditions at this section are computed with the same equations employed at the change in slope section i.e.,

$$y = 4.50 \text{ ft}$$

$$A = 4.50\ (100) = 450 \text{ sq ft}$$

$$V = \frac{50}{4.50} = 11.11 \text{ fps}$$

$$\frac{V^2}{2g} = \frac{11.11^2}{64.4} = 1.92 \text{ ft}$$

$$H = 4.50 + 1.92 = 6.42 \text{ ft}$$

$$P = 2\ (4.50) + 100 = 109 \text{ ft}$$

$$R = \frac{450}{109} = 4.13 \text{ ft}$$

$$S_f = \frac{(0.012 \times 11.11)^2}{2.21\ (4.13)^{4/3}} = 0.001214$$

Now between these two sections where $y = 4.27$ ft and $y = 4.50$ ft the average friction slope is

$$S_{f_{ave}} = \frac{0.001438 + 0.001214}{2} = 0.001326$$

The distance between the two sections is (from Equation 5-117)

$$\Delta L = \frac{H_2 - H_1}{S_o - S_{f_{ave}}}$$

$$= \frac{6.40 - 6.42}{.000095 - 0.001326} = 16.2 \text{ ft}$$

That is, the section where the depth is 4.50 ft is 16.2 ft upstream of the section where the slope changes.

In a similar manner, the distance between the sections where the depths are 4.50 ft and 5.00 ft (arbitrary choice) is computed. The results are listed in Table 5A-1. It is found that the flow is normal a distance approximately 44,000 ft above the change in slope.

The backwater calculations for the downstream reach are also presented in Table 5A-1. Here the computations start at the change in section and proceed downstream because the flow is supercritical. The computations show that the normal depth is reached approximately 1600 ft below the change in slope.

## 5A.4 ENERGY AND MOMENTUM COEFFICIENTS FOR RIVERS

In open channel flow problems it is common to assume that the energy coefficient $\alpha$ and the momentum coefficient $\beta$ are unity. What are values of $\alpha$ and $\beta$ for river channels?

From Equations 5-33 and 5-12

$$\alpha = \frac{1}{V^3 A} \int_A v^3 \, dA \tag{5A-1}$$

and

$$\beta = \frac{1}{V^2 A} \int_A v^2 \, dA \tag{5A-2}$$

In many wide channels, the distribution of velocities in the vertical is given by Equation 5-56 which is

$$\frac{v}{V_*} = 2.5 \ln (30.2 \frac{y}{k_s}) \tag{5A-3}$$

for fully turbulent (x = 1.0). The average velocity in the vertical is

$$V = \frac{1}{y_o} \int_0^{y_o} v \, dy \tag{5A-4}$$

and by employing Equation 5A-3

$$V \cong \frac{2.5 V_*}{y_o - \delta} \int_\delta^{y_o} \ln(\frac{y}{\delta}) \, dy \tag{5A-5}$$

Here, the upper limit of integration is $y_o$, the depth of flow and the lower limit is

$$\delta = \frac{k_s}{30.2} \tag{5A-6}$$

Table 5A-1. Computation of the backwater curve.

| y ft | A sq ft | V fps | $V^2/2g$ ft | H ft | P ft | R ft | n | $S_f$ | $S_{f_{ave}}$ | $H_2 - H_1$ ft | $\Delta L$ ft | L ft |
|---|---|---|---|---|---|---|---|---|---|---|---|---|
| At the change in slope | | | | | | | | | | | | |
| 4.27 | 427 | 11.71 | 2.13 | 6.40 | 108.5 | 3.93 | 0.012 | .001438 | -- | -- | -- | -- |
| $S_2$ backwater curve | | | | | | | | | | | | |
| 4.20 | 420 | 11.90 | 2.20 | 6.40 | 108.4 | 3.87 | 0.012 | .001519 | .001478 | -0.00 | 0.0 | 0.0 |
| 4.00 | 400 | 12.50 | 2.43 | 6.43 | 108 | 3.70 | | .001779 | .001649 | -0.03 | 10.9 | 10.9 |
| 3.50 | 350 | 14.28 | 3.17 | 6.67 | 107 | 3.27 | | .002738 | .002258 | -0.24 | 105.96 | 116.86 |
| 3.00 | 300 | 16.67 | 4.31 | 7.31 | 106 | 2.83 | | .004523 | .003630 | -0.64 | 716.7 | 833.56 |
| $M_2$ backwater curve | | | | | | | | | | | | |
| 4.50 | 450 | 11.11 | 1.92 | 6.42 | 109 | 4.13 | 0.012 | .001214 | .001326 | -0.02 | 16.2 | 16.2 |
| 5.00 | 500 | 10.00 | 1.55 | 6.55 | 110 | 4.54 | | .000867 | .001040 | -0.13 | 137.6 | 153.8 |
| 6.00 | 600 | 8.33 | 1.08 | 7.08 | 112 | 5.36 | | .000482 | .000674 | -0.53 | 914.6 | 1068.4 |
| 8.00 | 800 | 6.25 | 0.61 | 8.61 | 116 | 6.90 | | .000194 | .000338 | -1.78 | 6296.3 | 7364.7 |
| 10.00 | 1000 | 5.00 | 0.39 | 10.39 | 120 | 8.33 | | .000095 | .000144 | -1.78 | 36326.5 | 43691.2 |

$A = Wy$ $\quad V = \frac{Q}{A}$ $\quad P = 2y + W$ $\quad R = \frac{A}{P}$ $\quad S_f = \frac{n^2V^2}{2.21\ R^{4/3}}$ $\quad \Delta L = \frac{H_2 - H_1}{S_o - S_{f_{ave}}}$ $\quad L = \Sigma \Delta L$

the value of y for which Equation 5A-3 gives a zero velocity. The integration of Equation 5A-5 yields

$$\frac{V}{V_*} = 2.5 \left\{\frac{y_o}{y_o-\delta} \left(\ln\left(\frac{y_o}{\delta}\right) - 1\right)\right\} \tag{5A-7}$$

For a vertical section of unit width, the momentum coefficient is

$$\beta' = \frac{1}{v^2(y_o-\delta)} \int_{\delta}^{y_o} v^2 \, dy \tag{5A-8}$$

If we substitute Equations 5A-3 and 5A-7 into Equation 5A-8 and integrate the result is the expression

$$\beta' = \frac{1}{\left(\ln 11.11 \frac{y_o}{k_s}\right)^2} \frac{y_o}{y_o-\delta} \left\{\left(\ln \frac{y_o}{\delta}\right)^2 - 2 \ln \frac{y_o}{\delta} + 2 - \frac{2\delta}{y_o}\right\} \tag{5A-9}$$

Similarly, the energy coefficient for a vertical section unit width is

$$\alpha' = \frac{1}{V^3(y_o-\delta)} \int_{\delta}^{y_o} v^3 \, dy \tag{5A-10}$$

or

$$\alpha' = \frac{1}{\left(\ln 11.11 \frac{y_o}{k_s}\right)^2} \frac{y_o}{y_o-\delta} \left\{\left(\ln \frac{y_o}{\delta}\right)^2 - 3\left(\ln \frac{y_o}{\delta}\right)^2 + 6 \ln \frac{y_o}{\delta} - 6 + \frac{6\delta}{y_o}\right\} \tag{5A-11}$$

These equations (Equations 5A-9 and 5A-10) are rather complex, so a graph of $\alpha'$ and $\beta'$ vs $y_o/k_s$ has been prepared. The relations are shown in Figure 5A-3.

For the entire river cross section (shown in Figure 5A-4) Equation 5-33 can be written

$$\alpha = \frac{1}{\left(\frac{Q}{A}\right)^3 A} \int_0^W \int_0^{y_o} v^3 \, dy \, dz \tag{5A-12}$$

where W is the top width of the section, z is the lateral location of any vertical section, $y_o$ is the depth of flow at location z, and v is the local velocity at the position y,z. The total discharge is Q and the total cross-sectional area is A.

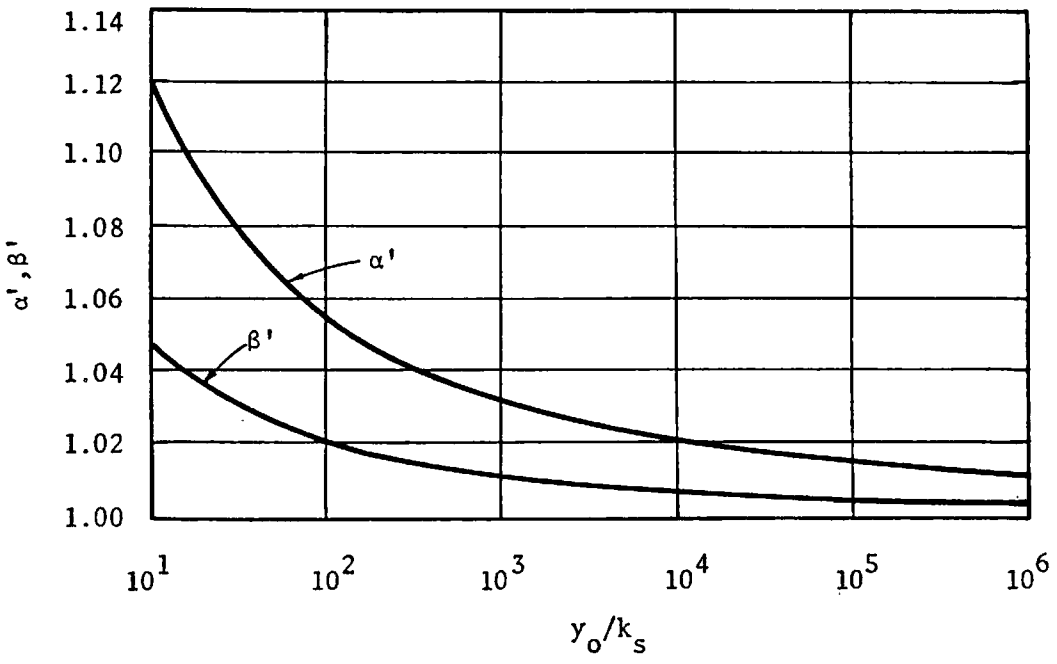


Figure 5A-3. Energy and momentum coefficients for a unit width of river.

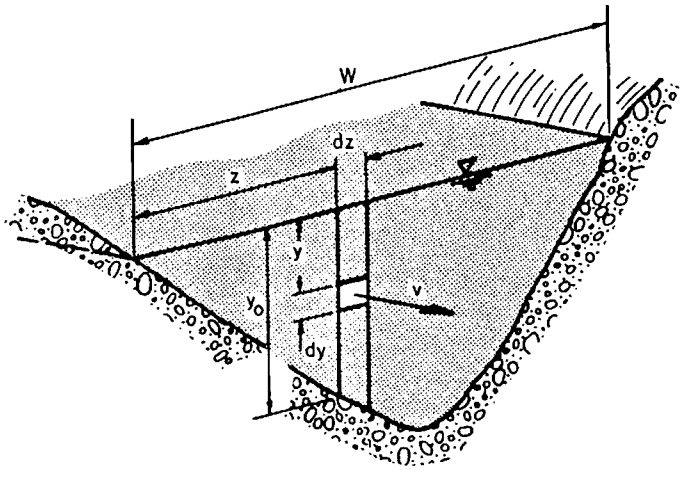


Figure 5A-4. The river cross section.

In Equation 5A-12 the portion

$$\int_0^{y_o} v^3 \, dy$$

is recognized as the integral portion of Equation 5A-10. That is

$$\int_0^{y_o} v^3 \, dy \cong \int_\delta^{y_o} v^3 \, dy$$

and

$$\int_\delta^{y_o} v^3 \, dy = \alpha' V^3 (y_o - \delta) \qquad (5A\text{-}13)$$

Here $\alpha'$ is the energy coefficient for the vertical section $dz$ wide and $y_o$ deep, $V$ is the depth-averaged velocity in this vertical section and $\delta = k_s/30.2$ (from Equation 5A-6).

Now, Equation 5A-12 can be written

$$\alpha = \frac{A^2}{Q^3} \int_0^W \alpha' V^3 (y_o - \delta) dz \qquad (5A\text{-}14)$$

Except for cases of low flow in gravel bed rivers, the term $\delta$ is very small compared to $y_o$ so

$$\alpha = \frac{A^2}{Q^3} \int_0^W \alpha' V^3 y_o dz \qquad (5A\text{-}15)$$

The discharge at a river cross section is determined in the field by measuring the local depth and two local velocities at each of approximately 20 vertical sections. In accordance with this general stream gaging procedure, Equation 5A-15 should be written

$$\alpha = \frac{A^2}{Q^3} \sum_i \alpha_i' V_i^3 y_{oi} \Delta z_i$$

or

$$\alpha = \frac{A^2}{Q^3} \sum \alpha_i' V_i^2 \Delta Q_i \qquad (5A\text{-}16)$$

Here, the subscript $i$ refers to the $i$-th vertical section, and $\Delta Q_i$ is the river discharge associated with the $i$-th vertical or

$$\Delta Q_i = V_i y_{oi} \Delta z_i$$

In a similar manner, the expression for $\beta$ is

$$\beta = \frac{A}{Q^2} \sum_i \beta_i' V_i \Delta Q_i \qquad (5A\text{-}17)$$

Now, with Equations 5A-16 and 5A-17 and Figure 5A-3 we are in a position to compute $\alpha$ and $\beta$ for any river cross section given the discharge measurement notes. An example is given below.

The information in Table 5A-2 is taken from the discharge measurement notes for Measurement No. 16 on the Rio Tigre at Las Piedritas in Venezuela.

The discharge measurement was made on August 18, 1969 during the peak flood event for the year. From Table 5A-2, the following values are obtained:

$Q = 5370$ cfs

$A = 1485$ sq ft

$W = 163$ ft

$\Sigma V_i \Delta Q_i = 21{,}070$ ft$^4$/sec$^2$

$\Sigma V_i^2 \Delta Q_i = 85{,}500$ ft$^5$/sec$^3$

The bed material at this gaging station (Simons et al., 1971a) has a $D_{50}$ of 0.33 mm and a $D_{67}$ of 0.45 mm and a gradation coefficient G of 3.27. If the value of $D_{67}$ is used for $k_s$, then for $y_o = 12.8$ ft (the maximum depth)

$$\frac{y_o}{k_s} = \frac{12.8}{0.45}(304.8) = 8700$$

and for $y_o = 1.1$ ft (the smallest non-zero depth)

$$\frac{y_o}{k_s} = \frac{1.1}{0.45}(304.8) = 750$$

If we use a mean $y_o/k_s$ of approximately 5000, then from Figure 5A-3, the average values for the energy and momentum coefficients are

$$\alpha' = 1.024$$

and

$$\beta' = 1.008$$

As it has been assumed that $\alpha'$ and $\beta'$ are constant across the river (for convenience), Equations 5A-16 and 5A-17 become

$$\alpha = \alpha' \frac{A^2}{Q^3} \sum_i V_i^2 \Delta Q_i \qquad (5A\text{-}18)$$

and

$$\beta = \beta' \frac{A}{Q^2} \sum_i V_i \Delta Q_i \qquad (5A\text{-}19)$$

With the values computed in Table 5A-2

Table 5A-2. Discharge measurement notes.[1]

| $y_{oi}$ ft | $\Delta z_i$ ft | $V_i$ fps | $\Delta A_i$ sq ft | $\Delta Q_i$ cfs | $V_i \Delta Q_i$ $ft^4/sec^2$ | $V_i^2 \Delta Q_i$ $ft^5/sec^3$ |
|---|---|---|---|---|---|---|
| 0.0 | 4.0 | 0.00 | 0.0 | 0.00 | 0.00 | 0.00 |
| 1.1 | 8.0 | 0.98 | 8.8 | 8.62 | 8.45 | 8.28 |
| 2.6 | 8.0 | 0.54 | 20.8 | 11.23 | 6.06 | 3.27 |
| 4.5 | 8.0 | 0.64 | 36.0 | 23.04 | 14.75 | 9.44 |
| 8.5 | 8.0 | 2.40 | 68.0 | 163.20 | 391.68 | 940.03 |
| 11.0 | 8.0 | 3.17 | 88.0 | 278.96 | 884.30 | 2803.24 |
| 11.6 | 8.0 | 4.02 | 92.8 | 373.06 | 1499.70 | 6028.80 |
| 12.0 | 8.0 | 4.06 | 96.0 | 389.76 | 1582.43 | 6424.65 |
| 12.8 | 8.0 | 3.78 | 102.4 | 387.07 | 1463.12 | 5530.61 |
| 12.6 | 8.0 | 3.74 | 100.8 | 376.99 | 1409.94 | 5273.19 |
| 12.4 | 8.0 | 3.78 | 99.2 | 374.98 | 1417.42 | 5357.86 |
| 11.6 | 8.0 | 4.71 | 92.8 | 437.09 | 2058.69 | 9696.45 |
| 11.4 | 8.0 | 4.30 | 91.2 | 392.16 | 1686.29 | 7251.04 |
| 10.8 | 8.0 | 4.90 | 86.4 | 423.36 | 2074.46 | 10164.87 |
| 10.6 | 8.0 | 4.63 | 84.8 | 392.62 | 1817.83 | 8416.56 |
| 10.9 | 8.0 | 4.32 | 87.2 | 376.70 | 1627.34 | 7030.13 |
| 11.4 | 8.0 | 3.89 | 91.2 | 354.77 | 1380.06 | 5368.42 |
| 11.8 | 8.0 | 3.10 | 94.4 | 292.64 | 907.18 | 2812.27 |
| 9.8 | 8.0 | 3.02 | 78.4 | 236.77 | 715.05 | 2159.44 |
| 6.4 | 7.0 | 1.69 | 44.8 | 75.71 | 127.95 | 216.24 |
| 3.8 | 5.5 | 0.00 | 20.9 | 0.00 | 0.00 | 0.00 |
| 0.0 | 2.5 | 0.00 | 0.0 | 0.00 | 0.00 | 0.00 |
| Total | 163.0 | | 1484.9 | 5368.74 | 21072.71 | 85494.77 |

[1]Simons et al., 1971b.

$$\alpha = 1.024 \frac{(1485)^2}{(5370)^3} (85500) = 1.247$$

$$\beta = 1.008 \frac{(1485)}{(5370)^2} (21070) = 1.094$$

These values for $\alpha$ (1.247) and $\beta$ (1.094) differ from unity by appreciable amounts. The difference may be important in many river channel calculations. If no data are available, the assumptions that $\alpha = 1.25$ and $\beta = 1.1$ should be used for river channels.

## 5A.5 AVERAGE PRESSURE AND ELEVATION AT A RIVER CROSS SECTION

In the absence of heat transfer, and shaft and shear work, the energy convected through a cross section of river with area A is

$$\int_A \gamma(\frac{v^2}{2g} + z)v \, dA$$

and the pressure work done on this cross section is

$$\int_A pv \, dA$$

The sum of the pressure work and the convected energy is

$$\int_A \gamma(\frac{v^2}{2g} + \frac{p}{\gamma} + z)v \, dA$$

Instead of using the definition Equation 5-32, we could write

$$\int_A \gamma(\frac{v}{2g} + \frac{p}{\gamma} + z)v \, dA = \{\frac{\alpha V^2}{2g} + \Omega(z_o + y_o)\}\gamma Q \qquad (5A\text{-}20)$$

where $\alpha$ is the kinetic energy correction factor defined by Equation 5-33 and $\Omega$ is a correction factor to be applied to the piezometric head. The terms $z_o$ and $y_o$ are the elevation of the bed above datum and the depth of flow respectively. According to Equations 5-33 and 5A-20 the expression for $\Omega$ must be

$$\Omega = \frac{1}{(z_o + y_o)VA} \int_A (\frac{p}{\gamma} + z)v \, dA \qquad (5A\text{-}21)$$

In straight reaches of river, the piezometric head does not vary appreciably from point to point in a cross section. Then the piezometric head at any point on the cross section can be used as the reference piezometric head. For example, at the water surface

$$\frac{p}{\gamma} + z = 0 + z_o + y_o \qquad (5A\text{-}22)$$

Using this equation in Equation 5A-21, we obtain

$$\Omega = \frac{1}{(z_o + y_o)VA} \int_A (z_o + y_o)v \, dA = \frac{1}{VA} \int_A v \, dA$$

or

$$\Omega = 1 \qquad (5A\text{-}23)$$

If the water surface at the cross section is not horizontal (as in a bend), then the piezometric head should be referenced to the point on the water surface which is at the average elevation of the water surface. Then $\Omega = 1$ for this case also.

In general, the assumption that

$$\Omega = 1$$

is satisfactory for rivers. Therefore, Equation 5-38 can be written

$$\frac{\alpha_1 V_1^2}{2g} + y_1 + z_1 = \frac{\alpha_2 V_2^2}{2g} + y_2 + z_2 + H_L \qquad (5A\text{-}24)$$

for a reach of river. Here $y_1 + z_1$ is the water surface level at section 1 and $y_2 + z_2$ is the water surface elevation at section 2.

# APPENDIX A-REFERENCES

Simons, D. B., Richardson, E. V., Stevens, M. A., Duke, J. H., and Duke, V. C., August 1971b, Streamflow, Groundwater and Ground Response Data, Hydrology Report, Vol. II, Venezuelan International Meteorological and Hydrology Experiment, Civil Engineering Dept., Colorado State University, Fort Collins, Colorado.

Simons, D. B., Richardson, E. V., Stevens, M. A., Duke, N. H., and Duke, V. C., October 1971a, Geometric and Hydraulic Properties of the Rivers, Hydrology Report, Vol. III, VIMHE, Civil Engineering Dept., Colorado State Univeristy, Fort Collins, Colorado.

# Chapter 6

# RESISTANCE TO FLOW

## 6.1 INTRODUCTION

Bed configuration and resistance to flow in alluvial rivers are functions of flow and channel conditions. The water surface level can increase or decrease in response to changes in either bed configuration or channel resistance. The factors governing these actions and responses in alluvial channels are numerous and complex and many interactions of the variables involved are not well understood. This chapter presents the current state-of-the-art on the fundamentals of resistance to flow, in particular it includes resistance to flow in sand, gravel, and cobble bed streams, and vegetated channels.

## 6.2 BASIC CONCEPTS FOR DESCRIBING RESISTANCE TO FLOW

There are many variables involved in the determination of resistance to flow. A general flow formula considering the major variables is

$$\phi(U, d, S, \rho, \mu, g, D, \sigma, \rho_s, S_p, S_R, S_c, f_s) = 0 \qquad (6\text{-}1)$$

where

$U$ = velocity
$d$ = depth
$S$ = slope of the energy grade line
$\rho$ = density of water
$\mu$ = apparent dynamic viscosity of water
$g$ = gravitational acceleration
$D$ = representative diameter of bed material
$\sigma$ = standard deviation of the size distribution of bed material
$\rho_s$ = density of sediment
$S_p$ = shape factor of the particles
$S_R$ = shape factor of the channel reach
$S_c$ = shape factor of the channel cross section
$f_s$ = seepage force in the bed of the channel

The effects of some of these factors on resistance to flow are known but it is difficult to consider them because of their complexity; the influence of others, however, is not known. With this in mind, Equation 6-1 can be transformed into

$$\frac{U}{U_*} = \phi\left(R_e, \frac{D}{d}, \frac{1}{R_w}, \frac{\tau}{\gamma' D}\right) \qquad (6\text{-}2)$$

where

$$\frac{U}{U_*} = \text{a measure of the resistance} = \frac{U}{\sqrt{gRS}}$$

$R_e$ = Reynolds number = $\frac{UR}{\nu}$

$\frac{D}{d}$ = relative roughness

$R_w$ = Reynolds number of the particle (related to fall velocity) = $\frac{wD}{\nu}$

$\frac{\tau}{\gamma_s' D}$ = Froude number related to the particle

With a rigid boundary $\gamma_s'$ representing the specific weight of a boundary particle and w, fall velocity, assumed to be equal to infinity, then $\frac{\tau}{\gamma_s' D}$ and $\frac{1}{R_w}$ are both zero, and Equation 6-2 reduces to

$$\frac{U}{U_*} = \phi(R_e, \frac{D}{d}) \tag{6-3}$$

Then $\frac{U}{U_*}$ can be transformed to

$$\frac{U}{U_*} = \frac{U}{\sqrt{gR}} \frac{1}{\sqrt{S}} = \frac{F_r}{\sqrt{S}} \tag{6-4}$$

where $F_r = \frac{U}{\sqrt{gR}}$ is the Froude number of the flow. Substituting the value of $\frac{U}{U_*}$ from Equation 6-3 and rearranging yields

$$S = F_r^2 \, f_1(R_e, \frac{D}{d}) \tag{6-5}$$

or

$$S = F_r^2 \, f_2(R_e), \, (\frac{D}{d})^n \tag{6-6}$$

Many formulas are of this form.

Surface Drag and Form Drag

Clearly in the case of a wide channel with a plane bed subjected to turbulent flow, the resistance to flow reduces to a function of $\frac{D}{d}$; or to skin friction, or surface drag. When bed forms occur a form drag must be added to the surface drag. Many studies and analyses have considered various ways of expressing form and surface drag. Two general approaches can be used.

Approach 1. A certain fraction of the energy is consumed overcoming the resistance due to surface drag and the remainder is used to overcome the form drag. This idea was generally developed in Europe

by Meyer-Peter and Müller (1948). If $S'$ corresponds to the fraction of the energy slope required to overcome surface drag and $S''$ the fraction required to offset form drag it is possible to write

$$S = S' + S'' \tag{6-7}$$

Approach 2. Considering a prism of flow over the bed of a wide river (Figure 6-1a) it is possible to define the hydraulic radius as

$$R = \frac{bh}{b}$$

If the numerator and the denominator of this ratio are multiplied by $\rho$ in such a way that $b\rho = A_o = 1$ and $bh\rho = V_o$

$$R = \frac{bh\ell}{b\rho} = \frac{V_o}{A_o} = \frac{V_o}{1}$$

where $b \times \rho = A_o$ is the unit area and $V_o$ is the volume superposed on this unit area, then the hydraulic radius represents the volume of a rectangular prism with a height equal to the depth of water. This concept of $R$ was first given by Einstein. "h" is defined as that part of this volume required to damp the turbulence generated by the boundary. If $V'$ corresponds to the necessary volume for damping the turbulence related to surface friction it is possible to define the volume $V''$ required to damp the turbulence attributed to bed forms so that

$$V = V' + V''$$

or from Figure 6-1b:

$$R = R' + R'' \tag{6-8}$$

It may be difficult to visualize the damping of the turbulence in the way defined but it is a fact that $R$ increases for increasing values of boundary resistance. The increase of the energy slope corresponding to an increase in the roughness is perhaps more difficult to understand. Specifically, the energy slope is a function of different factors and it can be kept constant by changing the hydraulic radius. For this reason Equation 6-8 is considered basic to future developments.

From Equation 6-8 the relations

$$\tau_o' = \gamma R'S \tag{6-9}$$

and

$$\tau_o'' = \gamma R''S \tag{6-10}$$

are formulated. Shear stress $\tau_o'$ represents the fraction of the total shear taken by the skin fraction or surface drag and the remaining part of resistance $\tau_o''$ represents the fraction of the total shear taken by the bed forms, it is frequently referred to as the form drag.

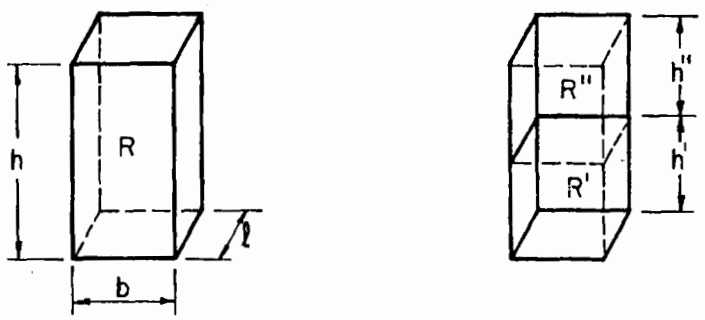


Figure 6-1. Visualization of hydraulic radius.

Additional resistance to flow caused by local accelerations or unsteadiness may be included in the resistance equation

$$\tau_o = \tau_o' + \tau_o'' \tag{6-11}$$

To eliminate the effects of local nonuniformity, both $\tau_o'$ and $\tau_o''$ can be evaluated based on the averaged characteristics of a channel reach. Equation 6-11 holds as long as the two components do not exert a mutual influence on one another.

Turbulence theory gives

$$U_* = \sqrt{\frac{\tau_o}{\rho}} \tag{6-12}$$

The term $U_*$ is the friction velocity and

$$U_*^2 = \left|\overline{u'v'}\right| \tag{6-13}$$

Though the dimension of $U_*$ is that of a velocity, the physical expression of it is different from velocity. It represents a variation of the fluctuation of turbulence around a point near the boundary of a channel.

From Equation 6-12

$$U_* = \sqrt{gRS} \tag{6-14}$$

$$U_*' = \sqrt{gR'S} \tag{6-15}$$

$$U_*'' = \sqrt{gR''S} \tag{6-16}$$

$$U_*^2 = U_*'^2 + U_*''^2 \tag{6-17}$$

For a channel with a flat bed, $R = R'$ because $R'' = 0$ and

$$U_* = U'_* \tag{6-18}$$

Common Parameters for Describing Resistance to Flow

Three most common parameters for describing the resistance to steady uniform flow are

(1) the Darcy-Weisbach friction factor, f,
(2) the Chézy resistance factor, C,
(3) the Manning roughness coefficient, n.

The Darcy-Weisbach formula, developed primarily for flows in pipes states that

$$h_f = f \frac{L}{D} \frac{U^2}{2g} \tag{6-19}$$

where $h_f$ is the friction loss associated with flow in pipes, f is the friction factor, L is the length of the pipe, D is the diameter of the pipe, U is the mean velocity of flow therein, and g is the acceleration of gravity.

Since $D = 4R$ and the energy gradient $S_E = \frac{h_f}{L}$, Equation 6-19 may be written in terms of friction factor as

$$f = \frac{8gRS_E}{U^2} \tag{6-20}$$

where R is the hydraulic radius. Noting that $U_*^2 = gRS_E$, Equation 6-20 yields

$$\frac{U}{U_*} = \sqrt{\frac{8}{f}} \tag{6-21}$$

Equation 6-21 can be applied to flow in open channels and sometimes it is presented as

$$\frac{r}{\sqrt{S_E}} = \sqrt{\frac{8}{f}} \tag{6-22}$$

or

$$f = \frac{E}{F_r^2} \tag{23}$$

The Chézy formula is expressed as

$$U = C\sqrt{RS_E} \tag{6-24}$$

where C is a resistance factor. The energy slope $S_E$ can be computed from

$$S_E = S_w - F_r^2 (S_w - S_b) \tag{6-25}$$

where

$S_w$ = slope of the water surface

$F_r^2 = \frac{U^2}{gd}$

U = mean velocity
d = depth of flow associated with $S_E$ and
$S_b$ = slope of the channel bottom

The use of $S_E$ is recommended because it reflects more accurately the state of flow at a particular location.

The Chézy resistance factor as expressed by Equation 6-24 is not dimensionless

$$C = \left| \frac{L^{1/2}}{T} \right|$$

Hence, it is common to assume

$$C = C' \sqrt{g} \tag{6-26}$$

and write

$$U = C' \sqrt{g} \sqrt{RS_f} = C' U_* \tag{6-27}$$

in this relation C' is dimensionless.

Substituting the value of U from Equation 6-24 in Equation 6-21 yields

$$\frac{C}{\sqrt{g}} = \sqrt{\frac{8}{f}} \tag{6-28}$$

or

$$C' = \sqrt{\frac{8}{f}} \tag{6-29}$$

The parameter $(\frac{C}{\sqrt{g}})$ is, in general, used to describe the resistance to flow in open channels.

Manning's formula is expressed in metric units as

$$U = \frac{1}{n} R^{2/3} S_E^{1/2} \tag{6-30}$$

or in the English system as

$$U = \frac{1.486}{n} R^{2/3} S_E^{1/2} \tag{6-31}$$

It can also be expressed as

$$C = \frac{1.486}{n} R^{1/6} \tag{6-32a}$$

$$C = \frac{R^{1/6}}{n} \tag{6-32b}$$

in the metric system. A similar expression can be obtained between C and f. Utilizing Equation 6-28

$$\frac{C}{\sqrt{8g}} = \frac{1}{\sqrt{f}} \tag{6-33}$$

Taylor and Brooks (1962) suggested the Darcy-Weisbach friction factor f be divided into two parts, that due to the grain roughness

$$f' = \frac{8gR'S_E}{U^2} \tag{6-34}$$

and that due to form roughness

$$f'' = \frac{8gR''S_E}{U^2}$$

In this case, the total friction factor

$$f = \frac{8gRS_E}{U^2} = f' + f'' \tag{6-35}$$

Using the same reasoning Bajorunas (1952) assumed that the Manning roughness coefficient n is composed of two parts

$$n = n' + n'' \tag{6-36}$$

where n' is due to the grain roughness and n'' is due to form roughness. From Equations 6-30 and 6-11 and noting that $\tau = \gamma S(R'+R'')$, the relation

$$R = R' \left(1 + \frac{n''}{n'}\right)^{3/2} \tag{6-37}$$

or

$$R = R' \left(\frac{n}{n'}\right)^{3/2} \tag{6-38}$$

is obtained.

Engineers have varying preferences for resistance parameters. The parameter f is used for both open channel and pressure flow. Consequently, the Task Committee (1963) recommended its use.

Use of Manning's n gives good results for fully rough and smooth conditions in rigid boundary channels but is less satisfactory in the transition range and for alluvial boundary flow, and its value is highly dependent on form of bed roughness. Disregarding these limitations, the Manning n is probably the most commonly used open channel flow resistance factor.

## Other Resistance to Flow Relations

Many resistance formulas have been proposed to determine the characteristics of flow; these are summarized in Table 6-1. However, the Chézy and Manning relations are the most commonly used.

Table 6-1. Other equations for resistance coefficients.

| Author | Definition |
|---|---|
| N. N. Pavlovsky (1925)<br>$C = \frac{Rx}{n}$ | C is the Chézy coefficient<br>n is the Manning coefficient<br>R is the hydraulic radius in meters<br>$x = 2.5\, n^{1/2} - 0.13 - 0.75\, R^{1/2}(n^{1/2} - 0.10)$ |
| G. H. Keulegan (1938)<br>$C = 8/f^{1/2}$ | C is the Chézy coefficient<br>f is the Darcy-Weisbach coefficient |
| A. E. Bretting (1948)<br>$1/f^{1/2} = 2 \log (k_s/14.83R)$ | f is the Darcy-Weisbach coefficient<br>$k_s$ is the equivalent sand grain diameter<br>R is the hydraulic radius |
| J. H. Thijsse (1949)<br>$1/f^{1/2} = 2.03 [\log (12.2R/0.282\delta + k_s)]$ | f is the Darcy-Weisbach coefficient<br>R is the hydraulic radius<br>$\delta$ is the thickness of the laminar sublayer<br>$k_s$ is a measure of the roughness |
| Powell (1950)<br>$C = 42 \log R/e$<br>(rough channel) | C is the Chézy coefficient<br>e is a measure of channel roughness<br>R is the hydraulic radius |
| A. D. Alfshul (1952)<br>$1/f^{1/2} = 1.8 \log [Re/Re(\Delta/d) + 7]$ | f is the Darcy-Weisbach coefficient<br>Re is the Reynolds number<br>$\Delta$ is a linear measure of roughness height<br>d is depth of flow |

Table 6-1. (Continued)

| Author | Definition |
|---|---|
| P. Ackers (1958)<br>$C = (32g)^{1/2}\log(14.8R/k_s)$ | C is the Chézy coefficient<br>$k_s$ is a measure of the amplitude of the roughness |
| W. W. Sayre and M. L. Albertson (1961)<br>$C/g^{1/2} = 6.06 \log (\frac{d_n}{x} + 2.6)$ | C is the Chézy coefficient<br>dn is normal depth<br>x is a general roughness parameter |
| H. J. Koloseus and Davidian (1961)<br>$1/f^{1/2} = {}_{0.2}{}_{9}\log [(0.56\ \lambda^{0.9}R)/k_s]$ | f is the Darcy-Weisbach coefficient<br>R is the hydraulic radius<br>$\lambda$ is a measure of the concentration of roughness elements<br>$k_s$ is a measure of the amplitude of the roughness elements |

Gunther Garbrecht (1961) lists and evaluates 22 Chézy coefficient formulas that have been used in Europe. The ones that have not been cited follow.

A. Salient formulas from turbulence theory

| | |
|---|---|
| von Kármán-Prandtl | $C = (8g)^{1/2}[2\ \log(2R/k_s) + 1.74]$ |
| V. Mises | $C = \frac{4.43}{0.0024 + (k'/2R)^{1/2}}$ |
| Bazin | $C = 87\ \frac{R^{1/2}}{m} + R^{1/2}$ |
| Agroskin | $C = \frac{1}{n} + 17.72\ \log R$ |
| Mostkow | $C = 22\ \log \frac{R}{\Delta} + 9.5\ \frac{\Delta}{R} + 1.5$ |
| Kutter | $C = 100\ \frac{R^{1/2}}{n} + R^{1/2}$ |

B. Empirical formulas

| | |
|---|---|
| Eytelwein | $C = 50.9$ |
| Hagen | $C = 43.7\ R^{1/6}$ (for large canals) |
| Hessle | $C = 25 + 12.5\ R^{1/2}$ |

Table 6-1. (Continued)

| Author | Definition |
|---|---|
| Lahmeyer | $C = 183.5\ R^{1/6}\ S^{1/6}$ |
| Saint-Venant | $C \sim 60$ |
| Humphreys and Abbot | $C \sim 5.35\ S^{2}$ |
| Beyerhans | $C \sim 27R^{1/5}$ |
| Hermanek ($U = C(DR)^{1/2}$) | $C = 30.7\ d^{1/2}$ ($d < 1.5$ m) |
| | $C = 34(d)^{1/4}$ ($1.50 \leqq d \leqq 6.0$) |
| | $C = 50.2 + 0.5\ d$ ($d > 6.0$ m) |
| Strickler | $C = (\text{Constant}/d_s^{1/6})R^{1/6}$ |
| Rinsum [$U = C(DS)^{1/2}$] | $C \sim k_s + 23$ |
| Eisner | $U = k_1 d_r \phi R^{1.5} - \xi^{-1}\ S^{0.5}\phi$ |

## 6.3 RESISTANCE TO FLOW IN OPEN CHANNELS WITH FLAT BED AND RIGID BOUNDARY

The simplest way to solve the resistance problem is by assuming the form drag and the wall effect are equal to zero. This is analogous to assuming a very wide bed with a rigid, plane bottom. Many formulas have been developed for this case. The effect of form drag may also be added to these approximations. Some of these approaches are summarized.

### The Semi-logarithmic Resistance Relations

The semi-logarithmic functions of resistance to flow according to Prandtl's (1926) mixing length theory are

$$u = \left(8.5 + 5.75 \log \frac{y}{k_s}\right) U_* \tag{6-39}$$

and

$$u = \left(5.5 + 5.75 \log \frac{yU_*}{\nu}\right) U_* \tag{6-40}$$

Equation 6-39 expresses the resistance to flow of a pipe with rough walls in the turbulent regime. The term $k_s$ is the equivalent sand roughness defined by Schlichting (1955) and $y$ is the distance from the wall where velocity $U$ is measured. Equation 6-40 expresses the resistance to flow of a pipe with a smooth boundary and turbulent flow.

Equations 6-39 and 6-40 can be integrated for different cross sectional shapes. The resulting mean velocity relations obtained for different shapes follow.

Circular cross section, smooth wall

$$\frac{U}{U_*} = 3.5 + 5.75 \log \frac{RU_*}{\nu} \tag{6-41}$$

very large rectangular cross section, smooth wall

$$\frac{U}{U_*} = 3.0 + 5.75 \log \frac{RU_*}{\nu} \tag{6-42}$$

circular cross section, rough wall

$$\frac{U}{U_*} = 6.5 + 5.75 \log \frac{R}{k_s} \tag{6-43}$$

very large rectangular cross section, rough wall

$$\frac{U}{U_*} = 6.00 + 5.75 \log \frac{R}{k_s} \tag{6-44}$$

rectangular cross section, rough wall and free surface

$$\frac{U}{U_*} = 6.25 + 5.75 \log \frac{R}{k_s} \tag{6-45}$$

where $R$ is the hydraulic radius, $U_*$ is the friction velocity and $\nu$ is the kinematic viscosity.

Equation 6-45 was presented by Keulegan (1938). The first parameter reflects the shape of the cross section. Coefficient 5.75 is a function of the universal constant $\kappa$ proposed by von Kármán (1930) and converts natural logs to logs. That is

$$\frac{2.3}{\kappa} = 5.75 \tag{6-46}$$

The semi-logarithmic formulas are widely used in hydraulics. They give a good approximation of the resistance to flow.

For practical use some of the parameters defined in a previous section are utilized in semi-logarithmic form.

From Chapter 3 (Simons and Sentürk, 1977) the logarithmic formula is

$$\frac{1}{\sqrt{f}} = 2.035 \log (R_e \sqrt{f}) - 0.91 \tag{6-47}$$

where $R_e = \frac{UR}{\nu}$ and $R$ are the hydraulic radius of the pipe or

$$\frac{1}{\sqrt{f}} = 2.0 \log (R_e \sqrt{f}) + 0.4 \tag{6-48}$$

where $R_e = \frac{Ur}{\nu}$ and r are the radius of the pipe. It is customary to express Equation 6-47 as

$$\frac{1}{\sqrt{f}} = 2.0 \log (R_e \sqrt{f}) - 0.8 \qquad (6\text{-}49)$$

Zegzhda (1939) was one of the first to attempt to apply these concepts to open channel flow. Since then extensive studies have been performed on this subject by many investigators. Their efforts to determine the Darcy-Weisbach parameter (f) are summarized in three categories.

1. The resistance to flow in open channels with fully developed roughness can be expressed by

$$\frac{1}{\sqrt{f}} = c \log (a \frac{R}{k_s}) \qquad (6\text{-}50)$$

where

$$\frac{k_s U_*}{\nu} > 70$$

2. The resistance in hydraulically smooth channels can be expressed as

$$\frac{1}{\sqrt{f}} = c \log (R_e \frac{\sqrt{f}}{b}) \qquad (6\text{-}51)$$

where

$$\frac{k_s U_*}{\nu} \leq 5$$

3. For "natural rough" (nonuniform grains) boundaries in the transition zone between hydraulically smooth boundaries and boundaries with fully developed roughness the equation

$$\frac{1}{\sqrt{f}} = c \log (a \frac{R}{k_s} + R_e \frac{\sqrt{f}}{b}) \qquad (6\text{-}52)$$

is applicable. In general, f is a function of the relative roughness, the Reynolds number, the shape of the cross section, and the parameters a, b, and c. For open channel, c is equal to 2.0 and 2.03. The proper values of a and b depend not only on the value of c, but also on the shape of the cross section of the channel. Table 6-2 shows the values of a and b for given values of c and cross sectional shape as suggested by various investigators. The only values applicable to the transition zone are those given by Colebrook and Bretting (1960) for circular channels. In Tables 6-3 and 6-4, Zegzhda (1938) and Ackers (1958) suggest $k_s$ values for rigid boundary conduits. However, for sand bed channels, Einstein (1950) suggested that $k \cong D_{65}$, Meyer-Peter (1948) suggests that $k_s \cong D_{90}$, and Simons and Richardson (1966) suggest that $k_s \cong D_{85}$.

Manning's Formula

In 1889 Manning presented an equation to approximate the average velocity in open channels (*). This formula defines the resistance to flow. The most useful forms are

$$U = \frac{1}{n} R^{2/3} S_E^{1/2} \qquad 6\text{-}30$$

in metric units, and

$$U = \frac{1.49}{n} R^{2/3} S^{1/2} \qquad 6\text{-}31$$

in English units.

Equation 6-30 can be transformed to

$$\frac{U}{U_*} = \frac{R}{n\sqrt{g}} \qquad (6\text{-}53)$$

for which n has the dimensions

$$|n| = TL^{-1/3} \qquad (6\text{-}54)$$

It is difficult to accept that n is a function of time. To overcome this anomaly it is customary to assume $n = \frac{n'}{\sqrt{g}}$. Substituting this value into Equation 6-54 yields

$$n' = L^{1/6} \qquad (6\text{-}55)$$

If n' is called n, Equation 6-55 becomes

$$n = L^{1/6} \qquad (6\text{-}56)$$

This dimension is accepted in general. The same result is achieved starting with Equation 6-45 which can be written as

(*)Manning's formula was first proposed in 1885 but was not published in its present form until 1889. Powel (1960) presented its chronological development as follows:

1868 - Gauckler proposed a formula of the form $U = \lambda R^{2/3} S^{1/2}$. This formula is valid for $S < 0.0007$.

1881 - Hagen, using the test results of Kutter, proposed the same formula for all values of S.

1885 - Manning proposed his formula.

1889 - Manning introduced barometric pressure in his formula $U = C\sqrt{RS}\,[R^{1/2} + \frac{0.22}{\sqrt{m}}(R - 0.15\ m)]$ where m is the atmospheric pressure in meters.

1890 - Flamant introduced Manning's formula in his book (1891).

1899 - Willcocks and Holt translate the formula into English units.

1911 - Buckley used the n values proposed by Flamant and the coefficient 1.486 to convert to English units.

$$\frac{U}{U_*} = 5.75 \log \frac{R}{k_s} \times 12.21 \qquad (6\text{-}57)$$

Combining Equations 6-57 and 6-53 yields

$$n\sqrt{g} = n' = \frac{\left(\frac{R}{k_s}\right)^{1/6}}{5.75 \log 12.21 \frac{R}{k_s}} k_s^{1/6}$$

or

$$n' = n = L^{1/6} \qquad 6\text{-}56$$

Also, Equation 6-53 can be written as

$$S = F_r^2 \frac{gn^2}{D^{1/3}} \left(\frac{D}{R}\right)^{1/3} \qquad (6\text{-}58)$$

Compared with Equation 6-6, Equation 6-58 shows that

$$n = f(R_e) \qquad (6\text{-}59)$$

However, n not only changes with Reynolds number but is a function of:

(1) the depth of flow
(2) the sediment transport (bed load, suspended load, and wash load)
(3) floating debris
(4) the geometry of the cross section
(5) the geometric pattern of scouring and silting in the channel
(6) the size of bed material
(7) the type and extent of vegetation on the banks
(8) the water temperature
(9) wind direction and magnitude.

In 1959 V. T. Chow published the detailed list of suggested n values given in Table 6-5.

The Chézy Formula

In 1769 Antoine Chézy a French engineer, was charged to study together with Leon Rodolphe Peronnet, navigation possibilities on the Canal de l'Yvette. He developed a simple formula for determining the average velocity in this water course. This formula is widely recognized by engineers. Chézy assumed that the drag force may be expressed in terms of the dynamic variables of resistance, viscosity and velocity i.e.,

$$\tau_o = f\rho \frac{U^2}{8} \qquad (6\text{-}60)$$

Table 6-5. Values of the roughness coefficient n (after Chow, 1959).

| Type of Channel and Description | Minimum | Normal | Maximum |
|---|---|---|---|
| A. Closed Conduits Flowing Partly Full | | | |
| A-1. Metal | | | |
| a. Brass, smooth | 0.009 | 0.010 | 0.013 |
| b. Steel | | | |
| 1. Lockbar and welded | 0.010 | 0.012 | 0.014 |
| 2. Riveted and spiral | 0.013 | 0.016 | 0.017 |
| c. Cast iron | | | |
| 1. Coated | 0.010 | 0.013 | 0.014 |
| 2. Uncoated | 0.011 | 0.014 | 0.016 |
| d. Wrought iron | | | |
| 1. Black | 0.012 | 0.014 | 0.015 |
| 2. Galvanized | 0.013 | 0.016 | 0.017 |
| e. Corrugated metal | | | |
| 1. Subdrain | 0.017 | 0.019 | 0.021 |
| 2. Storm drain | 0.021 | 0.024 | 0.030 |
| A-2. Nonmetal | | | |
| a. Lucite | 0.008 | 0.009 | 0.010 |
| b. Glass | 0.009 | 0.010 | 0.013 |
| c. Cement | | | |
| 1. Neat surface | 0.010 | 0.011 | 0.013 |
| 2. Mortar | 0.011 | 0.013 | 0.015 |
| d. Concrete | | | |
| 1. Culvert, straight and free of debris | 0.010 | 0.011 | 0.013 |
| 2. Culvert with bends, connections, and some debris | 0.011 | 0.013 | 0.014 |
| 3. Finished | 0.011 | 0.012 | 0.014 |
| 4. Sewer with manholes, inlet, etc., straight | 0.013 | 0.015 | 0.017 |
| 5. Unfinished, steel form | 0.012 | 0.013 | 0.014 |
| 6. Unfinished, smooth wood form | 0.012 | 0.014 | 0.016 |
| 7. Unfinished, rough wood form | 0.015 | 0.017 | 0.020 |
| e. Wood | | | |
| 1. Stave | 0.010 | 0.012 | 0.014 |
| 2. Laminated, treated | 0.015 | 0.017 | 0.020 |
| f. Clay | | | |
| 1. Common drainage tile | 0.011 | 0.013 | 0.017 |
| 2. Vitrified sewer | 0.011 | 0.014 | 0.017 |
| 3. Vitrified sewer with manholes, inlet, etc. | 0.013 | 0.015 | 0.017 |
| 4. Vitrified subdrain with open joint | 0.011 | 0.016 | 0.015 |
| g. Brickwork | | | |
| 1. Glazed | 0.011 | 0.013 | 0.015 |
| 2. Lined with cement mortar | 0.012 | 0.015 | 0.017 |
| h. Sanitary sewers coated with sewage slimes with bends and connections | 0.012 | 0.013 | 0.016 |

Table 6-5. (Continued)

| Type of Channel and Description | Minimum | Normal | Maximum |
|---|---|---|---|
| i. Paved invert, sewer, smooth bottom | 0.016 | 0.019 | 0.020 |
| j. Rubble masonry, cemented | 0.018 | 0.025 | 0.030 |
| B. Lined or Built-Up Channels | | | |
| B-1. Metal | | | |
| a. Smooth steel surface | | | |
| 1. Unpainted | 0.011 | 0.012 | 0.014 |
| 2. Painted | 0.012 | 0.013 | 0.017 |
| b. Corrugated | 0.021 | 0.025 | 0.030 |
| B-2. Nonmetal | | | |
| a. Cement | | | |
| 1. Neat, surface | 0.010 | 0.011 | 0.013 |
| 2. Mortar | 0.011 | 0.013 | 0.015 |
| b. Wood | | | |
| 1. Planed, untreated | 0.010 | 0.012 | 0.014 |
| 2. Planed, creosoted | 0.011 | 0.012 | 0.015 |
| 3. Unplaned | 0.011 | 0.013 | 0.015 |
| 4. Plank with battens | 0.012 | 0.015 | 0.018 |
| 5. Lined with roofing paper | 0.010 | 0.014 | 0.017 |
| c. Concrete | | | |
| 1. Trowel finish | 0.011 | 0.013 | 0.015 |
| 2. Float finish | 0.013 | 0.015 | 0.016 |
| 3. Finished, with gravel on bottom | 0.015 | 0.017 | 0.020 |
| 4. Unfinished | 0.014 | 0.017 | 0.020 |
| 5. Gunite, good section | 0.016 | 0.019 | 0.023 |
| 6. Gunite, wavy section | 0.018 | 0.022 | 0.025 |
| 7. On good excavated rock | 0.017 | 0.020 | |
| 8. On irregular excavated rock | 0.022 | 0.027 | |
| d. Concrete bottom float finished with sides of | | | |
| 1. Dressed stone in mortar | 0.015 | 0.017 | 0.020 |
| 2. Random stone in mortar | 0.017 | 0.020 | 0.024 |
| 3. Cement rubble masonry, plastered | 0.016 | 0.020 | 0.024 |
| 4. Cement rubble masonry | 0.020 | 0.025 | 0.030 |
| 5. Dry rubble or riprap | 0.020 | 0.030 | 0.035 |
| e. Gravel bottom with sides of | | | |
| 1. Formed concrete | 0.017 | 0.020 | 0.025 |
| 2. Random stone in mortar | 0.020 | 0.023 | 0.026 |
| 3. Dry rubble or riprap | 0.023 | 0.033 | 0.036 |
| f. Brick | | | |
| 1. Glazed | 0.011 | 0.013 | 0.015 |
| 2. In cement mortar | 0.012 | 0.015 | 0.018 |
| g. Masonry | | | |
| 1. Cemented rubble | 0.017 | 0.025 | 0.030 |
| 2. Dry rubble | 0.023 | 0.032 | 0.035 |
| h. Dressed ashlar | 0.013 | 0.015 | 0.017 |

Table 6-5. (Continued)

| Type of Channel and Description | Minimum | Normal | Maximum |
|---|---|---|---|
| i. Asphalt | | | |
| 1. Smooth | 0.013 | 0.013 | |
| 2. Rough | 0.016 | 0.016 | |
| j. Vegetal lining | 0.030 | --- | 0.500 |
| C. Excavated or Dredged | | | |
| a. Earth, straight and uniform | | | |
| 1. Clean, recently completed | 0.016 | 0.018 | 0.020 |
| 2. Clean, after weathering | 0.018 | 0.022 | 0.025 |
| 3. Gravel, uniform section, clean | 0.022 | 0.025 | 0.030 |
| 4. With short grass, few weeds | 0.022 | 0.027 | 0.033 |
| b. Earth, winding and sluggish | | | |
| 1. No vegetation | 0.023 | 0.025 | 0.030 |
| 2. Grass, some weeds | 0.025 | 0.030 | 0.033 |
| 3. Dense weeds or aquatic plants in deep channels | 0.030 | 0.035 | 0.040 |
| 4. Earth bottom and rubble sides | 0.028 | 0.030 | 0.035 |
| 5. Stony bottom and weedy banks | 0.025 | 0.035 | 0.040 |
| 6. Cobble bottom and clean sides | 0.030 | 0.040 | 0.050 |
| c. Dragline-excavated or dredged | | | |
| 1. No vegetation | 0.025 | 0.028 | 0.033 |
| 2. Light brush on banks | 0.035 | 0.050 | 0.060 |
| d. Rock cuts | | | |
| 1. Smooth and uniform | 0.025 | 0.035 | 0.040 |
| 2. Jagged and irregular | 0.035 | 0.040 | 0.050 |
| e. Channels not maintained, weeds and brush uncut | | | |
| 1. Dense weeds, high as flow depth | 0.050 | 0.080 | 0.120 |
| 2. Clean bottom, brush on sides | 0.040 | 0.050 | 0.080 |
| 3. Same, highest stage of flow | 0.045 | 0.070 | 0.110 |
| 4. Dense brush, high stage | 0.080 | 0.100 | 0.140 |
| D. Natural Streams (*) | | | |
| D-1. Minor streams (top width at flood stage < 100 ft) | | | |
| a. Streams on plain | | | |
| 1. Clean, straight, full stage, no rifts or deep pools | 0.025 | 0.030 | 0.033 |
| 2. Same as above, but more stones and weeds | 0.030 | 0.035 | 0.040 |
| 3. Clean, winding, some pools and shoals | 0.033 | 0.040 | 0.045 |
| 4. Same as above, but some weeds and stones | 0.035 | 0.045 | 0.050 |
| 5. Same as above, lower stages, more ineffective slopes and section | 0.040 | 0.048 | 0.055 |
| 6. Same as 4, but more stones | 0.045 | 0.050 | 0.060 |

(*)Also refer to Barne's work (1967).

Table 6-5. (Continued)

| Type of Channel and Description | Minimum | Normal | Maximum |
|---|---|---|---|
| 7. Sluggish reaches, weedy, deep pools | 0.050 | 0.070 | 0.080 |
| 8. Very weedy reaches, deep pools, or floodways with heavy stand of timber and underbrush | 0.075 | 0.100 | 0.150 |
| b. Mountain streams, no vegetation in channel, banks usually steep, trees and brush along banks submerged at high stages | | | |
| 1. Bottom: gravels, cobbles and few boulders | 0.030 | 0.040 | 0.050 |
| 2. Bottom: cobbles with large boulders | 0.040 | 0.050 | 0.070 |
| D-2. Flood plains | | | |
| a. Pasture, no brush | | | |
| 1. Short grass | 0.025 | 0.030 | 0.035 |
| 2. High grass | 0.030 | 0.035 | 0.050 |
| b. Cultivated areas | | | |
| 1. No crop | 0.020 | 0.030 | 0.040 |
| 2. Mature row crops | 0.025 | 0.035 | 0.045 |
| 3. Mature field crops | 0.030 | 0.040 | 0.050 |
| c. Brush | | | |
| 1. Scattered brush, heavy weeds | 0.035 | 0.050 | 0.070 |
| 2. Light brush and trees in winter | 0.035 | 0.050 | 0.060 |
| 3. Light brush and trees in summer | 0.040 | 0.060 | 0.080 |
| 4. Medium to dense brush in winter | 0.045 | 0.070 | 0.110 |
| 5. Medium to dense brush in summer | 0.070 | 0.100 | 0.160 |
| d. Trees | | | |
| 1. Dense willows, summer, straight | 0.110 | 0.050 | 0.200 |
| 2. Cleared land with tree stumps, no sprouts | 0.030 | 0.040 | 0.050 |
| 3. Same as above, but with heavy growth of sprouts | 0.050 | 0.060 | 0.080 |
| 4. Heavy stand of timber, a few down trees, little undergrowth, flood stage below branches | 0.080 | 0.100 | 0.120 |
| 5. Same as above, but with flood stage reaching branches | 0.100 | 0.120 | 0.160 |
| D-3. Major streams (top width at flood stage > 100 ft). The n value is less than that for minor streams of similar description because banks offer less effective resistance. | | | |
| a. Regular section with no boulders or brush | 0.025 | --- | 0.060 |
| b. Irregular and rough section | 0.035 | --- | 0.100 |

This relation may be applied equally well to flow in open channels, and pipes if the Darcy-Weisbach resistance coefficient (f) is evaluated properly for the different flow characteristics and the different shapes of channels.

Substituting Equation 6-60 into Equations 6-14 and 6-12 and rearranging gives

$$U = \sqrt{\frac{8\gamma}{f\rho}}\sqrt{RS_E} \qquad (6\text{-}61)$$

or

$$U = C\sqrt{RS_E} \qquad 6\text{-}24$$

with

$$C = \sqrt{\frac{8\gamma}{f\rho}} \qquad (6\text{-}62)$$

The term (C) is called Chézy's coefficient of resistance. It has the dimensions

$$C = \left|\frac{L^{1/2}}{T}\right|$$

But it is possible to define a dimensionless coefficient by assuming

$$C = C'\sqrt{g} \qquad 6\text{-}26$$

where C' is dimensionless.

Combining Equations 6-22, 6-28, and 6-45 yields

$$\frac{C}{\sqrt{g}} = 6.25 + 5.75 \log \frac{R}{k_s} + 5.75 \log 12.21 \frac{R}{k_s} \qquad (6\text{-}63)$$

and assuming g = 9.81, Equation 6-63 takes the form

$$C = 18 \log 12.21 \frac{R}{k_s} \qquad (6\text{-}64)$$

or

$$C = 18 \log 12.21 \frac{RU_*}{\nu} \times \frac{\nu}{k_s U_*}$$

Einstein has added a correction factor x to this formula and he changed it slightly as shown in Equation 6-79. Utilizing this relation Equation 6-64 yields

$$C = 18 \log 12.27 \frac{RU_*}{\nu} - 18 \log \frac{k_s U_*}{\nu} + 18 \log x \qquad (6\text{-}65)$$

where x is a function of $\frac{k_s U_*}{\nu}$; see Figure 6-2. The variation of Chézy's coefficient is shown in Figure 6-3.

A close examination of Figure 6-3 reveals that:

1. For values of $\frac{RU_*}{\nu} > 70$ the radius of curvature of the curves increases very rapidly and for $\frac{RU_*}{\nu} > 500$ it is practically equal to infinity.

2. For values of $\frac{kU_*}{\nu} < 3.63$ the bed is considered hydraulically smooth, the representative curves terminate when $\frac{k_s}{\delta} = 0.3129$.

3. The representative curves cross the axis of abscissa at different points according to different values of $\frac{RU_*}{\nu}$. However, $C = 0$ is a condition that cannot be realized.

4. It was shown in Chapter 3 (Simons and Sentürk, 1977) that for a surface to be hydraulically smooth it is sufficient that

$$\frac{U_* k_s}{\nu} \leq 5 \quad \text{or} \quad k_s \leq \frac{5\nu}{U_*} \qquad (6\text{-}66)$$

This condition leads to

$$k_s = \frac{5C\,\nu}{\sqrt{g}\,U}$$

Schlichting (1955) gives

$$k_s = 100 \frac{\nu}{U} \qquad (6\text{-}67)$$

for the average condition of a hydraulically smooth surface. Using this relation

$$\frac{U}{U_*} = 100 \frac{\nu}{U_*} \frac{1}{k_s}$$

or

$$\frac{C}{\sqrt{g}} = 100 \frac{1}{\frac{k_s U_*}{\nu}} \qquad (6\text{-}68)$$

Substituting the value of $\frac{k_s U_*}{\nu}$ taken from Equation 6-66 in Equation 6-68 yields

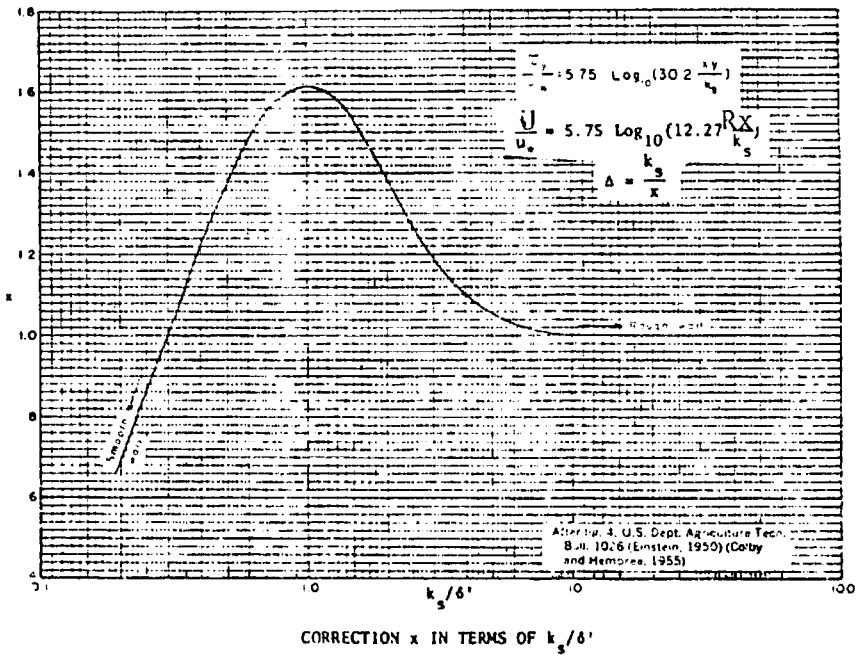


CORRECTION x IN TERMS OF $k_s/\delta'$

Figure 6-2. Correction factor in the logarithmic velocity distribution.

$$C = 113.5$$

in English units, and

$$C = 62.64$$

in metric units. This value of C corresponds to $\frac{RU_*}{\nu} \cong 1000$.

Strickler's Formula, Manning-Strickler's Formula, Lane's Formula

Strickler (1923) defined Manning's n as a function of particle size

$$n = \frac{D^{1/6}}{21.1} \tag{6-69}$$

where D represents the diameter in mm of the uniform sand used in performing the study. The experiments were conducted in a small flume, which had the experimental sand pasted on the bottom and walls. For that reason this equation cannot be used to predict the resistance to flow with a mobile bed.

Meyer-Peter and Müller (1948), considering a sand mixture, transformed Strickler's formula to

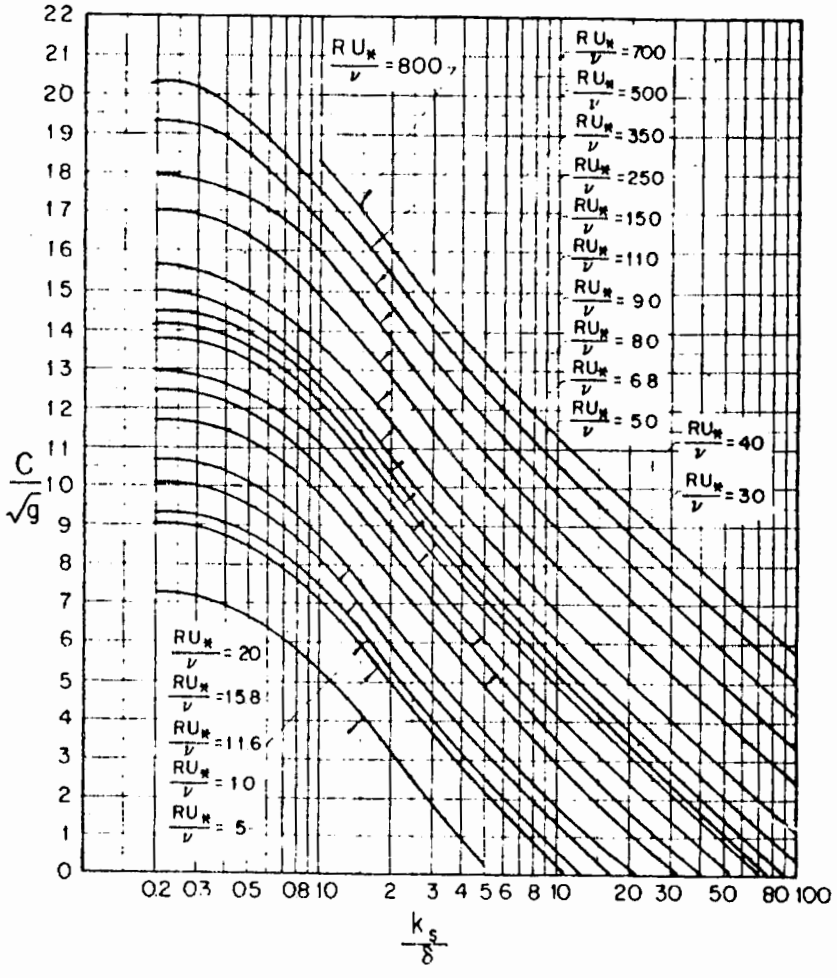


Figure 6-3. Variation of Chezy's coefficient as a function of $\frac{RU_*}{\nu}$, $\frac{k_s U_*}{\nu}$ and $\frac{k_s}{\delta}$.

$$n = \frac{D1/6}{90/26} \quad \text{(in metric units, D in m)} \tag{6-69a}$$

Different forms of Strickler's formula follows

$$n = \frac{D_{50}^{1/6}}{31.3} = 0.032\, D_{50}^{1/6} \quad (D_{50} \text{ in ft}) \tag{6-69b}$$

$$n = \frac{D_{65}^{1/6}}{75.75} = 0.0132\, D_{65}^{1/6} \quad (D_{65} \text{ in mm}) \tag{6-69c}$$

Keulegan (1938)

$$n = \frac{D_{50}^{1/6}}{46.9} \quad (D_{50} \text{ in ft}) \tag{6-69d}$$

in (1949) he suggested

$$n = \frac{D_{90}^{1/6}}{49.0} \quad (D_{90} \text{ in ft}) \tag{6-69e}$$

$$n = \frac{D_{65}^{1/6}}{29.3} \quad (D_{65} \text{ in ft}) \tag{6-69f}$$

This equation can be used to approximate Manning's coefficient when the bed is not paved with cobbles. Table 6-6 compares the results obtained by direct application of Equation 6-69a with corresponding measured values.

Lane and Carlson (1953), as a result of their San Luis Valley study, suggested the formula

$$n = \frac{D_{75}^{1/6}}{39} \tag{6-70}$$

where $D_{75}$ is measured in inches. The beds of the canals studied were paved with cobbles.

Substituting the value of n given by Equation 6-69a in Manning's equation yields

$$U = \frac{26}{g^{1/2}} R^{1/2} \left(\frac{R}{D_{90}}\right)^{1/6} S^{1/2}\, g^{1/2} \tag{6-71}$$

or

$$\frac{U}{U_*} = \frac{26}{g^{1/2}} \left(\frac{R}{D_{90}}\right)^{1/6} = 8.30 \left(\frac{R}{D_{90}}\right)^{1/6} \quad (*) \tag{6-72}$$

(*)The coefficient 8.30 in Equation 6-72 is obtained when working in metric measurements.

Table 6-6. Comparison of computed values of n determined from equation 69a with corresponding measured values (*).

| Name of River | $D90^{mm}$ (**) | n Computed | Measured |
|---|---|---|---|
| Clark Fork at St. Regis, Montana | | 0.030 | 0.028 |
| Clark Fork above Missoula, Montana | | 0.032 | 0.030 |
| Blackfoot River near Ovando, Montana | 280 | 0.031 | 0.031 |
| Coeur d'Alene River near Prichard | 650 | 0.036 | 0.032 |
| West Fork Bitterroot River near Conner, Montana | 265 | 0.031 | 0.036 |
| Wenatchee River at Plaine, Washington | 320 | 0.032 | 0.037 |
| Spokane River at Spokane, Washington | 360 | 0.032 | 0.038 |
| Middle Fork Flathead River near Essex, Montana | 285 | 0.031 | 0.041 |
| Grande Ronde River at la Grande, Oregon | 157 | 0.028 | 0.043 |
| Provo River near Hailstone, Utah | 310 | 0.032 | 0.045 - 0.073 |
| South Fork Clearwater River near Grangeville, Idaho | 440 | 0.034 | 0.051 |
| East Branch Au Sable River at Au Sable Forks, New York | 1500 | 0.041 | 0.055 |
| Rock Creek Canal near Darby, Montana | 375 | 0.033 | 0.060 |
| Merced River at Happy Isles Bridge near Yosemite, California | 550 | 0.035 | 0.065 |
| Boundary Creek near Porthill, Idaho | 375 | 0.033 | 0.073 |
| Rock Creek near Darby, Montana | 415 | 0.033 | 0.075 |

(*)Geological Survey Water-Supply Paper 1849 "Roughness Characteristics of Natural Channels."

(**)$D_{90}$ is assumed equal to $D_{84}$ (the value used in the original paper) and the $D_{84}$ value is introduced in Equation 69a. $D_{90}$ is in mm.

Equation 6-72 is called Manning-Strickler's equation and for the general case can be written as

$$U = \frac{C}{D^m} R^{(1/2 + m)} S^{1/2} \qquad (6\text{-}73)$$

where D is the representative diameter of the bed material in meters or feet. For C = 26 and m = $\frac{1}{6}$, Equation 6-73 reduces to Equation 6-71.

Monomial Type Formulas Describing the Resistance to Flow in General

The Monomial type formula has the form

$$\frac{U}{U_*} = k \left(\frac{R}{D_{90}}\right)^{1/m} \qquad (6\text{-}74)$$

Coefficient k and parameter m may be determined for each particular case. For values of k and m equal to 8.30 and 6, respectively. Equation 6-74 reduces to Manning-Strickler's formula given by Equation 6-72.

Lindquist (1933) gave Equation 6-74 with m = 6. Keulegan (1938) studied the variation of the resistance to flow and developed Equations 6-74 and 6-45. Eliminating $U/U_*$ between these relations yields

$$k \left(\frac{R}{D_{90}}\right)^{1/m} = 6.25 + 5.75 \log \frac{R}{D_{90}}$$

For m = 6, the mean value of k derived from this relation is 8.12(*), then Equation 6-74 becomes

$$\frac{U}{U_*} = 8.12 \left(\frac{R}{k_s}\right)^{1/6} \qquad (6\text{-}75)$$

Equation 6-75 can be used to estimate the resistance to flow for natural channels.

It is interesting to study the variation of the parameter m with the relative roughness. Figure 6-4 shows the variation of Equation 6-74 when written as

$$\log \frac{U}{U_*} = \log k + \frac{1}{m} \log \left(\frac{R}{D_{90}}\right) \qquad (6\text{-}76)$$

For k = 8.12 and m = 6, Equation 6-76 is plotted on Figure 6-4 yielding the straight line 1.1. If the flow takes place on a wide bed with flat bottom and a uniform roughness the characteristics of the flow can be expressed by Equation 6-45. For this case refer to curve 3.3 on Figure 6-4.

(*)cf. Figure 6-3.

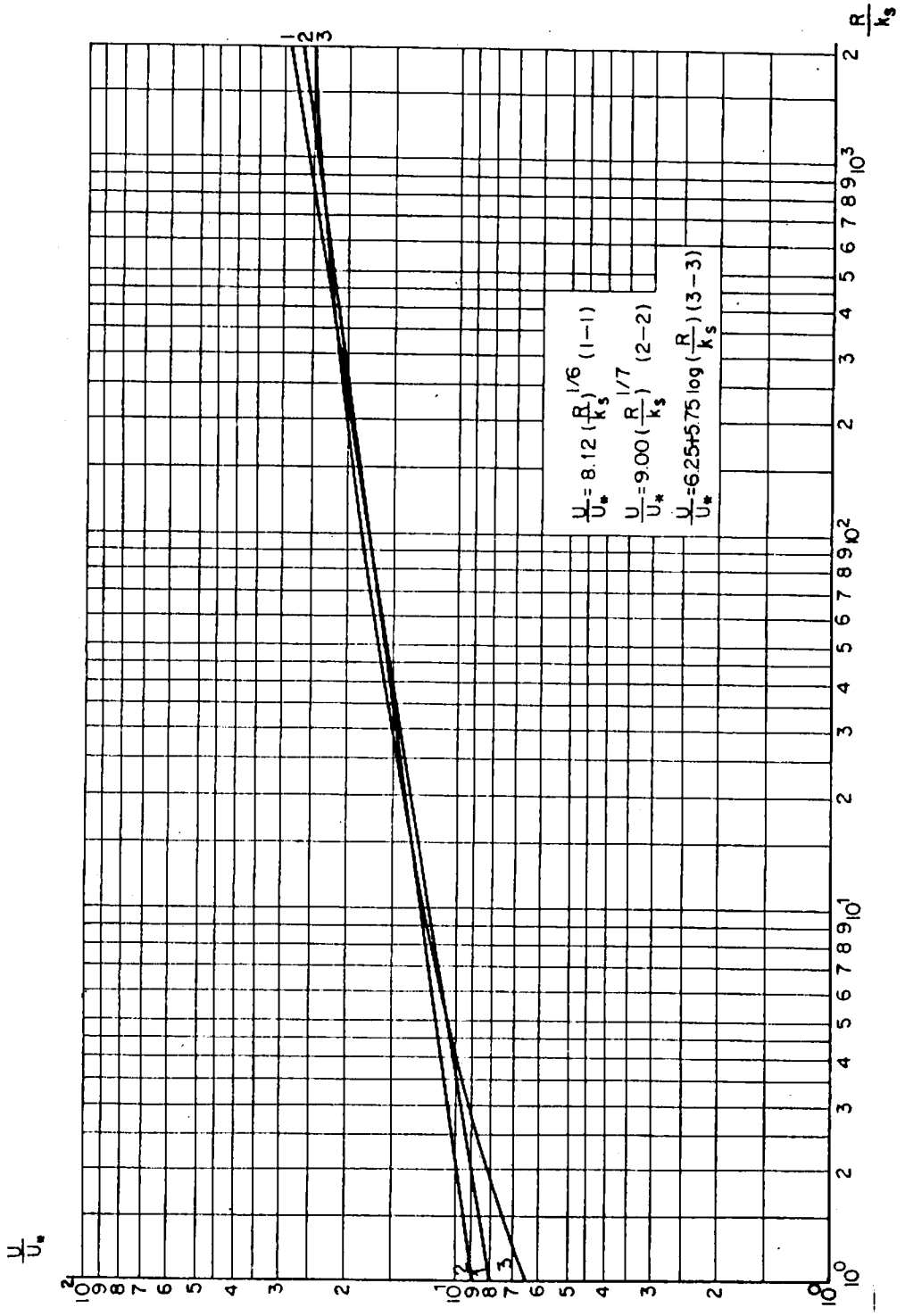


Figure 6-4. Variation of resistance to flow expressed by monomial type equations.

There is a difference between the straight line 1.1 and the curve 3.3, due to the variation in the value of the parameter m. In addition the straight line 2.2 represents Equation 6-77.

$$\frac{U}{U_*} = 9.0 \left(\frac{R}{k_s}\right)^{1/7} \tag{6-77}$$

There is an apparent overlapping of these three representative relations when

$$15 < \frac{R}{k_s} < 500 \tag{6-78}$$

Hence, it is possible to use Equation 6-77 or Equation 6-75 to define the resistance to flow in natural channels. An experimental method can be derived based on the preceding relations. If k and m in Equation 6-74 are determined directly in situ a monomial formula representing the variation of the resistance in this particular river can be obtained. This type of relation is very useful in physical and mathematical model studies. Utilizing field measurements and observations, engineering model studies can be conducted easily and accurately if the resistance to flow can be approximated by a monomial type formula. Example A illustrates this approach.

Example A

Extensive measurements were made on the Göksu River, Turkey, to define the variation of resistance to flow. Using these data determine the monomial formula representing this variation and compare the results obtained with results when utilizing different resistance formulas.

Data: The river data obtained by direct measurements are given in the following tables.

Table 6-7. Flow characteristics of the Göksu River, Turkey.

| U(m/sec) | R(m) | S | Q($m^3$/sec) |
|---|---|---|---|
| 0.37 | 0.94 | 0.0001112 | 24 |
| 0.45 | 1.08 | 0.0001125 | 42 |
| 0.70 | 1.37 | 0.0001800 | 83 |
| 1.00 | 1.64 | 0.0003000 | 148 |
| 1.44 | 2.09 | 0.0004280 | 270 |

Table 6-8. Sediment characteristics of the Goksu River, Turkey.

| | | | |
|---|---|---|---|
| $D_{35}$ = 0.0015 m | $D_{65}$ = 0.0027 m | $D_{90}$ = 0.003 m | $\gamma'_s$ = 1.7 t/$m^3$ |

Solution:

Values of $\frac{U}{U_*}$ and $\frac{R}{D_{90}}$ are computed and listed in Table 6-9.

Table 6-9. Values of $\frac{U}{U_*}$ and $\frac{R}{D_{90}}$, Göksu River, Turkey.

| U m/sec | R m | S | $U_*$ m/sec | $U/U_*$ | $R/D_{90}$ |
|---|---|---|---|---|---|
| 0.37 | 0.94 | 0.000112 | 0.03214 | 11.51 | 313 |
| 0.45 | 1.08 | 0.000113 | 0.03460 | 13.01 | 360 |
| 0.70 | 1.37 | 0.000180 | 0.04918 | 14.23 | 457 |
| 1.00 | 1.64 | 0.000300 | 0.06947 | 14.39 | 547 |
| 1.44 | 2.09 | 0.000428 | 0.09368 | 15.37 | 697 |

Values of $\frac{U}{U_*}$ and $\frac{R}{D_{90}}$ taken from Table 6-9 are plotted on Figure 6-5 as ordinate and abscissa values. The straight line representing the variation of the resistance of the Göksu River in this reach is then the straight line A-A shown in Figure 6-5. The monomial type formula corresponding to A-A in Figure 6-5 is

$$\frac{U}{U_*} = 4.6 \left(\frac{R}{D_{90}}\right)^{1/5.64}$$

The variation of the resistance characteristics computed using Manning's formula and Chézy's formula are tabulated in Table 6-10.

Table 6-10. Variation of coefficients n and c.

| U m/sec | C | n |
|---|---|---|
| 0.37 | 36.66 | 0.027 |
| 0.45 | 42.20 | 0.024 |
| 0.70 | 44.66 | 0.0236 |
| 1.0 | 45.25 | 0.024 |
| 1.44 | 49.16 | 0.023 |

Considering Strickler's formula

$$n = \frac{D_{90}^{1/6}}{26} = 0.015 \qquad (6\text{-}69a)$$

Utilizing the semi-logarithmic resistance formula

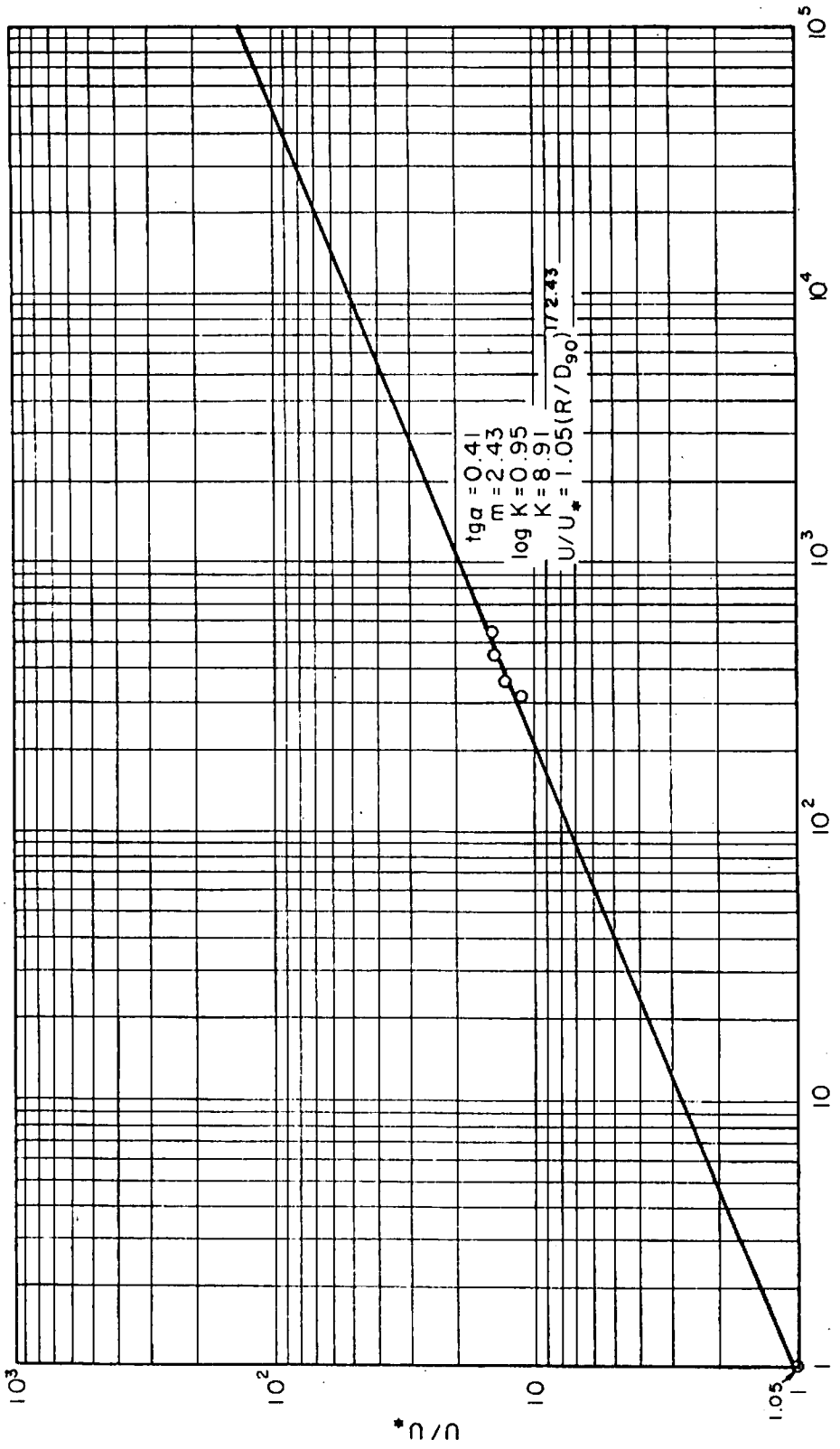


Figure 6-5. Variation of the resistance to flow for the Göksu River, Turkey.

$$C = 18 \log 12.21 \frac{RU_*}{\nu} - 18 \log \frac{D_{65}U_*}{\nu} + 18 \log x \qquad 6\text{-}65$$

and substituting the values of $\frac{RU_*}{\nu}$, $\frac{D_{65}U_*}{\nu}$ and $x$ based upon the data of Example A yields the results presented in Table 6-11.

Table 6-11. Variation of Chezy's and Manning's roughness coefficients computed from the semi-logarithmic relation, $\nu = 10^{-6}$ $m^2$/sec.

| R(m) | S | $U_*$(m/sec) | $\frac{RU_*}{\nu}$ | $\frac{D_{65}U_*}{\nu}$ | x | C | n |
|---|---|---|---|---|---|---|---|
| 0.94 | 0.000112 | 0.03214 | 30212 | 87 | 1 | 65.3 | 0.01516 |
| 1.08 | 0.000113 | 0.03460 | 37368 | 93 | 1 | 66.4 | 0.01525 |
| 1.37 | 0.000180 | 0.04918 | 67377 | 133 | 1 | 68.3 | 0.01543 |
| 1.64 | 0.000300 | 0.06947 | 113931 | 188 | 1 | 69.7 | 0.01558 |
| 2.09 | 0.000428 | 0.09368 | 195791 | 253 | 1 | 71.6 | 0.01579 |

Table 6-12 summarizes the results obtained using the different approaches.

Other Flow Formulas

Several investigators have suggested different formulas to determine the characteristics of the flow in open channels. Others have tried to define Chézy's coefficient C.

The performance of large concrete-lined irrigation canals was investigated by the U. S. Bureau of Reclamation (Tilp and Scrivner, 1964). As a result of its canal capacity test program, a design procedure was presented that utilizes the Manning equation. The Bureau's design procedure employs Figures 6-6, 6-7, and 6-8. The procedure suggested for design is outlined:

1. Determine the preliminary canal section using Manning's formula and assuming n from Figure 6-6.

2. Assume the water temperature that will exist at design flow and compute Reynolds number $R_e = 4RU/\nu$ for the preliminary section.

3. Enter Figure 6-7 with the computed value of $R_e$, project a vertical line upward to the average data curve, mark the intersection point 1 and read the value of f.

4. Enter Figure 6-7 with the value of f and locate point 2 at the intersection with the hydraulic radius line from the preliminary section.

5. Project a vertical line from point 2 and read Manning's n from the linear scale. If the n value from Figure 6-8 does not agree with the assumed value, repeat steps 1 through 5 with the value indicated by Figure 6-8.

In applying this method, the Reynolds number $R_e$, the slope S, and the Darcy-Weisbach friction factor f are dimensionless, the hydraulic radius R is in feet, the kinematic viscosity v has the units $ft^2/sec$, the average velocity U is in ft/sec, and the gravitational acceleration g is 32.2 $ft/sec^2$. For greater detail, refer to Tilp and Scrivner (1964).

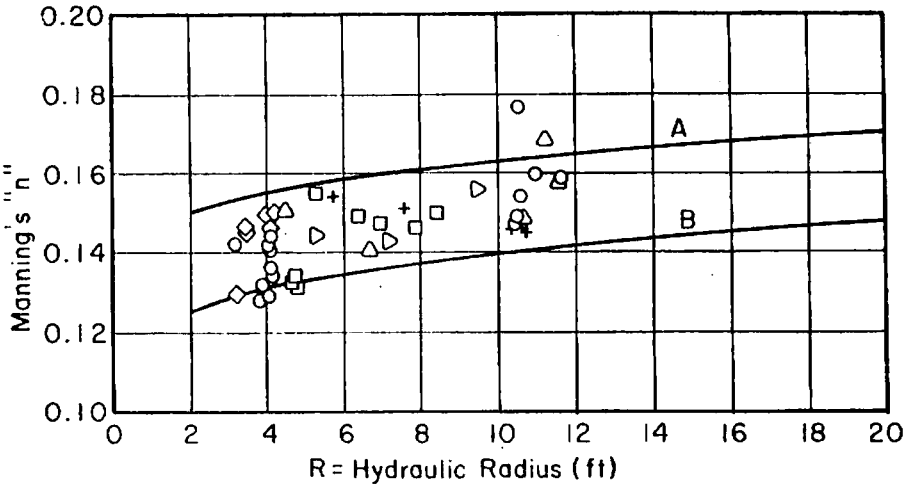


NOTES:

Curve A K = 0.010 ft Precast Pipe with Mortar Squeeze at Joints. Brick in Concrete Mortar (Normal Example).

Curve B K = 0.002 ft Monolithic Construction against Steel Forms Smooth Troweled Surface (Normal Example).

Figure 6-6. Relation between Manning's n and hydraulic radius R for different rigid surfaces (Tilp and Scrivner, 1964).

## 6.4 RESISTANCE TO FLOW IN SAND BED CHANNELS

The monomial formula expressing the variation of the resistance to flow for the Göksu River is based upon experimental results and closely approximates the measured values of resistance. Large discrepancies exist between the values of the resistance computed from Manning-Strickler's formula, the semi-logarithmic formula and the measured values of the resistance. In this particular case the Manning-Strickler formula and the semi-logarithmic formula give similar results. The difference between the measured and computed values of n may be attributed to the existence of bed forms and bars in the channel.

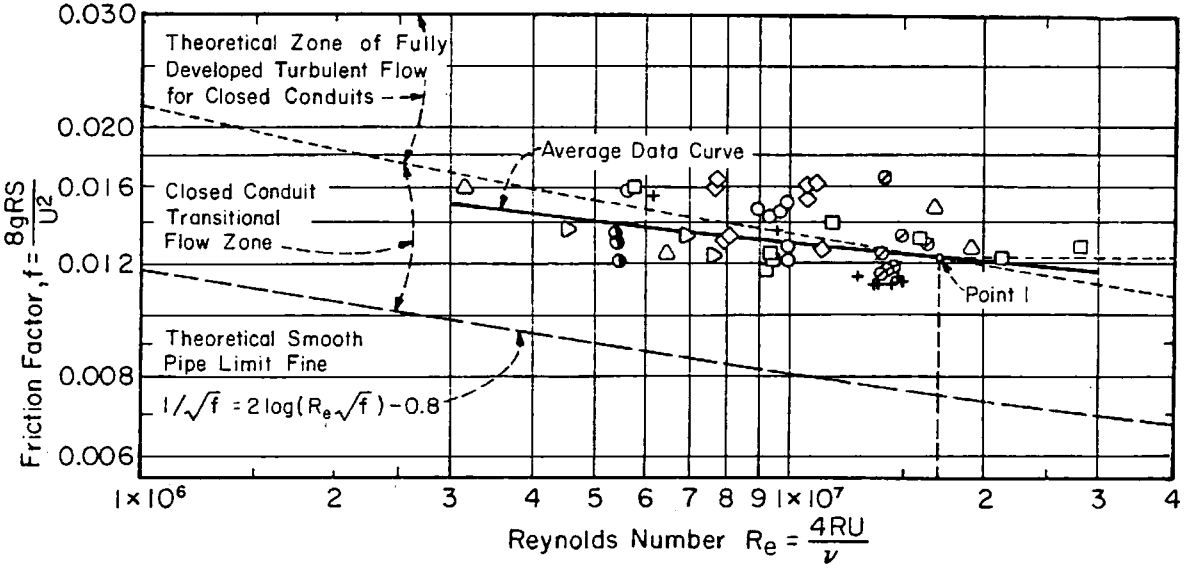


Figure 6-7. Resistance diagram showing the relation between friction factor f and Reynolds number $R_e$ for straight reaches of all canals (Tilp and Scrivner, 1964).

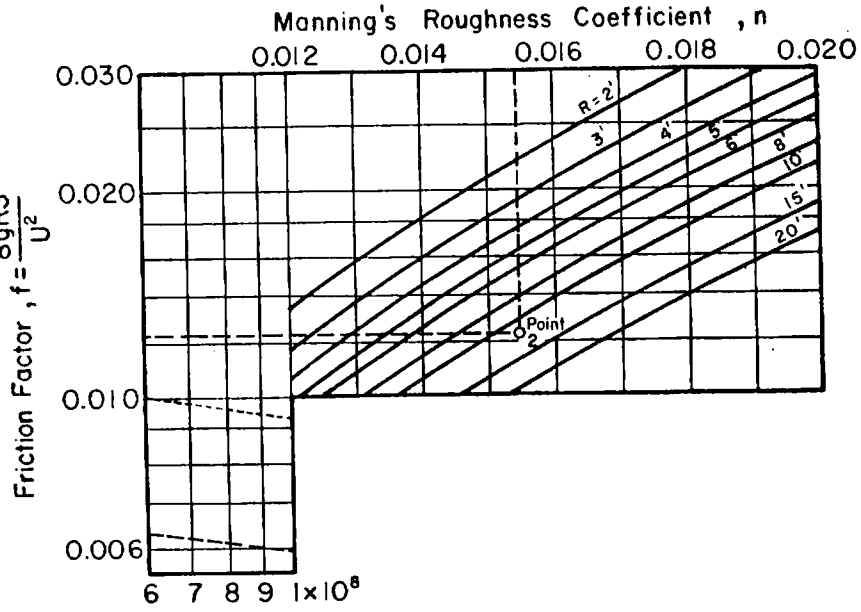


Figure 6-8. Resistance diagram showing the relation between friction factor f and Manning's roughness coefficient n for straight reaches of all canals (Tilp and Scrivner, 1964).

Table 6-12. Comparison of results obtained by application of different resistance formulas with measured values $U/U_*$.

| R(m) | Monomial Formula | Manning-Strickler Formula | Logarithmic Formula | Measured Value |
|---|---|---|---|---|
| 0.94 | 12.74(11)(*) | 21.63(88)(*) | 20.85(81)(*) | 11.51 |
| 1.08 | 13.06(0) (*) | 22.14(70)(*) | 21.20(63)(*) | 13.01 |
| 1.37 | 13.62(4) (*) | 23.03(62)(*) | 21.81(53)(*) | 14.23 |
| 1.64 | 14.07(2) (*) | 23.73(65)(*) | 22.25(55)(*) | 14.39 |
| 2.09 | 14.68(4) (*) | 24.71(61)(*) | 22.78(48)(*) | 15.37 |

(*)Values between brackets show the discrepancies from the measured values in percent.

Einstein's Approach for Solving the Problem of Resistance to Flow Over Movable Boundaries with Bed Forms

Einstein (1950) presented two relations for solving the problem of resistance to flow with movable boundaries and bed forms. The first relation applies to the resistance due to skin friction; the second utilizes graphics to define the resistance to flow caused by bed forms.

The first expression is similar to Equation 6-45 and is written

$$\frac{U}{U'_*} = 5.75 \log (12.27 \frac{R'}{k_s} x) \qquad (6\text{-}79)$$

where x is a correction factor that compensates for conditions where the channel bed is not fully rough. The value of x is given in Figure 6-2 as a function of $\frac{k_s}{\delta}$. The $\delta$ value is the thickness of the laminar sublayer equal to $\frac{11.6\nu}{U'_*}$. Due to the presence of suspended sediment, Equation 6-79 may require modification. When U is known, Equation 6-79 yields the value of R'.

The second component of the resistance is due to the effect of the bed forms. This form roughness or form drag is a function of flow. A small change in any variable affecting the form of bed roughness will cause a change in the bed roughness and the resistance to flow. Einstein (1950) pointed out that the form drag was related to the total sediment transport. Hence, he suggested a functional relation

$$\frac{U}{U''_*} = \phi(\psi') \qquad (6\text{-}80)$$

where $\psi'$ is the intensity of shear on the representative particles and

$$\psi' = \frac{\gamma_s - \gamma}{\gamma} \frac{D_{35}}{SR'} = \frac{\gamma'_s}{\gamma} \frac{D_{35}}{SR'} \qquad (6\text{-}81)$$

also $\psi'$ is the inverse of the Froude number related to the grain size.

The $\frac{U}{U''_*} = f(\psi')$ relationship as developed from field data is shown in Figure 6-9.

The resistance of different bed forms to flow is shown in Figure 6-5 as a single curve. It is probable that different portions of this curve correspond to different bed forms. However, Bishop, Simons and Richardson (1965) showed that the relation is not valid for upper regime flows in sand-bed channels and Sentürk (1975) pointed out that this curve is inadequate when $\psi'$ is smaller than 10.

Einstein and Barbarossa (1952) interpreted Figure 6-9 in a smaller way. The interesting point in Einstein's approach is that the factors governing the resistance are reduced to $\frac{\gamma R'S}{\gamma s' D_{35}}$ and $\frac{R'}{D_{65}}$. The first parameter is a Froude number and the second is the relative roughness. Comparing Equation 6-79 and Figure 6-9 with Equation 6-6 it is possible to see that the parameters previously used to define the resistance to flow are used by Einstein in their general form. The Reynolds number is replaced by the Reynolds number of the particle and the Froude number by the Froude number expressed in terms of the friction velocity.

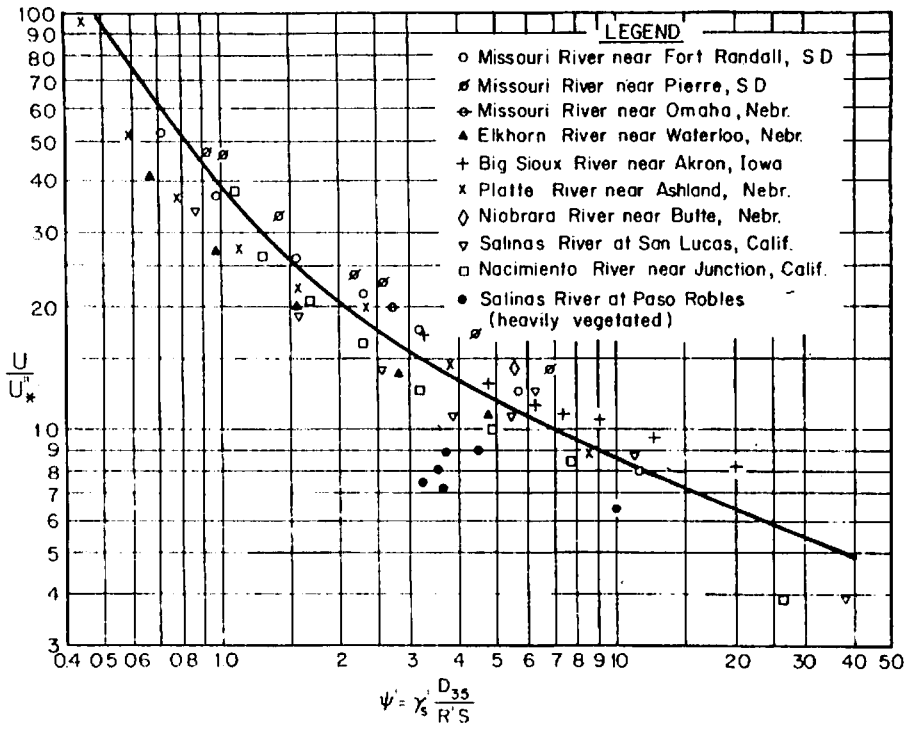


Figure 6-9. Friction loss due to channel irregularities as a function of sediment transport (after Einsten and Barbarossa, 1952).

A close inspection of Einstein's approach shows the importance of the variation of $U''_*$ on the resistance to flow. When the discharge increases in a meandering channel the sediment transport along the bed increases and the distortion or sinuosity decreases because the meanders progressively straighten. The value of $U''_*$ experiences a similar decrease.

Einstein's approach was checked with a limited amount of canal data from Pakistan. The variance did not exceed 0.018. Nordin (1964) has confirmed the value of this method. Harrison and Melema (1967) with data from the Missouri and the Mississippi Rivers found a good agreement between computed and measured results using Einstein's approach. However, when this relation is applied to natural water courses with small slopes that transport fine sand the discrepancies are large (Sentürk, 1945).

Using the foregoing method a mean stage discharge relationship for a river reach can be determined provided the characteristics of the reach and its bed material are known. The procedure suggested by Einstein and Barbarossa (1952) follows.

After surveying the selected reach, determine S, $D_{65}$, $D_{35}$ and the cross sectional dimensions of the average cross section of the channel. Then, two kinds of problems can be solved by applying Einstein's procedure:

1. With Q given determine R.
2. With R given determine Q.

To solve the first problem the following procedure is suggested:

Step 1. Assume a reasonable R'
Step 2. Apply Equation 6-79 and Figure 6-2 to determine U
Step 3. Compute $\psi'$ and then read $\frac{U}{U''_*}$ from Figure 6-5
Step 4. Compute $U''_*$ and then R"
Step 5. Compute R = R' + R" and determine the corresponding values of stage y and cross sectional area A
Step 6. Determine Q from Q = AU. If this value of Q matches the given value of the discharge, the problem is solved. If an appreciable difference exists between the complete and known value of Q choose another value for R' and repeat Steps 1 through 6 until agreement is achieved.

To solve the second problem:

Step 1. Assume a reasonable value of R'
Step 2. Apply Equation 6-79 and Figure 6-2 to determine U
Step 3. Compute $\psi'$ and then read $\frac{U}{U''_*}$ from Figure 6-5
Step 4. Compute $U''_*$ and then R"
Step 5. Compute R = R' + R". If this value of R agrees with the given discharge the problem is solved. Otherwise repeat the procedure until a solution is found. Then determine the corresponding values of stage y and cross sectional area A.
Step 6. Determine Q as Q = AU

The two approaches are computerized and the program, in FORTRAN IV language, is given in the appendix, of Simons and Sentürk, 1977.

Einstein's approach as interpreted by V. Vanoni

It is laborious to solve the problem of resistance to flow using the Einstein procedure previously explained. Vanoni and Brooks (1957) simplified the solution of the problem by using two parameters $\frac{U^3}{gvS}$, $\frac{U}{\sqrt{gk_s S}}$, see Figure 6-10a and an extension of this analysis, Figure 6-10b developed by Simons. This figure can be used to determine $U'_*$ without trial. The Einstein method of computation is illustrated in Examples B and C.

Evaluating Resistance to Flow by Adjusting Depth of Flow

It was verified by Simons and Richardson (1966) that resistance to flow and mean velocity can be estimated by using slope or depth adjustments. The depth adjustment takes into account the energy dissipation resulting from the form roughness and possible errors in depth measurements resulting from inclusion of the separation zones downstream from ripples and dunes in the total cross-sectional area of flow.

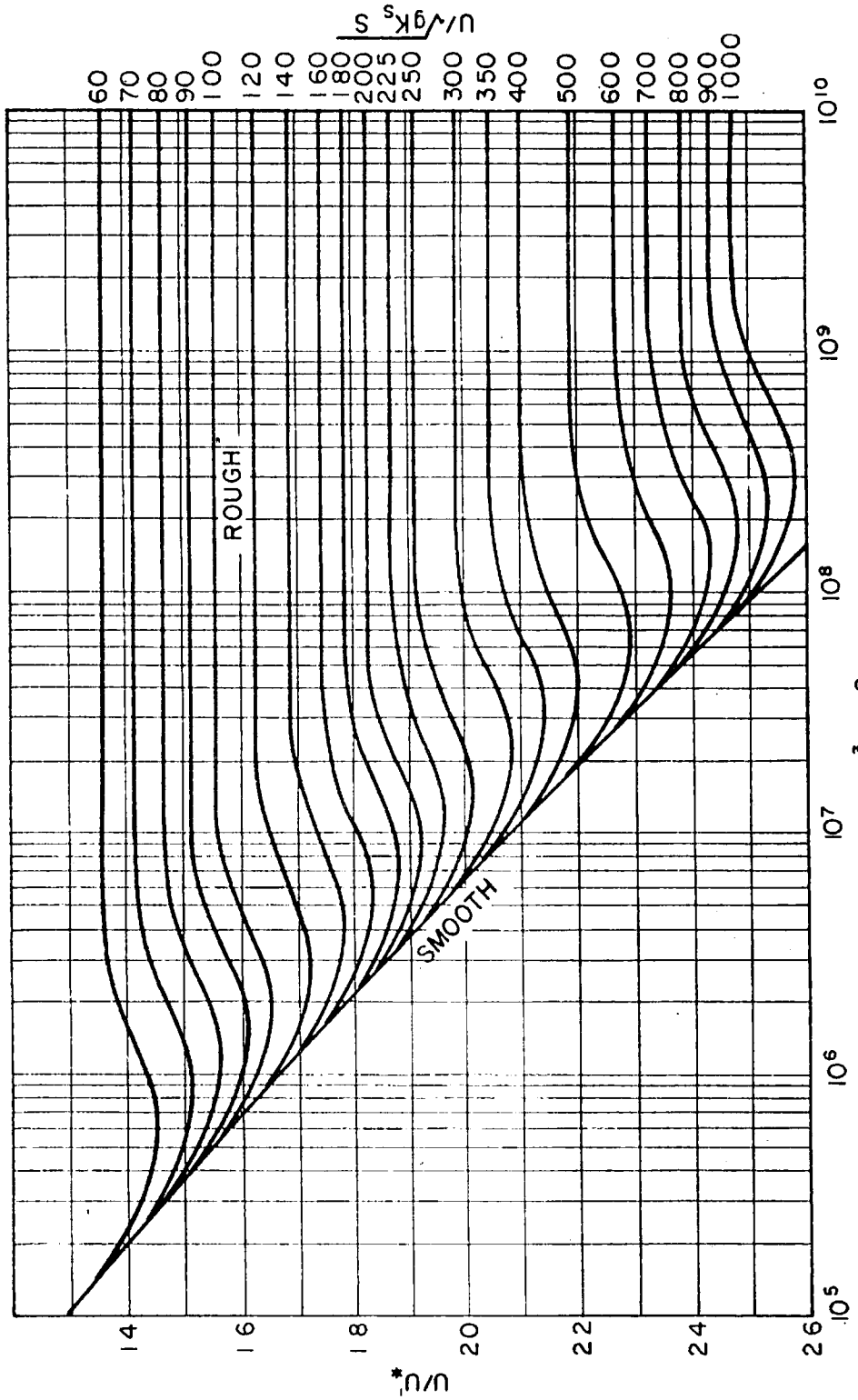


Figure 6-10a. Curves for the graphical solution of the Einstein-Barbarossa equations for determination of R'.

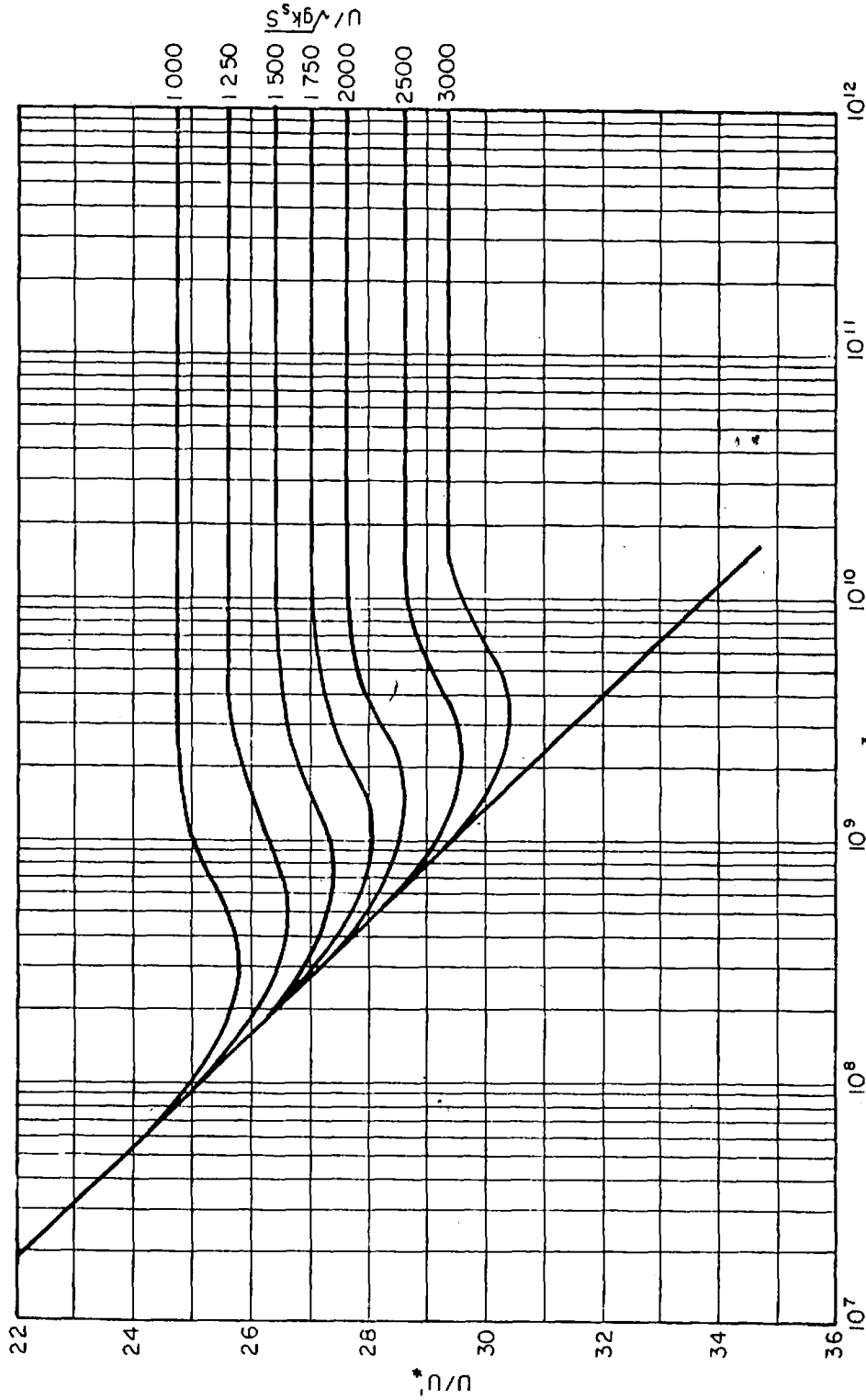


Figure 6-10b. Curves for the graphical solution of the Einstein-Barbarossa equations for determination of R'.

More specifically, the measured depth of flow includes part of the separation zones downstream from ripples and dunes. This part of the cross section does not effectively convey the water-sediment mixture. To verify this concept the roughness elements and their associated separation zones immediately downstream of ripples and dunes were observed, measured and photographed. Additionally, much attention was given to the flow pattern over the individual roughness elements. For example, downstream from the crest of each ripple and dune is a separation zone in which a part of the fluid rotates about a horizontal axis which passes through the mass of fluid within the zone of separation, as is shown in Figure 6-11.

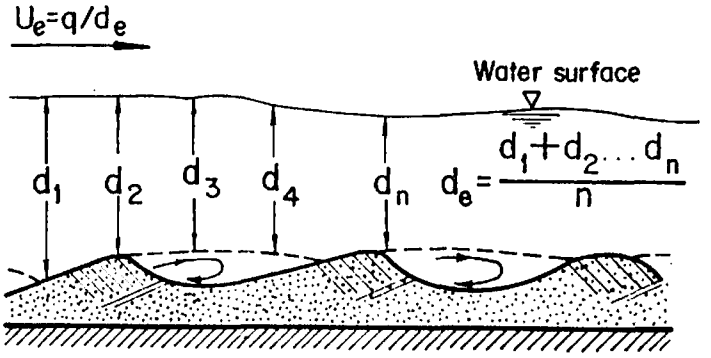


Figure 6-11. Sketch showing the flow pattern over two-dimensional ripples or dunes, effective depth ($d_e$) and effective velocity ($U_e = q/d_e$).

By careful measurement, it was determined that the length of these separation zones observed downstream from baffles placed in a wind tunnel (Nagabhushanaiah, 1961). These lengths were approximately 10-12 times the amplitude of the roughness element measured from trough to crest. A study of these separation zones suggested that average velocity based on Q/A and average depth based on the average distance from the water surface to the bed surface are perhaps misleading. An effective depth ($d_e$) reduced to compensate for the zones of separation, and an effective velocity may be defined correspondingly by applying the principle of continuity. The concept of an effective velocity and depth is further clarified by Figure 6-11 from which it can be seen that the effective depth,

$$d_e = \frac{d_1 + d_2 + d_3 + \ldots + d_n}{n} \tag{6-82}$$

and the effective velocity $U_e = q/d_e$.

The effective depth given in Equation 6-82 can be approximated in flumes by mapping the form roughness. This can be accomplished using sonic equipment and ejecting dye into the flow to define the limits of the separation zone. Knowing effective depth and velocity, the average velocity in the channel can be determined from continuity.

$$U = \frac{U_e d_e}{d} \tag{6-83}$$

This procedure is difficult to utilize. In addition, effective depth and velocity do not consider the increase in energy dissipation resulting from the form roughness. Therefore, in the next sections an adjusted depth (d') or hydraulic radius (R') and velocity (U') are defined that take both factors into account.

Adjusting Depth to Smooth Boundary Roughness

The adjustment of depth or hydraulic radius could be made relative to the depth or hydraulic radius associated with an average grain roughness of an alluvial sand bed or to other basic resistance curves (Simons and Richardson, 1966). However, the most general correction would be accomplished by correcting data for hydraulically rough channels, both rigid and alluvial, to fit a rigid-channel hydraulically smooth boundary relation such as the one presented by Tracy and Lester (1961). Their equation can be written as

$$C/\sqrt{g} = 5.75 \log \frac{R_e}{C/\sqrt{g}} + 2.38 \tag{6-84}$$

where $C/\sqrt{g}$ is the Chezy discharge coefficient for hydraulically smooth rigid open channels, $R_e$ is the Reynolds number, $UR/n$, which becomes $Ud/n$ for wide channels where sidewall effects are negligible.

Equation 6-84 indicates that the discharge coefficient is a function of depth, slope and temperature

$$C/\sqrt{g} = \phi(d'_s, S, T) \tag{6-85}$$

where $d'_s$ is the equivalent smooth-channel depth based on the same slope, $S$ is the discharge, and T is the temperature of the flow in degrees Fahrenheit. Simons and Richardson (1966) found that

$$C/\sqrt{g} = 8.4 \left[\log \frac{d'_s S^{1/3}}{3.52 - 1.415 \log T} + 4.132\right] \tag{6-86}$$

To develop a general method of adjusting the hydraulic radius of a particular run to the smooth-boundary relation, first assume that the change in the wetted perimeter $P$ is incorporated into the adjusted hydraulic radius. Then, from the continuity equation

$$Q = AU = A'U' \tag{6-87}$$

or

$$RU = R' \frac{P'}{P} U' = R'_s U' \tag{6-88}$$

The Chézy formula for smooth boundary or equivalent flow is

$$U' = C/\sqrt{g}\ \sqrt{gR'_s S} \tag{6-89}$$

Solving Equations 6-88 and 6-89 simultaneously for $R'_s$,

$$R'_s = \left[\frac{UR}{C/\sqrt{g}\ \sqrt{gS}}\right]^{2/3} \tag{6-90}$$

The correction to the hydraulic radius $\Delta R$ required to plot a particular run on the smooth boundary relation is

$$WR = R - R'_s = R - \left[\frac{UR}{C/\sqrt{g}\ \sqrt{gS}}\right]^{2/3} \tag{6-91}$$

or for channel conditions such that $R \cong d$,

$$\Delta d = d - \left[\frac{Ud}{C/\sqrt{g}\ \sqrt{gS}}\right]^{2/3} = d - \left[\frac{q}{C/\sqrt{g}\ \sqrt{gS}}\right]^{2/3} \tag{6-92}$$

Values of $\Delta R$ or $\Delta d$ can be computed using Equations 6-91 or Equation 6-92 and from these values $\Delta R$ versus R or $\Delta d$ versus d relations can be developed. Also the ratio of $\Delta d/d$ or $\Delta R/R$ can be computed and relations developed relating $C/\sqrt{g}$, $R_*$ and $\Delta d/d$ or $\Delta R/R$, where

$$R_* = R_e\ [C/\Delta g]^{-1} = \frac{U_* d}{\nu} \quad \text{or} \quad \frac{U_* R}{\nu} \tag{6-93}$$

It is then possible to use the $\Delta d$ versus d or $\Delta R$ versus R relation and the new resistance diagram to establish average velocity for a given boundary roughness. These relations and concepts will be developed and discussed for various boundary roughness in the following sections.

Evaluating Resistance to Flow in Open Channels with Flat Bed by Adjusting Depth of Flow

The resistance to flow in open channels with rigid boundaries or of plane movable boundaries formed of gravel and/or cobble bed was evaluated by adjusting depth of flow to smooth boundary roughness. Using the data obtained from different sources for various boundary roughness, the relations between $\Delta d$ and d for each of the families of boundary roughness and resistance diagrams relating $C/\sqrt{g}$, $R_* = U_* d/\nu$ and $\Delta d/d$ are prepared as outlined in the preceding section. The information and results are summarized in Table 6-13. More details can be found from Simons and Richard's (1966, 1971) works.

Table 6-13. Resistance functions in open channels of flat bed by adjusting depth of flows.

| Boundary Roughness | Source of Data | $\Delta d \sim d$ Relationship | $C/\sqrt{g}$, $R_*$ and $\Delta d/d$ Relationship |
|---|---|---|---|
| Baffle and cube | Sayer and Albertson (1963) (Flume) | Fig. 6-12 | Fig. 6-13 |
| Baffle and cube | Koloseus and Davidian (1961) (Flume) | Fig. 6-12 | Fig. 6-14 |
| Gravel and cobbles (B rock ~ 4" diam H rock ~ 2" diam) | Kharrufa (1962) (Flume) | Fig. 6-15 | Fig. 6-16 |
| Natural cobbles (*) (with 2", 1.5", diameters) | Lane and Carlson (1953) (Irrigational canals in the San Luis Valley, Colorado) | Fig. 6-17 | Fig. 6-18 |
| Natural gravel and cobble bed | Gravel and cobble bed rivers | Fig. 6-19 | Fig. 6-20 |
| Concrete channel (**) | Large concrete lined canals | Fig. 6-21 | Fig. 6-22 |

(*)The resistance relation holds as long as the bed material is stable. If a large discharge is turned into any of these canals, a boundary shear could develop that would cause significant movement of bed material and result in a little coarser bed material through transportation of some of the small particles and movement of large roughness elements into new positions. Also, a dune-bed configuration may develop that would be residual at lower discharges. In this case, the specific relations are no longer valid.

(**)These resistance relations may be used to design lined concrete channels.

Evaluating Resistance to Flow in Alluvial Sand Channels by Adjusting Depth of Flow

Sand-bed roughness is much more complex than the baffle, cube and rock roughness because sand-bed roughness is a function of flow. A small change in any variable affecting the form of bed roughness will cause a change in the bed roughness and the resistance to flow. However, $\Delta R$ versus $R$ or $\Delta d$ versus $d$ relations can be developed for each specific bed form shown in Figure 6-23.

For the 8-ft flume data, $d \cong R$, and the relations presented are in terms of $\Delta d$ and $d$. As can be seen in Equation 6-85, $C\sqrt{g}$ and hence, $\Delta d$ for a constant $q$ are a function of the slope and depth of the channel. Also, $\Delta d$ is more strongly dependent on slope when the bed form is dunes in the coarse sands.

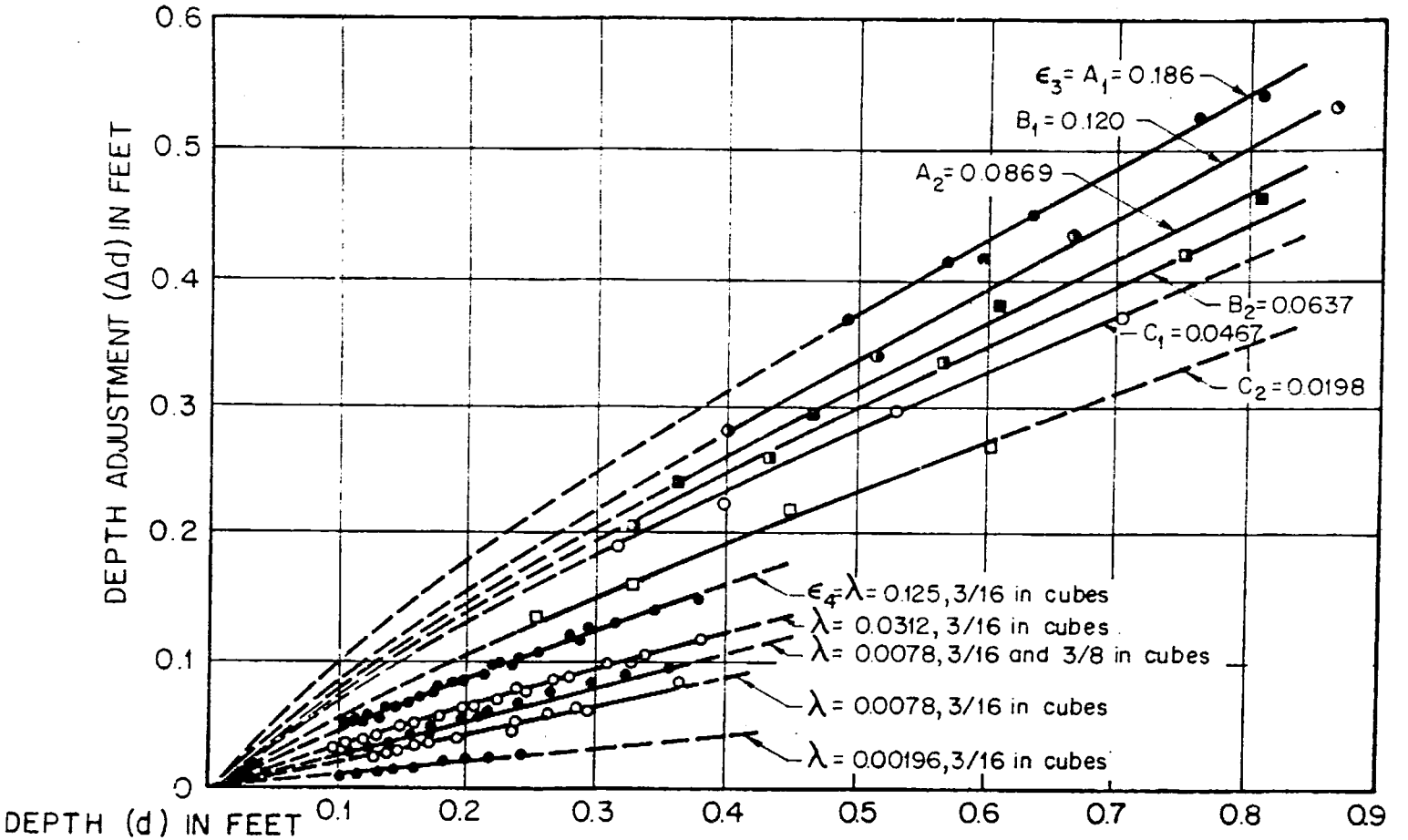


Figure 6-12. Depth adjustment (Δd) for baffle and cube roughness elements. $\epsilon_3$ refers to Sayre and Albertson's (1961) roughness coefficient, and $\epsilon_4$ refers to Koloseus and Davidian's roughness coefficient (after Simons and Richardson, 1966).

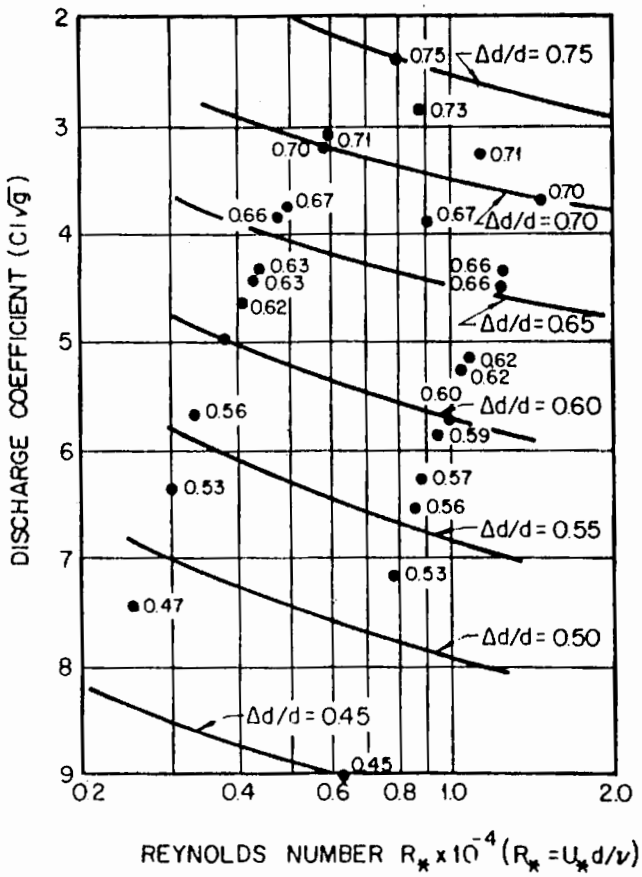


Figure 6-13. Resistance diagram relating $C/\sqrt{g}$, $R_*$, and $\Delta d/d$ for the baffle roughness (data from Sayre and Albertson, 1963)(after Simons and Richardson, 1966).

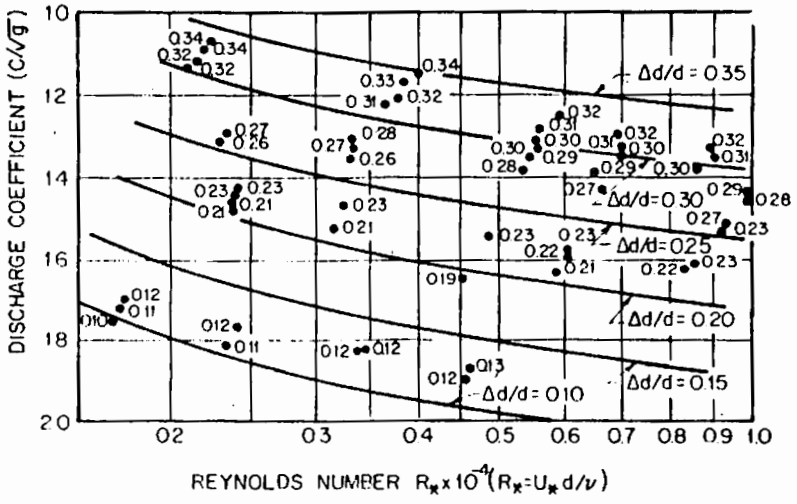


Figure 6-14. Resistance diagram relating $C/\sqrt{g}$, $R_*$, and $\Delta d/d$ for rock roughness of Kharrufa (1962)(after Simons and Richardson, 1966).

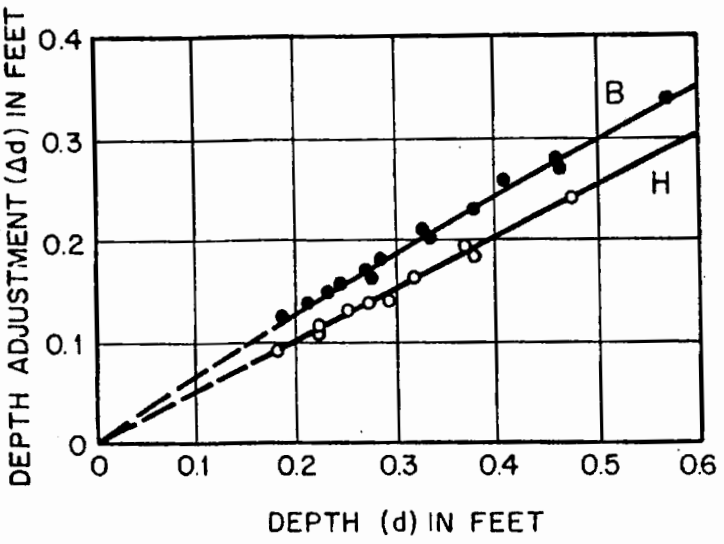


Figure 6-15. Relation between depth adjustment ($\Delta d$) and d for rock roughness in a flume. B and H rock roughness of Kharrufa (1962). Slope ranged from 0.001 to 0.09 foot per foot (after Simons and Richardson, 1966).

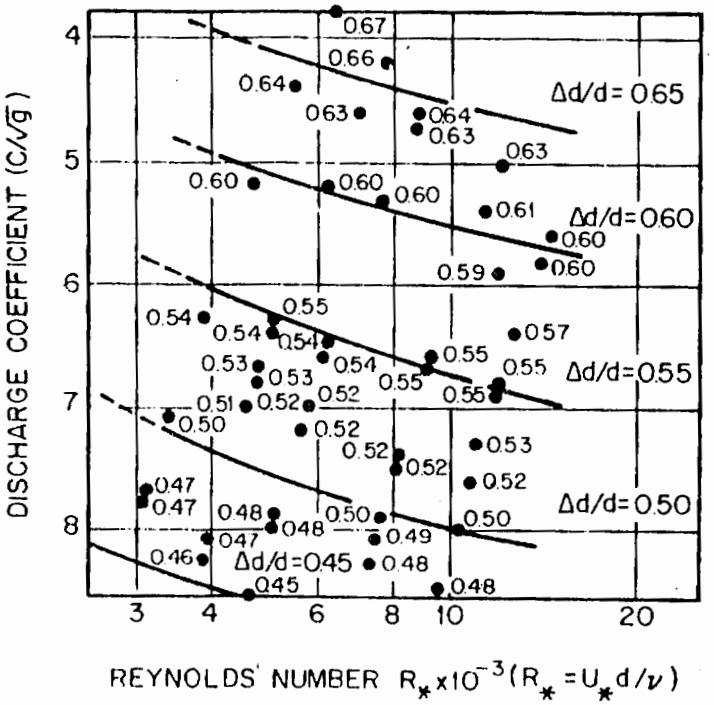


Figure 6-16. Resistance diagram relating $C/\sqrt{g}$, $R_*$, and $\Delta d/d$ for rock roughness of Kharrufa (1962)(after Simons and Richardson, 1966).

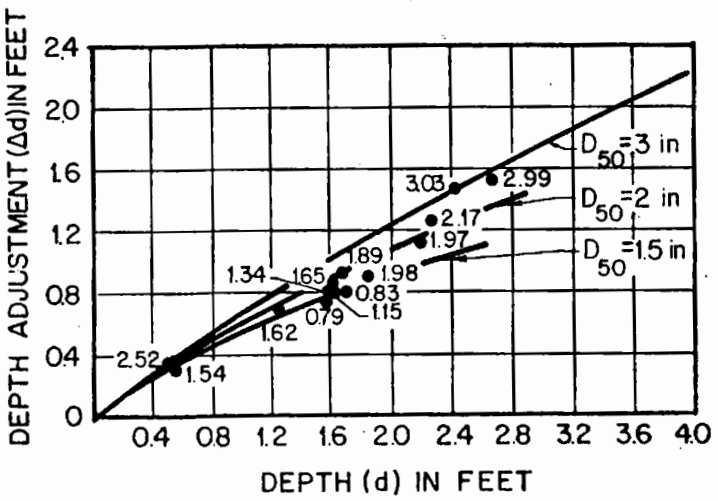


Figure 6-17. Relation between depth adjustment (Δd) and depth d for the San Luis Valley, Colorado, canals with cobble roughness (Lane and Carlson, 1953). The third variable is median diameter of the bed material, in inches (after Simons and Richardson, 1966).

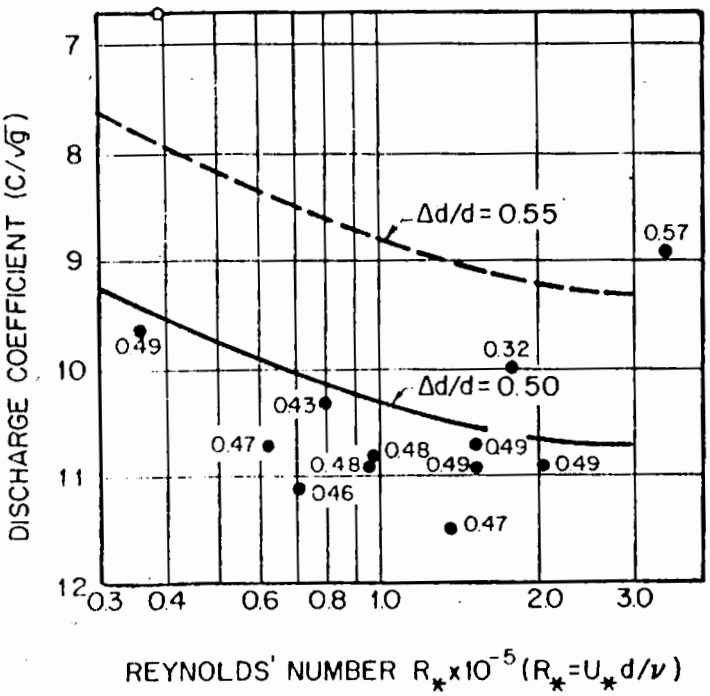


Figure 6-18. Resistance diagram relating $C/\sqrt{g}$, $R_*$, and $\Delta d/d$ for the San Luis Valley, Colorado, canals with cobble roughness (after Simons and Richardson, 1966).

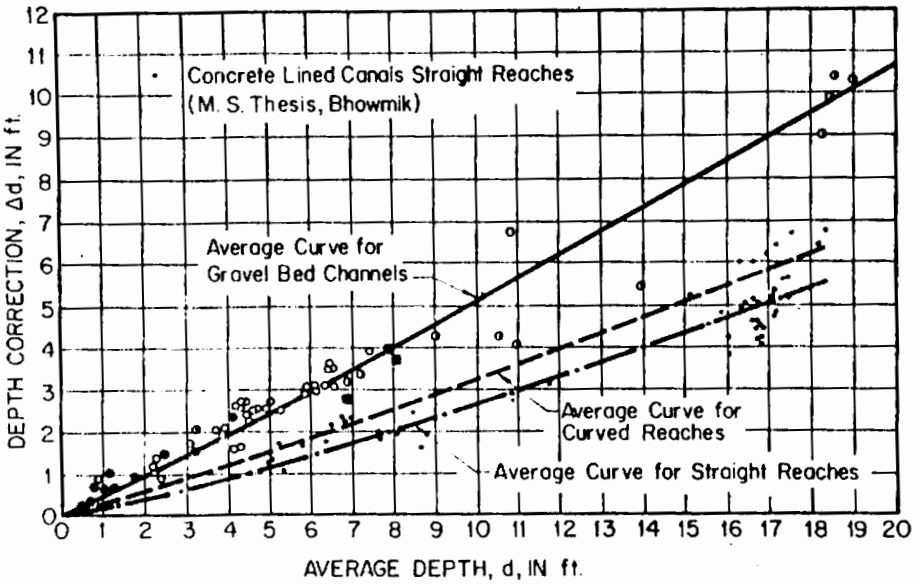


Figure 6-19. Relation between depth correction, $\Delta d$, and average depth, d (after Simons and Richardson, 1971).

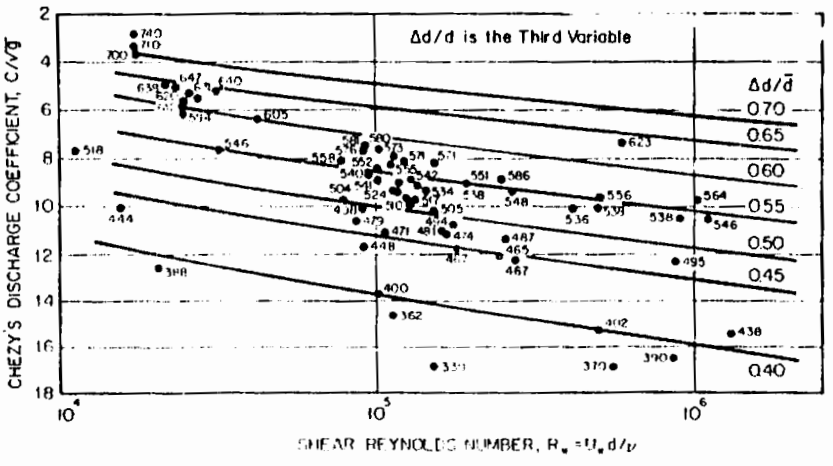


Figure 6-20. Resistance diagram relating $C/\sqrt{g}$, $R_*$ and $\Delta d/d$ (after Simons and Richardson, 1971).

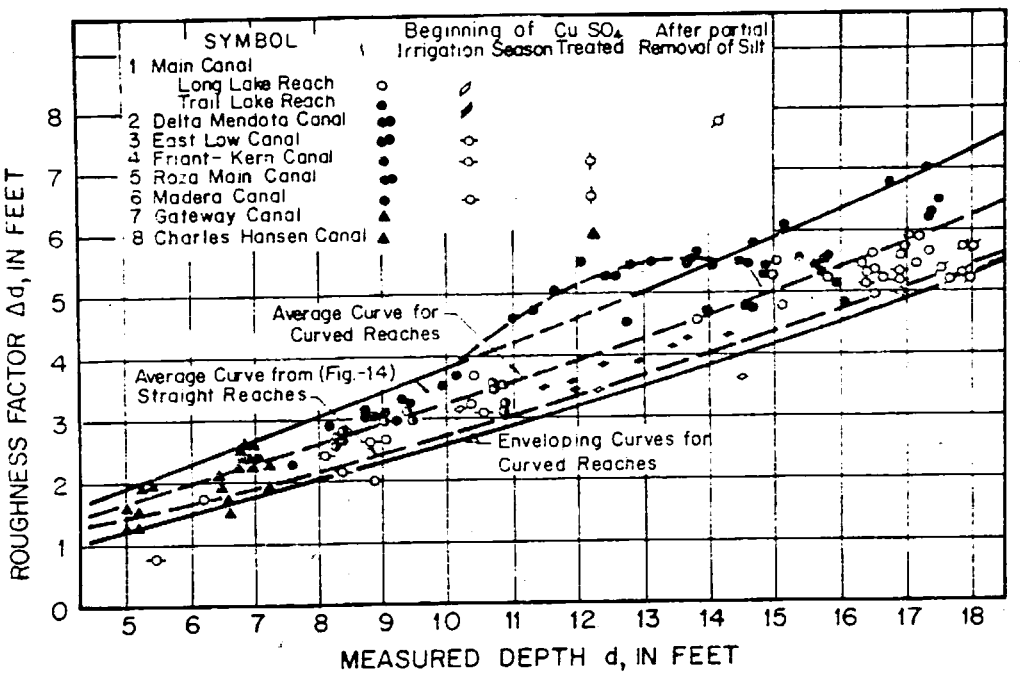


Figure 6-21. Relation between the roughness factor $\Delta d$, and the depth $d$ for curved reaches of all the canals (after Simons and Richardson, 1971).

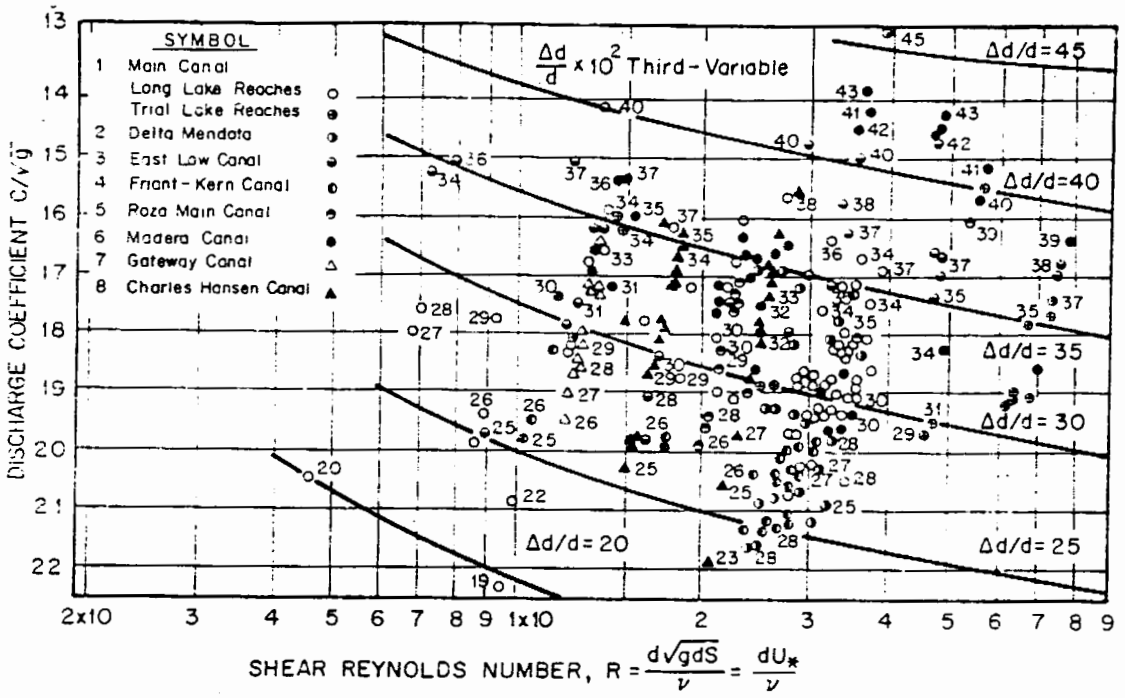


Figure 6-22. Resistance diagram relating $C/\sqrt{g}$, $R_*$ and $\Delta d/d \times 10^2$ for all the canals (after Simons and Richardson, 1971).

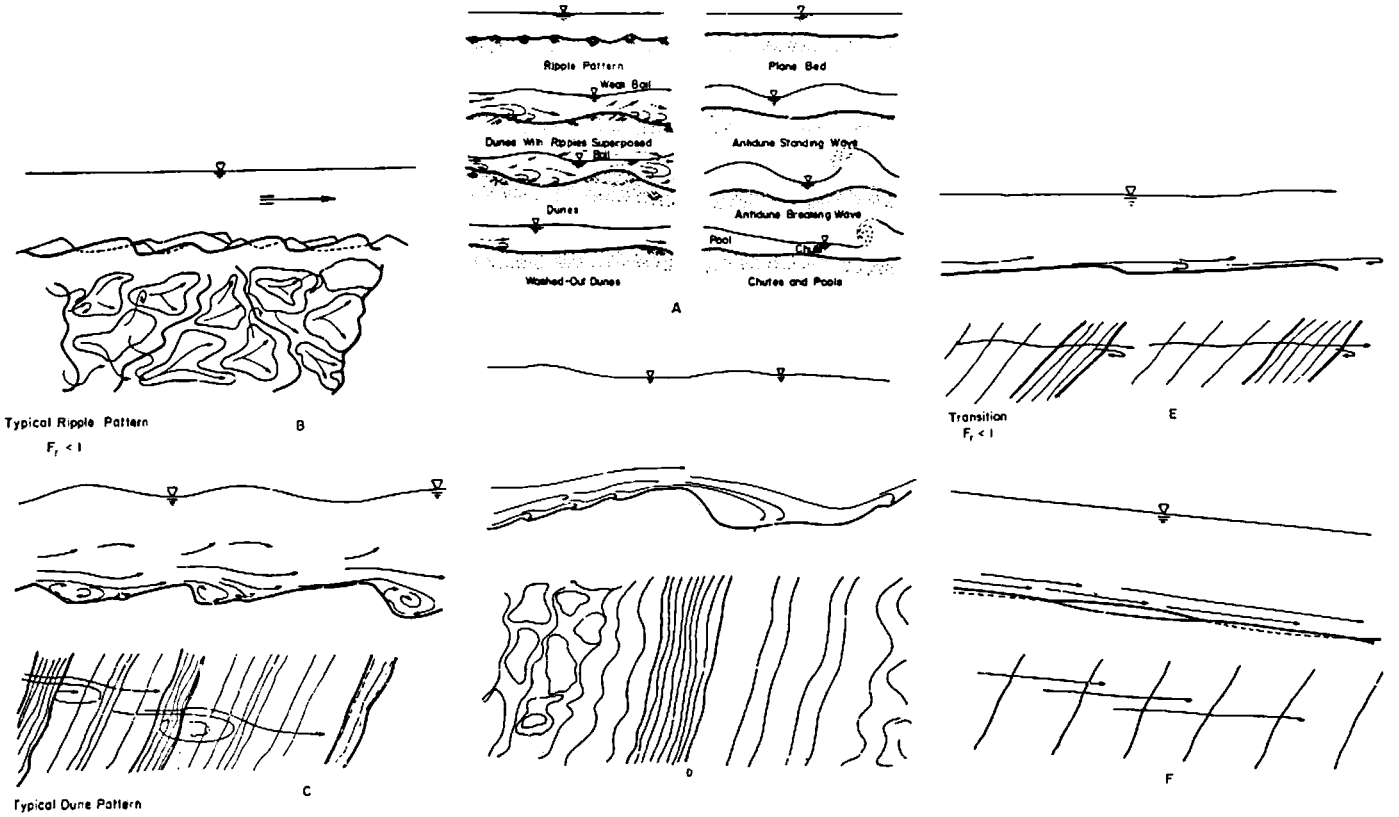


Lower flow regime bed flows.

Transition, ripples to dunes.

Lower flow regime, transition from dunes to plane bed.

Figure 6-23. Forms of bed roughness in sand channels.

The $\Delta d$ versus $d$ relations for plane-bed runs made in the 8-ft wide flume of Colorado State University using 0.19 mm sand, for ripple-bed runs using 0.19 mm, 0.27 mm, and 0.45 mm sand, and for dune-bed runs using 0.19 mm, 0.27 mm, 0.45 mm, and 0.93 mm sand, are given in Figures 6-24, 6-25 and 6-26 respectively. In these relations, $\Delta d$ is computed using Equations 6-86 and 6-92. A similar relation using slope as the abscissa for plotting antidune flow is given in Figure 6-27. Similar relations for the other forms of bed roughness and other bed materials can be developed.

Although the resistance diagram for the flume data could be more precise if separate diagrams were made for each form roughness and size of bed material, only one diagram has been prepared (see Figure 6-28). This diagram relates $C/\sqrt{g}$, $R_*$, and $\Delta d/d$ for all the ripple and dune flume data collected by Simons and Richardson (1966) at CSU. To show the possibilities of using this procedure to estimate the average velocity in sand-bed canals, the foregoing analysis was applied to the Punjab canal data reported by Simons (1957) and Pakistan canal data reported by Harza Engineering Co., International (1963). Relations based on these data were prepared in terms of the hydraulic radius, although the relations would be equally valid if expressed in terms of depth and a depth correction.

Figure 6-29 presents the $\Delta R$ versus $R$ relation for Pakistan canals, which, according to the relationship given in Figure 6-30, have a dune-bed roughness. The slope in the canals is a very significant third variable. The accompanying resistance relation for the Pakistan canals is presented in Figure 6-31.

Following an identical procedure, the $\Delta R$ versus $R$ relation for the Pakistan canals is presented in Figure 6-32 and the resistance diagram is given in Figure 6-33.

Similar relations were tested for field conditions using river-channel data. Very good results were obtained for channels having the same pattern throughout that is, dunes, plane bed, or antidunes. However, if multiple roughness patterns, transitional forms of roughness and other complicating factors occur, such as a braided stream, the accuracy of the method is greatly reduced unless each segment of channel width for which a particular bed form exists is considered.

Determination of Average Velocity of Flow

The preceding relations and equations offer two methods of estimating velocity by using the appropriate $\Delta d$ versus $d$ or $\Delta R$ versus $R$ relations, equations, and resistance diagrams. The procedures are outlined in the following paragraphs.

It is assumed that the depth or hydraulic radius is known or can be determined from $d$ versus $Q$ and $R$ versus $Q$ relations (Simons, 1957), that the slope is known or can be assumed on the basis of limits set by the $\Delta d$ versus $d$ relations, and that the form or roughness is known (rigid or alluvial). If the boundary is alluvial, the median

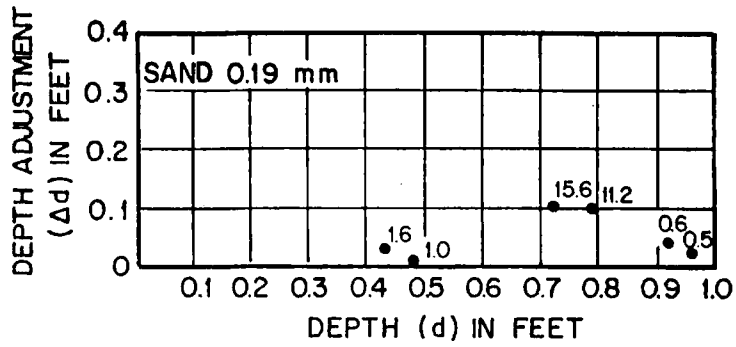


Figure 6-24. Relation between depth adjustment (Δd), depth (d), and slope (S x $10^4$) for plane sand bed in $D_{50}$ = 0.19 mm (after Simons and Richardson, 1966)(*).

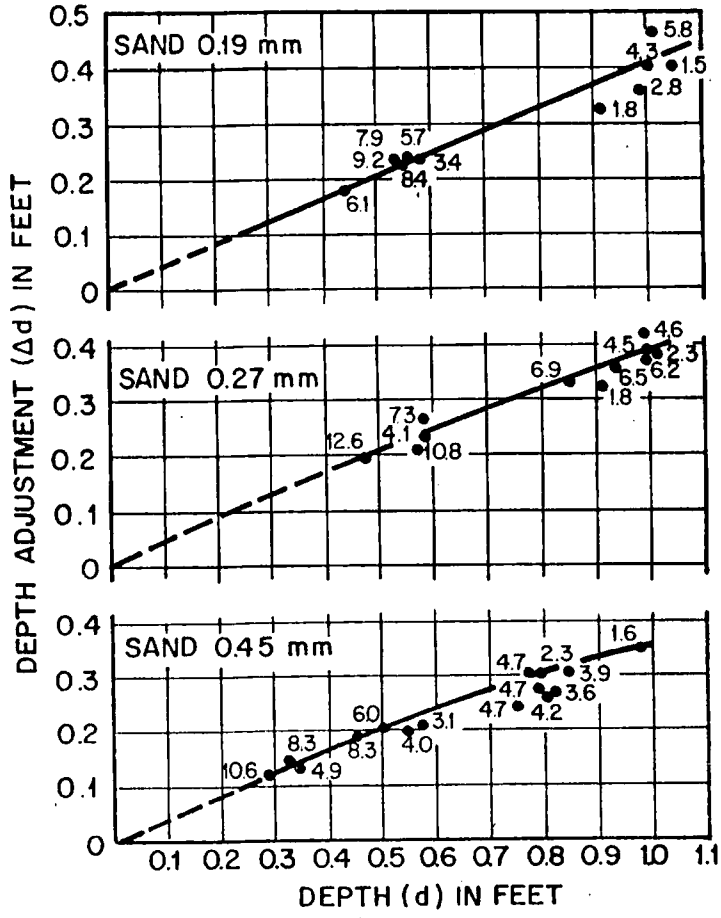


Figure 6-25. Relation between depth adjustment (Δd), depth (d), and slope (S x $10^4$) for the ripple-bed configuration in sands with $D_{50}$ = 0.19 mm, 0.27 mm, and 0.45 mm (after Simons and Richardson, 1966).

(*)Numbers beside the dots denote slope, S x $10^4$.

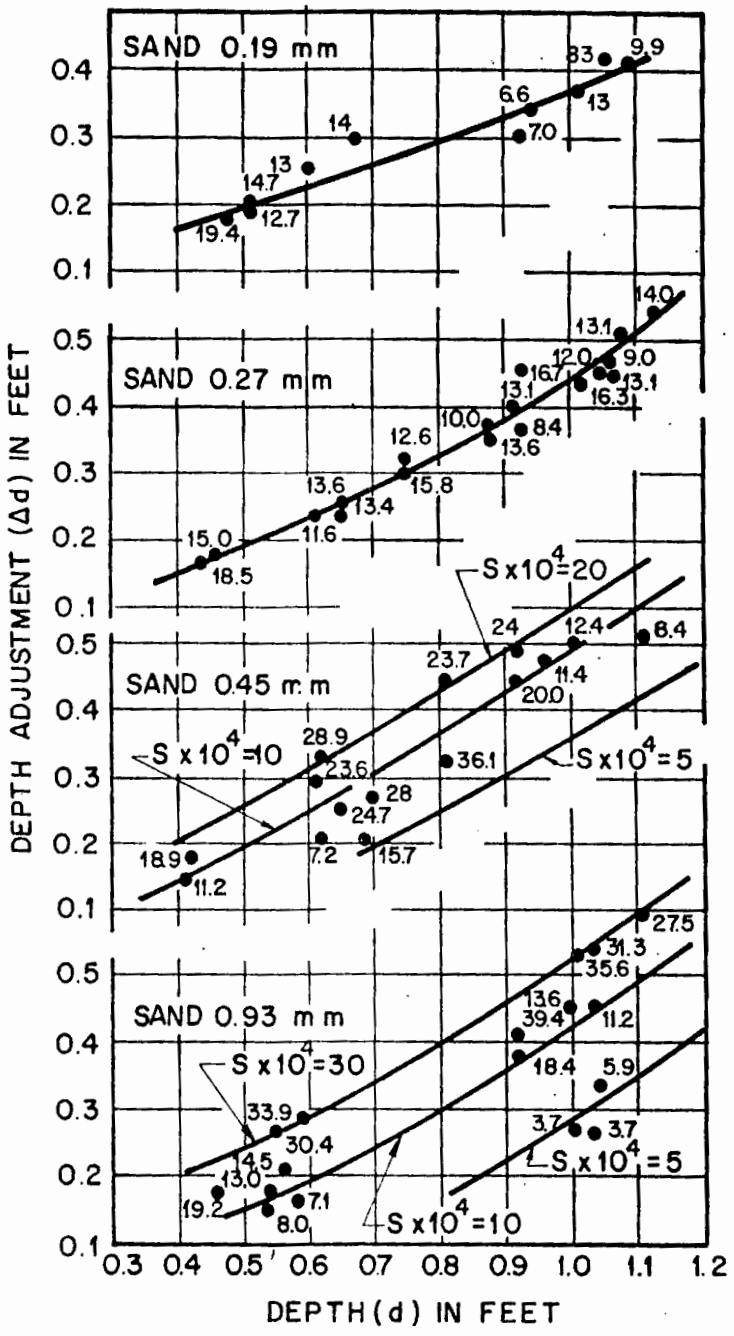


Figure 6-26. Relation between depth adjustment (Δd), depth (d), and slope (S x $10^4$) for the dune-bed configuration in sands with $D_{50}$ = 0.19 mm, 0.27 mm, 0.45 mm, and 0.93 mm (after Simons and Richardson, 1966). (Number beside the dots denotes slope S x $10^4$.)

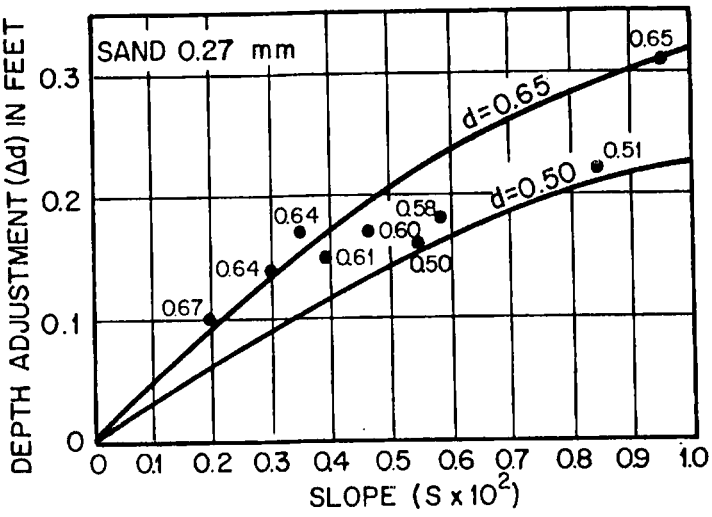


Figure 6-27. Relation between depth adjustment (Δd), depth (d), and slope ($Sx10^2$) for antidune flow in sand with $D_{50}$ = 0.27 mm (after Simons and Richardson, 1966). (Numbers beside the dots denote slope $Sx10^2$).

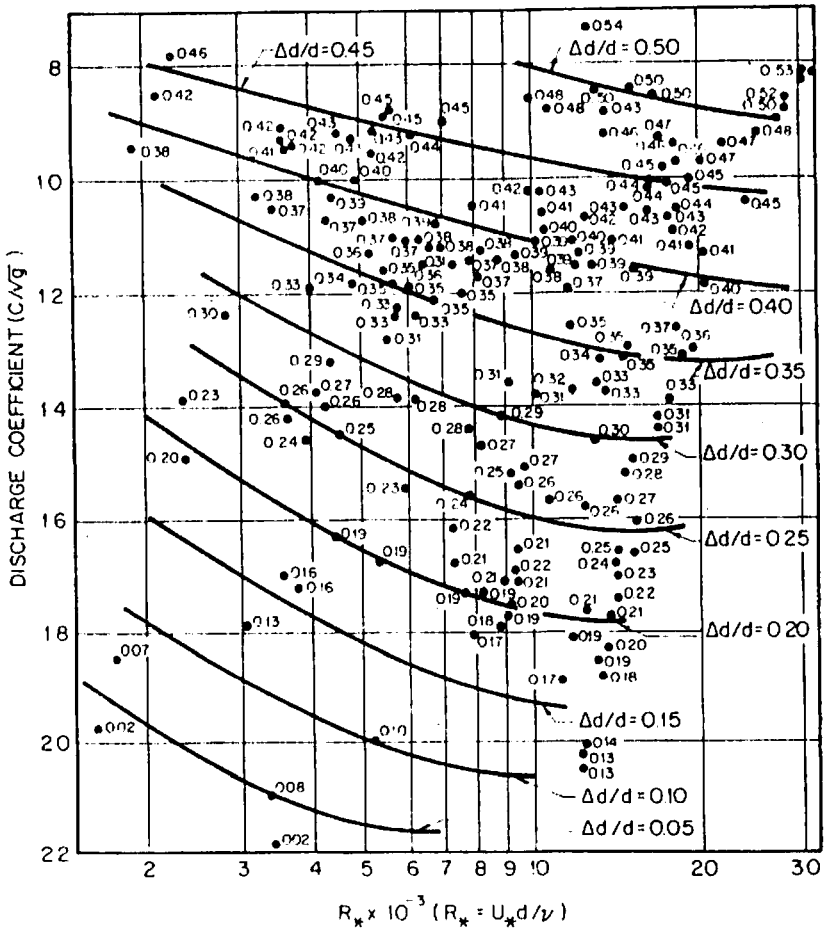


Figure 6-28. Resistance diagram relating $C/\sqrt{g}$, $R_*$, and $\Delta d/d$ for ripples and dunes. Data for sands 0.19 mm, 0.27 mm, 0.45 mm, and 0.93 mm in the 8-ft wide flume (after Simons and Richardson, 1966).

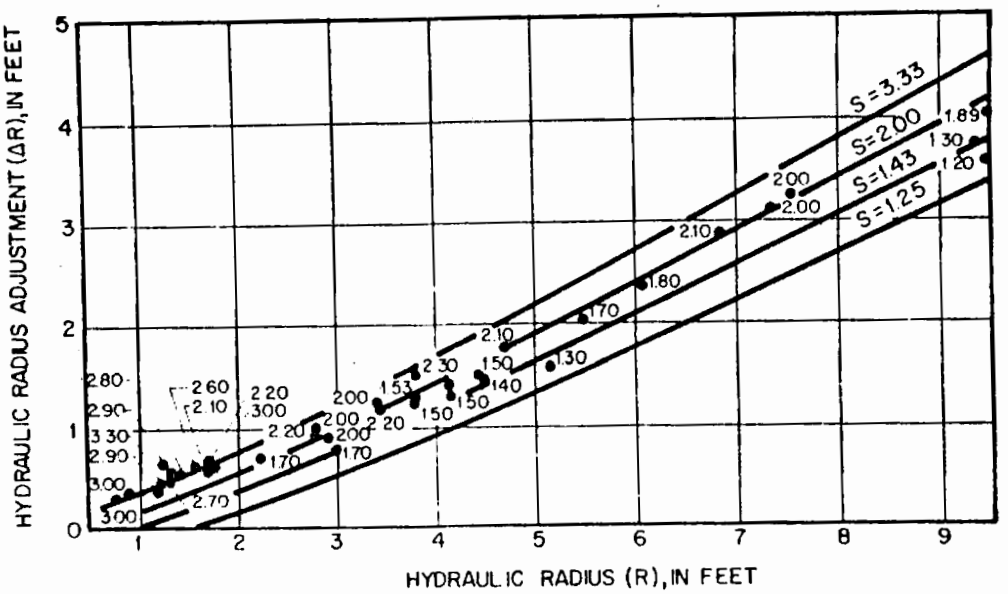


Figure 6-29. Relation between the hydraulic-radius adjustment ($\Delta R$), and slope ($S \times 10^4$) for Punjab canals (Simons, 1957)(after Simons and Richardson, 1966).

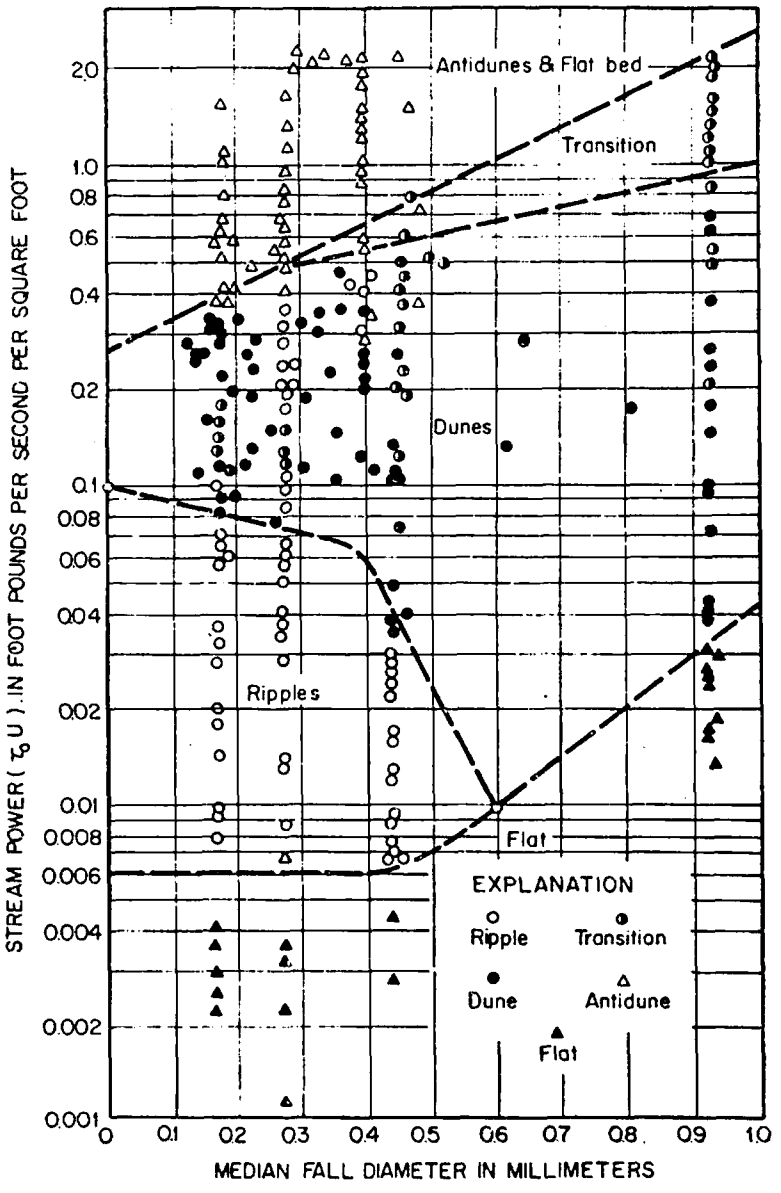


Figure 6-30. Relation of bed form to stream power and median fall diameter of bed sediment (after Simons and Richardson, 1966).

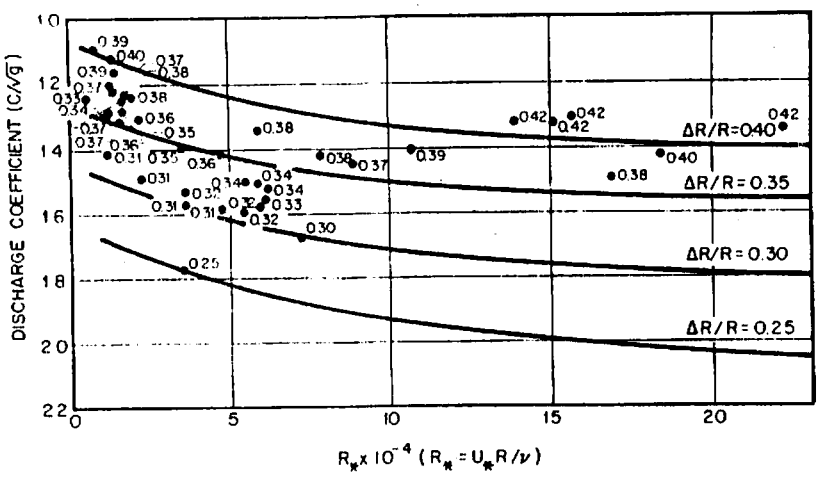


Figure 6-31. Resistance diagram relating $C/\sqrt{g}$, $R_*$, and $\Delta R/R$ for Punjab canals (Simons, 1957)(after Simons and Richardson, 1966).

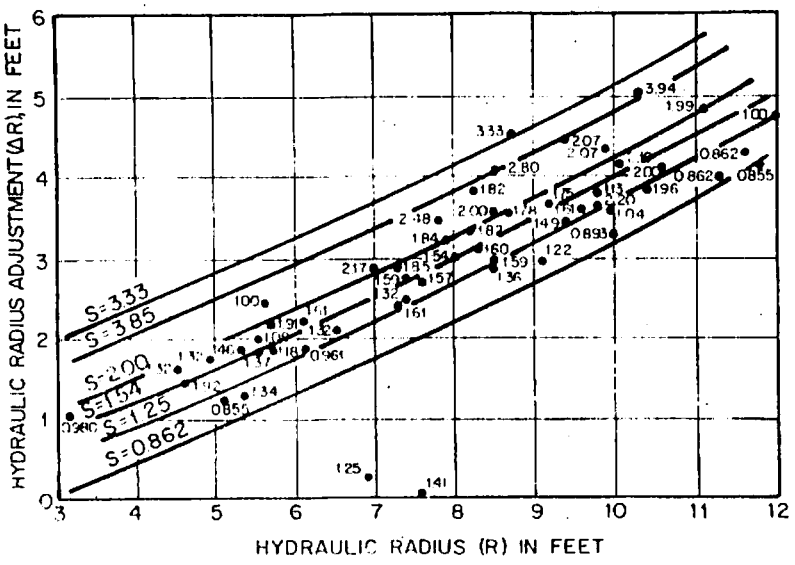


Figure 6-32. Relation between the hydraulic-radius adjustment ($\Delta R$), hydraulic radius (R), and slope ($S \times 10^4$) for Pakistan canals (Harza Engineering Co., Internat., 1963)(after Simons and Richardson, 1966).

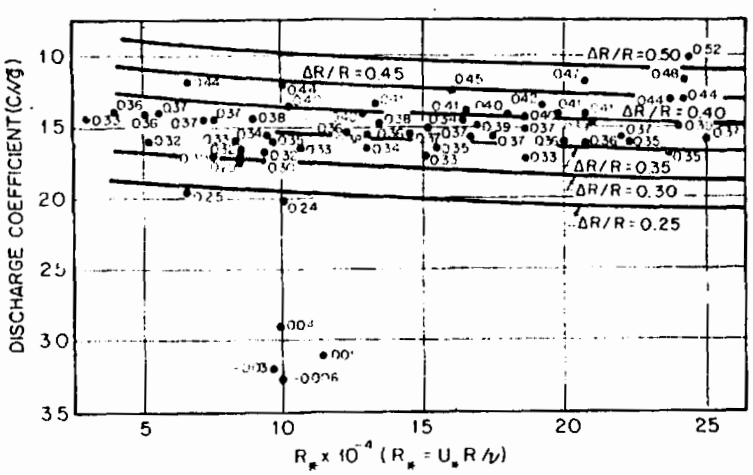


Figure 6-33. Resistance diagram relating $C/\sqrt{g}$, $R_*$, and $\Delta R/R$ for Pakistan canals (Harza Engineering Co., Internat., 1963)(after Simons and Richardson, 1966).

fall diameter of the bed material $D_{50}$ must also be known. For many channels only an estimate of $D_{50}$ is possible but this is usually adequate.

In the first method, if the depth d or hydraulic radius R, the slope S, and the temperature are known or assumed, $\Delta R$ or $\Delta d$ can be determined from the appropriate relation. Then $C/\sqrt{g}$ can be computed using Equations 6-84 or 6-86. Knowing $C/\sqrt{g}$, Equation 6-8 can be used to compute U', and U determined from Equation 6-88.

The second method of determining U, in the knowledge of d or R and of S is assumed, is as follows:

1. Read $\Delta d$ or $\Delta R$ directly from the appropriate $\Delta d$ versus d or $\Delta R$ versus R relation, in which slope may be a significant third variable.

2. Having determined a depth adjustment and knowing the corresponding values of S, d, or R, form roughness, and size of bed material when dealing with alluvial channels:

   A. Compute $\Delta d/d$ or $\Delta R/R$;
   B. Compute $R_* = U_* d/\nu$
   C. Enter the appropriate $C/\sqrt{g}$, $R_*$ relation in which $\Delta d/d$ or $\Delta R/R$ is the third variable, and read the value of $C/\sqrt{g}$ corresponding to the values of $R_*$ and $\Delta R/R$ or $\Delta d/d$.

3. Compute the average velocity from the relation $U = C/\sqrt{g} \cdot \sqrt{gRS}$, using $d = R$ where appropriate.

When determining the average velocity in a sand-bed channel, for which it has been necessary to assume a form of bed roughness prior to the determination of $\Delta d$ or $\Delta R$, it is necessary to compute the stream power, $\tau_o U$. Then with $D_{50}$ enter Figure 6-30 or some similar relation to determine whether the preselected roughness will occur. To conform with the selected bed roughness, it may be necessary to make another trial computation using a different slope and/or depth. For the design of a stable sand-bed canal, the bed material discharge is computed and compared with the desired bed-material discharge. If they are not approximately equal, the design should be modified by changing slope and/or depth without changing the form of bed roughness.

Example B

Determine the hydraulic radius and depth of flow which takes place in a rectangular flume 2.4 m (8 ft) wide using Simons and Richardson's method when U = 1.012 m/sec.

Data: $D_{35}$ = 0.37 mm, $D_{50}$ 0.45 mm, $D_{65}$ = 0.53 mm, $D_{85}$ = 0.70 mm, S = 0.00301, n = $1.03 \times 10^{-6}$ $m^2$/sec ($0.11 \times 10^{-4}$ $ft^2$/sec), $w_{50}$ = .060 m/sec, g = 9.805 m/$sec^2$, $q_s'$ = 1.68 T/$m^3$ and $w_{65}$ = 0.076 m/sec.

Solution:

1. Assume the bed form is dunes.

2. Assume $d = 1.27$ ft (to select an initial value a regime type relation $d = f(Q)$ may be utilized (see Appendix 6A).

3. Using Figure 6-26 determine $\Delta d$ equal to 0.70 and $\Delta d/d$ equal to 0.58.

4. Using Figure 6-28 determine $C/\sqrt{g}$

$$R_* = \frac{1.2\sqrt{32 \times 1.27 \times 0.00301}}{0.11 \times 10^{-4}} = 38.72 \times 10^3$$

$$\frac{C}{\sqrt{g}} \cong 8.9$$

5. Determine $U$ as

$$U = \frac{C}{\sqrt{g}} \sqrt{gdS} = 3.11 \text{ ft/sec} = 0.95 \text{ m/sec} < 1.012 \text{ m/sec}$$

6. Repeat the same steps using different $d$ while $U_{comp}$ is approximately equal to 1.012. This value of $d$ is equal to (*)

$$d = 1.32 \text{ ft}$$

or

$$R = 0.99 \text{ ft}$$

7. Determine $\tau U$ as

$$\tau U = 62.4 \times 0.99 \times 0.00301 \times 3.2 = 0.59$$

8. Using Figure 6-30 verify that the bed form for these flow conditions is dunes near the transition region. That is, with a slight increase in stream power the bed form would change from dunes to a transition condition between dunes on plane bed. Hence, adoption of the above design values entails some risk and a new design may be determined that avoids the foregoing problem.

Freeboard

Values of freeboard suggested for channel design are listed in Table 6-14 and Figure 6-34.

Manning Roughness Coefficient for Natural Sand-Bed Sediment

Most hydraulic engineers are used to working with the Manning n. Unfortunately, when dealing with natural sand-bed streams, many engineers select a Manning n that is valid for low flow but too large for high flow. They do not realize the fact that the bed form planes out at high flows with a subsequent significant decrease in Manning's n. Observations by Simons and Richardson (1966) on natural sand-bed

(*)In this example $C/\sqrt{g} \sim 9$, $U \sim 3.2$ ft/sec and $\Delta d/d = 0.53$.

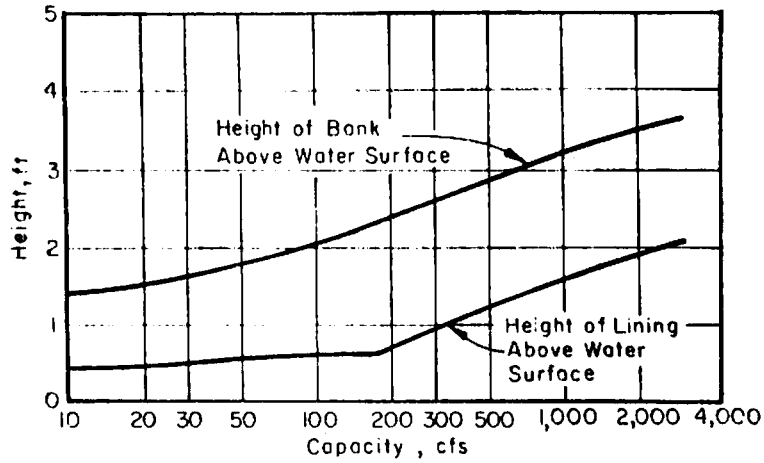


Figure 6-34. Recommended values of freeboard for lined channels (USBR).

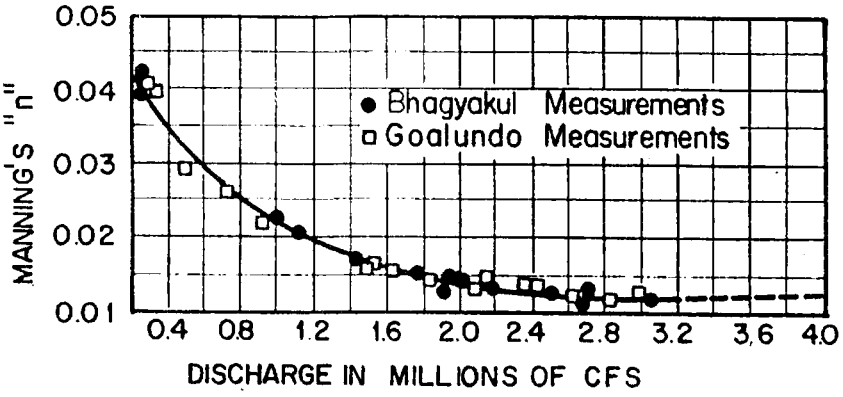


Figure 6-35. Decrease in Manning's n with discharge for the Padma River in Bangladesh.

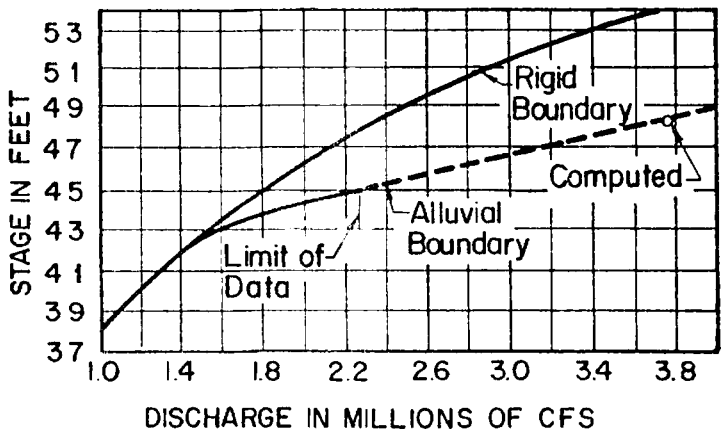


Figure 6-36. Stage discharge relation for the Brahmaputra River at Sirajganj, Bangladesh.

Table 6-14. Freeboard for man-made channels.

| | Freeboard ft | cm |
|---|---|---|
| 1. Lined Channels | | |
| Main channel | 0.49 | 15 |
| Secondary channel | 0.39 | 12 |
| Distributary | 0.16 | 5 |
| Elevated flume | 0.16 | 5 |
| 2. Earth Canals | | |
| Main flood channel (rural) | 2.46 | 75 |
| Main flood channel (residential area) | 3.28 | 100 |
| Drainage channel | 0.49 | 15 |
| Torrential channel | 3.28 | 100 |

streams with bed material having a median diameter ranging from 0.01 mm to 0.4 mm indicate that the bed planes out and resistance to flow may decrease whenever large flow occurs. Manning's n can change from values as large as 0.05 at low flow to as small as 0.012 at high flow. Other hydraulic engineers have also substantiated the small value of Manning's n for rivers and canals when flowing in upper regime.

Dawdy (1961) based upon the findings of Simons and Richardson (1966) found that the bed form changed from dunes to plane in many sand-bed streams of the southwest United States. Colby (1960) showed that a similar phenomena occurred on the streams of northern Mississippi. The change occurs on the Missouri River and the Mississippi River either as a result of change in temperature or when high flows occur. With a dune bed form, the reach of the Missouri River near Omaha, Nebraska, has a Manning n of 0.020, and with a plane bed the same reach has a Manning n of 0.015 (Corps of Engineers, 1968). In both cases discharge for the Missouri River was the same (about 33,000 cfs) but there was 20°F to 30°F decrease in water temperature. Beckman and Furness (1962) reported Manning's n as large as 0.031 for low flow and as small as 0.016 for high flow on the Elkhorn River in Nebraska.

Many rivers and canals in Bangladesh and Pakistan shift from dunes to plane with a consequential reduction in Manning's n. In Figure 6-21 the change that occurs in the Manning n with discharge is illustrated for the Padma River in Bangladesh. This decrease in n occurred as the dunes in the river changed to plane bed as discharge increased. The Hydrologic Directorate of the East Pakistan (now Bangladesh) Water and Power Development Authority (personal communication) found the value for Manning's n for high flows on the Brahmaputra River in Bangladesh to be 0.017. The effect of this value of Manning's n of the stage discharge relation is illustrated in Figure 6-36. The median diameter of the bed material for these Bangladesh rivers is fine sand (about 0.015 mm). Sand bed-streams in Eastern Venezuala that Simons has studied in cooperation with the Ministry of Public Works (MOP) also shifted from large values of Manning's n at low flows to small values of Manning's n at high flows.

Summary

Evaluating the resistance to flow of a movable bed is a very complex problem as illustrated in previous sections. Researchers have tried to simplify the problem assuming first that dimensionless parameters will define the phenomenon and afterwards that a single type of bed form develops on the channel bed. In reality, it is next to impossible to find a natural sand-bed channel with flow conditions such that only one form of bed roughness such as ripples or dunes form on the stream bed. Different bed forms may simultaneously form and their resistance to flow is quite different from the resistance computed using many resistance formulas. To the multiplicity of bed configurations one may also add the transitions which are governed by different factors.

In the lower regime, the resistance to flow is large and hence, the flow depth is large and the velocity is small for a given discharge. As the discharge increases the transition zones are encountered. The transition from ripples to dunes or from dunes to plane bed is accompanied by fluctuations in flow characteristics.

The importance of the bed forms has been considered in all of the methods presented herein. Engelund's (1967), Simons and Richardson's (1966), Richardson and Simons' (1967) and Sentürk's (1967-1973) approaches take explicit care of this effect, and the other approaches do implicitly.

Among the methods presented for estimating the resistance to flow in alluvial channels, no method is generally acceptable because of the tremendous uncertainties involved. However, Einstein and Barbarossa's (1952), Simons and Richardson's (1966), Richardson and Simons' (1967), Alan and Kennedy's (1969), and Sentürk's (1974) approaches have been validated using laboratory data and some field data. If field data pertaining to a particular problem are available, these methods should be tested and if necessary modified prior to their application.

A comparison of various formulas has shown that Einstein and Sentürk's approaches give approximately the same standard deviation when applied to streams. However, Sentürk's formula is more precise. In artificial sand-bed canals, Sentürk's approach and Simons and Richardson's (1966) approach give good results.

## 6.5 RESISTANCE TO FLOW IN COBBLE AND GRAVEL BED STREAMS

General

Traditionally civil engineers have not had to content with mountain rivers to any great extent. In recent decades, though, there has been an increasing human involvement with upland and mountain regions. Activities such as agriculture, forestry, recreation, reservoir construction, river regulation, and highway construction have encroached to a considerable degree on the upland enviroment. Examples of such development include the trans-Alaska oil pipeline, the Kielder scheme for interbasin transfers of water in England, irrigation channels in Nepal, and ski resorts in Colorado. Mountain rivers have felt increasing impacts of human activities and have also become the focus of engineering projects themselves.

At present little is known about the properties of such rivers so their response to development can not easily be predicted. However, there are many examples which have shown that poor development practices can quickly and seriously damage the physical, chemical, and biological environments of these rivers through erosion, siltation, increased flood magnitudes, pollution, destruction of fish spawning grounds, and so on. Consequently there is an urgent need to develop a knowledge of mountain rivers and to produce methods of management which will allow both the prediction and minimization of the impact of human activities.

The first step towards this goal requires that fundamental processes of river flow and channel adjustments be understood. The study that is used as an example here has been based on flume experiments and is intended to shed some light in the area of the processes of fluid mechanics which determine the resistance to flow in a channel. Quantification of the flow resistance is essential in any problem which requires knowledge of flow depth and velocity, such as flow routing or prediction of flood levels.

A mountain river is just one of the forms assumed by rivers which can be generally classified as gravel-bed, cobble-bed or boulder-bed rivers. In this section such rivers will be called just cobble-bed rivers for ease of reference. This section first considers the various types of cobble-bed rivers and the different approaches to describing their flow resistance and identifies the characteristic features of mountain rivers. Previous studies of mountain rivers are reviewed and then the theoretical approach of this study is developed. The flume experiments are described and a flow resistance equation is derived from the results. Finally a brief study of sediment transport in mountain rivers is presented.

Throughout this section the processes of flow are carefully considered. Consequently the derived equations, while inevitably semi-empirical in form, contain only terms which have definite physical meaning.

## Flow Resistance of Cobble-Bed Rivers

The purpose of a flow resistance equation is to relate the velocity of flow to all the other factors which might affect that velocity. Three coefficients are widely used to relate velocity to all relevent resisitive factors. They are Manning, Chézy and Darcy-Weisbach coefficients. The layer coefficient is the only one which is dimensionless and it is therefore used in this report. Darcy-Weisbach friction factor as defined for a channel cross section as follows

$$\left(\frac{8}{f}\right)^{0.5} = \frac{\bar{U}}{\bar{u}_*} \qquad (6\text{-}94)$$

where $\bar{U}$ = mean velocity of flow at the section and $\bar{u}_*$ = mean shear velocity at the section. Shear velocity at a point is defined as

$$\bar{u}_* = \left(\frac{\tau_o}{\rho}\right)^{0.5} \quad (6\text{-}95)$$

where $\tau_o$ = boundary shear stress at a point and $\rho$ = density of the fluid. In steady, uniform flow, mean shear velocity is

$$\bar{u}_* = (gRS)^{0.5} \quad (6\text{-}96)$$

where R = hydraulic radius, S = the energy gradient, which in this case equals the channel slope, and g = acceleration due to gravity (American Society of Civil Engineers, 1963; Henderson, 1966, p. 95).

The basic problem in flow resistance work is the determination of the resistance coefficient. Two approaches can be used but neither is yet completely satisfactory.

The first approach is to assign values based on experience. Aids to this method are tables of values which have been found to be common among open channels and sets of photographs of various channels allowing visual comparisons. Potential errors of this approach were large; subjective judgement lends to the assumption that the chosen coefficient applies to all discharges, dispite the large changes in flow resistance which actually occur as the discharge varies.

In the second approach the coefficient is calculated by some equation based on a theoretical description of the relevant process of flow. The potential for accuracy is greater but the method is inevitably more complex. At the present only simple flows have been described in this fashion.

This section uses the second approach, consequently the characteristics of cobble-bed rivers and various processes of flow resistance need to be identified. It is assumed that the boundary of a gravel-bed or cobble-bed river is composed of noncohesive material greater than about 10 mm (0.0328 ft) in diameter and that there are no significant outcrops of bedrock or patches of vegetation. This assumption restricts the theory to flows within the channel banks. Also assumed is the "only" significant bedforms are the pool/riffle sequence.

The velocity of flow is affected by the resistance of the boundary material, energy losses caused by distortions of the free surface and by changes in flow pattern related to channel cross-sectional shape, longitudinal profile and pattern or planform. Relative influence of these factors changed based on type of flow and type of channel, therefore the resistance coefficient has to be calculated by a different flow resistance equation in each different case. Areas of application of a given equation seem to be defined by the channel slope and the relative boundary roughness.

Small-scale roughness is defined as when the depth of flow is at least an order of magnitude larger than the height of the bed material. In such cases the roughness elements of the boundary act collectively

as one surface, exerting a frictional shear on the flow. The shear is translated into a velocity profile, the shape of which is determined by the roughness geometry, channel geometry, and any free surface distortions.

Large scale roughness is defined as when the depth is of the same order of magnitude as the bed material height. The velocity profile is completely disrupted and the roughness elements act individually, producing a total resistance based mainly on the sum of their form drags. Wall effects dominate the flow, so roughness geometry and distortions of the free surface around elements have most effect on the flow resistance. Channel geometry is indirectly important to the extent that it affects the flow around elements.

As the discharge varies the relative roughness can change by an order of magnitude. This variation of relative roughness allows for delineation of limiting relative roughness of the roughness scale. Figure 6-37 is a plot of resistance function $(8/f)^{0.5}$ against the logarithm of relative submergence $(R/S_{50})$; R is the hydraulic radius. The roughness height is represented by $S_{50}$, the size of the short axis of the bed material which is bigger than or equal to fifty percent of the short axis by count. The short axis is chosen since it more closely approximates the roughness height.

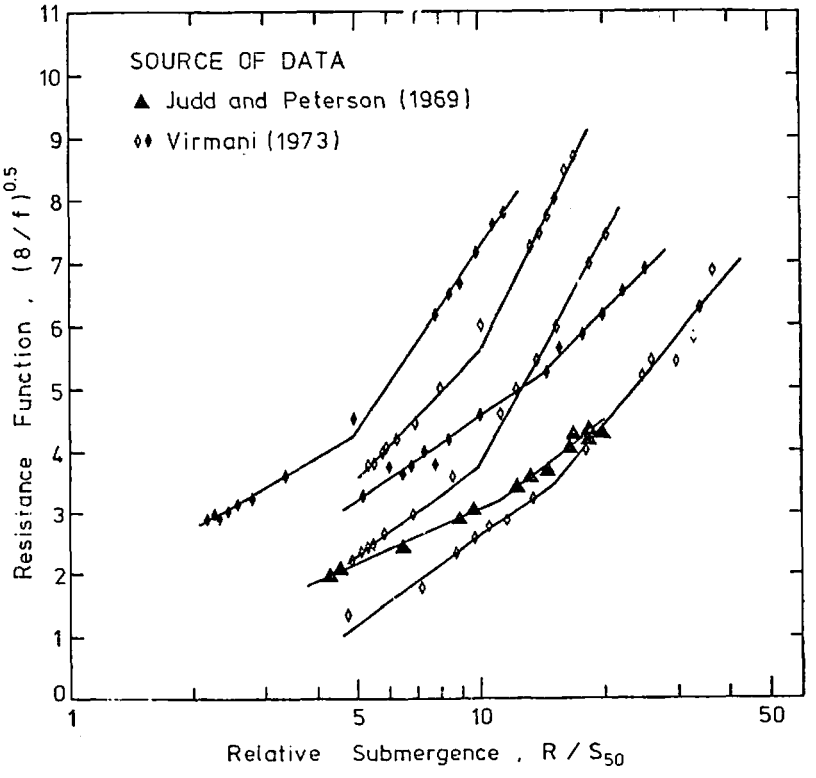


Figure 6-37. Variation of the resistance function with relative submergence at selected river sites.

At relative submergence greater than 10 to 15 the plots are straight lines. This region should correspond to small-scale roughness. At lower relative submergences a different set of straight line plots correspond to intermediate-scale roughness. According to the plots the resistance coefficient increases more slowly, as relative submergence decreases in the intermediate-scale roughness region, than in the region of small-scale roughness.

Insufficient field data exist to delineate the large-scale roughness region, but laboratory experiments by Bayazit indicate at lower relative submergence the resistance to flow increases more rapidly as relative submergence decreases.

The upper limit of small-scale roughness remains undefined. Relative submergence increases by either the depth boosted by increase discharge or the bed material decreases so as not to be classified by cobble or gravel. In both cases the boundary roughness characteristics would be sufficiently affected by bed forms. Therefore the type of flow and resistance equation cannot be classified solely in terms of the scale of the boundary material.

Different flow resistance equations may be required at times at the same section because of changes in the bed material characteristics. At low discharges armoring occurs. The finer sediment on the bed surface is removed until a protective layer composed of the larger material remains, overlying finer material. Typically the channel can then be classified as cobble-bed. At higher discharges the larger material is also removed and the finer material exposed classifying the channel as sand-bed. Consequently, different flow resistance equations are required at high and low discharges.

In addition to the differences in bed material characteristics caused by changes in the representative material, differences can be caused by bed material movement. Owing to the momentum extracted from the flow by the process of bed movement. Therefore a channel with a moving bed is likely to have a different resistance from an otherwise identical channel with a fixed bed.

In conclusion, roughness scale provides the simplest means of identifying the various types of channel flow and their characteristic processes of resistance but more detailed classifications depend on channel slope and bed material characteristics.

## Theoretical Approach to Flow Resistance

Flow resistance in mountain rivers is dominated by wall effects and is determined mainly by the profile drag of the elements. (Profile drag is the sum of form drag and skin friction, the latter being negligible compared with the former over the range of Reynolds numbers observed in rivers.) The drag of individual elements is determined by processes of fluid mechanics while the combined effects of the elements on the total drag of the boundary is determined by processes of wall geometry related to roughness geometry, and channel geometry.

The profile drag D on a single isolated element in a uniform flow of velocity U is related to a drag coefficient $C_D$ by

$$D = \frac{1}{2} \rho A_F U^2 C_D \qquad (6\text{-}97)$$

where $A_F$ = the frontal cross-sectional area of the body projected against the flow. The drag coefficient of a fully submerged element varies with the position of the separation point of the boundary layer about the element. That separation point position is mainly dependent on element shape, structure (surface texture and roundness), and by Reynolds number. For those elements which interact with the free surface, the drag coefficient also depends on the distortions of the surface and varies with Froude number and relative submergence.

Where the flow is both through and over a closely packed layer of elements, the picture is complicated by interactions between the elements. In order to calculate the flow resistance, the number of elements having siginificant drag and effects of neighboring elements and channel boundary on the flow past a given element must be known. Also how the bed movement effects the drag must be determined.

The factors which determine the flow resistance and the rate of change of flow resistance with discharge are as follows:

1. Reynolds number and element structure
2. Froude number and relative submergence
3. Roughness geometry
4. Channel geometry
5. Bed movement

The relative importance of these factors varies with depth and discharge.

Reynolds Number and Element Structure

The form drag of an element varies with the position of the separation point of the boundary layer on the element. The separation point position is dependent on the characteristics of the boundary layer, which in turn are determined by Reynolds number and element shape and structure.

When Reynolds numbers are less than a certain value, the boundary layer is laminar, even though the external flow is turbulent. As Reynolds number increases above the critical value, transition to turbulent boundary layer occurs. Laminar boundary layers have higher drag coefficient than turbulent boundary layers because of relative early separation. Qualitatively, the magnitude of the drag coefficient depends on the shape of the element. The critical Reynolds number at which transition begins varies with the surface texture of the element. Generally the rougher the surface, the lower the critical Reynolds number is. Another influencing factor is neighboring objects. The more concentrated the elements, the lower the critical Reynolds number is.

As the Reynolds number varies so does the drag coefficient. Therefore the Reynolds number must be accounted for in the resistance equation.

An element which protrudes through or nearly through the free surface causes distortions in the free surface which represents an energy loss and affect of the drag of the element. The drag generated in this fashion varies with Froude number and relative submergence.

Previous studies have been mainly concerned with the wave drag related to the pattern of waves around an element and have not considered the effects of larger distortions such as hydraulic jumps. Since hydraulic jumps are such an integral part of mountain rivers the contribution to drag cannot be neglected. Therefore this section includes effects of wave drag and hydraulic jump on total drag caused by free surface distortions around elements.

Wave Drag. Wave drag may be created by bridge piers with the depth large enough that the wall effects can be neglected and surface waves can develop freely around piers. The waves cause differences in depth, and therefore hydrostatic pressures, between upstream and downstream faces of each pier thereby creating a pressure drag. The wave pattern and drag change with Froude number and concentration of the piers.

Free Surface Drag of a Single Element. Pronounced free surface effects occur at relative submergences of less than about 1.6 and Froude numbers of less than 1.5. Generally the drag coefficient depends on gravitational forces and is a function of Froude number and relative submergence. At Froude numbers above 1.5, free surface distortion does not appear to contribute significantly to the drag, and viscous forces may be significant.

Moderate free surface effects occur at relative submergences of 1.6 to 4 and Froude numbers of less than 1.5. Both gravitational and viscous forces affect the drag coefficient so if the Reynolds number lies in the transitional range, the drag coefficient is a function of Froude number, Reynolds number, and relative submergence.

Negligible free surface effects occur once the relative submergence exceeds a value of about 4. Viscous forces predominate so the drag coefficient varies mainly with Reynolds number. Since a relative submergence of about 4 marks the limit between large-scale and intermediate-scale roughness, it seems likely that the physical explanation for that boundary is that it marks the relative submergence at which the effect of the elements on the free surface becomes negligible.

At Froude numbers less than 1.5 the drag coefficient, for a given Froude number, increases as the relative submergence decreases. On the other hand, for constant relative submergence, as Froude number increases the drag coefficient first rises to a peak value and then decreases. The Froude number corresponding to the peak drag coefficient varies with relative submergence.

The relative submergence obviously influences the mechanism by which free surface drag develops which suggests that the mechanism is related to the hydraulic jumps rather than surface waves.

Generation of Hydraulic Jumps. At low relative submergences (less than 0.5) the flow around an element resembles the flow about a bridge pier that there is no flow over the element. However, the flow about a bridge pier is not greatly affected by wall effects (except at very low depths) and a surface wave pattern can develop freely. In the flow about a roughness element, wall effects are very important and depths are shallow enough that changes in depth caused by distortions of the free surface can radically alter the local Froude number.

The various conditions under which a hydraulic jump occurs are shown in Figure 6-38. Localized supercritical flow can occur behind, along side, or in front of an element. The protrusion of the element through the water surface can create localized acceleration of the flow, which relative to the stationary wake (caused by the stagnation point) can cause an hydraulic jump. In the supercritical range a jump and its associated wave train are the principal cause of the free surface drag of protruding elements.

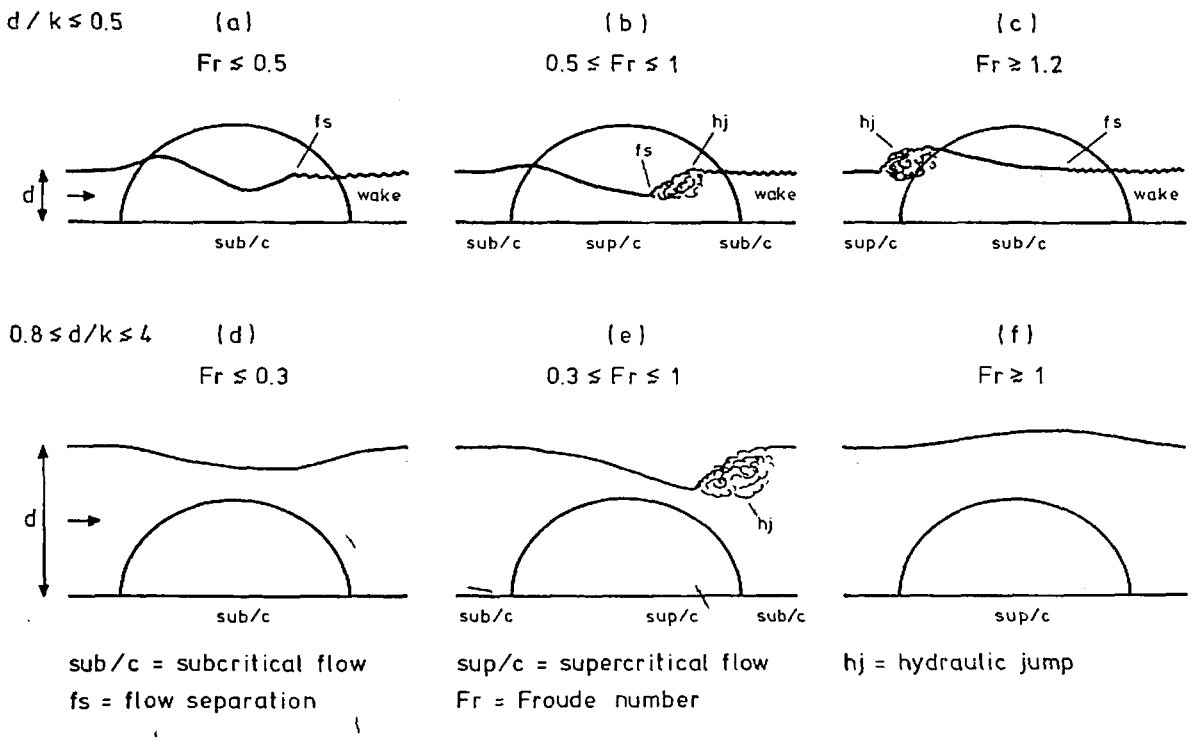


Figure 6-38. Theoretical free surface configurations for flow past a single roughness element of height k in the large-scale roughness region at various Froude numbers. Flow is from left to right.

The submerged element also can cause surface disturbances. Because of the relatively large differences between depths over the wall and over the element, large variations of local Froude number are possible.

For a given lateral width of hydraulic jump, the lower the mainstream Froude number, the greater is the amount of energy which must be lost in the hydraulic jump to decelerate the localized supercritical flow to the subcritical mainstream flow.

As the mainstream Froude number increases, the relative energy loss in the hydraulic jump decreases until, as the whole flow becomes supercritical, the jump disappears.

Free Surface Drag of a Rough Boundary. In rivers, increase of Froude number at a section is usually caused by increases of discharge and is usually accompanied by increase in depth and relative submergence. While the increase in Froude number might initially act to cause an increase in drag coefficient, that increase is likely to be masked entirely by the decrease in drag caused by the increasing relative submergence. Also, as Froude number continues to increase to near critical values, it acts to reduce the drag. As the depth increases the number of protruding elements decreases. Thus as Froude number, or discharge, increases at a section, both the drag of individual elements and the number of significant elements are likely to decrease, with the result that overall free surface drag should also decrease.

Free Surface Instabilities. Roll waves may appear at high Froude numbers classified as free surface instabilities. They can significantly affect local conditions by increasing depth and probably, promoting bed material movement and presumably represent an energy loss. However, on turbulent flows, roll waves do not develop until the Froude number approaches a value of two, and Froude numbers of this magnitude are unusual in natural channels. Also extreme rough boundaries deter the onset of roll waves, so free surface instabilities are unlikely to be important in mountain rivers.

Process of Wall Geometry

Roughness geometry, or the disposition of the elements on the boundary, determines the degree that each element affects the flow and the proportion of the bed material which has a significant effect on the flow. For nonuniform bed material it depends on the areal concentration of the elements and their size distribution and shape.

Roughness Concentration. Roughness concentration can be given as the ratio of either the average frontal cross-sectional area or, the average basal plan area of the elements, to the area of bed per element. Frontal concentration $\lambda_1$ is

$$\lambda_1 = \frac{\sum_1^n A_F}{A_{bed}} \tag{6-98}$$

and basal concentration $\lambda_2$ is

$$\lambda_2 = \frac{\sum_1^n A_B}{A_{bed}} \tag{6-99}$$

where $A_F$ = wetted frontal cross-sectional area, $A_B$ = basal plan area, and there are $n$ elements on an area of bed, $A_{bed}$. Basal concentration is related to the number of elements per unit area. Frontal concentration is related to the drag of the elements via Equation 6-97.

Various flume studies have shown that the relative influence of the roughness elements on the flow resistance depends mainly on their concentration. At low concentrations individual elements can exhibit their maximum resistance. At high concentrations the resistance of individual elements is reduced because of wake interference effects. Consequently the flow resistance of the boundary varies with roughness concentration. In a natural channel roughness concentration may change due to sediment erosion or deposition and depth change causes the wetted frontal cross-sectional area of an element altering the frontal concentration.

Effective Roughness Concentration. Calculation of effective roughness concentration must account for only those elements which project significantly into the flow. At low depths the effective roughness concentration will increase and the inverse is true for an increased depth. As depth increases the relative submergence increases and the roughness becomes small-scale, affecting the flow by boundary shear rather than by form drag.

Effective roughness concentration should therefore vary directly with relative roughness.

Bed Material Size Distribution. Nonuniform material causes the frontal concentration to initially rise as depth increased from zero, but it should begin to fall before all the elements are covered because smaller elements become submerged and are no longer included in the calculation. Similarly, the number of significantly projecting elements decreases and so therefore does the effective roughness concentration.

Bed Material Shape. Roughness shape affects the magnitude of the roughness concentration by determining the wetted frontal cross-sectional area of the elements. For the same depth different shape elements have very different wetted frontal cross-sectional area. The more cubical the element cross-section, the greater the concentration.

Number of Elements. Although not all the elements are included in the effective roughness concentration and the number decreases as the depth increases, that number is likely to be a function of the total number of elements on the bed.

The total number of elements on the bed is a direct function of the ratio of the area of the bed to the average basal plan area of the element. In turn the basal plan area is a function of the product of two axes of the element base, longstream axis $X_n$ and the cross-stream axis $Y_n$. With the section channel width $W$ and length $\Delta x$ the total number of boulders is

$$N = \frac{W\,\Delta x}{X_n\,Y_n} \tag{6-100}$$

Setting $\Delta x$ equal to $X_n$ gives a number characteristic of, but not necessarily equal to, the number of elements at a section

$$N = \frac{W}{Y_n} \tag{6-101}$$

It should therefore be possible to give an effective roughness concentration as some function varying directly with relative roughness, the rate of variation depending inversely on the roughness size distribution and the magnitude varying with roughness shape and $W/Y_n$.

Quantification of Roughness Geometry. The precise determination of an element axis depends on the method by which samples of bed material are aquired. The most practical and widely used method is that of Wolman (1954), in which individual elements are collected on a random basis from the surface layer of the bed material and their median axes measured. Once collected, the elements can be ranked by size, a cumulative percentage frequency curve is constructed and the median size of the median axis $D_{50}$ extracted. If the long and short axes are also measured, their median axes ($L_{50}$ and $S_{50}$, respectively) can be similarly derived.

It is assumed in this study that in natural channels the long, median, and short axes of an element correspond respectively to the cross-stream axis, longstream axis, and height.

Size distributions of natural sediments are often log-normal or nearly so. The simplest representation of the standard deviation T is

$$T = \log (D_{84}) - \log (D_{50}) \qquad (6\text{-}102)$$

$$T = \log \left(\frac{D_{84}}{D_{50}}\right)$$

As noted by Equation 6-102 the standard deviation is given as a logarithm, therefore it cannot be directly related to roughness size which has dimensions of length.

Channel Geometry

Channel geometry plays an important part in small-scale roughness, but not in large-scale roughness. Extreme wall roughness and shallow depths do not permit the development of secondary circulation at bends or changes of cross-sectional shape. The longitudinal bed profile is usually uniform. Consequently the effects of channel pattern or planform and bed profile can be neglected.

Channel cross-sectional shape can influence the variation of resistance with discharge. It is suggested that this shape effect acts via a relationship with the proportion of a channel cross section which is occupied by roughness elements, that proportion having a direct effect on the manner in which the flow loses energy.

Nerbich and Shulits (1964) showed that, with large-scale roughness and high concentration of elements, the flow is funnelled between the elements in jets and then impacts against downstream elements. The resulting energy loss and the distortions of the free surface, typical of tumbling flow, must considerably affect the flow velocity and resistance. However, the strength of the funneling effect must be a

function of the proportion of the channel cross section occupied by elements at a given discharge, thus, at any given discharge, the greater the proportion, the less the flow cross-sectional area and the more intense the funnelling effect. As a corollary, at any given section it would be expected that as discharge increases and the roughness elements are submerged, the proportion of channel occupied by elements would decrease and the funnelling effect becomes less intense.

This concept is illustrated using Figure 6-39 which shows a cross section of a channel with large-scale roughness. The shaded area represents that part of the roughness which lies below water. Total channel cross-sectional area is wd', where d' = depth from the free surface to the bed. If $A_w$ is the total wetted cross-sectional area of the roughness, the proportion of the channel cross section occupied by roughness is $A_w/wd'$. This parameter, here defined as the relative roughness area, is two-dimensional relative roughness.

Relative roughness area at a section decreases as depth increases but the relationship with depth must be different at different channel sections. Usually, as depth increases at a section, width also increases but the ratio of width to depth decreases. As the increase in depth brings into play more elements from the channel sides, it can be seen that the relative roughness area should vary directly with the ratio of width to depth.

The smaller the effective roughness concentration at any given depth, the smaller is the degree to which the elements project into the flow and the less is the funneling effect. Thus, if the effective roughness concentration decreases rapidly as depth increases, so should the relative roughness area decrease. It should therefore be possible to drive a relationship in which the relative roughness area changes with the ratio of width to depth and in which the rate of change is a function of the effective roughness concentration.

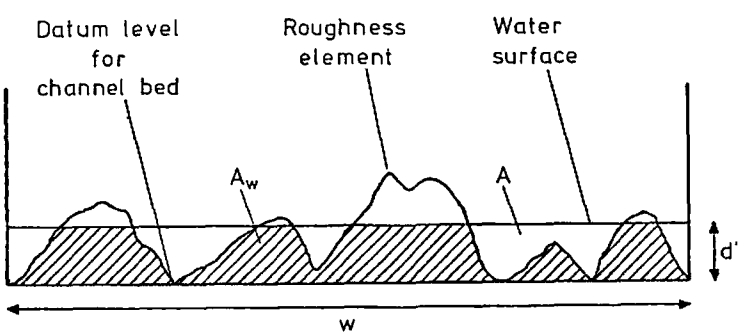


A = flow cross-sectional area

$A_w$ = wetted roughness cross-sectional area

$A + A_w = wd'$

$A_w/wd'$ = relative roughness area

Figure 6-39. Definition diagram for relative roughness area.

Assuming that the bed is composed of elements which are uniform in size, the area of flow A, above each element is

$$A = wd' \quad A_w \tag{6-103}$$

Experimental Work

In order to provide data with which to develop a flow resistance equation, a flume study was carried out. Measurements were made of flows over five different roughness beds at a variety of slopes and discharges. Most of the measurements were made with fixed beds but a few measurements were made using loose beds in order to study the effect of bed material movement on flow resistance.

The five roughness materials are classified as 0.5, 0.75, 1.5, 2.0, and 2.5 inch (respectively, 12.7, 19.05, 38.1, 50.8, and 63.5 mm), these figures referring approximately to the maximum size of each material. The 0.5, 0.75 and 1.5 inch materials were commercially available gravels, consisting of chips derived by crushing larger cobbles. The 2.0 and 2.5 inch materials consisted of cobbles which were collected by hand.

The size distributions of the materials were determined before the roughness beds were constructed. In an attempt to simulate Wolman's (1954) method of sampling coarse bed material, a sample of a hundred elements was collected on a random basis. The long, median and short axes of each element were measured and the relevant class size interval to which each axis corresponded was noted. The arrangement of the interval widths is one which has been found to be useful for river sediments (Bathurst, 1977).

Cumulative percentage frequency curves were plotted on log-probability paper (Figure 6-40). The distributions are approximately log-normal so the standard deviations of the distributions were calculated using Equation 6-102. Generally the distributions are more uniform than those of natural river sediments.

Intercept sphericity of each material was calculated based in turn on the 84, 50 and 16 percentile sizes of each axis. The ratios of long to short and median to short axes were also calculated. There are differences in shape between the chips and the cobbles but both have intercept sphericities similar to those measured by Miller (1958) in mountain rivers.

Densities of the packed materials (voids plus elements) were obtained by measuring the weight of a given volume of each material. Surface texture of the material was rough. The chips were angular and the cobbles were well rounded.

Froude number, $\bar{U}/(gd)^{0.5}$ varied from 0.189 to 1.927, covering the regions of subcritical, transcritical, and supercritical. Reynolds number $\bar{U}\ D_{50}/\nu$ varied from about $10^3$ to $4.4 \times 10^4$. This range lies below the critical Reynolds number marking the transition from laminar

to turbulent boundary layers on the elements and also in this range the drag coefficient varies little with Reynolds number. Reynolds number effects were therefore negligible.

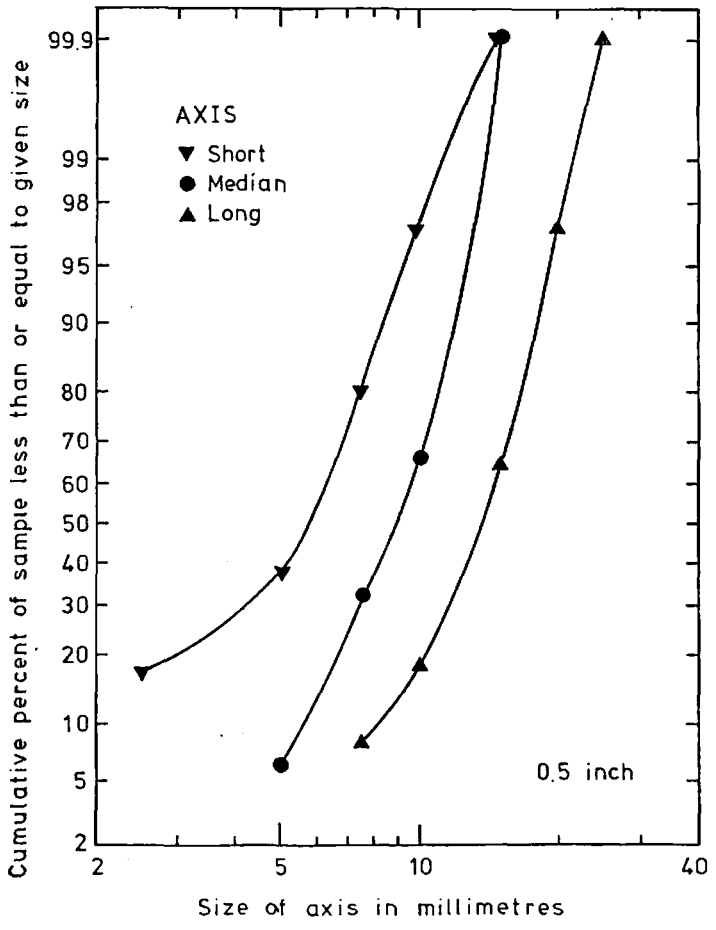


Figure 6-40. Cumulative percentage frequency curves for the long median and short axes of the 0.5 inch roughness material, plotted on a log-probability graph.

In calculating relative submergence it is assumed that the height of an element on the bed is equal to its short axis. This orientation is likely to have been adopted during hydraulic construction of the bed. However, because the bed of the flume was not constructed hydraulically this assumption is invalid. More probably the element height was nearer to the average of the long and the median axes.

An examination of the variation of resistance function $(8/f)^{0.5}$ with relative submergence indicates that there is a general decrease in resistance as relative submergence decreases. Bathurst showed that roughness concentration and its resistive effects change with relative submergence and therefore the concentration for only those boulders that protrude through the flow was calculated.

$$\lambda_1 = 0.139 \log \left(1.91 \frac{D_{84}}{R}\right) \qquad (6\text{-}104)$$

He further derived a resistance equation

$$\frac{\bar{u}}{(gRS)^{0.5}} = \left(\frac{8}{f}\right)^{0.5} = \left(\frac{R}{0.365D_{84}}\right)^{2.34} \left(\frac{w}{d}\right)^{7(\lambda_1 - 0.08)} \qquad (6\text{-}105)$$

Figure 6-41 shows Equation 6-105 and the data collected from flows over a fixed bed. The data points have a tendency to diverge at relative submergence of unity, possibly as a result of changes connected with the transition from large-scale to intermediate-scale roughness.

In the logarithmic region (Figure 6-41) there is a definite scatter of data points which is based partly on differences between the roughness beds and partly on Froude number. Values of Froude number are not given in the figure but examination of the data shows that, at a given relative submergence and for a given roughness bed, the flow resistance decreases as Froude number increases. The scatter is not so obvious in the semilogarithmic region (Figure 6-42) suggesting that the effect depends on a free surface drag which is present only while the roughness elements protrude through or nearly through the surface.

A more general equation than 6-105 would include additional terms to account for free surface drag and variations in roughness geometry. Also a replacement for the roughness concentration $\lambda_1$ is required. Although values of $\lambda_1$ calculated by Equation 6-104 are used in the plots of Figures 6-41 and 6-42, some of those values are negative. Strictly a negative value of $\lambda_1$ is physically meaningless since the elements are submerged and have zero frontal concentration.

Development of the Flow Resistance Equation

Most of the flow resistance is derived from the form drag of the roughness elements and the distortions to the flow around the elements. Consequently a flow resistance equation for mountain rivers has to account both for the processes of fluid mechanics by which the form drag is generated and for the processes of wall geometry by which the combined drag of the elements affects the flow resistance. More specifically the resistance varies with Reynolds number, Froude number, roughness geometry, channel geometry, and sediment movement where relevant. Analysis has shown that the flow resistance of large-scale roughness is likely to vary with relative roughness area, roughness geometry, Froude number, and possible Reynolds number. The flow resistance of intermediate-scale roughness should vary with relative roughness area, roughness geometry, and Reynolds number. The experimental data are used to qualify these relationships in a semiempirical fashion. The relationships are derived with river channels in mind but because of the one-dimensional nature of the flume flows the results should be applicable to any given vertical in a flow and therefore to overland flow.

Theoretical analysis, supported by the results of the flume study, suggests that, for the range of Reynolds numbers given by $4 \times 10^4 < \bar{U} D_{50}/\nu \; 2 \times 10^5$, resistance is likely to fall significantly as Reynolds number increases. However, if there are roughness elements protruding through the free surface, the effect is small by comparison, with Froude number effects related to the appearance of hydraulic jumps

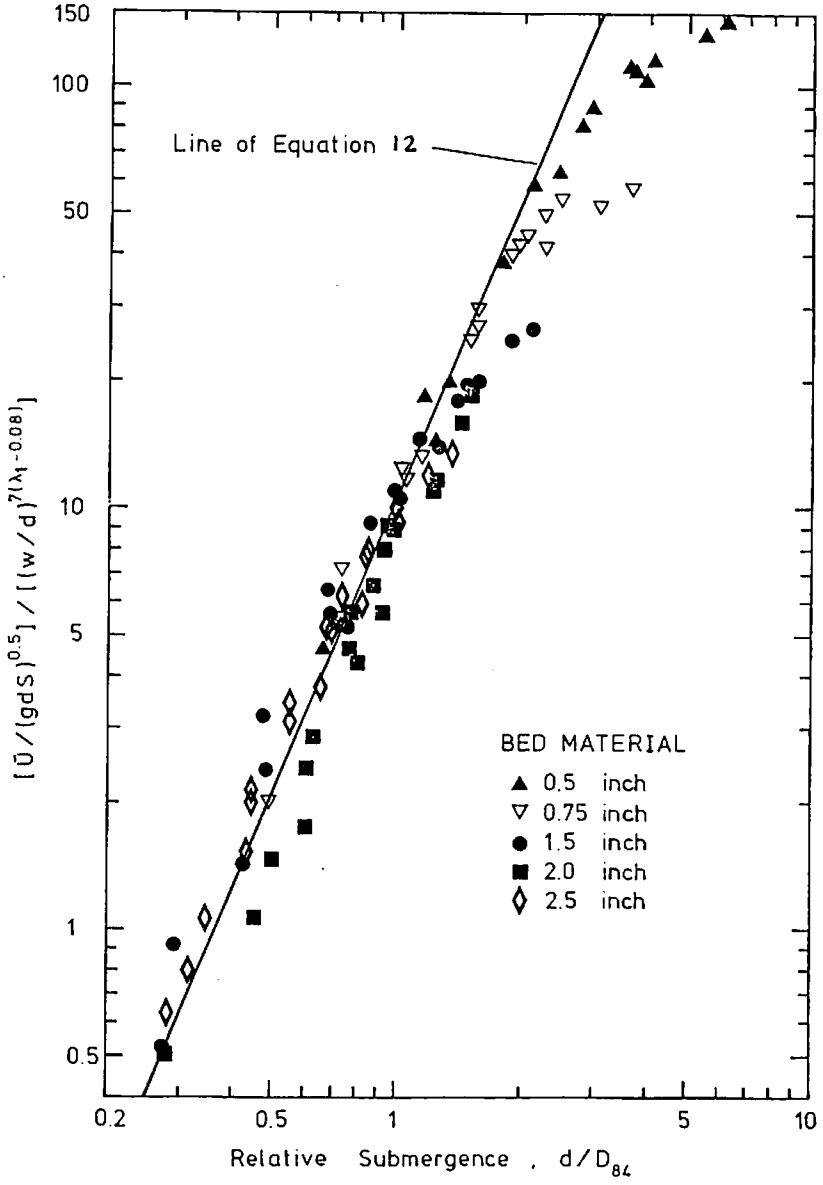


Figure 6-41. Variation of $[\bar{U}/(gdS)^{0.5}]/[(w/d)^{7(\lambda_1 - 0.08)}]$ with relative submergence for all the flows over the fixed roughness beds.

and the generation of free surface drag. For the bed as a whole, free surface drag decreases as Froude number and relative submergence increases. Once the elements are submerged, Froude number effects related to free surface drag are small but Froude number effects related to standing waves may be important.

The effect of roughness geometry can largely be described by a single parameter b the function of effective roughness concentration. This accounts for the variation of the roughness geometry both with depth and with bed material, although it does not make allowance for differing element shapes.

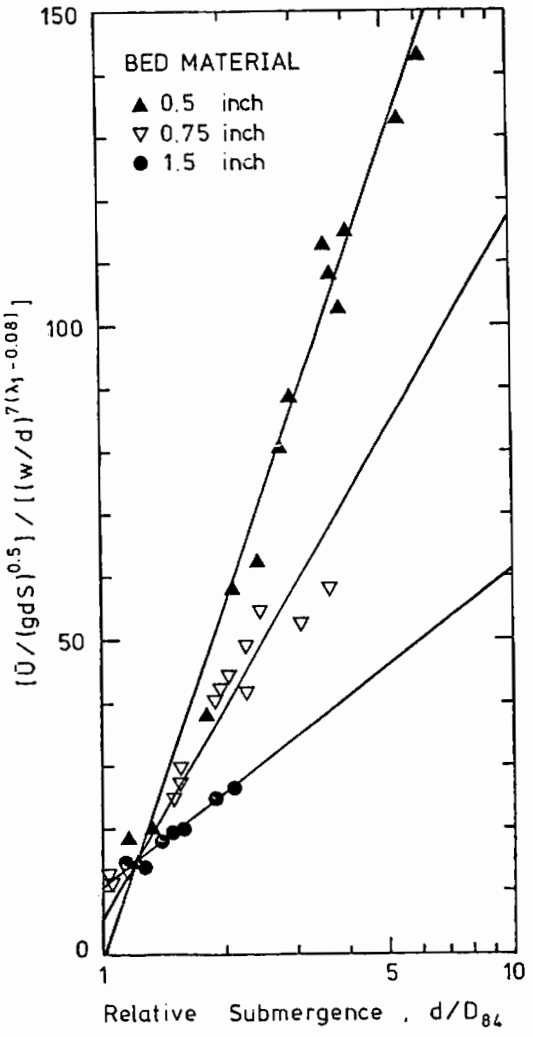


Figure 6-42. Variation f $[\bar{U}/(gdS)^{0.5}]/[w/d)^{7(\lambda_1 - 0.08)}]$ with relative submergence for all the flows over the fixed roughness beds with relative submergence of greater than unity.

$$b = [1.175 \left(\frac{Y_{50}}{w}\right)^{0.557} \left(\frac{d}{S_{50}}\right)]^{0.648\ \sigma^{-0.134}} \qquad (6\text{-}106)$$

Similarly the effect of channel geometry is accounted for by the relative roughness area $A_w/wd'$ which indicates the proportion of a channel cross section occupied by roughness and thence the degree of funneling of the flow. For river channels of homogeneous boundary material

$$\frac{A_w}{wd'} = \left(\frac{w}{d}\right)^{-b} \qquad (6\text{-}107)$$

Based on the analysis of the flume data, the resistance equation for large-scale roughness ($b < 0.755$) is

$$\frac{\bar{U}}{(gdS)^{0.5}} = \left(\frac{8}{f}\right)^{0.5}$$

$$= \left[\frac{0.28}{b}\ Fr\right]^{\log\ (0.755/b)}$$

$$\times\ \left[13.434\ \left(\frac{w}{Y_{50}}\right)^{0.492}\ b^{1.025}\ (w/Y_{50})^{0.118}\right]$$

$$\times\ \left[\frac{A_w}{wd'}\right] \qquad (6\text{-}108)$$

This equation does not apply where Reynolds number effects are significant, where there is bed material movement or where there is a system of standing waves. However, within its range of application the equation seems to work well as long as the various parameters, particularly the roughness sizes and the channel wetted perimeter, are derived or measured as in this study.

In spite of its complex form, Equation 6-108 contains relatively few parameters and can be applied using a simple iteration procedure. Comparison with independent river data shows that, when based on mean parameters of flow and with semiempirical equations describing relative roughness area and channel width, it can be used to calculate a mean resistance coefficient for a channel reach (see Figures 6-43, 6-44 and 6-45). Alternatively, in its more general form related to a single vertical through the flow, the equation can be applied to overland flow and to regions of large-scale roughness in channels where there are significant changes in boundary material and depth across a section.

The brief investigation of bed material movement shows that sediment transport equations developed for sand-bed rivers do not apply to mountain rivers. The flume data suggest that two of the hydraulic factors determining sediment movement are channel slope and bed material characteristics. Other studies, though, show that geomorphic factors, which determine the supply of sediment to the channel, are at least as important and future research should be directed towards identifying these factors.

Application of the Resistance Equation

The derived resistance equation was given in Equation 6-108. An iterative technique by which Equation 6-108 can be solved is demonstrated using the data of Virmani (1973).

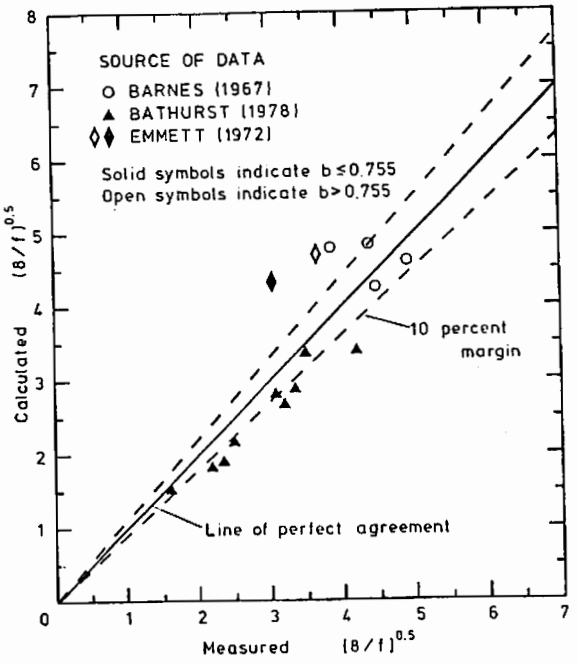


Figure 6-43. Comparison of values of the resistance function calculated using Equation 6-108 with measured values for flows at selected river sites.

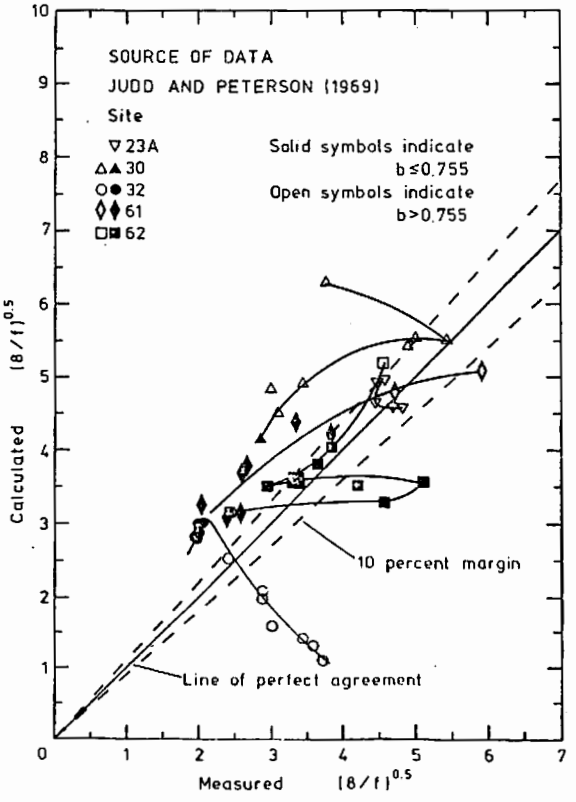


Figure 6-44. Comparison of values of the resistance function calculated using Equation 6-108 with measured values for flows at selected river sites.

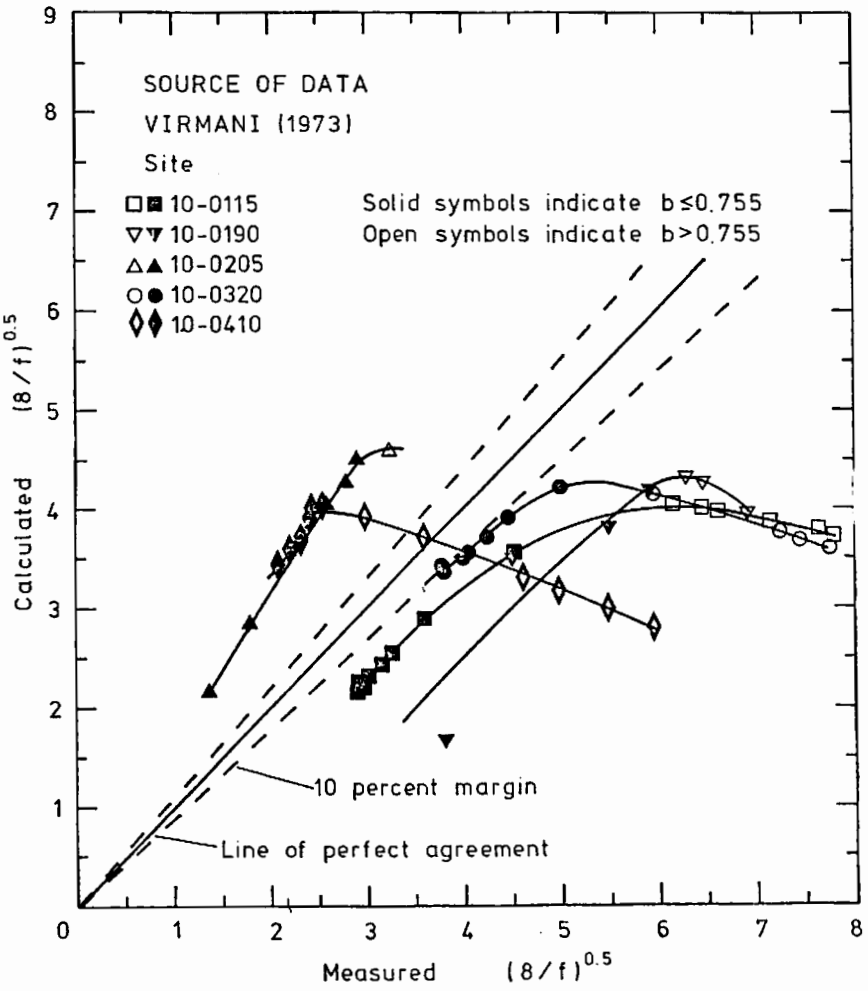


Figure 6-45. Comparison of values of the resistance function calculated using Equation 6-108 with measured values for flows at selected river sites.

A relationship between channel width w and mean depth d such as Equation 6-106, should first be delineated. Taking Virmani's site 10-0115 as an example, the data show that

$$w = 64.05\ d^{0.1858} \tag{6-109}$$

Thus the mean velocity $\bar{U}$ is related to discharge Q by

$$\bar{U} = \frac{Q}{64.05\ d^{1.1858}} \tag{6-110}$$

Substituting for w and $\bar{U}$ in Equation 6-108 and using Equation 6-109 to describe relative roughness area, depth is related to just discharge and the parameters of roughness geometry:

$$\frac{Q}{200.6\ d^{1.6858} S^{0.5}} = \left[\frac{0.001396\ Q}{b\ d^{1.6858}}\right]^{\log(0.755/b)} \times \left[104\ \left(\frac{d^{0.1858}\ 0.492_b 1.675 (d^{0.1858}/Y_{50})^{0.118}}{Y_{50}}\right)\right] \times \left[64.05\ d^{-0.8142}\right]^{-b} \tag{6-111}$$

where

$$b = \left[0.1158\ Y_{50}^{0.557}\ \left(\frac{d}{S_{50}}\right)^{0.8965}\right]\ 0.648\ \sigma^{-0.134} \tag{6-112}$$

Virmani's data show that

$$D_{50} = 0.144 \text{ m}$$

$$\sigma = 0.313$$

$$S = 0.0117$$

Assuming that $S_{50} = 0.57\ D_{50}$, and the cross-stream axis $Y_{50}$ is equal to $L_{50}$ and $L_{50} = D_{50}/0.57$, then

$$S_{50} = 0.0821 \text{ m}$$

$$Y_{50} = 0.253 \text{ m}$$

The calculated value of the function of effective roughness concentration b is therefore $0.7268\ d^{0.6787}$ (Equation 6-112). Substituting into Equation 6-111

$$\frac{Q}{21.7\ d^{1.6858}} = \left[\frac{0.00192\ Q}{d^{2.3645}}\right]^{\log(1.039/d^{0.6787})}$$

$$\times\ [204.5\ d^{0.0914}(0.7268\ d^{0.6787})^{1.969\ d^{0.02192}}]$$

$$\times\ \left[\frac{64.05}{d^{0.8142}}\right]^{-0.7267\ d^{0.6787}} \qquad (6\text{-}113)$$

The only two unknowns in this equation are discharge and depth, so specifying one allows the other to be calculated. Virmani's data show that at a discharge of 0.906 $m^3s^{-1}$ the depth is 0.146 m. If, however, the depth were unknown it could have been calculated by the following iterative technique.

The known value of discharge and a guessed value of depth are substituted into the right side of Equation 6-113. With depth set at, 1 m, for example, the value of the right side is 4.775. Equating this with the left side of the equation, and including the known value of discharge, a calculated value of depth equal to 0.0601 m is obtained.

Using this derived value as the new guessed value of depth for the right side of the equation, the next iteration gives a depth equal to 0.1134 m. Subsequent iterations give depths of 0.1546 m, 0.1623 m, and 0.1625 m. As the difference between the last two values is insignificant, the final value can be assumed to be the required value. Five iterations therefore seem to be sufficient for the calculation of depth and the result is about 10 percent in error relative to the measured value. By the use of Barnes' data (Water Supply Paper #1849) verification of this function can be made. Barnes' data provides Manning's friction factor for peak discharges in 14 rivers and 53 cross sections. Only 14 out of the 50 available river sites provide all the required information.

The cross sections were digitized in order to determine the geometric power relations. Then the routine calculated a depth by the resistance function and used this predicted depth and geometric power relations to determine Manning's friction factor. The results are presented in metric units, but the computer program can easily be converted to english units.

When the program was originally run the results were reasonable in predicting the depth, but it was felt that geometric differences between the flume studies and the field studies could be improved. Because of the large width depth ratio in the flume studies and smaller ratio in the field studies the adjustment must be of a channel shape nature. The area of concentration is the coefficient e because this constant accounts for resistance that is related to the width depth ratio and relative roughness. To determine e the data provided all the needed parameters and the computer program was altered to calculate an e coefficient for each of the 53 cross sections. Then the computer

package was used to determine an equation by use of nonlinear least square routine. The equation was based on the width depth ratio and relative submergence ($d/D_{84}$). The result was as follows

$$e = 1.902 \left[\frac{d}{D_{84}}\right]^{0.219} \left[\frac{w}{d}\right]^{0.615}$$

Figure 6-46 shows the relationship between measured e determined from the data and calculated e determined from the equation above. The scatter on this graph cannot be ignored but even with the scatter the improvement of the predicted depth was obvious and the comparison of measured depth and the calculated depth is shown in Figure 6-47. The improved coefficient e lowered the predicted values for depths above 3 meters. This figure shows that the predicted values worked very well with the adjustment of geometric differences.

In Figure 6-48 the area that was measured is plotted against the area calculated by the area power relation based on the depth. It should be noted that the power relations derived by the digitized cross sections were based on thalweg depth and not average depth. Some minor adjustment was required. By assuming that the average depth was equal to hydraulic radius, a correction equation was derived from the power relations. This correction equation was used in the width-depth equation in Bathurst's routine and for the area and wetted perimeter required by Manning's equation in order to determine friction factor.

Figure 6-49 shows the comparison measured Manning's friction factor with calculated friction factor. In the Manning's equation the hydraulic radius was determined from the geometric power relations for area and wetted perimeter. The scatter in this plot is probably due to the error involved with each individual component; as errors are combined the scatter is inevitable. The general trend does exist and it is evident that the predicted depth is not in error.

The discharge versus Manning friction factor is presented as a reference to other comparison presentations for different resistance functions. Comparing Figures 6-50 and 6-51 shows that the trend of the predicted and measured Manning's friction factor are the same. There are only 14 data points on Figure 6-49 because the 53 cross sections are all from 14 rivers having the same Manning's friction factor.

Figure 6-52 shows a comparison of discharge versus depth, both predicted and measured.

Figure 6-53 shows the comparison of relative submergence of calculated and measured depth. This graph shows that the resistance function predicted a large scale roughness when the channel was by definition large-scale and the same for intermediate scale roughness. It is important to note that relative roughness characteristics hold for true Bathurst resistance functions.

As is evident on the figures presented, the proposed resistance function is good for the cobble-bed channels. By slight adjustment of

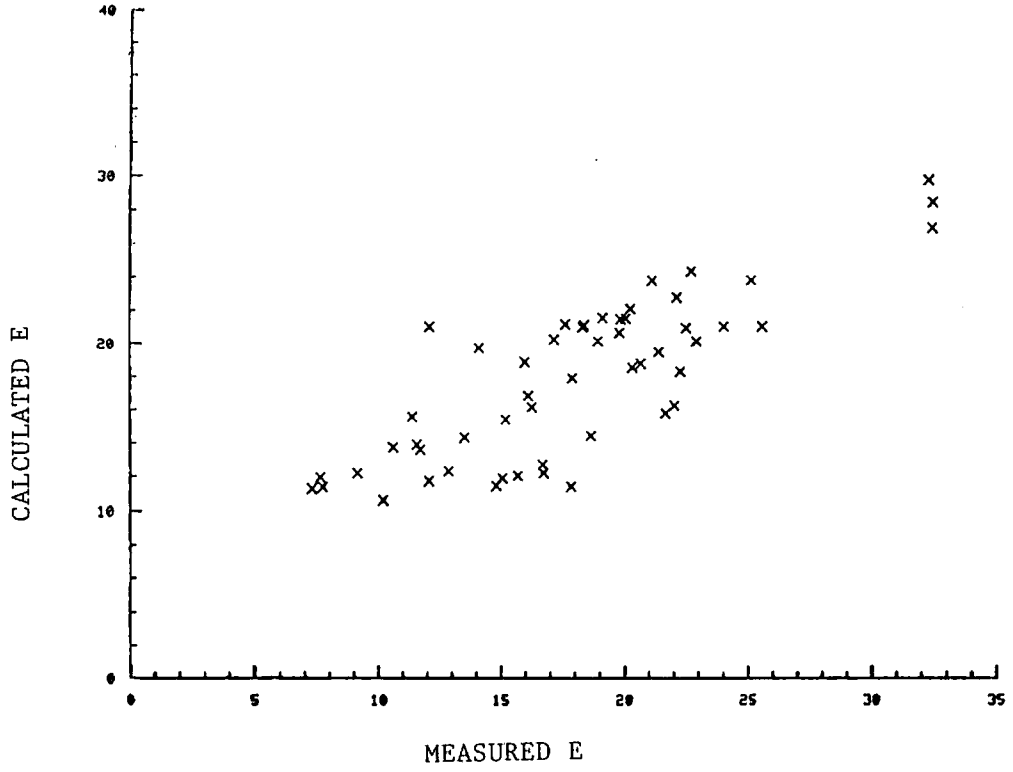


Figure 6-46. Comparison of coefficient e.

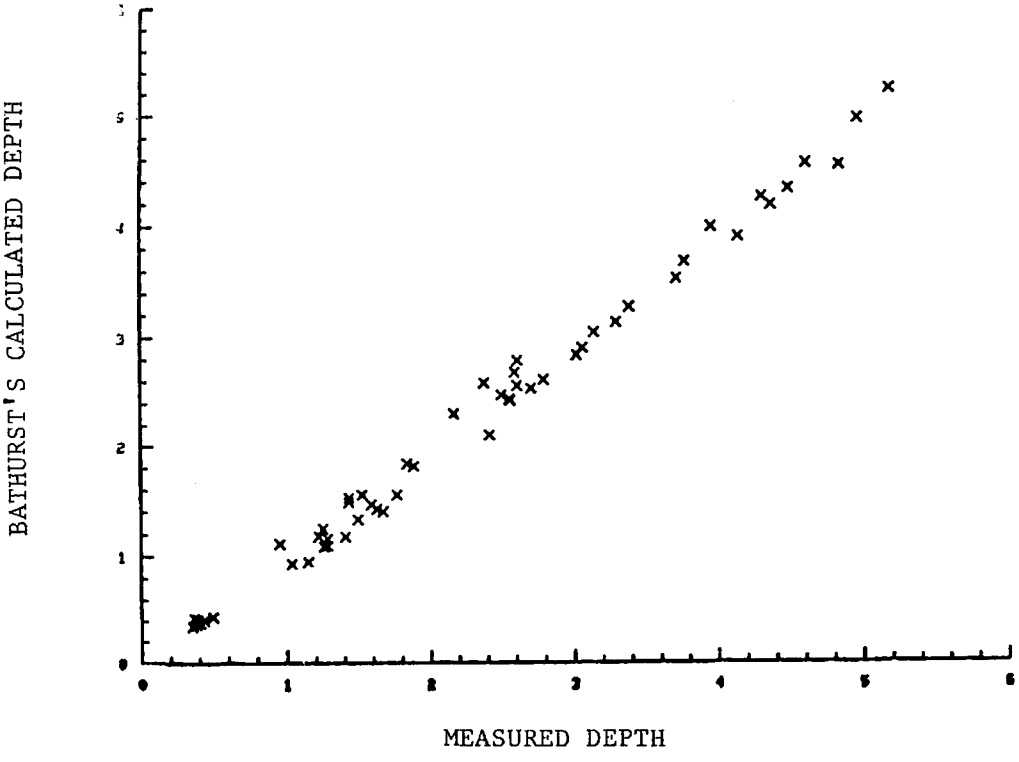


Figure 6-47. Comparison of depths.

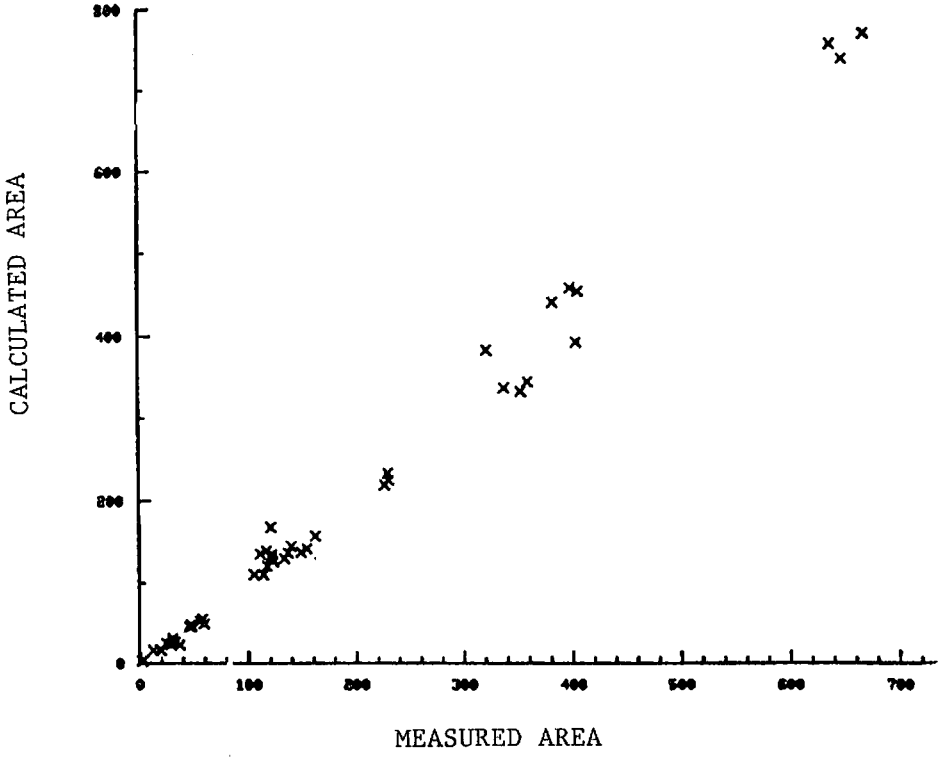


Figure 6-48. Comparison of areas.

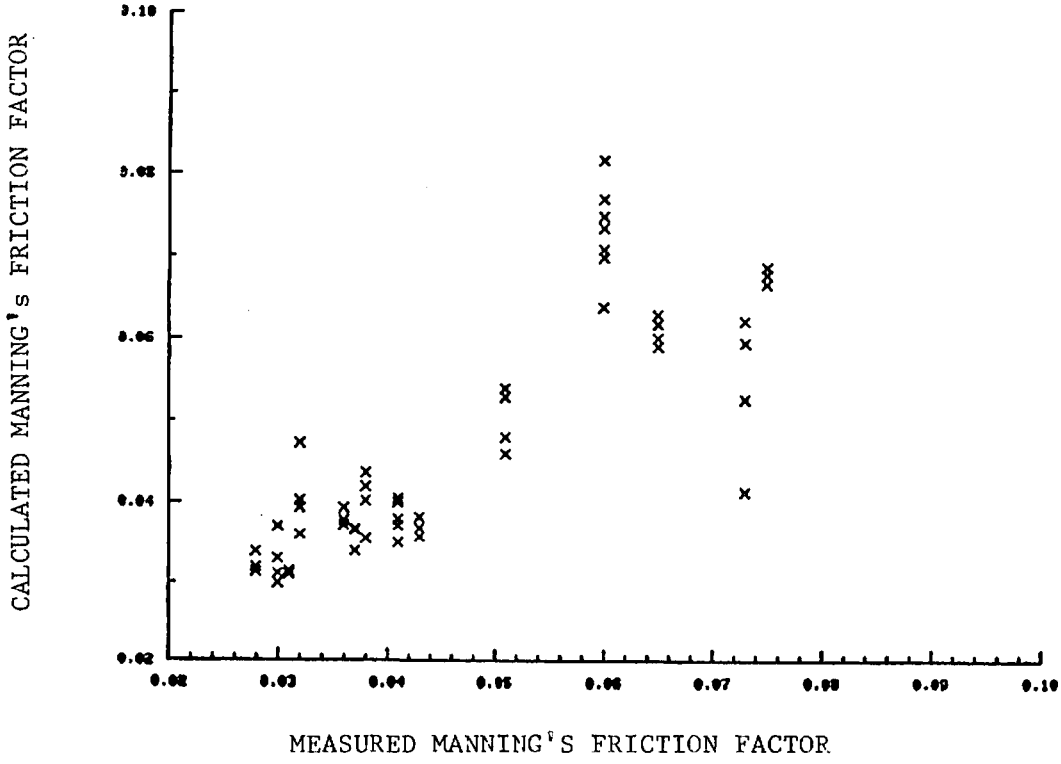


Figure 6-49. Manning friction factor comparison.

the channel shape factor it is evident that predictions are good. The coefficient equation e may be the calibration needed to properly adjust flume studies' results. Further tests must be done to determine if the coefficient equation for e holds for every cobble-bed or boulder-bed channels.

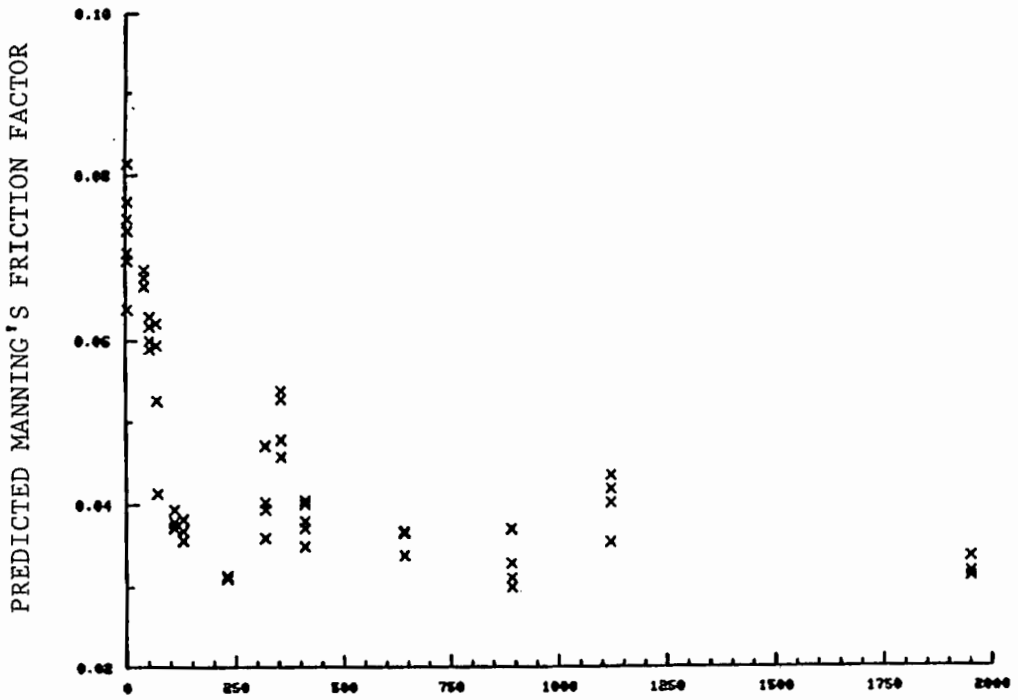


Figure 6-50. Discharge (cm) vs. Manning friction factor.

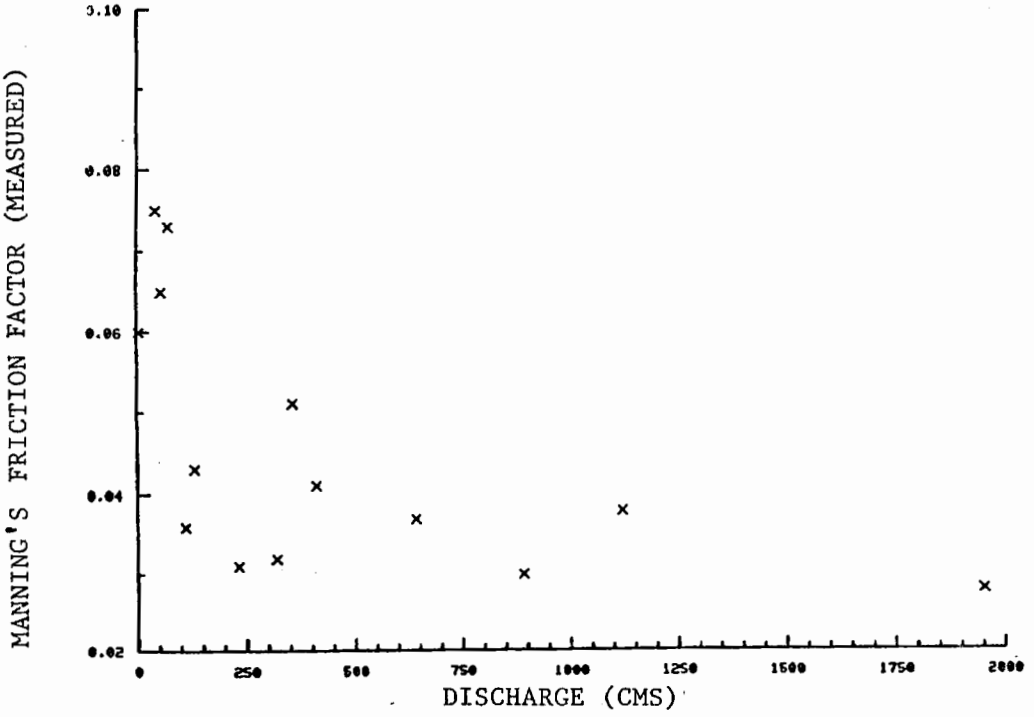


Figure 6-51. Discharge (cms) vs. Manning friction factor (measured).

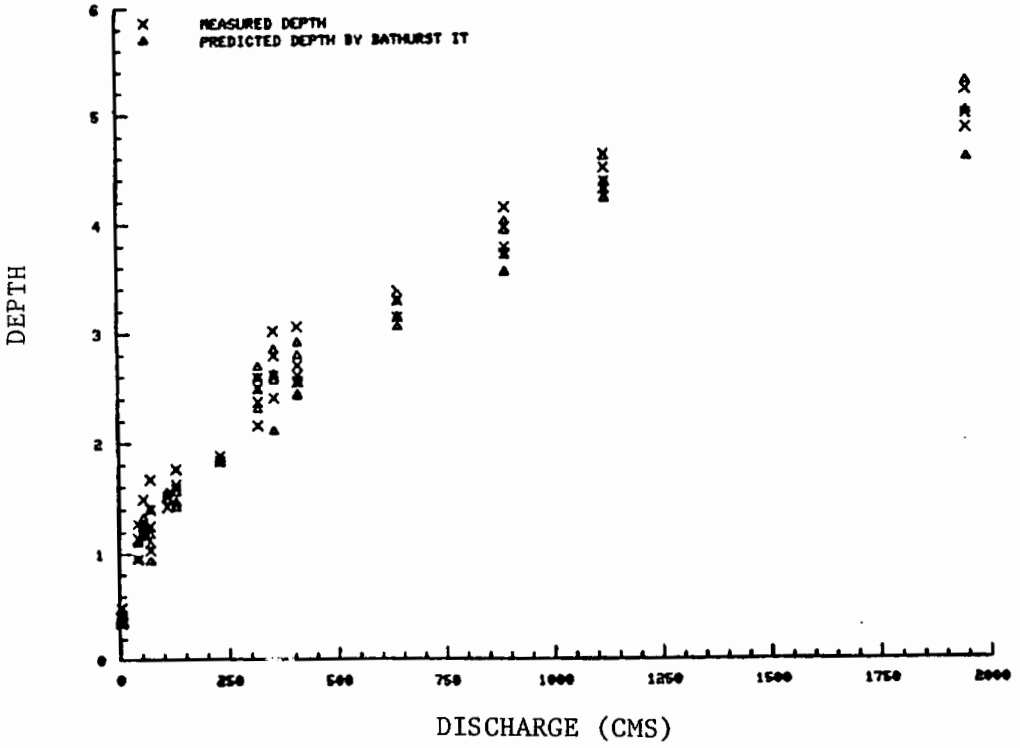


Figure 6-52. Discharge (cms) vs. depth (measured and predicted).

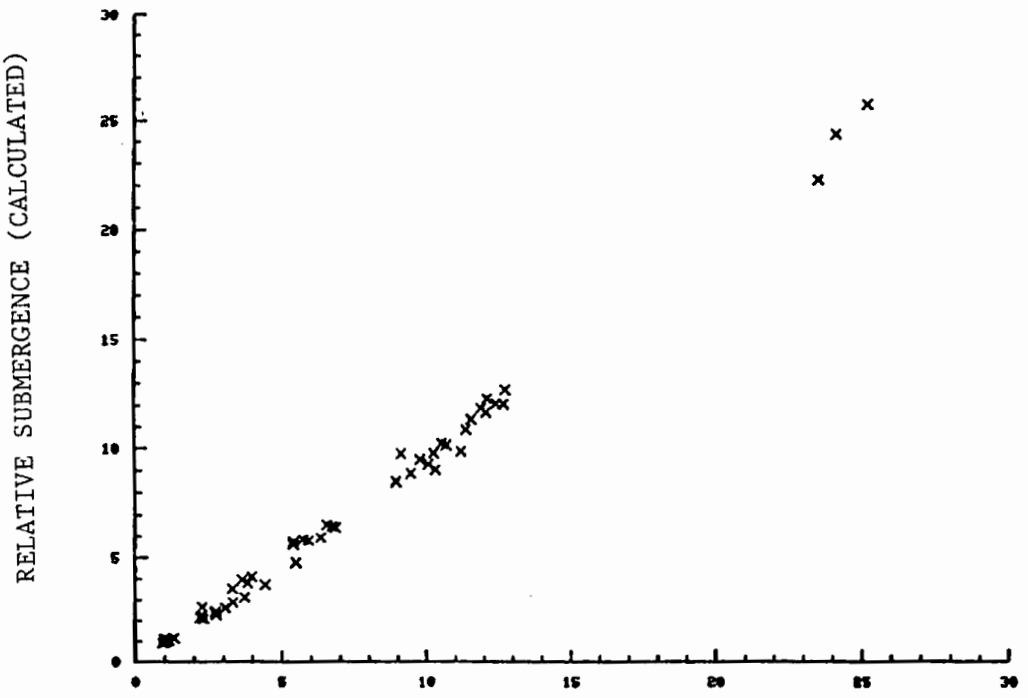


Figure 6-53. Comparison of relative submergence.

## 6.6 RESISTANCE TO FLOW IN VEGETATED CHANNELS

### General

Vegetation in open channels is often useful for the protection of channel banks and bottoms. At other times it grows uninvited and serves to obstruct ready disposal of storm water. Vegetation along roads or at appropriate points near construction areas can act to trap sediments and associated pollutants before storm water reaches a watercourse. To design water courses, determine the conveyance of drainage ditches, establish the resistance parameters for vegetated flood plains, or model the effect of the sediment trapping or releasing capacity of mats of vegetation, an adequate physical and mathematical description of flow in and over vegetation is required.

In the 1930's it was recognized that there was no quantitative information on the resistance to flow of vegetative channel linings. As a result, the U.S. Department of Agriculture, Soil Conservation Service established a program to test channels lined with various North American grasses and other plants for the purpose of determining their resistance and channel protective parameters. The bulk of the test results were reported in Cox and Palmer (1948), Ree and Palmer (1949), Cox (1962), and more recently Ree and Crow (1977). Eastgate (1966) carried out a series of tests on Australian grasses. The approach used to analyze the test results was to plot Manning's n which was defined through Equation 6-114 as a function of the product of the mean flow velocity and the hydraulic radius of the channel.

$$V = \frac{1}{n} R^{2/3} S^{1/2} \qquad (6\text{-}114)$$

In Equation 6-114 V is the mean velocity of flow, R is the hydraulic radius and S is the slope of the energy grade line, which for grassed channels often has a value close to the channel bed slope.

Most of the tests reported were in channels having bed slopes ranging from 1 to 20 percent. It was discovered that when Manning's n was plotted against the product VR for test flows in channels having similar stands of a particular species of grass, the points fell along a single line. Figure 6-54 summarizes much of the data. Furthermore, it was discovered that grasses could be classified into five broad categories, A through E. Each category could be represented by a characteristic curve as shown by the broken lines in Figures 6-54a, b, c and d. Figure 6-55 is taken from the "Handbook of Channel Design for Soil and Water Conservation" (USDA, 1954) and shows the relative position of the A, B, C, D and E curves. The curves are referred to as the retardance curves.

The retardance curves have been quite useful for the design of vegetated channels. Given a flow per unit width for a wide channel, where R is approximately equal to the flow depth $y_n$, Manning's n may be easily obtained from the appropriate retardance curve. For channels of narrow cross section where the hydraulic radius is substantially different from the flow depth, a somewhat more lengthy iterative

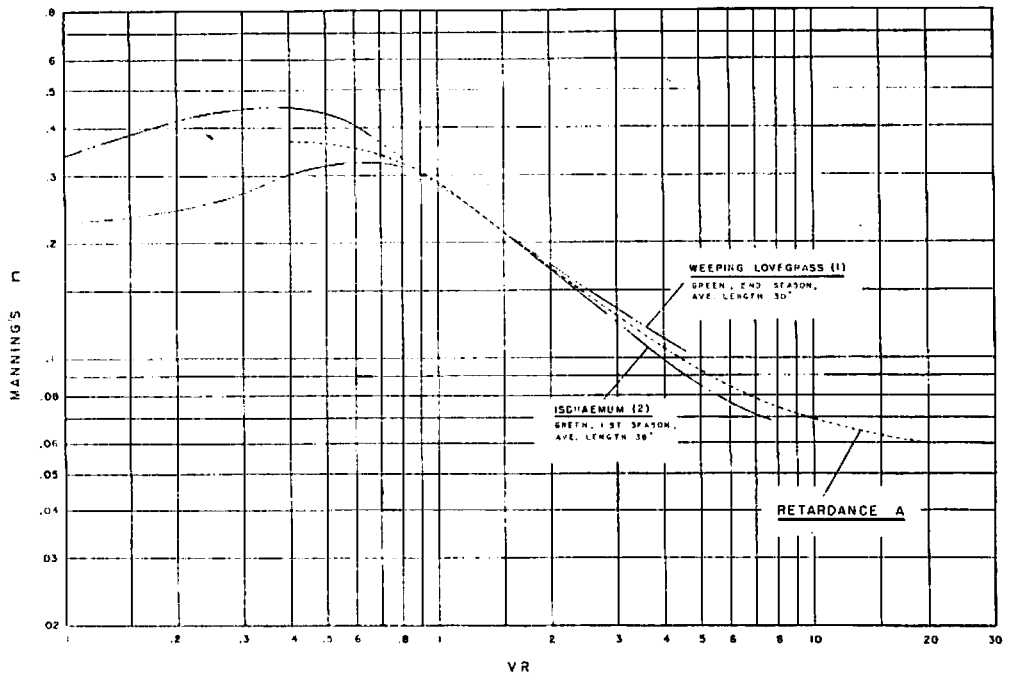


Figure 6-54a. Experimental results related to retardance A (very high vegetal retardance). English units.

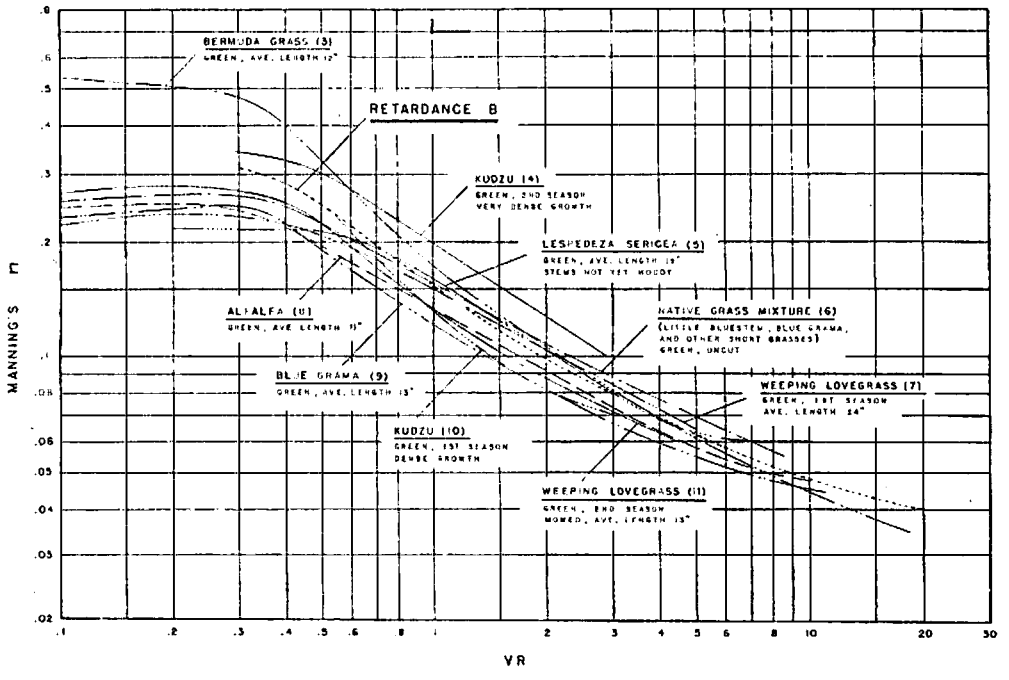


Figure 6-54b. Experimental results related to retardance B (high vegetal retardance). English units.

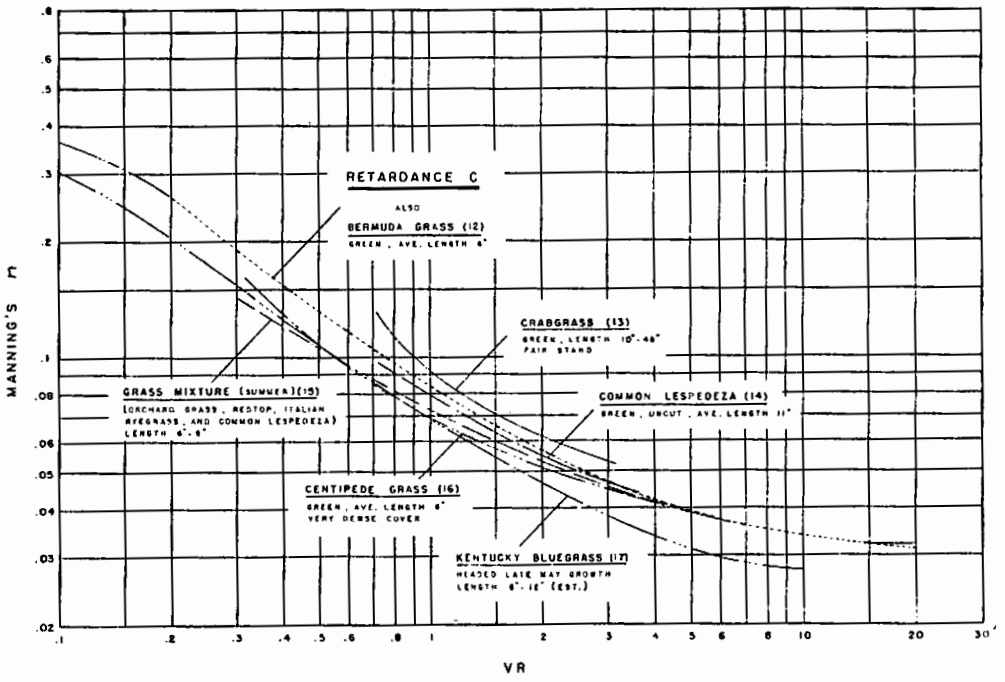


Figure 6-54c. Experimental results related to retardance C (moderate vegetal retardance). English units.

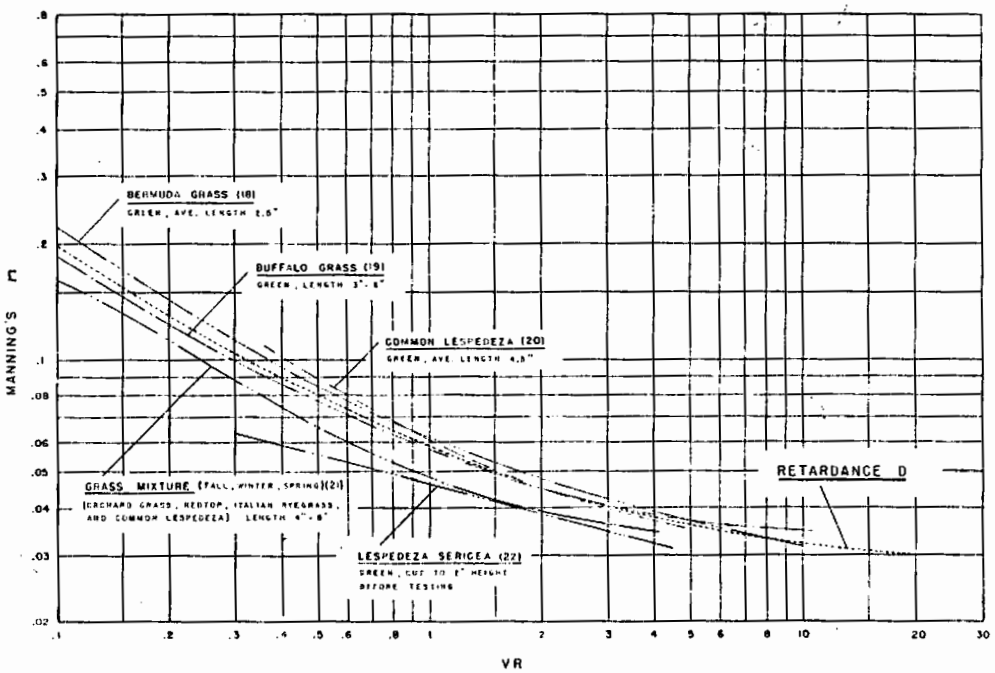


Figure 6-54d. Experimental results related to retardance D (low vegetal retardance). English units.

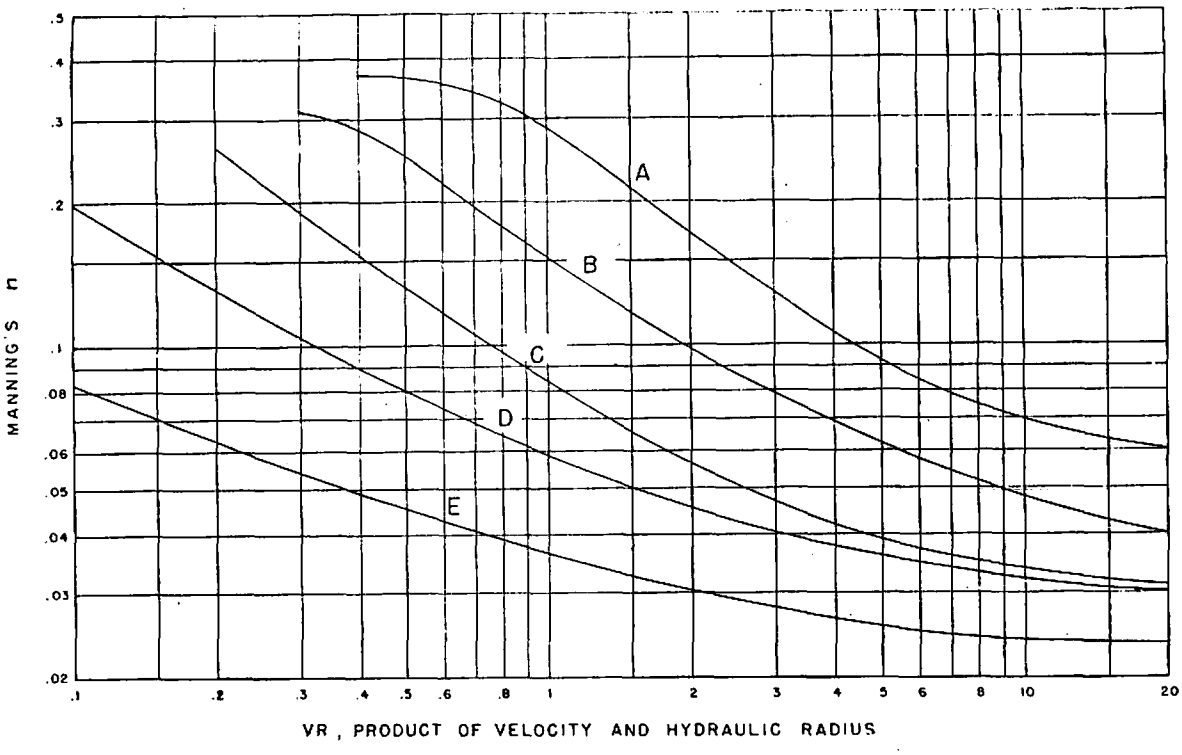


Figure 6-55. Retardance curves (Handbook of Channel Design for Soil and Water Conservation, 1954). English units.

procedure is required. This method is described in the "Handbook for Channel Design for Soil and Water Conservation" (1954) and in "Open Channel Hydraulics" by Ven-te Chow (1959). The "n-VR Method" as the retardance curve method is called (Palmer, 1945), is thus essentially a graphical method. It does not provide an adequate representation of the physical aspects of the flow, nor does it provide an algorithm which can be programmed for a programmable calculator or digital computer. Recently, two methods have been proposed to solve the channel retardance problem numerically.

Numerical Representation of the n-VR Method

Because of the difficulty of numerically solving for rapidly and gradually varies flow problems in vegetated channels using the graphical technique, Temple (1979), using an approach similar to subdividing overall roughness on alluvial beds in the grain and form roughness, subdivided the total roughness into a grain roughness and a form roughness. This approach led to an arbitrary roughness index between 1 and 10 and the expression

$$n_R = \exp \{0.01329\ C_I\ [\ln(R_v)]^2 - 0.09543\ C_I\ \ln(R_v) + 0.2971\ C_I - 4.16\} \quad (6\text{-}115)$$

reproduced the retardance curves shown in Figure 6-55. Equation 6-115 is valid only within the limits $n \leq (C_I + 1)/36$, $0.1 \leq R_v \leq 36$, $0.0 \leq C_I$

$\leq$ 10.0. In Equation 6-115 $n_R$ is the computed flow resistance coefficient, $R_v$ is a dimensionless parameter defined by $R_v = (VR/\nu_{74}) \times 10^{-5}$ where $\nu_{74}$ is the kinematic viscosity of water at 74°F and $C_I$ is a vegetal parameter which is arbitrarily set equal to 10 to match the retardance curve labeled A in Figure 6-55. The $R_v$ parameter is the Reynolds number and it happens that at 74°F the viscosity of water equals $10^{-5}$ $ft^2/sec$. This makes the numerical value of $R_v$ identically equal to the VR product in the English unit system.

The above approach is a purely empirical expression representing the retardance curves. In addition to the constraints listed above, it should not be used for slopes outside the 1 to 20 percent range, representing the range over which the original data was collected. It has been shown by Kouwen, Li, and Simons (1979) that for low slopes, the n-VR method breaks down because the retardance curves only collapse when substantial bending of the vegetation occurs. For low slopes there is not enough force to bend the vegetation. The same is true for very stiff vegetation on somewhat larger slopes. Kouwen and Unny (1973) modeled vegetation with flexible plastic strips. Their experiments showed that for low slopes and/or stiff roughness the friction factor was primarily dependent on the relative roughness. Kouwen and Li (1979) show that for this case, the retardance curves do not collapse to one line. Kao and Barfield (1976) also show n versus VR plots on which the data does not fall along one line.

Physically Based Resistance Function

Because the flow in and over vegetation is an extremely complicated process, it is not possible to construct a mathematical model which incorporates all aspects of the flow. However, it is possible to construct a resistance model which incorporates at least the basic flow and boundary parameters.

A great deal of work on resistance to flow in channels with rigid roughness elements of simple geometry has been reported in the literature. Much of this work is summarized by the ASCE task force on friction factors (1963) and by Rouse (1965). In general, the Darcy-Weisbach friction factor is related to the relative roughness through the logarithmic expression

$$\frac{1}{\sqrt{f}} = a + b \log (y_n/k) \qquad (6\text{-}116)$$

in which a and b are coefficients, $y_n$ is the normal depth of flow, k is the roughness height and f is as defined in the following equation.

$$V = \frac{1}{\sqrt{f}} \sqrt{8gy_nS} \qquad (6\text{-}117)$$

The logarithmic flow formula results from integrating the expression for the velocity profile of the flow over a rough boundary. This velocity profile is found to be logarithmic and can be explained by Prandtl's mixing-length hypothesis (see Schlichting, 1968).

For flow over flexible plastic roughness, Kouwen (1970) found that velocity profiles were logarithmic as well. Kouwen and Li (1979) present evidence that flexible plastic roughness elements adequately model the flow conditions over flexible natural vegetation. Eastgate (1966) measured velocity profiles over several Australian grasses and also found the velocity distribution to be logarithmic. This indicates that a logarithmic flow formula should also apply to flow over vegetation. Figure 6-56 shows a typical velocity profile for flow over vegetation. The velocity distribution is more or less uniform within the vegetation but plots as a straight line on semi-log paper above the vegetation as shown.

When any plastic or natural vegetation is subjected to a streamwise drag force, it will bend if sufficiently pliant. The amount of the bending depends on the applied force and the flexural stiffness of the roughness. When sufficient force is applied, the roughness may break. This aspect of vegetative resistance is what complicates the process beyond the rigid roughness case. The intercept of the velocity distribution with the y axis is at a distance y' from the channel boundary. Sayre and Albertson (1962) found that for rigid baffles, this intercept location is more or less fixed. For flexible roughness it is dependent on the degree to which the roughness bends. The more it bends, the lower the y-axis intercept y'. The reduction of the roughness height

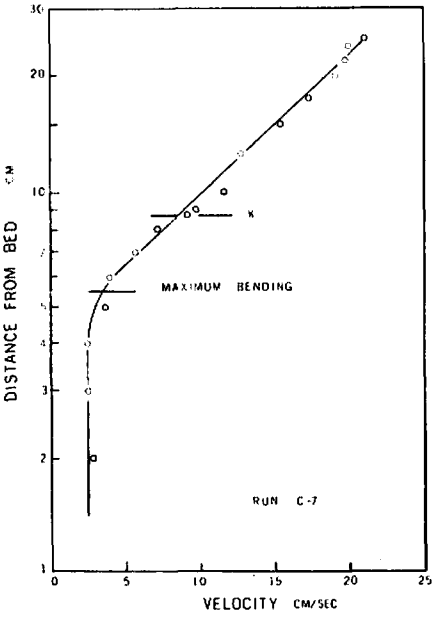


Figure 6-56. Typical velocity profile.

k and the y-axis intercept y' are found to be related to the same parameters so that the k in Equation 6-116 could be replaced by y' and the value of a would be different. It is thus necessary to be able to predict to what extent k (or y') will be reduced due to an imposed shear stress.

Figure 6-57 is a plot of $k/h$ versus $(MEI/\gamma y_n S)^{1/4}/h$ for plastic roughness. Both of these ratios are dimensionless, although M is dependent on the dimensional units used. In the above, h is the undeflected roughness height or average grass length, M is the relative density of the roughness and is evaluated as the stemcount per square meter, E is the elastic modulus of the stems, I is the stem cross-sectional moment of inertia, $\gamma$ is the weight density of water, $y_n$ is the normal depth, and S is the friction slope.

The value of the roughness height can be obtained through Figure 6-57 or the fitted line, Equation 6-118

$$k = 0.14\ h\ \left\{\left(\frac{MEI}{\gamma y_n S}\right)^{1/4} / h\right\}^{1.59} \qquad (6\text{-}118)$$

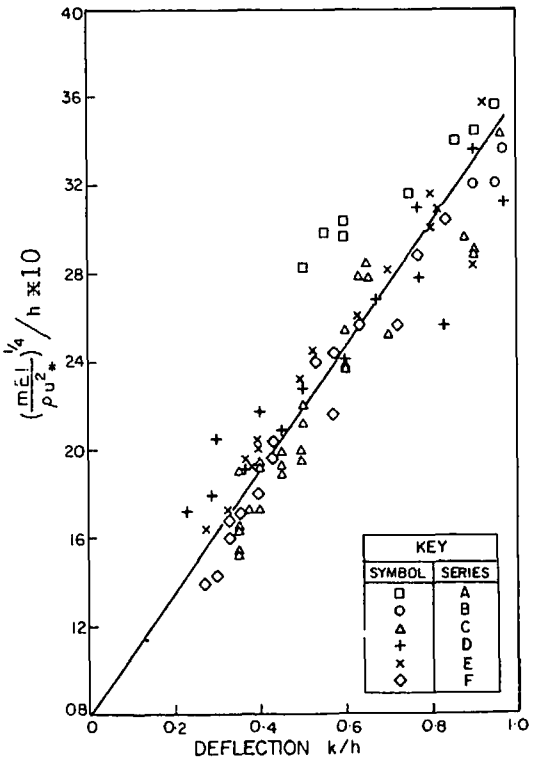


Figure 6-57. Plot of $[(MEI/\gamma y_n S)]^{1/4}$ versus deflection $k/h$.

The flow capacity of a vegetative channel having a depth of $y_n$, a channel slope S and a vegetation of average height h and stiffness MEI can not be determined by the following steps:

1. Calculate k through Equation 6-118,

2. Calculate $1/\sqrt{f}$ through Equation 6-116 using the proper values for a and b as described below,

3. Calculate the mean velocity V through Equation 6-117, and

4. Determine the flow for a channel sequence of width w through $Q = wy_nV$ and add the flow for the cross section segments.

As stated before, when artificial or natural flexible roughness is subjected to a shear stress, it bends. This bending alters the drag characteristics of the roughness and affects the a and b parameters in Equation 6-116. Figure 6-58 is a plot of $1/\sqrt{f}$ versus the log of $y_n/k$ for plastic roughness.

The data along the bottom line in Figure 6-58 is for roughness which is essentially erect and may be waving vigorously. The data above the bottom line is for roughness which is essentially prone. There is a shear stress or shear velocity $U_* = \sqrt{gy_nS}$ beyond which the data falls away from line 1. This shear velocity is denoted by $U_{*crit}$ and for plastic roughness was found to be related to the stiffness MEI through Equation 6-119.

$$U_{*crit} = .028 + 6.33\ (MEI)^2 \qquad \text{(elastic)} \qquad (6\text{-}119)$$

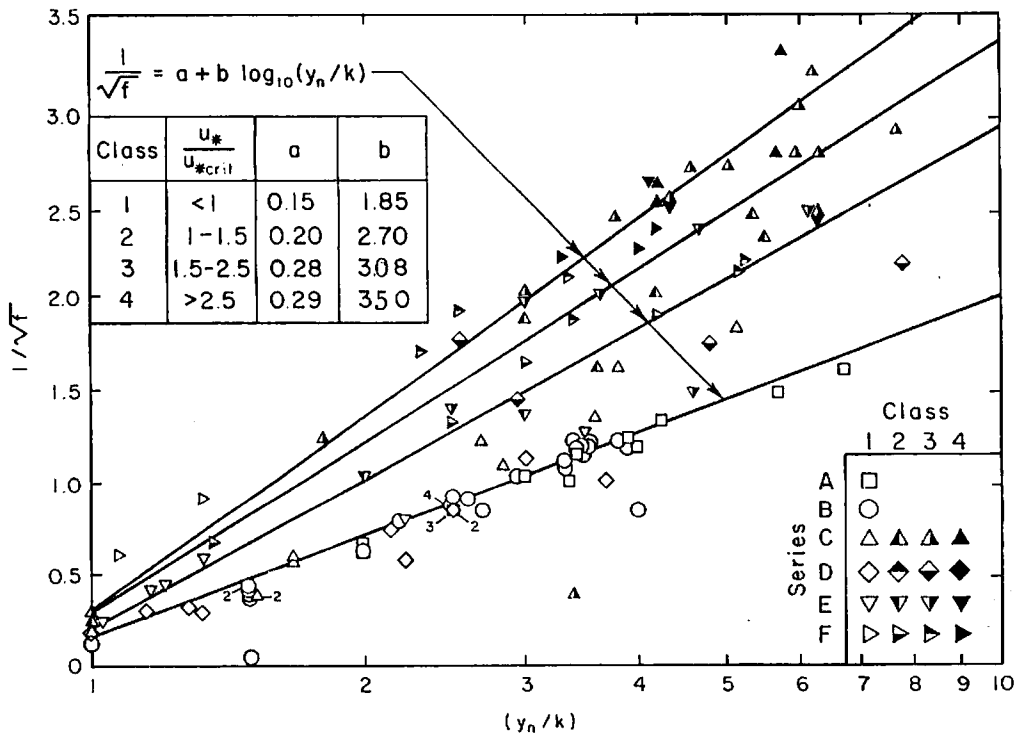


Figure 6-58. Friction factor versus relative roughness.

Since Equation 6-119 is not dimensionless, it can only be used in SI units i.e., $U_{*crit}$ in m/s and MEI in N-$m^2$. Natural vegetation will break when a critical shear velocity is reached. An analysis of Eastgatels (1966) data by Kouwen, Li and Simons (1979) indicates that this occurs when $U_{*crit}$ as given by Equation 6-120 is exceeded.

$$U_{*crit} = 0.23\ (MEI)^{0.106} \qquad \text{(plastic)} \qquad (6\text{-}120)$$

To determine the critical shear stress for a particular roughness, use the lower of the values given by Equation 6-119 or 6-120.

Furthermore, because there is a gradual transition from the erect to the fully prone condition, it is useful to subdivide the resistance relation for non-erect into three conditions. The classification scheme along with the appropriate values for a and b are given in Table 6-15. The conditions 1, 2, 3 and 4 refer to the numbered lines in Figure 6-58.

Table 6-15. Resistance classifications.

| Condition | Classification | Criteria | a | b |
|---|---|---|---|---|
| 1 | Erect | $U_*/U^*crit < 1.0$ | 0.15 | 1.85 |
| 2 | Prone | $1.0 < U_*/U^*crit < 1.5$ | 0.20 | 2.70 |
| 3 | Prone | $1.5 < U_*/U^*crit < 2.5$ | 0.28 | 3.08 |
| 4 | Prone | $2.5 < U_*/U^*crit$ | 0.29 | 3.50 |

Simulation of Retardance Curves

Equations 6-118, 6-119, or 6-120, 6-116 and 6-117 are used in that order to calculate Manning's n and the product of $Vy_n$. Manning's n is defined through the Manning formula in Equation 6-114. Values for the average vegetation height h and stiffness MEI for different vegetal covers are obtained from Table 6-16 which is based on the table classifying vegetal covers in the "Handbook of Channel Design for Soil and Water Conservation" (USDA, 1954). Using the values given in columns (2) and (3), the solid lines in Figure 6-59 are obtained for a 5 percent slope. The broken lines in that figure are the A, B, C, D and E retardance curves. The agreement between the lines is very good, especially with regard to their shape. Changing the slope has no effect on the position of these lines.

Table 6-16. Classification of vegetal covers as to degree of retardance (Handbook of Channel Design for Soil and Water Conservation, USDA, 1954).

| Retardance Class | Average Height h in millimeters | Stiffness MEI in Newtons-meters squared | Cover Type | Cover Condition | Calibrated Stiffness MEI in Newtons-meters squared |
|---|---|---|---|---|---|
| (1) | (2) | (3) | (4) | (5) | (6) |
| | | | Weeping lovegrass . . . . | Excellent stand, tall, (average 760 mm) | 200 |
| A | 910 | 300 | Yellow bluestem Ischaemum . . . . . | Do tall, (average 900 mm) | - |
| | | | Rhodes Grass (Australian). . . . . | Excellent stand (average 690 mm) | 140 |
| A/B | | | Kikuyu Grass . . . . . | Excellent stand Iaverage 420 mm) | 47 |
| | | | Kudzu . . . . . | Very dense growth, uncut | - |
| | | | Bermudagrass . . . . . | Good stand, tall, (average 300 mm) | 17 |
| | | | Native grass mixture (little bluestem, blue grama, and other long and short midwest grasses . . | Good stand, unmowed | 20 |
| B | 610 | 20 | Weeping lovegrass . . . . | Good stand, tall, (average 600 mm) | 30 |
| | | | Lespedeza sericea . . . . | Good stand, not woody, tall (average 500 mm) | 10 |
| | | | Alfalfa . . . . . | Good stand, uncut, (average 275 mm) | 4 |
| | | | Weeping lovegrass . . . . | Good stand, mowed, (average 330 mm) | 6 |
| | | | Kudzu . . . . . | Dense growth, uncut | - |
| | | | Blue grama . . . . . | Good stand, uncut, (average 330 mm) | 6 |
| | | | Bluegrass (Australian) . . | (average 340 mm) | 18 |
| | | | Dallas . . . . . | Uncut (average 760 mm) | 20 |
| B/C | | | African Star (Australian) . . . . . | (average 290 mm) | 4 |
| | | | Crabgrass . . . . . | Fair stand, uncut (250-1200 mm) | |
| | | | Bermudagrass . . . . . | Good stand, mowed (average 150 mm) | |
| | | | Common lespedeza . . . . . | Good stand, uncut (average 280 mm) | 3 |
| C | 200 | .5 | Grass-legume mixture--Summer (orchard grass, redtop, Italian ryegrass, and common lespedeza) . . . . | Good stand, uncut (100 to 125 mm) | |
| | | | Centipedegrass . . . . . | Very dense cover (average 150 mm) | 2 |
| | | | Kentucky bluegrass . . . . | Good stand, headed (150 to 300 mm) | |
| | | | Bermudagrass . . . . . | Good stand, cut to 64 mm | .15 |
| | | | Common lespedeza . . . . . | Excellent stand, uncut (average 114 mm) | .10 |
| | | | Buffalograss . . . . . | Good stand, uncut (75 to 150 mm) | .16 |
| D | 100 | .05 | Grass-legume mixture--fall, spring (Orchardgrass, redtop, Italian ryegrass, and common lespedeza . . . . | Good stand, uncut (100 to 125 mm) | .07 |
| | | | Lespedeza sericea . . . . | After cutting to 50 mm Very good stand | .015 |
| | | | Kikuyu (Australian) . . . | After cutting to 107 mm | .17 |
| | | | Kentucky Bluegrass . . . . | Cut to 75 mm | .10 |
| E | 40 | .005 | Bermudagrass . . . . . | Good stand, cut to 38 mm height | |
| | | | Bermudagrass . . . . . | Burned stubble | |

Note: Covers classified have been tested in experimental channels.
Covers were green and generally uniform.

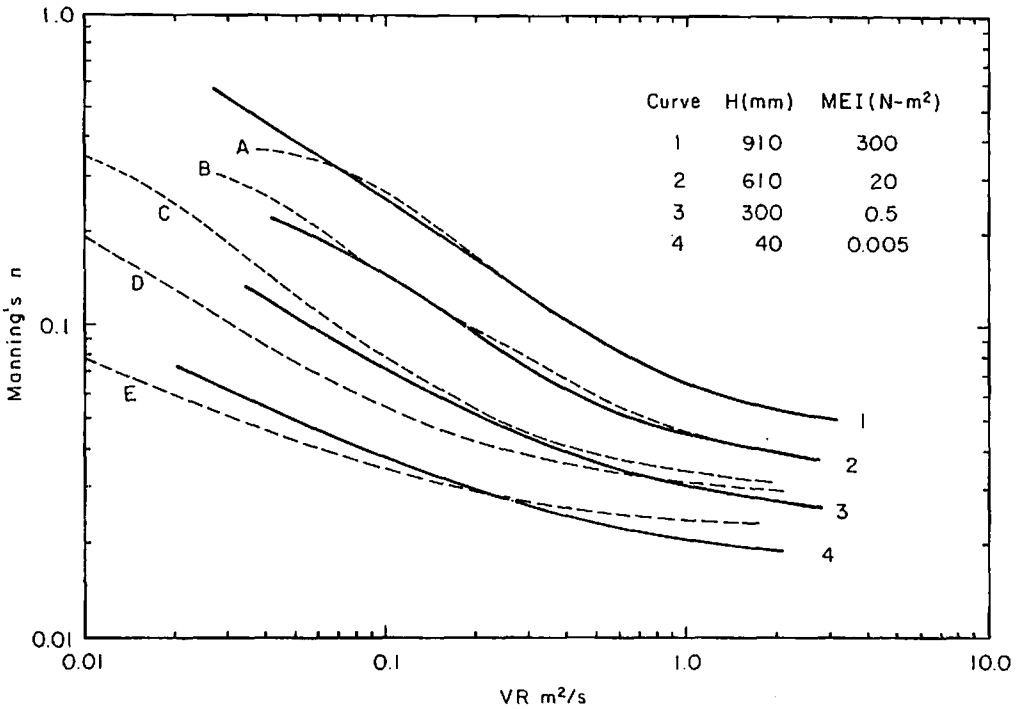


Figure 6-59. Comparison of retardance curves.

Figure 6-60 is a plot of n versus VR for particular vegetation with slope as the varied quantity. As can be seen, for slopes above 5 percent the model produces lines of n versus VR which coincide, but for smaller slopes there is a substantial increase in Manning's n. This is similar to the result obtained by Ree and Crow (1977) when they compared the retardance curves for Sudan grass or a 5 percent and .1 precent slope. Figure 6-61 is a reproduction of their Figure 57. The values of Manning's n differ by a large factor.

What the above discussion points out is that the n versus VR curves are valid only over a specific range of conditions as determined by the relative values of slope and MEI. It is, therefore, suggested that the n-VR method eventually be abandoned in favor of the new approach. Furthermore, with the advent of programmable calculators and compact computers, it is probably better to determine the flow capacity numerically.

## Computational Procedure

Given values for vegetation height h, stiffness MEI, slope S, and depth $y_n$, the velocity of flow may be calculated using the following work sheet.

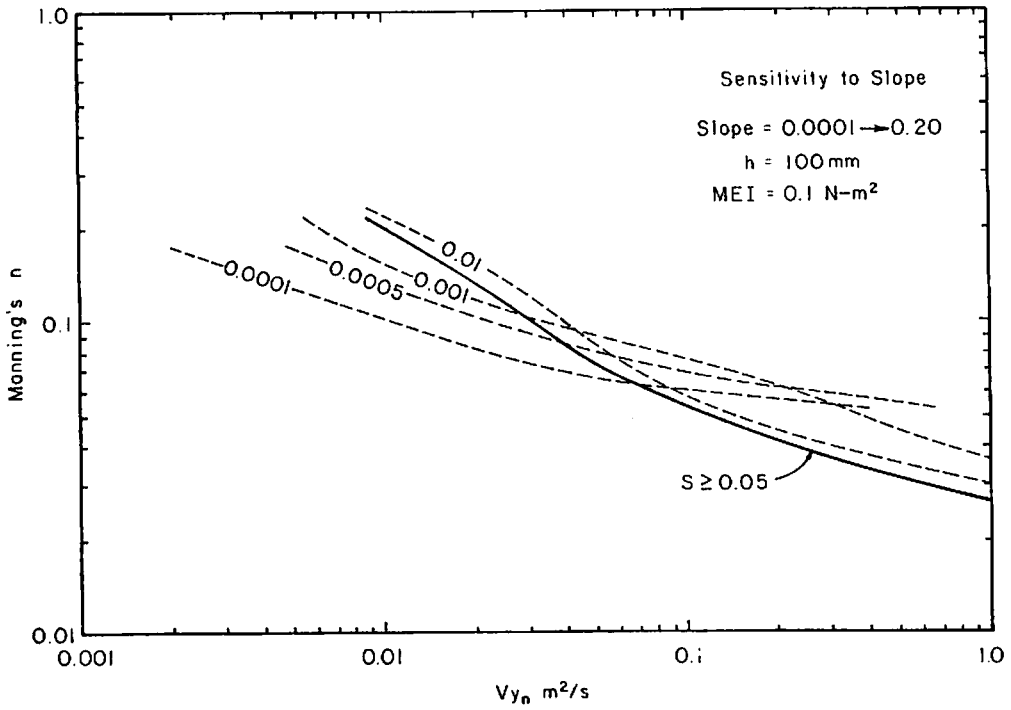


Figure 6-60. Effect of slope on resistance.

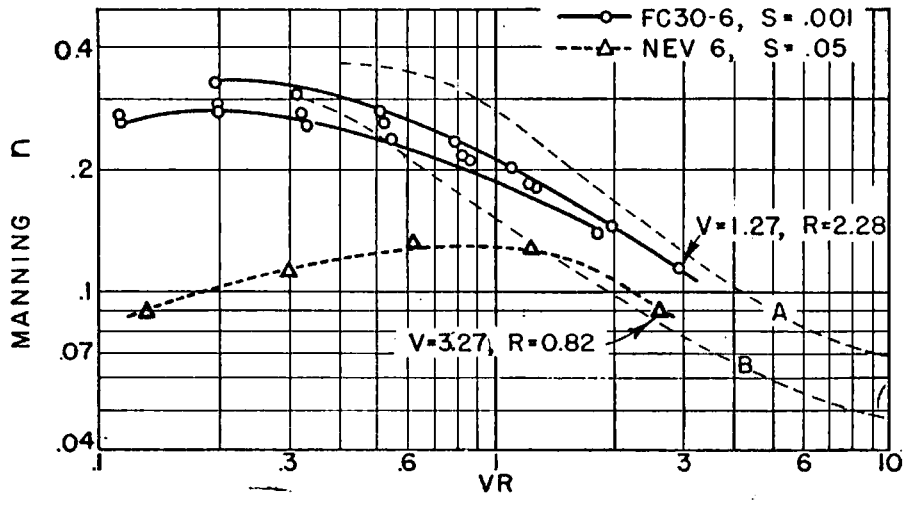


Figure 6-61. Retardance curves for Sudan grass (Ree and Crow, 1977). English units.

Work Sheet: Grassed Channels

INPUTS:

height of grass: ft x .3048, in x .0254 — $h$ = m

stiffness: (from Table 2) — MEI = $N - m^2$

channel slope: ft/ft, m/m — $S$ = m/m

depth: ft x .3048 — $y_n$ = m

OUTPUTS:

average boundary shear — $\tau_o = \gamma y_n S$ = Pa

shear velocity — $U_* = \sqrt{g y_n S}$ = m/s

critical shear stress

$U_{*crit}$ = minimum of

$0.0.28 + 6.33\ [MEI]^2$ = m/s

$0.23\ [MEI]^{0.106}$ = m/s

Minimum = m/s

classification — $U_*/U_{*crit}$ =

deflected grass height — $k = 0.14h\ \{(\frac{MEI}{\tau_o})^{.25}/h\}^{1.59}$ = m

if $h$ less than $k$, set $k = h$ — $k$ = m

$U_*/U_{*crit}$

| | | |
|---|---|---|
| 0 - 1 | $\frac{1}{\sqrt{f}} = 0.15 + 1.85 \log_{10}(y_n/k)$ | = |
| 1 - 1.5 | $\frac{1}{\sqrt{f}} = 0.20 + 2.70 \log_{10}(y_n/k)$ | |
| 1.5 - 2.5 | $\frac{1}{\sqrt{f}} = 0.28 + 3.08 \log_{10}(y_n/k)$ | |
| 2.5 - ∞ | $\frac{1}{\sqrt{f}} = 0.29 + 3.50 \log_{10}(y_n/k)$ | |

velocity — $V = \frac{1}{\sqrt{f}} \sqrt{8 g y_n S} = \frac{1}{\sqrt{f}} (2.83) U_*$ = m/s

$V \times 3.28$ = ft/s

$k/h$ =

$n = y_n^{1/6} / 8.86 \frac{1}{\sqrt{f}}$ =

$Vy_n$ =

## REFERENCES

Ackers, P., 1959, Resistance to fluids flowing in channels and pipes, Hydraulic Research Paper No. 1, HMSO, London, 1958; see also, discussion by P. Ackers of Relationship between pipe resistance formulas by W. L. Moore, J. of the Hydraulics Div., ASCE, Vol. 85, No. HY7, July, pp. 155-159.

Alan, M. S., and Kennedy, J. F., 1969, Friction factors for flow in sand-bed channels, Journal of the Hydraulics Division, ASCE, Vol. 95, No. HY6, Proc. Paper 6900, November, pp. 1973-1992.

American Society of Civil Engineers, 1963, Friction factors in open channels, Progress Report of the Task Force on Friction Factors in Open Channels of the Committee of Hydromechanics of the Hydraulics Division, E. Silberman, Chmn., Journal of the Hydraulics Division, ASCE, Vol. 89, No. HY2, Proc. Paper 3464, Mar., pp. 97-143.

Bajorunas, L., 1952, Discussion of River channel roughness, by H. A. Einstein and N. L. Barbarossa, Transactions, ASCE, Vol. 117, pp. 1140-1142.

Barnes, H. H., 1967, Roughness characteristics in natural channels, U.S. Geological Survey Water Supply Paper 1849.

Bathurst, J. C., 1977, Resistance to flow in rivers with stony beds, thesis presented to the University of East Anglia, Norwich, England, in 1977, in fulfillment of the requirements for the degree of Doctor of Philosophy.

Beckman, E. W., and Furness, L. W., 1962, Flow characteristics of Elkhorn River near Waterloo, Nebraska, U.S. Geological Survey Water Supply Paper 1498-B.

Bishop, A. A., Simons, D. B., and Richardson, E. V., 1965, Total bed material transport, ASCE Journal of Hydraulics Division, Vol. 91, HY2, CER64AAB-DBS-EVR21.

Bretting, A. E., 1948, A set of practical hydraulic formulas based on recent experimental research, International Association for Hydraulic Research, 2nd Meeting, No. 24, pp. 399-418.

Chow, V. T., 1959, Open Channel Hydraulics, McGrawHill, New York, NY.

Colby, B. R., 1960, Discontinuous rating curves for Pigeon Roost and Cuffawa Creeks in Northern Mississippi, U.S. Department of Agriculture, Agricultural Research Service Report 41-46, 31 p.

Colebrook, C. F., 1938, Turbulent flow in pipes with particular reference to the transition region between the smooth and rough pipe laws, Journal, Institute of Civil Engineers, Vol. 11, pp. 133-156.

Cox, M. B., 1962, Tests on Vegetated Waterways, Oklahoma Agricultural and Mechanical College Agricultural Experiment Station, Tech. Bull. No. T-15, September, pp. 1-23.

Cox, M. B. and Palmer, V. J., 1948, Results of tests on vegetated waterways and method of field application, Oklahoma Agricultural Experiment Station, Misc. Pub. No. MP-12, January, pp. 1-43.

Dawdy, D. R., 1961, Depth-discharge relations of alluvial streams - discontinuous rating curves, U.S. Geological Survey Water Supply Paper 1498-C, 16 p.

Eastgate, W. I., 1966, Vegetated stabilization of grassed waterways and dam bywashes, M. Eng. Sc. Thesis, Department of Civil Engineering, University of Queensland, St. Lucia, Queensland, Australia.

Einstein, H. A., 1950, The bedload function for sediment transportation in open channel flows, Technical Bulletin 1026, U.S. Department of Agriculture, Washington, D.C., 70 p.

Einstein, H. A. and Abdel-Aal, F. M., 1972, Einstein bedload function at high sediment rates, J. of the Hydraulics Div., ASCE, Vol. 98, No. HY1, January, pp. 137-152.

Einstein, H. A., and Barbarossa, N. L., 1952, River channel roughness, Transactions ASCE, Vol. 117, pp. 1121-1132.

Engelund, F. and Hansen, E., 1967, A monograph on sediment transport in alluvial streams, Teknisk Forlag, Copenhagen.

Graf, W. H., 1964, Gesetze der turbulenten geschwindigkeitsverteilung in geschlossenen rohern und offenen gerinnen, Schweizer Bauz., Jgg. 82, No. 53.

Harrison, A. S. Melema, W. J., 1967, Movable bed model for alluvial channel studies, International Association for Hydraulics Research, 12th Congress, Fort Collins, Colorado.

Harza Engineering Co., International, 1963, West Pakistan water and power development authority canal and head works observation program, 1962, Data tabulation, Chicago, Illinois, 322 p.

Henderson, F. M., 1966, Open Channel Flow, 1st ed., The Macmillan Co., New York, NY.

Kharrufa, N. S., 1962, Flume studies of steep flow with large graded natural roughness element, Logan, Utah, Utah State University, Department of Civil Engineering, Ph.D. Dissertation.

Keulegan, G. H., 1938, Laws of turbulent flow in open channels, Journal, National Bureau of Standards, Washington, D.C., Research Paper 1151, Vol. 21, December, pp. 707-741.

Koloseus, H. J. and Davidian, J., 1961, Flow in an artificially roughened channel, U.S. Geological Survey Paper 424-B, 25 p.

Kouwen, N., 1970, Flow retardance in vegetated open channels, Ph.D. Thesis, Department of Civil Engineering, Univ. of Waterloo, Waterloo, Ontario, Canada.

Kouwen, N. and Li, R. M., 1979, Biomechanics of vegetated channel linings, Journal of the Hydraulics Division, ASCE, in print.

Kouwen, N., Li, R. M., and Simons, D. B., 1980, Velocity measurements in a channel lined with flexible plastic roughness elements, Technical Report No. CER79-80NK-RML-DBS11, Department of Civil Engineering, Colorado State University, Fort Collins, Colorado.

Kouwen, N. and Unny, T. E., 1973, Flexible roughness in open channels, Journal of the Hydraulics Division, ASCE, Vol. 99, No. HY-5, Proc. Paper 9723, May, pp. 713-728.

Lane, E. W. and Carlson, E. J., 1953, Some factors affecting the stability of canals contructed in coarse granular materials, Proc. Minnesota International Hydraulics Convention, September.

Lindquist, M., 1933, On velocity formulas for open channel and pipes, Special Report, Third World Power Conference, Stockholm.

Meyer-Peter, E. and Müller, R., 1948, Formulas for bed load transport, Proc., 3rd Meeting of IAHR, Stockholm, pp. 39-64.

Nordin, C. F., 1964, Aspects of flow resistance and sediment transport, Rio Grande near Bernalillo, New Mexico, U.S. Geological Survey Water Supply Paper 1498-H.

Palmer, V. J., 1945, A Method for designing vegetated waterways, Agricultural Engineering, Vol. 26, No. 12, December, pp. 561-520.

Powel, R. W., 1960, History of Manning's formula, Journal of Geophysical Research, Vol. 65, No. 4.

Prandtl, L., 1926, Uber die ausgebildete turbulenz, Proc. of the 2nd International Congress of Applied Mechanics, Zürich.

Ree, W. O. and Crow, F. R., 1977, Friction factors for vegetated waterways of small slope, Agricultural Research Service, U.S. Department of Agriculture, ARS-S-151, January, pp. 1-56.

Ree, W. O. and Palmer, V. J., 1949, Flow of water in channels protected by vegetative linings, U.S. Soil Conservation Bulletin No. 967, February, pp. 1-115.

Richardson, E. V. and Simons, D. B., 1967, Resistance to flow in sand channels, Proc., International Association for Hydraulic Research, 12th Congress, Vol. 1, Fort Collins, Colorado, pp. 141-150.

Rouse, H., 1965, Critical analysis of open channel resistance, Journal of the Hydraulics Division, ASCE, Vol. 91, No. HY4, Proc. Paper 4387, pp. 1-25.

Sayre, W. W. and Albertson, M. L., 1961, Roughness spacing in rigid open channels, Journal of the Hydraulics Division, ASCE, Vol. 87, No. HY3, Proc. Paper 2823, May, pp. 121-150.

Sayre, W. W. and Albertson, M. L., 1962, Closure to Roughness spacing in rigid open channels, Journal of the Hydraulics Division, ASCE, Vol. 88, No. HY4, pp. 249-264.

Schlichting, H., 1955, Boundary Layer Theory, McGraw-Hill Book Co., Inc., New York, Pergamon Press Ltd. (translated from German, Grenz Schicht Theorie).

Schlighting, M., 1968, Boundary layer theory, McGraw-Hill, New York, NY.

Senturk, F., 1967, Mechanics of bed formation, La Houille Blanche No. 2.

Senturk, F., 1967, Détermination de la resistance d'un fond mobile sous l'action d'un ecoulement, IAHR 12th Congress, Fort Collins, Colorado.

Senturk, F., 1969, Nehir hidroligi, DSI Publication No. 66/X/64, Ankara.

Senturk, F., 1975, Discussion on current resistance to flow formulas, Teknik Bulten, No. 26, DSI, Ankara.

Simons, D. B., 1957, Theory and design of stable channels in alluvial material, Ph.D. dissertation, Department of Civil Engineering, Colorado State University, Fort Collins, Colorado.

Simons, D. B. and Richardson, E. V., 1966, Resistance to flow in alluvial channels, U.S. Geological Survey Prof. Paper 422-J.

Simons, D. B. and Richardson, E. V., 1971, Flow in alluvial sand channels, River Mechanics, ed. by H. W. Shen, Vol. 1, Chapter 9, 29 p.

Strickler, A., 1923, Beiträge zur frage der geschwindigheits - formel und der rauhigkeitszahlen für strome, kanale und geschlossene leitungen, (some contributions to the problems of the velocity formula and roughness factor for rivers, canals and closed conduits), Mitteilungen des Eidgenössischer Amtes fur Wassserwirtschaft, Bern, Switzerland, No. 16 g.

Task Committee, 1963, Friction factors in open channels, Journal of the Hydraulics Division, ASCE, Vol. 89, No. HY2, Proc. Paper 3464, March, pp. 97-143.

Taylor, R. H., Jr. and Brooks, N. H., 1962, Discussion of Resistance to flow in alluvial channels, by D. B. Simons and E. V. Richardson, Transactions, ASCE, Vol. 127, Part I, pp. 982-992.

Temple, D. M., 1979, Tractive force design of vegetated channels, Presented at the 1979 Summer Meeting of the ASAE and CSAE, University of Manitoba, Winnipeg, Canada.

Thijsse, J. Th., 1949, Formulae for the friction head loss along conduit walls under turbulent flow, International Association for Hydraulic Research, III-4, pp. 1-11.

Tilp, P. J. and Scrivner, M. W., 1964, Analyses and descriptions of capacity tests in large concrete-lined canals, U.S.B.R. Technical Memorandum No. 661, April, 195 p.

Tracey, H. J. and Lester, C. M., 1961, Resistance coefficients and velocity distribution-smooth rectangular channel, U.S. Geological Survey Water Supply Paper 1592-A, 18 p.

United States Bureau of Reclamation, 1960, Design of stable channels with tractive forces and competent bottom velocity, Sedimentation Section, Hydrology Branch, Division of Proj. Invest., Denver, Colorado, March.

USDA, Soil Conservation Service, 1954, Handbook of channel design for soil and water conservation," SCS-TP-61, Washington, D.C., pp. 1-34.

Vanoni, V. A. and Brooks, N. H., 1957, Laboratory studies of the roughness and suspended load of alluvial streams, Report E-68, California Institute of Technology, Pasadena, California, 121 p.

Virmani, J. K., 1973, The relationship between channel forming flows and the cross section shape, slope, and bed materials in large bed element streams, dissertation, Utah State University, Logan, Utah.

von Kármán, T., 1930, Mechanische äenlichtkeit und turbulentz, Proc. of the 3rd International Congress of Applied Mechanics, Stockholm, Vol. I.

Wolman, M. G., 1954, A method of sampling coarse river bed material, Transactions, America Geophysical Union, Vol. 35, No. 6, Part 1, December, pp. 951-956.

Zegzhda, A. P., 1939, Theoriia podobiia i metodika rascheta gidrotekhnicheskikh modelei, (theory of similarity and methods of design of models for hydraulic engineering), Gosstroiizdat, Leningrad.

# APPENDIX 6A

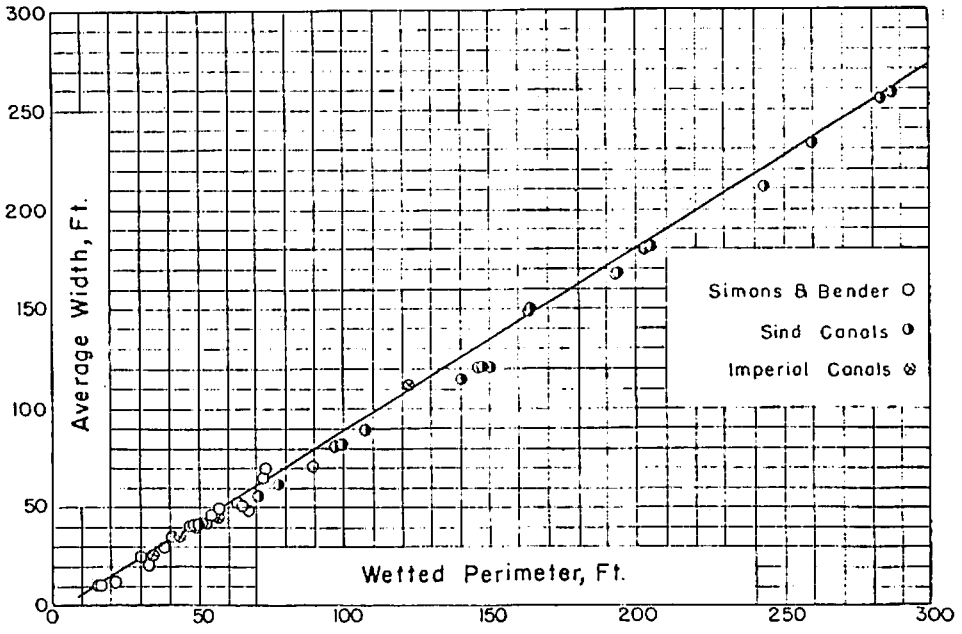


Figure 6A-1. Variation of hydraulic radius R with depth d.

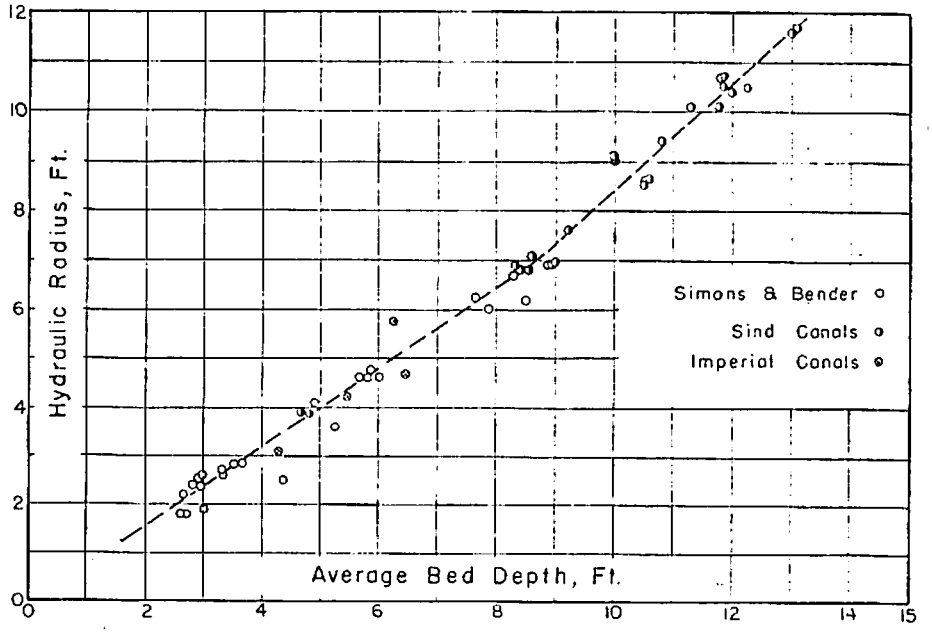


Figure 6A-2. Variation of average width w with wetted perimeter p.

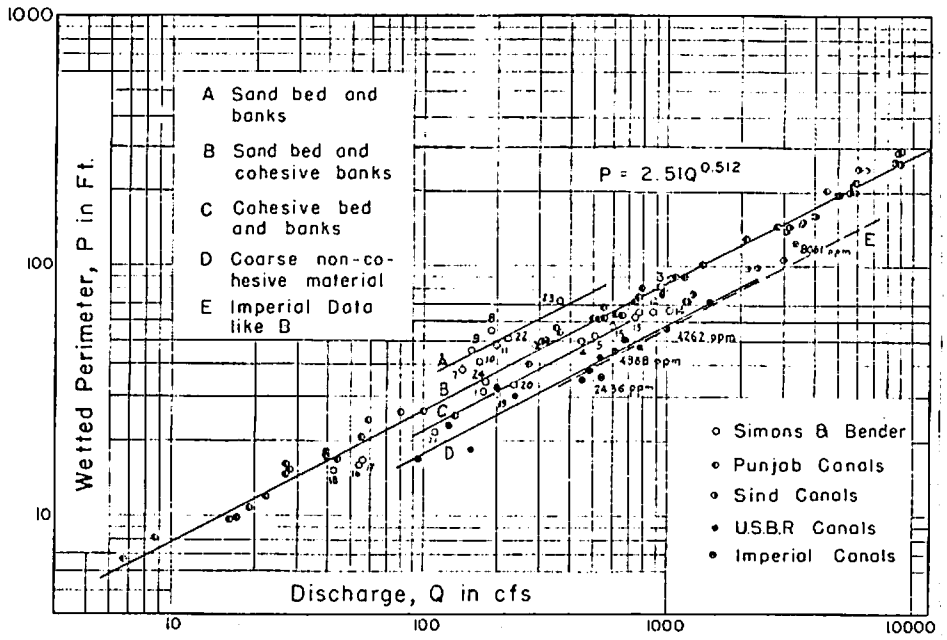


Figure 6A-3. Variation of wetted perimeter p with discharge q and type of channel.

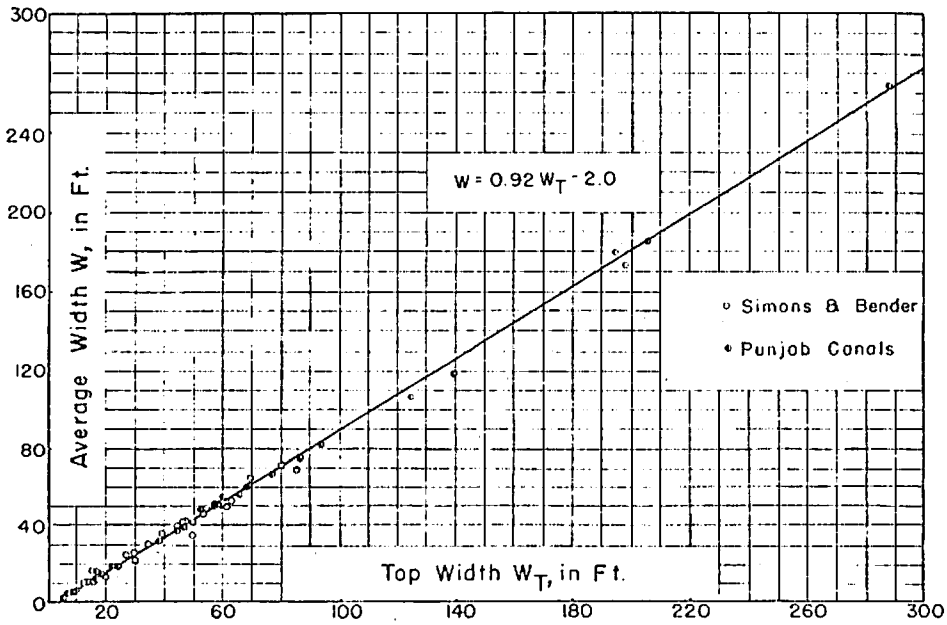


Figure 6A-4. Variation of average width w with top width $w_t$.

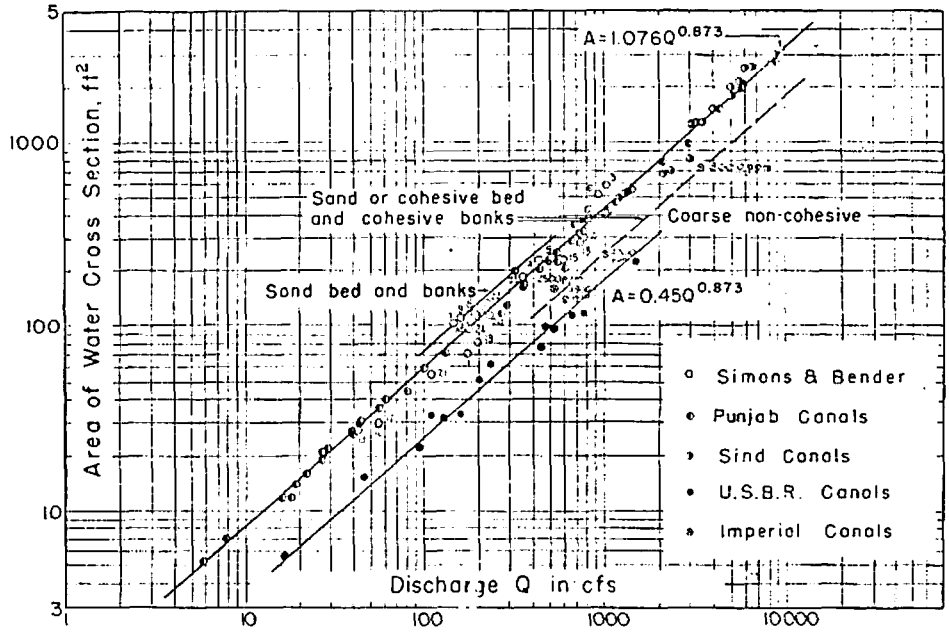


Figure 6A-5. Variation of hydraulic radius r with discharge q and type of channel, all data.

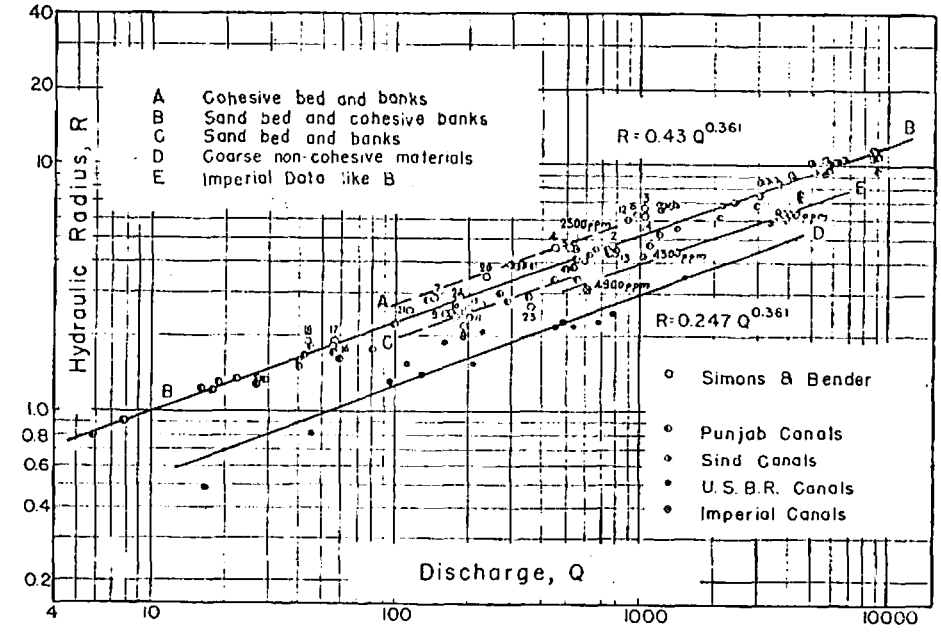


Figure 6A-6. Variation of area of water cross section a with discharge q and type of channel.

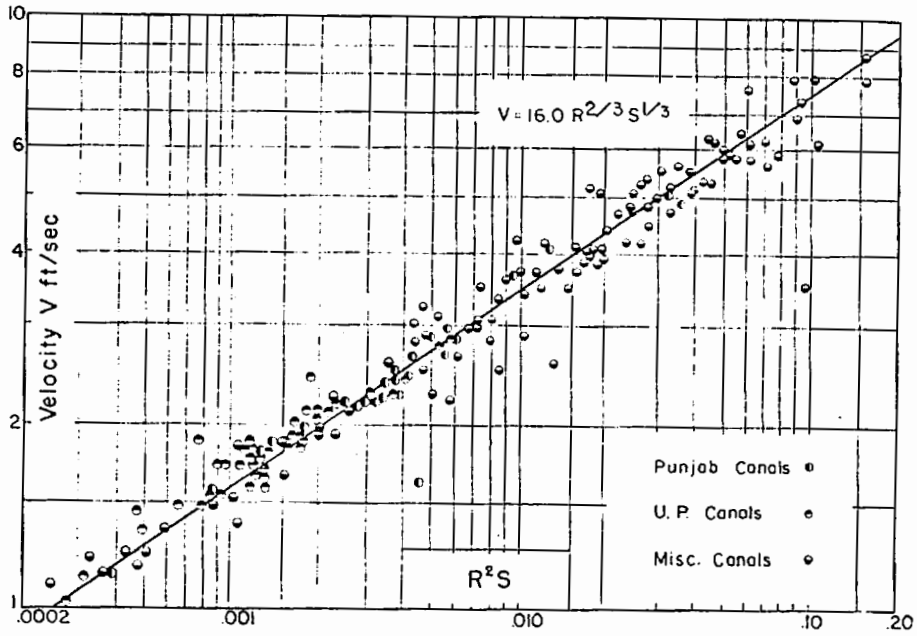


Figure 6A-7. Variation of average velocity v with $R^2S$, India date.

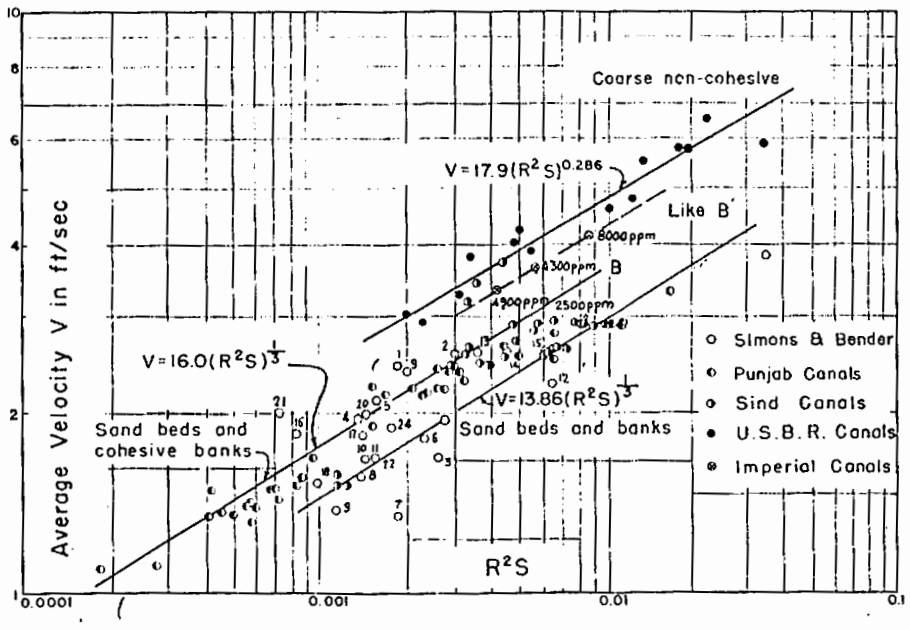


Figure 6A-8. Variation of average velocity v with $R^2S$ and type of channel, all data.

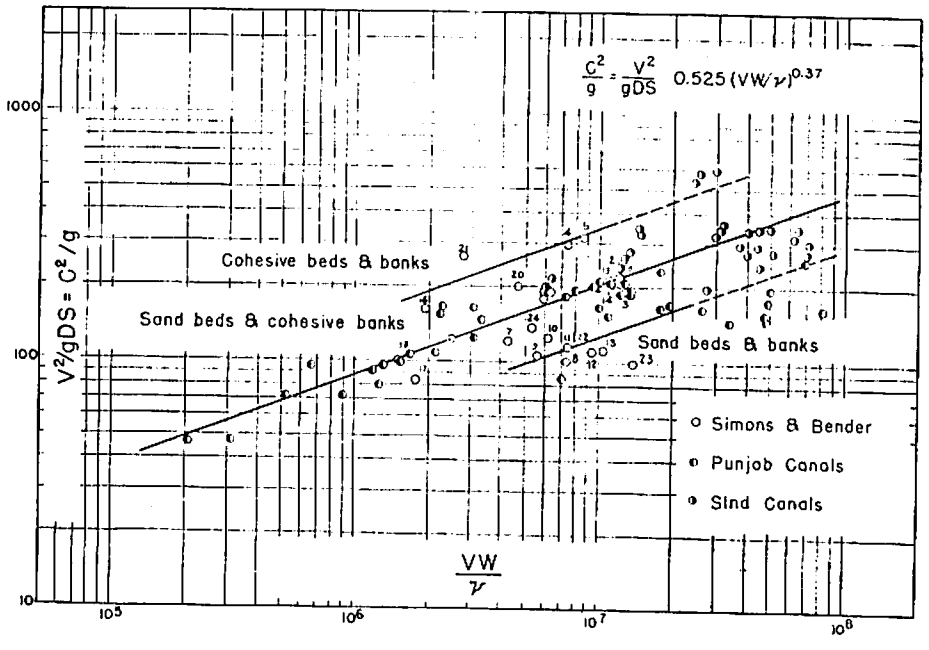


Figure 6A-9. Variation of $V^2/gDS$ with VW/v and type channel.

# CHAPTER 7

# SEDIMENT TRANSPORT

## 7.1 INTRODUCTION

Sediment is a major problem in control and utilization of surface waters. Various sediment problems are often encountered in design of irrigation and drainage canals, improvement or stabilization of rivers and floodways for navigation and in flood control, planning and design of reservoirs, maintenance of harbor channels, beach erosion, purification of public water supplies, and control of soil erosion on watershed areas.

This chapter is concerned with the basic ideas and findings upon which knowledge of sedimentation is based. Also methods of measurement and estimation of the sediment discharge of streams are reviewed and referenced.

### Terminology

A number of terms are frequently found in literature include

Bed layer. A flow layer, several grain diameters thick (usually two grains diameters) immediately above the bed.

Bedload. Sediment that moves by saltation (jumping), rolling, or sliding in the bed layer.

Bedload discharge (or bedload). The quantity of bed load passing a cross section of a stream in a unit of time.

Bed material (or bed sediment). The sediment mixture of which the streambed is composed.

Bed-material discharge (or bed-material load). That part of the total sediment discharge that is composed of grain sizes found in the bed and is equal to the transport capability of the flow.

Contact load. Sediment particles that roll or slide along in almost continuous contact with the streambed.

Density of water-sediment mixture. Bulk density which is mass per unit volume including both water and sediment.

Discharge weighted concentration. Dry weight of sediment in a unit volume of stream discharge, or the ratio of discharge of dry weight of sediment to discharge by weight of water sediment mixture.

Fine material load (or wash load). That part of the total sediment load that is composed of particle sizes finer than those represented in the bed. Normally the fine-sediment load is finer than 0.062 mm for a sand-bed channel. Silts, clays and sand could be considered as wash load in coarse gravel and cobble bed channels.

Load (or sediment load). Sediment that is being moved by a stream.

Saltation load. Sediment bounced along the stream bed by energy and turbulence of flow and by other moving particles.

Sediment (or fluvial sediment). Fragmental material that originates from weathering of rocks and is transported by, suspended in, or deposited by water.

Sediment concentration (by weight or by volume). Quantity of sediment relative to quantity of transporting or suspending fluid, or fluid-sediment mixture. Quantity may be by weight or by volume.

Sediment discharge (or sediment load). Quantity of sediment that is carried past any cross section of a stream in a unit of time. Discharge may be limited to certain sizes of sediment or to discharge through a specific part of the cross section.

Sediment yield. Total sediment outflow from a watershed or a drainage area at a point of reference and in a specified time period. This is equal to the sediment discharge from the drainage area.

Spatial concentration. Dry weight of sediment per unit volume of water-sediment mixture in place, or the ratio of dry weight of sediment to total weight of water-sediment mixture in a sample or unit volume of the mixture.

Velocity-weighted sediment concentration. Dry weight of sediment discharged through a cross section during unit time.

Suspended load (or suspended sediment). Sediment that is supported by upward components of turbulent currents and stays in suspension for an appreciable length of time.

Suspended-sediment discharge (or suspended load). Quantity of suspended sediment passing through a stream cross section above the bed layer in a unit of time.

Total sediment discharge. Total sediment discharge of a stream. It is the sum of suspended-sediment discharge and bedload discharge or the sum of bed material discharge and wash load discharge.

Total sediment load (or total load). Total sediment load of a stream. It is the sum of suspended load and bedload or the sum of bed-material load and wash load.

Wash-load discharge (wash load). That part of total sediment discharge that is composed of particle sizes finer than those represented in the bed and is determined by available bank and upslope supply rate.

Armoring of the bed. Natural equilibrium of the bed reached after the fine material is transported away by the flow resulting in the development of a thin layer of coarser particles at the bed surface.

Size frequency distribution. see Appendix 7A.

## Factors Affecting Sediment Transportation and Deposition

The amount of material transported or deposited in the stream under a given set of conditions is the result of the interaction of two groups of variables. The first group is composed of variables that influence quantity and quality of sediment brought down to that section of the stream. The second group consists of variables that influence the capacity of the stream to transport that sediment. A list of these variables is given below.

### Group 1 - Sediment Brought Down to the Stream

Quality. Size, settling velocity, specific gravity, shape, resistance to wear, state of dispersion, and cohesion.

Quantity. Geology and topography of watershed, magnitude, intensity, duration, distribution, and season of rainfall, soil condition, vegetal cover, cultivation and grazing, surface erosion and bank cutting.

### Group 2 - Capacity of Stream to Transport Sediment

Geometric Properties or Shape of Stream Prism. Depth, width, form, and alignment.

Hydraulic Properties of the Stream Channel. Slope, roughness, hydraulic radius, discharge, velocity, velocity distribution, turbulence, tractive force, fluid properties, and uniformity of discharge.

These variables are not all independent and in some cases the effect of a variable is not definitely known. Experience has shown that it is not possible to accurately compute a long-term record of the flow of a stream from other data. It is most practicable to measure the discharge over a long period of time and record the results. In a similar way, it is difficult to compute the supply of sediment that will be brought down to the stream because of complexity of the variables involved. The most accurate method to make such information available is to measure the sediment flow over a considerable time period. A few of the more commonly used methods for determining sediment yield were summarized by an ASCE Task Committee (1970).

The variables in the second group that deal with capacity of the stream to transport solids are more subject to mathematical analysis and prediction. These variables are closely related to the hydraulic variables controlling the capacity of streams to carry water which in turn are closely related to the forms of bed roughness of streams and their resistance to flow. Herein, the sediment transport equations that determine transport capacity of streams will be discussed. Since wash load is largely determined by the available upslope supply rate which is controlled by the variables of the first group, at best a sediment transport equation can to predict only the bed material load.

There is no clear distinction between wash load and bed material load. As a rule of thumb, engineers assume that bed-material load size

is equal to or greater than 0.0625 mm which is the division point between sand and silt. The sediment load consisting of grain sizes less than this size is considered wash load. A more reasonable criterion although not necessarily theoretically correct, is to choose a sediment size finer than 10 percent of the bed sample as the dividing size between wash load and bed material load. It is assumed that most of the wash load is transported through the system by streamflow and little wash load is deposited on or in the stream bed. Wash load thus deposited with the coarse material is usually a small fraction of the bed material.

The sum of bed material load and wash load becomes the total sediment load. Since the sediment-transport equations can determine merely the bed material load, total sediment load can be predicted only if the wash load is estimated by measurement, empirically, or by analytical relations.

Types of Sediment Movement

Sediment particles are transported by flow in one or a combination of the following ways: 1) rolling or sliding on the bed (surface creep), 2) leaping into the flow and coming to rest on the bed (saltation), and 3) supported by the surrounding fluid during its entire motion (suspension).

There is no clear distinction between saltation and suspension. However, this distinction is important for it serves to delimit two methods of hydraulic transportation which follow different laws i.e., traction and suspension. Of course, sediments may be transported partially as saltation and then suddenly be caught by the flow turbulence and transported in suspension. Sediments which move as surface creep or saltation and are supported by the bed, are called bed load. Sediments which are suspended and supported by flow, are called suspended load.

## 7.2 TRANSPORT CONCEPTS

Bed Load

When the flow over movable boundaries of a channel has hydraulic conditions that exceed the critical condition for motion of the bed material, sediment transport starts. If the motion of entrained particles is one of rolling, sliding, and sometimes jumping in the bed layer, this is commonly referred to as bedload transport or contact load.

Generally the amount of bed load transported by a large river is in the order of 5 to 25 percent of the suspended load. Although the amount of bed load may be small compared with total sediment load, it is important because it shapes the bed and influences channel stability, bed roughness form, and other factors.

DuBoys initiated the idea of the bed shear stress or tractive force in the analysis of bed load as early as 1879. Since then numerous bed load equations for relating the bedload discharge, flow condition, and

composition of the bed material have been proposed. Many of these equations look similar because they are derived under conditions of steady flow in graded channels and thus are only applicable under these conditions. There is a great need for research concerning the transport of sediment when flow is unsteady, nonuniform, and both slowly and rapidly varying with time.

Formulas Written as a Function of $(q - q_c)$

Many bed load equations are based on excess shear stress i.e., $\tau_o - \tau_c$, or $\tau_o ' \tau_c$. For example the DuBoy's relation

$$q_{bv} = K \tau_o (\tau_1 - \tau_c) \tag{7-1}$$

Replacing $(\tau)$ by $(q)$ it is possible to express these formulas in a more efficient form for direct use. The Manning's formula

$$q = \frac{1.486}{n} d^{5/3} S^{1/2} \tag{7-2}$$

or in metric units

$$q = \frac{1}{n} d^{5/3} S^{1/2} \qquad 7\text{-}2$$

for wide channels can be transformed to

$$dS = S^{7/10} \left(\frac{qn}{1.486}\right)^{3/5} = \frac{\tau_o}{\gamma} \tag{7-3}$$

Substituting $\tau_o$ from Equation 7-3 in Equation 7-1 yields

$$q_{bv} = K \frac{S^{1.4} \gamma^2}{(1.486/n)^{1.2}} q^{3/5} (q^{3/5} - q_c^{3/5}) \ (*) \tag{7-4}$$

where $q$ is the actual water discharge per unit width and $q_c$ is the discharge per unit width at channel slope $S_c$ where sediment transport begins.

Bed load equations with the general form of Equation 7-4 and equations that utilize average velocity have been proposed by various researchers. In fact, a large number of such formulas have been published but only a few are discussed.

Schoklitsch (1930) stated that the average bed shear stress in DuBoy's equation is a poor criterion when applied to field computations because the shear distribution in the channel cross section is nonuniform. He suggested two equations. First in 1934 he defined a critical value $q_c$ for the discharge after which sediment motion begins as

(*) In metric units this formula takes the form

$$q_{bv} = K \frac{S^{1.4} \gamma^2}{\left(\frac{1}{n}\right)^{1.2}} q^{3/5} (q^{3/5} - q_c^{3/5}) \tag{7-5}$$

$$q_c = 1.94 \cdot 10^{-5} \frac{D_s}{S^{4/3}}$$

and using this value he suggested

$$q_{bw} = \frac{7000}{D_s^{1/2}} S^{3/2} (q-q_c) \qquad (7\text{-}6)$$

to compute the bed load. Equation 7-6 is written in metric units and $q_{bw}$ represents the sediment discharge on a dry weight basis. Subsequently, Schoklitsch (1950) modified his first formula and proposed the relation

$$q_{bw} = 2500.00 S^{3/2} (q-q_c) \qquad (7\text{-}7)$$

where

$$q_c = 0.26 \left(\frac{\gamma_s'}{\gamma}\right)^{5/3} \frac{D_s^{3/2}}{S^{7/6}}$$

Meyer-Peter, Müller Formula

Meyer-Peter and Müller (1948), based on experiments with sand particles of uniform sizes, sand particles of mixed sizes, natural gravel, lignite, and baryta developed a formula similar in form to the DuBoy's formula.

The mechanics of sediment transport is explained in different manners by different authors. The stochastic approach was worked out by Einstein. Kalinske (1942) and Frijlink and Elderman (1961) attempted to determine the amount of shear taken by solid particles in their movement. Meyer-Peter assumed that energy slope is a characteristic of interaction between solid and liquid motion of a sediment laden flow. A given portion of the energy is consumed for solid transport and the remaining for liquid motion. A second assumption of Meyer-Peter is that similar parameters govern sediment transport and the beginning of motion. The results utilizing these assumptions are similar to DuBoy's but the method of solving problems is different.

Meyer-Peter and Müller's Sediment Transport Formula

The first sediment transport formula presented by Meyer-Peter was

$$\frac{q_{bw}^{2/3} S^{2/3}}{D_m} = c_1 + c_2 \frac{q_{bw}'^{2/3}}{D_m} \quad (*) \qquad (7\text{-}8a)$$

in which $q_{bw}'$ is the submerged weight of the transported sediment that equals $_{qs}\ \gamma'/\gamma$ and $c_1$ and $c_2$ are parameters. It should be noted that the relations

$$\left(\frac{\gamma_s R_s S}{D_m}\right) c = k \left(\frac{D_m}{Rs}\right)^{1/9} \qquad (7\text{-}8b)$$

and 7.8a are written as functions of $\frac{q_{bw}^{2/3} S^{2/3}}{D_m}$. (*)

If the motion of water in a conduit is considered, the resistance to flow can be expressed in different forms. Meyer-Peter used Strickler's formula and a compound resistance coefficient $k_s$ i.e.,

$$S_k = \frac{U^2}{k_r^2 R_s^{4/3}} \tag{7-9}$$

Considering only the resistance due to skin friction Equation 7-9 takes the form

$$S_r = \frac{U^2}{k_r^2 R_s^{4/3}} \tag{7-10}$$

and

$$\frac{S_r}{S} = \left(\frac{k_s}{k_r}\right)^2 \tag{7-11}$$

Combining Equations 7-8b and 7-8a and noting that both relations are a function of $\frac{q_{bw}^{2/3} S^{2/3}}{D_m}$ one obtains

$$\frac{\gamma R_s S}{D_m} = c_3 + c_4 \frac{q_{bw}'^{2/3}}{D_m} \tag{7-12}$$

Meyer-Peter assumed that since transport is mostly governed by skin friction

$$\frac{\gamma R_s S_r}{D_m} = c_3 + c_4 \frac{q_{bw}'^{2/3}}{D}$$

The value of $S_r$ can be obtained from Equation 7-9 and

$$\gamma \left(\frac{k_s}{k_r}\right)^2 \frac{R_s S}{D_m} = c_5 + c_6 \frac{q_{bw}'^{2/3}}{D_m} \tag{7-13}$$

(*)Equation 7-8a in its earliest form was written as:

$$\frac{q_{bw}^{2/3}}{D_m} = a_1 + a_2 \frac{q_{bw}'^{2/3}}{D_m}$$

At that time Meyer-Peter thought that an overall parameter may govern both, the beginning of motion and sediment transport.

Comparing Equation 7-13 and

$$q_{bw}^{2/3} = \gamma^{2/3}\, c^{2/3}\, (\frac{R_s}{D})^{1/9}\, R_s\, S^{1/3} \tag{7-14}$$

It should be noted that in Equation 7-14 $q_s^{2/3}$ is a function of $S^{1/3}$, and in Equation 7-13 the same quantity is a function of S. Hence, S in Equation 7-13 represents the total energy loss due to sediment transport and liquid motion but in Equation 7-14 S is only related to liquid motion. Noting that the sediment transport is mostly related to skin friction it is possible to write

$$S = S^{1/3}\, S_r^{2/3} \tag{7-15}$$

where S is the energy loss due to water and sediment transport and $S_r$ is the energy used to transport the solids. Substituting Equation 7-15 in Equation 7-12 yields

$$\frac{\gamma R_s S^{1/3} S_r^{2/3}}{D_m} = c_3 + c_4 \frac{q_{bw}'^{2/3}}{D_m} \tag{7-16}$$

From Equation 7-11 $S_r^{2/3} = (\frac{k_s}{k_r})^{4/3} S^{2/3}$. Substituting this value in Equation 7-16

$$\gamma(\frac{k_s}{k_r})^{4/3} \frac{R_s S}{D_m} = c_7 + c_8 \frac{q_{bw}'^{2/3}}{D_m} \tag{7-17}$$

It should be noted that Equation 7-14 shows that $k_s/k_r$ has an exponent of 2. Hence the exponent of $(k_s/k_r)$ varies between 4/3 and 2. If the mean value (3/2) expresses the phenomenon correctly then

$$\gamma(\frac{k_s}{k_r})^{3/2} \frac{R_s S}{D_m} = A + B \frac{q_{bw}'^{2/3}}{D_m} \tag{7-18}$$

This equation corrected according to experimental results is

$$\gamma(\frac{k_s}{k_r})^{3/2} R_s S = A'' \gamma_s' D_m + B''(\frac{\gamma}{g})^{1/3} q_{bw}'^{2/3} \tag{7-19}$$

Then substituting

$$A'' = 0.047,\ B'' = 0.25 \quad \text{and} \quad \gamma' = \gamma_s - \gamma$$

Equation 7-19 yields

$$\gamma(\frac{k_s}{k_r})^{3/2} R_s S_k = 0.047\, \gamma_s' D_m + 0.25\, \rho^{1/3}\, q_{bw}'^{2/3} \tag{7-20}$$

Figure 7-1 illustrates the usefulness of this relation. For a very wide cross section $R_s = d$ and if $k_s = k_r$ Equation 7-20 can be expressed as

$$\gamma dS = 0.047\ \gamma'_s D_m + 0.25\ \rho^{1/3}\ q'^{\,2/3}_{bw} \tag{7-21}$$

From Equation 7-21

$$\frac{\gamma dS}{\gamma'_s D_m} = 0.047 + \frac{0.25\ \rho^{1/3}}{\gamma'_s D_m}\ q'^{\,2/3}_{bw} \tag{7-22}$$

and when $q'_{bw} = 0$

$$\frac{\gamma dS}{\gamma'_s D_m} = 0.047 \tag{7-23}$$

This relation defines the beginning of motion according to Meyer-Peter, Müller. Equation 7-22 can be written in a dimensionless form as

$$\frac{q'_{bw}}{\rho U_*^3} = 8\ (1 - \frac{0.047}{\tau_*})^{3/2} \quad (*)$$

where

$$\tau_* = \frac{\rho U_*^2}{\gamma'_s D_m} \tag{7-24}$$

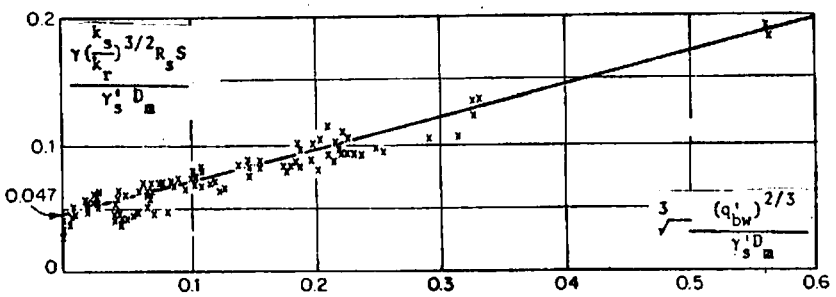


Figure 7-1. Meyer-Peter's bed load function.

On the other hand if

$$\tau_o = \gamma dS,\ \tau_c = 0.047\ \gamma'_s D_m \quad \text{and} \quad N = 8(\frac{g}{\gamma})^{1/2}\ \frac{\gamma}{\gamma'_s},$$

(*)Using the same parameters it is possible to write

Einstein transport formulas $\phi_* = \frac{q'_{bw}}{\rho U_*^3} \cdot \tau_*^{3/2}$

and $\psi_* = \frac{1}{\tau_*}\ f_1(R_*)$ (7-25)

where $R_* = \frac{U_* D_m}{\nu}$

and Kalinske's formula $\frac{q'_{bw}}{\rho U_*^3} = \tau$ (7-26)

then

$$q'_{bw} = (\tau_o - \tau_c)^{3/2} N$$

The DuBoys' formula is

$$q_{bv} = \tau_o(\tau_o - \tau_c)k \qquad (7\text{-}27)$$

The similarity between these two expressions is self evident. Definitions of variables and the meaning of symbols in Equation 7-20 are summarized

$\gamma$ = Specific weight of water ($T/m^3$)

$k_s$ = Roughness coefficient according to Strickler

$$k_s = \sqrt{\frac{U^2}{S\, R_s^{4/3}}}$$

$k_r$ = Roughness coefficient due to skin friction and is given by Strickler as

$$k_r = \frac{21.1}{D^{1/6}} \ (m^{1/3}/sec) \qquad (7\text{-}28)$$

Equation 7-28 was transformed by Meyer-Peter and Müller to

$$k_r = \frac{26}{D_{90}^{1/6}} \ (m^{1/3}/sec) \qquad (7\text{-}29)$$

to express the roughness due to a nonuniform bed material.

$R_s$ = Hydraulic radius of the bed (m)

$S$ = Energy gradient

$\gamma'_s = \gamma_s - \gamma$ ($T/m^3$)

$D_m$ = Representative diameter of bed material, defined as

$$D_m = \frac{\sum_{i} Di\Delta}{100} \quad (m) \qquad (7\text{-}30)$$

$\rho$ = Specific mass of water (ton · $sec/m^4$)

$q'_s$ = Rate of sediment discharge weighed under water ($T/m^3$ ·· sec/m)

Equation 7-20 has been coverted to English units by the Sedimentation Section, U.S. Bureau of Reclamation (1960). Methods and procedures to aid in the use of the USBR formulas have been developed. The USBR formulas are summarized. The relation for sediment transport is

$$q_{bw} = \left(\frac{\gamma_s}{\gamma_s-\gamma}\right)\left(\frac{g}{\gamma}\right)^{1/2}\left[0.0661\ \gamma\left(\frac{Q'}{Q}\right)\left(\frac{D_{90}^{1/6}}{n_b}\right)^{3/2} dS - 0.0076\ (\gamma_s-\gamma)\ D_m\right]^{3/2} \quad (7\text{-}31)$$

where $q_{bw}$ is the sediment discharge in tons per day per foot width, $Q'$ is the water discharge quantity that determines the bed load transport, $Q$ is the total water discharge, and $D_{90}$ and $D_m$ are in millimeters. The quantity $n_b$ is given by

$$n_b = n\left\{1 + \frac{2d}{B}\left[1 - \left(\frac{n_w}{n}\right)^{3/2}\right]\right\}^{2/3} \quad \text{(rectangular channel)} \quad (7\text{-}32)$$

$$n_b = n\left\{1 + \frac{2d(1+z^2)^{1/2}}{B}\left[1 - \left(\frac{n_w}{n}\right)^{3/2}\right]\right\}^{2/3} \quad \text{(trapezoidal channel)} \quad (7\text{-}33)$$

where $n$, $n_b$, and $n_w$ are roughness coefficients of the total channel, the bed, and the banks, respectively, $B$ is the top width, and $z$ defines the side slope, the ratio of horizontal distance to one unit vertically. The quantity $Q'/Q$ is given by

$$\frac{Q'}{Q} = \frac{1}{1 + \frac{2d}{B}\left(\frac{n_w}{n_b}\right)^{3/2}} \quad \text{(rectangular channel)} \quad (7\text{-}34)$$

and

$$\frac{Q'}{Q} = \left[1 + \frac{2d(1+z^2)^{1/2}}{B}\left(\frac{n_w}{n_b}\right)^{3/2}\right]^{-1} \quad \text{(trapezoidal channel)} \quad (7\text{-}35)$$

For water and quartz particles, Equation 7-31 reduces to

$$q_{bw} = 1.606\left[3.306\left(\frac{Q'}{Q}\right)\left(\frac{D_{90}^{1/6}}{n_b}\right)^{3/2} dS - 0.627\ D_m\right]^{3/2} \quad (7\text{-}36)$$

If the values of Q, d, S, B, n, $n_w$, and the grain size distribution of bed material are given, the bedload can be computed using Equation 7-31 or Equation 7-36.

Discussion of Meyer-Peter, Müller Formula

Applied to stable water courses the Meyer-Peter formula can give satisfactory estimates of sediment transport for sand and gravel material. The Meyer-Peter, Müller formula is based on two fundamental assumptions

1. The experimental sediment transport formula is based on $(q_{bw}{}^{2/3}S)$, which is changed to $q_{bw}{}^{2/3}S^{2/3}$.

2. The exponent for the ratio $(\frac{k_s}{k_r})^{3/2}$ utilized in Equation 7-17 is chosen arbitrarily.

When the variation of $k_r$ is between rather narrow limits the exponent $(\frac{3}{2})$ gives acceptable approximations. But when $k_r$ increases towards its extreme values the differences between observed and measured sediment discharge are large and results are questionable.

Einstein's Bed Load Equation

Einstein (1942, 1950) departed from the concepts of the DuBoys-type and Schoklitsch-type equations. His physical treatment of the problem considered at least two basic ideas which break with the past: 1) the critical criterion was avoided, because the critical condition for initiation of sediment motion is difficult to define and 2) bed load transport is related to the turbulent flow fluctuations rather than to the average values of forces the flow exerts on the sediment particles. Consequently, the beginning and ending of sediment motion is expressed with the concept of probability, which relates instantaneous hydrodynamic lift forces to the particle's submerged weight.

Based on experiments, Einstein found that there exists an intimate relationship between the bed material and the bed load.

1. A steady and intensive exchange of particles exist between the bed material and the bed load.

2. Particles are transported along the bed in a series of steps. The average step length is proportional to the particle size. A particular particle does not stay in motion continuously, but is deposited on the bed after a few steps.

3. The rate of deposition per unit area depends on the transport rate past a given section as well as the probability that the hydrodynamic forces are such that the particle may be deposited. On the other hand, the rate of erosion from this area depends on the number and properties of particles in the unit area and the probability that instantaneous hydrodynamic lift force on each particle is sufficiently large to move it. For stable bed conditions, the rate of deposition must be equal to the rate of erosion.

The number of particles of size $D$ that are deposited over a unit area per unit time can be expressed as

$$N_D = \frac{q_{bw} i_B}{(A_L D)(\gamma_s A_2 D^3)} = \frac{q_{bw} i_B}{A_L A_2 \gamma_s D^4} \tag{7-37}$$

where $q_{bw}$ is the bed load discharge in weight per unit time and width. The value of $q_{bw}$ can be subdivided into fractions $i_{Bw}$ according to particle size. The rate at which the given size moves through a unit width of channel cross section is $(q_{bw} i_{Bw})$. Particles with a given diameter $D$ are assumed to be performing individual steps of average

length ($A_L D$). These particles may be deposited anywhere between the given section and ($A_L D$) downstream, because by passing the given section they have already traveled an unknown part of the total step length ($A_L D$). The weight of such a particle is given by ($\gamma_s A_2 D^3$), thus the number of such particles deposited per unit time on a unit area of bed can be expressed as Equation 7-37.

Whether or not a particle of size D will be eroded from the bed surface depends on the availability of the particle and on the flow conditions. If the fraction of the bed sediment of a given size D is $i_{bw}$, then the number of such particles in a unit area of bed surface is given by $i_{bw}/(A_1 D^2)$ with $A_1$ being the constant of the grain area. If $p/t_1$ is the probability of such a particle being eroded during a unit time, the number of particles eroded per unit time and area is

$$N_e = \frac{i_{bw} p}{A_1 D^2 t_1} \tag{7-38}$$

where $t_1$ is the time consumed by each exchange and p is the probability for a particle to be eroded at any one spot, which corresponds to the fraction of the total time during which the local flow conditions are sufficient to remove the particle. No direct method is available for determining exchange time. Experimental evidence suggests that this quantity is a characteristic constant of the particle only and is proportional to the time necessary for the particle to settle in the fluid at a distance equal to its own size (Einstein, 1942)

$$t_1 \sim \frac{D}{w} \tag{7-39}$$

or

$$t_1 = A_3' \frac{D}{w} \tag{7-40}$$

The fall velocity was computed after Rubey (1933) as

$$w^2 = \frac{A_3'^2 \, Dg \, \gamma_s'}{A_3^2 \, \gamma} \tag{7-41}$$

Substituting this value of w Equation 7-40 yields

$$t_1 = A_3 \left[\frac{D\rho}{(\gamma_s - \gamma)}\right]^{1/2} \tag{7-42}$$

where $A_3 = 1.225$ for quartz particles greater than 1 mm and settling in water with a temperature of 16°C.

The probability of a particle being eroded during a unit time was given as

$$p_s = \frac{p}{t_1}$$

Then substituting this value of $t_1$ in Equation 7-42 yields

$$p_s = \frac{p}{A_3 \sqrt{\frac{\rho D}{\gamma_s - \gamma}}} \tag{7-43}$$

and

$$N_e = \frac{i_{bw}}{A_1 D^2} p_s = \frac{i_{bw} p}{A_1 D^2} \frac{[g(\rho_s - \rho)]^{1/2}}{A_3 [\rho D]^{1/2}} \tag{7-44}$$

For equilibrium the number of particles eroded must equal the number deposited i.e.,

$$\frac{q_{bw} i_{Bw}}{A_L A_2 \gamma_s D^4} = \frac{i_{bw} p}{A_3 A_1 D^2} \sqrt{\frac{g(\rho_s - \rho)}{\rho D}} \tag{7-45}$$

Then

$$\frac{q_{bw}}{\rho_s g} \sqrt{\frac{\rho}{g(\rho_s - \rho) D^3}} = \frac{q_{bw}}{\gamma_s} \sqrt{\frac{\gamma}{g \gamma_s D^3}} = \frac{i_{bw}}{i_{Bw}} \frac{A_2 A_L}{A_1 A_3} p \tag{7-46}$$

q and $\frac{q_{bw}}{\gamma_s} \sqrt{\frac{\gamma}{g \gamma_s' D^3}}$ is called $\phi$. The term $\phi$ is the transport rate function i.e.,

$$\phi = \frac{q_{bw}}{\gamma_s} \sqrt{\frac{\gamma}{g \gamma_s' D^3}} \tag{7-47}$$

The term $\phi$ can be expressed as

$$\phi = \frac{q_{bw}}{v \gamma_s} \sqrt{\frac{\rho v^2}{\gamma_s' D^3}} \tag{7-44}$$

Parameters $\frac{q_{bw}}{v \gamma_s}$, $\frac{\rho v^2}{\gamma_s' D^3}$ (*) and $\phi$ are dimensionless numbers.

Probability of erosion p as defined above may also be interpreted with all points of the bed statistically equivalent as the fraction of the bed on which at any time the lift on a particle of a given diameter D is sufficient to cause it to move. With this interpretation p may be used to calculate the distance $A_L D$ that a particle travels between consecutive places. If p is small, deposition of the particle is possible almost anywhere and $A_L$ equals a general constant $\lambda$ that has a value of about 100. However, if p is not small, deposition cannot occur on that part p of the bed where the lift force exceeds the particle weight. Thus, (1-p) particles are deposited and p particles

---

(*)The parameter $\frac{\rho v^2}{\gamma_s' D^3}$ is sometimes called the sedimentation parameter "Diametre sedimentalogique" in French. This term is encountered in many fields of sediment transport and particularly in equilibrium formulas.

are not deposited after traveling $\lambda D$. Of these, $p(1-p)$ particles are deposited after traveling $2\lambda D$ while $p^2$ particles are still not deposited, and so on. By averaging the distances traveled by individual particles, the travel distance can be expressed as

$$A_L D = \sum_{n=0}^{\infty} (1-p)\, p^n\, (n+1)\, \lambda D \tag{7-48}$$

The probability of a grain making the (n+1) jump is $(1-p)^n pn(n+1)$.

Then

$$\sum_{0}^{\infty} (1-p)\, p^n\, (n+1) = \Sigma(1-p)(n\, p^n + p^n) = 1+p+p^2+p^3+\ldots+p^n = \frac{1}{1-p}$$

and

$$A_L D = \sum_{n=0}^{\infty} (1-p)\, p^n\, (n+1)\, \lambda D = \frac{\lambda D}{1-p} \tag{7-49}$$

Substituting Equation 7-49 for $A_L D$ in Equation 7-46 and separating p yields the relation

$$\frac{p}{1-p} = \left[\frac{A_1 A_3}{A_2 \lambda}\right] \left(\frac{i_{Bw}}{i_{bw}}\right) \left\{\frac{q_{bw}}{\rho_s g} \sqrt{\frac{\rho}{\rho_s - \rho}} \sqrt{\frac{1}{gD^3}}\right\} \tag{7-50}$$

or

$$\frac{p}{1-p} = [A_*] \frac{i_{Bw}}{i_{bw}} \{\phi\} = A_* \phi_* \tag{7-51}$$

where $A_* = \dfrac{A_1 A_3}{A_2 \lambda}$

$$\phi_* = \frac{i_{Bw} q_{bw}}{i_{bw} g \rho_s} \sqrt{\frac{\rho}{\rho_s - \rho}} \sqrt{\frac{1}{gD^3}} \quad \text{and} \quad q_{bw} = q_s$$

The term $\phi$ as stated earlier is recognized as the intensity of bedload transport, or the transport rate function that is a dimensionless measure of bedload transport and is independent of stream size. If $\phi$ is equal in two different flows, the two rates of bedload transport are dynamically similar.

Probability That the Lift Force Is Larger Than the Submerged Weight of the Particle

As previously mentioned, the probability p is the probability of a particle being eroded, and hence is also the probability that the hydrodynamic lift force L on the particle is larger than its submerged weight

$$W' = g(\rho_s - \rho)\, A_2 D^3 \tag{7-52}$$

The lift force is expressed as

$$L = C_L A_1 D^2 \frac{\rho u^2}{2} \tag{7-53}$$

Einstein and El-Samni (1949) determined that the lift coefficient $C_L$ has a constant value of 0.178.

The flow velocity is based on the logarithmic velocity distribution formula (Equation 7-55)(*)

$$\frac{u}{u'_*} = 5.75 \log (30.2 \frac{y}{\Delta}) \tag{7-54}$$

where $u'_*$ is the shear velocity due to grain roughness and equals $\sqrt{gR'_bS}$, $R'_b$ is the bed hydraulic radius associated with the grain roughness, $\Delta$ is the apparent roughness of the bed surface and equals $k_s/x$ with $k_s \cong D_{65}$, and $x$ is determined from Figure 7-2 for values of $k_s/\delta = 11.6\ \nu/U_*$.

Comparing Equation 7-54 with Equation 7-55(*), it may be observed that $u_*$ is replaced by $u'_*$. Also, it may be recalled that the total resistance to flow is composed of two parts, surface drag and form drag. Transmission of shear to the boundary is accompanied by a transformation of flow energy into turbulence energy. The part of the energy corresponding to grain roughness is transformed into turbulence that remains for a short time in the immediate vicinity of the grains and has a great effect on the bed load.

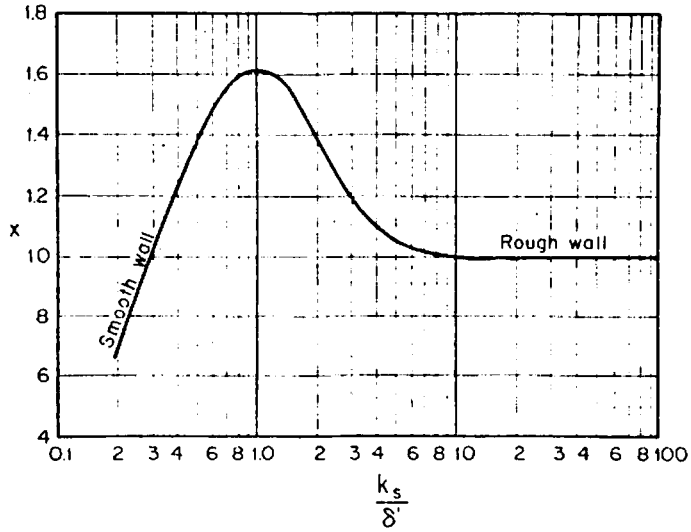


Figure 7-2. Correction factor in the logarithmic velocity distribution.

(*) $\frac{u}{U_*} = 5.75 \log (30.2 \frac{y}{k_s} x)$ (7-55)

Whereas, the other part of the energy corresponding to form resistance is transformed into turbulence at the interface between the wake and free streamflow or at a considerable distance from the grains. This energy does not significantly contribute to the bedload motion of the particles. Therefore, it has little effect on bed load transportation and explains the reason velocity distribution near a sediment grain in the bed surface is described by Equation 7-54.

From experiments, it is found that the velocity acting on all particles of a mixture must be measured at a distance 0.35X above the theoretical bed. Then from Equation 7-54, this velocity becomes

$$u = U_*' \; 5.75 \log \left(30.2 \frac{0.35X}{\Delta}\right) \tag{7-56}$$

or

$$u^2 = R_b' S g \; 5.75^2 \log^2 \left(10.6 \frac{X}{\Delta}\right) \tag{7-57}$$

where $X$ is the characteristic grain size of the mixture with

$$X = 0.77 \Delta \quad \text{if} \quad \Delta/\delta > 1.80$$

and

$$X = 1.39 \delta' \quad \text{if} \quad \Delta/\delta' < 1.80 \tag{7-58}$$

Using this knowledge, the instantaneous lift force may be determined by

$$L = 0.178 A_1 D^2 \frac{\rho}{2} R_b' S g \; 5.75^2 \log^2 \left(10.6 \frac{X}{\Delta}\right) (1+\eta) \tag{7-59}$$

where $\eta$ is a parameter that describes the fluctuation of velocity with time.

Quantity $p$ may be expressed as the probability that $W'/L$ is smaller than unity i.e.,

$$1 > \frac{W'}{L} = \left[\frac{1}{1+\eta}\right] \left\{\frac{\rho_s - \rho}{\rho} \frac{D}{R_b' S}\right\} \left(\frac{2A_2}{0.178 A_1 \; 5.75^2}\right) \frac{1}{\log^2 (10.6 X/\Delta)}$$

$$= \left[\frac{1}{1+\eta}\right] \{\psi\} (B)/\beta_x^2 \tag{7-60}$$

where

$$\psi = \frac{\rho_s - \rho}{\rho} \frac{D}{R_b' S}$$

$$\beta_x = \log \left(10.6 \frac{X}{\Delta}\right)$$

and

$$B = \frac{2A_2}{0.178 A_1 \; 5.75^2}$$

Here $\eta$ may be positive or negative but the lift is always positive so that from Equation 7-60

$$|(1-\eta)| > (B/\beta_x^2)\psi \tag{7-61}$$

Furthermore, Einstein (1950) suggested the use of two correction factors $\xi$ and Y. Bed material particles smaller than X are concealed by other particles or the laminar sublayer. Therefore, the lift they experience must be corrected by $\xi$. This hiding factor is a function of D/X and is obtained from Figure 7-3. The other correction factor Y describes the change in the lift coefficient for mixtures of sizes of bed material that contributes to various bed roughness conditions. Figure 7-4 gives the correction Y in terms of $D_{65}/\delta$. Introducing the two correction factors, Equation 7-61 becomes

$$\left|(1+\eta)\right| > \xi Y B' \psi \frac{\beta^2}{\beta_x^2} \tag{7-62}$$

where $B' = B/\beta^2$, $\beta$ = log 10.6, and $\xi$, Y, and $\beta^2/\beta_x^2$ are all unity for a uniform grain material and x = 1.

If $\eta$ varies according to the normal-error law and is expressed as $\eta = \eta_o \eta_*$ with $\eta_o$ being the standard deviation, then $\eta_*$ has the standard normal distribution with values of mean and standard deviations equal to zero and one, respectively. Squaring Equation 7-62 and letting $\eta = \eta_o \eta_*$, one obtains

$$\left(\frac{1}{\eta_o} + \eta_*\right)^2 > \xi^2 Y^2 \left(\frac{B'}{\eta_o}\right)^2 \left(\frac{\beta^2}{\beta_x^2}\right)^2 \psi 2 \tag{7-63}$$

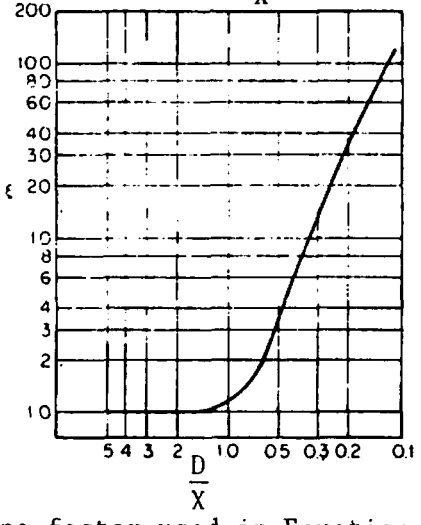


Figure 7-3. Hiding factor used in Equation 7-33 (after Einstein, 1950).

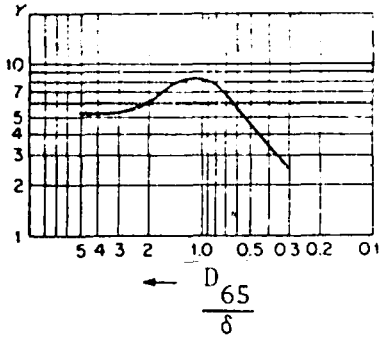


Figure 7-4. Pressure correction used in Equation 7-33 (after Einstein, 1950).

or

$$\left(\frac{1}{\eta_o} + \eta_*\right)^2 > B_*^2 \psi_*^2 \tag{7-64}$$

where $B_* = B'/\eta_o$ and $\psi_* = \xi Y(\beta^2/\beta_x^2)\psi$. The limiting case of motion may be written as

$$\left(\frac{1}{\eta_o} + \eta_*\right)^2 = B_*^2\psi_*^2 \tag{7-65}$$

or

$$[\eta_*]_{limit} = \pm B_*\psi_* - \frac{1}{\eta_o} \tag{7-66}$$

In order to minimize the errors the standard deviation of the fluctuations defined by Equation 7-66 must be small, then

$$B_* = \frac{B'}{\eta_o} \to \infty, \quad \frac{1}{\eta_o} \to \infty$$

then

$$-B_* \psi_* - \frac{1}{\eta_o} = -\infty$$

and

$$+B_* \psi_* - \frac{1}{\eta_o} \neq 0$$

If the random nature of $\eta_o$ satisfies the normal Gaussian error law, the probability that a grain will be lifted is

$$p = 1 - \frac{1}{\sqrt{\pi}} \int_{-B_* \psi_* - \frac{1}{\eta_o}}^{B_* \psi_* - \frac{1}{\eta_o}} e^{-t^2}\, dt \tag{7-67}$$

Equation 7-51 combined with Equation 7-67 yields

$$p = 1 - \frac{1}{\sqrt{\pi}} \int_{-B_* \psi_* - \frac{1}{\eta_o}}^{B_* \psi_* - \frac{1}{\eta_o}} e^{-t2}\, dt = \frac{A_*\phi_*}{1+A_*\phi_*} \tag{7-68}$$

where $A_*$, $B_*$, and $\eta_o$ are universal constants to be determined from experimental data. Using the data of Gilbert (1916) and of Meyer-Peter et al. (1934), $A_*$ and $B_*$ were determined to be 43.5 and 0.143, respectively. The value of $\eta_o = 0.5$ was determined by El-Samni. The resulting figure obtained by plotting Equation 7-68 is shown in Figure 7-5.

Figure 7-5 is utilized to compute bed load discharge. From the given characteristics of bed sediment and flow conditions the value of $\psi_*$ can be computed and the corresponding value of $\phi_*$ can be found from Figure 7-5. Then the bed load discharge per unit width for a given grain size $i_B q_{bw}$ can be determined from the known $\phi_*$ based on Equations 7-50 and 7-51. An example will be given when determination of the total bed material load is discussed.

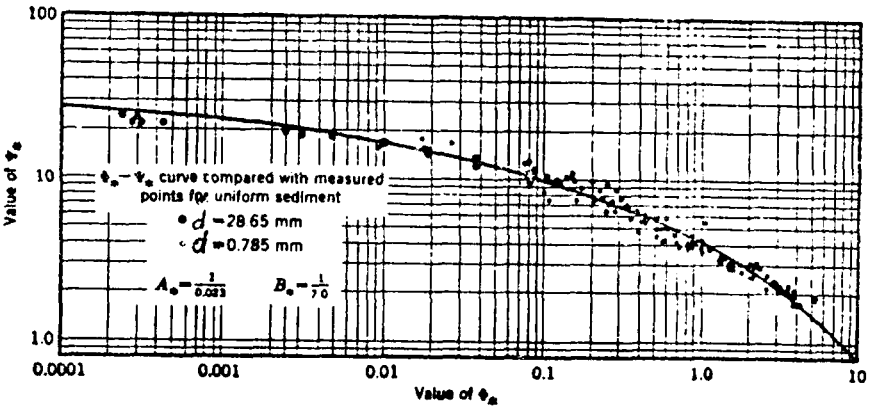


Figure 7-5. Einstein's $\phi_*$ - $\psi_*$ bedload function (after Einstein, 1950).

Equations Considering Bed Form Motion

In the lower flow regime when ripples and dunes cover the bed the ridges, owing to erosion of the upstream and deposition on the downstream slope, move downstream. If it is assumed that all the material moving as bed load is in continuous contact with the bed, the differential equation of bed load transport over ripple and/or dune beds is

$$\frac{\partial z}{\partial t} + \frac{1}{1-\lambda}\frac{\partial q_{bv}}{\partial x} = 0 \qquad (7\text{-}69)$$

in which $z$ is the elevation of the sand bed above a horizontal datum, $q_{bv}$ is the volume rate of bed load transport per unit width, $\lambda$ is the porosity of sand bed, and $x$ is distance in the direction of flow (Simons, 1965).

Using the transformation

$$\delta = x - U_s t \qquad (7\text{-}70)$$

where $U_s$ is the velocity of the sand wave in the direction of flow as shown in Figure 7-6 and assuming that $U_s$ and $q_{bv}$ variations are independent of time.

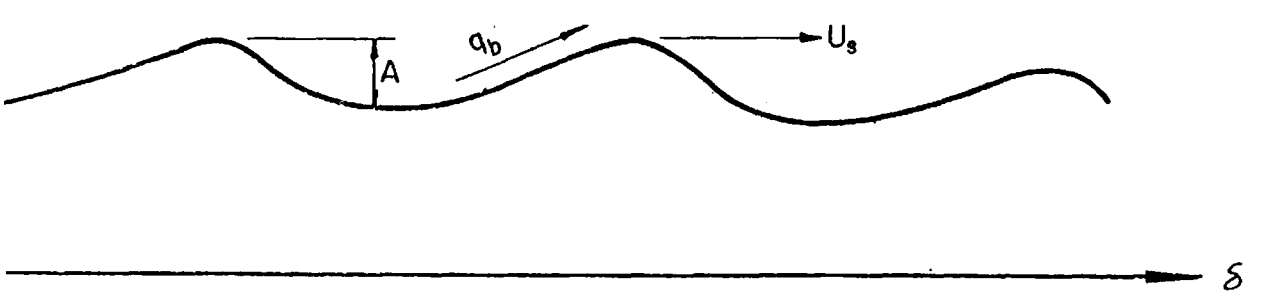


Figure 7-6. Sketch of bed load transport.

Then

$$\frac{\partial z}{\partial t} = \frac{\partial z}{\partial \delta}\frac{\partial \delta}{\partial t} = -U_s \frac{dz}{d\delta} \tag{7-71}$$

and

$$\frac{\partial q_{bv}}{\partial x} = \frac{\partial q_{bv}}{\partial \delta}\frac{\partial \delta}{\partial x} = \frac{dq_{bv}}{d\delta} \tag{7-72}$$

Substituting Equations 7-71 and 7-72 into Equation 7-69 yields

$$-U_s \frac{dz}{d\delta} + \frac{1}{1-\lambda} \frac{dq_{bv}}{d\delta} = 0 \tag{7-73}$$

Integrating Equation 7-73 gives

$$q_{bv} = (1-\lambda)\, U_s z + K \tag{7-74}$$

Noting that $K = 0$ because of boundary conditions and assuming that dunes and ripples have triangular shapes

$$q_{bv} = (1-\lambda)\, U_s \frac{A}{2} \tag{7-75}$$

where $A$ is the average amplitude of sand waves.

The differential equation of bed load transport Equation 7-69 was suggested by Exner (1925) and used by Simons et al. (1965) to develop the bed load equation (Equation 7-75). Simons (1967) mentions that with more sophisticated sonic equipment for measuring geometry and rate of movement of sand waves, the theory as given by Equation 7-75 provides an excellent method of determining the rate of bedload movement in rivers as well as a means of analytically defining bed-load discharge. Greater use could be made of this method to better understand sediment discharge and its importance to river hydraulics, behavior, and control.

Bed Load Equations Derived from Stochastic Models

Einstein (1937) developed the first stochastic model to describe the motion of a sediment particle that moves along the bed in a series of alternating transport and rest periods. His model has been modified by a number of researchers and similar models developed independently aid in understanding bed sediment motion. Shen (1971) has given a brief discussion of the works of Hubbell and Sayre (1964), Sayre and Hubbell (1965), Sayre and Conover (1967), Yang (1968), Grigg (1969), and Shen and Todorovic (1971).

Comparison of Bed Load Equations

Laursen (1956) reduced several well-known bed load equations into the following forms (Table 7-1).

Table 7-1. Original and reduced forms of bed load equations.

| Reporter | Original Form | Reduced Form | |
|---|---|---|---|
| DuBoys (1879) | $q_{bw} = A_1 \tau_o(\tau_o - \tau_c)$ | $= B_1 n^4 \frac{U^4}{d^{2/3}}$ | (7-76) |
| U.S. Waterways Expt. Station (1935) | $q_{bw} = \frac{A_5}{n}(\tau_o - \tau_c)^m$ | $= B_5 n^{2m-1} \frac{U^{2m}}{d^{m/3}}$ | (7-77) |
| Shields (1936) | $q_{bw} = \frac{A_6}{D_s} q S(\tau_o - \tau_c)$ | $= B_6 \frac{n^4}{D_s} \frac{U^5}{d^{2/3}}$ | (7-78) |
| Schoklitsch (1934) | $q_{bw} = \frac{A_2}{D_s^{1/2}} S^{3/2}(q - q_c)$ | $= B_2 \frac{n^3}{D_s^{1/2}} \frac{U^4}{d}$ | (7-79) |
| Meyer-Peter et al. (1934) | $q_{bw} = (A_3 q^{2/3} S - A_4 D)^{3/2}$ | $= B_3 n^3 \frac{U^4}{d}$ | (7-80) |
| Brown-Einstein (1950) | $q_{bw} = \frac{A_7}{D_s^{3/2}} \tau^3$ | $= B_7 \frac{n^3}{D_s^{3/2}} \frac{U^6}{d}$ | (7-81) |

In the above equations $A_1$ through $A_8$ and $B_1$ through $B_8$ are constants and $n$ is the Manning's roughness coefficient. Examining the reduced forms we can write the bed load equations in the general form

$$q_{bw} = K U^r d^s \tag{7-82}$$

where $K$ is an empirical coefficient that is a function of the characteristics of channel and bed sediment, and the exponents $r > 0$ and $s < 0$.

Conclusion

The goal of bedload equations is to predict the amount of bed load transport in a natural channel. With limited knowledge predicting the amount accurately is an extremely difficult task. Most bedload equations were derived from laboratory flumes and none have been thoroughly tested with field data due to the lack of sufficient field data, the cost, and measuring difficulty. Therefore, there is no way to determine the accuracy of applying the bedload equations presented here to large rivers. In other words, a bedload equation must be selected based on the investigator's experience usually without actual bed load measurements to verify it.

Suspended Load

Part of the sediment transported by the flow in streams is suspended in the flow. The weight of these sediment particles is continuously supported by fluid. Turbulence is the most important factor in suspension of sediment. Due to the particle weight there is

settling that is counter-balanced by irregular motion of the fluid particles introduced through turbulent velocity components.

Most earlier studies concerned with suspension of sediment are unacceptable when considered in relation to the present knowledge of fluid motion. Generally acceptable aspects of suspended sediment transport will be discussed in subsequent sections.

General Considerations

The suspended load discharge per unit width of channel $q_s$ for two-dimensional flow is given by the relations

$$q_{sv} = \int_a^d \bar{u}\,\bar{C}\,dy \tag{7-83a}$$

and

$$q_{sw} = \gamma_s \int_a^d \bar{u}\,\bar{C}\,dy \tag{7-83b}$$

where $\bar{u}$ and $\bar{C}$ are the time-averaged flow velocity and concentration, respectively, at distance $y$ above the bed and $a$ is the bed layer thickness. In Equation 7-83a $C$ is the sediment concentration by volume and $q_{sv}$ is calculated as the volume of sediment per unit time and width. Whereas in Equation 7-83b $q_{sw}$ is in weight per unit time and width. The discharge of sediment for the entire stream cross section $Q_s$ is obtained by integrating Equation 7-83 over the cross section. Then

$$Q_{sv} = Q\,\bar{C} \tag{7-84a}$$

and

$$Q_{sw} = \gamma_s\,Q\,\bar{C} \tag{7-84b}$$

where $\bar{C}$ is the average suspended sediment concentration by volume.

To integrate Equation 7-83 $u$ and $C$ must be expressed as a function of $y$. Turbulent velocity distribution over a movable bed is affected by sediment concentration. It will be seen later that the distribution of sediment concentration is also closely related to turbulent velocity. In other words, distributions of these two variables are closely interrelated. To apply the turbulent theory to the determination of sediment concentration either the turbulent velocity distribution in clear water is assumed or some correction factors are applied to the velocity distribution to account for interaction.

It should be pointed out that only that part of suspended load composed of bed-material load can be evaluated by applying sediment transport theory, since the wash load transport is determined by the available upslope supply rate. Thus, the relationships derived in the following sections for determining sediment concentration and suspended load are restricted to bed material load.

## Suspended Sediment Movement Under Equilibrium Conditions

Exchange Theory. Due to turbulent velocity fluctuations there is a continuous exchange of sediment particles across any arbitrary layer in the flow. In steady two-dimensional flow if the sediment concentration is steady and uniform (in the direction of flow), the average concentration at any level will be constant and the net average sediment flow through a layer parallel to the bed will be zero. Consider a unit area parallel to and at a distance $y$ from the bed. The sediment is of uniform size and falling under the influence of gravity at fall velocity $w$ so the average rate of settling through the unit area is

$$q_D = wC \tag{7-85}$$

where $C$ is the time-averaged concentration at $y$. To maintain an equilibrium profile, the quantity of sediment settling must be balanced by the upward sediment flow due to diffusion. Then combining Equation 7-85 with

$$g_1 = -\varepsilon_s \overline{\frac{dc}{dy}}$$

gives

$$wC + \varepsilon_s \frac{dC}{dy} = 0 \tag{7-86}$$

Integrating Equation 7-86 yields

$$C = C_a \exp(-w \int_a^y \frac{dy}{\varepsilon_s}) \tag{7-87}$$

where $C_a$ is a concentration of sediment with fall velocity $w$ at level $y = a$ above the bed. This equation is the O'Brien-Christiansen (1933) expression for the vertical distribution of suspended sediment.

The equation states that concentration is greatest at the bottom and smallest at the water surface. In order to determine the value of $C$ at a given $y$, $C_a$ and the variation of $\varepsilon_s$ with $y$ must be known.

For a two-dimensional steady uniform flow in an open channel $\tau$ at distance $y$ above the bed can be expressed as

$$\tau = \gamma S(d - y) = \tau_o(1 - \frac{y}{d}) \tag{7-88}$$

If the velocity distribution $u(y)$ is known, $\varepsilon_s$ can be expressed as a function of $y$ by means of Equations 7-84 and 7-88, and the Equation 7-87 can be solved for $C$.

Velocity distribution used with the sediment distribution relation may be a measured or calculated distribution. A convenient expression for $u$ is the well-known Prandtl-von Kármán velocity relation

$$\tau = \rho\kappa^2 y^2 (\frac{du}{dy})^2 \tag{7-89}$$

or

$$\frac{du}{dy} = \frac{U_*}{\kappa y}$$

From Equations 7-83, 7-88, and 7-89, it follows that

$$\varepsilon_m = \kappa U_* \frac{y}{d}(d - y) \tag{7-90}$$

and from Equation 7-84

$$\varepsilon_s = \beta \kappa U_* \frac{y}{d}(d - y) \tag{7-91}$$

Equations 7-90 and 7-91 indicate that $\varepsilon_m$ and $\varepsilon_s$ equal zero at the surface and bed, and attain maximum values at mid-depth. Substituting Equation 7-91 into Equation 7-86 (assuming a linear distribution for shear), Equation 7-88 and integrating yields

$$\frac{C}{C_a} = \left[\frac{d - y}{y} \frac{a}{d - a}\right]^{z_1} \tag{7-92}$$

where

$$z_1 = \frac{w}{\beta \kappa U_*} \tag{7-93}$$

Equation 7-92 known as the suspended sediment distribution equation was presented by Rouse (1937).

Figure 7-7 shows a family of curves obtained by plotting Equation 7-92 for different values of the exponent $z_1$. For low values of $z_1$ the sediment distribution is nearly uniform whereas for large $z_1$ values little sediment is found near the water surface. The particle size, specific gravity, and shape expressed as a fall velocity $w$ is directly related to this distribution of suspended sediment.

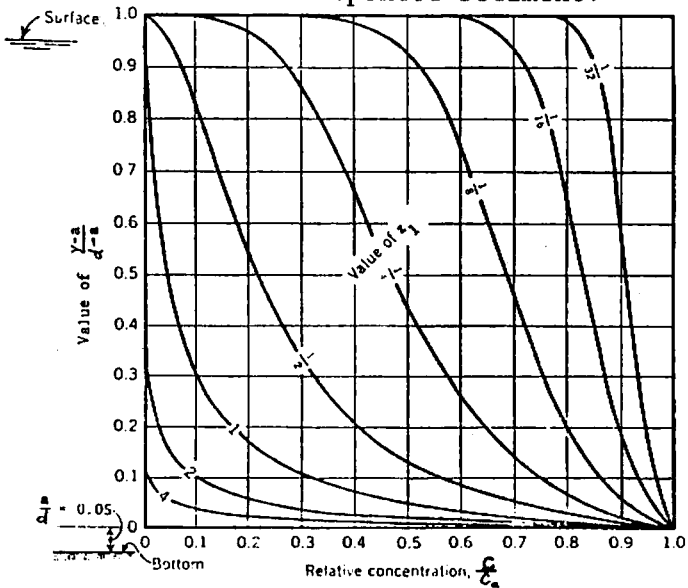


Figure 7-7. Graph of suspended load distribution equation for a/D=0.05 and several values of $z_1$ (after Vanoni, 1941)..

Einstein's Approach

One of the most widely recognized methods used to compute suspended sediment load is the one proposed by Einstein (1950). Assuming $\beta = 1$ and $\kappa = 0.4$ (for clear water) and replacing $U_*$ with $U_*'$ the shear velocity due to grain roughness (as explained before, see Equation 7-54) in Equation 7-92 the expression for $z_1$ can be reduced to

$$z_1 = z = \frac{w}{0.4\ U_*'} \tag{7-94}$$

Again recall Equation 7-83b

$$q_{sw} = \gamma_s \int_a^d \bar{u}\ \bar{C}\ dy$$

where $\bar{C}$ is the sediment concentration by volume of mixture. Expressing $C$ by weight, substituting the concentration distribution Equation 7-92 into Equation 7-83b, and expressing the velocity with the logarithmic velocity distribution relation (Equation 7-54), yields

$$q_{sw} = \int_a^d C_a \left(\frac{d-y}{y}\frac{a}{d-a}\right)^z\ 5.75\ U_*' \log\left(\frac{30.2y}{\Delta}\right)dy \tag{7-95}$$

where $\Delta$ is a correction factor, given in Figure 7-2. Replacing $a$ by the dimensionless ratio $E = a/d$, and using $d$ to normalize $y$ yields the relation

$$q_{sw} = \int_E^1 u\ C\ d\ dy'$$

$$= U_*' C_a \left(\frac{E}{1-E}\right)^z d5.75 \int_E^1 \left(\frac{1-y}{y}\right)^z \log\left(\frac{30.2y}{\Delta/d}\right) dy$$

$$= 5.75\ C_a U_*' d\left(\frac{E}{1-E}\right)^z \left[\log\left(\frac{30.2d}{\Delta}\right) \int_E^1 \left(\frac{1-y}{y}\right)^z dy \right. \tag{7-96}$$

$$\left. + 0.434 \int_E^1 \left(\frac{1-y}{y}\right)^z \ln y\ dy\right]$$

Since it was not possible to integrate this equation Einstein rewrote Equation 7-96 as

$$q_{sw} = 11.6\ U_*' C_a\ a\left[2.303 \log\left(\frac{30.2d}{\Delta}\right) \cdot I_1 + I_2\right] \tag{7-97}$$

and numerically integrated the terms $I_1$, and $I_2$ for various $E$ and $z$ values where

$$I_1 = 0.216 \frac{E^{z-1}}{(1-E)^z} \int_E^1 \left(\frac{1-y}{y}\right)^z dy$$

and (7-98)

$$I_2 = 0.216 \frac{E^{z-1}}{(1-E)^z} \int_E^1 \left(\frac{1-y}{y}\right)^z \ln y \, dy$$

The values of $I_1$ and $I_2$ in terms of E for values of z can be obtained from Figures 7-8 and 7-9.

Einstein (1950) assumed that the bed layer thickness is a = 2D and within this layer the suspension of material is impossible. However, this bed material is the source of the suspended load and the lower limit of the reference concentration $C_a$.

From bedload theory the bedload rate at which the given size D moves through unit width of channel cross section is $i_{Bw}q_{bw}$. Assuming the average velocity of bed load is $u_B$, the weight of particles of a given size per unit area is $i_{Bw}q_{bw}/u_B$ and the average concentration in the layer is $i_{Bw}q_{bw}/(u_B a)$. Then the assumption is made that the concentration in the bed layer is constant because the layer is only two diameters thick. However, a correction factor $A_5$ is utilized

$$C_a = \frac{A_5 i_B q_B}{a\, u_B} \tag{7-99}$$

The velocity $u_B$ is unknown. By setting $u_B \propto U_*'$ Einstein (1950) using experimental results established that $A_5 = 1/11.6$ and substituting this value in Equation 7-99 obtained

$$C_a = \frac{1}{11.6} \frac{i_{Bw}q_{bw}}{a\, U_*'} \tag{7-100}$$

The equation for suspended load discharge for each fraction $i_{ss}q_{sw}$, is derived from Equations 7-97 and 7-100 i.e.,

$$i_{sw}q_{sw} = i_{Bw}q_{bw}\left[2.303 \log\left(\frac{30.2d}{\Delta}\right) I_1 + I_2\right] \tag{7-101a}$$

$$= i_{Bw}q_{bw}[P_E I_1 + I_2]$$

where

$$P_E = 2.303 \log \frac{30.2d}{\Delta} \tag{7-102}$$

This equation relates bedload transport to suspended-load transport for all size fractions for which the bed-load function exists.

Equation 7-101a is dimensionally homogeneous and may be solved using any consistent system of units. The units of $q_s$ are weight per unit time and width.

Total Load

As defined earlier the total load is the sum of bedload and suspended load or the sum of bed material load and wash load. At low

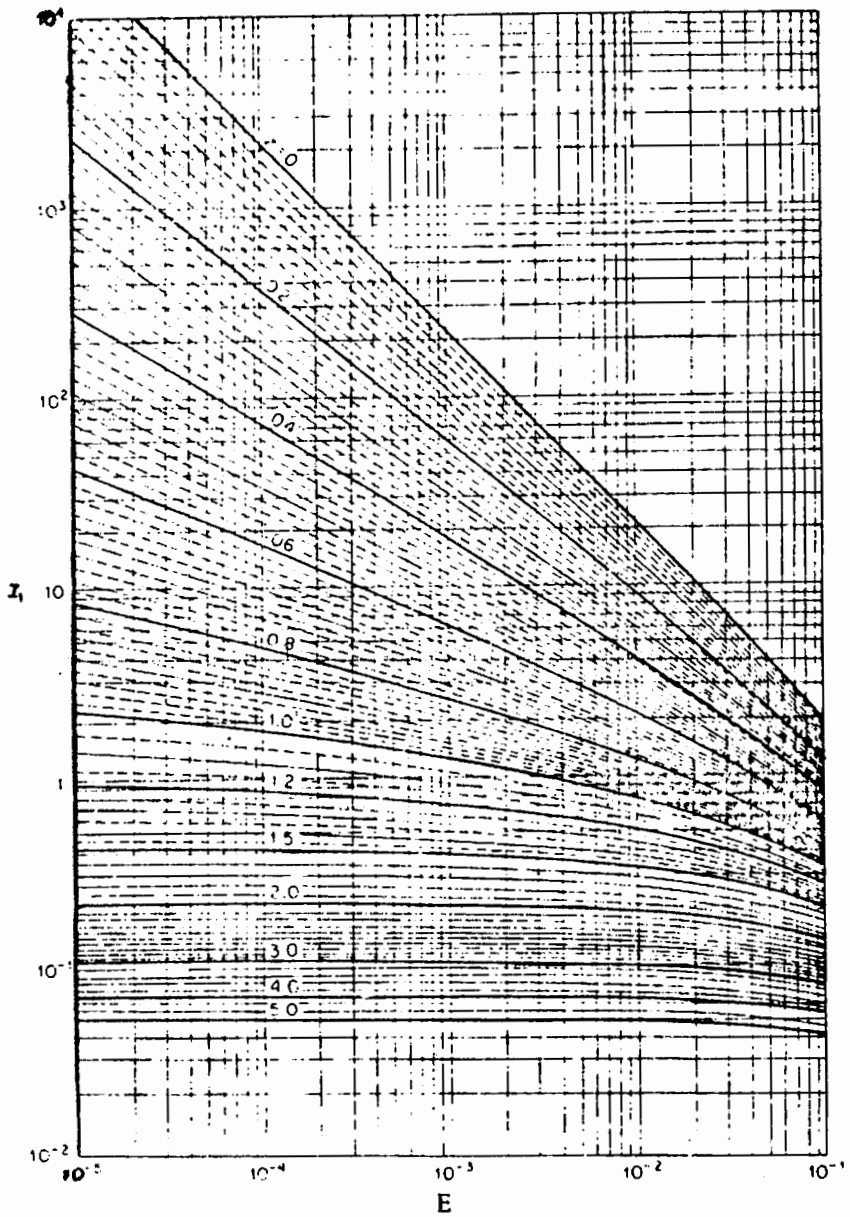


Figure 7-8. Function $I_1$ in terms of E for values of z (after Einstein, 1950).

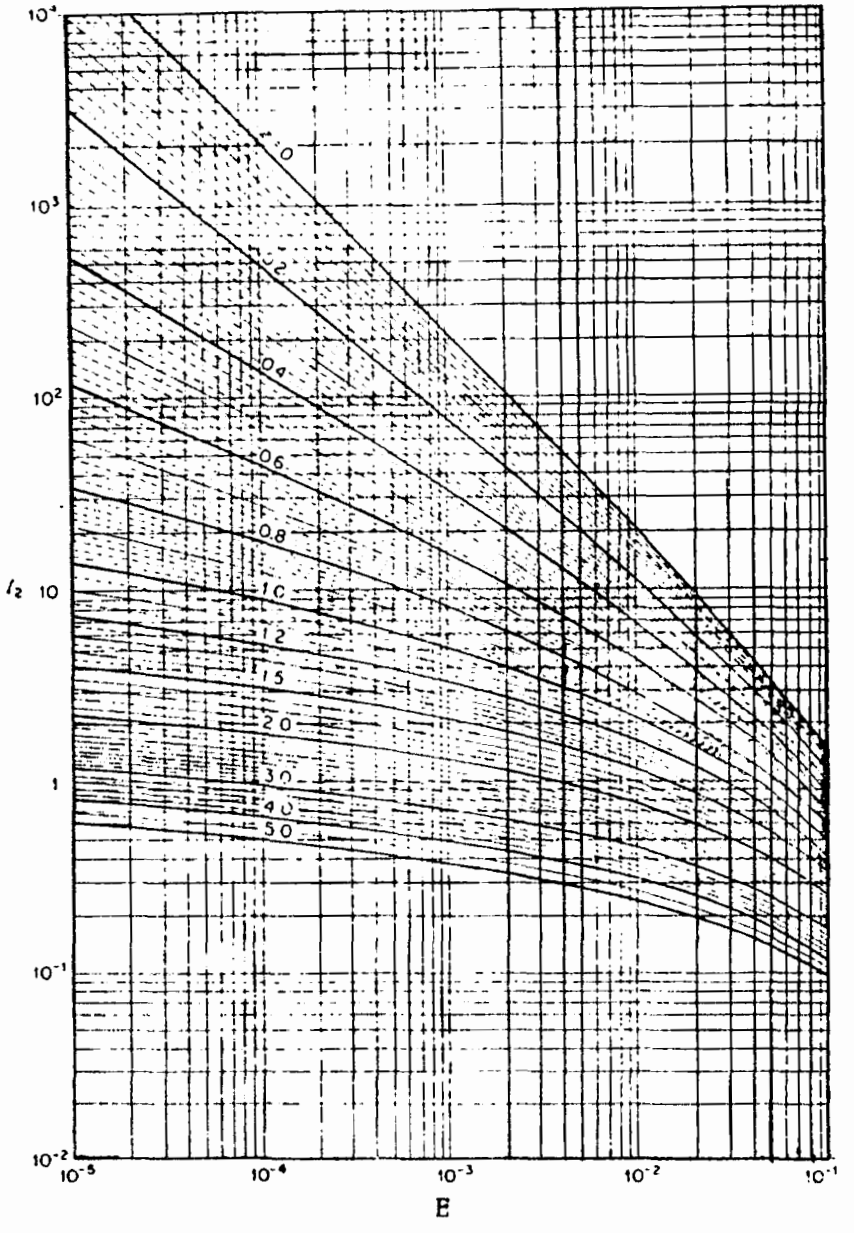


Figure 7-9. Function $I_2$ in terms of E for values of Z (after Einstein, 1950).

transport rates where most of the sediment moves in contact with the bed or in shallow flow, the bed load may approximate the total load. Conversely, in a deep river such as the Mississippi bedload may only total 10-20% of the total load.

In research work bed material load and wash load in a uniform flow is normally dealt with separately because the wash load is determined by available upslope supply rate and cannot be predicted by the transport capacity of the stream. Thus, only the bed material load that is made up of those solid particles consisting of grain sizes represented in the bed can be predicted by summing up the bedload and the suspended load. Note that this suspended load does not include the wash load.

Besides the indirect determination of bed material load by the addition of two fractions, the bed material load can be estimated by other methods.

Indirect Determinations of Bed Material Load

The indirect approach of determining the bed material load by summing up bedload and suspended load was initiated by Einstein (1950). As previously mentioned there is no sharp line dividing bedload and suspended load. However, at least two points warrant this division: 1) the differences in forms of transport requires two physically different models, and 2) the two loads are measured by different methods. The bed load is measured using suitable traps placed on or in the bed and the suspended load is measured by sampling the water-sediment mixture.

Einstein's Bed Load Function. The bed load function is defined by Einstein as a function that estimates the rate at which flow of any magnitude in a given channel will transport the individual sediment sizes of which the channel bed is composed. Following Einstein's definitions and concepts, bed load for a bed material that is of size D is

$$i_{Bw}q_{bw}$$

Suspended bed material load is

$$i_{sw}q_{sw}$$

and bed material load is the sum of suspended and bed material loads. More specifically

$$i_T q_T = i_{Bw} + i_{sw}q_{sw} \tag{7-103}$$

where $i_T$, $i_{bw}$, and $i_{sw}$ are specific percentages of suspended, bed and total loads for the given bed material size D. Utilizing Equations 7-101b(*) and 7-103

$$i_T q_T = i_{Bw}q_{bw}(1 + P_E I_1 + I_2) \tag{7-104}$$

(*) $$i_{sw}q_{sw} = \frac{0.4}{\kappa} i_{Bw}q_{bw}(P_E I_1 + I_2) \tag{7-101b}$$

where $P_E$ is a transport parameter, and $I_1$ and $I_2$ are integrals defined by Equation 7-98 and evaluated in Figures 7-8 and 7-9. Bed load discharge $i_{Bw}q_{bw}$ can be obtained from the $\phi_*$ compared with $\psi_*$ relation given in Figure 7-5. The relations for evaluating bed load and suspended load to establish Einstein's bed load function (Equation 7-104) have been extensively discussed in previous sections. The quantity $q_T$ is expressed as a dry weight per unit time and width. Equation 7-104 is dimensionally homogeneous and any consistent system of units may be used.

Application of Einstein's bed load function is complicated and laborious for practical use. In the original paper, Einstein (1950) gave a detailed sample calculation. An example will be presented later. Einstein's method represents one of the most detailed and comprehensive treatment of bed material transport from a fluid mechanics view point that is currently available.

Direct Determinations of Bed Material Discharge

In general researchers believe that bed material load is the summation of fractional loads. Despite this fact a group of investigators feel there is no need to distinguish bed load from suspended load, since the hydraulic forces involved are the same for both types of transport and thickness of bed layer or proper dmarcation between the bed load and suspended load is difficult to define. Also, direct approaches have some advantage over indirect approaches because of simpler application procedures especially for those relationships based upon available data. This procedure eliminates questionable assumptions involved in rational approaches. Furthermore, an empirical relationship between sediment rate and flow is relatively easy to apply and can provide the design engineer with an estimation that is of the correct order of magnitude. This is assuming the problem in question falls within the range of conditions used to establish the empirical relations.

In developing an empirical relationship, important variables such as the flow rate of water, the depth or hydraulic radius, the energy slope, and the properties of fluid and sediment must first be selected. Whether or not all these factors must be included in the analysis is subject to interpretation. In the analysis relative sensitivities of variables should be considered. For example, there is a general rule that sediment transport increases with flow velocity to the fourth power at low flow discharges and to the eighth power at high flow discharges (Shen, 1971). It is unlikely, therefore, that a simple relationship could be developed for all flow conditions. Recognizing this fact Colby (1964) developed different sediment discharge relationships with flow 0.1-ft, 1-ft, 10-ft, and 100-ft flow depths. Shen and Hung (1971) constructed a sediment-transport parameter and determined the sediment concentration as a function of Colby's parameter. Subsequently, Colby's and Shen and Hung's procedure will be discussed in more detail.

Colby's Approach. After investigating the effect of mean flow velocity, shear, shear velocity computed from mean velocity, stream power of flow, flow depth, viscosity, water temperature, and concentration of fine sediment on the bed material discharge per foot of channel

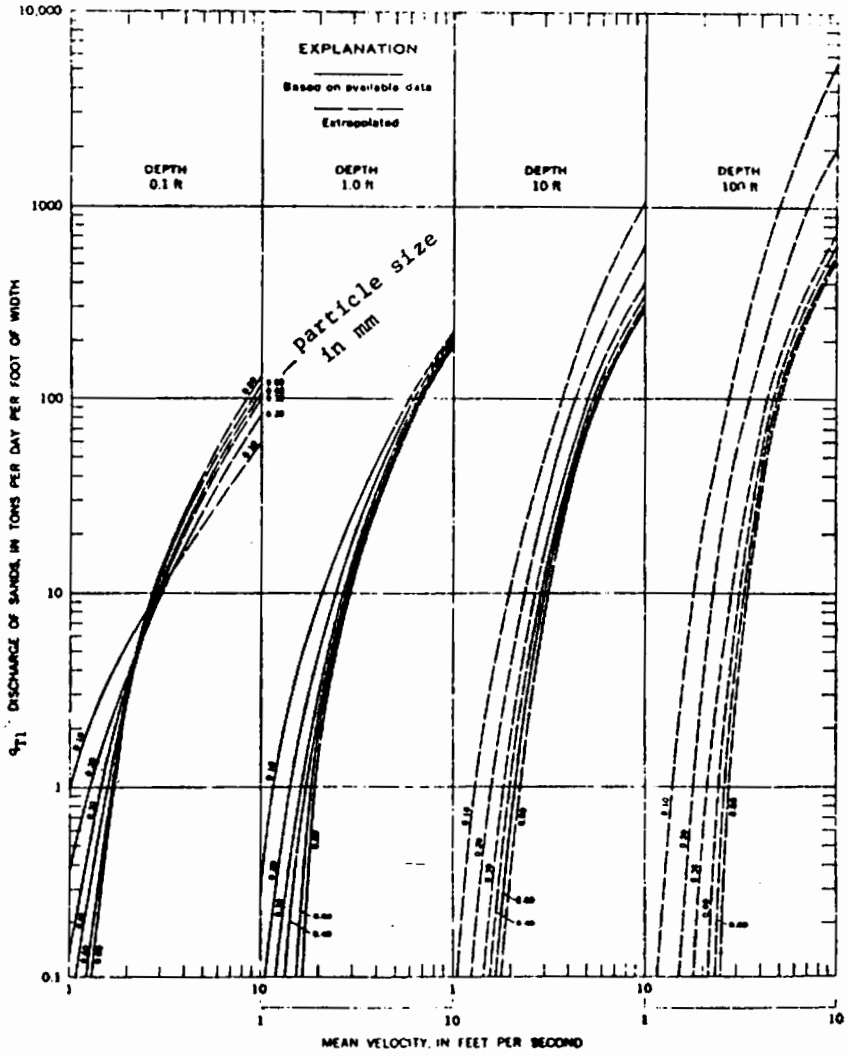


Figure 7-10. Relationship of discharge of sands to mean velocity for six median sizes of bed sands, four depths of flow, and a water temperature of 60°F (after Colby, 1964).

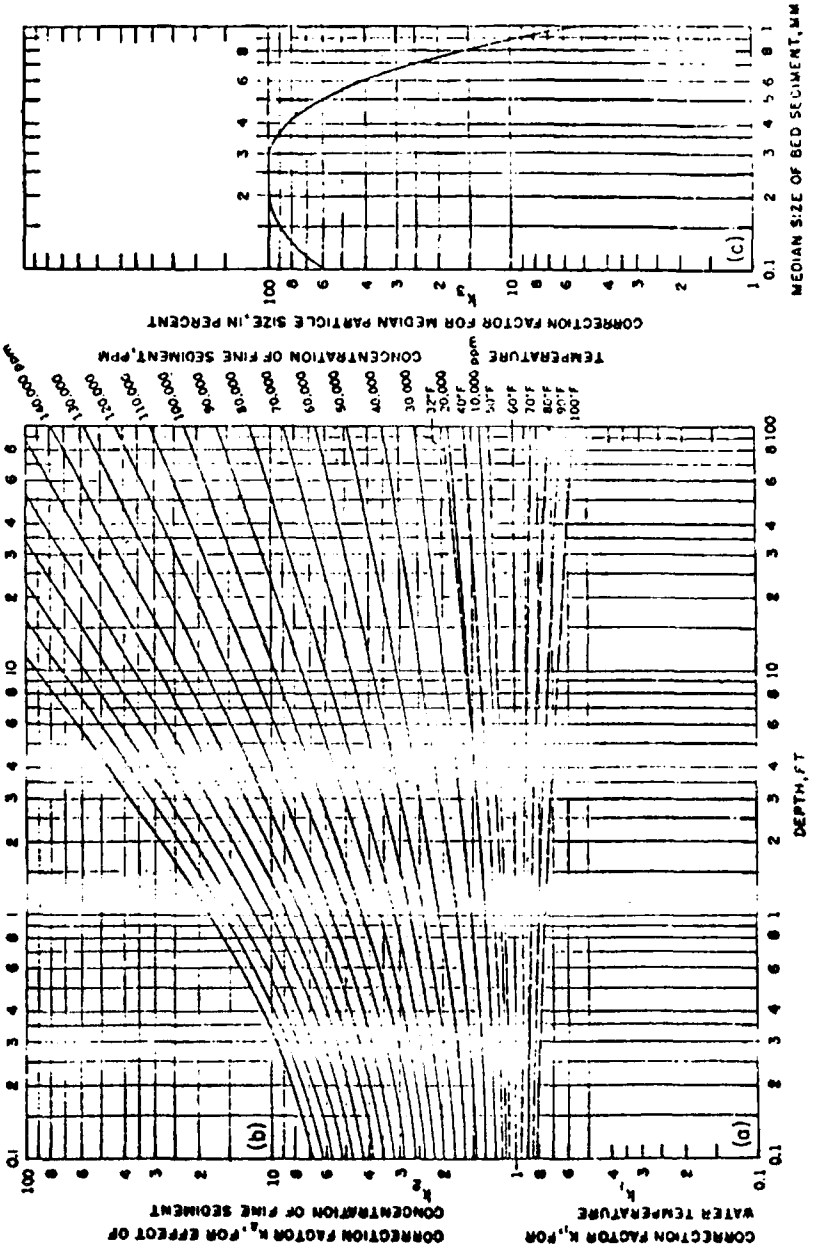


Figure 7-11. Approximate effect of water temperature and concentration of fine sediment on the relationship of discharge of sands to mean velocity (after Colby, 1964).

width, Colby (1964) developed four graphical relations shown in Figures 7-10 and 7-11 for determining the bed material discharge. In developing his computational curves Colby was guided by Einstein's bedload function (Einstein, 1950) and an immense amount of data from streams and flumes (Simons and Richardson, 1966). However, it should be understood that all curves for the 100 ft depth, most curves of 10 ft depth, and part of the curves of 1.0 ft and 0.1 ft (Figure 7-10), are not based entirely on data but are developed from limited data and theory.

In utilizing Figures 7-10 and 7-11 to compute the bed material discharge the following procedure is proposed: 1) the required data are mean velocity U, depth d, median size of bed material $D_{50}$, water temperature T, and fine sediment concentration $C_f$ and 2) uncorrected sediment discharge $q_{Ti}$ for the given U, d, and $D_{50}$ can be found from Figure 7-10 by first reading $q_{Ti}$ knowing U and $D_{50}$ for the two depths that brackets the desired depth. Then a logarithmic scale of depth versus $q_{Ti}$, is used to intepolate in order to determine the bed-material discharge per unit width for the actual d, U, and $D_{50}$; 3) two correction factors $k_1$ and $k_2$ shown in Figure 7-11a and 7-11b, respectively, account for the effect of water temperature and fine suspended sediment on the bedmaterial discharge. If the bed material size falls outside the 0.2 to 0.3 mm range, factor $k_3$ from Figure 7.11c is applied to correct for sediment size effect. True sediment discharge $q_T$ corrected for water temperature effect, presence of fine suspended sediment, and sediment size is given by

$$q_T = [1 + (k_1 k_2 - 1)\ 0.01\ k_3]\ q_{Ti} \qquad (7\text{-}105)$$

As Figure 7-5 shows, $k_1 = 1$ when the temperature is 60°F, $k_2 = 1$ when the concentration of fine sediment is negligible, and $k_3 = 1$ when $D_{50}$ lies between 0.2 mm and 0.3 mm.

In spite of many inaccuracies in the available data and uncertainties in the graphs, Colby found

> "...about 75 percent of the sand discharges that were used to define the relationships were less than twice or more than half of the discharges that were computed from the graphs of average relationship. The agreement of computed and observed discharges of sands for sediment stations whose records were not used to define the graphs seemed to be about as good as that for stations whose records were used."

Bishop Approach. This approach alters Einstein's (1950) $\phi_*$ compared with $\psi_*$ relationship so that it predicts bed material discharge.

In the Einstein procedure intensity of bed load transport is given by

$$\phi = \frac{q_{bw}}{v\gamma_s}\sqrt{\frac{\rho v^2}{\gamma_s'}\ \frac{1}{gD^3}} \qquad 7\text{-}47$$

and intensity of shear on a particle is given by

$$\psi = \frac{\rho_s - \rho}{\rho} \frac{D}{R_b' S} \qquad 7\text{-}60$$

In an abbreviated form Einstein's bed-load equation can be written as

$$\phi_* = f(\psi_*) \qquad (7\text{-}106)$$

where $\phi_* = (i_B/i_b)\,\phi$ and $\psi_* = \xi Y(\beta/\beta_x)^2\psi$. All symbols have been defined previously. The functional relation of Equation 7-106 is given by Figure 7-5 which permits calculation of bedload discharge $q_{bw}$.

Bishop, Simons and Richardson (1965) reasoned that the shear intensity parameter $\psi$ may be used to directly predict intensity of transport for bed material discharge $\phi_T$ given by

$$\phi_T = \frac{q_T}{\gamma_s} \sqrt{\frac{\rho}{\rho_s - \rho} \frac{1}{gD_{50}^3}} \qquad (7\text{-}107)$$

in which $q_T$ is the bed material discharge. Based on flume data for four different sands a functional relationship

$$\phi_T = f(\psi') \qquad (7\text{-}108)$$

was established and is shown in Figure 7-12 in which the shear intensity factor is

$$\psi' = \frac{\rho_s - \rho}{\rho} \frac{D_{35}}{R_b' S} \qquad (7\text{-}109)$$

Although the curves for each bed material size exhibit the same general trend, they differ by a considerable degree. These curves may be generally divided into three segments representing 1) the lower limb, 2) the segment of inflection, and 3) the upper limb except for 0.93 mm sand for which upper regime data were not available. The three segments correspond exactly with the lower flow regime (ripples and/or dunes), transition (bed configurations ranging from dunes to plane bed or antidunes), and upper flow regime (bed configurations including plane bed, standing waves, and antidunes) based on experimental evidence. The lower limbs of the curves are similar in shape to Einstein's $\phi_* - \psi_*$ curve and therefore part of the theoretical probability curve represented by Equation 7-67 was made to fit the data by choosing different values of $A_*$ and $B_*$ for different sands. The relation of $A_*$ and $B_*$ to the median diameter of the sand is given in Figure 7-13 which shows that $A_*$ and $B_*$ are not constant as assumed by Einstein (1950) but are a function of grain size. Data in the second and third segment of the curves cannot be predicted with Einstein's relation because in these regions the larger part of the bed material is transported in suspension.

To compute the bed material discharge for streams using this procedure the $\psi'$ value is calculated from available basic data and a corresponding value of $\phi_T$ is selected from Figure 7-12 by interpolation. The bed material discharge is then given by

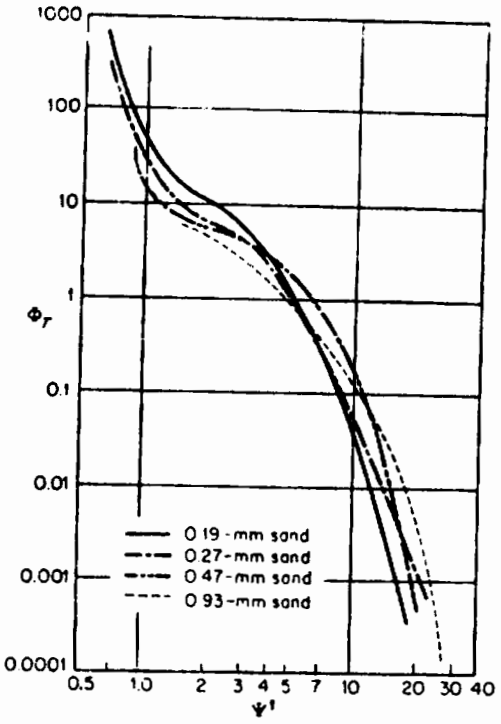


Figure 7-12. $\phi_T$ vs $\psi'$ relation for different sand sizes (after Bishop et al., 1965).

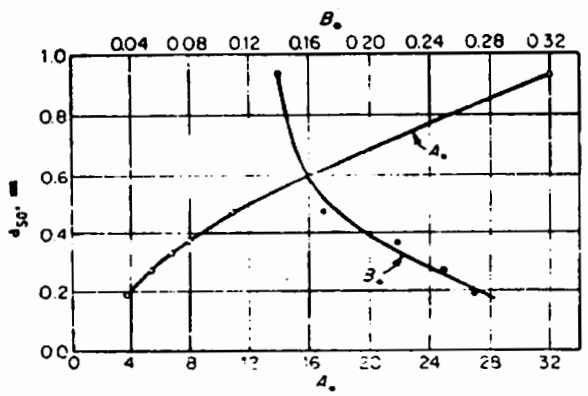


Figure 7-13. Scale constants $A_*$ and $B_*$ vs $D_{50}$ (after Bishop et al., 1965).

$$q_T = \phi_T \gamma_s \sqrt{\frac{\rho_s - \rho}{\rho} g D_{50}^3} \qquad (7\text{-}110)$$

where $q_T$ is the dry weight of sediment per unit time and width. Bed material transport computed by Equation 7-110 showed good agreement when compared with observed bed material discharges for streams such as the Rio Grande, Niobrara, Loup, and Colorado Rivers.

Calculation of Sediment Discharge from Stream Measurements

Normal measurements made on many streams include discharge measurements as well as suspended load measurements. Discharge measurements consist of determining depth and mean velocity at of selected verticals from which the total discharge Q and the cross sectional area A for the channel cross section may be calculated. Suspended load samples give the mean measured sediment concentration $C_s'$ at each or at least several of the verticals in which mean velocity is measured. Concentration $C_s'$ includes sediment of all grain sizes, wash load, and bed material load and is defined by

$$C_s' \int_{a'}^{d} udy = \int_{a'}^{d} Cudy \qquad (7\text{-}111)$$

where a' is the distance from the streambed to the sampler inlet tube. The region of cross section below a' forms what is referred to as the unsampled zone of the cross section. The part of the cross section above a' is called the sampled zone.

Suspended sediment measurements do not sample the sediment load in the unsampled zone that may include bedload and part of the suspended load. The modified Einstein procedure developed by Colby and Hembree (1955), the Colby method (1957), and the yet to be described Toffaleti method (1969) are methods for estimating the total sediment discharge once suspended load samples and other required data have been acquired.

Modified Einstein Procedure. Colby and Hembree (1955) and subsequently others proposed a modified Einstein procedure to obtain the total sediment transport rate in a river. The term modified Einstein procedure usually gives the impression that it serves the same purpose as the Einstein's (1950) procedure. Actually these two procedures although based on similar principles serve entirely different purposes. Einstein's procedure used mainly for design purposes (as well other equations that predict the bed material discharge), estimates bed material discharges for different river discharges based on channel cross section and sediment bed samples in selected uniform flow river reaches. The modified Einstein procedure on the other hand, estimates total sediment discharge (including wash load) for a given water discharge from measured depth-integrated suspended sediment samples, streamflow measurements, bed material samples, and water temperature for specific discharge at the cross section.

Major differences between the modified Einstein procedure (1955) and original Einstein procedure (1950) include:

1. The modified calculation is based on a measured mean velocity rather than on a calculated velocity from the given slope and depth is observed in each vertical in which velocity is measured.

2. The suspended load exponent $z$ in Equation 7-95 is determined from the observed $z$ value for a dominant grain size. Values of $z$ for other grain sizes are derived from that of dominant size and are assumed to vary with the 0.7 power of their fall velocity.

3. A slight change in the hiding factor is introduced and will be discussed later.

4. The depth $d$ is used to replace the hydraulic radius.

5. The value of Einstein's intensity of bedload transport is arbitrarily divided by a factor of two to fit the observed transport data more closely. There is some criticism on this point.

Application of the modified Einstein procedure is outlined as follows. Data needed are stream discharge $Q$, mean velocity $U$, cross sectional area $A$, stream width $B$, mean value $d_v$ of the depths at verticals where suspended sediment samples were taken, measured sediment discharge concentration $C'_s$, size distribution of the measured load $i_s$, size distribution of bed material at the cross section $i_b$, and water temperature $T$.

The next step is to calculate the suspended load discharge in the various size fractions per unit width in the sampled zone of the cross section $q'_{si}$. Allowing $q'_s$ to denote the sediment discharge through the unit width of sample zone, then

$$q'_s = \sum_i q'_{si} = C'_s \gamma Q'/B \tag{7-112}$$

where $Q'$ is the water discharge in the sampled zone. The relation between $Q'$ and $Q$ is given by

$$\frac{Q'}{Q} = \frac{\int_{a'}^{d_v} u\,dy}{\int_{o}^{d_v} u\,dy} \tag{7-113}$$

The term $a'$ is the distance from the streambed to the sampler inlet tube when sampling as closely as possible to the streambed. The value of $a'$ depends on the type of sampler used and if weights are used to position the sampler. If the point velocity is in the form of Equation 7-114(*) then

(*) $\frac{wDs}{v}$ (7-114)

$$\frac{Q'}{Q} = (1 - E') - 2.3 \frac{E' \log E'}{P_m - 1} \tag{7-115}$$

where $E' = a'/d_v$, and

$$P_m \cong 2.3 \log \frac{30.2\ xd}{D_{65}} \tag{7-116}$$

in which the quantity $x$ is found from Figure 7-2 and

$$\frac{u}{U'_*} = 5.75 \log (12.27 \frac{R'}{k_s} x) \tag{7-117}$$

by trial and error with $d$ replacing $R$. From Equations 7-112 and 7-115

$$q'_{si} = i_s \gamma C'_s q[(1 - E') - 2.3 \frac{E' \log E'}{P_m - 1}] \tag{7-118}$$

Bed load for a given size fraction per unit width of channel $i_{Bw}q_{bw}$ is computed next. Intensity of shear on the particles $\psi$ is calculated from the following equations

$$\psi = \frac{(\frac{\gamma_s}{\gamma} - 1)D_{35}}{(SR')} \tag{7-119}$$

$$\psi = \frac{0.4(\frac{\gamma_s}{\gamma} - 1)D_i}{(SR')} \tag{7-120}$$

where $D_i$ is the geometric mean particle size and $(SR')$ has been evaluated from the preceding step. The larger $\psi$ value is used to find $\phi_*$ from Figure 7-5 where $\psi$ replaces $\psi_*$. Then from the definition of $\phi_*$ (Equation 7-51),

$$i_{Bw}q_{Bw} = \frac{1}{2} \phi_* i_b \gamma_s \sqrt{\frac{\gamma_s}{\gamma} - 1} \sqrt{gD_i^3} \tag{7-121}$$

The term $\phi_*$ is arbitrarily divided by a factor of two to fit the observed river data more closely.

The next step involves computing the suspended load exponent $z'_i$ by trial and error for each size fraction. If the quantity $q'_{si}$ can be expressed by

$$q'_{si} = \int_{a'}^{d_v} C_i u dy \tag{7-122}$$

then using a procedure similar to the one for deriving Equation 7-101

$$\frac{q'_{si}}{i_{Bw}q_{bw}} = \frac{I_1(E,z')}{J_1(E,z')} [P_m J_1(E', z') + J_2(E',z')] \tag{7-123}$$

where

$$J_1(E',z') = \int_{E'}^{1} \left(\frac{1-y}{y}\right)^{z'} dy,$$

$$J_2(E',z') = \int_{E'}^{1} \left(\frac{1-y}{y}\right)^{z'} \ln y \, dy$$

and $I_1(E,z') = 0.216 \frac{E^{z'-1}}{(1-E)^{z'}} J_1(E,z')$ which is the same definition of $I_1$ as given by Equation 7-98. For simplicity of symbols, I, J equals $I(E,z')$, $J(E,z')$ and I', J' equals $I(E',z')$, $J(E',z')$, respectively. Then Equation 7-123 becomes

$$\frac{Q'_{si}}{i_{Bw}Q_{bw}} = \frac{B\, q'_{si}}{B(i_{Bw}q_{Bw})} = \frac{I_1}{J_1}(P_m J'_1 + J'_2) \tag{7-124}$$

The values of $I_1$, $I_2$, $J_1$, and $J_2$ can be obtained from Figures 7-8, 7-9, 7-14, and 7-15, respectively. In Equation 7-124 the quantity $(Q_{si}/i_{Bw}q_{bw})$ for each size fraction is known. The value of $z'_i$ can then be found by trial and error such that Equation 7-124 is balanced. In this manner the $z'_i$ value for each size fraction can be determined. However, Colby and Hembree (1955) discovered that the value of $z'_i$ can be related to fall velocities of sediment by

$$\frac{z'_i}{z'_1} = \left(\frac{w_i}{w_1}\right)^{0.7} \tag{7-125}$$

where $z'_1$ is obtained by solving Equation 7-123 for dominant grain size, and $w_i$ is fall velocity of a sediment grain of size $D_i$.

Total sediment discharge through the cross section $Q_{Ti}$ for a size fraction is then compared with

$$Q_{Ti} = Q'_{si}\frac{P_m J_1 + J_2}{P_m J'_1 + J'_2} \tag{7-126}$$

for the ranges of fine particle sizes and the relation

$$Q_{Ti} = i_{Bw}Q_{bw}(P_m I_1 + I_2 + 1) \tag{7-127}$$

is utilized to evaluate the transport of coarse particle sizes. Units of $Q_{Ti}$ are dry weight per unit time and any consistent system of units may be used. Theoretically, either Equation 7-126 or 7-127 can be used throughout the range of particle sizes. Practically, Equation 7-126 is limited to ranges of particle sizes for which $Q'_s$ can be determined with fair accuracy. Also Equation 7-127 is limited to ranges of particle sizes for which $i_B$ can be determined with reasonable accuracy. Another practical limitation on choice of equations is that a given

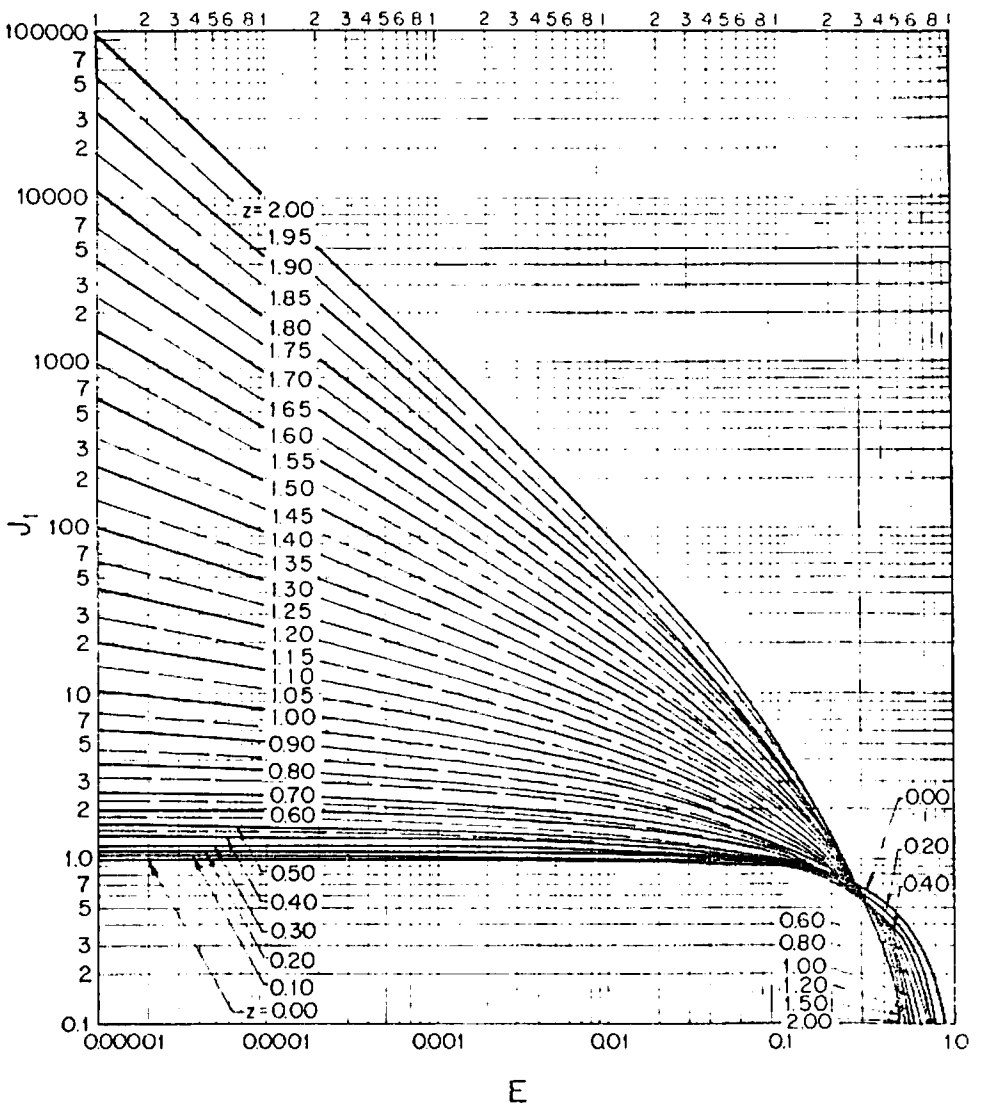


Figure 7-14. Integral $J_1$ in terms of E and z' (after Colby and Hembree, 1955).

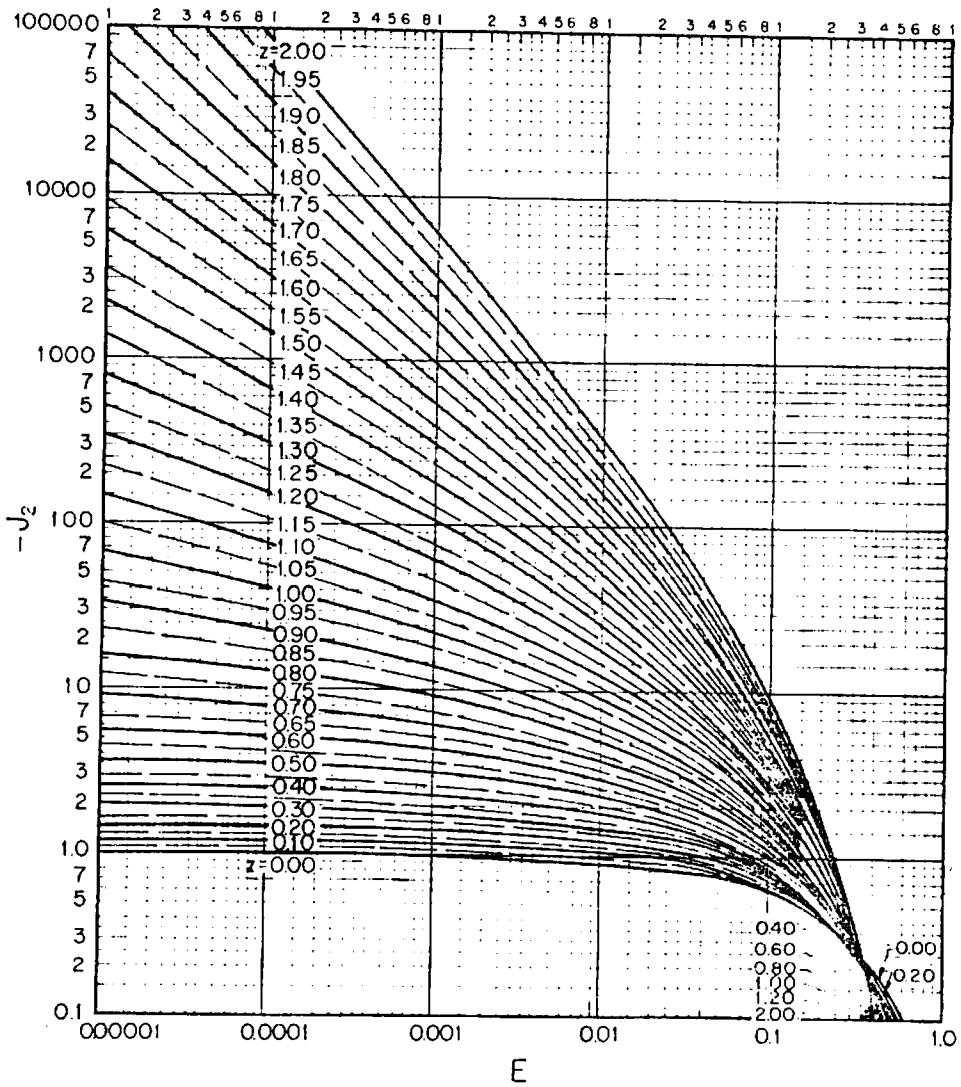


Figure 7-15. Integral $J_2$ in terms of E and z' (after Colby and Hembree, 1955).

percentage of variation in $z'$ changes computed sediment discharges more by Equation 7-126 when $z'$ is large and more by Equation 7-127 when $z'$ is small.

A change in the modified Einstein procedure to compute $z'$ was made by Lara (1966). Lara found that the $z'$ value determined by Equation 7-125 was not always representative. Further studies and analysis performed on the collected data showed that $z'$ values should be computed for those size ranges having significant quantities in both suspended and bed loads. The procedure to compute these values is by trial and error as described above. These $z'$ values are then plotted on logarithmic paper as a function of fall velocity $w$. When at least three points are plotted, the line of best fit for the relation $z' = aw^b$ can be computed by the method of least squares. From this relationship the $z'$ values can be determined for the other size ranges.

The modified Einstein procedure rendered very good predictions of the total load for the Niobarara and Loup Rivers, as demonstrated by Schroeder and Hembree (1956). Also, this theory should be generally applicable to streams of different character because much of the sediment discharge is actually measured. This is particularly true for streams of significant depth.

A numerical example that utilizes the modified Einstein procedure to compute total sediment discharge will be given later in this chapter.

Conclusions. Unmeasured sediment discharges for particular times and periods are often needed to supplement records of the measured suspended sediment discharge of streams. Among the three methods presented for computing the total sediment discharge the modified Einstein method is most widely used because it incorporates a maximum of measured data and is therefore quite reliable. The extrapolated suspended part of the load and estimated bed load is usually a small percentage of the total bed material load unless the flow depths are small. Its application to deep streams has been questioned (Toffaleti, 1969), but for small and medium size sand-bed streams, it is satisfactory.

## Comparison of Bed Material Load Equations and Field Applications

The bed material load equations are established for different conditions and use of these equations should be restricted to conditions for which the equations are applicable. Furthermore, very few direct measurements of total sediment discharge of rivers have been made. Most of the growing body of data on sediment discharge of rivers is obtained by adding an estimate of the unmeasured sediment discharge to that sediment measured with suspended load samplers. Although few attempts are discussed, a meaningful comparison of measured and calculated bed material load is difficult. Stall et al. (1958) compared field data collected from Money Creek with calculated results from approaches by Einstein (1950), DuBoys (1879), and Schoklitsch (1934). The latter method demonstrated fairly good (within 30 percent) agreement, whereas the former two methods gave values which were completely erroneous (about 200 percent for DuBoys' approach and 750 percent for Einstein's approach). However, there is some question as to whether the reported

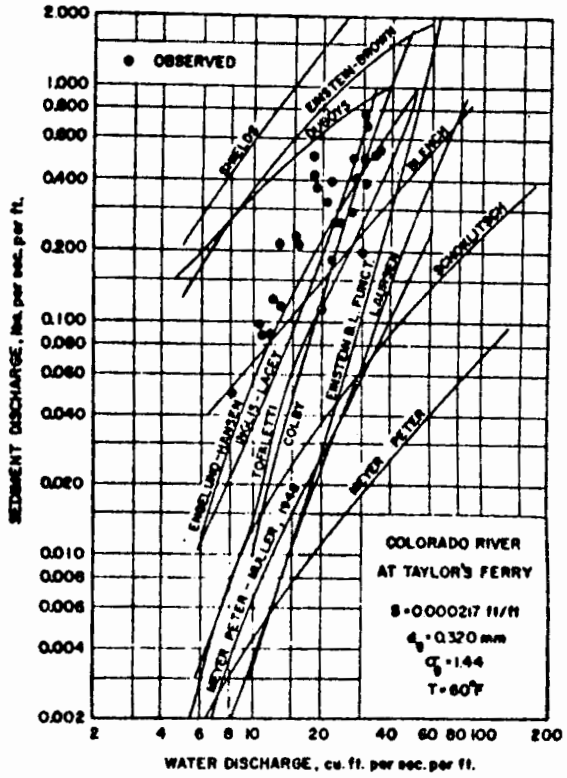


Figure 7-16. Sediment discharge as function of water discharge for Colorado River at Taylor's Ferry obtained from observations and calculations by several formulas (after Task Committee, 1971).

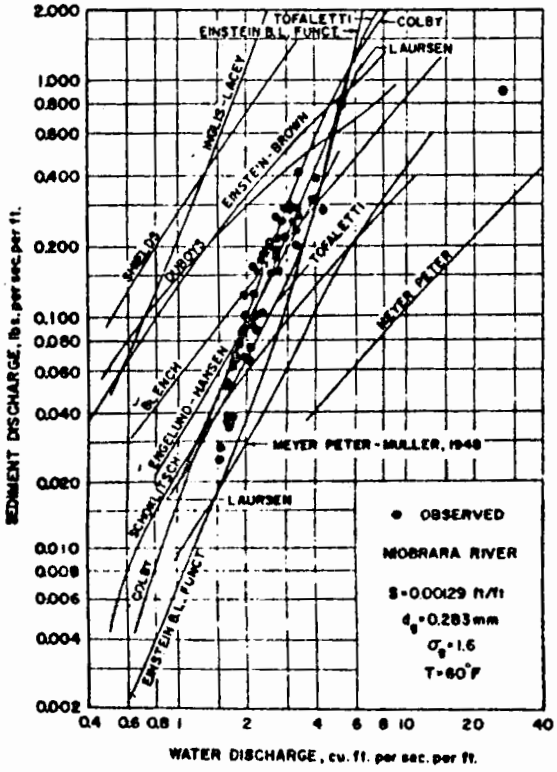


Figure 7-17. Sediment discharge as function of water discharge for Niobrara River near Cody, Nebraska, obtained from observations and calculations by several formulas (after Task Committee, 1971).

measured load is not merely bed load. This in turn would explain why in some cases Schoklitsch's equation, a pure bed load equation, provides a good estimate of bed material discharge and Einstein's bed load function for some cases, presents values which are apparently too high. An ASCE Task Committee (1971) used the field data from the Colorado River at Taylor's Ferry and Niobrara River near Cody, Nebraska to evaluate 13 sediment transport equations (Vanoni et al., 1960). They include formulas by Blench (1966), Colby (1964), DuBoys (1879), Einstein (1950), Brown-Einstein (1950), Englelund-Hansen (1967), Inglis-Lacey (1968), Laursen (1958), Meyer-Peter (1934), Meyer-Peter, Müller (1948), Schoklitsch (1935), Shields (1936), and Toffaleti (1969). Total bed material discharge for the Colorado River was calculated from suspended sediment samples utilizing the modified Einstein method and sediment discharge for the Niobrara River was measured directly. Figures 7-16 and 7-17 show the measured and calculated results. Formulas investigated that result in the best agreement with observed sediment discharge are those of Colby, Toffaleti, and Engelund-Hansen. Based on these comparisons it is clear that sediment discharge formulas cannot be expected to present precise results. Also, equations should only be applied to cases similar to those for which they have been verified.

The disagreement between calculated and observed sediment discharge in Figures 7-16 and 7-17 may be partly caused by large variations in important properties such as slope, bed material, and temperature. These variables as well as sediment load can vary with time and are not as constant as assumed in determining curves of Figures 7-16 and 7-17. However, in general the data in Figures 7-16 and 7-17 can be fitted roughly by a power relation of the form

$$q_T = aq^b$$

In analyzing field data because of the tremendous uncertainties in estimating sediment transport, it is difficult to make recommendations. Shen (1971) suggested the following procedures for analyzing field data.

When measured data are available the suitable procedures are

1. The modified Einstein method should be used to estimate unmeasured suspended load and bed load based on measured data.

2. Bed material load should be separated from wash load and analyzed.

3. Sediment transport equations that best agree with the measured data and used should be selected to estimate the sediment transport load for the design flow when actual measurement is not possible.

In the absence of measured data, the following relations are recommended:

1. Einstein's (1950) procedure should be used when the bed load is a significant portion of the total bed material load.

2. Colby's (1964) method should be used for rivers with flow depth less than or near ten feet.

3. Shen and Hung's (1971) method should be used for flumes and small rivers with shallow depths. This relation does not include depth as a variable, (Simons).

4. Use Toffaleti's (1969) method for large sand-bed rivers.

## 7.3 APPLICATION OF SEDIMENT TRANSPORT FORMULAS

There exists no better way to demonstrate the procedure of applying previously discussed relations than by sample calculations. Calculations of bed material load according to Meyer-Peter's (1948), Einstein's (1950), Colby's (1964), and Bishop's et al. (1965) methods and calculations of total sediment load by the modified Einstein procedure (Colby and Hembree, 1955) and the Colby method (Colby, 1957) will be presented.

### General Rules of the Choice of Test Reach, and of Determination of Data to be Used in Transport Formulas

#### Choice of Test Reach

To calculate or measure flow and sediment transport in a stream a test reach may be selected. This test reach should be sufficiently uniform in shape and sediment composition, with small effects such as sharp bends, sills, or excessive vegetation so that the reach can be treated as a uniform channel characterized by an overall slope and an average representative cross section. No important tributaries should join the river within or immediately above the test reach, and no significant diversions should occur therein.

#### Determination of Energy Slope

Slope determination is a difficult hydraulic measurements. In general the water surface is not parallel to the bottom of the river bed and is not possible to assume that that water level in a cross section is horizontal or a straight line. Under these circumstances accurate determination of energy slope is a real problem. Application of the following rules helps achieve the necessary accuracy

1. A datum line is chosen and the water profile in the cross section is determined relative to this line.

2. Two more cross sections (one upstream and one downstream) of the main section a minimum of 250 m (~ 820 ft) from this section should be chosen.

3. A floating object determines the main path of the flow between extreme sections.

4. Water stage on this path relative to the datum line is determined and this operation is repeated at least three times to determine the average value.

5. The distances separating up- and downstream sections from the main section is measured.

6. Upstream and downstream is calculated water level slope and compared with the main section slope. If the difference is more than ten percent, another reach is selected.

7. If the discharge of the river is known the mean velocity is determined using the continuity equation $Q = AU$. If $Q$ is unknown, $U$ is determined by measuring local velocities utilizing a current meter or some other suitable method. The velocity heads are added to the stage and $S$ is computed as

$$S = \frac{\Delta h + \frac{U_{up}^2 - U_{down}^2}{2g}}{L} \qquad (7\text{-}128)$$

where $\Delta h$ is the difference between the water stages and $L$ is the distance between up- and downstream cross sections

8. If a preliminary slope determination is required, the measurement may be taken along the side of the river but one should make certain that the measured water surface levels belong to a common stream line. In many instances it will be necessary to measure slope along the side or sides of a river because of river size and other complicating factors.

Sampling of Bed Material

A sieve analysis of bed material is usually necessary to determine $\sigma$, $D_{50}$, $D_m$, $D_{35}$, $D_{65}$, $D_{90}$, $D_{84}$ and etc. The following guidelines can be followed for sampling bed material.

1. When the bottom of the water course is dry
   a. Superficial bottom material of about $2D_{90}$ thickness should be removed using a shovel. The wash load material should be eliminated and this sample should be prepared for sieve analysis.
   b. Samples from the bed material over a depth of $d$ meters should be collected. The sampled depth $d$ is determined considering characteristics of the bed. The collected sampled material should represent the complete range of the material transported by the river.
   c. $D_{90}$ and $D_{65}$ must be determined from the first sample and $D_{50}$ from the second.

2. When water is flowing in the river
   a. One should attempt to locate an abandoned portion of river channel and collect samples from this reach for comparison.

b. Available material from the surface layer of the bottom should be sampled for sieve analysis. In general, wash load is retained by a sampler in this environment. The material thus collected is subjected to sieve analysis.
c. The result of this sieve analysis is used to determine particle size and particle size distribution.

## 7.4 SAMPLE CALCULATIONS

### Calculation of Sediment Discharge Using Transport Formulas

The application of various sediment transport theories follows.

#### Calculation of Bed Material Discharge by the Meyer-Peter, Müller Bed Load Function

The necessary data for calculation of bed-material discharge by Meyer-Peter's bed load function are: $\gamma_s$, $D_{90}$, $D_m$, S, Q, and the shape of the channel cross section. These data may be obtained as described previously. The technique of computation is illustrated.

#### Example A

Compute the rate of bed load transport in a stream, the characteristics of which are given

1. Characteristics of bed material

   $\gamma_s = 2.65\ T/m^3$

   Assume the particle size distribution is given by Figure 7.18.

2. Characteristics of the stream

   B = 110 m  S = 0.0005  z = 0.5
   d = 3.5 m  Q = 520 $m^3$/sec

3. Characteristics of the bed roughness

   Dune type bed forms are observed, $k_s = 35$ and $k_w = k_s$

Solution:

1. Compute, from Figure 7-18, the following characteristic grain sizes

   $D_{50} = 0.011$ m

$$D_m = \frac{5x0.00015+35x0.00065+10x0.0015+10x0.0028+10x0.00475+20x0.0085+10x0.018}{100}$$

   from which

   $D_m = 0.0046$ m

2. Compute $k_r$

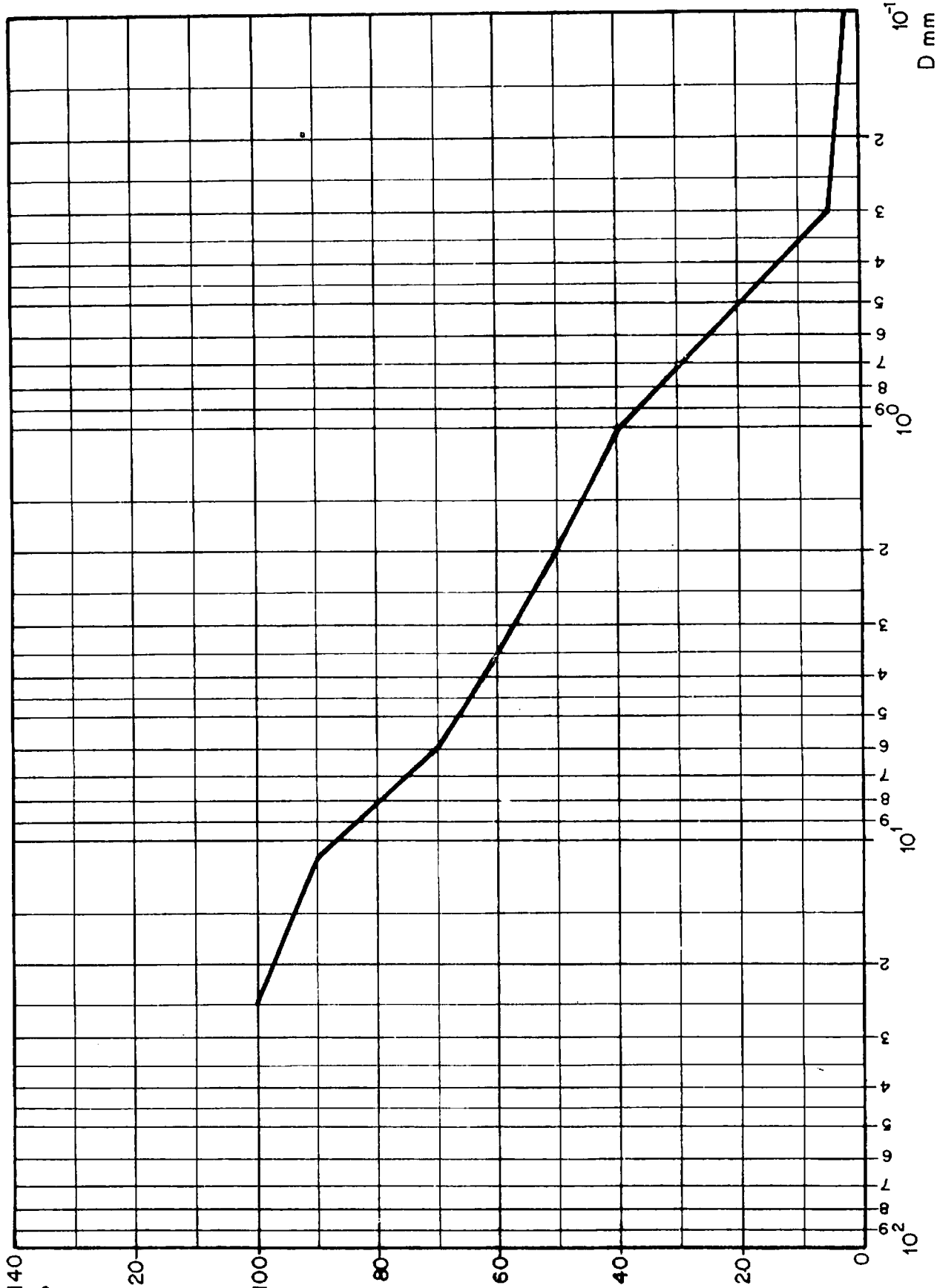


Figure 7-18. Particle size distribution of the bed material in Example A.

$$k_r = \frac{26}{(0.011)^{1/6}} = 55.13 \sim 55 \qquad 7\text{-}29$$

3. Compute $R_s$

Assume the influence of channel side slope is nill. Then

$$A = 110 \times 3.5 = 385 \text{ m}^2$$

$$P = 110 + 7 = 117 \text{ m} \quad \text{and} \quad \frac{A}{P} = R_s = 3.29 \text{ m}$$

4. Apply Equation 7-20:

$$\left(\frac{35}{55}\right)^{3/2} \times 3.29 \times 0.0005 = 0.047 \times 1.65 \times 0.0046 + 0.25\,(0.102)^{1/3} q_{bw}'^{\,2/3}$$

$$8.35 \times 10^{-4} = 3.57 \times 10^{-4} + 0.12\, q_{bw}'^{\,2/3}$$

from this relation

$$q_{bw}' = 2.52 \times 10^{-4} \text{ T/m sec} = 2.62 \times 10^{-1} \text{ kg/sec m}$$

and

$$Q_s' = 27.72 \text{ kg/sec}$$

5. To compute $(q_{bw}')$ for a hypothetical very wide channel, apply Equation 7-21 to the same problem and compare

$$1000 \times 3.5 \times 0.0005 = 0.047 \times 1650 \times 0.0046 + 0.25(102)^{1/3}$$

$$(q_{bw}'^{\,2/3}) = 1.30 \text{ kg/sec m}$$

and

$$\frac{(q_{bw}')_5}{(q_{bw}')_4} = 5.16$$

For simplicity engineers sometimes assume the canal is very wide. Hence, one should check the effect of shape of large sections on sediment transport since this assumption can lead to significant differences in the results in some cases.

Example B

Compute the rate of bed load transport in a laboratory channel, the characteristics of which are given

1. Use the characteristics of bed materials given in Example A.

2. Characteristics of the laboratory flume

$B = 1.00$ m  $S = 0.0005$

$d = 0.5$ m  $Q = 0.200 \text{ m}^3/\text{sec}$

$\nu = 10^{-6} \text{ m}^2/\text{sec}$  $z = 0$

Solution:

1. From Example A $D_{90} = 0.011$ m and $D_m = 0.0046$ m

2. From Example A $k_r = 55 = k_b$

3. The value of $k_w$ for glass = 100

4. Using Equation 7.129

$$q_b = 0.200 \frac{100^{3/2}}{2 \times 0.5 \times 55^{3/2} + 100^{3/2}} = 0.142 \text{ m}^3/\text{sec m} \quad (7\text{-}129)$$

5. Compute $R_s$ and $k_s$

$$q_b = q_s$$

$$U = \frac{0.2}{0.5} = 0.4 \text{ m/sec}$$

$$R_s = \frac{0.142}{0.4} = 0.355 \text{ m}$$

$$k_s = 0.4/(R_s^{2/3} S^{1/2}) = 35.68$$

6. Apply formula 20

$$1000\left(\frac{35.68}{55}\right)^{\frac{3}{2}} \times 0.355 \times 0.0005 = 0.047 \times 1.65 \times 0.0046 \times 10000 + 0.25(102)^{\frac{1}{3}} q_{bw}'^{\frac{2}{3}}$$

Because $q_s' < 0$ there is no bed material transport.

7. Solve the same problem using the USBR-Meyer-Peter, Müller formulas.

$$n_b = \left\{1 + \frac{2 \times 1.64}{3.28}\left[1 - \left(\frac{0.01}{0.018}\right)^{3/2}\right]\right\}^{2/3} 0.018 = 0.024 \quad 7\text{-}32$$

$$\frac{Q'}{Q} = \frac{1}{1 + \frac{2 \times 1.64}{3.28}\left(\frac{0.01}{0.018}\right)^{3/2}} = 0.79 \quad 7\text{-}34$$

$$q_{bw} = \left(\frac{2.65}{1.65}\right)\left(\frac{32.2}{62.4}\right)^{1/2}\left[0.0661 \times 62.4 \times 0.79 \frac{11^{1/6}}{0.024}\right]^{3/2}$$

$$\times 1.64 \times 0.0005 - 0.0076(102.96)\ 4.6\Big]^{3/2} \quad 7\text{-}31$$

Because $q_{bw} < 0$ there is no bed material transport.

Example C

Solve Example A applying the USBR-Meyer-Peter formulas

Solution:

1. $$n_b = n \left\{1 + \frac{2d(1+z^2)^{1/2}}{B} \left[1 - \left(\frac{n_w}{n}\right)^{3/2}\right]\right\}^{2/3} \qquad 7\text{-}33$$

$d = 11.48$ ft

$B = 360.89 = 360.89$ ft

$k_s = \frac{1}{n} = 35$

$n = 0.0286 \tilde{\sim} 0.029$

$n_w = n = 0.029$

using these values:

$$n_b = 0.029 \left\{1 + \frac{2x11.48\ (1 + 0.5^2)^{1/2}}{360.89} [1 - 1]\right\}^{2/3} = 0.029$$

2. $$\frac{Q'}{Q} = \frac{1}{1 + \frac{2x11.48(1 + z^2)^{1/2}}{360.89}} = 0.934 \qquad 7\text{-}35$$

3. $$q_{bw} = \frac{2.65}{1.65} \frac{32.2}{62.4}^{1/2} [0.0661 \times 62.4 \times 0.934 \left(\frac{11^{1/6}}{0.029}\right)^{3/2}$$

$$\times 11.48 \times 0.0005 - 0.0076\ (102.96)4.6]^{3/2}$$

and

$q_{bw} = 11.22$ ton/day/ft $= 0.426$ kg/m sec dry weight

or

$q'_{bw} = 0.265$ kg/m sec submerged weight.

4. Compared to the result of Example A, ($q_{bw} = 0.262$) a difference of 1 percent exists which can be attributed to the errors in the conversion of units.

Calculation of Bed Material Discharge by Einstein's Bed Load Function

Example D

The application of the Einstein procedure to a particular water course can be subdivided into three parts. The first part involves choice of a river reach and collection of required field data. The second part determines the required hydraulic parameters and the third part uses the results of the other parts to compute total bed material discharge.

## Description of the Test Reach

A test reach representative of the Big Sand Creek near Greenwood, Mississippi was used by Einstein (1950) to illustrate the application of his bed load function. His numerical example is reproduced here. For simplicity the effects due to bank friction are neglected. The original example may be referenced for the construction of the representative cross section and the consideration of bank friction. Characteristics of the channel cross section follow.

Channel slope was determined to be $S = 0.00105$. The relations of cross sectional area, hydraulic radius, and wetted perimeter versus stage for the representative cross section are given in Figure 7.19. For this wide and shallow channel the wetted perimeter is assumed to equal the surface width. The averaged values of the four bed material samples are given in Table 7-2, and grain size distribution is presented in Figure 7.20. Of these composite samples 95.8 percent of the bed material falls between 0.589 and 0.147 mm which is subdivided into four fractions. Sediment transport will be calculated for individual size fractions with selected representative grain sizes equal to the geometric mean grain diameter of each fraction. The kinematic water viscosity $\nu$ is $1.06 \times 10^{-5}$ $ft^2/sec$ and specific gravity of the sediment is 2.65.

Table 7-2. Bed material information for sample problem.

| Grain size distribution, mm | Average grain size mm | ft | % | Settling velocity mm/sec | fps |
|---|---|---|---|---|---|
| $D > 0.589$ | --- | --- | 2.4 | --- | --- |
| $0.589 > D > 0.417$ | 0.495 | 0.00162 | 17.8 | 5.20 | 0.195 |
| $0.417 > D > 0.295$ | 0.351 | 0.00115 | 40.2 | 3.75 | 0.148 |
| $0.295 > D > 0.208$ | 0.248 | 0.00081 | 32.0 | 2.70 | 0.100 |
| $0.208 > D > 0.147$ | 0.175 | 0.00058 | 5.8 | 1.70 | 0.064 |
| $0.147 > D$ | --- | --- | 1.8 | --- | --- |

$D_{35} = 0.29$ mm $= 0.000951$ ft

$D_{65} = 0.35$ mm $= 0.00115$ ft

## Hydraulic Calculations

Important hydraulic parameters were calculated according to Table 7-3. Table headings, their meanings, and calculations are explained with footnotes. Equation 7-130(*) and Figure 7-21 were used to evaluate the resistance to flow. Any similar relation discussed in Chapter 6 (Simons and Sentürk, 1977) can be utilized for the same purposes.

$$(*)\ \psi' = \frac{\gamma_s - \gamma}{\gamma} \frac{D_{35}}{SR'} = \frac{\gamma_s'}{\gamma} \frac{D_{35}}{SR'} \qquad (7\text{-}130)$$

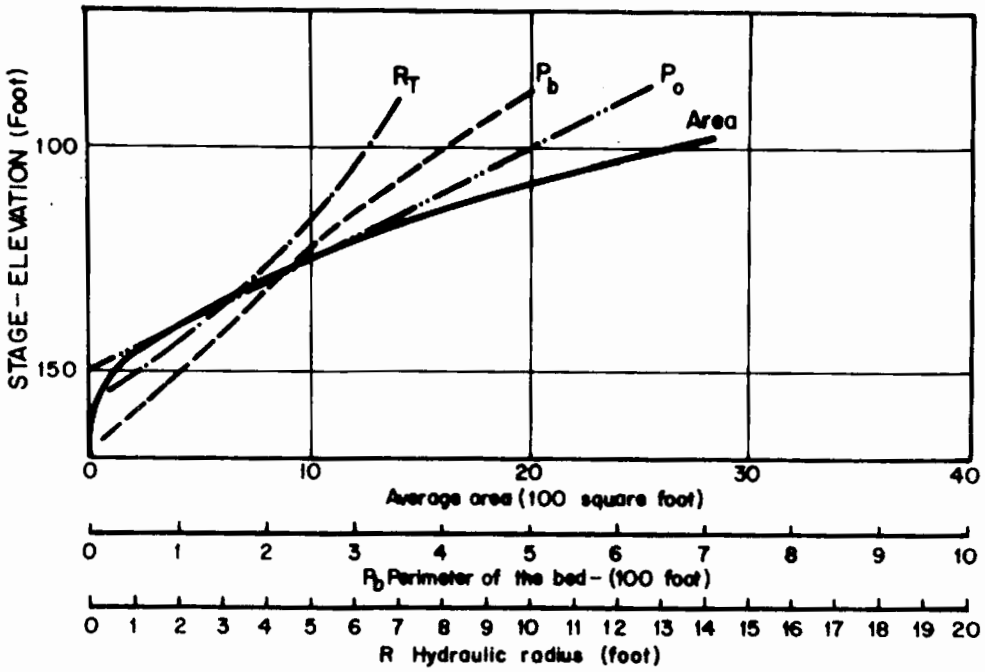


Figure 7-19. Description of the average cross section.

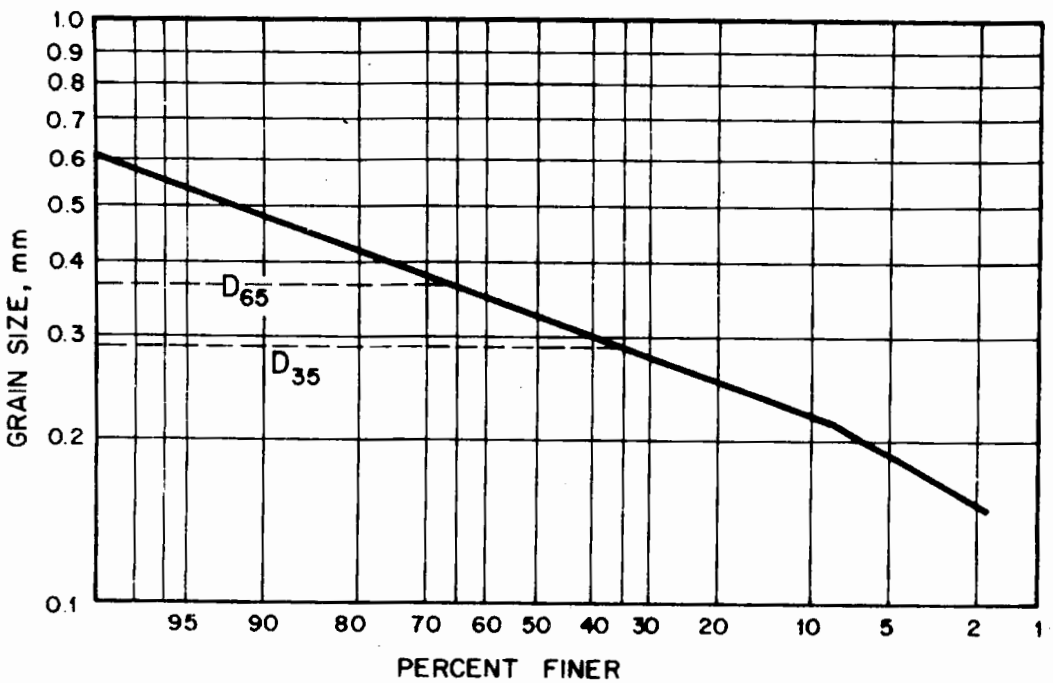


Figure 7-20. Grain size distribution of bed material.

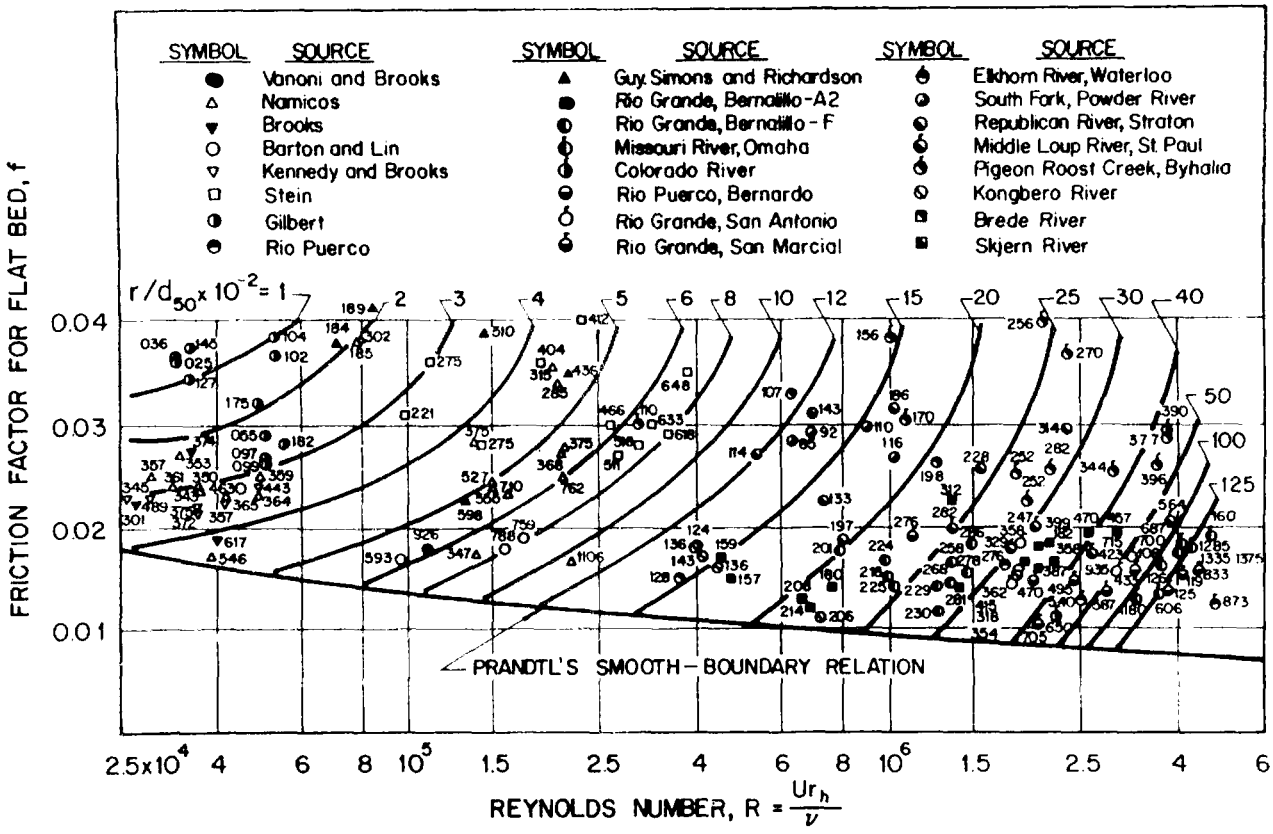


Figure 7-21. Friction-factors for flat-bed flows in alluvial channels, the number by each point is $R/D_{50} \times 10^{-2}$ (after Lovera and Kennedy, 1969).

Table 7-3. Hydraulic calculations for sample problem by applying the Einstein procedure (after Einstein, 1950).

| $R'_b$ | $U'_b$ | $\delta$ | $k_s/\delta$ | x | $\Delta$ | U | $\psi'$ | $\frac{U}{U''_{*b}}$ | $U''_{*b}$ | $R''_b$ | $R_b$ | $d_N R_b$ | Stage | A | $P_b$ | Q | X | Y | $\beta_x$ | $(\beta/\beta_x)^2$ | $P_E$ |
|---|---|---|---|---|---|---|---|---|---|---|---|---|---|---|---|---|---|---|---|---|---|
| 1 | 2 | 3 | 4 | 5 | 6 | 7 | 8 | 9 | 10 | 11 | 12 | 13 | 14 | 15 | 16 | 17 | 18 | 19 | 20 | 21 | 22 |
| 0.5 | 0.130 | 0.000946 | 1.22 | 1.59 | 0.000723 | 2.93 | 2.99 | 16.8 | 0.17 | 0.86 | 1.36 | 1.36 | 150.2 | 140 | 103 | 410 | 0.00132 | 0.84 | 1.29 | 0.63 | 10.97 |
| 1.0 | 0.184 | 0.000668 | 1.72 | 1.46 | 0.000783 | 4.44 | 1.49 | 27.0 | 0.16 | 0.76 | 1.76 | 1.76 | 150.9 | 240 | 136 | 1,065 | 0.000928 | 0.68 | 1.10 | 0.85 | 11.10 |
| 2.0 | 0.260 | 0.000474 | 2.45 | 1.27 | 0.000906 | 6.63 | 0.746 | 51.0 | 0.13 | 0.50 | 2.50 | 2.50 | 152.1 | 425 | 170 | 2,820 | 0.000693 | 0.56 | 0.91 | 1.27 | 11.30 |
| 3.0 | 0.318 | 0.000387 | 2.95 | 1.18 | 0.000966 | 8.38 | 0.498 | 87.0 | 0.10 | 0.30 | 3.30 | 3.30 | 153.3 | 640 | 194 | 5,380 | 0.000747 | 0.55 | 0.91 | 1.27 | 11.50 |
| 4.0 | 0.368 | 0.000334 | 3.49 | 1.14 | 0.001009 | 9.92 | 0.373 | 150.0 | 0.07 | 0.14 | 4.14 | 4.14 | 154.9 | 970 | 234 | 9,620 | 0.000785 | 0.54 | 0.91 | 1.27 | 11.70 |
| 5.0 | 0.411 | 0.000298 | 3.84 | 1.11 | 0.001036 | 11.28 | 0.299 | 240.0 | 0.05 | 0.07 | 5.07 | 5.07 | 156.9 | 1,465 | 289 | 16,550 | 0.000841 | 0.54 | 0.91 | 1.27 | 11.90 |
| 6.0 | 0.450 | 0.000273 | 4.26 | 1.08 | 0.001065 | 12.58 | 0.249 | 370.0 | 0.03 | 0.034 | 6.03 | 6.03 | 159.5 | 2,400 | 398 | 30,200 | 0.000824 | 0.54 | 0.91 | 1.27 | 12.04 |

[1]See the following for explanation of symbols, column by column:

(1) $R'_b$, ft (bed hydraulic radius due to grain roughness; values are assumed to cover the entire desired discharge range.

(2) $U'_{*b} = \sqrt{gR'_b S}$, fps, (shear velocity due to grain roughness).

(3) $\delta = 11.6\ \nu/U'_*$, ft, (thickness of laminar sublayer).

(4) $k_s = D_{65}$, ft, (roughness diameter).

(5) $x = f(k_s/\delta)$, (correction factor in the logarithmic velocity distribution).

(6) $\Delta = k_s/x$, ft, (apparent roughness diameter).

(7) $U = U'_b\ 5.75 \log (12.27\ R'_b/\Delta)$, fps, (average flow velocity).

(8) $\psi' = \frac{\rho_s - \rho}{\rho} \frac{D_{35}}{R'_b S}$ (intensity of shear on representative particles).

(9) $U/U'_{*b} = f(\psi')$.

(10) $U''_{*b}$, fps, (shear velocity due to form roughness).

(11) $R''_b$, ft, (bed hydraulic radius due to form roughness), from $U''_{*b} = \sqrt{gR''_b S}$.

(12) $R_b = R_b' + R_b''$, ft, (bed hydraulic radius), with no additional friction from the banks, $R_b$ represents the total hydraulic radius R.

(13) d, ft, (average flow depth), $d \cong R_b$ for wide shallow streams.

(14) Stage, ft, from description of cross section for $R = R_b$.

(15) A, $ft^2$, (cross-sectional area) for the given stage.

(16) $P_b$, ft, (bed wetted perimeter) for the given stage.

(17) $Q = AU$, cfs, (flow discharge), a stage-discharge relationship can be plotted by relating the computed Q to the stage.

(18) x, ft, (characteristic distance) $x = 0.77\ \Delta$ for $\Delta/\delta > 1.80$ and $x = 1.39\ \delta$ for $\Delta/\delta < 1.80$.

(19) $Y = f(k_s/\delta)$, (pressure correction term).

(20) $\beta_x = \log (10.6\ X/\Delta)$, (logarithmic function).

(21) $\beta^x = \log 10.6$.

(22) $P_E = 2.303 \log \frac{30.2d}{\Delta}$, (Einstein's transport parameter).

## Bed Material Discharge Calculations

The bed material transport is calculated for each representative grain size of the bed material at each given flow depth. For the summary of calculations, procedure, and results are presented in Table 7-4.

## Calculation of Bed Material Discharge by Colby's Method

### Example E

In applying the previously presented Colby method (1964), the necessary data include mean velocity, depth, median size or size distribution of bed material, water temperature, and fine sediment (wash load) concentration. Mean velocity and depth of flow may be determined using hydraulic calculations as described. However, to obtain the best results from calculations directly measured values of velocity and depth are utilized.

In order to compare the calculated results applying different methods the same sample problem used to illustrate Einstein's method is solved using the Colby method. The required data are taken from Table 7-3. In addition, water temperature and fine sediment concentration are assumed equal to 70°F and 10,000 ppm, respectively. For convenience the calculations are summarized in tables. Table 7-5 provides the calculations using median diameter of bed material and Table 7-6 presents the calculations for individual fractions using the bed material size distribution.

## Calculation of Bed Material Discharge by Bishop et al. Method

### Example F

Bishop, Simons and Richardson's (1965) method is applied to solve the same sample problem as the one solved by the Einstein procedure (1950). Again, table form is used (Table 7-7). Apparently the Bishop et al. method is very simple to apply.

Discussion of Sample Problems. The comparison of bed material discharge calculations for the sample problem using Einstein's (1950), Colby's (1964), Bishop et al. (1965), and Einstein and Abdel-Aal's (1972) methods are shown in Figure 7-22. The curves indicate that the sediment discharge increases rapidly with increasing water discharge. However, considerable deviations result from applying different methods. Since Einstein's method is basically derived from bed load measurements, application of this method to calculate bed material load is questionable when a large percent of bed material load is in suspension as in the sample problem.

Table 7-4. Bed material load calculations for sample problem by applying the Einstein procedure (after Einstein, 1950).

| $10^3 D$ | $10^2 i_b$ | $R_b'$ | $\psi$ | D/x | $\xi$ | $\psi_*$ | $\phi_*$ | $i_{Bw}q_{bw}$ | $i_B Q_B$ | $\Sigma i_B Q_B$ | $10^3 E$ | z | $I_1$ | $-I_2$ | $P_E I_1 + I_2 + 1$ | $i_T q_T$ | $i_T Q_T$ | $\Sigma i_T Q_T$ |
|---|---|---|---|---|---|---|---|---|---|---|---|---|---|---|---|---|---|---|
| 1 | 2 | 3 | 4 | 5 | 6 | 7 | 8 | 9 | 10 | 11 | 12 | 13 | 14 | 15 | 16 | 17 | 18 | 19 |
| 1.62 | 17.8 | 0.5 | 5.09 | 1.23 | 1.085 | 2.84 | 1.90 | 0.0266 | 118 | 396 | 2.08 | 2.38 | 0.078 | 0.44 | 1.42 | 0.0378 | 168 | 674 |
| | | 1.0 | 2.55 | 1.74 | 1.00 | 1.51 | 4.70 | 0.0658 | 387 | 1,561 | 1.84 | 2.65 | 0.131 | 0.74 | 1.72 | 0.0113 | 664 | 4,680 |
| | | 2.0 | 1.27 | 2.34 | 1.00 | 0.899 | 8.60 | 0.1204 | 884 | 3,735 | 1.35 | 1.88 | 0.240 | 1.27 | 2.44 | 0.294 | 2,160 | 30,900 |
| | | 3.0 | 0.849 | 2.17 | 1.00 | 0.590 | 12.8 | 0.1793 | 1,500 | 6,489 | 1.01 | 1.53 | 0.385 | 2.01 | 3.43 | 0.615 | 5,160 | 114,000 |
| | | 4.0 | 0.636 | 2.06 | 1.00 | 0.434 | 18.0 | 0.2521 | 2,500 | 10,646 | 0.784 | 1.33 | 0.560 | 2.80 | 4.76 | 1.20 | 12,100 | 330,000 |
| | | 5.0 | 0.509 | 2.02 | 1.00 | 0.347 | 22.5 | 0.3151 | 3,060 | 16,275 | 0.639 | 1.18 | 0.810 | 3.85 | 6.80 | 2.14 | 26,700 | 814,000 |
| | | 6.0 | 0.424 | 1.97 | 1.00 | 0.289 | 27.0 | 0.3781 | 6,500 | 26,743 | 0.537 | 1.08 | 1.09 | 4.90 | 9.23 | 3.49 | 60,000 | 1,961,000 |
| 1.15 | 40.2 | 0.5 | 3.38 | 0.871 | 1.29 | 2.47 | 2.45 | 0.0463 | 206 | | 1.47 | 2.86 | 0.117 | 0.68 | 1.62 | 0.0750 | 334 | |
| | | 1.0 | 1.81 | 1.24 | 1.05 | 1.12 | 6.50 | 0.1230 | 723 | | 1.24 | 2.02 | 0.210 | 1.19 | 2.16 | 0.266 | 1,560 | |
| | | 2.0 | 0.904 | 1.66 | 1.00 | 0.640 | 12.1 | 0.2289 | 1,680 | | 0.958 | 1.43 | 0.450 | 2.33 | 3.75 | 0.858 | 6,300 | |
| | | 3.0 | 0.602 | 1.54 | 1.00 | 0.419 | 19.0 | 0.3594 | 3,010 | | 0.714 | 1.17 | 0.830 | 3.85 | 6.72 | 2.42 | 20,300 | |
| | | 4.0 | 0.452 | 1.47 | 1.01 | 0.312 | 25.5 | 0.4824 | 4,880 | | 0.557 | 1.01 | 1.37 | 5.70 | 11.4 | 5.50 | 55,600 | |
| | | 5.0 | 0.361 | 1.44 | 1.01 | 0.249 | 31.5 | 0.5959 | 7,440 | | 0.454 | 0.90 | 2.12 | 8.10 | 18.1 | 10.8 | 135,000 | |
| | | 6.0 | 0.301 | 1.40 | 1.02 | 0.210 | 38.0 | 0.7188 | 12,400 | | 0.381 | 0.83 | 2.95 | 10.5 | 26.0 | 18.7 | 321,000 | |
| 0.814 | 32.0 | 0.5 | 2.56 | 0.617 | 2.25 | 3.06 | 1.75 | 0.0157 | 69.9 | | 1.04 | 1.94 | 0.230 | 1.29 | 2.26 | 0.0355 | 158 | |
| | | 1.0 | 1.28 | 0.875 | 1.26 | 1.946 | 7.90 | 0.0708 | 416 | | 0.880 | 1.36 | 0.520 | 2.60 | 4.21 | 0.298 | 1,750 | |
| | | 2.0 | 0.640 | 1.17 | 1.07 | 0.485 | 15.8 | 0.1417 | 1,040 | | 0.678 | 0.962 | 1.53 | 6.10 | 12.2 | 1.73 | 12,700 | |
| | | 3.0 | 0.428 | 1.09 | 1.11 | 0.329 | 23.5 | 0.2107 | 1,770 | | 0.506 | 0.786 | 3.35 | 11.0 | 28.6 | 6.03 | 50,500 | |
| | | 4.0 | 9.320 | 1.04 | 1.13 | 0.247 | 32.0 | 0.2870 | 2,900 | | 0.394 | 0.679 | 6.20 | 17.5 | 56.2 | 16.1 | 163,000 | |
| | | 5.0 | 0.256 | 1.02 | 1.15 | 0.201 | 39.5 | 0.3542 | 4,420 | | 0.321 | 0.608 | 9.80 | 25.5 | 92.2 | 32.7 | 407,700 | |
| | | 6.0 | 0.213 | 0.988 | 1.17 | 0.170 | 46.0 | 0.4125 | 7,090 | | 0.270 | 0.556 | 15.0 | 36.0 | 146.0 | 60.2 | 1,035,500 | |
| 0.574 | 5.8 | 0.5 | 1.80 | 0.435 | 5.40 | 5.16 | 0.58 | 0.00056 | 2.49 | | 0.736 | 1.23 | 0.720 | 3.35 | 5.63 | 0.00315 | 14 | |
| | | 1.0 | 0.902 | 0.619 | 2.18 | 1.16 | 6.2 | 0.00597 | 35.1 | | 0.621 | 0.870 | 2.44 | 8.10 | 20.2 | 0.121 | 709 | |
| | | 2.0 | 0.451 | 0.828 | 1.33 | 0.423 | 18.5 | 0.0178 | 131 | | 0.478 | 0.615 | 8.40 | 21.5 | 74.4 | 1.32 | 9,730 | |
| | | 3.0 | 0.301 | 0.768 | 1.47 | 0.308 | 25.0 | 0.02486 | 208 | | 0.357 | 0.503 | 19.3 | 41.0 | 183 | 4.55 | 38,100 | |
| | | 4.0 | 0.226 | 0.731 | 1.58 | 0.244 | 32.5 | 0.03128 | 316 | | 0.278 | 0.434 | 32.0 | 63.0 | 313 | 9.79 | 98,970 | |
| | | 5.0 | 0.180 | 0.717 | 1.61 | 0.198 | 39.5 | 0.03802 | 475 | | 0.226 | 0.389 | 51.0 | 91.0 | 517 | 19.7 | 245,000 | |
| | | 6.0 | 0.150 | 0.687 | 1.67 | 0.171 | 45.5 | 0.04379 | 753 | | 0.190 | 0.356 | 70.0 | 122 | 722 | 31.6 | 544,000 | |

[1]See the following explanation of symbols, column by column:

(1) D, ft, (represenative grain size).
(2) $i_b$, (fraction of bed material).
(3) $R_b$, ft, (bed hydraulic radius due to grain roughness),
(4) $\phi = \frac{\rho_s - \rho}{\rho} \frac{D_{65}}{R_b'}$ (intensity of shear on particle),
(5) D/X, for values of X
(6) $\xi = f(\frac{D_{65}}{X})$ (hiding factor).
(7) $\psi_* = \xi Y(\beta^2/\beta_*^2)\psi$ (intensity of shear on individual grain size), values of $Y(\beta^2/\beta_*^2)$.
(8) $\phi_* = f(\psi_*)$(intensity of sediment transport for individual grain size)
(9) $i_{Bw}q_{bw} = i_{bw}\phi_*\rho_s(gD)^{3/2}\sqrt{\frac{\rho_s - \rho}{\rho}}$ lb/sec-ft (bed load discharge per unit width for a size fraction).
(10) $i_{Bw}Q_{bw} = 43.2\ B\ i_{bw}q_{bw}$ tons/day, (bed load discharge for a size fraction for entire cross section), B = $P_b$.
(11) $\Sigma\ i_{Bw}Q_{Bw}$, tons/day (bed load discharge for all size fractions for entire cross section).
(12) E = 2(D/d)(ratio of bed layer thickness to water depth), for values of d.
(13) $z = \frac{w}{0.4u_*'}$, (exponent for concentration distribution), values of w and $u_*'$ are given.
(14) $I_1 = f(E,z)$(integral).
(15) $I_1^2 = f(E,z)$(integral).
(16) $P_E^2 I_1 + I_2 + I$.
(17) $i_T q_T = i_{Bw}q_{bw}(P_E I_1 + I_2 + 1)$, lb/sec-ft, (bed mateial load per unit width of stream for a size fraction.
(18) $i_T Q_T = 43.2\ B\ i_T q_T$, tons/day, (bed material load for a size fraction for entire cross section).
(19) $\Sigma\ i_T Q_T$, tons/day, (total bed material load for all size fractions).

Table 7-5. Bed material load calculations for sample problem by applying the Colby Method[1] (median diameter)

| d | B | U | $q_{Ti}$ | $k_1$ | $k_2$ | $k_3$ | $q_T$ | $Q_T$ |
|---|---|---|---|---|---|---|---|---|
| 1 | 2 | 3 | 4 | 5 | 6 | 7 | 8 | 9 |
| 1.36 | 103 | 2.93 | 14.5 | 0.92 | 1.20 | 99 | 16. | 1,648 |
| 1.76 | 136 | 4.44 | 50.0 | 0.91 | 1.21 | 99 | 56. | 7,616 |
| 2.50 | 170 | 6.63 | 135. | 0.91 | 1.22 | 99 | 150. | 25,500 |
| 3.30 | 194 | 8.38 | 220. | 0.90 | 1.23 | 99 | 243. | 47,142 |
| 4.14 | 234 | 9.92 | 325. | 0.90 | 1.25 | 99 | 365. | 85,410 |

[1]See the following for explanation of symbols, column by column:
(1) d, ft, (mean depth).
(2) B, ft, (surface width).
(3) U, fps, (average velocity).
(4) $q_{Ti}$, tons/day-ft (uncorrected sediment discharge per unit width of channel, for a given U, d, and $D_{50}$ (=0.32 mm) by logarithmic interpolation.
(5) $k_1 = f(d,T)$ (correction factor for temperature).
(6) $k_2 = f(d,C_f)$ (correction factor for fine sediment concentration).
(7) $k_3 = f(D_{50})$ (correction factor for sediment size).
(8) $q_T = [1 + (k_1 k_2 - 1) 0.01 k_3] q_{Ti}$, tons/day-ft, (true bed material discharge per unit width of stream).
(9) $Q_T = Bq_T$, tons/day, (bed material discharge for all size fractions for entire cross section).

Table 7-6. Bed material discharge calculations for sample problem by applying the Colby method[1] (individual size fraction).

| D | $10^2 i_b$ | d | B | U | $q_{T1}$ | $k_1$ | $k_2$ | $k_3$ | $q_T$ | $i_b q_T$ | $i_b Q_T$ | $\Sigma i_b Q_T$ |
|---|---|---|---|---|---|---|---|---|---|---|---|---|
| 1 | 2 | 3 | 4 | 5 | 6 | 7 | 8 | 9 | 10 | 11 | 12 | 13 |
| 0.495 | 17.8 | 1.36 | 103 | 2.93 | 12 | 0.92 | 1.20 | 62 | 13 | 2.3 | 237 | 1,710 |
| | | 1.76 | 136 | 4.44 | 40 | 0.91 | 1.21 | 62 | 43 | 7.7 | 1,050 | 6,908 |
| | | 2.50 | 170 | 6.63 | 112 | 0.91 | 1.22 | 62 | 119 | 21 | 3,570 | 22,780 |
| | | 3.30 | 194 | 8.38 | 193 | 0.90 | 1.23 | 62 | 205 | 37 | 7,180 | 45,560 |
| | | 4.14 | 234 | 9.92 | 265 | 0.90 | 1.25 | 62 | 288 | 51 | 11,900 | 77,640 |
| 0.351 | 40.2 | 1.36 | 103 | 2.93 | 15 | 0.92 | 1.20 | 92 | 16 | 6.4 | 659 | |
| | | 1.76 | 136 | 4.44 | 45 | 0.91 | 1.21 | 92 | 49 | 20 | 2,720 | |
| | | 2.50 | 170 | 6.63 | 120 | 0.91 | 1.22 | 92 | 132 | 53 | 9,010 | |
| | | 3.30 | 194 | 8.38 | 210 | 0.90 | 1.23 | 92 | 230 | 93 | 18,000 | |
| | | 4.14 | 234 | 9.93 | 290 | 0.90 | 1.25 | 92 | 323 | 130 | 30,420 | |
| 0.248 | 32.0 | 1.36 | 103 | 2.92 | 18 | 0.92 | 1.20 | 100 | 20 | 6.4 | 659 | |
| | | 1.76 | 136 | 4.94 | 53 | 0.91 | 1.21 | 100 | 58 | 19 | 2,580 | |
| | | 2.50 | 170 | 6.63 | 140 | 0.91 | 1.22 | 100 | 155 | 50 | 8,500 | |
| | | 3.30 | 194 | 8.38 | 240 | 0.90 | 1.23 | 100 | 266 | 85 | 16,500 | |
| | | 4.14 | 234 | 9.93 | 345 | 0.90 | 1.25 | 100 | 388 | 124 | 29,000 | |
| 0.175 | 5.8 | 1.36 | 103 | 2.92 | 23 | 0.92 | 1.20 | 97 | 25 | 1.5 | 155 | |
| | | 1.76 | 136 | 4.44 | 64 | 0.91 | 1.21 | 97 | 70 | 4.1 | 558 | |
| | | 2.50 | 170 | 6.63 | 163 | 0.91 | 1.22 | 97 | 180 | 10 | 1,700 | |
| | | 3.30 | 194 | 8.38 | 305 | 0.90 | 1.23 | 97 | 337 | 20 | 3,880 | |
| | | 4.14 | 234 | 9.92 | 420 | 0.90 | 1.25 | 97 | 471 | 27 | 6,320 | |

[1]See the following for explanation of symbols, column by column:

(1) D, mm, (representative grain size).

(2) $i_b$ (fraction, of bed material).

(3) d, ft, (average flow depth).

(4) B, ft, (top width).

(5) U, fps, (average velocity).

(6) $q_{T1}$, tons/day-ft, (incorrect sediment discharge per unit width by assuming the bed is composed entirely of one sand of size D) for a given U, D, and d.

(7) $k_1 = f(d,T)$ (correction factor for temperature).

(8) $k_2 = f(d,C_f)$ (correction factor for fine sediment).

(9) $k_3 = f(D)$ (correction factor for sediment size).

(10) $q_T = [1 + (k_1 k_2 - 1)\ 0.01\ k_3]\ q_{T1}$, tons/day-ft, (corrected bed material discharge per unit width by assuming the bed is composed entirely of one sand of size D).

(11) $i_b q_T$, tons/day-ft, (bed material discharge per unit width for a size fraction).

(12) $i_B Q_T = B\ i_b q_T$, tons/day, (bed material discharge for a size fraction for entire cross section).

(13) $\Sigma i_B Q_T$, tons/day, (bed material discharge for all size fractions for entire cross section.

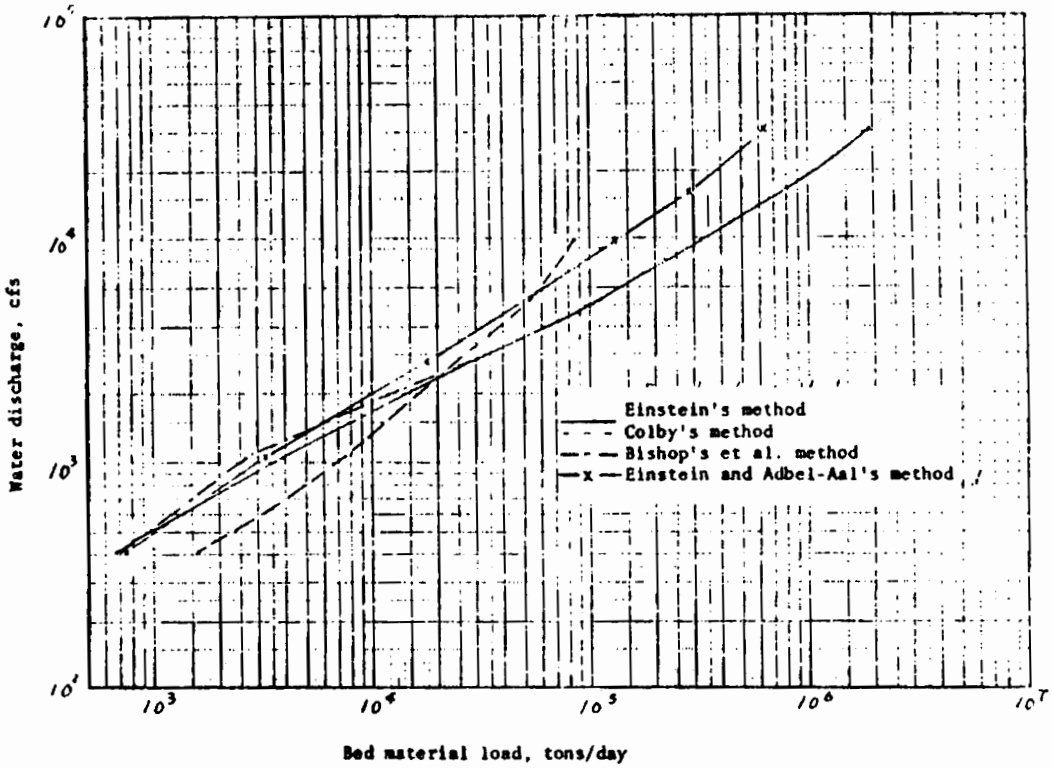


Figure 7-22. Water discharge compared with bed material discharge for sample problem.

Table 7-7. Bed material discharge calculations for sample problem by applying the Bishop et al. method.[1]

| $R_b'$ | B | $\psi'$ | $\phi_T$ | $q_T$ | $Q_T$ |
|---|---|---|---|---|---|
| 1 | 2 | 3 | 4 | 5 | 6 |
| 0.5 | 103 | 2.98 | 3.9 | 0.16 | 712 |
| 1.0 | 136 | 1.49 | 11. | 0.45 | 2,640 |
| 1.5 | 170 | 0.75 | 100. | 4.09 | 30,000 |

[1]See the following for explanation of symbol, column by column.

(1) $R_b'$ , ft, (bed hydraulic radius due to grain roughness), given in Table 7-3.

(2) B , ft, (top width), given in Table 7-3.

(3) $\psi' = \frac{\rho_s - \rho}{\rho} \frac{D_{35}}{R_b' S}$ (intensity of shear on particle), given by Equation 7-109.

(4) $\phi_T = f(\psi')$(intensity of bed material transport), given in Figure 7-20.

(5) $q_T = \phi_T \gamma_s \sqrt{g D_{50}^3 (\rho_s - \rho)/\rho}$ , lbs/sec-ft, (bed material discharge per unit width of stream), given by Equation 7-110.

(6) $Q_T = 43.2 \; B q_T$ , tons/day, (bed material discharge for entire cross section).

Einstein and Abedl-Aal's method considers the effect of suspended sediment on the turbulent intensity. According to this method suspended sediment damps turbulence, changes distribution of velocity and sediment concentration, and thus reduces transport capacity of flow. Application of this method is quite similar to the Einstein procedure except that the von Kármán constant $\kappa$ is a variable rather than a constant. Since more emphasis is placed on suspended sediment effects, the calculated results from Einstein and Abdel-Aal's method are more consistent than those from Einstein's method. Because the Bishop method and Einstein method mainly rely on the same principles, their results show good agreement. Bishop's method does give good results for flumes, canals and small sand-bed rivers and it is simple to apply. However, in general the Colby method is considered to be the most suitable model for this type problem.

## Calculation of Total Sediment Discharge from Stream Measurements

Once suspended load samples and other required data have been obtained, total sediment discharge can be calculated by the modified Einstein method (Colby and Hembree, 1955), the Colby method (1957), the Toffaleti method (1969), and others. A sample problem prepared by the Sedimentation Section of the Bureau of Reclamation (1955) is solved by the modified Einstein method and the Colby method. Details of the procedure follows.

## Calculation of Total Sediment Discharge by the Modified Einstein Procedure

### Example G

The basic data required for computations are water discharge $Q_2$= 230 cfs, mean velocity U = 2.08 fps, cross sectional area A = 111 $ft^2$, mean depth at the vertical where samples were taken $d_v$ = 1.22 ft (for most cases d and $d_v$ are very nearly the same), stream width B = 113 ft, water temperature T = 64°F, sampled mean sediment concentration, $C'_s$ = 262 ppm (by weight), a' = 0.3 ft (for hand sampler), and size distribution of the suspended sediment samples $i_s$ and size distribution of bed material samples $i_b$ are given in Table 7-8.

Although it is convenient to summarize the calculations in table form, some steps need further explanation because of the trial and error procedures. Computational sequence is computation of SR' and $P_m$, computation of $i_{bw}Q_{bw}$ (Table 7-9, col. 1-6), and computation of total sediment discharge (Table 7-9, (col. 7-19). In applying this method z' of col. 9 is determind by the trial and error procedure described later.

### Computation of SR' and $P_m$.

The logarithmic velocity distribution formula utilized is

$$\sqrt{SR'} = \frac{U}{5.75\sqrt{g}\log\left[\frac{12.27 \times d}{D_{65}}\right]} \qquad (7\text{-}131)$$

Table 7-8. Size distribution for sample problem.

| Size fraction (mm) | Average grain size | | | | Fall velocity w (fps) |
|---|---|---|---|---|---|
| | D(mm) | D(ft) | $i_s$(%) | $i_b$(%) | |
| 0.002 -0.0625 | 0.011 | 0.000036 | 22 | | 0.000296 |
| 0.0625-0.125 | 0.0884 | 0.00029 | 25 | | 0.0189 |
| 0.125-0.250 | 0.177 | 0.00058 | 42 | 38 | 0.0650 |
| 0.250-0.500 | 0.354 | 0.00116 | 11 | 50 | 0.151 |
| 0.500-1.000 | 0.707 | 0.00232 | | 5 | 0.258 |
| 1.000 -2.000 | 1.41 | 0.00464 | | 1 | 0.394 |
| 2.000 -4.000 | 2.83 | 0.00926 | | 1 | 0.574 |

$D_{65}$ = 0.00105 ft; $D_{35}$ = 0.00075 ft

where d = A/B = 0.98 ft. In Equation 7-131, the quantities $\sqrt{SR'}$ and x are unknown and will be determined by a trial and error procedure based on the additional relation shown in Figure 7-2. Assuming that x = 1.54, then from Equation 7-131

1. $\sqrt{SR'} = 0.0150\ (ft)^{1/2}$

2. $U_*' = \sqrt{gSR'} = 0.0851$ fps

3. $\delta = \frac{11.6\nu}{U_*'} = 0.00154$, for $\nu = 1.14 \times 10^{-5} ft^2/sec$

4. $k_s/\delta = D_{65}/\delta' = 0.695$ and

5. From Fig. 2, $x = f(k_s/\delta) = 1.54$.

No recomputation is necessary since the computed value is the same as the assumed value. Otherwise, steps 1 through 5 are repeated until agreement of assumed and computed values of x is achieved.

From Equation 7-116

$$P_m = 2.3 \log \frac{30.2 \times d}{D_{65}} = 10.7$$

As an alternative a graphical method was suggested by Colby and Hubbell (1961) for computation of SR' and $P_m$.

Computation of z' (for col. 9, Table 7-9)

The suspended-load exponent z' for a size fraction is calculated by trial and error so that Equation 7-124 is balanced. The procedure suggested by Colby and Hubbell (1961), Colby and Hembree (1955), and Lara (1966) are followed.

According to Colby and Hembree the z' value for dominant grain size of suspended load is calculated and the value of $z_i'$ for the other

Table 7-9. Total sediment discharge calculations by applying the modified Einstein procedure.

| Computation of $i_{Bw}Q_{bw}$ | | | | | | Total Sediment Discharge Computation | | | | | | | | | | | |
|---|---|---|---|---|---|---|---|---|---|---|---|---|---|---|---|---|---|
| $10^3D$ | $10^2i_b$ | $\psi$ | $\phi_*/2$ | $i_{Bw}q_{bw}$ | $i_{Bw}Q_{bw}$ | $10^2i_s$ | $Q'_s$ | $z'$ | E | $J_1$ | $-J_2$ | $J'_1$ | $-J'_2$ | $\frac{P_mJ_1+J_2}{P_mJ_1'+J_2'}$ | $I_1$ | $-I_2$ | $P_mI_1+I_2+1$ | $i_TQ_T$ |
| 1 | 2 | 3 | 4 | 5 | 6 | 7 | 8 | 9 | 10 | 11 | 12 | 13 | 14 | 15 | 16 | 17 | 18 | 19 |
| 0.036 | | | | | | 22 | 29 | 0.016 | 0.000074 | 1.00 | 1.03 | 0.75 | 0.40 | 1.27 | | | | 37 |
| 0.29 | | | | | | 25 | 32 | 0.33 | 0.00059 | 1.20 | 2.08 | 0.64 | 0.43 | 1.68 | | | | 54 |
| 0.58 | 38 | 5.50 | 0.255 | 0.00163 | 7.96 | 42 | 55 | 0.73 | 0.00118 | | | | | | 2.92 | 8.40 | 23.82 | 189 |
| 1.16 | 50 | 5.50 | 0.255 | 0.00605 | 29.54 | 11 | 14 | 1.34 | 0.00237 | | | | | | 0.51 | 2.13 | 4.33 | 128 |
| 2.32 | 5 | 6.80 | 0.147 | 0.000988 | 4.82 | | | 1.97 | 0.00474 | | | | | | 0.21 | 0.93 | 2.32 | 11 |
| 4.64 | 1 | 13.6 | 0.0122 | 0.000046 | 0.22 | | | 2.62 | 0.00947 | | | | | | 0.12 | 0.53 | 1.75 | |
| 9.26 | 1 | 27.2 | | | | | | | | | | | | | | | | |
| Total | 95 | | | | 42.54 | 100 | 130 | | | | | | | | | | | 419 |

[1]See the following for explanation of symbols, column by column:

(1) D, ft, (representative grain size).

(2) $i_b$ (fraction of bed material).

(3) $\psi$ (intensity of shear on particle), $\psi = \frac{\rho_s-\rho}{\rho}\frac{D_{35}}{R'S}$,

or $\psi = 0.4\frac{\rho_s-\rho}{\rho}\frac{D_i}{R'S}$,

where R'S is calculated from Step A; use larger $\psi$ value.

(4) $\phi_* = f(\psi)$ (intensity of sediment transport) with $\psi$ replacing $\psi_*$.

(5) $i_{Bw}q_{bw} = \frac{1}{2}\phi_* i_b\gamma_s\sqrt{\frac{\gamma s}{\gamma}-1}\sqrt{gD_i^3}$, lbs/sec-ft, (bed load discharge per unit width for a size fraction), given by

(6) $i_{Bw}Q_{bw} = 43.2\ B\ i_{Bw}q_{bw}$, tons/day, (bed load discharge for a size fraction for entire cross section).

(7) $i_s$ (fraction of suspended samples).

(8) $Q'_{si} = 43.2\ B\ q'_{Si} = 43.2\ B\ i_s\gamma C'_s Q[(1-E') - 2.3\frac{E'\log E'}{P_m-1}$

the sample zone, where $E' = a'/d_v$, and $P_m$ is given.

(9) z' (exponent for concentration distribution).

(10) $E = 2\frac{D}{d}$ (ratio of thickness of bed layer to mean depth).

(11) $J_1 = f(E,z')$ (integral).

(12) $J_2 = f(E,z')$ (integral).

(13) $J'_1 = f(E',z')$ (integral).

(14) $J'_2 = f(E',z')$ (integral).

(15) $P_mJ_1+J_2/(P_mJ'_1+J'_2)$.

(16) $I_1 = f(E,z')$ (integral).

(17) $I_2 = f(E,z')$ (integral).

(18) $P_mI_1+I_2+1$.

(19) $i_TQ_T$, tons/day, (total sediment discharge for a size fraction for entire cross section),

$i_TQ_T = Q'_{si}\frac{P_mJ_1+J_2}{P_mJ'_1+J'_2}$, for fine sediment.

$i_TQ_T = i_{Bw}Q_{bw}(P_mI_1+I_2+1)$, for coarse sediment.

size fractions are related to $z'$ by the 0.7 power of the fall velocities of the respective size fractions or by Equation 7-125. The trial and error graphical method for computation of $z'$, based on the properties of Equation 7-124 that was established by Colby and Hubbell (1961), is followed

1. The dominant grain size $D_1$ is selected. In this example $D_1 = 0.00058$ ft.

2. The d' value is computed; $d' = d \frac{0.00058}{D_1} = 0.98$ ft (cf. Figure 7-23).

3. The quantity $Q'_s/i_{Bw}Q_{bw} = 55/7.96 = 6.9$.

4. An approximation of the correct $z'$ value is taken from Figure 7-23a for the known $d'$ and $Q'_s/i_{Bw}Q_{bw}$ (Points A and B), which gives $z' = 0.79$.

5. For $E' = a'/d_y = 0.25$ and $z' = 0.79$ (Point C), the value $10\,J'_1 + J'_2 = 5.7$ is found from Figure 7-22b. Then

   $P_m J'_1 + J'_2 \cong P_m \left(\frac{10J'_1 + J'_2}{10}\right) = \frac{10.7 \times 5.7}{10} = 6.1$, which is the

   location of D on Figure 7-23b.

6. Point E locates a reference point where $10\,J'_1 + J'_2 = 8.0$. The distance D-E is determined and the same distance is measured from A to F in Figure 7-23a. (If point D is to the left of point E, point F is to the right of point A, and vice versa).

7. A vertical line through point F intersects a line for $d' = 0.98$ ft at point G, for which $z' = 0.76$. The difference between 0.76 and the first estimate of 0.79 is so small that no recheck is necessary. Otherwise, this new $z'$ value is used and steps 5 through 7 are repeated to obtain an accurate $z'_1$.

The $z'_1$ for the other size fractions is calculated by Equation 7-125

$$\frac{z'_i}{z'_1} = \left(\frac{w_i}{w_1}\right)^{0.7}$$

Additional values of $z'_1$ are listed in col. 9 of Table 7-9.

Lara (1966) found that the $z'$ value determined by the above equation was not always representative. His procedure follows

1. At least three size fractions which have significant quantities in both the suspended and bed loads are selected.

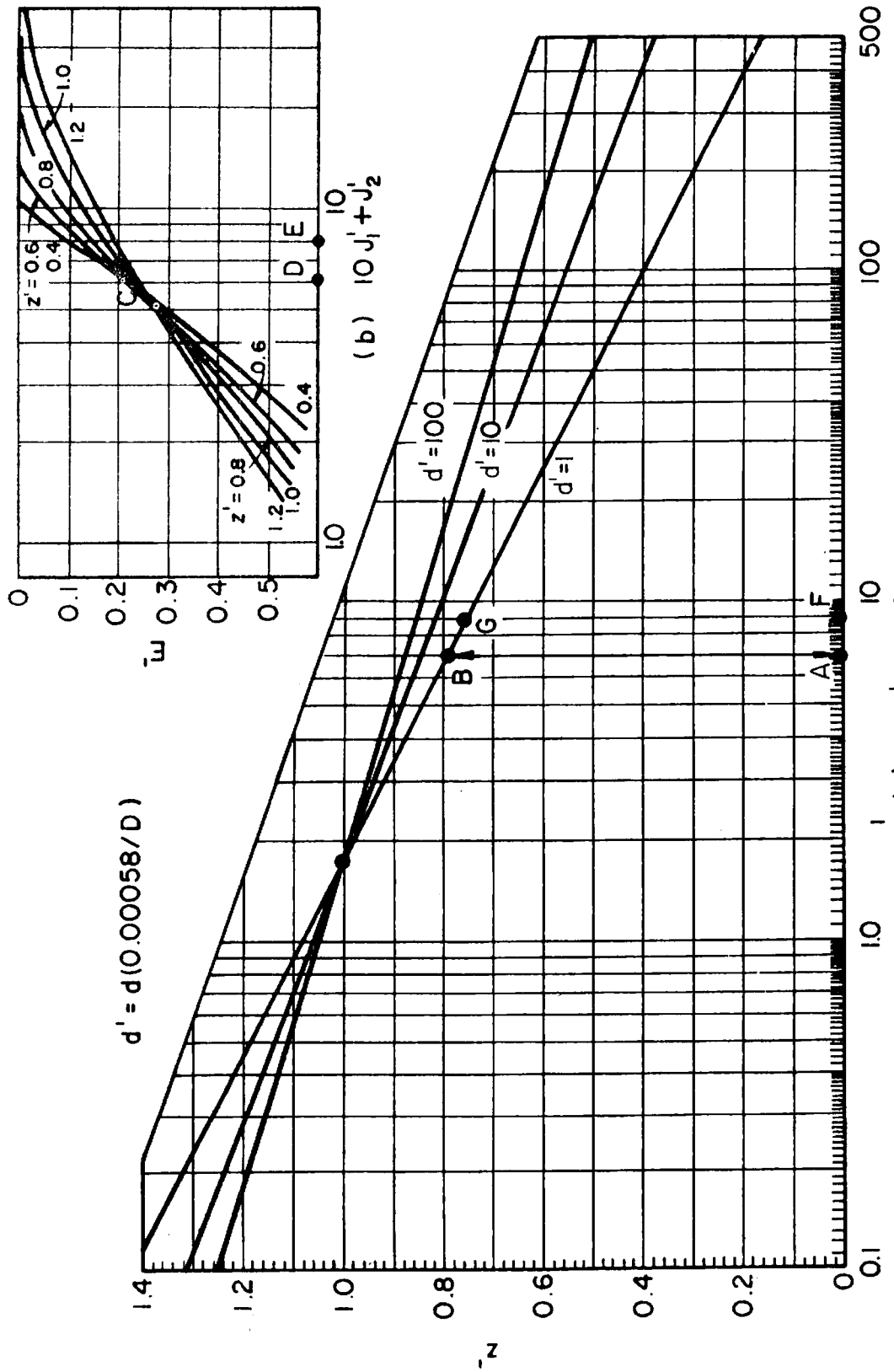


Figure 7-23. Nomograph for computing z' from $\frac{Q'_s}{i_{Bw}Q_{bw}} = \frac{I_1}{J_1}(P_m J'_1 + J'_2)$ (after Colby and Hubbell, 1961).

2. The $z_i'$ values for these fractions are found by applying Colby and Hubbell's procedure (Figure 7-23) as many times as required.

3. These calculated $z_i'$ values are plotted on the logarithmic paper as a function of the fall velocity w. A relation

$$z' = aw^b$$

that fits the plot can be found by the method of least squares or simply by eye. From this relationship $z_i'$ values can be determined for the other size ranges.

Lara's method for computing z' is preferred over Colby and Hembree's method. However, in this sample problem only two size fractions have significant quantities in both the suspended and bed loads. Thus, Colby and Hembree's method was utilized.

Calculation of Total Sediment Discharge by the Colby Method

Example H

Colby's (1957) method is used to compute the total sediment discharge of the sample problem solved by the modified Einstein procedure. The required data are 1) U = 2.08 fps, 2) B = 113 ft, 3) d = 0.98 ft, and 4) $C_S'$ = 262 ppm. The procedure follows

1. $q_{us}'$ = 3.1 tons/day-ft for the given velocity (Figure 7-24)

2. $C_r$ = 700 ppm for the given velocity and depth (Figure 7-25)

3. the correction factor = 0.72 for the availability ratio $C_s'/C_r$ = 262/700 = 0.374 (mean line of Figure 7-26)

4. The total unmeasured sediment discharge

$$Q_{us} = q_{us}' \times \text{correction factor} \times B$$

$$= 3.1 \times 0.72 \times 113 = 252 \text{ tons/day.}$$

5. The total sediment discharge is

$$Q_T = 43.2\ \gamma C_s' Q + Q_{us}$$

$$= 163 + 252 = 415 \text{ tons/day.}$$

The agreement between results calculated by the modified Einstein method and the Colby method is good. It is clear that the Colby method is much simpler than the modified Einstein method. However, Colby's method does not break down the sediment discharge into size fractions but as previously suggested analysis by fractions using the Colby method is possible even though not suggested by Colby.

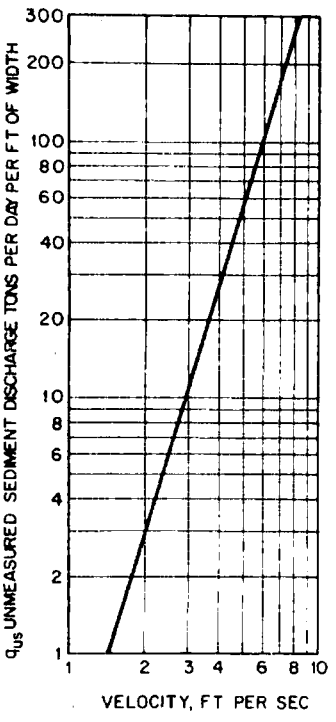


Figure 7-24. Relationship between unmeasured sediment discharge mean velocity (after Colby, 1957).

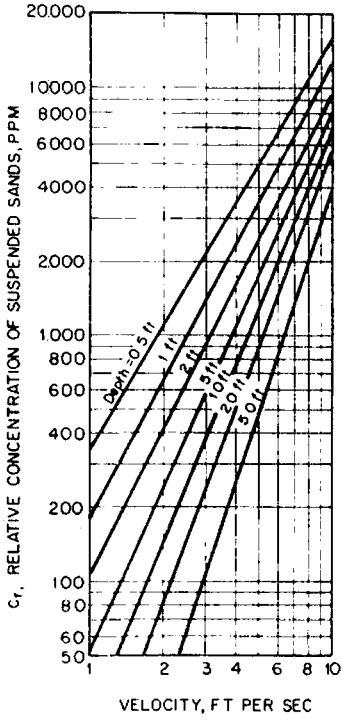


Figure 7-25. Relative concentrations of suspended sands for different depths and mean velocity (after Colby, 1957).

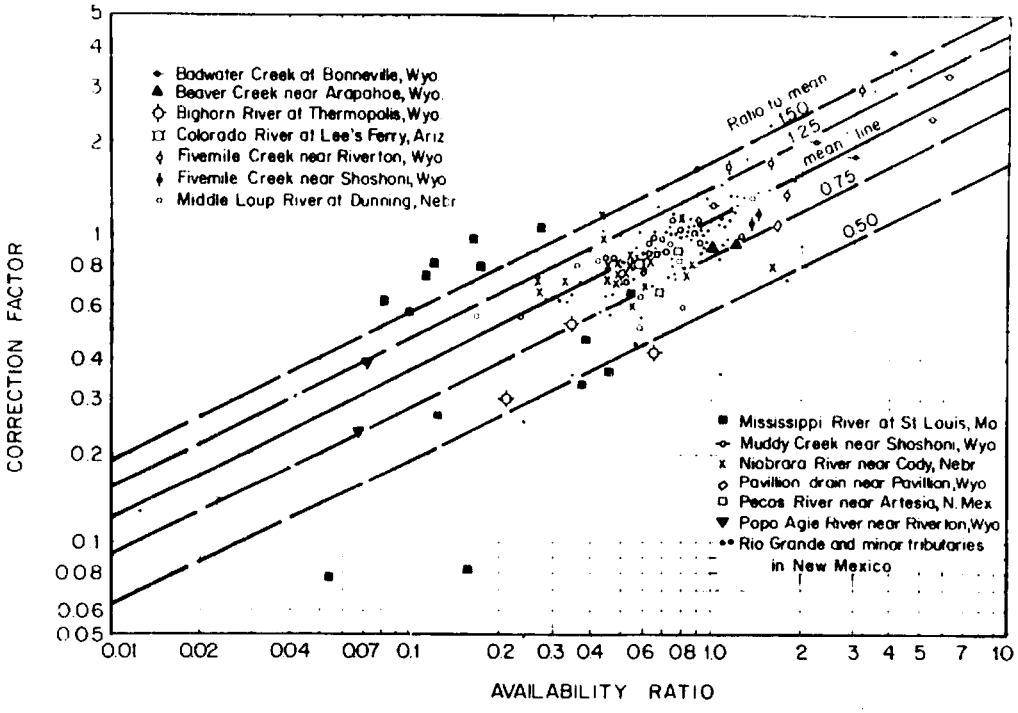


Figure 7-26. Variation of unmeasured sediment discharge adjusted for mean velocity with a measure of the availability of sands (after Colby, 1957).

## REFERENCES

Bishop, A. A., Simons, D. B., and Richardson, E. V., 1965, "Total Bed-Material Transport," J. of the Hydraulics Div., ASCE, Vol. 91, No. HY2, Mar., pp. 175-191.

Blench, T., 1966, "Mobile-Bed Fluviology," Dept. of Tech. Services, University of Alberta, Alb., Canada.

Colby, B. R., 1957, "Relationship of Unmeasured Sediment Discharge to Mean Velocity," Transactions, Amer. Geophy. Union, Vol. 38, No. 5, Oct., pp. 708-719.

Colby, B. R., 1964, "Practical Computations of Bed-Material Discharge," J. of the Hydraulics Div., ASCE, Vol. 90, No. HY2.

Colby, B. R., and Hembree, C. H., 1955, "Computation of Total Sediment Discharge, Niobrara River near Cody, Nebraska," U.S. Geol. Survey, Water Supply Paper 1357.

Colby, B. R., and Hubbell, D. W., 1961, "Simplified Methods for Computing Total Sediment Discharge with the Modified Einstein Procedure," U.S. Geol. Survey Water-Supply Paper 1593, 17 p.

DuBoys, M. P., 1879, "Etudes du Regime et Laction Exercee par les Eaux sur un Lit a Fond De Graviers Indefiniment Affouilable," Annales de Ponts et Chausses, Ser. 5, Vol. 18, pp. 141-195.

Einstein, H. A., 1937, "Der Geschiebetrieb als Wahrscheinlich-Keits Problem (the Bed-Load Movement as a Probability Problem)," Verlag Rascher, Zurich, 110 p.

Einstein, H. A., 1942, "Formulas for the Transportation of Bed-Load," Transactions, ASCE, Vol. 107.

Einstein, H. A., 1950, "The Bed-Load Function for Sediment Transportation in Open Channel Flows," U.S. Dept. Agric., Soil Conserv. Serv., T. B. No. 1026.

Einstein, H. A., and Abdel-Aal, F. M., 1972, "Einstein Bed-Load Function at High Sediment Rates," J. of the Hydraulics Div., ASCE, Vol. 98, No. HY1, Jan., pp. 137-152.

Einstein, H. A., and El-Samni, E. S., 1949, "Hydrodynamic Forces on a Rough Wall," Rev. Mod. Phys., Vol. 21, No. 3.

Englelund, F., and Hansen, E., 1967, "A Monograph on Sediment Transport in Alluvial Stream," Teknisk Vorlag, Copenhagen.

Exner, F. M., 1925, "Uber die Wechselwirkung zwischen Wasser und Geschiebe in Flussen," Sitzber, Akad. Wiss. Wien, Pt. IIa, Bd. 134.

Frijlink, H. C., and Elzerman, J. J., 1961, "Present State of the Investigations on Bedload Movement in Holland," Internationale d'Hydrólogie Scientifique, Assembleé Genéral de Druxelle.

Gilbert, K. G., 1914, "The Transportation of Debris by Running Water," U.S. Geol. Survey, Prof. Paper 86.

Grigg, N. S., 1969, "Motion of Single Particles in Sand Channels," U.S. Geol. Survey, Water Resources Div., Open File Report, Fort Collins, Colorado, p. 142.

Hubbell, D. W., and Sayre, W. W., 1964, "Sand Transport Studies with Radioactive Tracers," J. of the Hydraulics Div., ASCE, Vol. 90, No. HY3.

Kalinske, A. A., 1942, "Criteria for Determining Sand-Transport by Surface-Creep and Saltation," Transactions, Amer. Geoph. Union, Vol. 23, Pt. 2.

Lara, J. M., 1966, "Change in the Modified Einstein Procedure to Compute 'Z'," Sedimentation Sec., Hydrol. Branch, Bureau of Reclamation, U.S. Dept. of the Interior.

Laursen, E. M., 1956, "The Application of Sediment Transport Mechanics to Stable Channel Design," J. of the Hydraulics Div., ASCE, Vol. 82, No. HY4.

Laursen, E. M., 1958, "The Total Sediment Load of Streams," J. of the Hydraulics Div., ASCE, Vol. 84, No. HY1.

Meyer-Peter, E., Favre, H., and Einstein, A., 1934, "Neuere Versuchsresultate uber den Geschiebetrieb," Schweiz Bauzeitung, Vol. 103, No. 13.

Meyer-Peter, E., and Mûller, R., 1948, "Formulas for Bedload Transport," Proceedings, 3rd Meeting of Intern. Assoc. Hydra. Res., Stockholm, pp. 39-64.

Rouse, H., 1937, "Modern Conceptions of the Mechanics of Turbulence," Transactions, ASCE, Vol. 102.

Rubey, W. W., 1933, "Equilibrium-Conditions in Debris-Laden Streams," Transactions, Amer. Geophy. Union.

Sayre, W. W., and Conover, W. J., 1967, "General Two-Dimensional Stochastic Model for the Transport and Dispersion of Bed Material Sediment Particles," Proceedings, 12th Congress of Intern. Assoc. Hydra. Res., Fort Collins, Colorado.

Sayre, W. W., and Hubbell, D. W., 1965, "Transport and Dispersion of Labeled Bed Material--North Loup River, Nebraska," U.S. Geol. Survey Prof. Paper 433-C.

Schoklitsch, A., 1930, "Handbuch des Wasserbaues," Springer Vienna (2nd ed., 1950), English Translation (1937) by S. Shulits.

Schoklitsch, A., 1934, "Geschiebetrieb und die Geschiebefracht," Wasserkraft and Wasserwirtsch, Jgg. 39, Heft 4.

Schroeder, K. B., and Hembree, C. H., 1956, "Application of the Modified Einstein Procedure for Calculation of Total Sediment Load," Transactions, Amer. Geophy. Union, Vol. 37, No. 2, Apr., pp. 197-212.

Shen, H. W., 1971, "Wash Load and Bed Load," 1971, River Mechanics, Edited by H. W. Shen, Chapter 11, Fort Collins, Colorado, 30 p.

Shen, H. W., and Hung, C. S., 1971, "An Engineering Approach to Total Bed Mateial Load by Regression Analysis," Proceedings, Sedimentation Sym., Berkeley.

Shen, H. W., and Todorovic, P., 1971, "A General Stochastic Model for the Transport of Sediment Bed Material," presented at Intern. Sym. on Stochastic Hydraulics, University of Pittsburgh, Pennsylvania, May 31-June 2.

Simons, D. B., 1967, "River Hydraulics," Proceedings, 12th Congress of Intern. Assoc. Hydra. Res., Vol. 5, Fort Collins, Colorado.

Simons, D. B., Richardson, E. V., and Nordin, C. F., Jr., 1965, Bedload Equation for Ripples and Dunes," U.S. Geol. Survey Prof., Paper 462-H, 9 p.

Stall, J. B., Rupani, N. L., and Kandaswamy, P. K., 1958, "Sediment Transport in Money Creek," J. of the Hydraulics Div., ASCE, Vol. 84, No. HY1.

Task Committee on Preparation of Sedimentation Manual, 1970, "Chapter IV: Sediment Sources and Sediment Yields," J. of the Hydraulics Div., ASCE, Vol. 96, No. HY6, June, pp. 1283-1330.

Task Committee for Preparation of Sedimentation Manual, 1971, "Sediment Transportation Mechanics: H. Sediment Discharge Formulas," J. of the Hydraulics Div., ASCE, Vol. 97, No. HY4, Apr., pp. 523-567.

Toffaleti, F. B., 1969, "Definitive Computations of Sand Discharge in Rivers," J. of the Hydraulics Div., ASCE, Vol. 95, No. HY1, Jan., pp. 225-246.

Vanoni, V. A., 1941, "Some Experiments on the Transportation of Suspended Loads," Transactions, Amer. Geophy. Union, Vol. 20, Pt. 3, pp. 608-621.

Vanoni, V. A., Brooks, N. H., and Kennedy, J. F., 1960, "Lecture Notes on Sediment Transportation and Channel Stability," W. M. Keck Lab. of Hydraulics and Water Resources, California Inst. Techn., Rept. No. KH-R-1.

Yang, T., 1968, "Sand Dispersion in a Laboratory Flume," Ph.D. dissertation, Dept. of Civil Eng., Colorado State University, Fort Collins, Colorado.

# APPENDIX 7A

## 7A.1 SIZE FREQUENCY DISTRIBUTION

The most commonly used method to determine size frequency is mechanical or sieve analysis. In general the results are presented as cumulative size frequency curves. The fraction or percentage by weight of a sediment that is smaller or larger than a given size is plotted against particle size. From the size frequency curve it is possible to obtain:

$D_{35}$ is the size of sediment for which 35 percent of the sampler is finer. This size was specified by Einstein as a representative grain size of the sediment mixture.

$D_{40}$ is the size used by Schoklitsch to represent the mixture.

$D_{50}$ is the median diameter. It is naturally assumed that this size represents the sediment mixture. Shields used the $D_{50}$ size in his analysis of beginning of motion.

Physical evidence does not conclusively fix the size that represents a given sediment mixture. The choice is rather arbitrary.

$D_{65}$ is the size used by Einstein to express the roughness of a sediment mixture. It is also used by Sentürk (cf. Chapter 6, Simons and Sentürk, 1977) to represent the roughness in resistance formulas.

$D_{90}$ is the size chosen by Meyer-Peter and Müller to represent the roughness of a sediment mixture.

$D_{85}$ is the size used by Simons and Richardson in the formulas they established for the computation of the resistance to flow in sand bed channels.

$D_{84.1}$ and $D_{15.9}$ are the sizes derived from a probabilistic analysis. These sizes are used to define the geometric mean size and the gradation of the material.

$D_g$ is the geometric mean size (*).

$D_m$ is the mean diameter given by:

$$D_m = \frac{\Sigma \Delta_i D_i}{100} \qquad (7A\text{-}1)$$

(*)Will be explained later in this section.

where $\Delta i$ represents any portion of the percentages shown on the y-axis of Figure 7A-1 and $D_i$ represents the mean value of the sizes established by the extreme values of the interval $\Delta_i$. According to Figure 7A-1, $D_m$ is computed as follows

$$D_m = \frac{\Delta_1 D_1 + \Delta_2 D_2 + \Delta_3 D_3 + \ldots + \Delta_6 D_6}{100}$$

in which $D_m$ represents the mean size of the sample. In fact, the value of $D_m$ defined by Equation 7A-1 identifies the separation point between the two shaded areas in Figure 7A-1. It should not be assumed that the particle measure $D_m$ represents the hydraulic properties of the sediment mixture. The hydraulic properties of a sand mixture are related to: 1) the resistance to flow due to skin friction, and 2) the threshold condition which defines the beginning of transport. For each of these hydraulic properties the sand mixture reacts differently. If the beginning of motion is to be investigated, the sand particle representing the whole mixture may have a different size from the size that is important when evaluating resistance to flow of the mixture. Such representative sand sizes may be defined according to geometry of the size distribution diagram that describes the sand mixture.

The sediment size frequency distribution is essentially a probabilistic approach used to aid in describing the transported sediment and sediment mixture forming the bed of a river. Engineers most often express particle size by subgroups or intervals of sizes. The probability structure of such groupings may or may not follow the normal (Gaussian law). Sediment mixtures are affected by natural phenomena such as precipitation, floods, diversions, etc. It is possible to consider the effects of such phenomena on the characteristics of sediment and hence on canals and rivers.

A histogram or frequency pyramid (Figure 7A-2a) is a graphical method of representing size distribution. If the mathematical model can be visualized using graphics, it is easier to comprehend and if the grahics can be reduced to straight lines the results are simplier to apply.

Construction of a histogram that defines natural sorted sediments involves plotting sizes representing class intervals on the abscissa and the actual concentration or percent (by number, volume, or weight) of the total sample contained in each class interval on the ordinate (A-2a). If the class intervals are small, the histogram approaches a continuous curve. Choice of intervals depends on the sieves series chosen for mechanical analysis. Intervals provided in Table 7A-1 may be utilized.

If ordinates of successive classes are added and plotted successively against abscissa values, a cumulative distribution curve is obtained (Figure 7A-2b).

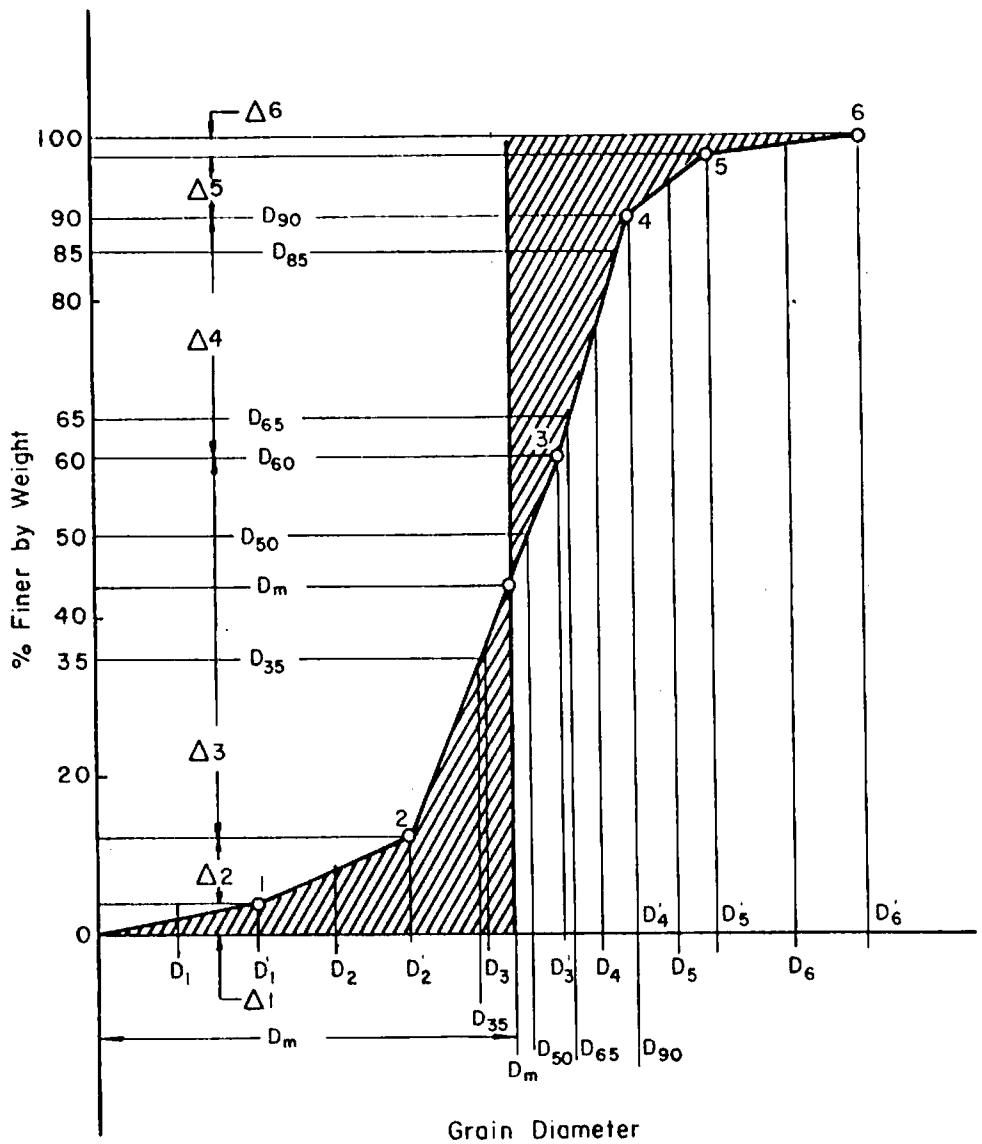


Figure 7A-1. Size frequency distribution curve showing $D_m$, $D_{35}$, $D_{50}$, $D_{65}$, $D_{85}$, and $D_{90}$.

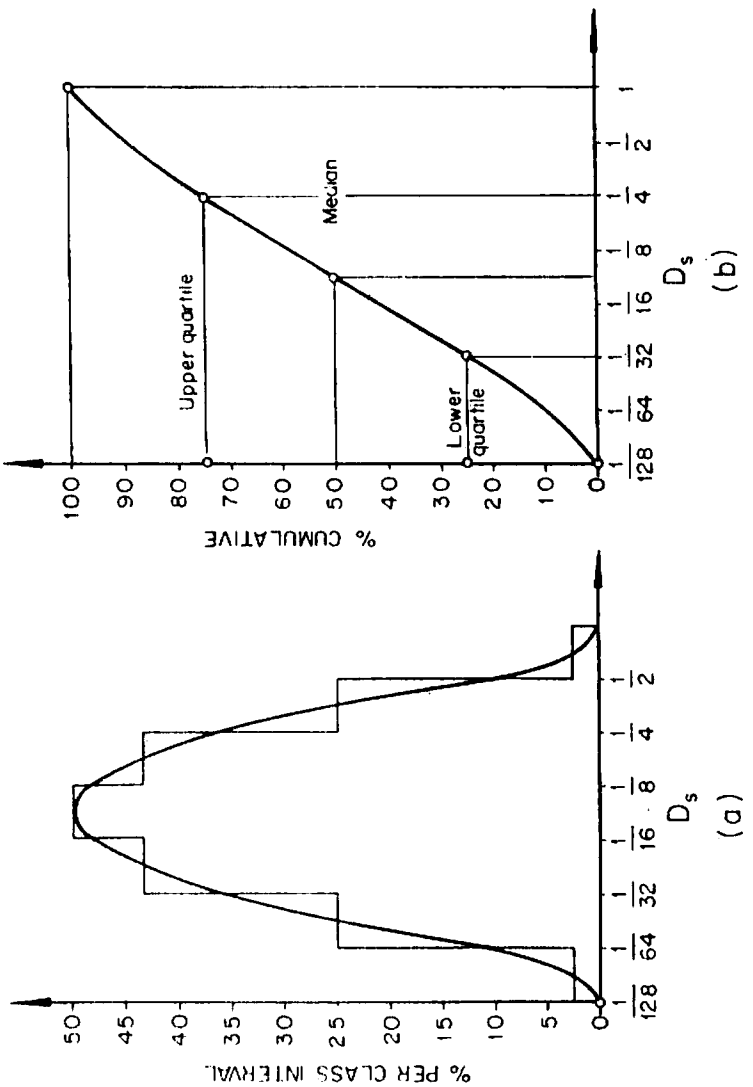


Figure 7A-2. Frequency curves.

TABLE 7A-1.
CALCULATION OF $\bar{x}$ AND $\sigma$ FOR SAMPLE OF n ITEMS OF GROUPED DATA

| % | Class Interval | Midpoint $x_i$ | Frequency $f_i(x)$ | $f_i(x)x_i$ | $f_i(x)x_i^2$ | $x_i-\bar{x}$ |
|---|---|---|---|---|---|---|
| 0 | 0.03 | 0.066 | 1 | 0.066 | $4.356 \times 10^{-3}$ | 0.1087 |
| 10 | 0.102 | 0.116 | 1 | 0.116 | $13.456 \times 10^{-3}$ | 0.0587 |
| 20 | 0.130 | 0.140 | 1 | 0.140 | $19.600 \times 10^{-3}$ | 0.0347 |
| 30 | 0.150 | 0.160 | 1 | 0.160 | $25.600 \times 10^{-3}$ | 0.0147 |
| 40 | 0.170 | 0.175 | 1 | 0.175 | $30.625 \times 10^{-3}$ | 0.0003 |
| 50 | 0.180 | 0.185 | 1 | 0.185 | $34.225 \times 10^{-3}$ | 0.0103 |
| 60 | 0.190 | 0.195 | 1 | 0.195 | $38.025 \times 10^{-3}$ | 0.0203 |
| 70 | 0.200 | 0.205 | 1 | 0.205 | $42.025 \times 10^{-3}$ | 0.0303 |
| 80 | 0.210 | 0.230 | 1 | 0.230 | $52.900 \times 10^{-3}$ | 0.0553 |
| 90 | 0.250 | 0.275 | 1 | 0.275 | $75.625 \times 10^{-3}$ | 0.1003 |
| 100 | 0.300 | | | | | |
| | | | n = 10 | $\Sigma f_i(x)x_i = 1.747$ | $\Sigma f_i(x)x_i^2 = 336.437 \times 10^{-3}$ | 0.4336 |

A mathematical model may be chosen to represent this curve. Experimental analysis shows that a similarity exists between the cumulative distribution diagram of Figure 7A-2 and the CDF (cumulative distribution function) of the standardized normal (Gaussian) distribution:

$$F_u(u) = \int_{-\infty}^{u} f_u(u)\, du$$

Distribution of particle size usually follows this relation. Einstein (1950) used this function to help explain the motion of particles on the bed of an alluvial channel.

The next step is to transform this curve to a straight line. Figure 7A-3 illustrates the use of normal probability paper as a means of transformation (Benjamin and Cornell, 1970). Characteristics of the CDF are such that between the ordinates 0.8413 and 0.1587 the normal distribution can be approximated by a straight line. The fifty percent value of the ordinate is midway between these two values. The diameter corresponding to the fifty percent ordinate is called the geometric mean size. The $D_{84.13}$ and $D_{15.87}$ sizes are equidistant from $D_g$. This distance is the standard deviation $\sigma_g$ and is given by

$$2 \log \sigma_g = \log D_{84.1} - \log D_{15.9}$$

from which

$$\sigma_g = \left(\frac{D_{84.1}}{D_{15.9}}\right)^{1/2} \qquad (7A\text{-}2)$$

or

$$\log \sigma_g = \log D_{84.1} - \log D_g = \log D_g - \log D_{15.9}$$

and

$$\sigma_g = \frac{D_{84.1}}{Dg} = \frac{D_g}{D_{15.9}} \ (*) \qquad (7A\text{-}3)$$

In general the straight line representing the CDF crosses the mechanical analysis curve at a diameter slightly different from $D_{84.1}$ or $D_{15.9}$. To compensate for this discrepancy a gradation coefficient is defined

$$G = \frac{1}{2}\left(\frac{84.1}{D_{50}} + \frac{50}{D_{15.9}}\right) \qquad (7A\text{-}4)$$

(cf. Example A-1 for the use of G). After $\sigma_g$ and $D_g$ are determined the representative line can be located on probability paper and $D_{35}$, $D_{65}$, etc. can be determined. The method explained above is only applicable to S-shaped size distribution curves. Those performing this graphical analysis should be cognizant of this important point.

(*)The value $D_g$ corresponds to $D_{50}$ only if the size distribution plots as a well-formed S curve. For this case $D_{50} = D_g$ and

$$\sigma_g = \frac{D_{84.1}}{D_{50}} = \frac{D_{50}}{D_{15.9}} \qquad (7A\text{-}5)$$

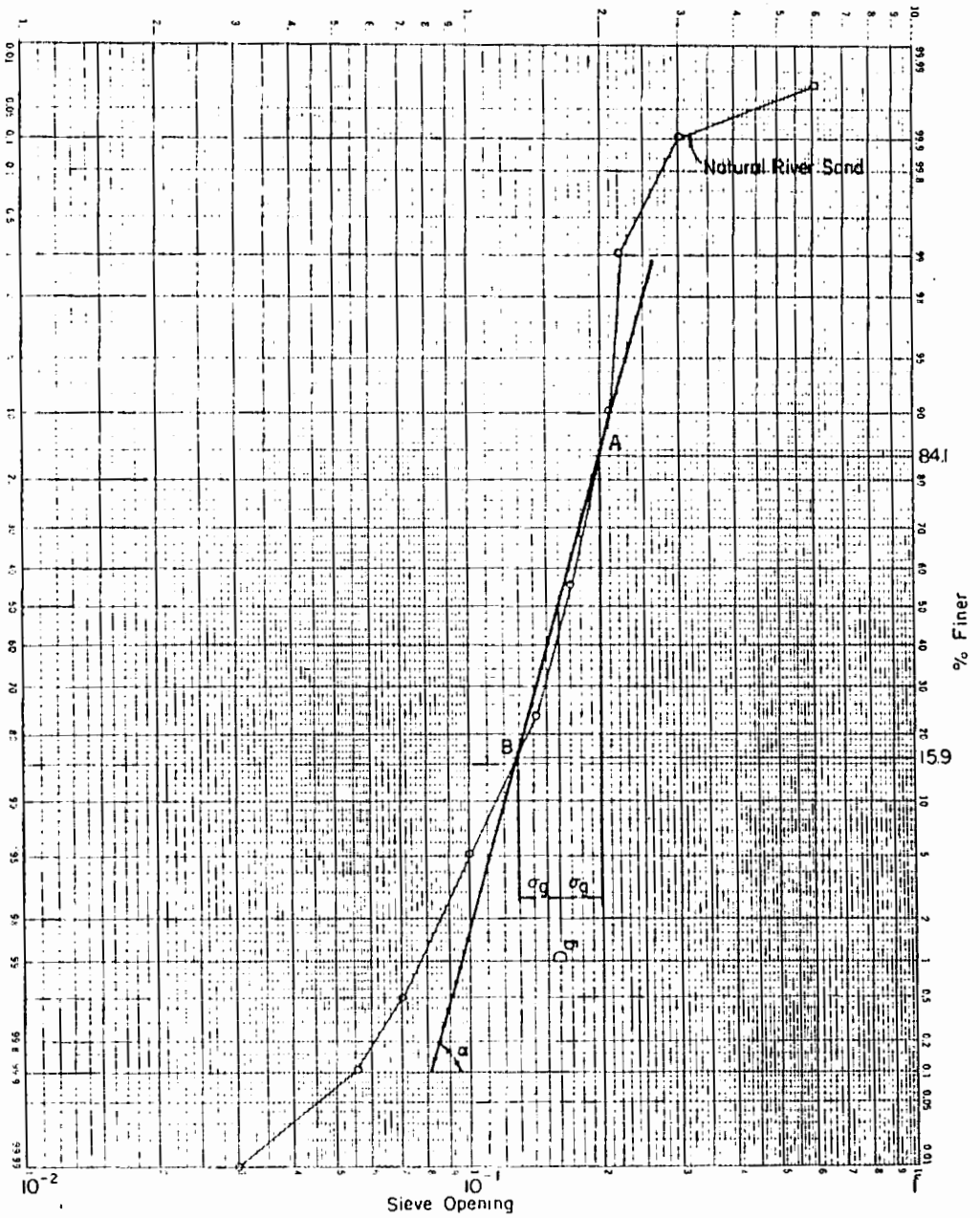


Figure 7A-3. Probabilistic analysis of sediment mixtures.

## 7A.2 QUARTILE AND MOMENT MEASURES

After the frequency curve is obtained, different particle diameters can be determined. Particles just larger than one-fourth of the distribution and particles just larger than the three-fourths of the distribution are defined as the limiting sizes for the first and the third quartile. Measures of spread are based on these quartile values.

The center of gravity of a given sediment mixture (moment of the first order) can be expressed as

$$\bar{x} = \frac{1}{n} \sum_{i=1}^{k} f_i(x)\, x_i \qquad (7A\text{-}6)$$

where

$x_i$ is the geometric mean of the $i^{th}$ class interval

$f_i(x)$ is the percentage of the total sample contained in $i^{th}$ class interval, and

$n = \sum_{i=1}^{k} f_i(x)$ is the total weight

$f_i(x) \geq 0$ and $f_1 \ldots f_k$ are called weighting factors and

$\bar{x}$ is the weighted arithmetic mean.

Moment measures are influenced by the complete gradation of the sand mixture from the coarsest to the finest grains. Second moment measures average spread of the curve and is expressed as the standard deviation of distribution. The mathematical representation of the second moment about the mean is the variance defined as

$$\sigma^2 = \frac{1}{n} \sum_{i=1}^{k} f_i(x)\, (x_i - \bar{x})^2$$

It should be noted that in some texts the $\frac{1}{n}$ term is replaced with $\frac{1}{n-1}$.

The term $\sigma$ is the standard deviation

$$\sigma = \left[\frac{1}{n} \sum_{i=1}^{k} f_i(x)\, (x_i - \bar{x})^2\right]^{1/2} \qquad (7A\text{-}7)$$

The standard deviation thus determined is not equal to the geometric standard deviation determined graphically as explained in the previous section.

The relation

$$M.D. = \frac{1}{n} \sum_{i=1}^{k} f_i(x)\, x_i - \bar{x}$$

defines mean deviation from the mean. Mean deviation from an arbitrary $x_o$ is

$$M.D._o = \frac{1}{n} \sum_{i=1}^{k} f_i(x)\, x_i - x_o$$

Example A-1

Mathematically $\bar{x}$, $\sigma^2$, $\sigma_g$, and M.D. are determined for bed material consisting of

| % finer | 0 | 10 | 20 | 30 | 40 | 50 | 60 | 70 | 80 | 90 | 100 |
|---|---|---|---|---|---|---|---|---|---|---|---|
| sieve opening (mm) | 0.03 | 0.102 | 0.13 | 0.15 | 0.17 | 0.18 | 0.19 | 0.20 | 0.21 | 0.25 | 0.30 |

and then the relation between $\sigma_g$ and $\sigma$ is developed.

Solution:

The solution of this example is self-explanatory, see Figure 7A-4 and Table 7A-1.

$$\bar{x} = \frac{1}{n} \sum f_i(x) x_i = \frac{1.747}{10} = 0.1747$$

Then

$$\sigma^2 = \frac{1}{n} \sum f_i(x)\, (x_i - \bar{x})^2 \qquad (7A\text{-}8)$$

and Equation 7A-8 can be written as:

$$n\,\sigma^2 = \sum f_i(x)\, x_i^2 - \frac{1}{n} \left[\sum f_i(x) x_i\right]^2 \qquad (7A\text{-}9)$$

Substituting

$$\sigma^2 = \frac{1}{10} \left(336.437 \times 10^{-3} - \frac{1}{10}\, 1.747^2\right) = 3.12361 \times 10^{-3}$$

$$\sigma = 0.056$$

and

$$M.D. = \frac{1}{n} \sum f_i(x)\, x_i - \bar{x} = \frac{0.4336}{10} = 0.043$$

Figure 7A-4 shows the size distribution curve of the sand mixture from which

$$D_g = 0.162$$

and

$$\sigma_g = 1.35$$

Using the previous definitions:

$$M.D. = \frac{(D_g - D_{15.9}) + (D_{84.1} - D_g)}{2} = \frac{D_{84.1} - D_{15.9}}{2}$$

$$= \frac{0.22 - 0.119}{2} = 0.05$$

and

$$\sigma_g = \sqrt{\frac{D_{84.1}}{D_{15.9}}} = 1.36$$

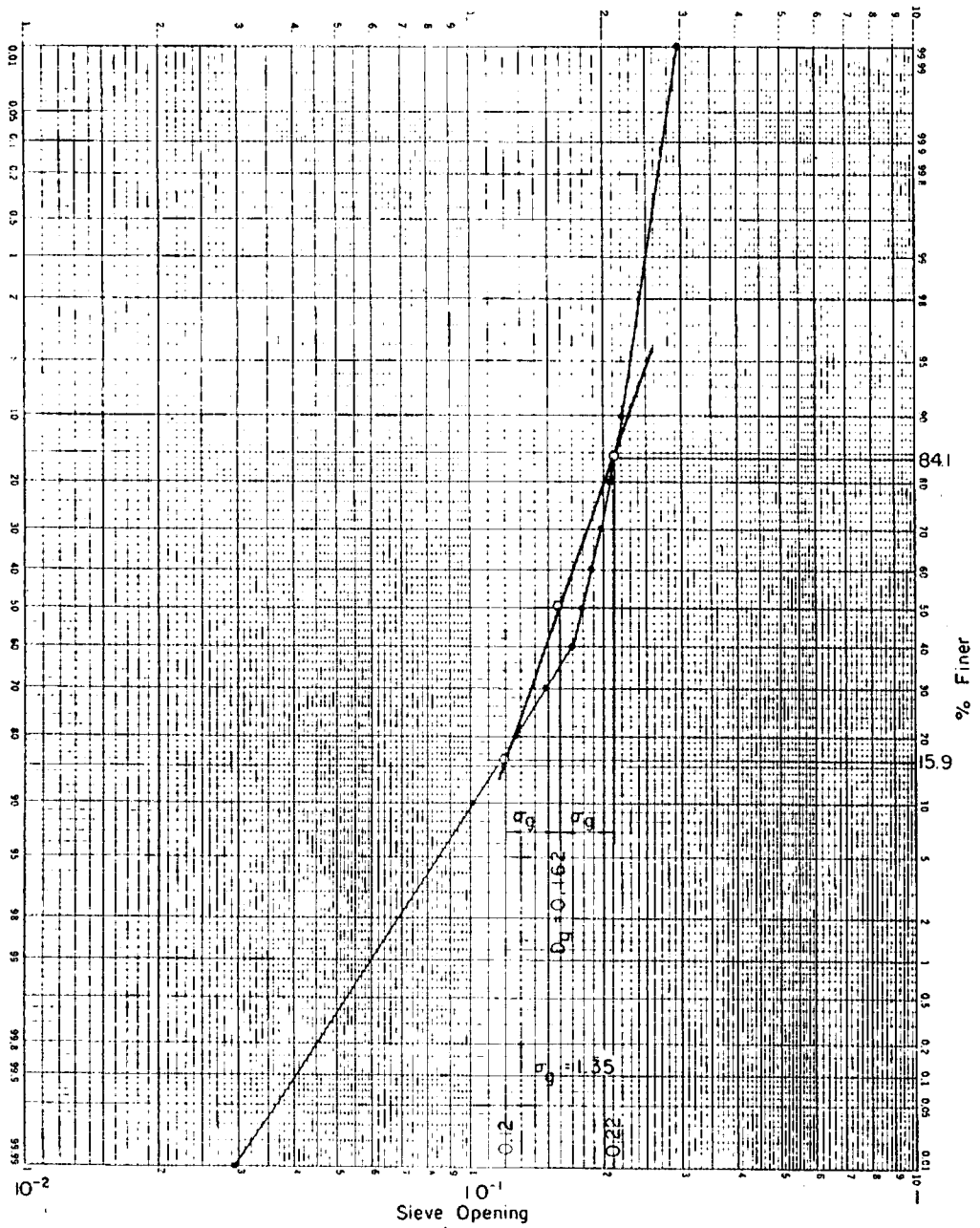


Figure 7A-4. Probabilistic analysis of sand mixture of Example A-1.

An explicit relation exists between M.D. and $D_g$ due to the common usage of the $D_{84.1}$ and $D_{15.9}$ sizes i.e.,

$$D_{M.D.} = D_{84.1} - M.D. = D_{15.9} + M.D.$$

and

$$D_{M.D.} \sim D_g$$

The gradation coefficient is equal to

$$G = \frac{1}{2}\left(\frac{0.220}{0.163} + \frac{0.163}{0.119}\right) = 1.36 \qquad 7A\text{-}4$$

Both $D_g$ and G are related to $D_{84.1}$ and $D_{15.9}$ and can be used to establish a straight line on log-log probability paper from which

$$D_{84.1} = G \times D_g = 1.36 \times 0.163 = 0.222$$

and

$$D_{15.9} = \frac{D_g}{G} = \frac{0.163}{1.36} = 0.120$$

## 7A.3 SHAPE DISTRIBUTION

Particle shape may be considered statistically as a distribution of geometric properties of the grain, rather than a cataloging of individual shapes of particles. Various schemes have been devised to obtain measurements and present data that are useful in defining particle shape. Two of these are 1)the triangle diagram of roundness grades of Szadeszky-Kardoss and 2)the shape classes of Zingg based on the three principal diameters a, b, and c of the particle (Krumbein and Pettijohn, 1938). A histogram of sphericity has also been presented that indicates the sphericity of particles. Sphericity is plotted on the abscissa and percentage on the ordinate.

Shape factor (sphericity or roundness) can be computed for bulk sediments and presented as frequency curves when either moment or quartile measures are used to describe the shape factor of the sediment.

## 7A.4 SPECIFIC WEIGHT OF DEPOSITED SEDIMENT

The specific weight of a sediment particle is in general different from that of an agglomeration of particles because of the spaces between the grains forming the agglomeration. When the particles are tightly packed they form a conglomerate such as pumice. If the particles are loose the conglomerate is subject to consolidation and the specific weight is variable with loading and time. The consolidation of sediment is an important soil mechanics problem. It is of interest to hydraulic engineers because the reservoir life varies as a function of deposition and consolidation. Consolidation concepts are used to convert sediment load (determined in units of weight) to volume of deposits in harbors, rivers, irrigation canals, etc. The specific weight of newly deposited sediments is about 0.1 $T/m^3$ (20 pounds per cubic foot). Specific weight

varies from 0.1 ~ 0.3 $T/m^3$ (20 ~ 60 lb/cf) for submerged silt and clay deposits in reservoirs. Larger values of 0.4 ~ 0.7 $T/m^3$ (75 ~ 125 lb/cf) apply to air-dried fine sediment. Dry sand ranges from 0.45 ~ 0.5 $T/m^3$.

Lana and Koelzer (1953) presented a formula for evaluating the variation of specific weight with time. Their relation states that

$$\gamma_m = \gamma_1 + B \log \theta \qquad (7A\text{-}10)$$

where $\gamma_m$ is the specific weight in pounds per cubic foot of a deposit with an age of $\theta$ years, $\gamma_1$ is the initial weight in $lb/ft^3$ corresponding to a 1-year consolidation period and B is given in Table 7A-2. When dealing with more than one class size it is suggested that a weighted combination of relative weights should be used.

Table 7A-2. Values of constant B in Equation 7A-10.

| Reservoir operation | Sand | | Silt | | Clay | |
|---|---|---|---|---|---|---|
| | $\gamma_1$ | $B_1^*$ | $\gamma_1$ | $B_2^*$ | $\gamma_1$ | $B_3^*$ |
| Sediment always or nearly submerged | 93 | 0 | 65 | 5.7 | 30 | 16.0 |
| Normal reservoir drawdown | 93 | 0 | 74 | 2.7 | 46 | 10.7 |
| Considerable reservoir drawdown | 93 | 0 | 79 | 1.0 | 60 | 6.0 |
| Reservoir emptied | 93 | 0 | 82 | 0.0 | 78 | 0.0 |

*B in $lb/ft^3$

Equation 7A-10 gives an approximation of specific weight. Other formulas and graphical charts are available but a reliable theoretical approach to the problem has not been developed (Report 9, U.S. Interagency Reports, Hembree, et al., 1952).

Richardson (1971) proposed two methods for determining average specific weight of sediment.

Method 1

1. Median particle size of each sample analyzed in a dispersed state is plotted against the instantaneous suspended-sediment discharge for the stream in tons per day.

2. For predetermined class intervals of suspended-sediment discharge the corresponding median particle sizes are taken from the curve and tabulated.

3. Samples are taken near the surface of submerged sediment deposits in order to establish a curve for specific weight of natural deposits before it becomes compacted by overlying layers. This information is plotted against mean particle size diameter to determine the relation between median particle size and specific weight of relatively unconsolidated sediment deposits.

4. Using specific weight from the curve developed in Step 3, the sediment discharge predicted in tons per day can be converted to acre-feet of sediment.

Method 2

This method uses the total size distribution of sediment load.

1. The sediment is divided into size fractions.

2. Specific weight of the deposit for each fraction is computed using size fraction weight and density of each size fraction.

3. Percentages of each size fraction are plotted against the suspended-sediment discharge in tons per day.

4 Best fit curves are drawn to average the information. Thus, the results are curves for sand, silt, and clay.

With the above data one can

1. Select class intervals of suspended sediment discharge in logarithmic progression,

2. Tabulate for each defined class interval the percentage of sand, silt, and clay as read from average curves for a given suspended sediment discharge,

3. Compile a frequency table of suspended sediment discharge from the daily sediment discharges on records this table can then be used to determine the different tonnages of suspended-sediment discharge in each class interval of suspended-sediment discharge, and

4. Compute the average percentage distribution of sand, silt, and clay from the tonnages and percentages in each class interval.

This fraction represents the inverse of the specific weight.

# APPENDIX B

## 7B.1 SEDIMENT TRANSPORT EQUATION FROM NONLINEAR REGRESSION ANALYSIS

Non-linear regression analysis was used by Jau-Yau Lu in his thesis to develop an equation that would be simpler and comparably or more accurate for calculating total bed material load (material larger than .062 mm in diameter) than the previous equations. Starting with dimensional analysis and omitting unnecessary factors Lu developed the equation

$$C_t = \phi_1 \left(\frac{V}{\sqrt{gD}}, \frac{wd}{v}, \frac{D}{d}, \frac{VD}{v}\right) \qquad (7B\text{-}1)$$

in which $C_t$ is the sediment concentration, $V$ is the mean flow velocity, $g$ is the gravitational acceleration, $D$ is the flow depth, $w$ is the particle fall velocity, $d$ is the particle diameter, and $v$ is the kinematic viscosity. First and last terms inside the brackets in Equation 7B-1 are Froude and Reynolds numbers respectively.

Using the physical principles of sediment transport and applying mathematical principles Lu determined that the first three terms in brackets in Equation 7B-1 are significant in determining the sediment concentration. However, he concluded that "...the sediment transport rate correlated with the Reynolds number only to the extent that Reynolds number correlated with the Froude number." Therefore omitting the Reynolds number from Equation 7B-1 and using it only as a reference to group his data Equation 7B-1 was modified into Equation 7B-2.

$$C_t = \phi_2 \left(\frac{V}{\sqrt{gD}}, \frac{wd}{v}, \frac{D}{d}\right) \qquad (7B\text{-}2)$$

Furthermore, Lu determined that the functional form of Equation 7B-2 is in the form of

$$\log C_t = P_1 + P_2 e^{P_3 F} + P_4 \log\left(\frac{wd}{v}\right) + P_5 \log\left(\frac{D}{d}\right) \qquad (7B\text{-}3)$$

where $P_1$, through $P_5$ are coefficients to be determined and $F$ is the Froude number $\frac{V}{\sqrt{gD}}$. Based on theory, coefficients in Equation 7B-3 were subject to the following limitations

$P_2 < 0$

$P_3 < 0$

$P_4 < 0$

$P_5 > 0$

Considering the limitations a non-linear least squares computer program was used to obtain a weighted least squares fit to the data. Program BMDO7R selects optimum values for coefficients to minimize the sum of squares of the differences between measured and calculated values of $C_t$.

Data Grouping

To calibrate his equation Lu carefully selected data from seven flume tests and seven river tests that appeared to be accurate. It turned out that the Froude number in all the river data was less than 0.8. So he considered only tranquil flow in his analysis and used flume data with Froude numbers smaller than unity for comparison.

For dividing the data into distinct groups Lu found that one group of rivers has Froude numbers of less than 0.2. This value was chosen as a dividing point and all the rivers with a Froude number of less than 0.2 were grouped together in Group I. Reynolds number of all of Group I was in the range of $10^6$-$10^7$. The rest of the rivers and the flumes that had a Froude number larger than 0.2 were divided according to the Reynolds number. Since a Reynolds number of $10^5$ separates fully turbulent from transition flow, Lu used this value as the dividing point. Therefore, Group II has a Froude number larger than 0.2 and a Reynolds number smaller than $10^5$ and Group III has the same Froude number and a Reynolds number of larger than $10^5$. Table 7B-1 shows the results of nonlinear regression analysis for the three groups.

Comparison with Other Formulas

To check the applicability of his analysis Lu compared his formulas with three other common formulas (Einstein's bed load function, Colby's, and Yang's). Reference should be made to Lu's original thesis for an explanation of each formula since the description is extensive. Figure 7B-1 and 7B-2 show typical comparison plots for flume and river data, respectively. Overall comparison of applicability of the non-linear regression equations is shown in Table 7B-2. The table demonstrates that this method is superior to the three others for the cases compared.

Application Example

There are innumerable applications for the "non-linear sediment transport equation" in sediment transport problems. However, for illustration purposes the following example is presented.

Based on dynamic and kinematic wave transmission models a stage-discharge curve was developed for the Mississippi River at Tarbert Landing (Figure 7B-3). The objective is to develop a sediment rating curve for the same river. This is done by first assuming a relationship of the kind

Table 7B-1. Final results of nonlinear regression analysis.

Equation Form: $Y = P1 + P2 \cdot e^{P3 \cdot X1} + P4 \cdot X2 + P5 \cdot X3$

in which $Y = \log(C_t)$, $X2 = \log(\frac{w \cdot d}{v})$ $X1 = F = \frac{V}{\sqrt{g \cdot d}}$, and $X3 = \log(\frac{D}{d})$

| Group | # of Data | F | log R | $s^2$ | Corr. $(y,\hat{y})$ | P1 | P2 | P3 | P4 | P5 |
|---|---|---|---|---|---|---|---|---|---|---|
| I | 104 | <0.2 | $\left.\begin{matrix}6.0\\ \\ 7.5\end{matrix}\right\vert$ | 0.0553 | 0.883 | 1.0027 | -4.0680 | -15.041 | -0.27675 | 0.46207 |
| II | 262 | $\geq$0.2 | <5.0 | 0.0560 | 0.916 | 3.8651 | -4.0711 | -4.8363 | 0.29139 | 0.02705 |
| III | 229 | $\geq$0.2 | $\geq$5.0 | 0.0555 | 0.885 | 2.5670 | -4.9855 | -4.0863 | 0.03739 | 0.41082 |

$C_t$ : P.P.M., Sediment Concentration

F : Froude number = $\frac{V}{\sqrt{g \cdot D}}$

w : fps, Fall Velocity of Particle

R : Reynolds number = $\frac{V \cdot D}{v}$

d : ft, Median Diameter of Particle

g : Gravitational Acceleration

v : $ft^2/sec$, Kinematic Viscosity

$s^2$ : Error Mean Square (from BMD07R)

V : fps, Average Velocity

P1, P2, P3, P4, and P5 : Coefficients

D : ft, Hydraulic Depth

Corr$(y,\hat{y})$ : Correlation coefficient between measured value, y, and predicted value, $\hat{y}$

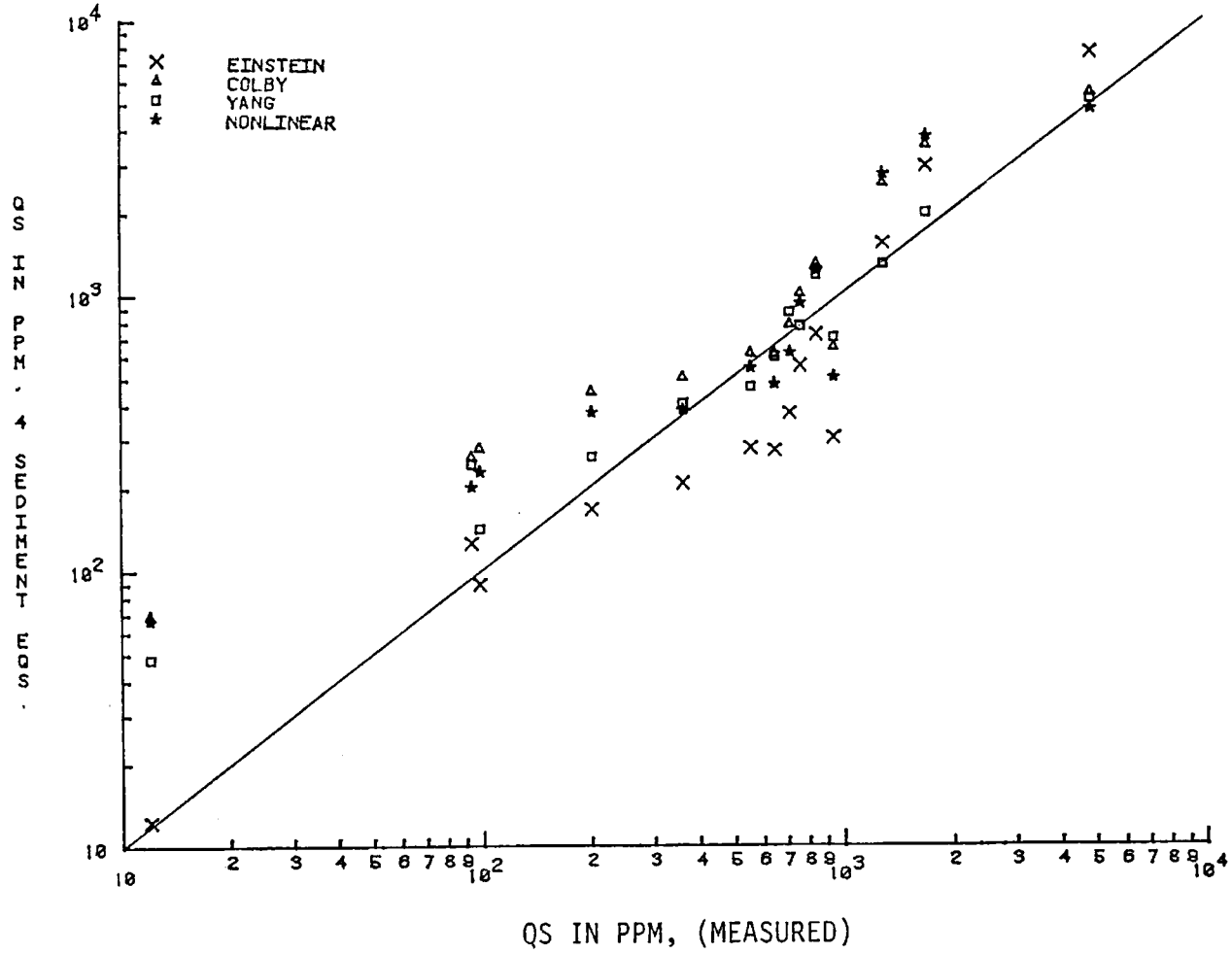


Figure 7B-1. Comparison of four sediment equations, CSU 8-ft flume, 0.27 mm.

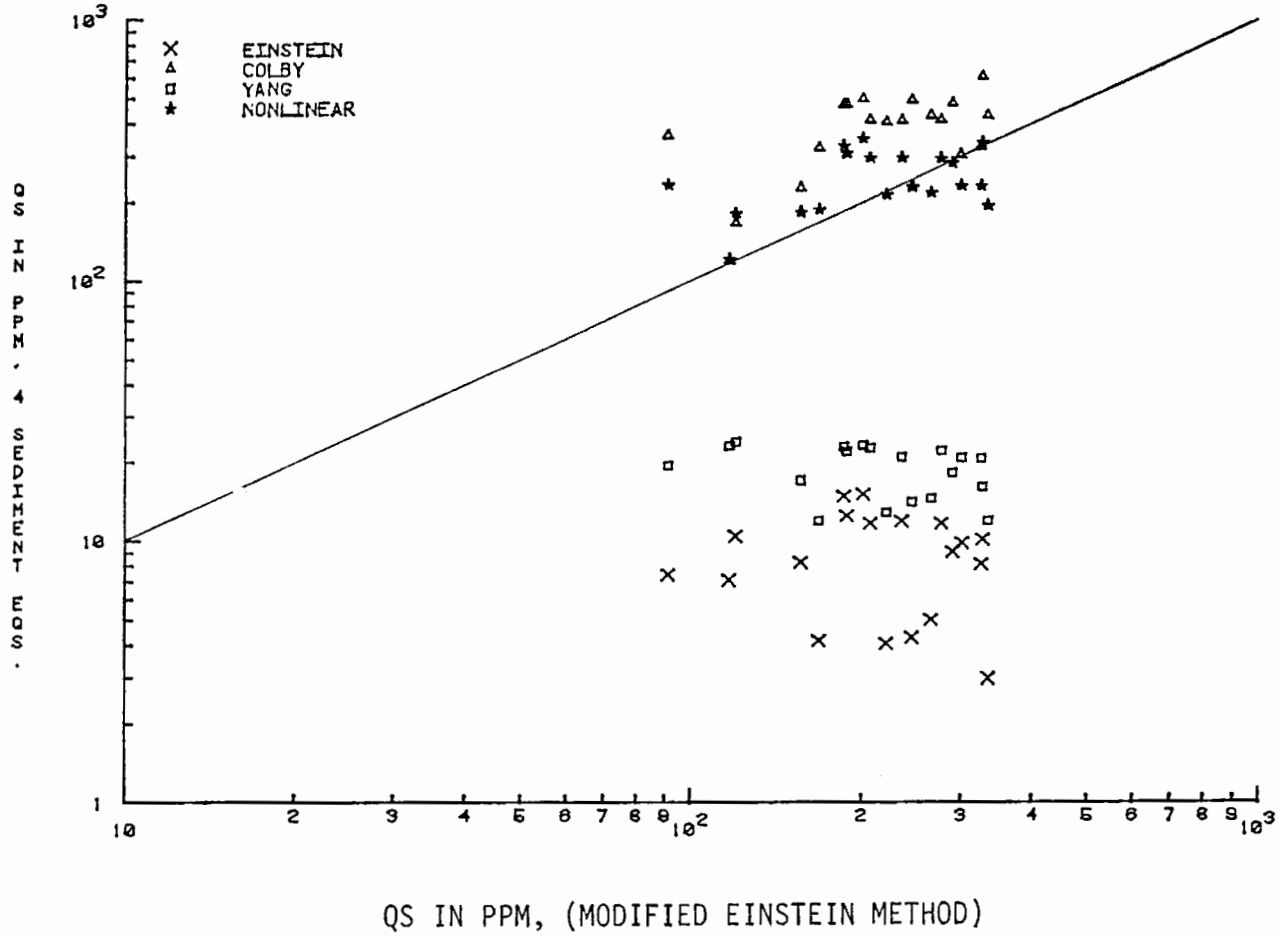


Figure 7B-2. Comparison of four sediment equations, Mississippi River, Tarbert Landing.

Table 7B-2. Qualitative comparison of four sediment transport equations as shown in Figures 1 to 4.

| Data | Figure | Einstein | Colby | Yang | Nonlinear |
|---|---|---|---|---|---|
| CSU, .19 mm | 4-19 | - | 0 | 0 | 0 |
| CSU, .27 mm | 4-20 | 0 | 0 | 0 | 0 |
| CSU, .45 mm | 4-21 | 0 | 0 | 0 | 0 |
| CSU, .93 mm | 4-22 | 0 | out of range | 0 | *+ |
| Middle Loupe River | 4-23 | - | 0 | 0 | 0 |
| Niobrara River | 4-24 | - | 0 | 0 | 0 |
| Rio Grande River, Sec. A-2 | 4-25 | - | - | - | 0 |
| Rio Grande River, Sec. F | 4-26 | - | -(0) | - | 0 |
| Mississippi River, St. Louis | 4-27 | - | 0 | - | + |
| Mississippi River, Tarbert Landing | 4-28 | - | + | - | 0 |
| Red River | 4-29 | - | -(0) | - | -(0) |
| Atchafalya River | 4-30 | - | 0 | - | 0 |

Symbol : 0 = close to the measured total bed material load
+ = too high
- = too low
-(0) = relatively lower, but still close to the measured total bed material load

*Effect of critical shear stress for incipient motion

# CHAPTER 8

# CHANNEL DESIGN

## 8.1 INTRODUCTION

Design of stable channels is important to engineers dealing with water resource utilization. Typically, there are three basic channels: natural streams, irrigation channels, and drainage ditches. The fundamental difference in design procedures for these channels concerns the uncertainty of flow magnitude. Natural channels must be concerned with magnitude and frequency of peak flows and large variation in flow. Irrigation channels are designed to safely carry a predetermined maximum discharge allowing for anticipated inflow from surface runoff. Variation in discharge for irrigation and drainage channels depends on availability and demand for water and is not as large or uncertain as in a natural stream. Drainage ditches typically have the smallest discharge range and the least uncertainty in flow magnitude.

It should be noted that evaluation of discharge design is not included in the scope of this course. However, assuming the design discharge is known, some techniques for designing a stable channel are presented. Additionally, utilization of vegetation and its impact on channel design and stability are discussed.

## 8.2 DESIGN OF STABLE CHANNELS: PERMISSIBLE VELOCITY AND TRACTIVE FORCE

Two major variables affecting channel design and sediment transport are velocity and shear stress. In reality determining shear stress is usually difficulty. Therefore velocity is often accepted as the most important factor when designing stable alluvial channels. If a maximum channel velocity is selected such that scouring occurs only for velocities greater than this value the problem would seem to be solved but often this is not a practical limit. Appreciable work has been devoted to developing the permissible velocity approach. Many methods have been suggested. However, experience has identified discrepancies in these procedures. For example, channels carrying sediment may be stable at velocities higher than the limiting velocity. Fortier and Scobey (1925) introduced a certain increase in their listed values of maximum permissible velocities when water was transporting colloidal silt (Table 8-1). Hence, how should permissible velocities be determined?

If clear water flows in a canal with alluvial boundaries, the resistance of these boundaries to the flow can be estimated by a formula of the form

$$\frac{U}{U_*} = a + b \log \frac{R}{D}$$

This relation is applicable to conditions before the beginning of motion. The value $U_*$ can be obtained from Meyer-Peter's or Shield's criterion when water temperature and the characteristics of the movable

Table 8-1. Maximum permissible velocities proposed by Fortier and Scobey (1926).

| Original material excavated for canals | n | Mean velocity, after Aging, of Canals (d ≤ 3 ft) | | | | | |
|---|---|---|---|---|---|---|---|
| | | Clear water, no detritus | | Water transporting colloidal silt | | Water transporting noncolloidal silts, sands, gravels or rock fragments | |
| | | ft/sec | m/sec | ft/sec | m/sec | ft/sec | m/sec |
| 1. Fine sand (colloidal) | .02 | 1.5 | 0.46 | 2.50 | 0.76 | 1.50 | 0.46 |
| 2. Sandy loam (noncolloidal) | .02 | 1.45 | 0.53 | 2.50 | 0.76 | 2.00 | 0.61 |
| 3. Silt loam (noncolloidal) | .02 | 2.00 | 0.61 | 3.00 | 0.91 | 2.00 | 0.61 |
| 4. Alluvial silt when noncolloidal | .02 | 2.00 | 0.61 | 3.50 | 1.07 | 2.00 | 0.61 |
| 5. Ordinary firm loam | .02 | 2.50 | 0.76 | 3.50 | 1.07 | 2.25 | 0.69 |
| 6. Volcanic ash | .02 | 2.50 | 0.76 | 3.50 | 1.07 | 2.00 | 0.61 |
| 7. Fine gravel | .02 | 2.50 | 0.76 | 5.00 | 1.52 | 3.75 | 1.14 |
| 8. Stiff clay (very colloidal) | .025 | 3.75 | 1.14 | 5.00 | 1.52 | 3.00 | 0.91 |
| 9. Graded, loam to cobbles, when noncolloidal | .03 | 3.75 | 1.14 | 5.00 | 1.52 | 5.00 | 1.52 |
| 10. Alluvial silt when colloidal | .025 | 3.75 | 1.14 | 5.00 | 1.52 | 3.00 | 0.91 |
| 11. Graded, silt to cobbles, when colloidal | .03 | 4.00 | 1.22 | 5.50 | 1.68 | 5.00 | 1.52 |
| 12. Coarse gravel (noncolloidal) | .025 | 4.00 | 1.22 | 6.00 | 1.83 | 6.50 | 1.98 |
| 13. Cobbles and shingles | .035 | 5.00 | 1.52 | 5.50 | 1.68 | 6.50 | 1.98 |
| 14. Shales and hard pans | .025 | 6.00 | 1.83 | 6.00 | 1.83 | 5.00 | 1.52 |

Table 8-2. Formulas that indicate the maximum permissible velocity for canals constructed in alluvium.

1. Mavis, et al. (1937)

$$(U_b) = \frac{1}{2} D^{4/9} \sqrt{\frac{\rho_s}{\rho} - 1} \qquad (8\text{-}1)$$

D in millimeters

$(U_b)$ = Maximum permissible velocity at the bottom, ft/sec

2. Carstens (1966)

$$\frac{U_b^2}{(\frac{\rho_s}{\rho} - 1)gD} = 3.61 \, (\tan\phi \cos\alpha - \sin\alpha) \qquad (8\text{-}2)$$

$\alpha$ = slope of plane bed, English units.

3. Neill (1967)

$$\frac{U_{per}^2}{(\frac{\rho_s}{\rho} - 1)gD} = 2.5 \, (\frac{D}{d})^{-0.20} \qquad (8\text{-}3)$$

English units.

4. Mirtskhulava, T. E.

$$U_{per} = (\log \frac{8.8d}{D}) \sqrt{\frac{2g}{0.44\sqrt{n}} (\gamma_s - \gamma) D} \qquad (8\text{-}4)$$

Metric units are required,

D > 2 mm

$$n = 1 + \frac{D}{0.00005 + 0.3D} \qquad (8\text{-}5)$$

and

$U_{per}$ = Maximum permissible mean velocity in mps

material are constant. If R is increased $U/U_*$ increases. But $U_*$ can be kept constant by decreasing slope accordingly. However, in this case U may increase with an increase in the R/D ratio. But no motion of particles is allowed on the channel bottom according to the permissive velocity criterion. Therefore the mean velocity's influence on the beginning of motion is difficult to accurately define and the permissible velocity method must be subjected to careful study before application to stable channel design problems.

Method of Maximum Permissible Velocity

If the adopted mean velocity is lower than maximum permissible velocity, the channel is assumed to be stable (Fortier and Scobey, 1926). The authors emphasized the importance of exercising judgment on each particular problem. Subsequently these limits were recommended by a Special Committee on Irrigation Research, ASCE. Since then many designs have been based on their suggested permissible velocities.

Table 8-1 summarizes the permissible velocities given by Fortier and Scobey (1926). Others have proposed additional relations for determination of maximum permissible velocities and several of these are presented in Table 8-2.

The use of Fortier and Scobey's table and formulas from Table 8-2 are illustrated in Example A.

Example A

A stable channel should be designed given the following data:

1. $Q = 10\ m^3/sec$, 2. the original material in which the canal is to be excavated is sandy loam, 3. the water transports noncolloidal silt, 4. the $D_{50}$ of the bed material is 2.5 mm, 5. $\gamma_s = 2.7\ T/m^3$, 6. $g = 10\ m/sec^2 = 32\ ft/sec^2$, 7. $\phi = 30°$, 8. $\alpha = 0.034$, and 9. $S = 0.0006$.

Solution

1. The maximum permissible velocity is determined from Tables 8-1 and 8-2. After Fortier and Scobey $U_{per} = 0.53$ m/sec $= 1.75$ ft/sec., after Mavis et al. $U_b = \frac{1}{2}\, 2.5^{4/9}\sqrt{1.7} = 0.979 \sim 0.98$ ft/sec. after Carstens

$$U_b = \sqrt{1.7 \times 32 \times \frac{2.5}{25.4 \times 12} \times 3.61(0.577 \times 0.99 - 0.00)} = 0.95 \text{ ft/sec}$$

The last two formulae give bottom velocities. These may be compared to the permissible velocity proposed by Fortier and Scobey when the depth d has been determined.

2. Using $U_{per} = 0.53$ m/sec (Fortier and Scobey).

$$A = \frac{10}{0.53} = 18.87\ m^2$$

3. Select $z = 1.5$ from Table 8-3.

Table 8-3. Suggested z values.

| Nature of Bank Material | z |
|---|---|
| Rock | 0.2 |
| Smooth or weathered rock, shell | 0.5 ~ 1.0 |
| Soil (clay, silt and sand mixtures) | 1.5 |
| Sandy soil | 1.5 |
| Silt and loam (loose sandy earth) | 2 |
| Fine sand | 3 |
| Flowing fine and other very fine material | >3 |
| Compacted clay | 1.5 |
| Noncohesive riprap material | see Figure 8-4 |

4. Excavating equipment will be used to form the channel. The dimension b may be checked taking into account the dimension of the equipment. Equation 8-6 is used for $\frac{b}{d}$

$$\frac{b}{d} = 4 - 1.5 = 2.5 \qquad (8\text{-}6)$$

and

$$b = 2.5d$$

5. Equations $b = 2.5d$ and $(b + 1.5d)\ d = 18.87$, $b = 5.43$ m, and $d = 2.17$ m are solved.

6. Results are checked with Equation 8-3

$$U_{per} = \sqrt{1.7 \times 32 \times 0.008 \times \left(\frac{0.008}{2.17 \times 3.28}\right)^{-0.20} \times 2.5}$$

$$= 2.05 \text{ ft/sec}$$

Then using Equations 8-5 and 8-4

$$n = 1 + \frac{0.0025}{0.00005 + 0.3 \times 0.0025} = 4.125 \qquad 8\text{-}5$$

$$U_{per} = \left(\log_{0.0025} \frac{2.17 \times 8.8}{}\right) \sqrt{\frac{20}{0.44 \times 4.125}\ (1.7)\ 0.0025} = 0.84 \text{ m/sec}$$

This analysis shows that Neill's Equation 8-3 results in the same range as Fortier and Scobey's.

The Mirtskhulava formula is very conservative. For $d = 2.17$ m and $U = 0.53$ m/sec, and U is 0.6d above the bed

$$\frac{U}{U_*} = 8.5 + 5.75 \log \frac{(1 - 0.6)\ 2.17}{0.0025} \quad \text{from which} \quad U_* = 0.0229$$

for $U = 0.53$ m/sec. Using $U_*$, the velocity at $d = D_{50}$ m above the bed is

$$U_b = 8.5 \times U_* = 0.1947 \text{ m/sec} = 0.639 \sim 0.64 \text{ ft/sec}$$

The Mavis equation and Carsten's equation give larger values than $U_b = 0.64$ ft/sec.

7. Using Manning's equation and choosing $n = 0.028$ for sandy loam

$$10 = \frac{18.27}{0.028} R^{2/3}\ 0.0006^{1/2}, \quad R = 0.48 \text{ m}$$

8. Determine $b$ and $d$ of the trapezoidal section using

$R = 0.48$ m and $A = 18.87$ m$^2$

$A = (b + 1.5d)\ d = 18.87$ and

$$R = \frac{18.87}{b + 2\sqrt{1 + z^2}} = 0.48 \text{ m}$$

from these relations

$b = 37.53$ m and $d = 0.49$ m

There are significant differences between these values and the preceding ones (Figure 8-1). Such differences are not acceptable even considering this aspect of engineering is more art and experience than science.

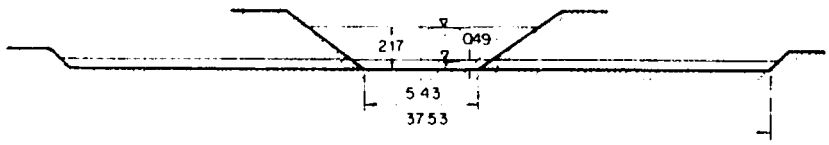


Figure 8-1. Stable canal section computed from the maximum permissible velocity method.

Method of Critical Shear Stress

The critical shear stress is given by

$$\tau_c = \gamma R S_E$$

which can also be expressed as $\tau_c = \rho U_*^2$. The criterion of beginning of motion established $U_*$ and $\tau$. This approach is not limited by uncertainties associated with the methods discussed in the previous section.

Shear stress $\tau$ is assumed constant at a point in the channel when hydraulic characteristics of flow and channel geometry remain constant. However according to Lane (1953) and others it varies in the cross section (Figure 8-2). Shear distribution is based upon a theoretical analysis that utilizes a membrane analogy and field data. But, if the channel is curved or if the geometry is different, the coefficients 0.75 and 0.97 as shown on Figure 8-2 are not valid. For example in bends, coefficients as high as 2.5 were measured by Ippen and Drinker (1962).

Based on the foregoing analysis and field studies, Figure 8-3 was prepared by Lane and Carlson (1953). For different values of $\frac{b}{d}$, values

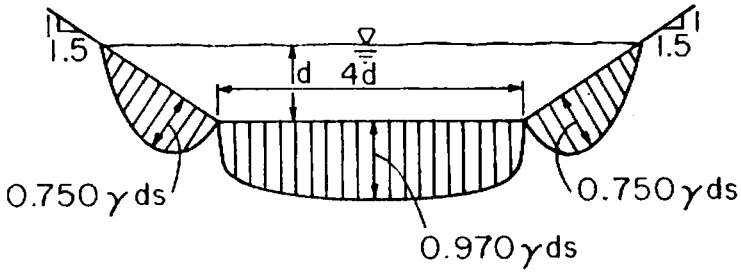


Figure 8-2. Maximum unit tractive force versus b/d.

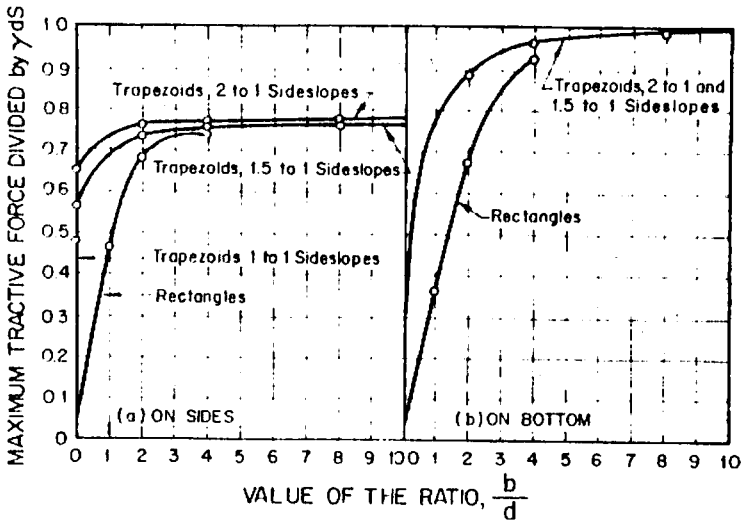


Figure 8-3. Variation of $\tau$ in a trapezoidal cross section.

of $\tau_c/\gamma dS_E$ are given for side slopes and channel bottom. Critical shear stress $\tau_c$ is given by Equation 8-6, $\frac{b}{d}$ is assumed or known and shear on the side slopes is estimated from Figure 8-3. The channel bottom is determined Figure 8-3 and angle of repose for noncohesive material is given in Figure 8-4. The tractive force method is illustrated by Example B.

Example B

A stable channel should be designed for the following conditions

1. $Q = 1.45\ m^3/sec$

2. The natural material in which the canal is excavated is fine gravel.
   $D_{35} = 0.7$ cm
   $D_{50} = 1.2$ cm
   $D_{65} = 1.8$ cm
   $D_{75} = 1.9$ cm
   $D_{85} = 1.95$ cm
   $D_{90} = 2.00$ cm

3. $\gamma_s = 2.7\ T/m^3$

4. $g = 9.81\ m/sec^2$

5. $S = 0.0006$

6. $n = 0.022$

Solution

1. From Figure 8-4 one can estimate the angle of repose of the natural alluvium defined above i.e.,

   $\phi = 36°$

if this material is considered angular. Then

$$\tan (36°) = 0.727$$

This angle corresponds to $z = 1.38$. For design purposes, $z = 1.5$ is selected, then $\theta = 33.69°$.

2. The critical shear stress on the sides of the channel is determined from Figure 8-43a. Assuming $\frac{b}{d} = 3.5$ then

   $\tau = 0.77\gamma Sd = 0.77 \times 0.0006d = 4.62 \times 10^{-4} d$

3. Coefficient K is computed from

$$K = \cos\theta \sqrt{1 - \frac{\tan^2\theta}{\tan^2\phi}} = 0.33 \qquad (8\text{-}7)$$

4. Critical shear stress is determined from Figure 8-5

$$\tau_c = 0.9 \text{ kg/m}^2$$

5. Permissible shear stress on the side slope is computed as

$$\tau_{ss} = 0.33 \times 0.9 = 0.297 \sim 0.3 \text{ kg/m}^2$$

6. For incipient motion

$$0.3 = 4.62 \times 10^{-4} d$$

and

$$d = \frac{0.3}{4.62 \times 10^{-4} \times 10^3} = 0.649 \sim 0.65 \text{ m}$$

7. The bottom width is

$$b = 3.5 \times 0.65 = 2.275 \sim 2.28 \text{ m}$$

8. From Manning's equation the discharge is

$$Q = \frac{2.12}{0.022} \times 0.60 \times 0.0245 = 1.42 \text{ m}^3/\text{sec}$$

where

$$A = (b + 1.5d)\, d = 2.12 \text{ and } R = 0.46$$

9. If more accuracy is needed the $\frac{b}{d}$ ratio is changed and the analysis is repeated until $Q = 1.45 \text{ m}^3/\text{sec}$ (cf. Example E).

Criteria for Cohesive Soils

The nature of cohesion is not well known. Therefore, formulae and procedures related to design of channels in cohesive soils are few.

Mirtskhulava has given a formula for computation of permissible velocity in canals excavated in cohesive soils

$$U_{per} = \log\left(\frac{8.8d}{D}\right) \sqrt{\frac{2gm}{2.6\gamma n}} \left[(\gamma_s - \gamma)\, D + 1.25\, c_f K\right] \qquad (8\text{-}8)$$

where

m = working condition coefficient of the aggregates, its value is equal to unity in normal cases

$$n = 1 + \frac{D}{0.00005 + 0.3D} \qquad 8\text{-}5$$

$c_f$ = the mean value of cohesion at the rupture "fatigue" limit

$$c_f \cong 0.035c \qquad (8\text{-}9)$$

c = factor of cohesion

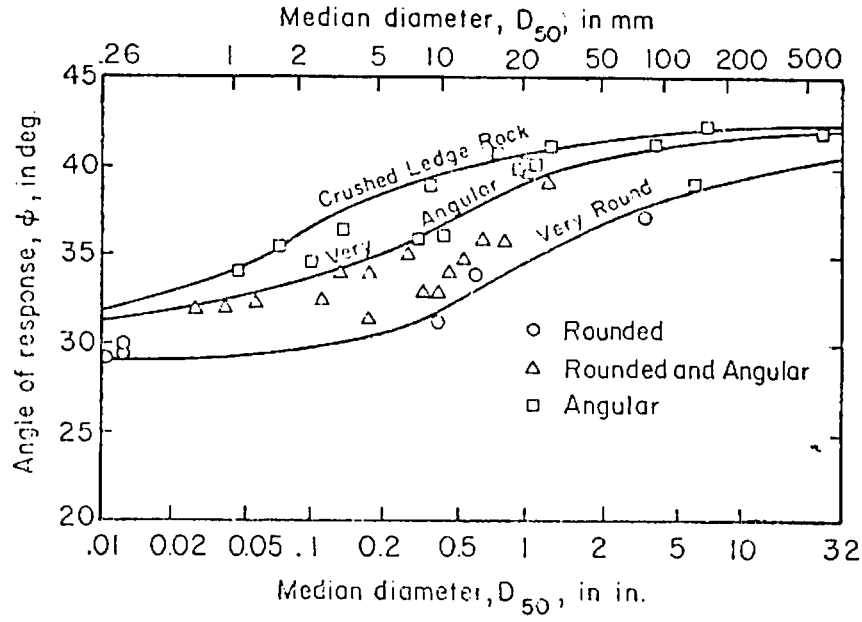


Figure 8-4. Angle of repose for dumped riprap (after Simons, 1956).

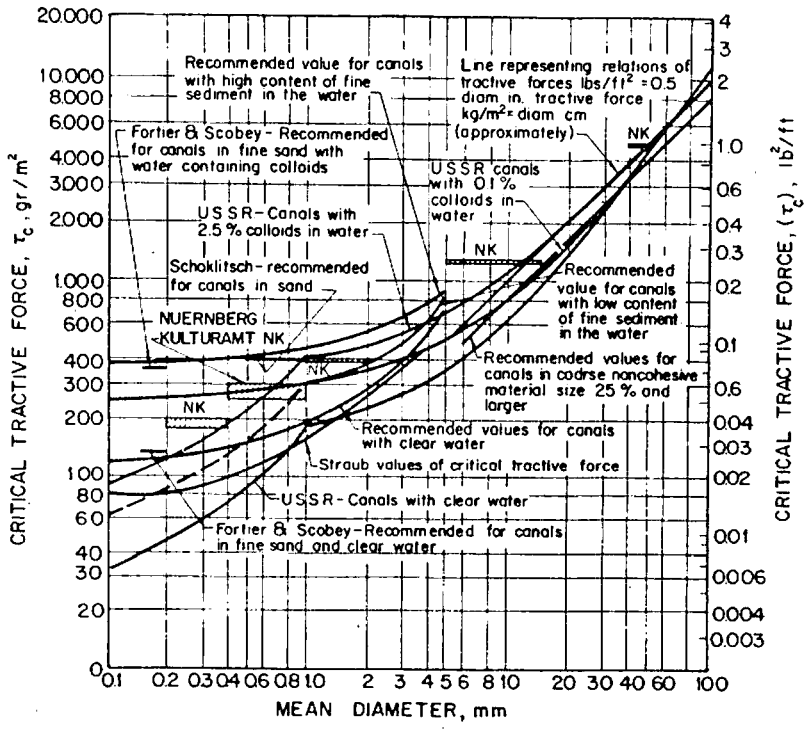


Figure 8-5. Critical shear stress as function of grain diameter (after Lane, 1953).

K = homogeneity factor. This factor is equal to unity when the soil is homogeneous. The value of K is selected in situ.

Mirtskhulava states that the permissible velocities computed by this formula are conservative.

Figure 8-6 provides another method for estimating maximum permissible velocities for cohesive soils. The permissible velocity is determined as a function of void ratio and is corrected by the factor given in Figure 8-6b which is a function of average depth.

The Ideal Stable Cross Section

The methods of maximum permissible velocity and critical shear stress when applied to trapezoidal sections take into account the maximum values of the mean velocity and the shear stress. But these values belong to the central part of the channel bottom or to the toe of the side slope. A more economical design is obtained when the mean values are considered and a partial lining is adopted (cf. Example E) or when the impending motion is assumed existent not only around the toe of the side slope but at every point on the wetted perimeter of the channel.

The U.S. Bureau of Reclamation has given an example for the computation of a cross section at incipient motion. Their procedure is reproduced.

Assuming that Figure 8-7 reproduces a stable cross section for the following conditions, then

1. Soil particles are in equilibrium on the channel bed. Thus stability is influenced by the component of their submerged weight acting normal to the bed.

2. Above the water surface the side slope of the channel is equal to the angle of repose $\phi$ of the bank material.

3. At the center of the channel $\theta = 0$.

4. Equilibrium of particles is assured when critical shear is equal to the component of the submerged weight of particles opposing motion.

5. Shear stress is obtained by multiplying the weight component of water over the elementary surface under consideration times the longtitudinal slope. The lateral component of shear is assumed negligible.

Consider the elementary surface $AB = 1 \cdot \sqrt{(\overline{dx}^2 + \overline{dy}^2)}$. Following assumption 5 the shear stress is equal to

$$\tau_c = \frac{\gamma y dx\, S}{\sqrt{\overline{dx}^2 + \overline{dy}^2}} = \gamma y S \cos\theta \qquad (8\text{-}10)$$

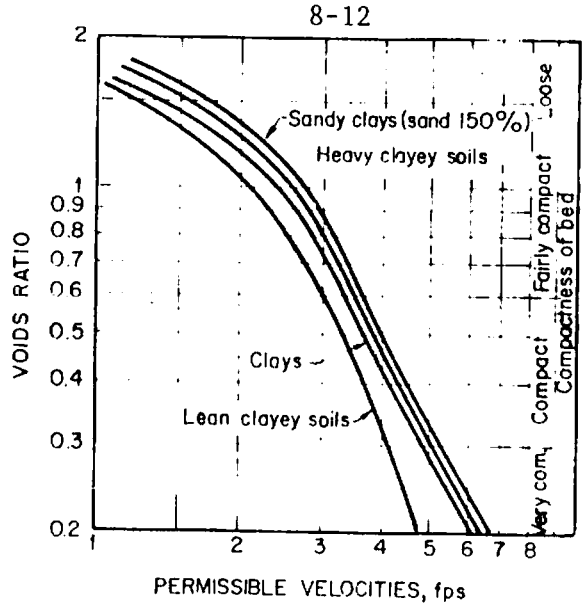


Figure 8-6a. Curves showing U.S.S.R. data on permissible velocities for cohesive soils, 1936.

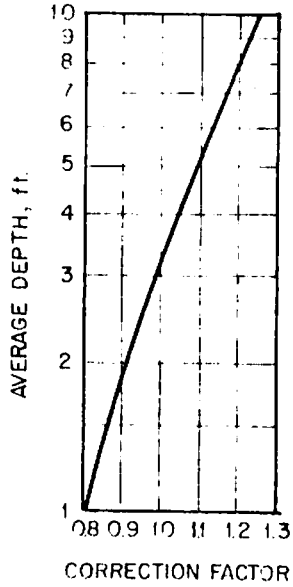


Figure 8-6b. Curves showing U.S.S.R. corrections of permissible velocity as a function of depth for both cohesive and noncohesive materials, 1936.

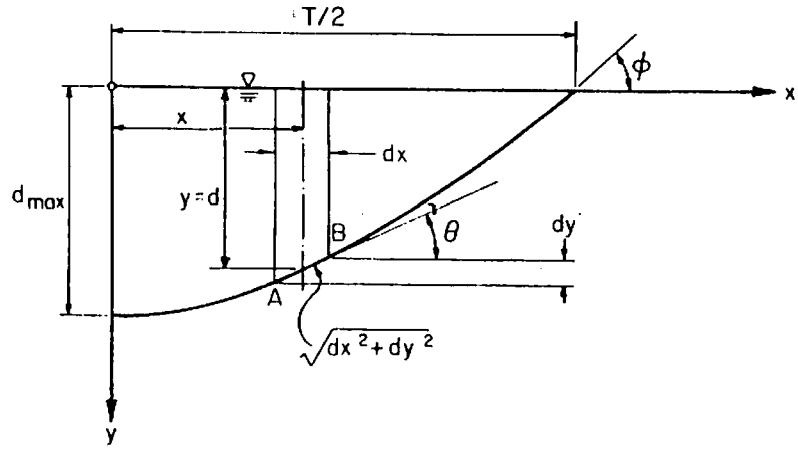


Figure 8-7. Elements of an ideal stable section

The tractive force or shear stress at the centerline of the channel is

$$\tau = \gamma d_{max} S$$

Corresponding shear stress on the sloping wetted surface is

$$\tau_{AB} = \gamma d_{max} SK$$

where K is given by

$$K = \frac{\tau_o}{\tau_c} = \cos\theta \sqrt{1 - \left(\frac{\tan\theta}{\tan\phi}\right)^2} = \sqrt{1 - \frac{\sin^2\theta}{\sin^2\phi}}$$

If $\tau_c \leq \tau_{AB}$ the cross section is stable. Therefore,

$$\gamma y \; S \cos\theta = \gamma d_{max} \; SK \tag{8-11}$$

is the minimum condition for equilibrium. Substituting K and $\theta = \tan^{-} \left(\frac{dy}{dx}\right)$ yields

$$\left(\frac{dy}{dx}\right)^2 + \left(\frac{y}{d_{max}}\right)^2 \tan^2\phi = \tan^2\phi \tag{8-12}$$

At the centerline of the channel, y is equal to $d_{max}$ and $x = 0$. With this condition solution of differential Equation 8-12 yields

$$y = d_{max} \cos \left(\frac{\tan\phi}{d_{max}} x\right) \tag{8-13}$$

This is a simple cosine curve used to define the channel cross sections given in Figure 8-7.

The U.S. Bureau of Reclamation (1951) has given the following relations to define the properties of the stable cross section

$$A = \frac{2d_{max}^2}{\tan\phi} \tag{8-14}$$

$$U = \frac{1}{n} \left[\frac{d_{max} \cos\phi}{E(\sin)\phi}\right]^{2/3} S^{1/2} \tag{8-15}$$

with

$$E(\sin\phi) \approx \left(\frac{\pi}{2}\right) \left(1 - \frac{1}{4} \sin^2\phi\right)$$

and

$$d_{max} = \frac{\tau_c}{0.97\gamma S} \tag{8-16}$$

then

$$\frac{T}{2} = \frac{\text{max}}{\tan\phi} \tag{8-17}$$

where T is the top width.

The product of A and U gives the discharge. If the given Q is different from the computed Q, the value of $d_{max}$ may be altered and a new discharge can be computed. This procedure is followed until computed and design discharges are equal. This procedure satisfies assumption 3 used for derivation of equations. When $Q_{given} > Q_{comp}$ a central section may be added to the cross section capable of delivering $(Q_{given} - Q_{comp})$ as shown in Figure 8-8.

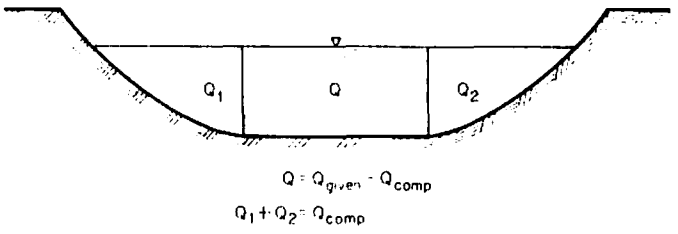


Figure 8-8. Central section added to a cross section.

Example C

Using the data from Example B the ideal stable section is determined, assuming $Q = 10\ m^3/sec$.

Solution

1. $$d_{max} = \frac{\tau_c}{0.97\gamma S}$$ Equation 8-16 and Figure 8-3

Given $\tau_c$ is equal to $0.9\ kg/m^2$

$$d_{max} = \frac{0.9}{0.97 \times 0.0006 \times 10^3} = 1.55\ m$$ 8-15

2. A is computed

$$A = \frac{2 \times \overline{1.55}^2}{0.73} = 6.58\ m^2$$ 8-13

3. U is computed

$$U = \frac{1}{0.022}\left[\frac{1.55\cos\phi}{\frac{\pi}{2}\left(1 - \frac{1}{4}\sin^2\phi\right)}\right]^{2/3} S^{1/2}$$ 8-14

$$U = 1.017 \sim 1.02\ m/sec$$

4. Q is computed

$$Q_{comp} = 1.02 \times 6.58 = 6.71 < 10.00\ m^3/sec$$

5. The discharge of central part is computed

$$Q_{cent} = 10.00 - 6.71 = 3.29 \ m^3/sec$$

6 The width of the central part B is computed using Manning's equation, noting that

$$A_{cent} = B \times 1.55 = \frac{Q_{cent}}{U}$$

so

$$B = \frac{0.022 \times 3.29}{1.55^{5/3} \times 0.0006^{1/2}} = 1.42 \ m$$

Empirical Relations for Stable Channel Design

Lacey (1929) published and then amended twice for a method for designing stable sandbed channels based on field data. Lacey's most common design relations are given in the following paragraphs and Table 8-5.

Field data systematically grouped and analyzed by Lacey yielded

$$U = a_1 R^{b_1} \tag{8-18}$$

with $a_1 = 1.17$ and $b_1 = 0.5$. Equation 8-18, that has a similar form to Kennedy's relation, takes the form

$$U = 1.17 R^{1/2} \tag{8-19}$$

This equation is in English units. According to Lacey, when Equation 8-19 applied to any type of sand-bed channel gives acceptable results and the canal designed accordingly is stable. In fact for large plains of mild slope and fine granular soil Lacey's method is reasonably successful. Lacey, furthermore defined a silt factor f expressed as

$$f = \left(\frac{a_1}{1.17}\right)^2 \tag{8-20}$$

The value of $a_1$ varies with type of material in which the canal is excavated. Then

$$U = 1.17\sqrt{Rf} \tag{8-21}$$

Lacey has given two additional equations similar to Equation 8-21. A recent one is

$$U = 1.15\sqrt{fR} \tag{8-22}$$

Table 8-4 summarizes the values of coefficient f proposed by Lacey.

For canals with the same hydraulic radius excavated in similar soil the product fR is constant. Possibilities exist that fP and fA

may be constant for constant values of velocity. From this point Lacey, using available field data showed that

$$Af^2 = 3.8\ U^5 \tag{8-23}$$

and

$$Qf^2 = 3.8U^6 \tag{8-24}$$

Lacey suggested two more relations to help define f. One is a function of Manning's n and the second is a function of the mean grain size $D_{50}$.

$$n = 0.022f^{0.2} \tag{8-25}$$

$$D_{50} = f^2/64 \tag{8-26}$$

Table 8-4. Values of silt factor f proposed by Lacey(*).

| Natural Soil | f |
|---|---|
| Lower Mississippi silt | 0.357 |
| Standard Kennedy silt | 1.00 |
| Medium sand | 1.31 |
| Coarse sand | 1.44 - 1.56 |
| Fine gravel | 2.00 |
| Large pebbles and coarse gravel | 4.68 |
| Small boulders, shingle and fine gravel | 6.12 |
| Medium boulders, shingle and fine gravel | 9.75 |
| Large boulders, shingle and fine gravel | 20.90 |
| Large stones | 38.60 |
| Massive boulders (D ~ 25 in.) | 39.60 |

(*)Raudkiwi, A. J. (1967)

$D_{50}$ in this formula is expressed in inches. When $D_{50}$ is given in millimeters Equation 8-26 takes the form

$$f = 1.59\sqrt{D_{50}} \tag{8-27}$$

In designing a stable channel using Lacey's method, for a given Q an f factor may be chosen according to the nature of the soil. Table 8-4 or one of the Equations 8-26 or 8-27 yields U. Using the value for U, A can be calculated from Equation 8-23 or R can be obtained from Equation 8-21

$$R = 0.7305\ U^2/f \tag{8-28}$$

Considering Equations 8-28 and 8-23

$$P = 3.8\ \frac{U^3}{0.7305\ f} \tag{8-29}$$

The wetted perimeter P is expressed as a function of mean velocity. It can also be expressed as a function of Q. When velocity U is eliminated from Equations 8-29 and 8-24

$$P = 2.668\ Q^{1/2} \tag{8-30}$$

Considering Equations 8-28, 8-25, and 8-24 it is possible to express the longitudinal slope S as a function of f and Q using Manning's relation

$$S = 0.00055\ f^{5/3}/Q^{1/6} \tag{8-31}$$

The set of relations proposed by Lacey for the computation of stable channel is summarized in Table 8-5 and channel design is illustrated in Example D.

Table 8-5. Lacey's formulae for computation of stable channels.

| | | | | | |
|---|---|---|---|---|---|
| 1) | $U = 1.15\sqrt{Rf}$ | (8-22) | 6) | $U = 0.794\ Q^{1/6} f^{1/3}$ | (8-32) |
| 2) | $R = 0.7305\ U^2/f$ | (8-28) | 7) | $R = 0.4725\ Q^{1/3}/f^{1/3}$ | (8-33) |
| 3) | $A = 3.8\ U^5/f^2$ | (8-23) | 8) | $A = 1.26\ Q^{5/6}/f^{1/3}$ | (8-34) |
| 4) | $P = 3.8\ \frac{U^3}{0.7305\ f}$ | (8-29) | 9) | $P = (8/3)\ Q^{1/2}$ | (8-35) |
| 5) | $S = 0.00044\ f^2/U$ | (8-31) | 10) | $S = 0.00055\ f^{5/3}/Q^{1/6}$ | (8-36) |

As an alternative to the Lacey equation refer to Figures 6A1-9, inclusive prepared by Simons (1963) at the end of Chapter 6 in Appendix 6A.

Example D

Given a discharge of 11,000 cfs and a bed material for which the median diameter is 0.23 mm and $\sigma = 1.5$, a stable channel should be designed using $a = 1/2$.

Solution

1. The silt factor should be determined using Equation 8-27

   $f = 1.59\ \sqrt{0.23} = 0.76$

   This value of f represents a minimum value. From experience $f = 0.89$.

2. Wetted perimeter P is determined using Equation 8-35

   $P = \frac{8}{3} \times 104.9 = 280$ ft

3. Bed slope S is determined using Equation 8-36

$$S = \frac{0.55 \times 10^{-3} \times .823}{4.72} = 9.59 \times 10^{-5}$$

4. Hydraulic radius R is determined using Equation 8-33

$$R = 0.4725 \left(\frac{11000}{0.89}\right)^{1/3} = 10.9 \text{ ft}$$

5. Wetted area A is determined using Equation 8-34

$$A = 1.26 \times 11000^{5/6} / 0.89^{1/3} = 3055 \text{ ft}^2$$

6. Velocity is determined

$$U = \frac{Q}{A} = \frac{11000}{3055} = 3.60 \text{ cfs}$$

Check this value with Equation 8-32

$$U = 0.794 \; 11000^{1/6} \; 0.89^{1/3} = 3.60 \text{ cfs}$$

7. Dimensions of the trapezoidal cross section are determined

$$\begin{cases} bd + \frac{1}{2} d^2 = 3055 \\ b + 2\sqrt{1.25}\, d = 280 \end{cases}$$

$$\begin{cases} b = 254 \text{ ft} \\ d = 11.6 \text{ ft} \end{cases}$$

8. Top width T is determined

$$T = 254 + 11.6 = 265.6 \sim 266 \text{ ft}$$

9. Manning's n is determined

$$n = \frac{1.49}{U} R^{2/3} S^{1/2}$$

$$n = \frac{1.49}{3.60} \times 10.9^{2/3} \times (0.0959 \times 10^{-3})^{1/2} = 0.0199 \sim 0.02$$

10. The bed form should be dunes. The design may be revised if necessary, otherwise the velocity may be too high causing excessive bank erosion.

Example E

A stable canal section should be designed for the following conditions

$Q = 1500\ m^3/sec$ $S = 0.001$ $D_{50} = 2.54\ cm$

$\gamma_s = 2.68\ t/m^3$ $g = 9.81\ m/sec$ $= 10^{-6}\ m^2/sec$

$n = 0.023$ (Figure 8-9)

If necessary the canal should be lined. The flow carries abundant sediment and the natural soil from which the canal is excavated ranges from graded loam to cobbles free from colloidal material.

Solution 1

Maximum permissible velocity

1. $U_{per} = 1.52$ m/sec is determined from Table 8-1

2. Maximum permissible velocity is determined from Equations 8-1 and 8-2 using the relations of Mavis and Carstens

$$U_b = \frac{1}{2}(25.4)^{4/9}\sqrt{1.68} = 2.7289 \sim 2.73\ ft/sec = 0.83\ m/sec$$

Using Carstens' relation

$$U_b = \sqrt{g \times \frac{1}{12} \times 1.68 \times 3.61(\tan\phi\cos\alpha - \sin\alpha)}$$

From Figure 8-4

$\phi = 35°$ for very round material
$\theta = 33.69°$ then $z = 1.5$
$S = \tan\alpha = 0.001$ and $\alpha = 0.057 \sim 0.06$. Then

$$U_{per} = \sqrt{32.2 \times \frac{1}{12} \times 1.68 \times 3.61\ (0.70 \times 0.99 - 0.001)}$$

$$= 3.36\ ft/sec = 1.02\ m/sec$$

These two values represent the velocity at the bed and may be checked after mean velocity is determined.

3. A is determined

$$A = \frac{Q}{U} = \frac{1500}{1.52} = 986.84 \sim 987\ m^2$$

4. $n = 0.023$

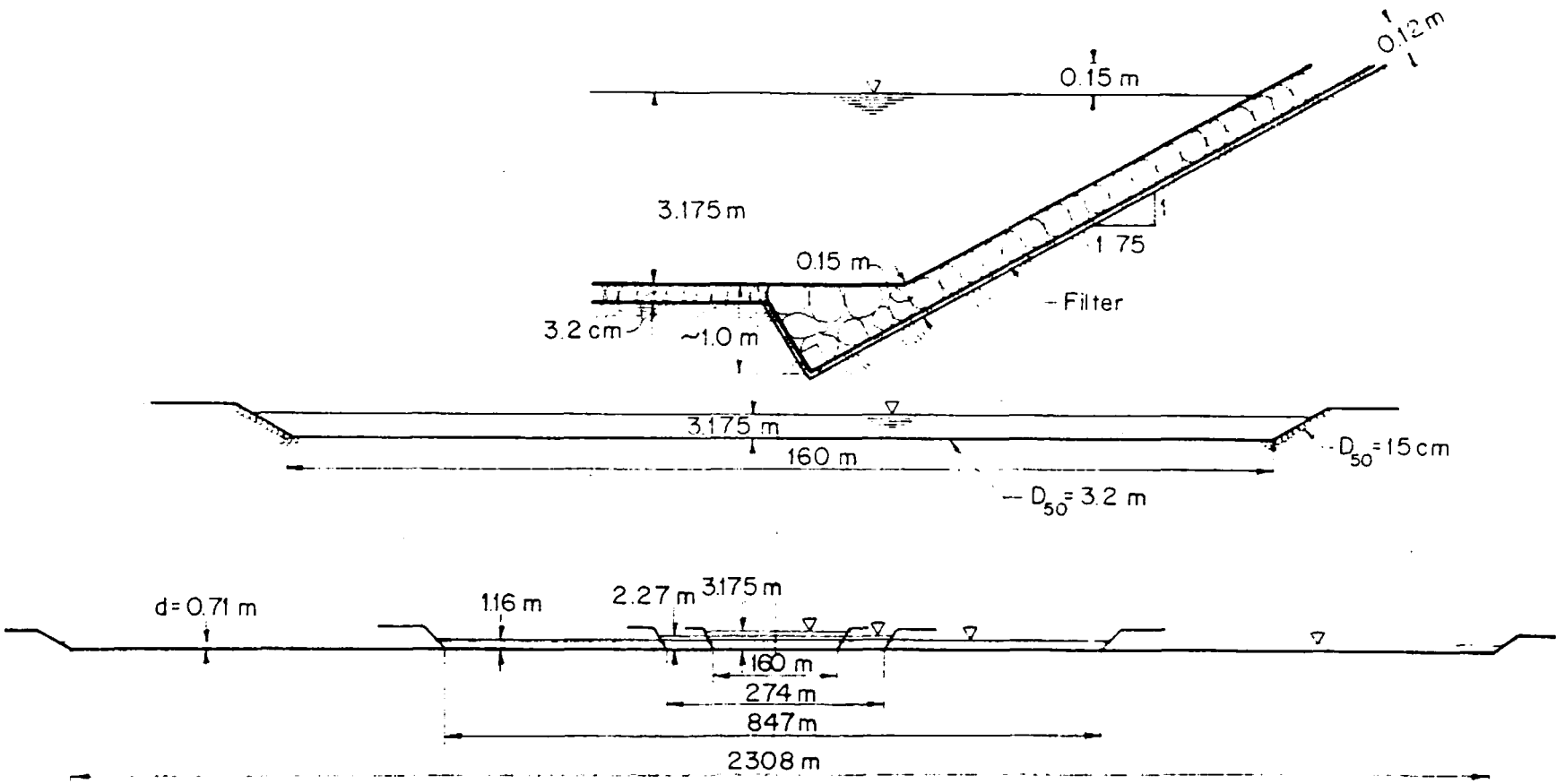


Figure 8-9. Cross section of the canal in Example E.

5. R from Manning's equation is determined

$$1.52 = \frac{1}{0.023} R^{2/3} 0.001^{1/2} \quad \text{and} \quad R = 1.16$$

6. For a trapezoidal section using

$$R = 1.16,\ A = 987\ m^2,\ \text{and}\ z = \frac{1}{1.5}$$

b and d are

$$b = 846.67 \qquad d = 1.16$$

7. Considering the equations given in Table 8-2 using Neill's equation

$$U_{per} = \sqrt{1.68 \times 32.2 \times \frac{1}{12} \times 2.5 \left(\frac{0.3048}{12 \times 1.16}\right)^{-0.2}}$$

$$= 4.92 \text{ ft/sec} = 1.50 \text{ m/sec}$$

Using Mirtshkulava's equation

$$n = 1 + \frac{0.0254}{0.00005 + 0.3 \times 0.0254} = 4.31 \quad \text{and}$$

$$U_{per} = \left(\log \frac{8.8 \times 1.16}{0.0254}\right) \sqrt{\frac{2 \times 9.81}{0.44 \times 4.31} 1.68 \times 0.0254}$$

$$= 1.73 \text{ m/sec}$$

Computing bottom velocity, assuming $k_s = 0.0254$

$$\frac{1.52}{U_*} = 8.5 + 5.75 \log \frac{1.16}{6} \times \frac{1}{0.0254}$$

Then $U_* = 0.112$ and

$$U_b = 0.112 \times 8.5 = 0.95 \text{ m/sec} = 3.12 \text{ ft/sec} \qquad (8\text{-}37)$$

This value of $U_b$ is approximately the same as that given by Carsten's equation but the value given by the Mavis equation is low.

Table 8-6 summarizes permissible velocities obtained using different approaches.

Table 8-6. Maximum permissible velocities.

| | |
|---|---|
| Mavis | $U_b = 0.83$ m/sec = 2.73 ft/sec |
| Carstens | $U_b = 1.02$ m/sec = 3.36 ft/sec |
| Fortier and Scobey | U = 1.52 m/sec = 4.99 ft/sec |
| Neill | U = 1.50 m/sec = 4.92 ft/sec |
| Mirtshkulava | U = 1.73 m/sec = 5.68 ft/sec |

U = 1.52 m/sec is the mean value of the velocities thus computed.

Solution 2

Critical shear stress method (cf. Example B)

1. Coefficient K is computed from Equation 8-7

$$K = \cos(33.69)\sqrt{1 - \frac{\tan^2 33.69}{\tan^2 35}} = 0.254$$

2. Critical shear is determined from Figure 8-5

$\tau_c = 2.2 \text{ kg/m}^2$

3. Permissible shear on the side slope is computed

$\tau_{ss} = 2.2 \times 0.254 = 0.5588 \cong 0.56$

4. For impending motion, assuming

$\frac{b}{d} > 10$

$\tau = 0.79\ \gamma SR = 0.79\ R \text{ kg/m}^2$

Then

$0.56 = 0.79\ R$ and $R = \frac{0.56}{0.79} = 0.71$

5. A and P are determined

$$Q = \frac{A}{0.023}\ 0.71^{2/3}\ 0.001^{1/2} = 1500 \text{ m}^3/\text{sec},$$

$A = 1641.35 \tilde{\sim} 1641 \text{ m}^2$ and

$P = 1641 \times 0.71^{-1} \cong 2311 \text{ m}$

6. Dimensions of the cross section are determined

$(b + 1.5d)\ d = 1641$

$b + 3.61\ d = 2311$ from which

$b = 2308.43$ and $d = 0.71$

Solution 3

Ideal stable section (cf. Example C)

1. $$d_{max} = \frac{2.2}{0.97 \times 0.001 \times 10^3} = 2.268 \sim 2.27 \text{ m}$$

2. $$A = \frac{2 \times \overline{2.27}^2}{0.7} = 14.72257 \sim 14.72 \text{ m}^2$$

3. $U = \frac{1}{0.023}\left[\frac{2.27 \times 0.819}{\frac{\pi}{2}(1 - \frac{1}{4} \times 0.329)}\right]^{2/3} 0.001^{1/2}$ 8-15

$U = 1.63$ m/sec

4. Compute Q is computed as

$Q_{comp} = 1.63 \times 14.72 = 23.99 \sim 24.0$ $m^3$/sec

$24.0 < 1500$

5. The discharge of the central part is computed as

$Q_{cent} = 1500 - 24 = 1476$ $m^3$/sec

6. Width B of the central part is computed as

$1476 = \frac{2.27B}{0.023} 2.27^{2/3} 0.001^{1/2}$

$B = 273.80 \sim 274$ m

7. $\frac{T}{2}$ is computed as

$\frac{T}{2} = \frac{d_{max}\pi/2}{\tan\phi} = 2.27 \times \frac{\pi}{2} \frac{1}{\tan 35} = 5.09$ 8-17

Summary of Results

Maximum permissible velocity method

$d = 1.16$ m

$b = 847$ m

$U = 1.52$ m/sec(*)

Critical shear velocity method

$d = 0.71$ m

$b = 2308$ m

$U = 0.91$ m/sec

Ideal stable cross section method

$d = 2.27$ m

$b = 279$ m

$U = 236$ m/sec

(*)The velocity $U = 1.52$ m/sec is used to compute b and d.

Lining

Cross sections as computed above are not economical and are not good conceptually from an engineering viewpoint. It is possible to obtain a more practical section by using a properly designed lining and a smaller section. For example

1. Choosing

$$\frac{b}{d} = 50$$

then

$$1500 = \frac{A}{0.023} R^{2/3} S^{1/2}$$

$$AR^{2/3} = 1090.98 \cong 1091$$

$$A = (b + 1.5d)d \quad \text{and} \quad b = 50d$$

$$P = 50d + 3.61d = 53.61d$$

$$R = \frac{51.5d^2}{53.61d} = 0.96d \quad \text{and} \quad R^{2/3} = 0.973d^{2/3}$$

$$AR^{2/3} = 51.5d^2 \times 0.973d^{2/3} = 50.1d^{8/3} = 1091$$

$$d = 3.175 \text{ m}$$

$$b = 158.75 \tilde{\sim} 160 \text{ m}$$

$$U = 2.89 \text{ m/sec}$$

2. Check this section for stability

$$R = 3.05 \text{ m}$$

$$\tau = 0.79 \gamma S \; 3.05 = 0.79 \times 1000 \times 0.001 \times 3.05 = 2.4095 \sim$$

$$2.41 \text{ kg/m}^2 \quad 2.41 > 0.56.$$

The channel section is not stable.

3. To choose riprap size for stabilization of the channel section, compute required riprap size for the bed using Meyer-Peter's criteria

$$\tau_c = \tau_b(\max) = 0.047 \; (S_s - 1)\gamma D_{50}$$

Assuming

$$S_s = 2.65 \text{ for the riprap}$$

$$D_{50} = \frac{2.41}{0.047 \times 1.65 \times 1000} = 0.031 \text{ m} \qquad (8\text{-}38)$$

this is a medium size gravel. The parameter should be checked

$$\frac{U_* D_{50}}{\nu} = \frac{\sqrt{gRS} \times D_{50}}{\nu} = 5362 > 200$$

The flow is fully turbulent. Hence, Equation 8-38 can be used. Acceptability of $D_{50}$ should be checked using SF = 1.2 following the procedure outlined in Riprap Design with Safety Factors (Simons and Sentürk, 1977, page 444) with the side slope specified.

4. Size of riprap may be checked using U.S. Army Corps of Engineers' approach. The following data will be used in solving the problem.

$\phi = 36°$ from Figure 8-4

$\theta = 33.69°$

$\alpha = \lambda = 0.06°$

$$u_r = 8.5\ U_* \qquad 8\text{-}37$$

$U_* = \sqrt{gRS} = \sqrt{9.81 \times 3.05 \times 0.001} = 0.172 \sim 0.17$ m/sec

$u_r = 8.5 \times 0.17 = 1.445 \sim 1.4$ m/sec $= 4.59$ ft/sec

$S_s = 2.65$

$k = D_{50} = 0.031$ m $= 0.10$ ft

Determination of the safety factor. From Equation 8-39

$$\eta = \frac{0.30\ u_r^2}{(S_s - 1)gk} \qquad (8\text{-}39)$$

$$\eta = \frac{0.30 \times \overline{4.59}^2}{(2.65 - 1) \times 32.2 \times 0.1} = 1.19$$

and from Equation 8-26

$$\beta = \tan^{-1}\left(\frac{\cos\lambda}{\frac{2\sin\theta}{\eta\tan\phi} + \sin\lambda}\right) \qquad 8\text{-}26$$

$$\beta = \tan^{-1}\left(\frac{0.999}{\frac{2 \times 0.555}{1.19 \times 0.727} + 1.05 \times 10^{-3}}\right) = 37.88°$$

The value of $\eta'$ is given by Equation 8-28 as

$$\eta' = \eta\left\{\frac{1 + \sin(\lambda + \beta)}{2}\right\} \qquad 8\text{-}28$$

$$\eta' = 1.19 \left(\frac{1 + \sin (0.06 + 37.88)}{2}\right) = 0.96$$

The safety factor for the rock is given by Equation 8-25 or

$$SF = \frac{\cos\theta \tan\phi}{\eta' \tan\phi + \sin\theta\cos\beta} = \frac{0.832 \times 0.727}{0.96 \times 0.727 + 0.555 \times 0.789}$$

$$= 0.533 < 1.6$$

This riprap is not stable. Hence, additional computations are required. These are tabulated in Table 8-7.

Table 8-7. Additional computations.

Choose $\theta = 33.69°$ $\tan\theta = \frac{1}{1.5}$ $\lambda = 0.06°$

| $D_{50}$ ft | $\phi$ degrees | $\tan\phi$ | $\eta$ | $\beta$ | $\eta'$ | SF |
|---|---|---|---|---|---|---|
| 0.10 | 36 | 0.727 | 1.19 | 37.88 | 0.96 | 0.533 |
| 0.50 | 40 | 0.839 | 0.238 | 10.20 | 0.14 | 1.05 |

Choose $\theta = 29.75$, $\tan\theta = \frac{1}{1.75}$ $\lambda = 0.06$

| | | | | | | |
|---|---|---|---|---|---|---|
| 0.50 | 40 | 0.839 | 0.238 | 11.37 | 0.143 | 1.20 |

The characteristics of the stable section are then

$b = 160$ m, $d = 3.175$ m, $z = 1.75$, $D_{50} = 0.50$ ft $= 0.15$ m

## 8.3 UTILITY OF VEGETATION AND ITS IMPACT ON CHANNEL STABILITY

### General

Stability of a stream, river, or canal refers to how channels accommodate the water and sediment inflow. "Most rivers if left completely to their own devices, will develop qualities that are at best inconvenient to man and his activities and at worst a threat to life and property," (Henderson, 1966). Thus man's interference with the natural response of rivers developed. More over, removal of natural vegetation in the drainage basins often aggrevated problems along streams and rivers.

There have been many efforts to stabilize channels and overcome these problems or in other words, to keep the river where it is. To accomplish this many devices are used depending on the local river

environment. Although various types of linings and jetties are the usual approach only the use of vegetation as an instrument of channel stabilization will be discussed.

The methods currently used to predict stability of a vegetative lining will be reviewed and evaluated in terms of physical significance. Also, a new approach based on the interaction of flow and vegetative properties will be suggested.

Since stability limits of vegetative channel linings are easily exceeded and vegetation is not suitable as a liner for permanent submergence, other forms of bank protection and their use in conjunction with vegetative linings will also be discussed.

## 8.4 METHODS OF DETERMINING STABILITY OF GRASSED CHANNELS

To date four methods to evaluate stability of grass lining have been proposed of which two are in general use.

### Maximum Permissible Velocity

Since about 1935, many flow tests over common American and Australian grasses have been performed and summarized by Cox and Palmer (1948), Ree and Palmer (1949), and Eastgate (1966). In each test depth of scour and general appearance of the channel was noted. Whenever conditions were such that unacceptable rates of scour and destruction of the channel lining occurred the mean velocity of flow was noted. Then the maximum mean velocity the channel withstood without significant damage was suggested as the maximum permissible velocity. Velocities tabulated in Table 3 of the "Handbook of Channel Design for Soil and Water Conservation" are reproduced in Table 8-8.

It should be noted that generally maximum permissible velocity is less for larger slopes. Also, velocities stated were often greatly exceeded without damaging the experimental channels from which the data was derived. Of course, these channels were usually prepared with great care and under ideal conditions resulting in vegetative linings of greater density and uniformity than those found in the field.

### Permissible Tractive Force

Because the removal of soil particles occurs when the force exerted on the particle exceeds the force resisting movement, it is more appropriate to base stability criteria on local boundary conditions. Furthermore, in the case of permissible velocity, local velocity that actually impinges on the particle and causes its movement is smaller than the mean velocity of flow. The discrepancy increases with depth. Figure 8-6b gives the appropriate correction for bare channels. Using the tractive force approach, this problem is circumvented since the tractive force calculated at any point on the channel boundary is the erosive agent.

Table 8-8. Permissible Velocities for Channels Lined with Vegetation.[1] The values apply to average uniform stands of each type of cover (USDA, 1954).

| Cover | Slope range[2] | Permissible velocity | |
|---|---|---|---|
| | | Erosion resistant soils | Easily eroded soils |
| | Percent | Ft per sec | Ft per sec |
| Bermudagrass | 0-5 | 8 | 6 |
| | 5-10 | 7 | 5 |
| | over 10 | 6 | 4 |
| Buffalograss<br>Kentucky bluegrass<br>Smooth brome<br>Blue grama | 0-5 | 7 | 5 |
| | 5-10 | 6 | 4 |
| | over 10 | 5 | 3 |
| Grass mixuture | [2]0-5 | 5 | 4 |
| | 5-10 | 4 | 3 |
| Lespedeza sericea<br>Weeping lovegrass<br>Yellow bluestream<br>Kudzu<br>Alfalfa<br>Crabgrass<br>Common lespedeza[4]<br>Sudangrass[2] | [3]0-5 | 3.5 | 2.5 |
| | [5]0-5 | 3.5 | 2.5 |

[1]Use velocities exceeding 5 feet per second only where good covers and proper maintenance can be obtained.

[2]Do not use on slopes steeper than 10 percent except for side slopes in a combination channel.

[3]Do not use on slopes steeper than 5 percent except for side slopes in a combination channel.

[4]Annuals--used on mild slopes or as temporary protection until permanent covers are established.

[5]Use on slopes steeper than 5 percent is not recommended.

For a vegetative lining, application of the tractive force approach becomes difficult. Figure 8-10 is a sketch of a typical distribution of velocity and shear in a vegetated channel. In the figure $u$ is the mean velocity at a distance $y$ from the bed and $\tau$ is the total shear at $y$ given by

$$\tau = \rho g \, (y_n - y) \, S \tag{8-39}$$

in which $y_n$ is the depth of flow. Subscript $n$ implies normal depth, thus uniform flow is referenced. When $y = 0$, the total bed shear $\tau = \tau_o = \rho g \, y_n \, S$.

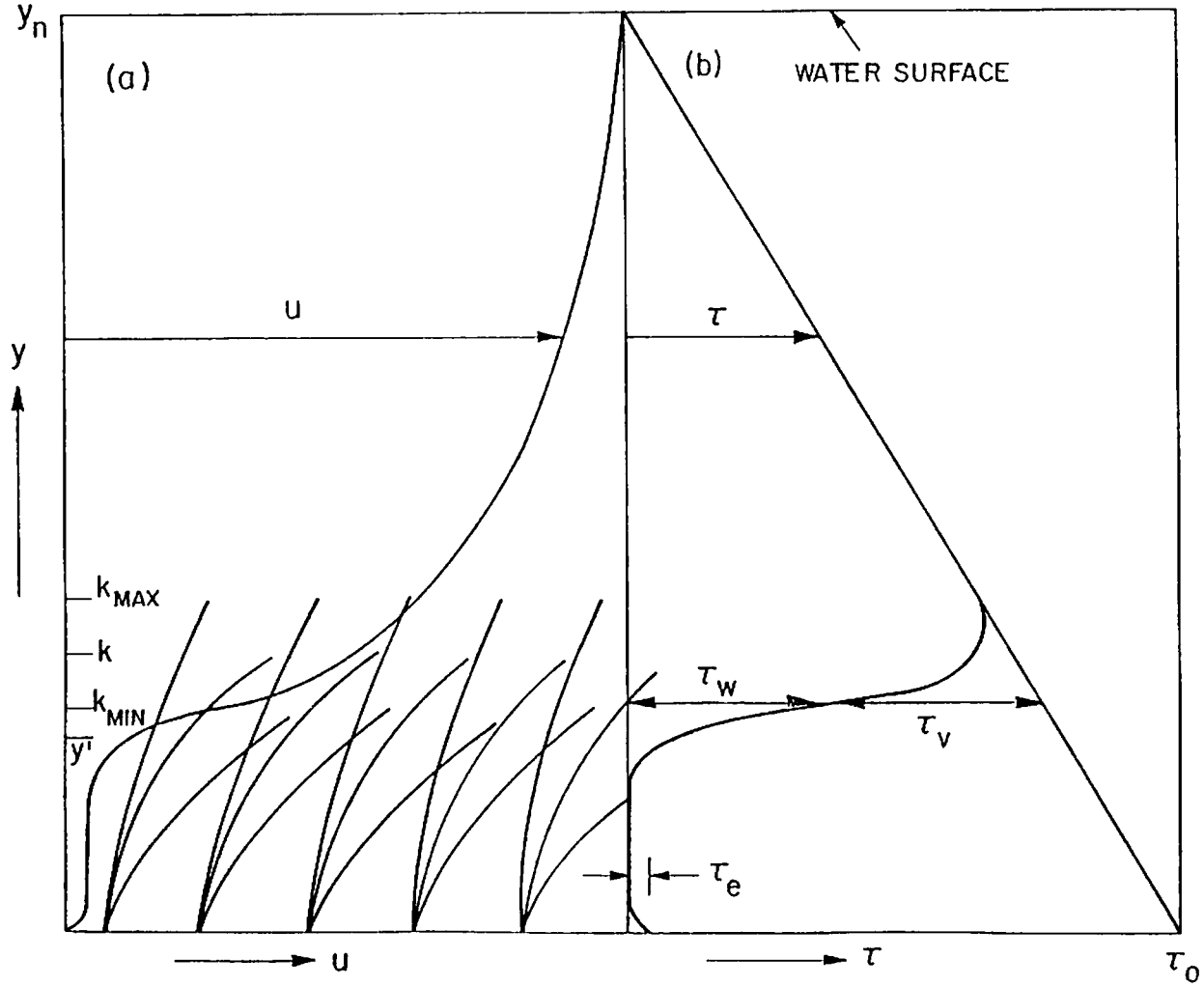


Figure 8-10. Distribution of shear and velocity in a vegetated channel.

Since drag exerted on vegetation by flowing water is proportional to $u^2$ for turbulent flow, much of the fluid shear is transferred to the vegetation at the tips where velocity is greatest. As the velocity is greatly reduced at lower levels in the vegetation, the amount of shear transferred by the fluid towards the bed is greatly reduced. If the vegetation is tall and stiff enough, a layer of virtually zero velocity gradient will exist. This implies zero fluid shear in this layer given by the Boussinesq expression for turbulent shear

$$\tau = \rho \varepsilon \frac{du}{dy} \tag{8-40}$$

where $\varepsilon$ is the virtual or eddy kinematic viscosity and $\rho$ the mass density of the liquid. As a result, the only shear acting on the soil is that required to reduce residual velocity $u_r$ to zero. In Eastgate's experiments $u_r$ seldom exceeded .3 m/s (1 ft/s) for slopes up to 7 percent. Such velocities are well below the lowest permissible velocity for bare soils and should never result in erosion among grass. Furthermore, it may be argued that the velocity gradient in this bottom layer is always smaller than the velocity gradient at similar distances from an unobstructed bed. It can thus be expected that for the situation shown in Figure 8-10 the effective shear $\tau_\varepsilon$ is always less than the permissible tractive force on a bare soil.

Temple (1979) suggested a method to quantify this effective shear by using the Taylor and Brooks (1962) logic of writing total shear as

$$\tau_o = \rho g y_n (S' + S'') \tag{8-41}$$

where $S'$ is the energy slope associated with the time average shear of the soil boundary and $S''$ is the drag of vegetal elements. Repeated application of Manning's equation yields

$$S' = (n_s/n)^2 \; S \tag{8-42}$$

and

$$S'' = (n_v/n)^2 \; S \tag{8-43}$$

where $n_s$ and $n_v$ are the Manning coefficients associated with soil and vegetative resistance respectively. Since $S = S' + S''$,

$$n = \sqrt{n_s^2 + n_v^2} \tag{8-44}$$

Temple then states that $n_s$ is relatively constant for a given soil. Thus in a vegetative channel $n_v$ is the varying factor. Temple suggests this implies a functional relation for $n_v$

$$n_v = n_v (C_I , R_V) \tag{8-45}$$

where $C_I$ is an emperical parameter describing vegetation and $R_V$ is a flow parameter. He writes a relation for $n$ with $C_I$ and $R_V$ as the variables to reproduce the A-E n-VR curves given in the Handbook of Channel Design for Soil and Water Conservation (USDA, 1954). Next Temple reasons that it is the vegetative stems ability to dissipate large turbulent eddies generated at the vegetation tips through waving that determines the erosion prevention characteristics of vegetation. He writes a functional relation

$$\tau_e = \rho g \, y_n \{[1 - f(C_F)] S' + g(C_F, C_I) \; S''\} \tag{8-46}$$

where $\tau_e$ is the effective shear stress at the soil-water interface, $C_F$ is an emperical parameter describing the potential of cover to dissipate turbulent eddies near the bed, $f(C_F)$ is a function describing the vegetal influence on turbulence generated at the soil boundary,

and $g(C_F,C_I)$ is a function describing the vegetal influence on the turbulence generated in the flow field by vegetal drag. Temple then states that $g(C_F,C_I)$ tends to zero because turbulence generated at some distance away from the bed would not effect conditions at the bed. He arbitrarily defines $f(C_F) = C_F$ resulting in

$$\tau_e = \rho g\, y_n\, S\, [(1 - C_F)\, (\frac{n_s}{n})] \qquad (8\text{-}47)$$

The $C_F$ values listed by Temple (1979) were obtained assuming a reference channel of depth 0.61 m (2 ft) and vegetated such that Manning's n fell on the C retardance curve. Using allowable tractive force for the soil in question as the effective shear stress, Equation 8-47 can be solved for $C_F$. Presumably S in Equation 8-47 was obtained through the Manning formula during calibration. The allowable tractive force for a soil type was obtained from Fortier and Scobey's (1926) data and recommendations.

Equivalent Stone Size

Parsons (1963) introduced the notion of an equivalent stone size to describe resistance of vegetation to destruction by flowing water. Using Ree and Palmer's (1949) tabulation of allowable velocities, slopes, and hydraulic radii Parsons computed the stone sizes required to give the same bank protection. Equivalent sizes are reproduced in Table 8-9.

This approach can give the designer familiar with capability of stone protection an appreciation of the protective capabilities of a vegetative liner. It also permits a ready comparison of costs.

Maximum Permissible Depth

Normann (1975) converted the Handbook's (USDA, 1954) values for permissible velocity to values for permissible depth. For a series of slopes he found permissible velocity's velocity. He then assumed the permissible velocity to be mean central velocity and using n-VR curves (USDA, 1954) he found n and R to match n versus VR. Next he set $d_{max} = R$ (R is the hydraulic radius) and then plotted $d_{max}$ versus slope for each vegetation.

Table 8-9. Equivalent stone sizes for Bermuda grass linings (Parsons, 1963).

| Condition of Bermuda grass | Allowable shear stress | Equivalent stone diameter |
|---|---|---|
| | Lb/sq. ft | Inches |
| Fair stand, short,[1] dormant | 0.9 | 2 |
| Good stand, kept short, dormant | 1.1 | 2 |
| Good stand, long,[2] dormant | 2.8 | 5.5 |
| Excellent stand, kept short, green | 2.7 | 5.5 |
| Good stand, long, green | 3.2 | 6.5 |

[1]Less than 5 inches high.

[2]Greater than 8 inches high.

Thus if channel slope and vegetation type are known, the value of permissible depth is easily determined from the charts. The remainder of the cross section is designed around this maximum depth.

Permissible Deflection

The tractive force method of determining channel stability incorporates the physical actions of particle removal at the bed. For channels in which erodable particles are also the particles directly affecting the resistance to flow, this approach is justifiable. It must be remembered however, that the mechanism of shear or momentum transfer is still embodied in the Boussinesq expression for shear (Equation 8-40). When shear is expressed as in Equation 8-39, it is an expression of the time average value of the Boussinesq shear which varies with respect to time. Thus when a large turbulent velocity component is near the bed, shear created by the large velocity gradient is the force removing the particle. Obviously magnitude of such a shear varies randomly as does the turbulent velocity creating it. While this instantanious shear cannot now by explicitly defined, two aspects of flow over and through vegetation are clearly evident from velocity profiles over grass and flexible linings.

1. When the grass remains relatively upright, velocity near the bed was seldom observed to exceed 0.3 m/s (1 ft/s) in any of Eastgate's (1966) experiments even though slopes ranged up to 7 percent.

2. For flow over plastic roughness and Eastgate's grass velocity below a distance $y'$ (the velocity intercept) was always small but the plastic strips waved downwards to about $y'$ under the action of large turbulent eddy velocities.

Therefore the lowest permissible velocity for any soil listed in Table 8-1 is .53 m/s (1.45 ft/s) thus it may be argued that any soil will be removed as long as $y'$ does not approach the bed. It has been observed that no large turbulent velocity components reach a level lower than $y'$ for data collected over plastic strips. Figures 8-11 and 8-12 are profiles of mean velocity, intensity of turbulence $\sqrt{u'^2}/u$, and eddy kinematic viscosity measured over flexible plastic roughness (Kouwen et al., 1980). In Figure 8-11 boundary shear is small, there is little deflection of the roughness, and $y'$ is located away from the bed along with the high velocities. In the figures $k_{max}$, $k$, and $k_{min}$ denote maximum, average, and minimum locations of roughness tips while waving up and down. In Figure 8-12 total shear is increased and the quantities $y'$, $k_{max}$, $k$, and $k_{min}$ are lowered. It should be noticed in both figures the proximity of $k_{min}$ to $y'$ but more important is the closeness of $k_{min}$ and $y'$ to the bed in Figure 8-12. This indicates that at times very high velocity particles of fluid exist near the bed setting up large shear forces. It is hypothesized that whenever $y'$ closely approaches the bed, large velocity gradients will intermittently exist near the bed and erosion results.

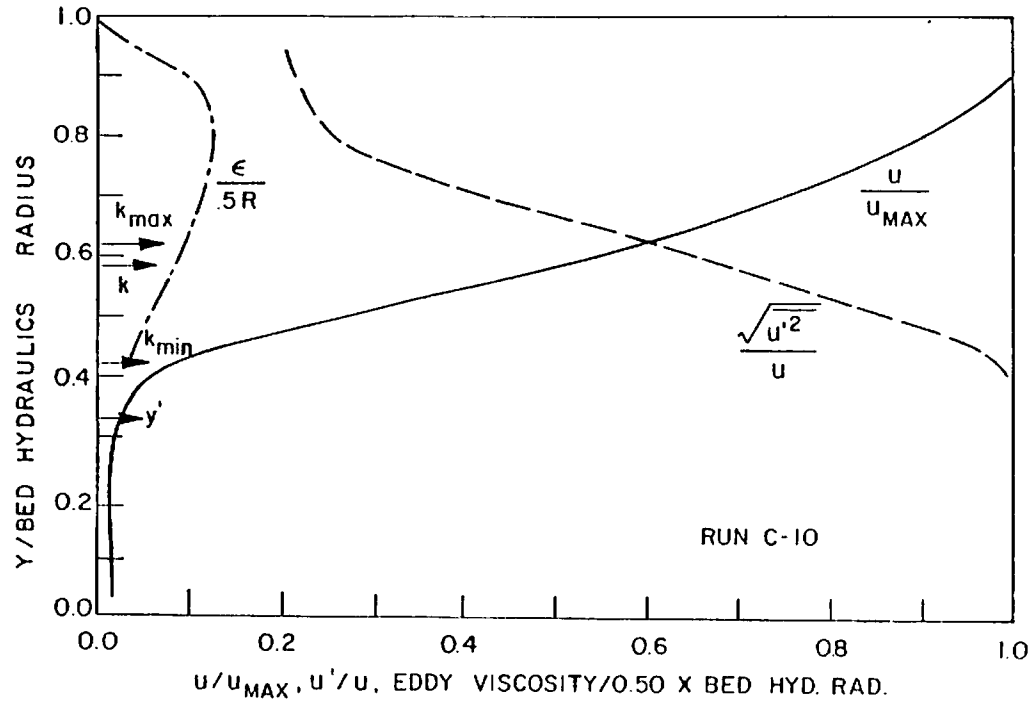


Figure 8-11. Velocity profile due to low shear.

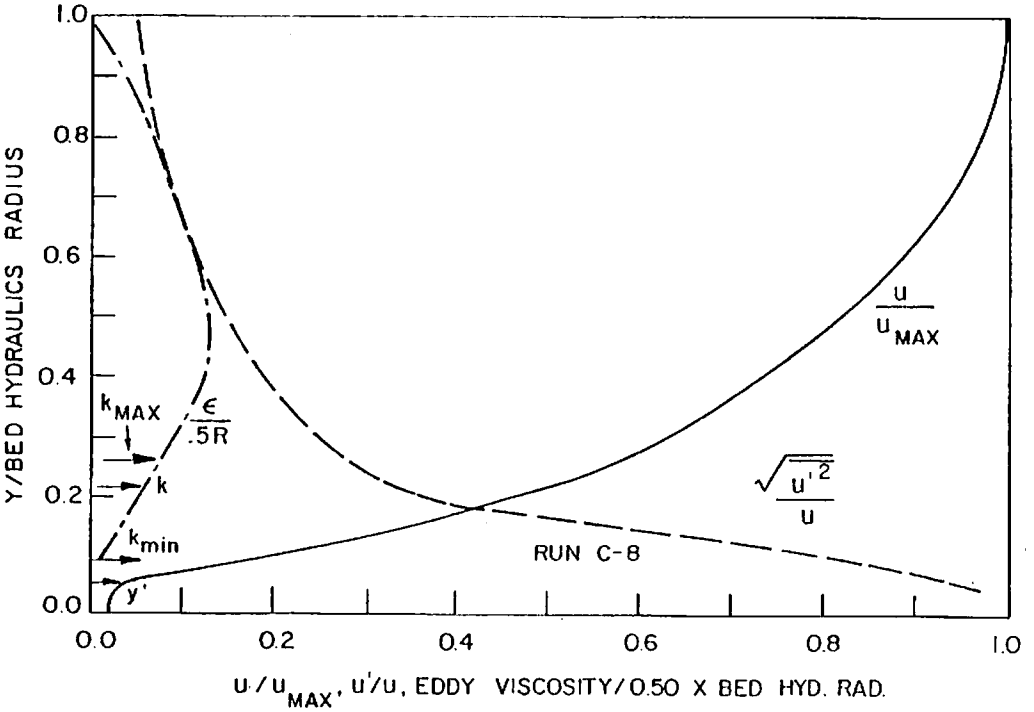


Figure 8-12. Velocity profile due to high shear.

A line drawn through the data for plot $y'/_h$ versus $k/_h$ for flexible plastic strips, intersects the horizontal axis at about $k/_h = .35$ indicating a negative $y'$ for values of $k/_h$ less than .35 (Figure 8-13). Physically this is impossible since $y'$ must be positive when the datum is taken to be the elevation of soil-water interface. In actual fact, the line would curve towards the origin of the graph. It is further hypothesized that the intersect of the line with the horizontal axis approximates the value of $k/_h$ below which large turbulent velocities occasionally penetrate the lining and cause erosion. Should this hypothesis be true, the Ree and Palmer (1949) and Cox and Palmer (1948) data summaries should show a significant change in the erosion rates when the ratio $k/_h$ becomes less than .35 for a given flow situation. In doing this it is assumed that the relationship $y'/_h$ as a function of $k/_h$ derived from plastic roughness is valid for real vegetation. It is implied that whenever a local shear is large enough to bend the lining to this degree, effective shear on the soil will be well above maximum permissible tractive force for most soils.

A perusal of the Ree and Palmer (1949) and Cox and Palmer (1948) data indicates the above stated hypothesis is true. Figure 8-14 consists of separate plots of the erosion rates versus the ratio $k/_h$ for long green Bermuda, short green Bermuda, Blue Grama, Buffalo, Weeping Lovegrass, and Alfalfa. The open points refer to experimental observations of scour which were followed by higher flows but with lower rates of scour. Cox and Palmer reported the experiments were run at successively higher flow rates. Often some erosion of loose material occurred at low flows followed by higher rates of flow with no or reduced rates of material removal. Obviously these conditions did not impair the channel stability. Solid points refer to erosion rates which increase with increasing flow. It is reasonable to conclude that these points indicate the condition at which failure of the lining was initiated. The plots in Figure 8-13 show that for long green Bermuda, Blue Grama, Buffalo, Weeping Lovegrass, and Alfalfa failure of the vegetal lining will usually result in $k/_h$ being less than .35. There is thus some variation for specific grasses. It appears that for short Bermuda grass failure is initiated when $k/_h$ becomes less than 0.60. Plots in Figure 8-14 show that above these critical values of $k/_h$ some and do not result in catastrophic failure of the lining.

In the deflection method, prediction was made solely on the physical, easily visualized behavior of the fluid and channel lining. This method is based on a rationalization of observed phenomena and the intermittency of the process is implicitly included. The approach is embodied in the degree to which the lining is deformed through the relation

$$k/_h = fn \left\{ \left( \frac{MEI}{\tau_o} \right)^{1/4} /_h \right\} \qquad (8\text{-}48)$$

given by Kouwen and Unny (1973) in which MEI represents stiffness of the lining and $\tau_o$ total boundary shear $\rho g\, y_n\, S$. Kouwen and Li (1980) list values for MEI and Kouwen et al. (1980) summarize the values.

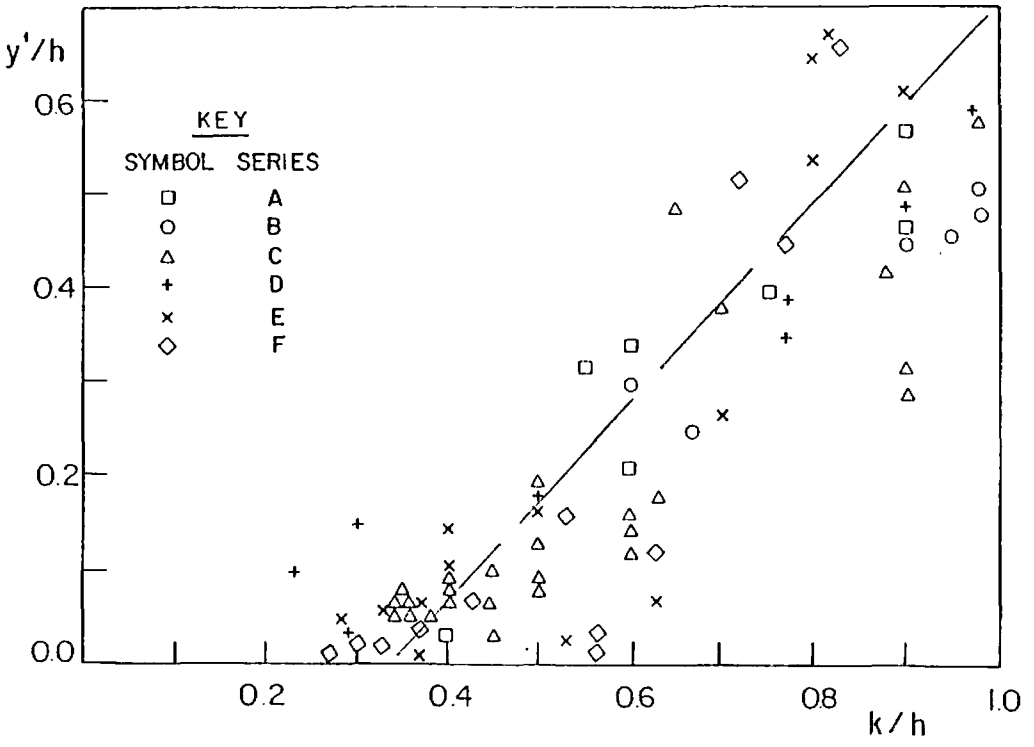


Figure 8-13. Plot of $y'/_h$ versus $k/_h$ for plastic roughness.

## 8.5 PRACTICAL CONSIDERATIONS

Is it well known that vegetative linings do not withstand large shear forces nor do they easily survive long periods of submergence. Thus, vegetative linings may be impractical and other linings such as concrete or rip rap might be utilized. Although design of such linings are not within the scope of this paper, often composite linings can be utilized to reduce costs. Such linings may consist of concrete or rip rap in areas of high shear or long term submergence and vegetation in the remainder of the cross section. Design of such linings are covered by Silberger (1959), Normann (1975), USDA (1954), and others. Ree (1951) describes tests in one such channel on a 10 percent slope.

Figure 8-15 is a reproduction of Ree's figure showing the dimensions and velocity distribution. Ree concluded that the usual practice of summing calculated discharge rates for the component parts of the cross section to give the capacity of a composite channel seems a valid method. Furthermore, he found that high velocities in the gutter section do not carry over appreciably to the grassed portion of the waterway and therefore concluded that observed scour at the junction cannot be attributed to excessively high velocities. However, based on the earlier discussion regarding the probably of high velocity eddies intermittently reaching the bed and causing erosion, it seems prudent to provide some sort of apron. The apron should be designed so that the velocity profile will be continuous across the joint thus preventing the

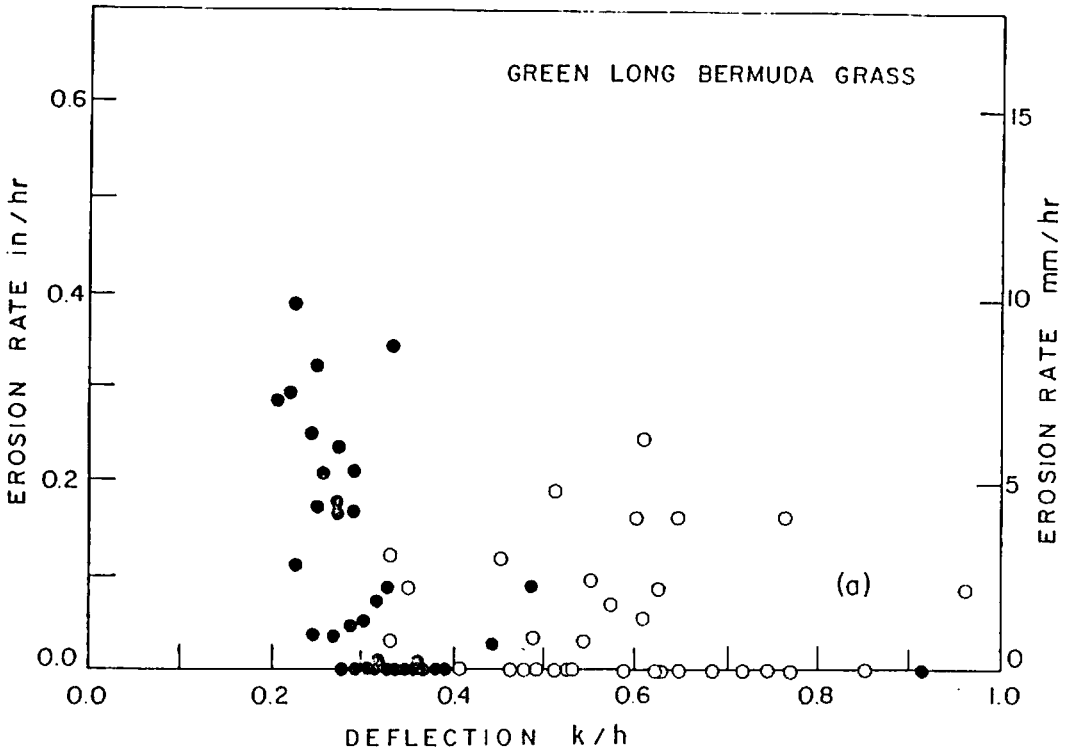


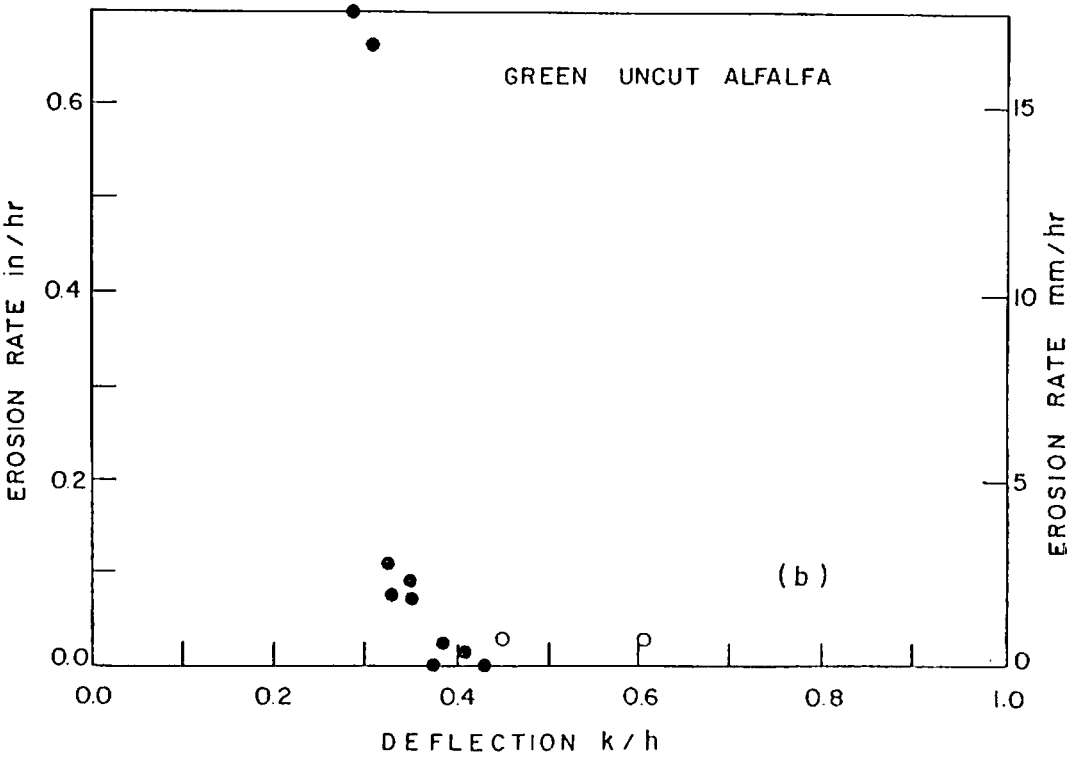


Figure 8-14. Plots of erosion rate as a function deflection of the vegetation.

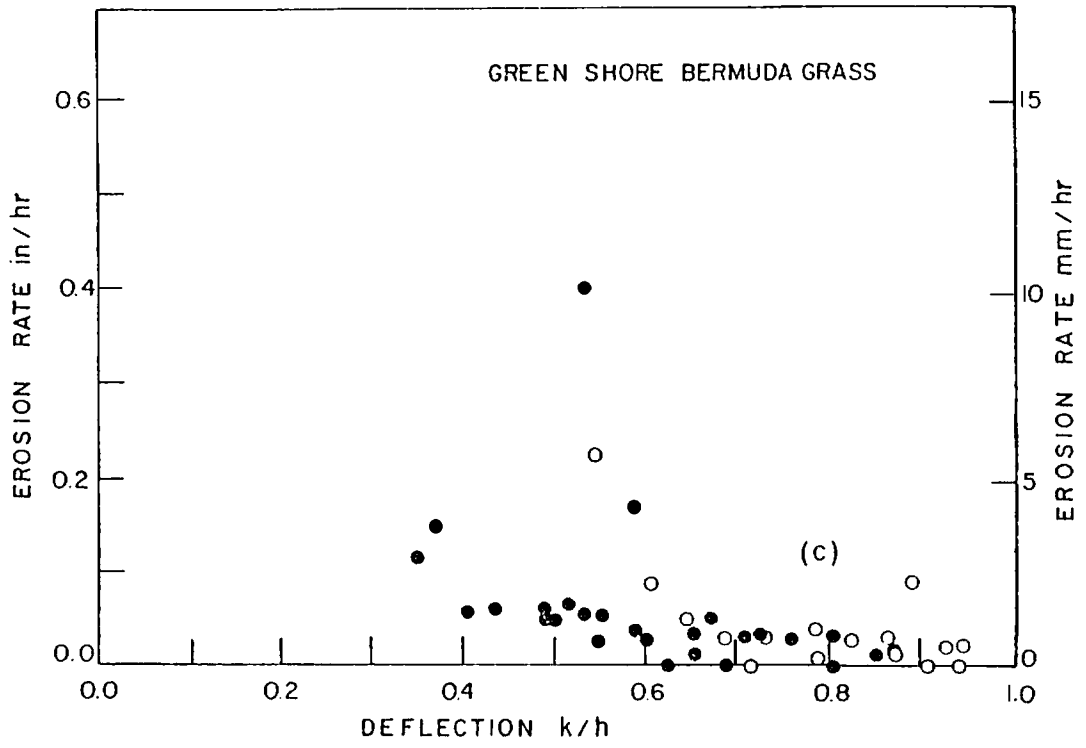


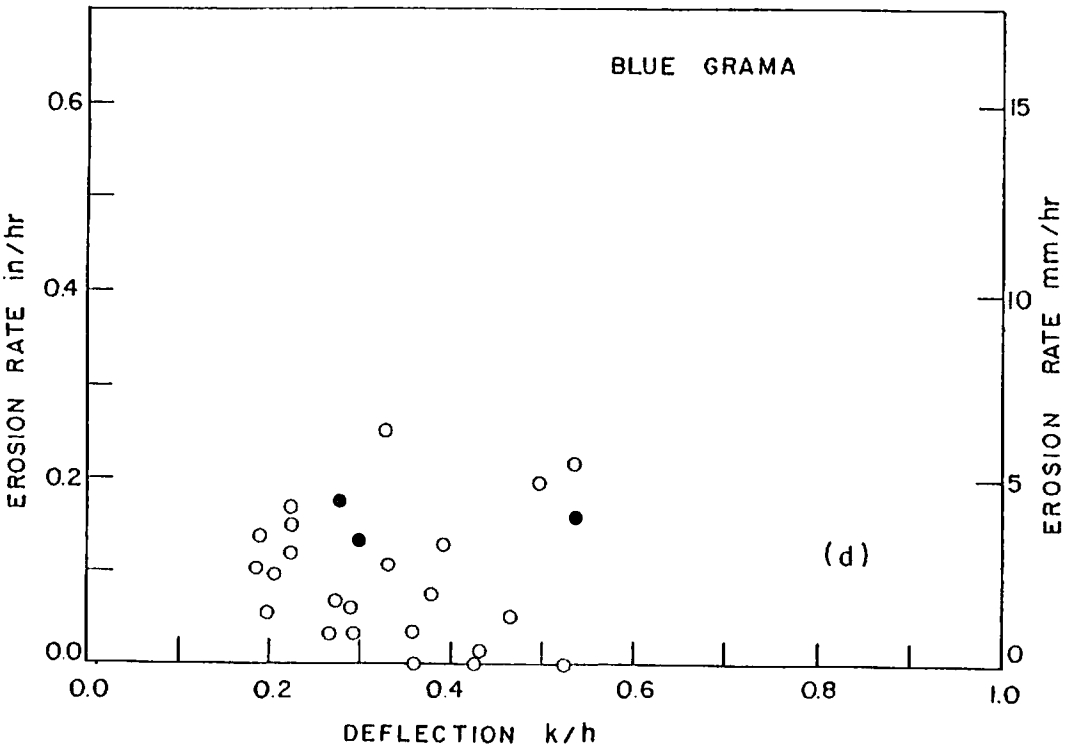


Figure 8-14. (Continued).

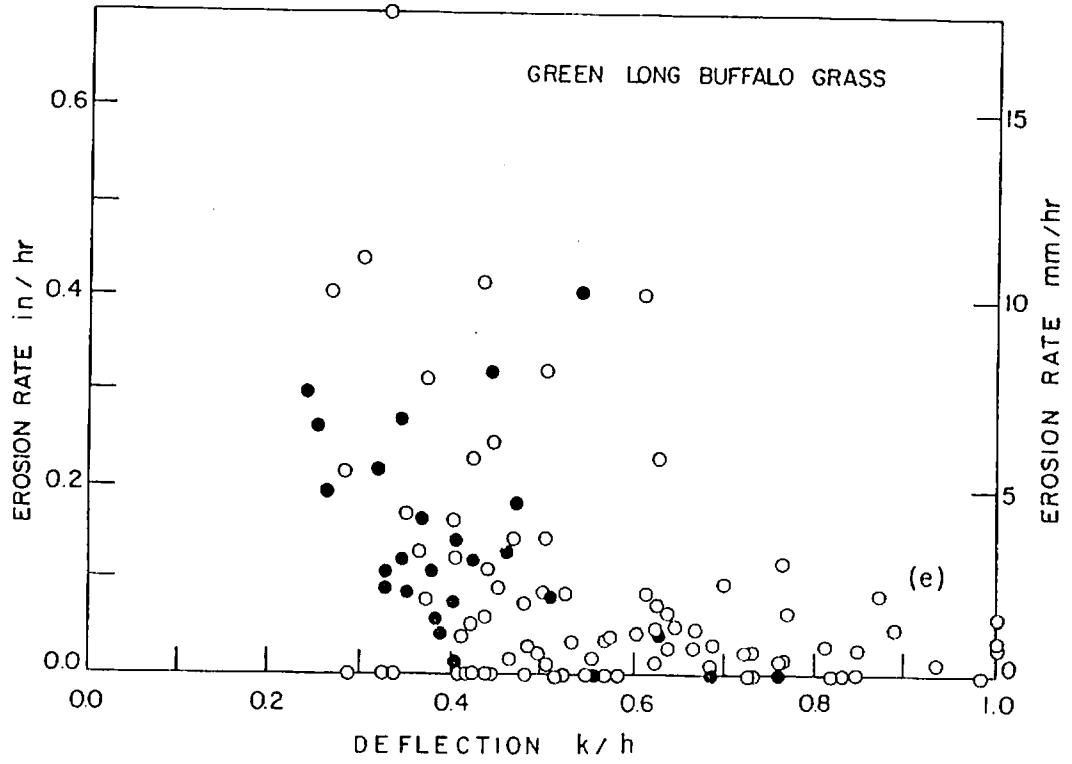


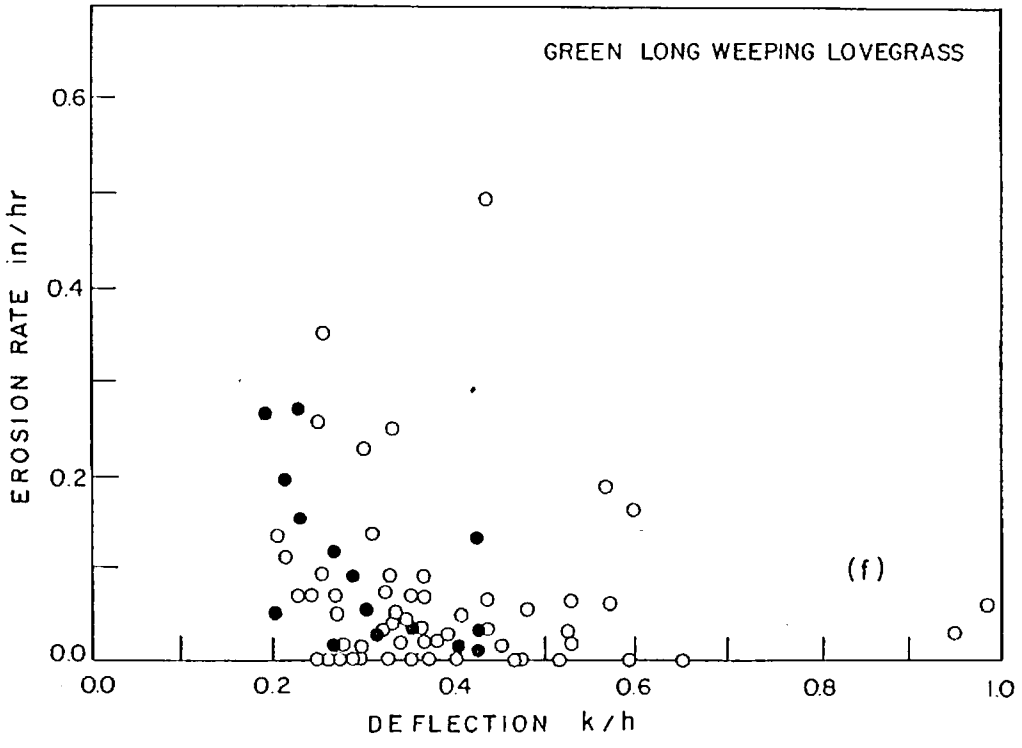


Figure 8-14. (Continued).

formation of a shear zone and its resulting turbulence. Figure 8-16 shows two examples of such junctions. The surface of the rigid lining should line up with y', the velocity intercept of the flowing water, at design depth.

The design of the rip rap or concrete part of the cross section should be according to accepted procedures as given in many manuals and textbooks.

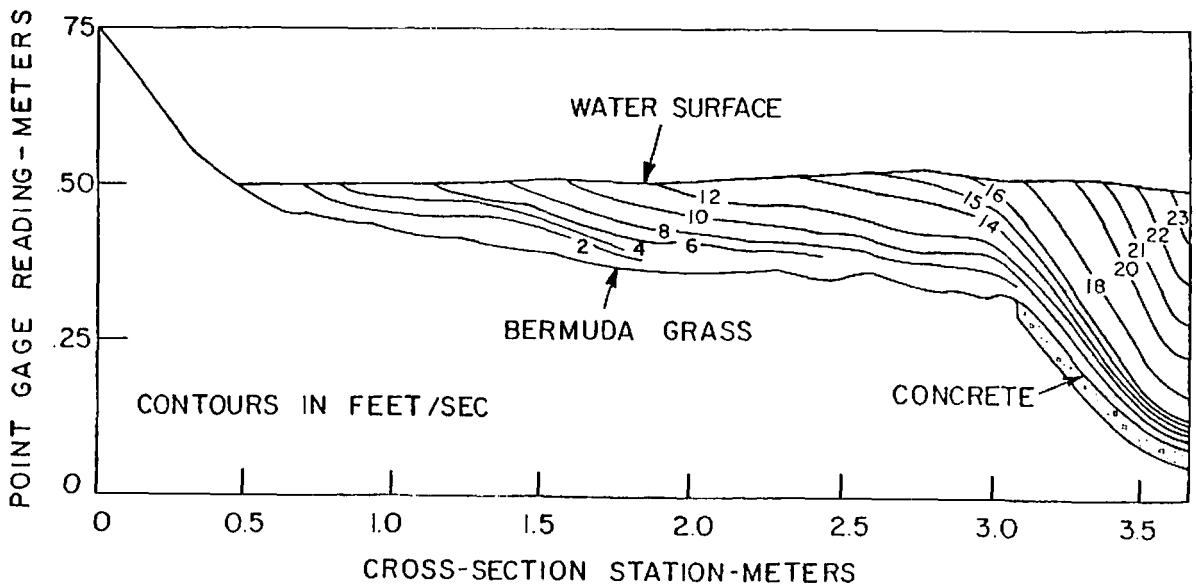


Figure 8-15. Dimensions and velocity distribution, Ree (1951).

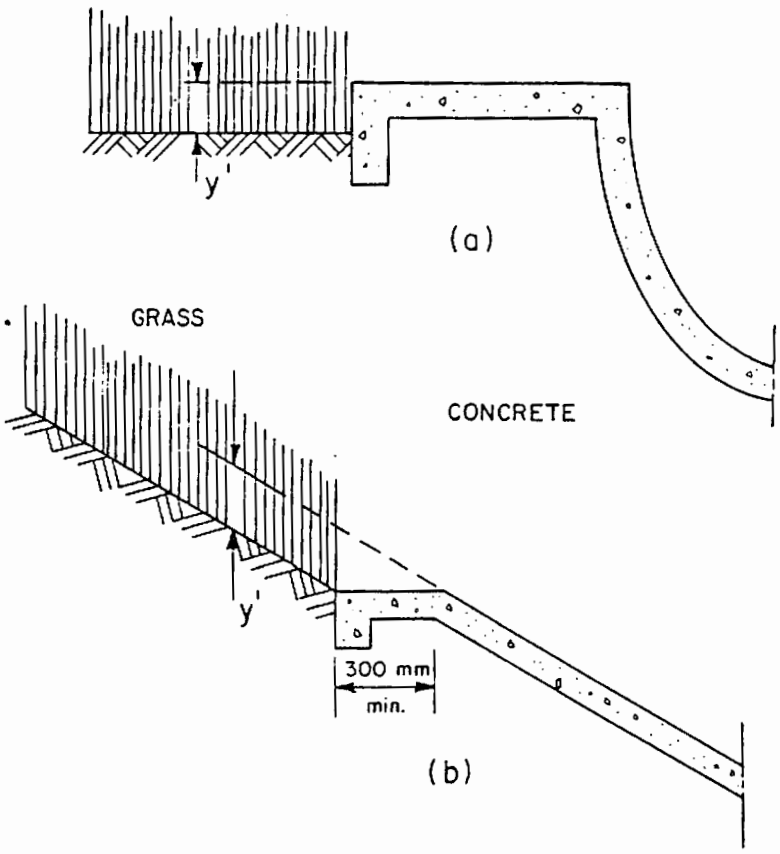


Figure 8-16. Detail of suggested grass to concrete junction.

## SYMBOLS

| Variable | Definition |
|---|---|
| $C_I$ | An empirical parameter describing vegetal conditions in the flow field |
| $C_F$ | An empirical parameter describing the potential of the vegetal cover to dissipate turbulent eddies in the immediate vicinity of the boundary |
| $d_{max}$ | Maximum channel depth |
| g | Acceleration due to gravity |
| h | Vegetation length |
| k | Deflected vegetation height |
| $k_{min}$ | Lowest point reached by tips of the vegetation while waving in the flow |
| $k_{max}$ | Highest point reached by tips of the vegetation while waving in the flow |
| n | Manning's coefficient |
| $n_s$ | Manning's coefficient associated with bare soil |
| $n_v$ | Manning's coefficient associated with vegetal drag |
| MEI | Aggregate value of relative vegetative stiffness |
| M | Stem count per square meter |
| E | Modulus of elasticity of vegetation |
| I | Moment of inertia of area of plant stems |
| S | Energy slope |
| S' | Energy slope associated with time average shear at the soil boundary |
| S" | Energy slope associated with drag on the vegetal elements |
| u | Mean velocity at a distance y from the bed |
| $u_r$ | A residual velocity of uniform distribution with y associated with flow through the vegetation |
| u' | Turbulent velocity in the direction of mean flow |
| y | Distance above the bed |

| Variables | Definition |
|---|---|
| $y_n$ | Normal depth |
| $y'$ | Velocity profile intercept with the y axis |
| $\varepsilon$ | Eddy or virtual kinematic viscosity |
| $\rho$ | Mass density of water |
| $\tau$ | Shear at distance y above the bed |
| $\tau_o$ | Total boundary shear |
| $\tau_e$ | Effective shear at the soil water interface |

## REFERENCES

Cox, M. B. and Palmer, V. J., 1948, "Results of Tests on Vegetated Waterways and Method of Field Application," Oklahoma Agricultural Experiment Station, Misc. Pub. No. MP-12, January, pp. 1-43.

Eastgate, W. I., 1966, "Vegetated Stabilization of Grassed Waterways and Dan Bywashes," M. Eng. Sc. Thesis, Department of Civil Engineering, University of Queensland, St. Lucia, Queensland, Australia.

Fenzi, K. N. and Davis, J. R., 1964, "Hydraulic Resistance Relationships for Surface Flows in Vegetated Channels," Trans. ASAE, Vol. 7, No. 1, pp. 46-55.

Fortier, S. and Scobey, F. C., 1926, "Permissible Canal Velocities," Transactions, ASCE, Vol. 89, pp. 940-956.

Henderson, F. M., 1966, "Open Channel Flow," MacMillan, New York.

Kouwen, N. and Li, R. M., 1979, "Biomechanics of Vegetative Channel Linings," Journal of the Hydraulics Division, ASCE, In print.

Kouwen, N., Li, R. M. and Simons, D. B., "On the Method for Designing Vegetated Waterways," Transactions, ASAE, In print.

Kouwen, N., Li, R. M. and Simons, D. B., 1980, "Velocity Measurements in a Channel Lined with Flexible Plastic Roughness Elements," Technical Report No. CER79-80NK-RML-DBS11, Department of Civil Engineering, Colorado State University, Fort Collins, Colorado.

Kouwen, N. and Unny, T. E., 1973, "Flexible Roughness in Open Channels," Journal of the Hydraulics Division, ASCE, Vol. 99, No. HY-5, Proc. Paper 9723, May, pp. 713-728.

Normann, J. M., 1975, "Design of Stable Channels with Flexible Linings," Hyd. Eng. Circ. No. 15, USDT, FHA, pp. 1-136.

Parsons, D. A., 1963, "Vegetative Control of Streambank Erosion," Proceedings, Federal Interagency Sedimentation Conference, Miscellaneous Publication No. 970, U.S. Department of Agriculture, pp. 130-136.

Raudkiwi, A. J., 1967, Loose boundary hydraulics, Commonwealth and International Library, publisher, R. Maxwell.

Ree, W. O. and Palmer, V. J., 1949, "Flow of Water in Channels Protected by Vegetative Linings," U.S. Soil Conservation Bulletin No. 967, February, pp. 1-115.

Ree, W. O., 1951, "Preliminary Report of Tests on a Grass Lined Channel with a Center Concrete Gutter Section," U.S. Department of Agriculture, Soil Conservation Service, pp. 1-12, Unpublished Report.

Silberger, L. F., 1959, "Streambank Stabilization," Agricultural Engineering, Vol. 40, No. 4, April, pp. 214-217.

Simons, D. B. and Sentürk, F., 1977, "Sediment Transport Technology," Water Resources Publications, Fort Collins, Colorado.

Taylor, R. H. and Brooks, N. H., 1962, "Discussion of Resistance to Flow in Alluvial Channels," by D. B. Simons and E. V. Richardson, Trans. ASCE, Vol. 127, Part I, pp. 982-992.

Temple, D. M., 1979, "Tractive Force Design of Vegetated Channels," Presented at the 1979 Summer Meeting of the ASAE and CSAE, University of Manitoba, Winnipeg, Canada, Paper No. 79-2068, pp. 1-20.

USDA, Soil Conservation Service, 1954, "Handbook of Channel Design for Soil and Water Conservation, SCS-TP-61, Washington, D.C., pp. 1-34.

# CHAPTER 9

# CHANNEL PROTECTION

## 9.1 INTRODUCTION

After studying the chapters on river mechanics and geomorphology, it should be clear that both short- and long-term changes may be expected on river systems as a result of natural and man-made influences. These changes can reduce navigability of the river and cause bank erosion and property losses that could involve litigation and legal expenses. Using a management plan to control river systems can minimize these adverse effects. Recommended structures and design methods for river control are presented.

Numerous types of channel protection and bank stabilization devices have evolved through past experience. Concrete, brick, willow and asphalt mattresses, sacked concrete and sand, riprap, grouted slope protection, sheet piles, timber piles, steel jack and brush jetties, angled and sloped rock-filled, earth-filled and timber dikes, automobile bodies, and concrete tetrahedrons have all been used in the practice of training rivers and stabilizing river banks. An extensive treatise on the subject of bank and shore protection was prepared by the California Division of Highways (1970). A large number of publications on river training and stabilization have been prepared by the Corps of Engineers, U.S. Soil Conservation Service, and U.S. Bureau of Reclamation. Many more publications on the subject exist in open literature. It is not intended that an exhaustive coverage of the various types of river control structures and methods of design be made in this section. Rather, the purpose is to recommend methods and devices that provide useful alternatives to the engineer for circumstances he is likely to encounter.

Generally, changes to river alignment, river cross section, training, and bank stabilization are confined to short reaches of the river. While methods for river training and bank stabilization discussed herein are applicable to short and long reaches of the river, they are not panacea to all problems associated with encroachments on rivers. Handbook-type analyses and designs usually lead to poor solutions of specific problems. Also, solution to a particular problem may generate problems elsewhere in the river system.

## 9.2 CHANNEL IMPROVEMENT

In some circumstances it could be advantageous to change river channel alignment as shown by the example (Figure 9-1a). This is assuming that alignment is fixed by constraints in the acquisition of the right-of-way.

To create better flow alignment, consideration is given to channel improvement as shown in Figure 9-1b. Similarly, consideration for improvement to the channel would also be advisable for a hypothetical lateral encroachment as depicted in Figure 9-1c. In either case, the designer's questions are how to realign the channel and what criteria should be used to establish the cross-sectional dimensions.

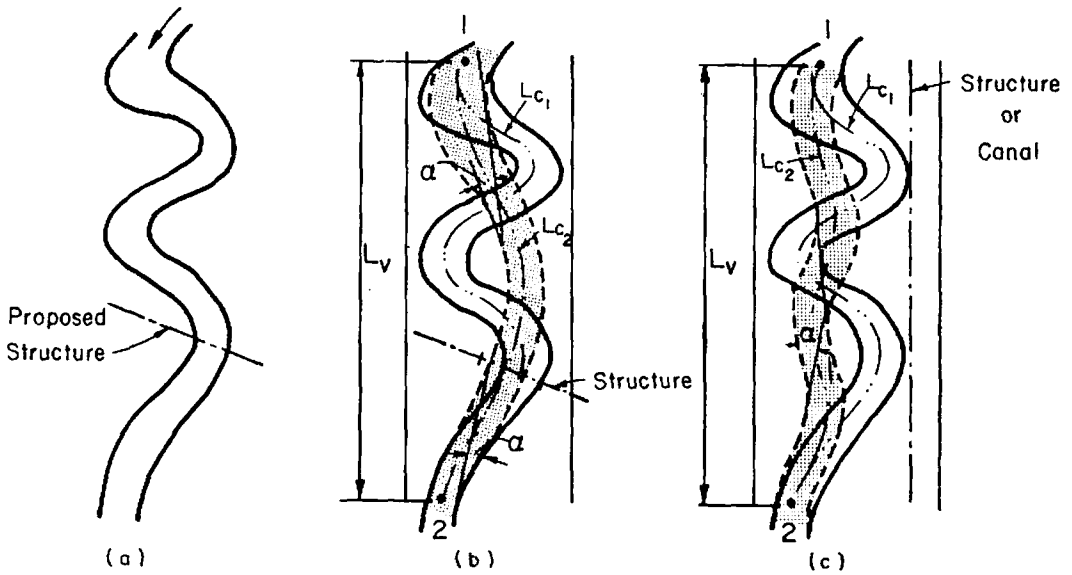


Figure 9-1. Encroachment on a meandering river.

A river channel may be realigned straight without curves or may include one or more curves. If curves are included, radii of curvature, number of bends, limits of rechannelization (hence length or slope of channel), and cross-sectional area are characteristics that must be determined by the designer. Different rivers have different characteristics and historical backgrounds with regard to channel migration, discharge, stage, geometry, and sediment transport and as indicated in the previous chapters, it is important for the designer to understand and appreciate river hydraulics and geomorphology when making decisions concerning channel improvement. It is difficult to state generalized criteria for channel improvement applicable to any river. Knowledge of river systems has not yet progressed to such a state as to make this possible. Nevertheless, it is important to provide some principles and guidelines for the design engineer.

As a general rule, the radii of bends should be made approximately equal to the mean radii of bends $r_c$ in extended reaches of the river. Angle $\alpha$ shown in Figure 9-1 between a line drawn tangent to the inside of two successive bends and the bank line in the crossing should be approximately 20 degrees. This enables a sufficient crossing length for the thalweg to swing from one side of the channel to the other. Generally, it is necessary to stabilize outside banks of the curves in order to maintain the new alignment. Depending upon crossing length, some amount of maintenance may be required to remove sandbars after large floods so that the channel does not develop new meander patterns in the crossings during normal flows.

Sinuosity and channel bed slope are related in the following manner. Bed elevations at the ends of the reach being rechannelized (designated 1 and 2, in Figure 9-1) are established by existing

conditions. Hence, total drop in bed elevation for new (subscript 2) and old channels (subscript 1) is the same.

$$\Delta z_1 = \Delta z_2 = \Delta z \tag{9-1}$$

Length of channel measured along the thalweg is labeled $L_c$. Thus, mean slope of the channel bed before rechannelization is

$$S_1 = \frac{\Delta z}{L_{c_1}} \tag{9-2}$$

and after rechannelization is

$$S_2 = \frac{\Delta z}{L_{c_2}} \tag{9-3}$$

Sinuosity is defined by the ratio of length of channel to length of valley or

$$P = \frac{L_c}{L_v} \geq 1 \tag{9-4}$$

Clearly,

$$P_1 = \frac{L_{c_1}}{L_{v_1}} \tag{9-5}$$

$$P_2 = \frac{L_{c_2}}{L_{v_2}} \tag{9-6}$$

but

$$L_{v_1} = L_{v_2} = L_v \tag{9-7}$$

and

$$\frac{\Delta z_1}{L_{v_1}} = \frac{\Delta z_2}{L_{v_2}} = \frac{\Delta z}{L_v} \tag{9-8}$$

Thus,

$$P_1 S_1 = \frac{L_{c_1}}{L_v} \cdot \frac{\Delta z}{L_{c_1}} = \frac{L_{c_2}}{L_v} \cdot \frac{\Delta z}{L_{c_2}} = P_2 S_2 \tag{9-9}$$

New channel slope and channel sinuosity are inversely related. If $P_2 < P_1$, then $S_2 > S_1$. The new channel alignment (hence $P_2$) can be chosen by the designer with due consideration given to radii of curvature, deflection angles, and tangent lengths between reversing curves. As previously indicated, consideration should also be given prevailing average conditions in the extended reach. New slope $S_2$ can be calculated from Equation 9-9 and the relationship

$$S_2 Q^{1/4} \leq 0.0017 \tag{9-10}$$

should be satisfied. If $S_1$ is of such magnitude that Equation 9-10 cannot be satisfied with still larger $S_2$, the possibility of the river changing to a braided channel because of steeper slope should be carefully evaluated. With steeper slope, there could be an increase in sediment transport that could cause degradation and the effect would be extended both upstream and downstream of the rechannelized reach. Meander patterns could change, considerable bank protection might be necessary to contain lateral migration that is characteristic of a braided channel, and if the slope is too steep, head cuts could develop which migrate upstream with attendant effects on the plane geometry of the channel. Even when changes in slope are not very large, a short-term adjustment of average river slope occurs consistent with the sediment transport rate, flow velocities, and roughnesses beyond the upstream and downstream limits of channel improvement. For small changes in slope the proportionality $QS \sim Q_s D_{50}$ tends toward equilibrium by slight increases in bed material size $D_{50}$ and adjustment in the sediment transport rate $Q_s$.

A small increase in new channel width could be considered that tends to maintain the same stream power in old and new channels. That is,

$$(\tau_o V)_1 = (\tau_o V)_2 \ . \tag{9-11}$$

With substitution of $\tau_o = \gamma RS$, $V = Q/A$, and $R = A/P \simeq A/W$, Equation 9-11 leads to

$$W_2 = \frac{S_2}{S_1} W_1 \tag{9-12}$$

Increase in width should be limited to about 10 to 15 percent. Wider channels would be ineffective and deposition would occur along one bank and the effort of extra excavation would be wasted. Furthermore, bar formation would be encouraged with resultant tendencies for changes in the meander pattern leading to greater maintenance costs of bank stabilization and removal of bars to hold the desired river alignment.

Depth of flow in the channel is dependent on discharge, effective channel width, sediment transport rate (because it affects bed form and channel roughness), and channel slope.

The foregoing discussion pertains to alluvial channels with fine-sized bed materials (sands and silts). For streams with gravel and cobble beds the concern is to provide adequate channel cross-sectional dimensions to convey flood flows. If the realigned channels are made too steep, there is an increased stream power with a consequent increase in transport rate of the bed material. Deposition of material in the downstream reaches tends to form gravel bars and encourages changes in the plan form of the channel. Short-term changes in channel slope can be expected until equilibrium is reestablished over extended reaches both upstream and downstream of the rechannelized reach. Bank stabilization to prevent lateral migration and periodic removal of gravel bars may be necessary.

## 9.3 RIVER TRAINING AND STABILIZATION

Various devices and structures have been developed to control river flow along a preselected path and stabilize the banks. Most have been developed through trial and error applications aided in some instances by hydraulic model studies. Rock riprap is probably the most widely used material to stabilize river banks and protect the side slopes of embankments. Because of its wide use and importance in river work a separate section is devoted to rock riprap. Other useful materials are discussed in this section.

Dikes, retards, and jetties are devices used to guide the river flow and to protect banks (Figure 9-2). In all instances the intent of the devices shown in Figure 9-2 is to cause resistance or obstruction to flow along the channel bank, thereby creating lower velocities to stop bank erosion, restrict the thalweg of the stream to the center portions of the channel, and if possible cause deposition of sediment along the bank where erosion previously occurred.

### Dikes

In general, dikes extend outward from the bank into the channel at right angles or angled thereto depending upon circumstances and particular success achieved in past experiences. Along straight reaches, dikes should be perpendicular to the bank and along sharp curves the dikes should be angled slightly downstream so as to deflect the flow toward the center of the channel. Some of the dikes are terminated with extensions parallel to the flow, forming L or T shapes, and are correspondingly referred as L or T heads.

There are two principle types of dikes, permeable and impermeable. Permeable dikes are those that allow flow through the dike but at reduced velocities, thereby preventing further erosion of the banks and causing deposition of suspended sediment from the flow.

Timber pile dikes. Timber pile dikes (also retards) may consist of closely spaced single, double, or multiple rows. There are a number of variations to this scheme. For example, wire fence may be used in conjunction with pile dikes to collect debris and thereby cause effective reduction of velocity. Double rows of timber piles can be placed together to form timber cribs, and rocks may be used to fill the space between the piles. Timber pile dikes are vulnerable to failure through

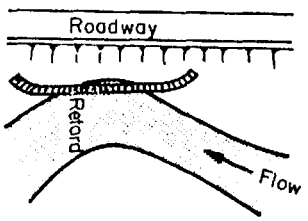


(a) Retards to protect in embankment

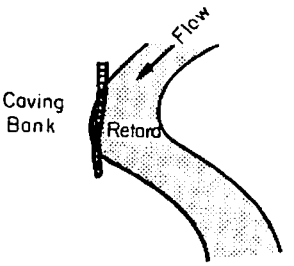


(b) Retard to prevent further bank caving

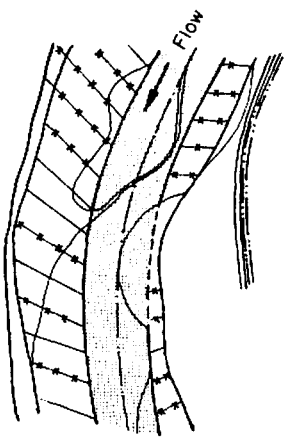


(c) Jetties to train the flow and protect the bank

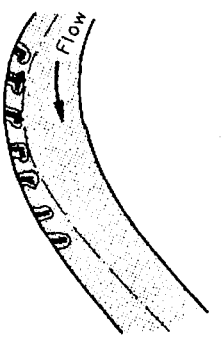


(d) Dikes to train the flow and protect the bank

Figure 9-2. Retards, jetties, and dikes to protect embankments and train channel flow.

scour. Piles can be driven to a large depth to achieve safety from scour or the base of the piles can be protected from scour with dumped rock in sufficient quantities to form a combination permeable and impermeable dike. Various forms of timberpile dikes are illustrated in Figure 9-3.

Arrangement of timber piles depends upon velocity of flow, quantity of suspended sediment transport, and depth and width of river. If the velocity of flow is large, timber pile dikes are not likely to be very effective and stabilization of the bank by other methods should be considered. On the other hand, in moderate flow velocities with high concentrations of suspended sediments, these dikes can be quite effective. Deposition of suspended sediments in the pile dike field is a necessary consequence of reduced velocities. If there is not sufficient concentration of suspended sediment in the flow or the velocities in the dike fields are too large for deposition, the permeable timber pile dikes will be only partially effective in training the river and protecting the bends.

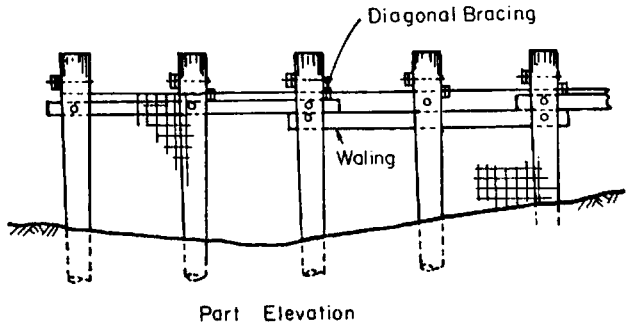


(a) Single row timber pile with wire fence

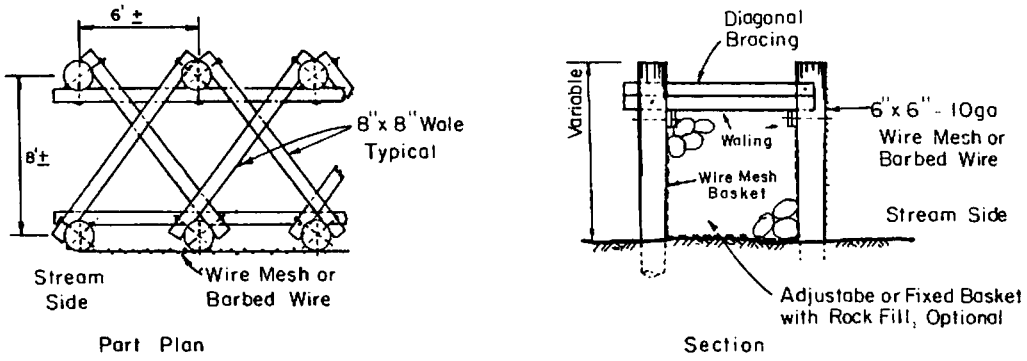


(b) Double row timber piles with rocks and wire fence

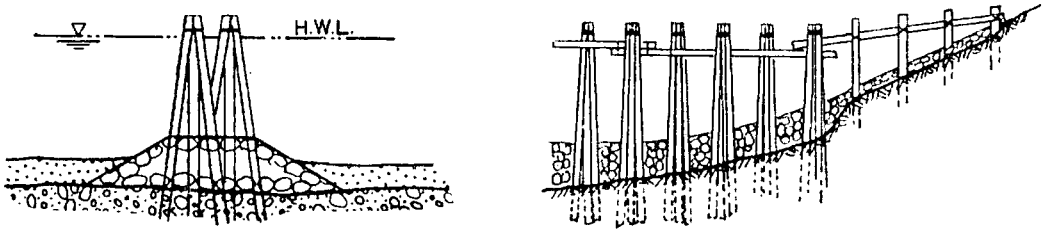


(c) Pile clusters

Figure 9-3. Timber pile dikes (retards would be similar).

The length of each dike depends on channel width, position relative to other dikes, flow depth, and available pile lengths. Generally, pile dikes are not used in large rivers where depths are great, although timber pile dikes have been used in the Columbia River. On the other hand, banks of wide shallow rivers can be protected with dikes. The spacing between dikes varies from 3 to 20 times the length of the upstream dike, with closer spacing favored for best results.

Stone-fill dikes. Stone-fill dikes are classed as impermeable dikes and do not depend on deposition of sediment between dikes nearly as much as permeable dikes. The principal function is to deflect flow

away from the bank and the dikes must be long enough to accomplish this purpose. The dikes may be angled downstream or upstream, or constructed normal to the bank. Variations such as a sloping dike with declining top elevation away from the bank, L or T head dikes, and curve dikes have been used. Stone-fill dikes are illustrated in Figure 9-4.

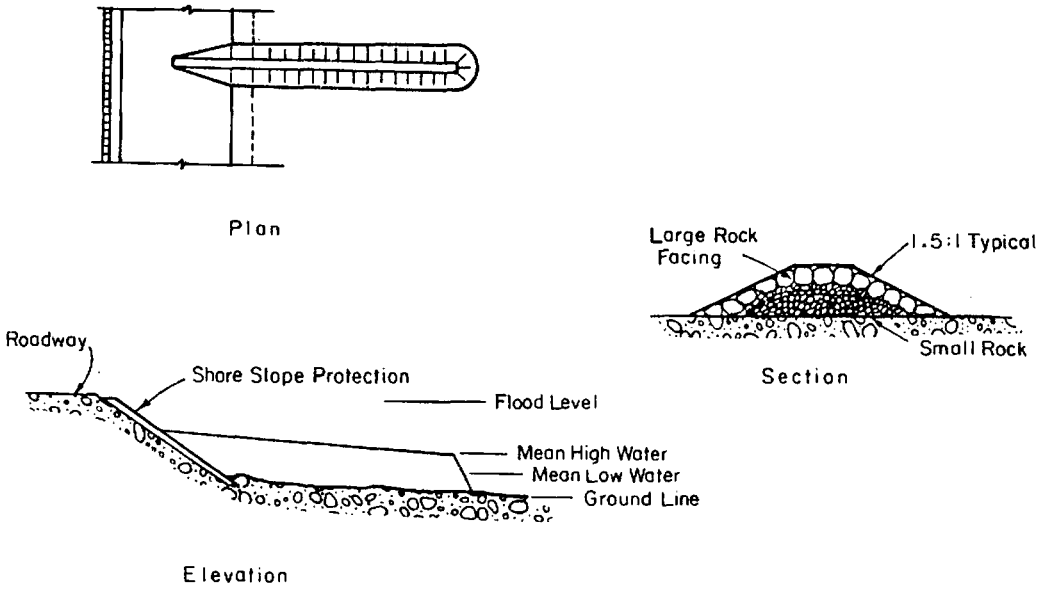


Figure 9-4. Typical stone fill dike.

Spacing between dikes may vary from 3 or 4 dike lengths to 10 or 12 dike lengths depending upon velocity and depth. Short dikes with long spacing are generally not useful for bank protection unless jacks or riprap are used to protect the bank between them.

Ends of the dikes are subjected to local scour and appropriate allowance should be made for loss of dike material into the scour hole. Rock size to be used for the dike depends on availability of material. Large rocks are generally used to cover the surface, while the internal section may be constituted with smaller rocks or earthfill. Side slopes of 1.5:1 and 2:1 are common.

Retards

Retards are permeable devices placed parallel to embankments and river banks to decrease stream velocities and prevent erosion.

Timber pile retards. Design of timber pile retards is essentially the same as the timber pile dikes discussed in the previous section and shown in Figure 9-2. The retards may be used in combination with bank protection works such as riprap to reduce the velocities sufficiently so that the riprap behind the retard is stable.

Steel jacks. These devices are basic triangular frames tied together to form a stable unit. The resulting framework is called a tetrahedron. Tetrahedrons are placed parallel to the embankment and cabled together with the ends of the cables anchored to the bank. Wire fencing may be placed along the row of tetrahedrons. In order to function well, there must be considerable debris in the stream to collect on the fence and suspended sediment concentration must be large enough for deposition behind the retard. Various forms of steel jacks may be assembled. Two types are shown in Figure 9-5. Jacks must be tied together with cable and must have tiebacks to deadmen set in the bank. Tiebacks should be spaced every 100 feet and space between jacks should not exceed their width.

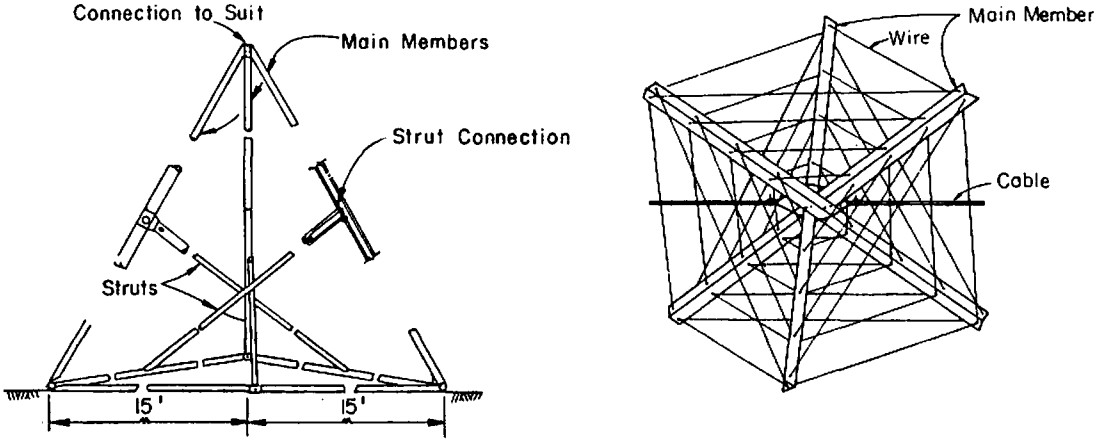


Figure 9-5. Steel jacks.

## Jetties

The purpose of a jetty field is to add roughness to a channel or overbank area in order to train the main stream along a selected path. Added roughness along the bank reduces the velocity and protects the bank from erosion. Jetty fields are usually made up of steel jacks tied together with cables. Both lateral and longitudinal rows of jacks are used to make up the jetty field as shown in Figure 9-6.

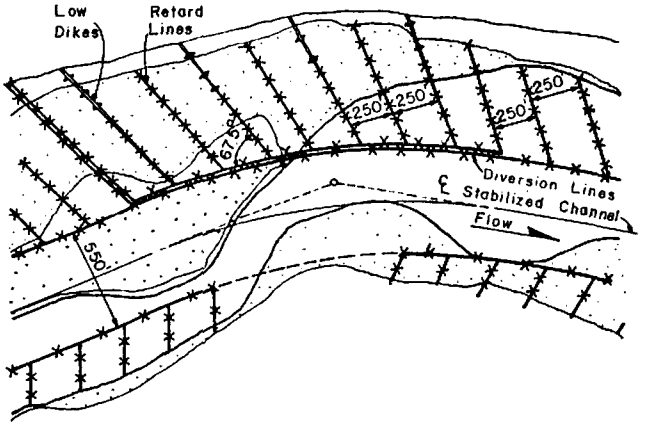


Figure 9-6. Typical jetty-field layout.

Lateral rows are usually angled about 45 to 70 degrees downstream from the bank. The spacing varies depending upon debris and sediment content in the stream and ranges from 50 to 200 feet. Jetty fields are effective only if there is a significant amount of debris carried by the stream and suspended sediment concentration is high.

When jetty fields are used to stabilize meandering rivers, it may be necessary to use jetty fields on both sides of the river channel because in flood stage the river may develop a chute channel across the point bar. A typical layout is shown in Figure 9-6.

Bank Protection

The term bank protection implies that the bankline has or is about to fail. In order to design bank protection properly, we must know how the bank fails. There are four principal ways in which a bank fails.

1. The erosion of soil particles on the bank either by the river currents or by waves.

2. Sloughing banks caused by excessive internal hydrostatic pressure in the bankline materials.

3. Slip-circle failures caused by the undermining of the toe.

4. Liquefaction and subsequent movement of the soil mass (called a flow slide).

The most common method of bank protection is with rock riprap. Sides of the bank or embankment are lined with large rocks to prevent erosion along the bank and at the toe. The next section in this chapter is devoted to riprap and further discussion is deferred. Other methods and devices are discussed in this section.

Rock-fill trenches. Rock-fill trenches are structures used to protect banks from caving caused by erosion at the toe. A trench is excavated along the toe of the bank and filled with rocks as shown in Figure 9-7.

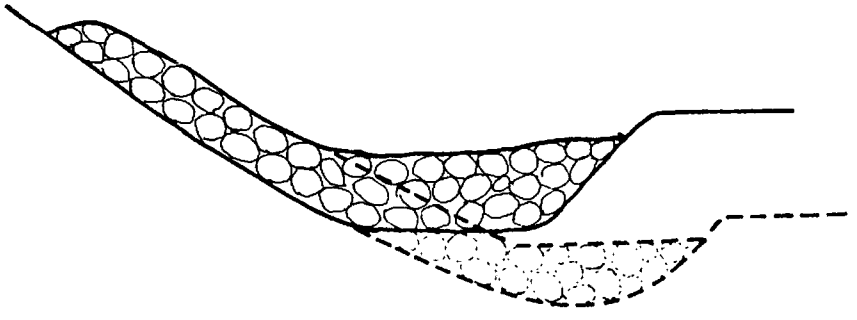

Figure 9-7. Rock-fill trench.

As the stream bed adjacent to the toe is eroded, the toe trench is undermined and rock fill slides downward to pave the bank. The size of trench to hold the rock fill depends on expected depths of scour. It is advantageous to grade the banks before paving the slope with riprap and placing rock in the toe trench. The slope should be at such an angle that the saturated bank is stable while the river stage is falling.

The rock-fill trench need not be at the toe of the bank. An alternative method is to excavate a trench above the water line along the top of the river bank and fill with rocks. Then as the bank erodes toward the trench, the rocks in the trench slide down and pave the bank. This method is applicable in areas of rapidly eroding banks of medium to large size rivers.

A variation of this method of toe protection is to pile rocks in a "window" along the bank line instead of excavating a trench. Then as the bank is scoured, rocks in the window drop down to pave the bank.

Rock-and-wire riprap. When adequate riprap size is not available, rocks of cobble sizes may be placed in wire mesh mats made of galvanized fencing and placed along the bank forming a mattress. Individual wire units are called baskets if the thickness is greater than 12 inches. Mattress implies a thickness no greater than 12 inches. Toe protection is offered by extending the mattresses into the channel bed as shown in Figure 9-8. As the bed along the toe is scoured, the mattress drops into the scour hole. Special wire baskets of manageable sizes are manufactured and sold throughout the United States. It should be noted that when rock-and-wire mattresses are used in streams transporting cobble and rocks, the wires of the basket can be cut rapidly which will destroy the intended protection along the base of the bank. Rusting of the wire mesh may also be a problem.

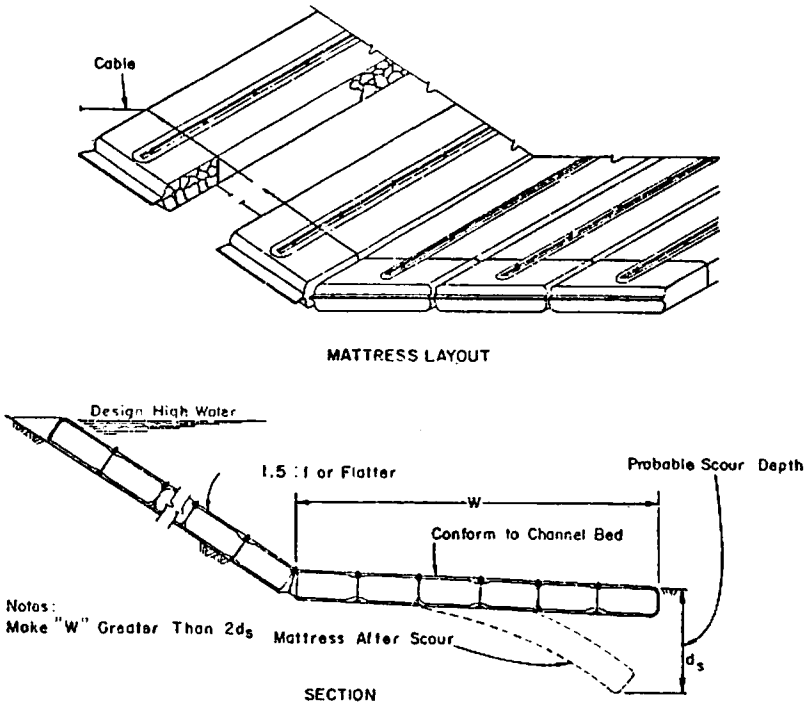


Figure 9-8. Rock and wire mattress.

Mats can be made up in large sizes in the field. Mats are flexible and can conform to scour holes that threaten bank stability. Mats should be linked together to prevent separation as subsidence takes place.

Articulated concrete mattress. Small precast concrete blocks held together by steel rods or cables can be used to form a flexible mat as shown in Figure 9-9.

Sizes of blocks may vary to suit the bank contour. It is particularly difficult to make a continuous mattress of uniform sized blocks to fit sharp curves. Open spacing between blocks permits removal of bank material unless a filter blanket of gravel or plastic filter cloth is placed underneath. For embankments that are subjected only to occasional flood flows the spaces between blocks may be filled with earth and vegetation can be established.

Use of articulated concrete mattresses has been limited primarily to the Mississippi River. This is due to the high cost of the plant required for placement of the mattress beneath the water surface. Thus, it is economically feasible to use articulated concrete mattresses only on rivers that require extensive bank protection. The expense of the installation plant is not a factor in the placement of articulated concrete mattresses above the water surface. Thus, paving the upper bank with articulated concrete mattresses has been used occasionally in the United States and Europe.

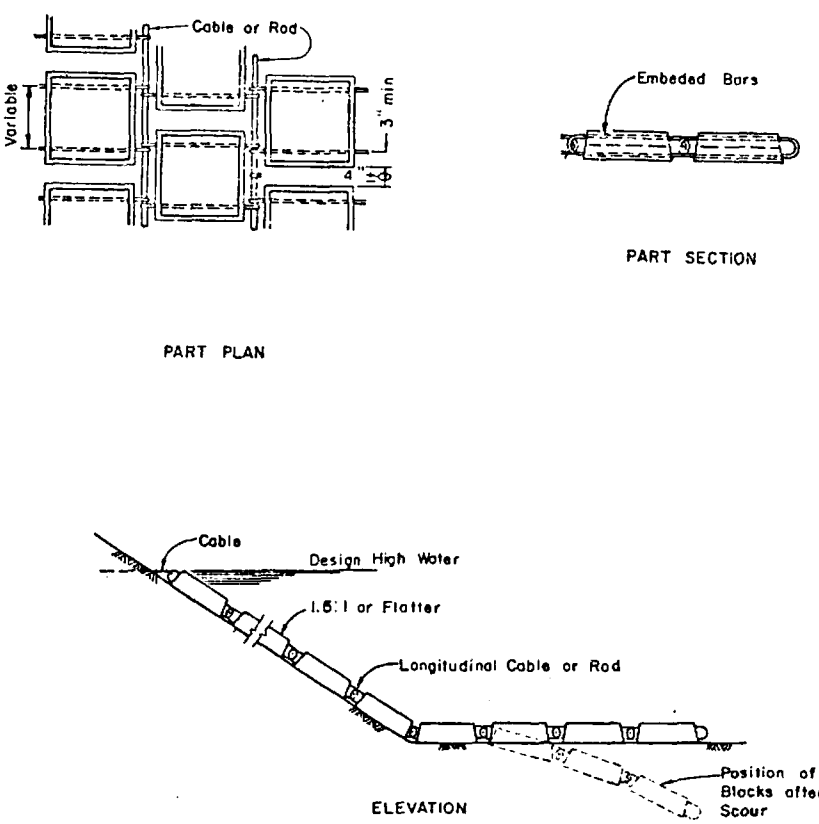


Figure 9-9. Articulated concrete mattress.

Other types of mattresses. Woven willow, brush, woven lumber, asphalt, and soil cement mattresses are other types that can be utilized. Concrete paving slabs are occasionally used. If the paving is extended well below the stream bed or if the entire cross section is lined with concrete paving, (especially for small channels) this form of bank paving is satisfactory.

Timber or concrete cribs. Timber and concrete cribs are sometimes used for bulkheads and retaining walls to hold embankments, particularly where lateral encroachment into the river must be limited. Cribs are formed by interlocking pieces in the manner shown in Figure 9-10. The crib may be slanted or vertical depending on height and is filled with rock or earth. Reinforced concrete retaining walls are alternatives to timber cribs. However, concrete retaining walls are expensive and are generally only used in special confined locations where space precludes other methods of bank protection. In constructing concrete retaining walls drainage holes (weep holes) must be provided. The foundation of these walls should be placed below expected scour depths.

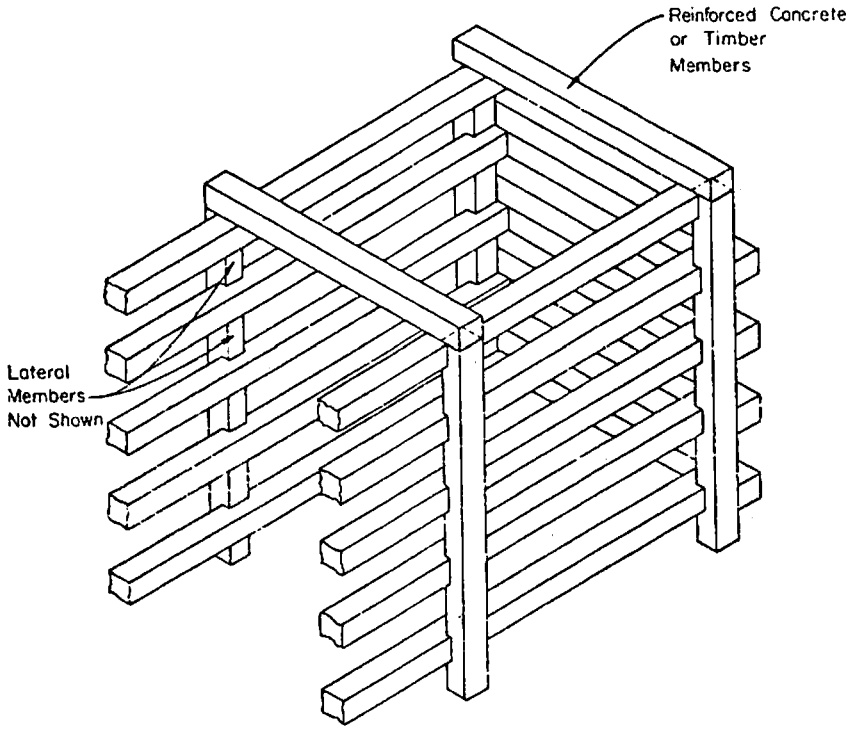


Figure 9-10. Concrete or timber cribs.

## 9.4 RIPRAP SIZE AND STABILITY ANALYSIS

When available in sufficient size, rock riprap is usually the most economical material for bank protection. Rock riprap has many other advantages over other types of protection. Rock riprap protection is flexible and local damage is easily repaired. Construction must be accomplished in a prescribed manner but is not complicated. Although

riprap must be placed to the proper level in the bed, there are no foundation problems. Appearance of rock riprap is natural and after a period of time vegetation will grow between the rocks. Wave runup on rock slopes is usually less than on other types. Finally, when the usefulness of the protection is finished, the rock is salvable.

The important factors to be considered in designing rock riprap protection are

1. Durability of the rock.
2. Density of the rock.
3. Velocity (both magnitude and direction) of the flow in the vicinity of the rock.
4. Slope of the bed or bankline being protected.
5. Angle of repose for the rock.
6. Size of the rock.
7. Shape and angularity of the rock.

The theoretical development of the relations between these important factors is presented in Appendix 9A. A summary of the equations for riprap design is given below.

Oblique Flow on a Side Slope

Consider flow along the nose of an embankment as shown in the diagrams of Figure 9-11.

At incipient motion, there is a balance of moments such that

$$e_2 W_s \cos\theta = e_1 W_s \sin\theta \cos\beta + e_3 F_d \cos\delta + e_4 F_\ell \tag{9-13}$$

where $e$ is the moment arm of each force.

Factor of safety S.F. of particles against rotation is then determined by the ratio of the moments.

$$\text{S.F.} = \frac{e_2 W_s \cos\theta}{e_1 W_s \sin\theta \cos\beta + e_3 F_d \cos\delta + e_4 F_\ell} \tag{9-14}$$

By following the development given in Appendix 9A, the following equations relating the safety factor for rock riprap on side slope where the flow has a non-horizontal velocity vector are obtained.

$$\text{S.F.} = \frac{\cos\theta \tan\phi}{\eta' \tan\phi + \sin\theta \cos\beta} \tag{9-15}$$

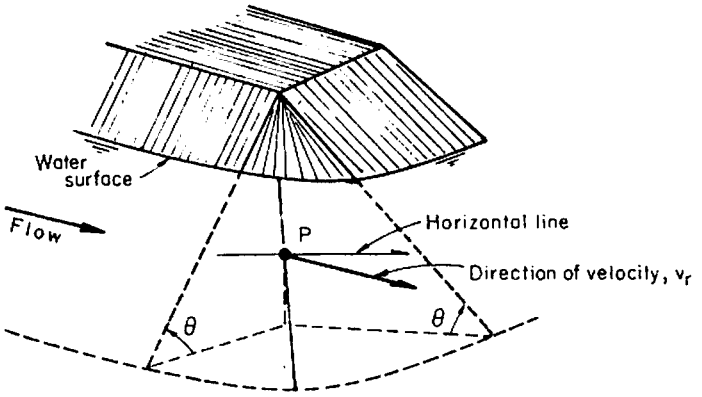


(a) General view

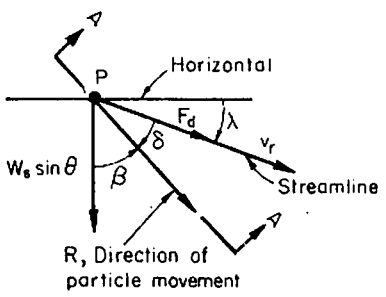


(b) View normal to the side slope

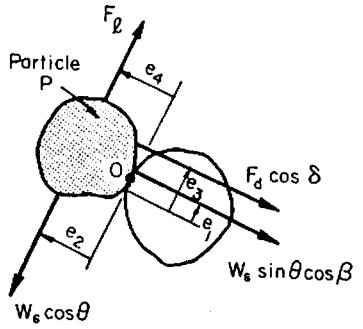


(c) Section A-A

Figure 9-11. Diagrams for the riprap stability analysis.

where

$$\eta' = \eta \left\{\frac{1 + \sin(\lambda+\beta)}{2}\right\} \tag{9-16}$$

$$\eta = \frac{21\ \tau_o}{(S_s - 1)\gamma D} \tag{9-17}$$

$$\beta = \tan^{-1} \frac{\cos\lambda}{\frac{2\ \sin\theta}{\eta\ \tan\phi} + \sin\lambda} \tag{9-18}$$

The angle $\lambda$ shown in Figure 9-11 is the angle between the horizontal and velocity vector (drag force) measured in the plane of the side slope.

The angles $\theta$ and $\beta$ are defined in Figure 9-11, $\phi$ is the angle of repose for dumped riprap, $\tau_o$ is the bed shear stress, $D$ is the representative rock size, $S_s$ is the specific weight of the rock, and $\eta'$ and $\eta$ are stability numbers.

In full-scale experiments with rock riprap below culvert outlets, Stevens (1969) developed the expression

$$D = \frac{\sum_{i=1}^{10} D_i^3}{10}^{1/3} \tag{9-19}$$

where

$$D_i(i=1) = \frac{D_0 + D_{10}}{2}$$

$$D_i(i=2) = \frac{D_{10} + D_{20}}{2}$$

$$\vdots$$

$$D_i(i=10) = \frac{D_{90} + D_{100}}{2}$$

for the representative grain size of riprap. The terms $D_0$, $D_{10}$, ..., $D_{100}$ are the sieve diameters of rock for which zero percent, 10 percent, ..., 100 percent of the material is finer by weight. The value of $D$ is greater than $D_{50}$ except for uniform materials. If all rock are one size, $D = D_{50}$. Representative grain size for riprap is discussed further in the appendix.

Horizontal Flow on a Side Slope

In many circumstances the flow angularity with the horizontal is small (i.e., $\lambda \tilde{\sim} 0$) and Equation 9-18 reduces to

$$\tan\beta = \frac{\eta \tan\phi}{2 \sin\theta} \tag{9-20}$$

and Equation 9-15 solved for $\eta$ becomes

$$\eta = \left(\frac{S_m^2 - (S.F.)^2}{(S.F.)S_m^2}\right) \cos\theta \tag{9-21}$$

where $S_m$ is the safety factor of rock particles rolling down the slope with no flow. Accordingly

$$S_m = \frac{\tan\phi}{\tan\theta} \tag{9-22}$$

Alternatively, the safety factor may be expressed as

$$S.F. = \frac{S_m}{2} \{(S_m^2\eta^2 \sec^2\theta + 4)^{1/2} - S_m\eta \sec\theta\} \tag{9-23}$$

Flow on a Sloping Bed

When considering flow along a plane bed sloping at an angle $\alpha$ with respect to the horizontal (Figure 9-12), the equations describing the stability of the riprap on the bed reduce to

$$S.F. = \frac{\cos\alpha \tan\phi}{\eta \tan\phi + \sin\alpha} \tag{9-24}$$

or

$$\eta = \cos\alpha \left[\frac{1}{S.F.} - \frac{\tan\alpha}{\tan\phi}\right] \tag{9-25}$$

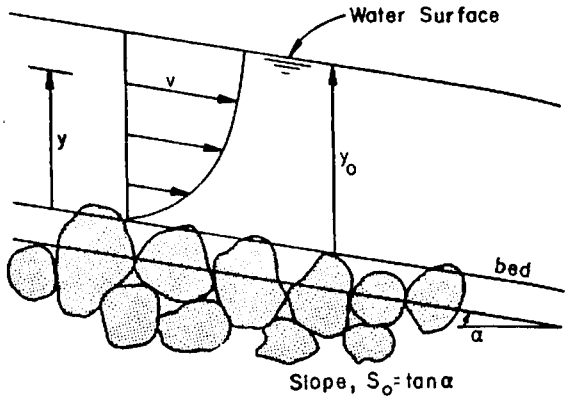


Figure 9-12. Definition sketch for riprap on a channel bed.

Flow on a Horizontal Bed

The most simple case is flow on a plane horizontal bed. In that case

$$S.F. = \frac{1}{\eta} \tag{9-26}$$

If the particles on a plane horizontal bed are in incipient motion, S.F. = 1 so $\eta = 1$ and from Equation 9-17

$$\frac{\tau_o}{(S_s - 1)\gamma D} = 0.047 \tag{9-27}$$

which is the Shields' criteria for incipient motion in fully developed rough turbulent flow. Use of foregoing analysis for determining riprap size is illustrated by numerical examples in the appendix at the end of this chapter.

University of Minnesota Method for Riprap Size Determination

A method to determine size of riprap to line the entire channel of small to intermediate sizes (6 to 1000 cfs) has been proposed by Anderson et al. (1970). The method applies to channels that are trapezoidal or triangular in shape and are essentially straight in alignment. The proposed equation relating size of riprap to discharge and channel geometry is

$$Q = \frac{1}{118} \frac{D_{50}^{5/2}}{S_o^{13/6}} \frac{P}{R} \qquad (9\text{-}28)$$

in which $P$ is the wetted perimeter and $R$ is hydraulic radius. Equation 9-28 is based on maximum shear stress related to rock diameter and Manning's equation of flow. It can be seen that for fixed channel size $P/R$ the riprap size is a function of $Q$ and $S_o$ so that a family of design curves can be made for fixed $P/R$ values.

Riprap Gradation and Placement

Riprap gradation should follow a smooth size distribution curve such as that shown in Figure 9-13. The ratio of maximum size to median size $D_{50}$ should be approximately 2.0 and the ratio between median size and the 20 percent size should also be about 2.0. This means that the largest stones would be 6.5 times the weight of the median size and small sizes would range down to gravels. Representative rock size $D$ for the gradation shown in Figure 9-13 is 1.25 $D_{50}$ (calculated using Equation 9-19) which is approximately equal to the $D_{67}$.

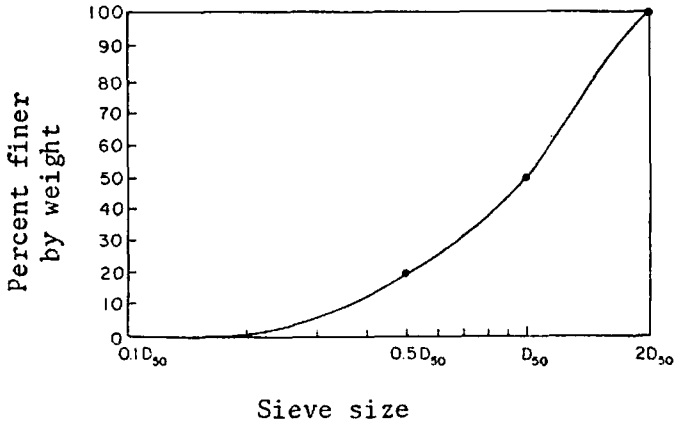


Figure 9-13. Suggested gradation for riprap.

With a distributed size range the interstices formed by larger stones are filled with smaller sizes in an interlocking fashion, preventing formation of open pockets. Riprap consisting of angular stones is more suitable than that consisting of rounded stones. Control of the gradation of the riprap is almost always made by visual inspection.

If it is necessary, poor gradations of rock can be employed as riprap provided the proper filter is placed between the riprap and the bank of bed material. Representative grain size of riprap is determined by Equation 9-19 and the filter is designed in accordance with the criteria given in the next section.

Riprap should be hard, dense, and durable to withstand long exposure to weathering. Visual inspection is most often adequate to judge quality but laboratory tests may be made to aid judgment of the field inspector.

Riprap placement is usually accomplished by dumping directly from trucks. If riprap is placed during construction of the embankment, rocks can be dumped directly from trucks at the top of the embankment. Rock should never be placed by dropping down the slope in a chute or pushed downhill with a bulldozer. These methods result in segregation of sizes. With dumped riprap there is a minimum of expensive hand work. Poorly graded riprap with slab-like rocks requires more work to form a compact protective blanket without large holes or pockets. Draglines with orange peel buckets, backhoes and other power equipment can also be used advantageously to place the riprap.

Hand placed rock riprap is another method of riprap placement. Stones are laid out in more or less definite patterns, usually resulting in a relatively smooth top surface. This form of placement is used rarely in modern practice because it is usually more expensive than the placement with power machinery.

Thickness of riprap should be sufficient to accommodate the largest stones in the riprap. With a well-graded riprap with no voids, this thickness should be adequate. If strong wave action is of concern, the thickness should be increased by 50 percent.

Filters for Riprap

Filters underneath the riprap are recommended to protect the fine embankment or riverbank material from washing out through the riprap. Two types of filters are commonly used, gravel filters and plastic filter cloths.

Gravel filters. A layer or blanket of well-graded gravel should be placed over the embankment or riverbank prior to riprap placement. Sizes of gravel in the filter blanket should be from 3/16 in. to an upper limit depending on the gradation of the riprap with maximum sizes of about 3 to 3-1/2 in. Thickness of the filter may vary depending upon riprap thickness but should not be less than 6 to 9 inches. Filters that are one-half the thickness of the riprap are quite satisfactory. Suggested specifications for gradation are as follows

$$\frac{D_{50}\ (\text{Filter})}{D_{50}\ (\text{Base})} < 40$$

$$5 < \frac{D_{15}\ (\text{Filter})}{D_{15}\ (\text{Base})} < 40$$

$$\frac{D_{15}\ (\text{Filter})}{D_{85}\ (\text{Base})} < 5$$

Plastic filter cloths. Plastic filter cloths are being used beneath riprap and other revetment materials such as articulated concrete blocks with considerable success. The cloths are generally in 100 ft rolls, 12 to 18 ft wide. Overlap of 8 to 12 inches is provided with pins at 2 to 3 ft intervals along the seam to prevent separation in case of settlement of the base material. Some amount of care must be exercised in placing riprap over the plastic cloth filters to prevent damage. Experiments and results with various cloth filters were reported by Calhoun, Compton, and Strohm (1971) in which specific manufacturers and brand names are listed. Stones weighing as much as 3000 lbs have been placed on plastic filter cloths with no apparent damage.

Filters can be placed subaqueously by using steel rods as weights fastened along the edges. Additional intermediate weights would assist in sinking the cloth in place. Durability of filter cloths has not yet been established because they have been in use only since around 1967. However, inspections at various installations indicate little or no deterioration had occurred in the few (1 to 4) years that have elapsed since test installations.

## Guide to Channel Improvement, River Training and Bank Stabilization

The type of channel improvement and devices used for training and bank stabilization depend upon river size with regard to width, depth, and discharge; type of rivers, that is, meandering, braided, or straight; sediment transport in terms of concentration and size distribution; length of river to be protected; availability of materials; environmental considerations; aesthetics; legal aspects; river use with regard to navigation, recreation, agriculture, and municipal and industrial purposes; and perhaps other factors.

Table 9-1 is offered as a guide to assist the engineer with regard to decisions for channel improvement and selection of type of bank protection and river training works. Rivers are first categorized as to size and type. The descriptors large, medium, and small are relative terms but should give no interpretive problems. Straight rivers are those with sinuosity less than 1.5 but long reaches between meander bends that are essentially straight may be included in the straight river classification. Because these long reaches are part of meander systems, stabilization and improvements may be required. This is the interpretation to be used in the table. The X in the box indicates that consideration should be given to use of that particular device.

Table 9-1. Guide for selection of methods and devices for river channel improvement and bank.

| Size of River | Type of River | Channel Improvement | Dikes | | | Retards | | Jetties | | Bank Protection | | | | | |
|---|---|---|---|---|---|---|---|---|---|---|---|---|---|---|---|
| | | | Timber | Stone-fill | Earth | Timber | Steel Jacks | Timber | Steel Jacks | Riprap | Rock Trench | Mattresses: Rock and Wire | Mattresses: Concrete | Mattresses: Other | Cribs |
| Large | Meandering | | X | X | ✲ | ✲ | | X | | X | X | ✲ | X | X | |
| | Braided | X | X | X | ✲ | ✲ | | X | | X | X | ✲ | X | X | |
| | Straight | | X | X | | ✲ | | X | | X | X | ✲ | | X | |
| Medium | Meandering | X | X | X | X | X | X | X | X | X | X | X | X | X | x |
| | Braided | X | X | X | X | X | X | X | X | X | X | X | X | X | X |
| | Straight | X | X | | | X | | X | | X | X | † | | X | X |
| Small | Meandering | X | | | | X | X | X | X | X | X | † | | X | X |
| | Braided | X | | | | X | X | X | X | X | X | † | | X | X |
| | Straight | X | | | | | | | | X | X | † | | X | X |

✲ Floodplain embankment protection

† Where large rocks for riprap are not available

Absence of a mark in the box indicates that the devices are not often used but could be considered in special circumstances. Additional remarks are noted on the table.

## 9.5 SCOUR AND DEGRADATION

Changes in bed level which affect construction and structures may be described by three types of interrelated phenomena.

1. Local scour, caused by local disturbances in the flow such as vortices and eddies. Examples are scour at the base of piers, dikes and other obstructions in a stream.

2. General scour due to contractions causing increasing velocities across the entire contracted width. Examples are scour at contracted stream channels caused by spur dikes, embankments, and accumulation of debris at bridge openings.

3. Degradation or aggradation of a stream channel over long lengths and time due to changes in controls, such as dams, changes in sediment content and changes in river geomorphology, such as changing from a meandering river to a braided stream.

These effects are in general additive so that local scour can occur while scour due to contraction is occurring and degradation or aggradation of the stream is taking place. Respective time scales for scour are progressively larger.

### Degradation and Aggradation

Degradation and aggradation of a river bed has been discussed in previous chapters and must be carefully considered. A long reach of river channel may be subjected to a general lowering or raising of the bed level over a long period of time. Prediction of ultimate degradation or aggradation of a stream can generally be made using mathematical models.

### General Scour

Scour at contractions occur because the flow area becomes smaller than the normal stream and average velocity and bed shear stress increase. Hence, there is an increase in stream power at the contraction and more bed material is transported through the contracted section than is transported into the section. As bed level is lowered velocity decreases, shear stress decreases, and equilibrium is restored when the transport rate of sediment through the contracted section is equal to the incoming rate.

Flows confined to the channel. Consider a situation where a normal river channel is narrowed by a contraction. Scour due to the contraction may be determined in the following manner (Nordin, 1971). The approach flow depth $y_1$ and average approach flow velocity $V_1$ result in

the sediment transport rate $q_{s1}$. Total transport rate to the contraction is $W_1 q_{s1}$ in which $W_1$ is width of the approach. If the water flow rate $Q_1 = W_1 q_1$ in the upstream channel is equal to the flow rate at the contracted section, then by continuity

$$q_2 = \frac{W_1}{W_2} q_1 \tag{9-29}$$

Here $q_1 = y_1 V_1$ and $q_2 = y_2 V_2$, and the subscript 2 refers to conditions in the contracted section. The sediment transport rate at the contracted section after equilibrium is established must be

$$q_{s2} = \frac{W_1}{W_2} q_{s1} \tag{9-30}$$

The relationships of $y$ and $V$ at sections 1 and 2 are shown in Figure 9-14 for constant $q_1$ and $q_2$.

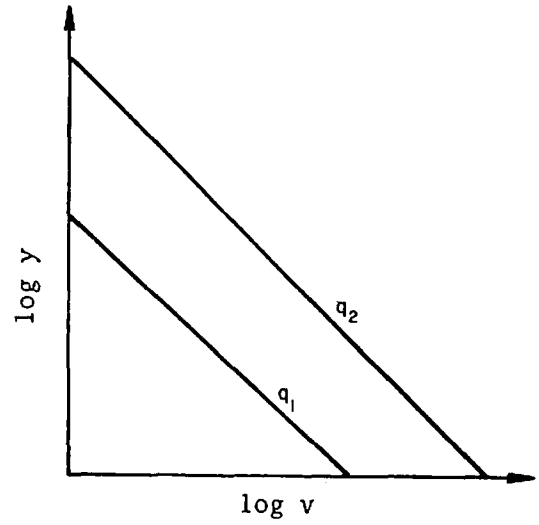


Figure 9-14. Unit discharge as a function of depth and velocity.

Utilizing a sediment transport equation it is possible to construct curves for transport rates of sediment of given median size as functions of flow depth and velocities. An illustration of such dependence is shown in Figure 9-15 using the Colby method.

Now the result of overlapping Figure 9-14 with Figure 9-15, is shown in Figure 9-16.

Depth of scour due to the contraction is then

$$y_s = y_2 - y_1 \tag{9-31}$$

Overbank flow with flow in the channel. Laursen (1960) developed an equation for scour at a contraction where in addition to channel flow there is overbank flow concentrating the contracted channel (designated by subscript 2). The equation to predict depth of flow at section 2 is

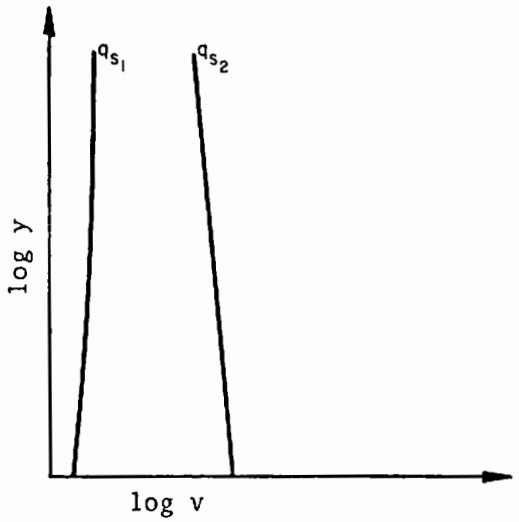


Figure 9-15. Sediment transport rate as a function of depth and velocity.

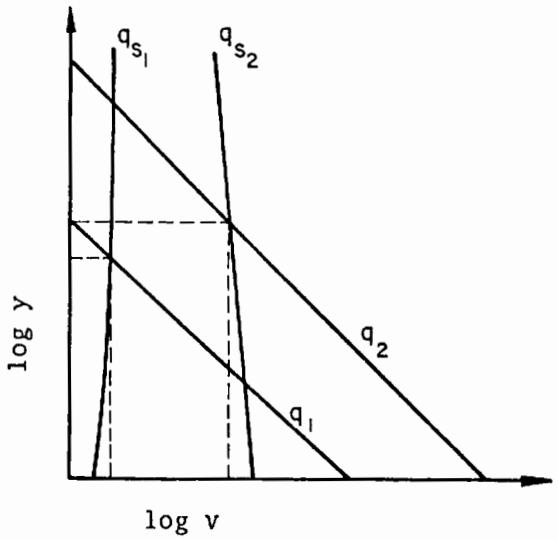


Figure 9-16. Determination of scour depth.

$$\frac{y_2}{y_1} = \left(\frac{Q_t}{Q_c}\right)^{6/7} \left(\frac{W_1}{W_2}\right)^{\frac{6(2+f)}{7(3+f)}} \left(\frac{n_2}{n_1}\right)^{\frac{6f}{7(3+f)}} \tag{9-32}$$

in which $Q_c$ is the approach channel flow rate and $Q_t$ is the contracted channel flow rate that is greater than the approach channel flow rate by the amount of flow on the floodplain. Variable n is the Manning roughness coefficient, W is the channel width, and exponent f is given below.

| $V_{*c}/\omega$ | f |
|---|---|
| < 0.5 | 0.25 |
| 1 | 1 |
| > 2 | 2.25 |

Here $V_{*c}$ is shear velocity in the approach channel and $\omega$ is fall velocity of bed material.

Overbank flow only. For scour at bridges on a floodplain where there is no sediment trasnport from upstream, Laursen (1963) proposed that

$$\frac{y_2}{y_1} = \left(\frac{W_1}{W_2}\right)^{6/7} \left(\frac{V_1^2}{120\, y_1^{1/3}\, D_{50}^{2/3}}\right)^{3/7} \tag{33}$$

where $y_1$, $V_1$, and $W_1$ are depth, velocity and width of the approach flow, $y_2$ is the general scour flow depth at the bridge and $D_{50}$ is median diameter of the bed materials at the bridge.

## Local Scour

Local scour occurs in the bed around piers and embankments due to the actions of vortex systems induced by obstructions to the flow. Local scour occurs in conjunction with or in the absence of degradation, aggradation, and scour due to contractions. There is need to understand the mechanism of local scour and calculation of potential scour depths, after which means may be considered in the design to eliminate or reduce its magnitude by suitable protective methods.

Mechanism of local scour. The basic mechanism causing local scour is the vortex of fluid resulting from pileup of water on the upstream edge and subsequent acceleration of flow around the nose of the pier or embankment. The action of the vortex is to erode bed materials away from the base region. If the transport rate of sediment away from the local region is greater than the transport rate into the region, a scour hole develops. As the depth is increased, strength of the vortex is reduced, transport rate is reduced, and equilibrium is reestablished and scouring ceases.

Flow field and vortex systems around a circular pier and approach embankment are illustrated in Figures 9-17 and 9-18. Although the vortex system is known to be the cause of local scour, it has not been possible as yet to calculate strength of the vortex and relate the velocity field with subsequent scour. Until further research and study makes this possible, average velocity and local depth of flow are used in the equations to predict local scour depths.

Local scour around embankments. A typical scour hole at an embankment and adjacent pier is illustrated in Figure 9-19.

The depth of scour varies with time because sediment transported into the scour hole from upstream varies, depending upon the presence or absence of dunes. The time required for dune motion is much larger than the time required for local scour. Thus, even with steady state conditions, depth of scour is likely to fluctuate with time when there are dunes traveling on the channel bed. Depth of the scour hole is more variable with larger dunes. When the crest of the dune reaches the

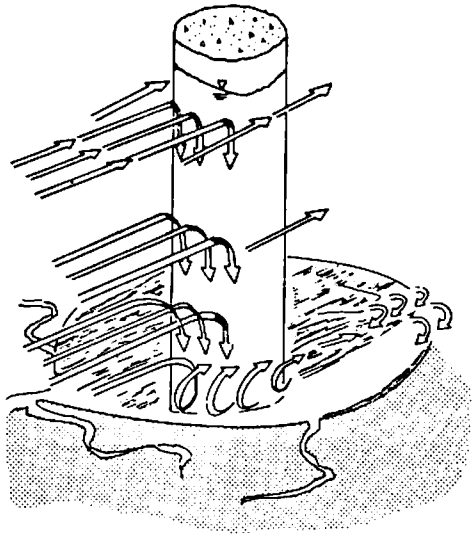

Figure 9-17. Schematic representation of scour at a cylindrical pier.

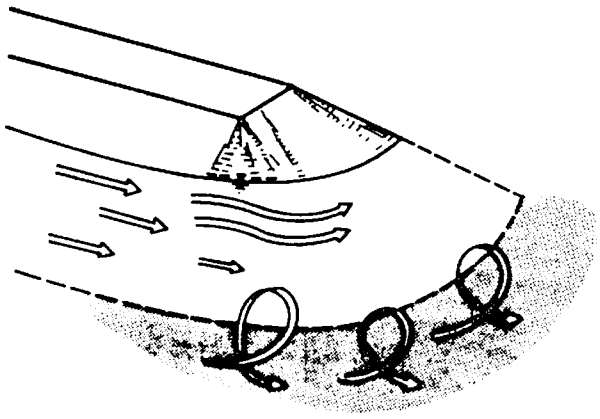

Figure 9-18. Schematic representation of scour at an embankment.

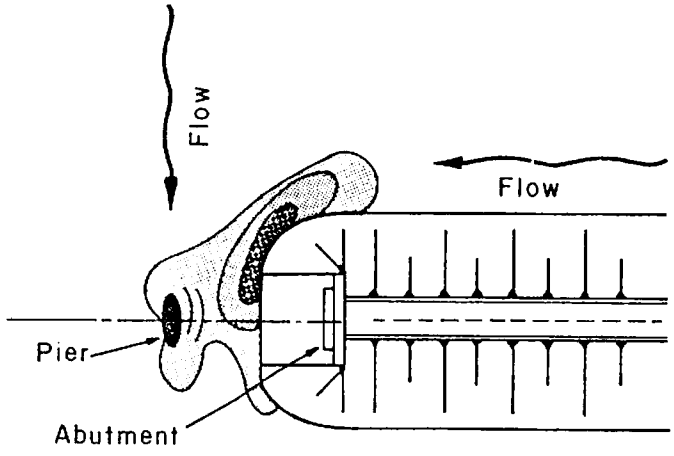


Figure 9-19. Typical scour at an embankment and adjacent pier.

local scour area, transport rate into the hole increases, the scour hole fills, and scour depth temporarily decreases. When a trough approaches, there is less sediment supply and the scour depth increases to try to reestablish equilibrium in sediment transport rates. A mean scour depth between these oscillations is referred to as equilibrium scour depth. It is not uncommon (as determined in laboratory tests) to find maximum depths to be 30 percent greater than equilibrium scour depths. The depth that would be reached if no sediment was transported into the scour hole is the clear-water scour depth.

Detailed studies of scour around embankments have been performed mostly in laboratories. There are very few case studies for scour at field installations. According to the studies of Liu et al. (1961) the equilibrium scour depth for local scour in sand at a spill slope when the flow is subcritical is determined by the expression

$$\frac{y_s}{y_1} = 1.1 \left(\frac{a}{y_1}\right)^{0.40} F_{r1}^{0.33} \tag{9-34}$$

where $y_s$ is equilibrium depth of scour measured from the mean bed level to the bottom of the scour hole, $a$ is embankment length (measured normal to the wall of a flume), $y_1$ is upstream depth, and $F_{r1}$ is the upstream Froud number determined as

$$F_{r1} = \frac{V_1}{\sqrt{gy_1}} \tag{9-35}$$

If the embankment terminates at a vertical wall and has a vertical wall on the upstream side, then the scour hole depth in sand nearly doubles (Liu, 1961 and Gill, 1972). That is,

$$\frac{y_s}{y_1} = 2.15 \left(\frac{a}{y_1}\right)^{0.40} F_{r1}^{0.33} \tag{9-36}$$

The lateral extent of the scour hole is nearly always determinable from depth of scour and natural angle of repose of the bed material.

Field data for scour at embankments for various size rivers are scarce but data collected at rock dikes on the Mississippi indicate that

$$\frac{y_s}{y_1} = 4 F_{r1}^{0.33} \tag{9-37}$$

determines the equilibrium scour depth for large $a/y_1$. Data are scattered primarily because equilibrium depths were not measured. Dunes as large as 20 to 30 feet high move down the Mississippi and associated time for dune movement is very large in comparison to time required to form local scour holes. Nevertheless, it is believed that these data represent the limit in scale for scour depths as compared to laboratory data and enables useful extrapolation of laboratory studies to field installations.

Accordingly, it is recommended that Equation 9-34 be applied to embankments with $0 < a/y_1 < 25$ and Equation 9-37 be used for $a/y_1 > 25$. The equations are shown in graphical form in Figure 9-20. In applying Equation 9-34, the embankment length a is measured from the high water line at the valley bank perpendicularly to the end of the embankment. If $a/y_1 > 25$, then scour depth is independent of $a/y_1$ and depends only on the approach Froude number and depth of flow. For $a/y_1 < 25$, as for example at dikes and short embankments, Equation 9-34 would apply.

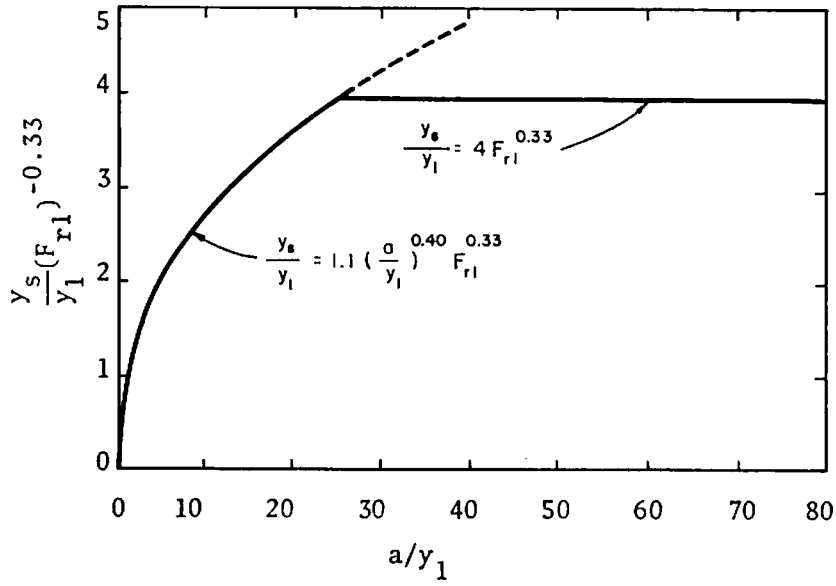


Figure 9-20. Recommended prediction equation for embankment scour.

It should be recalled that maximum depth of scour is about 30 percent greater than equilibrium scour depth. Lateral extent of scour can be determined from the angle of repose of the material and scour depth.

If the embankment is angled downstream, depth of scour is reduced because of the streamlining effect. Embankments that are angled upstream have deeper scour holes. Calculated scour depth should be adjusted in accordance with the curve of Figure 9-21 that is patterned after Ahmad (1953).

Local scour around piers. Local scour at piers in the flow is a result of vortex systems developed at the pier. The "horseshoe vortex system" is dominant at piers, causing deepest scour at the nose of the pier. The axis of this vortex or the vortex line is horizontal, and wraps around the base of the pier in the shape of a horseshoe. The high velocities scour the bed. The wake-vortex system has vertical axes and develops because of blockage of the flow by the pier. Wake vortices are commonly seen as "eddies". This vortex system suspends the scoured material and carries it downstream with the flow. Downstream of embankments, large wake vortices or eddies scour the downstream sides of the embankments, the river bank, and the stream bed. Wake vortices downstream of piers may create sufficient velocities to cause bed scour if the piers are wide. For most piers, however, little additional scouring is caused by wake vortices.

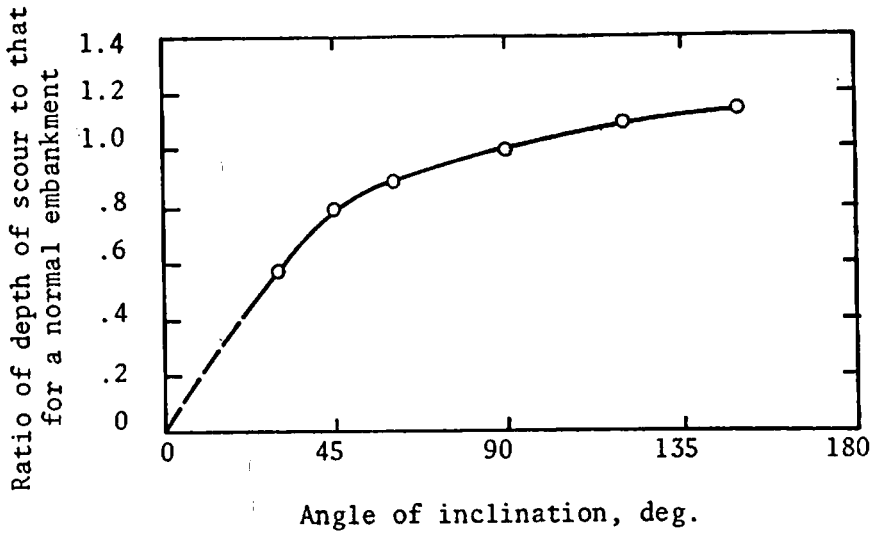


Figure 9-21. Scour reduction due to embankment inclination.

Shape of the pier is significant with respect to scour depth because it reflects the strength of the horseshoe vortex at the base of the pier. A blunt-nose pier causes the greatest scour depth. Streamlining the front end of the pier reduces the strength of the horseshoe vortex reducing the scour. Streamlining the downstream end of pier reduces the strength of wake vortices. Common shapes of piers are shown in Figure 9-22. Width of piers are labeled a and length designated $\ell$. Equilibrium of scour at the nose of square-nosed piers can be estimated with the equation

$$\frac{y_s}{y_1} = 2.2 \left(\frac{a}{y_1}\right)^{0.65} F_{r1}^{0.43} \tag{9-38}$$

where $y_1$ is upstream depth of flow and $F_{r1}$ is the Froude number. Scour depth for circular cylinders is

$$\frac{y_s}{y_1} = 2.0 \left(\frac{a}{y_1}\right)^{0.65} F_{r1}^{0.43} \tag{9-39}$$

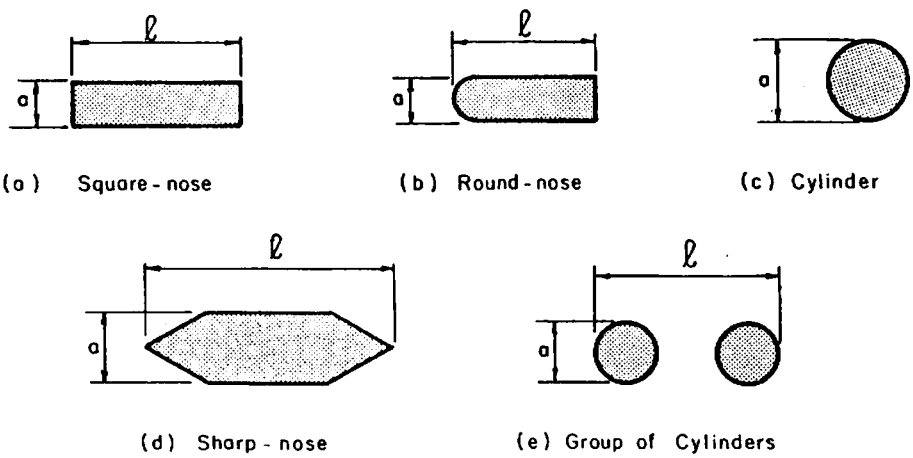


Figure 9-22. Common pier shapes.

The form of Equation 9-38 for square-nosed piers and Equation 9-36 for vertical-wall embankments are similar, although the variable a takes on different meanings. This similarity exists because the scour mechanisms for the two cases are similar.

Cylindrical piers have been widely investigated in the laboratory. Exponents in Equation 9-39 were determined from laboratory data shown in Figure 9-23. In this figure, the abscissa is labeled $(a/y_1)^3 F_{r1}^2$ to spread the data. It should be noted that

$$\{(\frac{a}{y_1})^3 F_{r1}^2\}^{0.215} = (\frac{a}{y_1})^{0.65} F_{r1}^{0.43} \qquad (9\text{-}40)$$

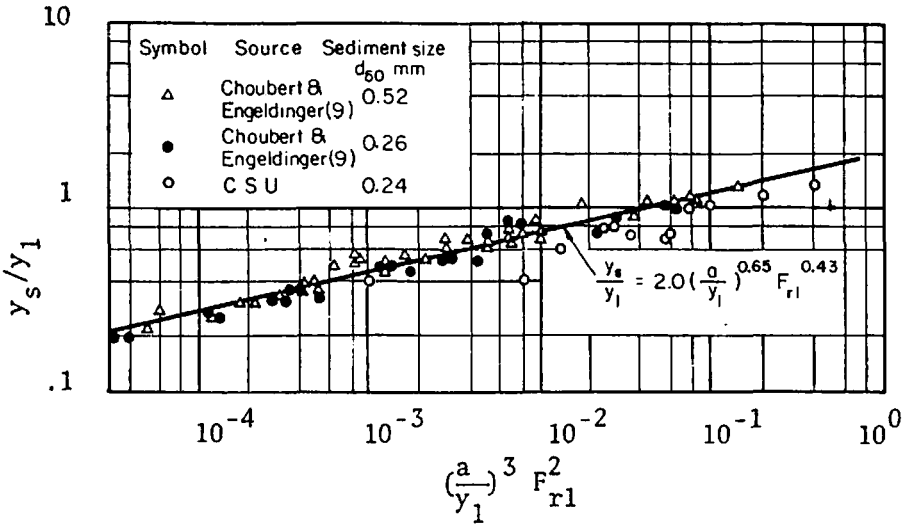


Figure 9-23. Results of laboratory experiments for scour at circular piers.

The scour depth decreases as a consequence of streamlining. Reduction in scour depth can be estimated from the value given in Table 9-2.

Table 9-2. Reduction in scour depths for equal projected widths of pier.

| Type of Pier | $y_s/y_s$ (square nose) |
|---|---|
| Square nose | 1.0 |
| Clyinder | 0.9 |
| Round nose | 0.9 |
| Sharp nose | 0.8 |
| Group of cylinders | 0.9 |

Pier alignment other than parallel with flow direction will create deeper scour holes because in effect the dimension a increases. In Table 9-3 multiplying factors to Equation 9-38 are given. Scour at single cylindrical piers is invariant to flow direction, but groups of cylindrical piers would be affected by flow angularity.

Table 9-3. Multiplying factors for scour depths with skewed flow direction.

| Angle of skew in degrees | $\ell/a = 4$ | $\ell/a = 8$ | $\ell/a = 12$ |
|---|---|---|---|
| 0 | 1.0 | 1.0 | 1.0 |
| 15 | 1.5 | 2.0 | 2.5 |
| 30 | 2.0 | 2.5 | 3.5 |
| 45 | 2.3 | 3.3 | 4.3 |
| 90 | 2.5 | 3.9 | 5.0 |

The concept of equilibrium scour depth also applies to scour around piers. It should be recalled that maximum scour depth at piers could be as large as 30 percent greater than equilibrium scour depth.

The base level to which scour depths can be referenced is not a trivial question. In some rivers, dune heights may be as large as 20 to 30 feet and $y_1$ would normally be measured from some level closer to the tops of the dunes. Scour depths on the other hand should be referenced nearer the trough of the dunes. The bed level for scour due to contractions is first calculated. This establishes $y_1$ and $F_{r1}$. The local scour depth is then referenced to that bed level.

Protection of Structures from Local Scour

Three basic methods may be used to protect structures from damage due to local scour. The first is to prevent damaging vortices from developing and the second is to provide protection at some level at or below the stream bed to arrest development of the scour hole. The third is to place the foundations of structures at such depth that the deepest scour hole will not threaten the stability of the structure. The last method is often very expensive and risk is involved because of the uncertainty associated with estimating additive effects of scour due to contraction and channel degradation.

Vortex reduction. As previously mentioned, streamlining the piers can reduce scour depth by 10 to 20 percent. Another method of reducing vortex strength at the pier is to construct barriers upstream of bridge piers with a cluster of piles for instance. While the piles are subjected to scour, failure of these piles is not damaging to the bridge. Debris can collect on the upstream piles keeping the nose of

the bridge pier relatively free of debris. Pileup of water at the upstream piles reduces the dynamic pileup of water at the pier and reduces the vortex strength at the pier. Spur dikes can be placed at the ends of approach embankments to reduce local scour at the bridge. Spur dikes were discussed in a previous section.

Bed protection. Riprap piled around the base of the pier is a common method of local scour protection. The principle is the same as toe trenches for bank protection. The region of the bed beyond the riprap pile scours and as the scour hole is formed, riprap slides down into the scour hole eventually armoring the side of the scour hole adjacent to the pier. An estimate of the depth of scour is needed to determine the quantity of riprap required for effective protection. Because of armoring, the effective depth of scour is less than that calculated by Equations 9-38 and 9-34. There are few studies to establish dependable guidelines, but 50 to 60 percent reduction in $y_s$ may be used as an estimate of final scour depth. By frequent inspection it can be determined whether the size and quantity of riprap used initially is adequate. If additional amounts of riprap are necessary, placement from the water surface may be possible in times of low flow with consideration given to the falling path of rocks in a flowing stream.

A structural concrete shelf placed at about $0.5\ y_s$, where $y_s$ is calculated from Equation 9-38, extending laterally from the pier, and completely surrounding the pier may be effective in limiting the scour depth. The lateral extent of the shelf should be about $0.3\ y_s \cot\phi$ where $\phi$ is the angle of repose of the bed material. While this method may be effective for $y_s < 20$ feet, it may become impractical for larger $y_s$.

Protective mattresses such as rock and wire have been suggested in the past and have been used in a few circumstances. While they may have merit where adequate size riprap may be scarce, anchoring and stabilization of the mattresses to conform with scour holes is usually difficult. Use of mattresses in conjunction with riprap may be quite effective, if the mattress performs essentially as a flexible filter blanket that deforms as scour holes develop.

## REFERENCES

Ahmad, M., 1953, Experiments on design and behavior of spur dikes: Proc. IAHR, ASCE Joint Meeting, Univ. of Minn., August.

Anderson, A. G., Paintal, A. S., and Davenport, J. T., 1970, Tentative design procedure for riprap-lined channels: Project Report No. 96, St. Anthony Falls Hydraulics Laboratory, Minneapolis, Minnesota, NCHRP Report 108, Highway Research Board, Washington, D.C.

Calhoun, C. C., Jr., Compton, J. R., and Strohm, W. E., Jr., 1971, Performance of plastic filter cloths as a replacement for granular filter materials: Highway Research Record Number 373, Transportation Research Board, January.

California Division of Highways, 1970, Bank and shore protection in California Highway Practice: Dept. of Public Works, November.

Laursen, E. M., 1960, Scour at bridge crossings: Jour. Hyd. Div., ASCE, Vol. 86, No. HY2, February, pp. 39-54.

Laursen, E. M., 1963, An analysis of relief bridge scour: Jour. Hyd. Div., ASCE, Vol. 89, No. HY3, May, pp. 93-118.

Liu, M. K., Chang, F. M., and Skinner, M. M., 1961, Effect of bridge construction on scour and backwater: Dept. of Civil Engineering, Colorado State University. Rept. No. CER60-MKL22, February.

Nordin, C. F., 1971, Graphical Aids for determining scour depth in long contractions: Unpublished Note (obtained from private communication), April.

Stevens, M. A., 1969, Scour in Riprap at culvert outlets: Ph.D. Dissertation, Dept. of Civil Eng., Colorado State University, Fort Collins, Colorado.

# APPENDIX 9A

## SAFETY FACTORS FOR RIPRAP - THEORETICAL DEVELOPMENT

### 9A.1 INTRODUCTION

In the absence of waves and seepage, stability of rock riprap particles on a side slope is a function of: 1) the magnitude and direction of the stream velocity in the vicinity of the particles, 2) angle of the side slope, and 3) the characteristics of the rock including geometry, angularity and density. Functional relations between the variables is developed below. This development closely follows that given by Stevens and Simons (1971).

Oblique Flow on a Side Slope

Consider flow along an embankment as shown in Figure 9A-1. The fluid forces on a rock particle identified as P in Figure 9A-1a result primarily from fluid pressures around the surface of the particles. The lift force $F_\ell$ is defined herein as the fluid force normal to the plane of the embankment. Lift force is zero when fluid velocity is zero. Drag force $F_d$ is defined as fluid force acting on the particle in the direction of the velocity field in the vicinity of the particle. The drag force is normal to the lift force and is zero when the fluid velocity is zero. The remaining force is the submerged weight of the rock particle $W_s$.

Rock particles on side slopes tend to roll rather than slide so it is appropriate to consider stability of rock particles in terms of moments about the point of rotation. In Figure 9A-1b the direction of movement is defined by the vector R. Point of contact about which rotation in the R direction occurs is identified as point "0" in Figure 9A-1c.

Forces acting in the plane of the side slope are $F_d$ and $W_s \sin\theta$ as shown in Figure 9A-1b. Angle $\theta$ is the side slope angle. Lift force acts normal to the side slope and the component of submerged weight $W_s \cos\theta$ acts normal to the side slope as shown in Figure 9A-1c.

At incipient motion, there is a balance of moments about the point of rotation such that

$$e_2 W_s \cos\theta = e_1 W_s \sin\theta \cos\beta + e_3 F_d \cos\delta + e_4 F_\ell \qquad (9A\text{-}1)$$

Moment arms $e_1$, $e_2$, $e_3$, and $e_4$ are defined in Figure 9A-1c and angles $\delta$ and $\beta$ are defined in Figure A1b.

The factor of safety S.F. of the particle P against rotation is defined as the ratio of the moments resisting particle rotation out of the bank to the submerged weight and fluid force moments tending to rotate the particle out of its resting position. Accordingly,

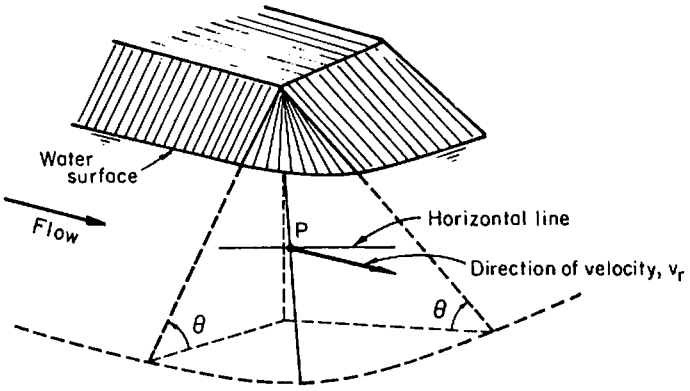


(a) General view

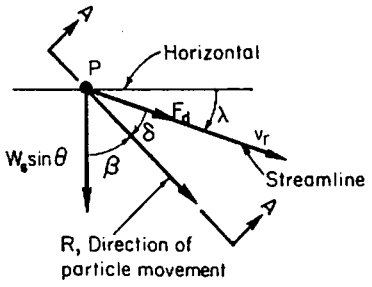


(b) View normal to the side slope

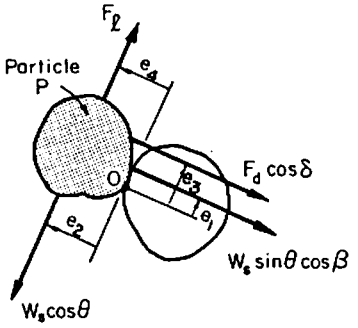


(c) Section A-A

Figure 9A-1. Diagram for the riprap stability conditions.

$$S.F. = \frac{e_2 W_s \cos\theta}{e_1 W_s \sin\theta \cos\beta + e_3 F_d \cos\delta + e_4 F_\ell} \qquad (9A\text{-}2)$$

If there is no flow and side slope angle is increased to the angle of repose $\phi$ for rock particles, the safety factor becomes unity. The no flow condition causes $F_d$ and $F_\ell$ to become zero. Then,

$S.F. = 1.0$

$\theta = \phi$

$\beta = 0$ deg

$\lambda = 0$ deg

$\delta = 90-\lambda-\beta$ (See Figure 9A-1b)

$\ell = 90$ deg

With these values, Equation 9A-2 reduces to

$$\frac{e_2 W_s}{e_1 W_s} \frac{\cos\theta}{\sin\theta} = 1 \tag{9A-3}$$

or

$$\tan\phi = \frac{e_2}{e_1} \tag{9A-4}$$

That is, the ratio of moment arms $e_2/e_1$ is characterized by the natural angle of repose $\phi$. Further, it is assumed that the ratio $e_2/e_1$ is invariant to the direction of particle motion indicated by angle $\beta$.

Dividing both numerator and denominator by $e_2 W_s$, Equation 9A-2 is transformed to

$$S.F. = \frac{\cos\theta \tan\phi}{\eta' \tan\phi + \sin\theta \cos\beta} \tag{9A-5}$$

in which

$$\eta' = \frac{e_3 F_d}{e_2 W_s} \cos\delta + \frac{e_4 F_\ell}{e_2 W_s} \tag{9A-6}$$

The variable $\eta'$ is called the stability number for the particles on the embankment side slope and is related to the Shields' parameter

$$\frac{\tau_o}{(S_s - 1)\gamma D}$$

Here $\tau_o$ is the average tractive force on the side slope in the vincinity of particle P, $\gamma$ is unit weight of water, and D is the diameter of the rock particles.

Angle $\lambda$ shown in Figure 9A-1b is the angle between the horizontal and velocity vector (or drag force) measured in the plane of the side slope. Then

$$\delta = 90 - \lambda - \beta \tag{9A-7}$$

so

$$\cos\delta = \cos(90 - \lambda - \beta)$$

$$= \sin(\lambda + \beta) \tag{9A-8}$$

Also $\sin\delta = \sin(90-\lambda-\beta)$

$$= \cos\lambda \cos\beta - \sin\lambda \sin\beta \qquad (9A\text{-}9)$$

It is assumed that moments of drag force $F_d$ and component of submerged weight $W_s\sin\theta$ normal to path R are balanced so that the direction of particle motion will be along R. Thus

$$e_3 F_d \sin\delta = e_1 W_s \sin\theta \sin\beta \qquad (9A\text{-}10)$$

It follows then from Equation 9A-9 and 9A-10 that

$$\sin\beta = \frac{e_3 F_d \sin\delta}{e_1 W_s \sin\theta}$$

$$= \frac{e_3 F_d(\cos\lambda \cos\beta - \sin\lambda \sin\beta)}{e_1 W_s \sin\theta} \qquad (9A\text{-}11)$$

or

$$\tan\beta = \frac{\cos\lambda}{\frac{e_1 W_s}{e_3 F_d}\sin\theta + \sin\lambda} \qquad (9A\text{-}12)$$

Stability number $\eta$ for particles on a plane bed ($\theta = 0$) with $\delta = 0$ would be

$$\eta = \frac{e_3 F_d}{e_2 W_s} + \frac{e_4 F_\ell}{e_2 W_s} \qquad (9A\text{-}13)$$

according to Equation 9A-6. Also, Equation 9A-5 becomes

$$S.F. = \frac{1}{\eta} \qquad (9A\text{-}14)$$

for flow over a plane flat bed.

For incipient motion conditions for flow over a plane flat bed, S.F. = 1.0 by definition so from Equation 9A-14 $\eta = 1.0$. When the flow along the bed is fully turbulent, the Shields' parameter for incipient motion has the value 0.047 according to Gessler (1971). That is, with $\eta = 1.0$,

$$\frac{\tau_o}{(S_s - 1)\gamma D} = 0.047 \qquad (9A\text{-}15)$$

For flow conditions other than incipient, $\eta$ is the ratio

$$\frac{1}{0.047} \quad \frac{\tau_o}{(S_s - 1)\eta D}$$

or

$$\eta = \frac{21\ \tau_o}{(S_s - 1)\gamma D} \tag{9A-16}$$

for convenience,

$$M = \frac{e_4 F_\ell}{e_2 W_s} \tag{9A-17}$$

and

$$N = \frac{e_3 F_d}{e_2 W_s} \tag{9A-18}$$

In terms of these new variables, Equation 9A-6 becomes

$$\eta' = M + N \cos\delta \tag{9A-19}$$

and Equation 9A-13 becomes

$$\eta = M + N \tag{9A-20}$$

Thus $\eta'$ and $\eta$ are related by the expression

$$\frac{\eta'}{\eta} = \frac{\frac{M}{N} + \cos\delta}{\frac{M}{N} + 1} \tag{9A-21}$$

Equation 9A-21 is represented graphically in Figure 9A-2.

The problem is to select the proper value of the ratio $M/N$ so that the stability factor on a side slope $\eta'$ can be related to the stability factor on a plane horizontal bed $\eta$, which in turn is related to the Shields' parameter. The assumption that drag force $F_d$ is zero means $M/N$ is infinite, $\beta$ is zero, and $\eta' = \eta$. The assumption of zero lift force $F\ell$ means $M/N$ is zero and $\eta'/\eta = \cos\delta$.

In considering incipient motion of riprap particles, the ratios $F_{\ell/Fd}$ and $e_4/e_3$ vary depending on the turbulent conditions of flow and the interlocking arrangement of the rock particles. In referring to Figure 9A-1c assume that

$$\frac{e_4}{e_3} \simeq 2 \tag{9A-22}$$

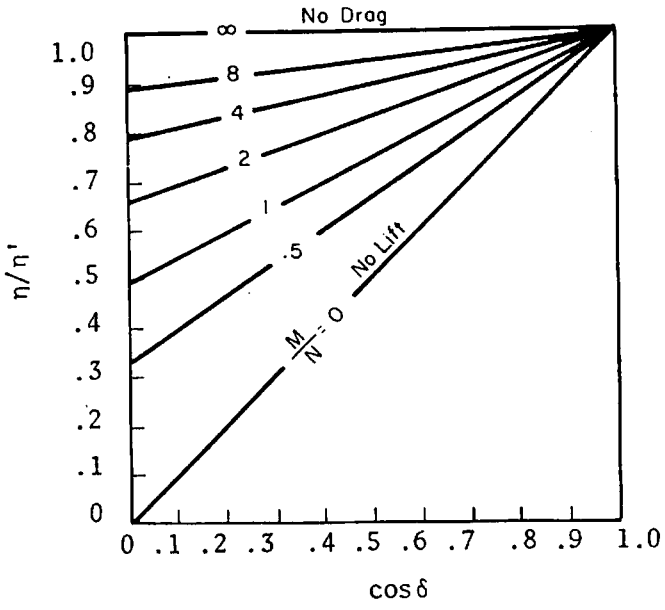


Figure 9A-2. Ratio of stability factors.

then a choice for $F_\ell/F_d$ is

$$\frac{F_\ell}{F_d} \simeq \frac{1}{2} \tag{9A-23}$$

so that

$$\frac{M}{N} = \frac{e_4}{e_3}\ \frac{F_\ell}{F_d} \simeq 1 \ . \tag{9A-24}$$

With M/N = 1, Equation 9A-21 becomes

$$\frac{\eta'}{\eta} = \frac{1 + \cos\delta}{2} \tag{9A-25}$$

or by using Equation 9A-8

$$\frac{\eta'}{\eta} = \frac{1 + \sin(\lambda+\beta)}{2} \tag{9A-26}$$

In Equation 9A-12, the term $e_1W_s/e_3F_d$ can be written

$$\frac{e_1W_s}{e_3F_d} = \frac{e2^{W_s}}{e_3F_d}\ \frac{e1}{e_2}$$

$$= \frac{1}{N}\ \frac{1}{\tan\phi} \tag{9A-27}$$

according to Equation 9A-18 and 9A-4. For M/N = 1, Equation 9A-20 becomes

$$N = \frac{\eta}{2} \tag{9A-28}$$

If we substitute Equations 9A-27 and 9A-28 into Equation 9A-12, the expression for $\beta$ becomes

$$\tan\beta = \frac{\cos\lambda}{\frac{2\sin\theta}{\eta\tan\phi} + \sin\lambda} \tag{9A-29}$$

In summary, the safety factor for rock riprap on side slopes where the flow has a non-horizontal velocity vector is related to properties of the rock, side slope, and flow by the following equations

$$S.F. = \frac{\cos\theta\ \tan\phi}{\eta'\tan\phi + \sin\theta\ \cos\beta} \tag{9A-30}$$

in which

$$\beta = \tan^{-1} \frac{\cos\lambda}{\frac{2\sin\theta}{\eta\tan\phi} + \sin\lambda} \tag{9A-31}$$

$$\eta = \frac{21\ \tau_o}{(S_s - 1)\gamma D} \tag{9A-32}$$

and

$$\eta' = \eta \left\{\frac{1 + \sin(\eta+\beta)}{2}\right\} \tag{9A-33}$$

Given rock size $D$ of specific weight $S_s$, angle of repose $\phi$, and a velocity field at an angle $\lambda$ to the horizontal producing a tractive force $\tau_o$ on the side slope of angle $\theta$, the set of 4 equations (Equations 9A-30, 9A-31, 9A-32, and 9A-33) can be solved to obtain the safety factor S.F. If S.F. is greater than unity, the riprap is safe from failure; if S.F. is unity, the rock is at the condition of incipient motion; and if S.F. is less than unity, the riprap will fail.

Horizontal Flow on a Side Slope

In many circumstances, the flow angularity with the horizontal is small i.e., $\lambda \simeq 0$. Then Equations 9A-31 and 9A-32 reduce to

$$\beta = \tan^{-1} \left\{\frac{\eta\ \tan\phi}{2\ \sin\theta}\right\} \tag{9A-34}$$

and

$$\eta' = \eta \left\{\frac{1 + \sin\beta}{2}\right\} \tag{9A-35}$$

When Equations 9A-34 and 9A-35 are substituted into Equation 9A-30, the expression for the safety factor for horizontal flow on a side slope is

$$S.F. = \frac{S_m}{2} \left\{\sqrt{\xi^2 + 4} - \xi\right\} \tag{9A-36}$$

in which

$$\xi = S_m \eta \sec\theta \tag{9A-37}$$

and

$$S_m = \frac{\tan\phi}{\tan\theta} \tag{9A-38}$$

If we solve Equations 9A-36 and 9A-37 for $\eta$, then

$$\eta = \left\{\frac{S_m^2 - S.F.^2}{S.F.\ S_m^2}\right\} \cos\theta \tag{9A-39}$$

The term $S_m$ is the safety factor for riprap on a side slope with no flow. Unless the flow is up slope, the safety factor for riprap cannot be greater than $S_m$.

Flow on a Plane Sloping Bed

Flow over a plane bed at a slope of $\alpha$ degrees in the downstream direction is equivalent to oblique flow on a side slope with $\theta = \alpha$ and $\lambda = 90°$.

Then according to Equation 9A-31, $\beta = 0°$ and from Equation 9A-33.

$$\eta' = \eta \left\{\frac{1 + \sin(90° + 0°)}{2}\right\} = \eta \tag{9A-40}$$

It follows from Equation 9A-30 that

$$S.F. = \frac{\cos\alpha \tan\phi}{\eta\tan\phi + \sin\alpha} \tag{9A-41}$$

for flow on a plane bed sloping $\alpha$ degrees to the horizontal. Alternatively solving for $\eta$ in Equation 9A-41

$$\eta = \cos\alpha \left\{\frac{1}{S.F.} - \frac{\tan\alpha}{\tan\phi}\right\} \tag{9A-42}$$

Flow on a Horizontal Bed

For fully developed rough turbulent flow over a plane horizontal bed ($\alpha = 0$) of rock riprap, Equation 9A-41 reduces to

$$S.F. = \frac{1}{\eta} \tag{9A-43}$$

If the riprap particles are at the condition of incipient motion, S.F. = 1 so $\eta = 1$ and from Equation 9A-32

$$\frac{\tau_o}{(S_s - 1)\gamma D} = 0.047 \tag{9A-44}$$

which is Shields' criteria for the initiation of motion.

9A.2 REPRESENTATIVE GRAIN SIZE FOR RIPRAP

The concept of a representative grain size for riprap is simple. A uniformly graded riprap with a median size $D_{50}$ scours to a greater depth than a well-graded mixture with the same median size. Uniformly distributed riprap scours to a depth at which the velocity is less than that required for the transportation of $D_{50}$ size rock. Well-graded riprap on the other hand develops an armor plate. That is, some of the finer materials including sizes up to $D_{50}$ and larger, are transported by high velocities leaving a layer of large rock sizes that cannot be transported under the given flow conditions. Thus, size of rock representative of the stability of riprap is determined by larger sizes of rock. Representative grain size D for riprap is larger than the median rock size $D_{50}$.

In studies of scour below culvert outlets, Stevens (1968) obtained the following expression for the representative grain size of well-graded materials

$$D = \left\{\frac{\sum_{i=1}^{10} D_i^3}{10}\right\}^{1/3} \tag{9A-45}$$

where

$$D_i(i=1) = \frac{D_0 + D_{10}}{2}$$

$$D_i(1=2) = \frac{D_{10} + D_{20}}{2}$$

$$\vdots$$

$$D_i(i=10) = \frac{D_{90} + D_{100}}{2}$$

The terms $D_0$, $D_{10}$, ..., $D_{100}$ are sieve diameters of riprap for which 0 percent, 10 percent, ..., 100 percent of the material is finer by weight.

Equation 9A-45 is equivalent to taking the arithmetic average of the sum of weights of individual rock sizes. In Stevens' studies (1968), the ratio of representative size to median size $D/D_{50}$ was varied between 1.005 and 2.25.

Recommended Representative Grain Size for Riprap

Computations of representative grain size D for the recommended gradation is given in Table 9A-1.

Table 9A-1. Data for suggested gradation.

| Percent finer | Sieve Dia. | i | $D_i$ |
|---|---|---|---|
| 0 | 0.25 $D_{50}$ | -- | -- |
| 10 | 0.35 $D_{50}$ | 1 | 0.28 $D_{50}$ |
| 20 | 0.50 $D_{50}$ | 2 | 0.43 $D_{50}$ |
| 30 | 0.65 $D_{50}$ | 3 | 0.57 $D_{50}$ |
| 40 | 0.80 $D_{50}$ | 4 | 0.72 $D_{50}$ |
| 50 | 1.00 $D_{50}$ | 5 | 0.90 $D_{50}$ |
| 60 | 1.20 $D_{50}$ | 6 | 1.10 $D_{50}$ |
| 70 | 1.60 $D_{50}$ | 7 | 1.50 $D_{50}$ |
| 90 | 1.80 $D_{50}$ | 9 | 1.70 $D_{50}$ |
| 100 | 2.00 $D_{50}$ | 10 | 1.90 $D_{50}$ |

Rock sizes in the last column of Table 9A-1 are used in Equation 9A-45 to determine representative grain size D. Computed D is

$$D = \left\{\frac{\sum_{i=1}^{10} D_i^3}{10}\right\}^{1/3}$$

$$= 1.25\ D_{50}$$

This effective grain size of the mixture corresponds to the size $D_{65}$ riprap.

Comparison of Representative Grain Sizes

In scour investigations, Stevens (1968) compared the scour produced in two different gradations of riprap having the same median diameter, $D_{50}$ = 1.2 in. Riprap gradations are shown in Figure A3 as curves 1-2 and 3-4.

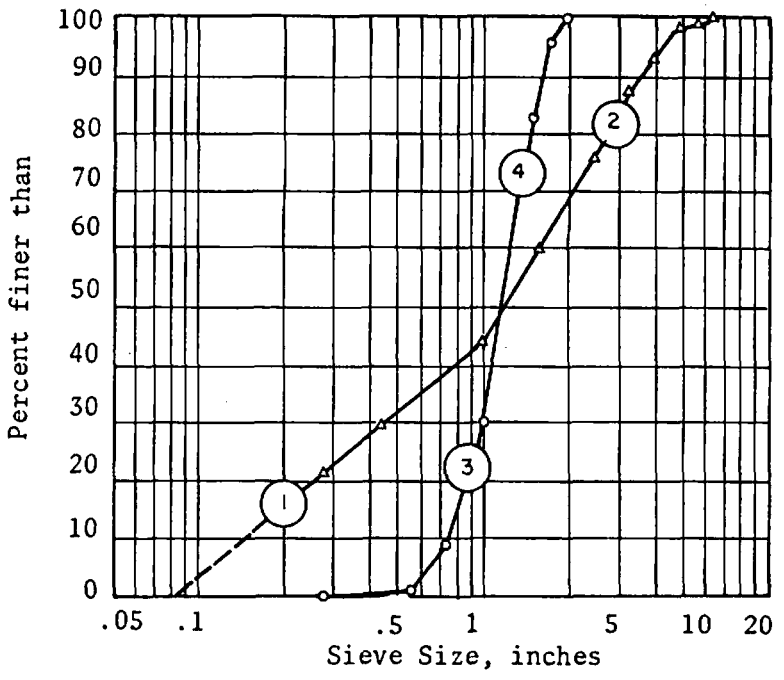


Figure 9A-3. Riprap gradations.

Sieve sizes of four segments of two gradation curves (segments 1, 2, 3, and 4) are listed in Table 9A-2.

Table A2. Data for selected gradations.

| Percent Finer | Curve 1 Dia. in. | Curve 2 Dia. in. | Curve 3 Dia. in. | Curve 4 Dia. in. |
|---|---|---|---|---|
| 0 | 0.08 | -- | 0.28 | -- |
| 10 | 0.15 | -- | 0.75 | -- |
| 20 | 0.26 | -- | 0.88 | -- |
| 30 | 0.46 | -- | 1.00 | -- |
| 40 | 0.80 | -- | 1.10 | -- |
| 50 | 1.20 | 1.20 | 1.20 | 1.20 |
| 60 | -- | 1.60 | -- | 1.28 |
| 70 | -- | 2.15 | -- | 1.35 |
| 80 | -- | 2.80 | -- | 1.45 |
| 90 | -- | 3.70 | -- | 1.60 |
| 100 | -- | 6.60 | -- | 2.00 |

From these data representative grain sizes for the four gradations are computed using Equation 9A-45. The representative grain size D and the ratio of representative diameter to median diameter $D/D_{50}$ are given in Table 9A-3 for the four gradations (Figure 9A-3).

Table 9A-3. Representative diameter for various gradations.

| Curve | D in. | $D/D_{50}$ |
|---|---|---|
| 1-2 | 2.70 | 2.25 |
| 3-2 | 2.71 | 2.26 |
| 1-4 | 1.21 | 1.01 |
| 3-4 | 1.27 | 1.06 |

Inspection of values in Table 9A-3 shows that larger sizes in the gradation have a dominant effect in determination of representative grain size. Thus, large sizes of a gradation are the important sizes for stability. Fines should not be neglected, however, since lack of fines necessitates using a filter under the riprap.

If a riprap gradation has a wide range of sizes, thickness of the riprap layer must be large enough to permit loss of some fines (armorplating) without uncovering protected materials (filter or bank material). Recommended thickness for the recommended gradation is $2D_{50}$ which is also $D_{100}$. For gradations with larger gradation coefficients thickness must be at least $D_{100}$. For larger gradation coefficients ($G > 3.0$) thickness can be increased to $1.5D_{100}$ to provide enough material for armorplating.

Effective Size for Log-normal Gradations

Cumulative distribution function of a log-normal distribution can be expressed as

$$F_X(x) = \int_o^x \frac{1}{\sigma_y x (2\pi)^{1/2}} \exp\{-1/2(\frac{\ln x - \mu_y}{\sigma_y})^2\}\, dx \qquad (9A\text{-}46)$$

where exp means raising the base of the natural log e to the power $(-1/2((\ln x-\mu_y)/\sigma_y)^2)$ and

x = particle diameter

Y = a normally (Gaussian) distributed variable

= lnx

$\mu_y$ = mean of Y

$\sigma_y$ = standard deviation of Y

The median value of x can be written

$$x_{med} = D_{50} = \exp(\mu_y)$$

Thus

$$\mu_y = \ln D_{50} \tag{9A-47}$$

Similarly

$$\sigma_y = \ln G \tag{9A-48}$$

where G is the gradation coefficient. It follows that the expression for mean size of bed material is

$$D_m = D_{50} \exp\{\tfrac{1}{2} (\ln G)^2\} \tag{9A-49}$$

Mahmood (1973) found that the distribution of other properties of bed material such as the projected area of the particle, the volume of the particle, or the surface area of the particle can also be represented by a log-normal distribution. The volume of a particle properties can be written

$$V = bx^3 \tag{9A-50}$$

where V = the volume of the particle

b = constant

x = particle diameter

Assuming a constant specific weight of sediment, particle weight can be represented by Equation 9A-50.

Weight of a bed material particle is important to particle stability. Thus, it is more meaningful to compute representative particle size based on weight of the particle than on diameter. From the expressions presented by Mahmood representative size of the bed material based on the weight of the particles is given by

$$D = D_{50} \exp\{\tfrac{3}{2} (\ln G)^2\} \tag{9A-51}$$

Ratio of mean weight size D to mean diameter size $D_m$ is given by

$$\frac{D}{D_m} = \frac{\exp\{\frac{3}{2} (\ln G)^2\}}{\exp\{\frac{1}{2} (\ln G)^2\}} \tag{9A-52}$$

which is always greater than one for nonuniform grain size distributions. For uniform distributions there is only one particle size and the means are identical.

9A.3 RELATION BETWEEN VELOCITY AND SHEAR

In order to design riprap it is necessary to relate tractive force acting on the riprapped bed or bank to the fluid velocity in the vicinity of the riprap. For fully turbulent flow the relation for the local velocity $v$ at a distance $y$ above the bed is given by

$$v = 2.5\ V_* \ln\ (30.2\ \frac{y}{D_c}) \qquad (9A\text{-}53)$$

in which $V_*$ is the shear velocity that is

$$V_* = (\frac{\tau_o}{\rho})^{1/2} \qquad (9A\text{-}54)$$

by definition. This velocity distribution equation was employed by Einstein (1950) in his bedload function research.

If we select velocity at distance $y = D$ above the bed as the reference velocity $v_r$ then

$$v_r = 2.5\ V_* \ln 30.2$$

or

$$v_r = 8.5\ V_* \qquad (9A\text{-}55)$$

From Equations 9A-54 and 9A-55 the relations between $v_r$ and $\tau_o$ is

$$\rho v_r^2 = 72\ \tau_o \qquad (9A\text{-}56)$$

This relation is valid only for uniform flow in wide prismatic channels in which flow is fully turbulent. For purposes of riprap design Equation 9A-56 can be employed when the flow is accelerating e.g., on the nose of a spur dike. The equation should not be used in areas where flow is decelerating or below energy dissipating structures. In these areas shear stress is larger than would be calculated by Equation 9A-56.

By substituting Equation 9A-56 into Equation 9A-66, the expression for stability factor $\eta$ becomes

$$\eta = \frac{0.30\ v_r^2}{(S_s-1)gD} \qquad (9A\text{-}57)$$

Average velocity in vertical $V$ is obtained from Einsteins logrithmic velocity equation with $x = 1$ for large riprap sizes. The expression can be written

$$V = 2.5\ V_* \ln\ (12.3\ \frac{y_o}{D}) \tag{9A-58}$$

in which $y_o$ is the depth of flow. Ratio of reference velocity $v_r$ to depth-average velocity is

$$\frac{v_r}{V} = \frac{2.5\ V_*\ \ln\ (30.2)}{2.5\ V_*\ \ln\ (12.3\ \frac{y_o}{D})}$$

or

$$\frac{v_r}{V} = \frac{3.4}{\ln(12.3\ \frac{y_o}{D})} \tag{9A-59}$$

Equation 9A-59 is obtained from Equations 9A-55 and 9A-58. The expression for the stability factor $\eta$ can be written in terms of depth-averaged velocity. From Equations 9A-57 and 9A-59

$$\eta = \frac{\beta V^2}{(S_s - 1)gD} \tag{9A-60}$$

in which

$$\beta = 0.30\ \{\frac{3.4}{\ln(12.3\ \frac{y_o}{D})}\}^2 \tag{9A-61}$$

As shown in Figure 9A-4 the value of $\beta$ varies from 0.30 for relatively shallow flows to 0.04 for $y_o/D = 1000$. Searcy (1967) uses the expression

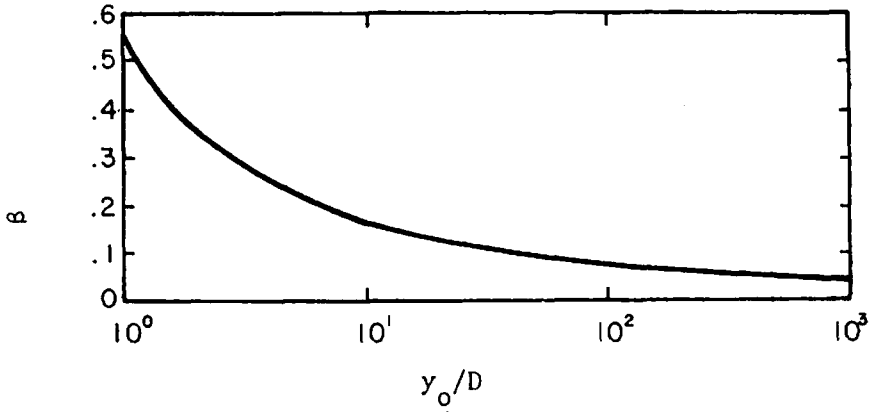


Figure 9A-4. Relation between $\beta$ and $y_o/D$.

$$\frac{v_s}{\bar{V}} = \frac{1}{0.958\ \log(\frac{y_o}{D}) + 1} \tag{9A-62}$$

to determine velocity "against the stone". Here $v_s$ is velocity against the stone, $\bar{V}$ is the mean velocity in the channel, and log is the logarithm to the base 10.

In wide channels depth-averaged velocity and mean velocity in the channel are nearly equal i.e., $V \simeq \bar{V}$. Then velocity against the stone is related to reference velocity by

$$\frac{v_r}{v_s} = \frac{v_r}{\bar{V}} \frac{V}{v_s}$$

or

$$\frac{v_r}{v_s} = \frac{3.4\{.958 \log(\frac{y_o}{D}) + 1\}}{\ln(12.3 \frac{y_o}{D})} \qquad (9A\text{-}63)$$

according to Equations 9A-59 and 9A-62. For values of $y_o/D$ between $1x10^0$ and $1x10^6$, the value of $v_r/v_s$ is nearly 1.4. By letting

$$\frac{v_r}{v_s} = 1.4 \qquad (9A\text{-}64)$$

the expression for stability factor $\eta$ (Equation 9A-57) becomes

$$\eta = \frac{0.60\ v_s^2}{(S_s - 1)gD} \qquad (9A\text{-}65)$$

In summary the following expressions for $\eta$ are equivalent

$$\eta = \frac{21\ \tau_o}{(S_s - 1)\gamma D} \qquad (9A\text{-}66)$$

$$\eta = \frac{0.30\ v_r^2}{(S_s - 1)gD} \qquad 9A\text{-}57$$

$$\eta = \frac{0.60\ v_s^2}{(S_s - 1)gD} \qquad 9A\text{-}65$$

and

$$\eta = \frac{\beta V^2}{(S_s - 1)gD} \qquad 9A\text{-}60$$

in which

$$\beta = 0.30 \left\{\frac{3.4}{\ln(12.3 \frac{y_o}{D})}\right\}^2 \qquad 9A\text{-}61$$

## 9A.4 RIPRAP DESIGN ON AN EMBANKMENT

When drawdown through a contraction is large there is an appreciable downslope component to the velocity vector on the nose of an embankment end or spur dike. This downslope component of velocity is illustrated in the model embankment shown in Figure 9A-5. The model study was reported by Simons and Lewis (1971). For the case shown in Figure 9A-5 the angle between the horizontal and velocity vector at point P is

$$\lambda = 20^\circ$$

A method of computing the streamlines and velocities around an embankment end is presented by Lewis (1972). If drawdown through the bridge is large, reference velocity $v_r$ in the vicinity of riprap can be as large as 6 fps.

Suppose that reference velocity is

$$v_r = 6 \text{ fps}$$

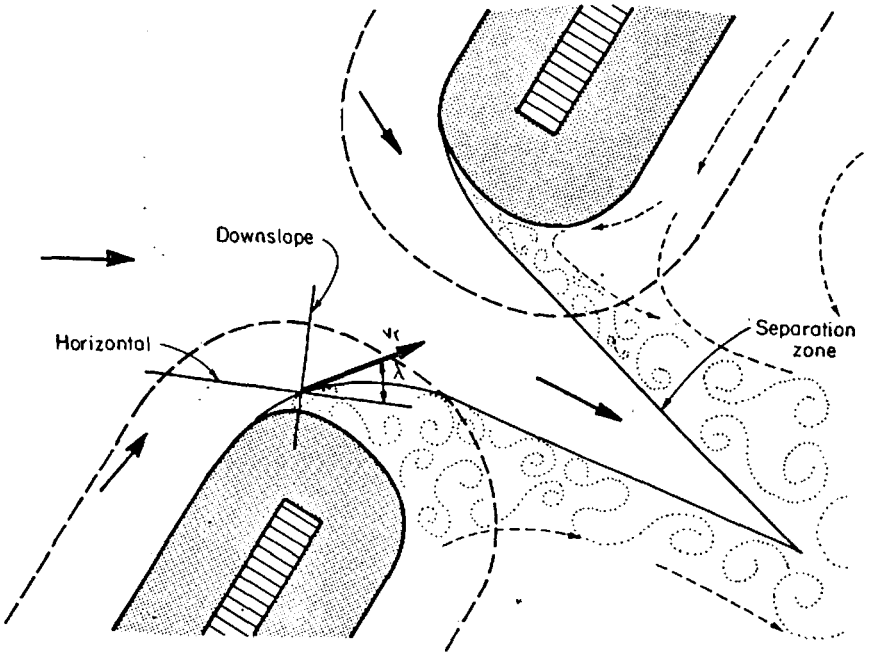


Figure 9A-5. Flow around an embankment end.

and embankment side slope angle is

$$\theta = 18.4°$$

which corresponds to a 3:1 side slope. If the embankment is covered with dumped rock of specific weight $S_s = 2.65$ and effective rock size $D = 1.0$ ft, the safety factor is determined in the following manner.

From Equation 9A-57

$$\eta = \frac{0.30\ v_r^2}{(S_s - 1)gD} = \frac{(0.30)(6)^2}{(2.65 - 1)(32.2)(1.0)} = 0.203$$

This dumped rock has an angle of repose of approximately 35° according to Figure 9A-9. Therefore,

$$\beta = \tan^{-1}\left\{\frac{\cos\lambda}{\frac{2\sin\theta}{\eta\tan\phi} + \sin\lambda}\right\} = \tan^{-1}\left\{\frac{\cos 20°}{\frac{2\sin 18.4°}{0.203\tan 35°} + \sin 20°}\right\} = 11°$$

and

$$\eta' = \eta\left\{\frac{1 + \sin(\lambda+\beta)}{2}\right\} = 0.203\left\{\frac{1 + \sin(20° + 11°)}{2}\right\} = 0.154$$

The safety factor for the rock is given by

$$S.F. = \frac{\cos\theta\tan\phi}{\eta'\tan\phi + \sin\theta\cos\beta} = \frac{\cos 18.4°\tan 35°}{0.154\tan 35° + \sin 18.4°\cos 11°} = 1.59$$

Thus, with a safety factor of 1.59 this rock is more than adequate to withstand the flow velocity.

By repeating the above calculations over the range of interest for D (with $\phi = 35°$), the curve given in Figure 9A-6 is determined. This curve shows that incipient motion rock size is approximately 0.35 ft and that the maximum safety factor is less than 2.0 on the 3:1 side slope.

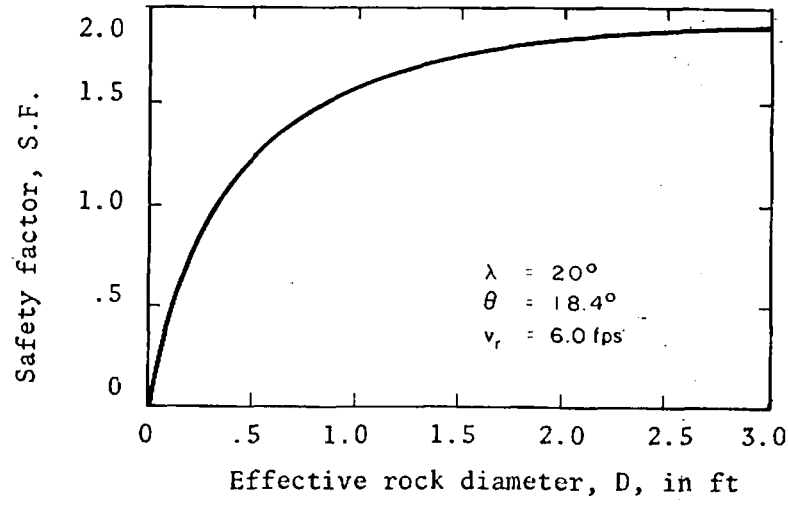


Figure 9A-6. Safety factors for various rock sizes on a side slope.

The safety factor of a particular side slope riprap design can be increased by decreasing side slope angle $\theta$. If side slope angle is decreased to zero then

$$S.F. = \frac{1}{\eta} = \frac{1}{0.203} = 4.93$$

The curve in Figure 9A-7 relates the safety factor and side slope angle of the embankment (for $\lambda = 20°$, $D = 1.0$ ft and $v_r = 6.0$ fps).

## 9A.5 DESIGN AID FOR SIDE SLOPE RIPRAP

When velocity along a side slope has a downslope component, sizing of riprap is accomplished by employing complex equations given in an earlier chapter. An example of sizing riprap using these equations is given in a following section. When the velocity along a side slope has no downslope component i.e., the velocity vector is along the horizontal, some simple design aids can be developed.

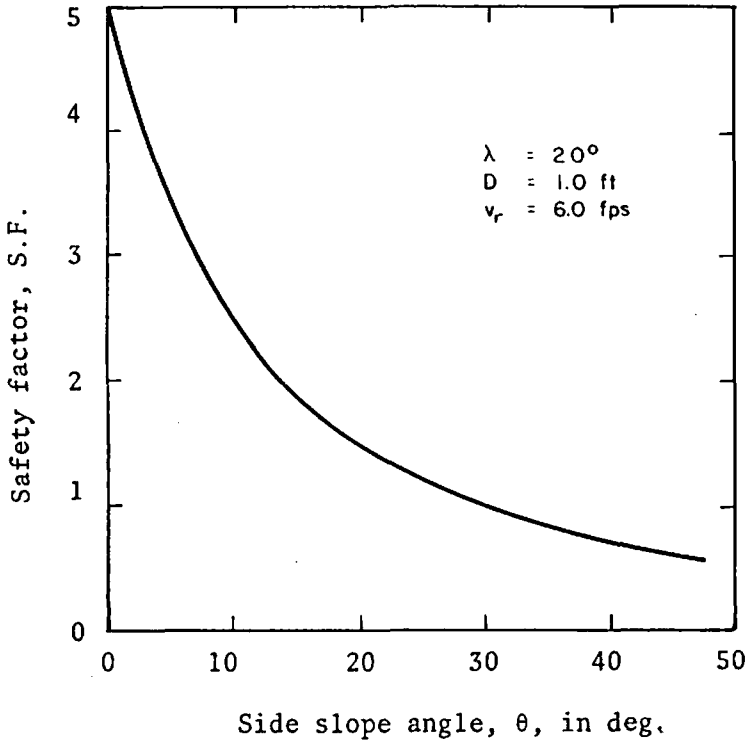


Figure 9A-7. Safety factors for various side slopes.

For horizontal flow along a side slope the equations relating safety factor, stability number, side slope angle, and angle of repose for the rock are

$$\eta = \left\{\frac{S_m^2 - (S.F.)^2}{(S.F.)\, S_m^2}\right\} \cos\theta \qquad (9A\text{-}67)$$

and

$$S_m = \frac{\tan\Phi}{\tan\theta} \qquad (9A\text{-}68)$$

Interrelation of variables in these two equations is represented in Figure 9A-8. Here specific weight of the rock is assumed 2.65 and a safety factor of 1.5 is employed.

Recommended safety factor for the design of riprap is

$$S.F. = 1.5$$

This recommendation is the result of studies of riprap embankment model data obtained by Lewis. These studies were reported by Simons and Lewis (1971).

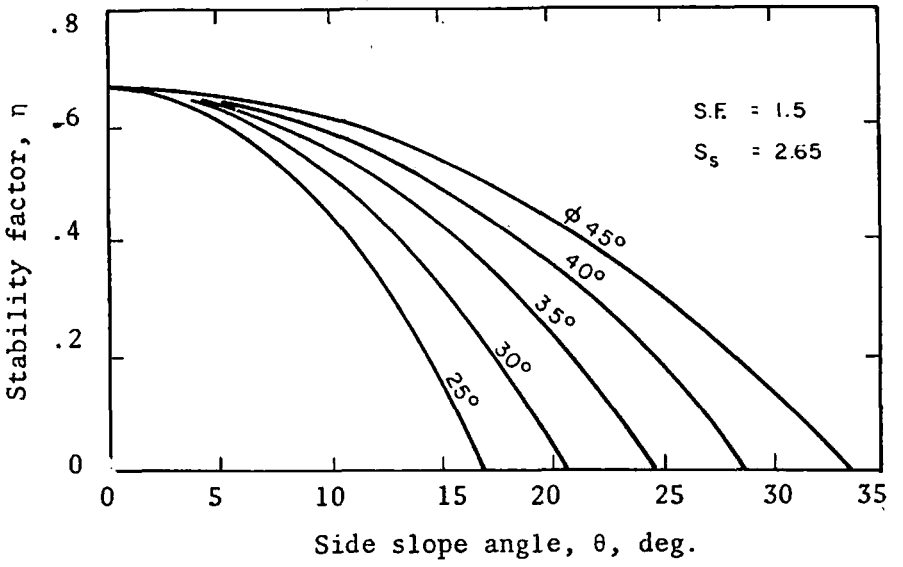


Figure 9A-8. Stability factors for a 1.5 safety factor for horizontal flow along a side slope.

The curves in Figure 9A-8 are computed in the following manner.

1. An angle of repose $\phi$ is selected e.g.,

   $$\phi = 45°$$

2. Side slope angle is then selected e.g.,

   $$\theta = 25°$$

3. $S_m$ is computed from Equation 9A-68

   $$S_m = \frac{\tan 45°}{\tan 25°} = 2.14$$

4. Then $\eta$ is computed from Equation 9A-67 with S.F. = 1.5

   $$\eta = \left\{\frac{(2.14)^2 - (1.5)^2}{(1.5)(2.14)^2}\right\} \cos 25° = 0.29$$

5. The above steps are repeated for the full range of interest for $\phi$ and $\theta$.

In a design problem side slope angle is known and angle of repose can be estimated (Figure 9A-9). With these values the stability factor is obtained from Figure 9A-8. For example if

$$\phi = 30°$$

and

$$\theta = 10°$$

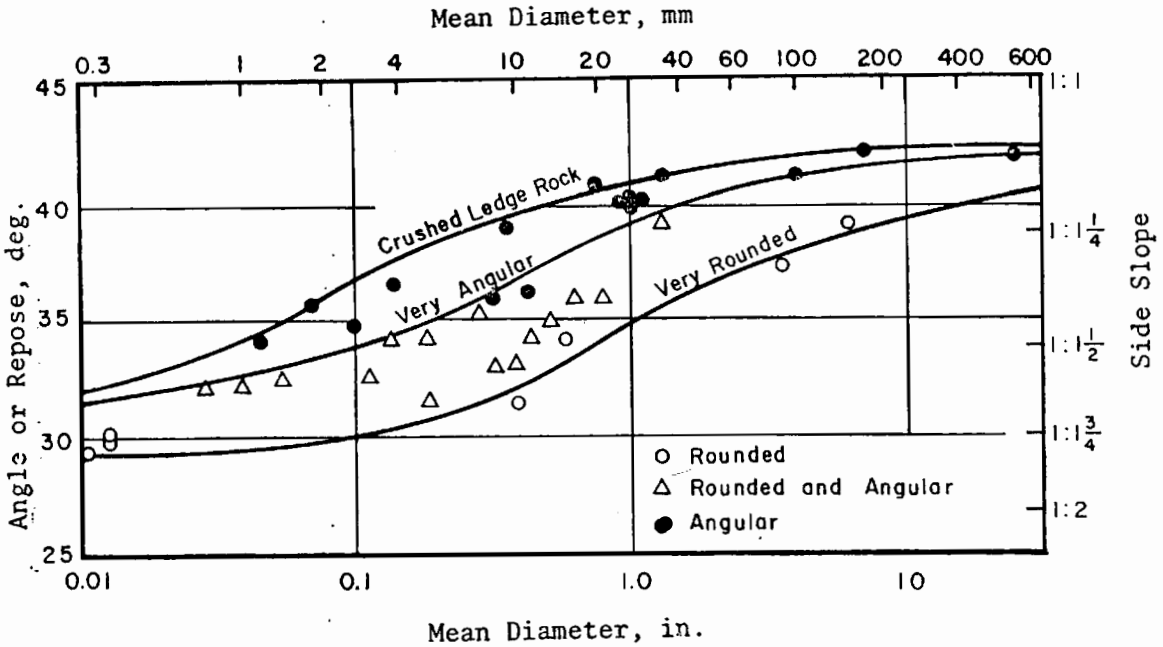


Figure 9A-9. Angle of repose.

then

$$\eta = 0.52$$

If the shear stress on the side slope is known,

$$D = \frac{21\ \tau_o}{(S_s - 1)\gamma\eta} \qquad (9A\text{-}69)$$

$$= \frac{21\ \tau_o}{(2.65 - 1)(62.4)\eta}$$

$$= 0.20\ \frac{\tau_o}{\eta}$$

In this example if

$$\tau_o = 2 \text{ psf}$$

then

$$D = \frac{(0.20)(2)}{(0.52)} = 0.77 \text{ ft.}$$

If the reference velocity on the side slope is known, then (from Equation 9A-57)

$$D = \frac{0.30\ v_r^2}{(S_s - 1)g\eta}$$

$$= \frac{0.30\ v_r^2}{(2.65 - 1)(32.2)\eta}$$

$$= .0056\ \frac{v_r^2}{\eta}$$

In this case, if

$$v_r = 6 \text{ fps}$$

$$D = \frac{(.0056)(6)^2}{0.52} = 0.40 \text{ ft.}$$

If average velocity $V$ and depth $y_o$ are known, more design aids should be prepared from Equations 9A-60 and 9A-61.

9A.6 FILTER DESIGN

Requirements for a gravel filter were given in an earlier lecture. Gradation of a filter should be such that

$$\frac{D_{50}(\text{Filter})}{D_{50}(\text{Base})} < 40 \qquad (9A\text{-}70)$$

$$5 < \frac{D_{15}(\text{Filter})}{D_{15}(\text{Base})} < 40 \qquad (9A\text{-}71)$$

and

$$\frac{D_{15}(\text{Filter})}{D_{85}(\text{Base})} < 5 \qquad (9A\text{-}72)$$

Filter Design Example 1

Considering a riprap blanket resting on base material and the properties of riprap and base material (Table 9A-4), a filter should be designed to be placed between the riprap and base material.

Table 9A-4. Sizes of materials.

| Base Material Sand | Riprap Gravel |
|---|---|
| $D_{85}$ = 1.50 mm | $D_{85}$ = 24 mm |
| $D_{50}$ = 0.75 mm | $D_{50}$ = 12 mm |
| $D_{15}$ = 0.38 mm | $D_{15}$ = 6 mm |

In accordance with the recommended sizes for filters, it should be noted that

$$\frac{D_{50}(\text{Riprap})}{D_{50}(\text{Base})} = \frac{12}{0.75} = 16$$

which satisfies expression 9A-70. Also

$$\frac{D_{15}(\text{Riprap})}{D_{15}(\text{Base})} = \frac{6}{0.38} = 16$$

which satisfies the requirement 9A-71. Moreover

$$\frac{D_{15}(\text{Riprap})}{D_{85}(\text{Base})} = \frac{6}{1.5} = 4$$

which satisfies the requirement 9A-72. Riprap itself satisfies the requirements for filter so no filter is needed.

Filter Design Example 2

The following filter design is taken from Anderson (1968). Properties of base material and riprap are given in Table 9A-5.

Table 9A-5. Sizes of materials.

| Base Material Sand | Riprap Rock |
|---|---|
| $D_{85}$ = 1.5 mm | $D_{85}$ = 400 mm |
| $D_{50}$ = 0.5 mm | $D_{50}$ = 200 mm |
| $D_{15}$ = 0.17 mm | $D_{15}$ = 100 mm |

The riprap does not contain sufficient fines to act as the filter because

$$\frac{D_{15}(\text{Riprap})}{D_{85}(\text{Base})} = \frac{100}{1.5} = 67$$

which is much greater than 5, the recommended upper limit (expression 9A-72). Also

$$\frac{D_{15}(\text{Riprap})}{D_{15}(\text{Base})} = \frac{100}{0.17} = 600$$

which is much greater than 40, the recommended upper limit (expression 9A-71).

Properties of the filter to be placed adjacent to the base are as follows

$$\frac{D_{50}(\text{Filter})}{D_{50}(\text{Base})} < 40$$

therefore

$$D_{50}(\text{Filter}) < (40)(0.5) = 20 \text{ mm}$$

$$\frac{D_{15}(\text{Filter})}{D_{15}(\text{Base})} < 40$$

therefore

$$D_{15}(\text{Filter}) < (40)(0.17) = 6.8 \text{ mm}$$

$$\frac{D_{15}(\text{Filter})}{D_{85}(\text{Base})} < 5$$

therefore

$$D_{15}(\text{Filter}) < (5)(1.5) = 7.5 \text{ mm}$$

$$\frac{D_{15}(\text{Filter})}{D_{15}(\text{Base})} > 5$$

therefore

$$D_{15}(\text{Filter}) > (5)(.17) = 0.85 \text{ mm}$$

Thus, with respect to the base

$$0.85 \text{ mm} < D_{15}(\text{Filter}) < 6.8 \text{ mm}$$

and $$D_{50}(\text{Filter}) < 20 \text{ mm}$$

Properties of the filter to be placed adjacent to the riprap are as follows

$$\frac{D_{50}(\text{Riprap})}{D_{50}(\text{Filter})} < 40$$

therefore

$$D_{50}(\text{Filter}) > \frac{200}{40} = 5 \text{ mm}$$

$$\frac{D_{15}(\text{Riprap})}{D_{15}(\text{Filter})} > 5$$

therefore

$$D_{15}(\text{Filter}) < \frac{100}{5} = 20 \text{ mm}$$

$$\frac{D_{15}(\text{Riprap})}{D_{15}(\text{Filter})} < 40$$

therefore

$$D_{15}(\text{Filter}) > \frac{100}{40} = 2.5 \text{ mm}$$

$$\frac{D_{15}(\text{Riprap})}{D_{85}(\text{Filter})} < 5$$

therefore

$$D_{85}(\text{Filter}) > \frac{100}{5} = 20 \text{ mm}$$

Thus, with respect to the riprap, the filter must satisfay these requirements

$$2.5 \text{ mm} < D_{15}(\text{Filter} < 20 \text{ mm}$$

$$D_{50}(\text{Filter}) > 5 \text{ mm}$$

$$D_{85}(\text{Filter}) > 20 \text{ mm}$$

These riprap filter requirements along with those for base material are shown in Figure 9A-10. Any filter with sizes represented by double cross-hatched area is satisfactory. For example, a good filter could have these sizes

$$D_{85} = 40 \text{ mm}$$

$$D_{50} = 10 \text{ mm}$$

$$D_{15} = 4 \text{ mm}$$

## 9A.7 STRAUB'S EQUATION FOR CLEAR-WATER SCOUR

Consider the long contraction shown in Figure 9A-11. In the wide approach reach at the cross section designated Section 1, average velocity is $V_1$, average depth of flow is $y_1$, and width is $W_1$. Flow-rate across Section 1 is

$$Q = V_1 y_1 W_1 \qquad (9A\text{-}73)$$

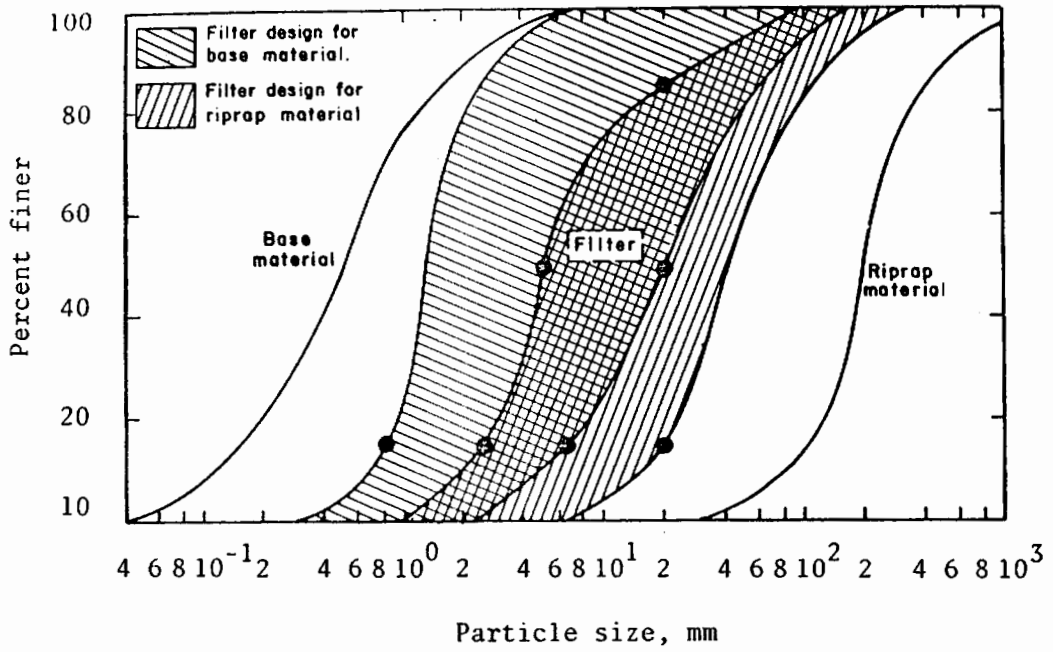


Figure 9A-10. Gradations of filter blanket for examples 2 (after Anderson et al., 1968).

In the contracted reach at the cross section designated Section 2, the average velocity is $V_2$, flow depth is $y_2$, and width is $W_2$. Flowrate across Section 2 is

$$Q = V_2 y_2 W_2 \tag{9A-74}$$

For a given flowrate $Q$ and a given contraction ratio $W_2/W_1$, depth ratio $y_2/y_1$ should be determined for a clear-water scour case.

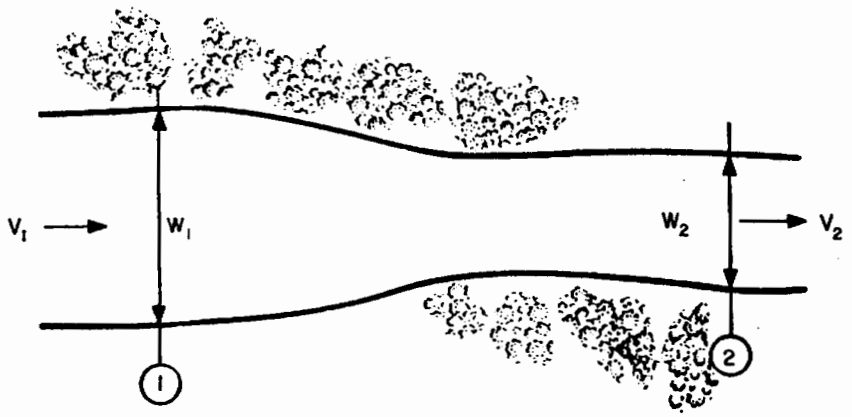


Figure 9A-11. Plan view of the long contraction.

In the clear-water scour case, there is no transport in the wide upstream section. Shear stress is less than critical shear stress (the shear stress causing initial movement of bed particles). That is,

$$\tau_1 = \gamma y_1 S_{f_1} < \tau_c \tag{9A-75}$$

Here $S_{f_1}$ is slope of the energy grade line at Section 1.

Assume for the time being that scour occurs in the long contraction. Scour will continue until bed shear stress in the long contraction has been reduced to critical shear stress. Then, at Section 2

$$\tau_2 = \tau c = \gamma y_2 S_{f_2} \tag{9A-76}$$

When this condition is reached there is no longer sediment transport at Section 2. Also, there is no sediment transport at Section 1 ($\tau_1 < \tau_c$). Hence the term clear-water scour is employed.

By utilizing Equations 9A-75 and 9A-76, the depth ratio is

$$\frac{y_2}{y_1} = \frac{S_{f_1}}{S_{f_2}} \frac{\tau_c}{\tau_1} \tag{9A-77}$$

Manning's equation can be employed to determine the friction slope ratio. Accordingly

$$\frac{S_{f_1}}{S_{f_2}} = (\frac{n_1}{n_2})^2 (\frac{V_1}{V_2})^2 (\frac{y_2}{y_1})^{4/3} \tag{9A-78}$$

so

$$\frac{y_2}{y_1} = (\frac{n_1}{n_2})^2 (\frac{V_1}{V_2})^2 (\frac{y_2}{y_1})^{4/3} (\frac{\tau_c}{\tau_1}) \tag{9A-79}$$

Velocity ratio $V_1/V_2$ is obtained by equating Equations 9A-73 and 9A-74 (constant discharge) or

$$\frac{V_1}{V_2} = \frac{y_2}{y_1} \frac{W_2}{W_1} \tag{9A-80}$$

By putting this ratio into Equation 9A-79 the expression

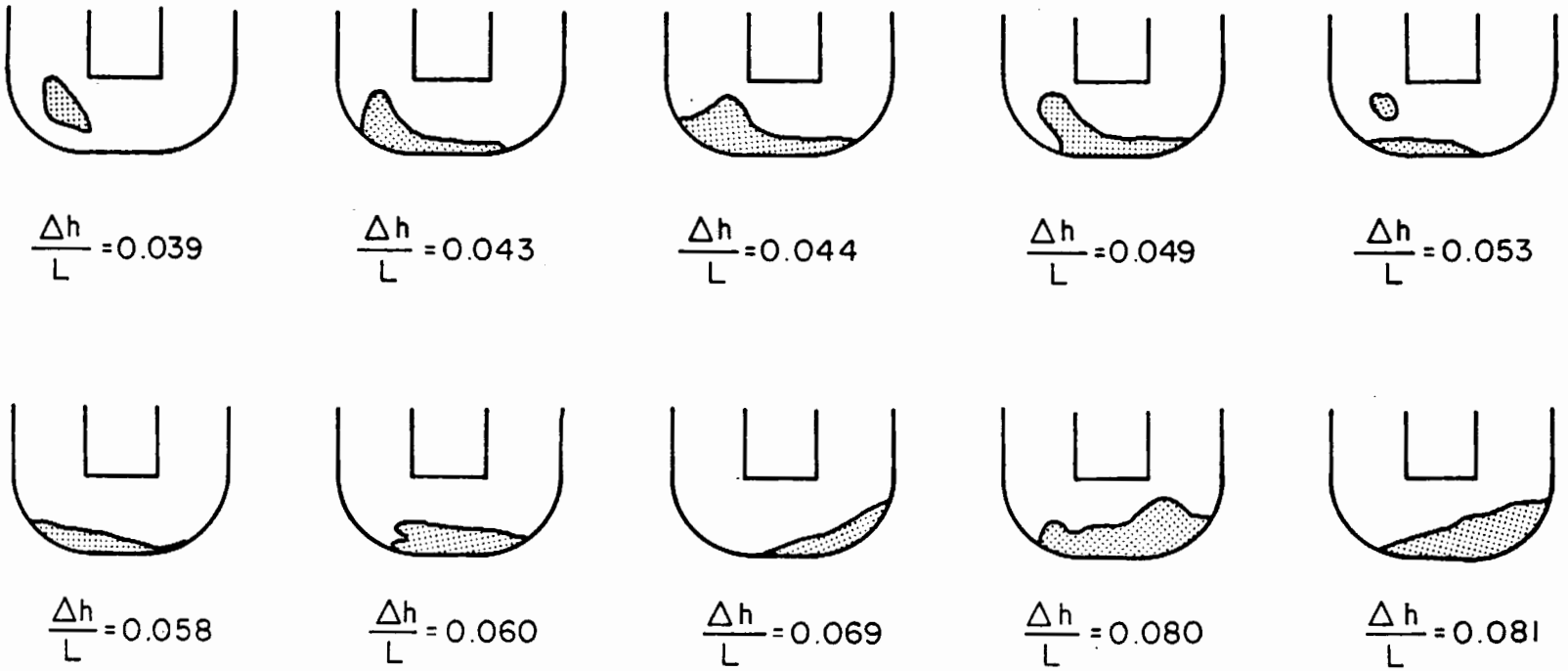


Figure 9A-12. Zones of failure on riprapped embankments.

$$\frac{y_2}{y_1} = \left(\frac{n_2}{n_1}\right)^{6/7}\left(\frac{W_1}{W_1}\right)^{6/7}\left(\frac{\tau_1}{\tau_c}\right)^{3/7} \qquad (9A\text{-}81)$$

is obtained for clear-water scour. If it is assumed that

$$n_1 = n_2$$

then Equation 9A-81 reduces to

$$\frac{y_2}{y_1} = \left(\frac{W_1}{W_2}\right)^{6/7}\left(\frac{\tau}{\tau_c}\right)^{3/7} \qquad (9A\text{-}82)$$

which is the form of the clear-water scour equation first developed by Straub (1940).

## 9A.8 DETERMINATION OF FLOW PARAMETERS ON AN EMBANKMENT

To apply the equations presented in the previous section on the design riprap bank protection, the flow parameters $\tau_o$ , $v_r$ , $v_s$ or $V$ , and $\lambda$ must be evaluated. Lewis (1972) developed an analytical model for determination of the complete velocity and depth distribution in the vicinity of embankments but application of this method is complex. Lewis pointed out, based on the model and analytical studies, that initial losses of the riprap protection occur at one or both zones on the embankment. One zone is near the flow separation point located approximately at midway around the upstream spill-slop. The other is along the embankment toe through the constriction. Riprap losses initially occurred on the upstream spill-slope for small constrictions ($\Delta h/L$ is small) and along the embankment toe for the severe constrictions ($\Delta h/L$ is large) as shown in Figure 9A-12. Here $\Delta h$ is the drop in water surface elevation through the bridge opening and $L$ is the horizontal distance shown in Figure 9A-13 with $\omega = 45$ deg.

For design purposes, estimation of velocities and depths in the entire bridge crossing is not necessary. It is adequate to determine riprap requirements for the most hazardous zones subject to failure. Then this riprap is used to protect the embankment. Flow parameters for determining required riprap at midway around the upstream spill-slope and along the embankment toe through the constriction are determined below. Sizes of riprap required to produce a safety factor of 1.5 at those two positions are computed and larger size rock is chosen for embankment protection.

### Determination of Flow Parameters at the Embankment Toe

Flow at the toe of the embankment is approximately horizontal and parallel to side slope (Figure 9A-13). For design purposes it is assumed that $\lambda = 0$ deg. Depth-averaged flow velocity at the two $V_t$ is related to depth-averaged velocity at the vena contracta $V_d$ by the curves in Figure 9A-14. The quantity $V_d$ is found using the expression

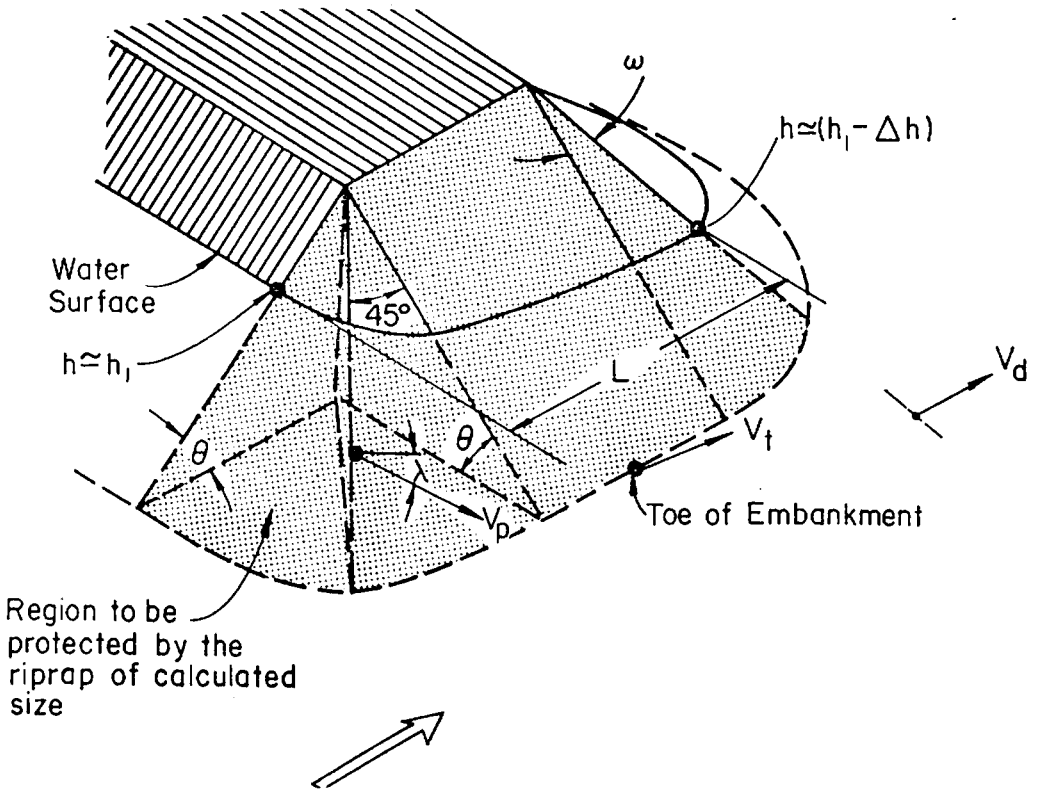


Figure 9A-13. Flow around a spill-through embankment nose.

$$V_d = (\alpha_1 V_1^2 + 2g\Delta h)^{1/2} \qquad (9A\text{-}83)$$

where $\alpha$ and $V_1$ are velocity head correction coefficient and mean velocity in the channel at the upstream section of maximum backwater, respectively and $\Delta h$ is total water surface drop through the bridge opening computed by the method recommended by the Federal Highway Administration (1970). Quantity L in Figure 9A-13 is estimated from geometry of embankment, stage at maximum backwater section $h_1$, and water surface drop $\Delta h$. Velocity at the toe velocity is then found from Figure A14.

Determination of Flow Parameters Midway Around the Upstream Spill-Slope

Depth-averaged velocity midway around the upstream spill-slope $V_p$ (Figure 9A-13) is related to vena contracta velocity $V_d$ and can be determined for given values of $V_p$ and $\Delta h/L$ using the relation in Figure 9A-14. The angle between the velocity vector and the horizontal line $\lambda$ is given in Figure 9A-15.

Application and Limitations

After values of $V_t$, $V_p$, and $\lambda$ are estimated from Figures 9A-14 and 9A-15, the riprap sizes for a given safety factor are determined at the toe and midway around the upstream spill-slope by employing Equations 9A-60 and 9A-61. Quantity $y_o$ in Equation 9A-61 is the local

flow depth. The larger of the two calculated riprap sizes should be used for embankment protection.

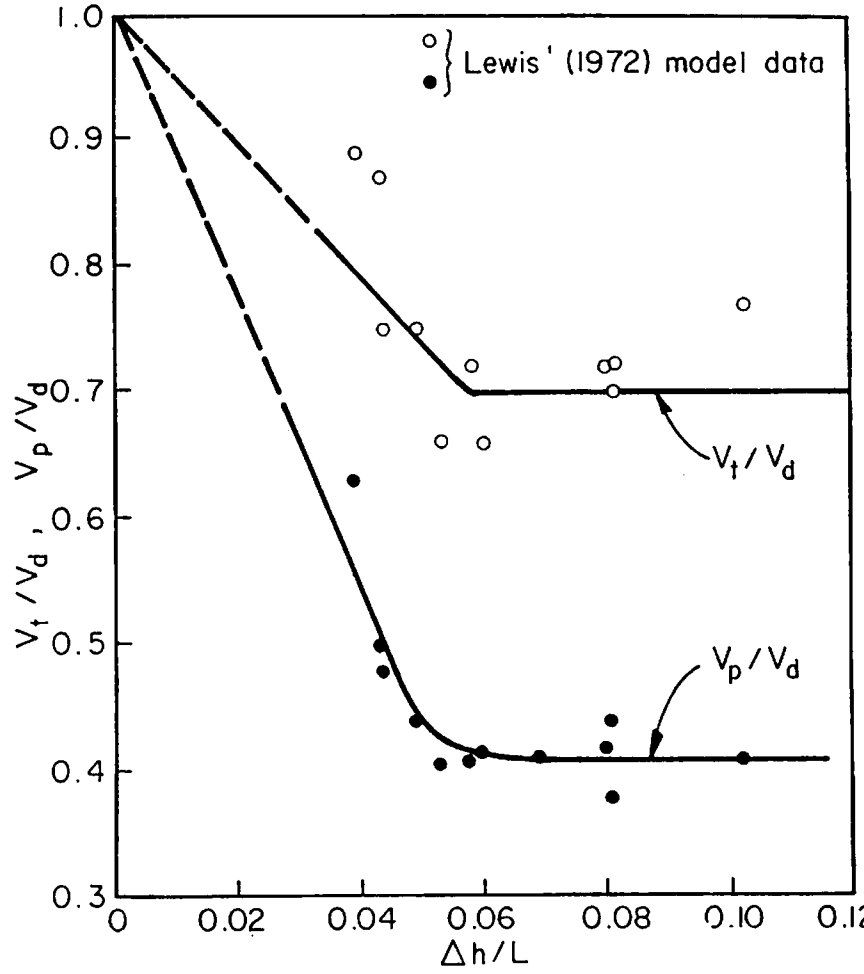


Figure 9A-14. Relation between relative velocities and the drop ratio.

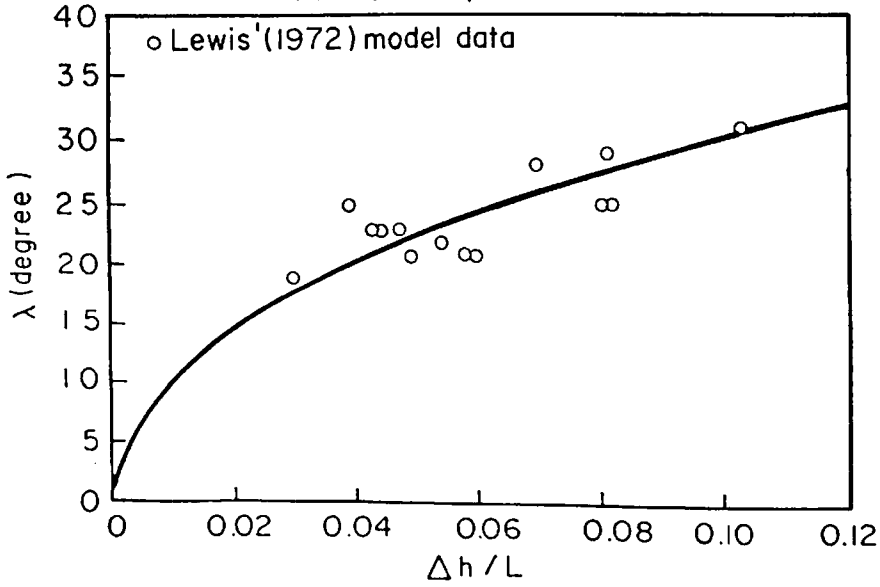


Figure 9A-15. Relation between $\lambda$ at midway around the upstream spill-slope and the drop ratio.

The design procedure given above has been applied to Lewis' model data. It was found that the procedure resulted in a built-in safety factor of approximately 1.2. However, the larger safety factor of 1.5 is recommended for embankments to allow for error in hydraulic predictions and for unknown scale effects which may exist in the models.

The region around the embankment nose requiring calculated riprap protection is shown in Figure 9A-13. Angle $\omega$ varies according to the relation given in Table 9A-6. The other region of the embankment may be protected by a smaller size riprap than the calculated one. A method for computing this size is given by Simons and Lewis (1971).

Table 9A-6. Termination angle for riprap protection.

| $\Delta h/L$ | $\omega$ degrees |
|---|---|
| 0 to 0.5 | 45 |
| .06 | 55 |
| .07 | 65 |
| .08 | 75 |
| .09 | 85 |
| .10 | 90 |

Figures 9A-14 and 9A-15 are developed from model data on spill-through embankments normal to the flow and require modifications when applied to other types of embankments.

## REFERENCES-APPENDIX 9A

Anderson, A. G., Paintal, A. S., and Davenport, J. T., 1968, Tentative Design Procedure for Riprap Lined Channels, Project Report No. 96, St. Anthony Falls Hydraulic Laboratory, University of Minnesota, Minneapolis.

Federal Highway Administration, 1970, Hydraulics of Bridge Waterways, Hydr. Branch, Bridge Div., Off. of Eng. and Oper., Hydr. Design Ser., No. 1, 2nd ed., U.S. Gov. Printing Office, Washington, D.C.

Lewis, G. L., 1972, Riprap protection of bridge footings, Ph.D. dissertation, Dept. of Civil Eng., Colorado State University, Fort Collins.

Mahmood, K., 1973, Lognormal Size Distribution of Particulate Matter, Journal of Sedimentary Petrology, Vol. 43, No. 4, December, pp. 1161-1166.

Searcy, J. K., 1967, Use of Riprap for Bank Protection, Hydr. Eng. Cir. No. 11, Hydraulics Branch, Bridge Division, Office of Engineering and Operations, Federal Highway Administration, Washington, D.C.

Simons, D. B. and Lewis, G. L., 1971, Flood Protection at Bridge Crossings, CER71-72DBS-GLL10, Colorado State University, Fort Collins.

Stevens, M. A. and Simons, D. B., 1971, Stability Analysis for Coarse Granular Material on Slopes, River Mechanics, H. W. Shen, ed., Chap. 17, Water Resources Publ., Fort Collins.

Straub, L. G., 1940, Approaches to the Study of Mechanics of Bed Movement, Iowa State University Studies in Engin. Bul. 20.

# Chapter 10

# UTILIZATION OF HYDROLOGIC INFORMATION SYSTEM

## 10.1 INTRODUCTION

Historical records are the most important source of data in studies of physical systems. This is particularly true in the case of river basin studies where a river is composed of numerous interacting natural and man-influenced physical processes. A river in turn influences the social and economic base of its river basin community by serving as a transportation route, providing water for domestic, agricultural and industrial uses, serving as a recreation site, providing hydropower generation, and functioning as a flood water drainage. The value of historical data depends greatly on the availability of data management techniques for extracting the largest amount of useful information for solving particular problems. A river basin manager and planner dealing with complex systems and their associated problems must view data management as a set of interacting components such as data acquisition, data storage and retrieval, and data processing and utilization. The block diagram in Figure 10-1 summarizes the relationships between these components. Following are the basic steps in this information flow diagram.

### Data Collection

The required data can be collected from many different sources, both internal and external to the organization. To insure against collecting redundant data, this task should be delegated to one data collection group.

### Data Reduction and Categorization

Many field observations become useful only when properly transcribed. Accurate data require care through all processing steps such as data annotation, tabulation and sorting. These constitute the basic functions of the data reduction and categorization task.

### Data Encoding and Verification

This task aims at minimizing the errors which can enter into the data. All data must be encoded to a form which can be used by the computer. Data verification can then be carried out through plotting, automatic screening, or statistical analysis. This step is extremely critical since the rest of the information system will assume clean and accurate data exists.

The data encoding and verification task constitutes the final stage of the Data Acquisition process.

### Data Base Organization

This task is concerned with the design of a storage system which is logically structured to physically store the collected data. The goal of this step is to minimize the turnaround time and cost in acquiring the necessary data from different sources.

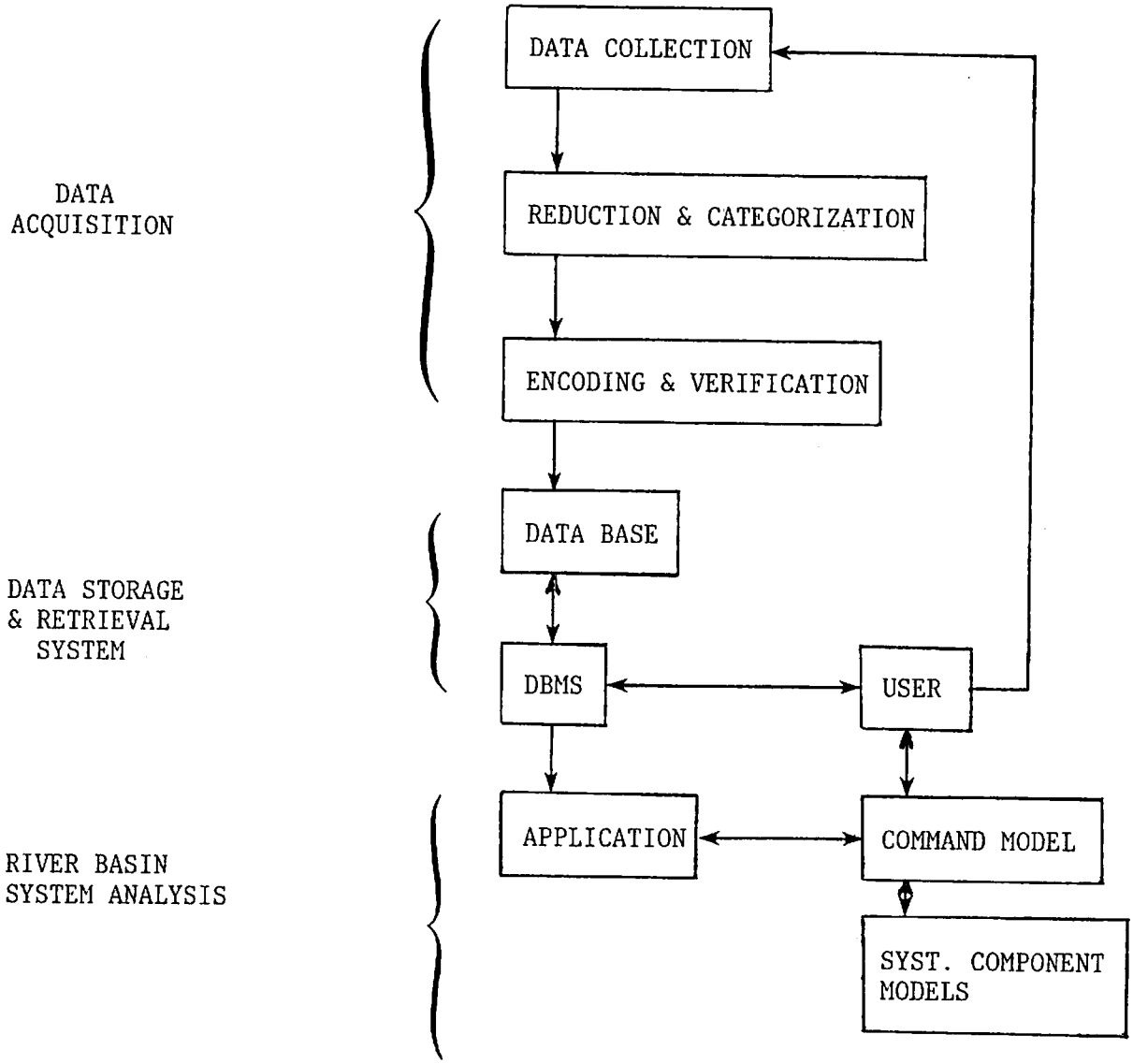


Figure 10-1. Relationship between data collection, processing and utilization.

Data Base Management System Design

A data base management system (DBMS) is a computer program package which assists users in retrieval and analysis of the required data set.

The data base and DBMS are two elements of the Data Storage and Retrieval System.

Application Data Files Organization

Each of these files contains a specific type of information that is retrieved from the data base and processed by the DBMS for use in a particular application such as river basin simulation, analysis, or planning.

Command Model

This is the link between the application data files and the various river system component models. It determines the order of computation based on the user selected options and transfers the information from one component model to the other.

System Component Models

Each model in this group represents one component process of the river system dynamics, or the simulation of one particular management scheme in the basin.

The number of application data files and their formats, the structure of the command model and of the various system component models are greatly affected by the design criteria of the information system.

In the subsequent sections, basic concepts used in the design of a data storage and retrieval system will be described and the actual implementation of these concepts to the design of the Yazoo Data Storage and Retrieval System for river system analysis will be discussed.

## 10.2 DATA STORAGE

Storage Mode

There are many ways to store historical data including charts, maps, microfilm and microfiche, computer cards, and magnetic recording devices. Because of the large volume of data that is required to describe a river system, a data storage and retrieval methodology is needed that will minimize the effort of creating, accessing, and updating such a large data bank. Table 10-1 gives a comparison of some data storage devices that are available for use. The first approach of providing digitized information for the computer is to record and store data on punched cards. A second approach is the combined use of magnetic tape and permanent files. The third approach is the use of disc-pack storage units. As Table 10-1 indicates, the use of the magnetic tape-permanent file devices is less costly, more reliable, and easier to use than the card storage approach.

Table 10-1. Comparison of cards, magnetic tape--permanent file data storage devices.

| System of Storage | Storage per 2000 card images | Cost per 2000 card images | Reliability | Updating | Retrieval/ Processing |
|---|---|---|---|---|---|
| Cards | Poor:<br>1 box = 160,000 characters | Poor:<br>$3.75 per 2000 cards box, or<br>$375. per 100 boxes<br>Hard to store | Poor:<br>Cards deteriorate with time and use. Possibility of unauthorized, or incorrect changes in data | Poor:<br>Manual updating requires large amounts of man hours possibility of errors | Poor:<br>Time consuming. Manual retrieval of data with no provision for processing |
| Tape | 1 tape = 120 boxes of cards | Tape: $12.00 per tape | Good:<br>Limit access to master tape. More than one tape can be created as a backup | Excellent:<br>System allows for quickly updating data directly | Excellent:<br>Both human and computer time efficient retrieval, with provisions for processing data in a number of ways. Data tape can be quickly searched for necessary data. Small storage space requirement. Approximately five times faster than reading cards |

If large amounts of storage are needed beyond that provided by a magnetic tape-permanent file system, a disc-pack storage device may be the best approach. Table 10-2 lists comparisons and approximate costs of magnetic tape-permanent file devices and disc-pack storage devices. As the table indicates, if a large, heavily-used data base is needed, then the disc-storage device is probably the best approach to data storage. Until that time the magnetic tape-permanent file approach is the best.

Handling and Storage of Magnetic Tape

Since increased quantities of hydrologic data are being stored on magnetic computer tape, the permanence and recoverability of this vital data are important. If data stored on magnetic tape are unrecoverable because of improper procedures or improper storage, the result could range from temporary inconvenience to complete failure of a research program.

The area in which the tape is used should approach, as closely as is practicable, a clean-room environment, which does not have airborne dust and lint. Air-conditioning filtration systems are available for this cleaning.

The work area should be designed to control temperature and humidity. Variations of temperature should remain within ±5° F (21° C) and a relative humidity of about 40 percent are suitable.

Smoking should not be allowed because ashes can contaminate the tape. Food and drink should be prohibited. Minute food particles can be transmitted easily to the tape and tape transports from the operator's hands.

Tape Storage

The hub is the strongest, most stable part of the reel. Reels should be handled by their hubs, and in storage they should be supported by their hubs. Therefore, the reel should be returned to its canister before being stored. The canister also gives protection from dust. For long-term storage, additional protection from dust and moisture can be gained by sealing the canister in a plastic bag.

To store more tape in a given area (reducing storage cost per unit), a plastic ring or collar may be used that wraps around the outer diameter of the reel. This allows the reel to be hung in the storage facility without the use of a standard canister.

Quality of wind is also important. A smooth wind offers built-in edge protection. Tapes in storage should be rewound at specific intervals, such as every 6 to 12 months, to relieve internal pressures. Modern tapes with polyester backings and advanced binders may not require periodic rewinding.

Table 10-2. Magnetic tape permanent file and disc storage comparison.

| | Storage | Cost | Access | Remarks |
|---|---|---|---|---|
| Magnetic tape-Permanent file | 19 million characters per tape | $12 per tape plus mounting | Unlimited when placed on permanent file | Good for data bases with limited users |
| Disc Pack | 1) Single Density 126 million characters | Lease- ~ $8800/year | Unlimited multiaccess unlimited | Best for data bases with many users that require that information be stored on the more accessible discs and not on the less accessible tapes |
| | 2) Double Density 224 million characters | Lease- ~ $10,000 year | Unlimited multiaccess | |
| | | Limited Access ~ $4-$5/hour both single and double density | 1 to 4 hour time blocks per day as contracted | |

Tape Handling

The tape should be protected while being transported. All incoming tape should be allowed to reach environmental equilibrium before being used. Tapes should remain in their canisters until they are placed on the tape drive and should be returned to their canisters immediately after use.

Empty reels should be inspected and cleaned thoroughly before tape is wound on them for storage.

A temperature greater than 130° F (54° C) and a relative humidity above 85 percent may cause layer-to-layer adhesion and some physical distortion.

To prevent fire, store the tape in a noncombustible area and make sure that no combustible materials are stored in the vicinity.

## 10.3 BASIC CONCEPTS OF A COMPUTERIZED DATA BASE SYSTEM

To the technicians of data base systems, a data base is a collection of physical records that are similarily defined and serve a single general application purpose. Examples of physical data bases are files of precipitation data, discharge data, or river stage data.

The next level in data base design is the definition of the logical data base in which cross-references are generated between physical files so that individual data need not be duplicated. An example of such a logical data base is a stage-discharge relationship data base in which the stage-discharge relationship at locations in the river are cross-referenced against the two physical files mentioned above river stage and discharge data bases.

A relatively simple data base management system (DBMS) can handle this type of organization, given appropriate design and support. When, however, additional levels of logical cross-referencing are defined, a pyramid-type structure results that greatly strains data base performance and requires a much more complex DBMS.

Careful structuring of data bases is the key. The following basic guidelines can be used for improving data base performance:

1. smaller files can accommodate a specific data management task better than a complex master file,

2. a large but seldom accessed data segment should be segregated into a separate file to reduce the overall file size and to improve access performance for most processing tasks, and

3. appropriate use of index and linkage can improve searching and sorting operations.

The activities essential for data base design can be listed as follows:

1. appropriate distribution of the data base structure across actual data files,

2. an activity-oriented positioning of data types within the data base structure,

3. specification of interrecord linkage tuned to processing requirements,

4. creation of indices to enhance access to data base records on the basis of given keys,

5. selection of pointer and linkage types, and

6. selection of access methods.

It is significant that each item in this list involves a choice between alternatives. These choices must be based on a careful analysis of the applications for which the structure is intended.

The concept of structure is central not only to understanding the rendering of data on storage media but to many areas of data base thinking in general. A data model aggregates all actual and possible informational inputs and outputs into a comprehensive conceptual representation. All data and, significantly, all their relationships are captured by the data model. A data structure is the rendering of that data model through the Data Description Language (DDL) of a DBMS. A storage structure refers to the configuration of data as they reside in an access method. An access method may be defined as any scheme used within a storage structure to store or retrieve records. Following are some basic access methods.

Physically Serial Access

This is the most rudimentary of access methods since no reference is made to record keys. In physically serial access, records are stored (or retrieved) by virtue of the "next" physical location on the storage media.

Physically serial access characterizes almost all access to magnetic tape (whether or not records happen to be in sequential order) and is often used in conjunction with other access methods on direct storage devices. Physically serial access to an indexed-sequential file, for example, retrieves records in sequential order.

Direct Access

In the direct access method, record keys correspond one-to-one with physical addresses; that is, given a record key, access is predetermined (whether for storage or for retrieval) to a unique storage location.

An important feature of the direct access method is that it obviates the necessity of looking in a table or index prior to record access; the physical location of the record is derived directly from the key itself.

Randomized Access

Randomized access is similar to the direct access method in that storage locations are derived directly from record keys; it is dissimilar in that storage locations are not available on a one-to-one basis with possible key values. Instead, a transformation algorithm of some nature is used to map a large number of potential key values into a smaller number of available storage locations. The randomized method allows a tailoring of the file size to the expected number of records, without significant loss of access speed, because the record location is still derived from the key.

Indexed Access

In the indexed access method, an index consists of key values paired on a one-to-one basis with pointers to the indexed records. Various organizations are possible for the index itself; the most commonly used in DBMS is the indexed-sequential.

In indexed-sequential organization, the indexed file and the index itself are both sequentially ordered on the basis of the same key field, usually called the primary key of the file. Since there is strict correspondence in record order, not all records in the indexed file need actually be represented by an index entry. Instead, indexed file records are often grouped into blocks and the highest key value in the block is then indexed. This arrangement is illustrated in Figure 10-2, which also presents an indexed-random indexing for the same file. In comparing the size of the respective indexes, it is evident that the indexed-sequential index is relatively compact. Furthermore, since both indexes are sequentially ordered, an indexed-sequential organization for the indexes themselves is possible; that is, index records can be grouped into blocks, which can then be indexed. For large files, this arrangement can be repeated a number of times, a scheme that greatly speeds record access.

## 10.4 CODASYL CONCEPTS OF DATA BASE MANAGEMENT

There are many data management techniques and capabilities that are widely common to DBMS. The CODASYL specifications are perhaps the most succinct currently available for implementing large-scale state-of-the-art data bases on existing hardware lines.

A CODASYL data base is described by a schema using facilities of the data description language (DDL). Within a given data base are areas, sets, and records reflecting the organization defined by the schema.

Areas, set types, and record types are named within the schema and are thus known to the DBMS. An area usually corresponds to a file. A record type is a named collection of data items; each record type describes actual occurrences (that is, records) in the data base.

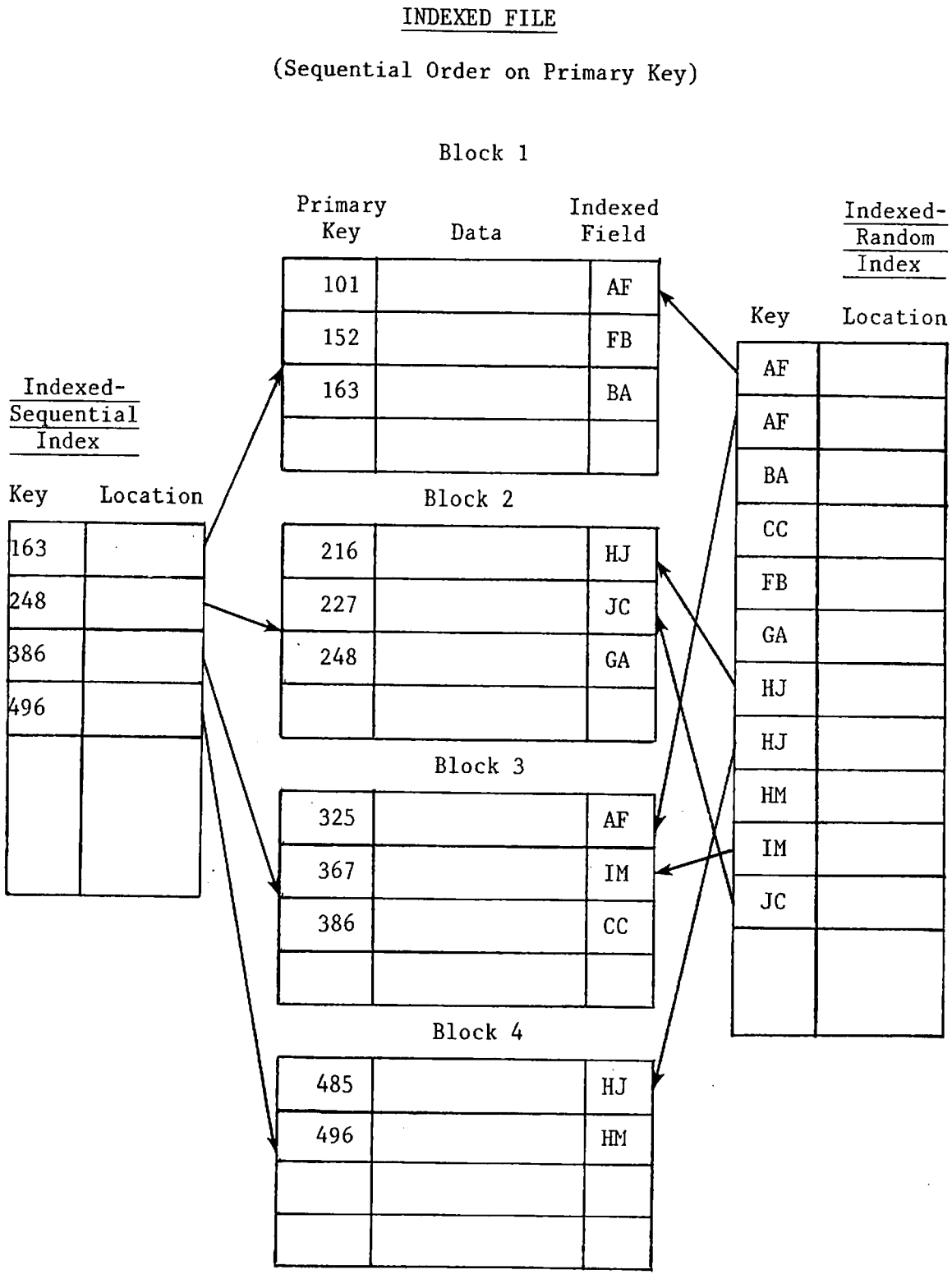


Figure 10-2. An illustration of indexed-sequential and indexed-random organizations.

Records that are related to one another may be collected into sets. A set type is defined to have one record type as owner and one or more record types as members. The same record type can be owner of multiple set types and member of multiple set types, but it cannot be both owner and member of the same set type.

The DDL description is used by a data description language analyzer in order to generate the actual schema that is used in creating and accessing the data base.

The other main component of the data management system is the data manipulation language (DML) which consists of a set of commands which perform the following kinds of functions: 1) opening and closing of the data bases; 2) creation and deletion of record occurrences; 3) setting of currency indicators; 4) addition and removal of record occurrences from sets; and 5) retrieval and storage of data from current record occurrences. Each DML command is a FORTRAN subroutine call. This permits direct user interaction with the data base via programs in the FORTRAN host language. The DML provides the link between the data base and the query language and application programs, thus allowing the planner to interact by means of non-procedural, natural language commands that require no knowledge of the physical or logical data base structure.

The conceptual design of a data base management system based on the above concepts can be summarized by the block diagram in Figure 10-3.

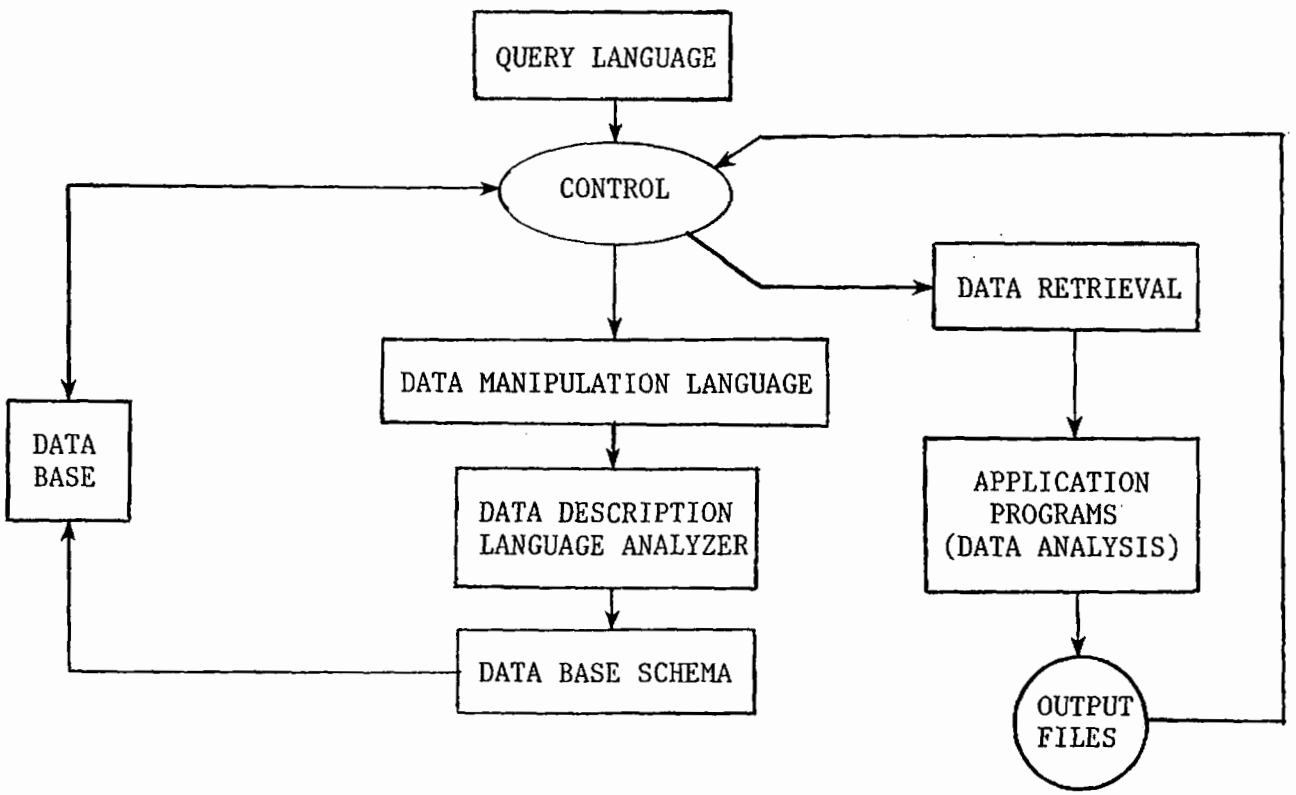


Figure 10-3. Conceptual design of a DBMS.

## 10.5 DATA STORAGE AND RETRIEVAL SYSTEM FOR RIVER BASIN ANALYSIS

The data storage and retrieval system should be capable of storing and managing all information obtained from the data acquisition phase and the data analysis phase. The efficiency of a data storage and retrieval system is important since it affects the availability and the quality of the input data for any level and type of analysis required in the basin. Therefore, the specific data base schema for each data category should be worked out to ease access, retrieval, and updating of data. A data management system should be established along with the data base to assist users in retrieval and reformatting of the data to obtain the desired information for the simulation and analysis of all or any part of the river basin under study. The data management system should be of a modular type and set up in an overlay structure to increase its flexibility in changing component elements and to reduce computer memory requirements.

The primary objective of such a data storage and retrieval system is to support multiple levels and types of analysis. The specific tasks involved in the development of the system are:

1. Identify general data needs for various levels and types of analysis considering water supply, flood control, sediment control, drainage and irrigation requirements, streambank erosion, water quality, reservoir operation, and environmental impacts.

2. Assemble and evaluate all of the available data from various agencies relating to climatology, hydrology, hydraulics, geomorphology, geology, water quality, land use, and such activities of man as hydraulic structures and river engineering works.

3. Standardize the time and space designation of data and develop a unified classification of data categories.

4. Establish the structure of the comprehensive data storage and retrieval system to include all data categories that are needed for multiple levels and various types of analyses.

5. Define a complete node system for location identification of all required data collection stations along the river channel system (including major tributaries and the watersheds).

6. Develop a data analysis package for incorporation into the data management system for extracting the maximum amount of information from the collected data.

## 10.6 A CASE STUDY: THE YAZOO DATA STORAGE AND RETRIEVAL SYSTEM

The following sections outline the application of the data storage and retrieval system for the Yazoo River Basin study conducted by Colorado State University for the Vicksburg District, U.S. Army Corps of

Engineers. Although many of the specific technical details of the data base management system are omitted, the general workings and capabilities of the system are presented and discussed.

## Characteristic Features of the Yazoo River Data Base Management System Structure

The Yazoo data base is set up to reflect the logical structure of the watershed and the river channel system under study. This hierarchical structure is coded by a node system, which is described in the next section, to ease the data indentification and retrieval task. The data base schema for the Yazoo River system is presented in Figure 10-4 which shows various data categories and their corresponding keys.

The data management system is a set of operating computer programs, established along with the data base to assist users in the retrieval and reformatting of the data to obtain the desired information for simulation and analysis of the river basin system. The overall package is of modular type and is set up in overlay (layered). This increases its flexibility in changing component elements and reduces computer memory requirements. The structure of the Yazoo River data management system is presented in Figure 10-5.

## Query Language

To help users who are not familar with computer systems, a simple query language for data retrieval and processing is developed. It consists of four groups of command statements written in ordinary language to guide the operations of the four-layered programs (i.e., GETDATA, PROCESS, OUTPUT, and UPDATE). The command language specifications for the Yazoo River data management system are presented in Simons, Li and Duong (1978).

To ensure an understanding of the use of various command statements for data retrieval and processing, samples of test cases are presented in the last section of this chapter. Each output is headed by a corresponding block of command statements.

## Data Processing Capability

At the present time, the following data processing options are available in the Yazoo data base management system:

1. Retrieve information at a gaging station.

2. Retrieve data at a gaging station by five different alternatives (station number, station name, station coordinates, node + river mile, river name + river mile).

3. Retrieve data for a particular data, year, or water year.

4. Retrieve data for a particuar time period (i.e., from date (x) to (y); from water year (x) to (y)).

5. Print or plot output results on paper or CRT tube.

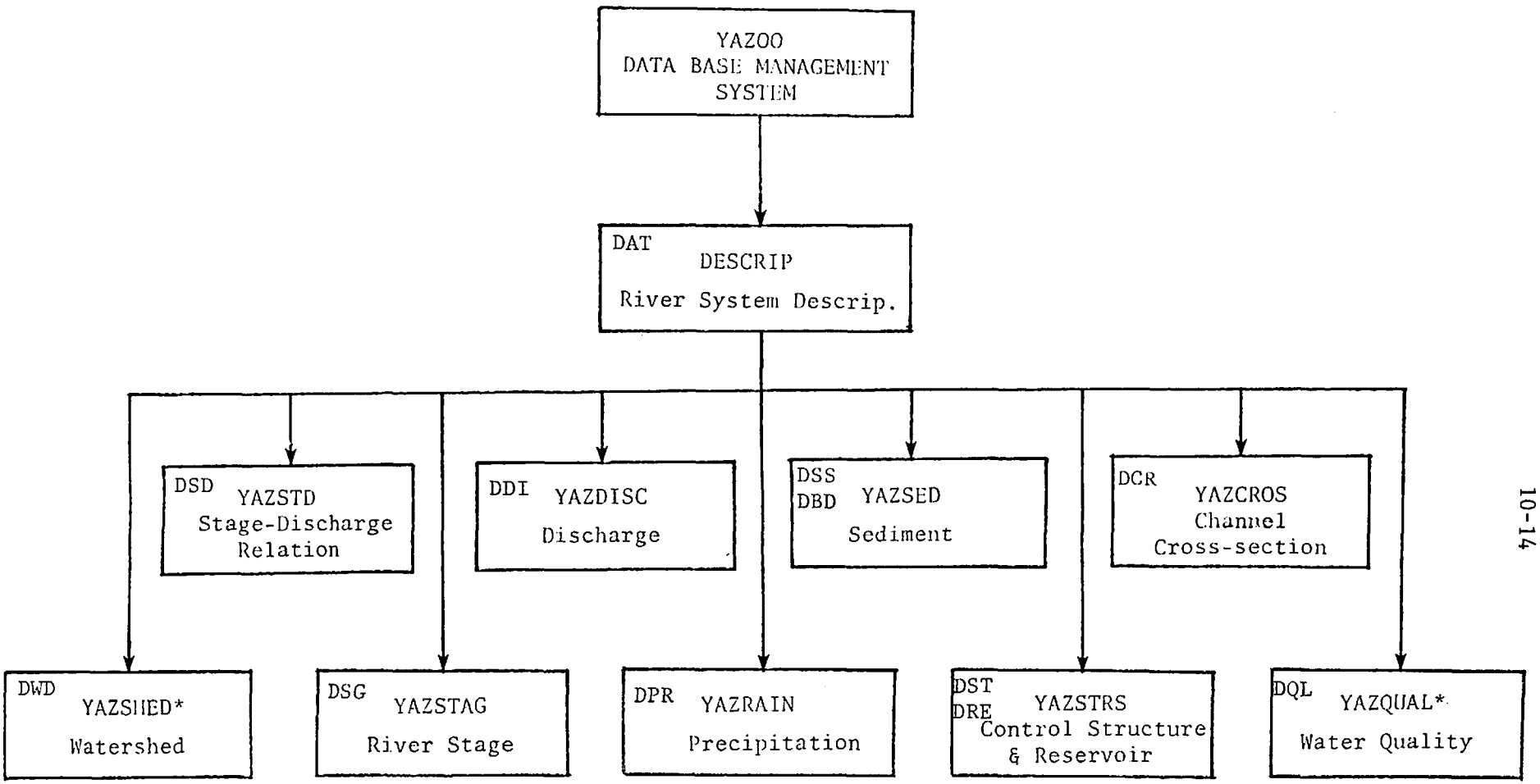


* Not presently in system

Figure 10-4. Structure of the Yazoo data base.

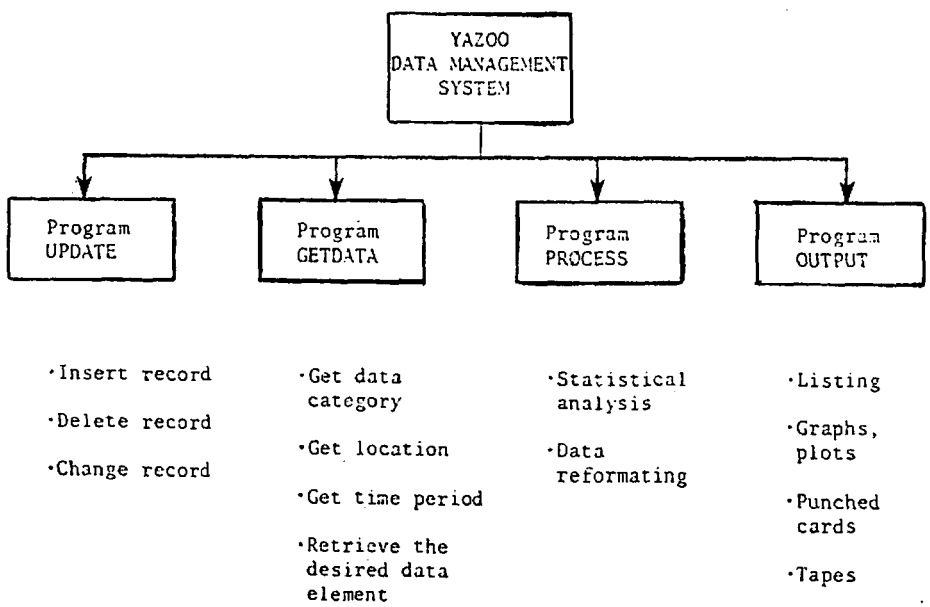


Figure 10-5. Overall structure of the Yazoo data management system.

6. Carry out elementary operations on data analysis, such as:
   a. flood frequency plot for a particular station (x),
   b. flow duration analysis for a particular station (x),
   c. stage-discharge plot for a particular station (x),
   d. cross section overlay plot for a particular station (x),
   e. discharge-hydrograph plot at a station (x),
   f. stage-hydrograph plot at a station (x),
   g. changing river stage with constant discharge,
   h. thalweg level plot for a river or segment of a river,
   i. basic statistical analysis
   j. regression analysis, and
   k. correlation analysis.

Other options for extracting additional useful information from the data can be added to the basic Yazoo data base management system.

The Node-system for Location Identificaton in the Yazoo River Basin

In order to speed access to information at specific stations, a uniform numbering sytem was developed. A group of four pairs of numbers is used to describe a node in the Yazoo River system starting at Vicksburg, node 00000000, and increasing going upstream. From right to left, the first pair indicates successive node numbers in the main stem of the river system; the next pair indicates the first-order tributary from the main stem, starting at the node defined by the pair on the right, and so on. The structure of the node-system for the Yazoo River system is presented in Figure 10-5. Thus, using a node-system, a particular gaging station can be defined by a downstream node and a stream-mile from that node. This makes the retrieval of data of a particular river segment or sub-basin simpler.

Data Categories in the Yazoo River Data Bank

Data stored in the Yazoo River data bank are separated into various categories and reside in various tape files for ease of maintenance and minimization of operating costs. Each data file contains all the gaging station information and the corresponding data elements. In the present version of the Yazoo River data bank, portions of the following data categories have been processed and put in storage for selected locations:

a. stage-discharge data,
b. daily discharge data,
c. suspended sediment data,
d. bed material data,
e. river cross-section information,
f. river control structure characteristics,
g. reservoir characteristics,
h. stage readings, and
i. meteorological information.

Watershed data will also be included in the Yazoo River data bank as soon as the data preparation and verification is completed.

Examples of the Utilization of the YAZOODB

This section contains some examples of data retrieval and analysis related to the needs of field personnel, engineers, and planners when dealing with large, complex river basin systems.

1. When designing a hydraulic structure, one of the first pieces of information needed is a flood frequency analysis. Figures 10-6a,b provide an example of flood frequency analysis carried out on the historical data of the Upper Yazoo River (Tallahatchie River) near Swan Lake, Mississippi, using three different analysis options.

2. The determination of the stage for a design discharge at a cross section is usually necessary for determining flood hazard and for hydaulic structure design. Figures 10-7a,b show the stage-discharge curves of the Yazoo River at Belzoni for 1973, using two different output options.

3. The trend for changing stage-discharge relations over time usually provides valuable information about the dynamics of a river at a particular location. Figure 10-8 is an overlay plot of stage-discharge curves of the Yazoo River at Belzoni for three consecutive years: 1973, 1974, and 1975.

4. Regression analysis is a simple, but very useful, technique used to derive the relationship between two sets of data. The computed analytical expression could then be used for short-term record extension. Figure 10-9 shows the derivation of the power function for stage-discharge data for the Tallahatchie River near Swan Lake for several years.

5. The change in river stage over time for some given discharge Q at one particular station could give some information concerning channel cross section geometry and the aggradation or degradation at a location. Figure 10-10a shows a plot of changing stage over time for Q of 5000 cfs for the Tallahatchie River near Swan Lake for several years. Figure 10-10b lists the corresponding values of the river stage for each year for Q of 5000 cfs for the same station.

6. In order to check the dynamics of aggradation or degradation it is always useful to plot the change in cross-sectional shape over time. Figure 10-11 is an overlay plot of cross-sectional data of the Yazoo River at river mile 82.90, upstream from Vicksburg, Mississippi.

7. Discharge data are needed to calibrate river system models which are used for the study of future behavior of the system. Thus, stage and discharge hydrographs are desired pieces of information for engineers and planners. In Figure 10-12 plots of hydrographs for the Tallahatchie River near Lambert for the calender years 1972, 1973 and 1974 are presented.

8. Examples similar to (7) above with outputs in a tabular format which are suitable for periodic reporting purposes during calender year 1973 and water year 1973 near Lambert and Swan Lake are presented in Figures 10-13 and 10-14, respectively.

9. Basic statistics are needed to understand the extreme events or for use in forecasting purposes. Thus, a way to get this information directly from historical data which are stored in the data bank is desirable. Figure 10-15 shows some typical outputs for basic statistical analysis.

10. Rainfall data are needed for water resources planning and for operation of watershed simulation models for basin system analysis. An example of the retrieval and a listing of daily rainfall data at Byhalia for calender year 1973 is shown in Figure 10-16. The results processing the retrieved data set to obtain cumulative rainfall is given by a plot in Figure 10-17.

11. Thalweg level plots can give engineers and planners some useful information on the variation of bed slope of a river or a segment of a river. This final example shows a plot of Thalweg level for a segment of the Yazoo River (from river mile 3. to river mile 100.) in August 1962 (Figure 10-18).

EXAMPLE 1a :

Input :

```
I>GET,DISCHARGE DATA
I>LOCATION,STATION LOCATED NR SWAN LAKE
I>TIME,ALL
I>PROCESS,PLOT,CUM FREQUENCY
```

Output :

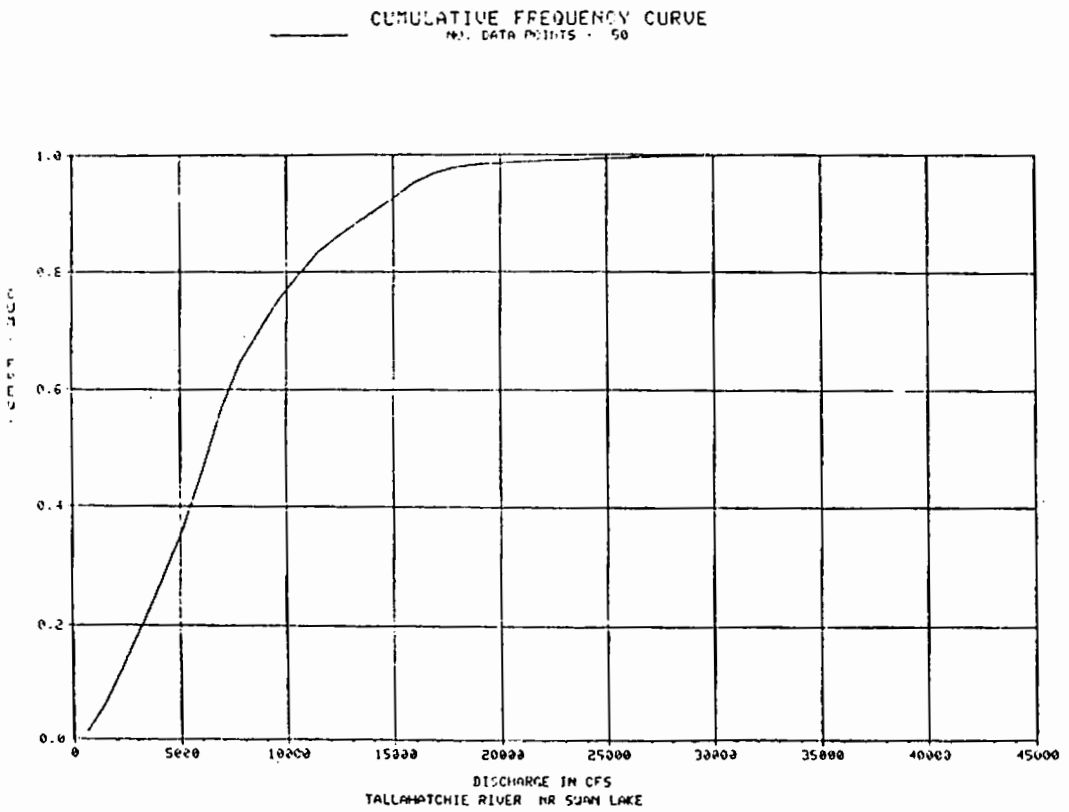


Figure 10-6a. All discharge data for cumulative frequency analysis for a gaging station.

EXAMPLE 1b:

Input:

```
I>GET,DISCHARGE DATA
I>LOCATION,STATION NUMBER 132D
I>TIME,ALL
I>PROCESS,PLOT,HISTOGRAM
```

Output:

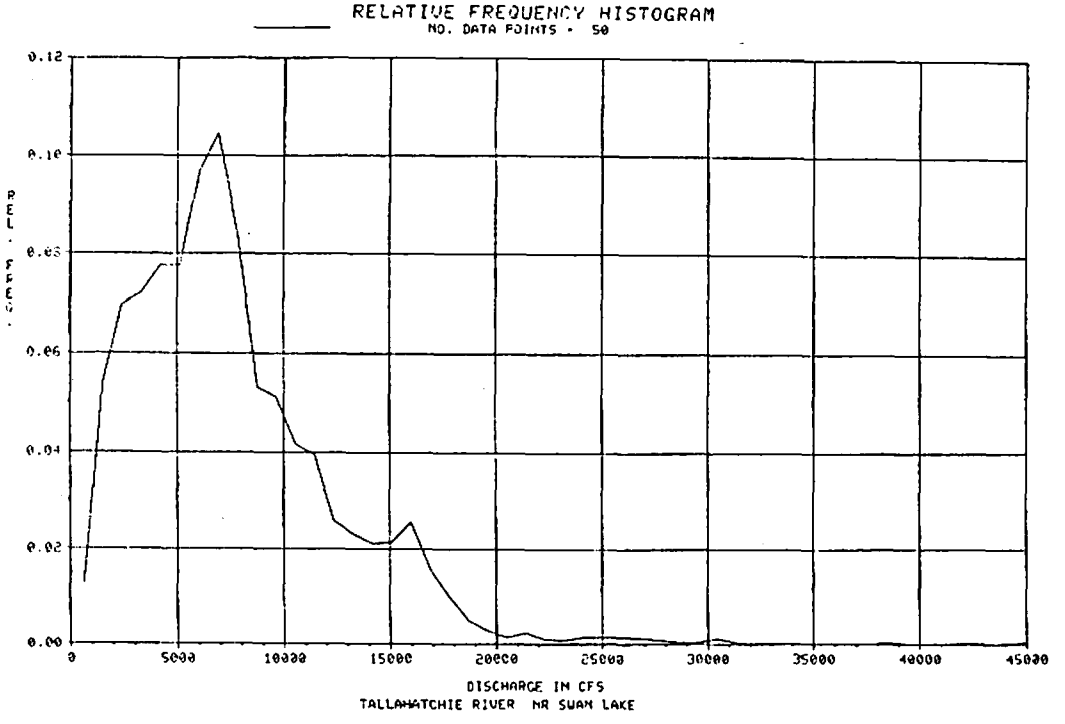


Figure 10-6b. All discharge data for a relative frequency histogram for a gaging station.

EXAMPLE 1c:

Input:

```
I>GET,DISCHARGE DATA
I>LOCATION,STATION ON TALLAHATCHIE RIVER
 AT I>219.10
I>TIME,ALL
I>PROCESS,LIST,FREQUENCY ANALYSIS
```

Output:

TABLE OF THE COMPUTED RELATIVE FREQUENCIES (PDF), AND THE CUMULATIVE FREQUENCIES (CDF)

TALLAHATCHIE RIVER NR SUAM LAKE

| NO. | RANGE | | MID-RANGE | OBS. FREQ. | CDF | PDF |
|---|---|---|---|---|---|---|
| 1 | ( 160.09 | 1063.52 ) | 612.80 | 65. | .01271 | .01271 |
| 2 | ( 1063.52 | 1967.76 ) | 1515.64 | 276. | .06669 | .05398 |
| 3 | ( 1967.76 | 2871.99 ) | 2419.87 | 356. | .13632 | .06963 |
| 4 | ( 2871.99 | 3775.43 ) | 3323.51 | 369. | .20849 | .07217 |
| 5 | ( 3775.43 | 4679.27 ) | 4227.35 | 397. | .28613 | .07765 |
| 6 | ( 4679.27 | 5583.10 ) | 5131.18 | 397. | .36378 | .07765 |
| 7 | ( 5583.10 | 6486.94 ) | 6035.02 | 495. | .46059 | .09681 |
| 8 | ( 6486.94 | 7390.78 ) | 6938.86 | 535. | .56523 | .10464 |
| ... | | | | | | |
| 45 | ( 39923.90 | 40832.73 ) | 40380.82 | 0. | .99941 | 0.00000 |
| 46 | ( 40832.73 | 41736.57 ) | 41284.65 | 0. | .99941 | 0.00000 |
| 47 | ( 41736.57 | 42640.41 ) | 42188.49 | 1. | .99961 | .00020 |
| 48 | ( 42640.41 | 43544.24 ) | 43092.33 | 0. | .99961 | 0.00000 |
| 49 | ( 43544.24 | 44448.08 ) | 43996.16 | 0. | .99961 | 0.00000 |
| 50 | ( 44448.08 | 45351.92 ) | 44900.00 | 2. | 1.00000 | .00039 |

EXAMPLE 2a :

```
I>GET*STAGE-DISCHARGE*DATA
I>LOCATION*STATION COORDINATES 33 10 02 90 29 35
I>TIME*YEAR 1973
I>PLOT


 DO YOU WISH THE RESULTS TO BE DISPLAYED ON THE TEKTRONIX SCREEN
I>NO


 DO YOU WISH THE RESULTS TO BE DISPLAYED BY A LINE PRINTER
I>YES
```

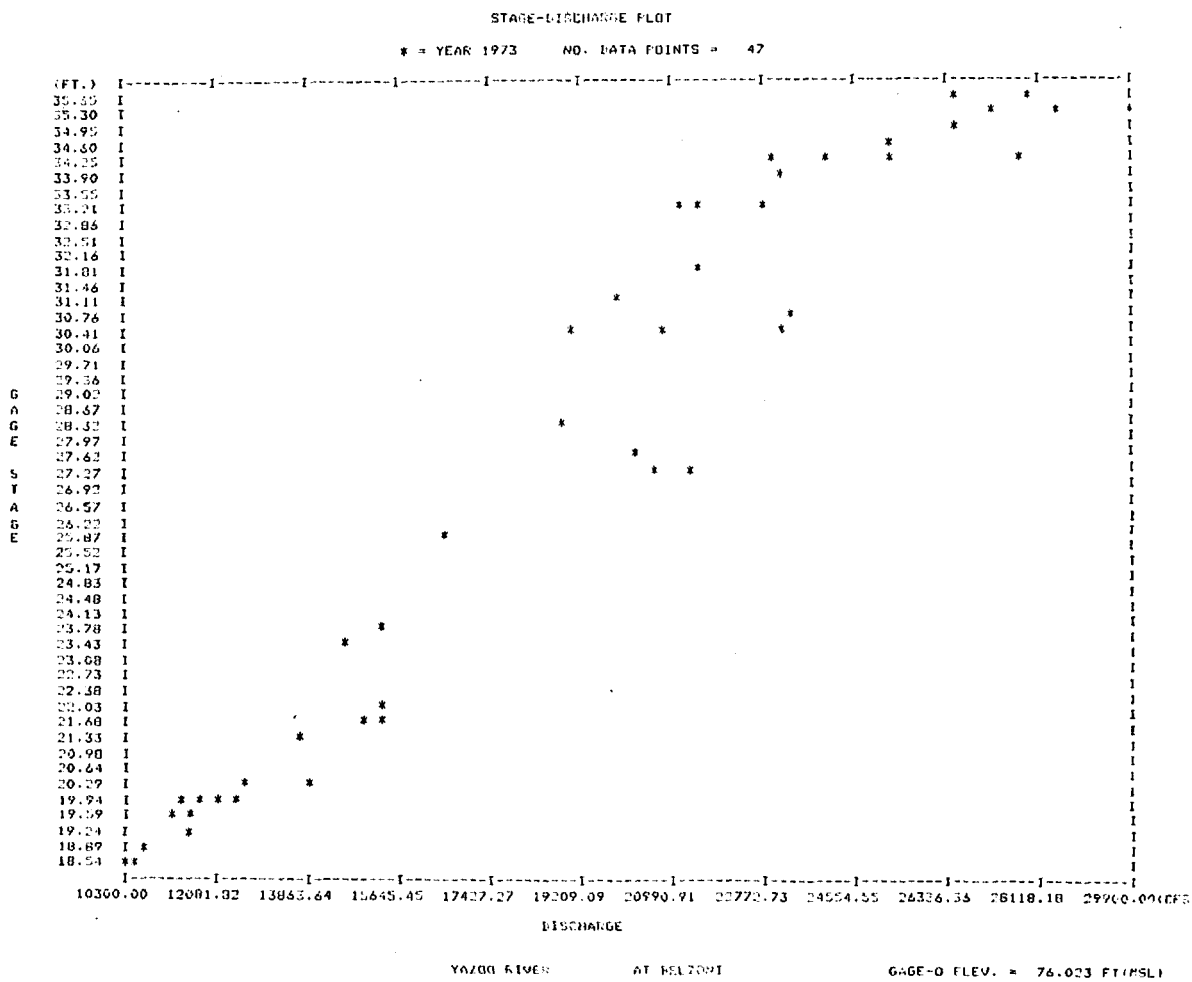


Figure 10-7a. Stage-discharge data plot for Belzoni by specifying its coordinates--33 10 02, 90 29 35--for 1973.

EXAMPLE 2b :

Input:

```
I>GET,STAGE-DISCHARGE DATA
I>LOCATION,STATION NUMBER 353
I>TIME,YEAR 1973
I>PLOT
```

Output:

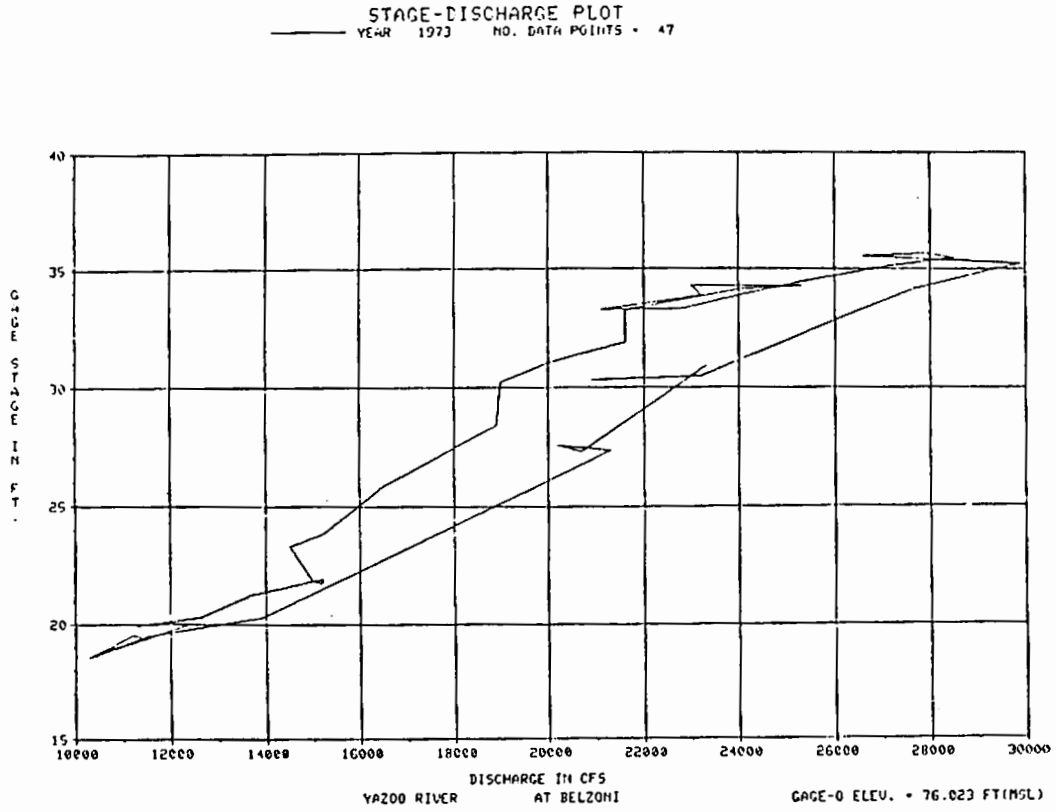


Figure 10-7b. Stage-discharge plot for a gaging station for a specified year.

EXAMPLE 3 :

Input:

```
I>GET,STAGE-DISCHARGE DATA
I>LOCATION,STATION COORDINATES 33 10 12,90 29 35
I>TIME,FROM YEAR 1973 TO 1975
I>PLOT
```

Output:

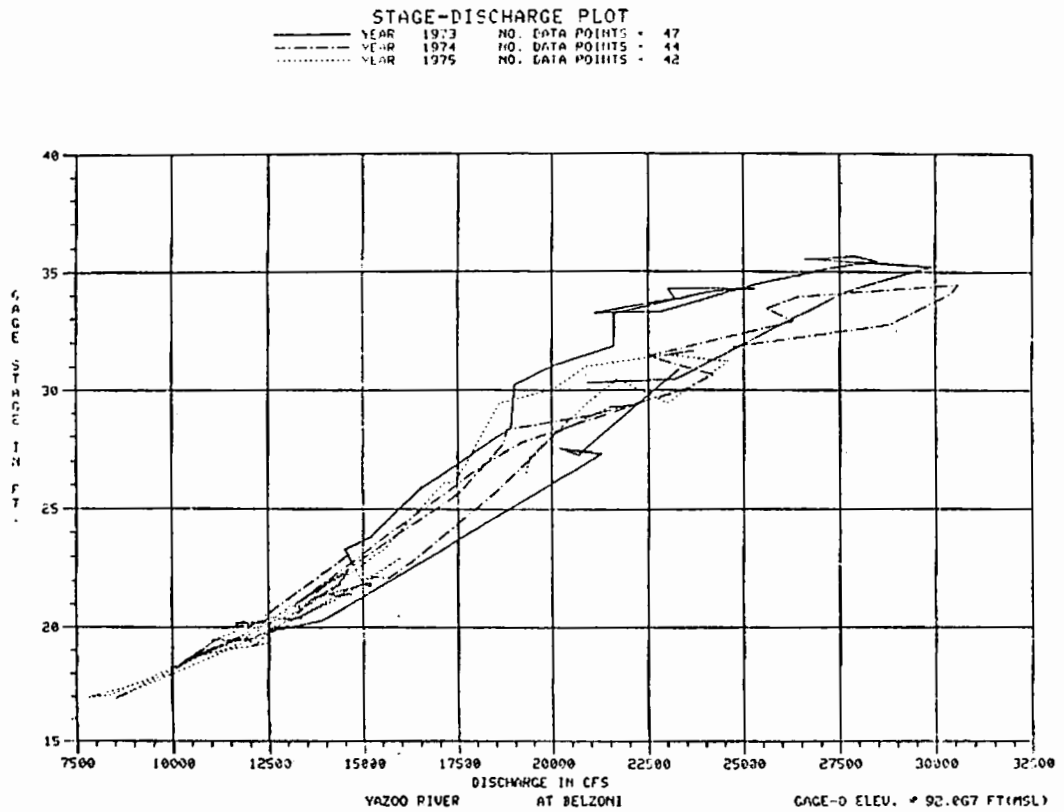


Figure 10-8. Stage-discharge plot for a gaging station for less than five years.

EXAMPLE 4 :

Input:

```
I>GET,STAGE-DISCHARGE DATA
I>LOCATION,STATION ON TALLAHATCHIE RIVER
 AT I>219.10
I>TIME,FROM YEAR 1970 TO 1976
I>PROCESS,LIST,REGRESSION ANALYSIS
```

Output:

```
                              YEAR = 1970
              REGRESSION EQUATION IS     Q =  31.36002((S).EXP( 1.8792))
CORRELATION COEFFICIENT =   .6913              STANDARD ERROR =   .314338

                              YEAR = 1971
              REGRESSION EQUATION IS     Q =  56.53675((S).EXP( 1.6504))
CORRELATION COEFFICIENT =   .9932              STANDARD ERROR =   .059618

                              YEAR = 1975
              REGRESSION EQUATION IS     Q =  33.21625((S).EXP( 1.8783))
CORRELATION COEFFICIENT =   .9848              STANDARD ERROR =   .068387

                              YEAR = 1976
              REGRESSION EQUATION IS     Q =  53.21398((S).EXP( 1.6994))
CORRELATION COEFFICIENT =   .9909              STANDARD ERROR =   .062539
```

Figure 10-9. Stage-discharge regression analysis for a gaging station for each year.

EXAMPLE 5a :

Input :

```
I>GET,STAGE-DISCHARGE DATA
I>LOCATION,STATION LOCATED NR SWAN LAKE
I>TIME,ALL
I>PROCESS,PLOT,CHANGING STAGE FOR Q=5000.
```

Output :

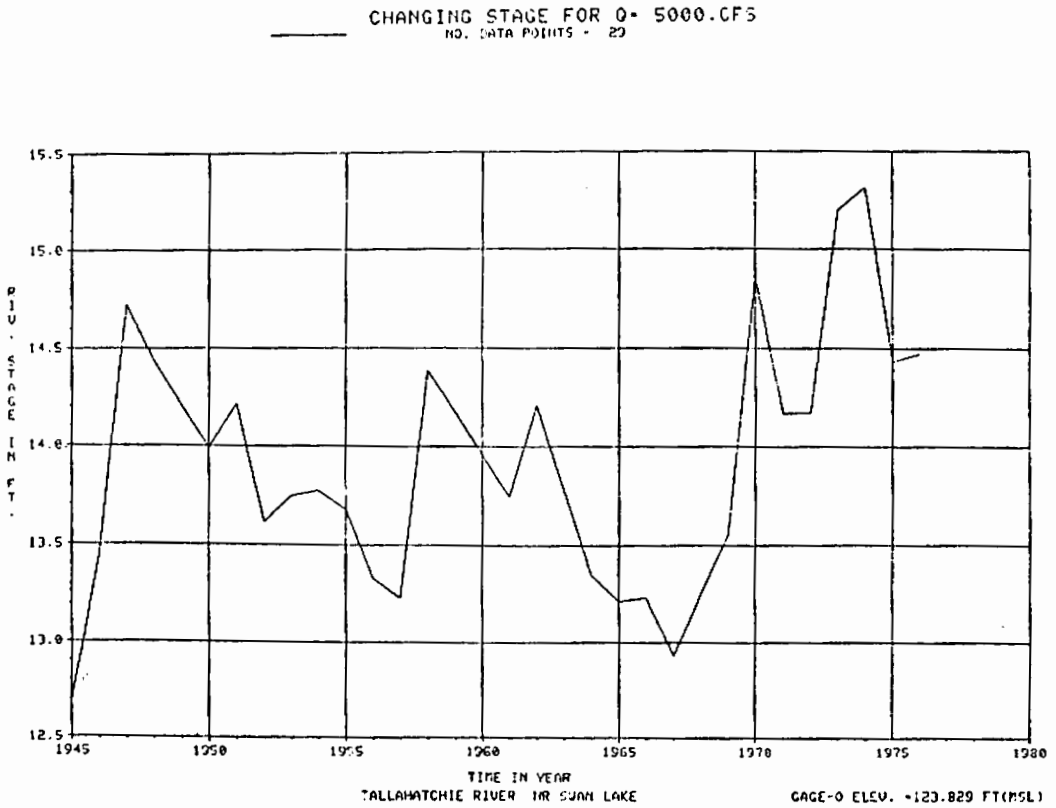


Figure 10-10a. Stage-discharge plot for a gaging station showing variation of river stage (in ft) for a given discharge (in cfs).

EXAMPLE 5b :

Input:

```
I>GET,STAGE-DISCHARGE DATA
I>LOCATION,STATION NUMBER 1320
I>TIME,ALL
I>PROCESS,LIST,CHANGING STAGE FOR Q=5000.
```

Output:

```
CHANGING RIVER STAGE FOR Q =   5000. CFS
  TALLAHATCHIE RIVER  NR SUMM LAKE
  (GAGE-0 ELEV. = 123.829 FT(MSL))

    YEAR          RIVER-STAGE IN FT

    1945              12.79
    1946              13.45
    1947              14.12
    1948              14.44
    1949              14.63
    1950              13.99
    1951              14.21
    1952              13.61
    1953              13.75
    1954              13.77
    1955              13.67
    1956              13.33
    1957              13.23
```

Figure 10-10b. Stage-discharge listing for a gaging station showing variation of river stage (in ft) for a given discharge (in cfs).

EXAMPLE 6 :

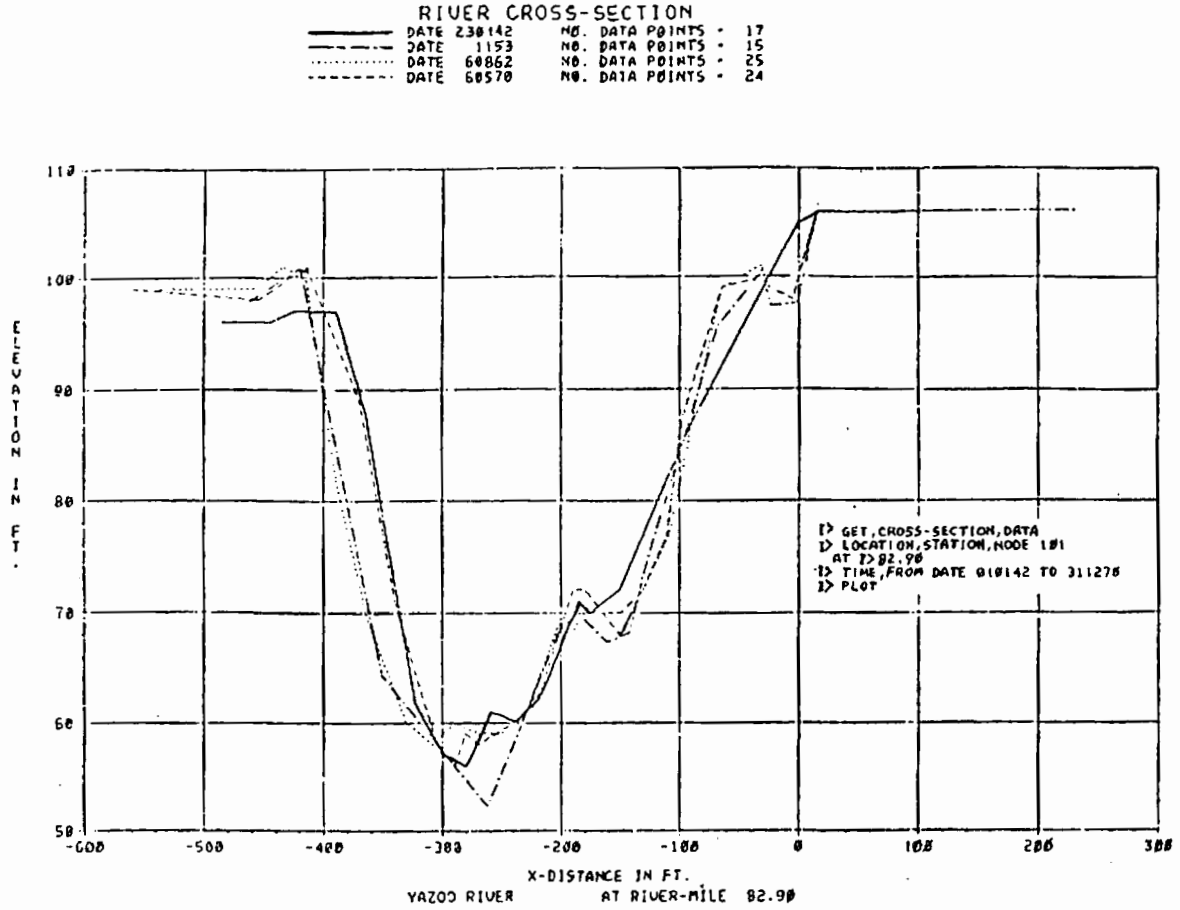


Figure 10-11. Plot of channel cross section of the Yazoo River at RM 82.90 for different dates.

EXAMPLE 7 :

Input :

```
I>GET,DISCHARGE DATA
I>LOCATION,STATION COORDINATES 34 10 50,90 12 55
I>TIME-FROM YEAR 1972 TO 1974
I>PLOT
```

Output :

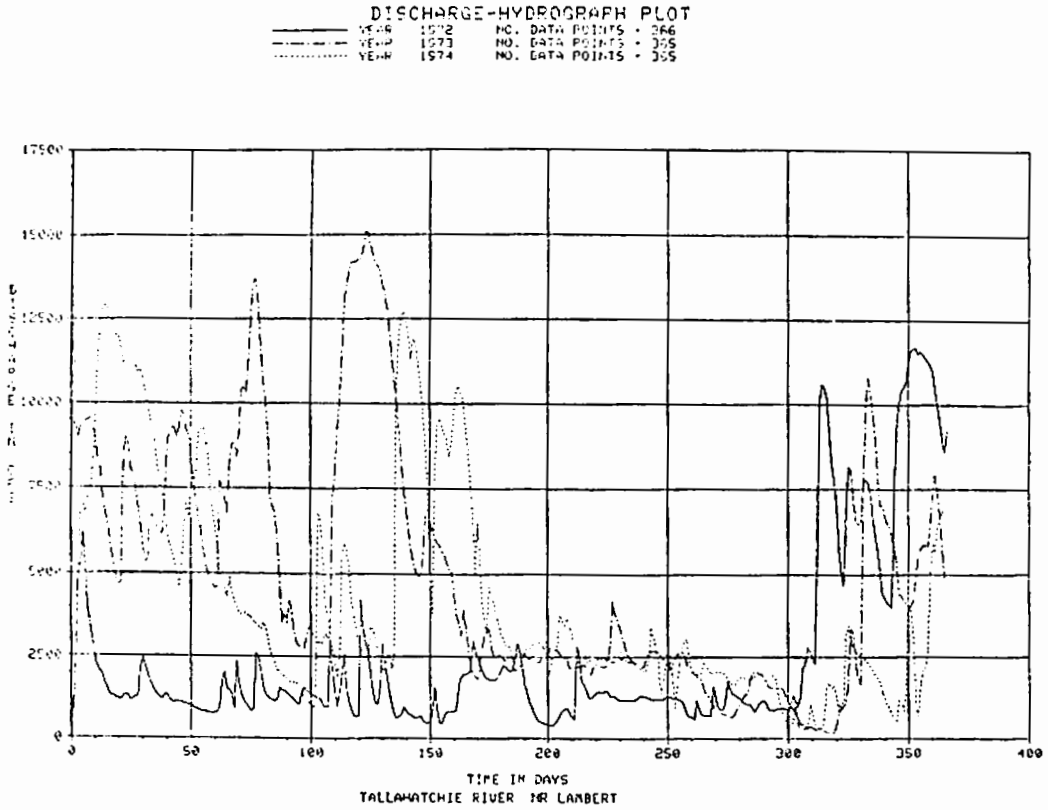


Figure 10-12. Discharge plot for a gaging station for a specified time.

EXAMPLE 8a:

Input:

```
I>GET,DISCHARGE,ALL INFORMATION
I>LOCATION,STATION LOCATED NR LAMBERT
I>TIME,YEAR 1973
I>DISPLAY
```

Output:

YAZOO RIVER SYSTEM DATA BANK

RIVER DISCHARGE DATA CATEGORY

| STATION NAME | STATN NO | DIST FR MOUTH | LATITUDE | LONGITUDE | GAGE ZERO(MSL) | DATA TYPE | NO YEARS |
|---|---|---|---|---|---|---|---|
| TALLAHATCHIE RIVER NR LAMBERT | 1328 | 253.20(MI) | 34 10 50 | 90 12 55 | 123.829(FT) | CONTI | 14 |

DAILY DISCHARGE FOR 1973

COMPUTED DAILY DISCHARGE IN CUBIC FEET PER SECOND

| DAY | JAN | FEB | MAR | APR | MAY | JUN | JUL | AUG | SEP | OCT | NOV | DEC |
|---|---|---|---|---|---|---|---|---|---|---|---|---|
| 1 | 9420. | 5380. | 4550. | 4220. | 14300. | 6050. | 2350. | 2200. | 2660. | 747. | 445. | 9760. |
| 2 | 9290. | 6580. | 4550. | 3530. | 14600. | 5890. | 2450. | 2250. | 2660. | 724. | 413. | 9020. |
| 3 | 8970. | 6700. | 7720. | 3250. | 15100. | 5810. | 2430. | 2230. | 2650. | 683. | 389. | 7930. |
| 4 | 9350. | 6500. | 7550. | 2910. | 15000. | 5620. | 2420. | 2210. | 2530. | 646. | 362. | 6970. |
| 5 | 9250. | 6330. | 7230. | 2830. | 14700. | 5540. | 2490. | 2120. | 2400. | 800. | 380. | 7030. |
| 26 | 7950. | 4950. | 6760. | 14000. | 4980. | 2530. | 2480. | 2240. | 1020. | 1250. | 1670. | 7370. |
| 27 | 7530. | 4760. | 6010. | 14200. | 5320. | 2480. | 2400. | 2190. | 878. | 1130. | 7070. | 7930. |
| 28 | 7020. | 4680. | 4740. | 14200. | 6710. | 2550. | 2150. | 2170. | 826. | 1030. | 9710. | 7250. |
| 29 | 6480. | 0. | 3500. | 14200. | 6700. | 2500. | 2160. | 2410. | 734. | 917. | 10400. | 6660. |
| 30 | 5870. | 0. | 3820. | 14300. | 6500. | 2410. | 2160. | 2550. | 700. | 788. | 10400. | 5720. |
| 31 | 5280. | 0. | 3500. | 0. | 6130. | 0. | 2170. | 2660. | 0. | 624. | 0. | 4910. |

MONTHLY STATISTICS

| | | | | | | | | | | | | |
|---|---|---|---|---|---|---|---|---|---|---|---|---|
| MEAN | 7620. | 7324. | 8432. | 6639. | 10010. | 3567. | 2476. | 2543. | 1972. | 1337. | 2038. | 6025. |
| MAX. | 9560. | 9810. | 13720. | 14320. | 15100. | 6050. | 2860. | 4200. | 2660. | 2050. | 10600. | 9760. |
| MIN. | 4630. | 4680. | 3500. | 2700. | 4900. | 1810. | 2150. | 1960. | 768. | 624. | 188. | 4040. |

TOTAL DISCHARGE FOR YEAR WAS 1823331. MEAN DISCHARGE FOR YEAR WAS 4995.4

HIGHEST DISCHARGE VALUE WAS 15100.CFS, OCCURRED ON MAY 3
LOWEST DISCHARGE VALUE WAS 188.CFS, OCCURRED ON NOV 14

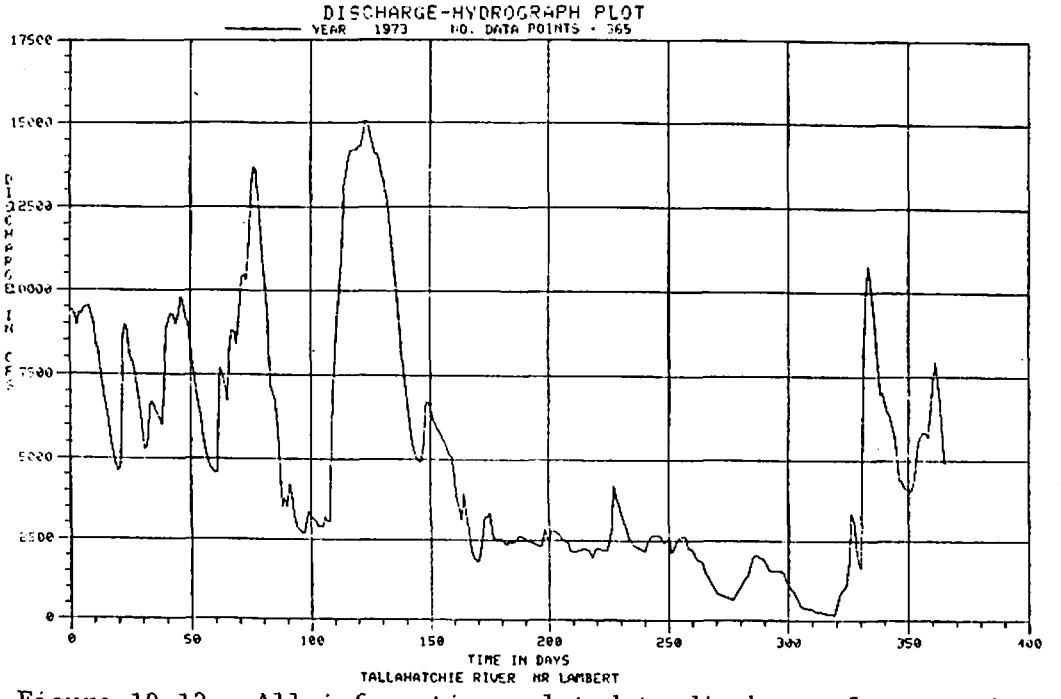


Figure 10-13. All information related to discharge for a gaging station for a specified year.

EXAMPLE 8b:

Input:

```
I>GET,DISCHARGE,ALL INFORMATION
I>LOCATION,STATION NUMBER 1320
I>TIME,WATER YEAR 1973
I>DISPLAY
```

Output:

YAZOO RIVER SYSTEM DATA BANK

RIVER DISCHARGE DATA CATEGORY

| STATION NAME | STATN NO | DIST FR MODE | LATITUDE | LONGITUDE | GAGE ZERO(MSL) | DATA TYPE | NO YEARS |
|---|---|---|---|---|---|---|---|
| TALLAHATCHIE RIVER NR SUAN LAKE | 1320 | 219.10(MI) | 33 51 35 | 90 16 35 | 113.384(FT) | CONTI | 14 |

DAILY DISCHARGE FOR WATER YEAR 1973

COMPUTED DAILY DISCHARGE IN CUBIC FEET PER SECOND

| DAY | OCT | NOV | DEC | JAN | FEB | MAR | APR | MAY | JUN | JUL | AUG | SEP |
|---|---|---|---|---|---|---|---|---|---|---|---|---|
| 1 | 6550. | 5880. | 19600. | 16100. | 22600. | 17400. | 10600. | 9300. | 15400. | 11300. | 9150. | 10600. |
| 2 | 7840. | 5560. | 19700. | 15700. | 21800. | 17100. | 10400. | 8970. | 15200. | 11230. | 8860. | 10500. |
| 3 | 6730. | 5420. | 18200. | 15800. | 21500. | 16800. | 10200. | 8700. | 15400. | 11000. | 8800. | 9400. |
| 4 | 6550. | 5400. | 17600. | 16100. | 21200. | 16600. | 9900. | 8440. | 15300. | 10900. | 8300. | 7250. |
| 5 | 6230. | 6170. | 17000. | 16100. | 20200. | 16300. | 9630. | 8660. | 15100. | 10880. | 8910. | 6710. |
| 26 | 6840. | 9380. | 15720. | 25900. | 18400. | 12600. | 11700. | 21100. | 12500. | 11320. | 10200. | 9490. |
| 27 | 6430. | 12140. | 16500. | 26200. | 17800. | 12200. | 11700. | 18700. | 12100. | 11600. | 10200. | 9490. |
| 28 | 6250. | 15200. | 17200. | 26700. | 17600. | 11800. | 10800. | 17600. | 11800. | 11300. | 10130. | 9440. |
| 29 | 6182. | 17000. | 17600. | 26720. | 0. | 11520. | 10300. | 16500. | 11600. | 10930. | 10100. | 9420. |
| 30 | 6480. | 18800. | 17600. | 25400. | 0. | 11200. | 9770. | 15400. | 11403. | 10300. | 10200. | 9400. |
| 31 | 6060. | 0. | 16800. | 23800. | 0. | 10900. | 0. | 14500. | 0. | 9640. | 10520. | 0. |

MONTHLY STATISTICS

| | OCT | NOV | DEC | JAN | FEB | MAR | APR | MAY | JUN | JUL | AUG | SEP |
|---|---|---|---|---|---|---|---|---|---|---|---|---|
| MEAN | 22833. | 12308. | 14501. | 10986. | 13872. | 17022. | 10804. | 9928. | 8738. | 7311. | 8483. | 11900. |
| MAX. | 28200. | 22600. | 17400. | 13100. | 21130. | 23500. | 11600. | 10500. | 10600. | 2050. | 10820. | 9760. |
| MIN. | 15700. | 15820. | 10500. | 8100. | 7710. | 11400. | 9640. | 8800. | 4720. | 624. | 188. | 19700. |

TOTAL DISCHARGE FOR YEAR WAS 4739890. MEAN DISCHARGE FOR YEAR WAS 12986.0

HIGHEST DISCHARGE VALUE WAS 28200.CFS, OCCURRED ON JAN 14
LOWEST DISCHARGE VALUE WAS 4720.CFS, OCCURRED ON SEP 10

DISCHARGE-HYDROGRAPH PLOT

YEAR 1973 NO. DATA POINTS = 365

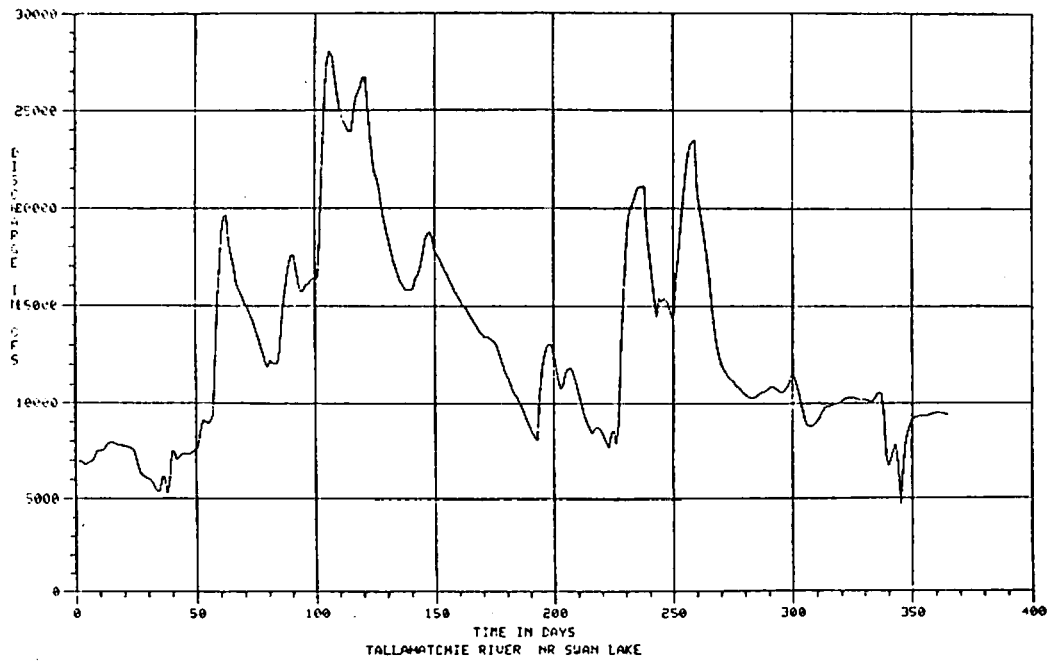


Figure 10-14. All information related to discharge for a gaging station for a specified water year.

EXAMPLE 9a :

Input:

```
I>GET,DISCHARGE DATA -
I>LOCATION,STATION NUMBER 123
I>TIME,DATE 191273
I>LIST
```

Output:

```
THE RIVER DISCHARGE FOR THAT DATE =  12726.CFS
```

EXAMPLE 9b :

Input:

```
I>GET,DISCHARGE DATA
I>LOCATION,STATION LOCATED AT GREENWOOD
I>TIME,FROM DATE 100473 TO 100573
I>PROCESS,LIST,MIN VALUE
```

Output:

```
THE MINIMUM VALUE IS   23100.00  WHICH OCCURRED ON APR 23,1973
```

EXAMPLE 9c :

Input:

```
I>GET,DISCHARGE DATA
I>LOCATION,STATION ON YAZOO RIVER
 AT I>166.00
I>TIME,FROM DATE 100473 TO 100573
I>PROCESS,LIST,MAX VALUE
```

Output:

```
THE MAXIMUM VALUE IS   31700.00  WHICH OCCURRED ON MAY 10,1973
```

Figure 10-15. Minimum value of discharge data for a gaging station for a specified time.

EXAMPLE 10a :

Input :

```
I>GET,PRECIPITATION DATA,DAILY
I>LOCATION,STATION NUMBER 1262
I>TIME,YEAR 1973
I>PLOT
```

Output :

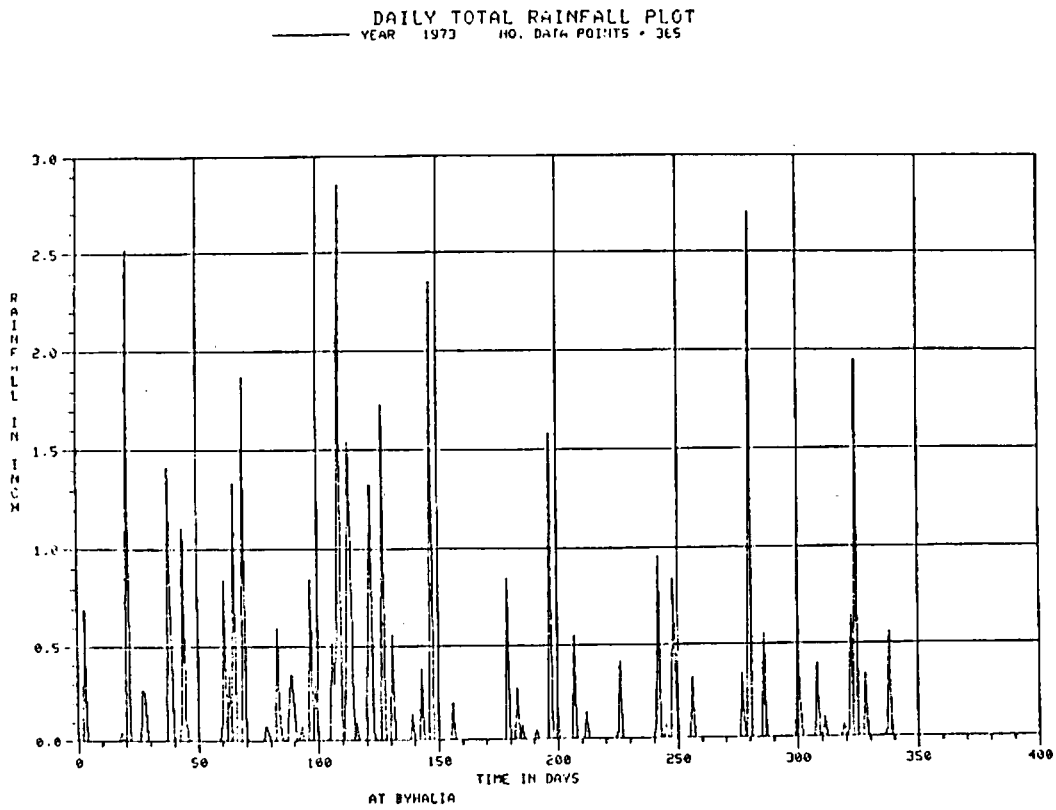


Figure 10-16. Daily precipitation plot for a gaging station for a specified year.

EXAMPLE 10b :

Input :

```
I>GET,PRECIPITATION DATA,DAILY
I>LOCATION,STATION NUMBER 1262
I>TIME,YEAR 1973
I>PROCESS,PLOT,CUM RAINFALL
```

Output :

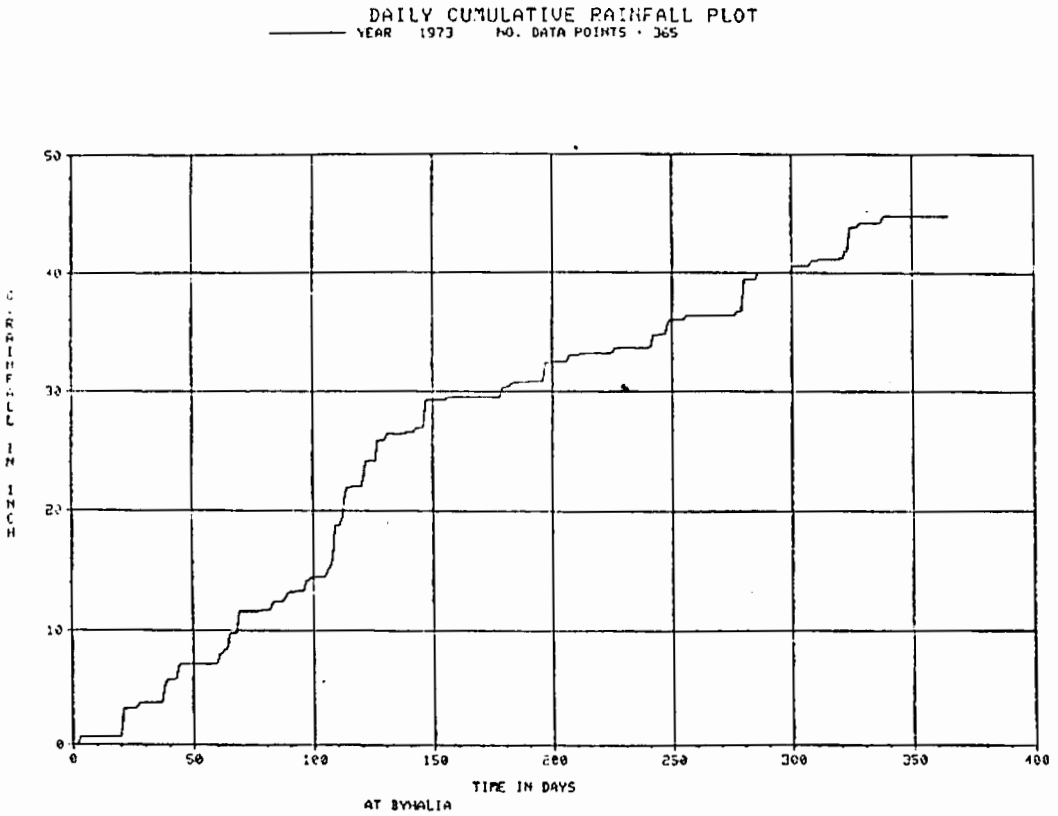


Figure 10-17. Daily precipitation and cumulative plot for a gaging station for a specified year.

EXAMPLE 11:

Input:

```
I>GET,CROSS-SECTION DATA
I>LOCATION,RIVER,YAZOO RIVER
I>TIME,DATE 999999
I>PROCESS,PLOT,THALWEG LEVEL
```

Output:

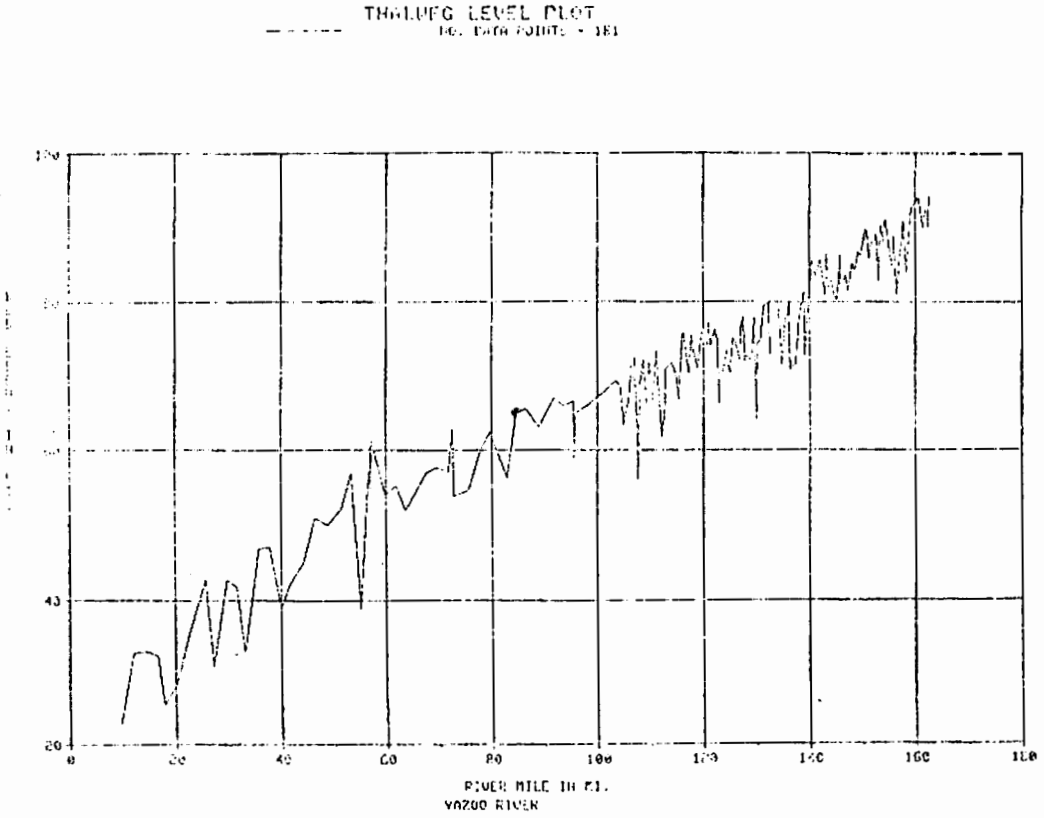


Figure 10-18. Cross section plot of the thalweg level for a river for a specified time.

## REFERENCES

Simons, D. B., Li, R. M., Brown, G. O., Chen, Y. H., Ward, T. J., Duong, N., and Ponce, V. M., 1978, Sedimentation Study of the Yazoo River Basin--Phase I General Report, reported prepared for U.S. Army Corp of Engineers, Vicksburg District, Vicksburg, Mississippi, June.

# Chapter 11

# WATER AND SEDIMENT ROUTING

## 11.1 INTRODUCTION

Decades ago behavior of water and sediment in alluvial channels was studied only in a qualitative manner or by highly simplified, statistical methods. With improved knowledge of the movement of water and sediment combined with the availability of high-speed digital computers, mathematical modeling of rivers has attracted increasing attention. Mathematical modeling of rivers usually involves a numerical technique to solve the differential equations for movement of water and sediment through a river reach. With proper calibration and adjustment of the model, one can eliminate many of the uncertainties involved and develop valuable information on present and future river conditions.

Flood routing is defined as the process of tracing by calculation the movement of a flood wave. In general, the problem consists of applying the principles of gradually varied unsteady open channel flow.

Two physical characteristics that are useful in describing flood waves are the rate of travel (flood wave celerity) and the rate of subsidence (flood wave attenuation). Attenuation of a flood wave can be accomplished by either longitudinal or lateral storage. Attenuation due to lateral storage is exemplified by the subsidence of a flood wave as it passes through a lake or reservoir. In the absence of lateral storage, such as the case of a flood wave moving through a prismatic channel of constant cross section, the wave attenuation is caused by longitudinal storage. The amount of longitudinal storage is directly related to the relative magnitude of various forces responsible for the wave movement. For instance, waves controlled primarily by gravity, friction, and the pressure gradient will attenuate slowly. Waves in which inertia is also significant will attenuate at a faster rate.

Movement of a flood wave is governed by the conservation principles of fluid mechanics. Conservation of mass is expressed by the equation of continuity and conservation of momentum by the equation of motion. These two equations constitute a system of partial differential equations for which no complete analytical solution is available. With the advent of the digital computer, numerical solutions are increasingly used to solve partial differential equations describing flood movement.

A numerical solution is based on the formulation of an algebraic analog of the partial differential equations. Independent variables (space and time) are represented discretely on the x-t plane such that dependent variables (discharge, velocity, stage) are either known or can be calculated at specified locations of the grid.

Early work on flood routing placed emphasis on specific problems which could be treated by an appropriate simplification of the equations of continuity and motion. For instance, if lateral storage is the predominant physical mechanism, such as in the passage of a flood wave through a lake or reservoir, the routing follows directly from the

equation of continuity alone, in effect disregarding the equation of motion. This is the basis of the level pool or Modified Puls reservoir routing method.

For stream channel routing, classical hydrology relied on the storage (or hydrologic) routing methods. These methods are aimed at simplifying the equation of motion by postulating a relationship between inflow, outflow, and storage in a channel reach, in lieu of the more complex partial differential equation. A linear algebraic relationship of this type is the basis of the Muskingum method, which has had wide application in engineering practice. The Muskingum method, however, cannot properly be regarded as a storage routing method, since it can be shown to be closely linked to hydraulic routing methods that take account of the equation of motion.

Equation of motion expresses the balance of inertia, surface, and body forces in a given direction. Inertia forces originate in the acceleration of motion, while surface forces are the longitudinal pressure gradient and shear resistance along the channel bottom. Body force is the gravitational component along the direction of motion. In flood routing applications, the question of relative magnitude of these various forces is often raised. If one or more forces are of negligible magnitude as compared with the remaining forces, they can be assumed equal to zero. This gives rise to approximate wave models, which are valid provided the neglected terms do not contribute appreciably to the solution. An important model of this sort is the kinematic wave that postulates the exact balance of gravity forces and bottom friction, neglecting the pressure gradient and inertia forces. An equally important model is the diffusive wave that considers the balance of gravity, bottom friction, and pressure gradient while also neglecting inertia forces.

Flood routing in natural river channels is subject to an additional degree of freedom imposed by the nonrigid boundary. An imbalance between sediment supply and transport capacity causes aggradation or degradation of the channel bed. Two additional equations are necessary in order to calculate the changes in bed elevation: 1) the equation of sediment continuity, and 2) the equation of sediment motion (sediment transport equation). By solving these two together with the equations describing the water phase (water continuity and motion), a solution for the unsteady flow of water and sediment in natural river channels can be obtained.

Owing to the large number of methods available no attempt is made here to provide a comprehensive treatment. Rather, emphasis is placed on the methods that have a sound theoretical basis. Criteria for selection of a method to solve a particular type of problem are given in the last section of this chapter.

## 11.2 CLASSIFICATION OF FLOOD ROUTING METHODS

The flood routing problem can be stated in the following terms: given a hydraulic system with a specified input discharge hydrograph, find the output discharge hydrograph. The system can be a channel reach, a lake or reservoir, or a combination of channel and reservoir.

In the most general case, the system is subject to the laws of unsteady flow in alluvial channels, which are expressed in terms of three governing equations: 1) the equation of water continuity, 2) the equation of motion, and 3) the equation of sediment continuity. Various simplifications are possible depending on whether certain features of the motion are predominant over others, or if an expedient mathematical solution to a simplified problem is desired. Thus, the neglect of the equation of sediment continuity results in the routing of water waves only. The further neglect of the equation of motion results in the routing of volumes of water, in effect disregarding the force balance.

For the purpose of clarity of presentation, the following classification is advanced.

1. Classification based on the quantity being routed.
   a. Water Routing. This refers to the routing of water waves only. It is governed by the equations of water continuity and motion.
   b. Water and Sediment Routing. This refers to the routing of water and sediment, therefore taking into consideration transient changes in sediment transport. The problem is formulated in terms of the three governing equations.

2. Water Routing: classification based on the predominant physical mechanism.
   a. Mass Balance. This refers to the routing of volumes of water, without considering the momentum balance. The problem is formulated only in terms of the equation of water continuity.
   b. Mass and Momentum Balance. This refers to the routing of water, considering both mass and momentum balance. The problem is formulated in terms of the equations of water continuity and motion. Alternatively, these two equations can be combined to form a second order convection-diffusion equation.

The term hydrologic (or storage) routing is often used in the literature to encompass a large class of routing methods which are primarily based on the storage equation i.e., lumped form of the water continuity equation. The term hydraulic routing refers to those methods that are based on a mass and momentum balance. Furthermore, some methods originally regarded as hydrologic have recently been shown to be linked to the more general hydraulic routing methods. The Muskingum method and its variations are a good example of this.

3. Mass and Momentum Balance: classification based on approximations to the equations of motion.
   a. Kinematic Wave Approximation. This method is based on the assumption that the pressure gradient and inertia terms in the equation of motion are negligible as compared with the gravity and bottom friction terms. This assumption leads to the kinematic wave equation, which is an equation of pure convection.

b. Diffusive Wave Approximation. This method is based on the assumption that the inertia (local and convective) terms of the equation of motion are negligible as compared with the gravity, bottom friction, and pressure gradient terms. This assumption leads to the diffusive wave equation which is an equation describing convective diffusion.
c. Dynamic Wave Routing. This method considers the complete equation of motion. It is often referred to as full dynamic routing. It is the most general model for flood routing.

The Muskingum method with improvement by Cunge (1969) can be shown to be based on a discretization of the convection-diffusion equation. Therefore, it can properly be classified as a diffusion wave model.

4. Water and Sediment Routing: classification based on the method of formulating the problem.
   a. Sequential Routing Method. The equations of water continuity and motion are solved as a first stage and changes in bed elevation are calculated using the sediment continuity equation in a second stage.
   b. Known-Discharge Method. Since the speed of the bed transients is several orders of magnitude smaller than that of water transients, water discharge can be assumed steady when modeling bed transients. The problem can be formulated in terms of the sediment continuity equation and the steady water surface profile (backwater) equation.

5. Classification based on the solution technique.
   a. Analytical Routing. The governing equations are solved strictly by analytical means. Examples are the diffusion analogy of Hayami and the linear routing of Dooge.
   b. Numerical Routing. The governing equations are solved by numerical methods, such as the method of characteristics, the finite difference method, and the finite element method.

## 11.3 NUMERICAL MODELING

The governing equations for describing water and sediment movement are presented in Chapter 5. This section presents several basic concepts regarding the use of finite difference methods in open channel flow computations. The emphasis throughout this section is on developing the proper background for a better understanding of numerical properties of finite difference solutions.

### Difference Equations

A difference equation is an algebraic equation relating values of one or more dependent variables (e.g., discharge Q or stage y) defined on a discrete domain of one or more independent variables (space x or time t). The discrete domain is represented as a grid system on the x-t plane.

The difference equation is obtained by the application of a certain finite difference scheme to the differential equation describing the problem under consideration. This procedure allows conversion of an analytical statement of the problem (for which a solution may be either difficult or impossible) into an algebraic statement for which a numerical solution can generally be made available.

Properties of numerical solutions are closely associated with properties of the differential equations from which they are derived. Therefore, the study of differential equations is the logical starting point in understanding the properties of numerical solutions. Differential equations can be of two types: 1) ordinary (one independent variable) and 2) partial (two or more independent variables). The differential equation that appears most commonly in hydraulic computations is the second order partial differential equation in two independent variables and one dependent variable. Accordingly, this type of equation will be discussed here in detail.

## Differential Equations

The second order partial differential equation can be derived by combining under the proper assumptions two first order partial differential equations of water continuity and motion. In general, the linear form of this equation is

$$A(x,y)\frac{\partial^2\phi}{\partial x^2} + B(x,y)\frac{\partial^2\phi}{\partial x\partial y} + C(x,y)\frac{\partial^2\phi}{\partial y^2} + D(x,y)\frac{\partial\phi}{\partial x} + E(x,y)\frac{\partial\phi}{\partial y} + F(x,y)\phi + G(x,y) = 0 \qquad (11\text{-}1)$$

in which $\phi$ = dependent variable, x,y = independent variables, and A, B, C, D, E, F, and G = coefficients. Equation 11-1 can be classified into the following three types: 1) elliptic, 2) parabolic, and 3) hyperbolic. The value of the discriminant $\Delta = B^2 - 4AC$ determines the type of equation, and with it, the properties of it solution. If $\Delta < 0$, the equation is said to be of elliptic type, if $\Delta = 0$, the equation is parabolic, and if $\Delta > 0$, the equation is of hyperbolic type. As an illustration of these concepts, consider first the Laplace equation for two-dimensional potential flow

$$\frac{\partial^2\phi}{\partial x^2} + \frac{\partial^2\phi}{\partial y^2} = 0 \qquad (11\text{-}2)$$

In Equation 11-2 the values of the coefficients of Equation 11-1 are A = 1, B = 0, and C = 1. Therefore, $\Delta = -4$, and the Laplace equation is of the elliptic type.

Consider another example, that of the convection-diffusion equation which is applicable to flood propagation problems. In its linear form, it is expressed as

$$\frac{\partial Q}{\partial t} + c\,\frac{\partial Q}{\partial x} - \mu\,\frac{\partial^2 Q}{\partial x^2} = 0 \qquad (11\text{-}3)$$

Equation 11-3 is parabolic, since $A = -\mu$, $B = 0$, and $C = 0$, leading to $\Delta = 0$. Furthermore, the linear wave equation

$$\frac{\partial^2 u}{\partial t^2} - c^2\,\frac{\partial^2 u}{\partial x^2} = 0 \qquad (11\text{-}4)$$

is of the hyperbolic type, since $A = -c^2$, $B = 0$, and $C = 1$, leading to $\Delta = 4c^2$

Elliptic equations are generally associated with equilibrium or steady-state problems in two spatial dimensions. For example, the velocity potential for steady flow of an incompressible inviscid fluid satisfies Laplace's equation and is the mathematical way of expressing the fact that the rate at which such fluid enters a given region is equal to the rate at which leaves it. The analytical solution of an elliptic equation is a function of the space variables x and y which satisfies the differential equation at every point of an area A inside a domain limited by a plane closed curve C (Figure 11-1), and satisfies certain conditions at every point of this curve. Those are termed the boundary conditions. Problems associated with elliptic equations are sometimes referred to as "boundary value" or "jury" problems.

Parabolic and hyperbolic equations are associated with unsteady problems in one spatial dimension. In contrast to the closed domain typical of the elliptic case, parabolic and hyperbolic problems are characterized by an "open" domain (Figure 11-2). Therefore, in addition to the differential equations, initial conditions ($t = 0$) and boundary conditions (e.g., $x = 0$) need to be specified. Problems associated with parabolic and hyperbolic equations are also referred to as "mixed initial-boundary value" or "marching" problems, the latter ostensibly because of the manner by which they propogate the solution forward from one time level to the next in a step-by-step fashion.

The essential difference between parabolic and hyperbolic equations is the number of solutions. Parabolic equations possess only one solution, while hyperbolic equations invariably lead to two solutions. The awareness of this difference can be significant in the study of the behavior of numerical solutions of parabolic and hyperbolic equations.

## Finite Difference Operators

A numerical solution by a finite difference method requires that the domain of the independent variables (space and time) be discretized into a finite number of grid points. The set of grid points within the domain is referred to as the grid system or grid configuration. Properties of the numerical solution, namely, stability, consistency, and convergence are determined by 1) the pattern and spacing of grid points, 2) the nature of the problem being solved, and 3) the structure of the finite difference "scheme" used to solve it.

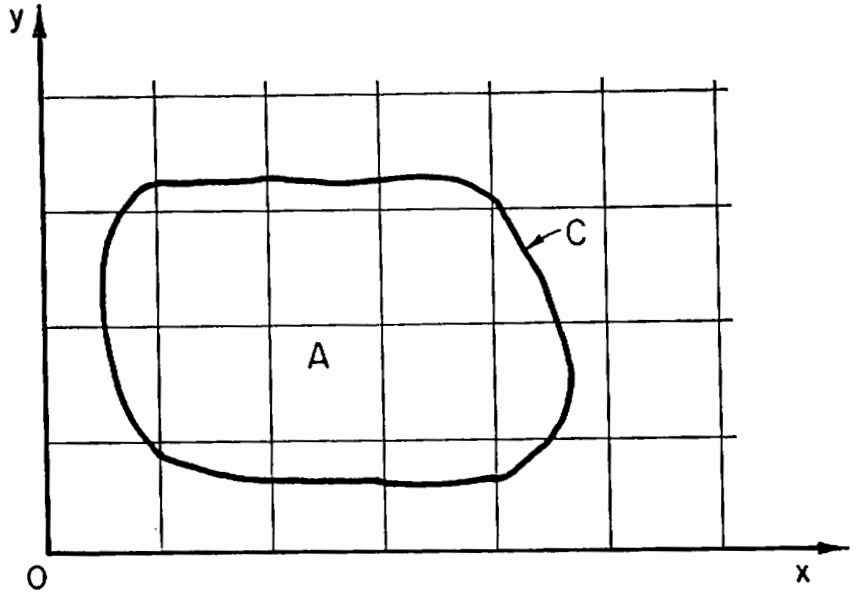


Figure 11-1. Schematic portrayal of the closed domain associated with elliptic equations.

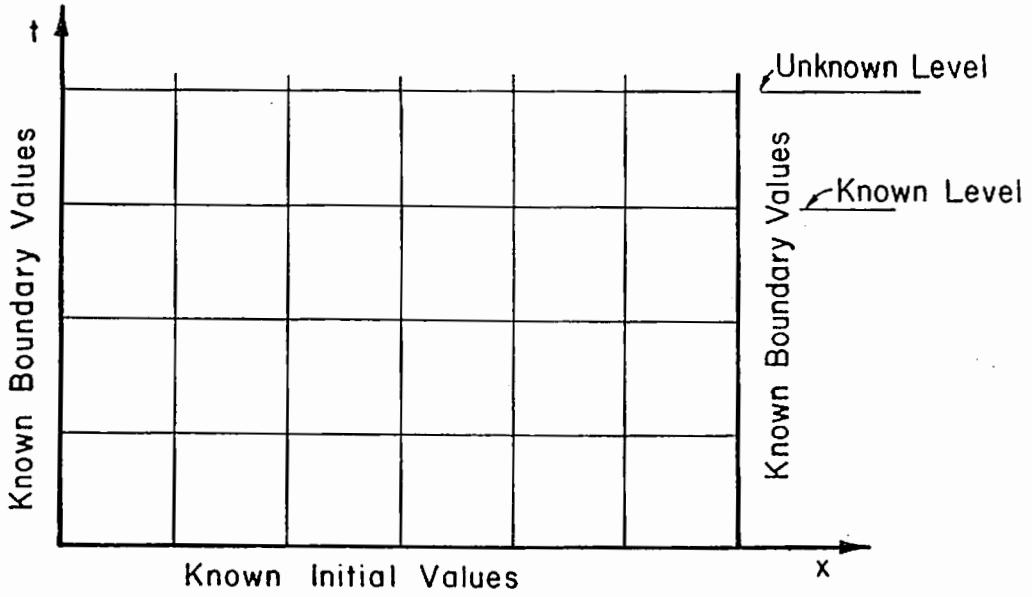


Figure 11-2. Schematical portrayal of the open domain associated with parabolic and hyperbolic equations.

A finite difference scheme is a computation molecule consisting of one or more finite difference operators. Difference operators can be of the following three types: 1) forward, 2) backward, and 3) central. For instance, the differential operator $\partial\phi/\partial x$ can be discretized on the $x$ domain around grid point $j$ using a forward difference operator $(\phi_{j+1}-\phi_j)/\Delta x$, a backward difference operator $(\phi_j-\phi_{j-1})/\Delta x$, or a central difference operator $(\phi_{j+1}-\phi_{j-1})/2\Delta x$, (Figure 11-3).

In order to study the properties of difference operators, the function $\phi$ is assumed to be expanded in Taylor series, leading to

$$\phi_{j+1} = \phi_j + \frac{\partial\phi}{\partial x}\Delta x + \frac{1}{2}\frac{\partial^2\phi}{\partial x^2}\Delta x^2 + \frac{1}{6}\frac{\partial^3\phi}{\partial x^3}\Delta x^3 + o(\Delta x^4) \qquad (11\text{-}5)$$

$$\phi_{j-1} = \phi_j + \frac{\partial\phi}{\partial x}\Delta x + \frac{1}{2}\frac{\partial^2\phi}{\partial x^2}\Delta x^2 + \frac{1}{6}\frac{\partial^3\phi}{\partial x^3}\Delta x^3 + o(\Delta x^4) \qquad (11\text{-}6)$$

The order of approximation (order of error) of the forward difference operator can be obtained from Equation 11-5

$$\frac{\partial\phi}{\partial x} = \frac{\phi_{j+1}-\phi_j}{\Delta x} + o(\Delta x) \qquad (11\text{-}7)$$

in which $o(\Delta x)$ denotes the order of error, given by the exponent of $\Delta x$.

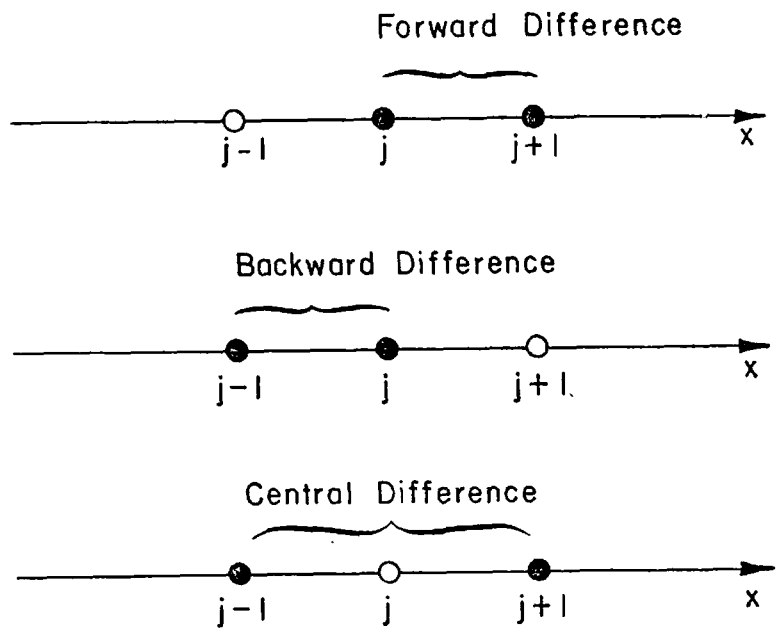


Figure 11-3. Difference operators.

Likewise, the order of error of the backward difference operator can be obtained from Equation 11-6

$$\frac{\partial \phi}{\partial x} = \frac{\phi_j - \phi_{j-1}}{\Delta x} + o(\Delta x) \tag{11-8}$$

Here again, the error is of first order. Finally, substracting Equation 11-6 from Equation 11-5

$$\frac{\partial \phi}{\partial x} = \frac{\phi_{j+1} - \phi_{j-1}}{2\Delta x} + o(\Delta x^2) \tag{11-9}$$

which shows that the error of the central difference operator is of second order.

On the basis of the foregoing analysis, it is concluded that the off-centered (forward and backward) difference operators lead to first order errors, while the central operator leads to second order errors. For the same grid spacing ($\Delta x$), second order errors are smaller than first order errors. Stated in more general terms, the higher the order of the error, the closer the approximation of the numerical solution to the analytical solution. This fundamental property of difference operators is of significant value in connection with the problem of stability, consistency and convergence to be diseussed later in this chapter.

## 11.4 TYPES OF FINITE DIFFERENCE SCHEMES

Finite difference schemes can be either explicit or implicit. Explicit schemes lead to a difference equation containing only one unknown variable. For instance, in Figure 11-4, the values of $\phi$ are known at time level $n$ and unknown at time level $(n+1)$. An explicit scheme for the diffusion equation

$$\frac{\partial \phi}{\partial t} = \mu \frac{\partial^2 \phi}{\partial x^2} \tag{11-10}$$

is

$$\frac{\phi_j^{n+1} - \phi_j^n}{\Delta t} = \mu \frac{\phi_{j+1}^n - 2\phi_j^n + \phi_{j-1}^n}{\Delta x^2} \tag{11-11}$$

from which the unknown value of $\phi_j^{n+1}$ can be calculated directly.

Implicit schemes lead to a difference equation containing more than one unknown variable. An implicit scheme for the diffusion equation is (Figure 11-5)

$$\frac{\phi_j^{n+1} - \phi_j^n}{\Delta t} = \mu \frac{\phi_{j+1}^{n+1} - 2\phi_j^{n+1} + \phi_{j-1}^{n+1}}{\Delta x^2} \tag{11-12}$$

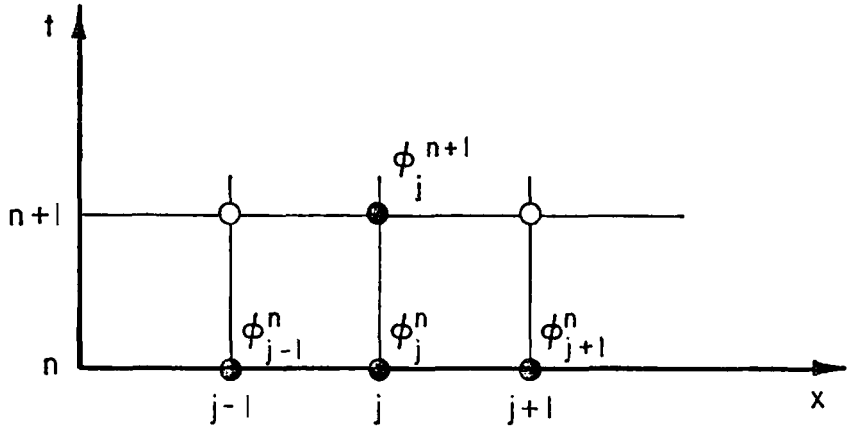


Figure 11-4. Grid configuration for an explicit scheme of the diffusion equation.

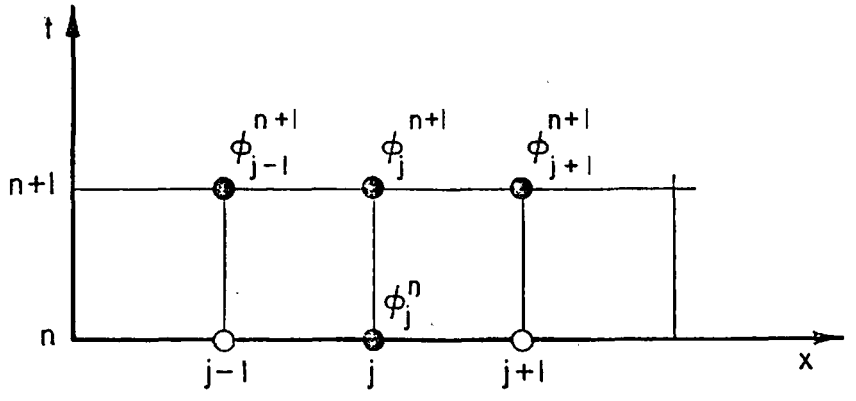


Figure 11-5. Grid configuration for an implicit scheme of the diffusion equation.

in which the unknowns occur in triads and the solution requires the inversion of a matrix.

Explicit Compared with Implicit Schemes. The choice between explicit and implicit schemes generally involves considerations of the cost of program development compared with the cost of program operation. Explicit schemes are easy to formulate and program for use with a computer, resulting in lower development costs. However, they are usually subject to a strict stability condition that effectively places an upper limit on the size of the time step that can be taken in practice.

Implicit schemes on the other hand are free from the stability condition usually imposed on explicit schemes. Therefore, there is no limitation on the size of the time step for stability reasons. The time step, however, cannot be chosen to be arbitrarily large. Care should be taken to ensure that the continuum problem is being properly discretized. For instance, large errors would result if a hydrograph of 24-hr duration (T=24) is simulated by using a time step of 12 hours ($\Delta t=12$).

Not all explicit schemes are subject to a stability condition. For instance, for convection-diffusion problems, unconditionally stable explicit schemes can be formulated. Furthermore, implicit schemes cannot be regarded as altogether free from stability problems. Instability due to nonlinear interation, roundoff errors, improper boundary conditions, etc. are often present in computations using an implicit scheme. The use of weighting factors (off-centering the temporal or spatial derivatives) is common in this connection, ostensibly to allow the operation of an otherwise unstable numerical scheme.

The advantage of being able to use a comparatively larger time step with implicit schemes is somewhat offset by the additional complications involved, including the need to solve large sets of simultaneous equations. Still, the choice between explicit and implicit schemes remains primarily one of cost, although convenience and efficiency play a significant role.

## 11.5 STABILITY AND CONVERGENCE

The properties of numerical solutions are conveniently discussed in terms of the concepts of stability and convergence. In order to illustrate these concepts, the following definitions are introduced. When D, $\Delta$, and N are the solution to the differential equation, the solution to the difference equation, and the numerical (actual) solution, respectively and the quantity ($\Delta$-N) is defined as the roundoff error. It exists because of the inability of the computer to carry out the numerical computations to an infinite number of decimal places. The quantity (D-$\Delta$) is the discretization error due to the finite distance between two neighboring grid points. Stability is associated with conditions such that the roundoff error is small throughout the region of integration. Convergence is related to the size of the discretization error.

### Stability

In general, stability refers to the ability of a numerical scheme to inhibit error growth. An unstable scheme is that in which a certain

type of numerical error (usually roundoff error) is allowed to grow unbounded until it eventually spoils the calculations. Causes of instability are related to 1) the type of differential equation (e.g., ordinary/partial, first order/second order, linear/nonlinear), 2) the type of continuum system (e.g., elliptic, parabolic, or hyperbolic in the case of linear second partial differential equations), and 3) the type of finite difference scheme (explicit or implicit).

Explicit schemes of hyperbolic systems are subject to the Courant-Friedrichs-Lewy stability criterion. This criterion states that for stability to be maintained, it is necessary that the domain of dependence of the difference equation encompass the domain of dependence of the differential equation (Figure 11-6). This leads to

$$\frac{\Delta x}{\Delta t} \geq c \tag{11-13}$$

in which c = phase velocity of the physical wave. For a given c and $\Delta x$, Equation 11-13 effectively imposes an upper limit on the size of $\Delta t$ that can be used in practice. This may often result in an inefficient computation due to the large number of time steps necessary to solve a particular problem.

In implicit schemes, the domain of dependence of the difference equation entirely encompasses the domain of dependence of the solution (Figure 11-7). Therefore, implicit schemes are not limited by the Courant-Friedrichs-Lewy criterion. Their unconditional stability allows the use of larger time steps than those usually possible with explicit schemes. The time step, however, cannot be chosen arbitrarily large. There is a practical limit dictated by the grid resolution above which accuracy would be considerably impaired. In order to remain within reasonable error bounds, experience dictates that the value of $T/\Delta t$ should be greater than 15.

Implicit schemes are not totally free from stability problems. Instabilities of a different nature (e.g., nonlinear interaction, improper boundary conditions) can sometimes plague computations using an implicit scheme. As an illustration of this fact, the Preissmann implicit scheme (Liggett and Cunge, 1975) when used in connection with the Saint Venant equations, can lead to instabilities for certain values of the weighting factor. In the Preissmann scheme, the spatial derivative $\partial\phi/\partial x$ is discretized as

$$\frac{\partial \phi}{\partial x} = \theta \frac{\phi_{j+1}^{n+1} - \phi_j^{n+1}}{\Delta x} + (1-\theta) \frac{\phi_{j+1}^{n} - \phi_j^{n}}{\Delta x} \tag{11-14}$$

in which $\theta$ = weighting factor, restricted in the range $0.5 \leq \theta \leq 1.0$. Within this range, the lower the value of $\theta$, the more the likelihood of instability. In practice, values of $\theta \leq 0.55$ are used to suppress any unstable tendencies which may tend to develop during the computations.

Consistency and Convergence

Consistency refers to the ability of a numerical scheme to produce a solution that approaches the analytical solution as the discretization

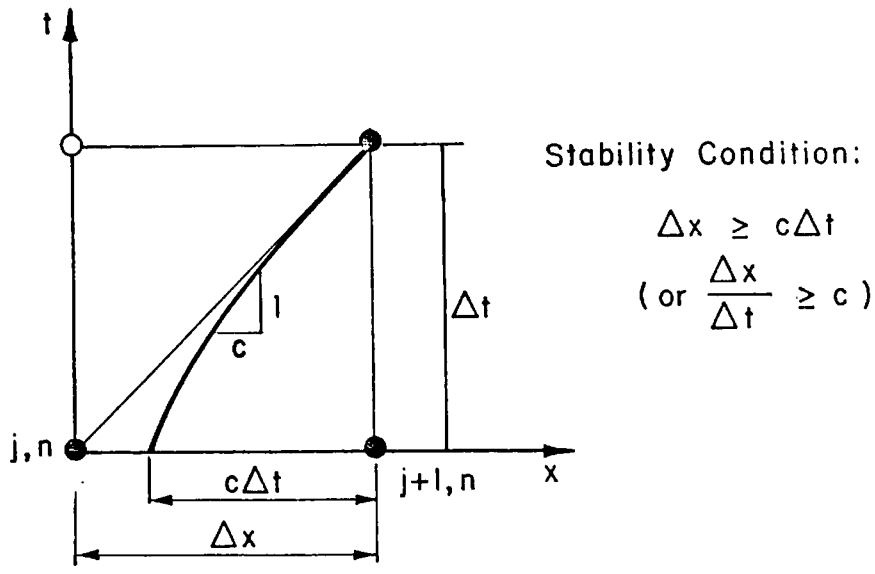


Figure 11-6. Schematic illustrating the stability condition of explicit schemes.

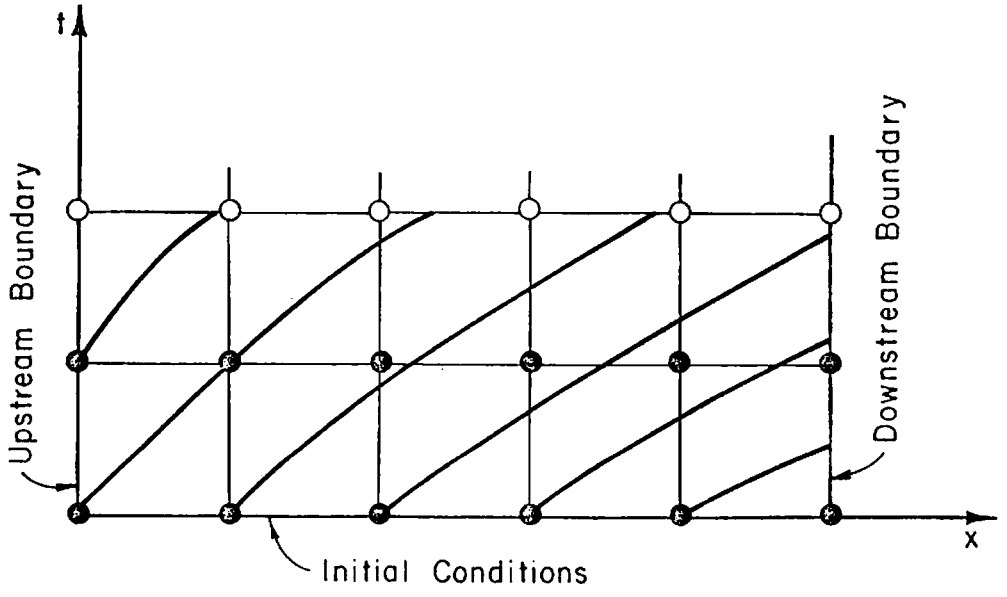


Figure 11-7. Characteristic structure illustrating the unconditional stability of implicit schemes.

is made exceedingly small. Convergence is a measure of the size of the discretization errors in any one numerical solution. These concepts are conveniently illustrated by the use of error portraits, as shown in Figure 11-8. In this figure grid resolution (spatial $L/\Delta x$ or temporal $T/\Delta t$) is plotted on the abscissas and convergence ratio R defined as the ratio of numerical to analytical solutions is plotted on the ordinates. The property of consistency is illustrated by comparing the error portraits of schemes labeled A and B. As the grid resolution increases, scheme A is shown to be consistent with the differential equation and the reverse is true of scheme B.

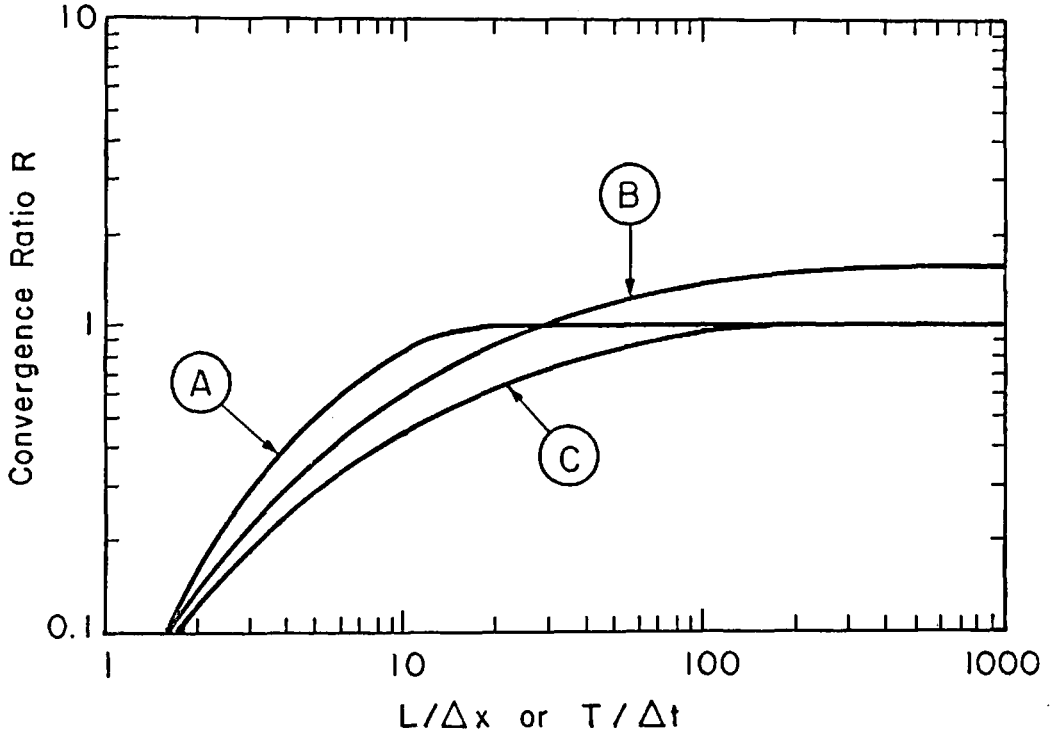


Figure 11-8. Schematic error portraits illustrating the concepts of consistency and convergence.

The property of convergence is illustrated by comparing the errors portraits of schemes A and C. While both schemes may be in error for low values of grid resolution, it is apparent that for the same accuracy, scheme C requires a much higher value of grid resolution. Scheme A is said to "converge faster" than scheme C.

In explicit schemes, convergence is usually associated with a certain grid configuration which is a function of the properties of the continuum problem. For instance, the convection equation

$$\frac{\partial C}{\partial t} + u \frac{\partial C}{\partial x} = 0 \qquad (11\text{-}15)$$

in which C = concentration, can be discretized using the upstream differencing scheme (Figure 11-9)

$$\frac{C_j^{n+1}-C_j^n}{\Delta t} + u\,\frac{C_j^n-C_{j-1}^n}{\Delta x} = 0 \qquad (11\text{-}16)$$

In this case, optimum convergence (R→1) is achieved when the computational time step $\Delta t$ equals the characteristic time step $\Delta t_c$ given as

$$\Delta t_c = \frac{\Delta x}{u} \qquad (11\text{-}17)$$

Since this is precisely the upper limit from the stability standpoint, it is common practice to set $\Delta t = 0.9\,\Delta t_c$, assuring both stability and reasonably adequate convergence properties.

In implicit schemes, convergence is associated with a certain combination of weighting factor and grid resolution. In general, the closer the weighting factor is to a central value (e.g., $\theta \rightarrow 0.5$), the better are the convergence properties of the numerical solution as illustrated by Figure 11-10.

Stability Compared with Convergence

Generally speaking, properties of stability and convergence are at odds in numerical modeling applications i.e., the more stable the model, the less convergent it is. Therefore, the task is to seek an optimum compromise between the conflicting demands of stability and convergence. To the extent that this can be done, numerical modeling remains a powerful tool for the solution of unsteady open channel flow problems.

## 11.6 WATER AND SEDIMENT ROUTING

The physical processes governing watershed and river responses are very complicated. Figure 11-11 illustrates some key elements in the mathematical modeling of watershed and river responses. As mentioned previously further approximation of system response utilizing numerical modeling techniques can be made by assuming the following conditions: 1) unsteady flow conditions by kinematic wave approximation, diffusion wave approximation, and dynamic wave approximation, and 2) known discharge conditions. For practical application to the design problems, a known discharge approach is usually valid due to relatively short study reaches and in adequacy of detailed information. A general numerical solution scheme was discussed in the last section. Characteristics of an alluvial river system can be evaluated utilizing these tools. River systems are dynamic and generally in a continuous state of change and the rate at which a streambed will degrade or aggrade can be estimated from sediment transport calculations. Evaluation of the spatial extent of change is related to the location of control points in the river. Use of degradation and aggradation analysis will provide the necessary information to 1) evaluate the stability of the hydraulic

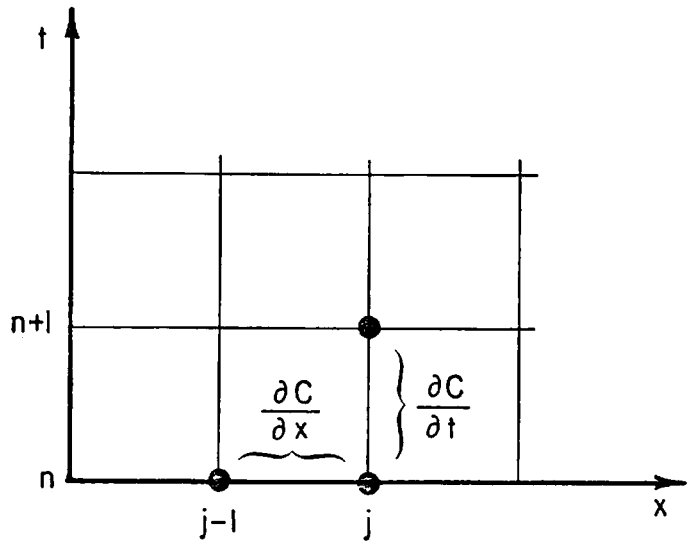


Figure 11-9. Grid configuration for the upstream differencing scheme of the convection equation.

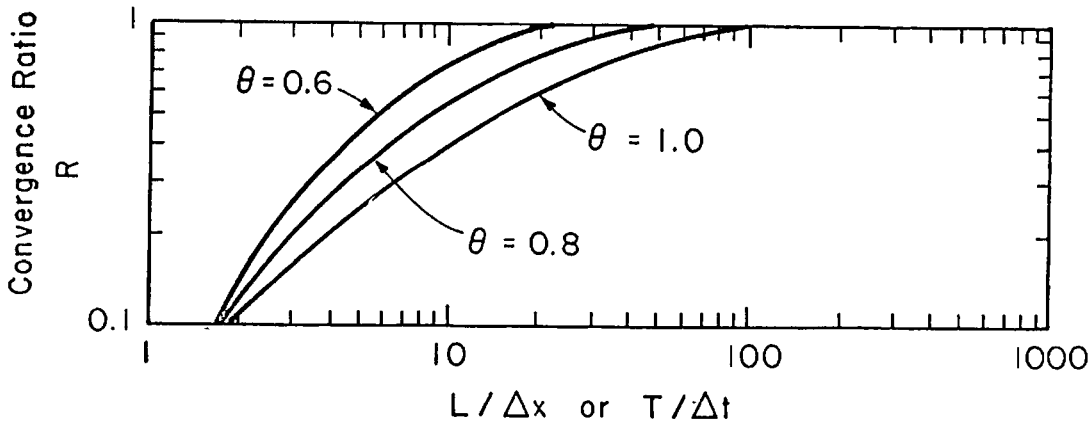


Figure 11-10. Schematic error portraits illustrating the effect of the weighting factor on convergence.

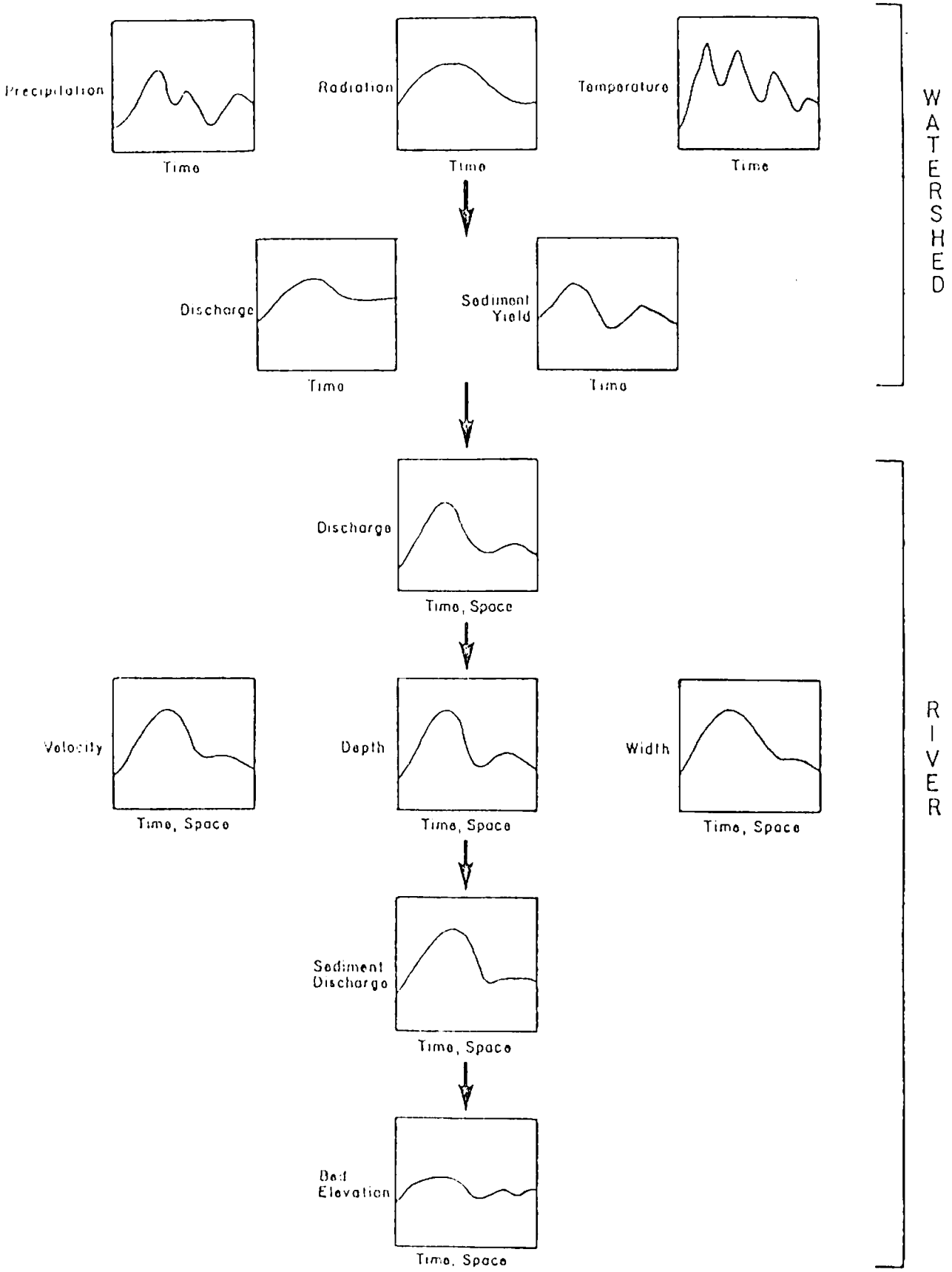


Figure 11-11. Key elements in the watershed and river analysis.

structures, 2) determine the lateral migration tendencies of the channels, 3) estimate the extent of expected general downstream channel scour., 4) determine the potential local scour around structures, and 5) estimate the long-term effects of sediment degradation and aggradation on the water surface profile.

A simple calculation of degradation or aggradation may be obtained using a method based on the sediment continuity equation. Assuming no lateral inflow, the sediment continuity equation may be written as

$$\frac{\partial Q_s}{\partial x} + (1 - \lambda) \frac{\partial A_s}{\partial t} = 0 \tag{11-18}$$

where $Q_s$ is volume sediment discharge, $\lambda$ is bed material porosity, $A_s$ is change in cross-sectional bed area, t is time, and x is distance. In simple finite difference formulations

$$\frac{\Delta Q_s}{\Delta x} + (1 - \lambda) \frac{\Delta A_s}{\Delta t} = 0 \tag{11-19}$$

Therefore, the change in area may be calculated as

$$\Delta A_s = - \frac{\Delta Q_s \Delta t}{\Delta x(1-\lambda)} \tag{11-20}$$

The change in $Q_s$ may be expressed as

$$q_{s_2} B_2 - q_{s_1} B_1 = \Delta Q_s \tag{11-21}$$

where $B_i$ is the channel width at Station i and $q_{s_i}$ is the sediment volume discharge per unit width at Station i. In addition, $\Delta_s$ may be expressed as

$$\Delta A_s = \frac{B_1+B_2}{2} \Delta z \tag{11-22}$$

where $\Delta z$ is the average change in bed elevation. Equating Equations 11-20 and 11-22 yields

$$\Delta z = - \frac{2\Delta Q_s \Delta t}{\Delta x(1-\lambda)(B_1+B_2)} \tag{11-23}$$

or using Equation 11-21

$$\Delta z = - \frac{2\Delta t(B_2 q_{s_2} - B_1 q_{s_1})}{\Delta x(1-\lambda)(B_1+B_2)} \tag{11-24}$$

This change in bed elevation is an average change over the entire $\Delta x$. If there is a control at the downstream end, the average change in bed elevation should be redistributed over $\Delta x$ giving no change at the downstream end and $2\Delta z$ at the upstream end. Equation 11-24 may be

used in conjunction with a transport equation to provide for dynamic slope. That is, if the water hydrograph is subdivided into several $\Delta$ts. The degradation-aggradation equation may be run for the first $\Delta t$ and the slope updated by $2\Delta z$. Then the new slope may be used in the transport equation to calculate a new value of $q_s$. This $q_s$ may then serve as input to the aggradation-degradation equation, and so forth.

Two examples of application of water and sediment routing techniques to solve engineering problem follow.

## 11.7 DEGRADATION BELOW A DAM (T OR C, WILLIAMSBURG WATERSHED, NEW MEXICO)

### General

Presented in this section is an analysis of degradation below the emergency spillway chute of the Site 8C, T or C, Williamsburg Watershed, New Mexico. The structure proposed by the Soil Conservation Service is a single-purpose flood retarding structure. The dam will be located in Mud Springs Canyon about one mile upstream from Williamsburg and about one and one-half miles from its confluence with the Ric Grande (USDA Soil Conservation Service, 1977).

The analysis involves the determination of the magnitude of degradation to be expected downstream from the emergency spillway chute during passage of the design hydrograph. Such an analysis is required to determine how far the baffled outlet end of the chute must extend below the present channel grade to accommodate degradation. In order to provide enough information for an adequate design three different conditions that depict the future water and sediment inflows to the dam prior to the occurrence of the freeboard hydrograph were considered in this study.

Case I considers that the reservoir is 90 percent filled with sediment resulting from a series of small floods, prior to the occurrence of the freeboard hydrograph. These small floods pass all of the flow through the principal spillway. Degradation due to the freeboard hydrograph would be negligible and total expected scour depth below the structure is equal to the general scour depth resulting from flows through the principal spillway.

Case II assumes that immediately following the closure of the dam, water storage has reached the top of the dam (EL. 4880.5') and the sediment storage capacity has enough room for the sediment yield associated with the freeboard hydrograph. Under this condition, the emergency spillway chute would pass the freeboard hydrograph with essentially clear water. This is because nearly all of the sediment will be trapped upstream of the flood retarding structure.

The third condition (Case III) represents the worst possible condition which assumes that after 85 years of operation, two 50-year floods and one 100-year flood occur prior to the passing of the freeboard hydrograph. Total expected scour is the sum of the general scour due to flows through the principal spillway for 85 years of operation

and the general and local scour resulting from a sequence of two 50-year floods, one 100-year flood, and the freeboard hydrograph. This condition is very unlikely to occur, yet constitutes the worst possible condition in determining the degradation below the emergency spillway structure.

Determination of the change in sediment storage is vital for evaluation of both Case I and Case III. This requires estimation of annual sediment yield and sediment yields resulting from various sizes of storms on the watershed. Sediment yield is determined by a combination of the Universal Soil Loss Equation modified by Williams (1975) and the Meyer-Peter, Müller bed load equation (USBR, 1960).

The magnitude of scour is determined utilizing a sediment routing procedure that considers size fractions of bed material. This computational procedure involves use of a sediment transport equation, sediment continuity equation, the armoring effect of coarse materials, and channel geometry equations. Hence, the mathematical model is developed according to physical principles governing water and sediment transport, degradation, and armoring processes. Both local scour immediately below the structure and general scour pivoting from a downstream control point are considered in the analysis.

Assuming the downstream control is located at the confluence with the Rio Grande (Station 161 + 70), a scour depth from the presence level of 15.1 feet is expected for the Case I condition. Under Case II, total scour depth from the present level is 18.9 feet. For the worst condition of Case III, estimated scour depth from the present bed level is 34.7 feet. In this case, the lowest bed elevation after experiencing the design floods is 4352.3 feet.

## Mathematical Model

Spatial Designation. The general layout and topographic map of the study site is given in Figure 11-12. The dam will be constructed of clayey sand and gravel and will be about 88 feet high with a 20-foot top width and a crest length of approximately 1920 feet. This would provide storage that would extend at least 3100 feet upstream of the dam. With this length of reservoir and noting that the median bed material diameter is 10 mm, nearly all of the incoming sediment will deposit upstream of the structure, unless the reservoir is filled with sediment. The principal spillway as planned is a 3'-0" x 4'-0" reinforced concrete box conduit, without control gates and is designed to pass a maximum flow rate of 400 cfs. If the structure functions properly, floodwater resulting from a 100-year flood would be stored in the reservoir temporarily and would slowly pass through the principal spillway. The emergency spillway consists of a concrete baffled chute having a width of 200 feet, a depth of 12.1 feet, and a crest elevation of 4468.4 feet. The side walls of the baffled chute were designed to accommodate a freeboard hydrograph discharge of 25,057 cfs and the blocks designed for two-thirds of the freeboard discharge, 16,700 cfs (USDA Soil Conservation Service, 1977). The proposed reservoir has a storage capacity of 2297 acre-feet. Of this 830 ac-ft are provided to store 100 years of sediment supply and 1467 acre-feet are for the flood water storage for

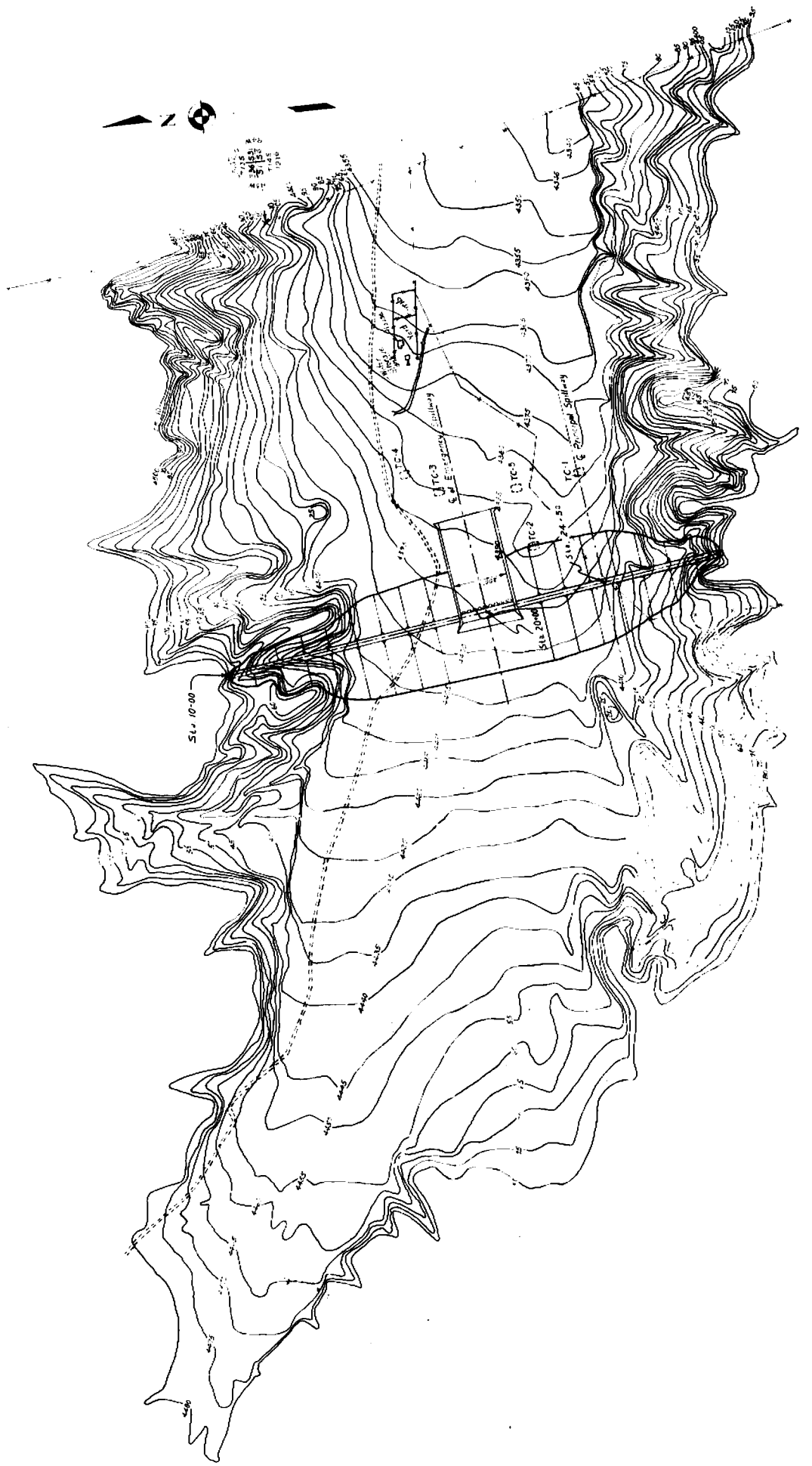


Figure 11-12. General layout and topographic map.

the 100-year flood with 24-hours duration. Assuming 90 percent trapping efficiency of the reservoir, a maximum sediment storage capacity of 2067 acre-feet can occur.

Stability of the emergency spillway baffled chute requires that it be designed so that the ultimate scour during the passage of the freeboard hydrograph does not cause failure of the structure. The purpose of the degradation study is to determine the ultimate scour below the baffled chute for the freeboard discharges so that proper design measures can be taken to assure the stability of the structure. This requires estimating both the local scour immediately below the structure and the general scour pivoting from a downstream control point. A mathematical model was developed to simulate these scour processes. Spatial arrangement of the structure for analysis utilizing the mathematical model is given in Figure 11-13.

Temporal Representation. In order to provide enough information for an adequate design, three conditions representing different sequences of water and sediment inflows to the dam prior to the occurrence of the freeboard hydrograph were considered. These three conditions were outlined in the previous section. For determining sediment inflow rates, an analysis of sediment yield is necessary.

Estimated annual sediment yield utilizing the procedure recommended by Agricultural Research Service (1976) is 8.4 acre-feet which is close to 8.3 acre-feet estimated by USDA Soil Conservation Service. However, total sediment yield consists of both wash load and bed material load. The procedure recommended by Agricultural Research Service (1976) gives the estimation of sediment yield for particles smaller than 2.0 mm. This size of particle is essentially the upper bound of the wash load considering the measured material size distribution for the watershed under investigation. Therefore, the total annual sediment yield should exceed 8.4 acre-feet.

The sediment yields from floods of various return periods were estimated using a combination of the Universal Soil Loss Equation Modified by Williams (1975) and the Meyer-Peter, Müller bed load sediment transport equation. The former relation determined wash load yield and the latter estimated bed material load. Computed results are tabulated in Table 11-1. The average ratio of the wash load sediment yield to the bed material load sediment yield is 2.24, which is close to 1.78 determined by the ratio of availability of wash load to bed material load indicated in the New Mexico Agricultural Experiment Station Research Report AES-RP-233.

The median size of flood was determined to have a return period of 2 years. Assuming that annual rainfall in the watershed is 10 inches and 4.2 percent of the rainfall becomes direct runoff considering weighted mean of various sizes of storms, annual runoff volume can be estimated as 451 acre-feet. Therefore, on the average, there will be approximately 1.61 floods equivalent to the median size flood within a year. Thus, annual sediment yield can be estimated to be 17.2 acre-feet. With the above information, temporal design of Case I, II, and III can be made.

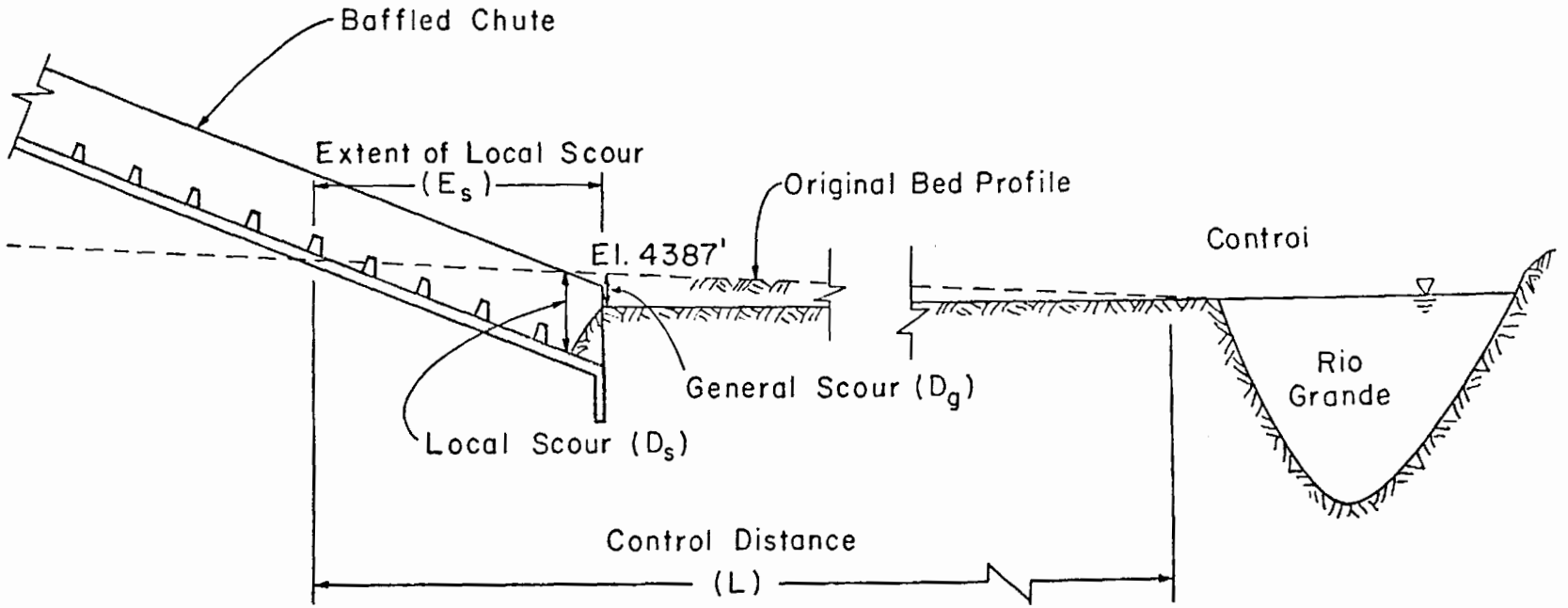


Figure 11-13. Spatial designation of the scour.

Table 11-1. Sediment yield computation.

| Return Period (yr.) | Runoff Volume* (ac-ft) | Runoff Peak** (cfs) | Wash Load (ac-ft) | Bed Material Load (ac-ft) | Total Yield (ac-ft) |
|---|---|---|---|---|---|
| 2 | 279.3 | 704.5 | 6.4 | 4.3 | 10.7 |
| 5 | 633.7 | 1598.5 | 15.9 | 9.7 | 25.6 |
| 10 | 913.0 | 2303.1 | 23.9 | 14.0 | 37.9 |
| 25 | 1310.4 | 3305.5 | 35.9 | 20.0 | 55.9 |
| 50 | 1621.9 | 4091.3 | 45.6 | 24.7 | 70.3 |
| 100 | 1976.4 | 4985.6 | 56.9 | 29.9 | 86.8 |
| Design Storm Inflow Hydrograph | 12265.0 | 30939.1 | 439.4 | 176.0 | 615.4 |

Note:

*Runoff volumes for the various return periods are 24-hour design storms.

**Runoff peaks are estimated by scaling runoff volumes according to the ratio of the peak flow to the runoff volume of the design storm inflow hydrograph.

Case I considers that the reservoir has filled with sediment to the maximum storage capacity prior to the occurrence of the freeboard hydrograph. It would require approximately 120 years to trap about 2067 acrefeet sediment in the reservoir. During this period, all flows pass through the principal spillway and are capable of inducing general scour only. When passing the freeboard hydrograph, the magnitude of scour would not be significantly increased because the sediment would also be delivered through the emergency spillway. This case would cause the smallest scour depth below the structure.

Case II assumes that immediately following the closure of the dam, water storage has reached the top of the dam (EL. 4480.5') and the sediment storage capacity has enough room for the sediment yield associated with the freeboard hydrograph. Potential sediment yield for the freeboard hydrograph is 615 acre-feet which is smaller than the reservoir sediment storage capacity of 2067 acre-feet. In this case, the temporal representation is limited to passing the freeboard flood. The design flood has a peak discharge of 25,057 cfs and a duration of 18 hours.

The third condition (Case III) simulates the worst possible condition. This assumes that after accumulating approximately 1462 acre-feet of sediment for a period of 85 years, two 50-year floods and one 100-year flood occur prior to the passing of the freeboard hydrograph. These two 50-year floods, one 100-year flood plus the design storm inflow hydrograph would reach the sediment storage capacity of 2067 acre-feet. Total expected scour depth is the sum of the general scour due to flows through the principal spillway for the 85-year period

and general and local scour resulting from a sequence of two 50-year floods, one 100-year flood and the freeboard hydrograph. This condition is unlikely to occur, yet constitutes the worst possible condition in determining magnitude of the degradation below the emergency spillway structure.

Governing Processes. Scour below a hydraulic structure is a complex problem. Dominant physical processes include water discharge, sediment transport, sediment routing, degradation, and armoring by sorting smaller sizes of sediment from coarse material. These processes are unsteady in nature. In order to simplify the problem, a known discharge model is used. The known discharge solution is appropriate in this study because of the short distance considered in the spatial arrangement of the structure and the channel.

Estimation of scour is made utilizing a procedure that routes sediment considering size fractions. This procedure includes the use of a bed load sediment transport equation for gravel streams (Meyer-Peter, Müller Bed Load Formula, USBR, 1960), the sediment continuity equation, the sediment supply equation, and the channel geometry equation. Only the bed load transport is considered. For flow through the principal spillway, only general scour is considered. For flow past the emergency spillway both local and general scour must be determined. Local scour and general scour are simulated interactively in a sequential manner within a time step. The time step used in the simulation is 15 minutes.

The baffled chute is usually designed to achieve an exit velocity less than critical velocity (Peterka, 1963). For a conservative estimation, a critical flow velocity is assumed for the terminal velocity. Because the current downstream channel is fairly steep (S = 0.026), the flow will reach normal depth in a short distance. If the downstream channel is eroded sufficiently flat, the flow from the baffled chute will join the downstream tailwater with approximately the normal flow depth as the water level.

## Channel Morphology

Based on the available information, the following information on channel morphology is derived for use in the mathematical model.

Representative Downstream Channel Cross Section. The representative cross section in the vicinity of the study site was developed by considering surveyed channel cross sections that are upstream of the crossing of I-25 near Station 125 + 70. The channel cross sections below this point are too wide and shallow. For a simple and conservative analysis, it is expedient to use data upstream of the intersection of I-25.

Figure 11-14 shows the relationship between wetted perimeter P and cross-sectional area A for the five sections. The representative relation considering these five cross sections is

$$P = 12.7\ A^{0.48} \qquad (11\text{-}25)$$

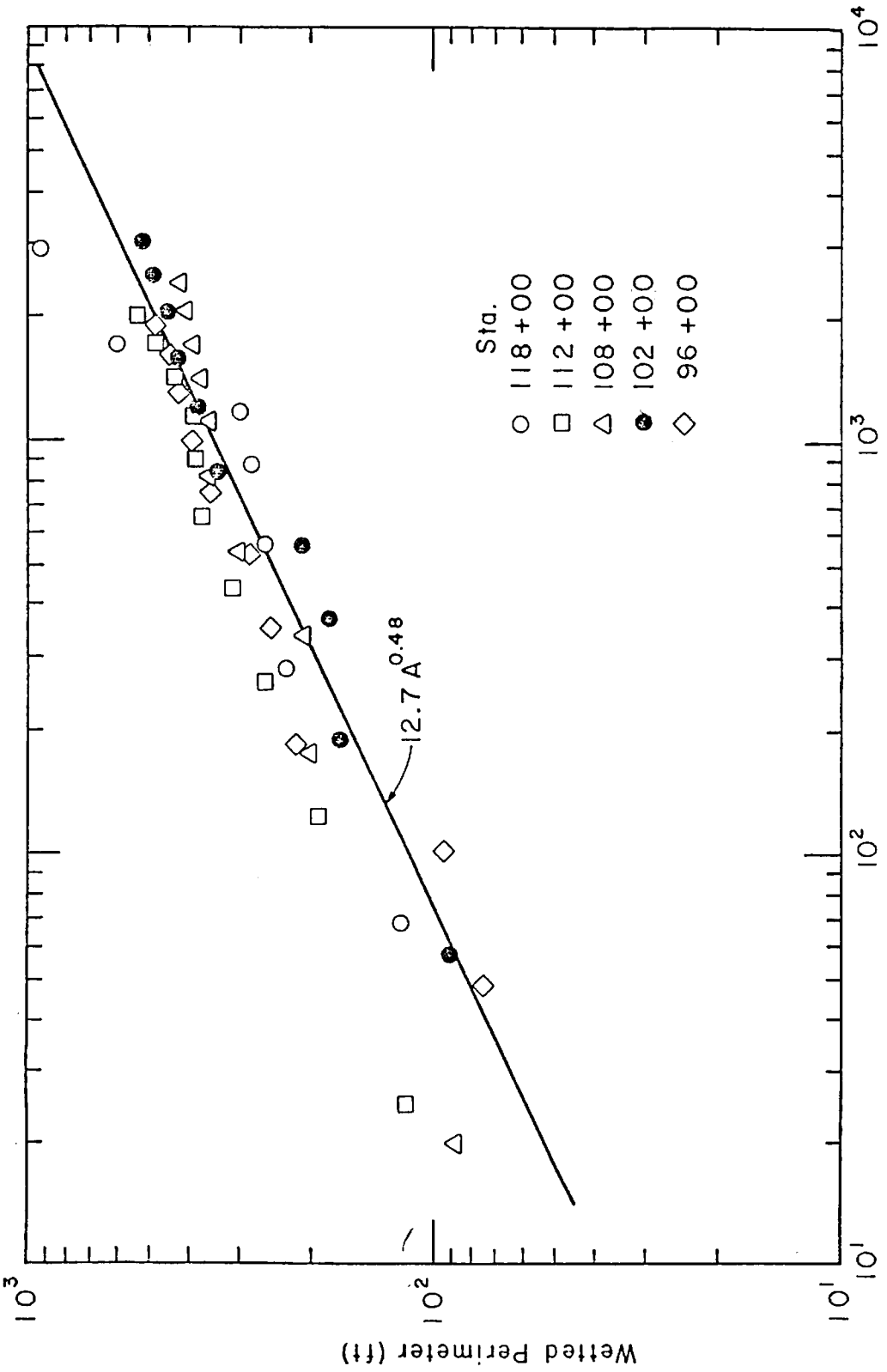


Figure 11-14. Wetted perimeter versus flow cross-sectional area relation.

Representative Bed Material Size. Bed material samples were collected upstream of the crossing of I-25 near 125 + 70 and within the potential scour area. The measured samples verified a highly heterogeneous distribution of bed material with respect to channel location and soil depth. Judging from location of samples, sampling depth, and range of sizes of bed material, it is concluded that sample No. TC-3.1 taken at Pit TC-3 is the most logical choice for representative bed material size because the median diameter and gradation coefficient for sample No. TC-3.1 are respectively $D_{50}$ = 6.0 mm and s = 5.9, which are close to the average of $D_{50}$ = 6.4 mm and s = 5.8 considering all samples. Figure 11-15 gives the representative bed material size distribution. Maximum particle size is assumed to be 100 mm. Field investigation confirmed that the above size distribution is a conservative estimate for determining scour potential.

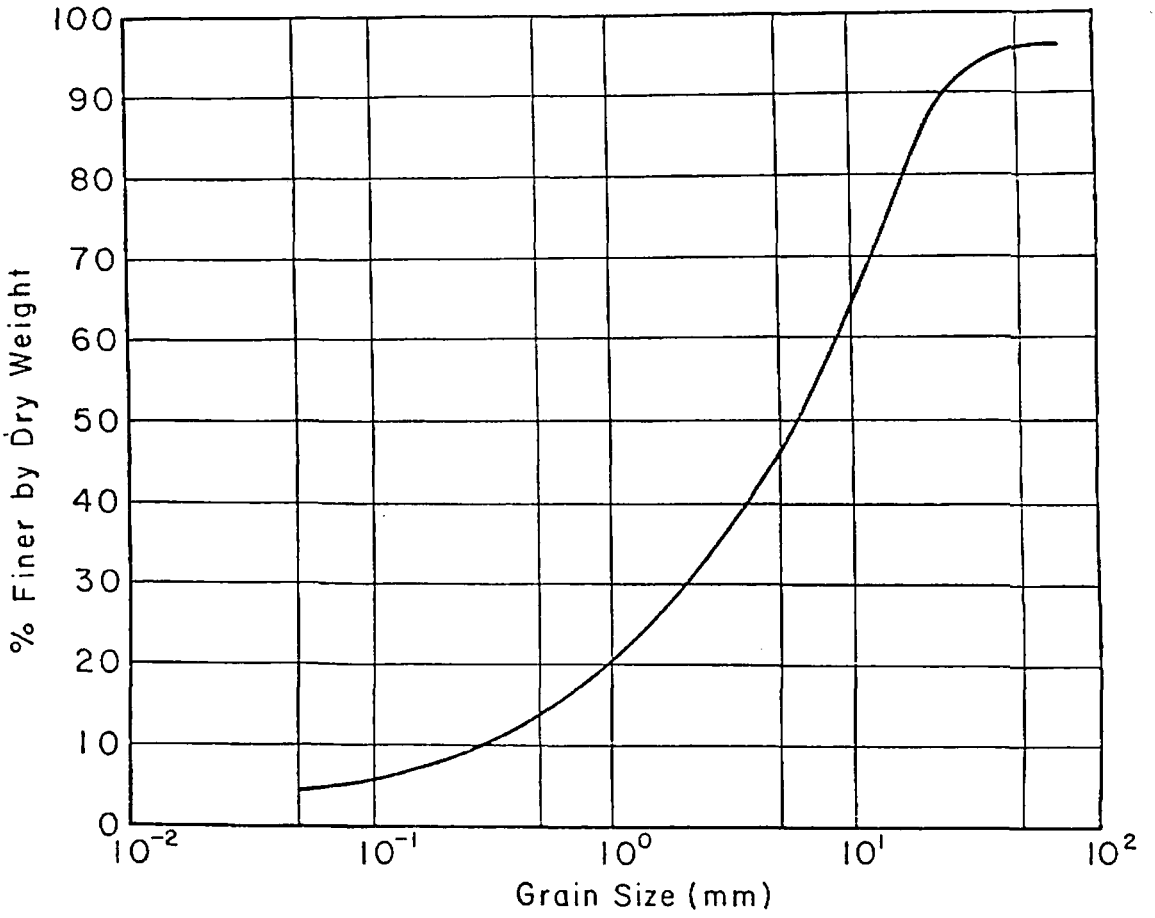


Figure 11-15. Representative bed material size distribution.

Channel Bed Slope and Control. Current slopes of the channel between consecutive stations were computed and the present channel bed profile downstream of the dam found to be fairly uniform to the crossing of Highway I-25 near Station 125 + 70. Channel bed slope becomes flatter downstream of this station. Average bed slope for the entire study reach (from 92+00 to 161+70) is 0.024. For a conservative estimation, representative channel bed slope before general degradation occurs

is assumed to be 0.026. This is the average slope upstream of Station 127 + 70. The friction slope may be less than the channel bed slope. However, for a safer design, it is assumed that friction slope of the downstream channel is equal to the channel bed slope. In other words, friction slope of the downstream channel before the general degradation occurs is 0.026.

Flow Resistance Coefficient. Considering stream power and median diameter, bed form of the channel is likely to be in the upper regime having essentially a plane bed (Simons and Sentürk, 1977). Manning roughness coefficient for a plane bed ranges from about 0.017 to 0.027. According to Chow (1959), Manning's roughness coefficient is 0.025 for the channel pattern and bed material sizes presented in the study reach. Furthermore, Manning's roughness coefficient is about 0.024 using the Strickler Formula (Simons and Sentürk, 1977). It is determined that a Manning roughness coefficient of 0.025 is satisfactory for analysis.

## Results of Analysis

Analysis shows that the ultimate scour depth is dependent on the water and sediment inflows to the reservoir prior to the occurrence of the freeboard hydrograph. Three cases defined in the temporal design were studied. The results demonstrate that the total scour depth for Case I is 15.1 feet after about 120 years of operation. For Case II, the passage of the freeboard hydrograph will cause a local scour of $D_s$ = 18.9 feet below the present bed level (EL. 4387), and the corresponding length $E_s$ of local scour will be 85.2 feet (Figure 11-13). Considering the effect of the assumed control at Station 161 + 70 (6970 feet from the structure), the general scour depth will be $D_g$ = 6.5 feet. The resultant mean particle sizes in the local scour hole and in the downstream channel will be about 25 mm and 11 mm, respectively. Final channel bed gradient indicated is 0.025. Figure 11-16 shows the time-lapse change of local and general scour. It should be noted that local scour depth defined in this study is measured from the present bed level. This local scour depth represents a combination of general scour and local scour according to definitions presented in some publications. Thus, the lowest expected bed level resulting from the spillway design flood is 4368.1 feet. This condition is not the worst condition considering scour potential.

The worst possible condition assumes that after 85 years of reservoir operation, two 50-year floods and one 100-year flood occur prior to the passing of the freeboard hydrograph. The 50-year floods and 100-year floods passing the spillway were scaled according to the design freeboard hydrograph utilizing runoff volumes. The assumed sequence of hydrographs after 85 years of operation is shown in Figure 11-17. General scour due to an 85-year operation is determined to be 12.0 feet. Local scour depth resulting from the assumed sequence of hydrographs will be 22.7 feet and the corresponding length of local scour will be 102.0 feet. Ultimate scour depth for this worst condition will be 34.7 feet. In this case, the lowest bed elevation after experiencing the design floods is 4352.3 feet. If the control of local scour is desired, an armor layer of rocks with size larger than 1.5 feet

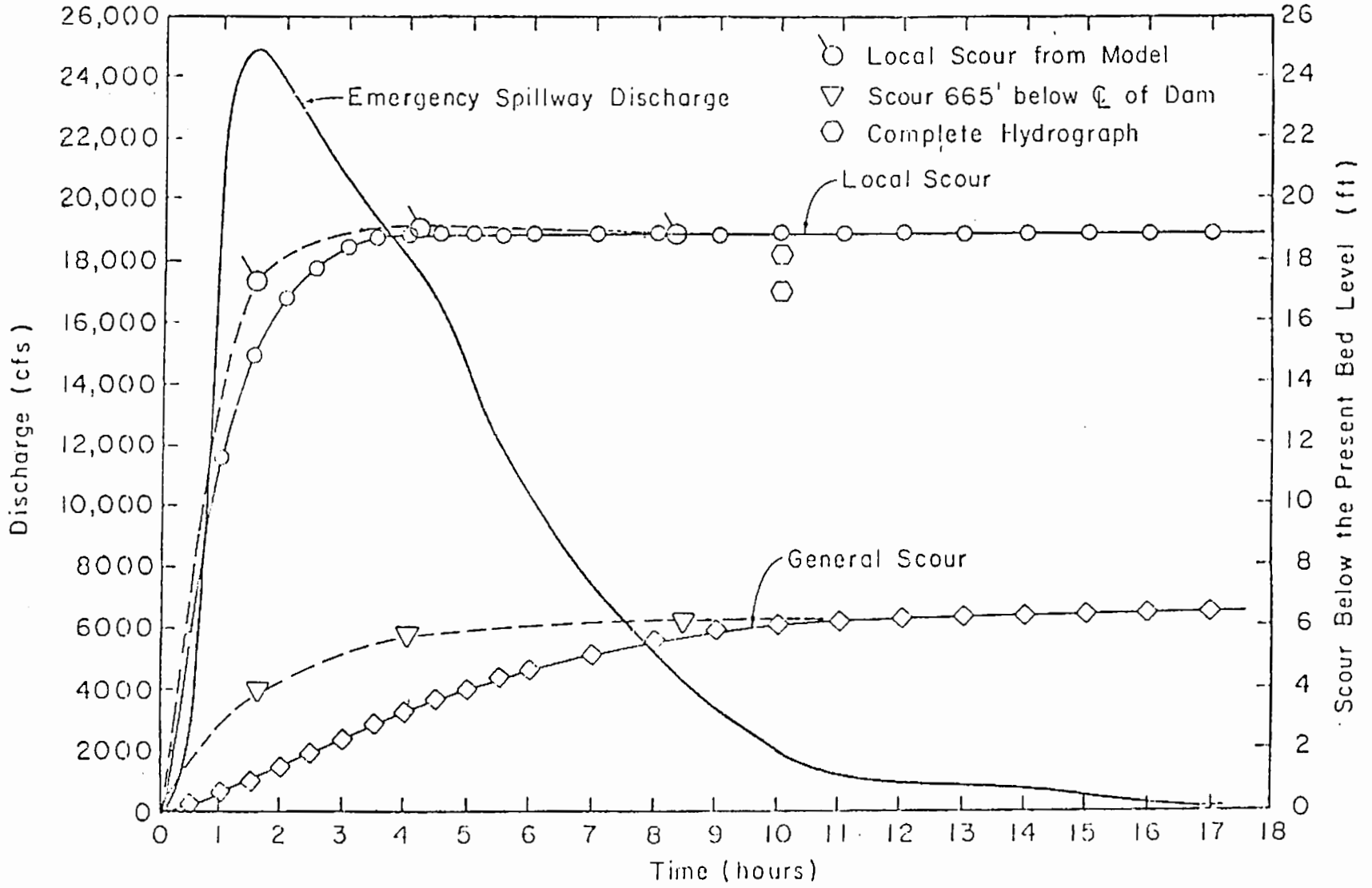


Figure 11-16. Local and general scour with the existing downstream control (6970 feet from the structure).

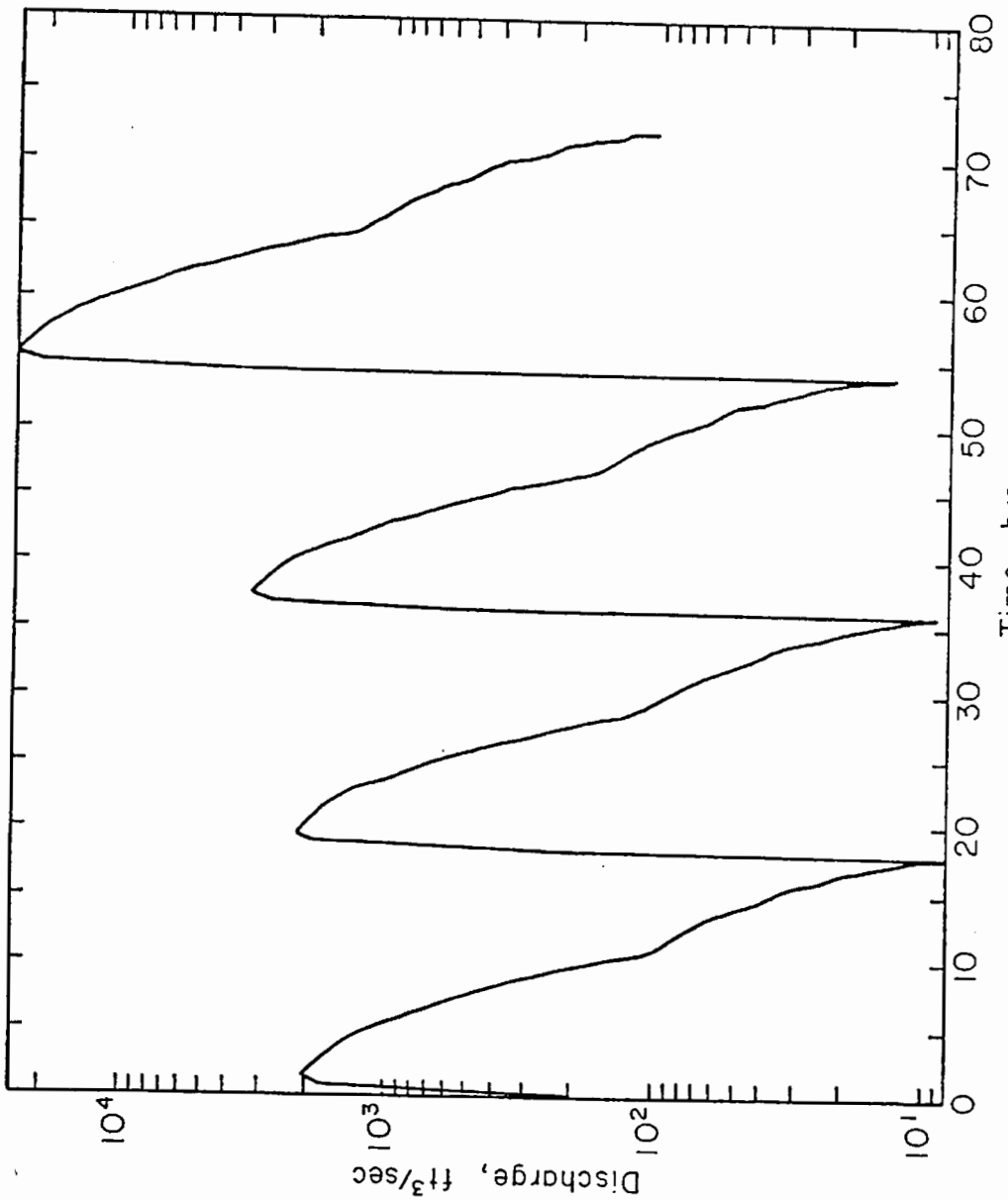


Figure 11-17. The assumed sequence of hydrograph after 85 years of operation.

and with a thickness of two rock diameters is required to pave an area approximately 100 feet long downstream of the structure and 12 feet below the present bed level. This size of riprap was determined using the Shields' criterion of incipient motion (Simons and Sentürk, 1977) and considering a safety factor of 1.5. The determination was based on the peak flow rate of the freeboard hydrograph. This peak flow rate will induce a tractive force of 5.02 $lb/ft^2$, which will cause motion of sediment particles smaller than 1.04 feet. If a safety factor of 1.5 is employed, the design armor layer rock size should be about 1.5 feet. If a soil cement is used, the size required would be about 3.3 feet, which is much larger than for rocks. This is because the specific gravity of soil cement (1.78) is smaller than that of rock (2.65), which makes the submerged weight of soil cement only half that of the submerged weight of the rock. Usually riprap protection requires a properly designed and placed gravel filter. Bed material in the current riverbed has an acceptable gradation for the filter. No additional effort is needed to prepare the gravel filter. Recommended design of the pavement control below the spillway is given in Figure 11-18.

In order to check the applicability of the mathematical model, a large-scale physical model (model scale 1:30) was utilized by a Federal agency to estimate the local and general scour for the design freeboard hydrograph (Case II). Results from both totally independent model approaches were extremely close (Figure 11-16), demonstrating a successful application of the mathematical model.

## 11.8 DEGRADATION AND AGGRADATION ASSOCIATED WITH GRAVEL MINING (SAN JUAN CREEK, CALIFORNIA)

### General

Presented in this section is an analyisis of erosion and deposition problems in San Juan Creek and Bell Canyon associated with Conrock gravel mining operations. A mathematical model for routing sediment by size fraction was developed and is utilized to estimate the erosion and deposition response of the stream and gravel pit subject to different hydrologic inputs and operational alternatives. Four engineering alternatives that consider rehabilitation of the Casper Regional Park and allow mining of sand and gravel are evaluated. Alternative I is a "do nothing" plan terminating the mining of sand and gravel. This alternative would allow natural healing processes in the form of aggradation to take place. No mitigation measure would be imposed on the existing stream. Alternative II is essentially the same as Alternative I except it permits a regular mining of sand and gravel. Alternative III proposes construction of a drop structure located near the upstream end of the gravel pit. Alternative IV proposes construction of a series of small gabion check dams near and upstream of the gravel pit boundary coupled with regular gravel mining.

The developed mathematical model has been calibrated using 1969 floods (January 25 and February 25, 1969) and validated utilizing the recent three storms (January 15-16, February 9-10 and March 4, 1978). Validation results are excellent. Evaluation of alternatives indicates that Alternative IV (a series of check dams) is the most feasible design for meeting the objectives.

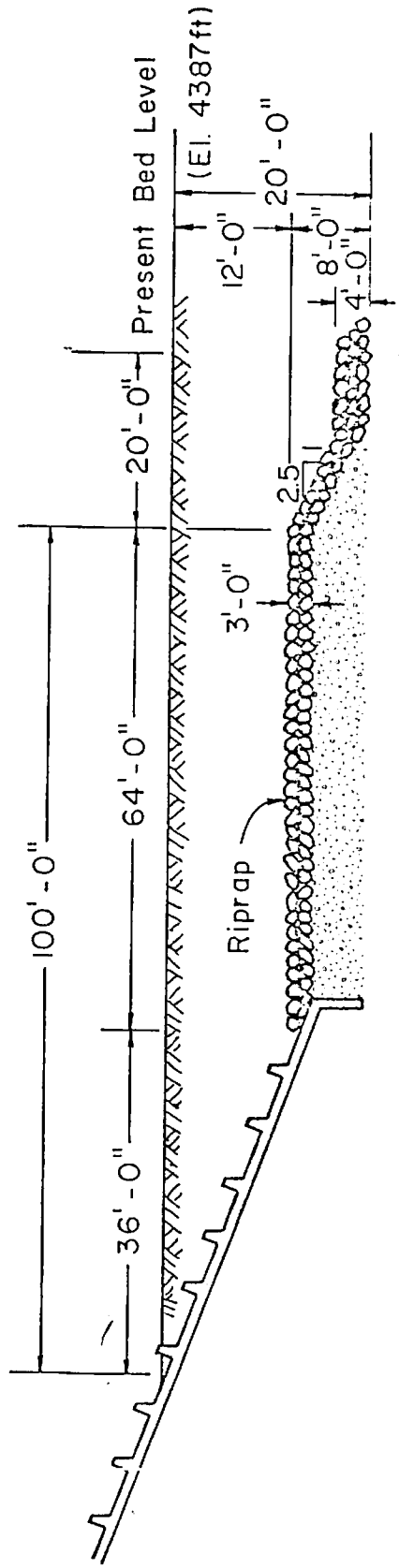


Figure 11-18. Sketch of the recommended design of control pavement.

## Hydrology

Flood Frequency. Utilizing the available flow records at the U.S. Geological Survey gaging station near San Juan Capistrano, California, a flood frequency analysis was made. Available records at this station are from October, 1928 to the present. The drainage area above this point is 106 square miles. Because the drainage area above Conrock gravel pit is only 77 square miles, flows entering the gravel pit are assumed to be proportional to the drainage areas above the two sites. According to Leopold, Wolman, and Miller (p. 251, 1964), the flood or bank-full discharge can be expressed as a power function of drainage area and the exponent of the equation varies from 0.65 to 0.8. For mean annual flow in humid regions, the exponent is about 1.0. In this study, a value of 1.0 is assumed. This assumption was also adopted by Camp Dresser and McKee (January, 1978). Figure 11-19 shows the plot of the flood frequency of peak flows for the two locations on San Juan Creek noted on the inset map on the figure. Location 1 is along San Juan Creek approximately at the upper edge of the gravel pit, and downstream of the Verdugo Canyon. Location 2 is at the U.S.G.S. gaging station. Our results are very close to those of Camp, Dresser and McKee (January, 1978).

Design Storms. Comparison of the 1969 flood hydrographs with the theoretical 100-year hydrographs by Camp Dresser and McKee for San Juan Creek immediately above the Conrock gravel pit was made by Camp Dresser and McKee (January, 1978) and is shown in Figure 11-20. As pointed out by Camp Dresser and McKee, the natural flood hydrographs may be of substantially longer duration than the classical hydrographs estimated by usually theoretical methods (Soil Conservation Service and Orange County Flood Control District). These floods may be capable of transporting considerably more sediment than the shorter duration floods utilizing the identified theoretical methods. For an adequate analysis of erosion and sedimentation, a better estimation of hydrograph shape is essential.

The best way to predict the flood hydrographs for the study site is to employ a more advanced theoretical approach involving rainfall-runoff relationships and numerical modeling techniques, such as the one developed by Simons et al. (1977). However, due to time and money constraints, a more practical means is used for estimating the hydrograph shapes for floods with various return periods. This method involves the development of a typical hydrograph normalized with respect to the flood peak. Figure 11-21 shows that the normalized hydrographs based on available data are sufficiently close and the hydrograph of January 25, 1969 is selected as the typical hydrograph. Design storms with different return periods are then estimated based on peak flow determined by Figure 11-8 and the typical hydrograph shown in Figure 11-21. The storm hydrograph on March 4, 1978 was not reported by the U.S.G.S. Only the peak discharge at Capistrano was given and it was estimated to be 12,000 cfs utilizing the slope-area method. The above-mentioned method was also used to obtain a hydrograph for the flood event of March 4, 1978.

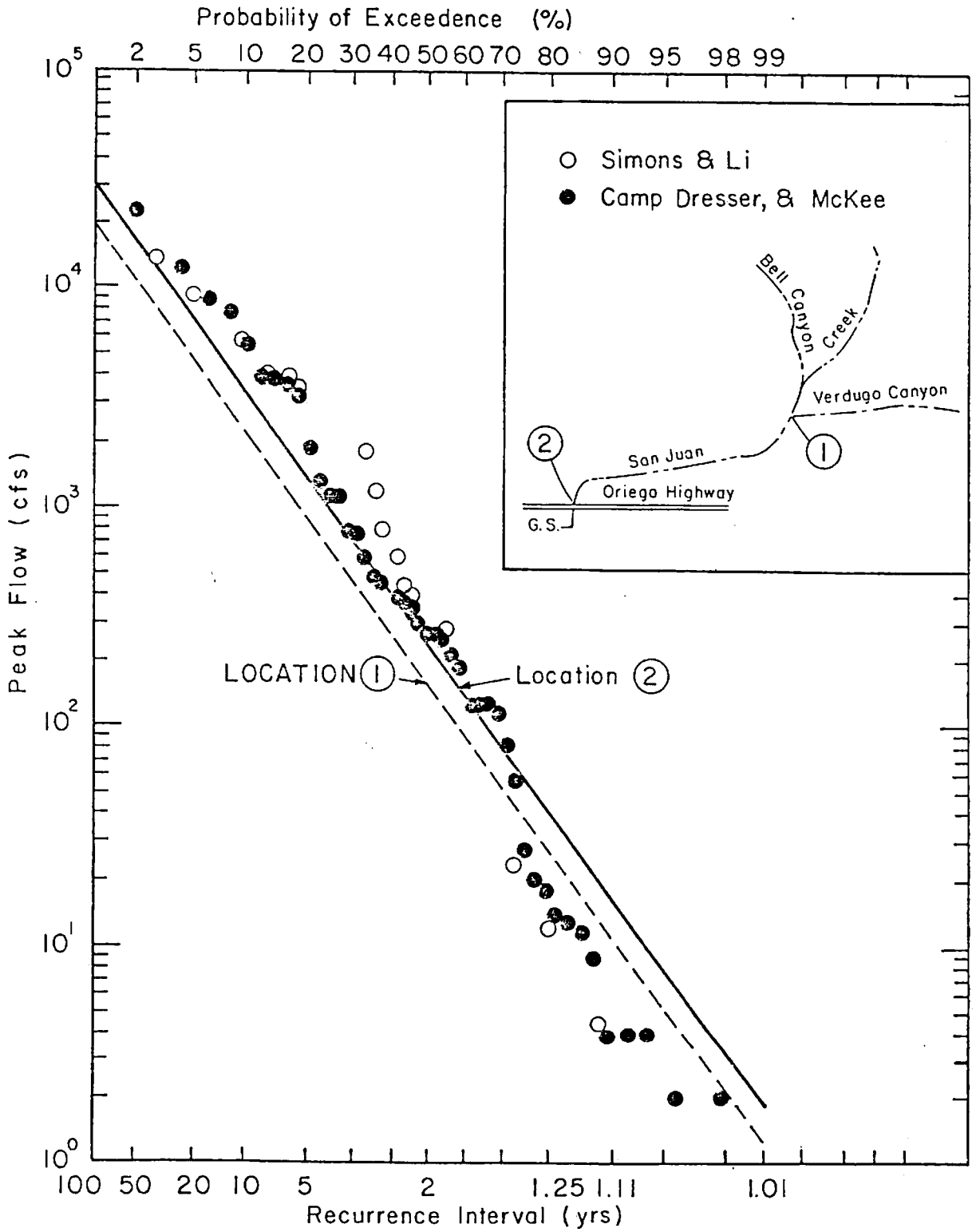


Figure 11-19. Frequency discharge relatonship for San Juan Creek (after Camp Dresser and McKee).

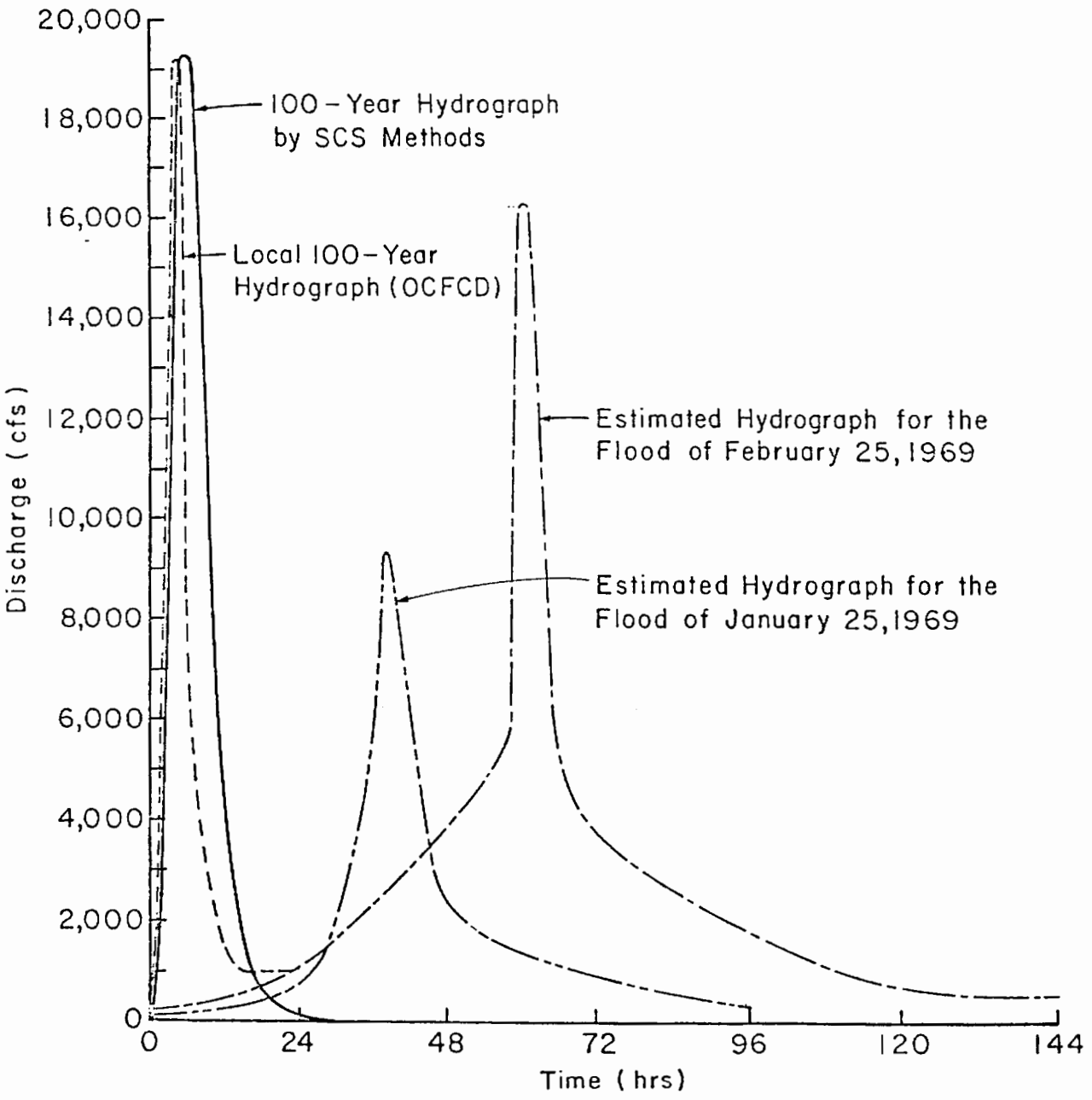


Figure 11-20. Comparison of the 1969 flood hydrographs with the theoretical 100-year hydrographs for San Juan Creek at its confluence with Bell and Verdugo Canyons (after Camp Dresser and McKee, January 1978).

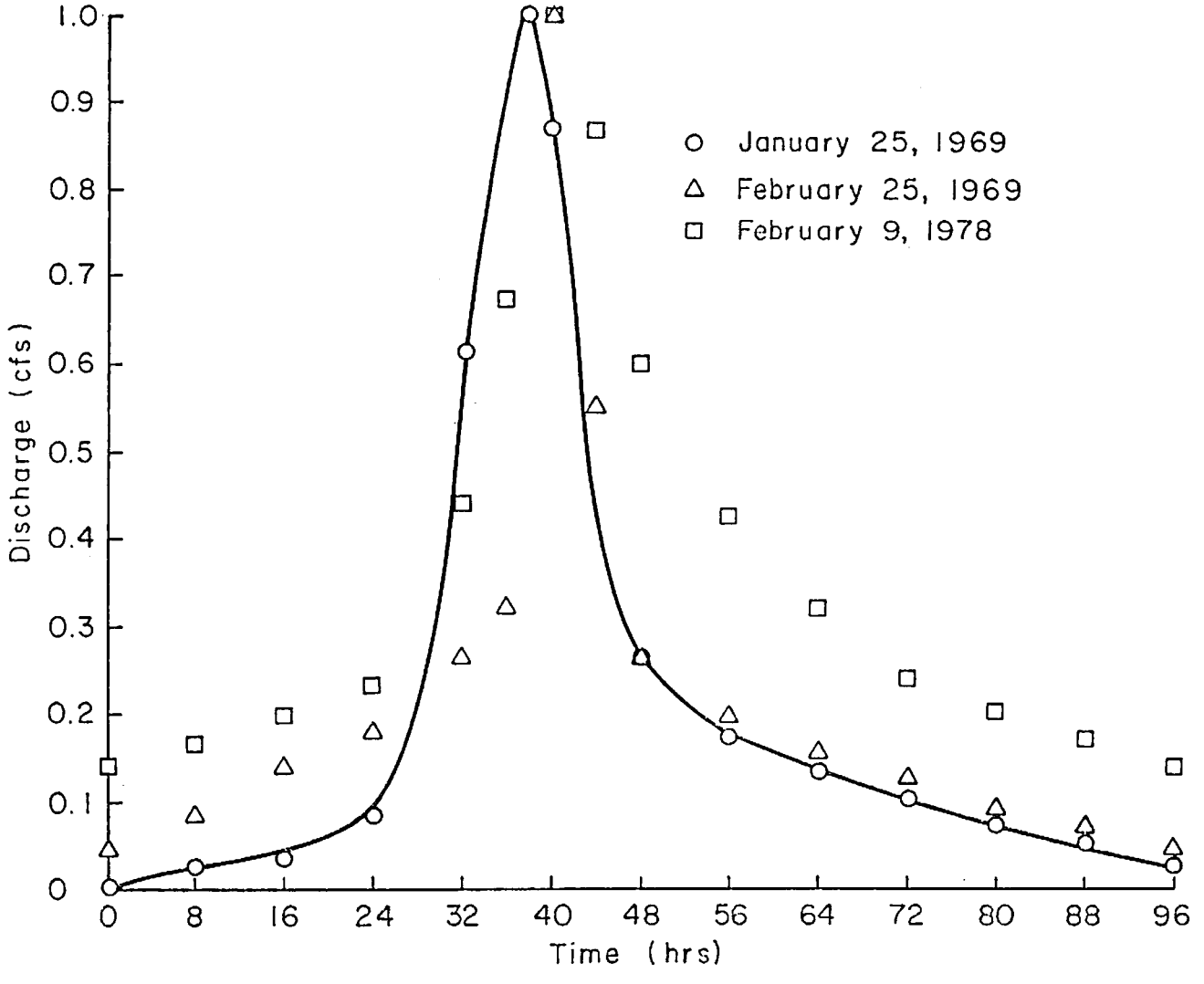


Figure 11-21. Normalized hydrographs.

Storm Events of January, February and March, 1978. Storms of January, February and March, 1978 have induced significant degradation along the San Juan Creek and Bell Canyon upstream of the Conrock gravel pit. These storms have provided considerable valuable data which should be used to test any suggested methodology for analyzing the stream and gravel pit response.

The storm of January 15 and 16, 1978 lasted about three days. It started on January 14 and ended on January 17. Measured hydrographs at the San Juan gage near Capistrano indicated very small discharges. Peak flow was only 210 cfs. It is suspected that the records were not accurate. An indirect check of the peak flow based on the material deposited in the gravel pit was made. This method utilized Shields Criterion of the incipient motion (Simons and Sentürk, 1977) with the assumption of a channel bed slope of 0.1 (the local bed slope immediately upstream of the gravel pit), a Manning's roughness of 0.03, and a channel width of 400 feet. Critical discharges large enough to move a specific size of sediment were determined. According to Camp Dresser and McKee (March, 1978), the coarsest particle of the material in the gravel pit after the January, 1978 storm was between 75 mm and 100 mm. Theoretical evaluation indicates that critical discharges to move the particle sizes between 75 mm and 100 mm range from 200 cfs to 300 cfs. These values are close to those measured near Capistrano. Thus, measured hydrographs near Capistrano were used to determine the hydrographs for the gravel pit. The small quantity of runoff resulting from large quantities of rain may be due to dry antecedent moisture conditions. A further study to relate rainfall and runoff relation is needed to develop more accurate information.

The storm of February 9-10, 1978 started on February 8, 1978 and ended on February 15, 1978. This storm was of a very long duration with two flow peaks. The hydrographs just upstream of the gravel pit were directly scaled from those measured near Capistrano utilizing the ratio of drainage areas.

The storm hydrograph of March 4, 1978 was unavailable. The estimated flow peak near Capistrano was between 10,000 to 13,500 cfs. A value of 10,500 cfs was adopted for this study (the peak flow entering the gravel pit is 7,600 cfs). Having the peak flow identified, the hydrograph was estimated by normalizing the hydrograph as described earlier.

The storm hydrographs of January, February, and March, 1978 are given in Figures 11-22, 11-23 and 11-24. These hydrographs were used in the validation of the developed mathematical model.

Stream and Gravel Pit Geometry

Detailed discussions of stream and gravel pit geometry have been presented by Camp Dresser and McKee (January and March, 1978). Measured profiles before and after each of the storms that occurred in early 1978 are plotted in Figure 11-25. For evaluation, a simplified geometry was assumed for the condition prior to the 1978 storms. The simplified geometry is given in Figure 11-26. This simplified geometry is very

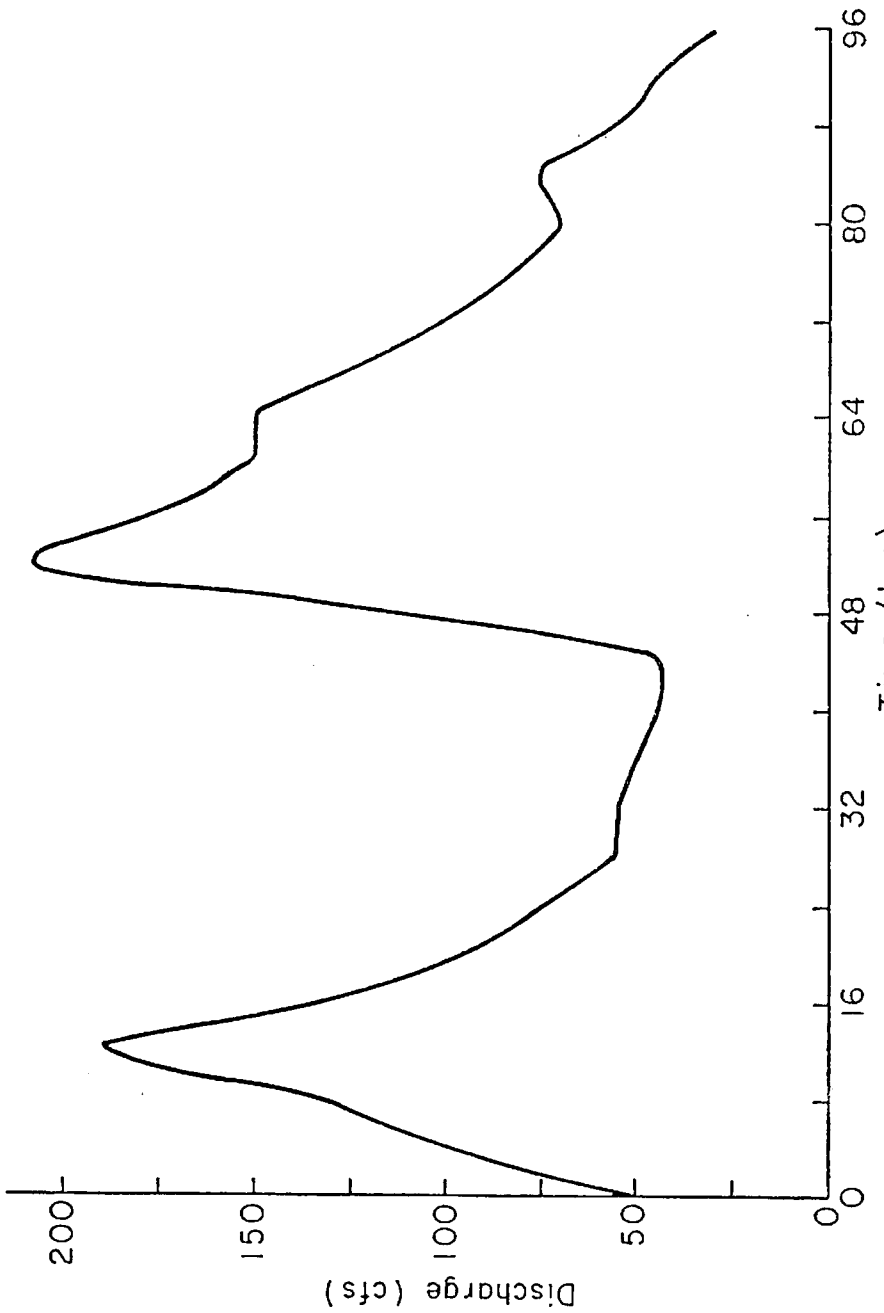


Figure 11-22. Storm hydrograph of January 1978.

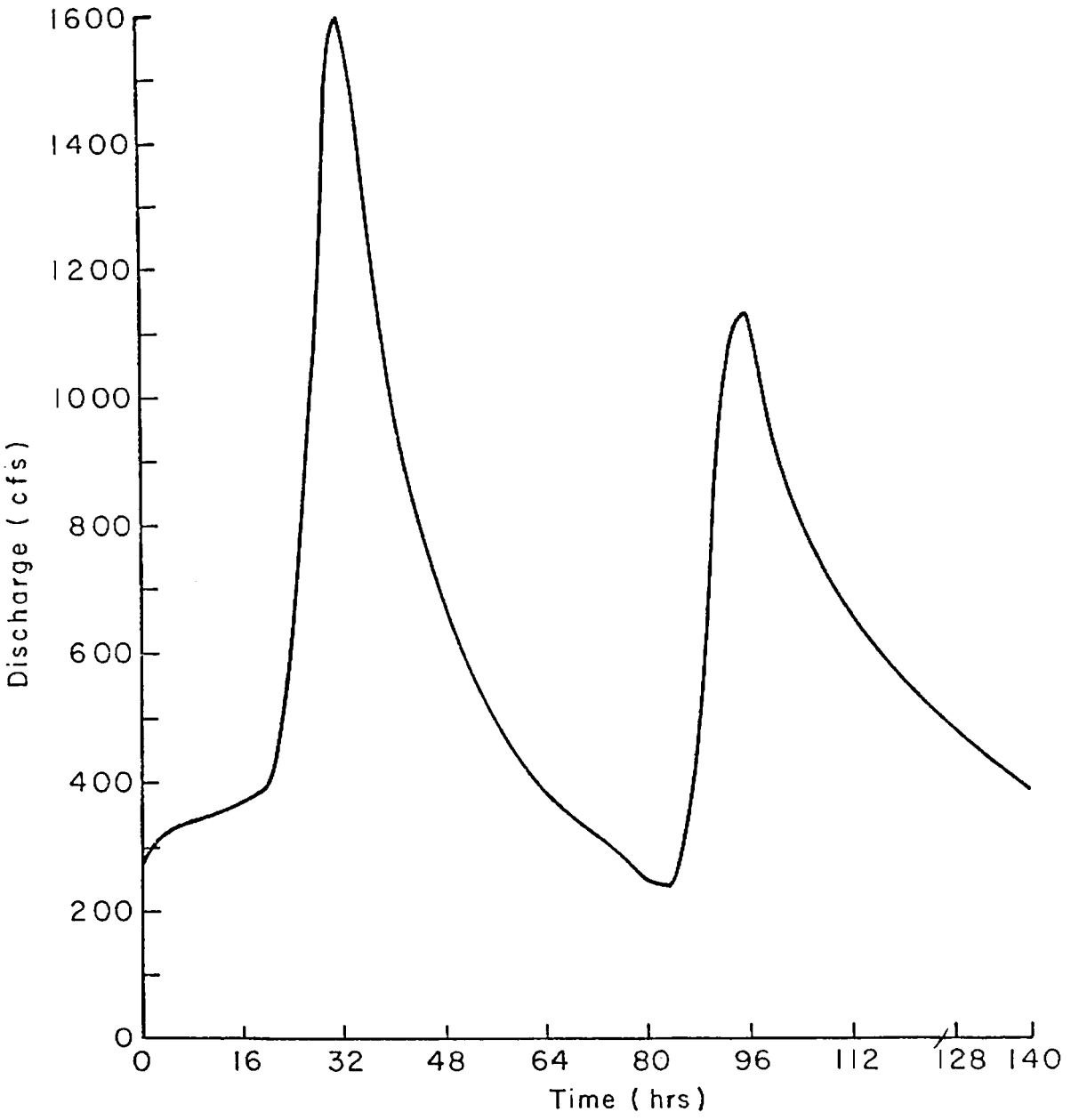


Figure 11-23. Storm hydrograph of February 1978.

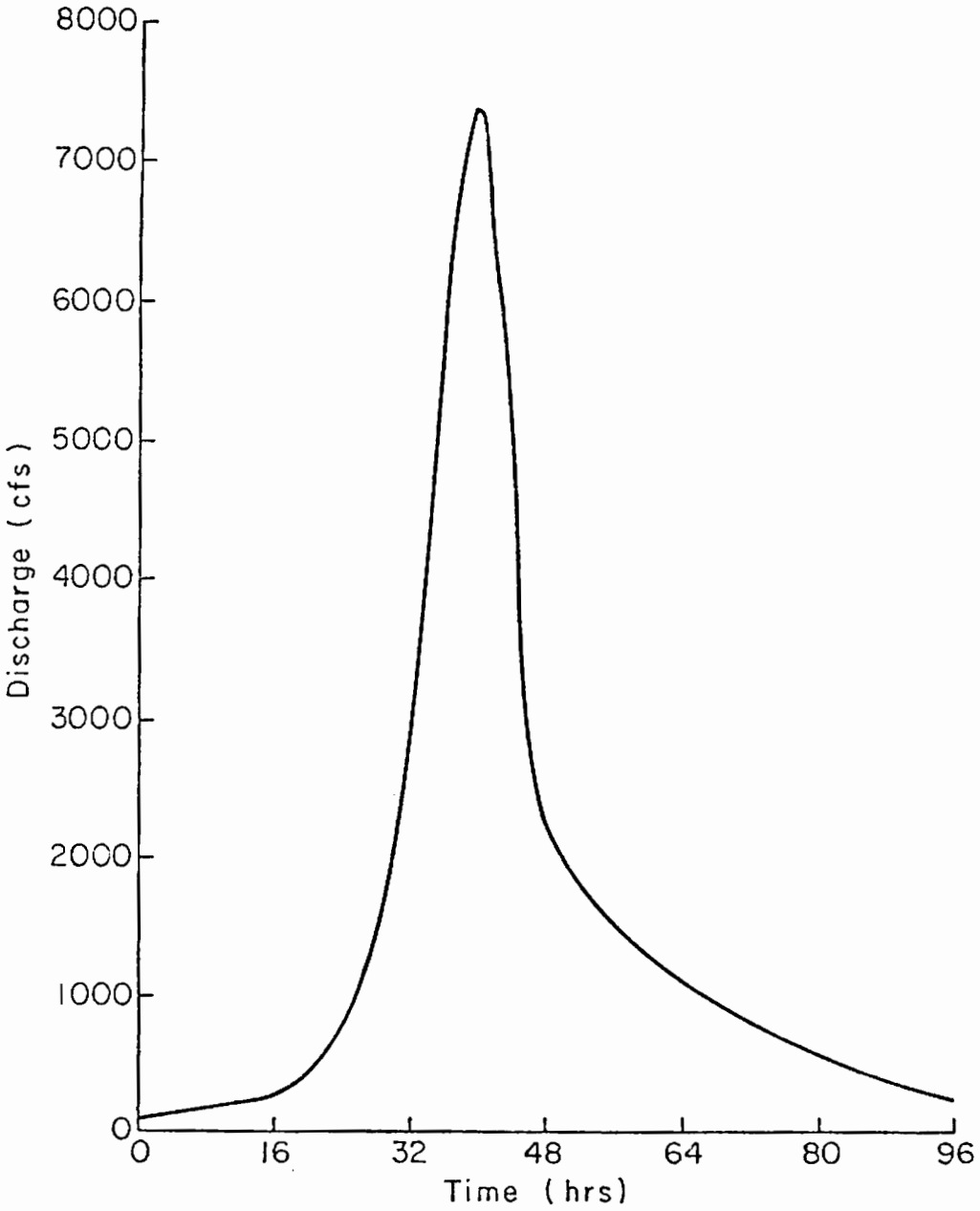


Figure 11-24. Storm hydrograph of March 1978.

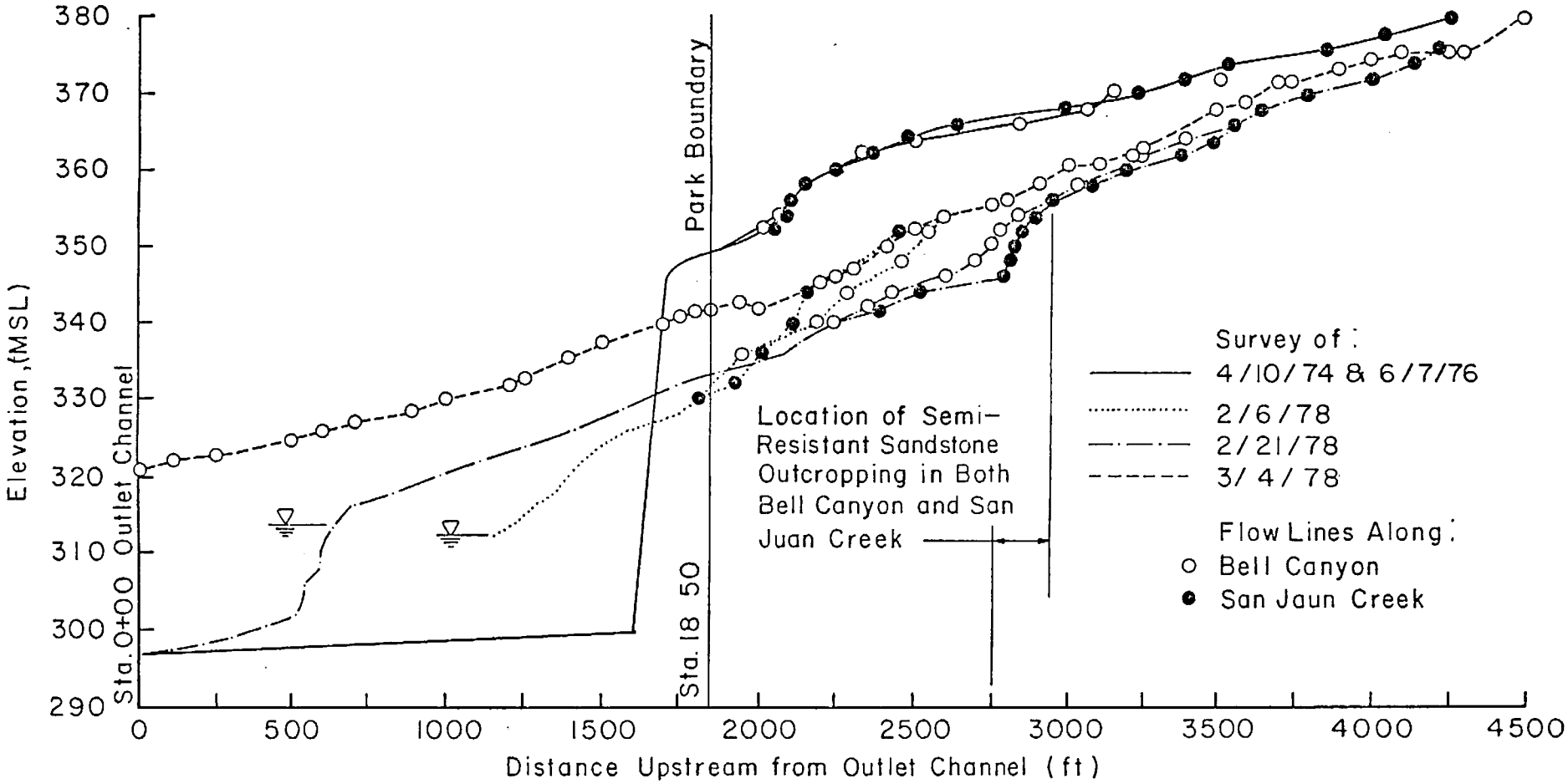


Figure 11-25. Measured bed profiles.

close to the actual conditions. The assumption of a 650-foot width in the gravel pit is consistent with the estimated volume of 6,500,000 tons of gravel and sand excavated since 1969. Assumption of a 400-foot width in San Juan Creek is consistent with the degradation width after the February 1978 storm. Width of channel usually increases during the degradation process, especially if there is erosion-resistant material and heavy armor on the bed. Dr. Mostafa (1978) assumed that the final channel width could reach 600.0 feet. Assumption of 400.0-foot width is appropriate for an average condition. In reality the channel is divided into three branches: San Juan Creek, Bell Canyon, and Verdugo Canyon shortly upstream of the Casper Regional Park boundary. Verdugo Canyon contributes only about 5 percent of total flow and is also limited in degradation due to a culvert that serves as a control. For all practical purposes Verdugo Canyon can be omitted from the analysis. The 400.0-foot width channel above the confluence of Bell Canyon and San Juan Creek implies that the sum of widths of these two creeks is 400.0 feet.

Based on the report by Camp Dresser and McKee (March, 1978) and the information provided by Dames and Moore, the channel and pit geometry after each of the storms occurring in early 1978 were compiled. Figure 11-26 shows the profile after each storm. Elevations at the original pit boundary and bed slopes are tabulated in Table 11-2. Measured data show that elevation at the original pit boundary (Station 16+00) was 327.0 feet after the January 1978 storm, 331.0 feet after the February 1978 storm, and 338.0 feet after the March 1978 storm.

Table 11-2. Geometry after 1978 storms.

| Storms | Elevation at the Original Pit Boundary (Station 16+00) (ft) | Average Bed Slope |
|---|---|---|
| January 1978 | 327.0 | 0.0310 |
| February 1978 | 331.0 | 0.0150 |
| March 1978 | 338.0 | 0.0118 |

Flow Resistance Coefficient

It is difficult to accurately estimate resistance to flow for a gravel channel. The size of gravel forming the streambed can change greatly as a consequence of degradation and aggradation processes. Resistance to flow changes accordingly.

Sediment Transport and Yield

Determination of sediment discharge is a difficult task but is the most important step in fluvial analysis of streams. Due to highly heterogeneous distribution of bed material, application of a transport highly heterogeneous distribution of bed material, application of a transport equation by size fraction is necessary for an adequate analysis.

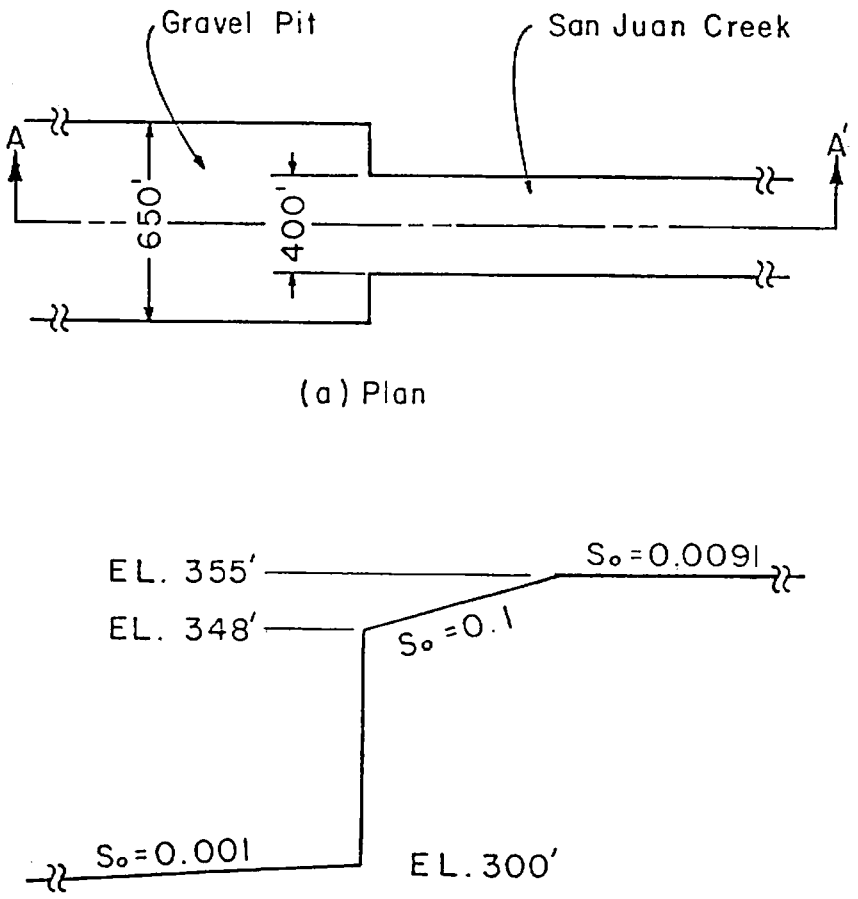


Figure 11-26. Simplified geometry before 1978 storms.

Representative Bed Material Size. Bed material samples of San Juan Creek were collected and analyzed by Dames and Moore. Size distributions of surface material was very uniform. Figure 11-27 shows that distribution of three composite samples is similar. The composite Sample A was selected as the typical bed material along the San Juan and Bell Canyon channels upstream of the gravel pit. Median diameter and gradation coefficient of the composite Sample A are very close to those averaged from the individual samples. Size distributions of transported material during two 1969 floods were determined from the samples in the gravel pit collected in 1976. The size distribution curve is shown in Figure 11-28.

Sediment Transport Rates. Available data on sediment transport rates either in the laboratory flumes or in the field have been collected in relatively flat channel systems and with a uniform sediment. Most of the available sediment transport equations are applicable for these conditions. Recent laboratory studies at Colorado State University by Li et al. (1977) on steep channel (5 percent to 25 percent bed slope) and gravel bed sediment transport indicated that a form of Meyer-Peter, Müller sediment transport equation is applicable for steep gravel bed streams. However, coefficients should be calibrated using measured data. The original Meyer-Peter, Müller equation accounts for the bed load only. The suspended portion of the bed material load plus the wash load delivered from upland area makes the coefficient of the transport equation larger than that originally proposed by Meyer-Peter, Müller.

According to Camp Dresser and McKee (January 1978) report records furnished by Conrock showed that in three years (1966 to 1969) 1,204,000 tons of sand and gravel were produced and sold. During these years, records of the U.S. Geological Survey at Highway 74 showed that the runoff was modest. It was assumed that the volume of the pits before the 1969 floods (Figure 11-26) represented the 1,204,000 tons of sediment. Thus the amount deposited by the flows of 1967 and 1978 was ignored. The above assumption of sediment yield produced by two 1969 floods was used to calibrate the sediment transport equation. The bulk rate of sediment was assumed to be 1.5. Calibrated results were then used later to validate the mathematical model using the 1978 floods. Figure 11-27 shows that the estimated size distribution of transported material is close to the measured. As a further check of validity of the developed discharge-sediment rating relation, a comparison of computed total sediment discharges with those determined by U.S.G.S. (1969) was made. Figure 11-29 verifies a good comparison of sediment discharge rates except the computed values are consistently higher than those determined by the U.S.G.S. It should be noted that sediment discharges computed in this study are total bed material loads upstream of the Conrock pit using a bed slope of 0.0091, width of 400 feet, and bed material size as shown in Figure 11-27, while the sediment discharge rates determined by the U.S.G.S. were made at the bridge on Highway 74 using measured suspended data.

Sediment Yields. The method of determining sediment transport developed in this study requires an additional assumption of a very large sediment supply from the upland area in order to determine the

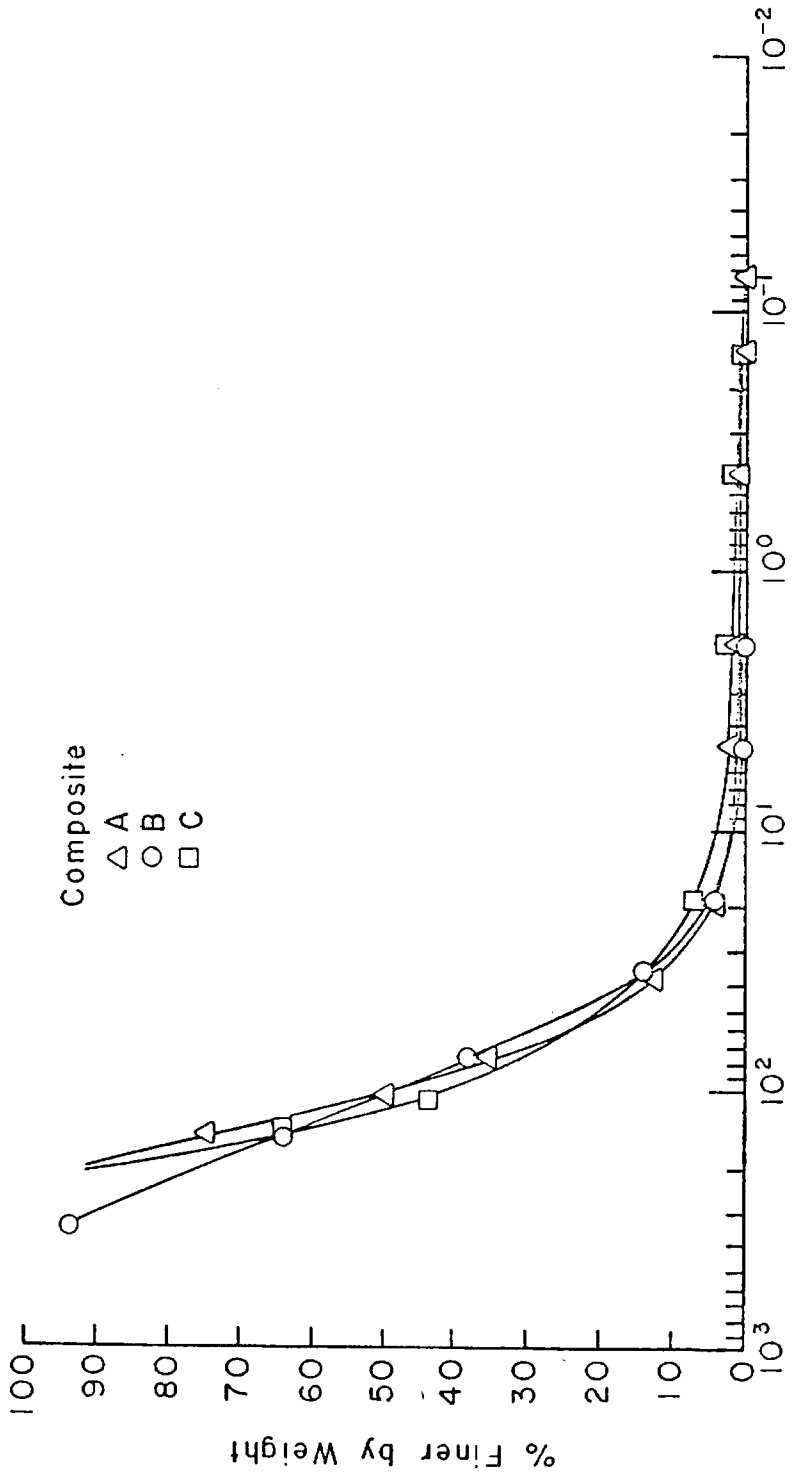


Figure 11-27. Size distribution of bed material in San Juan Creek.

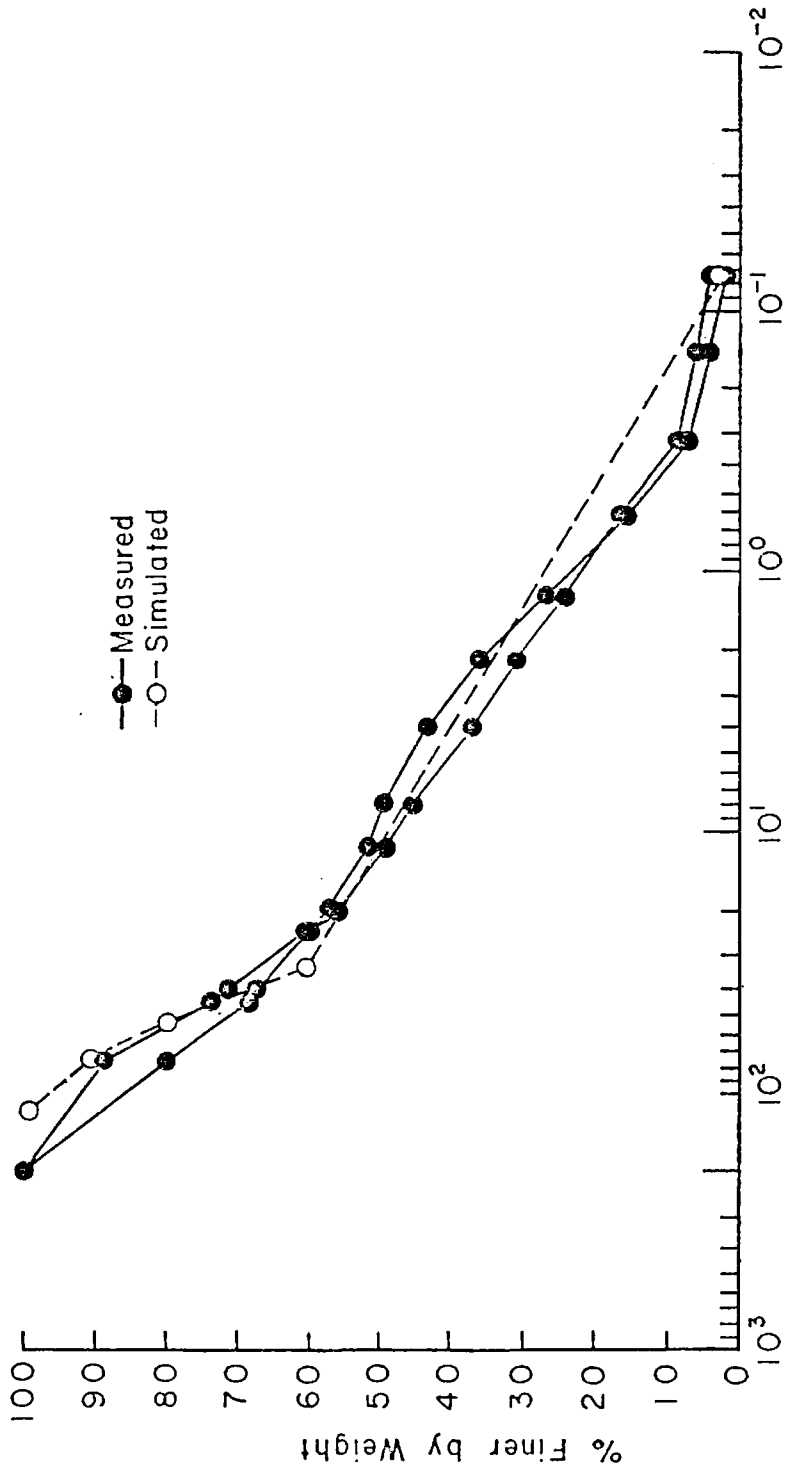


Figure 11-28. Size distribution of material in the gravel pit collected in 1976.

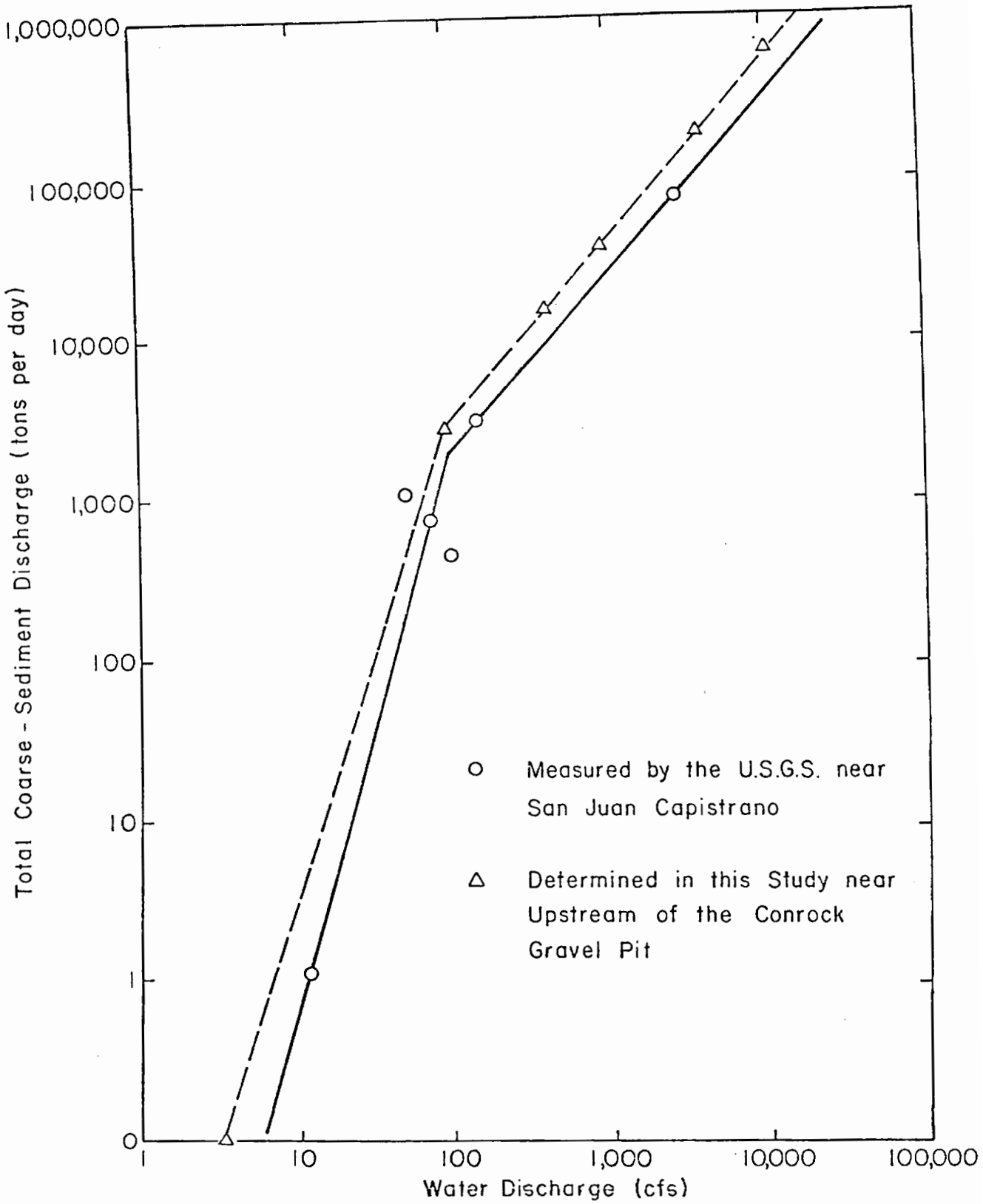


Figure 11-29. Relation between water discharge and total coarse-sediment discharge, San Juan Creek near San Juan Capistrano, California (after U.S.G.S., 1969).

sediment yield. According to the reports by Converse Davis Dixon Associates, Inc. (February and March 1978) ample sediment is available from the upland watersheds due to landslides and fire based on past records and geological information. Thus, the assumption of a large amount of sediment supply from upland area is reasonable. Hence, sediment yield during flood events is only limited to the channel carrying capacity.

Estimated sediment yields for floods with frequencies of 2, 5, 10, 15, 20, 25, 50, and 100 years are given in Table 11-3. The median size of flood has a return period of two years. For 42 years of records (1928 to 1969), average water yield upstream of the gravel pit is 7300 acre-feet. Thus, the average number of median size floods is 22.7 per year and the average annual sediment yield is 80,000 tons per year.

Table 11-3. Summary of sediment yield for San Juan Creek near Casper Park boundary.

| Flood Frequency (Return Period) (yr) | Peak Discharge (cfs) | Flow Volume (ac-ft) | Sediment Yield (tons) |
|---|---|---|---|
| 2 | 174 | 322 | 3,510 |
| 5 | 1,017 | 1,880 | 26,300 |
| 10 | 2,542 | 4,700 | 67,700 |
| 15 | 3,632 | 6,716 | 100,700 |
| 20 | 5,085 | 9,397 | 150,300 |
| 25 | 8,354 | 15,448 | 285,100 |
| 50 | 12,712 | 23,506 | 509,100 |
| 100 | 21,792 | 40,296 | 1,110,800 |

## Mathematical Model

Governing Processes. Degradation or head-cut upstream of the pit and deposition of material in the pit occur simultaneously. since this problem is very complicated, simplifying assumptions are needed to obtain solutions in a practical and economical way. The dominant physical processes include water runoff, sediment transport, sediment routing, degradation, aggradation, breaking and forming of the armor layer, etc. These processes are unsteady in nature. In order to simplify the problem, a known discharge assumption is used. The known discharge solution is appropriate in this study because of the short distance considered in the space. As mentioned earlier, for simplicity a simplified geometry representation as shown in Figure 11-26 was used.

Referring to Figure 11-30, temporal resolution of the degradation and aggradation processes considered in this study was treated in two separate conditions. For condition (a) transport rate in Zone II is much larger than in Zone I due to the local steep gradient (assuming a

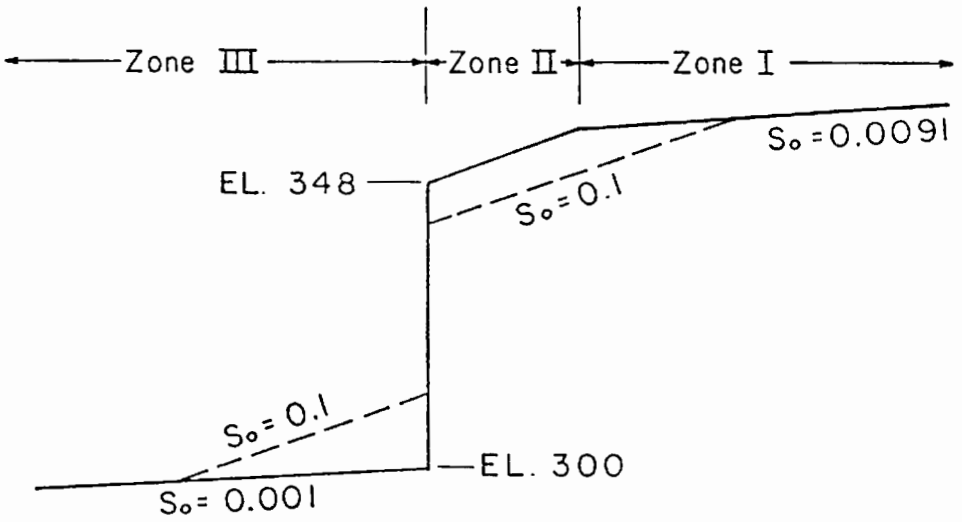


(a) Before the Joining of the Reaches Experiencing Degradation and Aggradation.

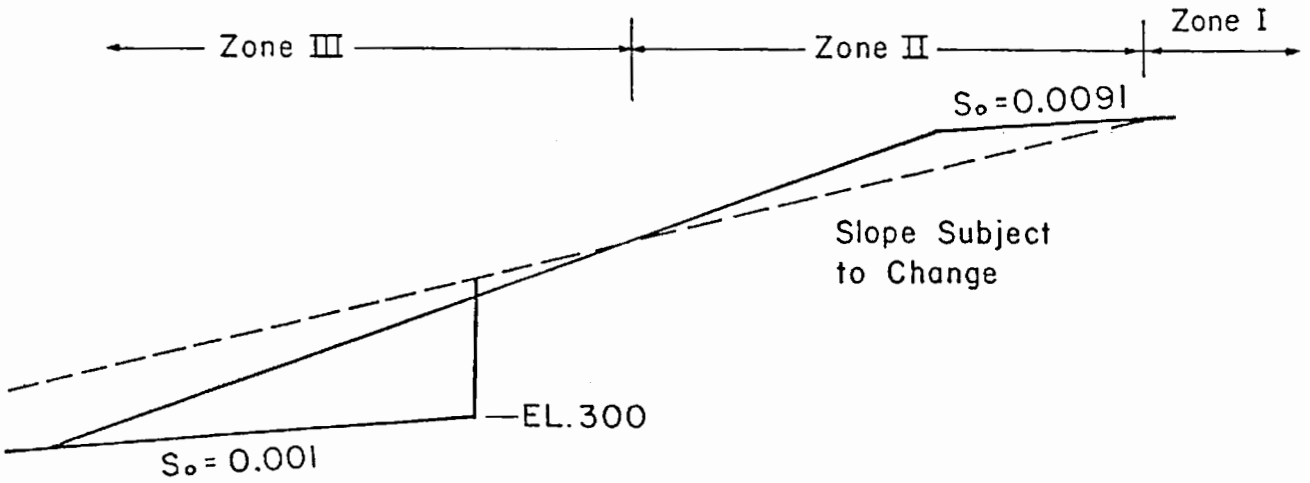


(b) After the Joining of the Reaches Experiencing Degradation and Aggradation.

Figure 11-30. Sketch of degradation and aggradation processes.

slope of 0.1 estimated from the bed profile prior to 1978 storms) and destruction of the armor layer on the bed of the channel. Degradation occurs in this reach. The bed material size of Zone II is assumed to be a mixture of the surface size distribution (Figure 11-27) and the size distribution described in the pit (Figure 11-28). The deposition and forming of a delta takes place in Zone I due to its negligible transporting capacity. The difference in sediment transport rates in Zones I and II for an increment of time would determine the new elevation of the downstream end of channel assuming a bed slope of 0.01. The growth of the delta can be determined as the amount of material transported into the pit. For simplicity, slope of delta is assumed to be 0.10 based upon the slope from the head of delta or shown after the February 9-10, 1978 storm. No lateral slope was assumed. As soon as the elevations of degrading and aggrading reaches meet, bed slope flattens as shown for conditions, (b) Under this condition, the delta grows both upstream and downstream and degradation should continue as evidenced by conditions after the February 1978 and March 1978 floods. The slope becomes flatter and the degree of degradation is reduced but it still proceeds slowly. The new slope and extent of degradation and/or aggradation were computed based on the difference in sediment transporting capacities in difference zones. The sediment transport rate in Zone II changes with the change in bed slope. Eventually, the pit should fill with new material if gravel mining is discontinued.

Simulation was made using time steps of four hours. The time lapse changes of elevation at the original gravel pit boundary (Station 16+00) are given in Figure 11-31. The simulation results are excellent when compared with field measurements. The comparison of simulated elevations and bed slopes with measured data (Table 11-2) are given in Table 11-4. Again, the results are excellent. One point worth mentioning is that the simulated results are the predicted results utilizing the calibrated sediment transport parameters based on the data of two 1969 storms.

Table 11-4. Comparison of simulated and measured results.

| Storms | Elevation at the Original Pit Boundary (Station 16+00) ft | | | Average Bed Slope | | |
|---|---|---|---|---|---|---|
| | Simulated | Measured | Error % | Simulated | Measured | Error % |
| January 1978 | 326.4 | 327.0 | 0.2 | 0.0339 | 0.0310 | 9.4 |
| February 1978 | 332.2 | 331.0 | 0.4 | 0.0138 | 0.0150 | 8.0 |
| March 1978 | 337.3 | 338.0 | 0.2 | 0.0110 | 0.0118 | 7.0 |

Evaluation of Design Alternatives

With the validated sediment transport equation and mathematical model, four engineering alternatives that consider rehabilitation of the Casper Regional Park and allow mining of sand and gravel are evaluated.

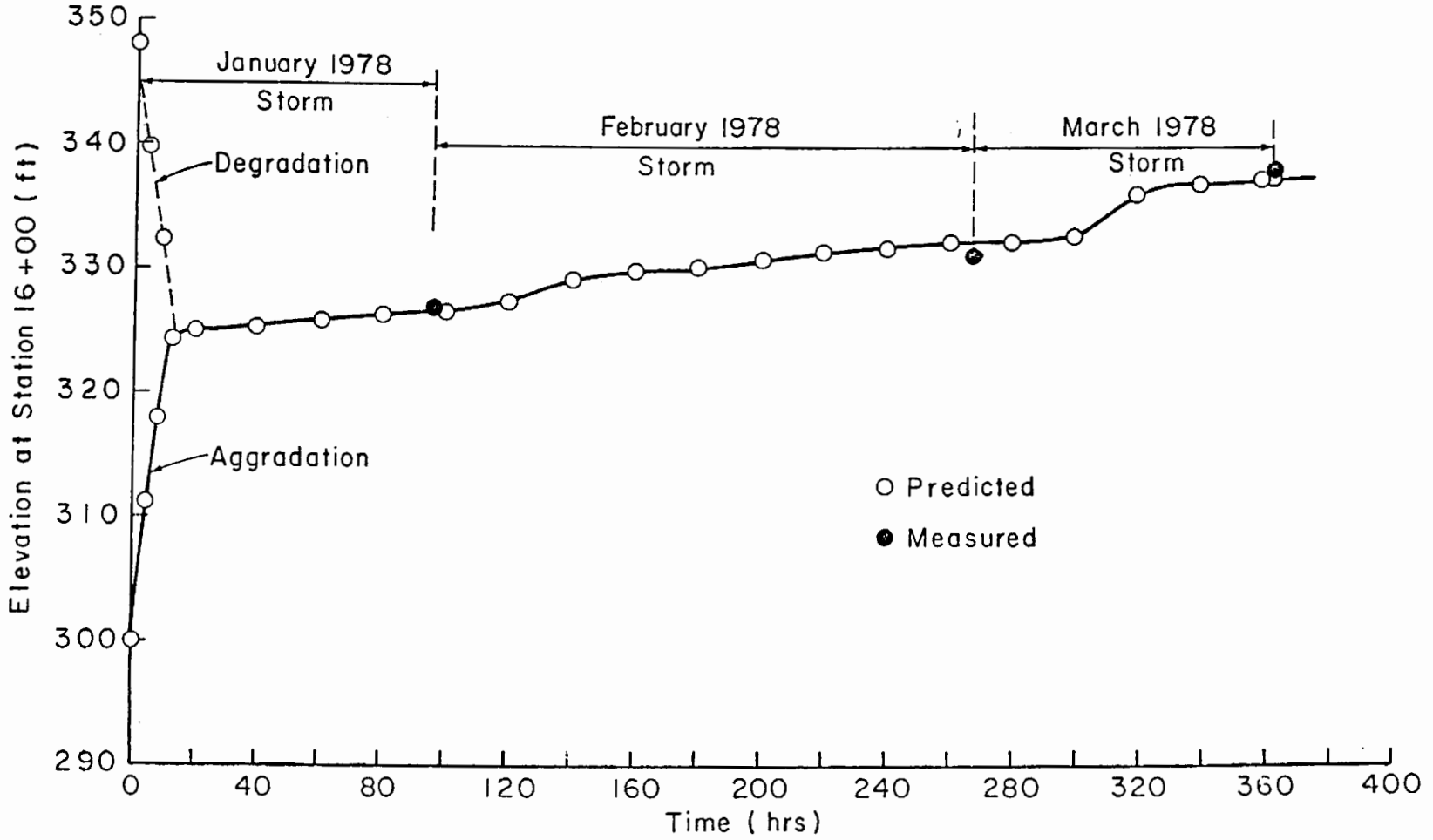


Figure 11-31. Time lapse changes of elevation at the original gravel pit boundary (Station 16+00).

Analysis in this study is simply to identify the most feasible solution, no attempt is made to provide detailed hydraulic design of the proposed structure. Results of the evaluation follow.

Alternative I. This is a "do nothing" and without gravel mining alternative. Applying this alternative, the gravel pit would be gradually filled up, the delta will continue to grow, and aggradation will complete restoration of grades to approximately original slopes in 75 years under average conditions. The above estimation was made by assuming an average annual sediment yield of 80,000 tons to fill the available space of 6,000,000 tons. Elevations of Station 16+00 after occurrence of individual storms with different return periods are given in Table 11-5. Available space for gravel is so large that it even requires approximately six 100-year floods to fill it up. Restoration of Casper Regional Park by natural processes requires a long period of time unless some large flood events occur in the future.

Table 11-5. Alternative I subject to floods with various return periods.

| Flood Frequency (Return Period) (yr) | Peak Discharge (cfs) | Flow Volume (ac-ft) | Elevation at the** Original Gravel Pit Boundary (Station 16+00)(ft) |
|---|---|---|---|
| 2 | 174 | 322 | 337.3 |
| 5 | 1,017 | 1,880 | 337.7 |
| 10 | 2,542 | 4,700 | 338.3 |
| 15 | 3,632 | 6,716 | 338.7 |
| 20 | 5,632 | 9,397 | 339.3 |
| 25 | 8,354 | 15,448 | 340.8 |
| 50 | 12,712 | 23,506 | 342.6 |
| 100 | 21,792 | 40,296 | 346.1 |

*Without gravel mining operation
**Start with computed elevation at 337.3

Alternative II. This alternative allows the continuation of gravel mining while providing the opportunity to heal degradation in Casper Regional Park naturally. The expected rate of gravel and sand mining is 1,000,000 tons per year. If additional supply after the March 4, 1978 storm is negligible, the gravel pit would be excavated within approximately three years to the geometry similar to that prior to the 1978 storms. Aggradation rate in the Casper Regional Park would be very slow, because the annual excavation rate is close to that produced by a 100-year flood event. Furthermore, some additional head cut should be expected along the current bed profile. Assuming that gravel pit dimensions after the removal of sand and gravel are similar to those prior to 1978 storms, the new head cut elevations at Station 16+00 for

various sizes of storms are given in Table 11-6. This alternative would induce worse problems that the Alternative I and certainly require a much longer period of time to restore the Casper Park.

Table 11-6. Alternative II and subject to floods with various return periods.

| Flood Frequency (yr) | Peak Discharge (cfs) | Flow Volume (ac-ft) | Elevation at the* Original Gravel Pit Boundary (Station 16+00)(ft) |
|---|---|---|---|
| 2 | 174 | 322 | 317.8 |
| 5 | 1,017 | 1,880 | 320.3 |
| 10 | 2,542 | 4,700 | 322.9 |
| 15 | 3,632 | 6,716 | 324.4 |
| 20 | 5,085 | 9,397 | 326.1 |
| 25 | 8,354 | 15,448 | 329.3 |
| 50 | 12,712 | 23,506 | 332.5 |
| 100 | 21,792 | 20,296 | 336.5 |

*With gravel operation
**Start with computed elevation at 337.3

Alternative III. This alternative would construct a drop structure near Station 16+00, approximately 250 feet downstream of the Conrock property line. The proposed structure would be a gabion check dam with crest elevation of approximately 355 feet. The equilibrium slope upstream of the dam would be close to the original gradient. If an equilibrium slope of 0.91 percent is assumed, it would provide a space for trapping approximately 1,870,000 tons of sediment and would take approximately 23 years, under average conditions, or two 100-year floods to fill up the degraded area completely. If the crest elevation of the drop structure is set at 348 feet it would take approximately nine years under an average rate to fill the sediment behind the structure. Although this alternative would allow continued gravel mining and provide the opportunity to heal the San Juan Creek and Bell Canyon gradually, the rate of restoration is still too slow. This would also terminate the gravel and sand supply to the gravel pit for a long time. This alternative is not attractive for the above reasons. A series of small dams to restore the park locally and control any further degradation may be a better alternative.

Alternative IV. This alternative would construct a series of small gabion check dams across San Juan Creek and Bell Canyon at space intervals. This arrangement would allow the stream to restore from degradation locally and to control any further head cutting. The proposed

engineering plan is shown in Figure 11-32. The three check dams are 2.5 feet high, approximately 1,400 feet apart, and each would trap approximately 37,300 tons of sediment if an equilibrium slope of 0.91 is assumed. This amount of sediment is close to one-half of the average annual sediment yield, thus, on the average, these three check dams would be filled up after approximately one and one-half years. This would be prior to the depletion of the sand and gravel in the pit and would continue to provide sand and gravel to the Conrock Pit. Of course, if any flood events larger than a 15-year return period occurs, the check dams would be filled up and the Conrock Pit would receive a supply of gravel and sand. After the Conrock Pit receives enough sand and gravel supply for another one and one-half years of operation, then the check dams can be built approximately 2.5 feet higher until the grade of the most downstream check dam has an elevation of about 355 feet. This requires the construction of 21 check dams over seven time periods. This scheme would first allow the stream to restore from degradation locally and to control any further head cutting and would eventually restore the degradated reach. In the meantime, the scheme still provides the supply of sand and gravel. Furthermore, this alternative would spread the capital cost of construction over a period of at least 30 years. This is the most feasible alternative.

The construction of the access road crossing in San Juan Creek is required for the park usage. This access road can be designed in such a way that it will also serve as a check structure. In addition, a low check structure can be implemented near the mouth of Bell Canyon to restore the canyon. The check dams for the access road and near the mouth of Bell Canyon would be approximately 10'0" high. In order to stabilize the gravel pit, an additional low check structure is required near Station 16+00. The available space upstream of the access road will trap approximately 600,000 tons of sediment. It will take about 7.5 years to restore the creek and the canyon, or one flood event with a return period longer than 50 years. In order to prevent further cutting, slope protection in the form of riprap would be required on the sharp bends in Bell Canyon and San Juan Canyon. Again, this scheme would allow the protection of the channel from further cutting and the restoration of the park in a reasonable period of time.

## Summary

This chapter reviews the classification of flood routing methods. Discusses the numerical methods and presents two examples of application of water and sediment routing techniques to real-world problems.

An introductory treatment of the properties of numerical solutions is given in this chapter. Difference equations are discussed in the context of the differential equations from which they are derived. The order of error of several finite difference operators of $\partial\phi/\partial x$ is calculated by using Taylor series. A finite difference scheme is defined as a computational molecule consisting of one or more finite difference operators. Difference schemes are classified into explicit and implicit.

Stability and convergence are discussed by focusing on the concepts of roundoff errors and discretization errors. Stability is related to

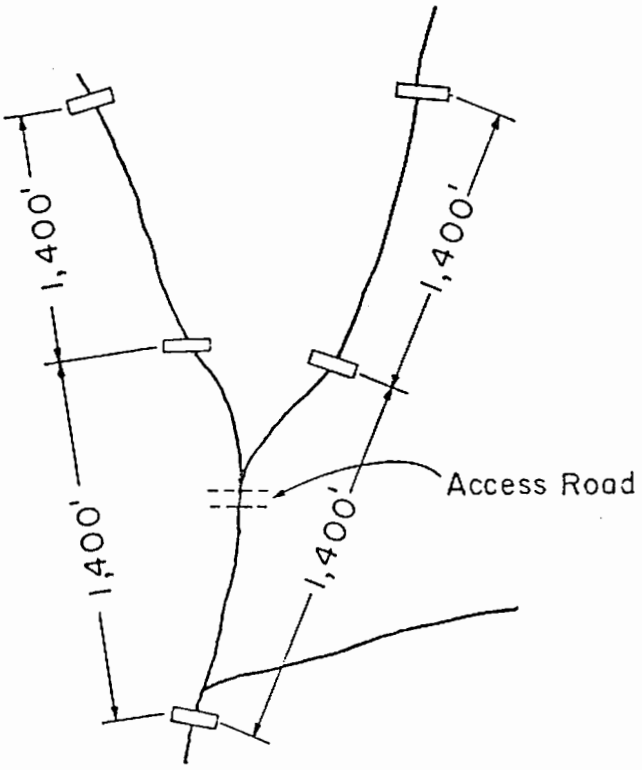


(a) Plan

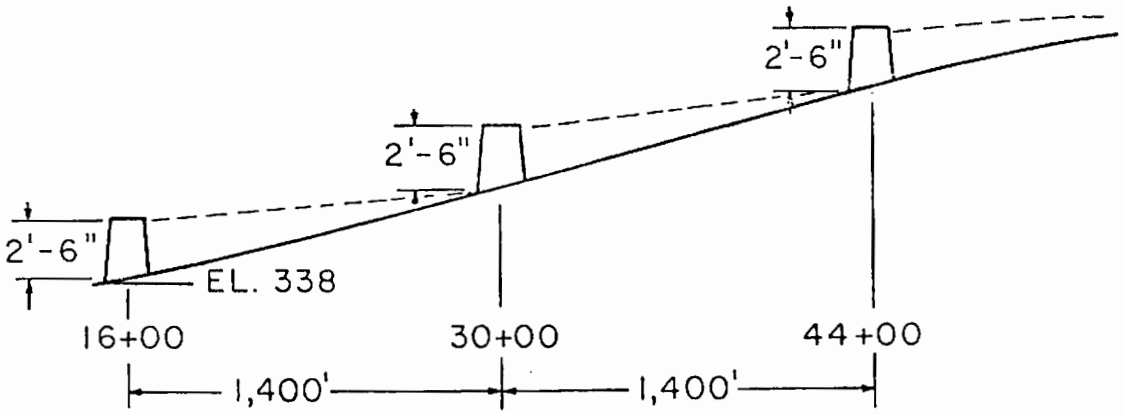


(b) Profile

Figure 11-32. Proposed engineering plan for Alternative IV.

roundoff error; convergence, to discretization error. An overview is given of the stability and convergence properties of finite difference schemes. Emphasis is placed on the difference between explicit and implicit schemes.

A mathematical model for routing sediment by size fraction was successfully developed and was utilized to estimate the local and general scour below an emergency spillway and to estimate the erosion and deposition response of the stream and gravel pit subject to different hydrologic inputs and operational alternatives.

## REFERENCES

Agricultural Research Service, 1976, Control of water pollution from cropland, Volumes I & II, Agricultural Research Service and Environmental Protection Agency, June.

Camp Dresser and McKee, 1978, Preliminary analysis of flood hazards resulting from an intermediate regional flood upstream from Conrock gravel pit, San Juan Creek, Orange County, California, Pasadena, California, January 6.

Camp Dresser and McKee, 1978, Supplemental report on erosion and deposition processes in and above Conrock gravel pit, San Juan Creek, Orange County, California, Consolidated Rock Company, Pasadena, California, March 20.

Chow, V. T., 1959, Open Channel Hydraulics, McGraw-Hill Book Company.

Converse Davis Dixon Associates, Inc., 1978, Geologic investigation of erosion sedimentation factors in Upper San Juan Creek, Orange and Riverside Counties, California, February and March 20.

Cunge, J., 1969, On the subject of a flood propagation computation method (Muskingum Method), IAHR Journal of Hydraulic Research, Vol. 7, No. 2, pp. 205-230.

Leopold, L. B., Wolman, M. G., and Miller, J. P., 1964, Fluvial Processes in Geomorphology, San Francisco, W. H. Freeman and Company, 522 p.

Li, R. M., Simons, D. B., Ward, T. J., and Steele, K. S., 1977, Hydraulic model study of flow control structures, Phase I Report, prepared for USDA Forest Service, Arizona.

Liggett, J. A. and Cunge, J. A., 1975, Numerical methods of solution of the unsteady flow equations, In Unsteady Flow in Open Channels, K. Mahmood and V. Yevjevich, eds., Water Resources Publications, Fort Collins, Colorado.

Mastafa, M. D., 1978, Erosion of San Juan Creek in the Vicinity of Caspter Regional Park, Environmental Management Agency (EMA), Orange County Design Division, Consulting Engineer, Huntington Beach, California.

Peterka, J. A., 1963, Hydraulic design of stilling basins and energy dissipators, USDI Bureau of Reclamation, July.

Simons, D. B. and Sentürk, F., 1977, Sediment Transport Technology, Water Resources Publication, Fort Collins, Colorado.

U.S. Bureau of Reclamation, 1960, Investigation of Meyer-Peter, Müller bedload formula, Sedimentation Section, Hydrology Branch, Division of Project Investigations, U.S. Department of the Interior, Bureau of Reclamation, June.

USDA Soil Conservation Service, 1977, Design engineers report - T or C, Williamsburg Watershed, Site 8C, Albuquerque, New Mexico, June.

USGS, 1969, Preliminary determinations of sediment discharge San Juan drainage basin, Orange and Riverside Counties, California, Openfile Report, Menlo Park, California, by C. G. Kroll and G. Porterfield, December.

Williams, J. R., 1975, Agricultural research service report ARS-S-40, June.

# CHAPTER 12

# SURFACE WATER HYDROLOGY

## 12.1 INTRODUCTION

The management of watersheds and river basins for optimum benefit of people in general requires complete knowledge of the interrelations between ecology and environment. The watersheds' response to developments, either natural or man-induced, must be projected correctly if the goal of wise use of our natural resources is to be met. The increasing interest in predicting watershed response has accelerated progress in mathematical modeling of water hydrographs and yields. Concern for protecting the natural environment has also increased research in the field of predicting watershed sediment yields. Further, degradation, aggradation and movement of sediment and other pollutants in watersheds are closely related to water movement. In fact, no sediment yield can be adequately predicted without the knowledge of water routing and yield. This chapter describes several methodologies for calculating water yield and storm water routing from watersheds being developed at the Engineering Research Center, Colorado State University, under the general direction of Daryl B. Simons and Ruh-Ming Li.

The physical processes governing watershed response are very complicated. Many past studies have utilized a statistical interpretation of observed response data. The unit hydrograph method for solving water routing and hydraulic geometry equations for stream morphology are examples of these types of studies. It is often difficult to predict the response of watersheds to various watershed developments or treatments using these methods because they are based on the assumption of homogeneity in time and space. Mathematical modeling using the governing physical processes may be used as an alternative means of estimating the time-dependent response of watersheds, with varying vegetative covers and land use, to precipitation. The principal advantage of the mathematical simulation approach is that the parameters that are used to vary watershed response may be physically defined. Such a definition enables the user to predict changes in watershed response arising from alterations in the watershed environment. The principal disadvantage of the simulation approach in comparison to purely statistical methods is the size and complexity of simulation models. However, the speed and availability of modern computers largely answers this problem. In addition, the availability of inexpensive and powerful hand-held programmable calculators places many sophisticated simulation methods in the hands of both researchers and application-oriented engineers.

Physical process simulation models represent the system being modeled by breaking down into its respective components. By dividing a system into its respective components, "lumping" of processes or parameters can be avoided. By simulating the selected phenomena through separate components, each individual process can be analyzed and refined or altered to meet the needs of the user. Consequently, as each process component is upgraded, the model becomes more representative of the physical system. Only a limited number of physical process models are presented. However, because they are physical process component models,

the processes involved are similar between the models. Differences do exist between some components, making some models more complex or versatile than others. Two modeling approaches are described below. Later sections discuss the physical processes used in these models and outline techniques that will enable the user to prepare input data and parameters. The selected water routing approaches are: 1) a high resolution watershed storm water routing and yield model, and 2) a simplified watershed storm routing and yield model. A number of other approaches are available, but research has shown that these contain the most sensitive physical processes.

The general approaches mentioned above share essentially the same basic physical process. The main differences are in formulation, implementation and degree of detail that may be represented. The high resolution model was first developed by Li (1974) and subsequently published by Simons, Li and Stevens (1975) and updated by Shiao (1978). This model routes storm runoff water from overland flow surfaces through the channel system of a watershed. This is done using mathematical formulations of the water continuity equations and certain assumptions about the flow momentum. This model is termed high resolution because it uses a finite difference solution technique to solve for water discharge at selected times and points on the overland flow surface and channel system. The watershed can be subdivided into numerous overland flow cascade surfaces and the channel can be represented by several connected segments in this model.

The simplified models in contrast to the high resolution model require a watershed to be represented by a channel and two contributing planes or a combination of two-plane and single plane watersheds connected by a channel system. This much simpler representation of the watershed provides for easier application, but may create problems if the watershed is extremely nonhomogeneous or anisotropic. This model uses an analytic formulation to route water from the overland flow planes (Simons, Li and Eggert, 1977). Use of the single two-plane one channel model is warranted for watersheds that are fairly homogeneous and are subject to spatially constant rainfall. The combined watershed model may be used for larger, more heterogeneous drainages that may be modeled as a group of different, yet internally homogeneous, subwatersheds.

## 12.2 SPATIAL REPRESENTATION OF WATERSHEDS

Because most watersheds are nonhomogeneous in topography, soils, vegetation, and other features, it is necessary to segment each watershed into units which can be treated as homogeneous. Similarly, the channel system in a watershed can be represented by one or more segments, each having a characteristic location, shape, slope, and roughness.

The location, area, length, and slope of each watershed unit is usually obtained from available topographic maps. The following steps can be used in collecting the geometric data from topographic maps. Two types of watershed segmentation are considered. For the high resolution model, the watershed is subdivided into square grids of a selected size

(Simons, Li and Ward, 1978). The size of these grids or cells is chosen to conform with the watershed geometry and to represent the accuracy of the input data and required output. Node points of the grid system represent sampling points where topographic, soils, and vegetative data are selected. The channel system is represented by straight line segments between the node points. The sampled information is processed by the computer to produce a segmented watershed of overland flow cells with corresponding length, slope, width, and soil and vegetative indices, and a channel system described by lengths, slopes, and locations. Gravity flow logic and cell and channel aspect are used to determine flow directions in the watershed. On a much smaller scale, the slope, lengths, widths and flow directions of roadways can be prepared from maps, construction plans, or field measurements. For the simplified watershed models consisting of planes and channels, a different approach is used to abstract the geometry for model input. This approach can be used on small or large watersheds. On large watersheds multiple sets of two plane-one channel watersheds may be present (Simons, Li and Spronk, 1978). A method is presented below that is applicable to single watersheds or subdivided watersheds.

## Geometric Representation for High Resolution Model

The first problem encountered in numerical modeling of watershed response is to determine representative response units for mathematical computations. Simons and Li (1975) have approached this problem by developing a watershed segmentation program based on a grid system. The grid size is chosen so that the watershed boundary and channel segments can be approximated by grid lines (Figure 12-1). The overland flow units are the grid units inside the watershed boundary and the channel units are segments of channel between grid intersection points.

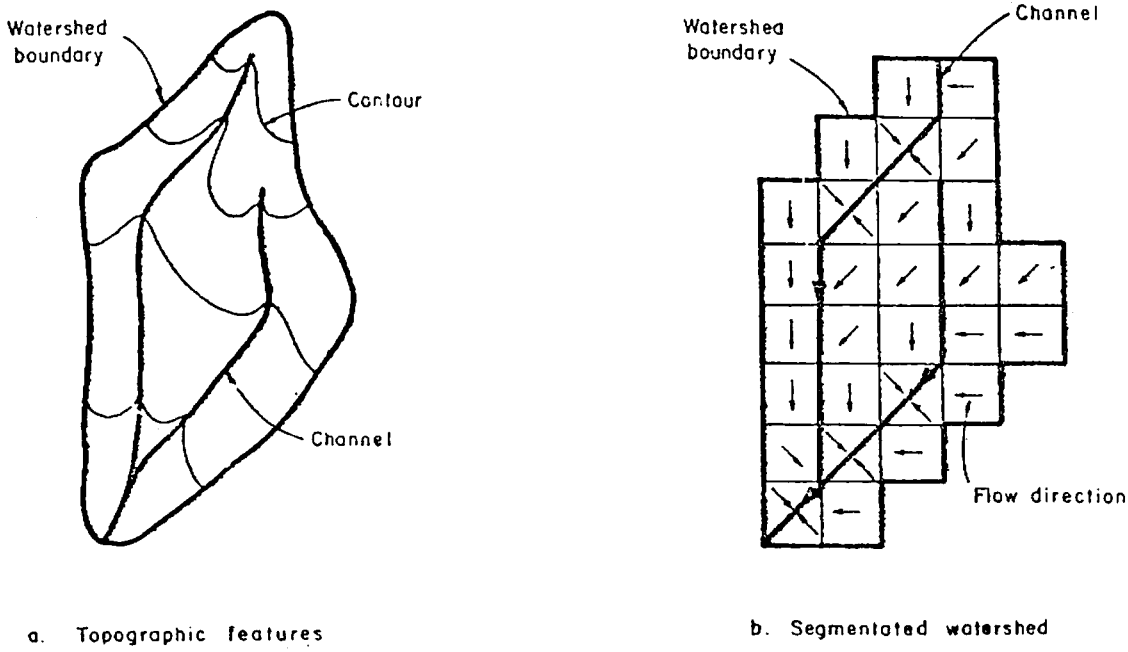


Figure 12-1. Example of watershed segmentation.

From the contour lines, the elevations of the land surface at the grid points are determined (Figure 12-2). These elevations, along with the locations and bed elevation of the stream channel, are inputs to the computer program. In addition to elevation data, vegetation and soil code numbers can be input for each grid point (Figure 12-2). The computer program then performs the following functions:

1. The slope and the slope azimuth of each overland flow unit are computed.

2. It is assumed that the water flows in the opposite direction of slope gradient to the next overland flow unit or to the adjacent channel. Thus, water cascades from overland unit to overland unit and then into the channel system. The program identifies the cascade sequence (arrows in Figure 12-1).

3. The computational sequence for flow is established by the program. The method employed is simply to follow the logic of gravity flow and flow continuity.

4. If data on the vegetation type, soil type, canopy cover density, and ground cover density are available, variations of these factors inside a watershed can be established in the program. This is executed by decoding the vegetation and soil codes and assigning previously input parameters to each type code. These parameters may include soil porosity, soil depth, and selected vegetation measures.

In order to save computer storage capacity and processing time in water and sediment routing computations, an additional computer program to combine small grid units into larger response units is developed. With this treatment, the flow is conceptually routed from overland flow units to channel units and to the selected watershed outlet.

This segmentation method is essential not only in water and sediment routing, but also for introducing the information from snowmelt computations, landslide hazard mapping, forest fire hazard mapping, forest inventory studies, and snow avalanche hazard identification into the routing model. Moreover, if such factors as soil properties, vegetation cover, type of management treatment, or rainfall vary within the watershed, these variations can be handled easily and with the least manual input by segmenting the watershed with a grid system. The developed segmentation method provides the input data on watershed geometry and computational sequence required for the simulation model to predict water and sediment routing and yield for small watersheds.

Often the manual determination of the response unit is preferable for non-computer oriented personnel. Such a manual determination should follow similar logic used in the computer segmentation method. The flow path can be drawn perpendicular to contour lines. Manual determination of the hydrologic response unit is subject to the individual's perception and can be time-consuming for application to complicated watersheds. It is recommended that manual determination be limited to small and simple watersheds.

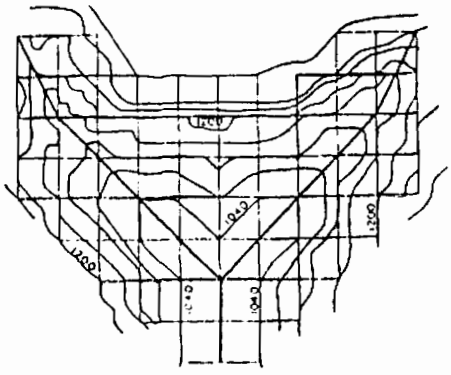

(a) Topographic Map Contour Interval = 40'

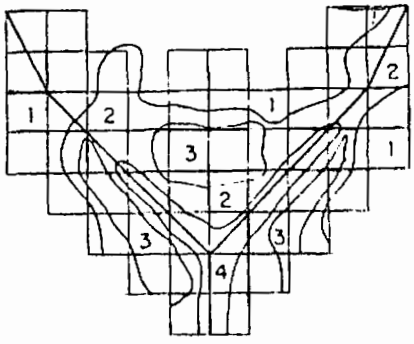


(b) Soils Map Numbers are soil type codes

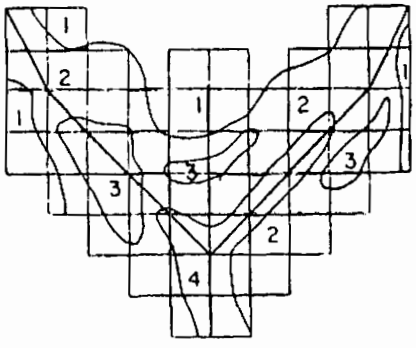


(c) Vegetation Map Numbers are vegetation type codes

Figure 12-2. Input data for hypothetical watershed.

Another characteristic of the channel system that must be numerically defined is the wetted perimeter-flow area relationship for each channel segment. This relationship is needed for use in water and sediment routing in the channel. The relationship is most often expressed in the power form as

$$P = a_1 A^{b_1} \qquad (12\text{-}1)$$

where $p$ is the wetted perimeter, $A$ is the flow area, and $a_1$ and $b_1$ are statistically determined values. Data needed for development of Equation 12-1 are measurements on the channel cross section. These measurements are the horizontal distance from a datum mark or a bank to a point in the channel and the elevation change between the point and the mark. In a complex application where many stream cross sections are involved, the values of $a_1$ and $b_1$ for each channel segment may be found by a fitting routine contained within the simulation program. As an alternative, $a_1$ and $b_1$ may be determined beforehand using a small programmable calculator.

Geometric Representation for Simplified Model

The two types of simplified watershed simulation use essentially the same geometric representation. The watershed must be subdivided in such a manner to allow approximation of the land surface by planes that extend to the watershed boundary with one or more interconnecting channels. The simpler of these two models uses an "open-book" representation wherein the watershed is transformed into a single two-plane unit with a central channel. The more complex model uses a number of such units in combination with single planes and interconnecting channel segments.

At Colorado State University two simplified models have been developed and are called ANAWAT and MULTWAT. The former is an acronym for Analytical Watershed Model and is a simpler single open-book representation. The latter name is an acronym for Multiple Watershed Model and is a more complex formulation. These acronyms are only introduced here to simplify later reference to these two model approaches. The basic method of transforming the contour map geometry into planes and channels, however, is the same for both models. This technique is described below for ANAWAT and then extended for MULTWAT. The process is illustrated by Figure 12-3 and presented in a step-by-step form below.

1a. Divide the watershed into units which can be considered homogeneous by using the available topographic, soil type, and vegetation type maps for the watershed. The size of the division is based on the resolution needed and the availability of data.

1b. Divide the watershed using the channel system. This division is often at the user's discretion, but should be based on homogeneity in the channel segment or its contributing side slopes. This homogeneity may be the channel segment gradient or similar soil types on the contributing side slopes.

2. Delineate the main channel in the unit. Extend the channels to at least the last distinct end points. Such an end point is often noted as the last distinct "V" on the contour line for tributary channels. In small watersheds determining the correct path along which to extend the channel may be difficult. In larger watersheds the extension of the channel may be apparent all the way to the basin boundary. Therefore, the extension of the channel for measurement purposes is arbitrary. A general rule may be:

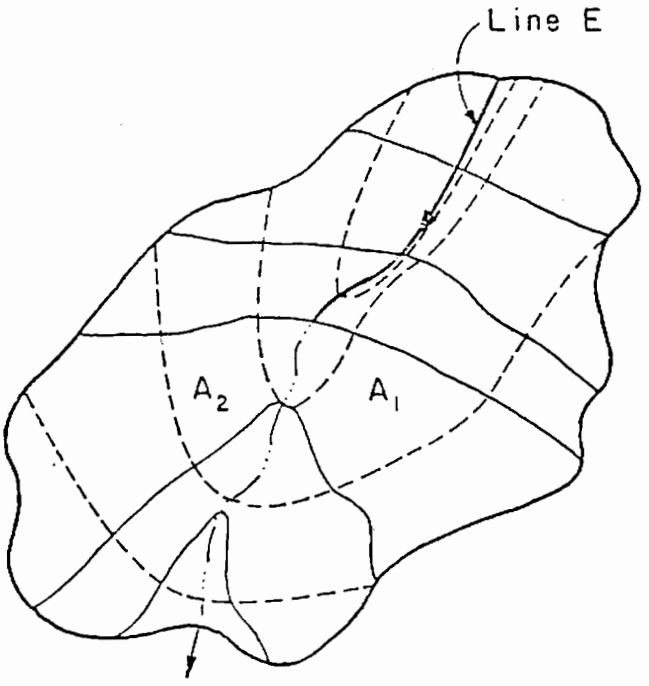


(a) Original Subwatershed Topographic Map

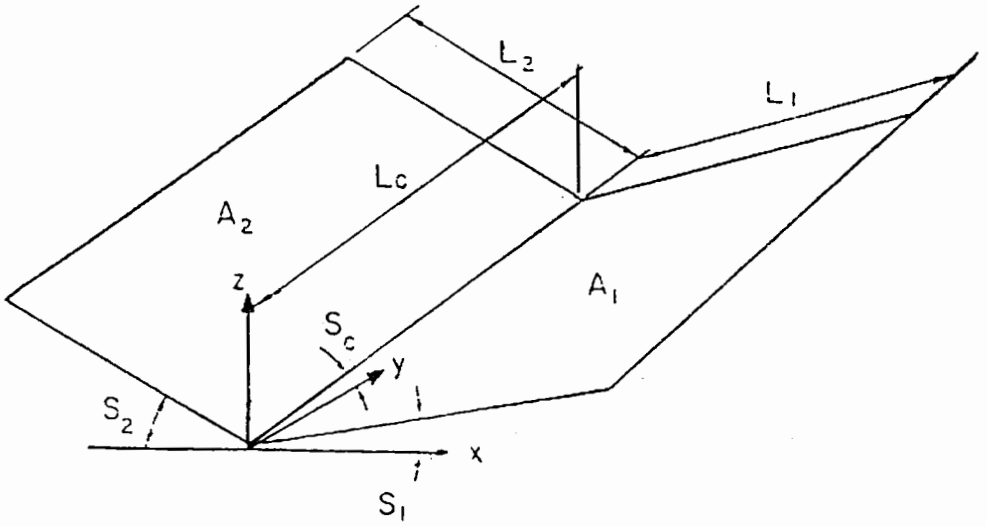


(b) Openbook Plane Representation

Figure 12-3. Geometric representation of a subwatershed unit.

(a) Small watersheds. Extend the channel to the last distinct "V" and no further.

(b) Medium sized watersheds. Extend the channel from the last "V" one-half the distance to the watershed boundary.

(c) Large watersheds. Extend the channel from the last "V" to the watershed boundary.

No distinction is made on watershed size as this is a factor that is dictated by experience. In general, a small watershed may have a maximum size of 100 acres, a medium watershed would be 100 to 1,000 acres, and a large watershed would be anyone over 1,000 acres.

If a channel extension is made, the extension must cross the contour elevations perpendicularly to insure that the water is following the shortest path to the channel. Measure the channel segment length.

3. Sketch in the boundaries between contributing side slopes for the different channel segments. The enclosed contributing areas are now the watershed subdivisions. Each channel has a left and right subdivision when looking downstream.

4. Determine the channel segment slope as the ratio of elevation difference at the channel end points to the channel length.

5. Determine the area of the left and right contributing subdivisions by using the channel as the dividing line. For small and medium sized watersheds, an artificial dividing line may need to be constructed as an extension from the assumed channel end point to the watershed boundary. Make sure this division remains perpendicular to the topographic contours.

6. Determine each subdivision width as sum of subdivision area divided by channel length as determined in Step 4.

7. Subdivide the channel into several (5-20) equally spaced sampling points. At each sampling point lay out sampling lines from the channel to the watershed or response unit boundary. Sampling lines are drawn perpendicular to contour lines and represent flow lines that cross equipotential lines in a flow net. The sampling lines are the potential routes water would follow when flowing across the subdivision. Determine the slope as elevation change on the sampling line. Take the product of sampling line length times slope; sum these products for the sampling lines in each response unit.

8. For small or medium sized watersheds, a single slope sampling line will be extended from the end point of the channel. This sampling line should coincide with the artificial dividing line constructed in Step 5. Because the area above the assumed

channel end point represents an overland flow plane, it is treated as being divided equally between the two response units. To do this, add the slope-length products for this sampling line to the summed slope-length products for each subdivision, then add the length of the sampling line to the summed lengths of the sampling lines of each subdivision. These additions will incorporate the effects of this headwater overland flow plane into each of the subdivisions.

9. Determine the average slope of each subdivision as the summed slope-length products for the unit divided by the summed sampling line lengths or

$$\bar{S} = \frac{\sum_{i=1}^{n} S_i \times \ell_i}{\sum_{i=1}^{n} \ell_i} \qquad (12\text{-}2)$$

where $\bar{S}$ is average of overland slope, n is number of sampling lines, $S_i$ is slope of line i, and $\ell_i$ is length of line i. The consistent step-by-step procedure presented above will provide a digitized watershed amenable to analysis by watershed modeling.

An example of the above procedure is presented below.

Example: Small Watershed (see Figure 12-4)

Area = 4.01 acres

Length of Channel to "V" = 418 feet

Slope of Channel to "V" = 0.108

| | (Acres) | Average Width Feet | Weighted* Average Slope |
|---|---|---|---|
| Left side | 2.64 | 275.5 | 0.172 |
| Right side | 1.37 | 142.4 | 0.205 |

*Includes artificial extension 192.5 feet long with slope of 0.26. Ten sampling lines were used.

As mentioned earlier, ANAWAT has the capability of simulating the storm water runoff from the single plane or from the "open book" geometry as shown in Figure 12-3. MULTWAT classifies the single plane units as planes and the "open book" units as subwatersheds. Storm water runoff hydrographs from the ANAWAT units serve as inputs to the interconnecting channel units. Water in the channels is routed by using a numerical solution to the nonlinear kinematic wave approximation. A method to account for channel losses due to infiltration is included in the channel routing procedure. The necessity of using a numerical channel routing routine rather than an analytical routine is due to the occurrence of kinematic shock. The analytical solution cannot be applied in situations where kinematic shock occurs.

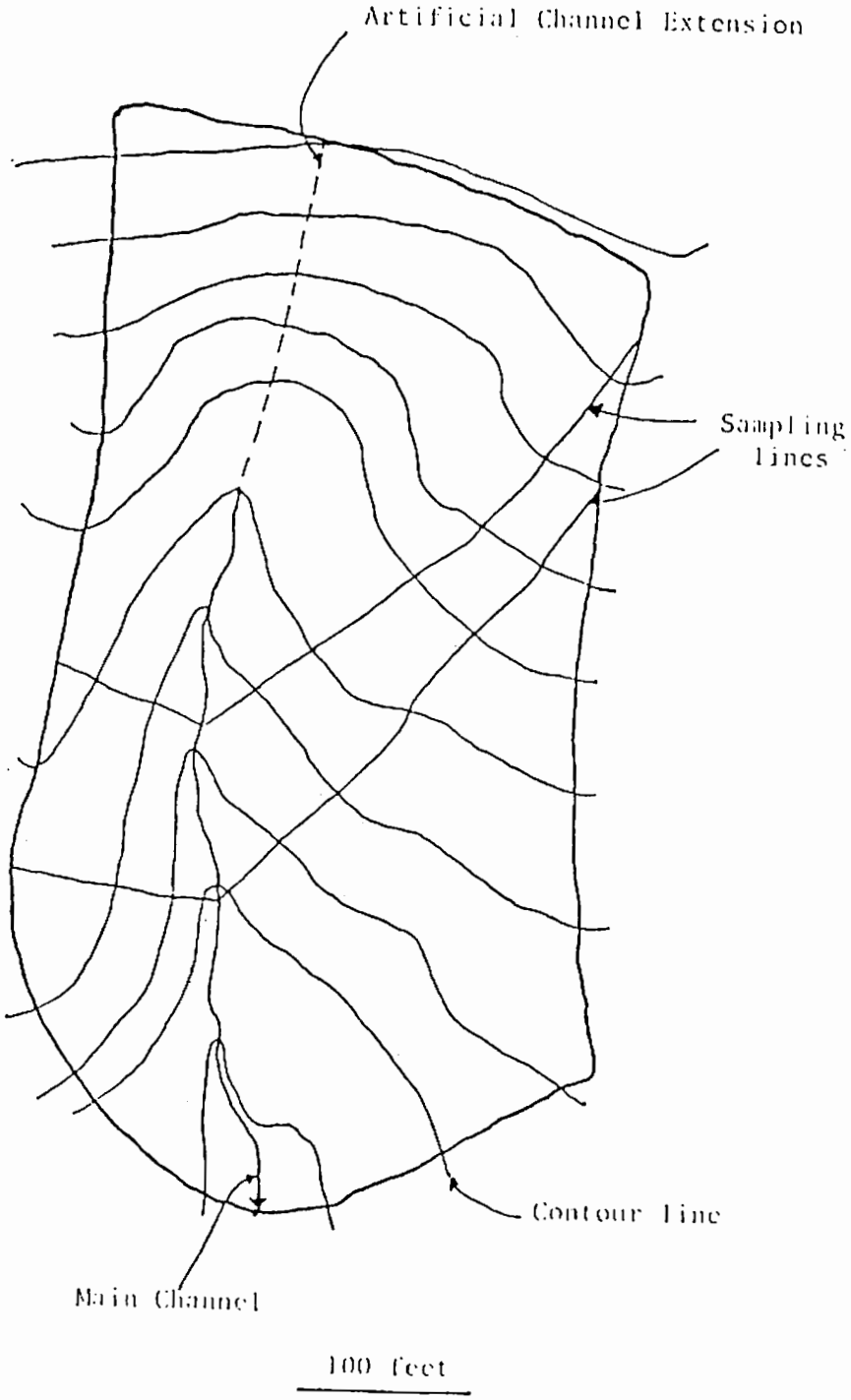


Figure 12-4. Important features for developing a small watershed representative geometry.

There are four types of response units in MULTWAT: 1) a single plane ANAWAT unit, 2) an "open book" ANAWAT unit, referred to as a subwatershed, 3) a channel, which is a large channel interconnecting the other units, and 4) a connection. A connection unit is used when only the lower part of a basin is being modeled and the response of the upstream portion of the basin is input as a hydrograph recorded or

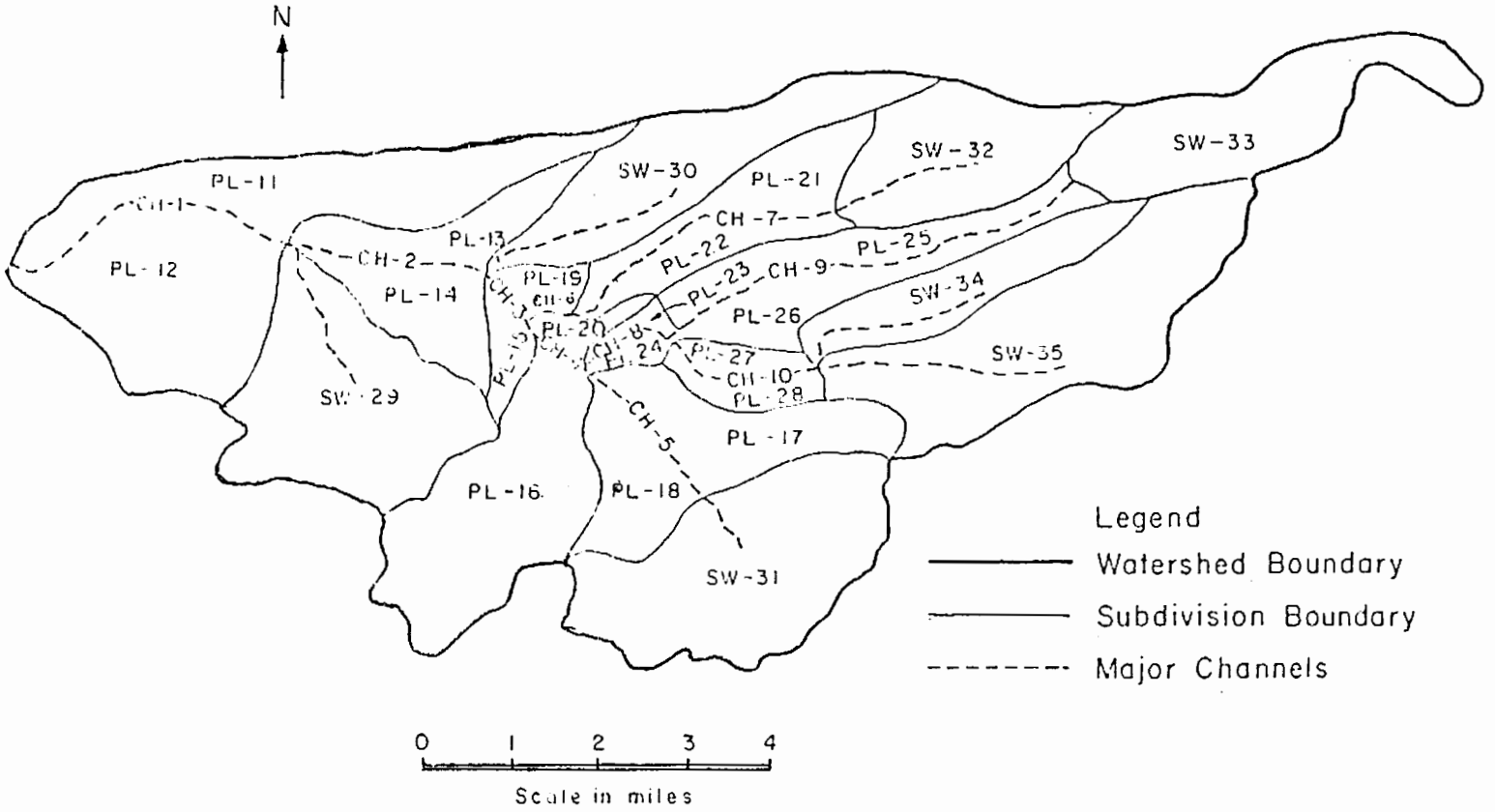


Figure 12-5. Response units for Walnut Gulch, Arizona, watershed.

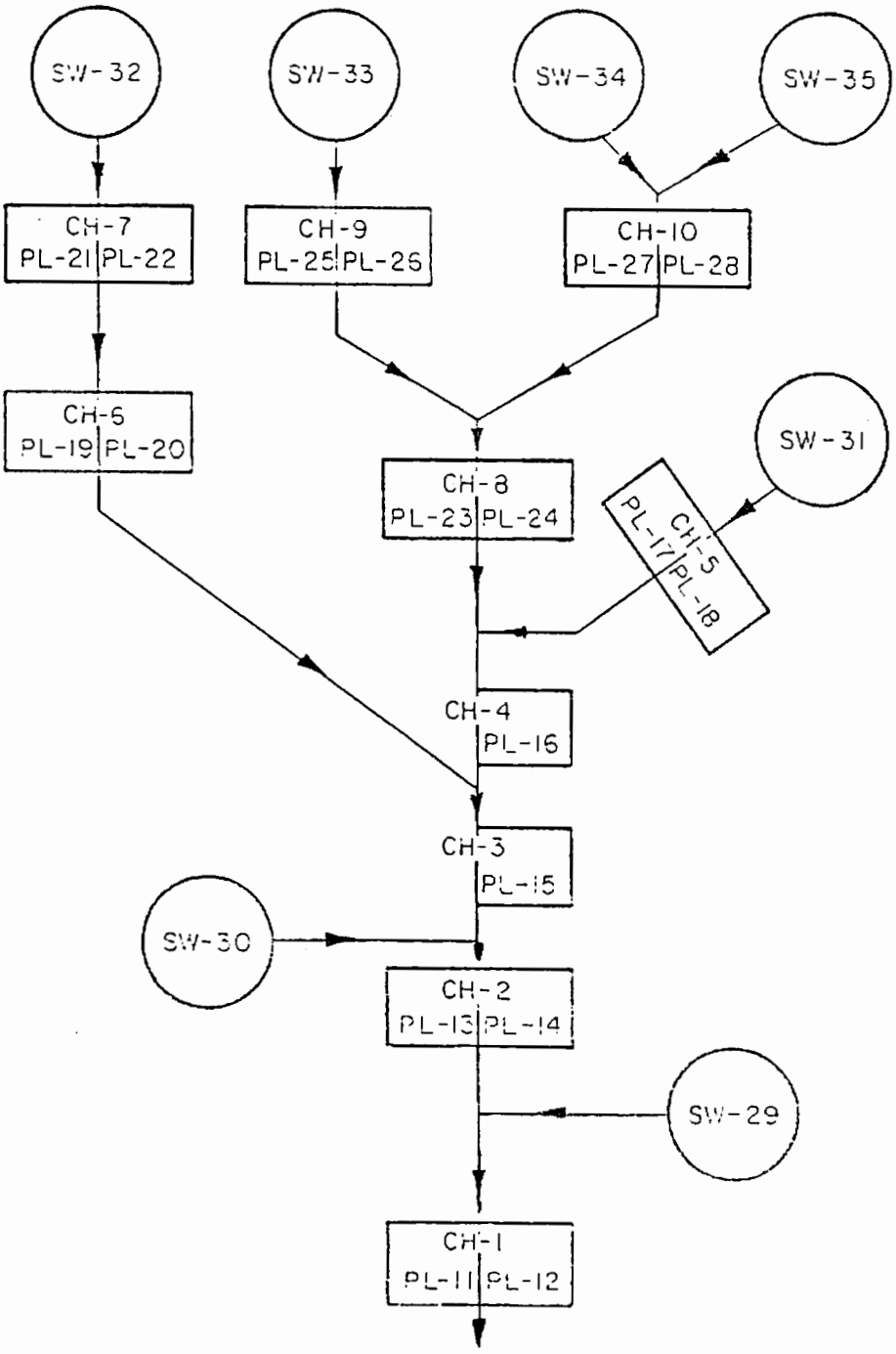


Figure 12-6. Schematic diagram of the Walnut Gulch response units.

simulated at the gaging station dividing the upper and lower parts of the basin. The method of obtaining the size and slope of planes and channels was given above. As an example of the transformation of a larger, more heterogeneous watershed into a system of planes and channels, Figure 12-5 shows a map of Walnut Gulch, Arizona, a watershed selected for development and testing of MULTWAT. The boundaries of the planes and subwatersheds are marked to illustrate how a large watershed can be represented by a system of these units interconnected by channel units. Figure 12-6 shows a schematic diagram of Walnut Gulch Watershed, represented by planes, subwatersheds, and channels.

## 12.3 MODEL COMPONENTS

As mentioned earlier, both the high resolution and simplified models contain essentially the same physical process components; however, the implementation of the process varies considerably due to the differences in water routing methods. The components and basic model structure are presented below. This discussion is a description of existing models, but may be used as a blueprint for the development of similar models.

### High Resolution Model

Once the watershed has been numerically defined by the above segmentation procedure, the overland flow units and channel flow units of the watershed can be determined. Simons and Li (1975) developed a watershed sediment model which is primarily applicable for surface erosion simulation. It simulates the land surface hydrologic cycle, sediment production, and water and sediment movement on small watersheds. Conceptually, the watershed is divided into an overland flow part and a channel system part. Different physical processes are important for the two different environments. In the overland flow loop, processes of interception, evaporation, infiltration, and overland flow water routing to the nearest channel are simulated. In a channel system loop, water contributed by overland flow is routed. A flowchart presenting the interrelationship of these processes is shown in Figure 12-7. A brief summary of the components is given below. The model described in Figure 12-7 also contains sediment routing and erosion components.

#### Overland Flow Loop

There are three components in the overland flow loop: interception, infiltration, and overland surface water.

*Interception Component*. In this component the interception amounts due to the crown and forest floor are computed and the net rainfall is determined from the rainfall input. The interception loss includes the constant interception storage and the continuous evaporation from interception surfaces. Evaporation is usually negligible during a storm. The interception storage is formulated to be a function of canopy cover density, ground cover density, and vegetation type.

*Infiltration Component*. This component of the model simulates the process of infiltration. The infiltration rate is computed by an approximation of Darcy's Law assuming that a distinct wetting front

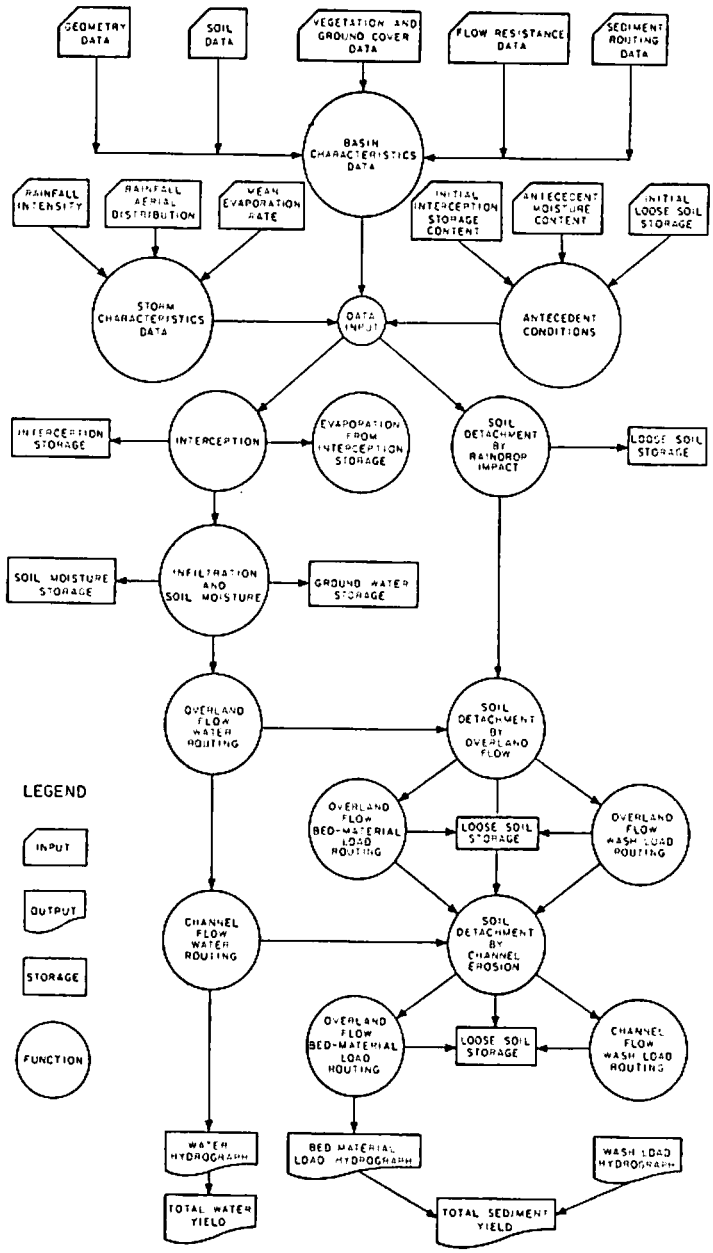


Figure 12-7. Flowchart for the watershed sediment and routing model.

exists and is formulated to be a function of saturated hydraulic conductivity, average capillary suction pressure, soil porosity, antecedent moisture content, and moisture content in the wetted zone. Therefore, the rate of rainfall excess can be determined from the net rainfall and infiltration rates.

Overland Surface Water Routing Component. With this component the overland surface water runoff resulting from the mean rainfall excess is routed to the nearest channel. The routing procedure is based on the continuity of water, a momentum equation of kinematic wave approximation, and a set of resistance functions for different hydraulic conditions. The total resistance to flow is assumed to be a sum of the drag

resistance due to ground cover and the shear stress acting on the soil bed. The computation is carried out by a nonlinear finite difference scheme developed by Li et al. (1975a) and computation results include the mean flow depth, bed shear stress and flow discharge at computation points as a function of time and space point.

Channel Water Routing Component. This component of the model routes the water down the creeks in the channel system and computes the hydrograph at the watershed outlet. The lateral water inflows to the channel system are the overland surface water flows. The channel water routing procedure and the finite difference scheme are similar to those used in the overland flow loop.

## Simplified Models

The simplified models contain the same physical processes listed above, but these routines are applied to subunits that are in general much larger than those of the high resolution model. In addition, these routines are uncoupled in the sense that they are used to calculate the process response for the entire event on a given unit before passing on to the next physical process. For example, infiltration for the entire storm is calculated before passing the entire rainfall excess function on to overland flow routing. This is as opposed to the time step by time step calculation of the high resolution model. Therefore, some resolution is sacrificed for a gain in computational speed.

The physical processes modeled for each type of unit are shown in Table 12-1. The processes involved in the plane and subwatershed units are identical except for the analytical channel routing performed for the subwatershed units. The only processes considered for the channel units are numerical routing and channel infiltration.

Table 12-1. Physical processes considered for each type of unit.

| | Plane | Subwatershed | Channel |
|---|---|---|---|
| Physical Processes Considered | 1. Interception | 1. Interception | 1. Channel Infiltration |
| | 2. Overland Infiltration | 2. Overland Infiltration | 2. Numerical Channel Routing |
| | 3. Analytical Overland Routing | 3. Analytical Overland Routing | |
| | | 4. Analytical Channel Routing | |

Much of the rain falling during the first part of a storm is intercepted by the vegetal ground cover. Precipitation intercepted by vegetation or other ground cover eventually evaporates, and the amount of rainfall reaching the soil surface is less than the recorded amount. The amount of interception loss depends on the percentage of the ground that is covered by canopy and ground cover, and their respective water holding capacities. It is assumed that interception starts at the beginning of a storm and continues until the potential intercepted volume is filled.

A portion of the rainfall reaching the ground moves through the soil surface into the soil. This process is defined as infiltration. The model used to simulate this process is based on the Green and Ampt infiltration equation (Li, Simons and Eggert, 1976).

Using an approximate explicit solution to the Green-Ampt equation for time varying rainfall given by Eggert, Li and Simons (1979), a function for infiltration with respect to time is developed. Thus, the infiltration occurring during a selected time period can be determined if the soil characteristics are known.

An analytical solution to the continuity, momentum, and cross section geometry equations is used to route water in the plane and subwatershed units. The method presented is identical to the routing scheme presented by Simons, Li and Eggert (1977). However, the routing of water with the conditions of continuous infiltration is developed and incorporated. Due to the assumed "open book" geometry, both overland and channel routing are required. Excess rainfall, the amount of rainfall not intercepted or infiltrated, serves as the input to the overland flow routing scheme. Results of the overland flow routing are then used as the lateral inflow into either a subwatershed or a channel unit.

The partial differential equations for overland flow are solved by the method of characteristics. The characteristic paths along which the solution is valid can be calculated in either the upstream or downstream direction. This allows a user to find the discharge at the downstream boundary for any given time.

A numerical procedure for water routing developed by Li, Simons and Stevens (1975a) is used for the channel units. Routing is accomplished by a second-order nonlinear scheme developed to numerically solve the kinematic wave equation. A numerical routing procedure rather than an analytical procedure is used for the channel units because analytic solutions are restricted by the formation of kinematic shock. Kinematic shock results when characteristic paths intersect. Physically this may be described as a faster moving parcel of water overtaking a slower moving parcel of water as they both travel downstream. Analytic solutions for problems that have kinematic shock display discontinuities in the hydrographs. Due to this restriction, a simple numerical routing procedure is necessary for the channel units.

Stability of a numerical procedure refers to whether the computational errors, due to the finite difference approximation of the partial differential equations, accumulate to an unbounded error. If

the errors do not grow unbounded, the procedure is stable. The numerical scheme that is used has proved to be unconditionally stable and can be used with a wide range of time to space increment ratios without loss of significant accuracy. However, the physical significance of the time and space intervals should be considered when selecting their values.

An infiltration routine is combined with the numerical channel routing procedure to account for channel seepage losses. The channel infiltration procedure is similar to the overland infiltration procedure because both are based on the Green-Ampt infiltration equation (1911). The major difference between the two routines is that the depth of the water in the channel situation cannot be neglected as in the overland situation.

This description has listed the components of a MULTWAT model. The same description applies to the simple ANAWAT model up to the numerical channel routing scheme. Since the single open book representation does not require an upstream inflow to any channel segment, a numerical channel routing is not required.

## 12.4 EXCESS RAINFALL ESTIMATION

A discussion of excess rainfall determination involves the processes of rainfall interception and infiltration. The formulation of these processes is the same for all of the models discussed in this chapter, therefore their discussion is combined in this section.

### Rainfall Interception

The amount of interception loss depends on the percentage of the ground that is covered by canopy and ground cover, their respective water holding capacities, as well as their initial moisture levels. The total intercepted volume can be written as

$$V_i = C_c V_c + C_g V_g \qquad (12\text{-}3)$$

in which $V_i$ is the total intercepted volume in depth, $C_c$ is the canopy cover density ($0 \leq C_c \leq 1$), $V_c$ is the potential volume of canopy cover interception in depth, $C_g$ is the ground cover density ($0 \leq C_g \leq 1$), and $V_g$ is the potential volume of ground cover interception in depth. The value of $V_i$ is dependent on the type of vegetation, height of vegetation (related to leaf areas), and the initial moisture level. The value of $V_g$ is a function of forest litter, grass and rock mulch, and the initial moisture level.

As the computations proceed through time, the rainfall is all intercepted until the potential volumes for ground and canopy cover are filled. This would constitute a series of net rainfall rates. Although interception losses are continuous over the storm period, it is assumed that the losses occur during the beginning period of the storm. A more detailed simulation of the interception process is given by Simons et al. (1975).

Infiltration of Unsteady Rainfall

In the determination of storm water runoff, an accurate estimation of storm water runoff is of critical importance. Not only the volume available for runoff, but the time history of the infiltration process is important if hydrographs are to be simulated. Because of its importance and its association with the soil surface, infiltration is one of the model processes most sensitive to man's activities in the watershed. Therefore, it is important that the process be modeled in such a way that parameters are sensitive to watershed development and utilization activities. However, it is equally important that the infiltration routine be time-efficient so that a digital computer simulation will remain economical.

In the past few years several authors: Bouwer, 1969; Li, Stevens and Simons, 1976; Bouwer, 1976; and Morel-Seytoux and Khanji, 1974 have discussed the applicability of the Green-Ampt (1911) equation to a variety of infiltration problems. In particular, Mein and Larson (1971) applied the equation to natural rainfall. Green and Ampt's formulation is particularly attractive since it is the simplest infiltration equation based on Darcy's Law. However, the method is somewhat more difficult to use than infiltration equations such as Horton's since the Green-Ampt equation is implicit with respect to time. This difficulty is particularly visible in watershed simulation when merging an infiltration routine with a finite difference surface water routing scheme.

Li, Stevens and Simons (1976) proposed a time-explicit solution to the Green-Ampt equation for the case of constant intensity rainfall. Since that time Eggert (1976) has presented a modification of that solution for unsteady rainfall, and Eggert, Li and Simons (1979) have indicated a further extension of the method to layered soils. The models discussed in this section share the time-explicit formulation of the Green-Ampt equation for unsteady rainfall. A version of MULTWAT using layered infiltration has also been developed.

The Green-Ampt infiltration model is a simple, physically based, two-parameter infiltration equation first proposed in 1911. It may be derived by direct application of Darcy's Law under the following assumptions:

1. A distinct piston wetting front exists.

2. The hysteresis effects in the soil properties are negligible.

3. The pressure effect of ponded water is negligible.

A Green-Ampt type equation may be written as

$$\frac{F}{\delta} - \ell n\left(1 + \frac{F}{\delta}\right) = \frac{Kt}{\delta} \qquad (12\text{-}4)$$

in which $F$ is infiltrated volume, $K$ is hydraulic conductivity of the soil in the wetted zone, $t$ is time, and $\delta$ is potential head parameter and is defined as

$$\delta = (\theta_w - \theta_i)\psi_{ave} \tag{12-5}$$

in which $\theta_w$ is moisture content of the soil after wetting, $\theta_i$ is antecedent moisture content, and $\psi_{ave}$ is the average suction head across the wetting front.

If at any time $t$ the infiltrated volume is $F(t)$, then at some later time $t + \Delta t$

$$F(t + \Delta t) = F(t) + \Delta F \tag{12-6}$$

in which $\Delta F$ is the change in infiltrated volume which occurred during time increment $\Delta t$. An expression for $\Delta F$ is obtained from Equation 12-6

$$\Delta F = F(t + \Delta t) - F(t) \tag{12-7}$$

Li et al. (1976a) developed the following method of solving for the infiltration rate. Their derivation yields

$$\frac{\Delta F}{\delta} - \ell n \left[\frac{\delta + F(t) + \Delta F}{\delta + F(t)}\right] = \frac{K}{\delta} \Delta t \tag{12-8}$$

Equation 12-8 is implicit with respect to $\Delta F$. However, the equation is simplified by expanding the logarithmic term in a power series (see Li et al., 1976b).

$$\ell n\left(1 + \frac{\Delta F}{\delta + F}\right) = \ell n\ 1 + \frac{\frac{2\Delta F}{\delta + F}}{2 + \frac{\Delta F}{\delta + F}} + \ldots \tag{12-9}$$

Truncating Equation 12-9 after the second term and substituting into Equation 12-8, one obtains

$$\frac{\Delta F}{\delta} - 2\left[\frac{\frac{\Delta F}{\delta + F}}{2 + \frac{\Delta F}{\delta + F}}\right] = \frac{K}{\delta} \Delta t \tag{12-10}$$

Equation 12-10 is simplified into a quadratic whose solution is (see Li et al., 1976a)

$$\Delta F = -\frac{(2F - K\Delta t)}{2} + \frac{[(2F - K\Delta t)^2 + 8K\Delta t(\delta + F)]^{\frac{1}{2}}}{2} \tag{12-11}$$

Only the positive root of Equation 12-11 has any physical significance. The average infiltration rate, $\bar{f}$, is obtained by dividing $\Delta F$ by $\Delta t$

$$\bar{f} = \frac{\Delta F}{\Delta t} \tag{12-12}$$

After accounting for the interception and infiltration losses, the rainfall excess $i_e$ can be determined. A rainfall event is commonly reported as a hyetograph i.e., a series of net rainfall intensities I, each lasting for a time increment $\Delta t$. Thus, if the net rainfall intensity is greater than the infiltration rate, the infiltration rate is subtracted from the net rainfall intensity to give the excess rainfall. If the net rainfall intensity is less than the corresponding infiltration rate, the infiltration rate equals the net rainfall intensity and there is no excess.

Bouwer (1969) and Brakensiek (1970) suggested an application of Green and Ampt equation to layered soils having equal layer thicknesses. Their basic concepts are easily implemented to modify Equation 12-11 to a form allowing calculation of the change of infiltrated volume within a given soil layer. The only additional complication is the increased amount of bookkeeping required to know the location of the wetting front.

Briefly, after Bouwer (1969), the total head loss $\Delta h_T$ through the soil layers to a wetting front that is assumed to be in the $k^{\underline{th}}$ layer may be written as

$$\Delta h_T = \sum_{i=1}^{k-1} \Delta z_i + \ell + \psi_{ave_k} \tag{12-13}$$

where $\Delta z_i$ is thickness of the $i^{\underline{th}}$ soil layer above the wetting front, $\ell$ is depth of penetration of the wetting front into the $k^{\underline{th}}$ layer below the base of the $k\text{-}1^{\underline{th}}$ layer, and $\psi_{ave_k}$ is average capillary suction head of the $k^{\underline{th}}$ layer. Additionally, the total head loss may be written in terms of Darcy's Law

$$\Delta h_T = q \left( \sum_{i=1}^{k-1} \frac{\Delta z_i}{K_i} + \frac{\ell}{K_k} \right) \tag{12-14}$$

where q is the Darcian flux which is equal by continuity for all layers behind the wetting front and $K_i$ is the hydraulic conductivity of the $i^{\underline{th}}$ layer. Equating the right-hand side of Equations 12-13 and 12-14, solving for q and using analysis similar to the homogeneous soil case, the change in infiltrated volume within the $k^{\underline{th}}$ layer may be expressed as

$$I = \frac{-[2F + K_k(2d_k - \Delta t)] + \{[2I + K_k(2d_k - \Delta t)]^2 + 8K_k \Delta t(F + c_k)\}^{\frac{1}{2}}}{2} \tag{12-15}$$

where

$$c_k = \phi_k \Delta S_k \sum_{i=1}^{k-1} \Delta z_i + \psi_{ave_k} - \sum_{i=1}^{k-1} \phi_i \Delta S_i \Delta z_i \tag{12-16}$$

$$S_k = S_{w_k} - S_{i_k}$$

and

$$d_k = \phi_k \Delta S_k \sum_{k=1}^{k-1} \frac{\Delta z_i}{K_i} - \frac{1}{K_k} \sum_{i=1}^{k-1} \phi_i \Delta S_i \Delta z_i$$

Above $S_{w_k}$ and $S_{i_k}$ are the degree of saturation of the wetted zone behind the wetting front and the initial degree of saturation for the $k^{\underline{th}}$ layer, respectively.

Equation 12-11 for homogeneous soils, and Equations 12-15 and 12-16 for layered soils are used to calculate the potential average infiltration rate $\bar{f}$ occurring during the time interval between $t$ and $t + \Delta t$. This calculation is carried out time increment by time increment throughout the event and compared to the corresponding rainfall intensity. If the rainfall intensity is greater than the average infiltration rate, the change in infiltration volume during $\Delta t$ is $\Delta F$. If the rainfall intensity is less than the average potential rate, the change in infiltration volume during $\Delta t$ is $r\Delta t$, where $r$ is the current rainfall intensity. Since $\Delta F$ for both layered and homogeneous soils is a function of the infiltrated volume at time $t$, the value of $\bar{f}$ during time increment $t$ to $t + \Delta t$ reflects periods of rainfall control as well as potential infiltration rate control. Therefore, although these methods appear somewhat more involved than Horton's and similar time-explicit approaches to infiltration calculations, the additional complexity can provide an inherently more accurate description of the infiltration process under unsteady rainfall. Further, these equations and the bookkeeping logic necessary for their use are easily programmed for incorporation into watershed simulations or into the more sophisticated programmable calculators for simple infiltration calculations using Equation 12-11.

## 12.5 WATER ROUTING

The largest difference between the high resolution watershed model and the simplified approaches is visible in the water routing methods. The basic theory for both kinds of model is the same; however, the solution techniques used for implementation of the theory are different. The simplified models use an analytical solution to the kinematic wave problem for both overland flow and the unbranched finger-tip channel between the planes of the open book or ANAWAT watersheds. In the high resolution and the connecting channels of MULTWAT, a numerical water routing scheme is used. Both schemes are based on the theory presented below.

### Governing Equations

Water runoff can be described by the equation of continuity, the equation of motion, and equations describing resistance to flow.

Continuity Equation. The equation of continuity for water is

$$\frac{\partial Q}{\partial x} + \frac{\partial A}{\partial t} = q_\ell \tag{12-17}$$

in which $Q$ is discharge, $x$ is downslope distance, $A$ is cross-sectional area of flow, $t$ is time, and $q_\ell$ is lateral inflow or outflow rate per unit length of channel. For overland flow, $q_\ell$ is rainfall excess, $A$ is depth of flow, and $Q$ is discharge per unit width of channel.

Momentum Equation. The momentum equation for a prismatic channel can be expressed as (Henderson, 1966)

$$S_f = S_o - \frac{\partial y}{\partial x} - \frac{1}{gA}\frac{\partial Q}{\partial t} - \frac{1}{gA}\frac{\partial}{\partial x}\left(\frac{Q^2}{A}\right) \tag{12-18}$$

in which $S_f$ is friction slope, $S_o$ is channel bed slope, $y$ is depth of flow, and $g$ is gravitational acceleration.

The assumption of the kinematic wave approximation is that the friction slope is equal to the channel bed slope. That is, the gradients due to local and convective accelerations are assumed to be negligible and the water surface slope is assumed to be equal to the bed slope. Then the simplified momentum equation is

$$S_o \tilde{\approx} S_f = f\frac{Q^2}{8gRA^2} \tag{12-19}$$

in which $f$ is the Darcy-Weisbach friction factor and $R$ is the hydraulic radius. By definition,

$$R = \frac{A}{P} \tag{12-20}$$

in which $P$ is wetted perimeter. Usually the wetted perimeter can be expressed as a power function of the flow area i.e.,

$$P = a_1 A^{b_1} \tag{12-21}$$

where $a_1$ and $b_1$ are constants.

If Manning's equation is used, the simplified momentum equation is

$$S_o \tilde{\approx} S_f = \frac{n^2 Q^2}{2.21\, R^{4/3} A^2} \tag{12-22}$$

in which $n$ is Manning's roughness coefficient.

Resistance Equations. In a natural watershed, the form resistance due to the ground cover is a very important component of the resistance to flow. The dependence of flow resistance on ground cover becomes further complicated depending on whether the ground cover is submerged or not. Rarely is the ground cover submerged in overland flow units. Therefore, in overland flow units one only needs to consider the resistance caused by flow through the ground cover. In channel flow units, the probability of submerging the ground cover is relatively great. Resistance is then considered as the resistance caused by flow through ground cover and flow over ground cover simultaneously.

Resistance to flow for the overland flow response units is generally expressed as a function of surfacing material, vegetation type and density of vegetation. Palmer (1946), Ree (1949), and Ree and Palmer (1949) conducted a series of experiments in channels with various types of grasses. More recently, Kouwen and Unny (1969), Phelps (1970), Wenzel (1970), Li and Shen (1973), and Chen (1976) carried the experimental studies further. Results indicate a functional relationship between the overall Darcy-Weisbach friction factor and flow characteristics as

$$f = \frac{K_t}{N_r} \tag{12-23}$$

in which $f$ is the overall Darcy-Weisbach friction coefficient, $N_r$ is the flow Reynolds number, $K_t$ is a constant describing the overall resistance. According to Chen (1976), this type of relationship can be used for a Reynolds number up to $10^5$. This would practically cover all of the possible overland flow conditions on natural surfaces.

The flow Reynolds number is defined as

$$N_r = \frac{QR}{A} \tag{12-24}$$

in which $\nu$ is the kinematic viscosity of water.

A review of literature suggests that the overall flow resistance of overland flow can be assumed as

$$K_t = K_\ell + (K_h - K_\ell)\, C_g^2 \tag{12-25}$$

in which $K_\ell$ is the parameter describing the minimum resistance ($C_g = 0.0$) and $K_h$ is the parameter describing the maximum resistance ($C_g = 1.0$).

In channel flow, the Darcy-Weisbach friction factor is often considered as a constant. Sometimes, the Chezy function equation is used in evaluating the overall resistance for overland flow and flow in rivers. By definition

$$C = \sqrt{\frac{8g}{f}} \tag{12-26}$$

in which C is Chezy's friction factor. Equation 12-26 shows that a constant value of f will give a constant value of C.

Manning's equation is frequently used by hydraulic engineers to describe flow in open channels. The Manning roughness coefficient is usually determined by measurement and can be expressed as a power function of flow discharge i.e.,

$$n = a_2 Q^{b_2} \tag{12-27}$$

in which $a_2$ and $b_2$ are constant.

Discharge and Flow Area Relation. In general, the cross-sectional area of the flow can be expressed as a power function of discharge

$$A = \alpha Q^{\beta} \tag{12-28}$$

in which $\alpha$ and $\beta$ are coefficients whose values depend on the shape of the channel, the friction slope, and the roughness of the wetted perimeter.

If the Darcy-Weisbach friction factor is used, the values of $\alpha$ and $\beta$ can be determined by substituting Equations 12-19, 12-20, 12-21, 12-23 and 12-24 into Equation 12-28. The solutions are

$$\alpha = \left( \frac{K_t \, a_1^2}{8 g S_f} \right)^{1/(3-2b_1)} \tag{12-29}$$

and

$$\beta = \frac{1}{3-2b_1} \tag{12-30}$$

For overland flows or flows in very wide channels, the wetted perimeter is constant so that $b_1 = 0$ and $\beta = 1/3$.

If Manning's equation is applied, the corresponding $\alpha$ and $\beta$ values are determined from Equations 12-20, 12-21, 12-22, 12-27 and 12-28. The results are

$$\alpha = \left( \frac{a_1^{4/3} \, a_2^2}{2.21 S_f} \right)^{3/(10-4b_1)} \tag{12-31}$$

and

$$\beta = \frac{3-3b_2}{5-2b_1} \tag{12-32}$$

If the Chezy friction equation is used, the corresponding $\alpha$ and $\beta$ values are determined by using Equations 12-19, 12-20, 12-21, 12-26 and 12-28. The values are

$$\alpha = \left(\frac{a_1}{C^2 S_f}\right)^{1/(3-b_1)} \tag{12-33}$$

$$\beta = \frac{2}{3-b_1} \tag{12-34}$$

For the kinematic wave approximation, the friction slope $S_f$ in Equations 12-29, 12-31 and 12-33 is equal to the bed slope $S_o$.

The problem of water routing is now a matter of solving Equations 12-17 and 12-28. These two equations can be solved either by an analytical method or a numerical method. The solution techniques follow.

Analytical Solutions

The analytical solutions of Equations 12-17 and 12-28 are available for some special cases (Eagleson, 1970; Kibler and Woolhiser, 1970; Harley et al., 1970; and Li et al., 1975b). For analytical solutions, it is common to express Equation 12-28 in the following form

$$Q = \alpha' A^{\beta'} \tag{12-35}$$

where

$$\alpha' = \left(\frac{1}{\alpha}\right)^{1/\beta} \tag{12-36}$$

and

$$\beta' = \frac{1}{\beta} \tag{12-37}$$

From Equations 12-17 and 12-35, one obtains

$$\alpha'\beta' A^{\beta'-1} \frac{\partial A}{\partial x} + \frac{\partial A}{\partial x} = q_\ell \tag{12-38}$$

This partial differential equation may be solved by the method of characteristics. The total differential of $A(x,t)$ is given by

$$dA = \frac{\partial A}{\partial t}\, dt + \frac{\partial A}{\partial x}\, dx \tag{12-39}$$

Equations 12-38 and 12-39 form a system of two equations in two unknowns, and may be written in matrix form as

$$\begin{bmatrix} \alpha'\beta' A^{\beta'-1} & 1 \\ dx & dt \end{bmatrix} \begin{bmatrix} \frac{\partial A}{\partial x} \\ \frac{\partial A}{\partial t} \end{bmatrix} = \begin{bmatrix} q_\ell \\ dA \end{bmatrix} \tag{12-40}$$

The characteristic paths along which the solution is valid are found by determining the loci of indeterminancy of the solution. These loci are obtained by equating the determinant of the coefficient matrix with zero. The resulting characteristic equation is

$$\frac{dx}{dt} = \alpha'\beta A^{\beta'-1} \tag{12-41}$$

Integrating Equation 12-41 with respect to time yields

$$x - x_o = \alpha'\beta' \int_{t_o}^{t} A^{\beta'-1}\, dt' \tag{12-42}$$

in which $x_o$ is initial distance and $t_o$ is initial time.

The invariants of this solution are found by substituting the right-hand side of Equation 12-40 for each column of the coefficient matrix and equating the determinant of the resulting matrix equal to zero. The invariants are

$$\frac{dA}{dt} = \frac{dQ}{dx} = q_\ell \tag{12-43}$$

or by integrating Equation 12-43

$$A - A_o = \int_{t_o}^{t} q_\ell\, dt' \tag{12-44}$$

or

$$Q - Q_o = \int_{x_o}^{x} q_\ell\, dx' \tag{12-45}$$

in which $A_o$ and $Q_o$ are initial values of area and discharge, respectively. By substituting Equation 12-44 into Equation 12-42, the following expression for the characteristic is obtained

$$x = x_o + \alpha'\beta' \int_{t_o}^{t} \left[A_o + \int_{t_o}^{\eta} q_\ell(\sigma)\, d\sigma\right]^{\beta'-1} d\eta \tag{12-46}$$

Theoretically, if the functional form of $q_\ell(\sigma)$ is known, then Equation 12-46 will give the characteristics in the x-t plane. Harley et al. (1970) noted that when $q_\ell(\sigma)$ is a histogram, then with reference, Equation 12-44 and 12-46 may be evaluated in pieces.

The procedure as outlined by Harley et al. (1970) is as follows (see Figure 12-8). From any point $(x_i, t_i)$ on characteristic C, the value of $x_{i+1}$ on C corresponding to time $t_{i+1}$ may be calculated by Equation 12-46.

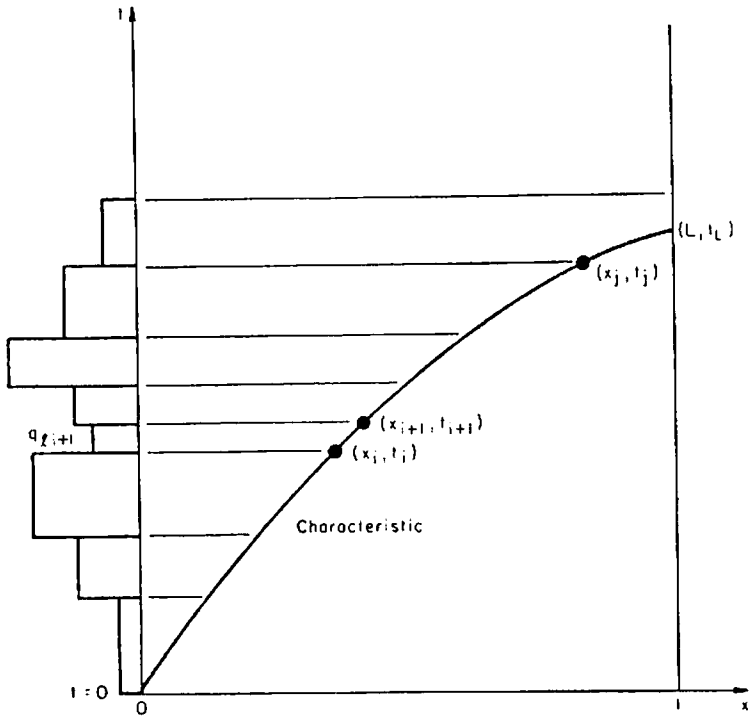


Figure 12-8. Schematic diagram of characteristic path.

$$x_{i+1} = x_i + \alpha'\beta' \int_{t_i}^{t_{i+1}} [A_i + q_{\ell i+1}(\eta - t_i)]^{\beta'-1} d\eta \qquad (12\text{-}47)$$

or

$$x_{i+1} = x_i + \frac{\alpha'}{q_{\ell i+1}} \{[A_i + q_{\ell i+1}(t_{i+1} - t_i)]^{\beta'} - A_i^{\beta'}\} \qquad (12\text{-}48)$$

for $q_{\ell i+1} \neq 0$, and

$$x_{i+1} = x_i + \alpha'\beta' A_i^{\beta'-1} (t_{i+1} - t_i) \qquad (12\text{-}49)$$

for $q_{\ell i+1} = 0$

From Equation 12-44 one obtains

$$A_{i+1} = A_i + q_{\ell i+1} (t_{i+1} - t_i) \qquad (12\text{-}50)$$

For a given plane of length L values of $x_{i+1}$ are calculated until $x_{i+1} \geq L$. The time of arrival of the characteristic at the downstream boundary $t_L$ is found by solving Equation 12-48 or Equation 12-49 for $t_L$ in terms of $t_j$ and $x_j$.

$$t_L = t_j + \frac{1}{q_{\ell i+1}} \left\{ \left[ \frac{q_{\ell i+1}(L-x_j)}{\alpha'} + A_j^{\beta'} \right]^{1/\beta'} - A_j \right\} \qquad (12\text{-}51)$$

for $q_{\ell i+1} \neq 0$, and

$$t_L = \frac{L-x_j}{\alpha'\beta' A_j^{\beta'-1}} + t_j \qquad (12\text{-}52)$$

Then, the discharge at the end of channel or overland flow reach is

$$Q_L = \alpha' A_L^{\beta'} \qquad (12\text{-}53)$$

Repeating the above solution, it is not difficult to route the water in terms of time and space. However, the timing of the outflow at the downstream boundary $t_L$ cannot be predetermined. Li et al. (1975a) suggested tracing the characteristic path backward from the downstream boundary for a desired $t_L$. Their method is simply to solve Equation 12-46 in terms of $t_o$. Or

$$\frac{L}{\alpha'\beta'} = \int_{t_o}^{t_L} \left[ \int_{t_o}^{\eta} q_\ell(\sigma)\, d\sigma \right]^{\beta'-1} d\eta \qquad (12\text{-}54)$$

As pointed out earlier, the continuity equation for overland flow has the same form as Equation 12-17. That is

$$\frac{\partial q}{\partial x} + \frac{\partial y}{\partial t} = e \qquad (12\text{-}55)$$

where $q$ is the overland flow discharge per unit width, $y$ is depth of overland flow, and $e$ is excess rainfall intensity. Also, analogous to Equation 12-35

$$q = \alpha_1 y^{\beta_1} \qquad (12\text{-}56)$$

where, using the Darcy-Weisbach resistance equation for overland flow

$$\alpha_1 = \frac{K_t}{8gS_o} \qquad (12\text{-}57)$$

and

$$\beta_1 = 3 \qquad (12\text{-}58)$$

Noting that the lateral inflow to the channel between the planes of the open-book watershed $q_\ell$ is simply the sum of overland flow discharge hydrographs from the two planes, the basis for an ANAWAT watershed model has been established. In fact, the routing of storm water in such a watershed may be accomplished using only the development

to this point. The overland and channel flow hydrographs may be determined with great resolution using Equations 12-44, 12-53 and 12-54. However, as examination of Equations 12-51 and 12-52 shows, $t_L$ the time at which the overland flow hydrograph points are known, is a function of rainfall, geometric and hydraulic parameters. Therefore, if the two planes are dissimilar, the times $t_L$ for the two overland flow hydrographs will not correspond, and in order to form the lateral inflow hydrograph to the channel, both overland flow hydrographs must be interpolated onto a common time base. This calculation presents no difficulties, but it is somewhat time consuming and introduces some error into the lateral inflow hydrograph. When using a programmable calculator method, this step must be performed; however, a computer provides sufficient storage for a more elegant method.

If $q_\ell(\sigma)$ in Equation 12-54 is in the form of a histogram, Equation 12-54 becomes a polynomial of degree $\beta$ that may be solved for $t_o$ when $t_L$ is selected. This allows the time points of the overland flow discharge hydrographs to be selected providing for simple addition of the hydrograph points to form the lateral inflow to the channel. Using the notation of Equations 12-55 and 12-56, the method is described below for overland flow.

Since $e(t)$ has the form of a histogram, excess rainfall during the $j^{\underline{th}}$ time increment $t_j - t_{j-1}$ is constant. In addition, the form of Equation 12-54 may be simplified by noticing the inner integration i.e., the integration on $\sigma$ is simply the difference between the cumulative excess at time $t_L$ and the cumulative excess at time $t_o$. That is

$$\int_{t_o}^{t_L} e(\sigma)\, d\sigma = E(t_L) - E(t_o) \tag{12-59}$$

where $E$ represents the cumulative excess.

With this notation in mind and taking advantage of the histogram form of $e(t)$, Equation 12-59 may be rewritten as

$$\begin{aligned}\frac{L}{\alpha_1\beta_1} = &\int_{t_K}^{t_L} [e_{k+1}\, t' - e_{k+1}\, t_k + E_k - e_{j+1}\, t_o + e_{j+1}\, t_j - Ej]^{\beta_1 - 1}\, dt' \\ &+ \sum_{i=j+2}^{k} \int_{t_{i-1}}^{t_i} [e_i\, t' - e_i\, t_{i-1} + E_{i-1} - e_{j+1}\, t_o + e_{j+1}\, t_j - E_j]^{\beta_1 - 1}\, dt' \\ &+ \int_{t_o}^{t_{j+1}} [e_{j+1}\, t' - e_{j+1}\, t_j + E_j - e_{j+1}\, t_o + e_{j+1}\, t_j - E_j]^{\beta_1 - 1}\, dt'\end{aligned} \tag{12-60}$$

Equation 12-60 consists of nothing more than a series of simple integrations of the form

$$\int (at' + b)^{\beta_1 - 1} \, dt' = \frac{1}{\alpha_1 \beta_1} (at' + b)^{\beta_1} \tag{12-61}$$

Integrating as in Equation 12-61 and introducing $A_i$ as defined below

$$A_i = -e_i \, t_{i-1} + E_{i-1} + e_{j+1} \, t_j - E_j \tag{12-62}$$

Equation 12-60 may be written as

$$\begin{aligned} \frac{L}{\alpha_1 \beta_1} = {} & \frac{1}{e_{k+1} \beta_1} \left[ e_{k+1} \, t' + A_{k+1} - e_{j+1} \, t_o \right]^{\beta_1} \Bigg|_{t_k}^{t_L} \\ & + \sum_{i=j+2}^{k} \frac{1}{e_1 \beta_1} \left[ e_i \, t' + A_i - e_{j+1} \, t_o \right]^{\beta_1} \Bigg|_{t_{i-1}}^{t_i} \\ & + \frac{1}{e_{j+1} \beta_1} \left[ e_{j+1} \, t' - e_{j+1} \, t_o \right]^{\beta_1} \Bigg|_{t_o}^{t_{j+1}} \end{aligned} \tag{12-63}$$

Since Equation 12-63 may be explicitly differentiated with respect to $t_o$, a Newton-Raphson technique provides a simple solution. The subroutine developed uses a second-order routine to speed convergence. The routine proceeds by rewriting Equation 12-63 as

$$\begin{aligned} f(t_o) = {} & -\frac{L}{\alpha_1 \beta_1} + \frac{1}{e_{k+1} \beta_1} \left[ e_{k+1} \, t' + A_{k+1} - e_{j+1} \, t_o \right]^{\beta_1} \Bigg|_{t_k}^{t_L} \\ & + \sum_{i=j+2}^{k} \frac{1}{e_1 \beta_1} \left[ e_i t' + A_i - e_{j+1} \, t_o \right]^{\beta_1} \Bigg|_{t_{i-1}}^{t_i} \\ & + \frac{1}{e_{j+1} \beta_1} \left[ e_{j+1} \, t' - e_{j+1} \, t_o \right]^{\beta_1} \Bigg|_{t_o}^{t_{j+1}} \end{aligned} \tag{12-64}$$

The first and second derivatives of $f(t_o)$ with respect to $t_o$ are, respectively

$$f'(t_o) = \frac{e_{j+1}}{e_{k+1}} \{[e_{k+1}\, t_L + A_{k+1} - e_{j+1}\, t_o]^{\beta_1 - 1} - [e_{k+1}\, t_k + A_{k+1} - e_{j+1}\, t_o]^{\beta_1 - 1}\} + \sum_{i=j+1}^{k} \frac{e_{j+1}}{e_i} \{[e_i\, t_o + A_i - e_{j+1}\, t_o]^{\beta_1 - 1} - [e_i\, t_{i-1} + A_i - e_{j+1}\, t_o]^{\beta_1 - 1}\} - [e_{j+1}\, t_{j+1} - e_{j+1}\, t_o]^{\beta_1 - 1} \quad (12\text{-}65)$$

and

$$f''(t_o) = \frac{e_{j+1}^2}{e_{k+1}} \{(\beta_1 - 1)\, [e_{k+1}\, t_L + A_{k+1} - e_{j+1}\, t_o]^{\beta_1 - 2} - [e_{k+1}\, t_k + A_{k+1} - e_{j+1}\, t_o]^{\beta_1 - 2}\} + \sum_{i=j+2}^{k} \frac{e_{j+1}^2}{e_i} (\beta_1 - 2) \{[e_i\, t_i + A_i - e_{j+1}\, t_o]^{\beta_1 - 2} - [e_i t_{i-1} + A_i - e_{j+1}\, t_o]^{\beta_1 - 2}\} + (\beta_1 - 1)\, (e_{j+1})\, [e_{j+1}\, t_{j+1} - e_{j+1}\, t_o]^{\beta_1 - 2} \quad (12\text{-}66)$$

The second-order Newton's method is based on truncating Taylor's series expansion of $f(t_o)$ about a trial value of $t_o$, defined as $t_o^*$, after the third term. Thus, $f(t_o)$ is written as

$$f(t_o) \simeq f(t_o^*) - (t_o - t_o^*)\, f'(t_o^*) + \frac{(t_o - t_o^*)^2}{2} f''(t_o^*) \quad (12\text{-}67)$$

Roots of $f(t_o)$ are then obtained by setting $f(t_o) = 0$ in Equation 12-67 and solving the resulting quadratic for $t_o$. This value of $t_o$ becomes the new estimate of the root and iterations continue until

$$\left| \frac{f(t_o^*)}{\frac{L}{\alpha_1 \beta_1}} \right| < \eta \quad (12\text{-}68)$$

where $\eta$ is some arbitrarily small convergence increment.

In this manner, $t_o$'s can be calculated corresponding to selected $t_L$'s. The values of $t_o$ contain some error due to Newton's method approximation; however, this error, unlike the error due to interpolation, may be precisely controlled by the specification of $\eta$.

The number of terms in the summation appearing in Equations 12-64, 12-65 and 12-66 are determined by using the histogram of the lateral inflow to subdivide the solution domain. This subdivision is accomplished by calculating the characteristics arising at the beginning of each new histogram element (Figure 12-9). Since the applications for which these routines are intended never exhibit kinematic shock, no characteristics in the solution domain intersect. Therefore, the characteristics calculated serve as a minimum set of bounds for those to be calculated by Equation 12-68. The number of terms in Equations 12-64 through 12-66 are immediately known by simply counting the number of histogram units crossed by the regions that are bounded by the characteristics having $t_L$'s on either side of the $t_L$ selected (Figure 12-9). Thus, the values of $k$ and $j$ for a given $t_L$ in Equations 12-64 through 12-66 are known.

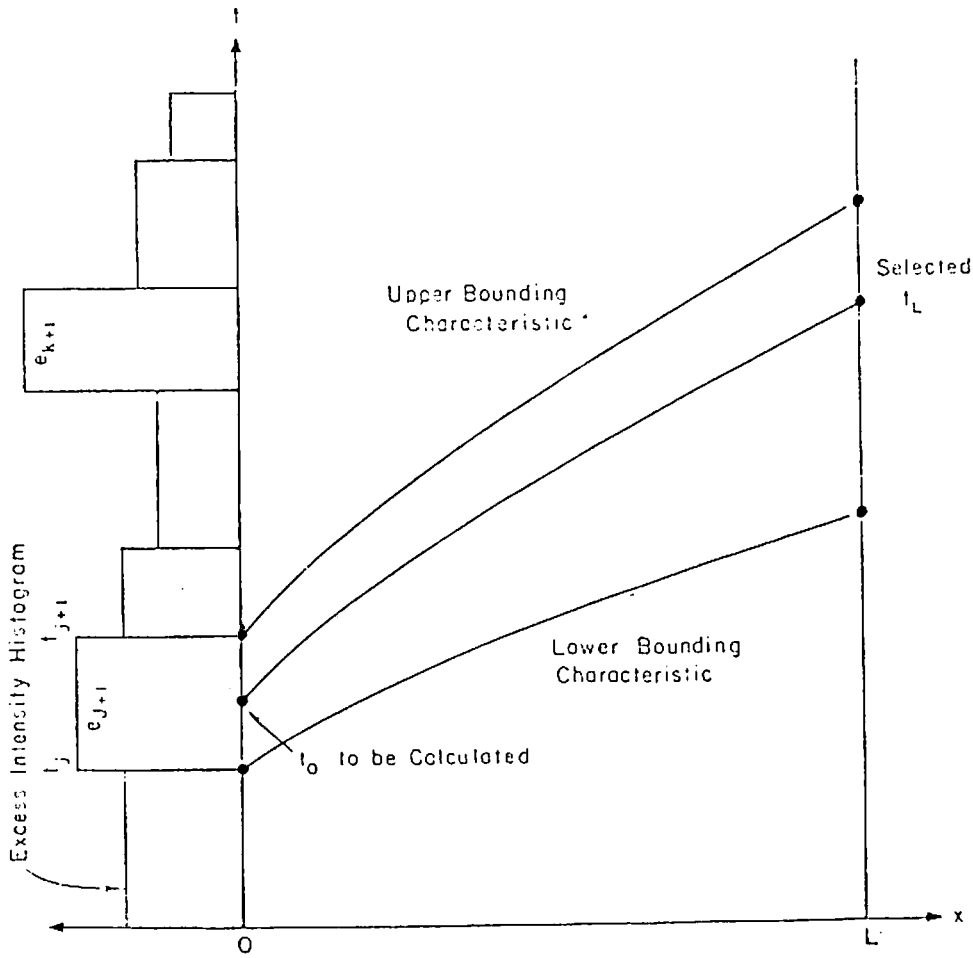


Figure 12-9. Method of characteristics solution domain illustrating upstream calculation of characteristics between bounding characteristics previously calculated in downstream direction.

This technique provides a rapid means of finding $t_o$'s corresponding to a given $t_L$. Three iterations of Newton's method have seemed sufficient for $\eta = 0.0001$. Knowing $t_o$ and $t_L$, the depth may be evaluated at the downstream boundary at time $t_L$ by using Equation 12-44. This depth is used to determine discharge at the downstream boundary at time $t_L$ by using Equation 35 with $q$ and $y$ substituted for $Q_\ell$ and $A$, respectively.

For the simplified formulation in the absence of channel cross-sectional data, it may be assumed that the planes meet to form a triangular channel as shown in Figure 12-10. The wetted perimeter of that channel $P$ (Figure 12-10) may be expressed as

$$P = \frac{A}{R} = r_1 + r_2 = (y^2 + t_1^2)^{\frac{1}{2}} + (y^2 + t_2^2)^{\frac{1}{2}} \qquad (12\text{-}69)$$

where the subscripts refer to plane 1 and plane 2. Since $t_1$ and $t_2$ may be expressed as

$$t_1 = \frac{y}{S_1} \quad ; \quad t_2 = \frac{y}{S_2} \qquad (12\text{-}70)$$

Equation 12-69 may be written

$$P = y \left(1 + \frac{1}{S_1^2}\right)^{\frac{1}{2}} + \left(1 + \frac{1}{S_2^2}\right)^{\frac{1}{2}} \qquad (12\text{-}71)$$

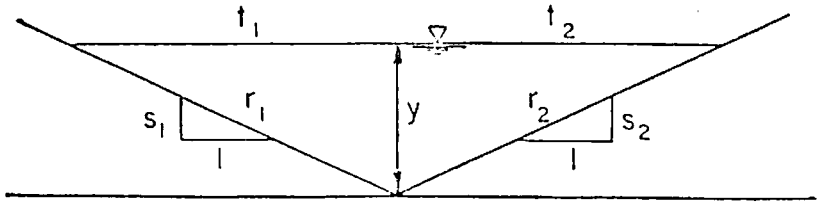


Figure 12-10. Definition sketch of triangular channel.

Referring to Figure 12-10, the cross-section area of the channel may be expressed as

$$A = \frac{1}{2}\, y\, (t_1 + t_2) \qquad (12\text{-}72)$$

or

$$A = \frac{1}{2}\, y^2 \left(\frac{1}{S_1} + \frac{1}{S_2}\right) \qquad (12\text{-}73)$$

Solving Equation 12-72 for $y$ and substituting the result into Equation 12-71 yields the following expression for $P$ in terms of $A$

$$P = a_1 A^{\frac{1}{2}} \tag{12-74}$$

with

$$a_1 = \left[\frac{2}{\left(\frac{1}{S_1} + \frac{1}{S_2}\right)}\right]^{\frac{1}{2}} \left[\left(1 + \frac{1}{S_1^2}\right)^{\frac{1}{2}} + \left(1 + \frac{1}{S_2^2}\right)^{\frac{1}{2}}\right] \tag{12-75}$$

and

$$b_1 = 1/2 \tag{12-76}$$

The $a_1$ and $b_1$ once calculated may then be used to obtain $\alpha'$ and $\beta'$ by substitution into either Equation 12-53 or 12-54. If channel cross-sectional data is available, $a_1$ and $b_1$ can be determined.

The above analytical solution is certainly desirable since there is no problem encountered in computational stability and convergence. Unfortunately, this analytical solution is often restricted for practical applications because of the kinematic "shock wave." The shock is represented by the intersections of characteristics in the x-t plane. This produces an abrupt increase in flow depth (Kibler and Woolhiser, 1970). An example of the kinematic wave shock is given in Figure 12-11. Li et al. (1976c) gives an in-depth discussion of this limitation. However, for a small watershed with simple geometry having two planes and one channel, the above analytical procedure can be used. Simons et al. (1977a) reported a simple watershed model using small programmable calculators based on the two-planes and one-channel representation of watersheds.

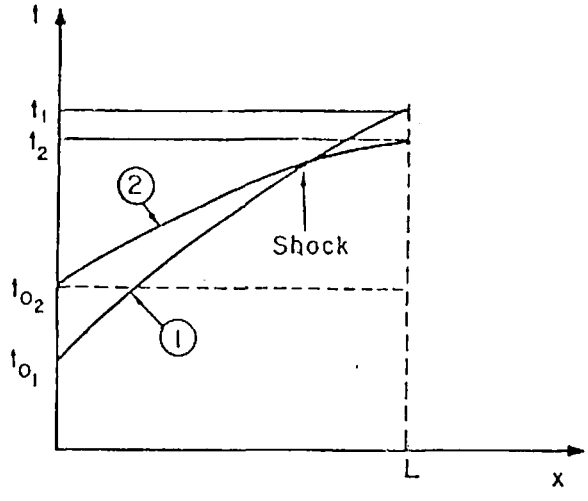


Figure 12-11. Schematic diagram of kinematic-wave shock formation.

Numerical Solution

Li et al. (1977b) and Simons (1977) developed a nonlinear scheme with an iterative procedure to solve a four-point implicit formulation of Equations 12-17 and 12-28. A linear scheme is used to obtain the initial estimate of the unknown discharge for the nonlinear scheme. The linear scheme may be used as is, with no iterations to solve for the unknown discharge, providing accuracy is satisfactory.

Nonlinear Scheme. The finite difference form of Equation 12-17 using quantities at all four points (see Figure 12-12) of the box scheme can be written as

$$\left[\frac{Q_{j+1}^{n+1}-Q_j^{n+1}}{\Delta x}(1-a)+\frac{Q_{j+1}^{n}-Q_j^{n}}{\Delta x}(a)\right]+\left[\frac{A_{j+1}^{n+1}-A_{j+1}^{n}}{\Delta t}(1-b)+\frac{A_j^{n+1}-A_j^{n}}{\Delta t}(b)\right]=\frac{(1-b)q_{\ell}{}_{j+1}^{n+1}+bq_{\ell}{}_{j}^{n+1}+(1-b)q_{\ell}{}_{j+1}^{n}+bq_{\ell}{}_{j}^{n}}{2} \qquad (12\text{-}77)$$

in which $Q_j^n$ is quantity $Q$ at grid point $x = j\Delta x$, $t = n\Delta t$, where $\Delta x$ is the space increment and $\Delta t$ is the time increment. Also, $a$ is the time weighting factor and $b$ is the space weighting factor where $0 \leq a \leq 1$ and $0 \leq b \leq 1$.

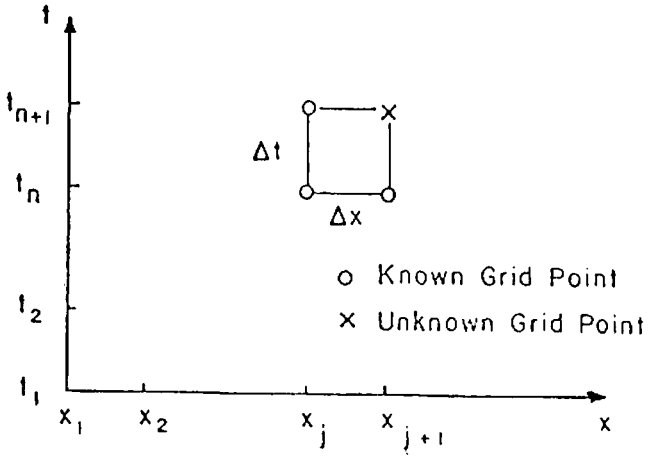


Figure 12-12. Rectangular network in x-t plane.

The unknowns in Equation 12-77 are $q_{j+1}^{n+1}$ and $A_{j+1}^{n+1}$, but they are related according to Equation 12-28. With these two equations, the two unknowns may be calculated. The boundary conditions required for this particular formulation are as follows: $Q(0,t)$ and $Q(x,0)$, or in other words, the discharge must be known or assumed along both the space axis $[Q(x,0)]$ and the time axis $[Q(0,t)]$. No downstream boundary conditions

are required. However, if there is a strong downstream control, the kinematic wave approximation no longer applies.

Either Q or A can be selected as the independent variable in the numerical procedure. As customary in backwater computations, the depth of flow (equivalent to A above) is chosen as the independent variable (see Henderson, 1966). However, Q is a better choice for the following reason. From Equation 12-28 one can derive

$$\frac{dA}{A} = \beta \frac{dQ}{d} \tag{12-78}$$

Since the value of $\beta$ is generally less than 1.0, if the discharge is computed incorrectly, the relative error in the flow area is smaller than the relative error in the discharge. On the other hand, the error in the discharge estimation is magnified if the numerical computations are performed on the flow area. From the physical viewpoint it is more appropriate to consider routing unit volumes of water rather than areas of flow.

From Equation 12-28

$$A_{j+1}^{n+1} = \alpha \, (Q_{j+1}^{n+1})^{\beta} \tag{12-79}$$

$$A_{j}^{n+1} = \alpha \, (Q_{j}^{n+1})^{\beta} \tag{12-80}$$

$$A_{j+1}^{n} = \alpha \, (Q_{j+1}^{n})^{\beta} \tag{12-81}$$

$$A_{j}^{n} = \alpha \, (Q_{j}^{n})^{\beta} \tag{12-82}$$

Equations 12-79 through 12-82 are substituted into Equation 12-77 and rearranged to yield

$$\begin{aligned} &\frac{\Delta t}{\Delta x} Q_{j+1}^{n+1} \, (1\text{-}a) + \alpha \, (Q_{j+1}^{n+1})^{\beta} \, (1\text{-}b) \\ &= \frac{\Delta t}{\Delta x} \left[ Q_{j}^{n+1} \, (1\text{-}a) \quad (Q_{j+1}^{n} - Q_{j}^{n}) \, (a) \right] \\ &+ \alpha \, (Q_{j+1}^{n})^{\beta} \, (1\text{-}b) - [\alpha (Q_{j}^{n+1})^{\beta} - \alpha (Q_{j}^{n})^{\beta}] \, (b) \\ &+ \frac{\Delta t}{2} \left[ (1\text{-}b) q_{\ell}{}_{j+1}^{n+1} + b q_{\ell}{}_{j}^{n+1} + (1\text{-}b) q_{\ell}{}_{j+1}^{n} + b q_{\ell}{}_{j}^{n} \right] \end{aligned} \tag{12-83}$$

The right-hand side of Equation 12-83 consists of known quantities and is represented by $\Omega$ i.e.,

$$\Omega = \frac{\Delta t}{\Delta x}\left[ Q_j^{n+1}(1-a) - (Q_{j+1}^n - Q_j^n)\ (a)\right] + \alpha(Q_{j+1}^n)^\beta(1-b)$$
$$- [\alpha(Q_j^{n+1})^\beta - \alpha(Q_j^n)^\beta](b)$$
$$+ \frac{\Delta t}{2}\left[(1-b)q_{\ell}{}_{j+1}^{n+1} + bq_{\ell}{}_j^{n+1} + (1-b)q_{\ell}{}_{j+1}^{n} + bq_{\ell}{}_j^{n}\right] \qquad (12\text{-}84)$$

Let $r = Q_{j+1}^{n+1}$ and $\theta = \frac{\Delta t}{\Delta x}$ so that the left-hand side of Equation 12-83 can be written as

$$f(r) = \theta(1-a)r + \alpha(1-b)r^\beta \qquad (12\text{-}85)$$

The solution to Equation 12-83 is the solution $r^*$ which satisfies the condition

$$f(r^*) = \theta(1-a)r^* + \alpha(1-b)r^{*\beta} = \Omega \qquad (12\text{-}86)$$

Equation 12-86 is nonlinear in $r^*$. An approximate solution to this nonlinear equation is obtained by the following iterative technique.

Let $r^k$ be the value of $r$ at the $k^{\underline{th}}$ iteration. Taylor's series expansion of function $f(r)$ around $r^k$ is

$$f(r) = f(r^k) + (r-r^k)f'(r^k) + 1/2(r-r^k)^2f''(r^k)$$
$$+ 1/6(r-r^k)^3f'''(r^k) + \ldots \qquad (12\text{-}87)$$

in which $f'(r^k)$, $f''(r^k)$, and $f'''(r^k)$ are the first, second and third derivatives of the function at $r^k$.

Dropping terms higher than third order, one obtains

$$f(r)\ \ f(r^k) + (r-r^k)f(r^k) + 1/2(r-r^k)^2f''(f^k) \qquad (12\text{-}88)$$

Iteration forces $f(r^{k+1})$ to approach the value of $\Omega$

$$\Omega = f(r^k) + (r^{k+1}-r^k)f'(r^k) + 1/2(r^{k+1}-r^k)^2f''(r^k) \qquad (12\text{-}89)$$

The solution of Equation 12-89 is

$$r^{k+1} = r^k - \frac{f'(r^k)}{f''(r^k)} \pm \left\{\left[\frac{f'(r^k)}{f''(r^k)}\right]^2 - \frac{2[f(r^k)-\Omega]}{f''(r^k)}\right\}^{\frac{1}{2}} \qquad (12\text{-}90)$$

in which

$$f(r^k) = \theta(1-a)r^k + \alpha(1-b)(r^k)^\beta \tag{12-91}$$

$$f'(r^k) = \theta(1-a) + \alpha\beta(1-b)(r^k)^{\beta-1} \tag{12-92}$$

$$f''(r^k) = \alpha\beta(\beta-1)(1-b)(r^k)^{\beta-2} \tag{12-93}$$

There are two solutions to Equation 12-90. It is advisable to choose the solution which gives a smaller value of $\left|f(r^{k+1})-\Omega\right|$. The iterations are continued until the absolute error $\left|f(r^{k+1})-\Omega\right|$ is less than some preassigned tolerance $\varepsilon$

$$\left|f(r^{k+1})-\Omega\right| \leq \varepsilon \tag{12-94}$$

An appropriate value for $\varepsilon$ is $0.01\Omega$.

The initial guess $r^o$ is the key to the speed of convergence to the correct numerical solution. The best way to determine $r^o$ is to use a linear scheme. The linear scheme may be used as the solution instead of going through the iterative, nonlinear scheme when accuracy is of less importance and when computer time has to be conserved.

Linear Scheme. The term $\frac{\partial A}{\partial t}$ in Equation 12-17 can be expressed as

$$\frac{\partial A}{\partial t} = \frac{\partial A}{\partial Q}\frac{\partial Q}{\partial t} \tag{12-95}$$

and from Equation 12-28

$$\frac{\partial A}{\partial Q} = \alpha\beta Q^{\beta-1} \tag{12-96}$$

Substitution of Equations 12-95 and 12-96 into 12-17 yields

$$\frac{\partial Q}{\partial x} + \alpha\beta Q^{\beta-1}\frac{\partial Q}{\partial t} = q_\ell \tag{12-97}$$

The finite difference form of Equation 12-97 can be expressed as

$$\frac{Q_{j+1}^{n+1} - Q_j^{n+1}}{\Delta x}(1-a) + \frac{Q_{j+1}^{n} - Q_j^{n}}{\Delta x}(a)$$

$$+ \alpha\beta\left[\frac{Q_j^{n+1} + Q_{j+1}^{n}}{2}\right]^{\beta-1}\left[\frac{Q_{j+1}^{n+1} - Q_{j+1}^{n}}{\Delta t}(1-b) + \frac{Q_j^{n+1} - Q_j^{n}}{\Delta t}(b)\right]$$

$$= \frac{1}{2}\left[(1-b)q_{\ell}{}_{j+1}^{n+1} + bq_{\ell}{}_{j}^{n+1} + (1-b)q_{\ell}{}_{j+1}^{n} + bq_{\ell}{}_{j}^{n}\right] \tag{12-98}$$

Solving for $r^o = Q_{j+1}^{n+1}$

$$Q_{j+1}^{n+1} = \left[\frac{1-a}{\Delta x} + \alpha\beta\left(\frac{Q_j^{n+1} + Q_{j+1}^n}{2}\right)^{\beta-1}\frac{(1-b)}{\Delta t}\right]^{-1}$$

$$\left\{\frac{Q_j^{n+1}}{\Delta x}(1-a) - \frac{Q_{j+1}^n - Q_j^n}{\Delta x}(a)\right.$$

$$-\alpha\beta\left(\frac{Q_j^{n+1} + Q_{j+1}^n}{2}\right)^{\beta-1}\left[-\frac{Q_{j+1}^n}{\Delta t}(1-b) + \frac{Q_j^{n+1} - Q_j^n}{\Delta t}(b)\right]$$

$$\left. + \frac{1}{2}\left[(1-b)q_{\ell}{}_{j+1}^{n+1} + bq_{\ell}{}_j^{n+1} + (1-b)q_{\ell}{}_{j+1}^{n} + bq_{\ell}{}_j^{n}\right]\right\} \qquad (12\text{-}99)$$

Equation 12-99 provides the best estimate for $r^o$ for the nonlinear scheme. However, Equation 12-99 is not applicable if both $Q_{j+1}^n$ and $Q_j^{n+1}$ are zero. In this case, use $\beta = 1$ in Equation 12-86.

$$r^o = \frac{\Omega}{(1-a)\theta + (1-b)\alpha} \qquad (12\text{-}100)$$

Li et al. (1977b) proved that weighting factors a and b must be less than or equal to 1/2 in order to insure stability. When a and b are both zero, this is a fully implicit scheme, which was developed by Li et al. (1975a). When a and b are equal to 1/2, it is a central implicit scheme. The central implicit formulation has been tested using Iwagaki's experimental data (Iwagaki, 1955). Figure 12-13 shows high correlation between experimental and computed results for the three events during different time durations. Li et al. (1975a) successfully applied the fully implicit scheme to a variety of flow conditions.

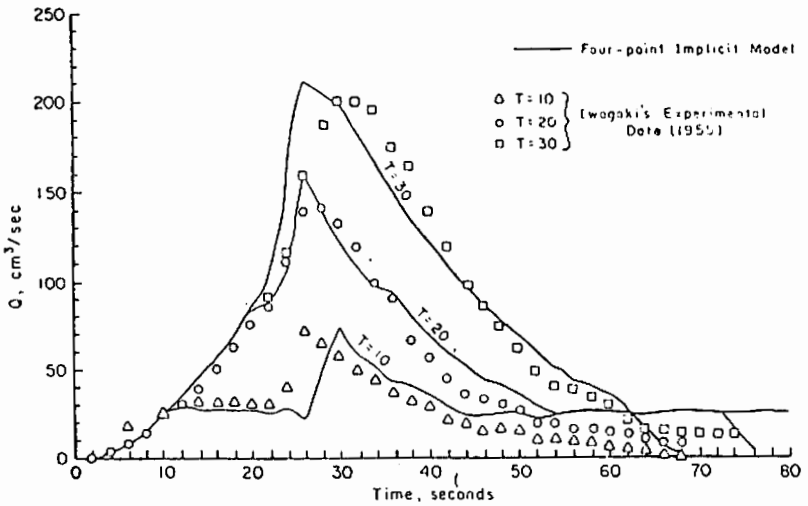


Figure 12-13. Comparison of the discharge hydrographs given by the four-point, central implicit model to Iwagaki's experimental data.

Other available numerical methods for kinematic wave approximation are given by Houghton and Kasahara (1968), Brakensiek (1967), Kibler and Woolhiser (1970), and Singh (1975). However, these methods are much more complicated and sometimes unstable in solution.

## 12.6 EXAMPLE OF APPLICATION

### Simplified Models

An example of the application of the single open-book model approach is provided by an event on Watershed 17 located in the Coconino National Forest near Flagstaff, Arizona. This watershed has an area of approximately 300 acres. This watershed is an area of heterogeneous topography partially forested in conifers. The modeled event was recorded on September 5, 1970. Figure 12-14 shows measured and calculated runoff. The agreement between measured and calculated runoff appears to be quite good. Some rudimentary calibration of K was performed to make the runoff volume agree with the measured volume, but Figure 12-14 represents a substantially uncalibrated result. Resistance for the main channel was guessed to correspond to a Manning's n of about 0.07 as reported by Chow (1959) for a cobble and boulder channel. The Manning's n was then converted to the Darcy-Weisbach friction factor.

As an example of application of the MULTWAT method to a large heterogeneous watershed, the model was used to simulate runoff from the Walnut Gulch watershed in southeastern Arizona. The spatial representation of the watershed appears in Figure 12-6 and the watershed map in Figure 12-5. Walnut Gulch is operated by the Agricultural Research Service and surrounds the historic town of Tombstone, Arizona. The study area consists of 57.7 square miles of uncultivated semiarid rangeland. Precipitation is measured with 93 recording rain gages spaced fairly evenly over the watershed. Runoff from the entire watershed and from nine subwatersheds is calculated from stage records collected at special flow measuring flumes.

The vegetation of Walnut Gulch consists of desert grasses and shrubs, and most of the soils are gravelly loam. Seventy percent of the annual precipitation of 11.5 inches occurs during high-intensity, short-duration thunderstorms in the late summer months.

The entire Walnut Gulch watershed (57.7 square miles) was modeled for two different storm events. The drainage areas (approximately 5.5 square miles) for several stock ponds were not included in the analysis since spillage was assumed to be negligible. The rainfall distributions for the response units were calculated by using an isohyetal map and individual gage records. United States Geological Survey topographical maps were used to determine the slopes and lengths of the units representing Walnut Gulch. The channel geometry parameters were obtained from a limited number of cross-sectional profiles. The comparison of the predicted and recorded hydrographs is shown in Figure 12-15. The agreement between predicted and recorded runoff is good considering the complexity and size of the watershed.

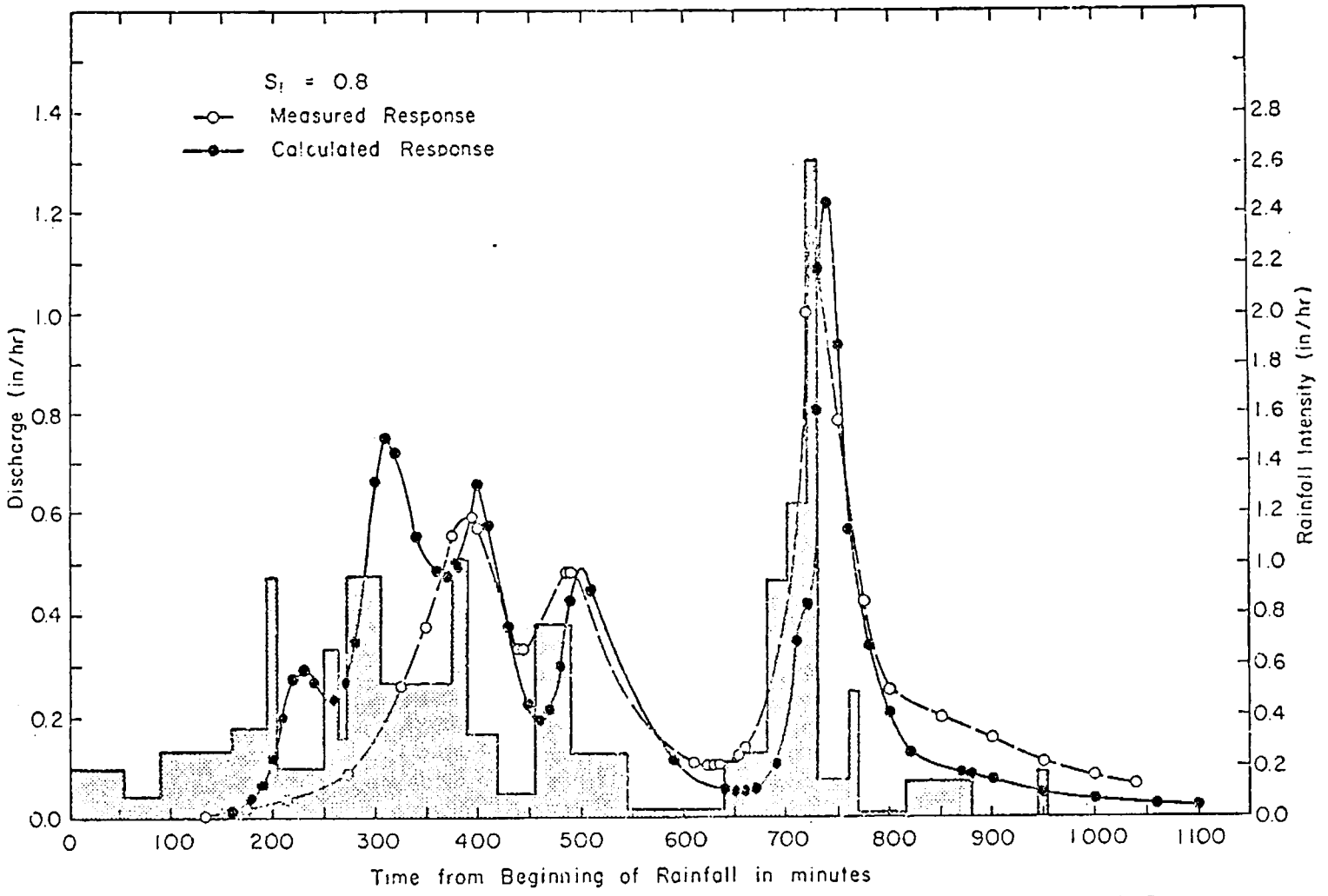


Figure 12-14. Rainfall-runoff response for Watershed 17, Coconino National Forest.

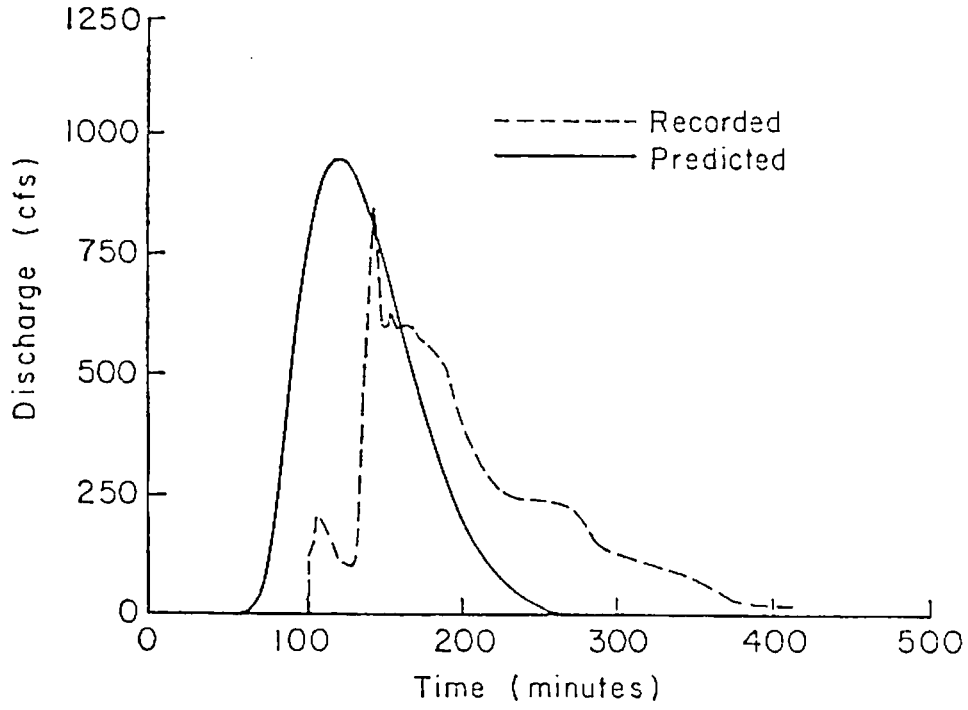


a. Runoff hydrograph for the storm of September 4, 1965, for the entire Walnut Gulch watershed.

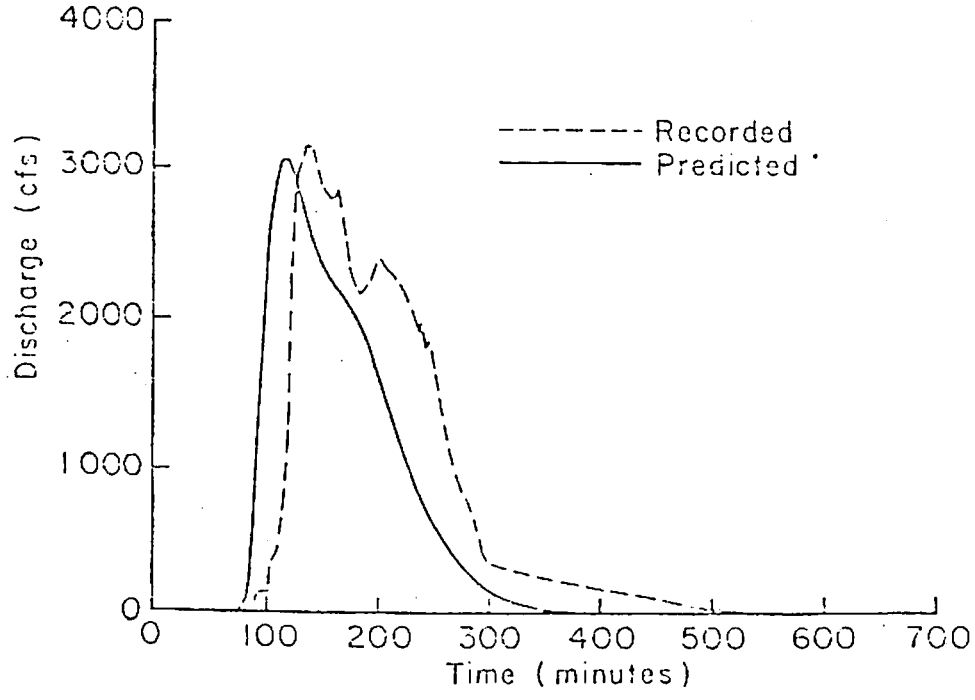


b. Runoff hydrograph for the storm of September 9, 1964, for the entire Walnut Gulch watershed.

Figure 12-15. Runoff hydrographs for the entire Walnut Gulch watershed.

## High Resolution Models

Water Routing Component. The high resolution is chiefly characterized by the water routing component. Two examples of applications of this component are presented.

Natural Channel. A flood hydrograph in the Rio Amana in Venezuela was used to test the applicability of the numerical method of flood routing in a natural channel. Both inflow and outflow hydrographs were measured in 1969 in the reach of river between El Tejero and the crossing of the Naturin-Tembledor Road (see Simons et al., 1971a). As described by Simons et al. (1971b), the reach is 47.1 miles long and has an average slope of 0.00146. The bank-full top width at the downstream station is approximately 70 feet. The measured $\alpha$ and $\beta$ values in the A versus Q relation are available at the downstream station. The values are $\alpha = 1.1$ and $\beta = 0.9$. For this reach it was assumed that $\beta$ remains a constant and $\alpha$ changes linearly with distance. The estimated value of $\alpha$ at the upstream station is 2.5, and the lateral outflow rate was approximately 0.26 $ft^3/s/mi$. The estimated upstream $\alpha$ value is much larger than the downstream value because of larger flow resistance and larger wetted perimeters for the same flow area in the upstream reach.

In Figure 12-16 the numerical solutions ($\Delta t = 2_h$ and $\Delta t/\Delta x = 0.58$ s/ft) agree with the measured results. The proposed numerical method is applicable in natural channels with steep gradients and slow-rising hydrographs because the kinematic wave approximation is applicable for such channels.

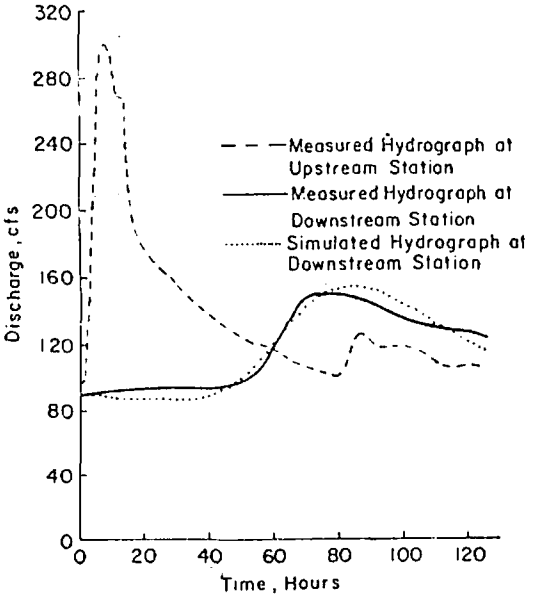


Figure 12-16. Flood routing in the Rio Amana in Venezuela.

Confined Catchment. The numerical model presented herein is valid for channel flows as well as overland flows. A catchment system is formulated by routing the overland flows to channels and then routing the flows through the channels. The numerical solutions for hydrographs from small catchments agree very well with the measured runoff. A

comparison of computed and measured hydrographs at the outlet of SPL1 parking lot at Johns Hopkins University is shown in Figure 12-17. The storm used in this analysis is 13SPL1, which was reported by Schaake (1965). The area of the parking lot was 0.39 acre. The catchment area consisted of the overland flow area and V-shaped channels. The lengths of overland flow paths varied from 20 to 36 feet and the overland slopes varied from 0.0167 to 0.019. The side slopes of V-shaped channels were 1:113. The lengths of these channels varied from 50 to 165 feet, and the channel slopes ranged from 0.0148 to 0.0213. In the numerical computations, $\Delta t = 1$ min and $7.3 \leq \Delta t/\Delta x \leq 30$ s/ft.

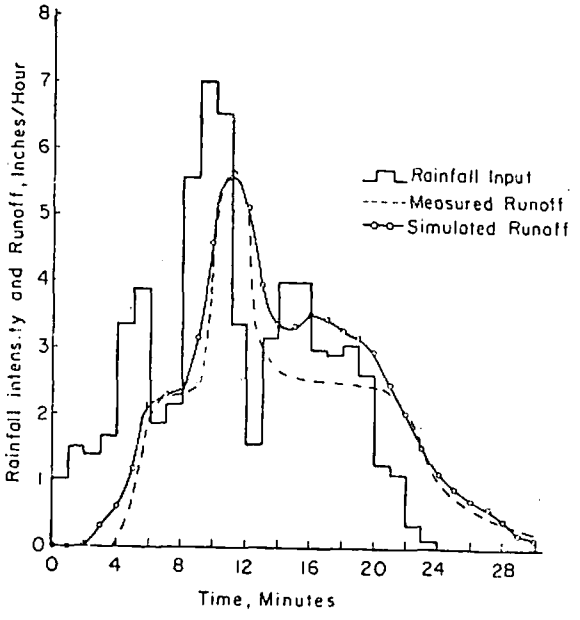


Figure 12-17. Runoff from SPL1 parking area, Johns Hopkins University.

The agreement between computed and observed hydrographs shown in Figure 12-17 indicates the usefullness of the proposed numerical model for time varient inflows and watershed modeling.

Simons et al. (1975) tested the applicability of their model on the Beaver Creek watershed in Arizona. Five runoff events in Watershed 1 and one runoff event in Watershed 17 were used.

Watershed 1 is a small drainage catchment with an area of 313.6 acres which has been clear cut. The five storm events used in this study for Watershed 1 occurred on November 22, 1965, November 24, 1965, November 25, 1965, September 6, 1967, and September 5, 1970. The latter is known as the "Labor Day" storm. This same storm is presented in Figure 12-14.

An example of the comparison between simulated and measured water hydrographs is shown in Figure 12-18. The agreement between the measured and the simulated water hydrographs is, for the most part, satisfactory. Because there is no measured sediment hydrograph, no comparison can be made. Other comparisons on water yield, peak water flow, time to peak water flow, and sediment yield are given respectively in Figures 12-19, 12-20 and 12-21. These figures show that the water

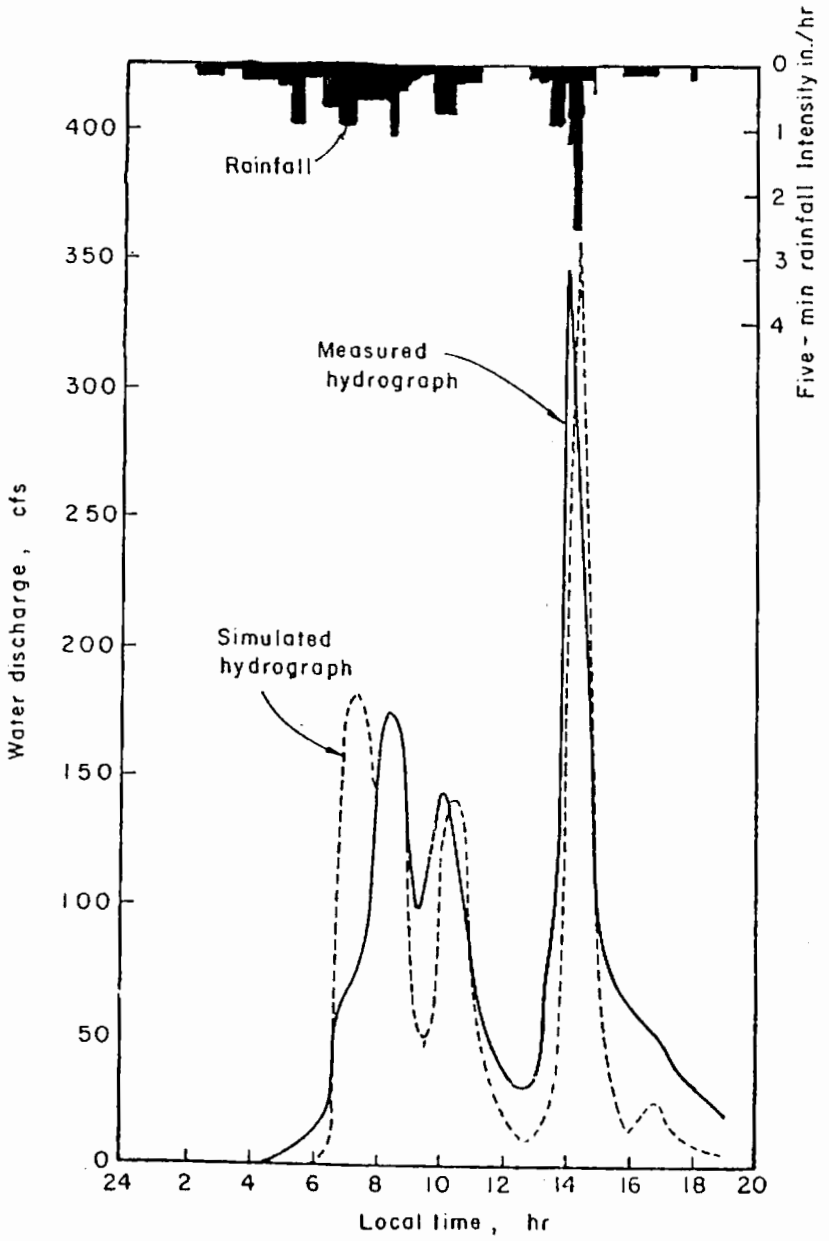


Figure 12-18. Water hydrograph from Watershed 17 for the September 5, 1970 storm (after Simons et al., 1975).

routing model simulated the shape, volume, peak flow, and time to peak flow of the six water hydrograph from Watershed 1 and Watershed 17 within approximately 30 percent. Satisfactory results were obtained for different size storms and in different watersheds by using only one set of model parameters. This verifies that the model could be used to synthesize missing data and to predict the response of watersheds to various types of watershed management practices. Also, it has been demonstrated that the model could be used to estimate flood flows from ungaged watersheds.

The transferability of the model is one of the main advantages of this physical process simulation model over conventional methods such as the Unit Hydrograph and Universal Soil Loss equation. For example, the Labor Day (September 5, 1970) storm produced approximately 2.2 times the surface runoff in Watershed 17 as in Watershed 1.

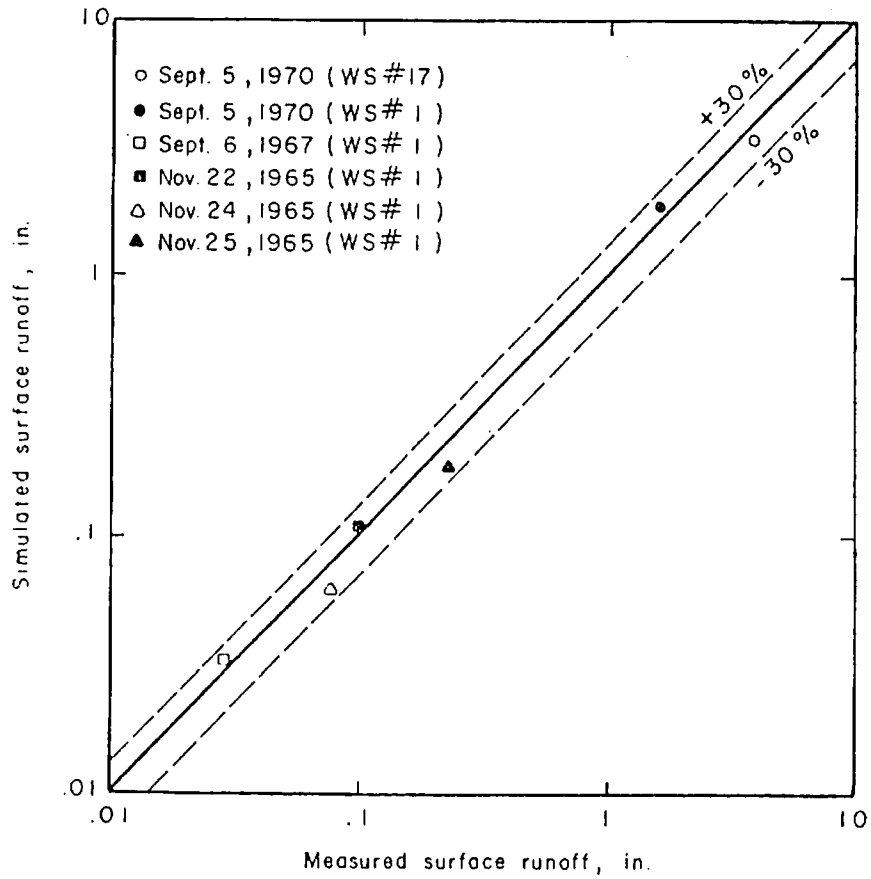


Figure 12-19. Comparison of measured and simulated water yield (after Simons et al., 1975).

An important aspect in watershed management is to predict watershed treatment effects. The vegetation treatment effects on water yield are estimated by changing the canopy cover density and the ground cover density in overland flow units. Based on the storms of September 5, 1970 and September 6, 1967, the effects of vegetation treatment on the water yield from Watershed 1 have been evaluated. As shown in Figures 12-22 and 12-23, for a constant and undisturbed ground cover of 65 percent, water yield and the peak flow rates from these two storms are increased as the canopy cover density is decreased.

The reduction in interception caused by removing the vegetation results in the increase of excess rainfall. These effects are much more pronounced in Watershed 1 for the smaller size of storm than for large storms like the Labor Day storm. The time to peak flow is shortened as the canopy cover is decreased for the small storm, but there is no change in time to peak flow for the large storm.

If a watershed is clear-cut and the forest litter, tree mulch, rocks, etc. are also removed in different degrees, or if the ground cover is seriously destroyed by a burning treatment, the associated response can be estimated by changing the ground cover density in overland flow units. The changes in water yield in Watershed 1 for the storms of September 5, 1970 and September 6, 1967, are shown in Figure 12-23. As the ground cover is decreased, the total surface runoff and

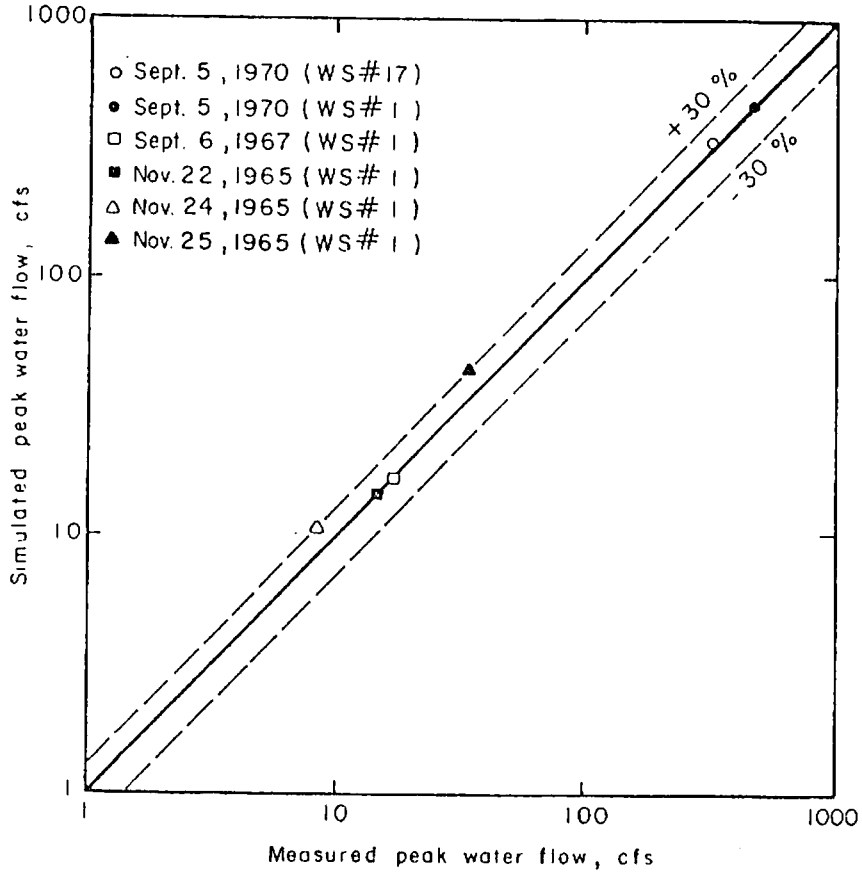


Figure 12-20. Comparison of measured and simulated peak water flows (after Simons et al., 1975).

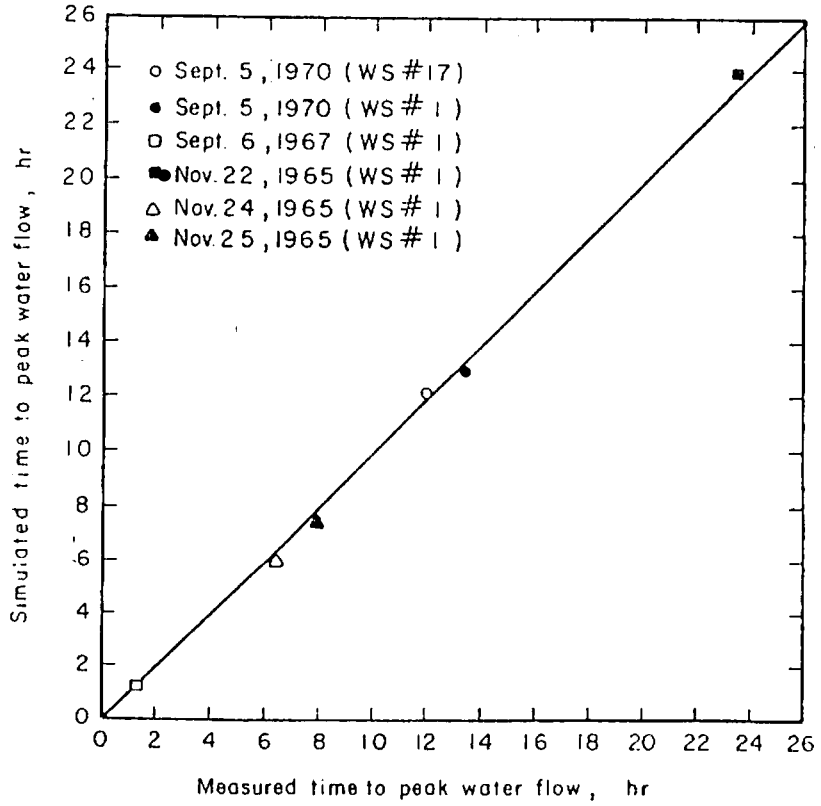


Figure 12-21. Comparison of measured and simulated time to peak water flow (after Simons et al., 1975).

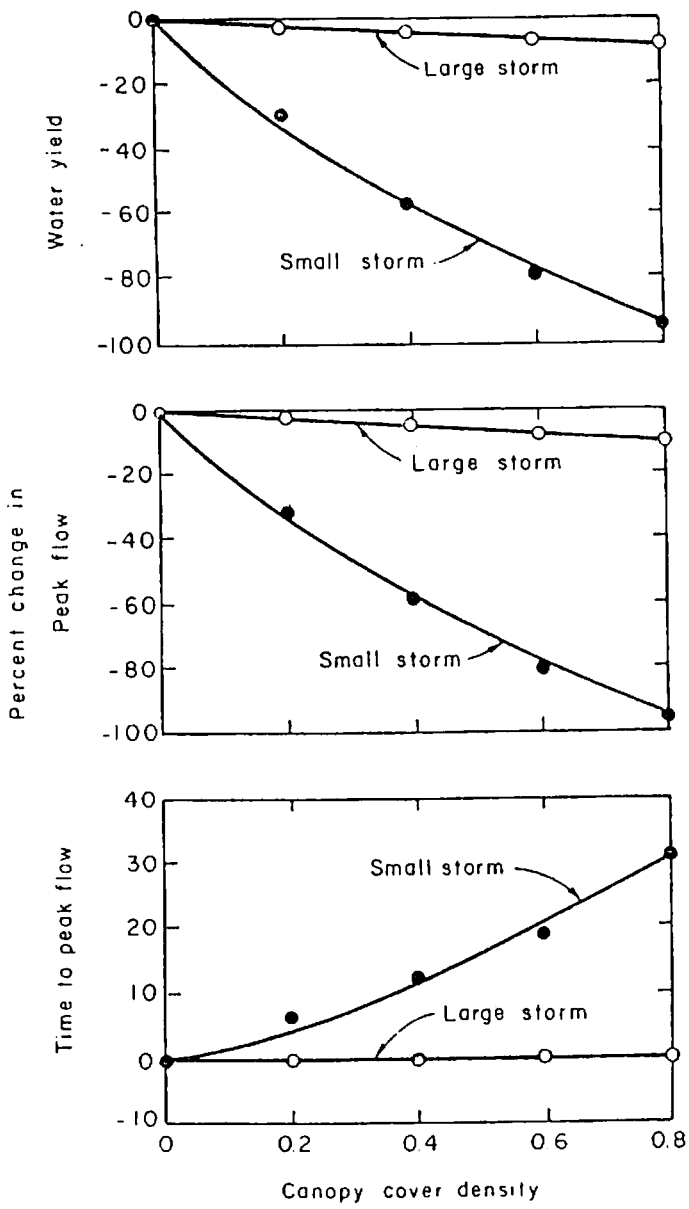


Figure 12-22. Effect of canopy cover density on the water hydrograph from Watershed 1 (after Simons et al., 1975).

peak water flow are increased moderately and the time to peak flow shortened slightly. The effect on water yield is more pronounced for a smaller storm.

## 12.7 PEAK FLOOD PREDICTION FOR AN ARID WATERSHED

### General

In the arid and semiarid west, normally low flowing or ephemeral streams can become raging torrents when swollen by runoff from intense thunderstorms. Because of the intermittency and random nature of such events, they cannot be analyzed using conventional flood frequency

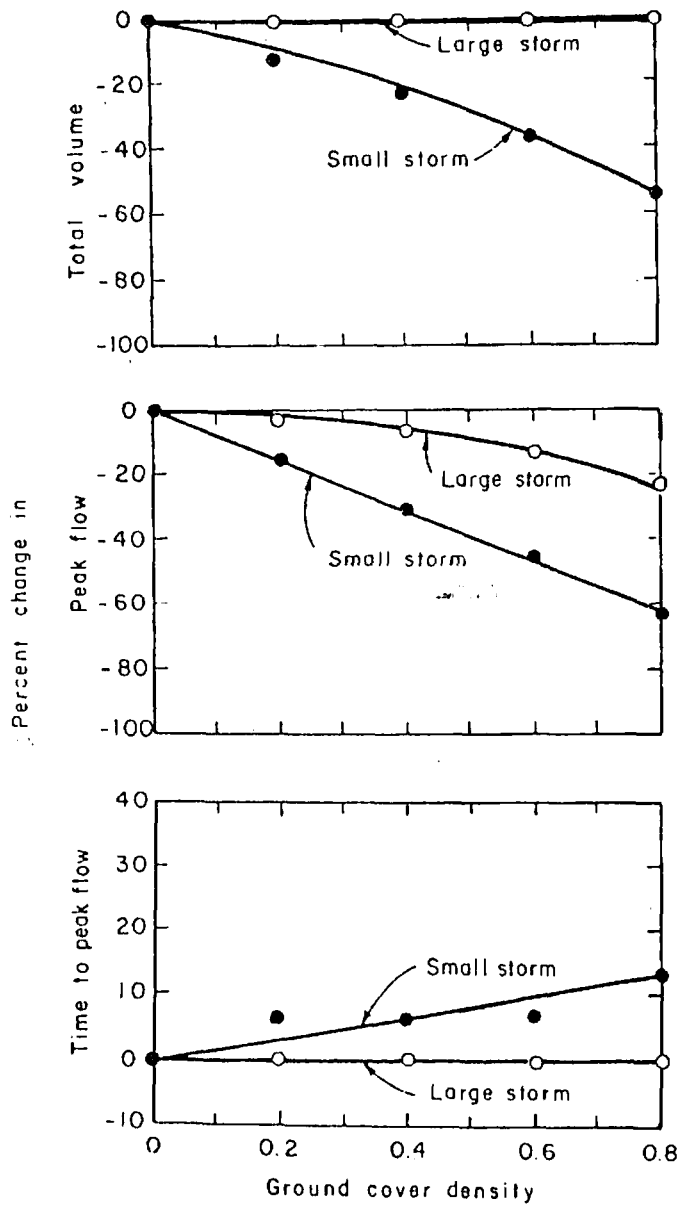


Figure 12-23. Effect of ground cover density on the water hydrograph from Watershed 1 (after Simons et al., 1975).

analyses as applied to larger streams or rivers. Instead the concept of probable maximum flood (PMF) is applied to estimate the absolute largest event that could occur based on present knowledge. Such a runoff does not coincide with what is termed the 100-year flood. It is usually many times larger. The PMF can be estimated utilizing several different techniques including analysis of the largest floods recorded. Here again such an approach is data dependent and may not completely represent the long-term system response. Another approach is to use the probable maximum precipitation (PMP) to generate a PMF. This generation can be from observed hydrograph similarities, such as a unit hydrograph, or through use of a rainfall-runoff simulation model. The simulation model is preferred if it is based on physical principles. In this

example, the multiple watershed model (MULTWAT) developed by Simons, Li and Spronk (1978) was used to determine the validity of a PMF hydrograph computed using other techniques. The primary purpose was for design of a diversion. Selection of a realistic PMF hydrograph is necessary in order to avoid high costs but provide the necessary safety in design. More details of this application are considered in the following segments.

## Model Application

### Background

On-site inspection of the watershed suggested that the PMF as calculated using an initial approach based on the average basin characteristics (U.S. Bureau of Reclamation, 1974) may be too large. The reasons for this were:

1. The upper half of the watershed is quite stable. It is armored with small rock and pebbles and shows no tendency to develop rills of gullies. Also, this part of the watershed is quite well protected with trees, shrubs, and in particular, a good growth of grass.

2. Topography of the watershed can be approximated by a series of three cascade sub-basins. The upper part of the basin is relatively flat with a ground cover density of approximately 70 percent and a canopy cover density of 15 percent. The middle sub-basin is very steep with 50 percent canopy cover density and 70 percent ground cover density and the lower sub-basin is relatively flat with a canopy cover density of 15 percent and a low ground cover density of approximately 40 percent. The shape and characteristics of the watershed indicate that the PMF hydrograph determined by the method given in "Design of Small Dams" is apt to be quite different from the one that considers the shape of the watershed and physical processes. It is anticipated that the peak flow will be smaller than the 31,800 cfs computed for the drainage area.

3. Observation of the dimensions of existing channels suggests that flows from the watersheds are not large. Observing the geometry of the channels at bends, it is possible to determine where maximum flow depths have undercut the vertical embankments at a height on the order of a few feet above the existing channel bank. Recent historic flows have probably not exceeded 4,000 cfs on the watershed. The maximum recorded flood of a nearby watershed (approximately 1,000 square miles) was 32,000 cfs.

Floods near the site are almost always the result of rainstorm rather than snowmelt. The prediction of flood hydrographs involves the consideration of such factors as: 1) amount, intensity, duration and temporal distribution of rainfall, 2) size, slope, and shape of the watershed, 3) soil conditions and vegetation, 4) channel size and shape, and 5) resistance to flow in watersheds and channels. The flood estimate in this example included the theoretical determination of peak flow, volume of flow, and the hydrograph at the site resulting from the

probable maximum precipitation (PMP). The PMF that results from applying the PMP to the watershed was estimated by assuming a flood equivalent to about 40 percent of the PMF and the antecedent rainfalls three to five days prior to the occurrence of the main flood. This required an assumption that the antecedent moisture condition is approximately equal to the field capacity that describes the moisture condition at which surface drainage is completed.

The PMP area rainfall correction and direct runoff were determined by methods currently employed by the U.S. Bureau of Reclamation (1974). Due to the distinct changes in slope from sub-basin to sub-basin, and because of the long, narrow-shaped watershed, the simplified procedure for obtaining the hydrograph developed by the Soil Conservation Service (U.S. Bureau of Reclamation, 1974) does not result in an acceptable hydrograph. A method that is based upon the governing physical processes was applied to obtain a more realistic answer.

Watershed Sedimentation

The drainage basin of the watershed has an area of about 11.2 square miles. Approximately 0.6 square mile in the upper portion drains to a closed basin and does not contribute runoff. It is assumed that the discharge from this basin would not contribute runoff to the project site even during the PMF. The highest elevation on the watershed approximates 8,700 feet with the lowest elevation near the proposed diversion dam approximating 6,500 feet. Typical average drainage basin slope for the watershed is approximately 5 percent. However, due to the distinct changes in slope from sub-basin to sub-basin, the average basin slope cannot represent the topographic features of the watershed adequately. There is a necessity to divide the watershed into sub-units. The watershed was divided into three subwatersheds, eight plane units, and six channel units (Figure 12-24). Each geometrical component of the subwatershed can be represented as an "open book" watershed. For subwatersheds and planes, analytical infiltration and water routing methods were utilized to obtain hydrographs. Hydrographs simulated on each of these units are combined by a numerical kinematic wave channel routing technique to form the total hydrograph for the watershed. The length, width and slopes of the segmented units are given in Table 12-2.

Probable Maximum Precipitation

Following the U.S. Bureau of Reclamation (1974) methodology for determining the PMP (page 53), the point rainfall of one-hour PMP was determined to be 11.0 inches. The ratio of area rainfall to point rainfall was estimated to be 0.8 (page 54). Thus, the area rainfall of the one-hour PMP is 8.8 inches. The one-hour thunderstorm PMF was selected over the 6-hour general storm because the one-hour thunderstorm would produce a high design peak flow.

The temporal distribution of the one-hour thunderstorm was based on the procedure suggested in the "Design of Small Dams" (page 543). The 15-minute intensities for the one-hour PMP are given in Table 12-3.

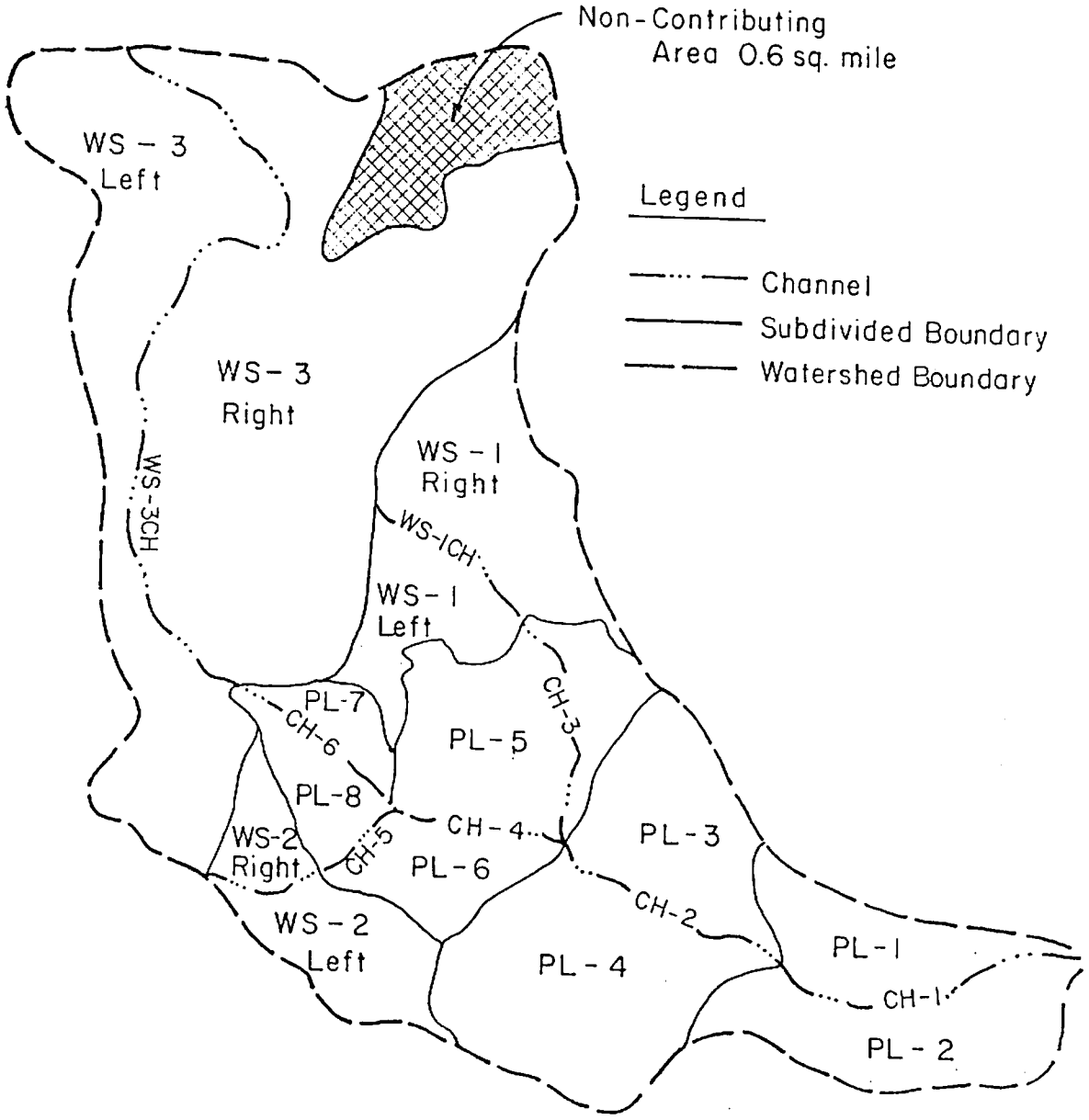


Figure 12-24. Watershed segmentation of the application area.

Direct Runoff

Peak rates of runoff are estimated to range from approximately 50 cubic feet per second (CF per square mile for the mean annual flood) to 500 cfs per square mile for the 50-year flood. The soils at the project site fall into Soil Conservation Service Hydrologic Groupings B and C. This hydrologic soil grouping is a four step rating indicating how much of a given rainfall will enter the soil profile and not run off. The hydrologic cover complex (vegetative cover) falls into the juniper-grass

Table 12-2. Geometry of the studied watershed.

| Unit | Length (ft.) | Width (ft.) | Slope |
|---|---|---|---|
| WS-1L | 2,342.72 | 4,760 | 0.0639 |
| WS-1R | 4,216.90 | 4,760 | 0.0404 |
| WS-1CH | 4,760.00 | | 0.0546 |
| WS-2L | 3,914.43 | 2,920 | 0.0523 |
| WS-2R | 1,814.01 | 2,920 | 0.0899 |
| WS-2CH | 2,920.00 | | 0.0685 |
| WS-3L | 2,444.25 | 19,960 | 0.0440 |
| WS-3R | 4,120.31 | 19,960 | 0.0394 |
| WS-3CH | 19,960.00 | | 0.0200 |
| PL-1 | 1,434.92 | 8,160 | 0.0458 |
| PL-2 | 2,289.04 | 8,160 | 0.0784 |
| CH-1 | 8,160.00 | | 0.0287 |
| PL-3 | 2,761.12 | 6,260 | 0.261 |
| PL-4 | 4,364.35 | 6,260 | 0.207 |
| CH-2 | 6,260.00 | | 0.0446 |
| CH-3 | 5,520.00 | | 0.189 |
| PL-5 | 5,369.17 | 4,050 | 0.273 |
| PL-6 | 2,271.57 | 4,050 | 0.315 |
| CH-4 | 4,050.00 | | 0.0778 |
| CH-5 | 2,360.00 | | 0.292 |
| PL-7 | 885.03 | 5,040 | 0.400 |
| PL-8 | 1,216.91 | 5,040 | 0.361 |
| CH-6 | 5,040.00 | | 0.137 |

Table 12-3. 15-minute rainfall intensities for one-hour probable maximum area rainfall.

| Time Minutes | Intensities in/hr |
|---|---|
| 15 | 10.56 |
| 30 | 7.04 |
| 45 | 3.52 |
| 60 | 14.08 |

category. The vegetative cover is mixed consisting of varying amounts of juniper, pinon, grass and cholla cover, or may be predominantly one of these types. Grass cover at the project site is generally heavier than that of desert grasses due to higher annual precipitation. Juniper-grass is typical of mountain slopes and mesas of intermediate elevations. Based on the above hydrologic soil cover complexes, the associated runoff curve numbers selected for use in the flood hydrograph computations approximated 85 for the one-hour, probable maximum precipitation occurrence. With this runoff curve number and the total rainfall of 8.8 inches, the direct runoff volume of the PMF is 7.0

inches (page 541 of "Design of Small Dams," 1974). Using the following soil parameters in the multiple watershed model: hydraulic conductivities in the wetted zone 1.0 in/hr for upper and middle subdrainages, 0.5 in/hr for the lowest subdrainage, porosity 0.4, initial degree of saturation 0.65, final degree of saturation 1.0, average suction head 2 inches, the estimated total water volume for the PMF over the duration of 6 hours is 6.96 inches. This value is very close to that determined by the runoff curve number.

Channel Characteristics

The channel cross-sectional data was utilized to determine the relationship between wetted perimeter and flow area. The channel resistance factors were estimated utilizing the information provided by Chow (1959) and Simons and Sentürk (1977). The estimated values of Manning's roughness coefficient n are 0.025 for the channel in the lowest sub-basin and 0.07 for the channels in the middle and upper sub-basins. There are trees, grass, cobbles and debris in the channel bottoms and banks of the middle and upper sub-basins.

Probable Maximum Flood Hydrographs

The computed PMF hydrograph based on the multiple watershed model is given in Figure 12-25. The peak flow of the PMF is 22,700 cfs and the duration of the flood is 6 hours. The shape of the determined hydrograph reflects the topographic features of the basin. The multiple peaks are very reasonable considering the series of three sub-basins. For quick comparison, the 100-year and probable maximum floods previously determined by the Soil Conservation Service method are given in Figure 12-26. The previous hydrographs are symmetrical in shape and fairly short in duration very different than those presented in Figure 12-27.

This PMF was determined by a physical process simulation model that routes water from subwatersheds and planes to channel networks. The rainfall input to the model was the one-hour PMP. The total PMF runoff volume was equal to 7.0 inches of runoff from the watershed. The simulated peak flow (PMF) is 22,700 cfs and the duration is about 6 hours. The shape of this second hydrograph is very reasonable, and is based on the analysis of three sub-basins. This 29 percent reduction in estimated flood peak could significantly reduce the diversion channel requirements. Also, there is little evidence of significant historical runoff from the upper 50 percent of the basin. If this observation was utilized in the analysis, the computed PMF would be even smaller than the reported value of 22,700 cfs. The general conclusion was that a large factor of safety (regarding peak flow) exists in the design of the diversion channel. As this above example indicates, use of old methods may not always provide the best analysis of a problem.

## 12.8 DATA NEEDS

The data needed for mathematical modeling of watershed response are dependent on the type of watershed, the objective of modeling and the type of model utilized. The data requirements summarized below are

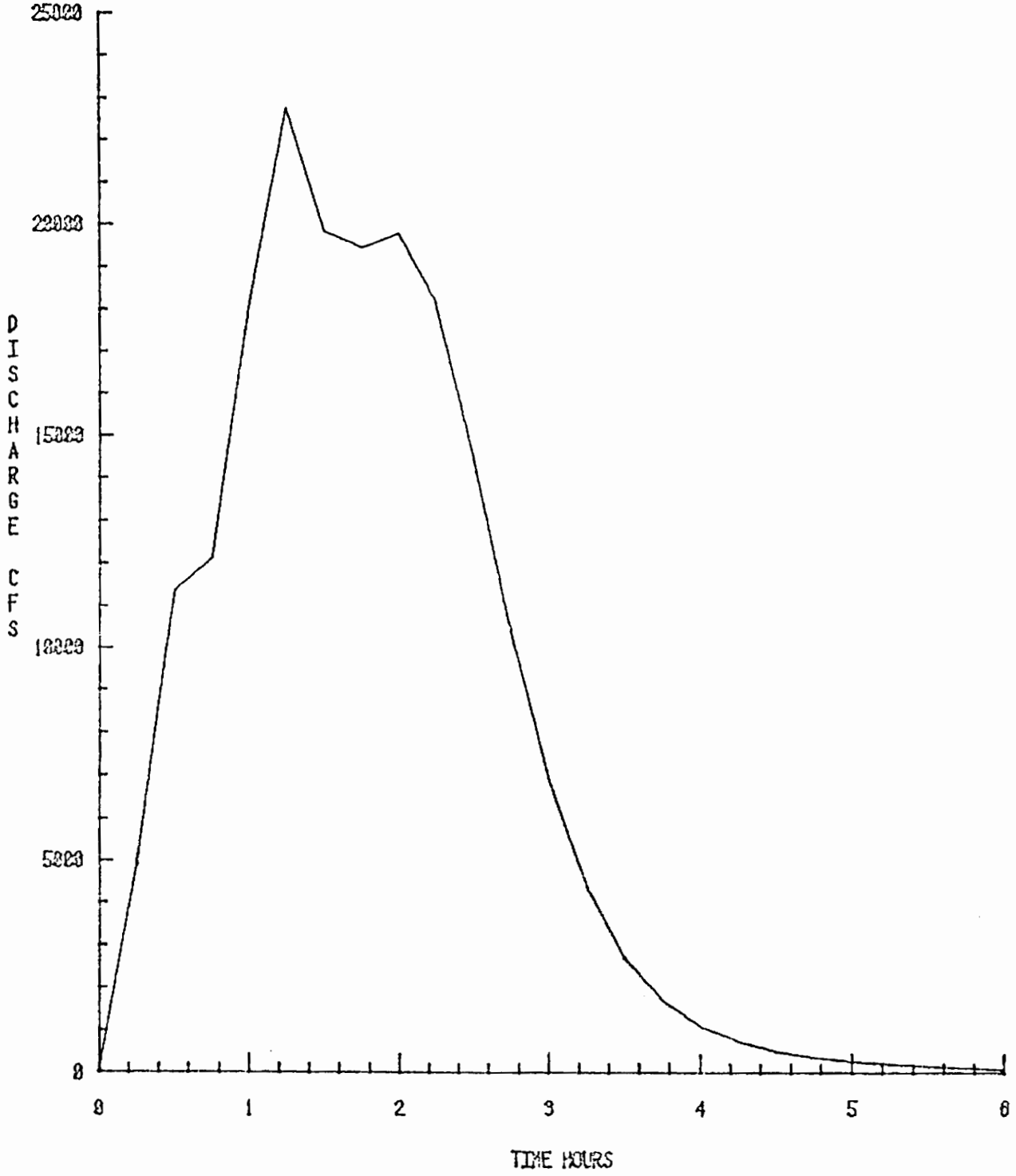


Figure 12-25. Hydrograph determined by MULTWAT.

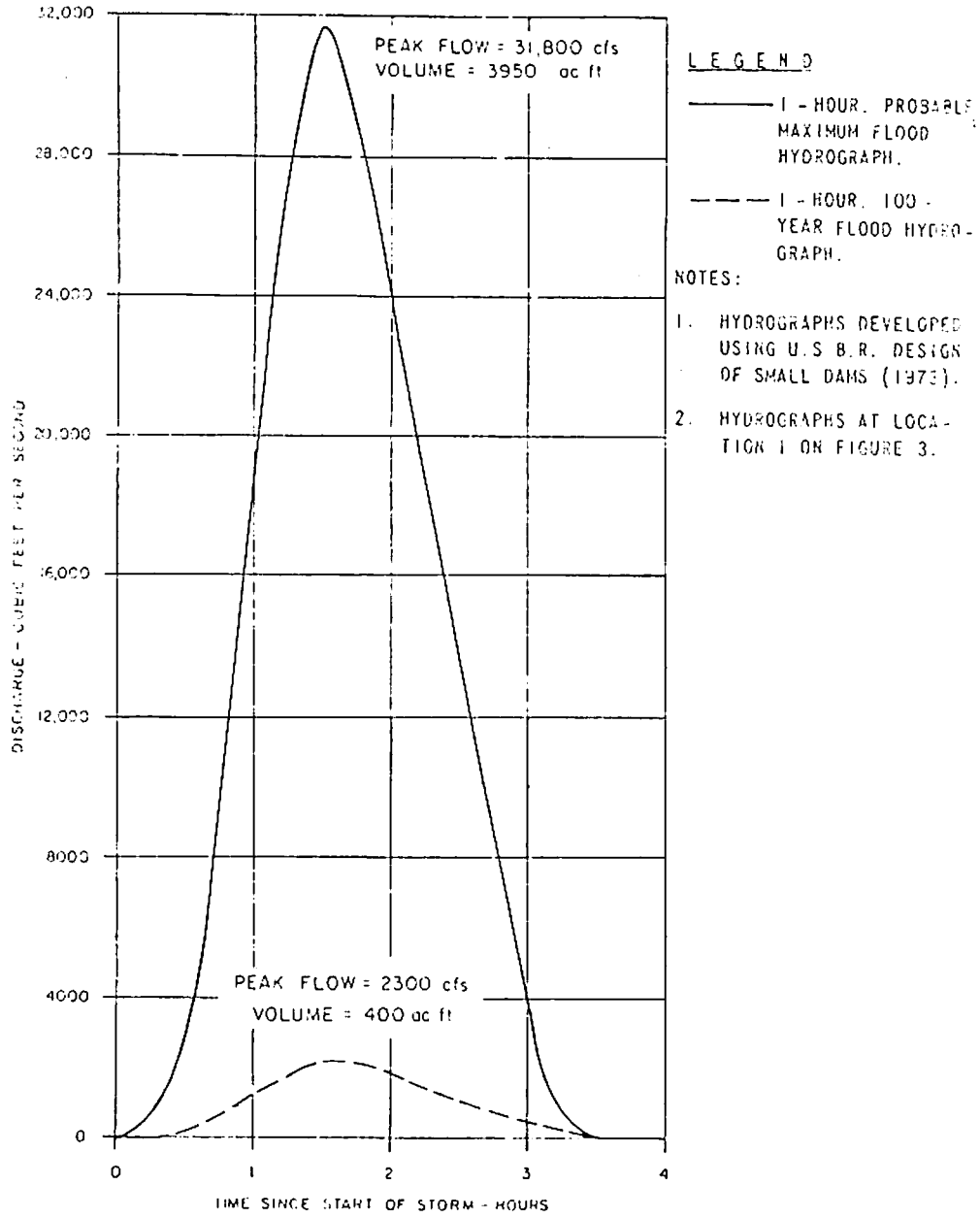


Figure 12-26. PMF as previously determined.

primarily for studying the major watershed response (water yield, sediment yield, and stream morphology) from small watersheds. The emphasis is made on the input data requirements of the watershed models presented in this chapter. However, additional data for other potential studies related to the watershed response are also identified.

There are two distinct types of data involved in the analysis. They are the model input data, which are required specifically for the model input, and the basic data (raw data), which are taken directly by field measurements. Generally, the model input data are obtained by retrieving and/or analyzing the raw data. The required model input data and basic data, and the supplementary data that are important to watershed study are summarized as follows.

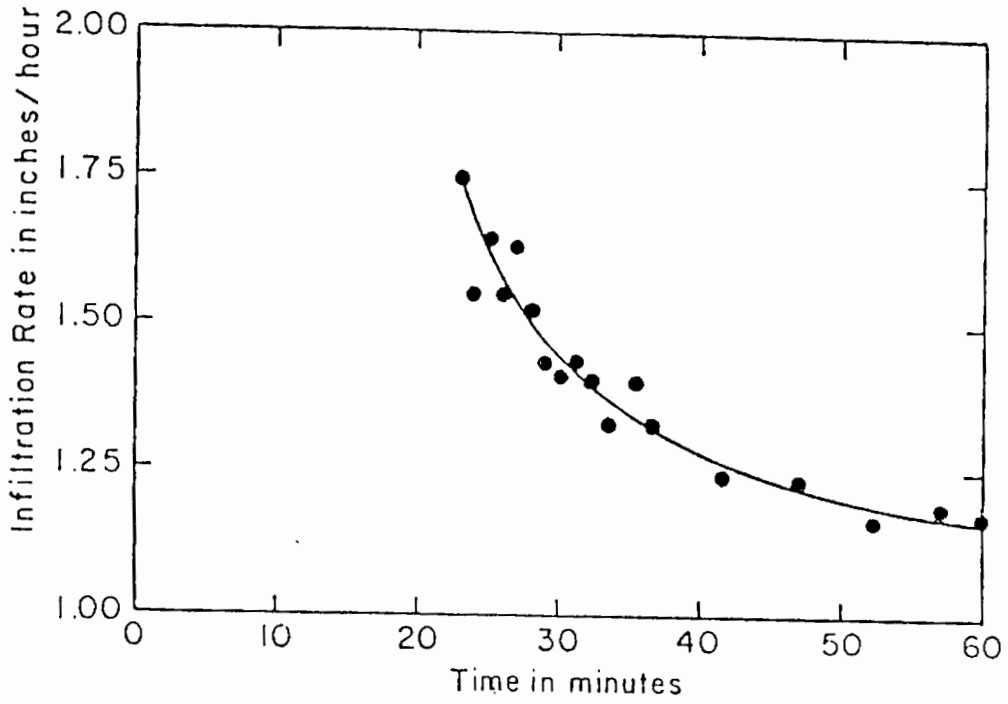


Figure 12-27. Infiltration rate data from Walnut Gulch, Arizona.

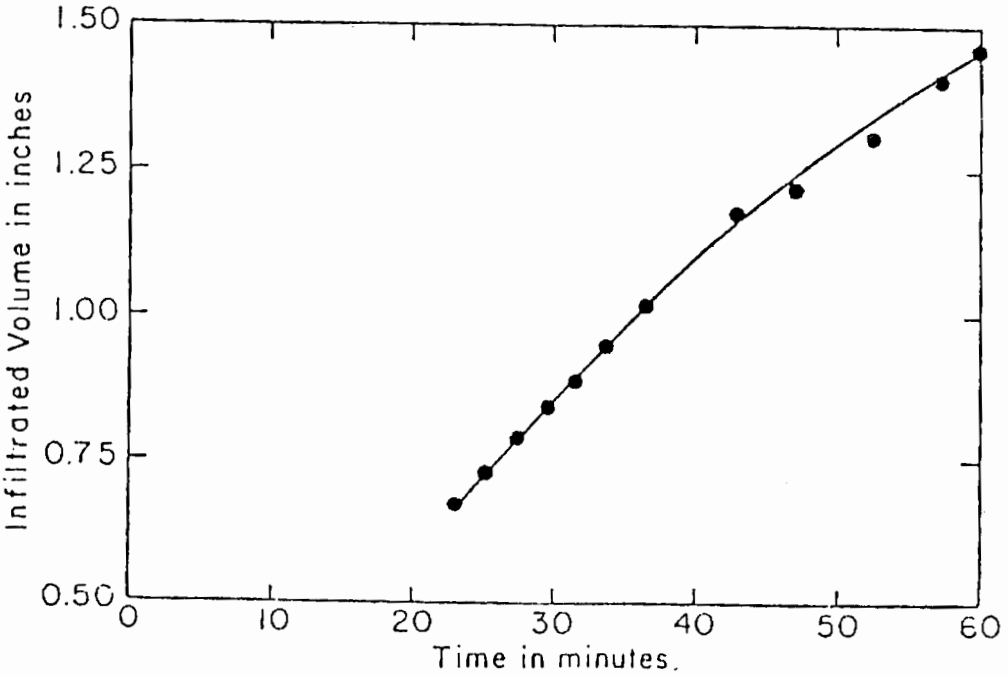


Figure 12-28. Infiltration volume data from Walnut Gulch, Arizona.

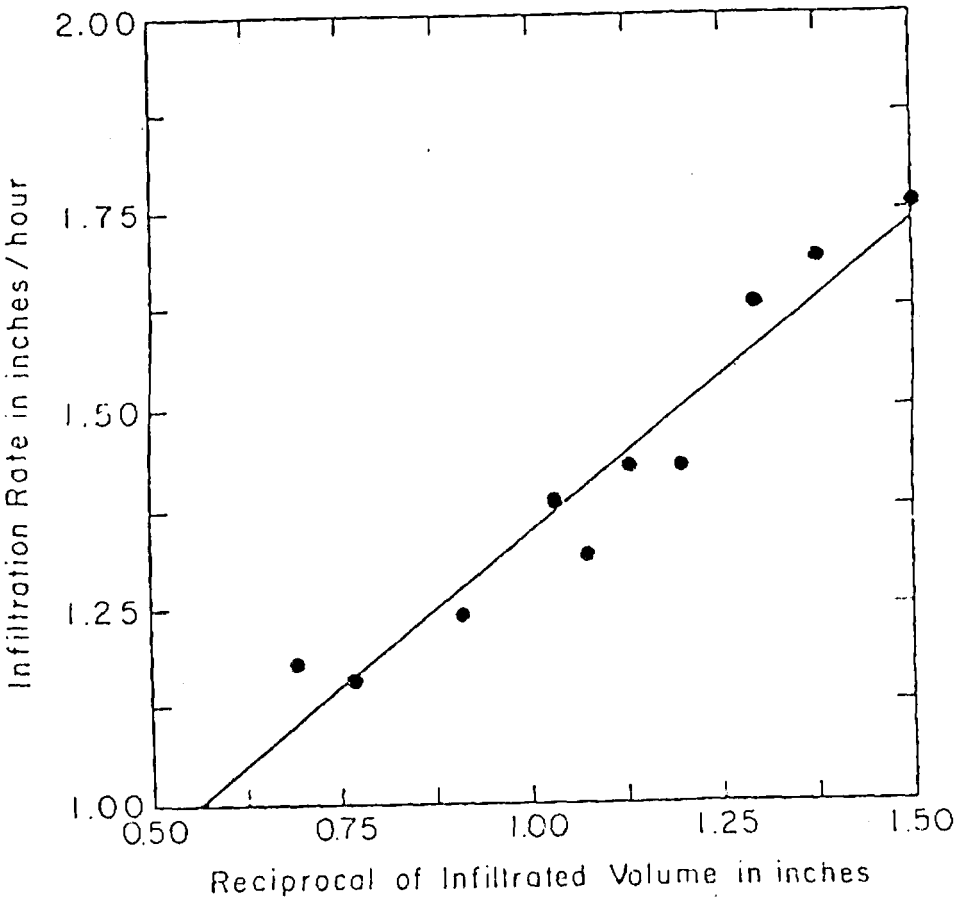


Figure 12-29. Plot of infiltration rate as a function of the reciprocal of infiltrated volume.

The first approximation of K may be obtained from U.S. Department of Agriculture, Soil Conservation Service field profile permeability tests. These tests give a range for the value of hydraulic conductivity for each soil class. Because values in Table 12-4 are saturated hydraulic conductivities, they must be divided by two to represent the conductivity in the wetted zone (Bouwer, 1969).

Because the hydraulic conductivity depends on texture, porosity and structure, as well as the viscosity of the water, a particular soil type may have different hydraulic conductivities as changes in these characteristics occur. Therefore, it is often difficult to assign conductivity values to each soil type. In general, though, clean sandy soils will have higher conductivities than plastic clay soils.

The range of values for $\psi_{ave}$, average capillary suction, for selected types of soils is shown in Table 12-5 (Eggert, 1976). Eggert shows a relationship between initial saturation and $\psi_{ave}$ which demonstrates that for a high initial saturation, the value of average capillary suction will be in the lower part of the given range, e.g.,

Table 12-4. Permeability (hydraulic conductivity) classes.

| Class | Rate in/hr | Representative Soil Type |
|---|---|---|
| very slow | < 0.06 | Clay |
| slow | 0.06 - 0.2 | Silty clay |
| moderately slow | 0.2 - 0.63 | Silty clay loam |
| moderate | 0.63 - 2.0 | Silt loam |
| rapid | 2.0 - 6.3 | Sandy loam |
| Very rapid | > 6.3 | Sand and gravel |

capillarity is destroyed. Though only a few soil types are listed in the table, a rough estimate for $\psi_{ave}$ can be made by associating the soil mixture found in the watershed to the most closely related soil listed in Table 12-5. It is necessary to specify soil types and distribution by use of a soil map so an effective value of $\psi_{ave}$ for the entire area being investigated can be obtained. Soil maps and textural descriptions can usually be obtained from soil surveys done by the U.S. Department of Agriculture, Soil Conservation Service.

Table 12-5. Average capillary suction for selected types of soil (after Eggert, 1976).

| Soil Type | Range of Average Capillary Suction (inches) |
|---|---|
| Nickel gravel-sand loam | 2.0 - 4.5 |
| Ida silt loam | 2.0 - 3.5 |
| Poudre fine sand | 2.0 - 4.5 |
| Plainfield sand | 3.5 - 5.0 |
| Yolo light clay | 5.5 - 10.0 |
| Columbia sandy loam | 8.0 - 9.5 |
| Guelph loam | 8.0 - 13.0 |
| Muren fine clay | 15.0 - 20.0 |

## Vegetative Cover

Ground and canopy cover densities determine rainfall interception volumes. Ground cover density is also used to compute overland flow resistance. Canopy cover density data can be acquired by on-site inspection or by use of aerial photography. If aerial photography is used, some on-site inspection is also needed for ground truth. Canopy cover and ground cover interception storage values are more difficult to determine. A starting point for estimating interception values is Table 12-6, from Zinke (1967). It is necessary to specify vegetation types and distribution by use of a vegetation map so that realistic interception volumes can be computed. There are tremendous ranges in the reported values making it sometimes difficult to select an appropriate number. Typical values for conifers average about 0.1 inches and ground cover interception is estimated at about 0.05 to 0.1. The interception depth is computed as the percent of cover times the selected interception value for the vegetative type.

## Climatic Data

Two types of climatic data are important in modeling of water and sediment yields. The most important is rainfall data; the other is temperature. Temperature is used to scale the hydraulic conductivity in the soil between various seasons of the year. Because hydraulic conductivity is a function of viscosity, as temperature rises so does the conductivity. Therefore, conductivities that represent winter rainfalls will be too low for summer storms. Since this is a scaling procedure, air temperatures themselves are not scaled but the corresponding water viscosities are. Because temperature change is such a widespread phenomena, use of temperatures from any nearby similar area is satisfactory.

The measurement of precipitation forms an integral part of watershed modeling. Information on precipitation amount, intensity, frequency, and duration is essential in determining the water and sediment yield from a watershed. The primary source of quality rainfall data is a network of recording rain gages. This data should consist of gage locations, time of recording, and volume or depth of rain at the recording time. From this information and records from standard rain gages, a spatial and temporal description of the storm can be developed from which the rainfall hyetograph for each modeled area is obtained. If gaged records are not available for an area, design storms can be generated from publications such as the U.S. Weather Bureau TP40 (Hershfield, 1961), and nondimensional accumulated volume-time curves. These design storms can then be used to derive a model to study watershed or road response to listic input.

## Channel and Flow Resistance Information

Channel data includes flow resistance coefficients, channel geometry parameters, and channel bed sediment characteristics. Flow resistance is estimated after a visual or photographic inspection of the flow surface.

Table 12-6. Some interception storage values reported for vegetation in the american literature*.

| Vegetation Element | Species | Storage Amount (mm) | (in.) |
|---|---|---|---|
| CONIFERS | Abies concolor Lindl. | 3.8 | 0.15* |
| | Mature | 6.6 | 0.26* |
| | Pole size | 7.6 | 0.30* |
| | Abies magnifica A. Murr. | 0.8 | 0.03 |
| | Pinus contorta Dougl. | | |
| | Pinus lambertiana Dougl. | 0.3 | 0.10* |
| | Pinus ponderosa | 3.0 | 0.12 |
| | Pinus ponderosa laws | 0.8-1.3 | 0.03-0.05 |
| | Second growth | 2.3 | 0.09* |
| | Mature | 2.3 | 0.09* |
| | Young (14 ft. high) | 0.3 | 0.01* |
| | Pinus radiata D. Don | 0.3-0.1 | 0.01-0.04 |
| | Pinus resinosa Ait. | 0.8 | 0.03 |
| | Picea rubens Sar. (30 yrs. old) | 9.1 | 0.36 |
| | Pinus storbus L. | 0.5 | 0.02 |
| | Tsuga canadensis (L) Carr. | 0.8-1.3 | 0.03-0.05 |
| HARDWOODS | Aesculus californica (Spach) Nutt. | | |
| | Fall and winter | 0.8 | 0.03 |
| | Spring and summer | 1.3 | 0.05 |
| | Citrus aurantium L. | | 0.04 |
| | Mixed hardwoods (Acer, Ulmus, Quercus, Betula) | 0.5-1.8 | 0.02-0.07 |
| | Mixed hardwoods West Virginia | | |
| | Quercus rubra L., Liviodendron Tulipifera L., etc.) | | |
| | Summer | 0.5 | 0.02 |
| | Winter | 0.2 | 0.006 |
| | Northern hardwoods | 2.0 | 0.08 |
| | Liquidamber stvraciflua L. | 0.8 | 0.034 |
| | All eastern N. American hardwood data | 0.03-1.6 | 0.001-0.064 |

Table 12-6. (continued)

| Vegetation Element | Species | Storage Amount (mm) | Storage Amount (in.) |
|---|---|---|---|
| SHRUBS | Adenostonma fasciculatum H & A | 1.3-1.5 | 0.05-0.06' |
| | Baccharis pilularis DC | 0.5-1.5 | 0.02-0.06' |
| | Ceanothu cuneatus (Hook) Nutt., Arctostaphylos mariposa Dudley | 1.5 | 0.06 |
| | Cercocarpus ledifolius Nutt. | 1.0 | 0.04' |
| | Photinia aributifolia Lindl. | 0.3-1.8 | 0.01-0.07' |
| | Quercus dumosa Nutt. Cercocarpus betuloides Nutt. | | |
| | Ceanothus crossifolius | 2.0 | 0.08 |
| GRASS | Annual grasses-Ca. | 1.0-1.5 | 0.04-0.06' |
| | Secale cereale L. | 1.3 | 0.05 |
| FOREST FLOOR | Liriodendron tulipfera L., Hicoria spp. Quercus coccinea Muenchh. | 1.4 | 0.057 |
| | Pinus ponderosa laws | | |
| | 20-24 yr | 2.3 | 0.09 |
| | 70-80 yr | 8.1 | 0.32 |
| | 140-160 yr | 11.2 | 0.44 |
| | Pinus radiata D. Don | | |
| | 5-10 yr | 0.5 | 0.02 |
| | 10-15 yr | 1.0 | 0.04 |
| | 15-20 yr | 1.8 | 0.07 |
| | 25-30 yr | 3.6 | 0.14 |

*Precipitation as rain unless indicated as snow(*) or artificial sprinkling(').

## General

### Model Input Data

The input data required for the simulation are different for different models. Described below are those for general purposes.

1. Geometry data include slope length, bed slope, wetted perimeter versus flow area relations, and computation sequence.

2. Soil data include the saturated hydraulic conductivity, average capillary suction pressure, soil porosity, and degree of saturation in the wetted zone.

3. Vegetation and ground cover data include canopy cover density, ground cover density, the typical interception storage capacity of canopy cover, and ground cover.

4. Flow resistance parameters are constants describing grain resistance and overall resistance. The overall resistance parameters for overland flow units should include parameters for both minimum and maximum resistance.

5. Storm characteristics include rainfall intensity and areal distribution of rainfall intensity if studying a large watershed.

6. Antecedent conditions include the antecedent soil moisture content.

### Basic Data

In order to have the model input data given in the previous section, the following basic data (raw data) are needed.

1. Topographic data include the topography survey map, aerial photographs, and channel geometry survey results. With these data, all the geometry data required for the model input can be determined for both overland flow areas and channels.

2. Soil data include soil survey maps indicating the aerial distribution of soil types, saturated hydraulic conductivity, average capillary suction pressure, soil porosity, and degree of saturation in the wetted zone.

3. Forest inventory data include total vegetation volume, total litter volume (or litter index), canopy cover density, ground cover density, areal distribution of vegetation type (can be estimated from aerial or color infrared photos), and interception storage capacity of a typical tree and a unit area of forest floor. From these forest inventory data, the vegetation and ground cover data for the model input can be easily determined.

4. Hydraulic data include flow discharge, depth, and velocity. These data are used to estimate the flow resistance parameters to evaluate the performance of the mathematical model.

5. Climatologic data include the rainfall record in either strip charts or hyetographs. The antecedent conditions can only be estimated if the interstorm water balance simulation is available.

6. Hydrograph data are needed for model calibration and simulation evaluation. These data include the water at the watershed outlet and the resultant channel profiles.

7. Watershed management data are very important for evaluating the watershed treatment effects. These data include the vegetation treatment data (clear-cut, patch-cut, or burning treatment) and the mechanical treatment data (check dam, logging road, windrow and skid trail, etc.).

Methods for Computing or Estimating Model Information

There are numerous and varied techniques for gathering and estimating information needed to operate a mathematical model. Experience has shown how some model parameters can be estimated from scanty data. Selected techniques are presented in the following section for determining these necessary parameters.

Soil Characteristics. Certain hydrologic properties of the soil must be obtained to properly model the infiltration process using the Green-Ampt model and soil size distribution. As a minimum, soil textural classifications are required. Parameters in the infiltration model include: the effect of hydraulic conductivity in the wetted zone K, the porosity $\phi$, the final ($S_w$) and initial ($S_i$) soil saturation, and the average capillary suction head $\psi_{ave}$. The Green-Ampt infiltration model can be rewritten as

$$i = K\ (1 + \frac{\delta}{F}) \qquad (12\text{-}101)$$

where $i$ is infiltration rate, $\delta$ is a grouping of soil parameters, F is infiltrated volume, and K is defined above. The $\delta$ parameter is $\delta = \psi_{ave}\ (S_w - S_i)\phi$. The effective hydraulic conductivity in the wetted zone is about one-half the hydraulic conductivity normally reported. It represents the infiltration rate when the soil nears saturation. Experience has shown that K is a more sensitive parameter than $\delta$. Therefore some of the parameters that make up $\delta$ can be roughly estimated if needed. Often $\phi$ is assumed as 0.5 and $S_w$ as 1.0. Better estimates of $\phi$ can be made, but the improvement in model accuracy is not usually marked. Values of $S_w$ are usually close to 1.0. The initial degree of saturation can be roughly estimated from antecedent rainfall conditions, temperature data, and a knowledge of the soil. Because this value is used for calibration in conjunction with the $\psi_{ave}$ value, only an intuitive realistic initial estimate is needed. Wet conditions are about 0.8 and greater, and dry is usually below about 0.3 or 0.4. The volumetric water content in the weighted zone $\theta_w$ is defined as

$$\theta_w = \phi S_w \qquad (12\text{-}102)$$

and can be used if water content data are available.

Unfortunately, except for soils which have undergone considerable laboratory study, soil data for values of $K$ and $\psi_{ave}$ are simply not available. Since soils are, in general, anisotropic and heterogeneous in their physical properties; conductivity, porosity, and capillary pressures may easily vary by significant amounts over very small areas (Carvallo et al., 1976). Therefore, the mathematical analysis based on data from one or two extensively studied samples may not be meaningful. Any watershed simulation requires calibration to attempt to compensate for neglected processes and inadequacies in theory. The parameters of this infiltration model, particularly $K$, are prime candidates for such calibration; therefore, good first estimates of $K$ and $\psi_{ave}$ are needed. To this end, the following, method for estimating $K$ and $\psi_{ave}$ is suggested.

If infiltrometer data are available, the following method can be used to obtain estimates of $K$ and $\delta$:

1. Plot the infiltration rate and infiltrated volume as a function of time. Figure 12-27 shows an example of plotted infiltrometer data from Walnut Gulch, Arizona.

2. Plot the infiltration rate versus the reciprocal of the infiltrated volume using the curves plotted in Step 1 of the procedure. Figure 12-28 shows the result of plotting this type of curve from data given in Figure 12-27.

3. The curve of infiltration rate as a function of the reciprocal of infiltrated volume is nearly a straight line, at least to the extent that the Green-Ampt equation represents the actual soil performance. If a straight line is fitted to this data, then the y-intercept is $K$, and the slope is $\delta K_w$. Thus, estimates of $K$ and $\delta$ can be obtained by measuring the slope and intercept of the line approximating the data. From Figure 12-29, the value of $K$ may be estimated as 0.78 inches per minute and $\delta$ as 1.22 inches.

As seen from Figure 12-29, a considerable amount of "noise" exists in this data. This "noise" may be due to a number of causes i.e., bubbling, inhomogeneities in the soil, or even a badly executed infiltrometer experiment. Whatever the cause, the scatter in the data makes fitting a straight line a difficult task.

A more precise estimate of these parameters using the same raw data could be obtained by using optimization techniques such as proposed by Li and Simons (1977). However, the use of these techniques, while more precise, suffers the same criticism as those mentioned earlier considering the wide spatial variability of soil characteristics. Therefore, while certainly not rigorous, the method proposed herein may be more consistent with available field data.

Overland flow resistance is defined using the Darcy-Weisbach friction factor as

$$f = \frac{K_t}{N_2} \tag{12-103}$$

where $f$ is the Darcy-Weisbach friction factor, $K_t$ is an overall flow resistance parameter, and $N_2$ is the Reynolds number of the overland flow. Reynolds number is the ratio of internal forces to viscous forces in flowing water. Overland flow resistance parameters will vary depending on the flow surface. Suggested values for the upper and lower overall resistance factors are given in Table 12-7 from Woolhiser (1975).

Table 12-7. Overall resistance parameters for overland flow.

| Surface | Range of Parameter |
|---|---|
| Concrete or Asphalt | 24 - 108 |
| Bare Sand | 30 - 120 |
| Graveled Surface | 90 - 400 |
| Bare Clay - Loam Soil (eroded) | 100 - 500 |
| Sparse Vegetation | 1000 - 4000 |
| Short Grass Prairie | 3000 - 10000 |
| Bluegrass Sod | 7000 - 40000 |

A forest floor may have a lower value of 100 for a bare soil surface and up to 40,000 for dense ground cover. Similarly a grain resistance Darcy-Weisbach friction factor is used in the models. A good estimate for the corresponding grain resistance parameter is in the range of 45 to 50.

An estimate of Manning's $n$ value can be used to determine a resistance parameter specifically for channel flow. The channel flow resistance parameter or Darcy-Weisbach friction factor $f$ can be related to Manning's $n$ as

$$f = \frac{116\ n^2}{R^{1/3}} \tag{12-104}$$

where $R$ is the hydraulic radius in feet of channel flow.

Channel geometry is usually determined by on-site measurements of cross sections. These measurements can be converted to sets of geometric relationships between depth, area, wetted perimeter, and top width. Recently, Simons, Li and Ward (1978) presented a method for acquiring channel cross section measurements from stream photographs.

Models being developed, used, and improved at Colorado State University are based on physical processes and therefore reflect changes in the natural system much more meaningfully than models based on regression analysis. This allows these process models to be widely used and easily transferable if the limitations of each model are recognized.

Computer based process models are a very useful tool in predicting and planning. However, more research is needed to perfect and simplify these models before they are widely accepted.

## REFERENCES

Bouwer, H., December 1969, Infiltration of Water into Non-uniform Soil, Journal of the Irrigation and Drainage Division, ASCE, Vol. 95, No. IR4, pp. 451-462.

Bouwer, H., March 1976, Infiltration into Increasingly Permeable Soils, Journal of the Irrigation and Drainage Division, ASCE, Vol. 102, No. IR1, pp. 127-136.

Brakensiek, D. L., 1967, Kinematic Flood Routing, ASAE, Vol. 10, No. 3, pp. 340-343.

Brakensiek, D. L., September 1970, Discussion of Infiltration of Water into Non-uniform Soils, by H. Bouwer, Journal of the Irrigation and Drainage Division, ASCE, Vol. 96, No. IR3, pp. 358-360.

Carvallo, H. O., Cassel, D. K., Hamnand, J., and Bauer, A., January 1976, Spatial Variability of In Situ Unsaturated Hydraulic Conductivity of Maddock Sandy Loam, Soil Science, Vol. 121, No. 1.

Chen, C. L., March 1976, Flow Resistance in Broad Shallow Greased Channels, Journal of the Hydraulics Division, ASCE, Vol. 102, No. HY3, pp. 307-322.

Chow, V. T., 1959, Open Channel Hydraulics, McGraw-Hill Book Company, New York.

Eagleson, P. S., 1970, Dynamic Hydrology, McGraw-Hill Book Company, New York.

Eggert, K. G., 1976, Modeling the Unsteady Infiltration Process, M.S. Thesis, Colorado State University, Fort Collins, Colorado.

Eggert, K. G., Li, R. M., and Simons, D. B., September 1979, Time Explicit Formulation of the Green-Ampt Infiltration Equation, Proceedings of the XVIIIth International Congress of the IHRA in Italy.

Green, W. H. and Ampt, G. A., May 1911, Studies on Soil Physics Part 1: The Flow of Air and Water through Soils, Journal of Agriculture Science.

Harley, B. M., Perkins, F. E., and Eagleson, P. S., A June 1970, Modular Distributed Model of Catchment Dynamics, MIT, Department of Civil Engineering, Hydrodynamics Laboratory Report No. 133.

Henderson, F. M., 1966, Open Channel Flow, Macmillan, New York.

Hershfield, M. T., 1961, Rainfall Frequency Atlas of the U.S.

Houghton, D. P. and Kasahara, A., 1968, Nonlinear Shallow Fluid Flow Over an Isolated Ridge, Communication on Pure and Applied Mathematics, Vol. XXI.

Iwagaki, Y., 1955, Fundamental Studies on Runoff Analysis by Characteristics, Disaster Prevention Research Institute Bulletin No. 10, Kyoto University, Kyoto, Japan.

Kibler, D. F. and Woolhiser, D. A., 1970, The Kinematic Cascade as a Hydrologic Model, Hydrology Paper No. 39, Colorado State University, Fort Collins, Colorado.

Kouwen, N. and Unny, T. E., June 1969, Flow Retardance in Vegetated Channels, Journal of Irrigation and Drainage Division, ASCE, Vol. 95, No. IR2, pp. 329-342.

Li, R. M., 1974, Mathematical Modeling of Response from Small Watershed, Ph.D. Dissertation, Department of Civil Engineering, Colorado State University, Fort Collins, Colorado.

Li, R. M. and Shen, H. W., May 1973, Effect of Tall Vegetation on Flow and Sediment, Journal of Hydraulics Division, ASCE, Vol. 99, No. HY5, pp. 793-814.

Li, R. M. and Simons, D. B., August 1977, In-Field Estimation of Infiltration Parameters, Colorado State University Report prepared for U.S. Department of Agriculture Forest Service, Rocky Mountain Range and Experiment Station, Flagstaff, Arizona, CER76-77RML-DBS43.

Li, R. M., Simons, D. B., and Eggert, K. G., December 1976, Process Model of Infiltration and Subsurface Flow Routing, Colorado State University, Report CER76-77RML-DBS-KGE20, prepared for USDA Forest Service, Rocky Mountain Forest and Range Experiment Station, Flagstaff, Arizona

Li, R. M., Simons, D. B., and Eggert, K. G., December 1976a, Process Model of Infiltration and Subsurface Flow Routing, Colorado State University, Report CER76-77RML-DBS-KGE20, prepared for USDA Forest Service, Rocky Mountain Forest and Range Experiment Station, Flagstaff, Arizona.

Li, R. M., Simons, D. B., Shiao, L. S., and Chen, Y. H., August 1976c, On Kinematic Wave Approximation for Flood Routing, Rivers 76, Vol. 1, 3rd Annual Symposium on Inland Waterways for Navigation, Flood Control and Water Diversion, Colorado State University, Fort Collins, Colorado, pp. 377-398.

Li, R. M., Simons, R. K., and Simons, D. B., 1976b, A Generalized Kinematic Wave Approximation for Flood Routing, paper submitted to Journal of Hydraulics Division, ASCE, for possible publication.

Li, R. M., Simons, D. B., and Stevens, M. A., 1975a, Nonlinear Kinematic Wave Approximation for Water Routing, Water Resources Research, Vol. 11, No. 2.

Li, R. M., Simons, D. B., and Stevens, M. A., July 1975b, On Overland Flow Water Routing, Proceedings of the National Symposium on Urban Hydrology and Sediment Control, Lexington, Kentucky.

Li, R. M., Stevens, M. A., and Simons, D. B., June 1976, Solutions to Green-Ampt Infiltration Equations, Journal of the Irrigation and Drainage Division, ASCE, Vol. 102, No. IR2, pp. 239-248.

Mein, R. G. and Larson, C. L., 1971, Modeling the Infiltration Component of the Rainfall-Runoff Process, Water Resources Research Center, Minneapolis.

Morel-Seytoux, H. J. and Khanji, J., August 1974, Derivation of an Equation of Infiltration, Water Resources Research, Vol. 10, No. 4, pp. 795-800.

Palmer, V. J., 1946, Retardance Coefficients for Low Flow in Channels Lined with Vegetation, Trans. AGU, Vol. 27, pp. 187-197.

Phelps, H. O., August 1970, The Friction Coefficient for Shallow Flows over a Simulated Turf Surface, Water Resources Research, Vol. 6, No. 4, pp. 1220-1226.

Ree, W. O., 1949, Hydraulic Characteristics of Vegetation for Vegetated Waterways, Agricultural Engineers, Vol. 30, No. 4, pp. 184-189.

Ree, W. O. and Palmer, V. J., 1949, Flow of Water in Channels Protected by Vegetative Linings, USDA Soil Conservation Service Technical Bulletin No. 967.

Schaake, J. C., Jr., June 1965, Synthesis of the Inlet Hydrograph, Tech. Report 3, Storm Drainage Project, Johns Hopkins University, Baltimore, Maryland.

Simons, D. B. and Li, R. M., 1975, Watershed Segmentation by a Digital Computer for Mathematical Modeling of Watershed Response, Colorado State University, Report CER75-76DBS-RML9, prepared for USDA Forest Service, Rocky Mountain Forest and Range Experiment Station, Flagstaff, Arizona.

Simons, D. B., Li, R. M., and Eggert, K. G., April 1977, Storm Water and Sediment Runoff Simulation for Upland Watersheds Using Analytical Routing Technique, Volume I--Water Routing and Yield, Colorado State University, Report CER77-78DBS-RML-KGE16, prepared for USDA Forest Service, Rocky Mountain Forest and Range Experiment Station, Flagstaff, Arizona.

Simons, D. B., Li, R. M., and Eggert, K. G., April 177a, Simple Water Routing and Yield Model Using a Small Programmable Calculator, Colorado State University, Report CER76-77DBS-RML-KGE52, prepared for USDA Forest Service, Rocky Mountain Forest and Range Experiment Station, Flagstaff, Arizona.

Simons, D. B., Li, R. M., and Spronk, B. E., April 1978, Storm Water and Sediment Runoff Simulation for a System of Multiple Watersheds, Vol. I--Water Routing and Yield, Draft Report prepared for USDA Forest Service, Rocky Mountain Forest and Range Experiment Station,

Simons, D. B., Li, R. M., and Stevens, M. A., August 1975, Development of Models for Predicting Water and Sediment Routing and Yield from Storms on Small Watershed, USDA Forest Service, Rocky Mountain Forest and Range Experiment Station.

Simons, D. B., Li, R. M., and Ward, T. J., December 1978, Estimation of Parameters that Describe Channel Geometry for Watershed Modeling, Colorado State University Draft Report prepared for USDA Forest Service, Rocky Mountain Forest and Range Experiment Station, Flagstaff, Arizona.

Simons, D. B., Richardson, E. V., Stevens, M. A., Duke, J. H., and Duke, V. C., August 1971a, Venezuelan International Meterological and Hydrological Experiment, VIMHEX, Hydrology Report, Vol. II, Streamflow, Groundwater and Ground Response Data, Civil Engineering Department, Colorado State University, Fort Collins, Colorado.

Simons, D. B., Richardson, E. V., Stevens, M. A., Duke, J. H., and Duke, V. C., October 1971b, Geometric and Hydraulic Properties of the Rivers, VIMHEX, Hydrologic Report, Vol. III, Civil Engineering Department, Colorado State University.

Simons, D. B. and Senturk, F., 1977, Sediment Transport Technology, Text, Water Resources Publications, P.O. Box 303, Fort Collins, Colorado.

Simons, R. K., 1977, A Modified Kinematic Approximation for Water and Sediment Routing, M.S. Thesis, Colorado State University, Fort Collins, Colorado.

Singh, V. P., 1975, A Distributed Approach to Kinematic Wave Modeling of Watershed Surface Runoff, Proceedings of National Symposium on Urban Hydrology and Sediment Control, July 28-31, University of Kentucky, pp. 227-236.

U.S. Bureau of Reclamation, 1974, Design of Small Dams.

Woolhiser, D. A., 1975, Simulation of Unsteady Overland Flow, In Unsteady Flow in Open Channels, edited by K. Mahmood and V. Yevjevich, Water Resources Publications, Fort Collins, Colorado.

Wenzel, H. G., 1970, The Effects of Raindrops Impact and Surface Roughness on Sheet Flows, WRC Research Report No. 34, University of Illinois, Water Resources Center, Urbana, Illinois.

Zinke, P. J., 1967, Forest Interception Studies in the United States, Forest Hydrology, W. E. Sopper, Editor, Pergamon Press, Oxford.

# CHAPTER 13

# WATERSHED SEDIMENT YIELD

## 13.1 INTRODUCTION

Increased demands on natural resources have produced beneficial and adverse impacts on watershed systems. Activities such as timbering, road building, mining, and agricultural uses have sometimes created adverse impacts on soil and water systems. Assessment of these impacts often demands quantitative as well as qualitative evaluations. One such evaluation is sediment yield or change in sediment yield brought about by such activities. Qualitative response of the system can be deduced from an understanding of controlling physical processes and the influence specific activities have on these processes. Quantitative responses such as change in sediment yield per acre require some type of mathematical expression or model. Such an expression should relate measures of key physical processes to the sediment yield. In this manner the model or expression would be sensitive to changes in controlling processes and reflect quantifiable natural or man-induced changes in the system.

This chapter discusses various models for estimating sediment yield from watersheds. Physical process simulation models are emphasized and example applications are presented. Models are used to estimate or predict sediment yields resulting from natural or disturbed watershed lands taking into account important physical processes such as raindrop splash, overland flow erosion, channel erosion, and movement of the different sediment size fractions. The models presented herein do not account for gully- or landslide-generated sediment yields. One important aspect of model development and operation is data. Without adequate data, testing and verification of models before application to real situations may produce erroneous results unrepresentative of actual conditions. Understanding model operations and controlling physical processes allows rapid delineation of erroneous data. Model development, keeping physical processes and data needs in the forefront, can produce realistic accurate methods for estimating sediment yield from watersheds.

## 13.2 TYPES OF APPROACH

Numerous approaches can be used to determine sediment yield from natural or disturbed land surfaces. Of interest are those approaches that utilize mathematical models. One category of mathematical models is the "black box," or lumped parameter model. Another category is based on regression equations as typified by the Universal Soil Loss Equation. Both types interpret input-output relations using simplified forms that may or may not have physical significance. Processes related to the movement of water and sediment through the watershed are grouped into coefficients. A classic example is the rational formula for estimating peak discharge i.e., $Q = CiA$ where $Q$ is peak discharge, $i$ is rainfall input, $A$ is the drainage area, and $C$ is the runoff coefficient that represents all hydrologic processes. Although lumped parameter and regression models are often used, the parameters may not

accurately represent observable physical characteristics. Another disadvantage is that some models do not consider physical environment dynamic with respect to time and location.

Another approach is through the use of stochastic models. If rainfall events, watershed response, and runoff events are stochastic i.e., probabilistic in nature, the processes of sediment yield are also stochastic. However, stochastic models are difficult to apply (Shen and Li, 1976) and do not readily show response of a watershed undergoing changes as a result of various land use activities. Most hypotheses used in stochastic models have not been tested by field data. Because Woolhiser and Blinco (1975) indicated that knowledge in applying stochastic models to sediment yield from watersheds is primitive, stochastic models are not considered in this chapter.

The physical process simulation model is another type of model in which the governing processes controlling sediment yield are formulated and analyzed separately to provide model sensitivity to land management alternatives. This type of model will be discussed in detail in this chapter.

## Regression Models

Among the methods available to estimate sediment yield, regression models are perhaps the simplest to use. Validity of regression models is dependent on data availability. Therefore application of regression models is substantially restricted if there is insufficient data.

Musgrave (1947) analyzed soil loss measurement for approximately 40,000 storms occurring on fractional plots in the United States. Results of his study indicated that

$$A_s = I^{1.75} K L^{0.35} S^{1.35} C_g \quad . \tag{13-1}$$

where $A_s$ is the annual soil loss per unit area, I is the maximum 30 minute intensity with a return period of two years, K is the numerical value that is proportional to the soil erodibility, L is the slope length, S is the percent slope, and $C_g$ is the ground cover.

This equation is usually applicable to long-term average soil losses for an extensive area. In order to extend the Musgrave equation to estimate short-term soil loss rates for localized areas, extensive data collection and analyses were made by Wischmeier and Smith (1960). Their efforts led to the development of a more refined soil loss equation, the Universal Soil Loss Equation (USLE). Since then, the USLE has been applied to all types of watersheds and is perhaps the most comprehensive and popular regression model for estimating soil loss. It is discussed in the following sections.

Williams and Berndt (1972) recognized that application of the Universal Soil Loss Equation is limited to soil loss and developed another procedure for computing sediment yields from watersheds. They introduced a runoff factor instead of rainfall energy into the Universal

Soil Loss Equation to estimate soil loss and a delivery ratio to estimate sediment yield. Later Williams (1975) used the modified Universal Soil Loss Equation with a decay function to estimate sediment yield from watersheds. The modified Universal Soil Loss Equation is

$$A_s \simeq 95\ (Q_v \cdot q_p)^{0.56}\ K\ LS\ CP \qquad (13\text{-}2)$$

where $Q_v$ is runoff volume in acre-ft and $q_p$ is the peak flow rate in cubic feet per second. The decay function is

$$A_s \simeq A_o\ e^{-Bt}\ d_s \qquad (13\text{-}3)$$

where $A_o$ is the sediment yield in the upstream section, B is the routing coefficient, t is the travel time between sections, and $d_s$ is the soil particle diameter. Although promising in that it uses more easily understood physical quantities, this storm-basis method is subject to some of the same disadvantages as the original USLE.

Universal Soil Loss Equation

The most widely used regression model is the Universal Soil Loss Equation (USLE). The U.S. Department of Agriculture began to study soil loss approximately 1930 when the first ten Federal-State Cooperative Stations began operation. Thirty-two additional stations were established in the next 25 years. Measurements of precipitation, runoff, and soil loss associated with these 42 stations (in 23 states east of the Rocky Mountains) were collected continuously for periods of from 5 to 30 or more years. Field plots were rectangular to facilitate typical flow row spacings for cultivated units. A plot 72.6 feet long on nine percent uniform slope in bare fallow soil and tilled to break surface crusts was arbitrarily selected to serve as a reference for evaluation.

Six major factors to describe rainfall R, soil erodibility K, slope-length L, slope steepness S, cropping and management C, and supplemental erosion-control practices such as contouring or terracing P, were used to develop the Universal Soil Loss Equation. This model is based on field data collected from the plots described above and from rainfall simulation data. The USLE model is

$$\underline{E} = R\ K\ L\ S\ C\ P \qquad (13\text{-}4)$$

where L, S, C, and P are all dimensionless. Computed soil loss $\underline{E}$ has a time period of R and soil loss dimension of K. Smith and Wischmeier (1957), Meyer (1971), and Wischmeier (1973) provide detailed descriptions of this equation and its terms.

The rainfall factor R is dependent on parameter EI and the product of kinetic energy of the storm times maximum 30-minute rainfall intensity. Maximum 30-minute intensity is twice the greatest amount of recorded rainfall in any 30 consecutive minutes. The storm energy E was computed from a relationship between E and rainfall intensity. An iso-erodent map to indicate values of R for nearly all locations in the 37 states east of the Rocky Mountains was developed by Wischmeier and Smith (1965) based on data collected by the U.S. Weather Bureau.

In general the R factor must be predicted on a probability basis. Frequency distributions of annual, seasonal, or annual-maximum storm EI values follow the log-normal type of curve typical of hydrological data.

Soil erodibility factor K was found by Wischmeier et al. (1971) to be a function of percent of silt, percent of coarse sand, soil structure, permeability of soil, and percent of organic matter. The soil erodibility nomograph is shown in Figure 13-1.

Slope length factor L was defined as the ratio of soil loss from a particular slope length to soil loss from a 72.6-foot plot length with all other conditions the same. Slope length was defined as the distance from the point of overland flow origin to the point where either slope decreases to the extent that deposition begins or runoff water enters a well defined channel (Smith and Wischmeier, 1957). Effect of slope length on soil loss is primarily a result of increased potential due to greater accumulation of runoff on the longer slopes.

Slope steepness factor S was found by Smith and Wischmeier (1957) to be a function of actual slope steepness. Cropping-management factor C was defined as the ratio of soil loss from land cropped under specific conditions to corresponding loss from tilled, continuously fallow ground. The factor ranging from approximately zero to 1.0 depends on type of vegetation cover, crop season, and other management techniques. According to Wischmeier and Smith (1965) continuous corn is 63 percent as erodible as continuous fallow during the first month after seeding, but it is only 26 percent as erodible as fallow when mature.

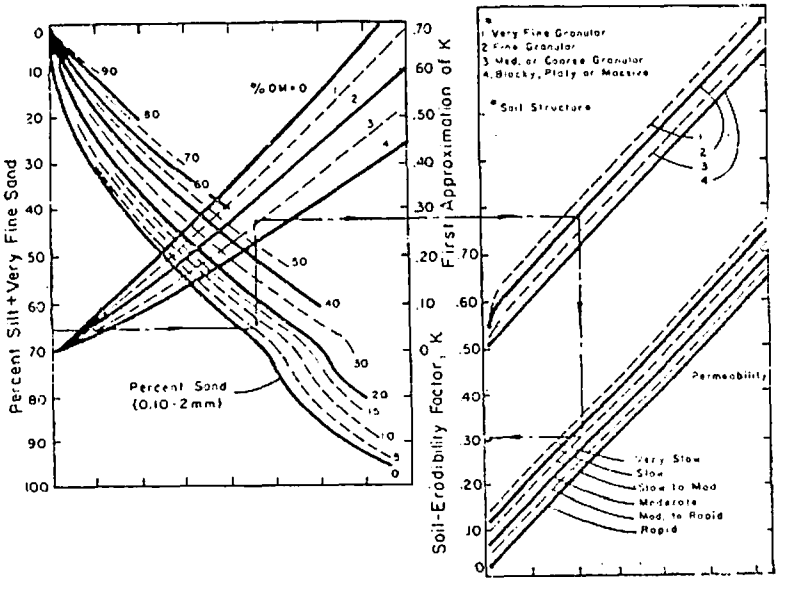


Figure 13-1. Soil erodibility nomograph used to determine factor K for specific topsoils or subsoil horizons. Solutions are in tons per acre (from Wischmeier et al., 1971).

Small grains are approximately 50 percent as erodible as continuous fallow during the first month after seeding but are only about 5 percent as erodible near maturity. Wischmeier and Smith (1965) presented a table to show the relative erodibilities of several crops (corn, grain, and grass) for different crop sequences and yield levels at various stages of crop growth.

Erosion-control practice factor P accounts for the effect of conservation practices such as contouring, strip-cropping, and terracing on erosion. It is valuable as the ratio of soil loss using one of these practices to the loss using straight row farming up and down the slope. Terracing is generally the most effective conservation practice for decreasing soil erosion.

Wischmeier (1972) presented a method including graphical aids for determining the cover and management factor (cropping-management factor, C). The cropping-management factor can be divided into three distinct types of effects as follows: Type I-effects of canopy cover, Type II-effects of mulch or close growing vegetation in direct contact with the soil surface, and Type III-tillage and residual effects of the land-use.

Type I-Canopy Cover

Leaves and branches that do not directly contact the soil are effective only as canopy cover. A canopy can intercept falling raindrops but waterdrops falling from the canopy may regain an appreciable velocity, although not the terminal velocities of free-falling raindrops. Therefore, canopy cover reduces rainfall erosivity by reducing impact energy at the soil surface. Amount of reduction depends on height and density of the canopy. Figure 13-2 shows the canopy factor as a function of height and density of the canopy. Canopy factors for various percentages of cover at heights of 0.5, 1.0, 2.0, and 4.0 meters may be obtained directly from this graph.

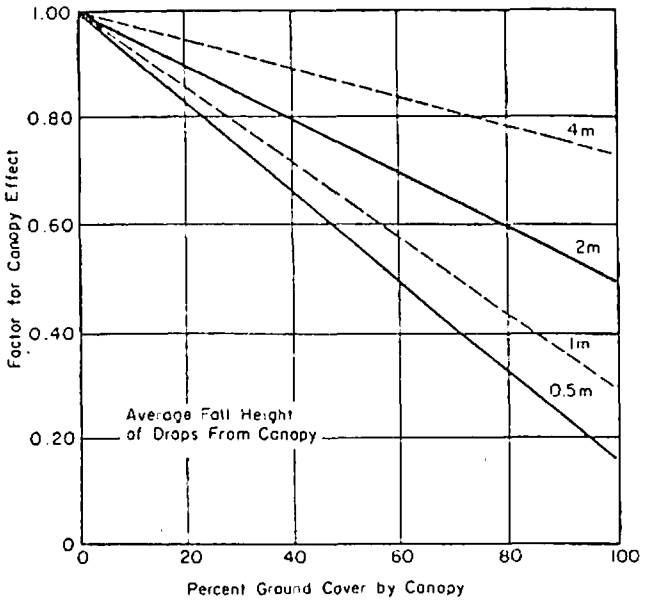


Figure 13-2. Influence of vegetal canopy on effective-EI (after Wischmeier, 1972).

Type II-Mulch and Close Growing Vegetation

A mulch at the soil atmosphere interface is much more effective than an equivalent percentage of canopy cover. Because intercepted raindrops have no remaining fall-height to the ground, their impact on the soil surface is eliminated. A mulch that makes a good contact with the ground also reduces runoff velocity which greatly reduces the potential of runoff to detach and transport soil material.

Substantial rainulator data are not available on erosion-reducing effectiveness of various amounts and types of mulches used on cropland and construction sites. Extrapolation of these data to other mulches and close covers such as those associated with range or woodland is facilitated by expressing them on the basis of percent surface cover rather than tons per acre. This conversion, and a preliminary summarization of data are reflected in the relationship curve shown in Figure 13-3.

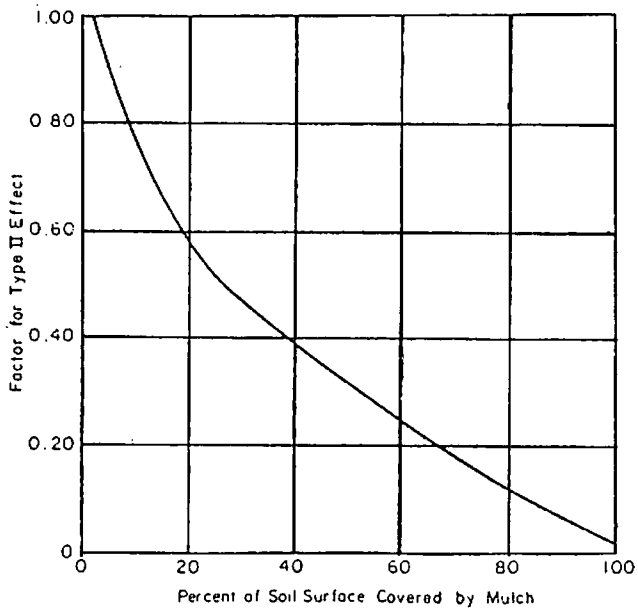


Figure 13-3. Effect of plant residues or close-growing stems at the soil surface (after Wischmeier, 1972).

Type III-Residual Effects of the Land Use

This category includes residual effects of land use on soil structure, organic matter content and soil density, effects of tillage or lack of tillage on surface roughness and porosity, roots and subsurface stems, biological effects, and probably other factors. This factor can be evaluated from Figure 13-4 by knowing the percent of root network in the topsoil relative to a good rotation meadow. This percent of root network is often a difficult value to estimate. Overall C factor can be evaluated by the product of three subfactors i.e., Type I, II, and III subfactors.

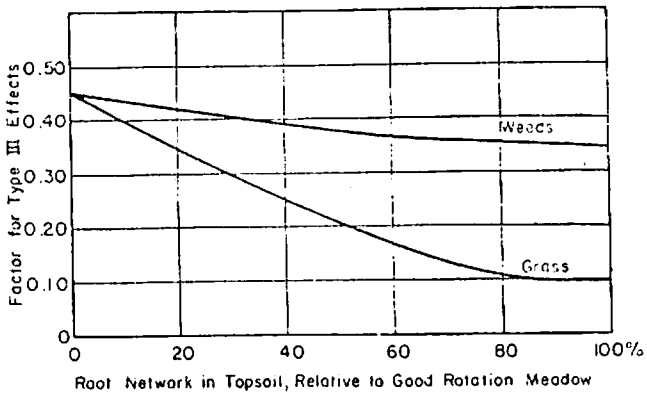


Figure 13-4. Type III effects on undisturbed land areas (after Wischmeier, 1972).

Although widely used, the USLE approach has some important limitations. Until recently the approach was most applicable for estimating long term soil yields.

Wischmeier (1973) discussed confidence in the equation's predictions. As previously indicated, some of the terms in the soil loss equation are themselves functions of several significant parameters and must be derived by separate formulas and subroutines. Therefore, the complete equation could not be derived as a single least-squares fit to the 10,000 plot-years of basic data and overall statistical confidence limits could not be computed by the usual analysis of variance technique. Wischmeier did obtain an indication of confidence limits using the equation, iso-erodent map, EI distribution curves, slope effect chart, and soil-loss ratio table to predict long-term average annual soil losses on 189 plots for which he had a total of approximately 2300 plot-years of soil loss records. The 189 individual plot predictions deviated from corresponding measured soil losses by an average of 1.4 tons per acre per year which is approximately 12 percent of the 11.3-ton overall-average soil loss for the sample. About 84 percent of the deviations were within two tons per year but the variance indicated that about five percent of such predictions may be in error by as much as 4.6 tons or 40 percent of the average soil loss for the sample plots.

There is strong evidence of 20- to 22-year cycles in rainfall patterns. The iso-erodent map and EI distribution curves were derived from 22 years of rainfall records that represent full cycles and therefore can be used to predict long-term average losses. Thus the predicted values in the foregoing comparison are long-time averages while the actual data with which they were compared represent specific time periods (some as short as five years). Since cyclical changes in rainfall patterns tend to be geographically widespread and most of short-term locational studies in the sample were approximately

concurrent, the effects of deviations from long-term average rainfall and seasonal distribution of erosive rainstorms would not have averaged out. For 2300 plot-years in the sample, the equation overpredicted by an average of 0.4 ton per acre per year. Of the 88 deviations of one ton or more 59 were from comparisons representing less than half of the normal rainfall cycle. Therefore, use of the USLE for short-term comparisons may be in error.

Confidence bands on predictions by the equation are the narrowest for silt, silt loam and loam soils, uniform slopes of from five to twelve percent (lengths not exceeding 400 feet), and consistent croping systems that are directly represented by lines in the soil-loss-ratio graph. Beyond these limits significant extrapolation errors become more likely, but the predictions are believed to have sufficient accuracy for most applications over a much wider range of conditions. The equation's accuracy for predicting long-term average soil loss for a given situation is limited by lack of available data to evaluate individual terms rather than by the model itself. Therefore, overall attainable prediction accuracy is continuously improving as research provides data for accurate evaluation of the factors over a wider range of conditions.

The Universal Soil Loss Equation is designed to predict average annual soil losses by sheet and rill erosion on upslope areas such as farmland and construction sites. It can be helpful for prediction of contributions from these sources to downstream sediment loads but capabilities and limitations for this use must be recognized. It is an erosion equation and is not designed to predict deposition. Its predictions do not include sediment contributions from gully erosion or landslides, and it does not include factors to account for sediment losses or gains between the field and stream or reservoir. These items must be evaluated separately.

Another problem with the USLE or other types of regression models is the models' dependence on large amounts of data for development. As previously mentioned, approximately 10,000 plot-years of data from the central and eastern United States were used to develop the equation. However, in the semi-arid west collection of this amount of data may take centuries because the number of rainfall events that occur over an area in a year and the number of data collection sites are limited in the west and most other forested watersheds. In addition the tree growth is a long and slow process and its effect on water and sediment yield is prolonged. It is difficult to collect large amounts of data for wildland conditions. Another drawback to regression type equations as previously mentioned, is their relative stationarity in time and space. In other words the data are restricted to a certain collection period at selected locations and do not necessarily represent long term variations in the system. Therefore, use of regression equations to predict sediment yields outside the range of the data base can be unwarranted.

## 13.3 BASIC SEDIMENT ROUTING AND YIELD EQUATIONS

### General

Sediment yield from watersheds is governed by general physical processes. Governing equations and methods of solution for water

routing were discussed in the previous chapter. In addition to the continuity equation for water and the momentum equation, additional equations are refined for sediment routing. Of primary importance is the sediment continuity equation and corresponding sediment transport formulae. Another basic principle is that sediment yield is directly proportional to either transport or supply. In general if supply is greater than transport capacity, the transport capacity controls yield and vice versa. Sediment supply is considered to develop from raindrop impact detachment and flow detachment and basic equations are applicable to overland and channel flow. Another important aspect is the use of the sediment continuity equation to account for aggradation or degradation of the land or channel surface. In all models sediment yield is considered for individual size fractions.

Sediment Continuity Equation

The sediment continuity equation can be expressed as

$$\frac{\partial G_s}{\partial x} + \frac{\partial CA}{\partial t} + (1-\lambda)\frac{\partial PZ}{\partial t} = g_s \tag{13-5}$$

in which

$$C = \frac{G_s}{Q} \tag{13-6}$$

and $G_s$ is total sediment transport rate by volume per unit time, $C$ is sediment concentration by volume, $Z$ is depth of loose soil, $\lambda$ is soil porosity, and $g_s$ is lateral sediment inflow.

Sediment load can be considered for different sizes and the continuity equation can be divided into $N$ parts or

$$\frac{\partial G_{si}}{\partial x} + \frac{\partial C_i A}{\partial t} + (1-\lambda)\frac{\partial PZ_i}{\partial t} = g_{si} \tag{13-7}$$

$$i = 1, \ldots, N$$

in which $i$ is the size fraction index and $N$ is the number of size fractions and

$$C_i = \frac{G_{si}}{Q} \tag{13-8}$$

$$C = \sum_{i=1}^{N} C_i \tag{13-9}$$

and

$$Z = \sum_{i=1}^{N} Z_i \tag{13-10}$$

Sediment Transport Equations

Sediment transport equations are used to determine the sediment transport capacity for a specific set of flow conditions. Different transport capacities can be expected for different sediment sizes. For each sediment size, the transport rate includes the bedload transport rate and suspended load transport rate. The following equations are adopted to determine the sediment transport capacity for each size.

The Meyer-Peter, Müller equation a simple and commonly used bedload transport equation (USBR, 1960) is

$$q_b = \frac{12.85}{\sqrt{\rho\ \gamma_s}} (\tau\ -\ \tau_c)^{1.5} \tag{13-11}$$

in which

$$\tau_c = \delta_s(\gamma_s - \gamma)d_s \tag{13-12}$$

In Equations 13-11 and 13-12 $q_b$ is the bedload transport rate in volume per unit width for a specific size of sediment, $\tau_c$ is critical tractive force, $\rho$ is density of water, $\gamma_s$ is specific weight of sediment, $\gamma$ is specific weight of water, $d_s$ is size of sediment, and $\delta_s$ is a constant dependent on flow conditions. Gessler (1965) showed that $\delta_s$ should be 0.047 for most flow conditions. If rilling develops on the overland flow surface, the value of $\delta_s$ should be reduced.

Although it is not necessary to use the Meyer-Peter, Müller equation, an equation should be chosen that is applicable to the field conditions. According to Shen (1971) the general bedload function can be expressed in the following functional form of

$$q_b = a_4\ (\tau_o - \tau_c)^{b_4} \tag{13-13}$$

in which $a_4$ and $b_4$ are constants.

Flow discharge $Q$ and flow area $A$ are determined by water routing procedures described in the previous chapter. The corresponding value of $\tau_o$ is computed below. Mean velocity is in general

$$V = Q/A \tag{13-14}$$

Boundary shear stress acting on the grain is

$$\tau_o = \frac{1}{8} \rho f_o\ V^2 = \frac{1}{8} \rho \frac{K_o}{N_r} V^2 \tag{13-15}$$

where $\rho$ is density of flowing water, $f_o$ is the Darcy-Weisbach friction factor, $K_o$ is flow resistance related to grain, and $N_r$ is the flow's Reynolds number.

The sediment concentration profile that relates sediment concentration with depth above the bed (Einstein, 1950) can be written as

$$\frac{C_\xi}{C_a} = \left(\frac{R-\xi}{\xi}\,\frac{a'}{R-a'}\right)^w \tag{13-16}$$

in which $C_\xi$ is sediment concentration at distance $\xi$ from the bed, $C_a$ is the known concentration at a distance $a'$ above the bed, and $w$ is a parameter defined as

$$w = \frac{V_s}{\kappa U_*} \tag{13-17}$$

In Equation 13-17, $V_s$ is the settling velocity of the sediment particles, $\kappa$ is the von Karman constant (assumed 0.4), and $U_*$ is shear velocity of the flow defined as

$$U_* = \left(\frac{\tau_*}{\rho}\right)^{1/2} \tag{13-18}$$

It should be noted that

$$\tau_* = \frac{1}{8}\, f\rho V^2 \tag{13-19}$$

where $f$ is the overall Darcy-Weisbach resistance factor.

A logarithmic velocity profile is commonly adopted to describe velocity distribution in turbulent flows. A useful equation is

$$\frac{u_\xi}{U_*} = B + 2.5\ \ell n\ \left(\frac{\xi}{\eta_s}\right) \tag{13-20}$$

in which $u_\xi$ is point mean velocity at distance $\xi$ from the bed, $B$ is a constant dependent on roughness, and $\eta_s$ is roughness height.

The integral of suspended load above the $a'$ level in the flow is obtained by combining Equations 13-16 and 13-20 or

$$q_s = \int_{a'}^{R} u_\xi C_\xi \xi = C_a U_* \int_{a'}^{R} \left[B + 2.5\ \ell n\left(\frac{\xi}{\eta_s}\right)\right]\left(\frac{R-\xi}{\xi}\,\frac{a'}{R-a'}\right)^w d\xi \tag{13-21}$$

By letting

$$\sigma = \frac{\xi}{R} \tag{13-22}$$

and

$$G = \frac{a'}{R} \tag{13-23}$$

the equation becomes

$$q_s = \int_{a'}^{R} u_\xi C_\xi d\xi = C_a U_* \int_{a'}^{R} [B + 2.5 \ln(\frac{\xi}{\eta_s})](\frac{R-\xi}{\xi}\frac{a'}{R-a'})^w d\xi \quad (13\text{-}24)$$

According to Einstein (1950), concentration near the "bed layer" $C_a$ is related to the bedload transport rate $q_b$ by expression

$$q_b = 11.6\ C_a U_* a' \quad (13\text{-}25)$$

in which $a'$ is defined as thickness of the bed layer that is twice the size of sediment or $2d_s$.

Average flow velocity $V$ is defined

$$V = \frac{\int_0^R u_\xi d\xi}{\int_0^R d\xi} \quad (13\text{-}26)$$

Using Equation 13-20 yields

$$\frac{V}{U_*} = B + 2.5 \ln (\frac{R}{\eta_s}) - 2.5 \quad (13\text{-}27)$$

Einstein (1950) defined the two integrals in Equation 13-24 as

$$I_1 = \int_G^1 (\frac{1-\sigma}{\sigma})^w d\sigma \quad (13\text{-}28)$$

and

$$I_2 = \int_G^1 (\frac{1-\sigma}{\sigma})^w \ln\sigma\ d\sigma \quad (13\text{-}29)$$

Integrals $I_1$ and $I_2$ cannot be integrated in closed form for most values of $w^1$ so numerical integration is necessary. An efficient numerical method of determining $I_1$ and $I_2$ was developed by Li (1974).

Substitution of Equations 13-25, 13-27, 13-28, and 13-29 into 13-24 yields

$$q_s = \frac{q_b}{11.6}\frac{G^{w-1}}{(1-G)^w}[(\frac{V}{U_*} + 2.5)\ I_1 + 2.5\ I_2] \quad (13\text{-}30)$$

Total load per unit width of channel is

$$q_t = q_b + q_s \quad (13\text{-}31)$$

Equation 13-31 gives total load per unit width of channel for a uniform size of sediment in the bed. When considering transport by different sizes and the entire width of channel, sediment transport capacity of the ith size fraction of a sediment mixture would be

$$G_{ci} = P\, P_{ai}\, q_t \tag{13-32}$$

in which $G_{ci}$ is sediment transport capacity for the ith size, and $F_{ai}$ is the adjusted fraction of the ith size sediment as determined in the next section.

Equations for Sediment Supply

Sediment supply rate is another determining factor in actual sediment yield. Simons et al. (1975) stated that sediment supply depends on the initial depth of loose soil left from previous storms, the amount of soil detachment by raindrop impact, and the amount of soil detachment by flow.

Soil Detachment by Raindrop Impact

Raindrop impact is a primary source of kinetic energy for detaching soil from any unprotected land surface. Ellison (1944) made a comprehensive study about raindrop splash. Law and Parson (1943), Young and Wiersma (1973), and Mutchler (1967) greatly contributed to the study on detachment by raindrop impact. The conclusion drawn from these studies is that soil detachment is a function of erosivity of rainfall and erodibility of soil particles. Erosivity is directly related to the energy produced by raindrop impact and is generally formulated as a power function of rainfall intensity, droplet size, cover condition, and terminal velocity of the drop. More recently, Carter et al. (1974) reported energy produced by raindrop impact is also a function of air temperature, season of the year, and storm duration. Potential rate of soil detachment by raindrop impact is assumed as a power function of rainfall intensity given by Meyer (1971) or

$$D_r = a_5 I^{b_5} \left(1 - \frac{Z_w}{Z_m}\right)(1-C_g)(1-C_c) \tag{13-33}$$

in which $I$ is rainfall intensity, $a_5$ is a parameter depending on soil characteristics, and $b_5$ is a constant ($b_5 \cong 2.0$, see Meyer, 1971). The term $Z_w$ is depth of water plus loose soil depth, and $Z_m$ is the maximum penetration depth of raindrop splash. According to Mutchler and Young (1975), $Z_m$ can be equal to three times the median raindrop size. Median raindrop size is often expressed as a power function of rainfall intensity. Therefore, $Z_m$ can be written as

$$Z_m = 3(2.231^{0.182}) \tag{13-34}$$

with $Z_m$ in millimeters.

Equation 13-33 is valid when $Z_w$ is less than $Z_m$. When depth of loose soils plus water depth is greater than $Z_m$, $D_r$ is zero or

$$D_r = 0, \text{ if } Z_w > Z_m \tag{13-35}$$

If tree branches are high, drops from leaves can regain terminal velocity and erosive potential. However, the usually extensive ground

cover under trees protects the surface. Canopy cover density $C_g$ in Equation 13-33 should be that portion that effectively protects the soil surface from raindrop impact.

Potential rate of loose soil detachment $D_r$ is expressed in units of depth per unit time. Thus, the amount of loose soil available for transport from raindrop splash is

$$Z_i = F_i D_r \Delta t \tag{13-36}$$

where $Z_i$ is depth of available loose soil and $F_i$ is original percentage of sediment size in a given size fraction $i$.

Percentage of each size fraction on the surface changes over time due to armoring or lagging of the non-eroded sizes. Water transports smaller sediment sizes more easily and leaves larger size fractions behind. Thus, percentages of surface material need adjustment each time step. If total loose soil depth is greater than $D_a$ (the thickness of the armor layer), adjusted percentages $F_{ai}$ can be written

$$F_{ai} = \frac{Z_i}{Z} \tag{13-37}$$

If total loose soil depth $Z$ is less than $D_a$, then adjusted percentages must account for the layer of undisturbed soil that is distributed according to original percentages plus loose soil that covers it or

$$F_{ai} = \frac{1}{D_a} [Z_i + F_i (D_a - Z)] \tag{13-38}$$

Thickness of the armor layer can be determined as the maximum size of particles in motion. It is usually assumed that $D_{84}$ (the size of sediment for which 84 percent of the sample is finer by weight) is the representative size of the armor layer.

Soil Detachment by Surface Runoff

The amount of soil detached by surface runoff is determined by comparing total sediment transport capacity to total amount of available loose soil. Total sediment transport capacity is

$$G_c = \sum_{i=1}^{N} G_{ci} \tag{13-39}$$

By substituting total sediment transport capacity $G_c$ into the transport rate in Equation 13-5, total potential change in loose soil can be determined as

$$\Delta Z^P = \frac{\partial Z}{\partial t} \Delta t \tag{13-40}$$

where $\Delta Z^P$ is change in loose soil.

If $\Delta Z^p \geq -Z$, loose soil storage is enough for transport and no detachment of soil by surface runoff is expected. Soil is detached if $\Delta Z_p \leq -Z$ and the amount of detachment is

$$D = D_f[\Delta Z^p + Z] \tag{13-41}$$

in which $D$ is total amount of runoff detached soil and $D_f$ is defined as a detachment coefficient runoff with values ranging from 0.0 to 1.0 depending on soil erodibility. As an example if the flow were over a nonerodible surface, the value for $D_f$ would be zero. In a river where the riverbed is always loose, $D_f$ would be unity.

The new amount of loose soil should be further modified as

$$Z_{Ti} = Z_i + D\,F_i \tag{13-42}$$

in which $Z_{Ti}$ is the total amount for size fraction $i$.

Numerical Procedure for Sediment Routing

The following numerical procedure for sediment routing is used to couple equations governing sediment motion with the water routing procedure presented in the previous chapter.

Sediment transport capacity is determined by Equation 13-32 for a given sediment size with flow conditions obtained by water routing. Potential sediment load concentration for a given sediment size $i$ is then

$$C_i^p = \frac{G_{ci}}{Q} \tag{13-43}$$

Using the same finite difference approximation as that in the water routing procedure, potential change in loose soil storage for a given sediment size is determined by utilizing Equations 13-7 and 13-43. That is

$$\Delta z_i^p = \frac{1}{(1-\lambda)p}\{\theta[G_{si_j}^{n+1} - C_i^p\,Q_{j+1}^{n+1})(1-a) + (G_{s_i}^{n} - G_{si_j}^{n})a]$$

$$- [(C_i^p\,A_{j+1}^{n+1} - C_{i_{j+1}}^{n}\,A_{j+1}^{n})(1-b) + (C_{i_j}^{n+1}\,A_j^{n+1} - C_{i_j}^{n}\,A_j^{n})b]$$

$$+ \frac{\Delta t}{2}[(1-b)g_{si_{j+1}}^{n+1} + bg_{si_j}^{n+1} + (1-b)g_{si_{j+1}}^{n} + bg_{si_j}^{n}]\} \tag{13-44}$$

where $\theta$ is $\Delta t/\Delta x$.

Sediment transport rate is dependent on both the available supply of sediment and transporting capacity of the flow. If $\Delta Z_i^p \geq -Z_i$, the availability is greater than the transporting capacity. Consequently, the bed material load transport rate is equal to the transporting capacity or

$$C_{i_{j+i}}^{n+1} = C_i^p \tag{13-45}$$

and the actual change in $Z_i$ is

$$\Delta Z_i = \Delta Z_i^p \tag{13-46}$$

If $\Delta Z_i^p < -Z_i$, availability of material is less than transporting capacity. The transport rate is limited by availability of loose soil and the bed material concentration is therefore,

$$\begin{aligned} C_{i_{j+1}}^{n+1} = \{&(1-\lambda)pZ_i + \frac{\Delta t}{2}[(1-b)g_{si_{j+1}}^{n+1} + bg_{si_j}^{n+1} \\ &+ (1-b)g_{si_{j+1}}^{n} + bg_{si_j}^{n}] + \theta[gsi_j^{n+1}(1-a)-(G_{si_{j+1}}^{n} - G_{si_j}^{n})a] \\ &+ C_{i_{j+1}}^{n} A_{j+1}^{n}(1-b)-(C_{i_j}^{n+1}A_j^{n+1}-C_{i_j}^{n}A_j^{n})b\} / [A_{j+1}^{n+1}(1-b)+\theta Q_{j+1}^{n+1}(1-a)] \end{aligned} \tag{13-47}$$

and

$$\Delta Z_i = Z_i \tag{13-48}$$

Sediment transport rate $G_{si}$ is determined by

$$G_{si_{j+1}}^{n+1} = C_{i_{j+1}}^{n+1} Q_{j+1}^{n+1} \tag{13-49}$$

and the amount of loose soil available at the next time increment is

$$Z_{i_{k+1}} = Z_{i_k} + \Delta Z_i \tag{13-50}$$

where k designates the time period. If the finite difference scheme weighting factors a and b are zero the above sediment routing scheme becomes identical to that reported by Simons et al. (1975). The main concept for determining actual sediment transport rate follows the paper by Shen (1971) and is depicted in Figure 13-5. This figure indicates that actual sediment transport rate for a particle size is determined by the smaller of the following two quantities: transporting capacity or the availability considering all sources of supply. Usually the transport rates of smaller particle size are controlled by supply and the transport rates for coarser particles are dictated by transporting capacities.

The above equations indicate the key physical processes that must be considered in sediment routing and yield. If models are simplified or altered in any manner, the general physical processes remain the same except minor adjustments made to account for simplifying assumptions or other alterations. The following sections briefly describe various sediment routing and yield physical process models. Similarities and differences for each model type are presented along with limited examples.

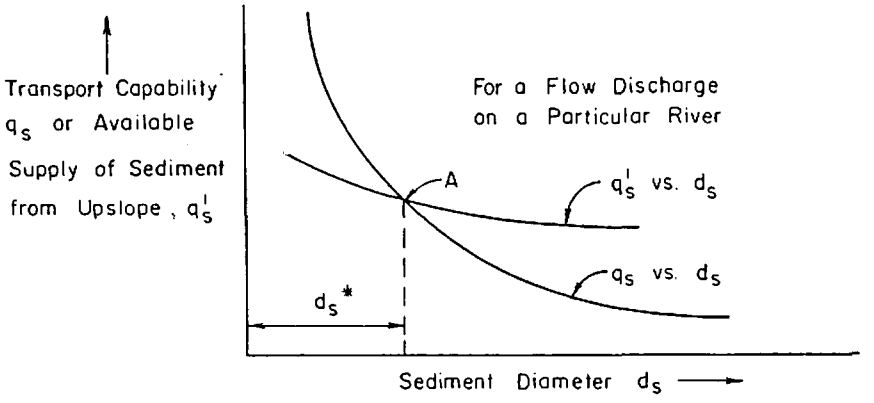


Figure 13-5. Concept of controlling sediment transport rates (after Shen, 1971).

## 13.4 MODEL APPLICATION

The combination of hydrologic models such as those presented in the chapter on surface water hydrology and the sediment routing procedure form a series of models for predicting sediment yield. Two levels of resolution have been utilized. Brief description of approaches follows.

### High Resolution Model

Once the watershed has been numerically defined by the segmentation procedure, overland flow units and channel flow units in the watershed can be determined. Simons, et al. (1975) developed a watershed sediment model that is primarily applicable for surface erosion simulation. The land surface hydrologic cycle, sediment production, and water and sediment movement on small watersheds are simulated. Conceptually the watershed is divided into an overland flow section and a channel system section. Different physical processes are important for the two different environments. In the overland flow loop processes of interception, evaporation, infiltration, raindrop impact detachment of soil, erosion by overland flow, and overland flow water and sediment routing to the nearest channel are material load movement. The amount of soil detachment by raindrop splash is assumed to be a simple power function of rainfall intensity. Soil detachment by surface runoff is considered as the result of bed material load movement. Local transporting capacity of bed material load is assumed to be a function of local effective bed

shear stress and a combination of Meyer-Peter, Müller's bed load equation and Einstein's suspended load procedure is used for the sediment transport equation. Wash load pickup rate is formulated to be a function of bed shear stress and the amount of available loose soil. The sediment routing procedure is primarily based on the continuity equation for sediment (wash load and bed material load by size fraction) and the computation is carried out by a finite difference numerical procedure coupled with the overland surface water routing.

Simplified Models

Simplified models contain the same physical processes listed above but these model components are applied to subunits that are in general much larger than those of the high resolution model.

Many successful applications of the developed models have been performed including small experimental plots, small watersheds, medium-sized watersheds, and large and mixed watersheds. Selected examples follow.

Beaver Creek Watersheds, Arizona

Simons, Li and Stevens (1975) tested applicability of the high resolution watershed model on the Beaver Creek Watershed in Arizona. Five runoff events in Experimental Watershed 1 and one runoff event in Experimental Watershed 17 were used.

Watershed 1 is a small drainage catchment with an area of 313.6 acres which has been cleared of trees. The five storm events modeled for Watershed 1 occurred on November 22, 1965; November 24, 1965; November 25, 1965; September 6, 1967; and September 5, 1970. The latter is known as the Labor Day storm which is one of the largest on record. Watershed 17 has an area of 287.4 acres. The only storm available for testing is the Labor Day storm.

Agreement between measured and simulated water hydrographs was satisfactory. Because there was no measured sediment hydrograph, no comparison could be made. Comparisons of simulated and measured sediment yields are given in Figure 13-6 which show that the water and sediment routing model simulated sediment yield from Watershed 1 and Watershed 17 within approximately 30 percent. Satisfactory results were obtained for different size storms and in different watersheds by using only one set of model parameters. This verifies that the model could be used to synthesize missing data and predict the response of watersheds to various types of watershed management practices. The model could be used to estimate flood flows and corresponding sediment yields from ungaged watersheds.

Transferability of the physical process model is one of its main advantages over conventional methods such as the Unit Hydrograph and Universal Soil Loss Equation. The Labor Day storm produced approximately 2.2 times more surface runoff in Watershed 17 than in Watershed 1 but only about 0.4 times more sediment yield. There was more surface runoff and less sediment yield in Watershed 17 because it is longer and narrower and its average slope is less than that of Watershed 1.

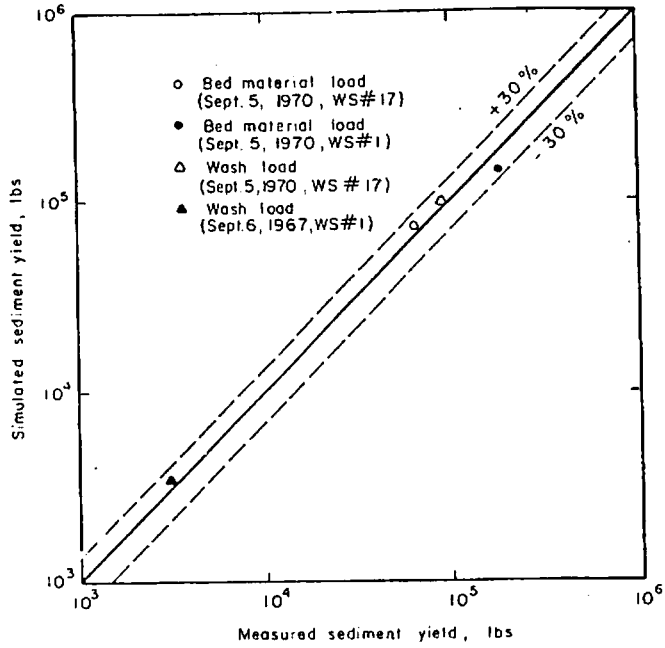


Figure 13-6. Comparison of measured and simulated sediment yields (after Simons et al., 1975).

Computed sediment hydrographs for the large Labor Day storm and for a small storm (November 22, 1965) on Watershed 1 are given in Figures 13-7 and 13-8. Shapes of sediment and water hydrographs are similar for the large storm but differ for the small storm. For the small storm tested, the peak of the sediment hydrograph occurs earlier than the water hydrograph peak because sediment supply rate is greater in the early stage of surface runoff. This effect is not significant for a larger storm.

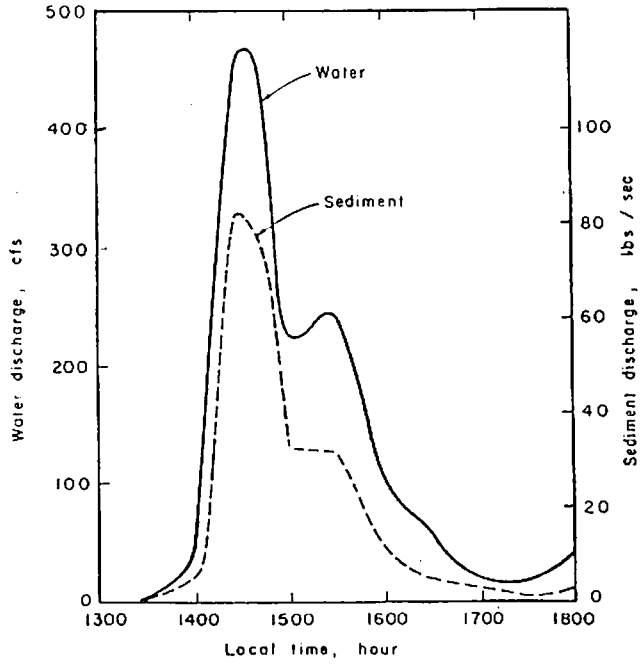


Figure 13-7. Computed hydrographs for the September 5, 1970 storm on Watershed 1 (after Simons et al., 1975).

An important task of watershed management is to predict results of selected treatment effects. Vegetation treatment effects on sediment yields are estimated by changing canopy cover density and ground cover density of overland flow units. Effects of vegetation treatment on the water and sediment yields from Watershed 1 were evaluated based on storms of September 5, 1970 and September 6, 1967. As shown in Figure 13-9, for a constant and undisturbed ground cover of 65 percent, sediment yield and peak flow rates and timing from these two storms are increased as the canopy cover density is decreased.

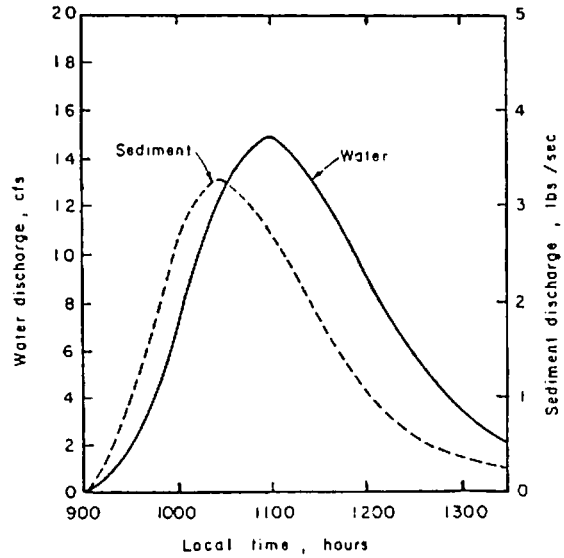


Figure 13-8. Computed hydrographs for the November 22, 1965 storm on Watershed 1 (after Simons et al., 1975).

Reduction in interception caused by removing vegetation results in an increase of excess rainfall and raindrop soil detachment. These effects are much more pronounced in Watershed 1 for the smaller storm than for large storms.

If a watershed is clear-cut and the forest litter, small brush, grass, and rocks are removed to varying degrees or if the ground cover is seriously destroyed by a burning treatment, the associated response can be estimated by changing ground cover density in overland flow units. Changes in sediment yields for Watershed 1 from the storms of September 5, 1970 and September 6, 1967 are shown in Figure 13-10. As ground cover is decreased, sediment yield and peak sediment flow are increased greatly and the time to peak flow is shortened slightly. Effect on water yield is more pronounced for a smaller storm but nearly the same effects on sediment yield are obtained for both small and large storms.

Ground cover density is an important factor in controlling sediment yields. If a watershed is subjected to clear-cut treatment but there is proper management of ground cover, the sediment yield may not be significantly increased.

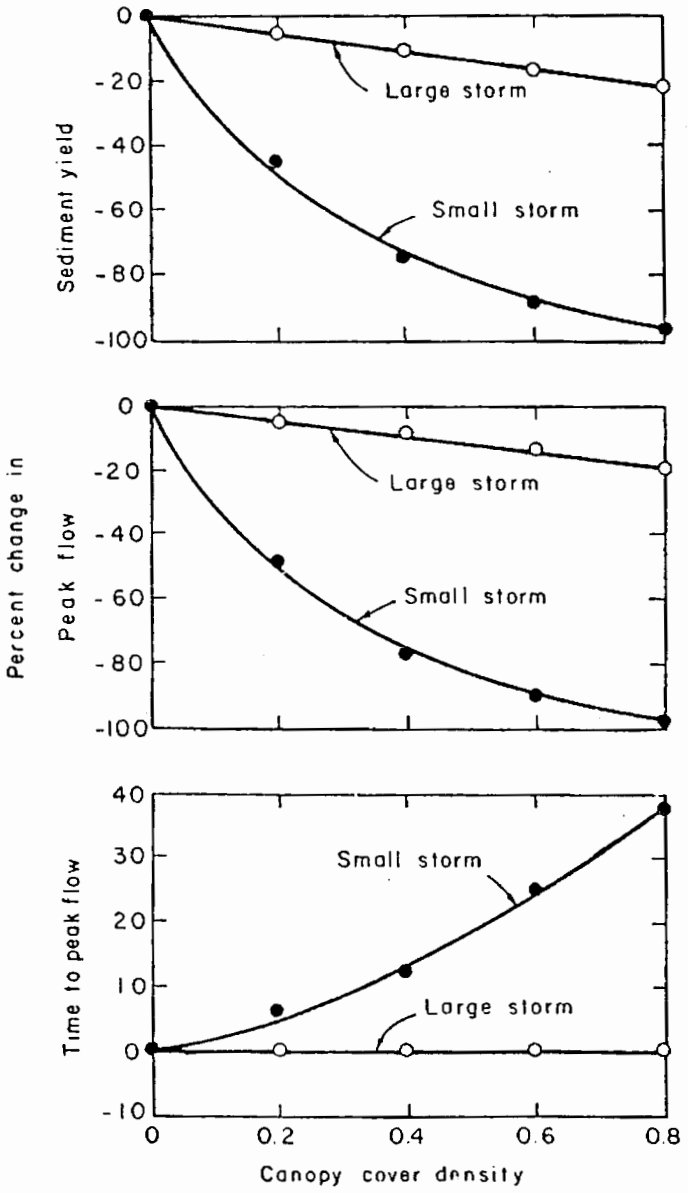


Figure 13-9. Effect of canopy cover density on the sediment hydrograph from Watershed 1 (after Simons et al., 1975).

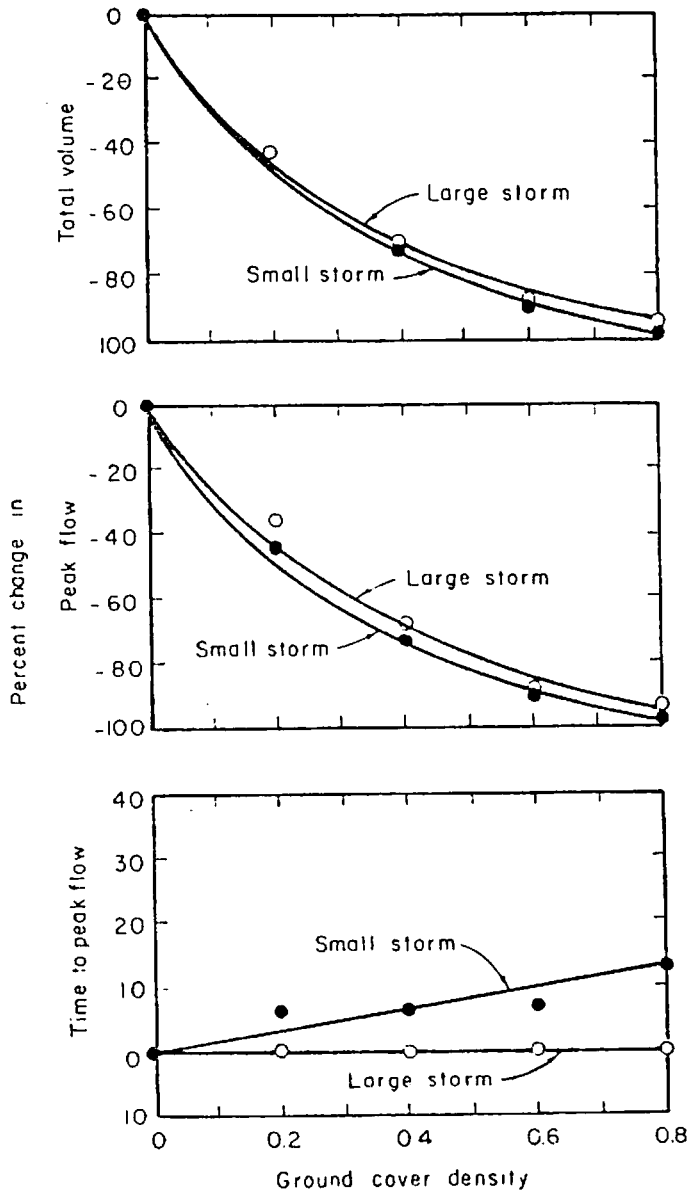


Figure 13-10. Effect of ground cover density on the sediment yield from Watershed 1 (after Simons et al., 1975).

Watershed near Watkinsville, Georgia

Sediment runoff data were not available for Walnut Gulch so another watershed was used to test the sediment yield portion of the multiple watershed model. The only watersheds with sufficient sediment data available were two small agricultural watersheds, each about three acres in area, located near Watkinsville, Georgia. Several storms were used to calibrate the model on one of the watersheds. Calibrated parameters were then combined with the available data for the remaining storms for both watersheds. Comparison of simulated and measured sediment yield appears in Figure 13-11.

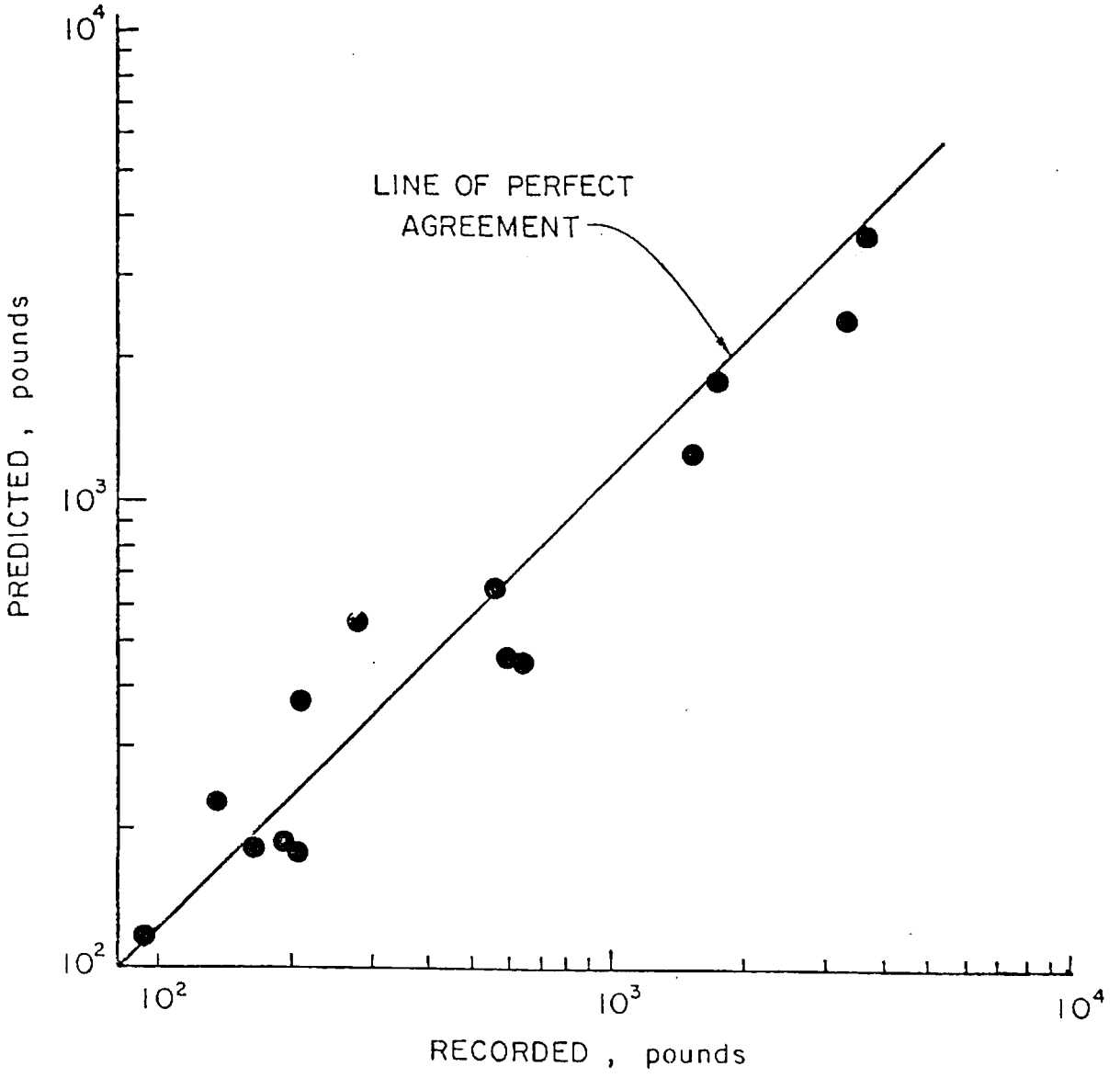


Figure 13-11. Comparison of simulated and recorded sediment yields for Watkinsville Georgia Watershed.

These results again indicate spatial and temporal predictive capabilities. Sediment yield was estimated by considering different size fractions. This also provides useful information for estimating water pollutants attached to the sediment.

## 13.5 DATA NEEDS

Data needed for mathematical modeling of watershed response are dependent on type of watershed, objective of modeling, and type of model utilized. Data requirements summarized herein are primarily for studying major watershed response (water yield, sediment yield, and stream morphology) from small watersheds. Emphasis is placed on input data requirements of the watershed models presented in this paper.

There are two distinct types of data involved in the analysis which include model input data that are specifically required for the model input and basic data (raw data) that are directly taken from field measurements. Generally, the model input data are obtained from retrieving and/or analyzing the raw data. Required model input data, basic data, and supplementary data important to watershed study are summarized in section 12.8 of the previous chapter.

## 13.6 ESTIMATION OF DATA

In addition to the hydrologic characteristics of the area as described in the previous chapter on surface water hydrology, sediment information is needed for modeling. Three types of sediment data are required to model sediment yield. These are size analysis, detachment coefficients, and a sediment transport coefficient.

Sediment size data should be on-site size distributions and transported material distributions. Use of both distributions aids in model calibration in order to confirm that the model is transporting correct size fractions from correct sediment supply. Size distributions are obtained from sieve analyses of duplicate samples. Common size breakdowns are given in Table 13-1. Particle size distribution for the in-situ soil is needed to determine the resultant sediment transport. If it is unavailable, an estimate of the $D_{50}$ sediment size is needed. Some information may be available from USDA Soil Conservation Service Reports or state soil surveys. Textural classification is one rudimentary method for estimating a $D_{50}$ sediment size and aggradation or size distribution. This requires use of a clay-silt-sand chart (Figure 13-12). Entering the chart with a textural class name, a point is selected in a central part of the class name polygon. The corresponding percent sand, percent silt, and percent clay values are used to plot a gradation curve. In Figure 13-12 silt percent is the difference between 100 percent and the sum of sand and clay percentages. The percents are plotted as 100 percent finer than 2 mm (coarse sand), silt percent plus clay percent finer than 0.05 mm (silt), and clay percent finer than 0.002 mm (clay). The gradation curve consisting of three points (sand, silt, and clay) can be described for mathematical purposes by $D_{50}$ and G the gradation coefficient. The gradation coefficient is defined as

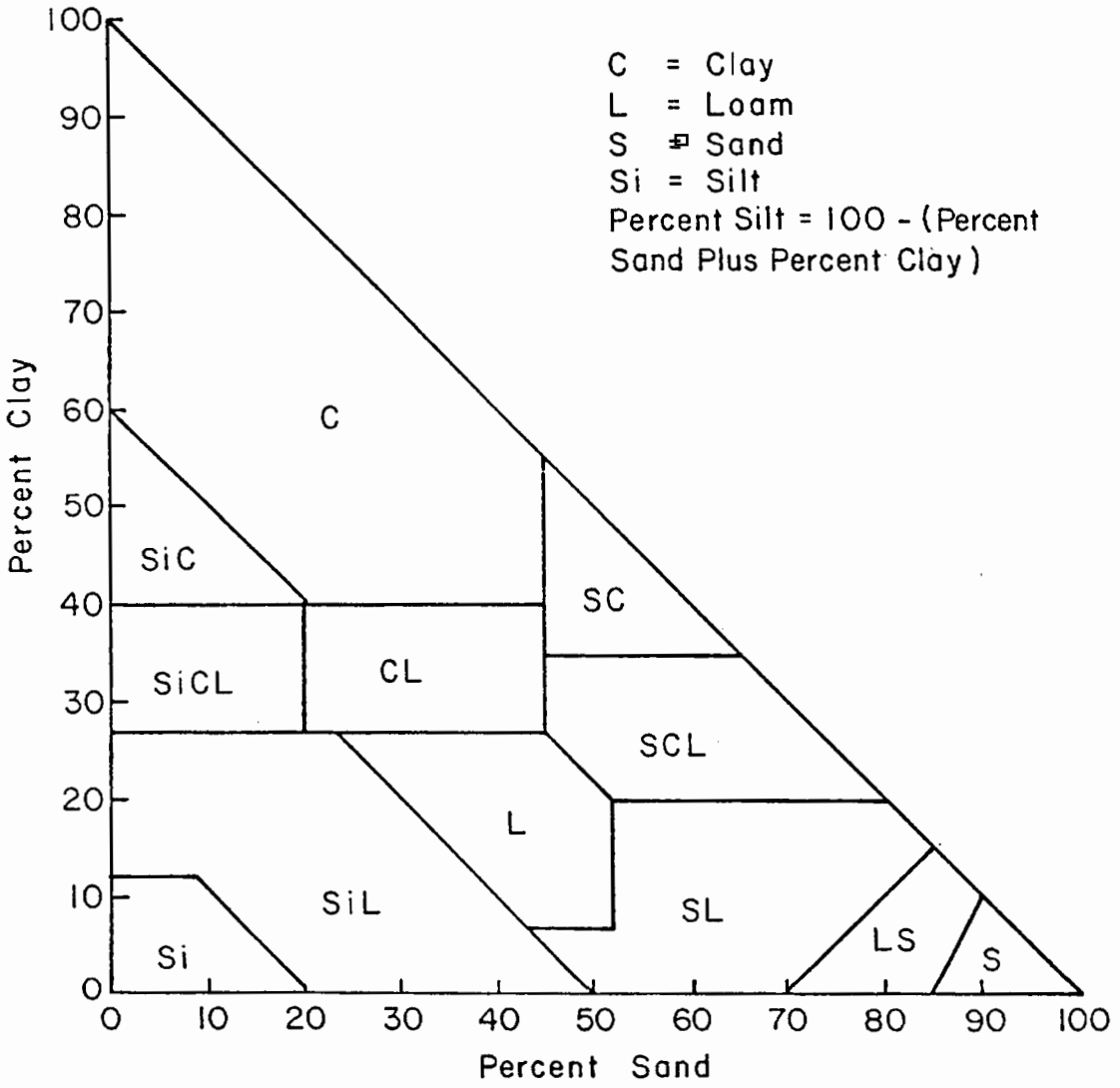


Figure 13-12. Soil textural classification graph for estimating size fractions.

Table 13-1. Common size breakdowns for sand, silt and clays.

| Class | Size in mm | |
|---|---|---|
| | Rouse, 1951 | Typical Soil Conservation Service Reporting |
| very coarse sand | 2-1 | 2-1 |
| coarse sand | 1-.5 | 1-.5 |
| medium sand | .5-.25 | .5-.25 |
| fine sand | .25-.125 | .25-.10 |
| very fine sand | .125-.062 | .10-.05 |
| coarse silt | .062-.031 | .05 |
| medium silt | .031-.016 | |
| fine silt | .016-.008 | to |
| very fine silt | .008-.004 | .002 |
| coarse clay | .004-.002 | less than |
| medium clay | .002-.001 | .002 |
| fine clay | .001-.0005 | |
| very fine clay | .0005-.0024 | |

$$G = \frac{1}{2}\left(\frac{D_{84.1}}{D_{50}} + \frac{D_{50}}{D_{15.9}}\right) \tag{13-51}$$

where $D_{84.1}$ and $D_{15.9}$ are the sizes at which 84.1 and 15.9 percent of the sample is finer (Simons and Sentürk, 1977). For example when a soil is classified as a clay loam it may be 31 percent sand and 32 percent clay which indicates 37 percent silt (Figure 13-12). The corresponding gradation curve is shown in Figure 13-13. A practical lower limit below which particles are very small is 0.00024 mm. This size is the lower limit on clay sizes (Simons and Sentürk, 1977). In this example, gradation is equal to 8.1 (reasonable for watershed) because $D_{15.9}$ equals 0.0014 mm, $D_{50}$ equals .0097 mm, and $D_{84.1}$ equals 0.09 mm. Using the $D_{50}$ and G values, a computed gradation curve can be developed as shown in Figure 13-13. The computed distribution can be found using three points, $D_{15.9}$, $D_{50}$, and $D_{84.1}$. If $D_{50}$ is known then

$$D_{84.1} \simeq D_{50} \cdot G \tag{13-52}$$

and

$$D_{15.9} \simeq \frac{D_{50}}{G} \tag{13-53}$$

Comparison of synthetic and assumed (from textural classification) distributions shows that the computed curve may be off for the smaller and larger fractions. This discrepancy is reasonable as the techniques are applicable to soil samples that have lognormal size distributions (Simons and Sentürk, 1977). If the sample does not closely follow such a distribution then deviations at the large and small size fractions may be expected. Therefore, if actual or assumed distributions are available, they should be used in preference to the computed type. If a computed type is used, possible errors must be recognized. Although a

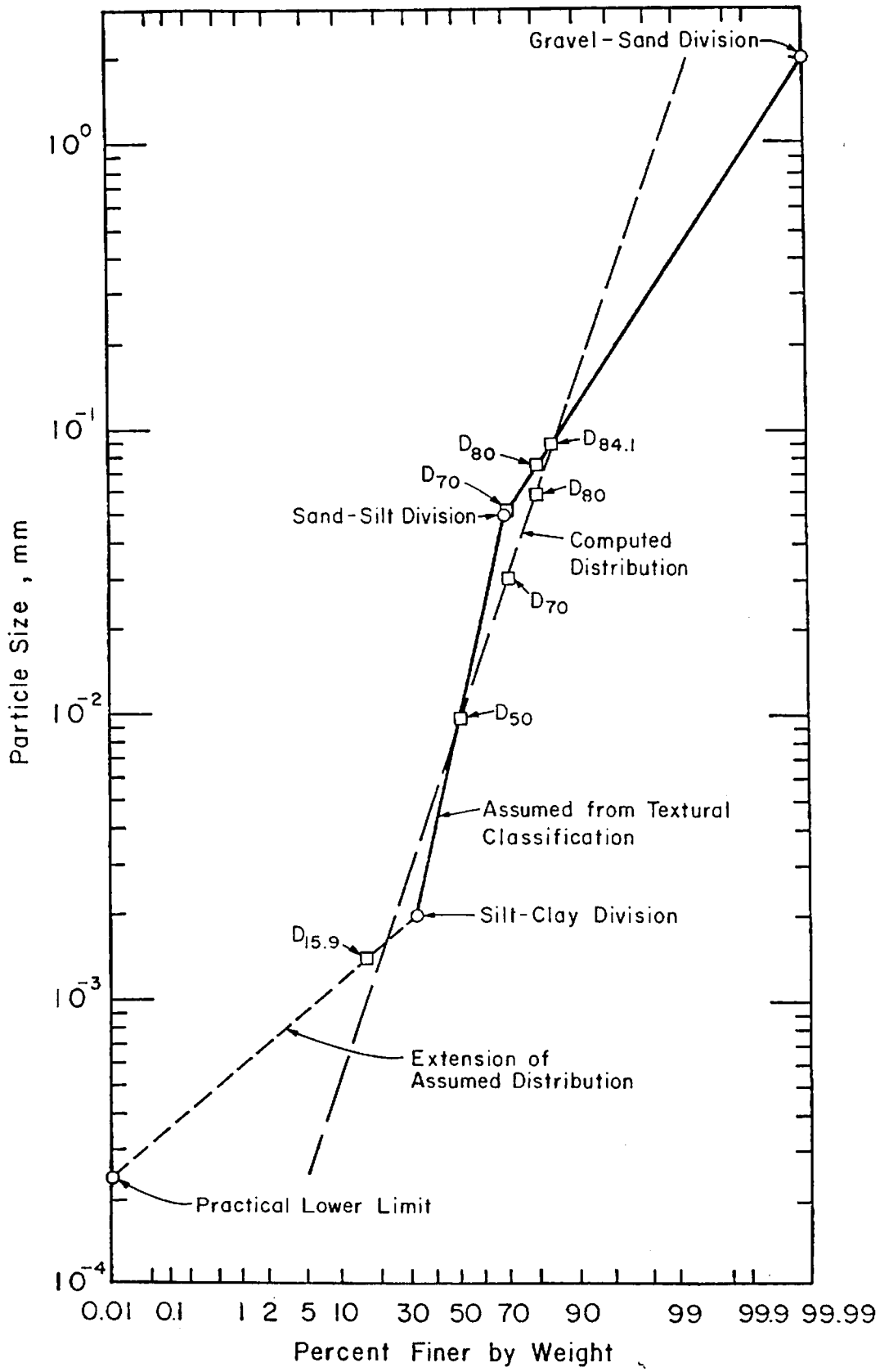


Figure 13-13. Assumed and computed size distributions derived from soil texture classification.

rough approximation, it does provide an initial estimate of size distribution. If more than one textural name is used to represent a soil type then the constructed gradation curves must be composited.

Once a size distribution has been chosen, it is necessary and desirable to subdivide distribution into representative size fractions. A rough estimate of transport using the $D_{50}$ size is possible, but because the models are formulated for different size fractions more information is gained when multiple size fractions are employed. Size distribution may be subdivided into numerous representative values (five to twenty) that are often employed. For example, if the sample in the previous discussion (Figure 13-13) is to be subdivided into ten representative fractions of 10 percent each then the following computations are required. Representative size is computed as

$$\bar{D}_i = \sqrt{D_i \times D_{i-1}} \qquad (13\text{-}54)$$

where $D_i$ is the geometric mean or representative size of the fraction, $d_i$ is the upper limit size of the fraction, and $D_{i-1}$ is the lower limit size of the fraction. From Figure 13-13 representative size for the $D_{80}$ fraction of 10 percent (i.e., $D_{70}$ to $D_{80}$) is 0.062 mm because $D_{80}$ is 0.075 mm and $D_{70}$ is 0.052 mm. As a comparison, the computed gradation curve suggests a value of 0.042 mm for this size fraction ($D_{70}$ = 0.03 mm and $D_{80}$ = 0.06 mm). Representative size of 0.062 mm is used in transport computations and the size fraction of 10 percent is used to modify the total transport rate. Although this is a rather crude approach, it does provide a method for developing useful model inputs from sparse data. Actual sieve samples of transported materials provide a check of the model and assumed input distribution by determining if the transported material is equal to or finer than the on-site material. If it is not, an explanation is necessary.

In addition to on-site soil samples and size distributions, other soil information includes soil detachment coefficients for raindrop splash and overland flow. These two coefficients are used in determining sediment supply. Raindrop splash and overland flow detachment coefficients are initially estimated but are often subsequently calibrated. Rainfall splash detachment coefficient $a_1$ is a function of soil type, soil structure, moisture conditions, and cohesion. Moldenhauer and Long (1964) have studied raindrop splash detachment resulting from simulated rainfall striking a soil target 7.6 cm in diameter. The amount of soil splash resulting from these targets has been replotted with rainfall intensity for several soil types. Figure 13-14 is a replotting of the fitted lines presented by Moldenhauer and Long (1964) as related to the square of rainfall intensity. Although approximate in nature, the corresponding $a_1$ values do allow a first estimate of the raindrop splash detachment coefficient for several soil types. Values suggested here are based on only one experiment and should be used with caution as other influences such as cohesion may decrease these values by a factor of 10 or even 100. From previous experience, a factor of at least 10 is recommended for the reduction.

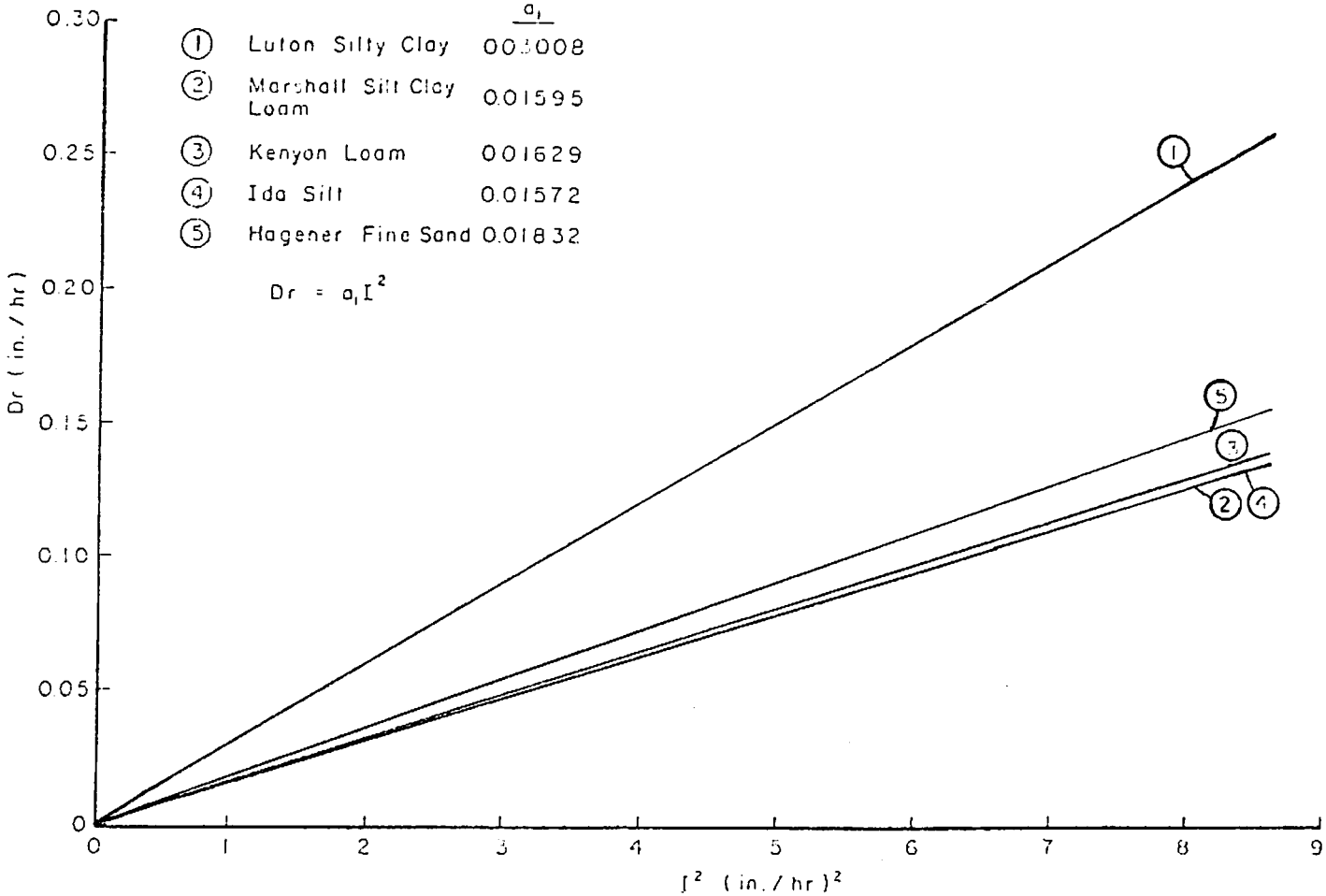


Figure 13-14. Soil detachment rate compared with rainfall intensity squared.

Because the raindrop splash detachment coefficient is usually insensitive in the models for many applications, a value of around 0.001 is often adequate for use.

The runoff detachment coefficient $D_f$ is also difficult to estimate and often needs to be calibrated. One tentative approach for estimation of the $D_f$ value uses the erosivity index K from the Universal Soil Loss Equation. Knowing soil particle size distribution, percent organic material, soil texture, and permeability rate, K can be determined from Figure 13-14. Once K is selected a value of $D_f$ can be estimated from

$$D_f \simeq \frac{K(D_s)^2}{0.63} \qquad (13\text{-}55)$$

where $D_s$ is the representative sediment size in millimeter. This technique is most applicable when several sediment sizes are being used to estimate sediment yield. If only one representative size is used, the $D_f$ value should increase on the order of 3-5 times.

An example of this approach for determining $D_f$ can be developed from Figure 13-13. If $D_{50}$ of 0.0097 mm is used as the representative size, silt plus very fine sand is about 54 percent, organic material is chosen at a realistic value of two percent, sand (.1-2 mm) is about 16 percent, soil structure is fine granular, and permeability (hydraulic conductivity) is slow to moderate, then the corresponding value of K from Figure 13-14 is about 0.28. This yields a $D_f$ of 0.00004 which may be increased or decreased but provides a realistic starting point for model adjustment. It should be noted that $D_f$ ranges from 0 to 1, and therefore if $D_f$ is computed to be greater than 1 it should be reduced to 1.0. The last coefficient needed in sediment transport is the dimensionless critical shear stress parameter $\delta$. This coefficient dictates which sediment sizes will be transported. Lower $\delta$ values increase transport of larger, previously stable, particle sizes. Values of $\delta$ range between about 0.01 and 0.06. A good first estimate is 0.047 (Gessler, 1965). If rilling develops, $\delta$ should be lower because the flow is more concentrated and more erosive. The $\delta$ value can be calibrated by comparing simulated transport material size distribution and measured distribution. The value of $\delta$ is then adjusted to match these distributions as close as possible. Sometimes it is necessary to subdivide larger and smaller fractions of the on-site distribution to provide a better fit.

In all cases where parameters are properly chosen, computer simulation results will provide realistic estimates of sediment yield. When field data is available, model parameters should be calibrated using the observed response. In this manner the system will feedback and provide the user with better future estimates of input parameters.

## 13.7 SUMMARY

This chapter has presented current techniques and selected specific models used for estimating sediment yield from watersheds, small sites, and roadways. Physical process type models are strongly advocated

because they are responsive to management activities, are transferable between areas (if the limitations on each model are respected), and can be easily updated or changed. Although other models for different levels of analysis were discussed, physical process models are more useful than regression models for several reasons. However, further research is needed in order to provide potential users with easy to understand and apply methodologies.

## REFERENCES

Carter, C. E., Greet, J. D., Braud, H. J. and Floyd, J. M., 1974, Raindrop Characterisitics in South Central United States, Trans. ASAE, pp. 1033-1037.

Einstein, A. H., 1950, The Bed Load Function for Sediment Transportation in Open Channel Flows, United States Department of Agriculture Technical Bulletin, No. 1026.

Ellison, W. D., May 1944, Studies of Raindrop Erosion, Agricultural Engineering, pp. 181-182.

Gessler, J., 1965, The Beginning of Bed-Load-Movement of Mixtures Investigated as Natural Armoring in Channels, (Translated by Prych, E. A., W. M. Keck Laboratory of Hydraulics and Water Resources, CIT).

Law, J. Q. and Parson, D. A., 1943, The Relation of Raindrop Size to Intensity, Trans. AGU, Vol. 24, pp. 452-459.

Li, R. M., 1974, Mathematical Modeling of Response from Small Watershed, Ph.D. Dissertation, Department of Civil Engineering, Colorado State University, Fort Collins, Colorado.

Meyer, L. D., 1971, Soil Erosion by Water on Upland Areas, Chapter 27, Vol. II,, River Mechanics edited by H. W. Shen, Colorado State University, Fort Collins, Colorado.

Musgrave, G. W., July 1947, The Quantitative Evaluation of Factors in Water Erosion: A First Approximation, Journal of Soil Water Conservation, Vol. 2, No. 3, pp. 133-138.

Mutchler, C. K., May-June 1967, Parameters for Describing Raindrop Splash, Journal of Soil and Water Conservation, pp. 91-94.

Mutchler, C. K. and Young, R. A., June 1975, Soil Detachment by Raindrops, Proceedings of the Sediment-Yields Workshops, Oxford, Mississippi, USDA, ARS-S-40, pp. 113-117.

Shen, H. W., 1971, Wash Load and Bed Load, Chapter 11, River Mechanics edited and published by H. W. Shen, Colorado State University, Fort Collins, Colorado.

Shen, H. W. and Li, R. M., 1976, Watershed Sediment Yield Model, Chapter 21, Stochastic Application to Water Resources, edited by H. W. Shen, Water Resources Publication Company, Fort Collins, Colorado.

Simons, D. B., Li, R. M. and Stevens, M. A., 1975, Development of Models for Predicting Water and Sediment Routing and Yield from Storms on Small Watersheds, prepared for USDA Forest Service, Rocky Mountain Forest and Range Experiment Station, Flagstaff, Arizona.

Simons, D. B. and Sentürk, F., 1977, Sediment Transport Technology, Water Resources Publication, Fort Collins, Colorado.

Smith, D. D. and Wischmeier, W. H., 1957, Factors Affecting Sheet and Rill Erosion, Trans. AGU, Vol. 38, pp. 889-896.

United States Bureau of Reclamation, June 1960, Investigation of Meyer-Peter, Müller Bed Load Formulas, Sedimentation Section, Hydrology Branch, Division of Project Investigations, U.S. Department of the Interior, Bureau of Reclamation.

Williams, J. R. and Berndt, H. D., December 1972, Sediment Yield Computed with Universal Equation, Journal of Hydraulics Division, ASCE, Vol. 98, No. HY12, pp. 2087-2097.

Wischmeier, W. H., 1972, Estimating the Cover and Management Factor for Undisturbed Areas, Paper presented at the Sediment Yield Workshop, USDA Sed. Lab., Oxford, Mississippi.

Wischmeier, W. H., 1973, Upslope Erosion Analysis, Chapter 15, Environmental Impact on Rivers, edited and published by H. W. Shen, Colorado State University, Fort Collins, Colorado.

Wischmeier, W. H., Johnson, C. B. and Cross, B. V., 1971, A Soil-Erodibility Nomograph for Farmland and Construction Sites," Journal of Soil and Water Conservation, Vol. 26, No. 5, pp. 189-193.

Wischmeier, W. H. and Smith, D. D., 1960, Predicting Rainfall-Erosion Losses from Cropland East of the Rocky Mountains, Agriculture Handbook, No. 282, ARS, USDA.

Wischmeier, W. H. and Smith, D. C., 1965, Predicting Rainfall-Erosion Losses from Cropland East of the Rocky Mountains, Agriculture Handbook, No. 282, USDA.

Woolhiser, D. A. and Blinco, P. H., June 1975, Watershed Sediment Yield--A Stochastic Approach, Present and Prospect Technology for Predicting Sediment Yields and Sources," Agriculture Research Service, U.S. Department of Agriculture, ARS-S-40, pp. 264-273.

Young, R. A. and Wiersma, J. L., 1973, The Role of Rainfall Impact on Soil Detachment and Transport, Water Resources Research, Vol. 9, pp. 1629-1636.

# CHAPTER 14

## STAGE-DISCHARGE RELATIONSHIP

The basic hydraulic engineering curriculum deals with rigid-boundary open-channel flow very well. Backwater programs are extensively used in relating hydraulic parameters such as stage, discharge, velocity, resistance to flow and slope. The backwater analysis works fairly well for a rigid boundary channel. From this type of computation a unique stage-discharge relationship can be developed for a particular location along a river. Observations of stage and discharge are often plotted and a unique relationship is often developed even when a number of these observations seem to fall some distance from the curve. Rating tables are the tabular equivalent to the single-value rating curve. A common explanation for points falling off the curve is "scatter" of data or measurement errors. Hypothetical rating curves for both rigid-boundary and alluvial channels are shown in Figure 14-1. The rigid-boundary stage-discharge relationship can be very uniform without much scatter or discontinuities. The alluvial channel rating curve can exhibit a large amount of scatter or discontinuities.

The relationship between stage and discharge is usually called a discharge rating curve. In general a discharge rating curve is developed by making several discharge measurements and then plotting the observed stage versus the measured discharge. However, experience indicates that measurements of stage and discharge do not necessarily form a one-to-one relationship. It is difficult to obtain a very meaningful discharge rating curve simply from a statistical analysis.

A number of phenomena exist that cause a stage-discharge relation to be non-unique. These phenomena have been discussed in engineering literature and are reviewed in this chapter.

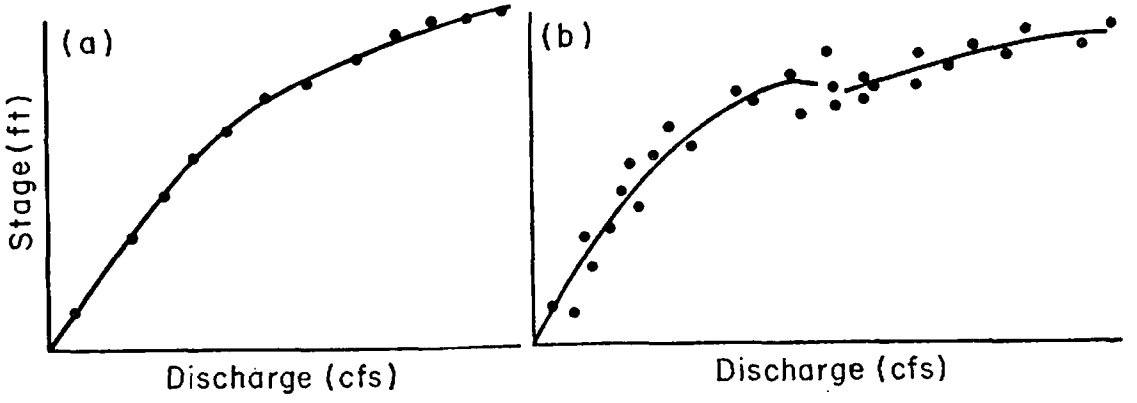


Figure 14-1. Hypothetical rating curves for rigid boundary (a) and alluvial channels (b).

The major phenomena that cause "scatter" or discontinuities in stage-discharge relations are listed below.

1. Changes in alluvial bed form (Simons and Richardson, 1962; Dawdy, 1961).

2. Scour or fill (Simons et al., 1973; Al-Shaik-Ali et al., 1978).

3. Variable energy slope due to unsteady, nonuniform flow (Henderson, 1963, 1966; Fread, 1973; Simons et al., 1977).

Other factors that can affect stage-discharge relations, such as measurement errors, vegetation, ice, backwater, overbank storage, etc., do exist, but are not discussed in this chapter. Each of the three major topics listed above is discussed with respect to stage-discharge relations. Examples and some techniques regarding the mathematical representation or interpretation of these phenomena are given.

## 14.1 THE EFFECT OF ALLUVIAL BEDFORMS ON STAGE-DISCHARGE RELATIONS

An alluvial channel differs from a rigid-boundary channel in that the stream bed is subject to movement and changes in shape whenever the shear stress exerted by flowing water is sufficient to cause sediment transport. Most natural rivers, unless carved out of solid rock, are alluvial. Even rivers with massive boulder beds can be considered alluvial streams under some flow conditions.

Two regimes of flow are defined when discussing bedforms. These two regimes are lower regime and upper regime. Lower regime generally occurs when the stream power and velocity are low, and vice-versa for upper regime. The bedforms that develop for lower and upper regime flow are listed in Table 14-1 and graphically illustrated in Figure 14-2.

Manning's $n$ is a commonly used resistance-to-flow parameter. A general relationship between Manning's $n$ and bedform illustrates the large changes in resistance to flow that can be experienced in an alluvial river (Figure 14-3). This change in resistance to flow causes respective changes in velocity and stage.

During low flow in an alluvial stream lower regime bedforms such as ripples or dunes may be present. As the flow increases, the bedforms change to upper regime, such as plane bed or antidunes. When this occurs, the discharge may increase significantly without much of an increase in stage. A comparison between a rigid boundary and an alluvial stage-discharge relation is shown in Figure 14-4.

During low flow a number of rivers in Bangladesh and Pakistan are in lower regime with ripples and dunes. When flows increase sufficiently, the bed begins to plane out and resistance to flow drops. This decrease in Manning's $n$ on the Padma River in Bangladesh is shown in Figure 14-5. A stage-discharge relation for the same river is shown in Figure 14-6. These figures demonstrate the dramatic change in Manning's

Table 14-1.

| | Lower Regime Bedforms | | Upper Regime Bedforms |
|---|---|---|---|
| 1. | Plane bed without sediment motion | 1. | Plane bed with sediment motion |
| 2. | Ripples | 2. | Standing waves |
| 3. | Dunes with ripple superposed | 3. | Antidunes |
| 4. | Dunes | 4. | Chutes and pools |
| 5. | Washed out dunes or transition | | |

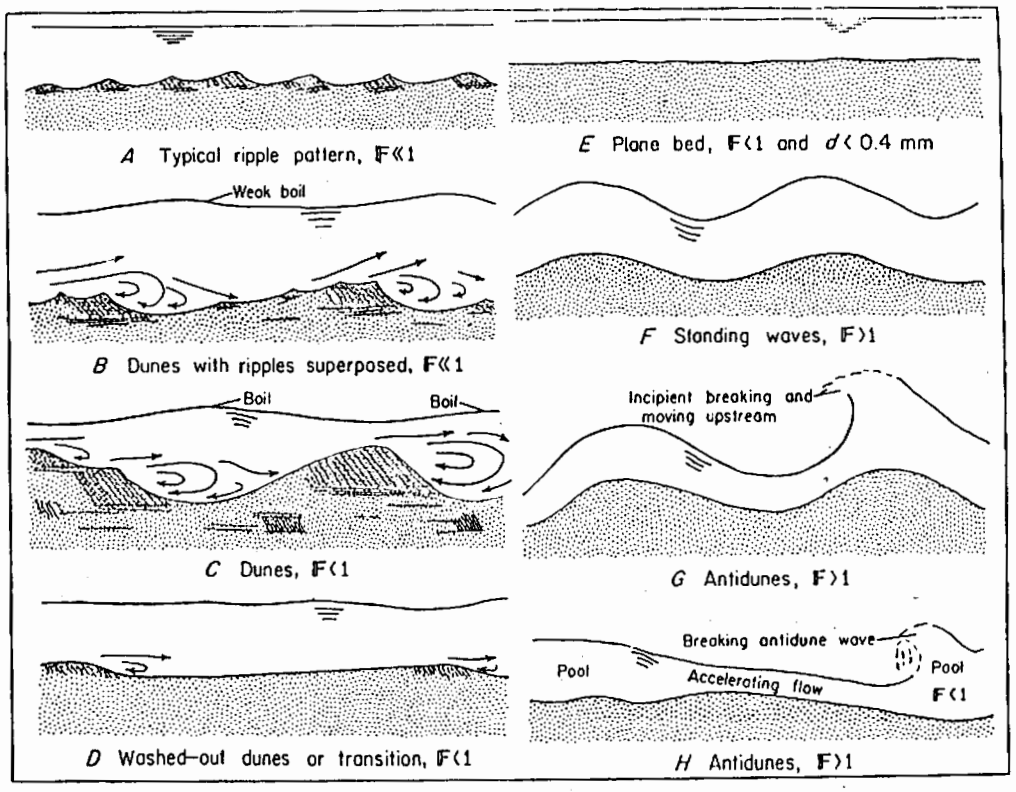


Figure 14-2. Forms of bed roughness in alluvial channels.

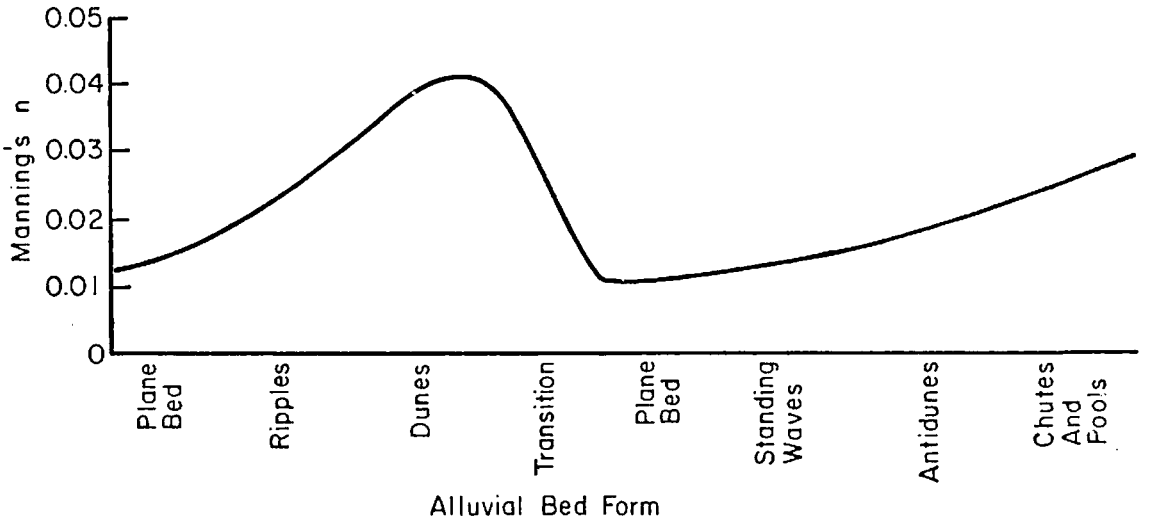


Figure 14-3. Variation of Manning's n with changing alluvial bedform.

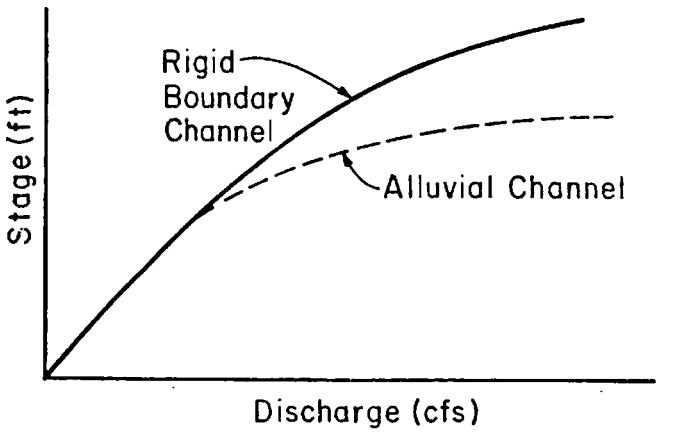


Figure 14-4. Comparison of rigid boundary and alluvial channel stage-discharge relationship.

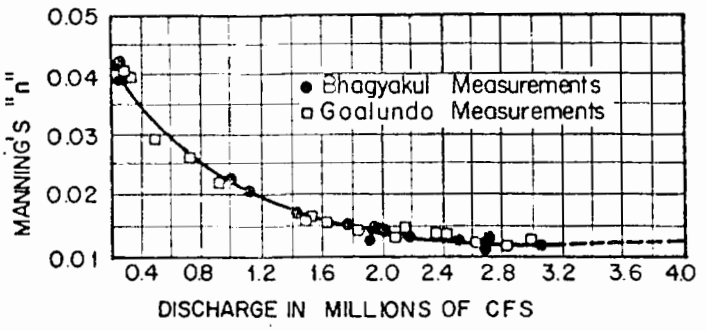


Figure 14-5. Decrease in Manning's n with discharge for the Padma River in Bangladesh (from Simons and Senturk, 1977).

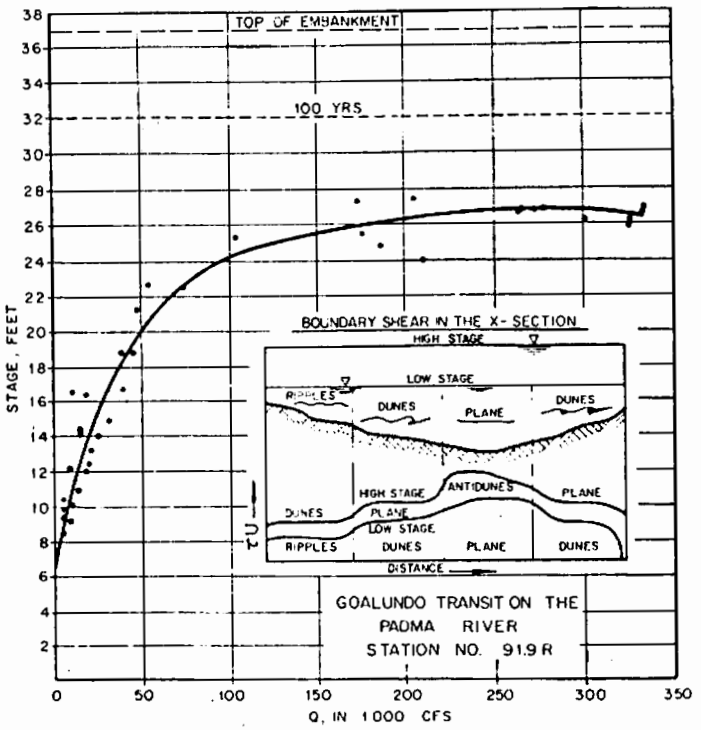


Figure 14-6. Stage-discharge relation for the Padma River, Bangladesh (from Simons and Senturk, 1977).

n of about 300%. The corresponding change in stage is very small even though discharge increased from about 150,000 cfs to over 300,000 cfs.

Examples of changing alluvial bedform and its effect on stage-discharge relations are also common in the United States. Dawdy (1961) observed that the bedform changed from dunes to plane bed in many streams in the southwestern portion of the country. Colby (1960) recognized a similar situation in Mississippi. The Omaha District of the Corps of Engineers (1968) reported that the Mississippi River has changed from dunes to plane bed with a corresponding drop in resistance to flow and stage at a constant discharge of 33,000 cfs because of a 20° F to 30° F decrease in water temperature. This decrease in water temperature increased water viscosity, changing sediment transport characteristics as well as regime of flow. Beckman and Furness (1962) observed a Manning's n of 0.31 for low flow and 0.16 for high flow on the Elkhorn River in Nebraska.

## 14.2 DISCONTINUITIES IN STAGE-DISCHARGE RELATIONS DUE TO BEDFORM CHANGES

The stage-discharge relation given for the Padma River (see Figure 14-6) is a fairly smooth curve with some "scatter." In many streams a discontinuity in the rating curve can be detected, especially when observations of bedform are made at the time of a discharge measurement. Dawdy (1961) concentrated on these discontinuities. Beckman and Furness (1962) and Colby (1960) also contributed to the understanding of discontinuous rating curves. Dawdy (1961) chose to show the discontinuity by relating hydraulic radius and velocity in the form of a graph. Figure 14-7 reproduces his graph, showing a distinct discontinuity on the Republican River at Stratton, Nebraska.

It is readily seen that a distinct increase in velocity occurs at a hydraulic radius of about 1 foot. He concludes that this and many other locations that exhibited discontinuities were the result of changing from lower to upper regime.

Beckman and Furness (1962) show the actual discontinuous rating curve for the Elkhorn River near Waterloo, Nebraska (see Figure 14-8). Their observations include the bedform at the time of the discharge measurement. This type of information is extremely helpful when developing a rating curve. The figure shows that two curves should be drawn, one for lower regime flow and one for upper regime flow. The observations when the bed was in a state of transition lie between the upper and lower regime clusters. The fact that both upper and lower regimes, as well as transition bed forms, can exist at the same discharge may be due to water temperature changes as noted on the Missouri River, or other factors such as suspended load concentrations.

## 14.3 HYSTERESIS PHENOMENON IN STAGE-DISCHARGE RELATIONS DUE TO CHANGING BED FORMS

Bedform changes are the result of changing stresses on the bed due to some unsteady nature of the flow or temperature, etc. The bed is continually trying to reach some equilibrium state. When the hydraulic conditions are in a state of change, the corresponding change in

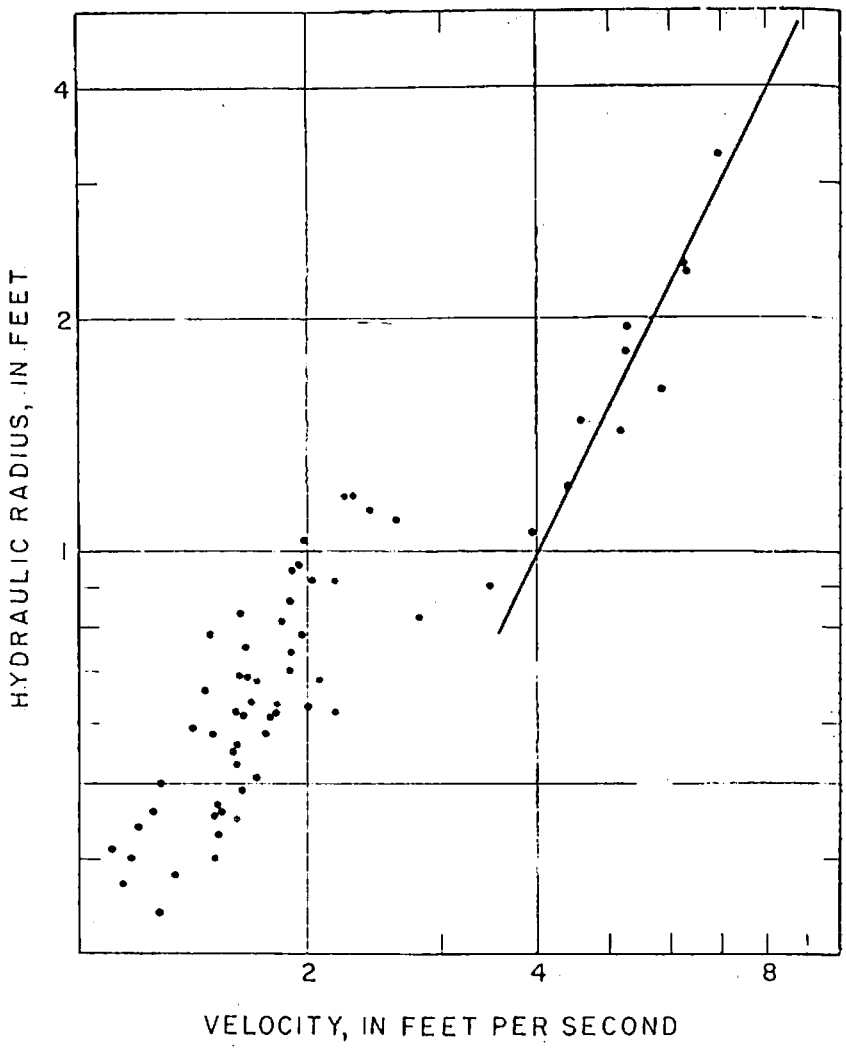


Figure 14-7. Relation of velocity to hydraulic radius for Republican River at Stratton, Nebraska (after Dawdy, 1961).

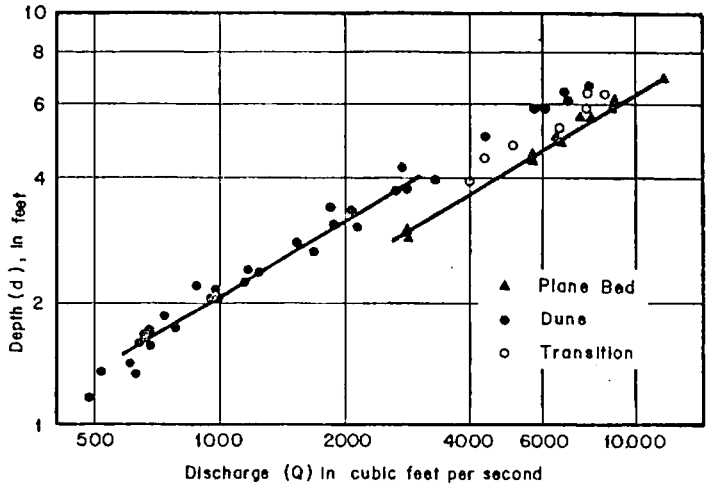


Figure 14-8. Relation of depth to discharge for Elkhorn River near Waterloo, Nebraska (after Beckman and Furness, 1962).

bedforms tends to lag behind. This time lag causes a hysteresis effect in a stage-discharge relation on a flow event by event basis. Senturk (1969) tried to mathematically explain the process of hysteresis effects in bedform changes. Simons and Richardson (1962) show the hysteresis effect using laboratory data. This looping effect can be quite complex depending on a number of criteria. A number of experiments were performed covering a range of flow conditions. The results of six of the data sets are now briefly discussed.

The first experiment was in lower regime flow with a median fall diameter of the bed material at 0.45 mm. The initial discharge was low and was increased and decreased in a stepwise manner, allowing about 45 minutes of constant discharge between each step. The initial bedforms were small dunes with ripples superposed. As the discharge was increased, the ripples were washed out and larger dunes formed. As the discharge was decreased the bedforms gradually returned to the original configuration. The depth discharge relation shows a smaller depth on the rising limb and a large depth on the falling limb for the same discharge (see Figure 14-9). This can be explained by bedform changes as caused by changes in discharge with time. As the flow increased, the roughness increased as dunes formed. This increase in roughness, however, did not have time to fully develop before discharge was increased again. In other words, on the rising limb the resistance was smaller than the depth, velocity, etc. would be under equilibrium conditions because the bed did not have time to fully reach a new equilibrium.

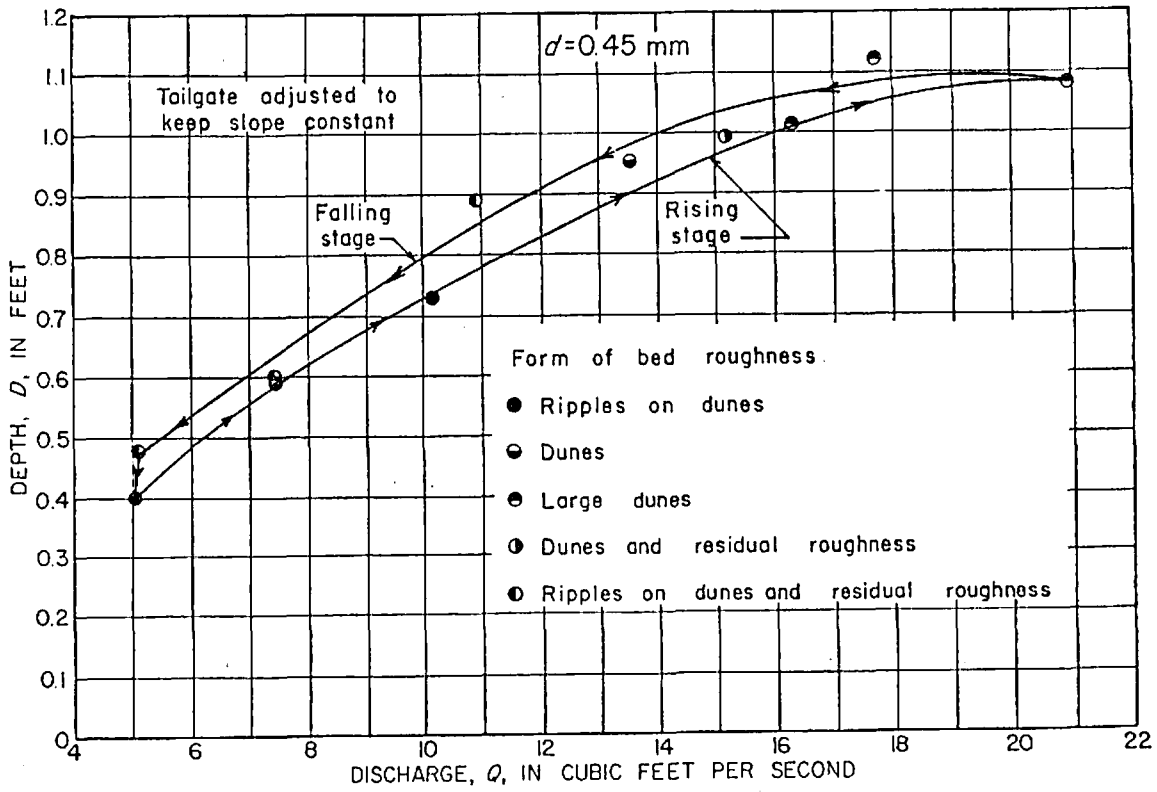


Figure 14-9. Relation of depth to discharge for lower flow regime when channel slope is constant (after Simons and Richardson, (1962).

The opposite is true on the recession limb in that the resistance was larger than the hydraulic conditions would dictate, causing depths to be deeper than for equilibrium conditions. The depth at the end of the run was larger than at the beginning for the same discharge. After a few hours of constant discharge, the depth decreased to the original value.

The next run did not utilize tailgate control at the downstream end of the flume so the slope of the energy gradient varied with discharge. The median bed material diameter was 0.28 mm. The initial bed roughness consisted of ripples. With increasing discharge the bed changed to dunes and then to a transition state. As the discharge decreased, the bed reverted to dunes, ripples on dunes, and finally ripples (see Figure 14-10). Again, the depth on the rising limb was less than the depth on the recession limb. Near the high end of the depth-discharge relation both the rising limb and recession limb are nearly the same.

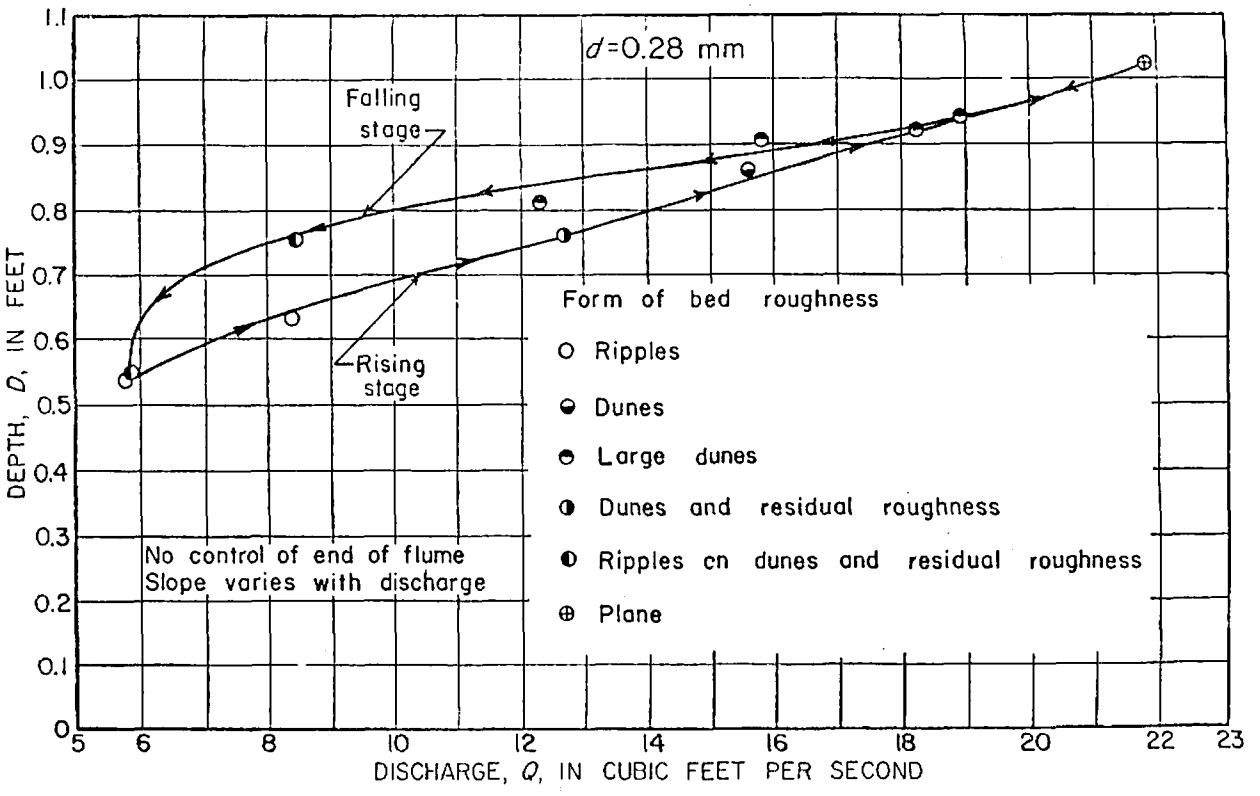


Figure 14-10. Relations of depth to discharge for lower- and upper-regime flow when the variation of slope with discharge is small (after Simons and Richardson, 1962).

The run shown in Figure 14-11 started with similar initial conditions, but the channel slope was steep, so more upper regime conditions were experienced. As the discharge increased the resistance to flow also increased as the bed changed to large dunes. While still on the rising limb, the bed went through transition and on to plane bed

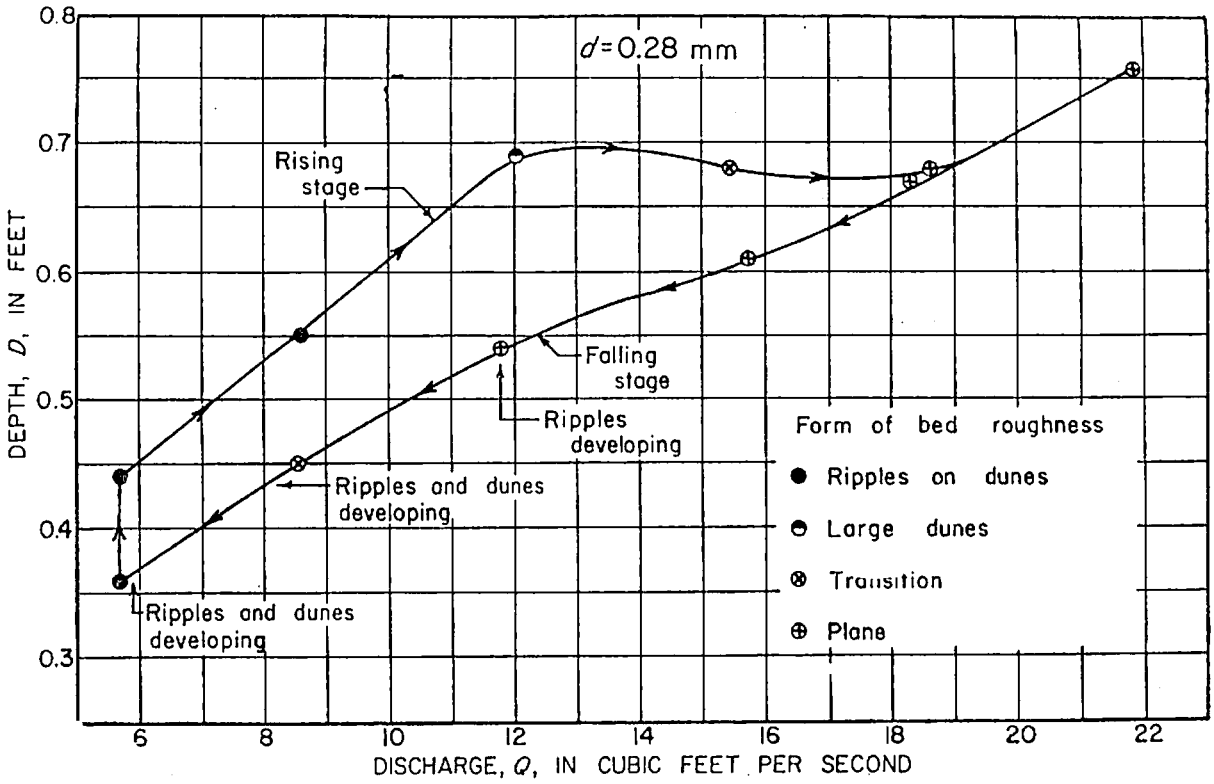


Figure 14-11. Relation of depth to discharge for lower- and upper-regime flow when the variation of slope with discharge is moderate (after Simons and Richardson, 1962).

with a corresponding decrease in depth. On the recession limb the bed went back through transition to dunes and ripples. The hysteresis loop in this case is opposite of the others since the depth on the rising limb was greater than on the recession limb. This difference is due to the fact that resistance to flow was increasing on the rising limb as ripples with dunes developing changed to large dunes. Before the rising limb was over and the bed went plane, the resistance to flow decreased, as did the depth. The resistance to flow and the depth remained lower for the rest of the recession limb.

The experiment shown in Figure 14-12 was similar to the previous one, except the median bed material size was 0.45 mm instead of 0.28 mm. No tailgate control was used. Dunes were initially present on the bed. As the discharge increased the bed changed from dunes to standing waves and the resistance to flow and depth decreased substantially. Through the remainder of the rising limb no major resistance to flow changes occurred as the bed remained in upper regime going from standing waves to plane bed. The bed remained in upper regime about halfway down the recession limb. Both the rising limb and recession limb were nearly the same since no major changes in resistance were encountered. Further down the recession limb dunes began to form and the resistance began to increase. The dunes were larger on the recession limb at low flow than on the rising limb, causing the depth-discharge relation to cross over itself. As the discharge decreased to the minimum, the depth returned

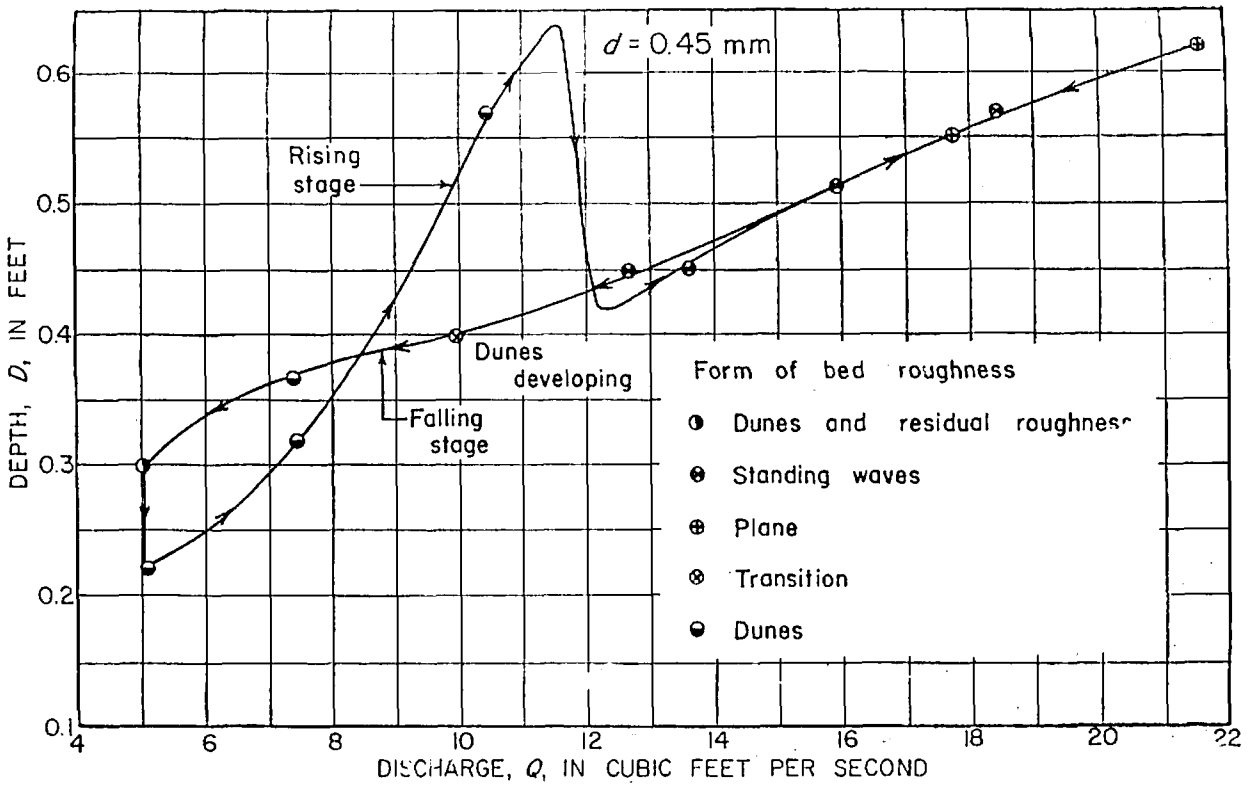


Figure 14-12. Relation of depth to discharge for lower- and upper-regime flow when the variation of slope with discharge is large (after Simons and Richardson, 1962).

to the initial depth after the bedforms changed to the initial configuration and level of resistance to flow.

Another experiment was performed to show the effect of a downstream channel constriction at high flows similar to the situation that might exist in a channel upstream of a bridge, culvert or natural constriction (see Figure 14-13). The initial flow is rapid with standing waves and antidunes and low resistance to flow. As the discharge increased, the flow became more tranquil due to the increasing influence of the constriction downstream. The bed changed from upper regime to ripples on dunes and then to large dunes. As the discharge decreased, large residual dunes continued for a time, causing the depth on the recession limb to be greater than on the rising limb for the lower regime bedforms. As the discharges decreased towards initial conditions, the effect of the constriction reduced, allowing the velocity of flow to increase. The bed changed back to upper regime conditions with the remainder of the recession limb being the same as the rising limbs, since resistance to flow was essentially the same. The depth-discharge relation in this case is practically the opposite of those developed and shown in Figures 14-10 and 14-11.

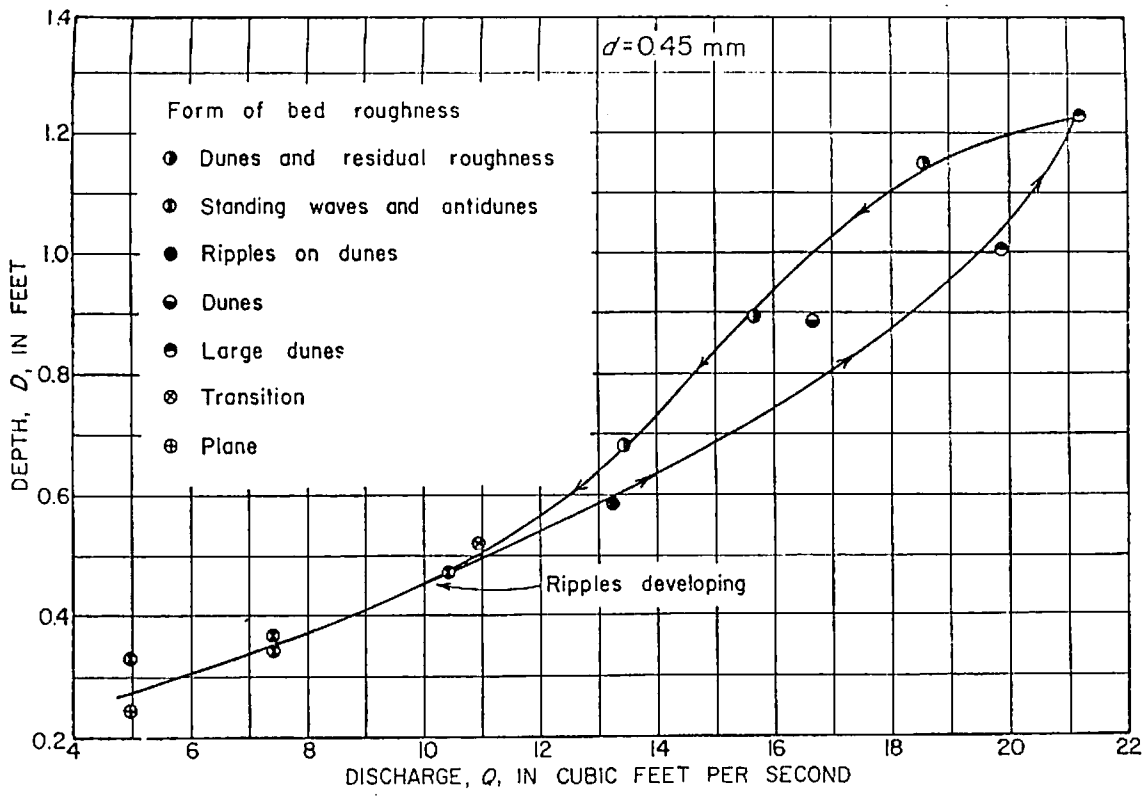


Figure 14-13. Relation of depth to discharge for upper- and lower-regime flow when slope varies inversely with discharge (after Simons and Reichardson, 1962).

The final experiment showed the depth-discharge relation when only upper regime flow occurs. This is shown in Figure 14-14. The initial bedforms were standing waves and antidunes. As the discharge increased, antidunes became stronger. The depth discharge relation followed an almost straight line without major changes in bedform or resistance to flow for both the rising and recession limbs.

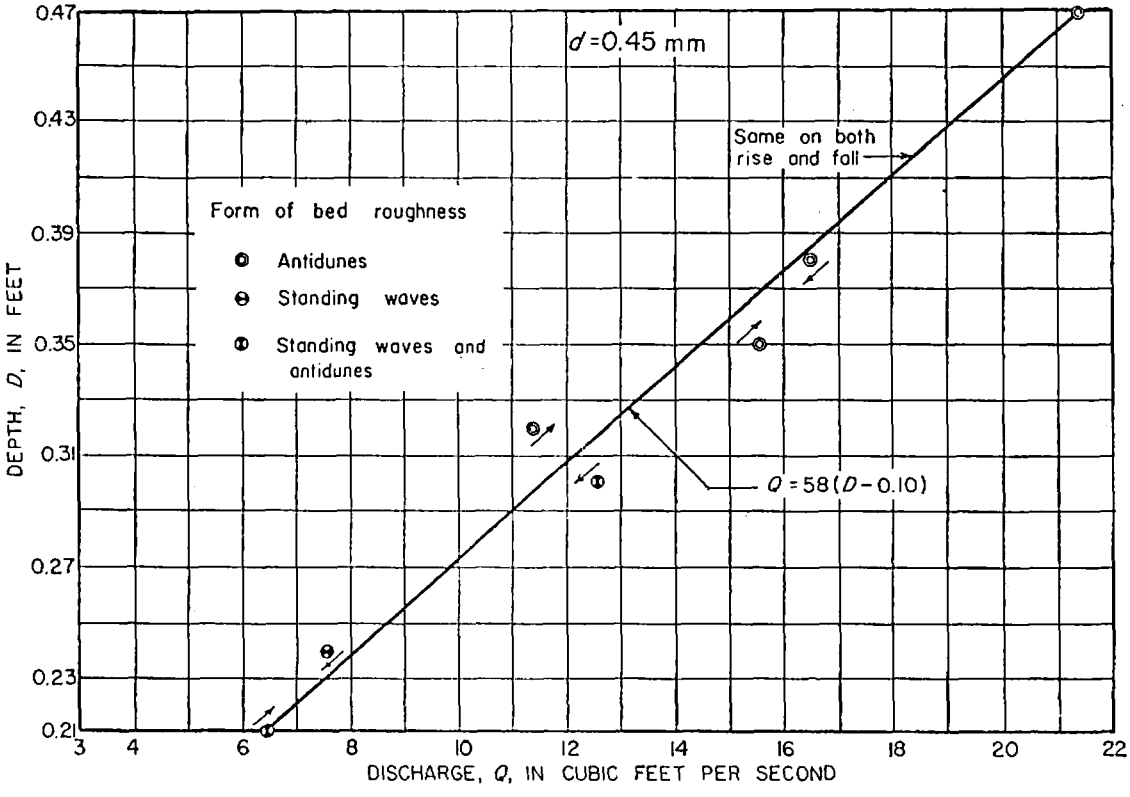


Figure 14-14. Relation of depth to discharge for upper-regime flow (after Simons and Richardson, 1962).

These experiments demonstrate that the depth-discharge relationship depends on the occurrence of changes in bedform which can drastically change resistance to flow and depth for a given discharge. The depth-discharge relation also depends on bed-material size and on the rate of change of discharge with time. When the discharge and hydraulic conditions are changing faster than corresponding bedforms seeking equilibrium, residual resistance effects cause different depths for the same discharge. Large changes in resistance to flow and depth occur when the bed changes from lower to upper regime or vice-versa. When the entire flow occurs on upper regime bedforms, the depth discharge is almost a straight line without much difference on the rising and recession limbs. Because of the unlimited possibilities, an infinite number of depth-discharge relationships is possible.

Theoretical explanations of why bedforms exist or follow the form and changes they do have been made, but due to the complexity of the

phenomena, results are not always as good as one might hope. Several attempts have been made to predict bedform and potential changes. Such work is helpful in explaining and predicting changes in resistance to flow due to changes in alluvial bedform. A summary of several methods used in predicting bedforms, as well as methods for predicting resistance to flow for alluvial streams where bedform changes are likely, is presented in Simons and Senturk (1977). A treatment of this important subject is left to the reader due to time and space limitations. Application of these principles is helpful in the understanding and application of stage-discharge relations.

## 14.4 EFFECT OF GRAVEL, SAND OR SILT TRANSPORT IN DEPTH-DISCHARGE RELATIONS OF COBBLE AND BOULDER BED RIVERS

A paper by Al-Shaik-Ali et al. (1978) discusses the effect of gravel, sand or silt transport in cobble and boulder bed streams on resistance to flow. An example given is of the 1976 Big Thompson Flood in Colorado. A high-intensity thunderstorm caused a flood of record on the Big Thompson River. The estimated discharge was more than three times higher than the previous record flood. The bed material of the river is small to large boulders. During the flood flow conditions verified the existence of antidunes leading to the fact that the bed was behaving as a sand bed stream with large quantities of smaller-sized sediment flowing over and through the boulders.

Laboratory experiments were conducted in a small flume to demonstrate the effect of sand in a gravel bed. A constant discharge was released over a bed of gravel in a small flume with the depth being monitored. For the same discharge finer sediment particles were fed into the flume so that the gravel bed was impregnated with sand. The depth dropped by a factor of about 1/2 while velocity doubled. The results are shown schematically in Figure 14-15. The experiments and observations indicate that even a boulder bed stream can behave as a sand bed stream in flood events when finer sediment is being transported in large quantities. This phenomenon has a profound effect on the stage-discharge relation that may have been assumed to be an almost rigid boundary channel.

## 14.5 EFFECT OF SCOUR AND FILL ON STAGE-DISCHARGE RELATIONS

Scour and fill have an obvious effect on stage-discharge relations. When a river is degrading or scouring the stage must decrease for a given discharge and when aggradation occurs the stage increases for a given discharge. An alluvial channel may be in a state of apparent continual aggradation or degradation, but often during a flood event both aggradation and degradataion are taking place. As the discharge, velocity and sediment transport capacity increase on the rising limb of a hydrograph, the bed may begin to scour. By using a fixed stage-discharge relation, one would underestimate the amount of discharge due to the decrease in bed elevation. As the discharge passes the peak and declines, sediment may begin to deposit on the bed so that the discharge could be overestimated by the same stage-discharge relation. A study by

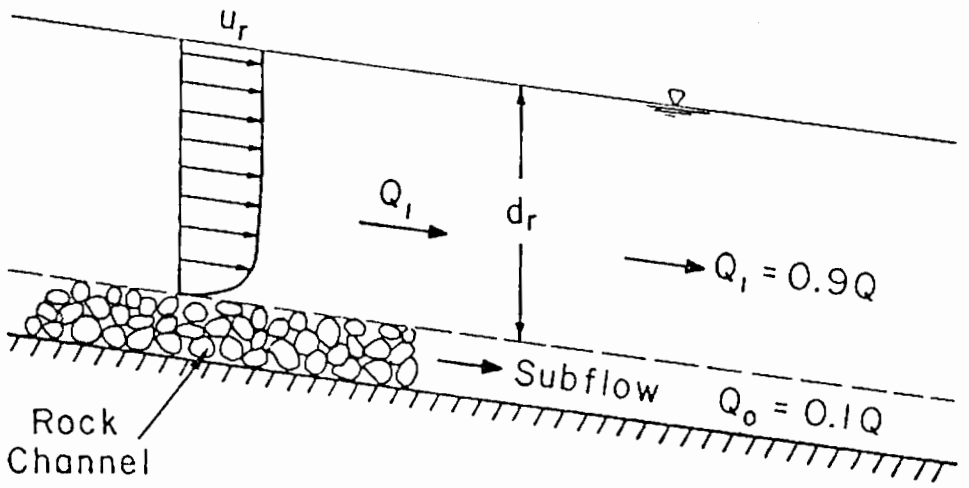


(a) Before Sediment Feeding

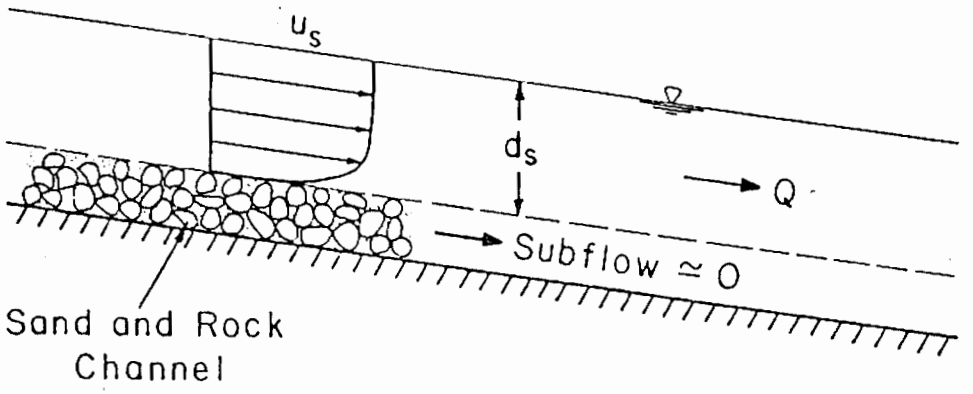


$d_s \approx 0.5\, d_r$

$u_s \approx 2u_r$

(b) After Sediment Feeding

Figure 14-15. Schematic illustration of a rock channel before and after sediment feeding (after Al-Shaik-Ali et al., 1978).

Li et al. (1979) demonstrated the problem that is encountered by ignoring scour or fill in stage-discharge relations. Various techniques, including a statistical approach, rigid boundary backwater and a sediment routing technique, were applied to two reaches of the Yazoo River in Mississippi. One case involved a relatively stable reach of river, while the other was unstable. All three models are relatively accurate for the stable reach. However, the sediment routing model that considers the physical processes of open channel flow and fluvial geomorphology is the only feasible approach to predict the response of an active river.

## Case Studies

The Yazoo River in Mississippi was selected for study due to the availability of data for that area. Two reaches of the river were carefully analyzed: a stable reach near Locopolis and an unstable reach at the Fort Pemberton cutoff near Greenwood. Historically, the bed elevation in the stable reach has not changed substantially. However, the bed of the unstable reach degraded up to 20 feet during 1973 and 1974. This degradation was caused by the removal of a dam in the cutoff that allowed a large portion of the Yazoo River flow to bypass the Greenwood Bendway. The changing behavior of the river discharge and sediment transport at this unstable reach makes prediction of flood stage from discharge data difficult. This is especially true for models that are based entirely on historical data since they cannot adjust to the new flow conditions. Selection of these two reaches allows evaluation of the reliability of the three models.

## Description of Models

### Stage-Discharge Relationship Model

The relationship between stage and discharge is called a discharge rating curve. Generally, a discharge rating curve is obtained by making several discharge measurements and then plotting the observed stage compared with the measured discharge. In reality, experience indicates that measurements of stage and discharge do not form a one-to-one relationship. Many rivers, especially those with a flatter gradient, display by hysteresis loop in the stage-discharge relationship due in part to dynamic effects and changing bed forms, Equation (14-1). Since these relationships can normally only be determined using water and sediment routing models, the following relation is commonly used to determine the stage at a given location along the river from the corresponding discharges

$$q = \alpha' (y - y_o)^{\beta'} \tag{14-1}$$

where $q$ = discharge, $y$ = stage, and $\alpha'$ and $\beta'$ are time-invariant coefficients. The unknown coefficients $\alpha'$ and $\beta'$ were estimated by least-squares regression techniques based on historical records.

### Rigid Boundary Backwater Model

A known-discharge model developed by the authors was used in this study. Characteristic features of this model follow.

Known Discharge. This model assumes that during any one time period, water discharge is constant along a reach of river, except where lateral inflows occur, i.e., a steady flow is assumed. Although a model of this type cannot predict the dynamic effects that an unsteady flow model can, it requires considerably less computer time. Also, the model is able to calculate flood stages, and provide a practical method to evaluate water surface profiles over long time periods. The time increments on the input hydrographs vary from a few hours to a month or longer, depending on the flow conditions and the desired accuracy of the results. In this study, a time increment of one day was used.

River Geometry. The only river geometry data required by the model are digitized channel cross sections and the river distance between cross sections. The model uses the digitized channel cross sections to determine geometric equations that define conveyance, width, and area of channel as a function of water depth.

Backwater Calculations. The backwater curve is determined by starting at a known downstream water surface elevation and calculating the upstream water surface elevation using a first-order Newton-Raphson approximation to solve the total head equation at each successive cross section. For a rigid boundary model the cross-sectional shape is assumed to be unaltered during the simulation.

### Sediment Routing Model

In addition, a sediment routing capability is added to the backwater model described above; additional features of this model follow.

Uncoupled Routing. Water and sediment routing are uncoupled, making the bed profile constant during one time increment. Changes in the bed profile due to sediment movement are made at the end of the time increment.

Sediment Transport. The bed material sediment transport at each cross section was calculated using a transport equation derived from river sediment discharge measurements.

Since both process models are using the same backwater calculations, any difference in results is due solely to the higher level of physical processes modeled considering sediment movement.

## Calibration of Models

### Calibration Data

All three models were calibrated using the same data. In the unstable Fort Pemberton reach, the calibration period was from April 12, 1973, to February 23, 1974 (318 days). In the stable Locopolis reach,

the calibration period was from January 1, 1971, to December 31, 1972 (731 days). The calibration data included observed discharges and stages at Fort Pemberton and Locopolis. The sediment routing model also utilized the observed bed elevations at Fort Pemberton.

Stage-Discharge Relationship

Measured discharge and observed stage data from the two test reaches for the specified times were used to estimate the unknown parameters, $\alpha'$ and $\beta'$, that minimized the mean-square-error of the estimates. Regression constants and the coefficient correlation R are as follows:

Unstable reach: $\alpha' = 1783.7782$, $\beta' = 0.75383$, $R = 0.901$

Stable reach: $\alpha' = 0.28715$, $\beta' = 3.14017$, $R = 0.991$

It is clear that the stage-discharge relationship is very easy to calibrate and use.

Rigid Boundary Backwater Model

The river stage computed by this rigid boundary model was calibrated by adjusting the estimated channel roughness coefficient, Manning's n. Manning's n was calibrated by multiplying a constant with the estimated n value for the main channel and overbanks. The model was then run with flow data from the calibration periods and error between the observed and computed water surface was determined. The process was repeated with different values of the constant until no reduction in error resulted.

Manning's n for the Fort Pemberton reach was determined to be 0.031. At the Locopolis reach it was necessary to allow Manning's n to vary with discharge, since there appeared to be large differences in head loss in the reach at different flow levels. The calibrated Manning's n varies as a power function of discharge, and is about 0.018 for the extreme high flow and approximately 0.040 for the low flow. These values are reasonable considering the hydraulics of the fluvial system.

Sediment Routing Model

The sediment routing model was calibrated at Fort Pemberton by adjusting both Manning's n and sediment input into the cutoff. Sediment input had to be calculated because a weir, a low submerged dam, is located at the upstream end of the cutoff. This weir traps sediment upstream. Sediment input was adjusted until the computed bed elevation at four sections directly downstream of the weir matched as closely as possible the observed bed changes. Figure 14-16 shows a plot of observed and computed bed elevations at the four locations. As indicated, the computed bed profile for February 23, 1974, closely matches the observed bed profile. The calibrated Manning's n had a value of 0.030, which is only 3-1/3 percent lower than the value obtained from the backwater curve model.

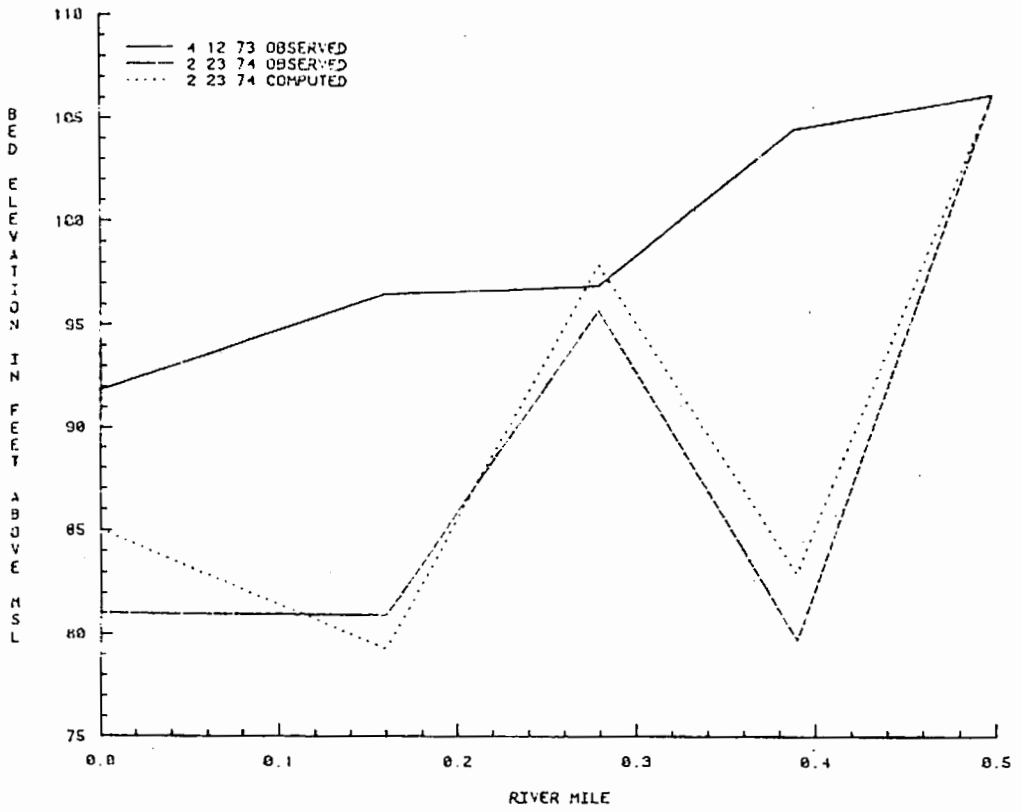


Figure 14-16. Observed and computed bed elevation at Fort Pemberton (1 foot = 0.305 m).

In the Swan Lake-Locopolis reach, there was not enough cross-sectional data to calibrate the sediment transport; therefore, only Manning's n was calibrated with the sediment trasport at its normal value. Again, in this reach the n value changed only slightly from the backwater model, varying from 0.042 at low flows to 0.02 at extreme high flows.

Inference can be made from the above description that calibration of the physical process models requires significantly more data and effort to develop and calibrate than the statistical stage-discharge model. However, once the physical process model is developed and calibrated, less data are required for the application.

## Verification of Models

To verify the results of the calibration, an additional run utilizing each model was made for each reach using the calibration results. These runs were made for the periods immediately following the calibration period. At Fort Pemberton, the verification time period was from February 24, 1974, to December 31, 1974 (311 days). At Locopolis, the time period was from January 1, 1973, to December 31, 1974 (730 days). Figures 14-17 through 14-22 show plots of the measured and computed stage at Fort Pemberton and Locopolis for the verification period.

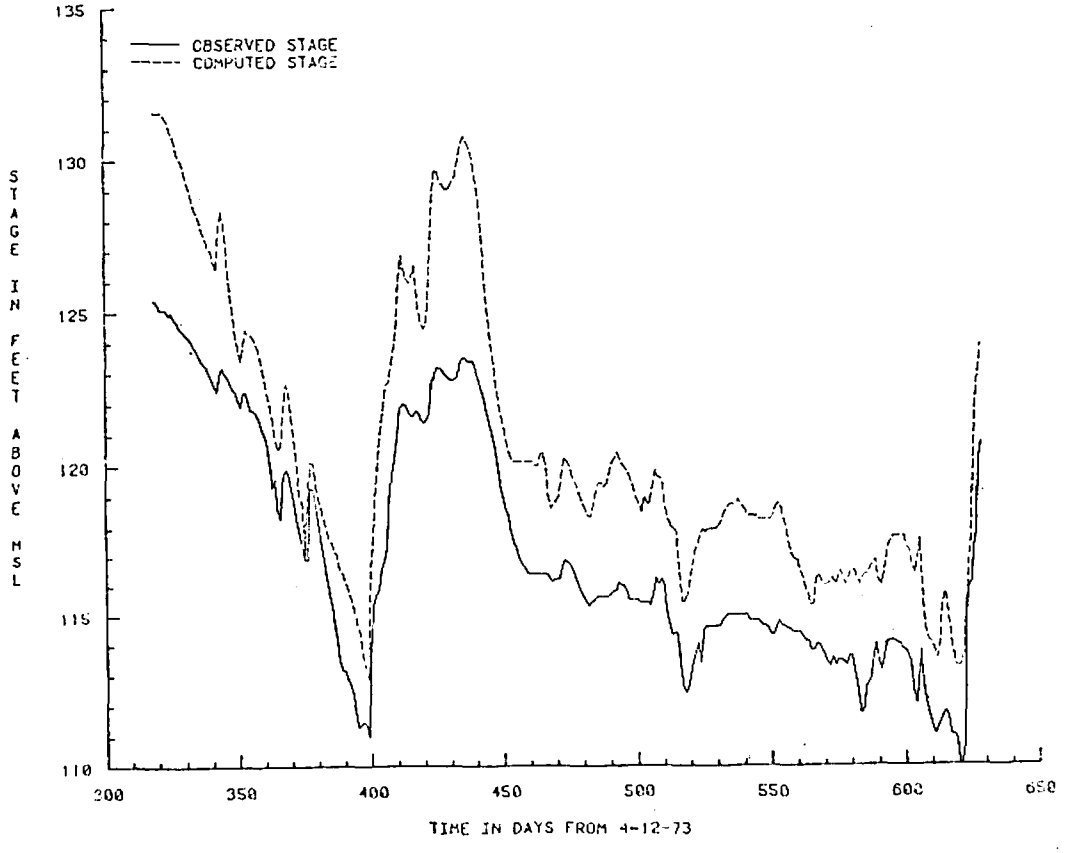


Figure 14-17. Statistical model verification at Fort Pemberton.

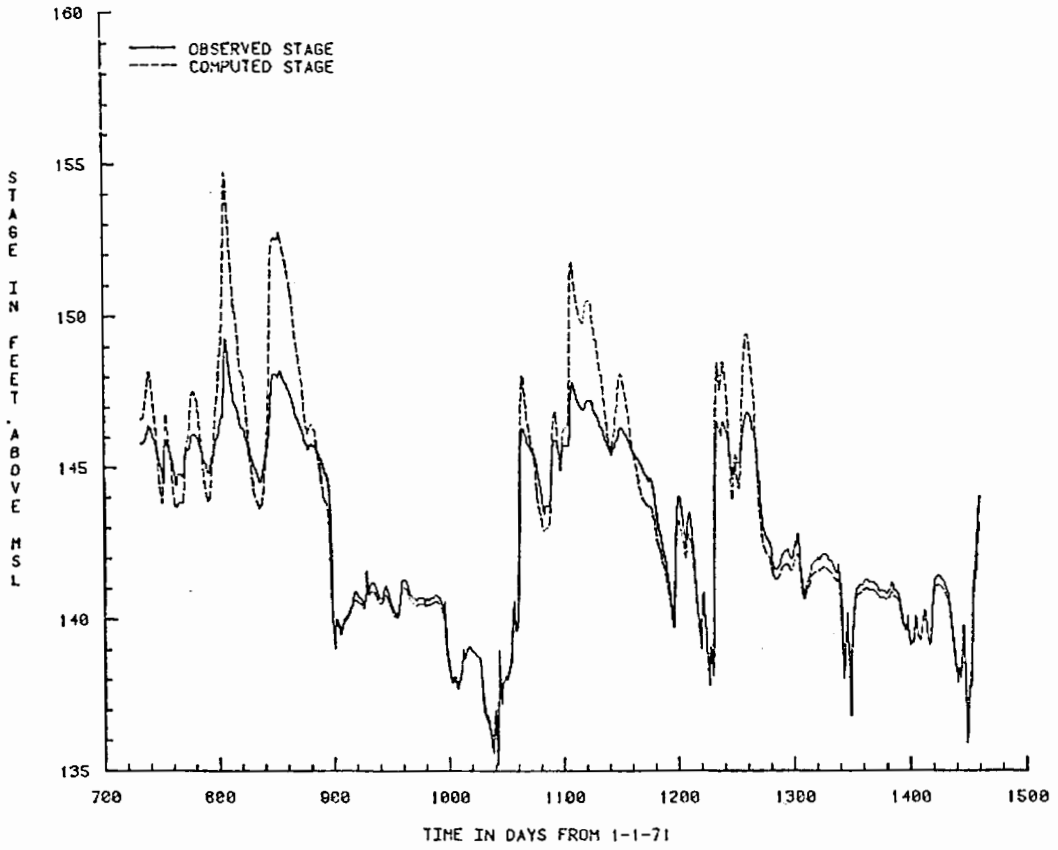


Figure 14-18. Statistical model verification at Locopolis (1 foot = 0.305 m).

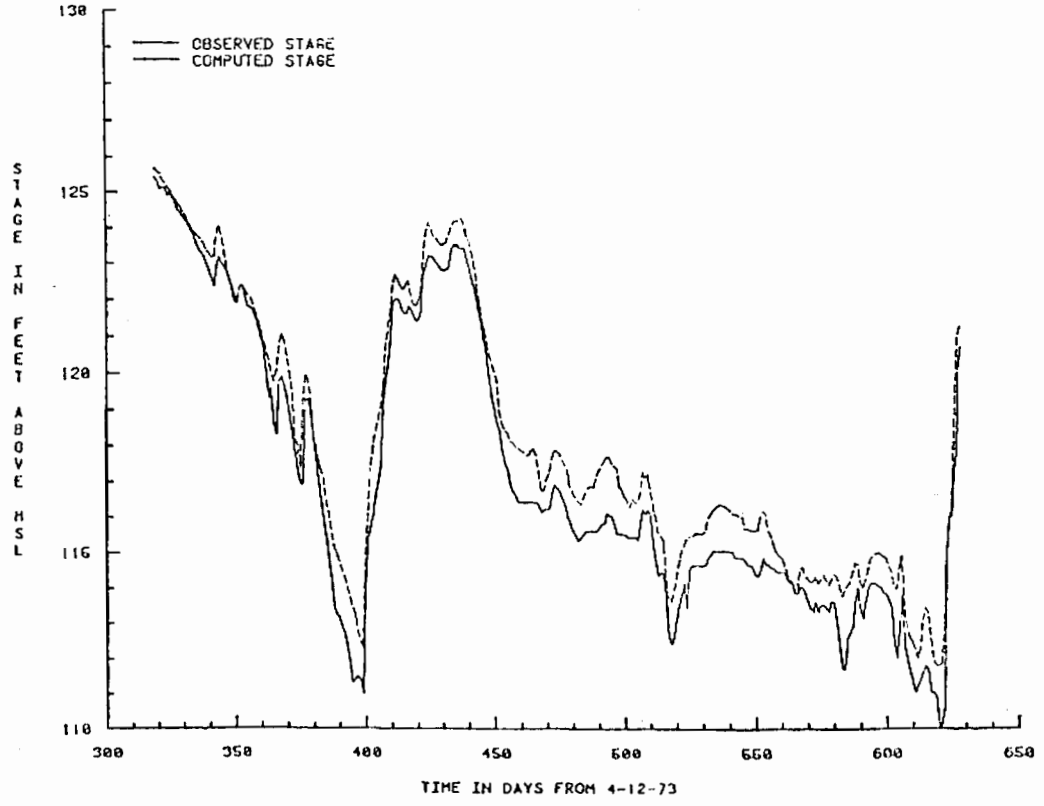


Figure 14-19. Rigid boundary model verification at Fort Pemberton (1 foot = 305 m).

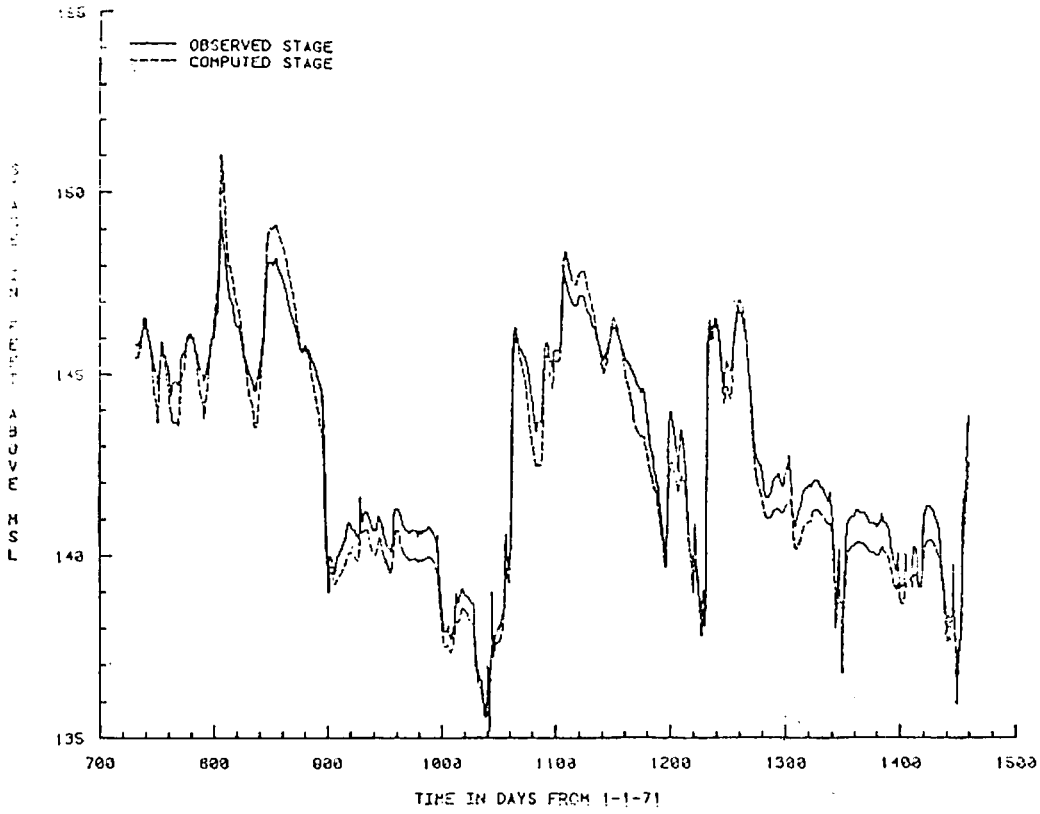


Figure 14-20. Rigid boundary model verification at Locopolis (1 foot = 305 m).

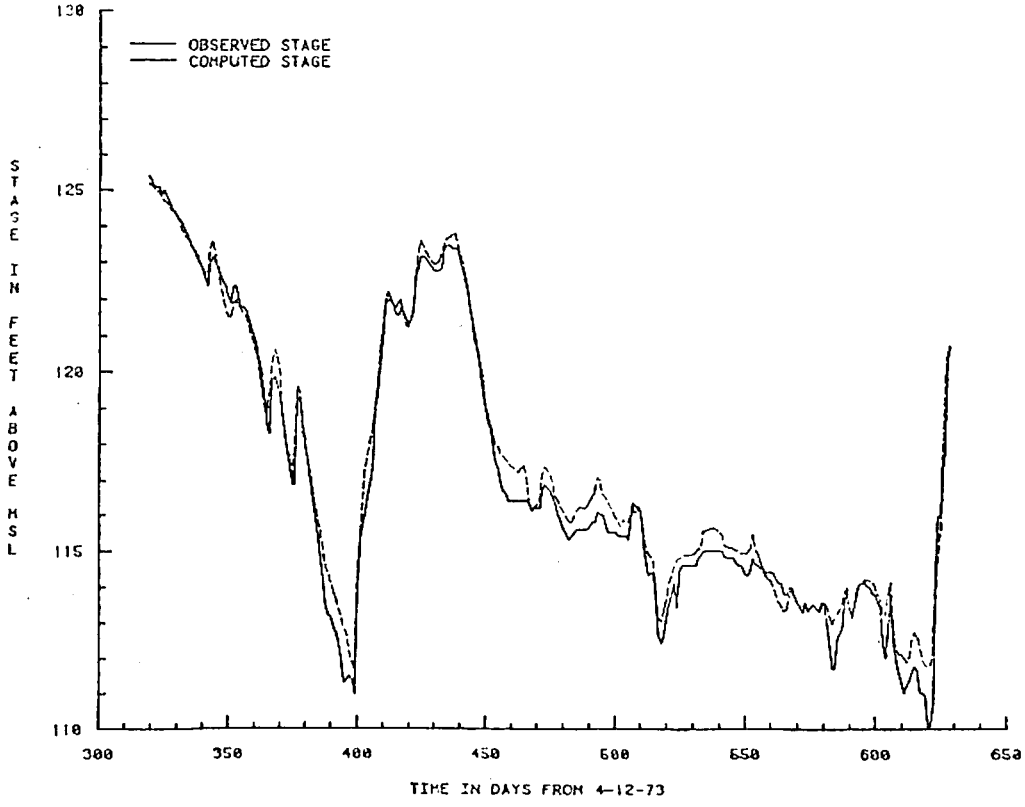


Figure 14-21. Sediment routing model verification at Fort Pemberton (1 foot = 0.305 m).

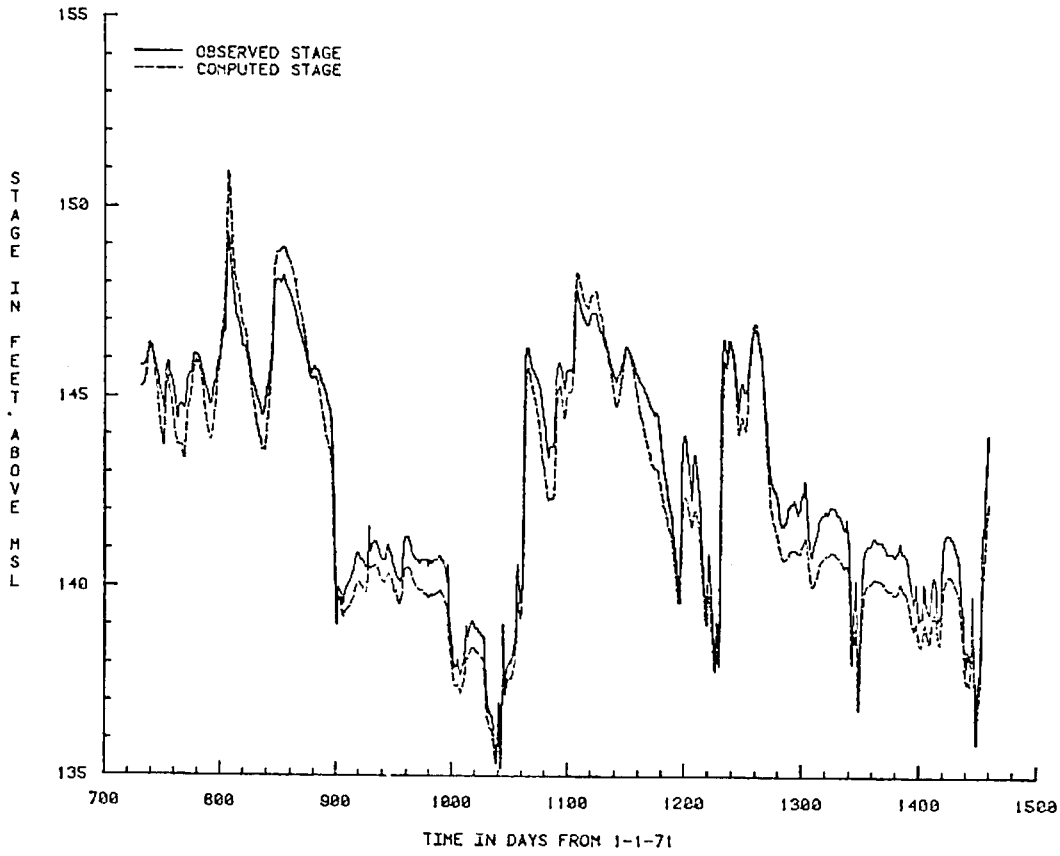


Figure 14-22. Sediment routing model verification at Locopolis (1 foot = 0.305 m).

## Comparison of Methods

For comparison purposes, model error is defined as the difference between observed and predicted stage for each day. Figures 14-23 and 14-24 show the relative frequency distribution of error for the verification periods and Table 14-2 lists the statistics of the absolute error for each method.

As indicated in the figures and table, all three methods have approximately the same mean error for Locopolis, but the process models have much lower maximum errors than the stage-discharge statistical relationships. Since there are few channel changes in this reach, the results of the two process models, rigid boundary and movable bed, are essentially the same. At Fort Pemberton the sediment routing model is clearly better than the simple backwater model, assuming a rigid boundary bed, and is superior to the statistical approach because the sediment routing model predicts and adapts to changes in river conditions related to sediment movement and deposition. The stage-discharge statistical and rigid boundary models, however, are based only upon limited historical conditions and cannot adapt to a changing environment.

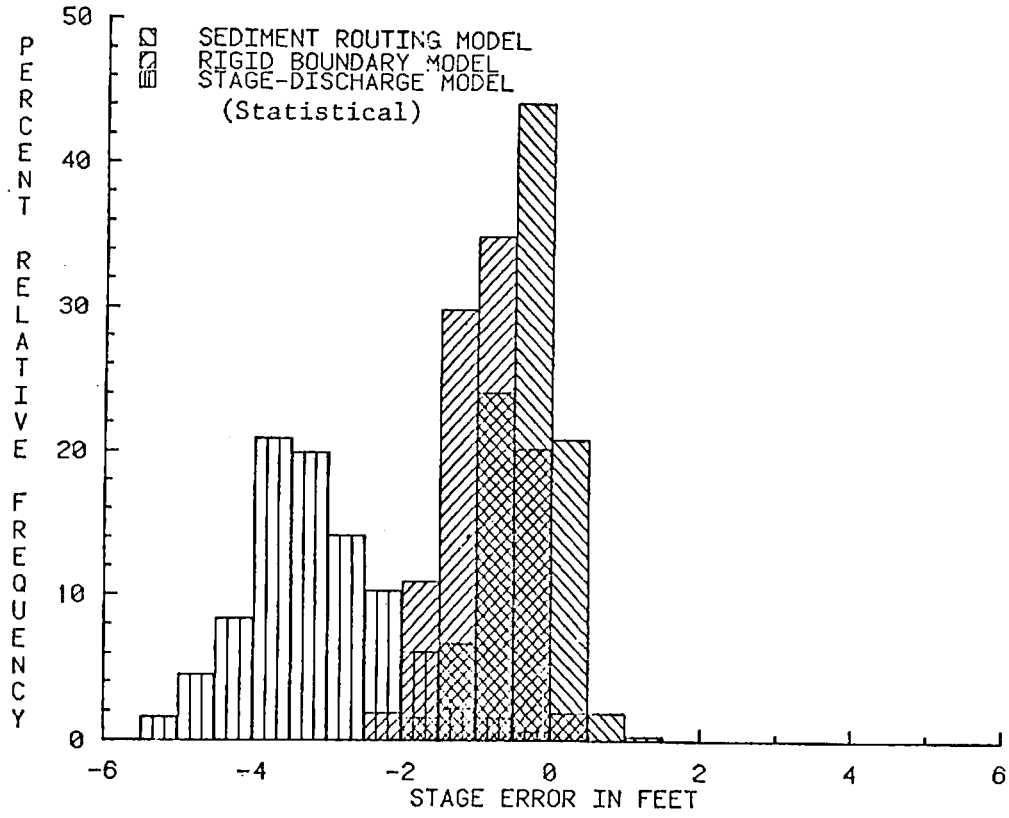


Figure 14-23. Model error fequency at Fort Pemberton (1 foot = 0.305 m).

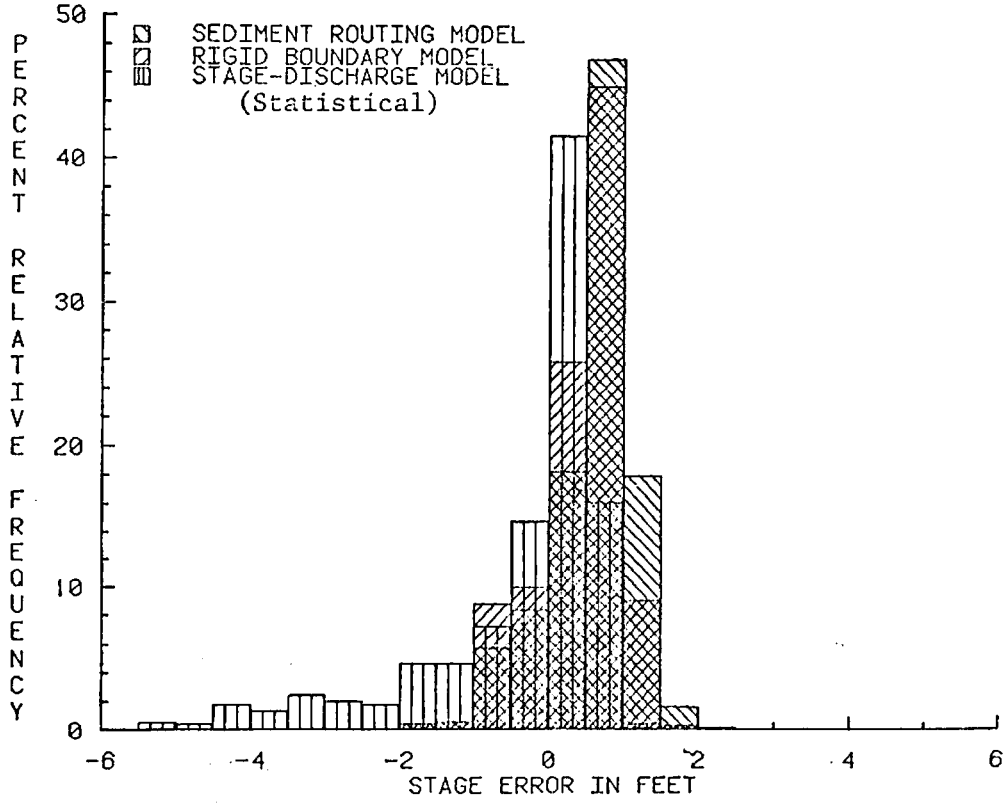


Figure 14-24. Model error frequency at Locopolis (1 foot = 0.305 m).

TABLE 14-2

Statistics of Absolute Model Errors

| | Error in Feet | | | |
|---|---|---|---|---|
| | Calibrated | | Verification | |
| | Mean | Maximum | Mean | Maximum |
| Stage-Discharge Model | | | | |
| Fort Pemberton | 2.56 | 10.38 | 3.47 | 7.27 |
| Locopolis | 0.33 | 2.56 | 0.80 | 5.48 |
| Rigid Boundary Model | | | | |
| Fort Pemberton | 0.90 | 3.97 | 0.92 | 2.39 |
| Locopolis | 0.29 | 2.27 | 0.62 | 1.91 |
| Sediment Routing Model | | | | |
| Fort Pemberton | 0.88 | 3.60 | 0.45 | 1.78 |
| Locopolis | 0.34 | 2.12 | 0.74 | 2.21 |

Computer central processor times on the Cyber 172 at Colorado State University, required for one run on both test reaches, were 10, 140 and 240 seconds for the stage-discharge, backwater, and sediment routing models, respectively. While the stage-discharge model needed to be run once, the process models required several runs to calibrate.

Another study was presented by Simons et al. (1973) on rivers in Venezuela. A significant amount of deviations in stage-discharge relations were observed. These deviations were attributed to changes in bed elevation due to scour or fill, changes in energy gradeline slope and lags in bedform roughness. Data indicated that a shift curve applied to a single valued reference rating curve could be used to reduce errors in estimating discharge from stage measurements. The shift curve was developed as a function of peak discharge and time after the peak.

## 14.6 DYNAMIC EFFECTS ON STAGE-DISCHARGE RELATIONS DUE TO UNSTEADY, NONUNIFORM FLOW IN BOTH RIGID AND ALLUVIAL CHANNELS

A hysteresis looping effect in stage-discharge relations is also caused by dynamic effects. Accelerations in the unsteady, nonuniform flow change the friction slope so that on the rising limb of a hydrograph the friction slope is greater than the bed slope and depth is less than for steady flow, while the opposite is true of the recession limb. Figure 14-25 shows this effect on a hypothetical river.

The literature offers various documentation and mathematical explanations of this phenomenon (see Henderson, 1963, 1966; Fread, 1973; and Simons, 1977). Data showing this looping effect was presented by Fread on the Mississippi River and was used by Simons in showing how a

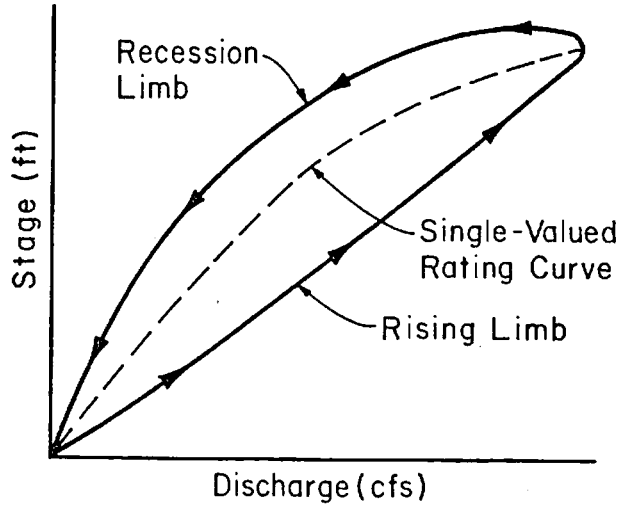


Figure 14-25. Stage-discharge relation with dynamic effects.

solution of the full dynamic momentum equation can account for the hysteresis loop in stage-discharge relations.

## 14.7 SOLUTION OF THE FULL DYNAMIC MOMENTUM EQUATION TO DESCRIBE THE STAGE-DISCHARGE RELATION

The full dynamic momentum equation can be written as (see Henderson, 1966)

$$S_f = S_o - \frac{\partial y}{\partial x} - \frac{1}{gA}\frac{\partial Q^2/A}{\partial x} - \frac{1}{gA}\frac{\partial Q}{\partial t} \qquad (14\text{-}2)$$

in which $S_f$ is the friction slope, $S_o$ is the channel bed slope, $y$ is the depth of flow, $x$ is the downstream distance, $g$ is the gravitational acceleration, $A$ is the cross-sectional area of flow, $Q$ is the discharge, and $t$ is the time. Each term of Equation 14-2 can be solved in terms of the known input hydrograph.

## 14.8 CONVERSION FROM DISCHARGE TO STAGE

When a discharge hydrograph is known, often the stage hydrograph is desired. One may wish to know how high the water will rise during a flood. For this case a model is formulated to convert a single discharge hydrograph to the corresponding stage hydrograph considering dynamic effects.

The Manning's equation is used to relate discharge to hydraulic parameters.

$$Q = \frac{1.486}{n} AR^{2/3} S_f^{1/2} \qquad (14\text{-}3)$$

The hydraulic radius, $R$, is defined as $A/P$ in which $P$ is the wetted perimeter. The wetted perimeter can be written as a power function of flow area

$$P = a_1 A^{b_1} \tag{14-4}$$

in which $a_1$ and $b_1$ are constants. Therefore, Manning's equation may be written as

$$Q = \frac{1.486}{n a_1^{2/3}} A^{(5-2b_1)/3} S_f^{1/2} \tag{14-5}$$

or

$$A = \frac{n a_1^{2/3}}{1.486}^{3/(5-2b_1)} (S_f^{-1/2})^{3/(5-2b_1)} Q^{3/(5-2b_1)} \tag{14-6}$$

Often Manning's $n$ varies with discharge and can be written in a power relation

$$n = a_3 Q^{b_3} \tag{14-7}$$

Next, each of the terms in Equation 14-2 are expressed in terms of the known input hydrograph.

The water surface slope $\partial y/\partial x$ may be determined as follows. The depth of flow can be expressed as a power function of the flow area

$$y = a_4 A^{b_4} \tag{14-8}$$

in which $a_4$ and $b_4$ are constants.

By taking the partial derivative of Equation 14-8 with respect to x one obtains

$$\frac{\partial y}{\partial x} = a_4 b_4 A^{b_4 - 1} \frac{\partial A}{\partial x} \tag{14-9}$$

An expression for $\partial A/\partial x$ is found by taking the partial derivative of Equation 14-6 with respect to $x$.

$$\frac{\partial A}{\partial x} = \left(\frac{n a_1^{2/3}}{1.486}\right)^{3/(5-2b_1)} (S_f^{-1/2})^{3/(5-2b_1)} \left(\frac{3}{5-2b_1}\right) Q^{(-2+2b_1)/(5-2b_1)} \frac{\partial Q}{\partial x} \tag{14-10}$$

Next, the term $\partial Q/\partial x$ is expressed in terms of the input discharge hydrograph through the continuity equation for the case of no lateral inflow or outflow (see Chow, 1959).

$$\frac{\partial Q}{\partial x} + \frac{\partial A}{\partial t} = 0 \tag{14-11}$$

The partial derivative of the flow are with respect to time is determined using Equation 14-6.

$$\frac{\partial Q}{\partial x} = -\frac{\partial A}{\partial t} = -\left(\frac{na_1^{2/3}}{1.486}\right)^{3/(5-2b_1)} (S_f^{-1/2})^{3/(5-2b_1)}$$

$$\left(\frac{3}{5-2b_1}\right) Q^{(-2+2b_1)/(5-2b_1)} \frac{\partial Q}{\partial t} \tag{14-12}$$

This expression is now substituted into Equation 14-10 which is then related to the water surface slope using Equation 14-9. The resultant expression for the water surface slope is

$$\frac{\partial y}{\partial x} = a_4 b_4 A^{b_4-1} \left(\frac{1.486}{na_1^{2/3}}\right)^{-6/(5-2b_1)}$$

$$\left(\frac{3}{5-2b_1}\right)^2 Q^{(-4+4b_1)/(5-2b_1)} S_f^{-3/(5-2b_1)} \frac{\partial Q}{\partial t} \tag{14-13}$$

The next term in the full dynamic momentum equation (Equation 14-2) to be found is the convective acceleration term, $1/(gA)\ \partial Q^2/A/\partial x$. Using Equation 14-5 an expression for $\partial Q^2/A/\partial x$ is derived.

$$\frac{\partial Q^2/A}{\partial x} = \left(\frac{1.486}{na_1^{2/3}}\right)^2 \left(\frac{7-4b_1}{3}\right) S_f A^{(4-4b_1)/3} \frac{\partial A}{\partial x} \tag{14-14}$$

The term $\partial A/\partial x$ is given in Equation 14-10.

From Equation 14-11 on obtains

$$\frac{\partial Q}{\partial x} = -\frac{\partial A}{\partial t} \tag{14-15}$$

The term $\partial A/\partial t$ is found by taking the partial derivative of Equation 14-6 with respect to time.

$$\frac{\partial A}{\partial t} = \left(\frac{n a_1^{2/3}}{1.486}\right)^{3/(5-2b_1)} (S_f^{-1/2})^{3/(5-2b_1)}$$

$$\left(\frac{3}{5-2b_1}\right) Q^{(-2+2b_1)/(5-2b_1)} \frac{\partial Q}{\partial t} \qquad (14\text{-}16)$$

Substitution of Equation 14-16 into Equation 14-15 and then substitution of the resulting expression into Equation 14-10 and finally substitution of this result into Equation 14-14 gives the desired equation

$$\frac{\partial Q^2/A}{\partial x} = -\left(\frac{7-4b_1}{3}\right)\left(\frac{3}{5-2b_1}\right)^2 \frac{\partial Q}{\partial t} \qquad (14\text{-}17)$$

The final term of the full dynamic momentum equation is the local acceleration, $\partial Q/\partial t$. This term is known since the input hydrograph $Q(o,t)$ is given.

$$\frac{\partial Q}{\partial t} \simeq \frac{\Delta Q}{\Delta t} \qquad (14\text{-}18)$$

Expressions for all of the terms in the full dynamic momentum equation, Equation 14-2, have been derived and are substituted into Equation 14-2.

$$S_f = S_o - \frac{\partial y}{\partial x} - \frac{1}{gA}\frac{\partial Q^2/A}{\partial x} - \frac{1}{gA}\frac{\partial Q}{\partial t} \qquad (14\text{-}19)$$

$$S_f = S_o + a_4 b_4 A^{b_4-1}\left(\frac{1.486}{n a_1^{2/3}}\right)^{-6/(5-2b_1)}\left(\frac{3}{5-2b_1}\right)^2 Q^{(-4+4b_1)/(5-2b_1)}$$

$$S_f^{-3/(5-2b_1)} \frac{\partial Q}{\partial t} + \frac{1}{gA}\left(\frac{7-4b_1}{3}\right)\left(\frac{3}{5-2b_1}\right)^2 \frac{\partial Q}{\partial t} - \frac{1}{gA}\frac{\partial Q}{\partial t} \qquad (14\text{-}20)$$

Before Equation 14-20 can be solved for $S_f$, the area term in the factor $1/(gA)$ and in the water surface slope term are converted to discharge through Equation 14-6.

$$S_f - S_o - a_4 b_4\left(\frac{1.486}{n a_1^{2/3}}\right)^{(-3-3b_4)/(5-2b_1)}\left(\frac{3}{5-2b_1}\right)^2 Q^{(-7+4b_1+3b_4)/(5-2b_1)}$$

$$S_f^{(-3-3b_4)/(10-4b_1)} \frac{\partial Q}{\partial t} + \frac{1}{g}\frac{\partial Q}{\partial t}\left[1 - \left(\frac{7-4b_1}{3}\right)\left(\frac{3}{5-2b_1}\right)^2\right]$$

$$\left(\frac{n a_1^{2/3}}{1.486}\right)^{-3/(5-2b_1)} Q^{-3/(5-2b_1)} S_f^{\frac{1}{2}(3/(5-2b_1))} = 0 \qquad (14\text{-}21)$$

This equation can be solved by the well known Newton-Raphson technique.

Once the friction slope has been determined the depth may be related to the known discharge. First, the flow area is calculated from the discharge by Equation 14-6 and then the depth of flow is related to the cross-sectional area of flow by a power function given in Equation 14-8.

## 14.9 CONVERSION FROM STAGE TO DISCHARGE

Generally the stage hydrograph is known and the corresponding discharge hydrograph is desired. A method is shown below for converting a stage hydrograph to the corresponding discharge hydrograph with dynamic effects. The formulation is similar to the previous section. The known input is now $y$ expressed as a function of time and hence the partial derivative of $y$ with respect to time is $\frac{\partial y}{\partial t} \simeq \frac{\Delta y}{\Delta t}$. Again each term in the full dynamic momentum equation is expressed as a function of the known inputs.

Using Equation 14-8, and assuming lateral inflow is zero, the continuity equation may be written as (Note: $(1/b_4-1)$ does not equal $1/(b_4-1)$).

$$\frac{\partial Q}{\partial x} + (1/b_4)a_4^{-1/b_4} y^{(1/b_4-1)} \frac{\partial y}{\partial t} = 0 \qquad (14\text{-}22)$$

By taking the partial derivative of Equation 14-5 with respect to $x$ and utilizing Equation 14-8

$$\frac{\partial Q}{\partial x} = \left(\frac{1.486}{n a_1^{2/3}}\right) S_f^{1/2} \left(\frac{5-2b_1}{3}\right) A^{(2-2b_1)/3} (1/b_4)a_4^{-1/b_4} y^{(1/b_4-1)} \frac{\partial y}{\partial x} \qquad (14\text{-}23)$$

The expression is then substituted into the continuity equation, Equation 14-22 yielding

$$\frac{\partial y}{\partial x} = - \frac{\partial y}{\partial t} \left(\frac{1.486}{n a_1^{2/3}}\right)^{-1} S_f^{-1/2} \left(\frac{3}{5-2b_1}\right) A^{-(2-2b_1)/3} \qquad (14\text{-}24)$$

Next, the convective acceleration term $(1/gA \frac{\partial Q^2/A}{\partial x})$ is put in terms of of the known input data. The term $\frac{\partial Q^2/A}{\partial x}$ was defined in Equation 14-14. The term $\partial A/\partial x$ can be related to the water surface slope

$$\frac{\partial A}{\partial x} = (1/b_4)a_4^{-1/b_4} y^{(1/b_4-1)} \frac{\partial y}{\partial x} \qquad (14\text{-}25)$$

The water surface slope was previously derived in Equation 14-24. This expression is then substituted into Equation 14-25 which is in turn substituted into Equation 14-14.

$$\frac{\partial Q^2/A}{\partial x} = - \ (1/b_4)a_4^{-1/b_4} \ y^{(1/b_4-1)} \left(\frac{1.486}{na_1^{2/3}}\right)\left(\frac{7-4b_1}{5-2b_1}\right) A^{(2-2b_1)/3} \ S_f^{1/2} \ \frac{\partial y}{\partial t} \tag{14-26}$$

The local acceleration term is determined by taking the partial derivative of Equation 14-5 with respect to time and using Equation 14-8.

$$\frac{\partial Q}{\partial t} = \ (1/b_4)a_4^{-1/b_4} \ y^{(1/b_4-1)} \left(\frac{1.486}{na_1^{2/3}}\right)\left(\frac{5-2b_1}{3}\right) \ S_f^{1/2} \ A^{(2-2b_1)/3} \ \frac{\partial y}{\partial t} \tag{14-27}$$

Again, the expressions describing the water surface slope and local and convective accelerations are substituted into the full dynamic momentum equation, Equation 14-2. The terms involving A are converted to y through Equation 8.

$$S_f = S_o + \left(\frac{1.486}{na_1^{2/3}}\right)^{-1}\left(\frac{3}{5-2b_1}\right)\left[a_4^{-1/b_4} \ y^{1/b_4}\right]^{-(2-2b_1)/3} \ S_f^{-1/2} \ \frac{\partial y}{\partial t}$$

$$+ \frac{1}{g} \ (1/b_4)a_4^{-1/b_4} \ y^{(1/b_4-1)} \left(\frac{1.486}{na_1^{2/3}}\right)\left(\frac{7-4b_1}{5-2b_1}\right)\left[a_1^{-1/b_4} \ y^{1/b_4}\right]^{(-1-2b_1)/3}$$

$$S_f^{1/2} - \frac{1}{g} \ (1/b_4)a_4^{-1/b_4} \ y^{(1/b_4-1)} \ \left(\frac{1.486}{na_1^{2/3}}\right)\left(\frac{5-2b_1}{3}\right)$$

$$\left[a_4^{-1/b_4} \ y^{1/b_4}\right]^{(-1-2b_1)/3} \ S_f^{1/2} \ \frac{\partial y}{\partial t} \tag{14-28}$$

After multiplying $S_f^{1/2}$ and letting $Z^2 = S_f$ one obtains a cubic equation.

$$Z^3 + Z^2 \ \frac{1}{g} \ (1/b_4)a_4^{-1/b_4} \ y^{(1/b_4-1)} \left(\frac{1.486}{na_1^{2/3}}\right)\left[a_4^{-1/b_4} \ y^{1/b_4}\right]^{(-1-2b_1)/3}$$

$$\frac{\partial y}{\partial t}\left[\frac{5-2b_1}{3} - \frac{7-4b_1}{5-2b_1}\right] - ZS_o - \left(\frac{1.486}{na_1^{2/3}}^{-1}\right)\frac{3}{5-2b_1}$$

$$\left[a_4^{-1/b_4} \ y^{(1/b_4)}\right]^{-(2-2b_1)/3} \ \frac{\partial y}{\partial t} = 0 \tag{14-29}$$

This equation may be solved using a routine which solves a third order polynomial. The value obtained for Z is then squared in order to determine the friction slope, $S_f$.

Once the friction slope has been determined and knowing the depth, the corresponding value for discharge can be calculated. The flow area is calculated using Equation 14-8 and the discharge is calculated using Equation 14-5.

## 14.10 TEST RESULTS OF DYNAMIC STAGE-DISCHARGE RELATION

In order to validate the model an observed stage hydrograph is read into the model to calculate a discharge hydrograph which is then checked against observed discharges. Fread (1973) gave data of this type and two sets of data are run through the model developed in this paper.

Figure 14-26 shows an observed stage hydrograph on the Mississippi River at Red River Landing which is input to the model. The simulated discharge hydrograph is compared to the observed discharge hydrograph in Figure 14-27. The simulated and observed stage-discharge relation is shown in Figure 14-28. For the rising limb of a floodwave the friction slope is larger than the bedslope and hence the corresponding stages are smaller. During the falling limb of a floodwave the friction slope is smaller than the bedslope and hence the corresponding stages are larger. This hysteresis loop is due to dynamic effects. Also, shown in Figure 14-26 is the simulated stage hydrograph which uses the simulated discharge hydrograph as input. Thus the applicability of both the stage to discharge model and the discharge to stage model is established.

A stage hydrograph on the Mississippi River at Tarbert Landing was used as input to the model as further verification. Figure 14-29 shows the comparison of simulated and observed discharge hydrographs. Figure 14-30 shows that the comparison of simulated and observed data agree closely.

## 4.11 CONCLUSIONS

Some of the major phenomena affecting stage-discharge relations have been discussed. These include alluvial bed form changes, scour and fill and dynamic effects due to unsteady, nonuniform flow. Sometimes a unique, single-value rating curve can be developed for rigid boundary channels. However, dynamic effects can cause a hysteresis loop in the stage-discharge relation. The relative strength of dynamic effects are inversely proportional to the bedslope and directly proportional to the rate of rise or fall of the stage or discharge. A mathematical tool was presented based on the full dynamic momentum equation that accounts for this phenomenon. The dynamic effects also play a role in alluvial boundary stage discharge relations.

The effect of alluvial bed form changes can produce discontinuity in a stage discharge relation. The discontinuity usually appears when the streambed changes from lower to upper regime and resistance to flow decreases markedly. Hysteresis looping is also encountered due to a lag in bed form roughness response to changing hydraulic conditions. An

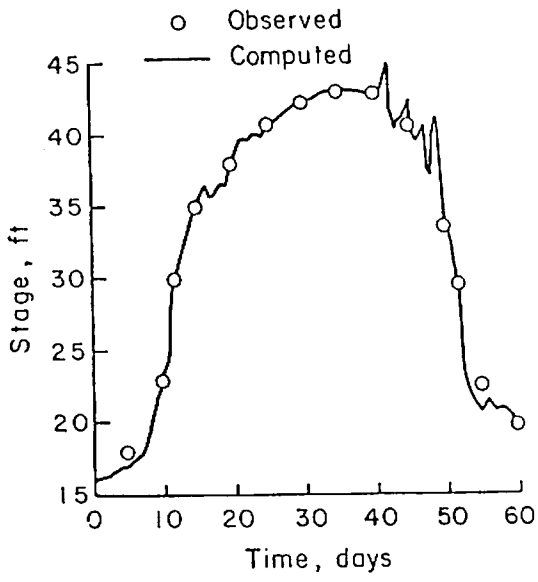


Figure 14-26. Stage hydrograph, Mississippi River at Red River Landing, LA. (3/11/63-5/13/63).

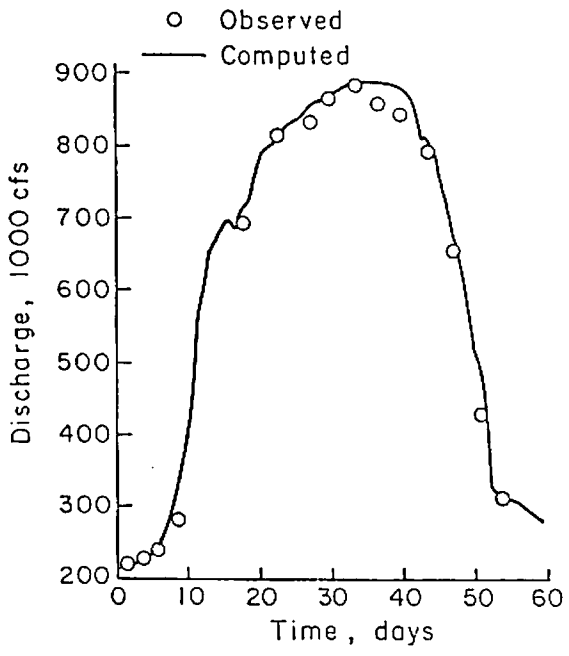


Figure 14-27. Discharge hydrograph for Mississippi River, Red River Landing, LA. (3/11/63-5/13/63).

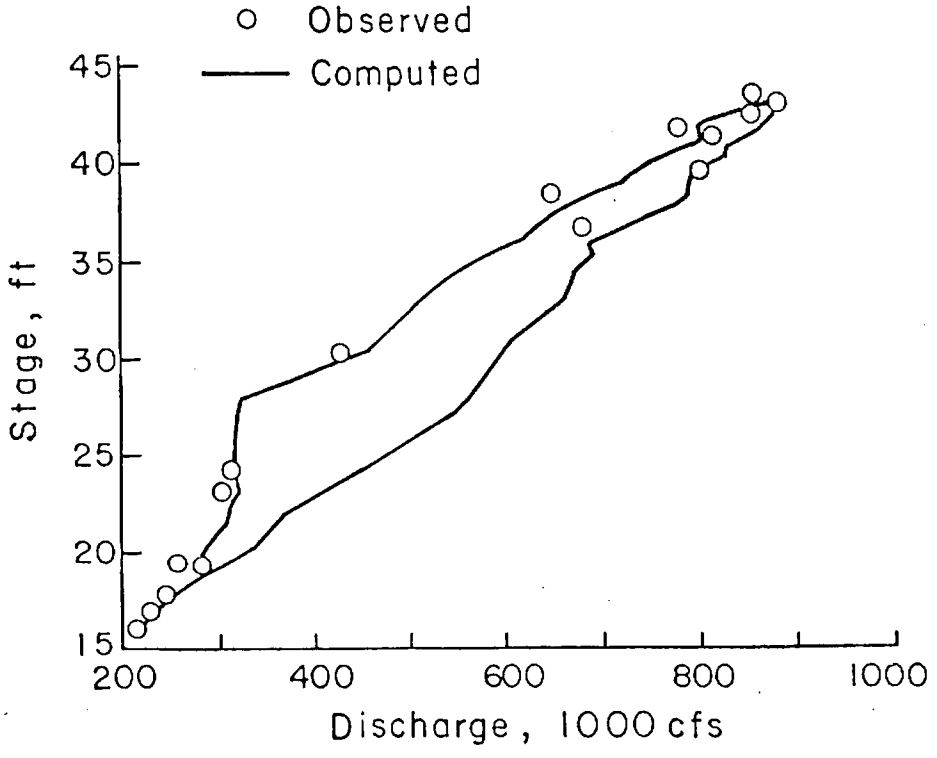


Figure 14-28. Stage-discharge relation for Mississippi River, Red River Landing, LA (3/11/63-5/13/63).

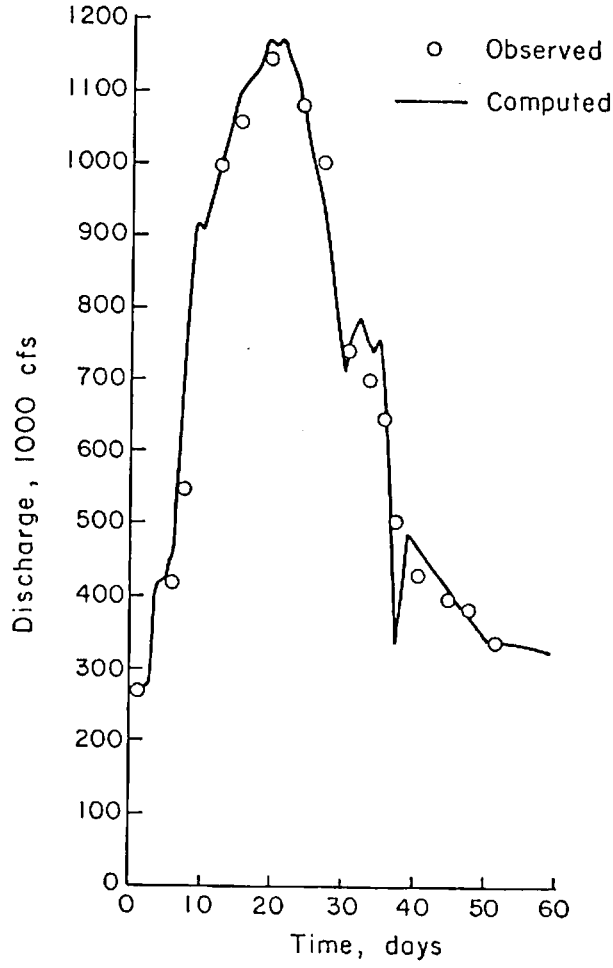


Figure 14-29. Discharge hydrograph for Mississippi River, Tarbert Landing, LA (2/9/66-4/11/66).

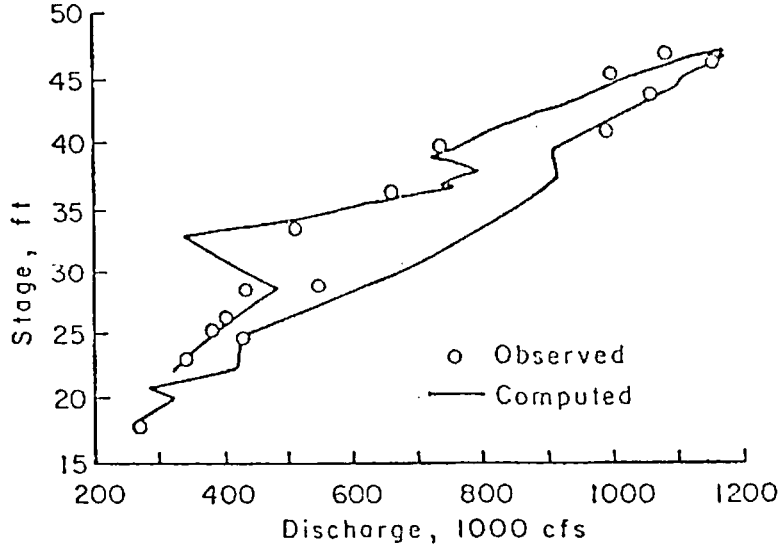


Figure 14-30. Stage-discharge relation for Mississippi River, Tarbert Landing, LA (2/9/66-4/11/66).

investigation of alluvial bed form prediction methods and corresponding resistance to flow analysis is recommended to the reader.

Scour and fill changes stage discharge relations by changing the bed elevation of the stream. Sediment transport techniques are required to best evaluate stage-discharge relations for streams where bed elevation changes are significant.

The resistance to flow and water depth over a boulder bed stream can be significantly reduced due to the transport of large quantities of silt and sand changing the bed to upper regime flow conditions at high flows. Discharge estimation from a previously developed stage-discharge relation can have a significantly high rate of error under these conditions.

Unfortunately a combination of all these phenomena is possible and is likely to some extent in all alluvial rivers. Even apparent rigid boundary channels can be subject to these phenomena when conditions dictate. The relationship between stage and discharge is highly complex and requires a thorough understanding of hydraulics and sediment principles to avoid significant errors. Tools are available to aid in the understanding and application of these processes on stage-discharge relations.

## REFERENCES

Al-Shaik-Ali, K. S., Simons, D. B., and Li, R. M., 1978, Effect of Sediment on Resistance to Flow in Cobble and Boulder Bed Rivers, Civil Engineering Dept., Colorado State University, Fort Collins, Colorado, CER77-78KSA-DBS-RML-46.

Beckman, E. W., and Furness, L. W., 1962, Flow Characteristics of Elkhorn River near Waterloo, Nebraska, U.S. Geological Survey Water Supply Paper 1498-B.

Colby, B. R., 1960, Discontinuous Rating Curves for Pigeon Roose and Cuffawa Creeks in Northern Mississippi, U.S. Department of Agriculture, Agricultural Research Service Repot 41-46, 31 p.

Corps of Engineers, 1968, Missouri River Channel Regime Studies, MRD Sediment Series No. 13A, Omaha, Nebraska.

Dawdy, D. R., 1961, Depth-Discharge Relations of Alluvial Streams -Discontinuous Rating Curves, U.S. Geological Survey Water Supply Paper 1498-C, 16 p.

Fread, D. L., November 1973, A Dynamic Model of Stage-discharge Relations Affected by Changing Discharge, NOAA Technical Memorandum NWS Hydro 16.

Henderson, F. M., July 1963, Flood Waves in Prismatic Channels, Journal of the Hydraulics Division, ASCE.

Henderson, F. M., 1966, Open Channel Flow, Macmillan, London.

Li, R. M., Brown, G. O. and Simons, D. B., 1979, Computer Simulation of River Stages, Colorado State University, Fort Collins, prepared for Summer Computer Simulation Conference in Toronto, Canada.

Senturk, F., 1969, Nehir Hidroligi, DSI Publication No.: 66/X/64, Ankara.

Simons, D. B., and Richardson, E. V., 1962, The Effect of Bed Roughness on Depth-Discharge Relations in Alluvial Channels, Geological Survey Water Supply Paper 1498-E, U.S. Government Printing Office, Washington.

Simons, D. B., and Senturk, F., 1977, Sediment Transport Technology, Text, Water Resources Publications, Fort Collins, Colorado.

Simons, D. B., Stevens, M. A. and Duke, J. H., May 1973, Predicting Stages on Sand-Bed Rivers, Journal of the Waterways, Harbors and Coastal Engr. Division, ASCE, Vol. 99, No. WW2, Proc. Paper 9731, pp. 231-243.

Simons, R. K., 1977, A Modified Kinematic Approximation for Water and Sediment Routing, M.S. Thesis, Department of Civil Engineering, Colorado State University, Fort Collins, Colorado.

Simons, R. K., Li, R. M., and Simons, D. B., 1977, On Stage Discharge Relation of Rivers, Proceedings Congress IAHR, Baden-Baden.

# CHAPTER 15

# RESERVOIR SEDIMENTATION

Through the mid 20th century, most reservoirs designed to provide storage space for sediment considered accumulation to occur from the "bottom up." That is, dead storage was filled first and then the active storage. As reservoirs were resurveyed, this notion was found to be erroneous. In some cases, years passed before any noticeable depletion of dead storage occurred, while the active space was being filled continuously. It was realized that, not only the volume, but the pattern of deposition had to be taken into account in order to insure that the reservoir was not under designed (allocated active storage space is depleted faster than anticipated) or over designed (dams constructed higher than needed due to anticipated accumulation at the base). Current knowledge concerning the prediction of both volume and location of deposition is discussed below.

## 15.1 TYPES OF RESERVOIRS

It is important to recognize that different types of reservoirs typically affect sediment flow and deposition in varied ways. Methodologies for predicting deposition patterns seldom provide an explicit statement of the type of reservoir for which the method is applicable. Prior to discussing specific methodologies, some general delineations between types of reservoirs are established for communicative purposes. The characteristics used for categorization are operation and width.

### Operation

From a general standpoint, three major classifications appear to be appropriate when addressing sediment deposition: normally ponded, semi-dry, and run-of-the-river.

#### Normally Ponded

Normally ponded reservoirs range from small ranch and farm ponds to large multi-purpose reservoirs. Their primary characteristic influencing sediment deposition is the lack of continuous through flow coupled with an intense mixing zone at the river-reservoir juncture. The majority of time, they are operated at or near the top of a conservation pool. After the inertia of the incoming flow is dissipated in the mixing zone, the movement of water through the reservoir is fairly quiescent and dependent on those factors causing circulation. During times of high flow (floods) and, correspondingly, high sediment inflow, the outflow is characteristically less than the inflow. This creates a rise in stage and movement of the mixing further upstream. All coarse material is trapped and the fine sediment distribution is a function of reservoir and sediment characteristics.

#### Semi-Dry

These reservoirs usually do not have a conservation pool and they do not have a dead storage space. During times of low or no inflow,

they are empty, and all deposited material is exposed. During high inflows and times when they contain water, they behave in much the same manner as a normally ponded reservoir. Trap efficiencies fluctuate over a wide range.

Run-of-the-river

The run-of-the-river condition is where outflow is dependent and of the same order of magnitude as inflow. All flow is primarily from the head of the reservoir to the dam. Flow can be approximated by river hydraulics methods which take into account the backwater profiles. Reservoirs where these conditions exist are usually used for navigation and, sometimes, power production. They are characterized by short detention times, trap efficiencies less than 100 percent, relatively high flow velocities, and significant reentrainment of deposited material.

Width

This geometric characteristic is basically an indication of the tendency for shortcircuiting. For lack of better criteria at the present time, the following categories are established:

Narrow. The reservoir is approximately the same width as the channel.

Moderately Wide. Width of the reservoir is approximately the same as that of the meander pattern.

Wide. Reservoir is wider than the meander belt.

## 15.2 VOLUME OF DEPOSITION

Early work in the area of reservoir sedimentation dealt with determining the volume of deposition. Methodologies were sought which provided a reservoir's trap efficiency (TE) without regard to the sediment distribution. Dominant parameters which relate to trap efficiency are:

Detention (Retention) Time. This is the average time a particle of water will remain in the reservoir and is calculated by dividing the volume of the reservoir by the through flow under equilibrium conditions.

$$\text{Detention Time} = \text{Reservoir Capacity/Inflow} = C/I$$

The longer a particle of sediment remains in a reservoir, the more time it will have to settle from suspension. Therefore, the greater the detention time is, the greater the trap efficiency. It should be noted that the capacity is the volume of water in the reservoir and not the maximum possible volume of water.

Sediment Characteristics. Basically, this factor relates to the different fall velocities of the different sizes of sediment, although

flocculation and hindered settling have a marked effect. The greater the fall velocity of a particle, the faster it will leave suspension. Therefore, the larger the particle size, the larger the trap efficiency will tend to be. The clay and finer silt are the most likely to escape. The sand and course silt fractions seldom reach the reservoir outlet. The only instances where this is not true is when the reservoir is nearly full of sediment or when the reservoir is operating at extremely low stages. In both cases, the river-reservoir juncture is near the dam.

Flow Velocity. Sediment tank design considered trap efficiency to be a function of only the two factors discussed above. Neglecting the effect of the velocity of flow is usually attributable to designing the facilities for low flow through velocities and thus, minimal suspension due to turbulence. In some reservoirs this assumed quiescent flow does not exist at all cross sections. The effect is a decrease in the perceived fall velocity and a corresponding decrease in trap efficiency.

Depth of Reservoir. Although the depth of reservoir affects stratification and circulation patterns, the fall distance of a particle is the major consideration here. Simply, the further a particle has to fall, the longer it will remain in suspension.

Shortcircuiting. This phenomena reflects as a deviation from plug flow and is caused by reservoir operation, density flow, wind, reservoir geometry, etc. Once run-of-the-river conditions do not exist, shortcircuiting will have a definite effect on the trap efficiency. Basically, it will create differences in detention time for different elements of water. The average detention time is less representative of the reservoir flow. This is a complex phenomena which is extremely difficult to account for precisely.

To date, most methods formulated to predict trap efficiencies are based on empirical correlations utilizing one or more of the first three factors discussed i.e.,

$$TE = f[(C/I)(w_i)/\bar{U}]$$

where $C/I$ = capacity-inflow ratio

$w_i$ = fall velocity of fraction $i$

$\bar{U}$ = the average through flow velocity

Several of these methodologies are discussed below.

Brune and Allen (1941)

Brune and Allen made one of the first studies of trap efficiency. They related the C/W ratio to the percent of eroded soil caught in the reservoir (Figure 15-1), where $C$ is the capacity of the reservoir in acre-feet and $W$ is the area of the watershed in square miles. The C/W ratio is intended to be a measure of the detention time of the reservoir. Two basic problems exist with this ratio.

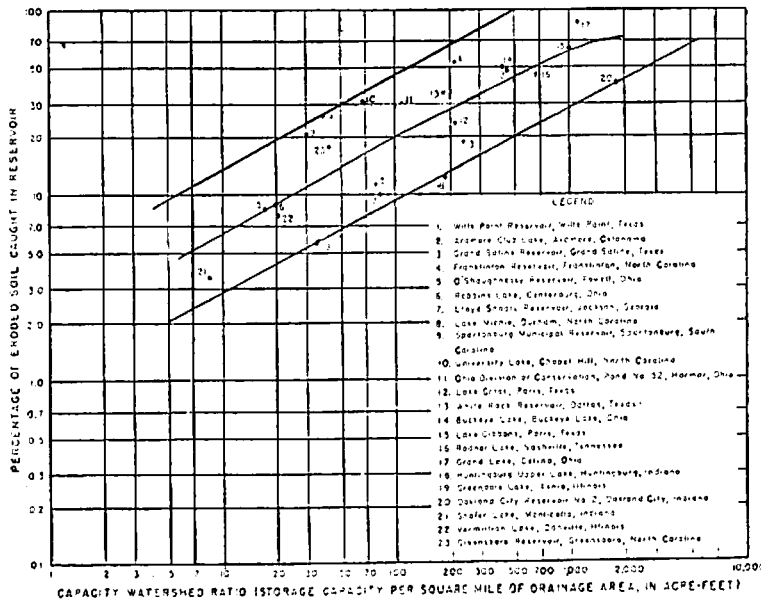


Figure 15-1. Percentage of eroded soil caught in reservoir as related to C/W ratio.

1. The watershed area can not be directly correlated to the inflow.

2. The capacity does reflect the reservoir volume, however, the reservoir capacity used should be the capacity for a given stage and not the maximum capacity of the reservoir. Another problem with the Brune and Allen analysis is that they used the amount of soil eroded and compared it to the reservoir accumulation to determine trap efficiency. The amount of sediment eroded from the watershed is usually less than that which is in the inflow to the reservoir. This would make the trap efficiencies determined by Brune and Allen lower than actual. Brown (1943) corrected the procedure to consider actual sediment inflow (Figure 15-2). The points are still scattered reflecting problems in the use of the C/W ratio.

Churchhill (1948)

Churchill correlated trap efficiency with a sedimentation index (Figure 15-3). The sedimentation index is equal to the ratio of the retention period to the mean velocity of flow through the reservoir. This analysis did take into account two of the prominent factors affecting trap efficiency and the scatter of points is significantly decreased. Borland (1971) applied this method using different data and found reasonable correlation.

Brune (1953)

Brune concluded that the data needed to use Churchill's procedure i.e., information needed to determine period of retention and the mean

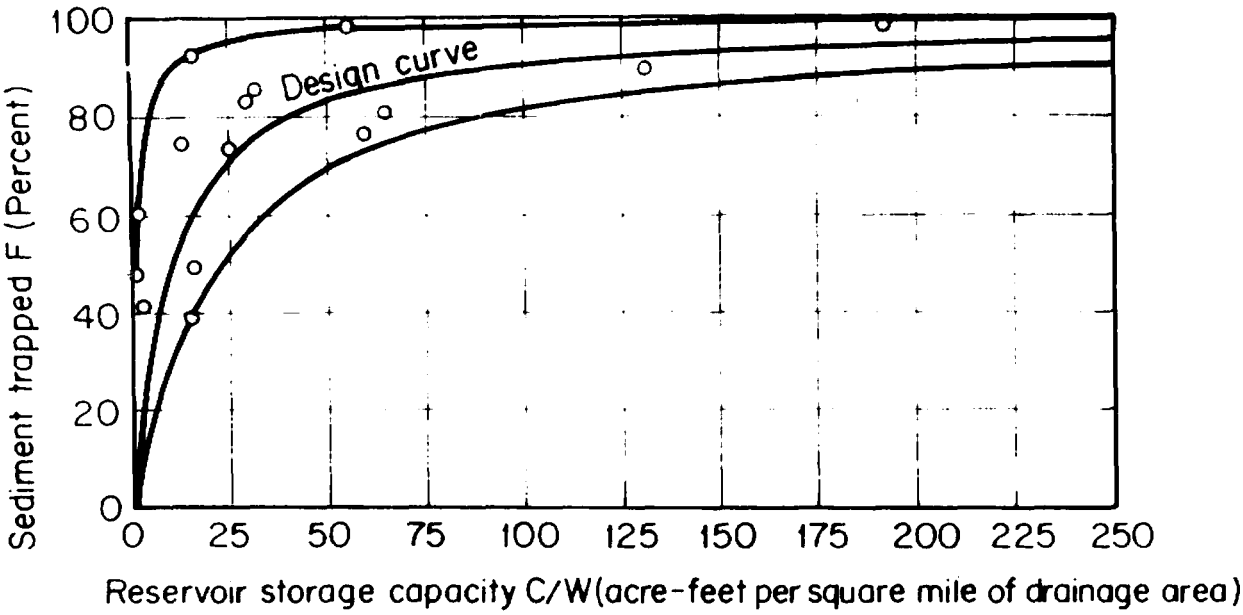


Figure 15-2. Trap efficiency as related to C/W ratio.

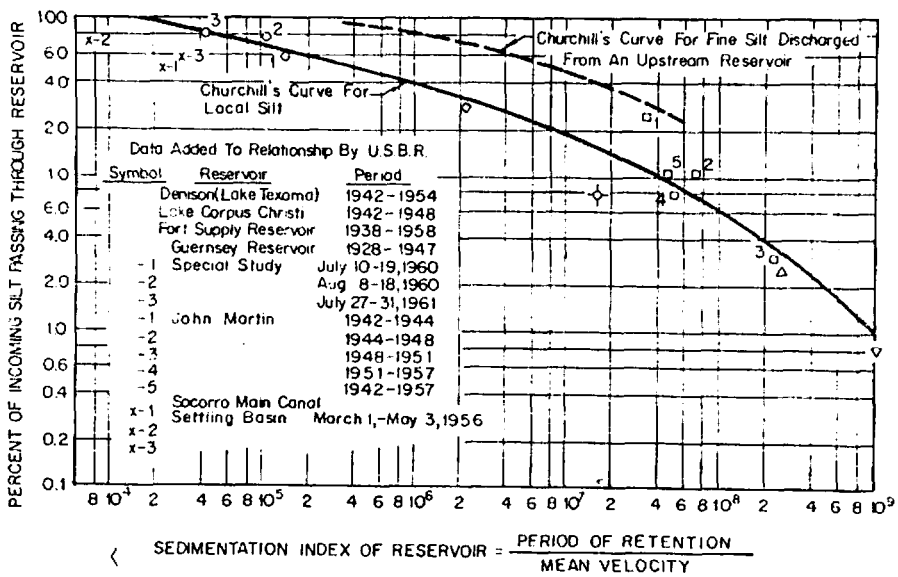


Figure 15-3. Percent of sediment passing through reservoir as related to sedimentation index.

velocity, was not readily available. He then developed a relationship between the trap efficiency and the reservoir capacity-inflow (C/I) ratio which is depicted in Figure 15-4. Here the C/I ratio is intended to be a measure of the detention time. The curve gave reasonable results, but Borland (1971) determined that Churchill's procedure was more precise. This procedure basically correlates the trap efficiency to the retention time and thus, considers one less factor than Churchill considered.

Karaushev (1966)

Karaushev developed an expression for trap efficiency in small reservoirs.

$$TE = 1 - [1 - (C/I)]\, e^{\left[\frac{-\phi(C/I)}{1-(C/I)}\right]} \qquad (15\text{-}1)$$

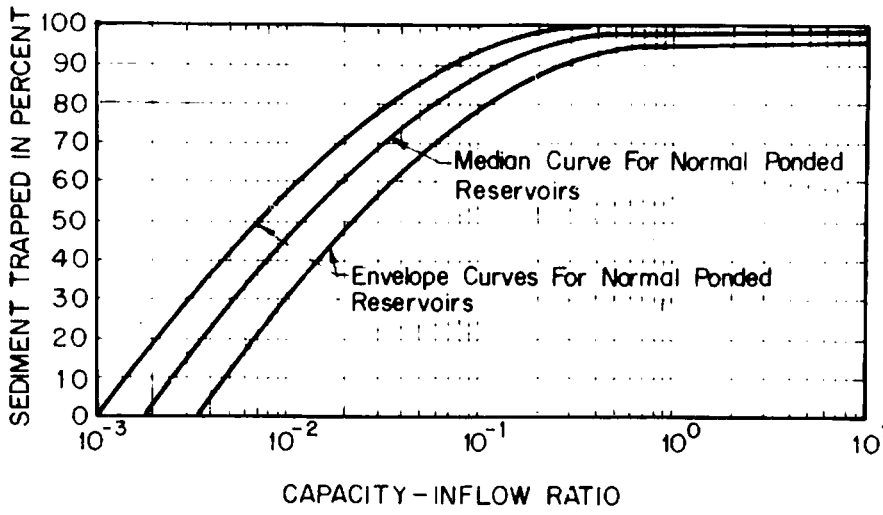


Figure 15-4. Trap efficiency as related to C/I ratio.

where $\phi = \frac{\bar{w}\, T_s}{\bar{h}}$

$\bar{w}$ = mean fall velocity of the transported sediment

$T_s$ = duration of spill over period in seconds

$\bar{h}$ = the mean depth of the reservoir.

The relationship is depicted graphically in Figure 15-5. The derivation of the relationship is not completely explained. A qualitative interpretation of the parameters follows.

1. C/I: As before, an increase in the C/I ratio produces an increase in trap efficiency.

2. $\bar{w}$ and $\bar{h}$: Sediment characteristics and reservoir depth are considered for the first time. The faster the particle falls, the sooner it will be removed from suspension; the further it has to fall the longer removal will take. These factors are taken into account by the parameter $\phi$ and produce the expected changes in trap efficiency.

3. $T_s$: The longer a spill-over occurs, the greater its mean flow velocity through the reservoir and greater are the chances that a particle of sediment will escape. $T_s$, as utilized in the equation, creates an increase in $\phi$, thus causing a decrease in trap efficiency. This anomoly is not explained.

The method does point out that sediment characteristics do influence the trap efficiency. This indicates that a family of curves are warranted for both Churchill's and Brune's methods.

Lopez (1978)

Lopez's analytical model to predict deposition patterns includes a determination of the sediment reaching the dam. If it is assumed that

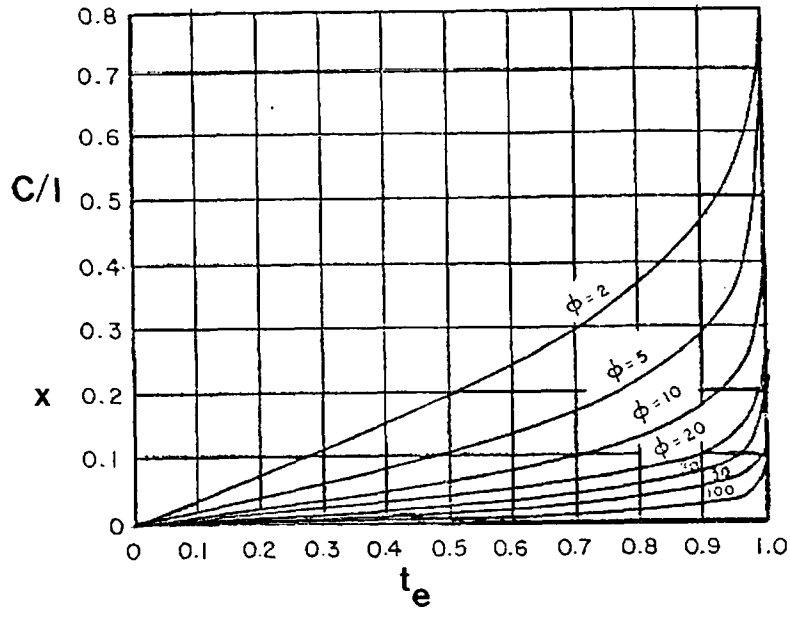


Figure 15-5. Trap efficiency as related to C/I and $\phi$.

this material exits the reservoir, the trap efficiency can be calculated. This and similarly derived models are the only analytical methods which provide a measure of trap efficiency. Their limitations will be discussed in a later section on analytical models.

## 15.3 PATTERNS OF DEPOSITION

Predictions of the patterns of deposition entail not only volume determination, but the location in the reservoir where the volume is depleted.

### Ideographic Deposition

General consensus among researchers working in the area of reservoir sedimentation is that the factors influencing sediment distribution characteristically create two basic formations: the delta and the bottom deposit (Figure 15-6). Predictions of deposition in reservoirs usually divide the formations and the characteristics that produce them into two separate categories and consider their development to be independent. The following paragraphs summarize the current state of knowledge with respect to each.

### Delta Deposits

The bed load and the coarse suspended load are usually transported at a rate commensurate with the existing capability of the stream. Once this capability is decreased by the expansion of the flow area at the river-reservoir juncture, a deposition occurs which is termed delta development. How this development proceeds depends on the distribution and amount of material being transported and how the flow is altered as it enters the reservoir. The flow of the river into the reservoir is most closely approximated by the dynamics of plane jet flow of water

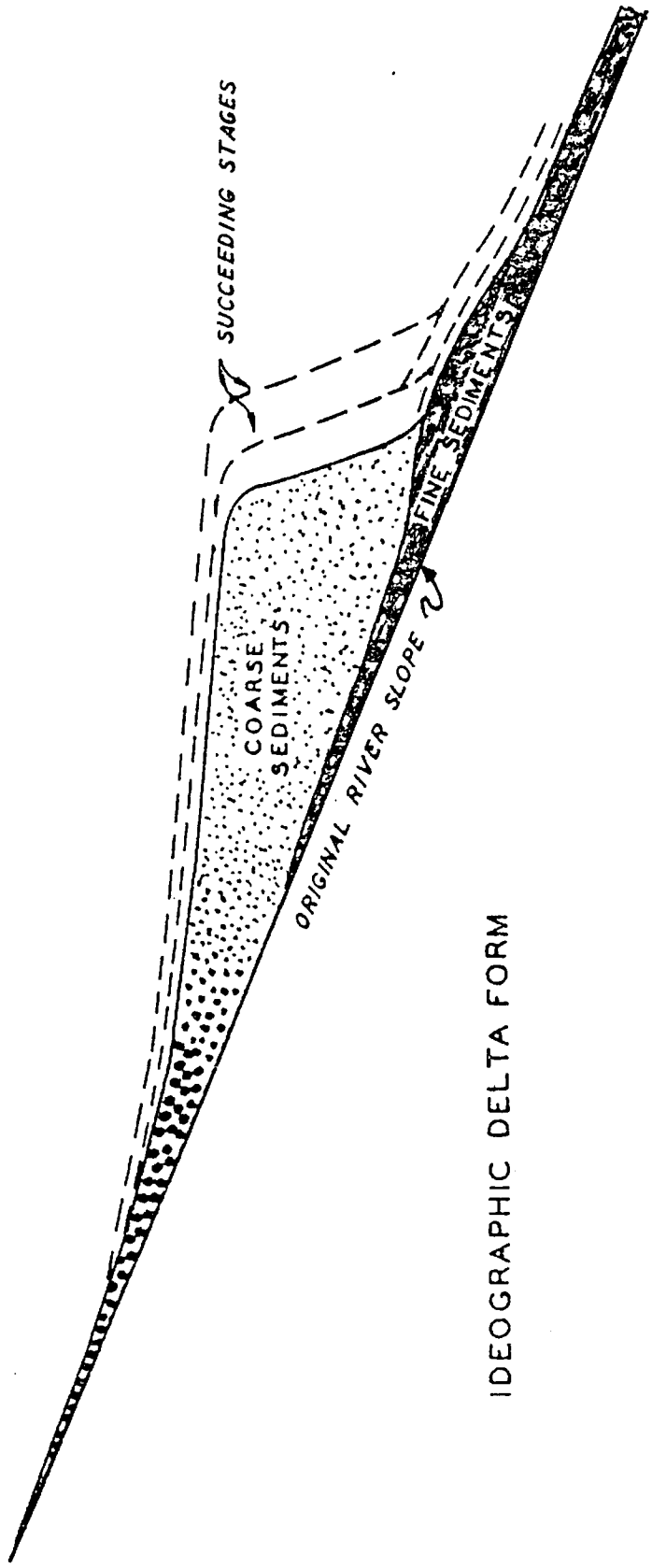


Figure 15-6. Ideographic delta form.

into water. Bates (1953) defines a delta as a sedimentary deposit built by jet flow into or within a permanent body of water. This process is schematically depicted in Figure 15-7 (Daily and Harleman, 1973).

Theoretical analysis of jet flow does provide insights into the general character of jet diffusion, but does not define precise velocity distributions, rates of entrainment of surrounding fluid, and jet dimensions. It has been necessary to resort to semi-empirical approaches to determine the aforementioned characteristics (Daily and Harleman, 1973).

Superimposing the results of these studies on the inflow of a river into a reservoir is complicated by several factors.

1. Inflow is unsteady. This affects both the jet characteristics and the location of the river-reservoir juncture.

2. Reservoir geometry tends to restrict the jet expansion in the narrower impoundments.

3. Deposition and erosion of material acts to alter the geometry. Vertical changes are depicted in Figure 15-8 (Harrison, 1952).

4. Differences in the densities of the reservoir water and the inflow alters the results of theoretical/laboratory studies which assume equal densities.

As a result of the gap between theory and reality, it has been necessary to rely heavily on field and laboratory observations in determining the growth characteristics of deltas.

In 1951, representatives of the Missouri River Division visited 12 reservoirs during low stage conditions in order to observe delta formations (Bondurant, 1955). Prior to the visual investigation, the team made a rather comprehensive review of existing literature. They summarized the state-of-the-art as follows:

> ...data were restricted almost wholly to such information on volume and profiles as were obtained from reservoir capacity surveys. In lieu of more reliable information, an ideographic concept (Figure 15-6) appeared to be generally accepted. Briefly, this concept assumes that deposition begins at the upstream limits of backwater effect with the deposition of the largest particles in the transport entering the reach. Deposition is considered to occur progressively downstream, with increasingly finer particles being deposited as the average velocity of flow is decreased, until, shortly after entering the reservoir, all material of the size of fine sand or larger must have been deposited.....It was recognized, of course, that this idealistic pattern would be complicated by the forward growth of the sand deposits over previously deposited silts, encroachment of one material over another due to fluctuations in pool level, and local erosion (re-working) of deposits during periods of low pool levels.

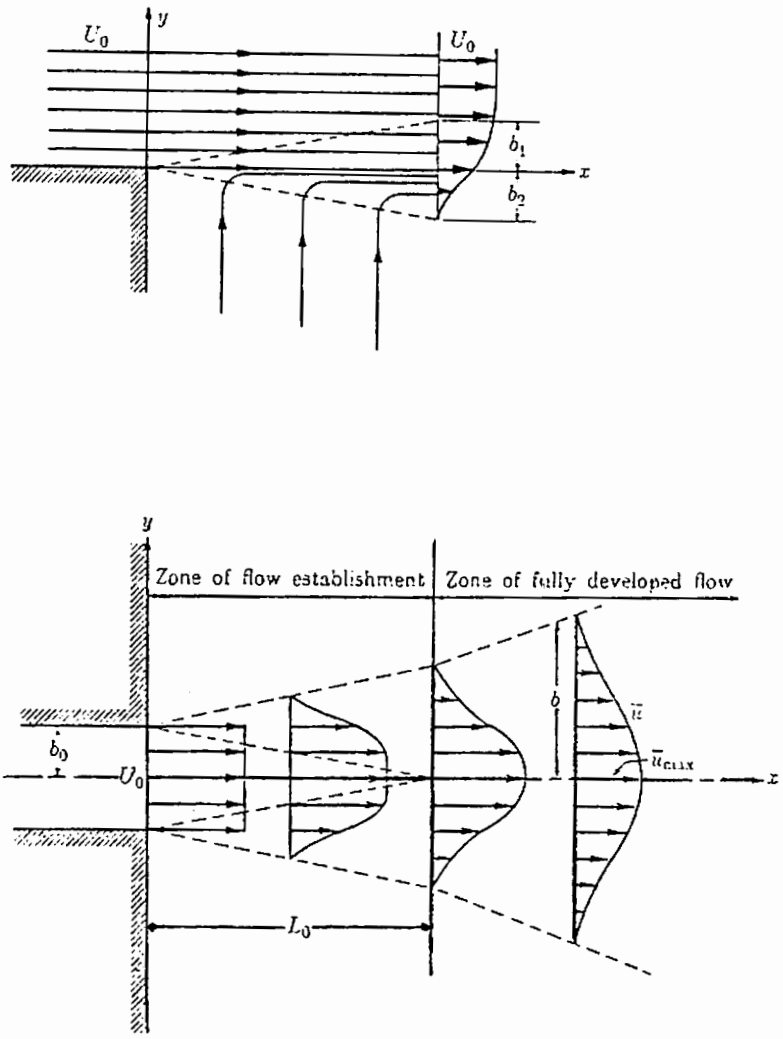


Figure 15-7. Development of similar velocity profiles in a plane jet.

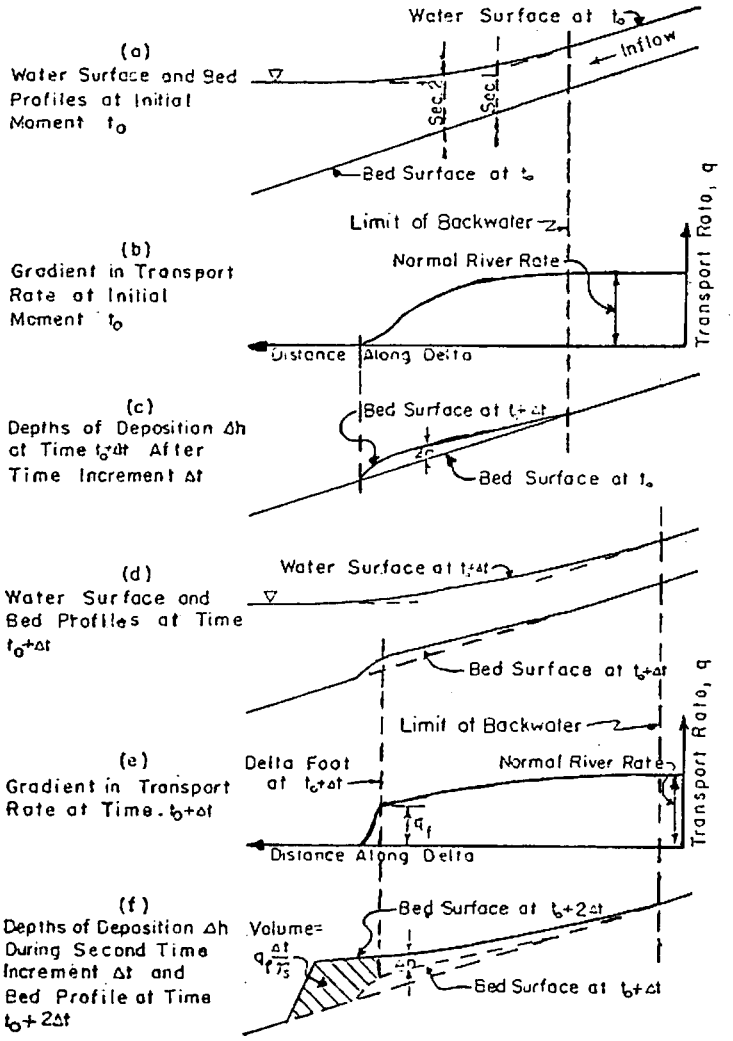


Figure 15-8. Theoretical water - surface and bed profiles of an alluvial river entering a reservoir.

Wright (1977), based on the work of past investigators of the deltaic process, concluded that a finite number of river-mouth types exist and that the variability can best be understood by considering the influence of primary forces in conjunction with modifying forces. The three primary forces are:

1. Inertia and associated turbulent diffusion

2. Turbulent bed friction

3. Buoyancy

The flow patterns associated with these dominant forces are depicted in Figures 15-9, 15-10, and 15-11. If present at all, inertia dominated flow is short lived in a reservoir due to deposition. Turbulent bed friction is dominant and results in the characteristic pattern depicted in Figure 15-12.

As the deposition process continues, repeated avulsions tend to distribute the deltaic material laterally as well as longitudinally. Laboratory experiments by Chang (1967) revealed that the delta will grow laterally approximately as fast as it does longitudinally. This is indicative of a tendency of the deltaic process to deplete storage space progressively from the river-reservoir juncture toward the dam.

Bottom Deposits

The patterns of deposition of bottom deposits are much more complex than those of the delta. The delta formation is controlled primarily by the sediment load and reservoir operation, while the bottom deposits are influenced by these factors plus the circulation within the reservoir. The intricacy of the circulation patterns within the reservoir makes predicting the deposition process of the finer grained material extremely difficult. Bondurant (1944) summed up the knowledge of these deposits as follows:

> Sediments of silt and clay sizes are considered to be transported, in an undefined manner, beyond the point where it is known that density flows sometimes result in clay materials being transported throughout the length of the reservoir to be deposited in front of the dam or perhaps to be discharged through the outlets.

Our knowledge has been increased very little since that synopsis.

Predicting Patterns of Deposition

The purpose of these models is to provide the planner with insight into the disposition of sediment collected in the reservoir as a function of time. Both empirical and analytical methods have been developed.

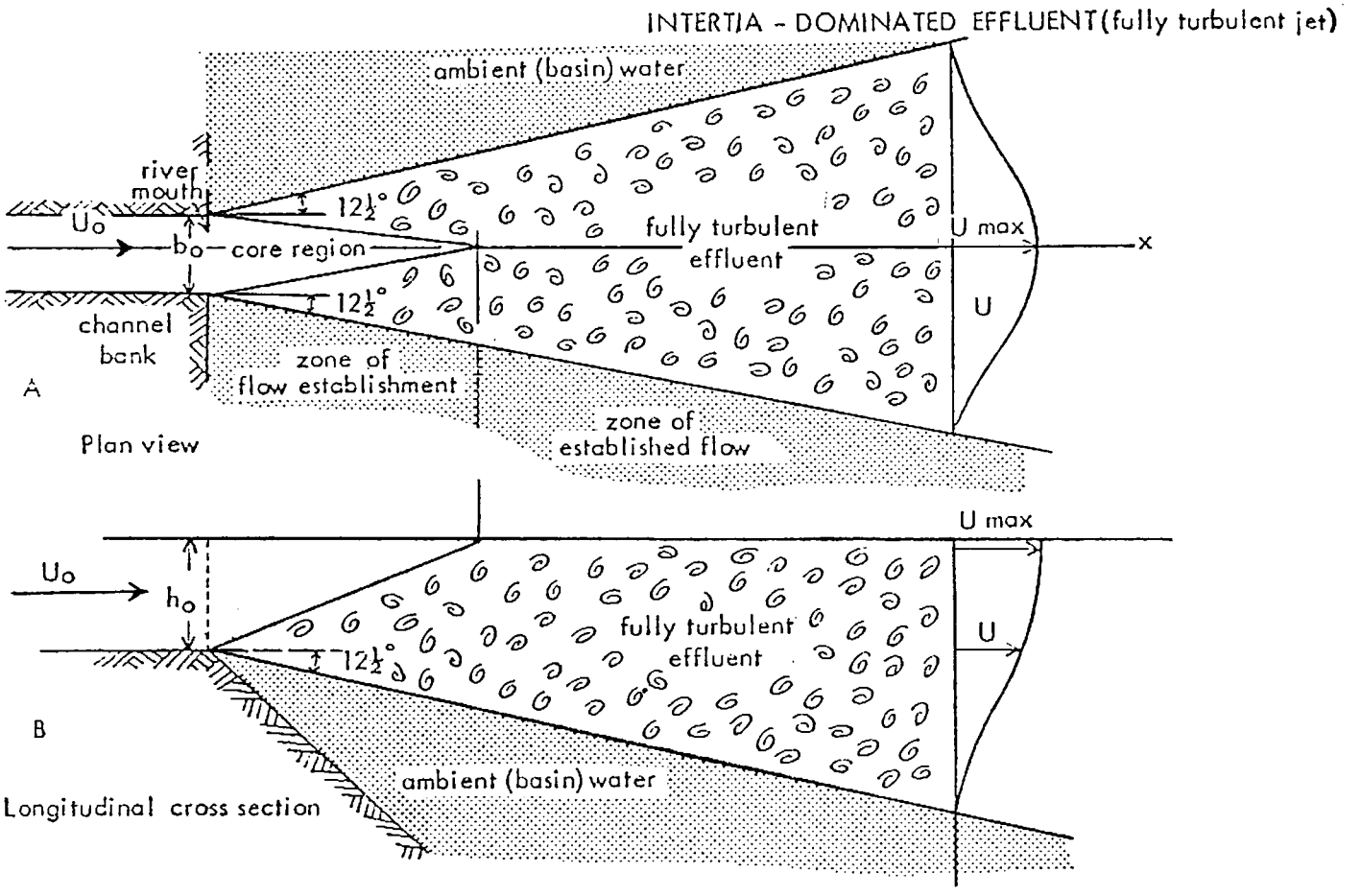


Figure 15-9. Inertia dominated effluent.

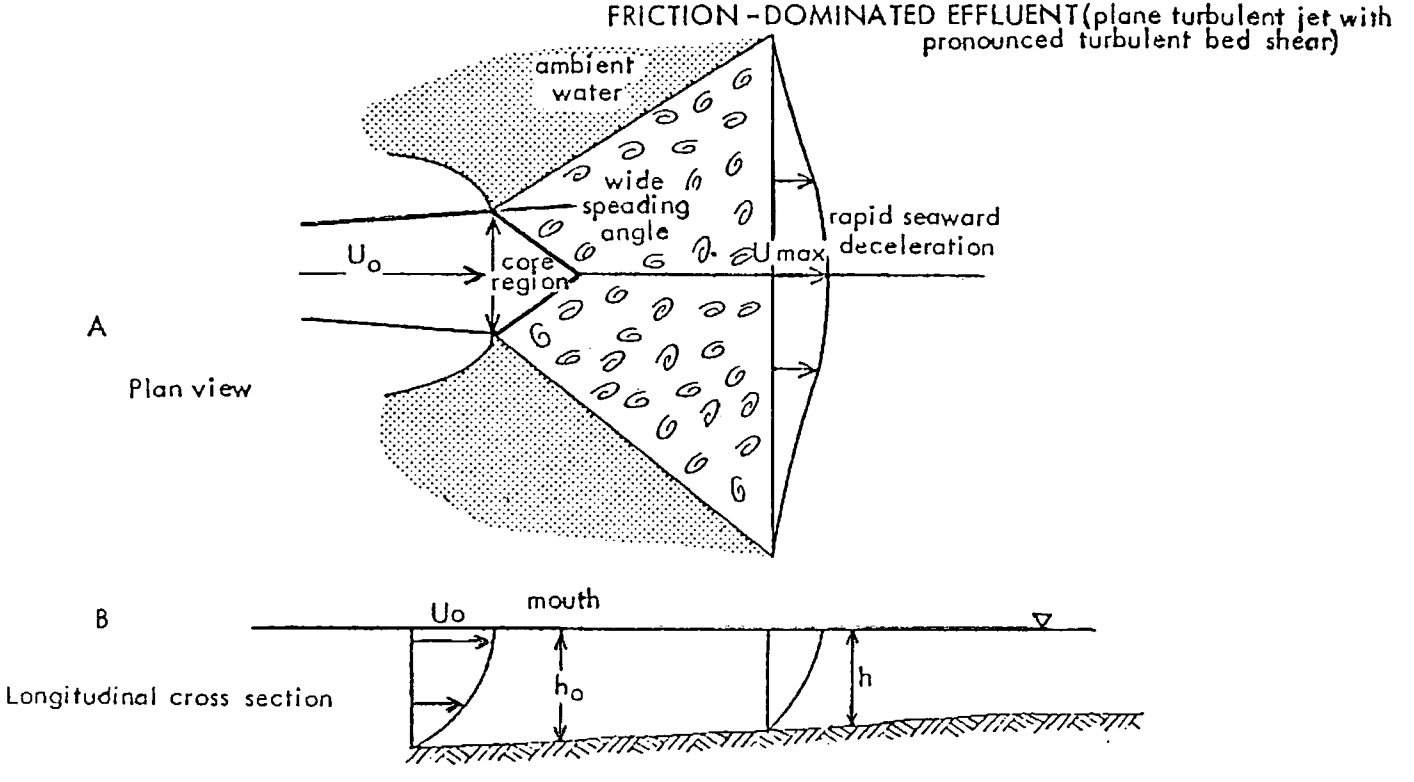


Figure 15-10. Friction dominated effluent.

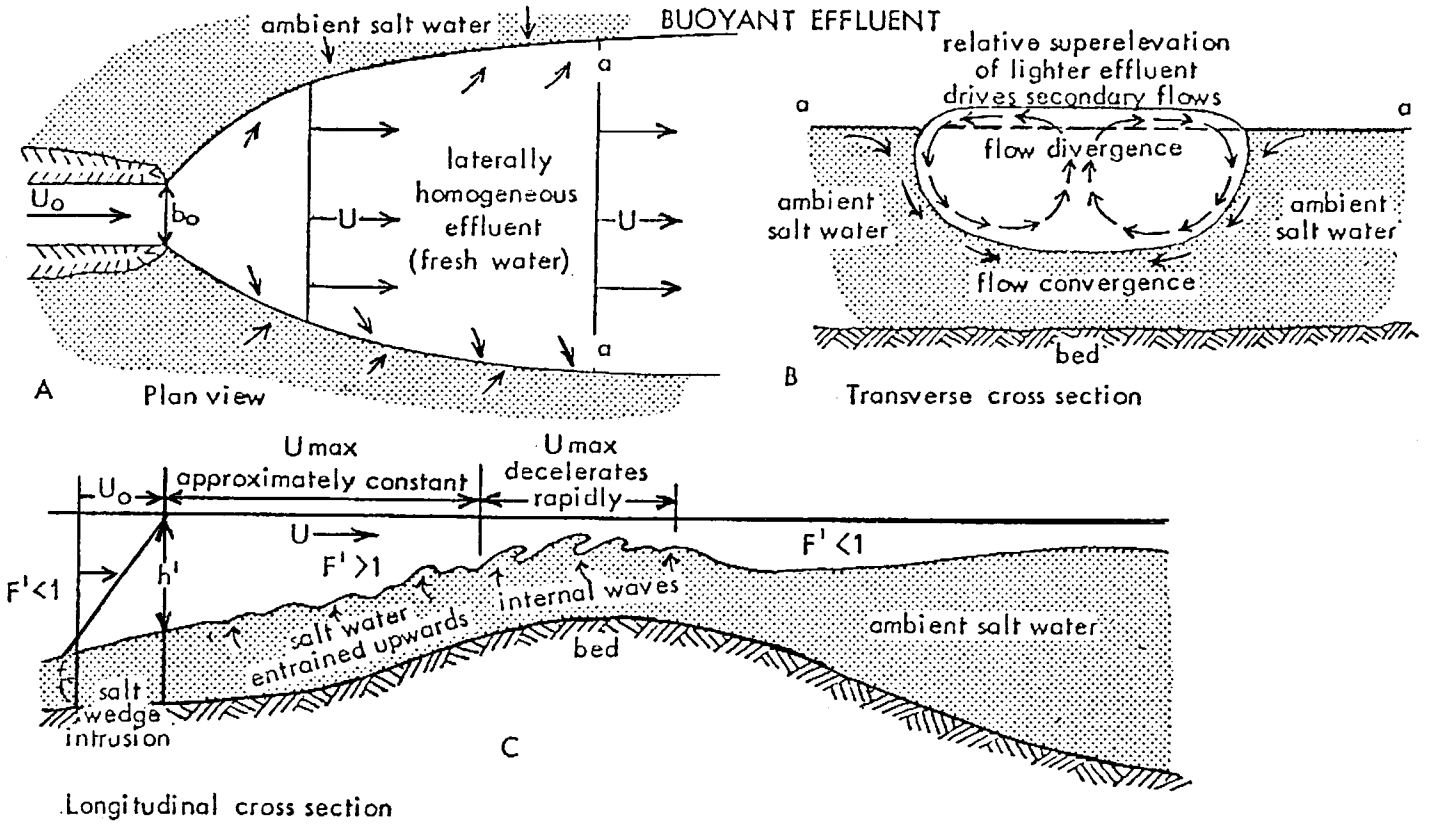


Figure 15-11. Buoyant effluent.

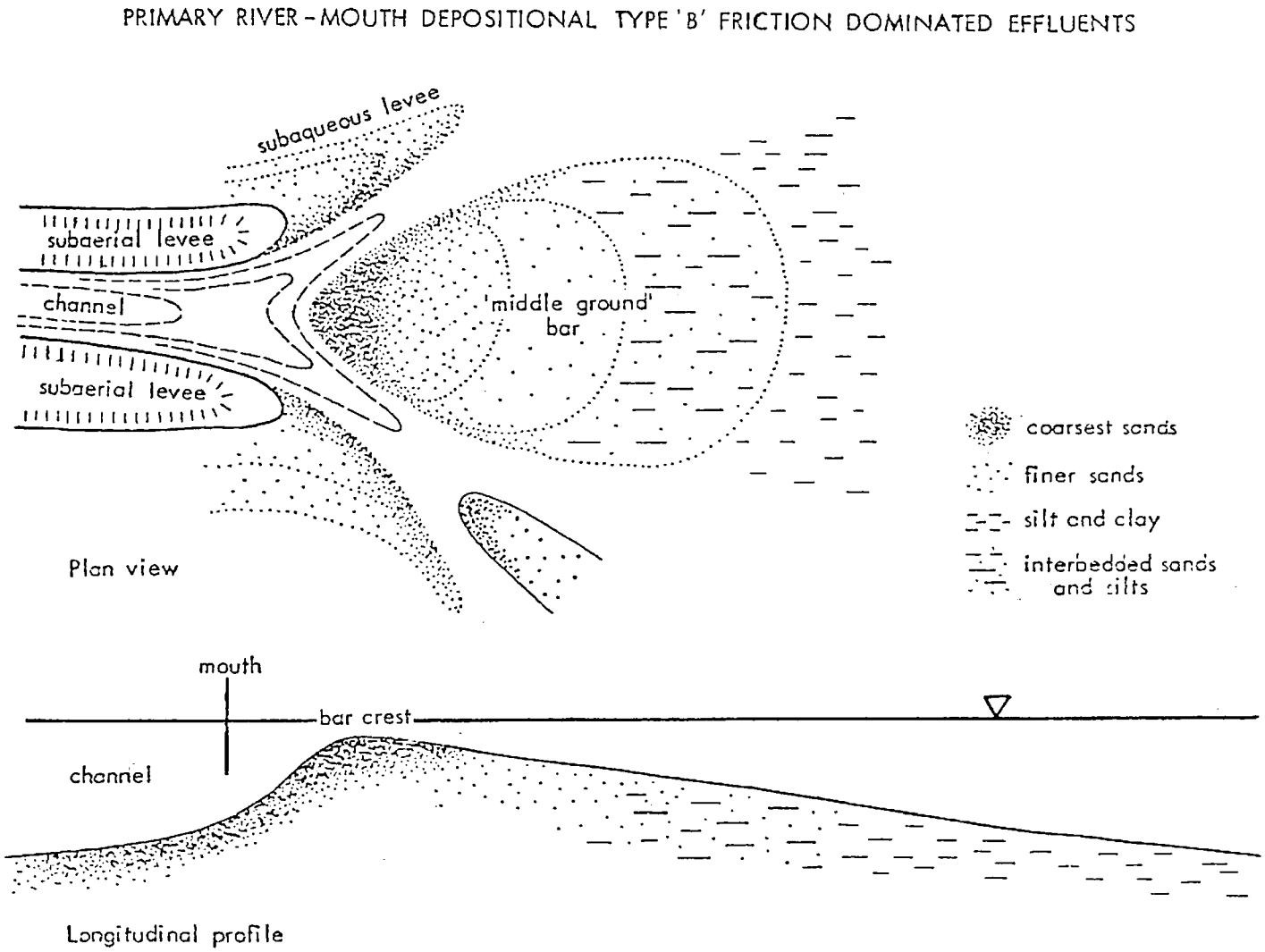


Figure 15-12. River-mouth deposition/friction dominated effluent.

This is probably the most extensive visual study of reservoir deltas ever conducted. Their observations revealed the following:

1. Deposits entering relatively wide basins projected into the basins instead of spreading laterally.

2. Massive deposits of clays were frequently associated with delta formations. In some instances, characteristically deltaic formations appeared to consist almost wholly of clays.

3. The deposits noted appeared to consist primarily of either sands or clays. Although it appears obvious that silt size materials must have been present, they were not identified in appreciable quantities. It is probable that mechanical analyses of the deposits would have disclosed a greater proportion of silts than was apparent visually.

4. The channels of inflowing streams frequently appeared to have shifted over the surface of the deposits in a series of avulsions rather than by progressive meandering.

5. Bedding of the deposits was frequently quite complex.

6. Numerous small lenses of various materials, some of them definitely discontinuous, were noted in the banks of channels scoured into the deposits.

7. Channels eroded into sand deposits tended to develop a symmetrical meander and, in at least one instance, were reported to be dimensionally in accord with the Lacey formula (Lacey, 1946). Channels eroded in clay tended to be straight.

8. Clay deposits, even when soft and unconsolidated, were highly resistant to erosion.

9. An appreciable quantity of gravel, sometimes in bar formation and sometimes scattered, was noted in the channel of the South Canadian River arm of the Conchas Reservoir well towards the downstream end of the exposed portion of the delta. This gravel was lying over a considerable depth of previously deposited sediments.

10. Boundaries of maximum experienced pool levels and backwater reaches could not be determined during the reconnaissance; however, backwater deposits appeared to be much less extensive than anticipated. Characteristic aggradation deposits i.e., deposits lying above the limits of normally experienced pool levels, appeared generally to be limited to boundaries of the maximum experienced pool.

11. Where extensive deposits were found in or above backwater reaches, they were invariably associated with other characteristic phenomena such as an aggrading stream, extensive vegetation, or constructions, either topographic or man made.

Empirical Models

Empirical models are based on observations of existing reservoirs. Data is analyzed to discover general trends of deposition under varying conditions in order to provide procedures for predicting effects in planned reservoirs. This empiricism is characterized by a lack of specific knowledge of the actual processes related to sediment deposition. The more representative the planned development is of the data used in developing a methodology, the better the results of the study will be. It is imperative that methodologies not be extrapolated to situations beyond those by which a procedure was developed.

Comparison. The simplest empiricism is generally comparison. When observations of reservoirs constructed in similar basins (those with like soil characteristics, cover, slopes, climate, etc.) reflect an absence of sediment related problems, it is reasonable to assume that a proposed reservoir with similar basin characteristics will not be subjected to adverse sediment effects. The Tennessee Valley is an excellent example of a basin where reservoir sedimentation is essentially not a problem (TVA, 1968). It stands to reason that other reservoirs constructed in this basin or similar basins will not be adversely affected within a reasonable period of analysis. A detailed study of the volume and patterns of accumulation is not warranted. In other basins where sediment has created adverse effects within the economic life of reservoirs, the reservoir designer must include sediment considerations as part of his analysis.

This basic method of analysis should provide a means of excluding in depth studies in some situations. On the other hand, it will warrant more precise methodologies where sediment is characteristically a problem.

Area Increment Method (1953). This effort by Cristofano (1953) represents the first attempt to distribute the sediment in accordance with actual observations. Recognizing that the sediment does not fill from bottom to top, but at all elevations, Cristofano made the assumption that deposition could be approximated by reducing the reservoir area at each elevation by a fixed amount. The progressive filling of the reservoir using this purely mathematical method is depicted schematically in Figure 5-13.

The method does better approximate the actual sediment deposition pattern than the "bottom up" assumption, but does not account for the various factors which determine the pattern. Actual patterns will vary widely from those predicted using this method. It tends to be conservative for the estimation of the dam height and unconservative for the allocation of active storage space.

Empirical Area-Reduction Method (1958). This is probably the most widely known and used method for predicting sediment deposition. Borland and Miller (1958) used the resurveys of 30 reservoirs to develop a relationship between percentage of reservoir depth and percentage of sediment deposited for reservoirs of different shapes as per Figure 15-14. The shape of the reservoir is defined by M which is the

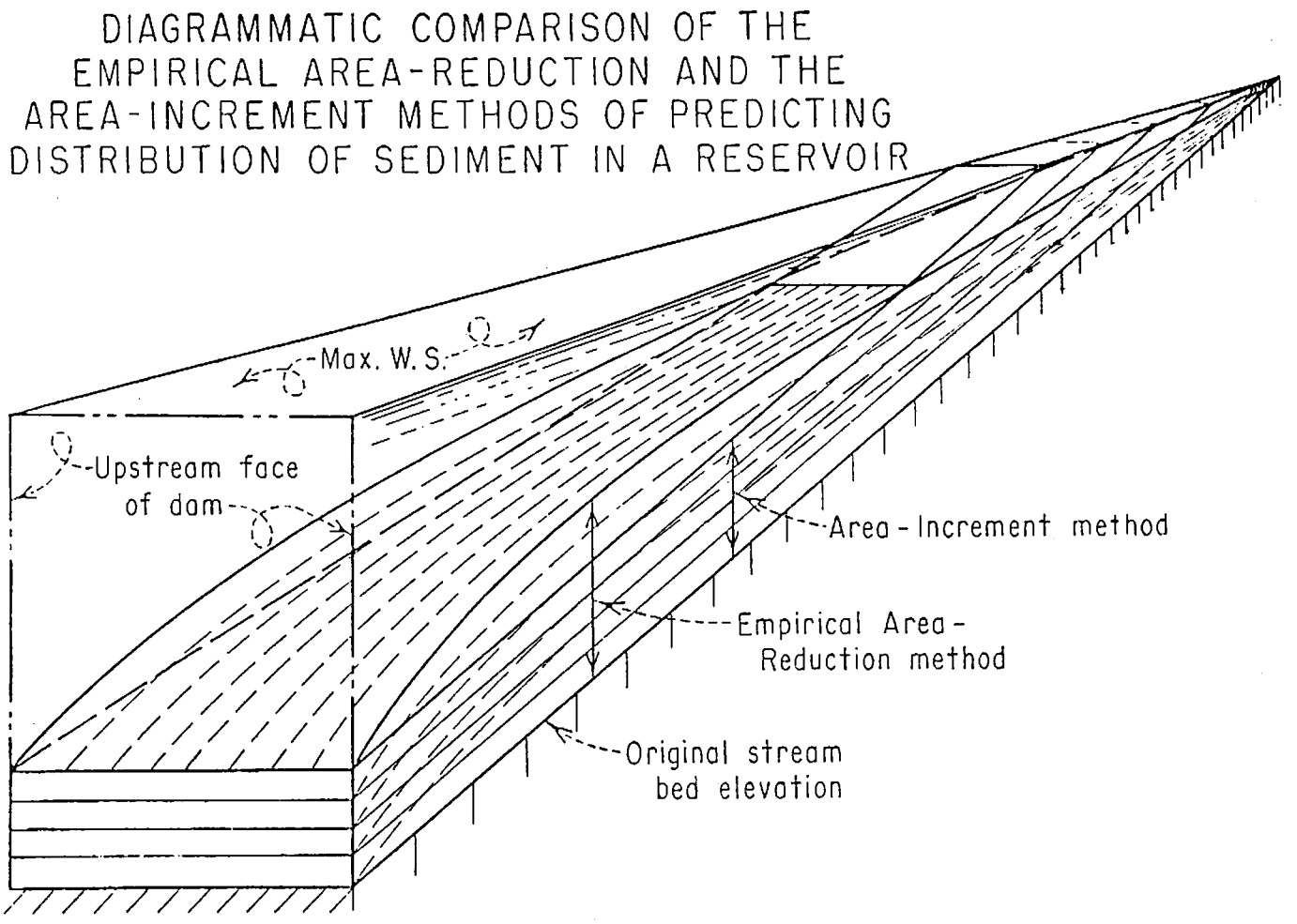


Figure 15-13. Empirical area-reduction/area increment comparison.

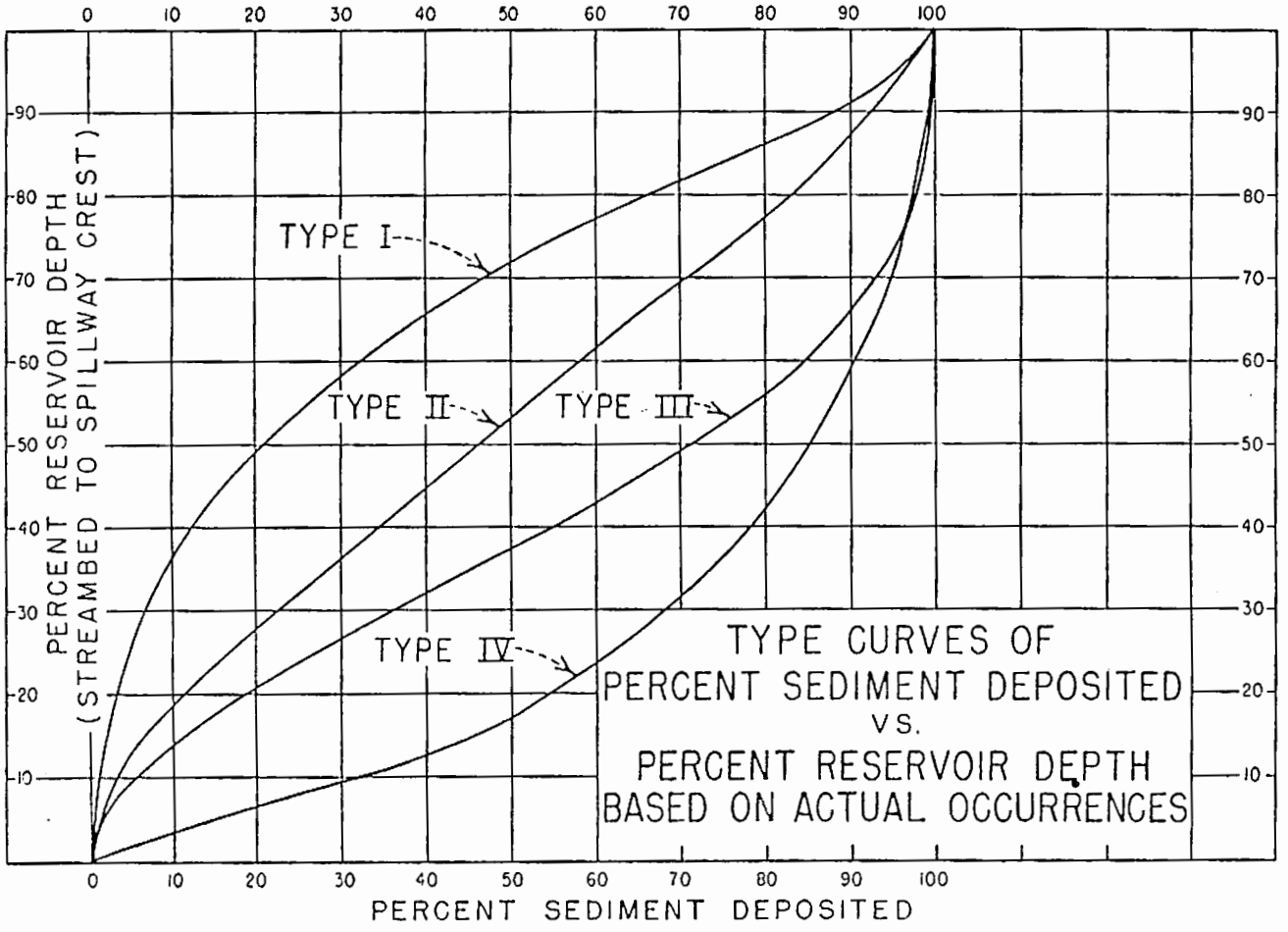


Figure 15-14. Empirical area-reduction method type curves.

reciprocal of the slope (n) of the plot of depth versus reservoir capacity on log-log paper as depicted in Figure 15-15. The general reservoir types are listed in Table 15-1.

Table 15-1. General reservoir types.

| Value of M | Reservoir Type | Standard Classification |
|---|---|---|
| 1.0-1.5 | Gorge | IV |
| 1.5-2.5 | Hill | III |
| 2.5-3.5 | Flood Plain-Foothill | II |
| 3.5-4.5 | Lake | I |

Once the reservoir is classified, the remainder of the process is mathematical. The projected sediment inflow is distributed in accordance with the type of reservoir it most closely resembles. The characteristic shape of the deposition profile is depicted in Figure 15-13.

The method does allow for deposition to occur in accordance with distributions found in existing reservoirs, which is a better basis than found with the Area Increment Method. It still does not include the effect of all factors which determine the deposition patterns, but assumes all the factors are related to reservoir geometry. The sediment characteristics and physical processes unique to each reservoir are not accounted for. Results will usually be more accurate than those obtained using the Area Increment Method, but can be expected to vary widely from actual observations. Predictions will usually be conservative and unconservative in the same manner as the Area Increment Method.

Pool-Elevation Duration Method (1969). Hobb's (1969) method is based on the premise that reservoir operation and the sediment gradation are two of the most important factors influencing the sediment distribution. It also assumed that:

1. When reservoir elevations are between the maximum and minimum inflowing sediment transported by medium and moderate floods will be deposited over an extended period of time according to a statistical order of coincidence.

2. The regulation of rare floods and the resulting deposition at higher elevations will be similar.

The procedure requires that the geometry of the reservoir be known in order that elevation/capacity data can be developed. The planned operating schedule is needed in order to develop a pool-elevation duration graph. It is also necessary to project the amount of sediment expected to accumulate in the reservoir and percentage of that sediment which is sand. Based on the percentage of time that the reservoir is at or below a given stage, an index is developed for each elevation. Figure 15-16 is a plot of these indices versus the cumulative percent of total accumulation with the data plotted reflecting actual measurements in the reservoirs indicated. The sand scale is derived from Figure 15-17 which reflects data from 11 reservoirs.

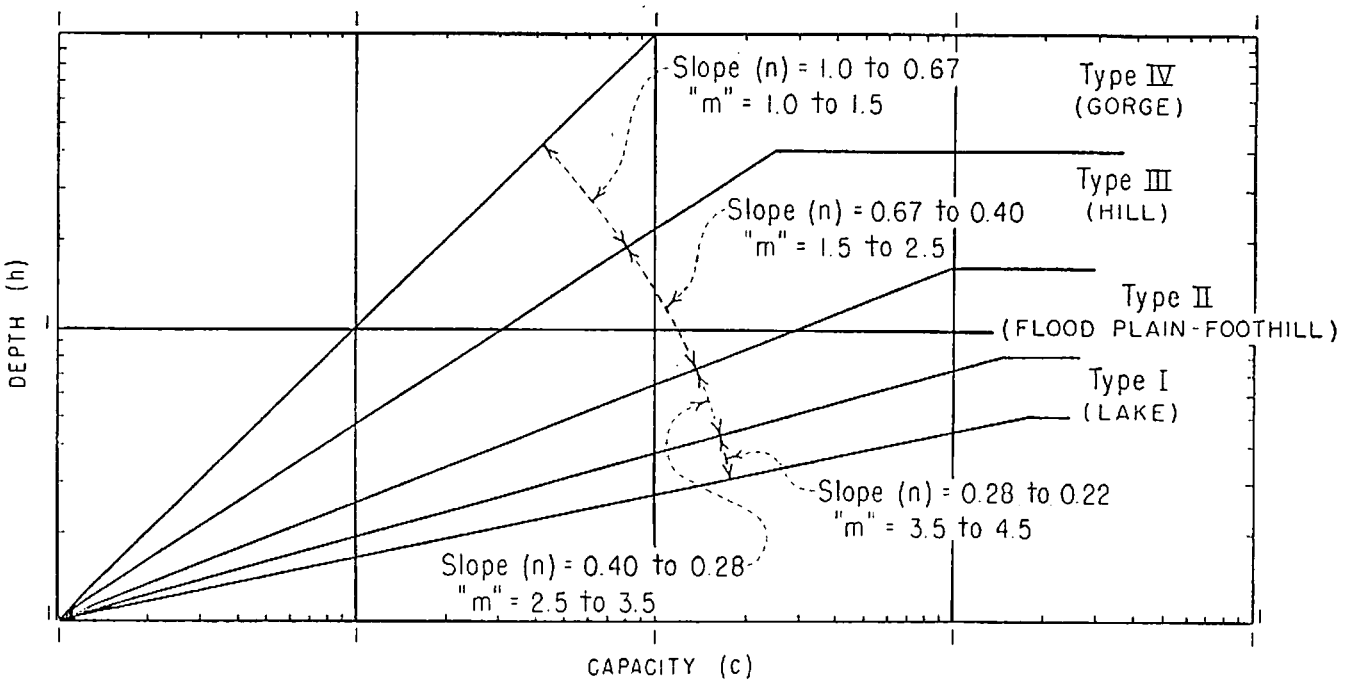


CLASSIFICATION OF RESERVOIRS
BY
DEPTH VERSUS CAPACITY
RELATIONSHIP

Figure 15-15. Reservoir type determination.

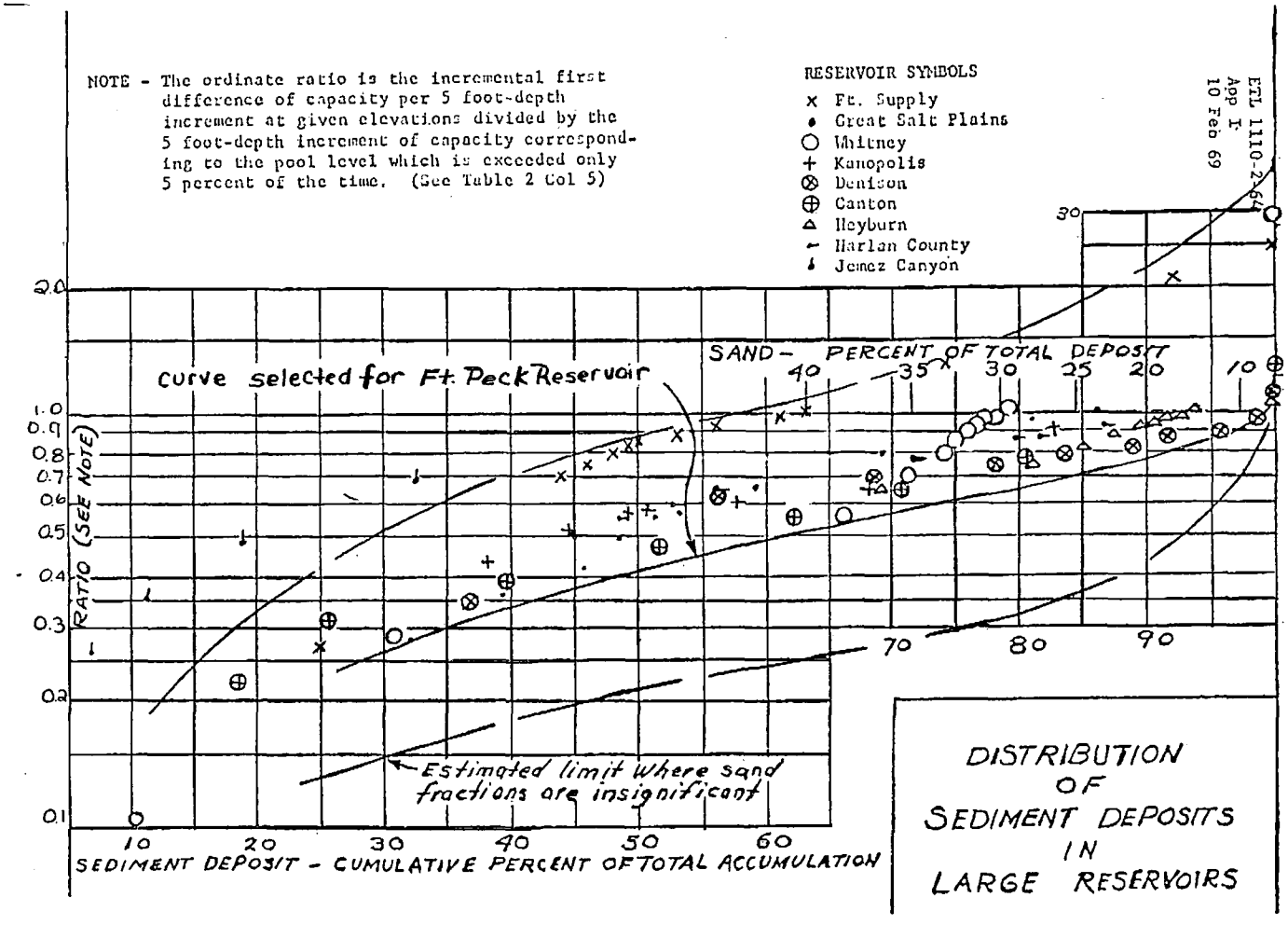


Figure 15-16. Distribution of sediment deposits in large reservoirs.

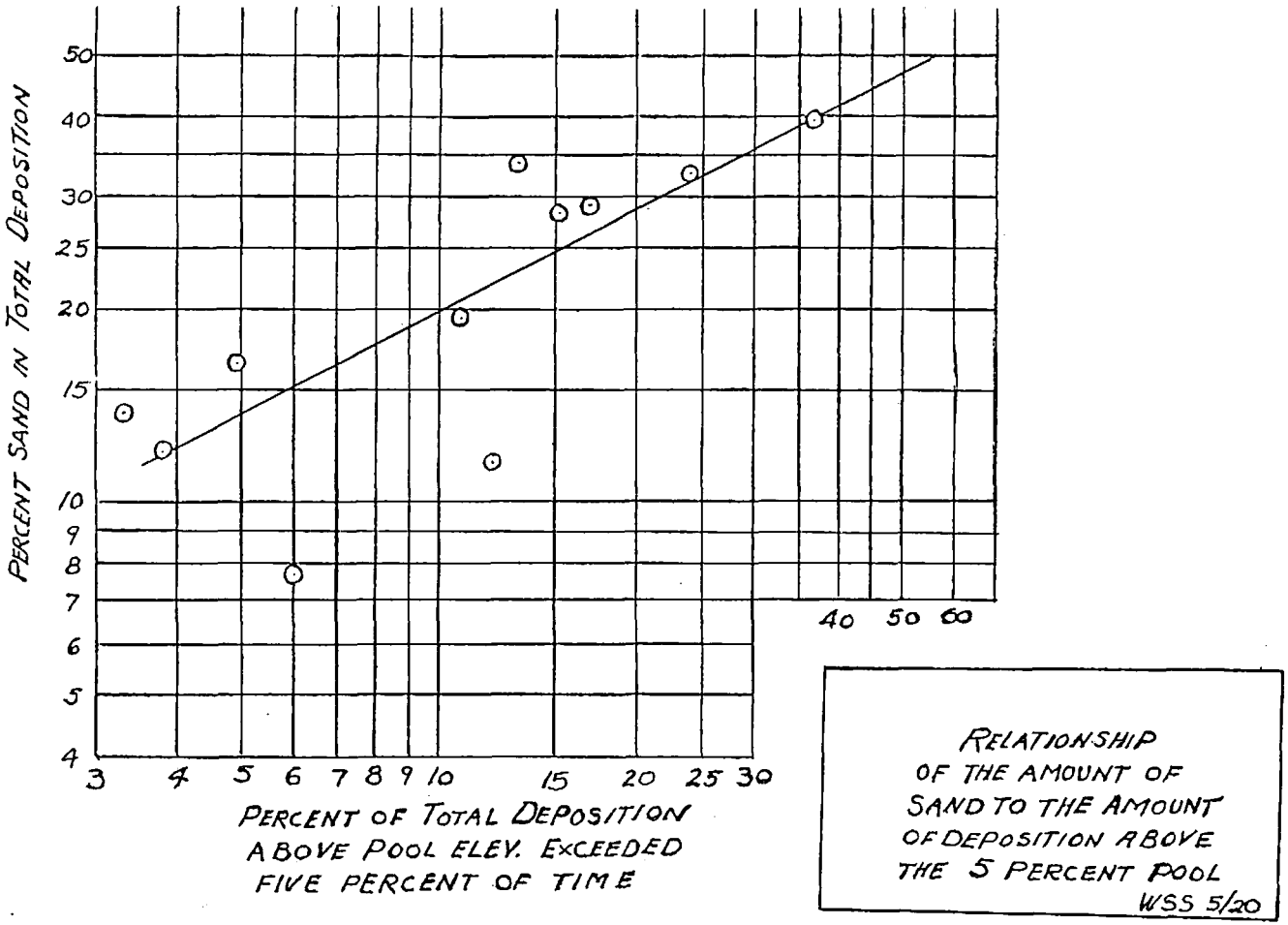


Figure 15-17. Amount of sand vs. deposition above 5 percent pool.

Based on the sand scale as the initial plotting point, a curve of the general shape of existing curves is drawn. The index and cumulative accumulation is read. The upper envelope is based on the maximum reasonable percent of sand in the deposition and the lower limit is estimated for deposits where sand is an insignificant percentage.

The Fort Peck Reservoir curve was drawn based on four percent sand. The results compared favorably with actual measurements and can be seen in Table 15-2.

The geometry is considered as it relates to reservoir capacity. The percentage of sand versus other depositional material, reflects a concern for sediment characteristics. Reservoir operation is considered on a time/stage basis.

As it stands now, the method is based on limited data. If this method is to be considered reliable for general application, much more testing is required. No evidence has been found that indicates use or verification since it was published in 1969.

Garde, Swamee, and Dalvi Method (1978). The authors developed a scheme for predicting progressive delta formation using the ideographic delta profile as a model (topset and foreset slopes). The focal point of the method is an empirically derived equation which is used to estimate the progressive loss of capacity (Swamee and Garde, 1977).

$$\frac{V_s}{V_o} = \frac{(t/t_*)^m}{[1+(t/t_*)^{m/n}]^n} \qquad (15\text{-}2)$$

where $V_o$ = initial volume

$V_s$ = volume of sediment deposited in t years

$t_*$ = time in years since reservoir operation began

$t_*$, m, and n = constants for a given reservoir

$t_*$ = time when $V_s = V_o$ (reservoir full with sediment)

m = slope of $V_s/V_o$ versus t on log-log paper

n represents the departure from a straight line of the plot of $V_s/V_o$ versus t at approximately $V_s/V_o$ equal to .6. From analysis of reservoirs that have completely filled, n equals approximately .25.

Once the constants are established in Equation 15-2, the sediment can be distributed in the reservoir at any time in accordance with Figure 15-18. This is accomplished using the assumed geometry defined in the figure and empirical relationships between the geometric variables and t, $t_*$, and $V_v$ (the cumulative volume of inflow per unit width of reservoir at full reservoir level). These relationships are based on limited data.

Table 15-2. Estimate of distribution of sediment deposits using pool-elevation duration method.

Estimate of Distribution of Sediment Deposits in Fort Peck Reservoir Missouri River, Montana

| Pool Elev. Duration (Percent of Time)[1] | Elev (Ft MSL) | Depth (Ft) | First Diff of Capacity Ac-Ft/5-ft Depth Increment) | Ratio[2] (col. 4 ÷ 1,125,000) | Sediment Distribution | |
|---|---|---|---|---|---|---|
| | | | | | Estimated (Σ%) | Measured (Σ%)[3] |
| 1 | 2 | 3 | 4 | 5 | 6 | 7 |
| 10 | 2,117 | 84.0 | 236,000 | 0.27 | 30.0 | 32.0 |
| 20 | 2,116.5 | 143.5 | 580,000 | 0.52 | 65.0 | 78.5 |
| 30 | 2,195 | 162.0 | 722,600 | 0.64 | 79.0 | 92.0 |
| 40 | 2,208 | 175.0 | 828,000 | 0.74 | 88.0 | 95.5 |
| 50 | 2,212 | 179.0 | 862,000 | 0.77 | 90.0 | 97.8 |
| 60 | 2,218 | 185.0 | 915,000 | 0.81 | 94.0 | 98.8 |
| 70 | 2,225 | 192.0 | 987,000 | 0.88 | 97.0 | 99.5 |
| 80 | 2,230 | 197.0 | 1,030,000 | 0.92 | 98.5 | 99.8 |
| 90 | 2,236 | 203.0 | 1,090,000 | 0.97 | 99+ | |
| 95 | 2,240 | 207.0 | 1,125,000 | 1.00 | 99.5 | 99.95 |
| 100 | 2,248 | 215.0 | 1,200,000 | 1.07 | 100.0 | 100.0 |

[1] Percent of time pool was at or below corresponding elevation shown in Column No. 2.
[2] Ratio is 1.0 at the 95 percent pool.
[3] Values from Item No. 26 of Reservoir Sediment Data Summary (see Curve 3 Figure 15-1).

The method does attempt to account for the general form of delta development, but the analysis has neglected consideration of key factors relating to that development. Shortcomings of the methods are as follows:

1. Method is based on data from only nine reservoirs.

2. Reservoir operation is not considered. The maximum depth of water is the only stage referenced.

3. The total inflow of sediment is computed, but no account is made of the various size fractions. All sediment is considered to form the delta.

4. The distribution of sediment is based strictly on geometry. Continuity of the sediment is not maintained at each time increment as no effort is made to match total sediment deposited to the capacity of that part of the reservoir filled.

5. The value of parameters needed to define topset and foreset slopes at each time increment vary over a wide range. The uncertainty involved in assuming values for these parameters limits the application of the method in reservoir design.

6. The authors make no mention of the type of reservoir modeled. Without investigating each reservoir, it appears that the method relates to a normally ponded condition, where a large percentage of the inflowing sediment is sand or larger.

Based on the degree of empiricism used, more data from existing reservoirs must be included before the method is used for prediction of deposition profiles in reservoirs under design. The types of reservoirs for which it is applicable must be clearly delineated.

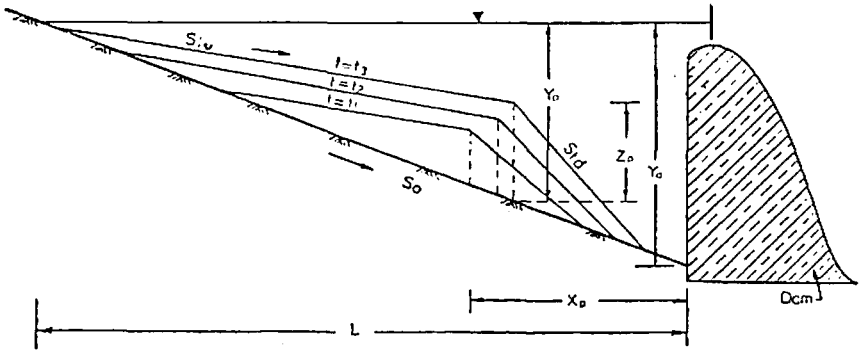


Figure 15-18. Representative section of deposition profiles.

Mangla Reservoir Sedimentation (1973). The method presented (Szechowycz and Qureshi, 1973) takes into account those known characteristics of delta formation as a function of time in order to predict the useful life of a reservoir. The method is applied to the Mangla Reservoir in West Pakistan. Key points of the method follow.

1. Sediment inflow concentration and composition are established by field tests. Composition is considered to be constant at all flows, but the concentration is fitted to an equation of the general form

$$Q_s = aQ \qquad (15\text{-}3)$$

where $Q_s$ = sediment load
$a$ = a parameter
$Q$ = total inflow

2. The specific weight of the sediment was calculated using the Lane and Koelzer (1953) formula. An average value was used for all sediment.

3. Reservoir operation is considered to be deterministic and cyclic on an annual basis. Elevations were allowed to range between the normal pool level and a projected drawdown level.

4. The delta was considered to be formed starting at the river-reservoir juncture. During high flow, the delta would progressively move into the reservoir from this juncture. The sand and 25 percent of the silt particles were considered to form the delta. The delta slope was based on a dominant discharge, the coarse load, median size of the coarse load, channel width, and depth of the dominant discharge.

5. The pattern of deposition of the fine fractions (the clay and 75 percent of the silt) is not determined except that they are deposited downstream from the delta formation. The percentage trapped is determined using the method developed by Brune (1953).

This method is the only empirical procedure discussed which bases the deposition pattern in the reservoir on the characteristics of the processes which occur rather than attempting to correlate a future pattern to the profiles formed in existing reservoirs. Even though the processes are based on empirical evidence and treated empirically within the model, they provide a better representation of the sedimentation process than do the correlation models discussed. By being able to discern the characteristics of the reservoir being planned, the associated processes can be accounted for, producing a model with reasonable predictive capabilities.

Analytical Models

An analytical model indicates the use of appropriate equations of flow and sediment movement to describe the processes affecting sediment deposition. This type model requires an exact knowledge of the mechanics of the processes and an ability to represent these processes and their interactions mathematically. Due to the complexity of the system, a totally analytical deposition model has not been formulated. Empiricism has been used to bridge the gaps where adequate analytical expressions are lacking. Viable analytical techniques to date have been offshoots of the mechanics of rivers. Both flow and sediment transport techniques have been adapted to the reservoir system. As a result of this general trend, the methods can only be applied up to the point where the flow in the reservoir can be approximated by an enlarged river. This basically limits their use to narrow, run-of-the-river reservoirs. The patterns of flow in other types of reservoirs are extremely difficult to formulate analytically.

An important characteristic of these methods is that they require calibration and verification. The parameters of the various equations must be manipulated until the model can reproduce observations in the

field. These parameters usually can take on a wide range of values making calibration difficult. As a result, application for predicting deposition in a planned reservoir is extremely limited.

A major problem associated with the extrapolation of river mechanics to the reservoir is the accuracy of river sediment formulas to accurately predict river responses. The following statement summarizes their reliability in a river system:

> There have been many equations developed for the estimation of bed material transport. The variation in the magnitude of the bed-material discharge that these equations predict is tremendous. For the same discharge, the predicted discharge can have a 100 fold difference between the smallest and the largest value. This should not be unexpected given the number of variables, the interrelationship between them, the difficulty of measuring many of the variables, and the statistical nature of bed material transport (Karaki, Mahmood, Richardson, Simons, and Stevens, 1974).

Application of such formulas to a more complex system can only decrease their reliability.

Analytical models have characteristically taken two basic forms (Lopez, 1978)

1. Type I: A simplified form of the differential equation representing flow continuity is used to make backwater computations and, thus, flow at various cross sections. Basic sediment transport equations are used to route the sediment inflow. The sediment deposited in a given reach is the difference between the transport capacity at the beginning and end of the reach. Specific methodologies have been developed by Fowler (1957), Thomas (1970), Yucel and Graft (1973), Asada (1973), and Hurst and Chao (1975).

2. Type II: The differential equations depicting the one-dimensional equations of continuity of water and sediment and the momentum equation for sediment-laden water are used in conjunction with sediment transport and bed friction equations. The equations are solved at specified time intervals using numerical techniques. The solution can be coupled or uncoupled. A coupled solution solves the flow and sediment transport equations together at each step. In the uncoupled solution, the flow is determined first and, based on these calculated flows, the sediment is routed through the reservoir. Chang and Richards (1971), Garde and Swamee (1972), and Lopez (1978) employed these principles in developing models.

The following paragraphs describe various analytical techniques which represent the different approaches. They are presented to point out the importance of establishing the dominant processes, clarify the methodologies, and review some of the pertinent equations utilized.

Merrill Models (1974). Merrill attempted to predict deposition patterns in reservoirs by assuming that the process could be modeled by the two dimensional diffusion equation

$$\frac{\partial C}{\partial t} = k_x \frac{\partial^2 C}{\partial x^2} + k_y \frac{\partial^2 C}{\partial y^2} \qquad (15\text{-}4)$$

where C = the sediment concentration
x and y = the longitudinal and lateral directions, respectively
t = time
$k_x$ and $k_y$ = the diffusion coefficients in the x and y directions, respectively

The reservoir is divided into two dimensional cells to facilitate the finite-difference solution to Equation 15-4. The depth of each cell is not considered to affect the diffusion process and is considered explicitly as it relates to volume and concentration.

At $t = 0$, a slug of sediment is introduced at the head of the reservoir. This volume of sediment is held constant for the entire period of analysis. The sediment is diffused by an iterative process until a predetermined trap efficiency is satisfied. At this time it is assumed that all sediment in suspension settles to a location immediately below its present position. This additional thickness is added to the previous elevation assigned to a cell and, thus, the new reservoir shape is acquired.

An increase in the sophistication of the solution process does not always correlate directly with improved results. The author does look at the problem in two dimensions and even varies trap efficiency as the capacity of the reservoir is depleted. Beyond these two desirable features, not much positive can be said about the model formulation

1. Reservoir operation is not considered. The pool elevation is held constant over a long period of analysis (ten years minimum).

2. No real effort is made to distinguish between the different sediment characteristics. Sand and the larger silt particles will obviously not diffuse as rapidly as they will settle from suspension. These settling properties are not considered. The diffusion coefficients used are the same for all fractions and all directions. No distinction is made between the consolidation properties of the different fractions.

3. The two reservoirs modeled received a sediment load which was predominantly fine grained, making the bottom type deposit predominant. The effect of density flow was not considered.

4. The paramount shortcoming of this method is the assumption that the movement and deposition of sediment within the reservoir can be viewed totally as a diffusion process. Diffusion is of minor importance when compared to other processes affecting sediment distribution. The fall velocities

alone will out weight the effect of such an assumed diffusion process. The method allows only the sediment to flow through the water without considering the movement of water with the sediment entrained.

It must be said that this proposed model is an excellent example of knowing the answer, choosing a method of solution, and making that method reproduce the answer. Any agreement between model output and observed data has to be the result of coefficient selection and selective empiricism.

Analytical Step Method (1957). This is a Type I model. It is one of the earliest attempts to route sediment through a reservoir using analytical relationships. The procedure relates the difference between the sediment transport capabilities of a river under natural conditions to those existing after the reservoir is in operation. It is based on the following relationship developed by Rouse

$$C = \phi\left[\frac{U_*}{w}, h\right] \tag{15-5}$$

where $C$ = sediment concentration
$U_*$ = shear velocity
$w$ = fall velocity
$h$ = depth of flow

The depth is considered to be of less significance than $U_*/w$ and is neglected. It is assumed that the concentration ratio will be

$$\frac{C_n}{C_1} = \phi\,\frac{U_{*n} \cdot w_1}{w_n \cdot U_{*1}} \tag{15-6}$$

where 1 denotes the cross section at the river-reservoir juncture and n is any delineated cross section downstream from 1. If the different fractions are routed separately, then the fall velocity at any section is constant. Therefore

$$\frac{C_n}{C_1} = \phi\,\frac{U_{*n}}{U_{*1}} \tag{15-7}$$

$U_{*1}$ corresponds to a fully saturated condition. $C_1$ usually does not reflect the fully saturated suspended load due to limitations on the source of the wash load. Assuming that $U_*$ critical, corresponding to a fully saturated condition, is a constant for a given particle size within the normally experienced limits of an alluvial channel, it is determined graphically by plotting $U_{*1}$ versus $C_1$ for several rivers. It is the value that $U_{*1}$ has when $C_1$ becomes a constant. Then

$$\frac{C_n}{C_1} = \phi(U_{*n}) \tag{15-8}$$

and $U_{*1}$ is a constant for each size fraction. Given the inflow concentration $C_1$ and that

$$U_* = \sqrt{ghS} \tag{15-9}$$

where g = gravitational constant
S = water surface slope

and h and S are determined from backwater computations, then the difference in sediment transport at the beginning and end of a reach gives the sediment deposited within the reach. The sediment is distributed and the new channel and flow characteristics are used to calculate the backwater profile and sediment transport capabilities for the next iteration.

The method was applied in the design phase to a run-of-the-river, the Dardanelle Reservoir, a navigation and power pool on the Arkansas River. Due to the possible variations in the method and the various assumptions which create large discrepancies in the final results, the method was deemed of questionable reliability (Corps of Engineers, Little Rock District, 1957).

Several key factors are accounted for in this methodology, but it is of limited use unless it is calibrated using field data and the validity of the assumptions is verified.

Lopez Model (1978). This work represents a rigorous attempt to account for the flow and sediment characteristics, the reservoir geometry, and reservoir operation in predicting the volume and pattern of deposition in a reservoir using the Type II approach. The procedure developed consists of two steps.

1. The routing of water through the entire system, which is depicted schematically in Figure 15-19, uses the gradually varied, unsteady flow and momentum equations for sediment-laden water. The flow equation is expressed as

$$\frac{\partial Q}{\partial x} + \frac{\partial A}{\partial t} + \frac{\partial Ad}{\partial t} - q_L = 0 \tag{15-10}$$

where Q = discharge of sediment-laden water
A = cross-sectional area of the channel
Ad = volume of deposition or erosion of sediment per unit length of channel
$q_L$ = lateral inflow of sediment-laden water into the stream
x = distance along the channel bed measured in the downstream direction
t = time
$\partial Ad/\partial t$ is considered much less than $\partial A/\partial t$ and the equation becomes

$$\frac{\partial Q}{\partial x} + \frac{\partial A}{\partial t} - q_L = 0 \tag{15-11}$$

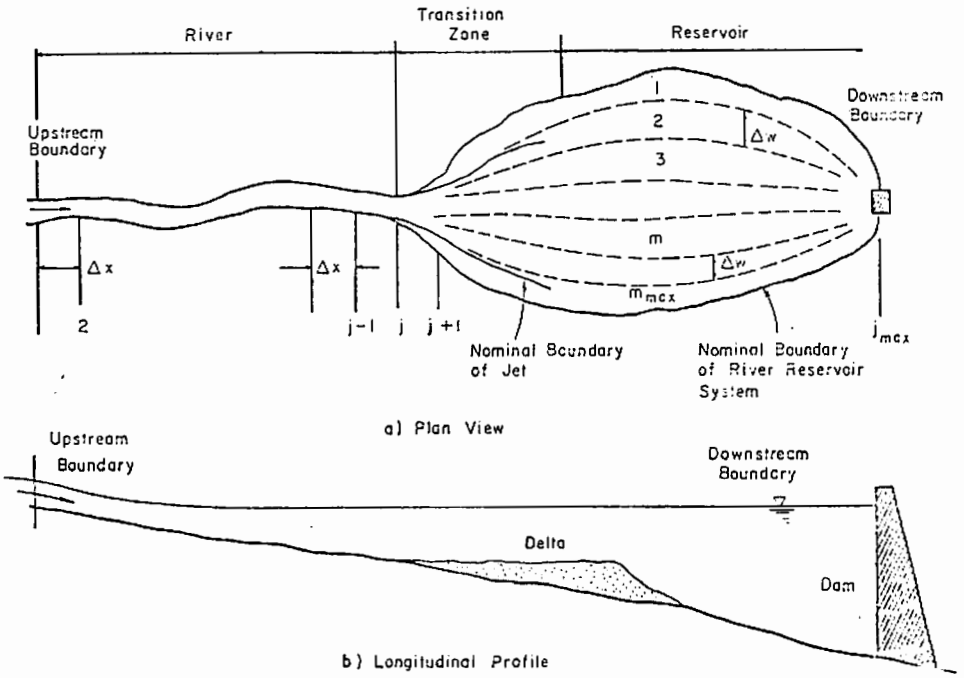


Figure 15-19. The river-reservoir system i.a.w., the Lopez Model.

The momentum equation for sediment-laden water is

$$\frac{\partial(\rho\beta QV)}{\partial x} + \frac{\partial(\rho Q)}{\partial t} + gA\frac{\partial(\rho h)}{\partial x} = \rho gA(S_o - S_f) + \rho Q_L V_L \quad (15\text{-}12)$$

where $V$ = mean flow velocity
$g$ = gravitational constant
$\rho$ = density of sediment-laden water
$\beta$ = momentum correction factor for velocity distribution
$h$ = flow depth
$S$ = friction slope
$V_L$ = velocity component of the lateral flow in the x-direction

It is assumed that $\partial\rho/\partial x = \partial\rho/\partial t = 0$ and the equation becomes

$$\frac{\partial(\beta QV)}{\partial z} + \frac{\partial Q}{\partial t} + gA\frac{\partial h}{\partial x} = gA(S_o - S_f) + q_L V_L \quad (15\text{-}13)$$

These equations are solved using a linear-implicit scheme of finite differences for each x over each t given the discharge at the upstream boundary and the outflow at the downstream boundary (the dam). The results give Q and h at each specified cross section. For this step the entire system is treated as a single channel.

Flow in the transition region is considered to be representative of a two-dimensional submerged jet. The velociety changes associated with jet expansion are accounted for by using jet theory in conjunction with some simplifying assumptions.

2. The second step uses the flow rates determined in step one to route the sediment within the reservoir system. The basic equation used is the sediment continuity equation

$$\frac{\partial Q_s}{\partial x} + P\frac{\partial Ad}{\partial t} + \frac{\partial AC_s}{\partial t} - q_{SL} = 0 \quad (15\text{-}14)$$

where $Q_s$ = total sediment load in units of volume per unit time
$P$ = volume of sediment in a unit volume of bed layer
$C_s$ = average sediment concentration in the cross section on a volume basis
$q_{SL}$ = lateral sediment inflow into the stream

The reservoir is divided into m channels as per Figure 15-19. The total flow at a cross section is divided into these channels by multiplying the total flow by the conveyance of the sub-channel divided by the conveyance of the entire channel. The sediment continuity equation becomes

$$\frac{\partial Q_{s_m}}{\partial x} + P_m \frac{\partial Ad_m}{\partial t} + \frac{\partial AC_s}{\partial t} - q_{s_m} + q_{s_{(m-1)}} = 0 \qquad (15\text{-}15)$$

$$\forall\ m = 1, 2 \ldots\ldots m_{max}$$

where $q_{s_m}$ = sediment transfer between channels

The $q_{s_m}$ terms are evaluated by first solving the continuity equation for flow between channels $q_m$ at the various cross sections in the divided reservoir and then substituting them into the equation representing lateral discharge

$$q_{s_m} = C'_s \Big|_{aa'} q_m + k_{yd} \frac{\partial C'_s}{\partial y} \qquad (15\text{-}16)$$

where $C'_s$ = suspended sediment concentration in the longitudinal direction at section aa'

$k_y$ = diffusion coefficient for the sediment particles in the laterial direction

$d$ = average flow depth

$\frac{\partial C'_s}{\partial y}$ = suspended sediment concentration gradient in the lateral direction

In order to evaluate $P$ that varies according to sediment gradation, the specific weight of the deposited sediments is considered a variable (weight/volume). Equation 15-15 becomes

$$\frac{\partial Q_{s_m}}{\partial x} + \gamma_{d_m} \frac{\partial Ad_m}{\partial t} + \gamma_{s_m} \frac{\partial AC_s}{\partial t} - q_{s_m} + q_{s_{(m-1)}} = 0 \qquad (15\text{-}17)$$

Now $Q_{s_m}$ and $q_{s_m}$ are expressed in units of weight per unit time and $\gamma_{s_m}$ is the specific weight of the transported sediment (assumed to be 165.36 lb/ft based on a specific gravity of 2.65). Different size fractions are routed separately and $\gamma_{d_m}$ is corrected at each time step.

The boundary condition needed to solve Equation 15-17 is the inflow sediment hydrograph. The inflowing sediment $Q_s$ is related to the inflow velocity $U$ by the following relationship

$$Q_s = eu^f \qquad (15\text{-}18)$$

where $e$ and $f$ are parameters which have to be calibrated from field surveys or from available equilibrium data. This correlation is made for each sediment size considered.

The values of all variables are known except for $Ad_m$. Equation 15-17 can now be solved for all sub-channels in all reaches for each $\Delta t$.

Problems associated with the use of this method follows

1. This method relates to a system where the dominant movement of water is through the reservoir at each lateral cross section and the reservoir system is merely an expanded channel. This situation is limited to narrow, run-of-the-river type impoundments.

2. It neglects the effect of density flow.

3. The process of delta formation is not addressed. The approach used may closely approximate a narrow reservoir, but the avulsion process must be considered in the wider reservoirs.

4. The density of the deposited sediment is considered and modified after each t to account for redistribution of sediment sizes in each reach, but the consolidation with time of undisturbed sediment is not considered.

5. The friction slope is considered constant across the entire cross section which is a difficult assumption to satisfy in the field.

6. The uncoupled routing process neglects the effect of the change of water density on flow within the reservoir.

7. If all assumptions made satisfy the reservoir system being modeled, calibration of the model becomes a major effort
   a. The value of Manning's n has to be determined for each subsection of the system.
   b. Jet width constants must be determined.
   c. The sediment transport parameters e and f must be determined for each sediment size fraction.
   d. The diffusion coefficient must be specified.

This is no easy task. Many computer runs are needed for the process of choosing parameters and then verifying the results by checking the model's ability to reproduce a known deposition pattern.

The model analytically accounts for several of the important processes affecting reservoir sedimentation. By following the method one can develop an understanding and appreciation for the mechanics of flow and deposition in a reservoir. The method is limited in application to systems for which the assumptions are approximately satisfied i.e., narrow run-of-the-river reservoirs. When assumptions are satisfied application is difficult due to calibration requirements. Its application for predicting the deposition in reservoirs under design is severely limited due to the requirement of model verification using existing data. Nevertheless, the model provides valuable insights into the complexities of the reservoir system.

## 15.4 CONCLUSIONS

Volume of deposition has been reasonably correlated to average detention time in normally ponded reservoirs. The run-of-the-river and

semi-dry reservoirs have not been adequately addressed. Due to the relative independence of deltaic deposition from the effects of reservoir circulation, delta formation and characteristics are much better understood than those of the bottom deposits.

The analytically derived methodologies are limited to run-of-the-river conditions in narrow reservoirs. Their application is further limited by the requirements of extensive calibration and verification. Application in the design phase of a reservoir project is tenuous at best. Empirical methods developed to predict deposition patterns are based on limited data and, for the most part, attempt to translate patterns in existing reservoirs to planned reservoirs without due consideration of the unique characteristics of the proposed project. The procedure used to predict deposition in the Mangla Reservoir deviates from the general trend utilized in the development of empirical models in that the processes, rather than reservoir resurveys, were utilized to predict patterns.

## REFERENCES

Asada, H., June 11-15, 1973, Prediction of Sediment Bed Profile in Reservoir and River Bed Deformation: A Practical Method and Some Examples of Calculation, Int. Congr. on Lg. Dams, 11th, Trans., Quest 40-43 Pap., and Geo. Rep., Madrid, Spain, V. 1, pp. 381-402.

Bates, C. C., September 1953, Rational Theory of Delta Formation, Am. Assn. Pet. Geol. Bull., Vol. 37, pp. 2119-2162.

Bondurant, D. C., June 1955, Report on Reservoir Delta Reconnaissance, Corps of Engineers, Missouri River Division Sediment Series No. 6.

Borland, W. M., 1971, Reservoir Sedimentation, River Mechanics, H. W. Shen, ed., Water Resources Publications, Fort Collins, Colorado.

Borland, W. M. and Miller, C. R., April 1958, Distribution of Sediment in Large Reservoirs, Proceedings, ASCE, V. 84, No. HY2, Paper 1587, pp. 1587-1 to 1587-18.

Brown, C. B., 1943, Discussion of Sedimentation in Reservoirs by B. J. Witzig, Proceedings, ASCE, V. 69, No. 6, pp. 793-815, 1493-1499.

Brune, G. M., June 1953, Trap Efficiency of Reservoirs, Transactions, Am. Geophysical Union, U. 34, Mo. 3, pp. 407-418.

Brune, G. M. and Allen, R. E., 1941, A Consideration of Factors Influencing Reservoir Sedimentation in the Ohio Valley Region, Transactions, Am. Geophysical Union, V. 30, pp. 649-655.

Chang, Hai-Yain, 1967, Hydraulics of Rivers and Deltas, Ph.D. dissertation, Department of Civil Engineering, Colorado State University, Fort Collins, Colorado.

Chang, F. F. M. and Richards, D. L., June 1971, Deposition of Sediment in Transient Flow, Proceedings, ASCE, V. 97, No. HY6, June 1971.

Churchill, M. A., 1948, Analysis and Use of Reservoir Sedimentation Data, Proceedings of the Federal Interagency Sedimentation Conference, U.S. Bureau of Reclamation, Denver, Colorado, pp. 139-140.

Corps of Engineers, Little Rock District, October 1957, Project Design Memorandum No. 6, Sedimentation-Part IV, Dardanelle Reservoir, Corps of Engineers, Little Rock District, Little Rock, Arkansas.

Cristofano, E. A., September 1953, Area Increment Method for Distributing Sediment in a Reservoir, U.S. Bureau of Reclamation, Albuquerque, New Mexico, September 1953.

Daily and Harleman, 1973, Fluid Dynamics, Addison-Wesley Publishing Company, Inc., Reading, Mass.

Fowler, L. C., November 1957, Determination of Location and Rate of Growth of Delta Formations, Corps of Engineers, Missouri River Division Sediment Memorandum No. 6, Omaha, Nebraska.

Garde, R. J. and Swamee, P. K., 1973, Analysis of Aggradation Upstream of a Dam, Proceedings, IAHR, International Symposium on River Mechanics, V. 1, Bangkok.

Garde, R. J., Swamee, P. K., and Dalvi, M. E., November 1978, Estimation of Progressive Deposition in Reservoirs, Proceedings of the 47th Research Session of the CBIP, Hubli-Dharwar, Karnataka, V. 1.

Harrison, A. S., 1952, Deposition at Heads of Reservoirs, Proceedings, Fifth Hydraulics Conference, State University of Iowa, Bulletin 34, pp. 199-225.

Hobbs, B. L., July 7, 1969, Forecasting Distribution of Sediment Deposits in Large Reservoirs, Engineer Technical Letter, No. 1110-2-64, O.C.E.

Hurst, A. J. and Chow, P. C., 1975, Sediment Deposition Model for Tarbela Reservoir, Symposium on Modeling Techniques, 2nd Annual Symposium of the Waterways, Harbors and Coastal Engineering Division, V. 1, pp. 501-520.

Karaki, S., Mahmood, K., Richardson, E. V., Simons, D. B., and Stevens, M. A., September 1974, Highways in the River Environment Hydraulic and Environment Design Considerations, Colorado State University, Fort Collins, Colorado, 1974.

Karaushev, A. V., 1966, Silting of Small Reservoirs and Ponds-Theory and Calculation Method, Am. Geophysical Union, Soviet Hydrology, Selected Papers, No. 1, pp. 35-46.

Lacey, G., 1946, A General Theory of Flow in Alluvium, Inst. C.E., 5518.

Lane, E. W. and Koelzer, V. A., 1953, Density of Sediments Deposited in Resevoirs, Report No. 5 of a Study of Methods Used in Measurement and Analysis of Sediment Loads in Streams, St. Paul, U.S. Eng. Dist. Sub. Office Hydr. Lab., University of Iowa, Iowa City, Iowa.

Lopez, J. L., 1978, Mathematical Modeling of Sediment Deposition in Reservoirs, Ph.D. dissertation, Colorado State University, Fort Collins, Colorado.

Merrill, W. M., August 1974, Reservoir Sedimentation: A Computer Simulation, The Kansas Water Resources Institute, University of Kansas.

Swamee, P. K. and Garde, R. J., 1977, Progressive Deposition of Reservoir Capacity Due to Sedimentation, Research Report of the Hydraulic Engineering Section of the Department of Civil Engineering, University of Roorkee.

Szechowyez, R. W. and Qureshi, M. M., September 1973, Sedimentation in Magla Reservoir, Proceedings, ASCE, V. 99, No. HY9, Paper 10033, pp. 1551-1572.

Thomas, W. A., 1970, A Digital Model for Simulating Sediment Movement in a Shallow Reservoir, Proceedings of a Seminar on Sediment Transport in Rivers and Reservoirs, The Hydrologic Engineering Center, U.S. Army Corps of Engineers, 1970.

TVA, 1968, Sedimentation in TVA Reservoirs, Tennessee Valley Authority, Report No. 0-6693, Knoxville, Tenn., February 1968.

Wright, L. D., January 1977, Sediment Transport and Deposition at River Mouths, Geol. Soc. Bull. 88, pp. 857-868.

Yucel, O. and Graft, W., 1973, Bedload Deposition and Delta Formation: A Mathematical Model, Lehigh Univeristy, Fritz Engineering Laboratory Report No. 384.1.

*U.S. GOVERNMENT PRINTING OFFICE: 1980-0-721-379/173